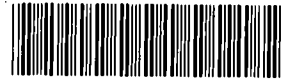


SANDIA REPORT

SAND94-0472/1 • UC-721

Unlimited Release

Printed August 1997



TL0006046

**SANDIA NATIONAL
LABORATORIES
TECHNICAL LIBRARY**

Porosity, Single-Phase Permeability, and Capillary Pressure Data from Preliminary Laboratory Experiments on Selected Samples from Marker Bed 139 at the Waste Isolation Pilot Plant

Volume 1 of 3: Main Report, Appendix A

Susan M. Howarth, Tracy Christian-Frear

Prepared by
Sandia National Laboratories
Albuquerque, New Mexico 87185 and Livermore, California 94550

Sandia is a multiprogram laboratory operated by Sandia
Corporation, a Lockheed Martin Company, for the United States
Department of Energy under Contract DE-AC04-94AL85000.

Approved for public release; distribution is unlimited.

**Sandia National Laboratories**

276 p, in
various pagings

Issued by Sandia National Laboratories, operated for the United States Department of Energy by Sandia Corporation.

NOTICE: This report was prepared as an account of work sponsored by an agency of the United States Government. Neither the United States Government nor any agency thereof, nor any of their employees, nor any of their contractors, subcontractors, or their employees, makes any warranty, express or implied, or assumes any legal liability or responsibility for the accuracy, completeness, or usefulness of any information, apparatus, product, or process disclosed, or represents that its use would not infringe privately owned rights. Reference herein to any specific commercial product, process, or service by trade name, trademark, manufacturer, or otherwise, does not necessarily constitute or imply its endorsement, recommendation, or favoring by the United States Government, any agency thereof, or any of their contractors or subcontractors. The views and opinions expressed herein do not necessarily state or reflect those of the United States Government, any agency thereof, or any of their contractors.

Printed in the United States of America. This report has been reproduced directly from the best available copy.

Available to DOE and DOE contractors from
Office of Scientific and Technical Information
P.O. Box 62
Oak Ridge, TN 37831

Prices available from (615) 576-8401, FTS 626-8401

Available to the public from
National Technical Information Service
U.S. Department of Commerce
5285 Port Royal Rd
Springfield, VA 22161

NTIS price codes
Printed copy: A13
Microfiche copy: A01

Porosity, Single-Phase Permeability, and Capillary Pressure Data from Preliminary Laboratory Experiments on Selected Samples from Marker Bed 139 at the Waste Isolation Pilot Plant

Volume 1 of 3: Main Report, Appendix A

Susan M. Howarth
Tracy Christian-Frear

Geohydrology Department 6115
Sandia National Laboratories
Albuquerque, NM 87185

ABSTRACT

Three groups of core samples from Marker Bed 139 of the Salado Formation at the Waste Isolation Pilot Plant (WIPP) were analyzed to provide data to support the development of numerical models used to predict the long-term hydrologic and structural response of the WIPP repository. These laboratory experiments, part of the FY93 Experimental Scoping Activities of the Salado Two-Phase Flow Laboratory Program, were designed to (1) generate WIPP-specific porosity and single-phase permeability data, (2) provide information needed to design and implement planned tests to measure two-phase flow properties, including threshold pressure, capillary pressure, and relative permeability, and (3) evaluate the suitability of using analog correlations for the Salado Formation to assess the long-term performance of the WIPP. This report contains a description of the borehole core samples, the core preparation techniques used, sample sizes, testing procedures, test conditions, and results of porosity and single-phase permeability tests performed at three laboratories: TerraTek, Inc. (Salt Lake City, UT), RE/SPEC, Inc. (Rapid City, SD), and Core Laboratories-Special Core Analysis Laboratory (Carrollton, TX) for Rock Physics Associates. In addition, this report contains the only WIPP-specific two-phase-flow capillary-pressure data for twelve core samples.

The WIPP-specific data generated in this laboratory study and in WIPP field-test programs and information from suitable analogs will form the basis for specification of single- and two-phase flow parameters for anhydrite marker beds for WIPP performance assessment calculations.

ACKNOWLEDGMENTS

The authors thank Joanne Fredrich (formerly with TerraTek, Inc., now with Sandia National Laboratories), Nancy Brodsky (formerly with RE/SPEC, Inc., now with Sandia National Laboratories), and Joel Walls of Rock Physics Associates for their contributions to this work. We also thank Rick Beauheim, Kurt Larson, and Peter Davies for their thorough review and thoughtful comments on this report. The authors also thank Sally Woerner, Tina Johnson, and Rick Bower of Tech Reps, Inc. for their help with the figures, tables, and technical editing.

TABLE OF CONTENTS

1.0 SUMMARY	1
2.0 INTRODUCTION AND FRAMEWORK FOR INVESTIGATION	3
2.1 Background	3
2.2 Marker Bed 139 Description	5
2.3 Salado Two-Phase Flow Laboratory Program–Preliminary Laboratory Experiments.	5
2.4 Net Effective Stress	8
2.5 Report Organization	9
3.0 MARKER BED 139 TEST SPECIMENS	11
3.1 Test Specimen Selection	11
3.2 Test Specimen Preparation and Description	17
4.0 POROSITY	19
4.1 Effective Porosity	19
4.1.1 Test Procedures	19
4.1.2 Histograms and Probability Distributions	19
4.1.3 Effect of Stress on Effective Porosity	25
4.1.4 Relationship between Zone Classification and Effective Porosity	25
4.2 Total Porosity	27
4.2.1 Test Procedures	27
4.2.2 Histograms and Probability Distribution	27
4.2.3 Relationship between Total and Effective Porosity	27
4.2.4 Relationship between Zone Classification and Total Porosity	29
4.3 Grain Density	29
4.3.1 Test Procedures	29
4.3.2 Histogram and Probability Distribution	30
5.0 PERMEABILITY	33
5.1 Test Procedures	33
5.1.1 Single-Phase Gas Permeability	33
5.1.2 Single-Phase Liquid Permeability	35
5.2 Test Results	35
5.2.1 Single-Phase Gas Permeability	35
5.2.1.1 Histograms and Probability Distributions	36
5.2.1.2 Relationship between Zone Classification and Gas Permeability .. .	40
5.2.1.3 Relationship between Confining Stress and Gas Permeability	40
5.2.2 Single-Phase Liquid Permeability	42
5.2.2.1 Histograms and Probability Distributions	42
5.2.2.2 Relationship between Zone Classification and Liquid Permeability. .	43
5.2.2.3 Relationship between Confining Stress and Liquid Permeability .. .	43
5.2.3 Comparison of Gas and Liquid Permeability	48
5.2.4 Comparison of Vertical and Horizontal Permeability	49

TABLE OF CONTENTS (Continued)

6.0	CAPILLARY PRESSURE	51
6.1	Test Procedures	51
6.1.1	Centrifuge Tests	52
6.1.2	Mercury Injection Tests	53
6.2	Test Results	53
6.2.1	Centrifuge Tests	54
6.2.2	Mercury Injection Tests	55
6.2.3	Comparison of Results from Centrifuge and Mercury Injection Tests	65
6.3	Determination of Threshold Pressure	65
6.4	Comparison of MB139 Mercury Injection Capillary Pressure Data to Brooks-Corey and van Genuchten Correlations	77
7.0	RELATIONSHIPS BETWEEN MEASURED PARAMETERS	79
7.1	Single-Phase Gas Permeability versus Porosity and Grain Density	79
7.2	Single-Phase Gas Permeability versus Threshold Pressure	79
8.0	CONCLUSIONS	83
8.1	WIPP-Specific Porosity and Single-Phase Permeability Measurements	83
8.1.1	Porosity	83
8.1.2	Permeability	83
8.2	Application of Test Results for Design and Implementation of Two-Phase Flow Tests	84
8.3	Suitability Using Analog Correlations for WIPP PA Calculations	85
9.0	RECOMMENDATIONS	87
9.1	WIPP-Specific Porosity and Single-Phase Permeability Measurements	87
9.2	Application of Test Results for Design and Implementation of Two-Phase Flow Tests	87
9.3	Technical Basis for Specification of Single- and Two-Phase Flow Parameters for PA Calculations	88
10.0	REFERENCES	91

APPENDICES

- A. Data Report: Rock Physics Associates (Core Laboratories)
- B. Data Report: RE/SPEC Inc.
- C. Data Report: TerraTek Inc.
- D. Marker Bed 139 Brine Recipe Documentation
- E. PA Parameter Package: Salado Data/Parameters: Anhydrite Two-phase Parameters. Tracy Christian-Frear to SWCF-A. January 31, 1996.
- F. Memorandum: S.W. Webb to P. Vaughn, August 29, 1995

LIST OF FIGURES

1. Stratigraphy of the Salado Formation in the vicinity of the WIPP underground excavations	4
2. The five zones of MB139, shown in an idealized core section.	6
3. Salado Two-Phase Flow Laboratory Program roadmap.	7
4. Location of boreholes for test specimens	12
5. Flow diagram for tests performed on Marker Bed 139 specimens	18
6a. Effective porosity at 0.0 MPa net effective stress histogram	21
6b. Effective porosity at 0.0 MPa net effective stress cumulative frequency plot	21
7a. Effective porosity at 3.4 MPa net effective stress histogram	22
7b. Effective porosity at 3.4 MPa net effective stress cumulative frequency plot	22
8a. Effective porosity at 6.0 MPa net effective stress histogram	23
8b. Effective porosity at 6.0 MPa net effective stress cumulative frequency plot	23
9a. Effective porosity at 10.0 MPa net effective stress histogram	24
9b. Effective porosity at 10.0 MPa net effective stress cumulative frequency plot	24
10. Effective porosity versus net effective stress	26
11. Effective porosity versus Marker Bed 139 stratigraphic zone	26
12a. Total porosity histogram	28
12b. Total porosity cumulative frequency plot	28
13. Effective porosity versus total porosity	29
14. Total porosity versus Marker Bed 139 stratigraphic zone	30
15a. Grain density histogram	31
15b. Normalized grain density cumulative frequency plot	31
16a. Gas permeability histogram for 1.6, 2.0, and 3.4 MPa net effective stress	37
16b. Normalized cumulative frequency plot for 1.6, 2.0, and 3.4 MPa net effective stress	37
17a. Gas permeability histogram for 5.6 and 6.0 MPa net effective stress	38
17b. Normalized cumulative frequency plot for 5.6 and 6.0 MPa net effective stress	38

LIST OF FIGURES (Continued)

18a. Gas permeability histogram for 9.6 and 10.0 MPa net effective stress	39
18b. Normalized cumulative frequency plot for 9.6 and 10.0 MPa net effective stress	39
19. Gas permeability versus Marker Bed 139 stratigraphic zone	41
20. Gas permeability versus net effective stress	41
21a. Liquid permeability histogram for 1.6 and 2.0 MPa net confining stress	44
21b. Normalized cumulative frequency plot for 1.6 and 2.0 MPa net effective stress	44
22a. Liquid permeability histogram for 5.6 and 6.0 MPa net confining stress	45
22b. Normalized cumulative frequency plot for 5.6 and 6.0 MPa net effective stress	45
23a. Liquid permeability histogram for 9.6 and 10.0 MPa net confining stress	46
23b. Normalized cumulative frequency plot for 9.6 and 10.0 MPa net effective stress	46
24. Liquid permeability versus MB139 stratigraphic zone	47
25. Liquid permeability versus net effective stress	47
26. Liquid permeability versus gas permeability	48
27. Gas vertical permeability versus horizontal permeability	49
28a. Centrifuge capillary pressure versus brine saturation: Sample 6	56
28b. Centrifuge capillary pressure versus brine saturation: Sample 8	56
28c. Centrifuge capillary pressure versus brine saturation: Sample 12	57
28d. Centrifuge capillary pressure versus brine saturation: Sample 14	57
28e. Centrifuge capillary pressure versus brine saturation: Sample 22	58
28f. Centrifuge capillary pressure versus brine saturation: Sample 24	58
29a. Comparison of centrifuge and mercury injection capillary pressure: Samples 5 and 6, 140° contact angle	66
29b. Comparison of centrifuge and mercury injection capillary pressure: Samples 5 and 6, 180° contact angle	66
30a. Comparison of centrifuge and mercury injection capillary pressure: Samples 7 and 8, 140° contact angle	67
30b. Comparison of centrifuge and mercury injection capillary pressure: Samples 7 and 8, 180° contact angle	67

LIST OF FIGURES (Continued)

31a. Comparison of centrifuge and mercury injection capillary pressure: Samples 11 and 12, 140° contact angle	68
31b. Comparison of centrifuge and mercury injection capillary pressure: Samples 11 and 12, 180° contact angle	68
32a. Comparison of centrifuge and mercury injection capillary pressure: Samples 13 and 14, 140° contact angle	69
32b. Comparison of centrifuge and mercury injection capillary pressure: Samples 13 and 14, 180° contact angle	69
33a. Comparison of centrifuge and mercury injection capillary pressure: Samples 21 and 22, 140° contact angle	70
33b. Comparison of centrifuge and mercury injection capillary pressure: Samples 21 and 22, 180° contact angle	70
34a. Comparison of centrifuge and mercury injection capillary pressure: Samples 23 and 24, 140° contact angle	71
34b. Comparison of centrifuge and mercury injection capillary pressure: Samples 23 and 24, 180° contact angle	71
35. Centrifuge capillary pressure data versus brine saturation: all samples (log-linear)	72
36. Mercury injection capillary pressure data versus brine saturation: all samples (log-linear)	73
37. Capillary pressure data: all samples (Cartesian)	74
38. Capillary pressure data: all samples (log-linear)	75
39. Comparison of measured MB139 mercury injection capillary pressure data (140° contact angle) to median parameter values used in determining the two-phase flow capillary pressure curve in performance assessment	78
40. Gas permeability versus effective porosity	80
41. Gas permeability versus grain density	80
42. Comparison of measured MB139 gas threshold entry pressure to Davies' (1991) correlation.	81

LIST OF TABLES

1.	Summary of Successful Preliminary Laboratory Tests Performed	2
2.	Borehole Locations	13
3a.	Detailed Summary of Information for Each Test Sample at Core Laboratories . . .	14
3b.	Detailed Summary of Information for Each Test Sample at RE/SPEC Inc	15
3c.	Detailed Summary of Information for Each Test Sample at TerraTek, Inc	16
4.	Summary of Petrographic Analysis Results	17
5.	Summary of Effective Porosity Data Results	20
6a.	Summary of Gas Permeability Data Results	36
6b.	Statistical Summary of Gas Permeability and Log of Gas Permeability	36
7.	Summary of Gas Permeability Data Results by Zone	40
8.	Summary of Liquid Permeability Data Results	43
9.	Capillary Pressure Conversion Constants Used in this Study	54
10.	Summary of Centrifuge Capillary Pressure Data	54
11a.	Mercury Injection Capillary Pressure Data for Sample 5	59
11b.	Mercury Injection Capillary Pressure Data for Sample 7	60
11c.	Mercury Injection Capillary Pressure Data for Sample 11	61
11d.	Mercury Injection Capillary Pressure Data for Sample 13	62
11e.	Mercury Injection Capillary Pressure Data for Sample 21	63
11f.	Mercury Injection Capillary Pressure Data for Sample 23	64
12.	Summary of Two-Phase Flow Data Results for Mercury Injection Cores	76

1.0 SUMMARY

Three groups of core samples from Marker Bed 139 (MB139) of the Salado Formation at the Waste Isolation Pilot Plant (WIPP) were analyzed to provide data to support development of the numerical models that are used to predict the long-term hydrological and structural response of the WIPP repository. These laboratory experiments, part of the FY93 Experimental Scoping Activities of the Salado Two-Phase Flow Laboratory Program, were designed to (1) generate WIPP-specific porosity and single-phase permeability data, (2) provide information needed to design test equipment and implement planned tests to measure two-phase flow properties including threshold pressure, capillary pressure, and relative permeability, and (3) evaluate the suitability of using analog correlations for the Salado Formation to assess the long-term performance of the WIPP. This report contains a description of the borehole core samples, the core preparation techniques, sample sizes, testing procedures, test conditions, and the results of porosity and single-phase permeability tests performed at three laboratories: RE/SPEC, Inc. (Rapid City, SD), TerraTek, Inc. (Salt Lake City, UT), and Core Laboratories—Special Core Analysis Laboratory (Carrollton, TX) for Rock Physics Associates. In addition, this report contains the only WIPP-specific two-phase flow data that exist; capillary pressure data for twelve core samples are included. The type and number of tests performed at each laboratory are summarized in Table 1 at the end of this section.

This report is intended to present the data collected during the Experimental Scoping Activities portion of the Salado Two-Phase Flow Laboratory Program. The WIPP-specific data generated in this laboratory study, combined with WIPP field-test programs and information from suitable analogs, will form the basis for specification of single- and two-phase flow parameters for WIPP Performance Assessment (PA) calculations. A separate document is planned that will contain recommendations for single- and two-phase flow parameters for anhydrite marker beds for the WIPP PA calculations.

The effective porosity of 42 samples tested ranged from 0.4 to 2.7%; total porosity of three samples ranged from 0.4 to 1.6%. Results of tests to determine the magnitude of the difference between total and effective porosity for specific samples were inconclusive. A slight reduction in effective porosity was observed when increasing confining stress was applied to a sample. Gas permeability ranged from a minimum of $5.0 \times 10^{-20} \text{ m}^2$ at 10 MPa net effective stress to a maximum of $8.3 \times 10^{-16} \text{ m}^2$ at 2 MPa net effective stress. Permeability decreased as net effective stress was increased, and an increasing gas permeability trend occurred with increasing effective porosity.

The simulated MB139 brine was found unsuitable for liquid flow tests on MB139 core samples; it caused dissolution of test specimens, resulting in order-of-magnitude increases in permeability. Liquid permeability measurements performed using odorless mineral spirits (OMS) agreed well with Klinkenberg-corrected gas permeability.

Air-brine threshold pressures determined from the mercury injection capillary pressure tests ranged from 0.33 to 0.78 MPa (48 to 113 psi). Air-brine threshold pressures from the centrifuge capillary pressure test could not be determined exactly. Residual liquid saturation ranged from 0.8 to 17.4%. The threshold pressure results from cores tested in this study are within the range that would be predicted from the Davies' (1991) correlation for anhydrite.

Table 1. Summary of Successful Preliminary Laboratory Tests Performed

Laboratory	RE/SPEC	TerraTek	Core Laboratories	Total
Total Porosity	0	3	0	3
Effective Porosity	0	14	28	42
Gas Permeability	2	6	23	31
Liquid Permeability	2	3	0	5
Capillary Pressure Centrifuge	0	0	6	6
Capillary Pressure Mercury Injection	0	0	6	6
Petrography XRD	9	6	15	30
Petrography Thin Sections	9	6	15	30

2.0 INTRODUCTION AND FRAMEWORK FOR INVESTIGATION

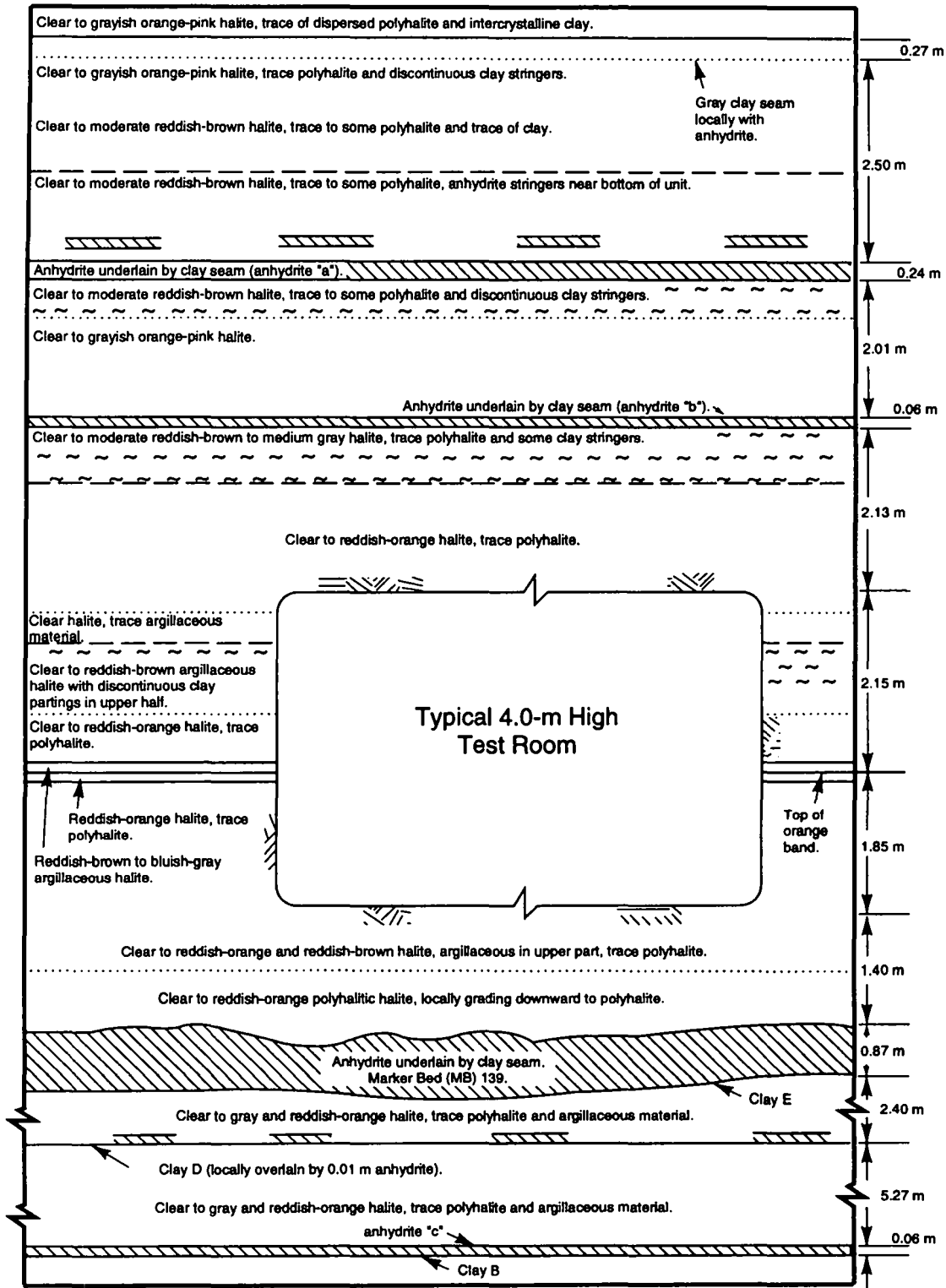
2.1 Background

The WIPP is the U.S. Department of Energy's (DOE's) planned repository for transuranic (TRU) waste generated by United States defense programs. This underground research and development effort is generating the technology base for the safe disposal of TRU waste in bedded salt. The Salado Formation was chosen for the repository in part because of salt's very low permeability and its natural ability to creep under the effects of stress, ultimately encapsulating and isolating the waste.

The Salado Formation consists of thick halite layers with interbeds of minerals such as clay and anhydrite, as shown in Figure 1. The polycrystalline Salado salt and anhydrite layers contain small quantities of brine in intragranular fluid inclusions and as intergranular (pore) fluid. It is important to quantify the amount of brine in the Salado Formation and to determine its mobility and flow properties because the accumulation and subsequent migration of significant quantities of brine in the repository might lead to problems that affect the salt's ability to isolate waste.

Salado rock and flow parameters describe its ability to transmit and store fluids. Permeability data from in situ tests indicate that the anhydrite and impure halite interbeds within the Salado Formation have higher permeability, by 1 to 2 orders of magnitude, than the pure halite intervals (Beauheim et al., 1991; 1993). Numerical flow simulations and sensitivity analyses show that the anhydrite interbeds could be the primary flow path for brine moving into the repository and the path for waste-generated gas and contaminated brine flowing outward into the formation (Davies et al., 1991). Thus the role of the anhydrite interbeds in the long-term hydrological response of the WIPP facility has become an issue that involves the initial state of the material, the mechanism(s) and potential for brine and gas flow in the material, and the influence of excavation-induced and/or gas-pressure-induced damage on these flow parameters.

About 45 siliceous or sulfatic laterally continuous units exist within the Salado Formation; these include Marker Bed 138 and MB139, which are in the vicinity of the repository horizon (Borns, 1985). MB139, an approximately 1-m thick anhydrite interbed that lies approximately 1 m below the planned waste storage rooms, is a potential gas and brine flow path. Although permeability values of 5×10^{-17} to 8×10^{-20} m² have been inferred from in situ borehole tests in MB139 (Beauheim et al., 1991; 1993), laboratory examination and testing of the anhydrite interbed material have been extremely limited until this study.



TRI-6334-257-4

Figure 1. Stratigraphy of the Salado Formation in the vicinity of the WIPP underground excavations.

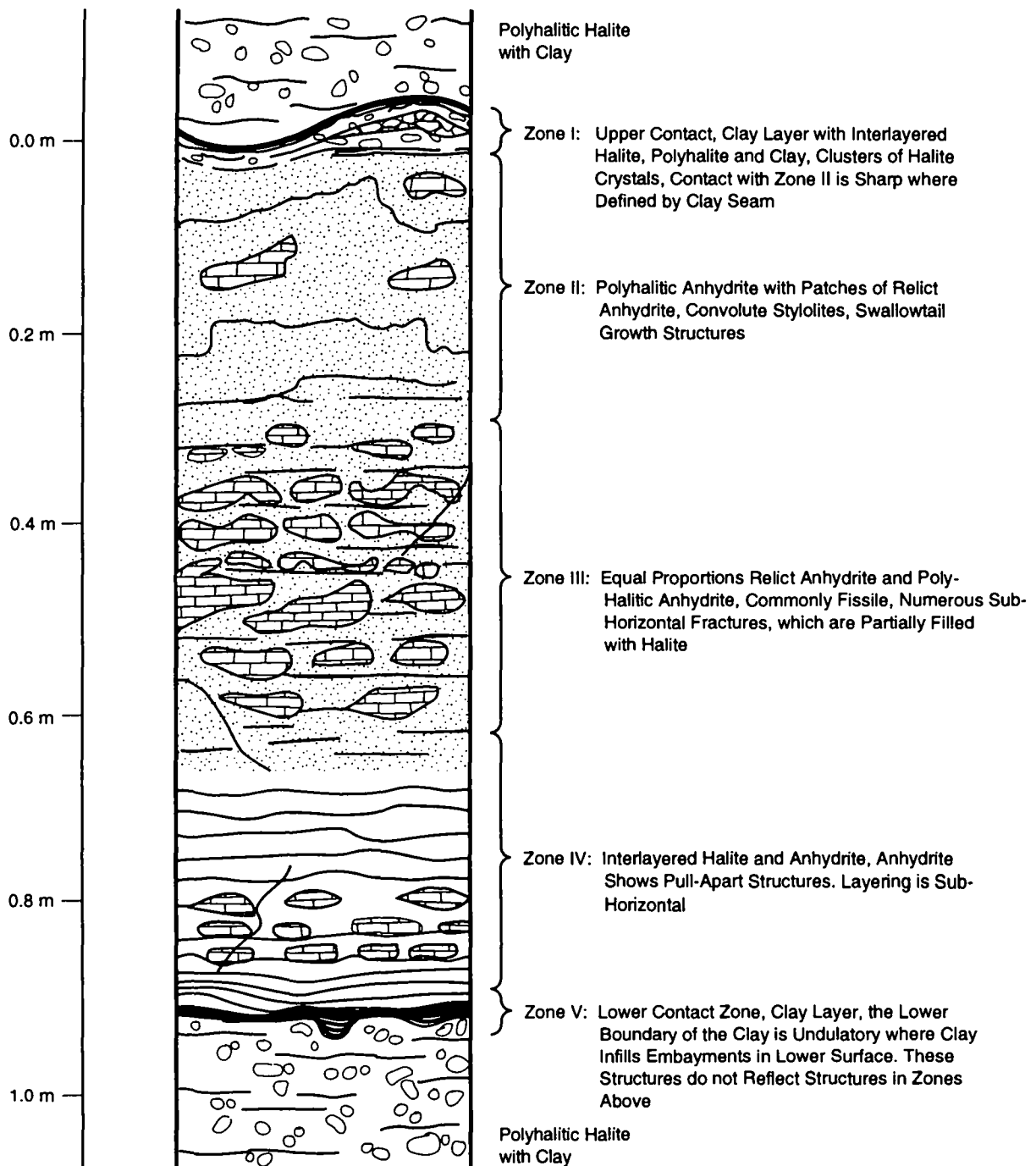
2.2 Marker Bed 139 Description

Within the Salado Formation, MB139 is one of 45 siliceous or sulfatic units that are traceable in the repository subsurface for several kilometers but may not be recognizable in every borehole. The approximately 0.4- to 1.25-m thick unit is located approximately 1 m below the planned repository interval, as shown in Figure 1. The bed is described as a microcrystalline anhydrite with moderate reddish orange/brown to light and medium grey coloring. As further described by Borns (1985) and Fredrich and Zeuch (1996), MB139 exhibits an undulatory upper surface with vertical amplitudes of approximately 0.5 m (20 in.) and wave lengths of about 0.6 to 1.8 m (2 to 6 ft). A "swallowtail" pattern, consisting of halite growths within the anhydrite, is common in the upper part of the marker bed. Locally, hairline, clay-filled low-angle fractures are located in the lower part of the unit. A thin halite layer is commonly found close to the lower contact, and clay "E" is situated at the base of the unit.

Borns (1985) studied core taken from five 10-cm (4-in.) boreholes drilled from Room 4 at the WIPP; MB139 was then mesoscopically divided into five stratigraphic zones. Zone I, termed the Upper Contact Zone, was described as the "upper contact, clay layer with inter-layered halite, polyhalite and clay, clusters of halite crystals; contact with Zone II is sharp where defined by clay seam." Zone II, termed the Massive Polyhalitic Anhydrite, was described as "polyhalitic anhydrite with patches of relict anhydrite, convolute stylolites, swallowtail growth structures." Zone III, termed the Mixed Anhydrite and Polyhalitic Anhydrite, was described as containing "equal proportions relict anhydrite and polyhalitic anhydrite, commonly fissile, numerous sub-horizontal fractures, which are partially filled with halite." Zone IV, termed the Laminated Anhydrite with Halite, was described as "inter-layered halite and anhydrite; anhydrite shows pull-apart structures, layering is sub-horizontal." Zone V, termed the Lower Contact Zone, was described as the "lower contact zone, clay layer; the lower boundary of the clay is undulatory where clay infills embayments in lower surface; these structures do not reflect structures in zones above." An idealized core section on which the five zones are identified and described is shown in Figure 2.

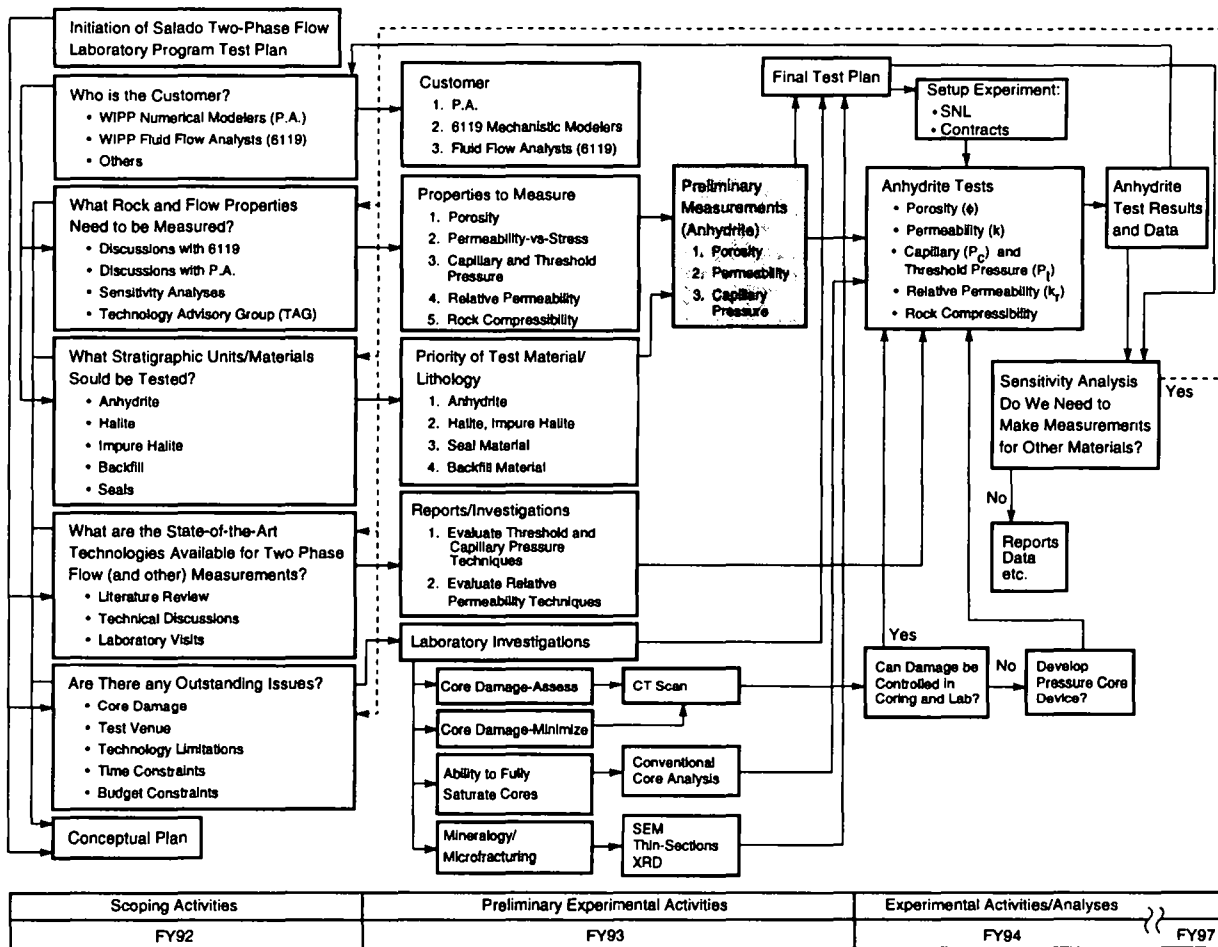
2.3 Salado Two-Phase Flow Laboratory Program--Preliminary Laboratory Experiments

The tests reported here were part of preliminary experimental activities of the Salado Two-Phase Flow Laboratory Program as described in Howarth (1993). As shown in Figure 3, these preliminary measurements (anhydrite) experiments are an integral part of the Salado



TRI-6334-220-0

Figure 2. The five zones of MB139, shown in an idealized core section (after Borns, 1985).



TRI-6119-125-0

Figure 3. Salado Two-Phase Flow Laboratory Program roadmap (Howarth, 1993).

Two-Phase Flow Program. The preliminary laboratory test matrix was designed to provide a wide variety of information regarding the rock and flow properties of MB139, including total and effective porosity, gas and liquid permeability, permeability anisotropy, and mercury injection and centrifuge capillary pressure. Porosity and permeability tests were performed under various stress conditions to evaluate stress sensitivity. In addition, the suitability of using a synthetic brine for liquid permeability tests and the compositional and hydrological heterogeneity of MB139 were investigated.

Porosity and gas permeability are two fundamental, measurable rock properties. Simple methods exist to measure these rock properties. Ultimately, developing relationships between the more difficult-to-measure properties and effective porosity and/or gas permeability is desirable. Therefore, when possible, effective porosity and/or gas permeability measurements were made on all core samples tested within the scope of the preliminary laboratory experiments. In addition, specimens were categorized according to Borns' (1985) stratigraphic zone classification system to assess whether correlations between stratigraphic zone and porosity and/or permeability exist within MB139.

Standard petrographic analysis, including x-ray diffraction (XRD) and scanning electron microscopy (SEM), was used to describe the mineral composition. This analysis consists of a description of the assemblage of each sample, which includes a modal analysis of the phases present, a description of primary (growth fabrics, reworking, etc.) and secondary (replacement mineral growth, overprinting, relic minerals, fracture infilling, etc.) textures, and a description of fracture or pore systems present and observed. Section 3 contains a brief summary of the petrographic analysis performed in conjunction with the porosity, permeability, and capillary pressure tests. Details of these and other petrographic analyses performed as part of the Salado Two-Phase Flow Laboratory Program are found in Holcomb et al. (1995) and Fredrich and Zeuch (1996).

2.4 Net Effective Stress

Measurements of effective porosity and permeability were performed while confining pressure, and in some cases pore pressure, was applied to the test specimen. As described in Howarth (1993), the effective stress law is used to describe the appropriate stress state of a rock by defining a relationship between internal pore pressure, P_p , and confining stress, σ , for any given material property or process. A generalized effective stress law is presented in Equation 1.

$$P = G(\sigma - \alpha P_p) \quad (1)$$

The classic definition for net effective stress, σ' , is shown in Equation 2 (Warpinski and Teufel, 1992).

$$\sigma' = \sigma - P_p \quad (2)$$

For Equations 1 and 2:

- P = the specific material property or process (i.e., permeability, deformation, rock compressibility, or capillary pressure)
- G = generalized function which describes the effect of stress on the property or process
- σ = external confining stress on the sample (for hydrostatic conditions, $\sigma = P_{conf}$)
- P_{conf} = confining pressure
- P_p = pore pressure
- α = poroelastic parameter that relates stress and pore pressure
- σ' = net effective stress.

The classic definition for net effective stress is the effective stress law when $\alpha = 1.0$. In this definition, the net effective stress is given by $\sigma - P_p$, and σ is assumed to be constant, thereby resulting in a linear effective stress law. This definition, widely used in soil and hard rock analysis, is used to quantify the stress state imposed on test specimens analyzed for this report. In all cases where confining pressure was applied to test specimens for this study, the applied confining stress, P_{conf} , was hydrostatic. Therefore the net effective stress, σ' , is defined by Equation 3 for this report. Further investigation of the net effective stress law for these tests was beyond the scope of this study.

$$\sigma' = P_{conf} - P_p \quad (3)$$

2.5 Report Organization

The following sections present the results of measured rock and flow properties from the preliminary laboratory experiments. In addition to summarizing the petrographic analyses, Section 3 describes the test specimens and details of the borehole cores from which

the test specimens were taken. Section 4 contains a description of the porosity and grain density test methods, procedures, and results. Similarly, Section 5 describes the single-phase gas and liquid permeability test methods, procedures, and results. A description of the capillary pressure test methods, procedures, and results, including threshold pressure, is found in Section 6. Relationships between measured parameters are found in Section 7. Conclusions are found in Section 8, and Section 9 contains recommendations. Section 10 contains the references. Results of the petrographic analyses are reported in a separate document (Fredrich and Zeuch, 1996).

The unabridged final data and analysis reports from Rock Physics Associates (incorporating data from Core Laboratories in Carrollton, TX), RE/SPEC, and TerraTek are included in Appendices A, B, and C, respectively. In some instances, inconsistencies remain between the raw data and/or calculated values from test laboratory notebooks and worksheets and the data reported in the final data and analysis reports exist. Therefore an errata sheet that identifies inconsistencies is included at the beginning of each appendix. Copies of the laboratory notebooks/worksheets are retained in the Sandia WIPP Central Files (SWCF) records center.

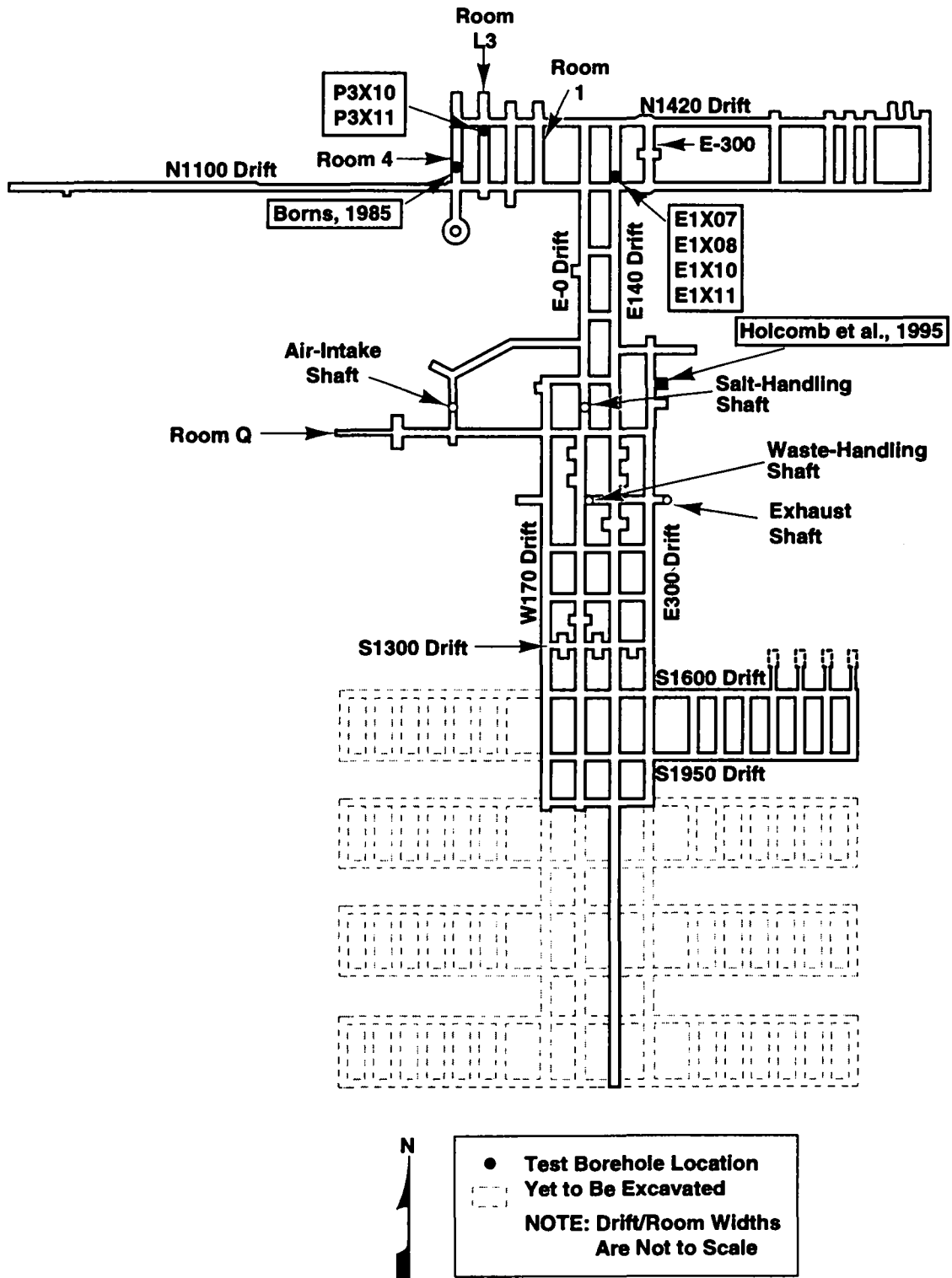
3.0 MARKER BED 139 TEST SPECIMENS

3.1 Test Specimen Selection

The intent of the test specimen selection process was to select groups of cores that represent a distribution of MB139 physical textures. However, only Borns' (1985) stratigraphic Zones II, III, and IV were recovered in their entirety from all holes during the coring process. In most cases, the whole cores broke during coring or recovery. Breaks occurred at the upper and lower contact zones (Zones I and V, respectively), and a specimen could not be cut from either the Zone I or Zone V remaining whole cores. In these cases, there appeared to be pre-existing fractures at the contact zones, consistent with observations of stress-sensitive fracturing along marker bed contacts in the vicinity of older excavated rooms. In other cases, the contact zone was so thin that a truly representative test specimen of Zone I or V could not be cut. Because of the different composition of Zones I and V and the possible existence of pre-existing fractures, the flow properties for Zones I and V might vary from the more intact portions of MB139.

To obtain samples that would withstand the core preparation and finishing process, test samples were cut from competent portions of the borehole core (also referred to here as whole core). The test specimens were cut from whole core taken from six underground boreholes at the WIPP: E1X07, E1X08, E1X10, E1X11, P3X10, and P3X11. Locations of the six boreholes are shown in Figure 4, together with locations of the cores studied by Holcomb et al. (1995) and Borns (1985). Table 2 is a cross-reference guide that contains borehole coordinates and elevation from mean sea level (MSL).

Tables 3a, 3b, and 3c summarize information about each specimen, including designation of the laboratory that performed the tests, the borehole number from which the specimen was taken, the sample number at the test laboratory, zone classification, depth (from borehole collar) at which the specimen was cut from the whole core, specimen bulk volume, flow direction (with respect to the bedding plane) during permeability testing, and grain density. Tables 3a, 3b, and 3c contain information from Core Laboratories, RE/SPEC, and TerraTek, respectively. Porosity, permeability, and threshold pressure test results and anhydrite content for each core are presented in Tables 3a, 3b, and 3c and are discussed in Sections 4, 5 and 6, respectively. Zone classifications were determined during consultation with D. J. Borns and were based on review of photographs showing the locations where test specimens were extracted from whole cores.



TRI-6330-129-10

Figure 4. Location of boreholes for test specimens.

Table 2. Borehole Locations

Borehole Number	Borehole Coordinate North (ft)*	Borehole Coordinate East (ft)**	Borehole Elevation at Collar (ft MSL)
E1X07	10830.61	7064.48	1302.46
E1X08	10998.45	7064.97	1303.09
E1X10	10992.22	7064.80	1303.12
E1X11	10988.49	7065.02	1303.14
P3X10	11103.34	6385.30	1297.27
P3X11	11101.62	6385.46	1297.26

* To convert this coordinate to the New Mexico State Plane Coordinate System (Gonzales, 1989), add 490,000.00 to the coordinate value given here. For example, the north coordinate of E1X07 is 500,830.61 in the New Mexico State Plane Coordinate System.

** To convert this coordinate to the New Mexico State Plane Coordinate System (Gonzales, 1989), add 660,000.00 to the coordinate value given here. For example, the east coordinate of E1X07 is 667,064.48 in the New Mexico State Plane Coordinate System.

Table 3a. Detailed Summary of Information for Each Test Sample at Core Laboratories

Lab	Bore Hole No.	Sample No.	Zone	Depth (feet)	Flow Dir.	Bulk Vol (cc)	*Grain Den. (g/cc)	Effective Porosity			** Gas Permeability			Anhydrite Cont.		Thres. Press. 140 d (MPa)	Res. Brine Sat. (%)
								3.4 MPa (%)	6 MPa (%)	10 MPa (%)	3.4 MPa (m ²)	6 MPa (m ²)	10 MPa (m ²)	XRD (wt%)	TS (vol%)		
CL	E1X10	1	2	4.5	H	11.88	2.64	0.60									
CL	E1X10	2	2	4.5	H	10.7	2.59	0.80	0.70		6.50e-19	4.60e-19	2.30e-19	80	82		
CL	E1X10	3	2	5	H			0.60									
CL	E1X10	4	2	5	H	12.69	2.62	0.90	0.90		1.30e-18	8.80e-19	6.50e-19	73	72		
CL	E1X10	5	3	5.25	H	12.45	2.62	0.70	0.60		5.10e-19	3.80e-19	1.80e-19	56	67	0.541	
CL	E1X10	6	3	5.25	H	12.43	2.62	0.70			5.80e-19	3.00e-19	5.00e-20				
CL	E1X10	7	3	5.25	V	12.65	2.95	1.10	1.00		9.50e-19	5.50e-19		99	99	0.78	
CL	E1X10	8	3	5.25	V	12.98	2.95	1.10	1.00		8.20e-19	4.90e-19	1.40e-19				
CL	E1X10	9	3	5.5	H	12.65	2.85	0.90			4.70e-19			92	93		
CL	E1X10	10	3	5.5	H	12.65	2.94	1.00			1.10e-18	1.80e-19					
CL	E1X10	11	3	5.75	H	12.53	2.89	1.70	1.70	1.60	1.80e-18	1.60e-18	1.10e-18	93	95	0.45	
CL	E1X10	12	3	5.75	H	12.93	2.92	1.40	1.30		1.40e-18	1.00e-18	7.30e-19				
CL	E1X10	13	3	5.75	V	12.7	2.96	1.60	1.50	1.50	1.60e-18	3.10e-19		97	82	0.753	
CL	E1X10	14	3	5.75	V	10.78	2.95	1.20	1.10		6.10e-19	3.10e-19	1.70e-19				
CL	E1X10	15	4	6.25	V	12.6	2.96	1.00	0.90		5.90e-19	1.30e-19	6.40e-20	96	100		
CL	E1X10	16	4	6.25	V	12.37	2.96	0.60									
CL	E1X11	17	2	4.5	H	11.38	2.63	0.80			4.00e-19	3.40e-19	1.00e-19	54	60		
CL	E1X11	18	2	4.5	H	11.88	2.63	1.80									
CL	E1X11	19	3	4.75	H	12.91	2.72	0.90			4.70e-19	3.20e-19	1.00e-19	68	71		
CL	E1X11	20	3	4.75	H	12.83	2.79	0.90	0.80		3.90e-19						
CL	E1X11	21	3	5	H	12.04	2.82	1.10	1.00		7.70e-19	5.70e-19	2.60e-19	66	64	0.329	
CL	E1X11	22	3	5	H	12.29	2.69	1.40	1.30		1.50e-18	8.40e-19					
CL	E1X11	23	3	5.25	H	12.62	2.65	2.10			1.30e-18	5.90e-19		54	69	0.397	
CL	E1X11	24	3	5.25	H	12.2	2.67	1.40	1.40		1.50e-18	5.70e-19					
CL	E1X11	25	3	5.25	V	13	2.61	0.90	0.80		2.00e-18	5.60e-19	2.90e-19	69	83		
CL	E1X11	26	3	5.25	V	12.93	2.74	1.60			2.20e-18	7.50e-19	3.30e-19				
CL	E1X11	27	4	5.75	H	12.72	2.75	1.60	1.40	1.20				85	44		
CL	E1X11	28	4	5.75	H	13.67	2.91										
CL	E1X11	29	4	5.75	V	12.69	2.96	0.80									
CL	E1X11	30	4	5.75	V	12.72	2.96	1.00			1.50e-18	5.90e-19		99	100		

* Grain densities from effective grain volume measurements.

** Pressure values are net effective stress; gas permeabilities are Klinkenberg corrected.

Table 3b. Detailed Summary of Information for Each Test Sample at RE/SPEC Inc.

Lab	Bore Hole No.	Sample No.	Zone	Depth (feet)	Flow Dir.	Bulk Vol (cc)	*Grain Den. (g/cc)	Permeability (pressure values are net effective stress)						Anhydrite Content	
								Gas (Klinkenberg Corrected)			Liquid **			XRD (wt%)	TS (vol%)
								1.6 MPa (m ²)	5.6 MPa (m ²)	9.6 MPa (m ²)	1.6 MPa (m ²)	5.6 MPa (m ²)	9.6 MPa (m ²)		
RS	P3X11	5-2-SP1	2	5.50	H	823.5		3.20e-18	1.70e-18	1.40e-18	5.30e-17				
RS	P3X11	5-2-SP1T	2	5.50	H	12.62	2.73							18	
RS	P3X11	5-2-SP1B	2	5.50	H	13.97	2.73							6	
RS	P3X10	6-SP2	3	5.70	H	820.5									
RS	P3X10	6-SP2T	3	5.70	H	14.59	2.69							55	
RS	P3X10	6-SP2B	3	5.70	H	13.19	2.57							45	
RS	P3X11	5-3-SP3	4	7.05	H	813.00		1.60e-17	8.90e-18	5.10e-18	7.90e-17	4.30e-17	2.60e-17		
RS	P3X11	5-3-SP3T	4	7.05	H	14.97	2.53							55	
RS	P3X11	5-3-SP3B	4	7.05	H	17.88	2.70							59	
RS	P3X11	5-3-2-TS1-1	3	5.93	H										70
RS	P3X11	5-3-2-TS1-2	3	5.93	V										46
RS	P3X11	5-3-2-TS1-3	3	5.93	V										49
RS	P3X11	5-3-2-TS1-4	3	5.93	V									60	
RS	P3X10	5-3-2-TS2-1	2	5.28	H										68
RS	P3X10	5-3-2-TS2-2	2	5.28	V										43
RS	P3X10	5-3-2-TS2-3	2	5.28	V										58
RS	P3X10	5-3-2-TS2-4	2	5.28	V									47	
RS	P3X11	6-TS3-1	4	7.60	H										96
RS	P3X11	6-TS3-2	4	7.60	V										90
RS	P3X11	6-TS3-3	4	7.60	V										67
RS	P3X11	6-TS3-4	4	7.60	V									72	

* Grain densities from effective grain volume measurements.

** All liquid permeabilities are scoping calculations.

Table 3c. Detailed Summary of Information for Each Test Sample at TerraTek, Inc.

Lab	Bore Hole No.	Sample No.	Zone	Depth (feet)	Flow Dir.	Bulk Vol (cc)	* Grain Den. (g/cc)	Porosity		Permeability (pressure values are net effective stress)						Anhydrite Content	
								Total (%)	Eff. (%)	Gas (Klinkenberg Corrected)			Liquid**			XRD (wt%)	TS (vol%)
										0 MPa	2 MPa (m ²)	6 MPa (m ²)	10 MPa (m ²)	2 MPa (m ²)	6 MPa (m ²)		
TT	E1X08	A	2	3.82	H	822.8	2.65		1.90	8.20e-18	5.70e-18	5.00e-18	6.70e-18	5.70e-18	5.30e-18		
TT	E1X08	B	3	4.66	H	776.8	2.60		0.50	1.30e-17	7.40e-18	4.60e-18					
TT	E1X08	C	4	5.53	H	819.6	2.72		1.00	4.60e-18	2.60e-18	2.00e-18	3.60e-18	2.40e-18	1.80e-18		
TT	E1X08	EP1	2	3.57	H	83.47	2.56	1.40	1.30								
TT	E1X08	EP2	3	4.4	H	84.39	2.66		0.80								
TT	E1X08	EP3	3	5.12	H	83.54	2.58	0.40	0.40								
TT	E1X08	EP4	4	5.93	H	83.35	2.88	1.60	1.60								
TT	E1X08	PX1	2	4.07												70	6
TT	E1X08	PX2	3	4.93												32	62
TT	E1X08	PX3	4	5.78												98	80
TT	E1X07	D	2	4.32	H	803.8	2.71		0.70	1.50e-19	5.90e-20	5.50e-20					
TT	E1X07	E	3	4.82	H	843.1	2.71		1.50	8.30e-16	3.00e-16	1.50e-16					
TT	E1X07	F	4	5.38	H	815.3	2.88		1.00	1.10e-18	6.90e-19	5.70e-19	1.10e-18	6.10e-19	5.10e-19		
TT	E1X07	EP5	2	4.07	H	84.85	2.64		1.90								
TT	E1X07	EP6	2	4.57	H	84.04	2.70		2.70								
TT	E1X07	EP7	3	5.07	H	83.73	2.80		0.60								
TT	E1X07	EP8	4	5.66	H	84.52	2.75		1.60								
TT	E1X07	PX4	2	4.07												7	50
TT	E1X07	PX5	3	5.07												62	66
TT	E1X07	PX6	4	5.8												81	82

* Grain densities from effective grain volume measurements.

** All liquid permeabilities are scoping calculations.

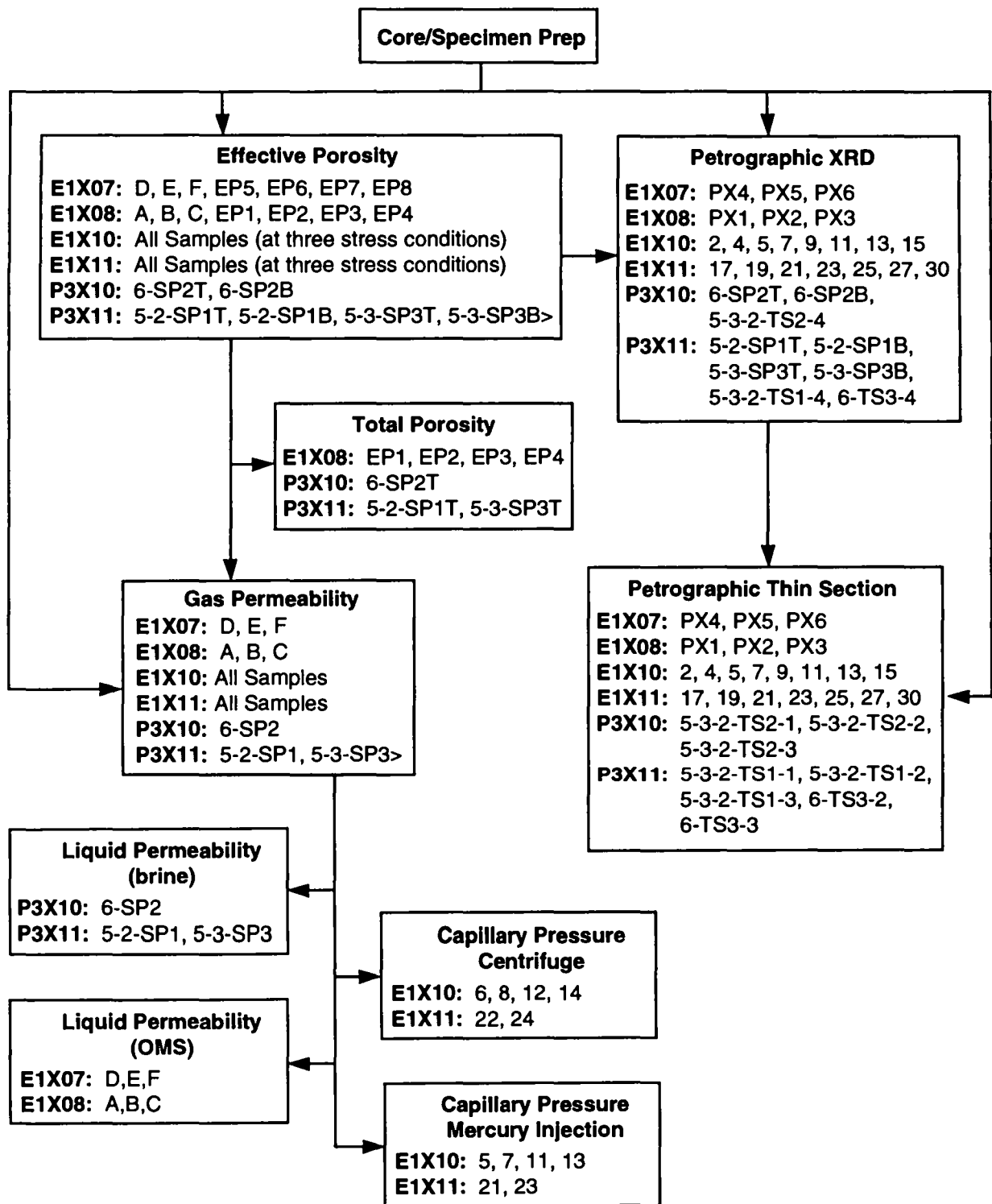
3.2 Test Specimen Preparation and Description

All test specimens used in this study were taken from 10- or 15.2-cm (4- or 6-in.) diameter core drilled through MB139 from six different underground locations. All samples were cut and prepared according to SNL-approved procedures. Prior to the tests conducted at RE/SPEC and TerraTek, the mineralogical composition of the test samples was uncertain and there was concern that some clays might be present. Because overdrying of clays can cause increases in porosity and permeability that are not indicative of natural, in situ conditions (Bush and Jenkins, 1970), the specimens at TerraTek and RE/SPEC were dried under controlled temperature and humidity conditions (65° C and 45% humidity). Subsequent compositional analysis at TerraTek and RE/SPEC revealed that clays were not present in measurable quantities; therefore Core Laboratories personnel were instructed to dry their specimens in a vacuum oven at 104° C until the weight stabilized to within 0.001 gram over a 24-hour period.

Figure 5 is a flow diagram that shows the tests performed on the specimens. As previously stated, developing relationships between the more difficult-to-measure properties and effective porosity and/or gas permeability was desired, so, when possible, effective porosity and/or gas permeability measurements were made on all core samples tested within the scope of this program. Table 4 contains a summary of the results of x-ray diffraction (XRD) and thin-section petrographical analysis performed on samples from the six boreholes. The list of "other" minerals included carbonate (predominately magnesite), polyhalite, carbon, or pyrite. RE/SPEC and TerraTek both analyzed for polyhalite, a dominant constituent in five of the twelve samples analyzed by these two laboratories, but Core Laboratories did not. (Note that RE/SPEC subcontracted petrographic work to the South Dakota School of Mines, Core Laboratories subcontracted to Omni Laboratories, and TerraTek subcontracted some analysis to the University of Utah and performed the remainder in house.) Details of the petrographic analysis are contained in Fredrich and Zeuch (1996).

Table 4. Summary of Petrographic Analysis Results

Mineral	XRD (Mean Weight %)	Thin Section (Mean Volume %)
Anhydrite	65	70
Other	35	30



TRI-6115-149-1

Figure 5. Flow diagram for tests performed on Marker Bed 139 specimens.

4.0 POROSITY

Porosity is a measure of the void space or storage capacity of a rock. Effective porosity is the ratio of the interconnected pore volume to bulk volume. Total porosity is the ratio of interconnected and non-interconnected pore space to bulk volume. A summary of the results of total and effective porosity tests is given in Tables 3a, 3b, and 3c. Results of effective and total porosity tests are presented and discussed below. Successful measurements of both total and effective porosity were made on three MB139 samples by TerraTek. Effective porosity was measured on an additional 42 samples. RE/SPEC porosity measurements could not be qualified as required by SNL WIPP Quality Assurance procedures and thus are not included here. In most cases, a particular core specimen subsequently underwent such additional testing as gas or liquid permeability, capillary pressure, or petrography upon completion of effective porosity tests, as shown in Figure 5.

4.1 Effective Porosity

Effective porosity was successfully measured on 28 specimens at Core Laboratories and 14 specimens at TerraTek, Inc. The data are shown in Tables 3a, 3b, and 3c.

4.1.1 Test Procedures

Effective porosity was determined at Core Laboratories under the direction of Rock Physics Associates using the CMS 300 system, which directly measures pore volume using the Boyle's law helium expansion technique and the autoporosimeter to measure grain volume. As shown in Table 3a, effective porosity was measured while the samples were subject to 3.4, 6.0, and 10.0 MPa net effective stress. Details regarding test procedures at Core Laboratories are found in Appendix A.

Effective porosity was determined at TerraTek using Archimedes' principle to determine bulk volume and a porosimeter (using the Boyle's Law helium expansion technique) to measure grain volume. The specimens were not subject to confining stress during the tests. Details regarding test procedures at TerraTek are found in Appendix C.

4.1.2 Histograms and Probability Distributions

Effective porosity was successfully measured on 42 specimens; 14 at TerraTek under

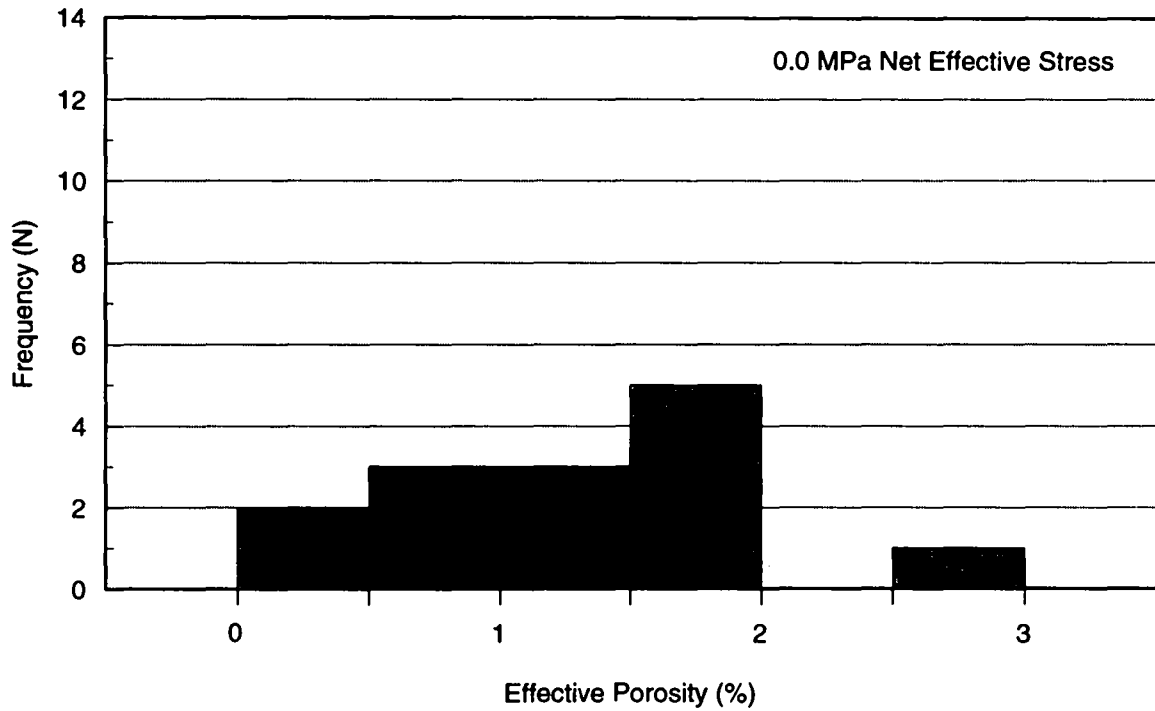
zero confining stress (zero net effective stress) conditions, and 28 at Core Laboratories under three stress conditions. Effective porosity for zero confining stress ranged from 0.4 to 2.7% with a mean of 1.2% and is shown as a histogram in Figure 6a and as a cumulative frequency in Figure 6b.

Effective porosity was measured on 28 cores at a net effective stress of 3.4 MPa. Effective porosity ranged from 0.6 to 2.1% with a mean of 1.1%. The porosity data for the specimens tested under 3.4 MPa net effective stress are shown as a histogram in Figure 7a and as a probability distribution in Figure 7b. Effective porosity was successfully measured on 16 of the 28 specimens under a net effective stress of 6.0 MPa. At 6.0 MPa net effective stress, effective porosity ranged from 0.6 to 1.7 % with a mean of 1.1%. The porosity data for the specimens tested under 6.0 MPa net effective stress are shown as a histogram in Figure 8a and as a probability distribution in Figure 8b. Effective porosity was successfully measured on three of the 16 specimens, previously tested under 3.4 and 6.0 MPa net effective stress conditions, at a net effective stress of 10.0 MPa. At 10.0 MPa net effective stress, effective porosity ranged from 1.2 to 1.6% with a mean of 1.5%. The porosity data for the specimens tested under 10.0 MPa net effective stress are shown as a histogram in Figure 9a and as a cumulative frequency in Figure 9b.

Table 5 summarizes the effective porosity data for all net effective stress conditions. All porosity measurements ranged between 0.4 and 2.7%, independent of confining stress conditions. The effect of stress on effective porosity is discussed in Section 4.1.3.

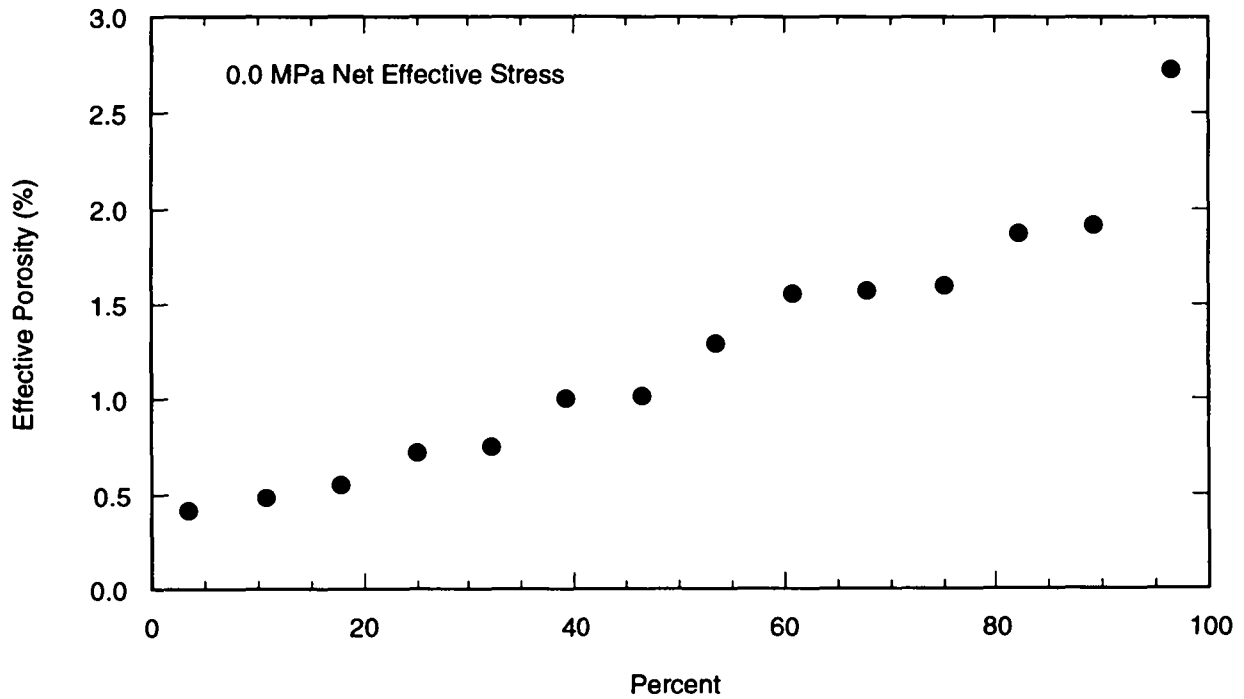
Table 5. Summary of Effective Porosity Data Results

		Porosity				
		Total	Effective			
		(%)	0 MPa (%)	3.4 MPa (%)	6 MPa (%)	10 MPa (%)
Minimum	0.4	0.4	0.6	0.6	1.2	
Maximum	1.6	2.7	2.1	1.7	1.6	
Sum	3.4	17.4	31.4	17.3	4.4	
Points	3	14	28	16	3	
Mean	1.1	1.2	1.1	1.1	1.5	
Median	1.4	1.2	1	1.0	1.5	
Std. Deviation	0.63	0.66	0.4	0.32	0.20	
Variance	0.4	0.44	0.16	0.10	0.04	



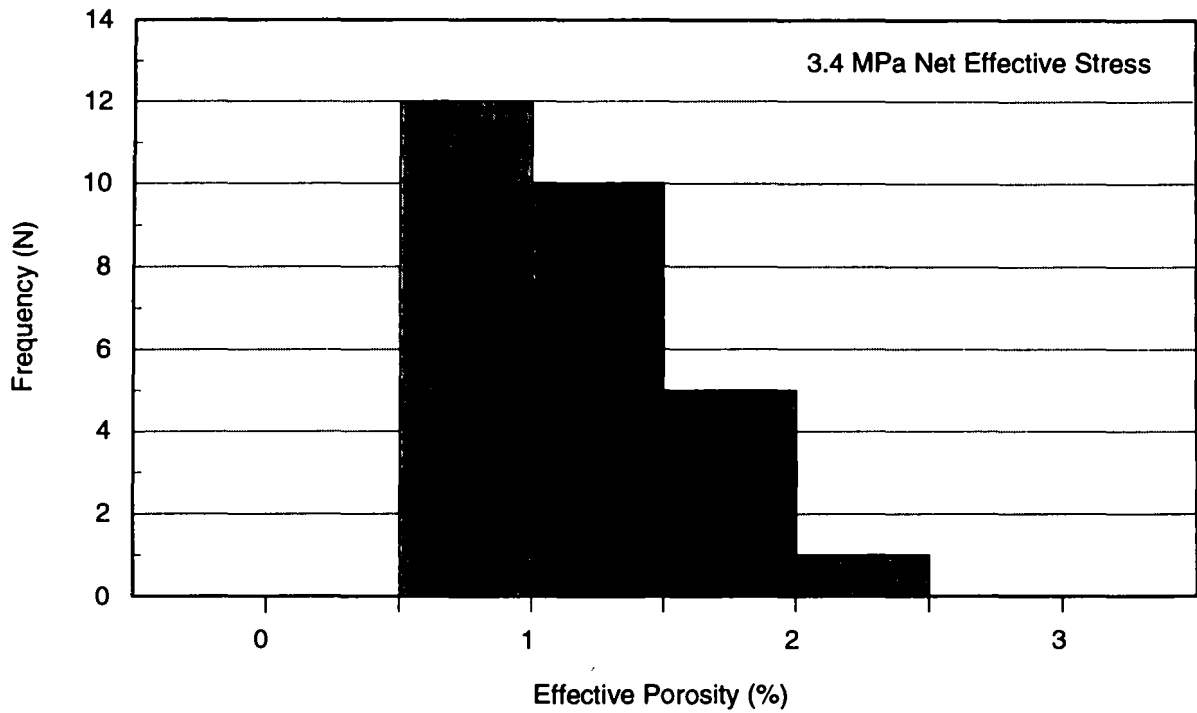
TRI-6115-150-0

Figure 6a. Effective porosity at 0.0 MPa net effective stress histogram.



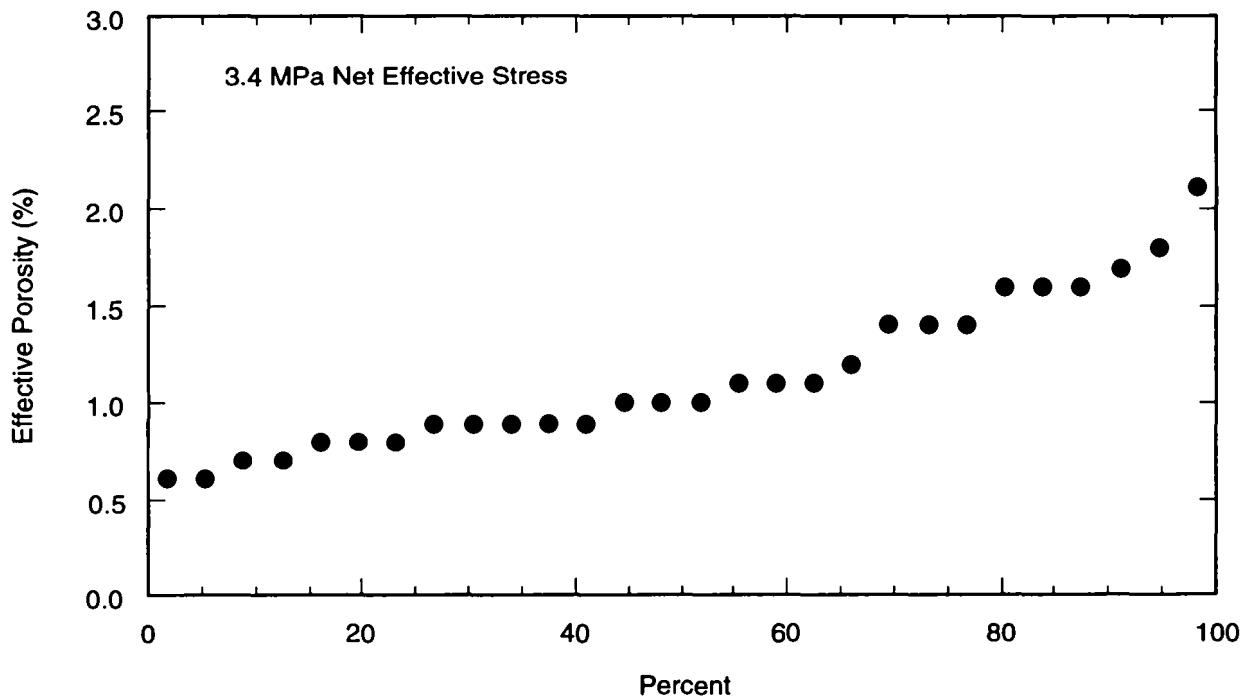
TRI-6115-154-0

Figure 6b. Effective porosity at 0.0 MPa net effective stress cumulative frequency plot.



TRI-6115-151-0

Figure 7a. Effective porosity at 3.4 MPa net effective stress histogram.



TRI-6115-155-0

Figure 7b. Effective porosity at 3.4 MPa net effective stress cumulative frequency plot.

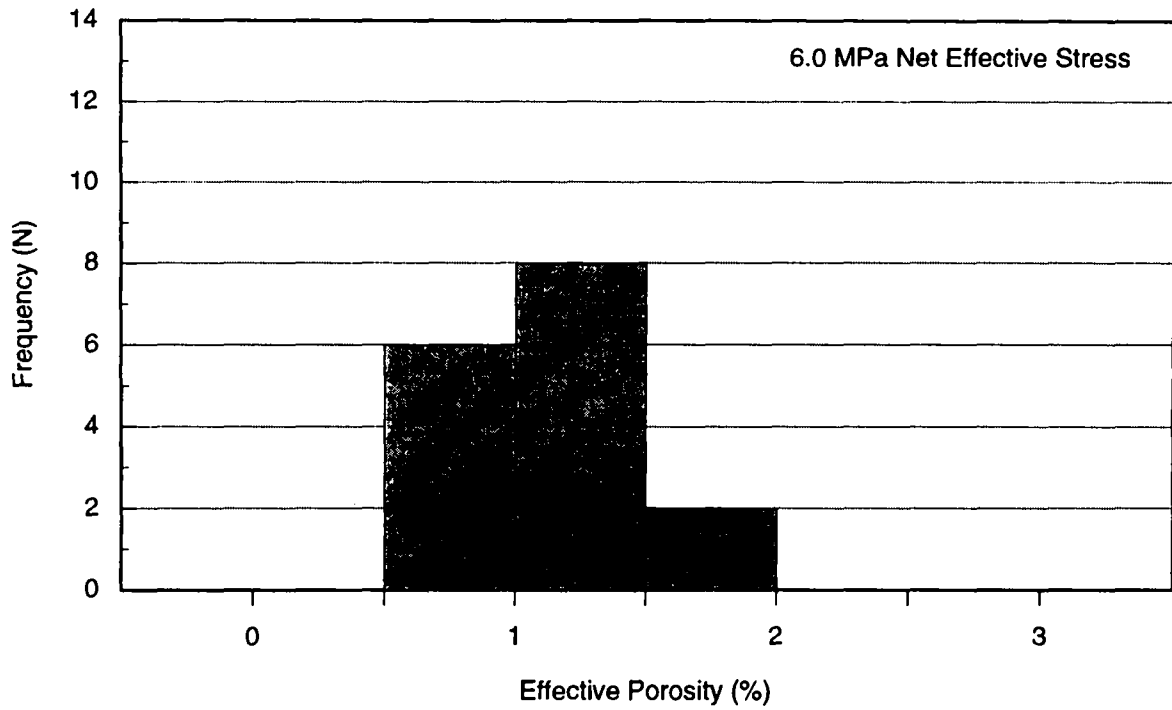


Figure 8a. Effective porosity at 6.0 MPa net effective stress histogram.

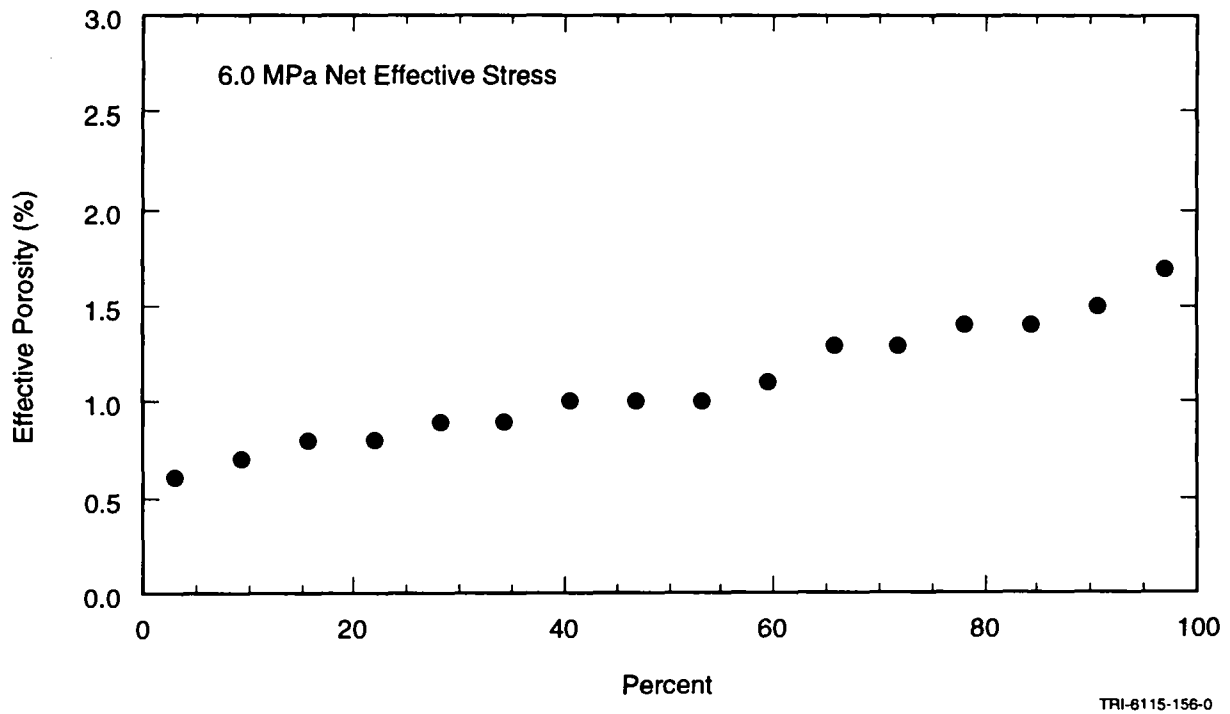
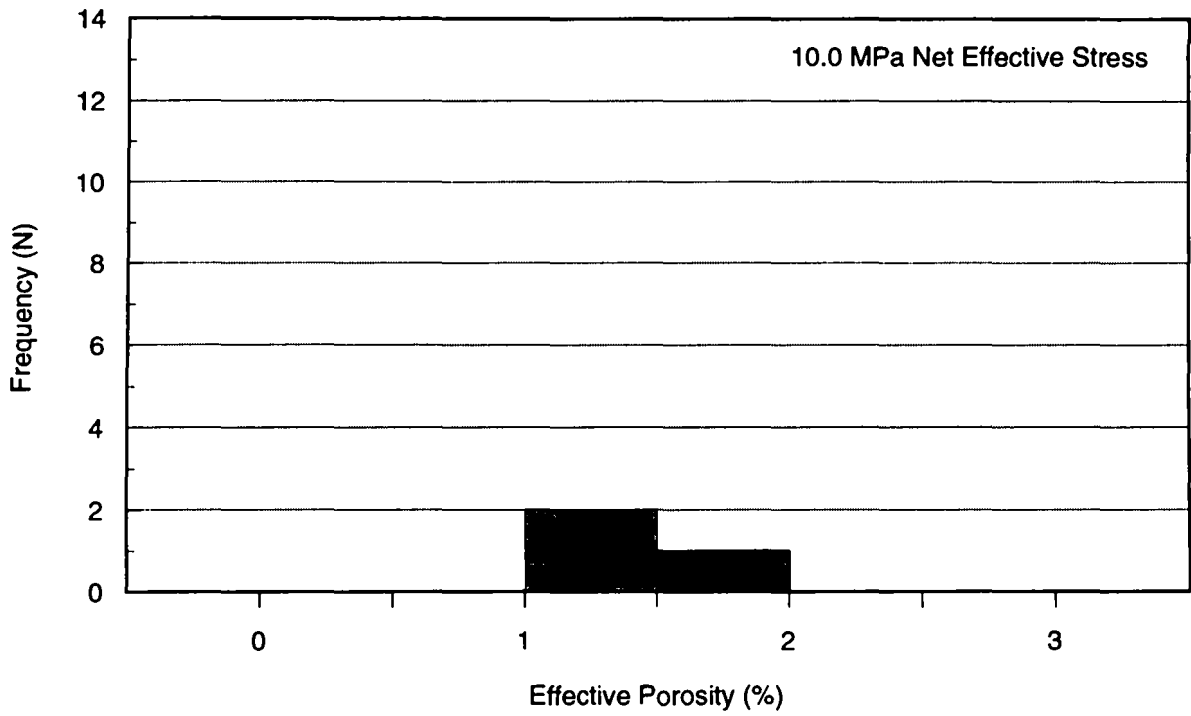
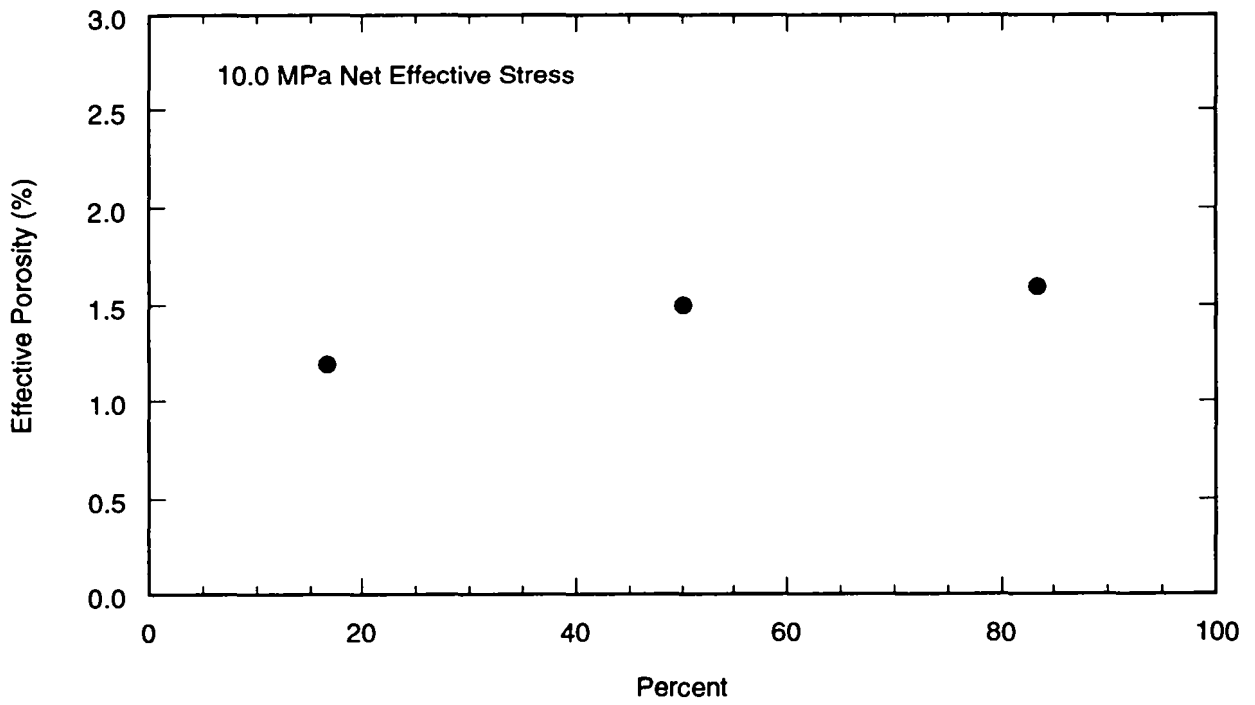


Figure 8b. Effective porosity at 6.0 MPa net effective stress cumulative frequency plot.



TRI-6115-153-0

Figure 9a. Effective porosity at 10.0 MPa net effective stress histogram.



TRI-6115-157-0

Figure 9b. Effective porosity at 10.0 MPa net effective stress cumulative frequency plot.

4.1.3 Effect of Stress on Effective Porosity

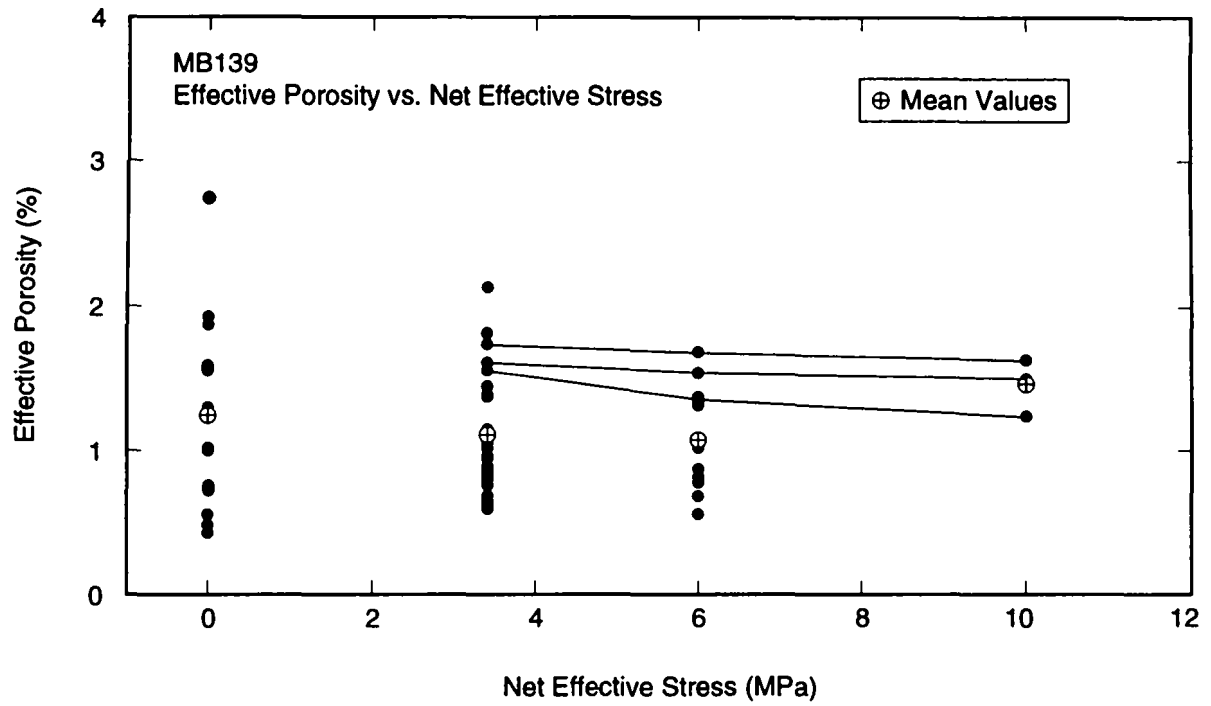
Twenty-eight specimens were tested under different hydrostatic confining stress conditions. Effective porosity was successfully measured on all 28 specimens at a net effective stress of 3.4 MPa, on 16 of the 28 specimens at a net effective stress of 6.0 MPa, and on three of the 16 specimens at a net effective stress of 10.0 MPa. Figure 10 shows the effective porosity versus net effective stress for all samples tested at TerraTek and Core Laboratories. The graph shows the range of measured effective porosity values at each net effective stress and the mean effective porosity at each net effective stress. Note that these data are for two different sets of cores: (1) the specimens tested at TerraTek at 0.0 MPa, and (2) the specimens tested at Core Laboratories at 3.4, 6.0, and 10.0 MPa. None of the specimens tested at TerraTek is included in the set of cores tested at Core Laboratories.

Increasing the net effective stress on the specimens caused the porosity either to remain constant or to decrease. This trend is illustrated in Figure 10 for the three Core Laboratories' specimens, Samples 11, 13, and 27, for which effective porosity was successfully measured at 3.4, 6.0, and 10.0 MPa net effective stress conditions. The decrease in porosity corresponding to an increase in net effective stress from one stress level to the next was ≤ 0.1 porosity units for all specimens except for Sample 27. For Sample 27, the effective porosity decreased by 0.2 porosity units when the net effective stress was increased from 3.4 to 6.0 MPa and by 0.2 porosity units when the net effective stress was increased from 6.0 MPa to 10.0 MPa.

4.1.4 Relationship between Zone Classification and Effective Porosity

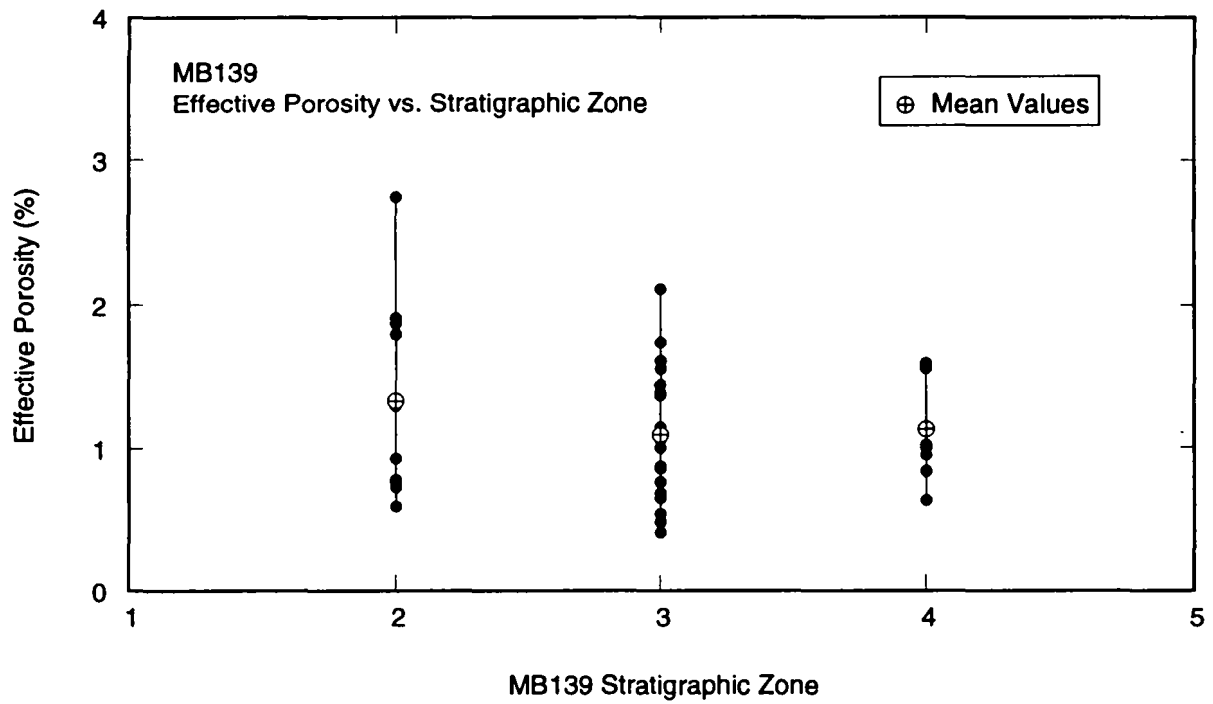
The core samples were classified according to the five stratigraphic zones described in Section 3.2. Zone classifications for core samples are listed in Tables 3a, 3b, and 3c. The data are shown in Figure 11. Specimens were cut only from Zones II, III, and IV. Zones I and V, the upper and lower contact zones, respectively, are thin compared to Zones II, III, and IV. Also, because of the presence of clay interlayers, Zones I and V fracture during the coring process; therefore intact specimens could not be cut from within those sections of whole core.

As Figure 11 shows, the range of effective porosity values is largest for Zone II cores and smallest for Zone IV cores; a slight trend suggests that Zone III has lower effective porosity than Zones II and IV. However, insufficient data exist to draw definitive conclusions regarding correlations between Borns' (1985) MB139 stratigraphic zone



TRI-6115-160-0

Figure 10. Effective porosity versus net effective stress.



TRI-6115-158-0

Figure 11. Effective porosity versus Marker Bed 139 stratigraphic zone.

classifications and effective porosity. The properties of Zones I and V are expected to be more representative of fractured rock and therefore likely to have greater porosity than Zones II, III, or IV.

4.2 Total Porosity

The total porosity data are summarized in Table 3c and discussed in the following sections. Because of the small number of total porosity data points generated, a sufficient data base from which to develop significant trends does not exist.

4.2.1 Test Procedures

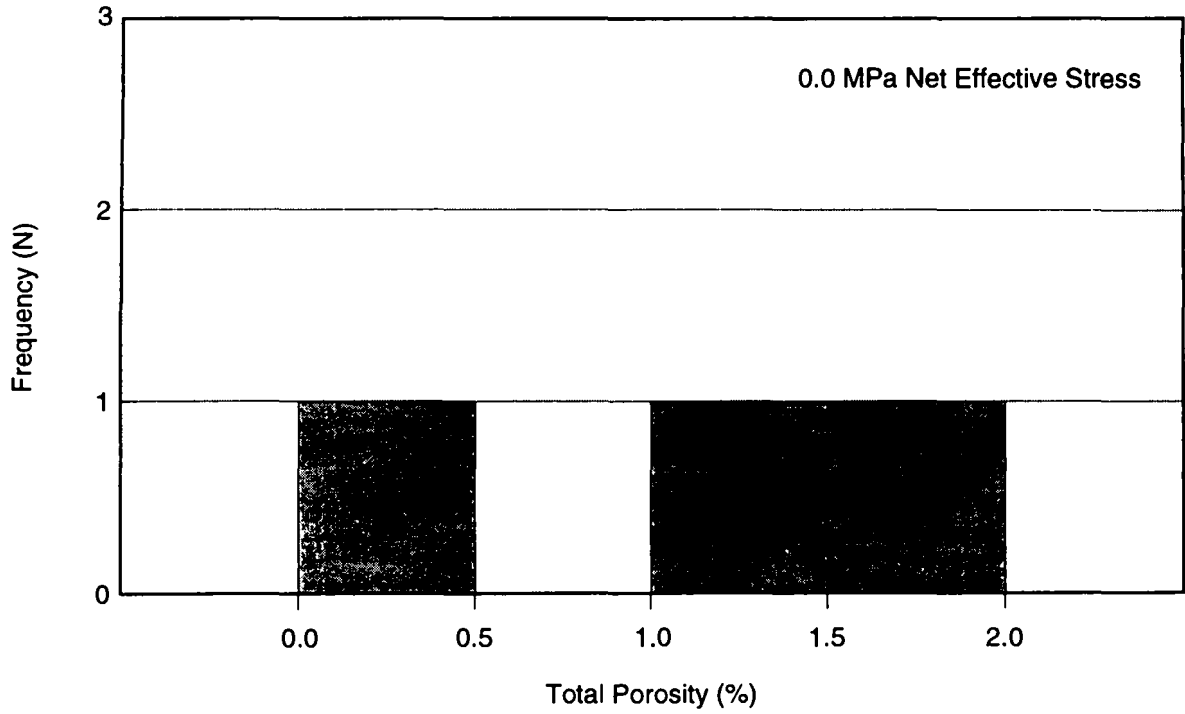
Total (interconnected plus non-interconnected) porosity was measured on four specimens at TerraTek. The specimens were not subject to confining stress during these tests. Of the four tests performed, only three are considered to have produced useable data because significant portions of Sample EP2 were lost during the pulverization process. The effective porosity of each of these samples was measured prior to measuring total porosity. Total porosity was determined at TerraTek by powdering the test specimens and determining the grain density. Details regarding the test procedures are found in Appendix C.

4.2.2 Histograms and Probability Distribution

Total porosity was successfully measured at TerraTek on three samples for which effective porosity was also measured. Total porosity values ranged from 0.4 to 1.6%, with a mean of 1.1%. The total porosity data are shown as a histogram in Figure 12a and as a probability distribution in Figure 12b.

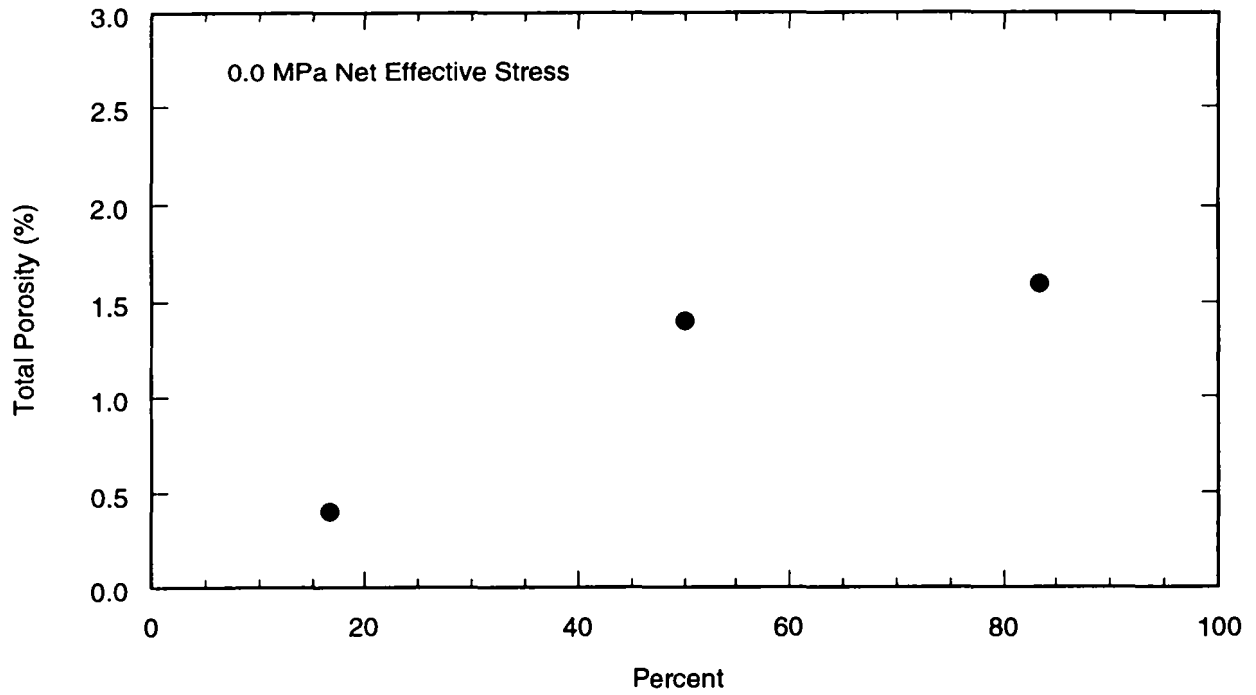
4.2.3 Relationship between Total and Effective Porosity

Figure 13 illustrates the relationship between total and effective porosity for the three samples on which both tests were performed. As expected, total porosity is greater or equal to effective porosity for all three samples. Note however that in Sample EP1, for which total porosity was greater than effective porosity, the difference was less than the corresponding experimental error (see Tables 6 and 7 of Appendix C). Sufficient data do not presently exist to draw definitive conclusions regarding correlations between total and effective porosity.



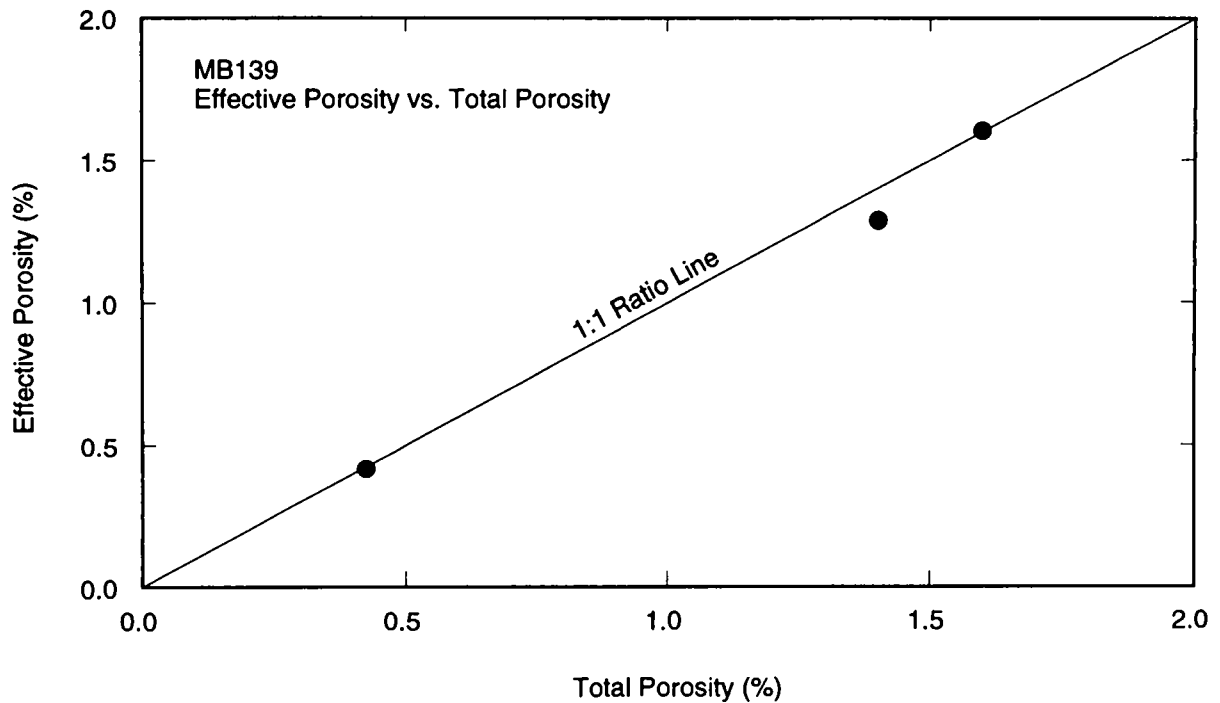
TRI-6115-186-0

Figure 12a. Total porosity histogram.



TRI-6115-185-0

Figure 12b. Total porosity cumulative frequency plot.



TRI-6115-161-0

Figure 13. Effective porosity versus total porosity.

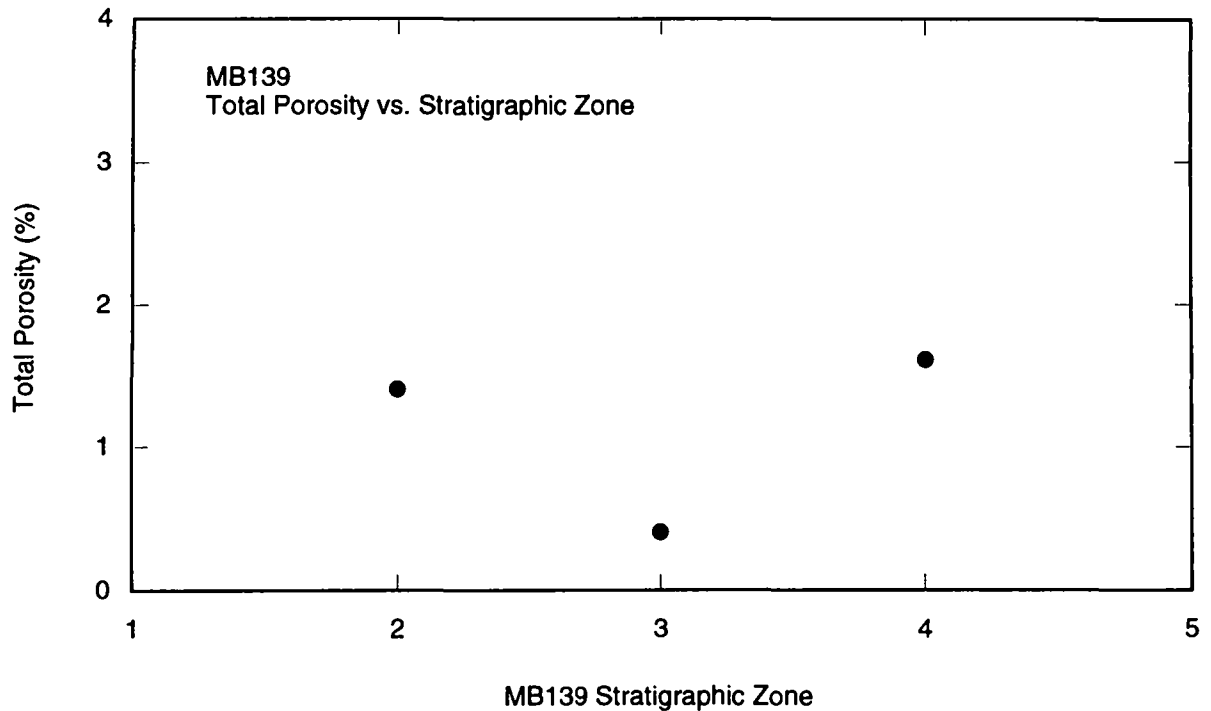
4.2.4 Relationship between Zone Classification and Total Porosity

The three total porosity specimens were classified according to the five MB139 stratigraphic zones described in Section 3.2. Zone classification for each specimen is listed in Table 3, and the data, are shown in Figure 14. Total porosity was measured only on specimens cut from Zones II, III, and IV. As Figure 14 shows, the data suggest that Zone III has lower total porosity than Zones II and IV. However, at this time insufficient data exist from which to draw definitive conclusions regarding correlations between Borns' (1985) MB139 stratigraphic zone classifications and total or effective porosity.

4.3 Grain Density

4.3.1 Test Procedures

Grain density was calculated for 49 cores by dividing the weight of the dry specimen by the grain volume measured using a porosimeter and the Boyle's law helium expansion technique. As shown in Table 3, the grain density values ranged from 2.53 to 2.96 g/cm³,



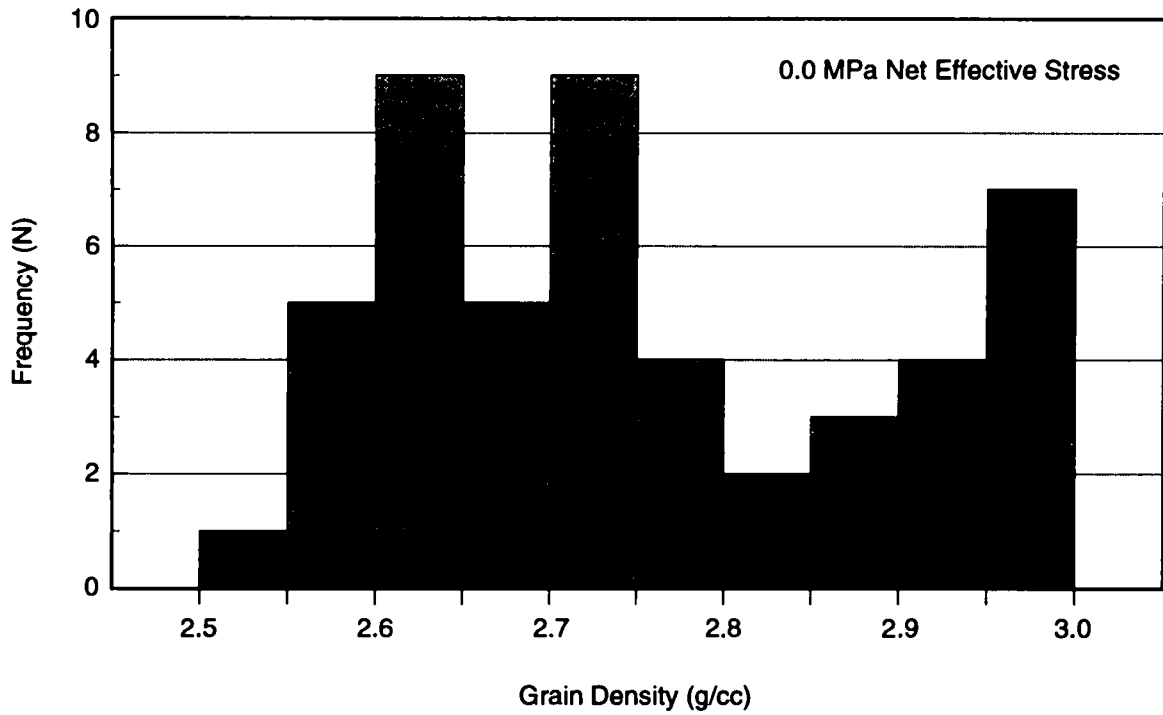
TRI-6115-159-0

Figure 14. Total porosity versus Marker Bed 139 stratigraphic zone.

with a mean of 2.75 g/cm³. The specific gravity of pure anhydrite is 2.89 to 2.98 g/cm³, and these results illustrate the wide variability in anhydrite content within MB139.

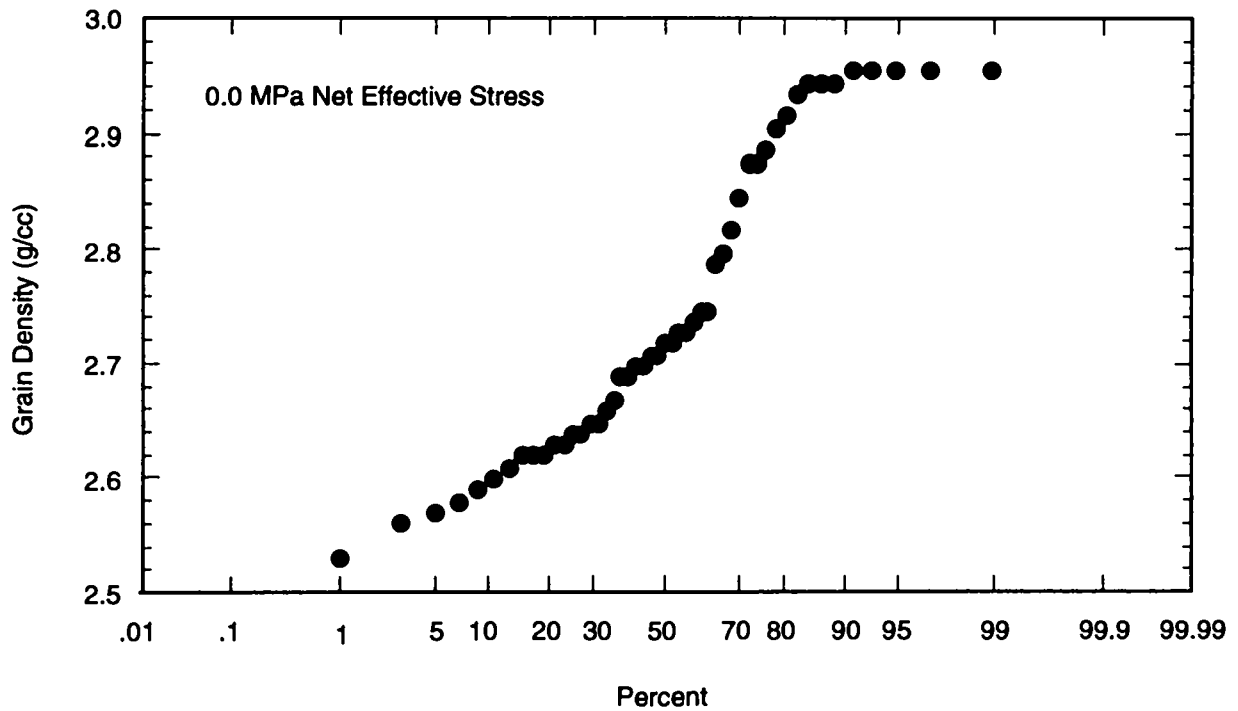
4.3.2 Histogram and Probability Distribution

Distributions of grain density data are shown as a histogram in Figure 15a and as a cumulative frequency plot in Figure 15b. As Figure 15a illustrates, the marker bed exhibits a bimodal distribution of grain density. Approximately 75% of the samples are composed of anhydrite and other minerals, and approximately 25% are nearly pure anhydrite.



TRI-6115-162-0

Figure 15a. Grain density histogram.



TRI-6115-199-0

Figure 15b. Normalized grain density cumulative frequency plot.

5.0 PERMEABILITY

The permeability test matrix was designed to provide MB139 permeability data, to investigate the effects of confining stress on gas and liquid permeability and possible differences between horizontal and vertical (with respect to the bedding plane) gas permeability, and to assess the suitability of using synthetic MB139 brine versus a known nonreactive liquid for liquid permeability tests. Gas permeability was measured using the steady-state method on 39 specimens at the three test laboratories. Successful gas permeability measurements including correction for gas-slippage effects were made on 31 specimens. Successful liquid permeability measurements were conducted on five of the 31 specimens.

The results of the gas and liquid permeability tests performed under various net effective stress conditions are summarized in Tables 3a, 3b, and 3c. Twenty-three successful measurements were made on the 29 tested specimens, which were cut and oriented so that the flow direction was parallel to the bedding plane to measure horizontal permeability. Eight successful measurements were made on ten specimens, which were cut and oriented so that the flow direction was perpendicular to the bedding plane to measure vertical permeability. Five successful liquid permeability tests were conducted. Three specimens were tested at TerraTek using odorless mineral spirits (OMS) as the saturant; three specimens were tested at RE/SPEC, producing two successful tests, using a simulated MB139 brine as the saturant.

5.1 Test Procedures

5.1.1 Single-Phase Gas Permeability

The test matrix for each test laboratory was designed to measure permeability at three different suites of net effective stress. The values of 2, 6, and 10 MPa were chosen to represent a wide range of in situ stress conditions, assuming that the MB139 specimens obey the classical net effective stress law described in Section 2.4 of this report. (For example, the 2 MPa value reflects conditions where the difference between the lithostatic and the pore pressures is 2 MPa.)

RE/SPEC was the first laboratory to perform permeability tests on the MB139 samples. Significant uncertainty existed on the range of gas permeability values expected and on the appropriate values of pore pressure and confining pressure to be applied.

Therefore permeability tests were conducted at RE/SPEC at 2, 6, and 10 MPa confining pressure with 0.4, 0.7, and 1.0 MPa inlet pore pressure and 0.1 MPa outlet pore pressure at each confining pressure step. To ensure reproducible results, each test was repeated twice at each inlet pore pressure.

To provide data comparable to that from the other laboratories, the net effective stress was calculated at each confining pressure from the average pore pressure, as shown in Equation 4, using the raw RE/SPEC data contained in Appendix B. For example, for the tests performed at 2 MPa confining pressure, the average pore pressures were 0.25 MPa, 0.4 MPa, and 0.55 MPa. The average pore pressure for this suite, 0.4 MPa [i.e., (0.25 MPa + 0.4 MPa + 0.7 MPa)/3], was then calculated. Using the confining pressure and the average pore pressure, the net effective stress, 1.6 MPa [i.e., (2.0 MPa - 0.4 MPa)] was determined. This method was repeated for the 6.0 and 10.0 MPa confining pressure data, and the corresponding permeability results for RE/SPEC are presented in Table 3b at 1.6, 5.6, and 9.6 MPa net effective stress. Results from RE/SPEC indicated that permeability measurements can be made at specified effective stress. Therefore the net effective stresses chosen for subsequent tests were 2, 6, and 10 MPa.

$$P_p = (P_{inlet} + P_{outlet}) / 2 \quad (4)$$

Because of equipment limitations at Core Laboratories, the lowest net effective stress that could be imposed on the cores was 3.4 MPa; therefore permeability was measured at 3.4, 6.0, and 10.0 MPa at this test facility. TerraTek performed permeability tests at the three specified net effective stress values of 2.0, 6.0, and 10.0 MPa. In some cases, equipment resolution capabilities were exceeded at Core Laboratories, which precluded completion of tests at higher net effective stress conditions.

Ten of the specimens tested at Core Laboratories were cut perpendicular to the bedding plane of MB139. The other 20 Core Laboratories specimens and all specimens tested at RE/SPEC and TerraTek were cut parallel to the MB139 bedding plane. In the general discussion of gas and liquid permeability test results, the results are presented independent of flow orientation with respect to bedding plane. Section 5.2.4 contains a comparison of gas permeability results related to flow orientation.

The test conditions and procedures used at Core Laboratories, RE/SPEC, and TerraTek are described in detail in Appendices A, B, and C, respectively.

5.1.2 Single-Phase Liquid Permeability

Single-phase, steady-state liquid permeability was measured for five specimens at three net effective stress conditions: three at TerraTek at 2.0, 6.0, and 10.0 MPa net effective stress; two at RE/SPEC at 1.6, 5.6, and 9.6 MPa net effective stress. Prior to the liquid permeability tests, gas permeability was measured on each specimen so that direct comparisons could be made between the liquid permeability and the Klinkenberg-corrected gas permeability: the measured liquid permeability should be equal to the Klinkenberg-corrected gas permeability (Klinkenberg, 1941).

To address concerns about the possibility of brine composition affecting the permeability of a test specimen (e.g., causing local dissolution of the specimen), liquid permeability tests were performed at TerraTek using odorless mineral spirits (OMS), a non-reactive liquid. These tests were performed at RE/SPEC using a simulated MB139 brine, SB-139-95B. This brine was formulated according to the recipe contained in Appendix D.

5.2 Test Results

5.2.1 Single-Phase Gas Permeability

The results of the Klinkenberg-corrected, single-phase gas permeability measurements are detailed in Tables 3a, 3b, and 3c and summarized in Tables 6a and 6b. All gas permeability data presented in Tables 3a, 3b, and 3c have been rigorously verified and are considered "good" data. Explanation and discussion of data excluded from Tables 3a, 3b, and 3c are found at the beginning of Appendix A, B, or C for Core Laboratories, RE/SPEC, or TerraTek, respectively.

For simplicity, in Table 6b the results for gas permeability tests performed at 1.6, 2.0, and 3.4 MPa are grouped together and in this discussion are referred to as the 2 MPa data. Similarly, the 5.6 and 6.0 MPa data are combined and referred to as the 6 MPa data, and the 9.6 and 10.0 MPa data are combined and referred to as the 10 MPa data. Gas permeability ranged from a minimum of $1.5 \times 10^{-19} \text{ m}^2$ to a maximum of $8.3 \times 10^{-16} \text{ m}^2$ for the 2 MPa tests, $5.9 \times 10^{-20} \text{ m}^2$ to $3.0 \times 10^{-16} \text{ m}^2$ for the 6 MPa tests, and, $5.0 \times 10^{-20} \text{ m}^2$ to $1.5 \times 10^{-16} \text{ m}^2$ for the 10 MPa tests. The high permeability of Sample E, tested at TerraTek, appears to be an anomaly. It is not known whether the core was damaged or its high permeability occurred naturally. The log of gas permeability values are also summarized in Table 6b.

5.2.1.1 Histograms and Probability Distributions

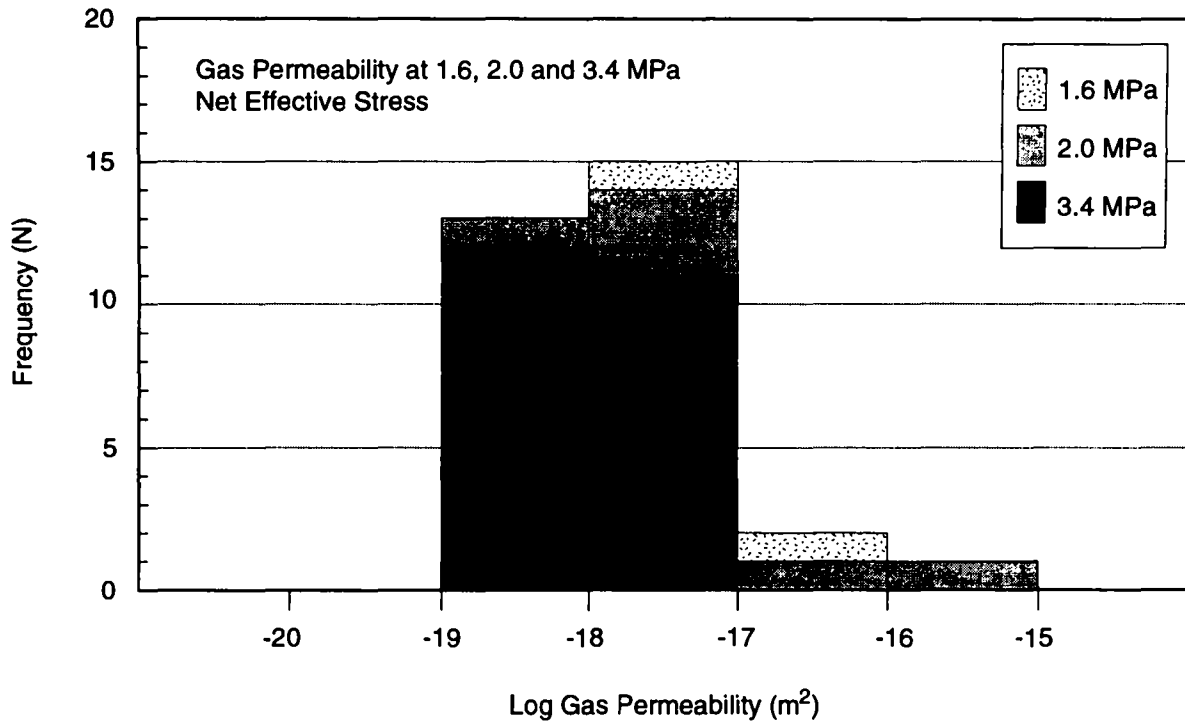
The histogram and associated cumulative frequency plots for the 2, 6, and 10 MPa data are shown in Figures 16, 17, and 18, respectively. The permeability distribution appears to be log normal. A log-normal distribution is expected because permeability depends on pore-size distribution, and pore-size distribution is typically log-normal for rocks (Freeze, 1975).

Table 6a. Summary of Gas Permeability Data Results

Gas Permeability (Klinkenberg Corrected)							
	1.6 MPa (m ²)	2 MPa (m ²)	3.4 MPa (m ²)	5.6 MPa (m ²)	6 MPa (m ²)	9.6 MPa (m ²)	10 MPa (m ²)
Minimum	3.2×10^{-18}	1.5×10^{-19}	3.9×10^{-19}	1.7×10^{-18}	5.9×10^{-20}	1.4×10^{-18}	5.0×10^{-20}
Maximum	1.6×10^{-17}	8.3×10^{-16}	2.2×10^{-18}	8.9×10^{-18}	3.0×10^{-16}	5.1×10^{-18}	1.5×10^{-16}
Sum	1.9×10^{-17}	8.5×10^{-16}	2.4×10^{-17}	1.1×10^{-17}	3.3×10^{-16}	6.5×10^{-18}	1.7×10^{-16}
Points	2	6	23	2	27	2	20
Mean	9.7×10^{-18}	1.4×10^{-16}	1.1×10^{-18}	5.3×10^{-18}	1.2×10^{-17}	3.2×10^{-18}	8.5×10^{-18}
Median	9.7×10^{-18}	6.4×10^{-18}	9.5×10^{-19}	5.3×10^{-18}	5.7×10^{-19}	3.2×10^{-18}	2.8×10^{-19}
Std. Deviation	9.1×10^{-18}	3.4×10^{-16}	5.5×10^{-19}	5.1×10^{-18}	5.8×10^{-17}	2.7×10^{-18}	3.4×10^{-17}
Variance	8.3×10^{-35}	1.1×10^{-31}	3.0×10^{-37}	2.6×10^{-35}	3.4×10^{-33}	7.1×10^{-36}	1.2×10^{-33}

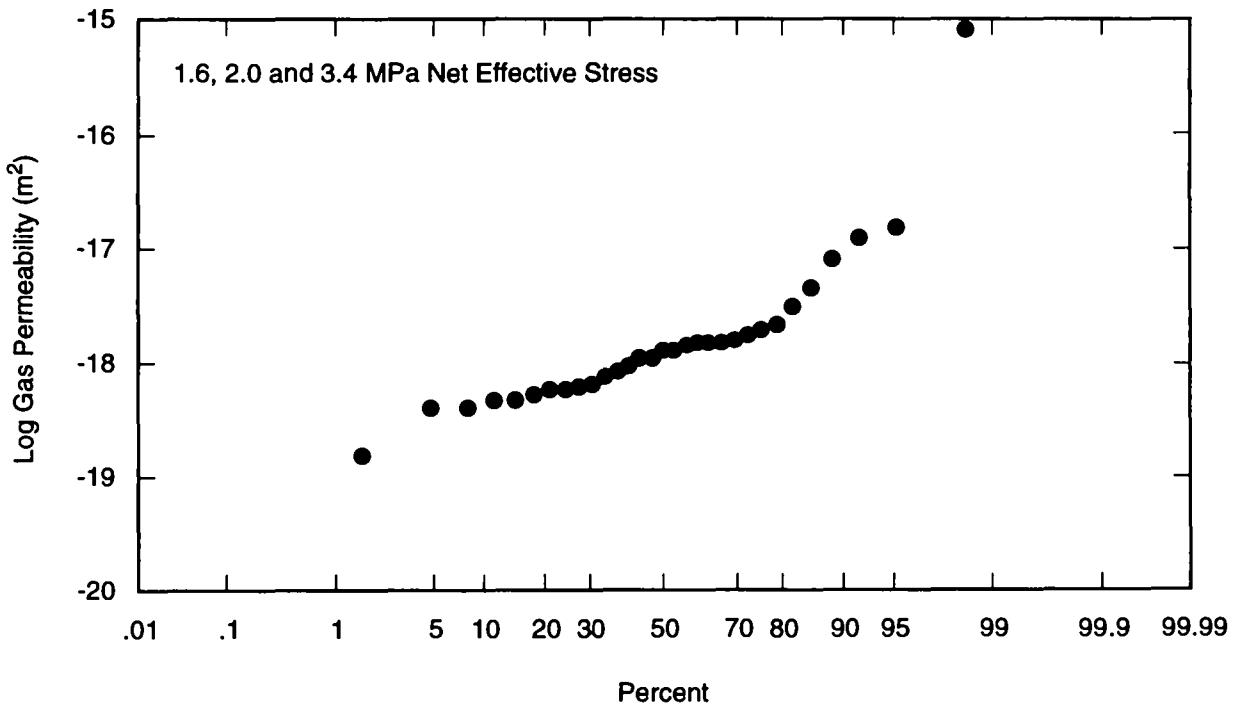
Table 6b. Statistical Summary of Gas Permeability and Log of Gas Permeability (Klinkenberg Corrected)

	Gas Permeability			Log (Gas Permeability)		
	2 MPa (m ²)	6 MPa (m ²)	10 MPa (m ²)	2 MPa (m ²)	6 MPa (m ²)	10 MPa (m ²)
Minimum	1.5×10^{-19}	5.9×10^{-20}	5.0×10^{-20}	-18.84	-19.23	-19.30
Maximum	8.3×10^{-16}	3.0×10^{-16}	1.5×10^{-16}	-15.08	-15.52	-15.82
Sum	9.0×10^{-16}	3.4×10^{-16}	1.8×10^{-16}	-552.29	-524.43	-402.17
Points	31	29	22	31	29	22
Mean	2.9×10^{-17}	1.2×10^{-17}	8.0×10^{-18}	-17.82	-18.08	-18.28
Median	1.3×10^{-18}	5.7×10^{-19}	3.1×10^{-19}	-17.89	-18.24	-18.51
Std. Deviation	1.5×10^{-16}	5.6×10^{-17}	3.2×10^{-17}	0.67	0.69	0.83
Variance	2.2×10^{-32}	3.2×10^{-33}	1.1×10^{-33}	0.45	0.48	0.69



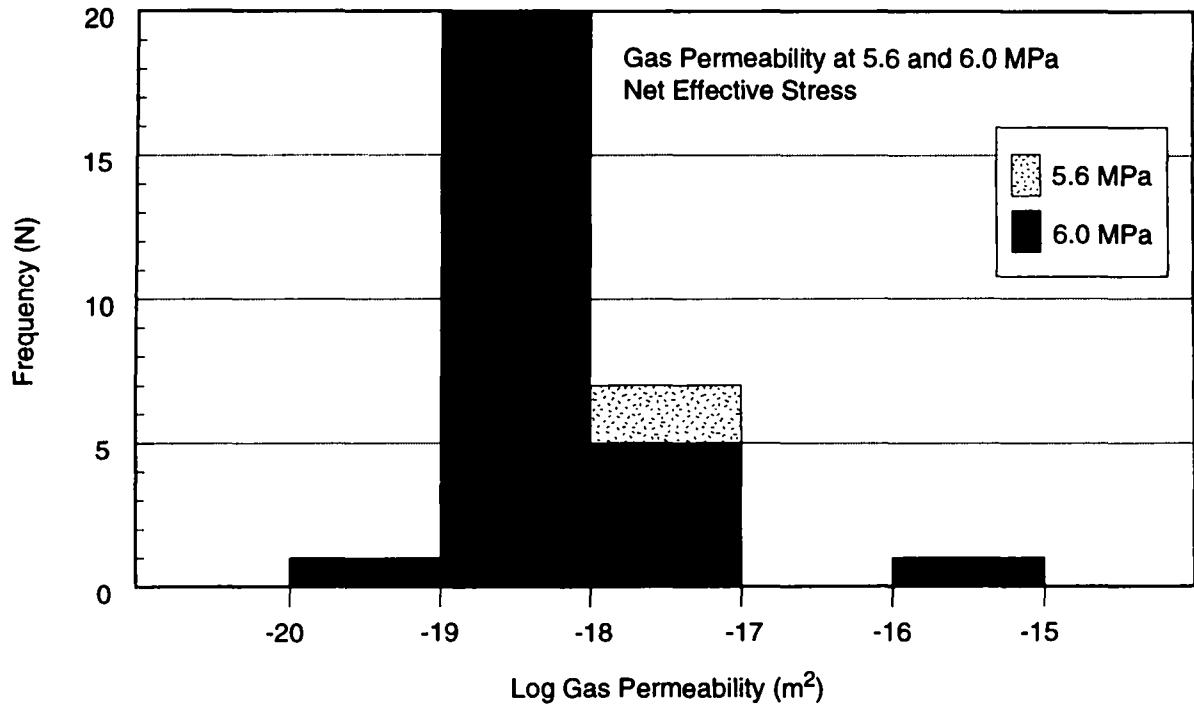
TRI-6115-164-0

Figure 16a. Gas permeability histogram for 1.6, 2.0, and 3.4 MPa net effective stress.



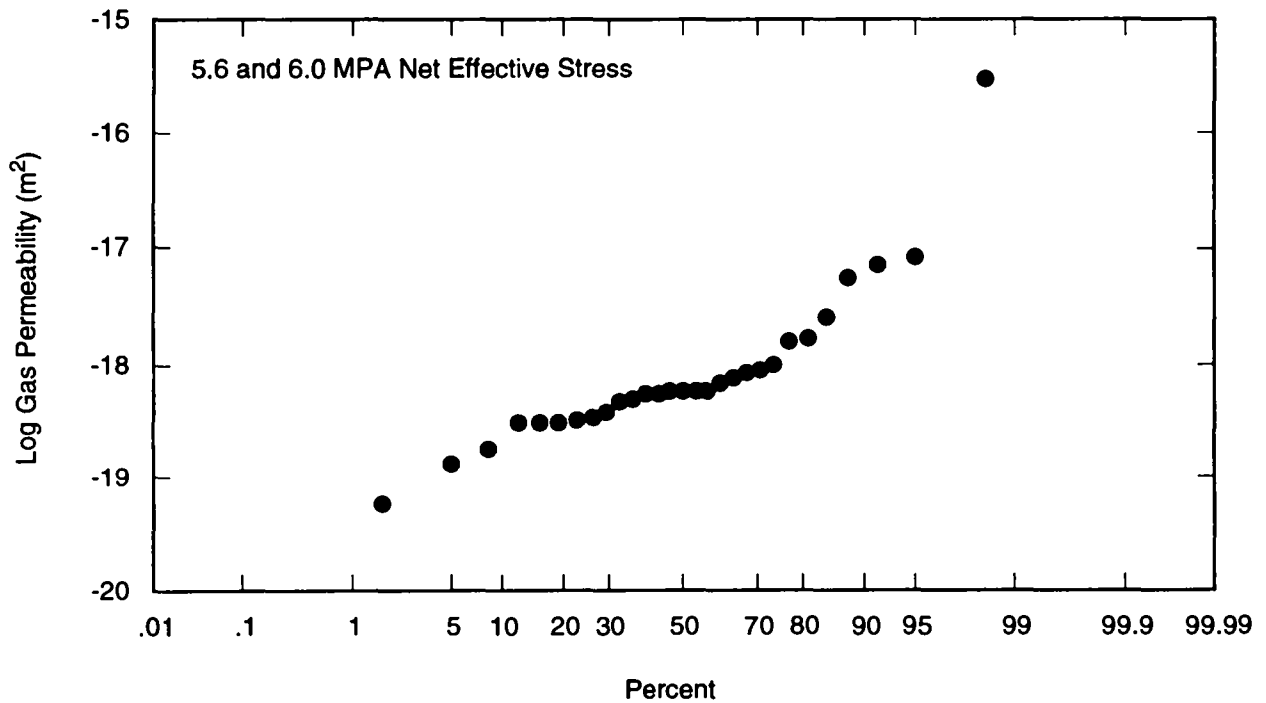
TRI-6115-167-0

Figure 16b. Normalized cumulative frequency plot for 1.6, 2.0, and 3.4 MPa net effective stress.



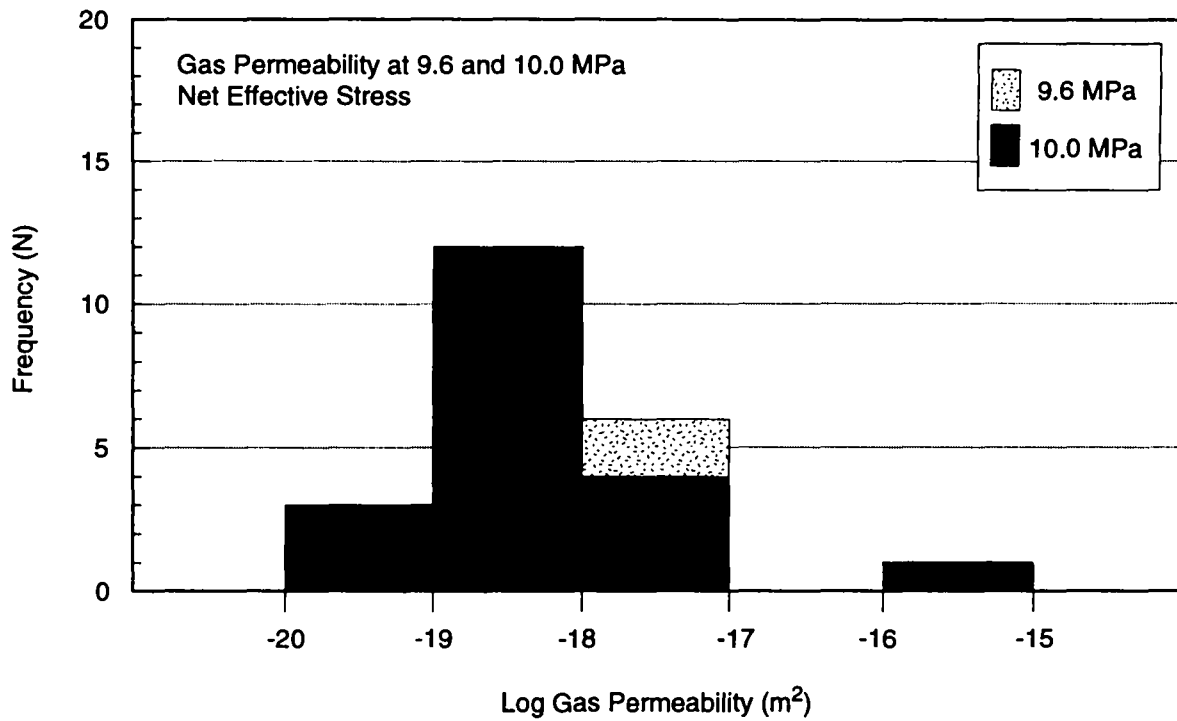
TRI-6115-165-0

Figure 17a. Gas permeability histogram for 5.6 and 6.0 MPa net effective stress.



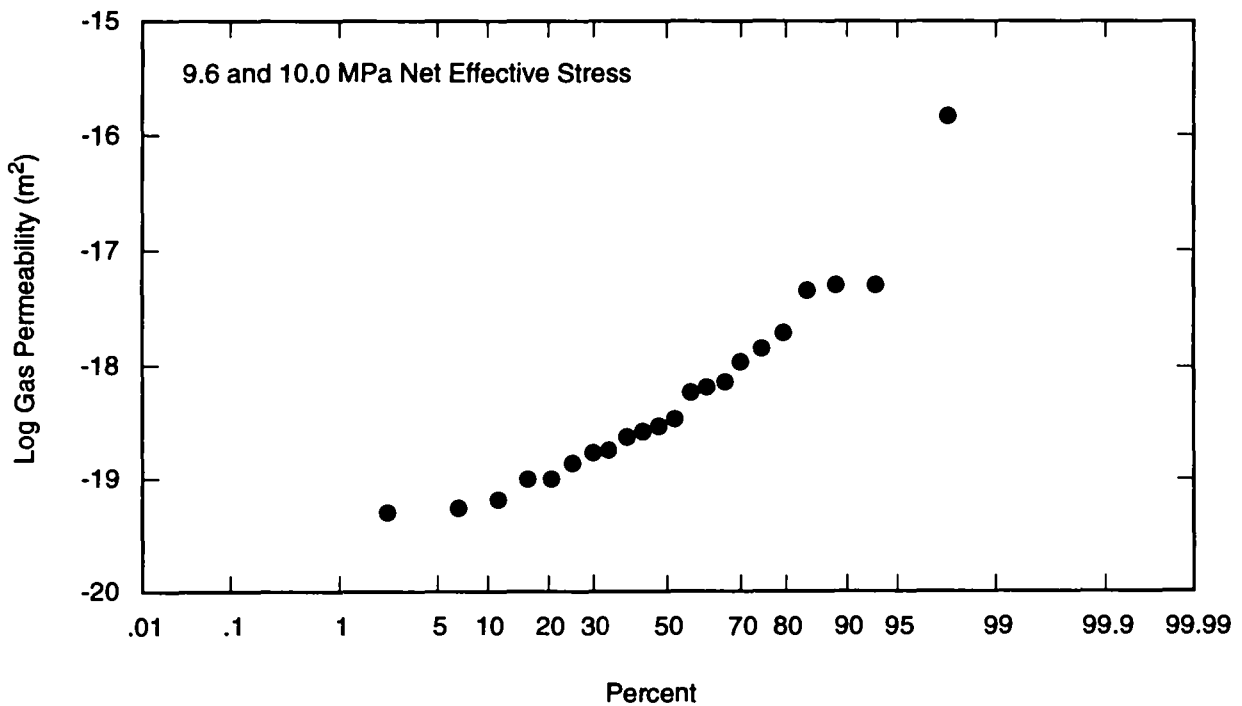
TRI-6115-168-0

Figure 17b. Normalized cumulative frequency plot for 5.6 and 6.0 MPa net effective stress.



TRI-6115-168-0

Figure 18a. Gas permeability histogram for 9.6 and 10.0 MPa net effective stress.



TRI-6115-169-0

Figure 18b. Normalized cumulative frequency plot for 9.6 and 10.0 MPa net effective stress.

5.2.1.2 Relationship between Zone Classification and Gas Permeability

Figure 19 shows a plot used to evaluate gas permeability for the 2 MPa data among MB139 Stratigraphic Zones II, III, and IV. The results are summarized in Table 7. No specimens were cut from Zones I or V. No definitive distribution is evident from the gas permeability data; however, the data suggest that the permeability of Zone IV is slightly higher than Zones II and III, if the anomalously high permeability data from TerraTek's Sample E are excluded. The flow properties of Zones I and V are expected to be more representative of fractured rock and are therefore likely to have greater permeability than Zones II, III, or IV.

Table 7. Summary of Gas Permeability Data Results by Zone at 2 MPa Net Effective Stress

Zone	Number of Data Points	Minimum Permeability (m ²)	Maximum Permeability (m ²)	Median Permeability (m ²)
II	6	5.9×10^{-20}	5.7×10^{-18}	9.6×10^{-19}
III	20	3.9×10^{-19}	3.0×10^{-16}	1.2×10^{-18}
IV	5	5.9×10^{-19}	8.9×10^{-18}	1.5×10^{-18}

5.2.1.3 Relationship between Confining Stress and Gas Permeability

Gas permeability tests were successfully conducted on 31 specimens under hydrostatic confining stress conditions. Gas permeability was successfully measured on 31 specimens at the 2 MPa net effective stress level, on 29 of the 31 specimens at the 6 MPa net effective stress level, and on 22 of 29 specimens at the 10 MPa net effective stress level.

Figure 20 is a graph showing Klinkenberg-corrected gas permeability versus net effective stress for 31 specimens. The graph shows the range of measured gas permeability values at each net effective stress and the median gas permeability at each net effective stress. The near-horizontal lines on Figure 20 connect the gas permeability data for some specimens. Attempts were made at each test laboratory to measure gas permeability at three net effective stresses. In some cases, however, equipment resolution capabilities were exceeded at Core Laboratories, precluding the completion of tests at higher net effective stress conditions.

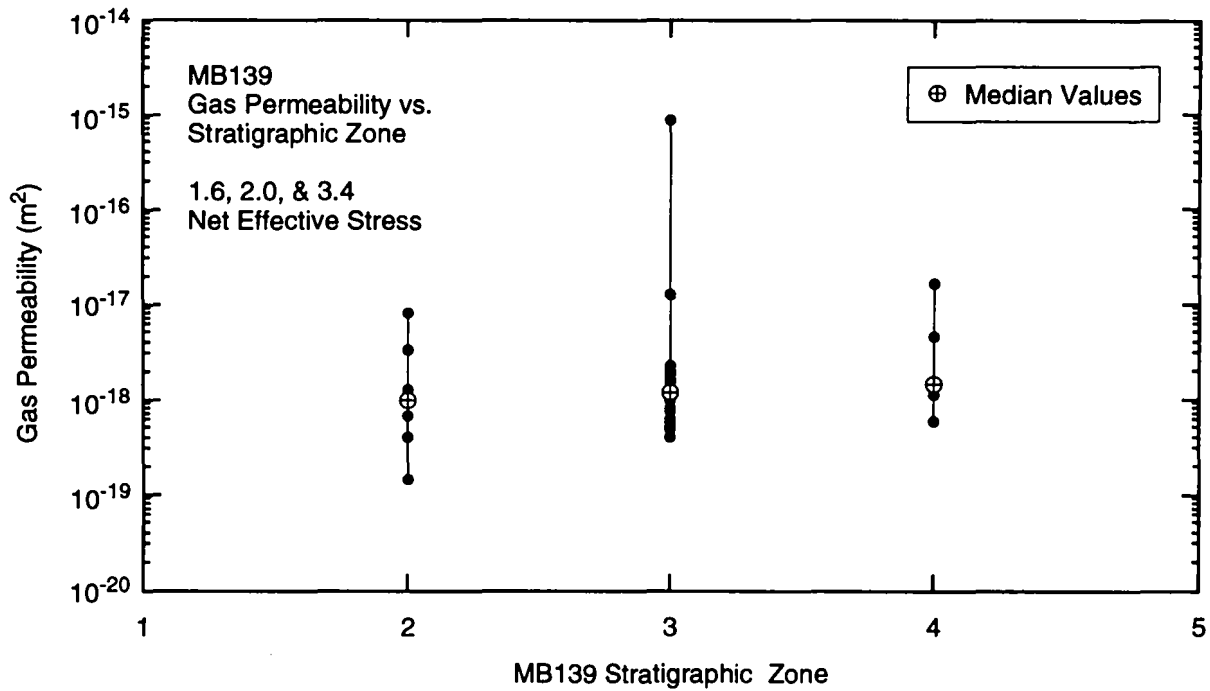


Figure 19. Gas permeability versus Marker Bed 139 stratigraphic zone.

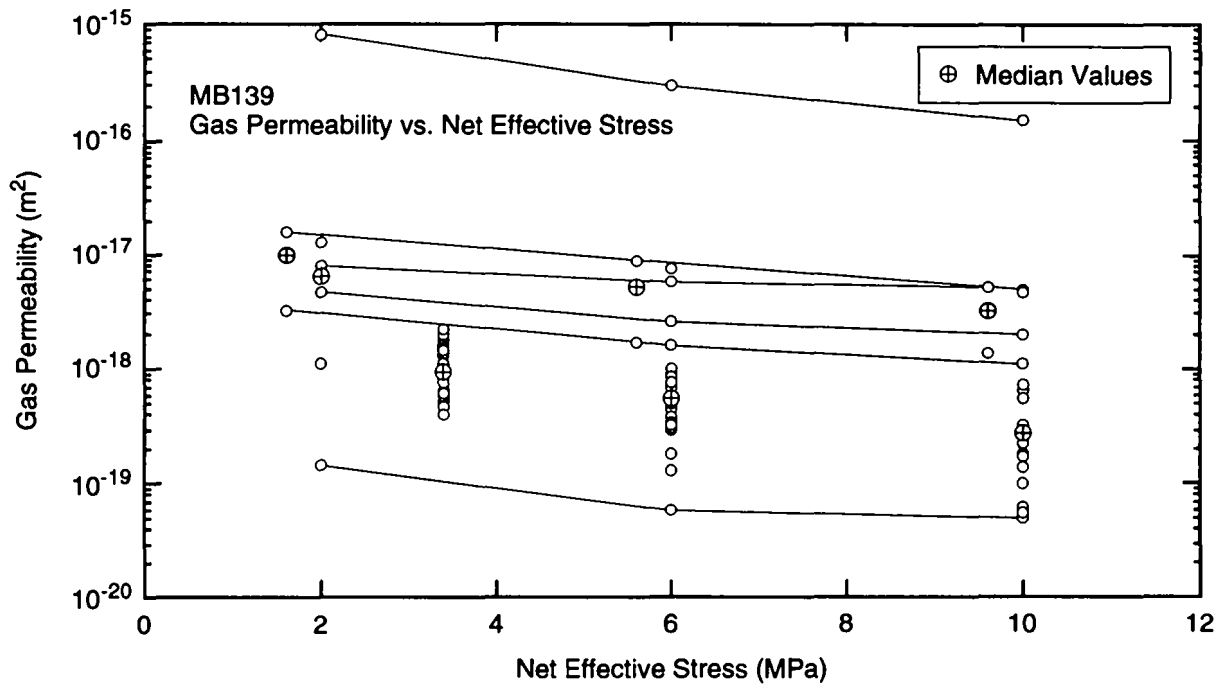


Figure 20. Gas permeability versus net effective stress.

Increasing the net effective stress on a specimen caused the gas permeability to decrease in all cases. The decrease in Klinkenberg-corrected gas permeability corresponding to an increase in net effective stress from 2 to 10 MPa ranged from a factor of 1.6 to 11.6, with a mean of 4.0.

5.2.2 Single-Phase Liquid Permeability

Single-phase, steady-state liquid permeability was measured for five specimens: three at TerraTek and two at RE/SPEC. Prior to the liquid permeability tests, gas permeability was measured for each specimen so that direct comparisons could be made between the liquid permeability and the Klinkenberg-corrected gas permeability: the measured liquid permeability should equal the Klinkenberg-corrected gas permeability (Klinkenberg, 1941). Results of the liquid permeability tests are summarized in Tables 3b and 3c.

Liquid permeability tests were designed to be conducted using the steady-state method with fully saturated test specimens. However, both test laboratories reported difficulties related to saturating the test specimens. RE/SPEC observed during the saturation process that noticeable dissolution of both specimens occurred, indicating that brine composition was not compatible with the rock. A careful review of the raw TerraTek liquid permeability data showed that only "preliminary" data were included; in some cases, it was reported that specimens were over 100% saturated with OMS, which is not possible. Therefore the liquid permeability data reported here should be considered only as "scoping data." Although the liquid permeability data provide useful information for designing and implementing future liquid and relative permeability tests, the data do not meet applicable quality standards necessary for use within the WIPP Performance Assessment (PA) program.

5.2.2.1 Histograms and Probability Distributions

Results of single-phase liquid permeability measurements performed at RE/SPEC and TerraTek are shown in Tables 3b and 3c and summarized in Table 8. RE/SPEC measured liquid permeability for two specimens at 1.6 MPa net effective stress but was able to measure liquid permeability on only one core at 5.6 and 9.6 MPa net effective stress because of mechanical failure. TerraTek measured liquid permeability for all three samples at 2.0, 6.0, and 10.0 MPa net effective stress. Measured liquid permeabilities ranged from a minimum of $5.1 \times 10^{-19} \text{ m}^2$ to a maximum of $7.9 \times 10^{-17} \text{ m}^2$ at the lower net effective stress levels. The lowest measured permeability of $5.1 \times 10^{-19} \text{ m}^2$ was at 10.0 MPa net effective stress.

Table 8. Summary of Liquid Permeability Data Results

	Liquid Permeability					
	1.6 MPa (m ²)	2 MPa (m ²)	5.6 MPa (m ²)	6 MPa (m ²)	9.6 MPa (m ²)	10 MPa (m ²)
Minimum	5.3×10^{-17}	1.1×10^{-18}	4.3×10^{-17}	6.1×10^{-19}	2.6×10^{-17}	5.1×10^{-19}
Maximum	7.9×10^{-17}	6.7×10^{-18}	4.3×10^{-17}	5.7×10^{-18}	2.6×10^{-17}	5.3×10^{-18}
Sum	1.3×10^{-16}	1.1×10^{-17}	4.3×10^{-17}	8.7×10^{-18}	2.6×10^{-17}	7.6×10^{-18}
Points	2	3	1	3	1	3
Mean	6.6×10^{-17}	3.8×10^{-18}	4.3×10^{-17}	2.9×10^{-18}	2.6×10^{-17}	2.5×10^{-18}
Median	6.6×10^{-17}	3.6×10^{-18}	4.3×10^{-17}	2.4×10^{-18}	2.6×10^{-17}	1.8×10^{-18}
Std. Deviation	1.8×10^{-17}	2.8×10^{-18}		2.6×10^{-18}		2.5×10^{-18}
Variance	3.4×10^{-34}	7.9×10^{-36}		6.6×10^{-36}		6.1×10^{-36}

The histogram and associated cumulative frequency plots for the 2, 6, and 10 MPa data are shown in Figures 21, 22, and 23, respectively. The permeability distribution appears to be log normal. A log-normal distribution is expected because permeability depends on pore-size distribution, and pore-size distribution is typically log-normal for rocks (Freeze, 1975).

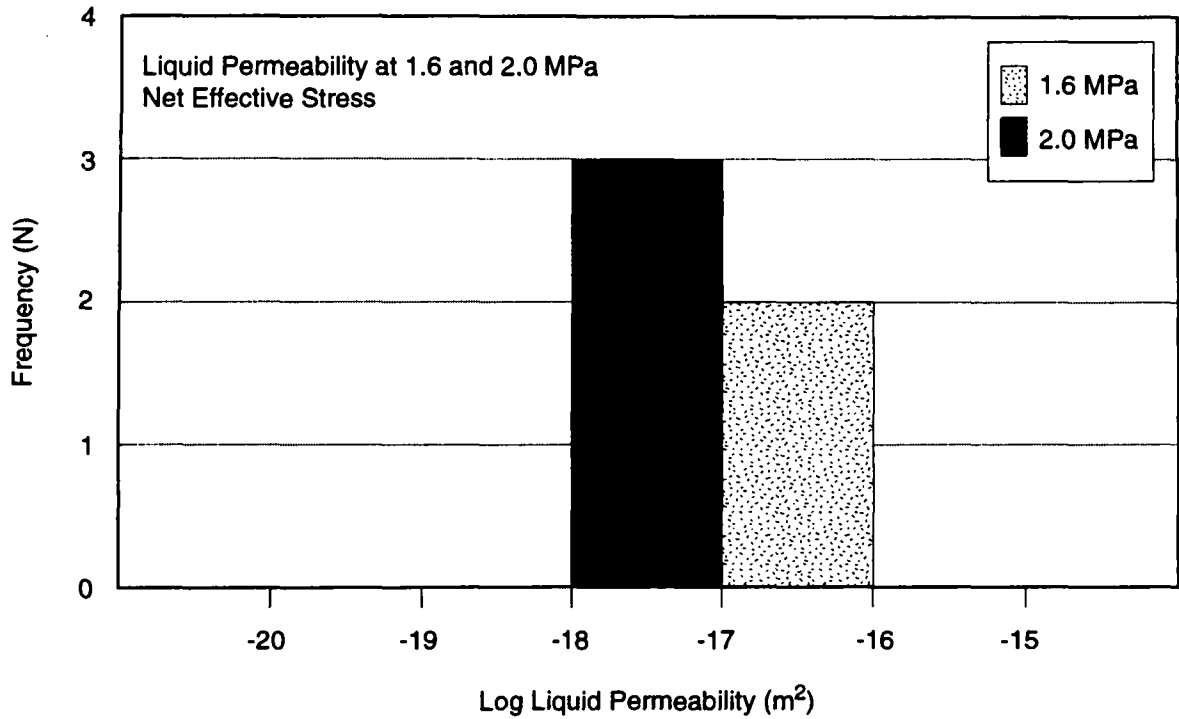
5.2.2.2 Relationship between Zone Classification and Liquid Permeability

A plot of liquid permeability for the 2 MPa data among MB139 Stratigraphic Zones II and IV is shown in Figure 24. No specimens were cut from Zones I or V, and no successful measurements were made from Zone III.

Zone II permeabilities for net effective stress at 2 MPa ranged from 6.7×10^{-18} to 5.3×10^{-17} m² with a median value of 3×10^{-17} m². Zone IV permeabilities ranged from 1.1×10^{-18} to 7.9×10^{-17} m² with a median value of 3.6×10^{-18} m². There are not sufficient data from which to draw conclusions regarding liquid permeability distribution within the MB139 zones.

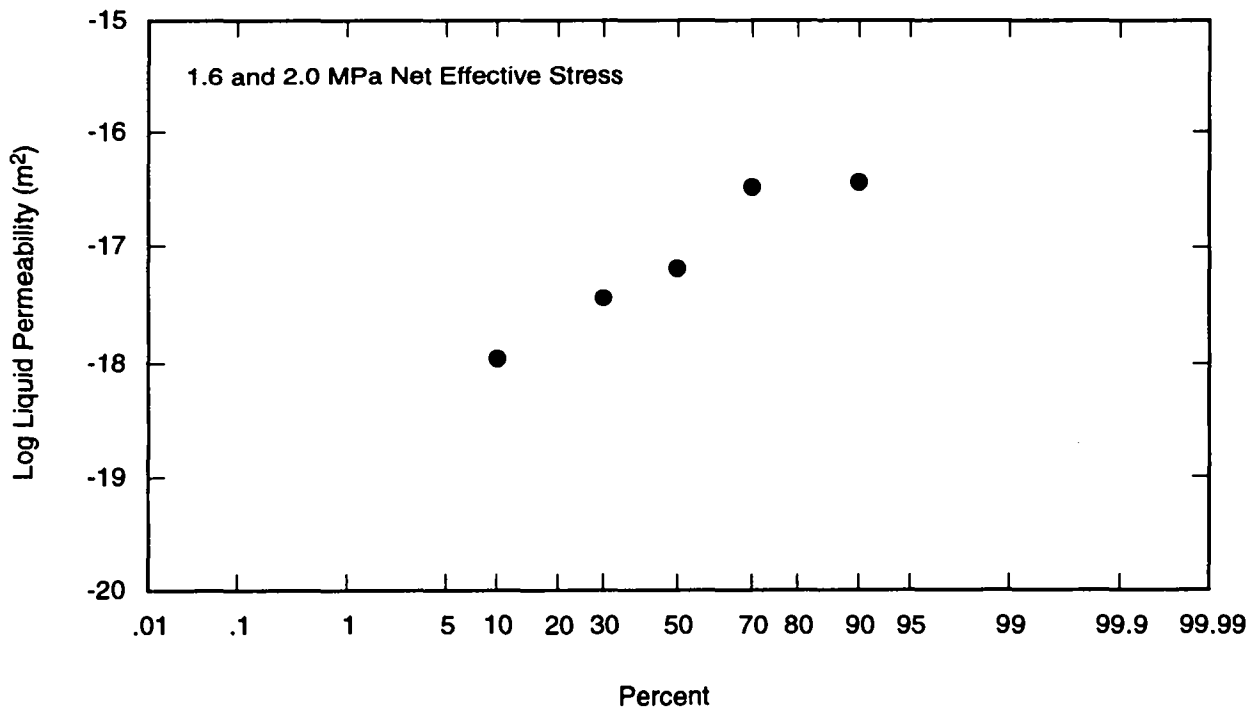
5.2.2.3 Relationship between Confining Stress and Liquid Permeability

Figure 25 is a graph showing liquid permeability versus net effective stress for the five specimens. The graph shows the range of measured liquid permeability values at each net effective stress. The line on Figure 25 shows the general trend of the gas permeability data for the four specimens measured at three different net effective stresses.



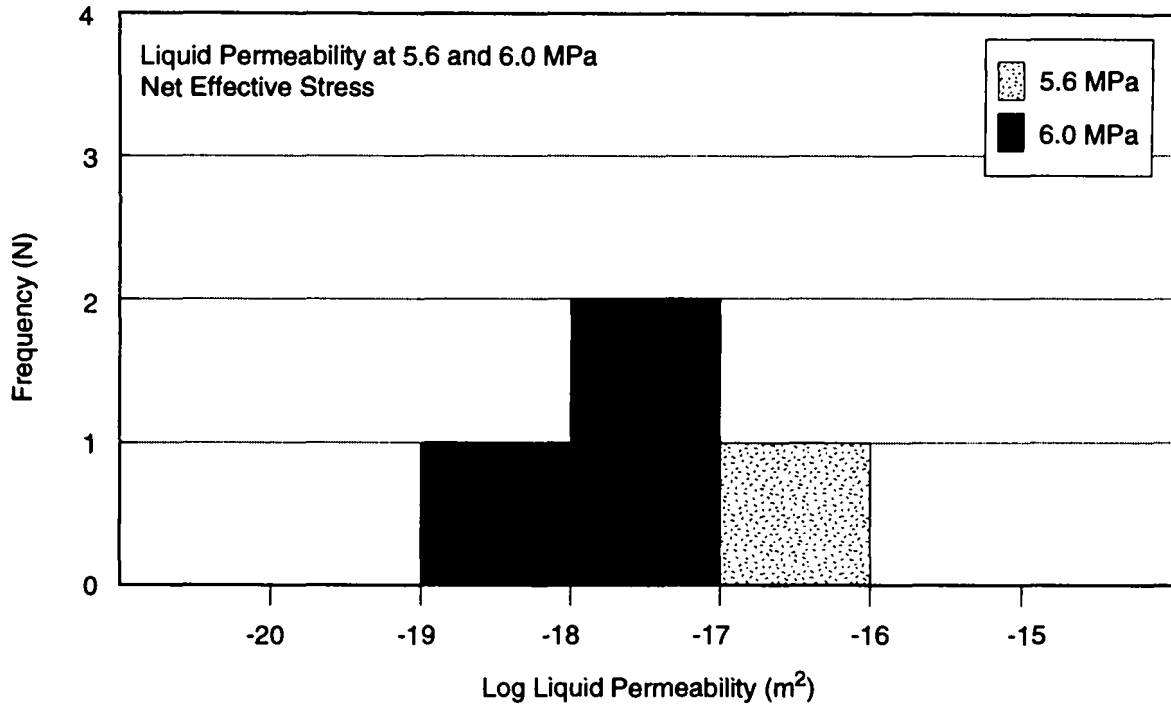
TRI-6115-170-0

Figure 21a. Liquid permeability histogram for 1.6 and 2.0 MPa net confining stress.



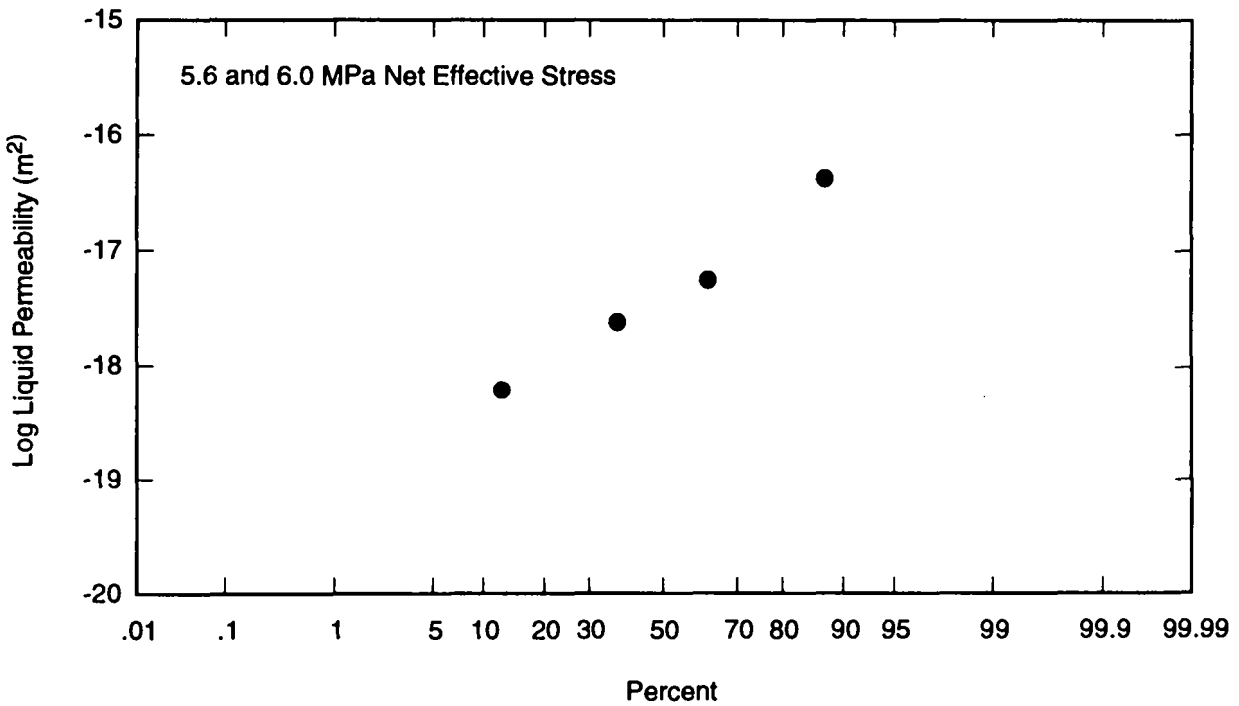
TRI-6115-173-0

Figure 21b. Normalized cumulative frequency plot for 1.6 and 2.0 MPa net effective stress.



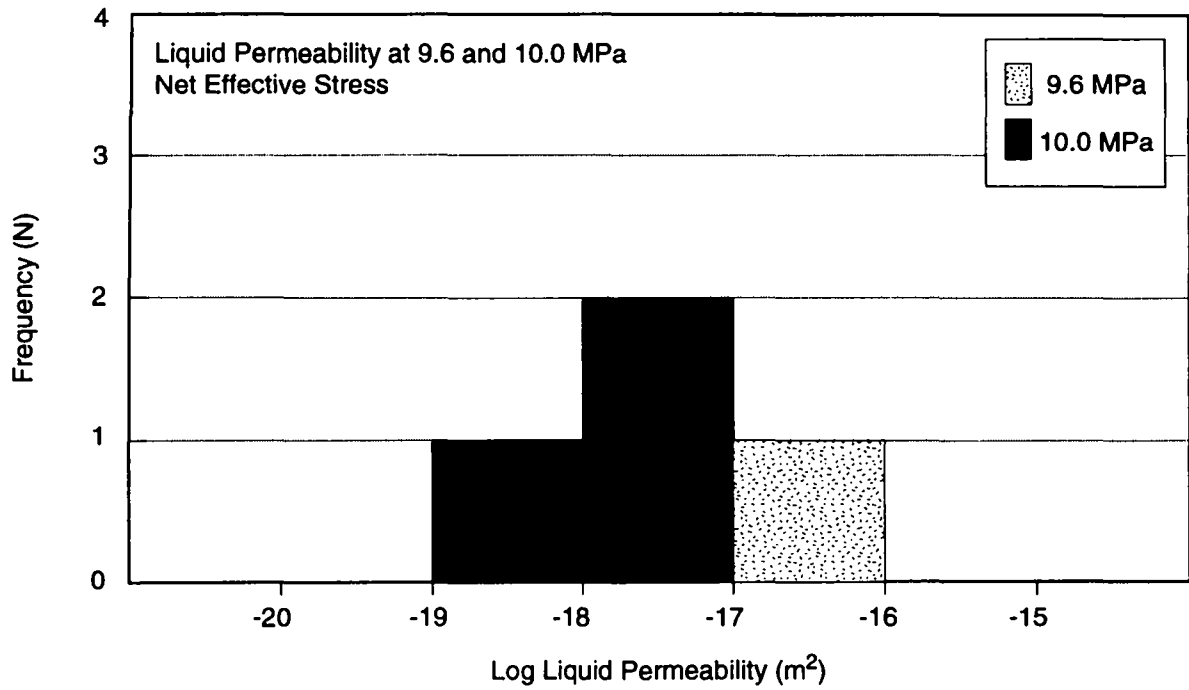
TRI-6115-171-0

Figure 22a. Liquid permeability histogram for 5.6 and 6.0 MPa net confining stress.



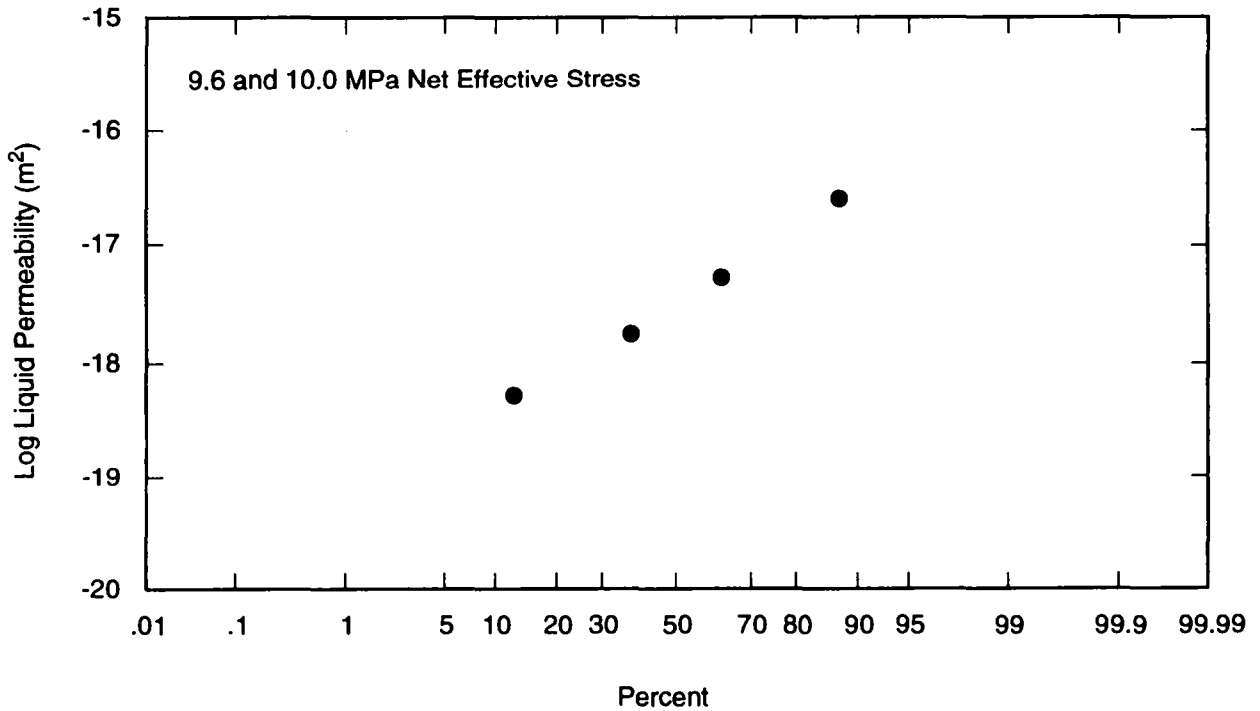
TRI-6115-174-0

Figure 22b. Normalized cumulative frequency plot for 5.6 and 6.0 MPa net effective stress.



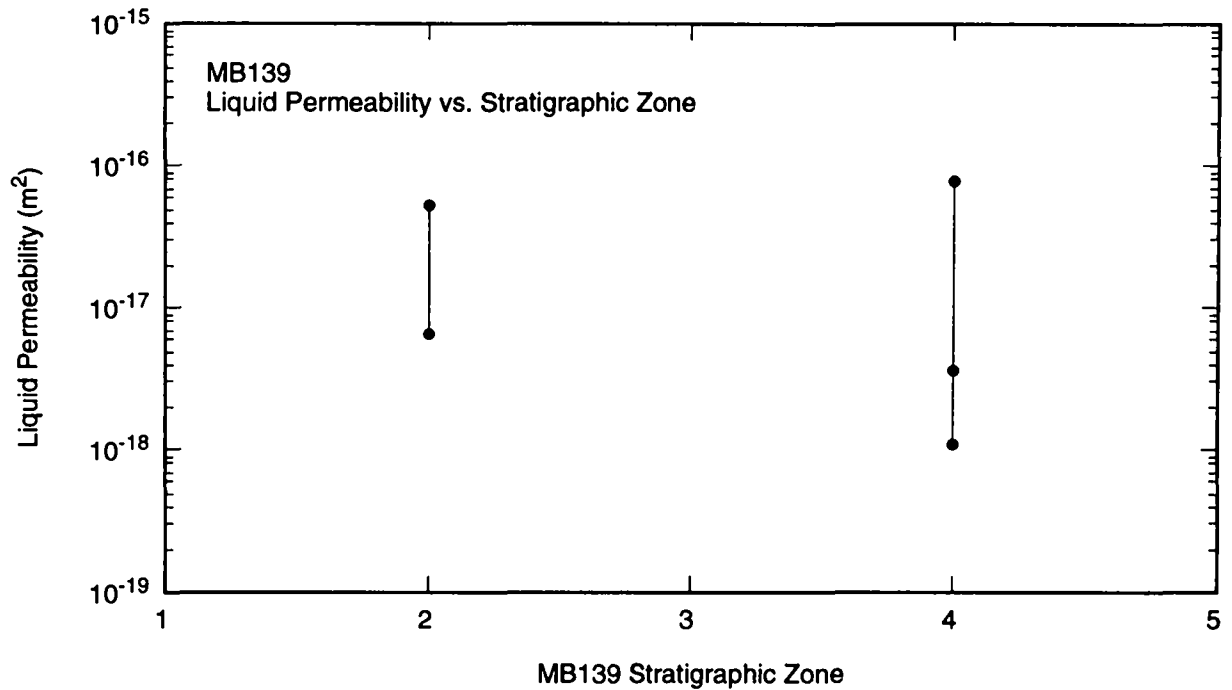
TRI-6115-172-0

Figure 23a. Liquid permeability histogram for 9.6 and 10.0 MPa net confining stress.



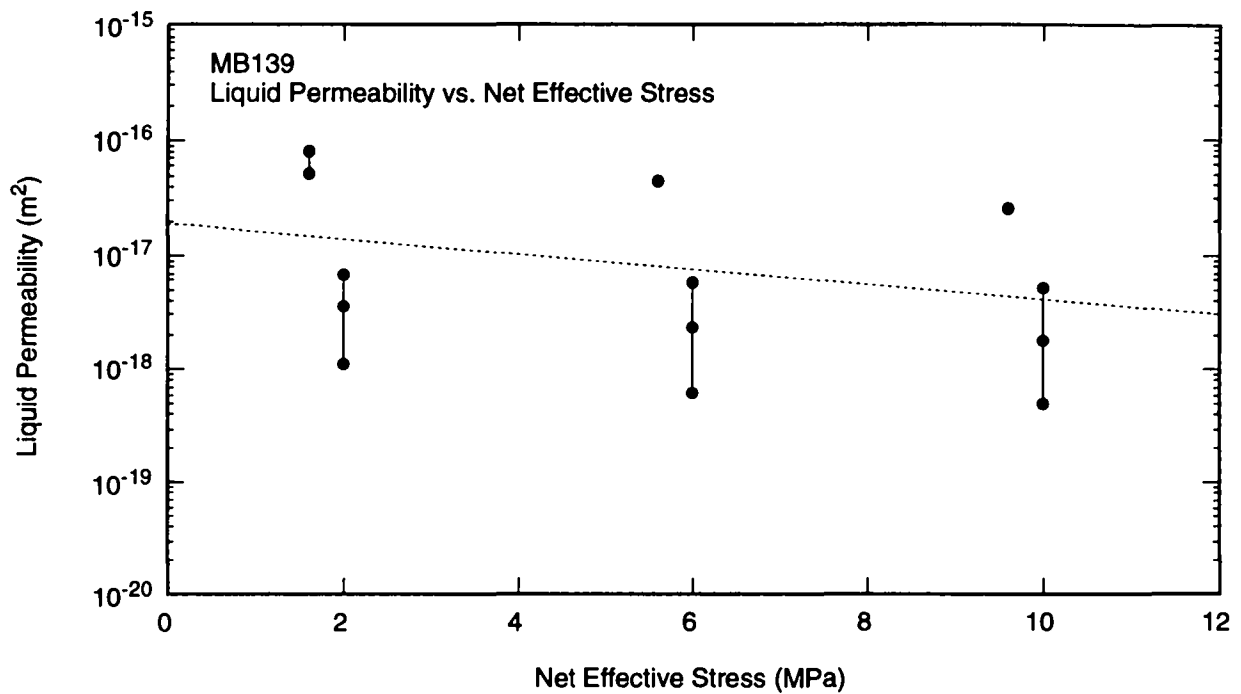
TRI-6115-175-0

Figure 23b. Normalized cumulative frequency plot for 9.6 and 10.0 MPa net effective stress.



TRI-6115-177-0

Figure 24. Liquid permeability versus Marker Bed 139 stratigraphic zone.



TRI-6115-179-0

Figure 25. Liquid permeability versus net effective stress.

As expected, liquid permeability decreases as the net effective pressure is increased. The range of the magnitude of permeability decrease with an 8.0 MPa increase in net effective stress is less than for the gas permeability samples. However, at this time there are insufficient data from which to draw definitive conclusions regarding the decrease in liquid permeability with increasing net effective stress.

5.2.3 Comparison of Gas and Liquid Permeability

Figure 26 shows a plot of liquid permeability versus Klinkenberg-corrected gas permeability for the five cores for which gas and liquid permeability were measured. As expected, the liquid permeability measurements made with OMS show a nearly one-to-one agreement with the Klinkenberg-corrected gas-measured permeabilities. However, liquid permeability measurements performed with brine as the saturant show a significant difference from the gas permeability measurements. The significantly higher liquid permeabilities of the brine-saturated specimens were most likely caused by dissolution of the specimen, which resulted in an increase in the interconnected pathways.

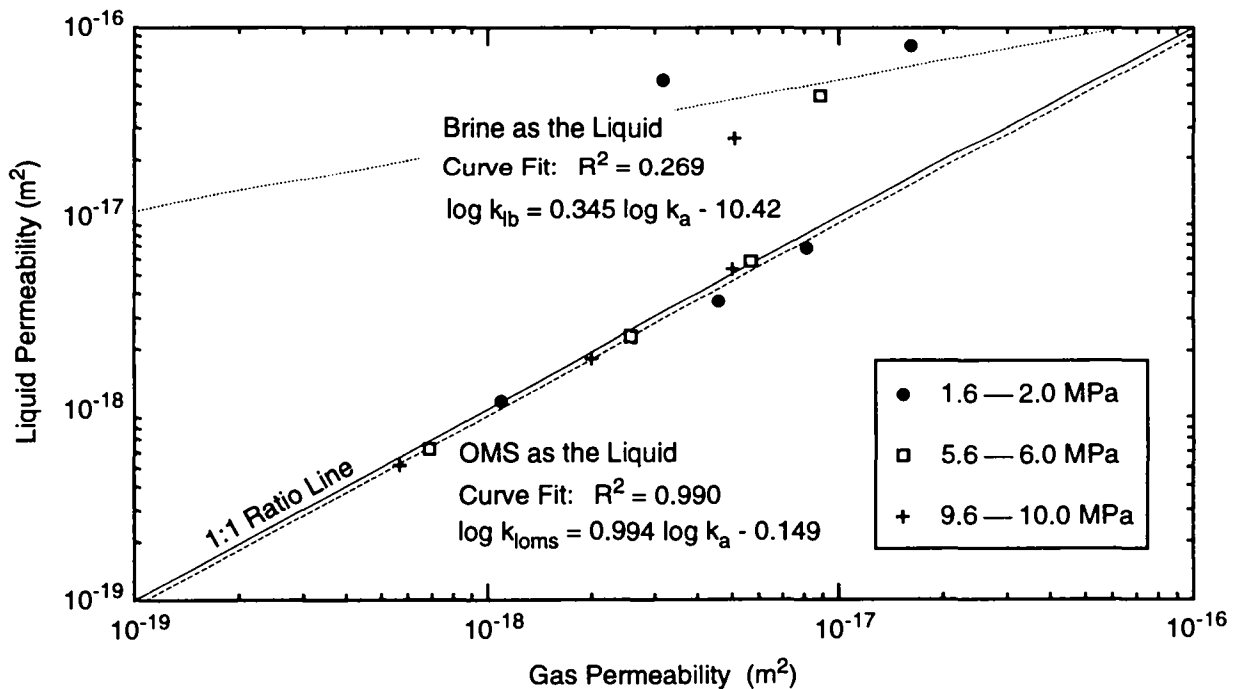
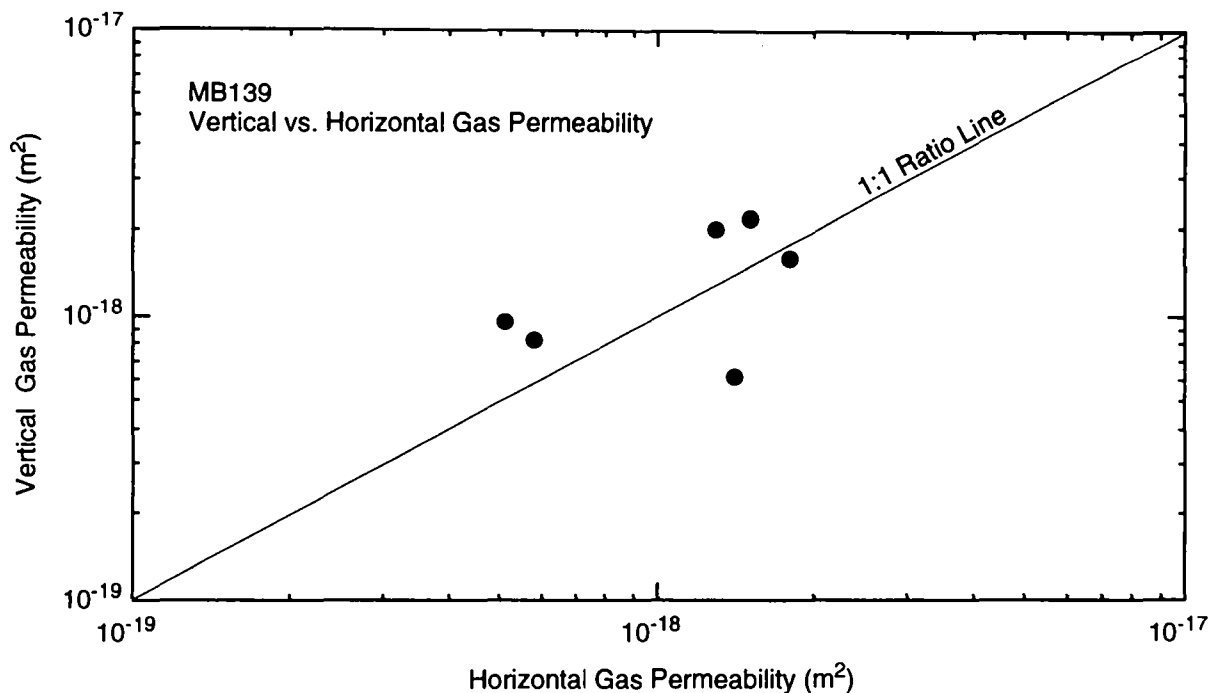


Figure 26. Liquid permeability versus gas permeability.

5.2.4 Comparison of Vertical and Horizontal Permeability

To evaluate anisotropy within the marker bed, Core Laboratories cut specimens from the same depth from whole cores oriented parallel and perpendicular to the bedding plane of MB139. The flow direction orientation with respect to the MB139 bedding plane is shown in Tables 3a, 3b, and 3c for each specimen. The "H" designates horizontal flow (i.e., flow parallel to the bedding plane), and the "V" designates vertical flow (i.e., flow perpendicular to the bedding plane).

Figure 27 shows a cross-plot of vertical and horizontal permeability made at 3.4 MPa net effective stress for six pairs of specimens that were drilled at Core Laboratories. The pairings were as follows: E1X10 Samples 5 and 7, E1X10 Samples 6 and 8, E1X10 Samples 11 and 13, E1X10 Samples 12 and 14, E1X11 Samples 23 and 25, and E1X11 Samples 24 and 26. Figure 27 shows the measurements with a one-to-one ratio line indicating where the data would fall if the horizontal and vertical permeabilities were the same. The limited data results suggest that anisotropy in MB139 is not apparent; horizontal and vertical permeability are the same, within experimental error parameters.



TRI-6115-180-0

Figure 27. Gas vertical permeability versus horizontal permeability.

6.0 CAPILLARY PRESSURE

This report contains the only WIPP-specific two-phase flow data that exist. Capillary pressure tests were performed on twelve cores from the Core Laboratories' set of 2.5-cm (1-in.)-diameter specimens using the centrifuge and mercury injection techniques. The objective of the capillary pressure tests was to use two conventional oil and gas laboratory techniques (high-speed centrifuge and mercury injection), assess whether either was applicable for MB139 samples, and compare the results from the two techniques. Six pairs of specimens with comparable orientation, depth, porosity, and permeability values were selected from the Core Laboratories specimens. One specimen from each pair underwent centrifuge capillary pressure tests and the other specimen underwent mercury injection capillary pressure tests. Neither the centrifuge nor the mercury injection tests were performed under confining stress.

Details about the test procedures, raw data, and analysis are presented in Appendix A. Because this is the only report containing the results of two-phase flow tests on Salado rock, this section is more detailed than the previous sections in which the single-phase data were presented. This section contains the raw data converted from test conditions to repository conditions and presents the data in tabular and graphic formats. This section also contains comparisons of data from the two techniques from adjacent core samples, compilation of the data generated by each technique, and compilation of the results from all twelve tests.

6.1 Test Procedures

Using x-ray photos, quantitative x-ray diffraction data, and porosity and permeability data, six pairs of specimens used in the capillary pressure tests were selected from the 30 specimens tested at Core Laboratories. Two characteristics comprised the selection criteria: (1) adequate permeability and porosity for testing, and (2) same orientation, depth, and reasonable similarity between the two samples in each pair as evidenced from the x-ray photos, diffraction data, and porosity and permeability data. The six selected pairs were: Samples 5 and 6; 7 and 8; 11 and 12; 13 and 14; 21 and 22; and 23 and 24. After selection, axial x-ray computer tomography (CT) slices were made at two orientations on each core to provide additional evidence for comparison purposes. The odd-numbered core from each pair was tested using the mercury injection method; the even-numbered core was tested using the centrifuge.

6.1.1 Centrifuge Tests

A high-speed centrifuge was used to determine the drainage capillary pressure curves for six samples using decane (a non-reactive hydrocarbon) to pressures up to about 3.45 MPa (500 psi). The centrifuge method is nondestructive, yields reproducible results, and can provide data for both drainage and imbibition curves. During a drainage test (non-wetting phase [gas] displacing wetting phase [liquid]), a core is fully saturated with the liquid and placed on a semipermeable membrane inside a centrifuge rotor's coreholder. A low rotation rate is selected, and the core is spun. The high acceleration rate increases the force field on the fluids, in effect subjecting the core to an increased gravitational field (Bass, 1987). The volume of liquid is measured as the core is rotated until the volume of expelled liquid is constant. An average value of brine saturation is calculated using a method such as that of Hassler and Brunner (1945) for the core at each rotation rate, and the rotation speed is converted into force units in the center of the sample. A higher rotation rate is selected, and the steps are repeated. If the test system has different surface tension behavior than in situ, the results are converted using standard correction factors.

Decane was chosen as the wetting phase fluid for the centrifuge tests because it is available in a very pure form, will not react with water-soluble minerals found in the specimens, and has a well-documented surface tension (24 dynes/cm at 25°C). The dry samples were fully saturated with 99%-pure decane, then placed in a high-speed centrifuge with calibrated collection tubes located below each sample. The decane volume in the collection tubes was read manually using a strobe light synchronized to the speed of the spinning rotor. These tests were performed at ambient temperature and at zero confining stress.

The equilibrium time between speed changes was at least 24 hours. Collection tubes had an original volume of 1 cm³ and were subdivided into 0.025 cm³ divisions, readable to 0.01 cm³. Because the porosity of the specimens was very low and greater volume resolution was desired, small Plexiglass rods with cross-sectional areas approximately half that of the collection tubes were inserted in the collection tubes. This ballast volume reduced the volume resolution to approximately 0.0125 per division, readable to 0.005 cm³.

The Hassler-Brunner (1945) and the Rajan (1986) methods were used to reduce the data and generate the capillary pressure curves from the produced volume and rotation speed data. Correction factors were then applied to the reduced data to correct from the decane-air test conditions to the desired brine-air in situ conditions.

6.1.2 Mercury Injection Tests

With the mercury injection method, a dry core sample is submersed in a chamber containing mercury and then evacuated. Volumes of mercury, a non-wetting liquid, are then incrementally forced into the core under pressure. The volume of mercury injected at each pressure is used to determine the non-wetting phase saturation, and the process is repeated until the entire capillary pressure curve is obtained (Bass, 1987). Because a mercury-air system is used, the mercury surface tension behavior is converted to that of the in situ fluids. This is a destructive method for determining capillary pressure.

The test system used at Core Laboratories measured the volume injected at each pressure from 0 to 345 MPa (0 to 50,000 psi). This test was destructive to the samples; the mercury-filled samples were discarded after the tests. Tests were conducted by an automated system that recorded all data on a computer data logger. Data reduction was performed using software provided by the manufacturer of the two-sample Micromeritics Autopore II 9220, which is a standard machine for testing porous ceramics, rocks, and similar materials.

6.2 Test Results

Conversion of capillary pressure data from one fluid system to another (e.g., air-decane to air-brine or air-mercury to air-brine) is performed using the following equation as described in Section 4.5 of Appendix A.

$$P_{c2} = P_{c1} \left(\frac{T_2 \cos \phi_2}{T_1 \cos \phi_1} \right) \quad (5)$$

where

P_c = capillary pressure

T = surface tension

ϕ = contact angle at the fluid/solid interface (subscripts refer to the different fluid systems).

Table 9 contains the values for surface tensions and contact angles used in this study. As described in Appendix A, to convert air-decane capillary pressure to that of an air-brine system, air-decane capillary pressure is multiplied by 3. Similarly, to convert air-mercury capillary pressure to that of an air-brine system, air-mercury capillary pressure is multiplied by 5.2 or 6.7, depending on whether 140° or 180° is used for the contact angle conversion.

Table 9. Capillary Pressure Conversion Constants Used in this Study

Fluid System	Surface Tension (T) (dynes/cm)	Contact Angle (ϕ) (degrees)
air-decane	24	0
air-brine	72	0
air-mercury	485	140 or 180

6.2.1 Centrifuge Tests

The results of the centrifuge capillary pressure tests, converted from the air-decane test conditions to the WIPP in situ air-brine conditions, are presented in Table 10. Data were reduced using the Hassler-Brunner method (Hassler and Brunner, 1945). The initial pressure plotted for each of the six samples is 0.0345 MPa (5 psi), which corresponds to a rotation speed of 1,720 rpm; the final pressure for each specimen was 4.48 MPa (650 psi), which corresponds to a rotation speed of 17,660 rpm. The initial rotation speed was selected because high threshold entry pressures were expected; the final rotation speed was a function of equipment limitations.

Table 10. Summary of Centrifuge Capillary Pressure Data

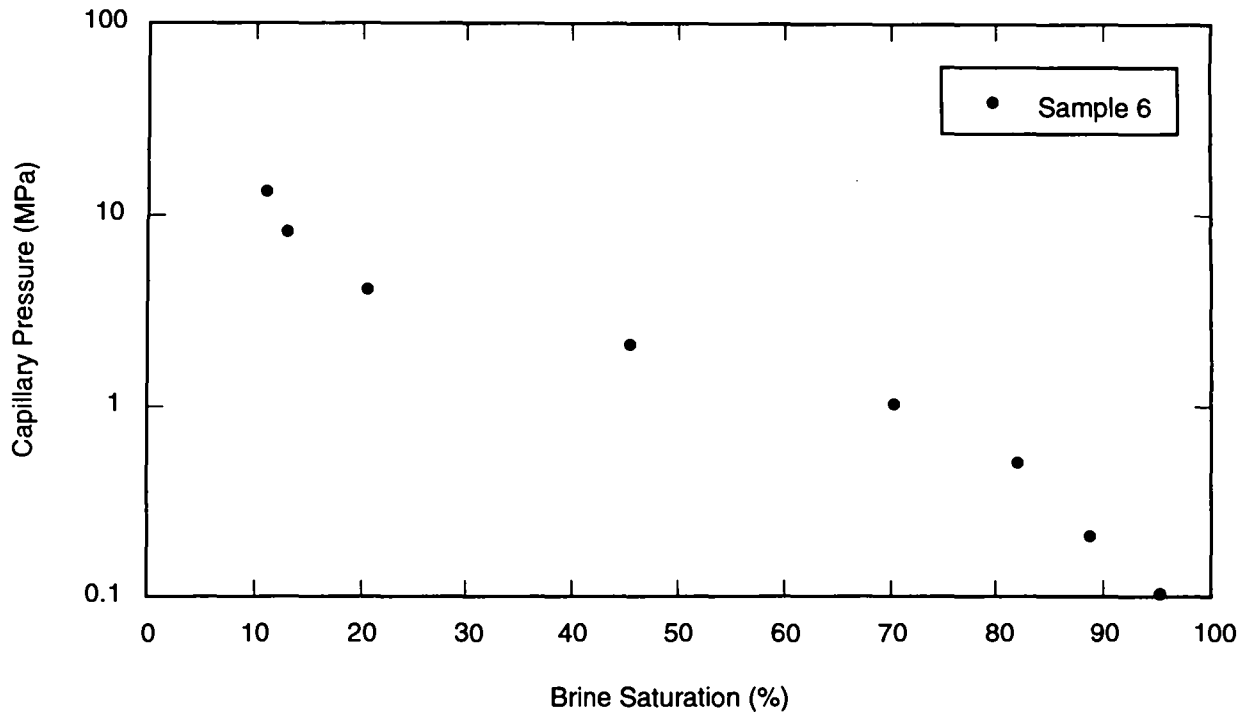
Capillary Pressure (MPa)	Capillary Pressure (psi)	Sample 6 Brine Saturation (%)	Sample 8 Brine Saturation (%)	Sample 12 Brine Saturation (%)	Sample 14 Brine Saturation (%)	Sample 22 Brine Saturation (%)	Sample 24 Brine Saturation (%)
0.10	15	95.2	86.9	91.5	85.2	90.7	94.4
0.21	30	88.7	86.4	88.6	85.1	90.1	90.5
0.52	75	82.0	84.6	81.8	84.5	87.0	78.5
1.03	150	70.3	80.5	70.2	82.3	76.2	61.9
2.07	300	45.5	68.3	42.0	73.6	46.5	40.2
4.14	600	20.7	32.1	21.4	48.6	30.1	25.9
8.28	1200	13.0	17.8	13.0	45.1	20.8	24.0
13.45	1950	11.1	10.7	10.6	44.5	17.6	23.6

The Hassler-Brunner method was used because it is applicable when the samples are small enough that the ratio of distance from centrifuge axis to top end of the sample divided by the distance from the centrifuge axis to bottom end of sample is greater than 0.7 (for details see Appendix A, page 6). This condition was met for all samples tested at Core Laboratories using the centrifuge. The results from the Hassler-Brunner method were compared to the results from the Rajan method (Rajan, 1986). The differences between the calculated end face saturations were typically less than 1% of the pore volume measured at 3.45 MPa (500 psi) net effective stress using the CMS-300 test apparatus.

The decane (oil) saturation at 0.0345 MPa (5 psi) capillary pressure ranged from approximately 85 to 95% for the six samples. Therefore the threshold entry pressure was less than 0.0345 MPa (5 psi). Residual liquid saturations at 4.48 MPa (650 psi) ranged from approximately 11 to 45%. Based on the general shape of the centrifuge capillary pressure curves, exhibiting a concave downward shape (or "knee") at 80 to 90% liquid saturation, a bimodal or multimodal pore size distribution is suggested. Except for Sample 14, the relatively low final liquid saturations suggest that these specimens did not contain significant microporosity. The centrifuge capillary pressure curves for Samples 6, 8, 12, 14, 22, and 24 are presented in Figures 28a through f, respectively. All data presented in these figures were converted from the air-decane test conditions to the air-brine system to represent in situ WIPP conditions.

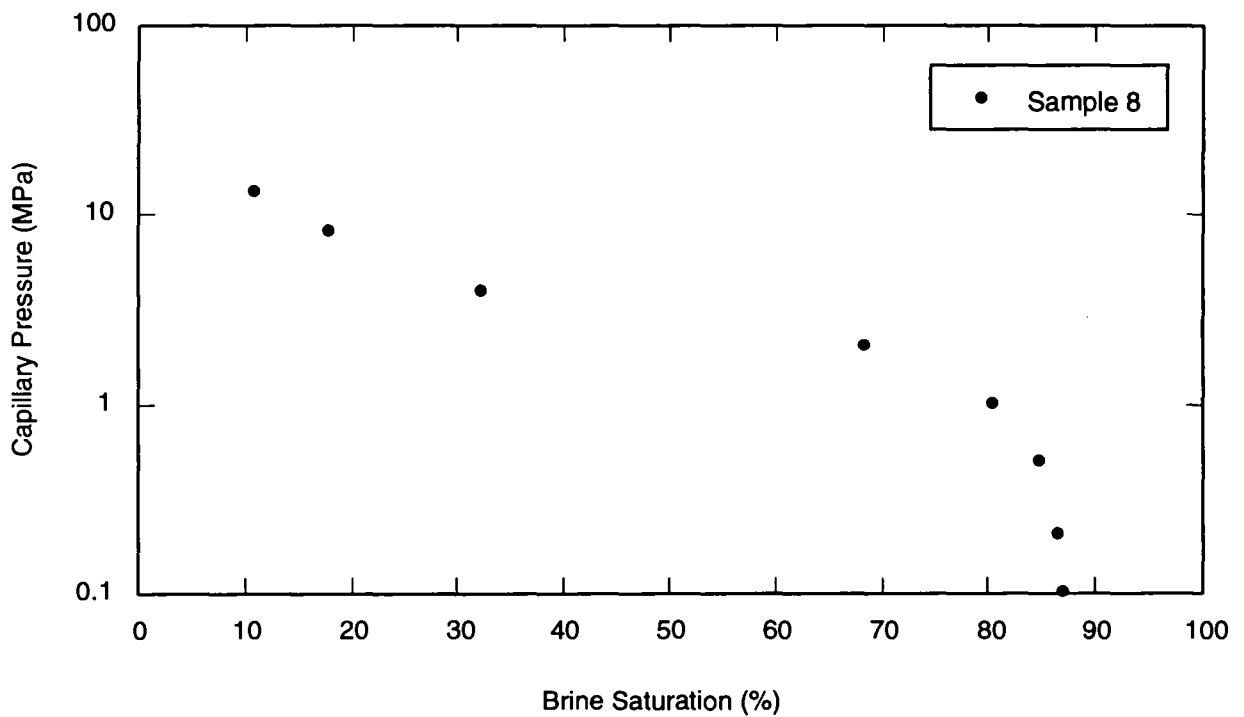
6.2.2 Mercury Injection Tests

Results of the mercury injection capillary pressure tests are presented in Tables 11a through f for Samples 5, 7, 11, 13, 21, and 23, respectively. Each table presents the mercury-air test conditions data corrected to the air-brine system representing the in situ WIPP conditions. The data were corrected using both the 140° and 180° contact angles as recommended by Good and Mikhail (1981), and both sets of results are included in each table for comparison. Pore volumes for the mercury injection specimens were measured using the CMS-300 at 3.45 MPa (500 psi) net effective stress, consistent with the centrifuge pore volumes. The starting pressure for the mercury injection was about 0.010 MPa (1.5 psi), and the final pressure was approximately 345 MPa (50,000 psi), which results in a complete capillary pressure curve from 100% wetting-phase saturation to a residual wetting-phase saturation.



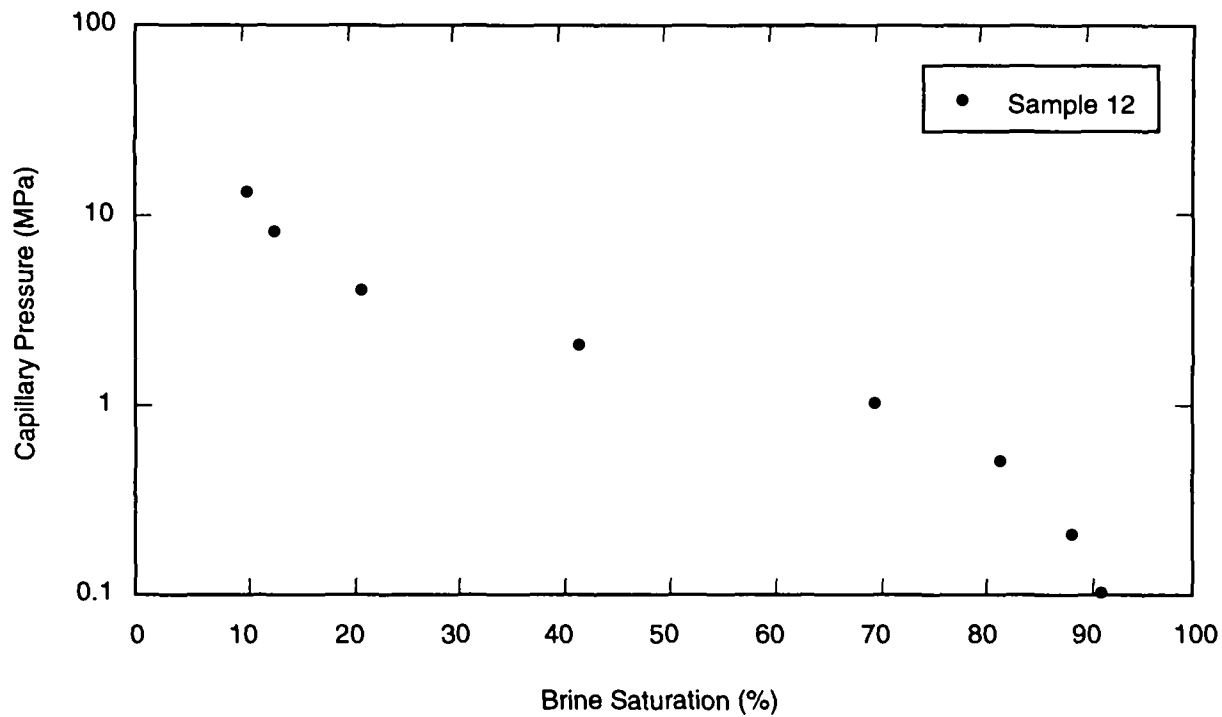
TRI-6115-204-0

Figure 28a. Centrifuge capillary pressure versus brine saturation: Sample 6.



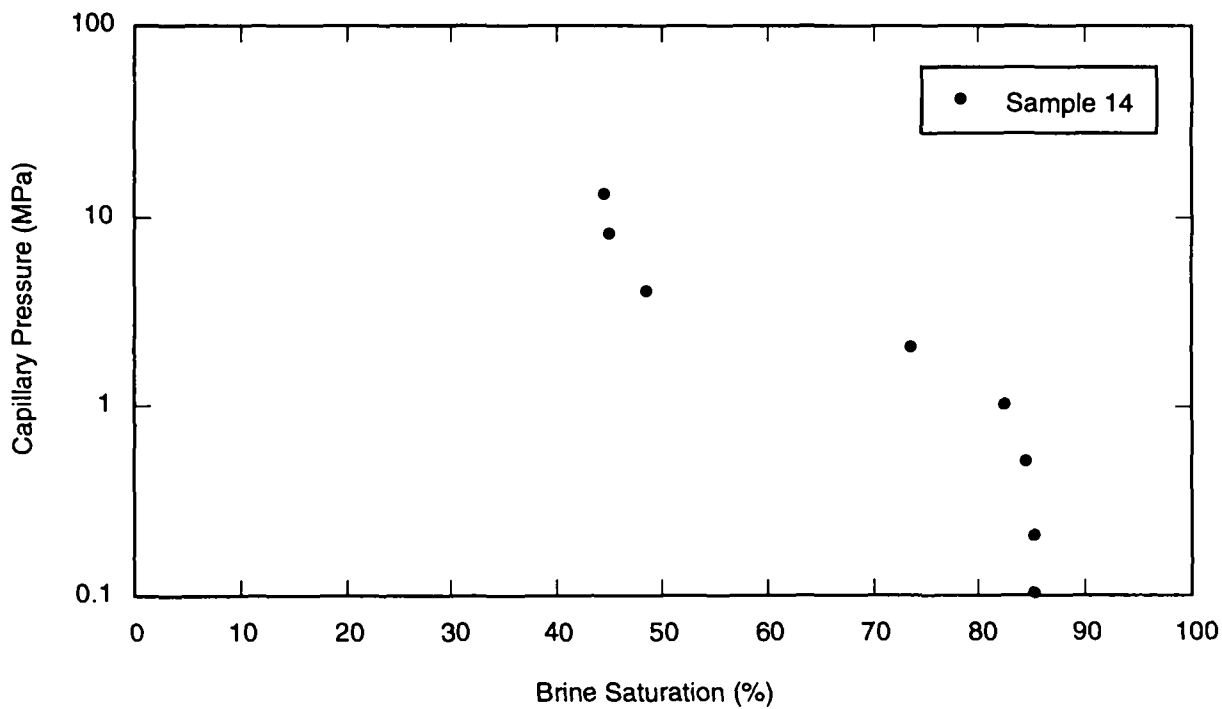
TRI-6115-205-0

Figure 28b. Centrifuge capillary pressure versus brine saturation: Sample 8.



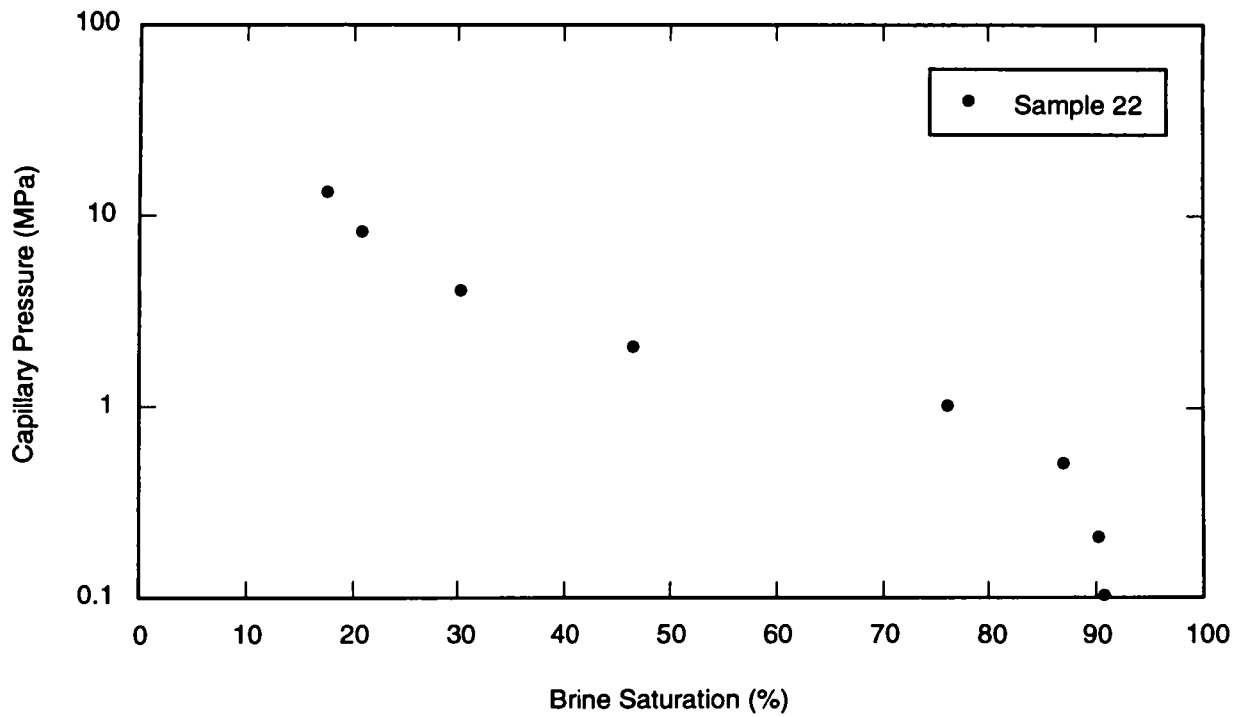
TRI-6115-200-0

Figure 28c. Centrifuge capillary pressure versus brine saturation: Sample 12.



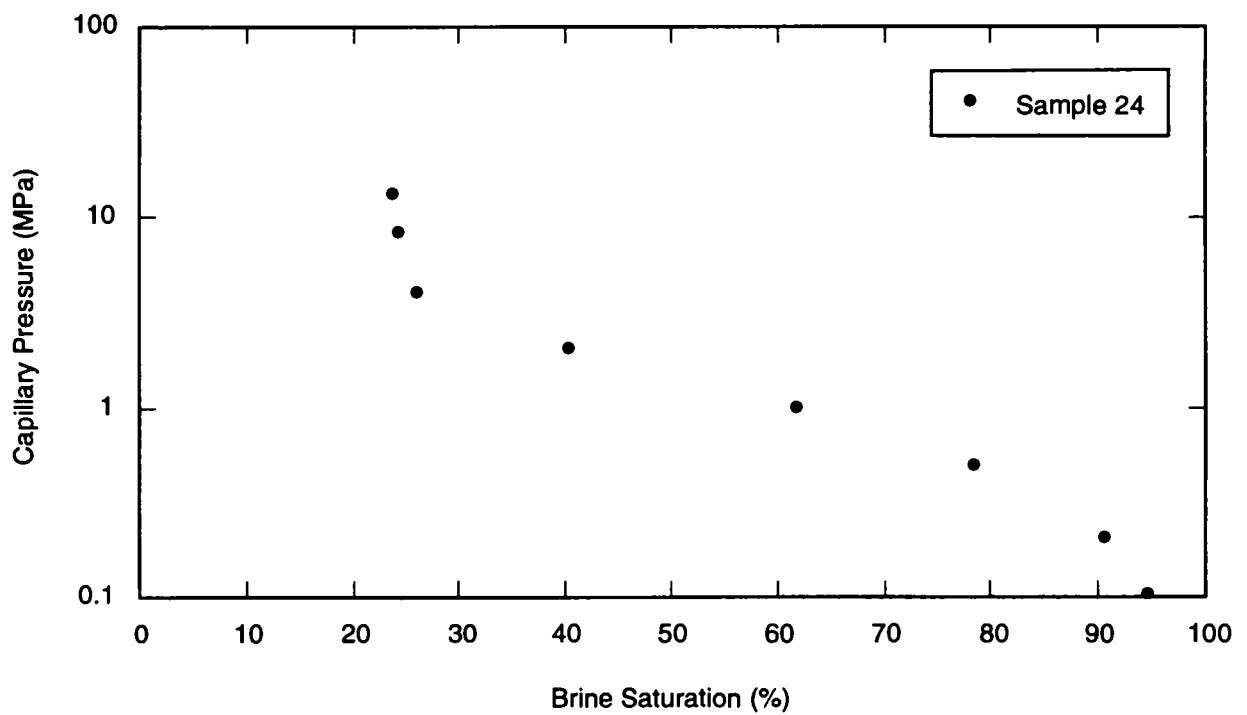
TRI-6115-201-0

Figure 28d. Centrifuge capillary pressure versus brine saturation: Sample 14.



TRI-6115-202-0

Figure 28e. Centrifuge capillary pressure versus brine saturation: Sample 22.



TRI-6115-203-0

Figure 28f. Centrifuge capillary pressure versus brine saturation: Sample 24.

Table 11a. Mercury Injection Capillary Pressure Data for Sample 5

Brine Saturation (%)	140° Contact Angle Capillary Pressure		180° Contact Angle Capillary Pressure		Brine Saturation (%)	140° Contact Angle Capillary Pressure		180° Contact Angle Capillary Pressure	
	(MPa)	(psi)	(MPa)	(psi)		(MPa)	(psi)	(MPa)	(psi)
100	0.002	0.3	0.002	0.23	40.1	3.3	484	2.6	371
100	0.004	0.58	0.003	0.44	36.1	4.7	676	3.6	518
100	0.008	1.2	0.006	0.89	36.1	5.7	825	4.4	632
100 *	0.012	1.7 *	0.009	1.3 *	32.1	6.7	968	5.1	742
96	0.016	2.3	0.012	1.8	28.1	9.3	1351	7.1	1035
96	0.024	3.5	0.019	2.7	28.1	13.3	1931	10.2	1479
92	0.033	4.8	0.026	3.7	24.1	16.7	2416	12.8	1850
92	0.047	6.8	0.036	5.2	16.1	20	2897	15.3	2219
88	0.06	8.7	0.046	6.7	12.1	26.6	3860	20.4	2957
88	0.076	11	0.057	8.2	12.1	33.3	4830	25.5	3700
88	0.097	14	0.076	11	12.1	40	5795	30.6	4440
88	0.131	19	0.1	15	8.1	46.7	6765	35.7	5182
84	0.017	24	0.12	18	8.1	53.3	7725	40.8	5917
84	0.21	31	0.17	24	8.1	60	8708	46	6671
84	0.24	35	0.19	27	8.1	66.5	9643	50.9	7387
84	0.27	39	0.21	30					
80	0.41	59	0.31	45					
80	0.53	77	0.41	59					
76	0.67	97	0.51	74					
68	1	145	0.77	111					
60	1.3	193	1	148					
56	1.7	243	1.3	186					
44.1	2.1	311	1.6	238					
40.1	2.7	387	2	296					

* Threshold entry pressures and residual brine saturations.

Table 11b. Mercury Injection Capillary Pressure Data for Sample 7

Brine Saturation (%)	140° Contact Angle Capillary Pressure		180° Contact Angle Capillary Pressure		Brine Saturation (%)	140° Contact Angle Capillary Pressure		180° Contact Angle Capillary Pressure	
	(MPa)	(psi)	(MPa)	(psi)		(MPa)	(psi)	(MPa)	(psi)
100	0.004	0.58	0.003	0.45	45.4	5.7	823	4.4	631
100	0.008	1.2	0.006	0.89	40.3	6.7	965	5.1	739
100 *	0.012	1.7 *	0.009	1.3 *	35.1	9.3	1354	7.2	1037
97.4	0.016	2.3	0.012	1.8	29.9	13.3	1933	10.2	1481
97.4	0.024	3.5	0.019	2.7	24.7	16.6	2411	12.7	1847
94.8	0.033	4.8	0.026	3.7	19.5	20	2894	15.3	2217
92.2	0.047	6.8	0.036	5.2	14.3	26.7	3864	20.4	2960
92.2	0.06	8.7	0.046	6.7	14.3	33.3	4825	25.5	3696
92.2	0.076	11	0.057	8.2	14.3	40	5790	30.6	4435
89.6	0.103	15	0.076	11	11.7	46.6	6758	35.7	5177
89.6	0.14	20	0.1	15	11.7	53.3	7723	40.8	5916
87	0.17	24	0.13	19	11.7	60	8705	46	6668
87	0.21	31	0.17	24	11.7	66.8	9683	51.2	7417
87	0.24	35	0.19	27					
87	0.27	39	0.21	30					
84.4	0.4	58	0.31	45					
81.8	0.54	78	0.41	60					
79.2	0.67	97	0.51	74					
76.6	1	146	0.77	112					
74	1.3	195	1	149					
71.4	1.7	241	1.3	185					
66.2	2.1	310	1.6	237					
61	2.7	386	2	296					
55.8	3.3	483	2.6	370					

* Threshold entry pressures and residual brine saturations.

Table 11c. Mercury Injection Capillary Pressure Data for Sample 11

Brine Saturation (%)	140° Contact Angle Capillary Pressure		180° Contact Angle Capillary Pressure		Brine Saturation (%)	140° Contact Angle Capillary Pressure		180° Contact Angle Capillary Pressure	
	(MPa)	(psi)	(MPa)	(psi)		(MPa)	(psi)	(MPa)	(psi)
100	0.004	0.58	0.003	0.44	37.9	5.7	824	4.4	632
100	0.008	1.2	0.006	0.89	36.3	6.7	968	5.1	742
100	0.012	1.7	0.009	1.3	33.1	9.3	1351	7.1	1035
100 *	0.016	2.3 *	0.012	1.8 *	29.9	13.3	1931	10.2	1479
98.4	0.024	3.5	0.019	2.7	28.3	16.7	2415	12.8	1850
98.4	0.033	4.8	0.026	3.7	28.3	20.0	2897	15.3	2219
96.8	0.047	6.8	0.036	5.2	26.7	26.6	3860	20.4	2957
96.8	0.060	8.7	0.046	6.7	25.1	33.3	4830	25.5	3700
96.8	0.076	11	0.057	8.2	23.5	40.0	5795	30.6	4439
96.8	0.10	15	0.08	11	23.5	46.7	6765	35.7	5182
96.8	0.13	19	0.10	15	23.5	53.3	7725	40.8	5917
96.8	0.17	24	0.12	18	23.5	60.1	8708	46.0	6671
95.2	0.21	31	0.17	24	23.5	66.5	9643	50.9	7387
93.6	0.24	35	0.19	27					
92.1	0.27	39	0.21	30					
85.7	0.41	59	0.31	45					
80.9	0.53	77	0.41	59					
79.3	0.67	97	0.51	74					
72.9	1.0	145	0.8	111					
66.5	1.3	193	1.0	148					
61.8	1.7	242	1.3	186					
57	2.1	311	1.6	238					
50.6	2.7	387	2.0	296					
41	3.3	484	2.6	371					

* Threshold entry pressures and residual brine saturations.

Table 11d. Mercury Injection Capillary Pressure Data for Sample 13

Brine Saturation (%)	140° Contact Angle Capillary Pressure		180° Contact Angle Capillary Pressure		Brine Saturation (%)	140° Contact Angle Capillary Pressure		180° Contact Angle Capillary Pressure	
	(MPa)	(psi)	(MPa)	(psi)		(MPa)	(psi)	(MPa)	(psi)
100 *	0.004	0.58*	0.003	0.45 *	40	4.7	677	3.6	519
98.2	0.008	1.2	0.006	0.89	40	5.7	823	4.4	631
96.4	0.012	1.7	0.009	1.3	36.4	6.7	967	5.1	741
96.4	0.016	2.3	0.012	1.8	32.8	9.3	1351	7.1	1035
96.4	0.024	3.5	0.019	2.7	29.2	13.3	1932	10.2	1480
92.7	0.033	4.8	0.026	3.7	25.5	16.7	2418	12.8	1852
92.7	0.047	6.8	0.036	5.2	20.1	20.0	2896	15.3	2218
92.7	0.060	8.7	0.046	6.7	20.1	26.6	3863	20.4	2959
90.9	0.08	11	0.057	8.2	16.4	33.3	4826	25.5	3697
90.9	0.10	15	0.08	11	16.4	40.0	5794	30.6	4439
90.9	0.13	19	0.10	15	16.4	46.6	6750	35.7	5171
90.9	0.17	24	0.13	19	14.6	53.2	7718	40.8	5912
87.3	0.21	31	0.17	24	14.6	60.0	8705	46.0	6669
85.5	0.24	35	0.19	27	14.6	66.5	9649	51.0	7392
85.5	0.27	39	0.21	30					
78.2	0.40	58	0.30	44					
76.4	0.53	77	0.41	59					
74.6	0.66	96	0.51	74					
70.9	1.0	145	0.8	111					
65.5	1.3	193	1.0	148					
61.8	1.7	241	1.3	185					
58.2	2.1	309	1.6	236					
49.1	2.7	386	2.0	296					

* Threshold entry pressures and residual brine saturations.

Table 11e. Mercury Injection Capillary Pressure Data for Sample 21

Brine Saturation (%)	140° Contact Angle Capillary Pressure		180° Contact Angle Capillary Pressure		Brine Saturation (%)	140° Contact Angle Capillary Pressure		180° Contact Angle Capillary Pressure	
	(MPa)	(psi)	(MPa)	(psi)		(MPa)	(psi)	(MPa)	(psi)
100	0.004	0.58	0.003	0.45	28.7	4.7	677	3.6	519
100 *	0.008	1.2 *	0.006	0.89 *	26.2	5.7	823	4.4	631
97.4	0.012	1.7	0.009	1.3	26.2	6.7	967	5.1	741
97.4	0.016	2.3	0.012	1.8	21.1	9.3	1351	7.1	1035
94.9	0.024	3.5	0.019	2.7	18.5	13.3	1932	10.2	1480
94.9	0.033	4.8	0.026	3.7	16	16.7	2418	12.8	1852
94.9	0.046	6.7	0.036	5.2	13.4	20.0	2896	15.3	2218
94.9	0.060	8.7	0.046	6.7	10.9	26.6	3863	20.4	2959
94.9	0.076	11	0.057	8.2	10.9	33.3	4827	25.5	3698
94.9	0.10	15	0.08	11	10.9	40.0	5794	30.6	4439
92.3	0.13	19	0.10	15	8.3	46.6	6750	35.7	5171
92.3	0.17	24	0.13	19	8.3	53.2	7718	40.8	5912
92.3	0.21	31	0.17	24	8.3	60.0	8705	46.0	6669
92.3	0.24	35	0.19	27	8.3	66.5	9649	51.0	7392
92.3	0.27	39	0.21	30					
87.3	0.40	58	0.30	44					
82.2	0.54	78	0.41	59					
77.1	0.66	96	0.51	74					
64.3	1.0	145	0.8	111					
56.7	1.3	193	1.0	148					
51.6	1.7	241	1.3	185					
44	2.1	309	1.6	236					
33.8	2.7	386	2.0	296					

* Threshold entry pressures and residual brine saturations.

Table 11f. Mercury Injection Capillary Pressure Data for Sample 23

Brine Saturation (%)	140° Contact Angle Capillary Pressure		180° Contact Angle Capillary Pressure		Brine Saturation (%)	140° Contact Angle Capillary Pressure		180° Contact Angle Capillary Pressure	
	(MPa)	(psi)	(MPa)	(psi)		(MPa)	(psi)	(MPa)	(psi)
100	0.004	0.58	0.003	0.45	19.4	3.3	483	2.6	370
100 *	0.008	1.2 *	0.006	0.89 *	13.2	4.7	677	3.6	518
97.5	0.012	1.7	0.009	1.3	11.9	5.7	823	4.3	630
97.5	0.016	2.3	0.012	1.8	10.7	6.6	964	5.1	739
97.5	0.024	3.5	0.019	2.7	10.7	9.3	1353	7.2	1037
96.3	0.033	4.8	0.026	3.7	10.7	13.3	1933	10.2	1481
93.8	0.047	6.8	0.036	5.2	9.4	16.6	2411	12.7	1847
93.8	0.060	8.7	0.046	6.7	9.4	20.0	2894	15.3	2217
93.8	0.08	11	0.057	8.2	9.4	26.6	3864	20.4	2960
93.8	0.10	15	0.08	11	8.2	33.3	4825	25.5	3696
92.5	0.14	20	0.10	15	8.2	39.9	5789	30.6	4435
92.5	0.17	24	0.12	18	8.2	46.6	6758	35.7	5177
91.3	0.21	31	0.17	24	8.2	53.3	7723	40.8	5916
91.3	0.24	35	0.19	27	8.2	60.0	8704	46.0	6668
90.1	0.27	39	0.21	30	8.2	66.8	9682	51.2	7417
87.6	0.40	58	0.31	45					
80.1	0.54	78	0.41	60					
73.9	0.67	97	0.51	74					
61.5	1.0	146	0.8	112					
51.6	1.3	195	1.0	149					
44.2	1.7	241	1.3	185					
34.2	2.1	309	1.6	237					

* Threshold entry pressures and residual brine saturations.

6.2.3 Comparison of Results from Centrifuge and Mercury Injection Tests

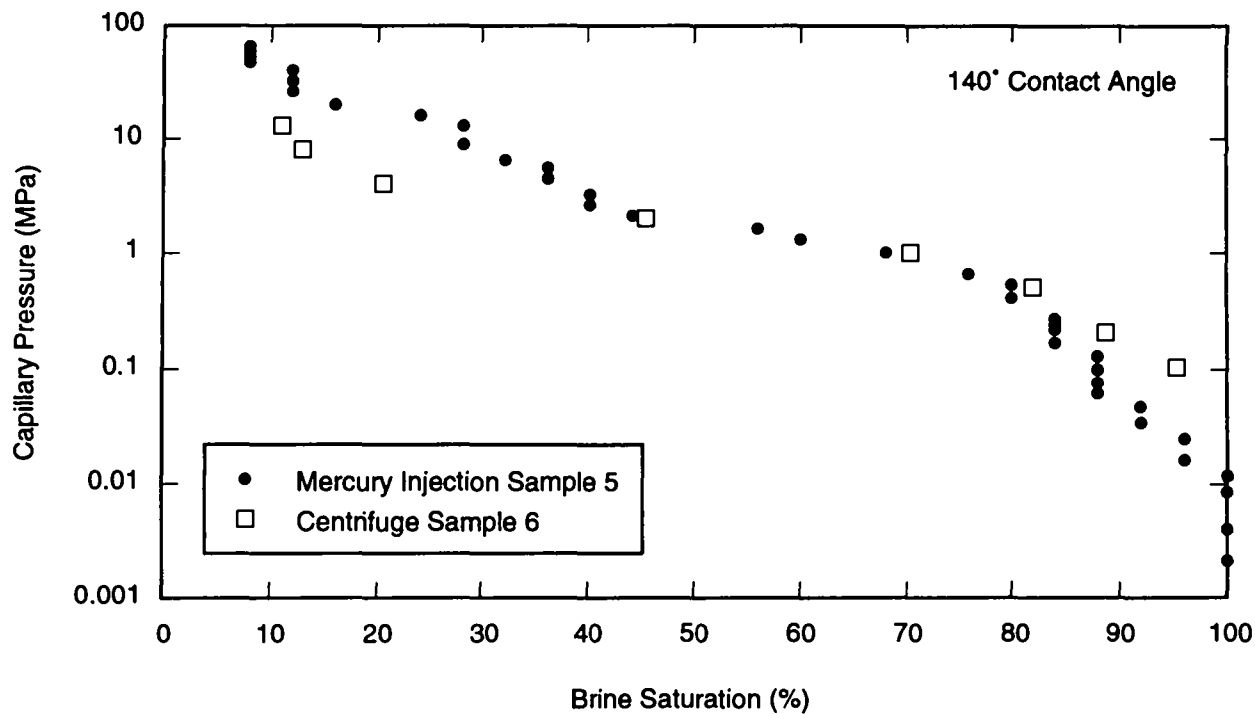
Figures 29 through 34 show the comparisons of capillary pressure results for the six pairs of core samples. The top graphs (a) of Figures 29 through 34 show the air-brine (converted) centrifuge data plotted with the 140° contact angle air-brine (converted) mercury injection data. The bottom graphs (b) show the same air-brine (converted) centrifuge data plotted with the 180° contact angle air-brine (converted) mercury injection data. The difference in the capillary pressure results, when converted to an air-brine system using 140° or 180° for the contact angle, is not significant.

Figure 35 is a plot of all the air-brine (converted) centrifuge capillary pressure data, and Figure 36 is a plot of all the air-brine (converted) mercury injection capillary pressure data using a contact angle of 140°. Figure 37 is a Cartesian plot of all the capillary pressure data from Figures 35 and 36, and Figure 38 is a log-linear plot of the same data.

The mercury injection method has the advantage of producing capillary pressure data over the full saturation range, but it is a slow method and tests cannot be performed under confining stress conditions. In addition, the mercury injection method is destructive and no further tests can be performed on the cores. The faster centrifuge method was unable to capture the high brine saturation data because of equipment hardware constraints that precluded the use of very low spin rates. Although these centrifuge capillary pressure tests were performed using an apparatus that could not impose confining stress on samples, newer generation centrifuges are now available that can test cores under prespecified stress conditions. Both the mercury injection and centrifuge test apparatus have sample size limitations, which currently allow only small specimens to be tested.

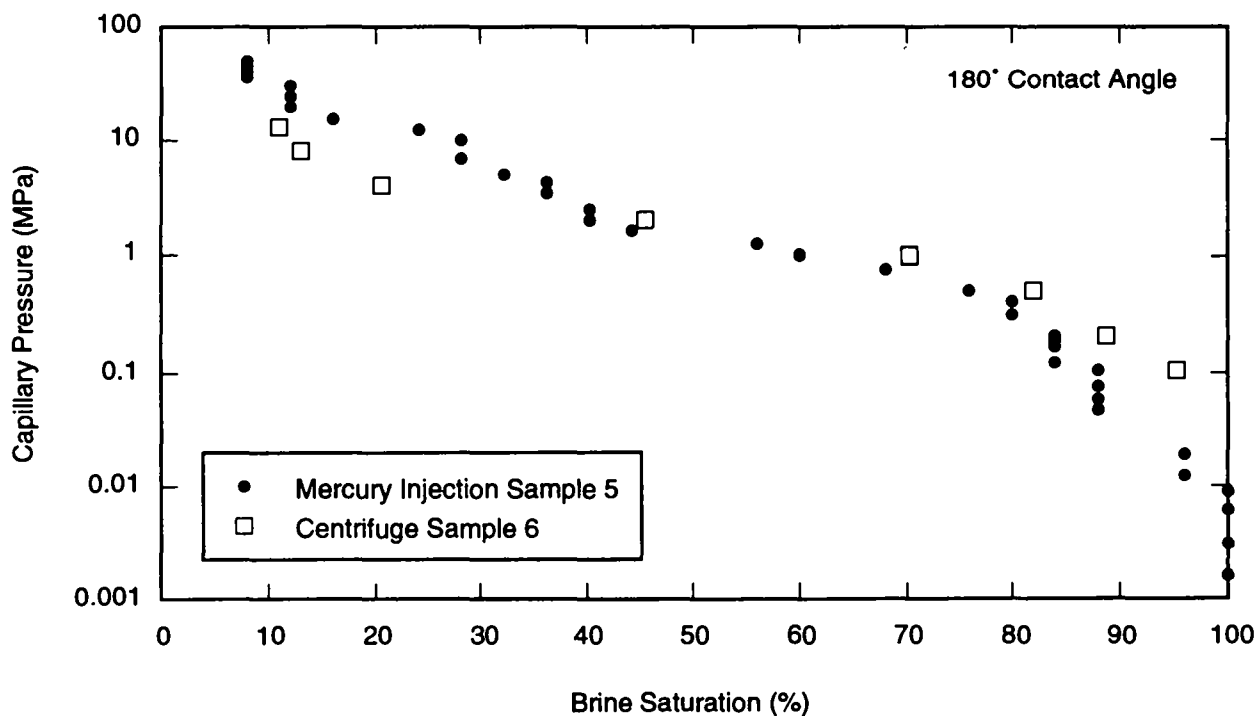
6.3 Determination of Threshold Pressure

As described by Davies (1991), some investigators define threshold pressure as the capillary pressure associated with first penetration of a nonwetting phase into the largest pores near the surface of the medium. Others define threshold pressure as the capillary pressure associated with the incipient development of a continuum of the nonwetting phase through a pore network, providing gas pathways not only through relatively large pores, but also through necks between pores. Defining threshold pressure as corresponding to first penetration of a nonwetting phase into the largest pores near the surface of the medium means that threshold pressure is equal to the capillary pressure at a brine saturation of 1.0.



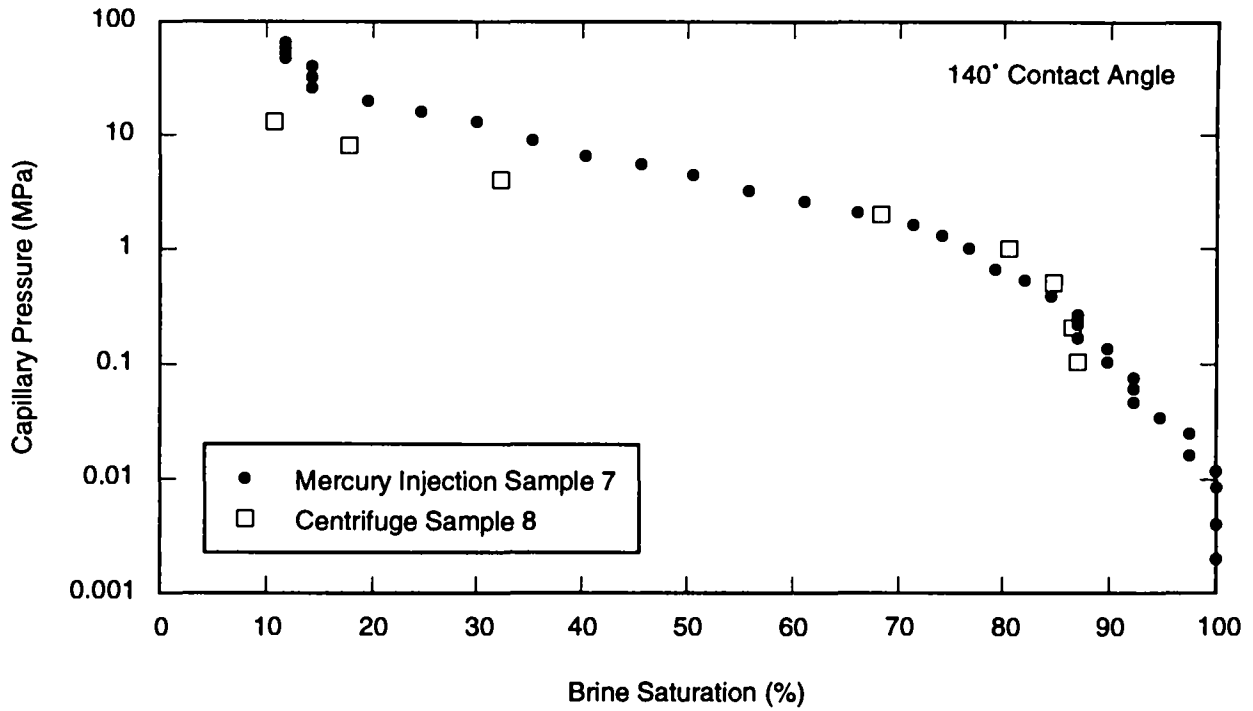
TRI-8115-224-0

Figure 29a. Comparison of centrifuge and mercury injection capillary pressure: Samples 5 and 6, 140° contact angle.



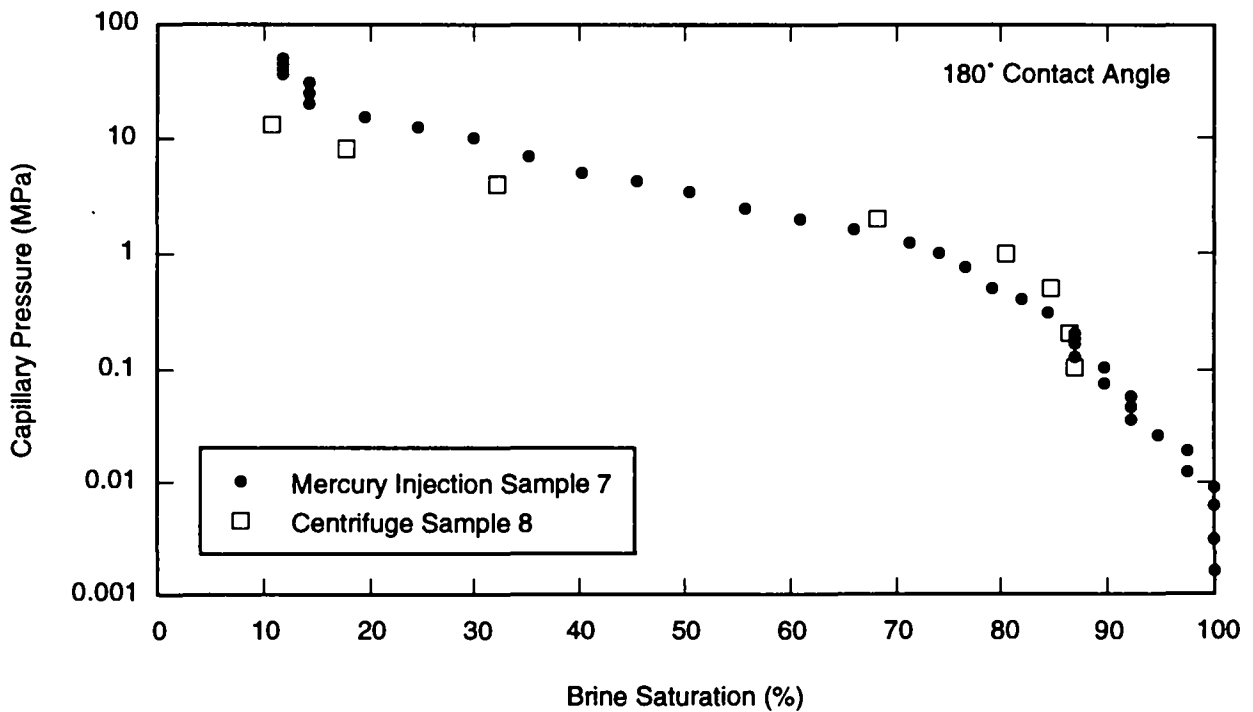
TRI-8115-225-0

Figure 29b. Comparison of centrifuge and mercury injection capillary pressure: Samples 5 and 6, 180° contact angle.



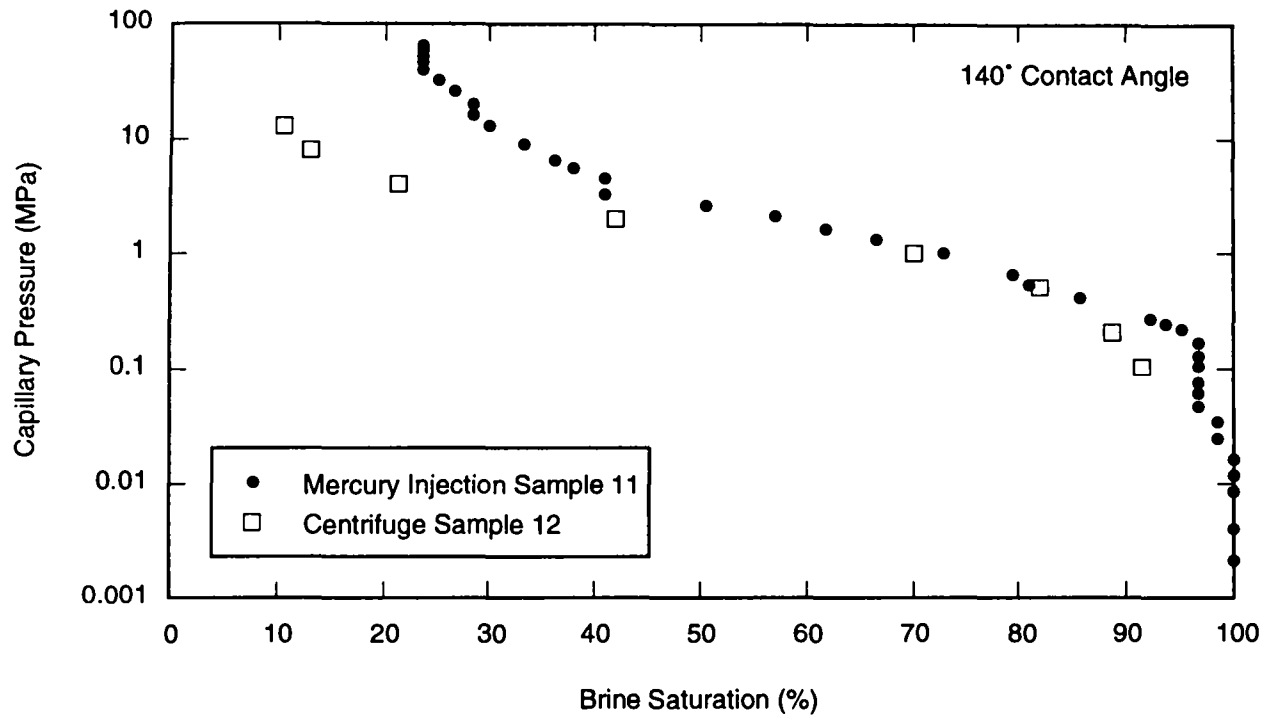
TRI-6115-226-0

Figure 30a. Comparison of centrifuge and mercury injection capillary pressure: Samples 7 and 8, 140° contact angle.



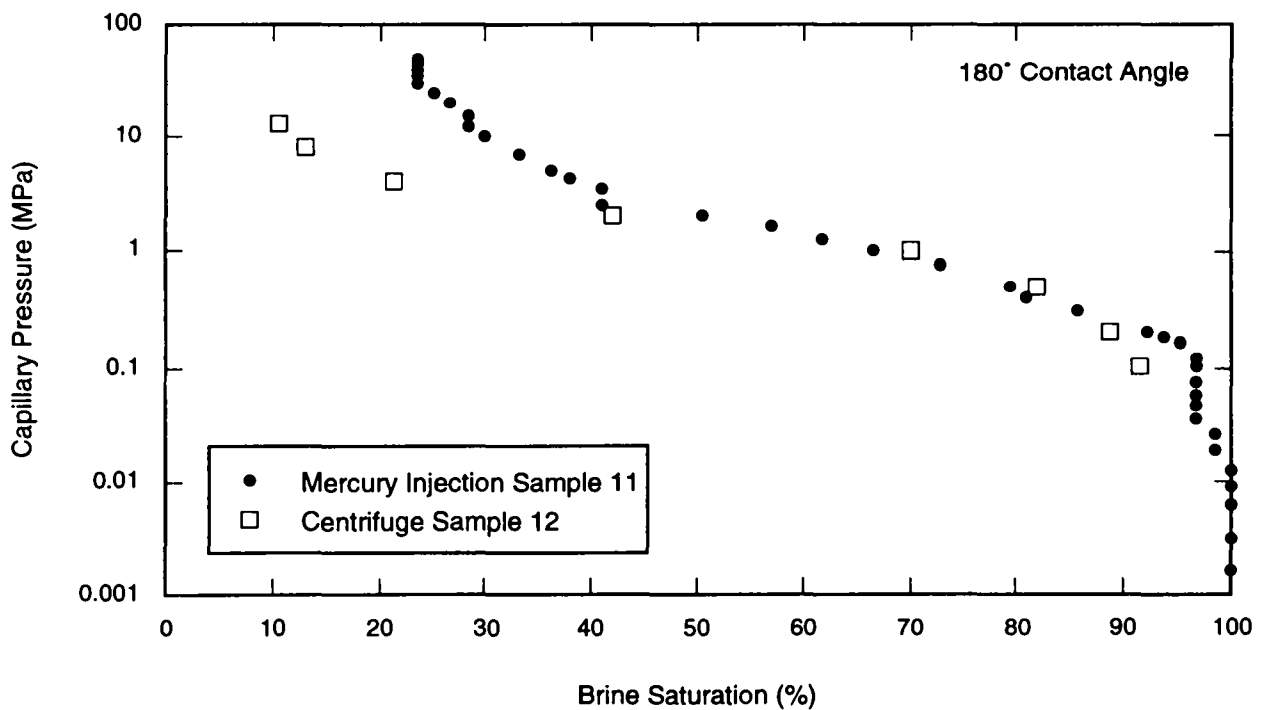
TRI-6115-227-0

Figure 30b. Comparison of centrifuge and mercury injection capillary pressure: Samples 7 and 8, 180° contact angle.



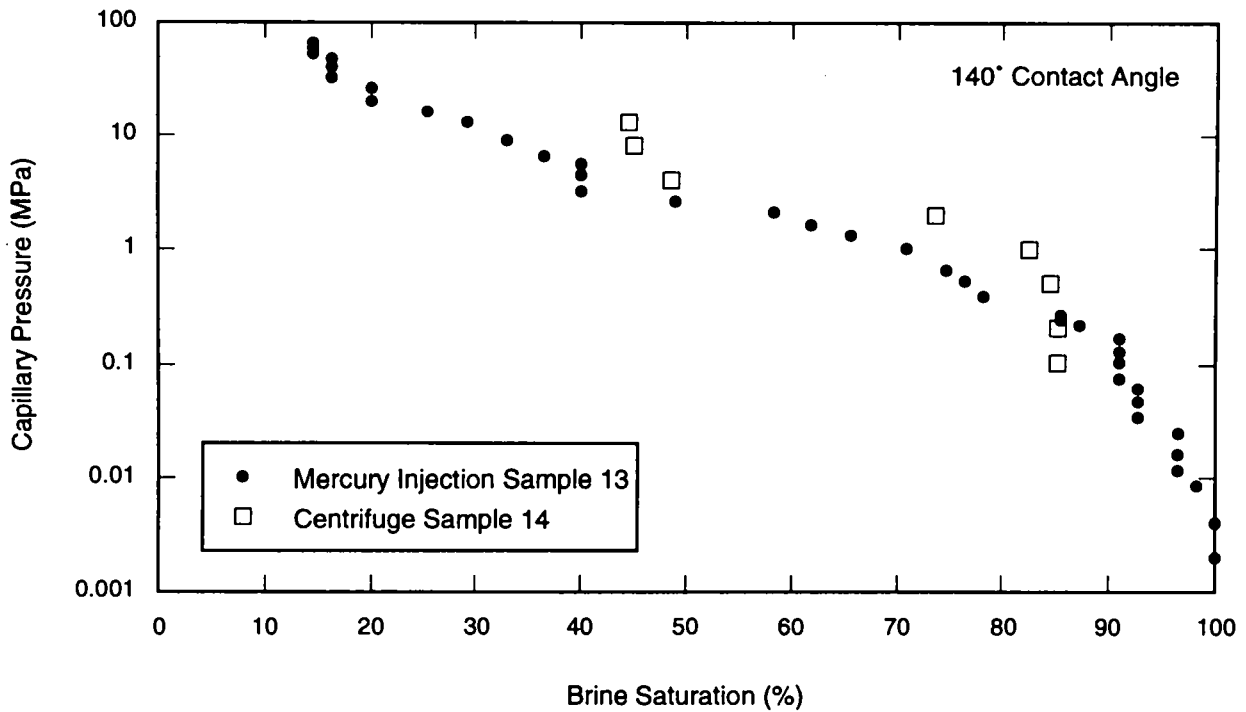
TRI-6115-228-0

Figure 31a. Comparison of centrifuge and mercury injection capillary pressure: Samples 11 and 12, 140° contact angle.



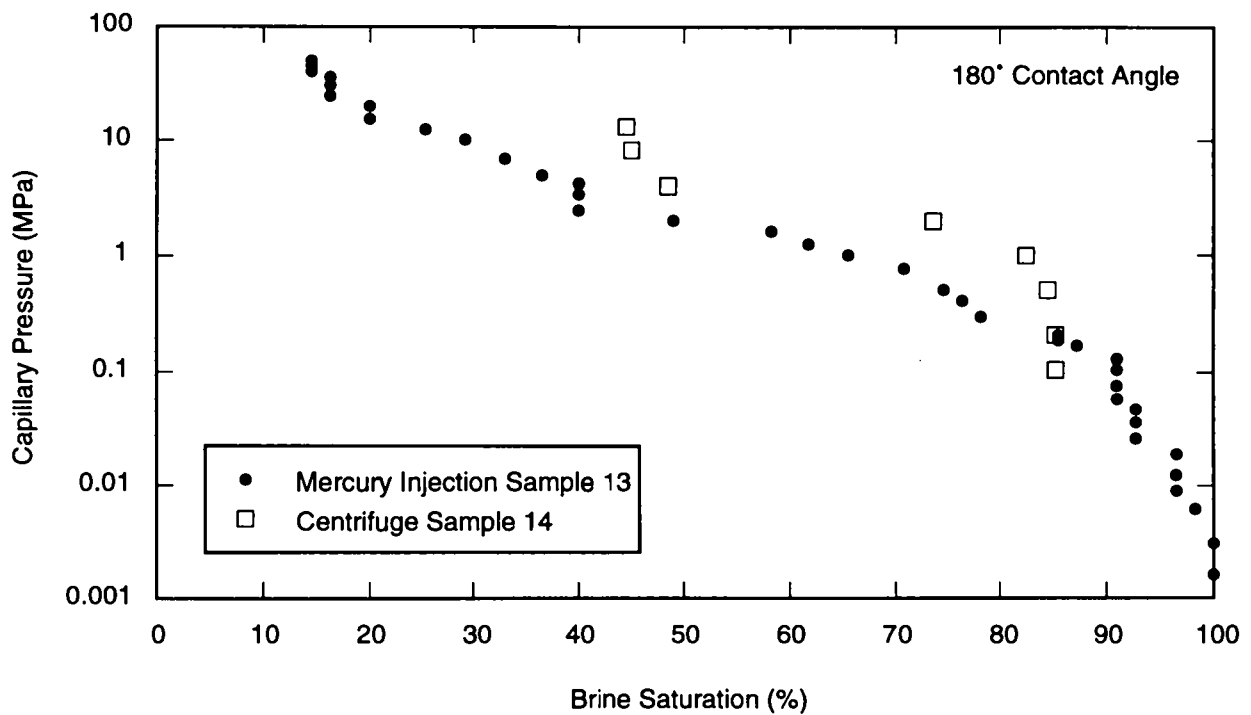
TRI-6115-229-0

Figure 31b. Comparison of centrifuge and mercury injection capillary pressure: Samples 11 and 12, 180° contact angle.



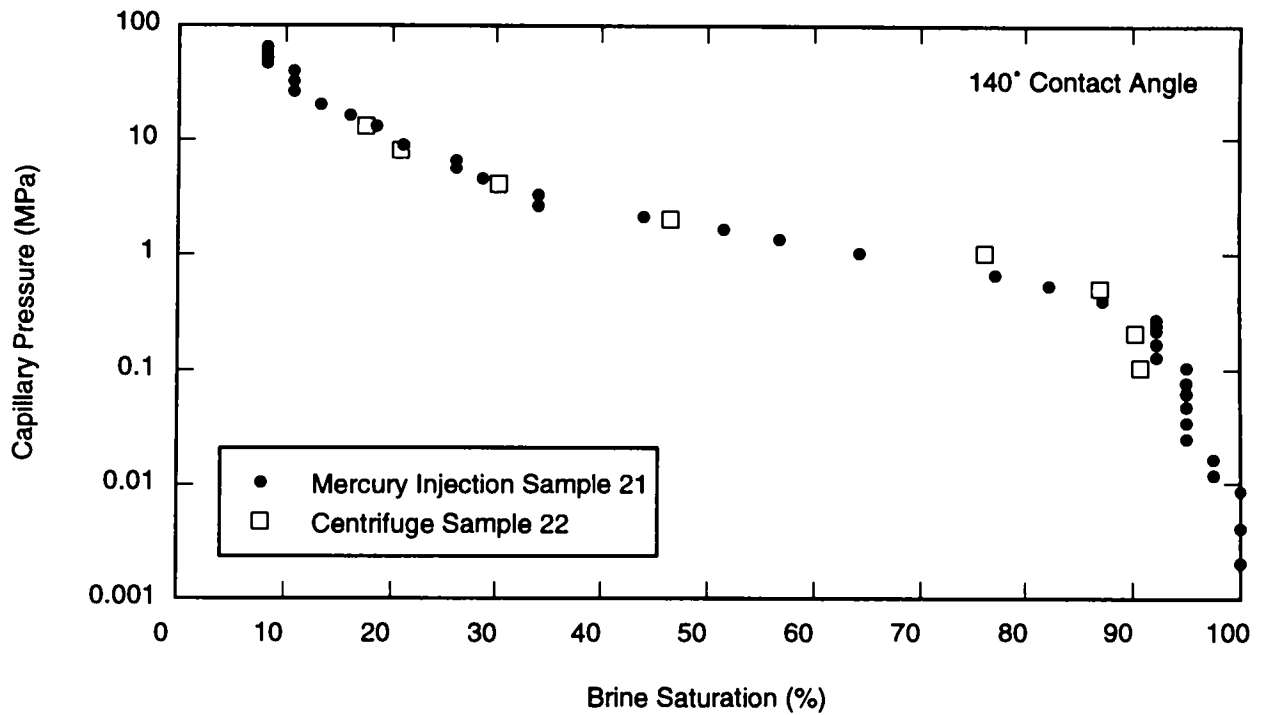
TRI-6115-230-0

Figure 32a. Comparison of centrifuge and mercury injection capillary pressure: Samples 13 and 14, 140° contact angle.



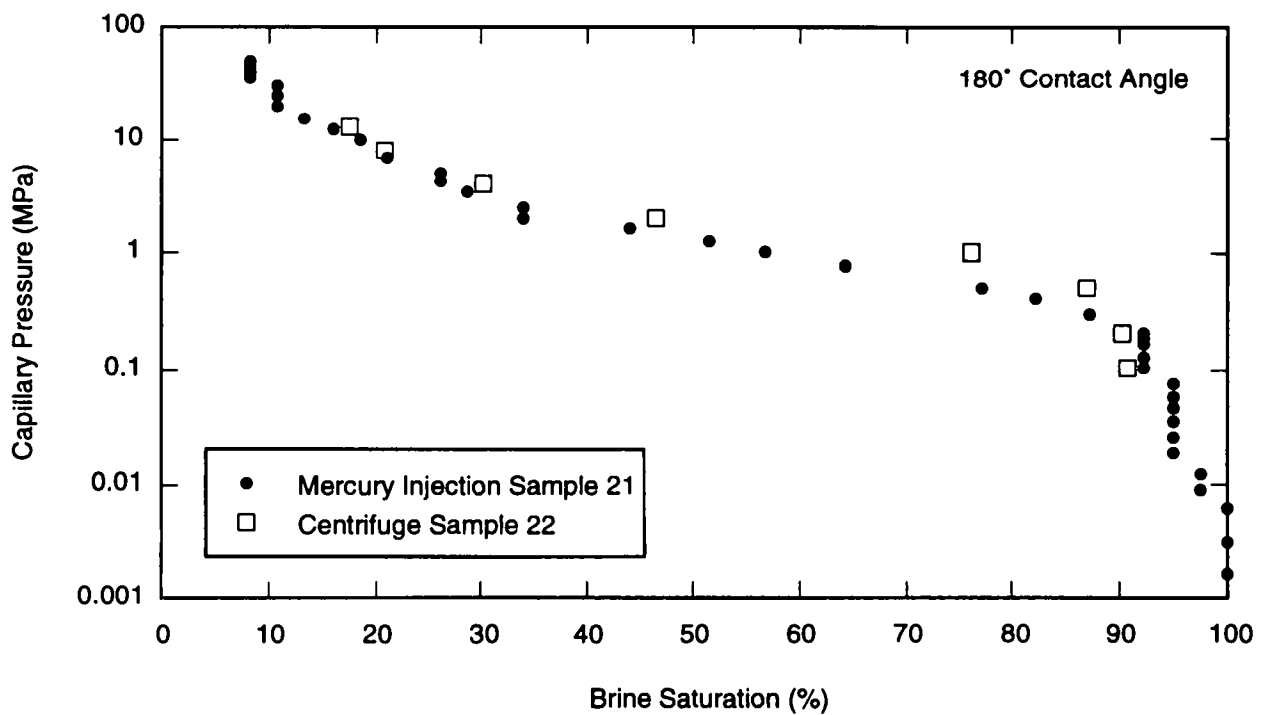
TRI-6115-231-0

Figure 32b. Comparison of centrifuge and mercury injection capillary pressure: Samples 13 and 14, 180° contact angle.



TRI-6115-232-0

Figure 33a. Comparison of centrifuge and mercury injection capillary pressure: Samples 21 and 22, 140° contact angle.



TRI-6115-233-0

Figure 33b. Comparison of centrifuge and mercury injection capillary pressure: Samples 21 and 22, 180° contact angle.

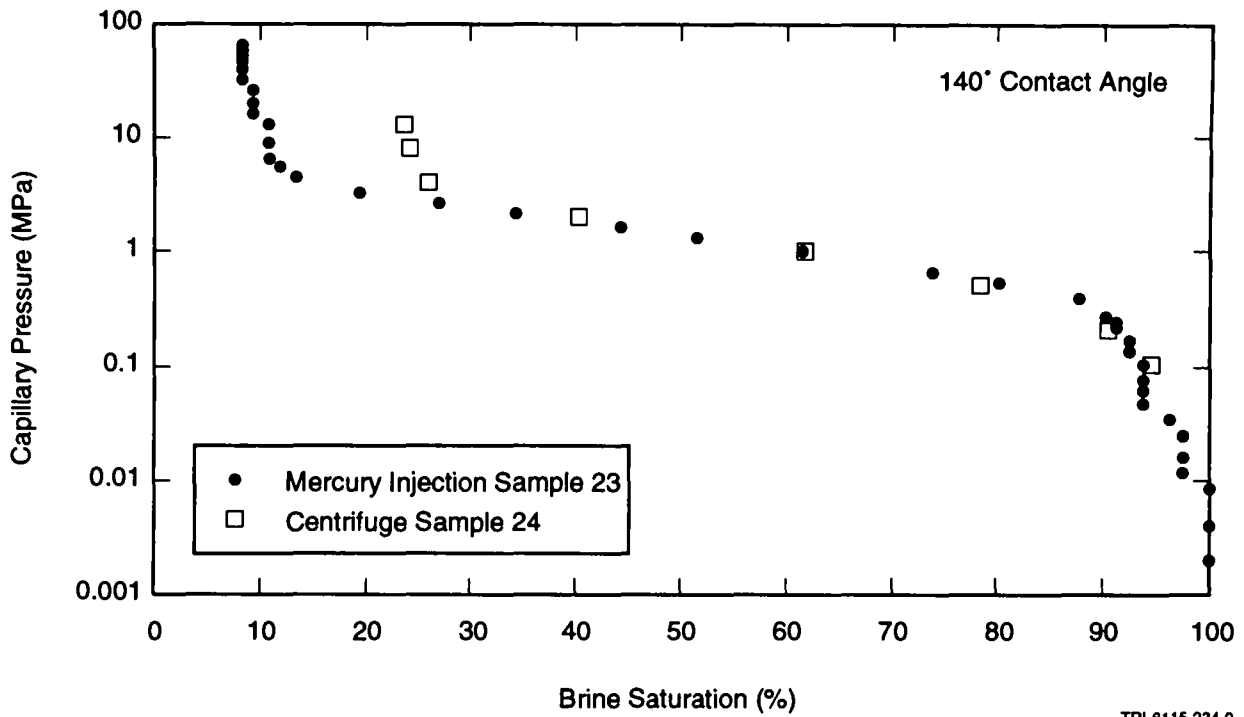


Figure 34a. Comparison of centrifuge and mercury injection capillary pressure: Samples 23 and 24, 140° contact angle.

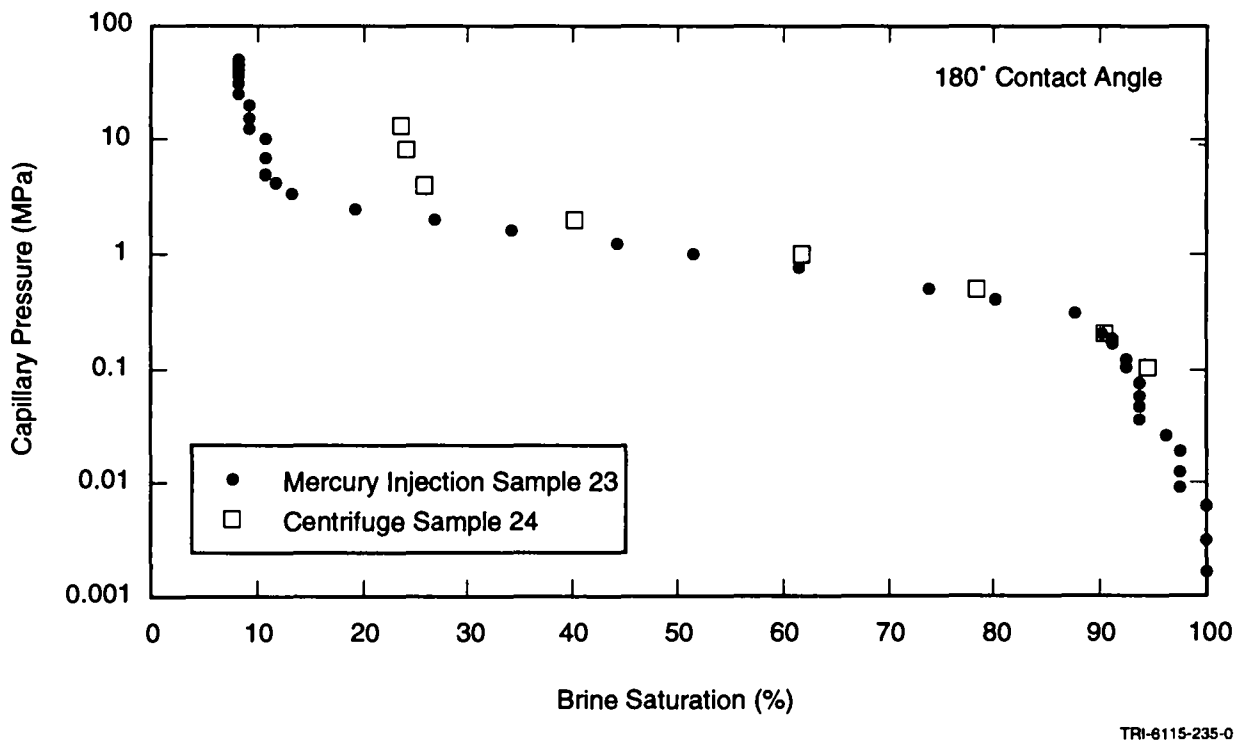
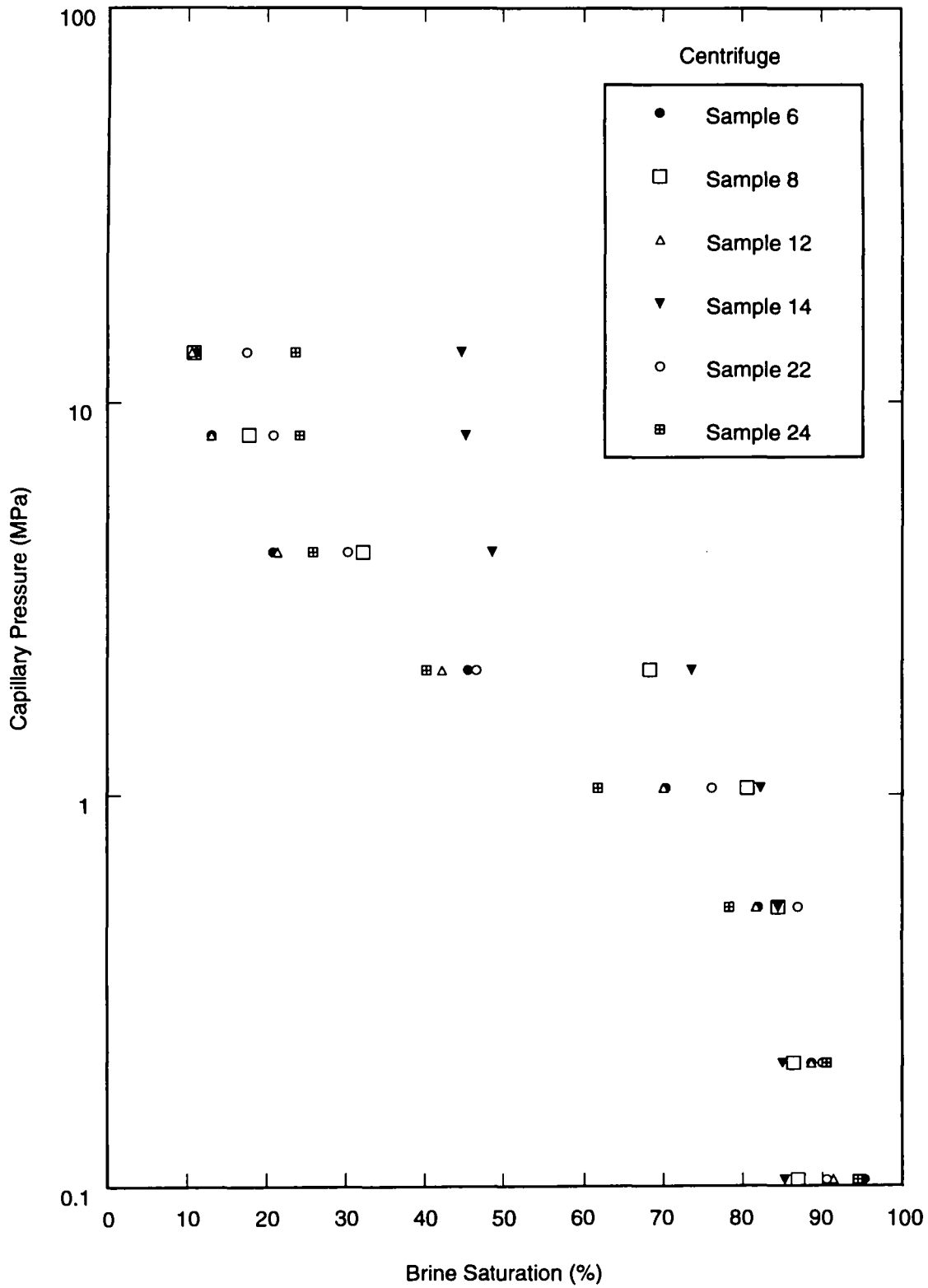


Figure 34b. Comparison of centrifuge and mercury injection capillary pressure: Samples 23 and 24, 180° contact angle.



TRI-6115-236-0

Figure 35. Centrifuge capillary pressure data versus brine saturation: all samples (log-linear).

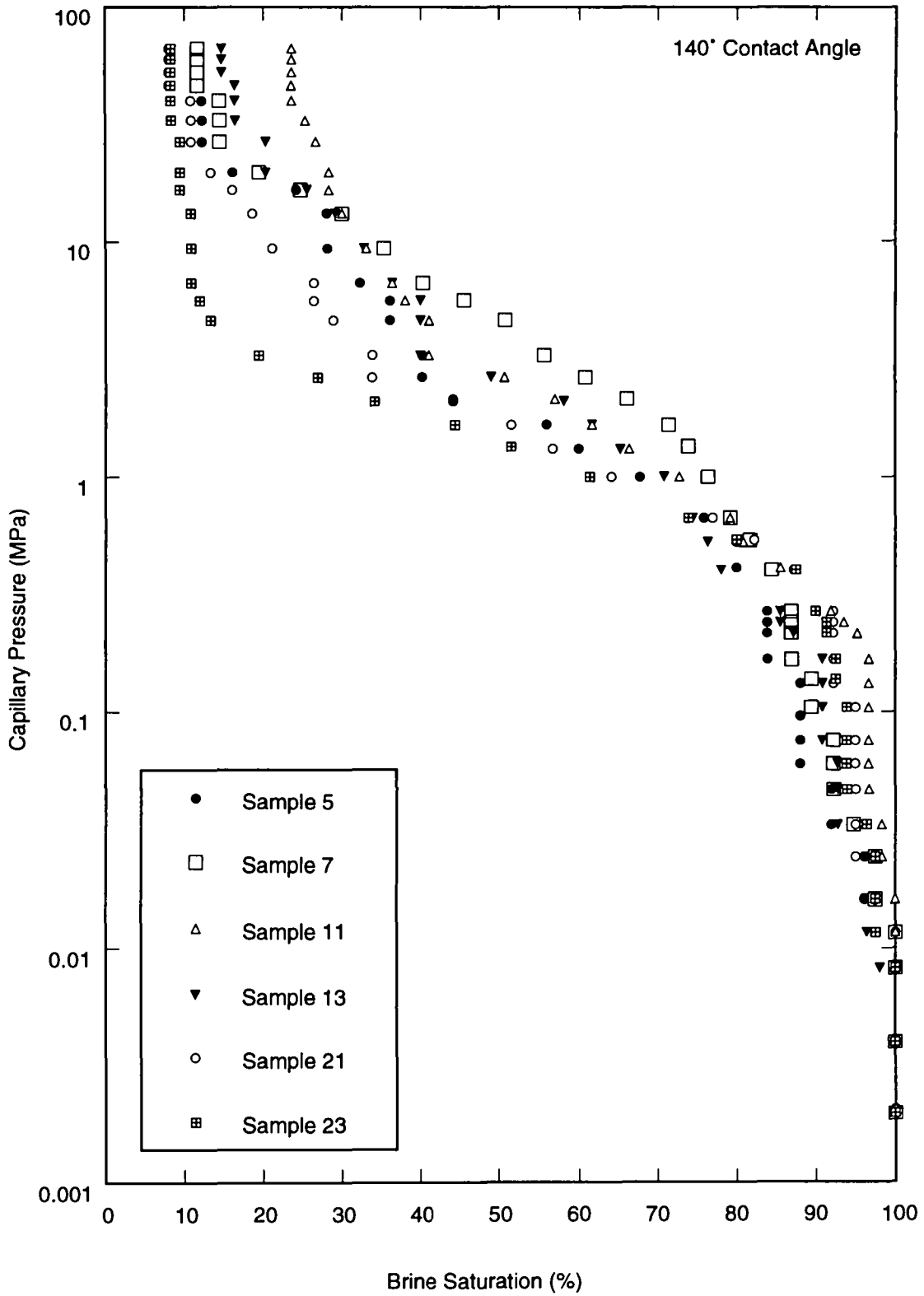
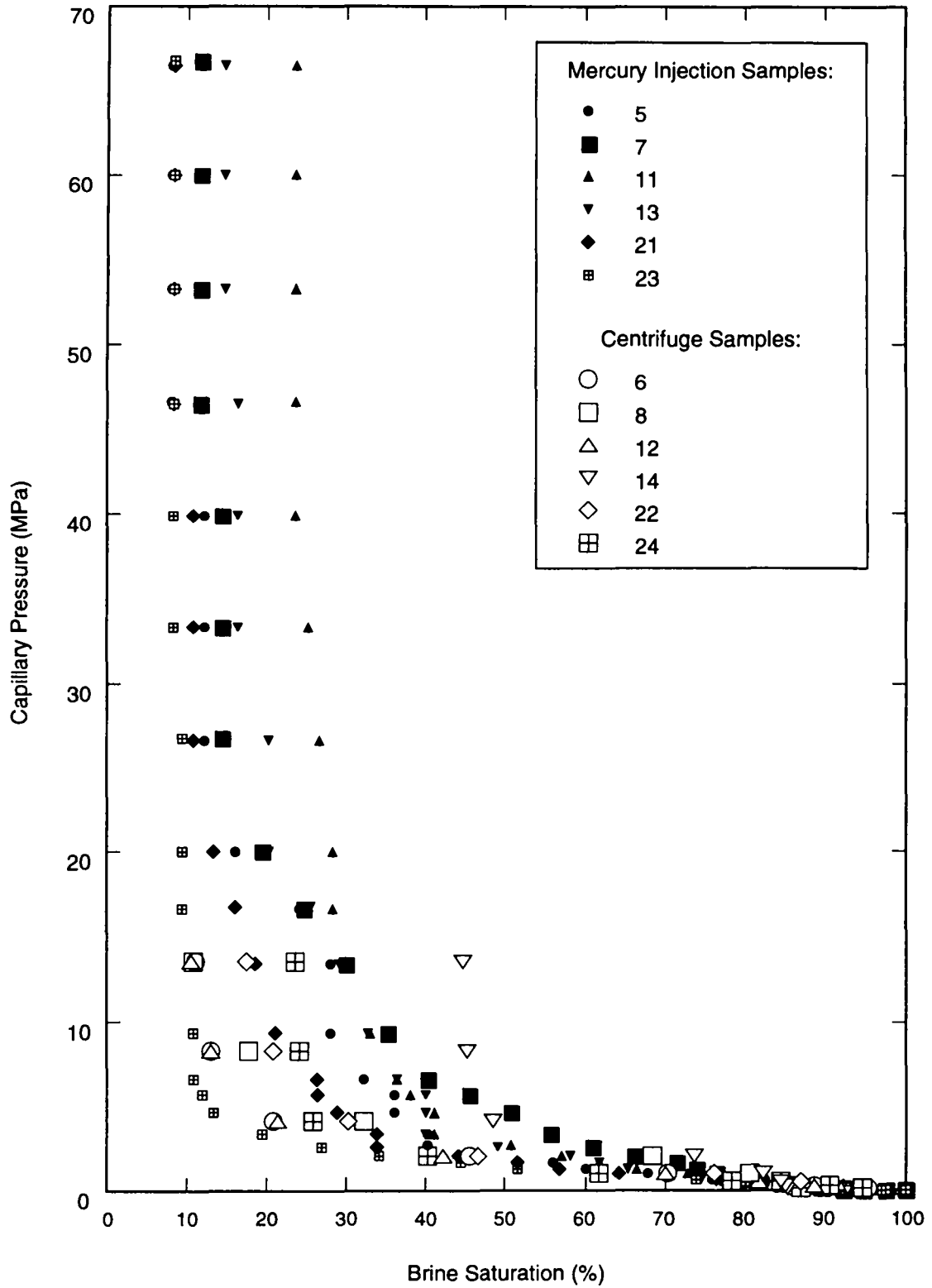
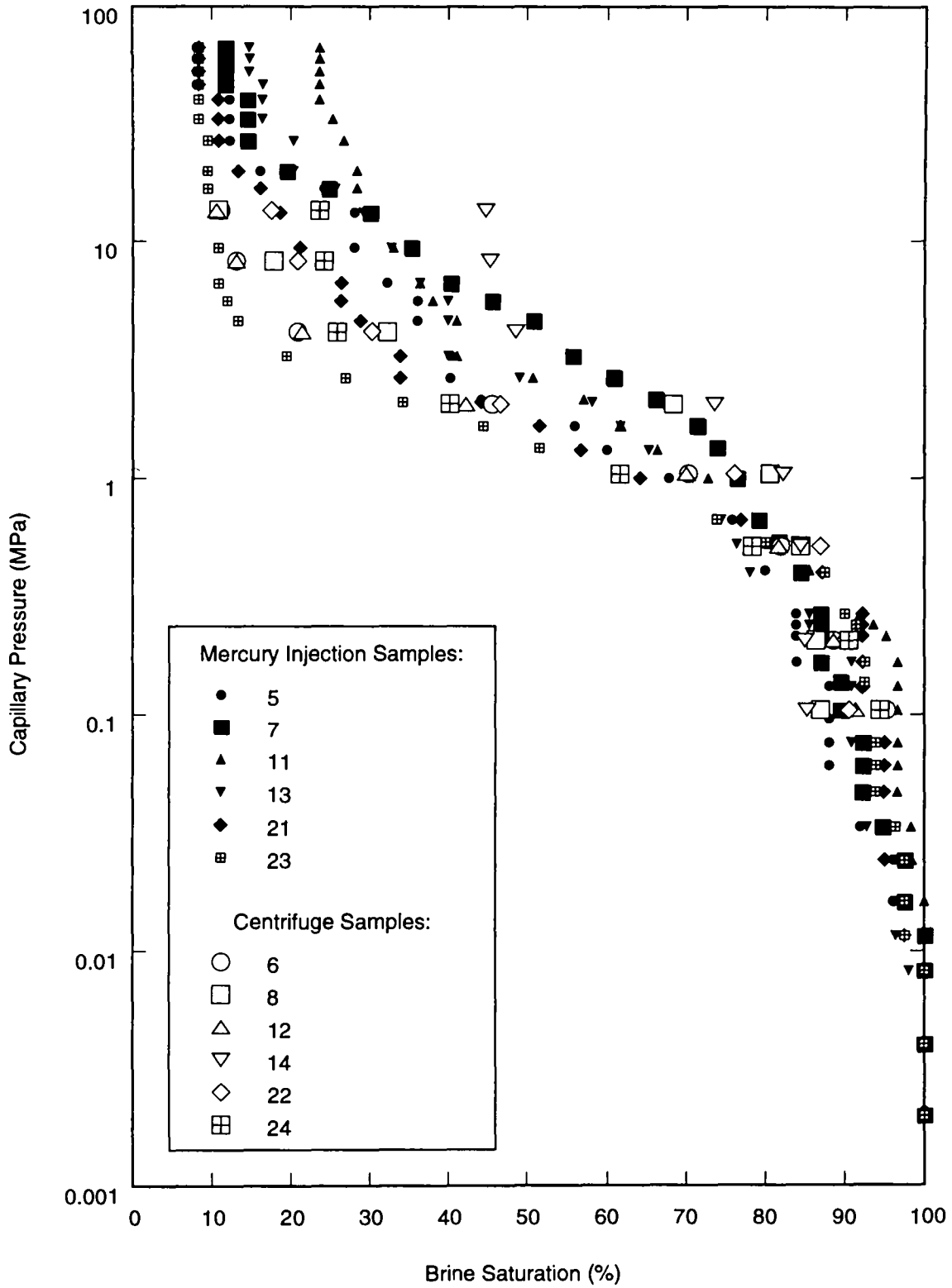


Figure 36. Mercury injection capillary pressure data versus brine saturation: all samples (log-linear).



TRI-6115-238-0

Figure 37. Capillary pressure data: all samples (Cartesian).



TRI-6115-239-0

Figure 38. Capillary pressure data: all samples (log-linear).

Defining threshold pressure as corresponding to the incipient formation of a continuum of the nonwetting phase through the pore network means that threshold pressure is equal to the capillary pressure at a saturation equal to the critical gas saturation. In other words, threshold pressure is equal to the capillary pressure at which the relative permeability to the gas phase begins to rise from its zero value, corresponding to the incipient development of interconnected gas flow paths through the pore network.

The present study is concerned with quantifying the potential for flow of waste-generated gas outward from the WIPP repository. This process will likely require that outward flowing gas penetrate and establish a gas-filled network of flow paths in the surrounding formation. Therefore the term gas threshold displacement pressure, shortened here to *threshold pressure*, will be defined as the pressure associated with the incipient formation of a continuous network of gas flow paths. The pressure corresponding to the initial penetration of the nonwetting phase (gas) into the largest pores near the surface of the medium will be termed the *gas entry pressure* in this report.

Table 12 contains a summary of the two-phase flow data for the mercury injection cores, including sample number, effective permeability, gas entry pressure, threshold pressure residual fluid saturations, and the Brooks and Corey Lambda parameter. The gas entry pressures reported in Table 12 are taken from the 140° contact angle corrected data reported in Tables 11a through 11f as the capillary pressure at the last 100% wetting-phase saturation. Likewise the residual brine saturations reported in Table 12 are also taken from the data reported in Tables 11a through 11f as the brine saturation value.

Table 12. Summary of Two-Phase Flow Data Results for Mercury Injection Cores

Sample Number	Permeability (m ²) 3.4 MPa Net Effective Stress	Gas Entry Pressure (psi/MPa) 140° Contact Angle	Gas Entry Pressure (psi/MPa) 180° Contact Angle	Residual Brine Saturation (%)	Threshold Pressure (psi/MPa) 140° Contact Angle	Residual Liquid Saturation (%)	Residual Gas Saturation (%)	Lambda
5	5.1 × 10 ⁻¹⁹	1.7/0.012	1.3/0.009	8.1	78/0.54	7.3	11.6	0.655
7	9.5 × 10 ⁻¹⁹	1.7/0.012	1.3/0.009	11.7	113/0.78	7.0	7.8	0.664
11	1.8 × 10 ⁻¹⁸	2.3/0.016	1.8/0.012	23.5	65/0.45	17.4	1.4	0.558
13	1.6 × 10 ⁻¹⁸	0.6/0.004	0.5/0.003	14.6	109/0.75	10.9	19.7	0.652
21	7.7 × 10 ⁻¹⁹	1.2/0.008	0.9/0.006	8.3	48/0.33	0.8	2.5	0.491
23	1.3 × 10 ⁻¹⁸	1.2/0.008	0.9/0.006	8.2	58/0.40	6.8	3.2	0.842

The values for threshold pressure, residual liquid saturation, residual gas saturation, and lambda reported in Table 12 were derived using an iterative trial-and-error solution technique documented in Appendix E. These values are consistent with the Brooks and Corey and the van Genuchten-Parker definitions.

6.4 Comparison of MB139 Mercury Injection Capillary Pressure Data to Brooks-Corey and van Genuchten Correlations

Figure 39 presents a plot of the six mercury injection capillary pressure curves (corrected using a 140° contact angle) shown in Figure 36 with the Mixed Brooks and Corey (see Appendix F) and van Genuchten correlations used in WIPP Performance Assessment (PA) calculations of 1992. The values for input parameters for these correlations are the median values for anhydrite used in the 1992 WIPP PA (Sandia WIPP Project, 1992) and are shown on Figure 32. The van Genuchten correlation shows a better fit to general shape of the capillary pressure curves, especially in the high brine-saturation region of the graph, than does the Mixed Brooks and Corey correlation. However, values from the high brine-saturation region approach experimental resolution. Therefore, the use of one correlation over the other cannot be recommended.

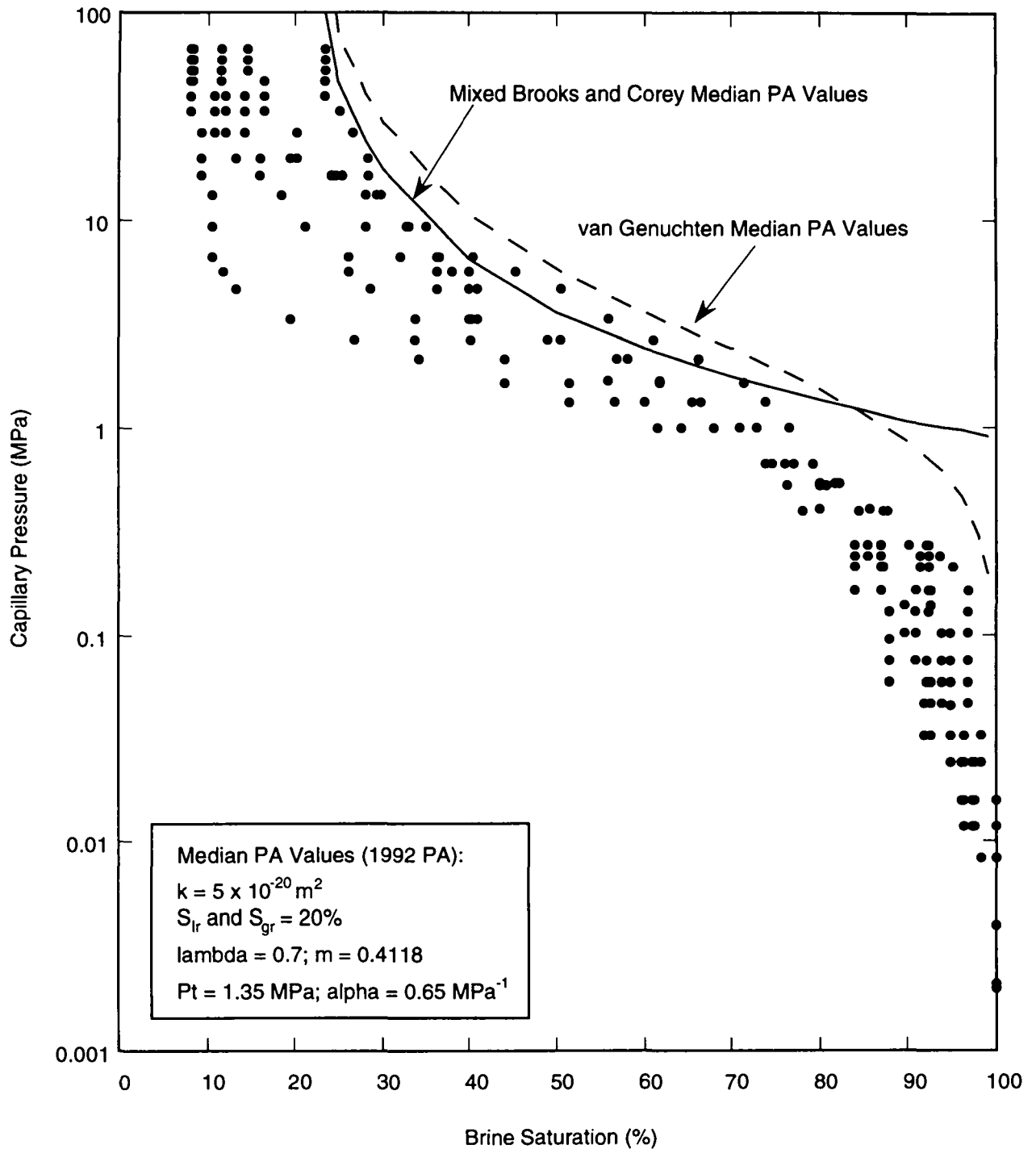


Figure 39. Comparison of measured MB139 mercury injection capillary pressure data (140° contact angle) to median parameter values used in determining the two-phase flow capillary pressure curve in performance assessment.

7.0 RELATIONSHIPS BETWEEN MEASURED PARAMETERS

7.1 Single-Phase Gas Permeability versus Porosity and Grain Density

Figures 40 and 41 are log-linear cross-plots of gas permeability versus effective porosity and grain density, respectively. As illustrated in Figure 40, there is a trend of increasing Klinkenberg-corrected gas permeability, k_g , with increasing effective porosity, ϕ_{eff} , as described by Equation 6.

$$\log k_g = -0.416\phi_{eff} - 18.59 \quad (6)$$

No apparent correlation exists between the gas permeability and grain density, as illustrated by the gas permeability versus grain density cross-plot in Figure 31. Sufficient data were not available to determine if a relationship existed between total and effective porosity or between total porosity and single-phase gas permeability.

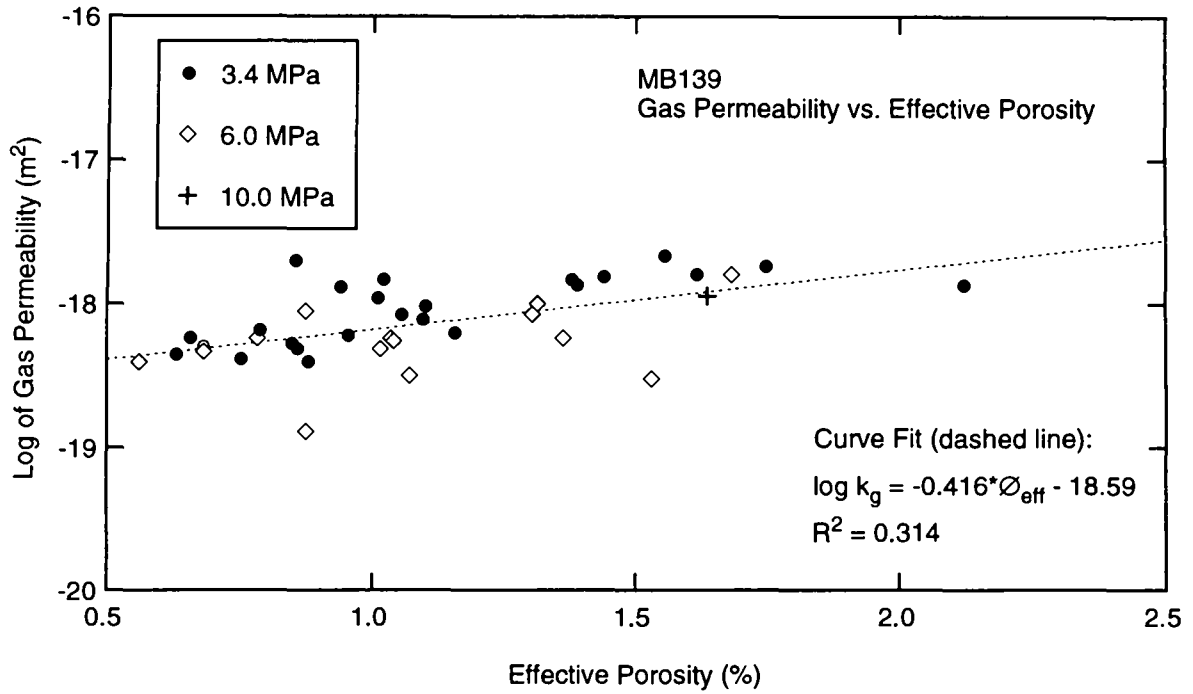
7.2 Single-Phase Gas Permeability versus Threshold Pressure

Figure 42 is a cross-plot of air-brine threshold pressure versus Klinkenberg-corrected gas permeability. The results from cores tested in this study are shown with the Davies' (1991) correlation for all rock and for anhydrite. The Davies' (1991) correlation for all rock types, Equation 7, relates threshold pressure, P_t , to intrinsic permeability, k .

$$P_t(\text{MPa}) = 5.6 \times 10^{-7} [k(\text{m}^2)]^{0.346} \quad (7)$$

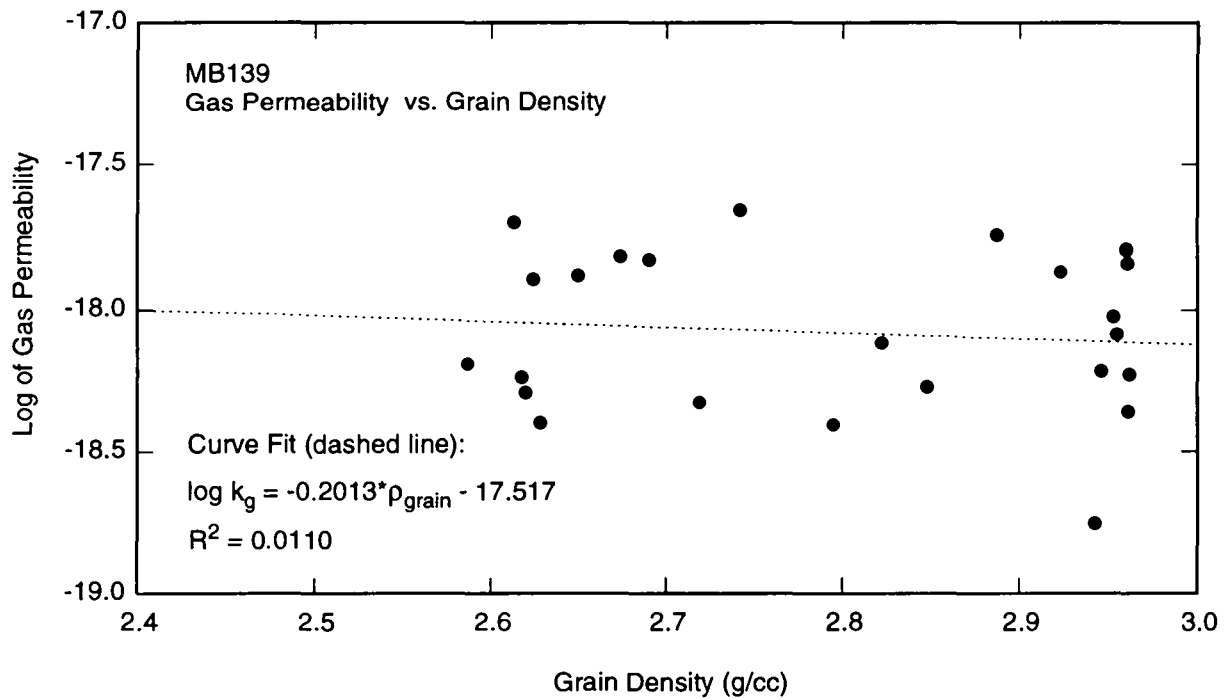
This correlation, used in the 1992 WIPP PA calculations, was developed prior to the initiation of the Salado Two-Phase Flow Program using data from a variety of consolidated rock lithologies including carbonate, anhydrite, shale, and sandstone. The Davies' correlation was considered the best available analog-based correlation for relating intrinsic permeability to threshold pressure, and uncertainties regarding its applicability to the Salado provided the impetus for this work.

The Davies' (1991) correlation for anhydrite appears to be adequate for relating threshold pressure and permeability for anhydrite, based on the tests conducted for this study.



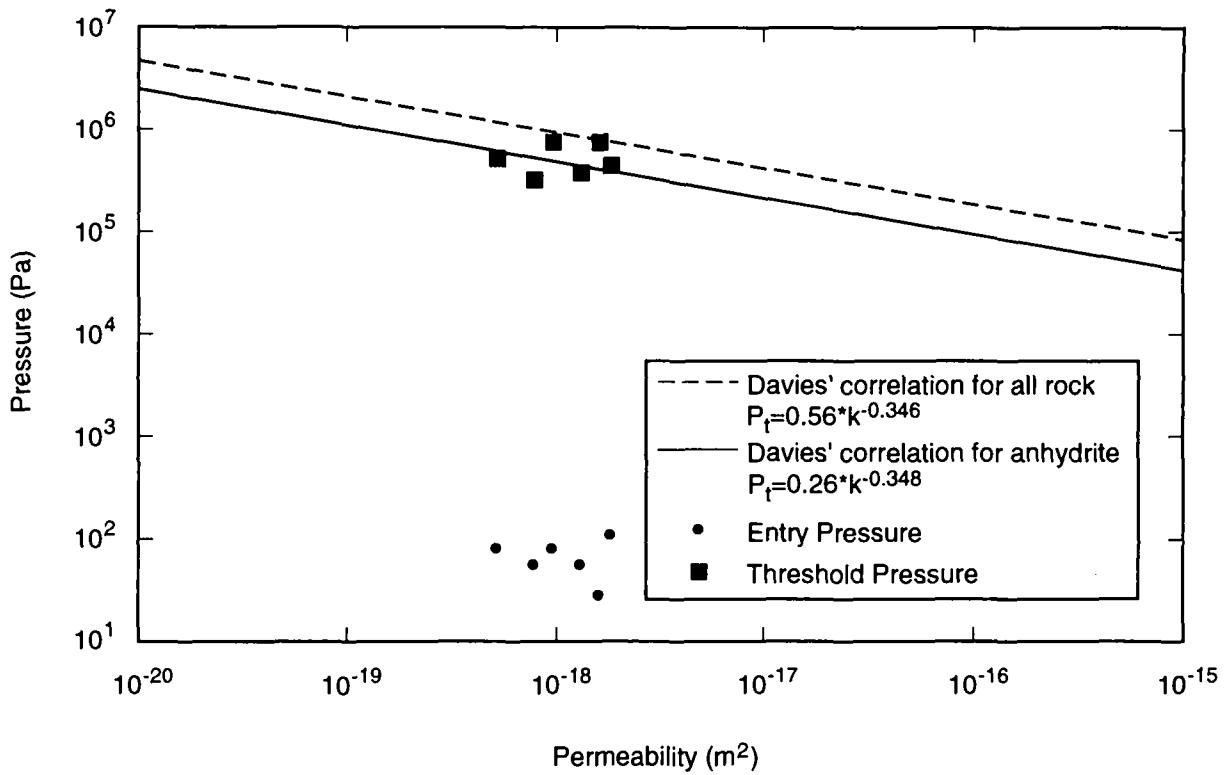
TRI-6115-184-0

Figure 40. Gas permeability versus effective porosity.



TRI-6115-182-0

Figure 41. Gas permeability versus grain density.



TRI-6115-241-0

Figure 42. Comparison of measured MB139 gas threshold entry pressure to Davies (1991) correlation.

8.0 CONCLUSIONS

The laboratory experiments and results reported here comprise the Preliminary Measurements (Anhydrite) portion of the Preliminary Experimental Activities of the Salado Two-Phase Flow Laboratory Program. These measurements were made to (1) generate WIPP-specific porosity and single-phase permeability data; (2) provide information needed to design test equipment and implement planned tests to measure two-phase flow properties, including relative permeability, threshold pressure, and capillary pressure; and (3) evaluate the suitability of using analog correlations for the Salado Formation to assess the long-term performance of the WIPP. Section 8.1 summarizes conclusions about the measurement of porosity and single-phase permeability of WIPP-specific material (anhydrite), Section 8.2 summarizes information from these tests that will be used for designing and implementing the two-phase flow tests, and Section 8.3 summarizes conclusions regarding the suitability of using analog correlations for the anhydrite marker beds in WIPP PA calculations.

8.1 WIPP-Specific Porosity and Single-Phase Permeability Measurements

8.1.1 Porosity

Effective porosity, measured on 42 samples, ranged from 0.4 to 2.7%; total porosity, measured on three of the 42 samples, ranged from 0.4 to 1.6%. The magnitude of difference between total and effective porosity could not be determined because of the limited amount of data and experimental error.

A slight reduction in effective porosity occurred when increasing confining stress was applied to a sample. In general, Zone III samples exhibited slightly higher effective porosity than Zone II and IV samples; no porosity measurements were made in Zone I or V rock. Because of the presence of pre-existing fractures in Zones I and V and/or differences in composition between Zones I and V and Zones II, III, and IV, the porosity of Zones I and V is expected to be more representative of fractured rock and therefore is likely to be higher than the rock recovered from Zones II, III, and IV.

8.1.2 Permeability

Gas permeability ranged from a minimum of 5.0×10^{-20} m² at 10 MPa net effective stress to a maximum of 8.3×10^{-16} m² at 2 MPa net effective stress. For all specimens tested,

permeability decreased as net effective stress was increased. Differences between vertical and horizontal permeability were within experimental error bounds. In general, Zone IV samples exhibited slightly higher permeability than Zone II and III samples; no permeability measurements were made in Zone I or V rock. Because of the presence of pre-existing fractures in Zones I and V and/or differences in composition between Zones I and V and that of Zones II, III, and IV, the permeability of Zones I and V is expected to be more representative of fractured rock and therefore higher than rock recovered from Zones II, III, and IV.

The relationship between effective porosity and gas permeability was linear; however, insufficient total-porosity data were available to define a relationship between total porosity and gas permeability. No trend existed between gas permeability and grain density, nor between gas permeability and threshold pressure resulting from the mercury injection capillary pressure tests.

8.2 Application of Test Results for Design and Implementation of Two-Phase Flow Tests

The design and implementation of a test program and development of experimental apparatus for measuring two-phase flow properties is highly dependent on the expected magnitude and range of single-phase flow properties (Christiansen and Howarth, 1995). The porosity of MB139 is very low, especially compared to sandstones and other rocks for which flow properties are routinely measured. Because capillary pressure and relative permeability are directly related to saturation and therefore to porosity and pore volume, accurate porosity measurements are essential. The Boyle's law helium expansion technique was used to measure porosity for this study and yielded acceptable results.

The gas and liquid permeability tests reported here were successfully performed using the steady-state technique when a non-reactive fluid was used. The magnitude and range of intrinsic permeability results from these tests also support the use of transient methods that would decrease the amount of time necessary for each test.

The simulated MB139 brine (recipe found in Appendix D) is not suitable for liquid flow tests on MB139 core samples. Dissolution of specimens which resulted in order-of-magnitude increases in permeability occurred when the simulated MB139 brine recipe was used. Liquid permeability measurements performed using odorless mineral spirits (OMS) agreed well with Klinkenberg-corrected gas permeability. Liquid permeability measurements

performed using the simulated MB139 brine did not agree with Klinkenberg-corrected gas permeability.

Both the centrifuge and mercury injection methods were suitable for measuring capillary pressure on samples from MB139. Although the decane-air centrifuge data and the mercury-air mercury injection data must be converted to air-brine data, introducing possible error, the air-brine corrected capillary pressure for tests conducted using the mercury injection technique agreed well for 140° and 180° contact angles, especially at higher wetting-phase saturations. Either the Hassler-Brunner or Rajan data reduction method for determining end face saturations for capillary pressure curves for centrifuge data could be used; no significant difference existed in the calculated capillary pressure because the sample lengths were short.

Air-brine threshold pressures determined from the mercury injection test results ranged from 0.33 to 0.78 MPa (48 to 113 psi). Air-brine gas entry pressures could not be determined exactly from the centrifuge capillary pressure test data. Residual liquid saturation results determined from the mercury injection technique ranged from 0.8 to 17.4%. The residual liquid saturations determined from the centrifuge tests should not be used in WIPP PA calculations because centrifuge hardware limitations precluded tests at sufficiently high spin rates to define the residual liquid saturations properly.

8.3 Suitability Using Analog Correlations for WIPP PA Calculations

As shown in Figure 42, the air-brine threshold pressure versus Klinkenberg-corrected gas permeability data from measurements made in this study are within an acceptable range that would be predicted from the Davies' (1991) anhydrite correlation; this correlation appears to be adequate for relating threshold pressure and permeability for Salado anhydrite.

The capillary pressure and threshold pressure data measured on MB139 samples do not match the characteristic curves that result from the Brooks and Corey or van Genuchten correlations, as shown in Figure 29. The general shape of the van Genuchten capillary pressure characteristic curve is similar to that of the actual MB139 capillary pressure curves. However, values from the high brine-saturation region approach experimental resolution. Therefore, the use of one correlation over the other cannot be recommended.

9.0 RECOMMENDATIONS

Based on the preliminary tests and results summarized in this report, the recommendations in Sections 9.1 and 9.2 should be considered in the development of future test programs and experimental procedures. Section 9.3 contains recommendations and considerations that should be made regarding the compilation and development of a technical basis for specification of single- and two-phase flow parameters for WIPP PA calculations.

9.1 WIPP-Specific Porosity and Single-Phase Permeability Measurements

- The net effective stress law should be determined for MB139. MB139 permeability and porosity tests should be performed under appropriate confining stress conditions.
- Anisotropy in permeability of MB139 should be investigated further.
- Porosity and single-phase permeability should be measured on core specimens from Zones I and V of MB139 to determine the flow properties of those zones.

9.2 Application of Test Results for Design and Implementation of Two-Phase Flow Tests

- If capillary pressure is measured using a centrifuge, the selected system must be one that can accommodate sufficiently slow spin rates such that the threshold entry pressure could be determined.
- Capillary pressure should be measured on MB139 samples using apparatus that allows confining stress to be exerted on samples during the test to verify the estimated effect of stress on threshold entry pressures and capillary pressure characteristic curves for MB139 samples.
- The simulated MB139 brine (recipe found in Appendix D) should not be used for flow tests on MB139 core-scale specimens.
- Both the centrifuge and mercury injection methods were suitable for testing samples from MB139; however, only small samples can be tested using existing hardware at commercial laboratories. The porous plate method should also be investigated for use in measuring threshold and capillary pressure of MB139 rocks because larger, more representative samples could be tested and WIPP-specific brines and appropriate gas could be used.

9.3 Technical Basis for Specification of Single- and Two-Phase Flow Parameters for PA Calculations

The development of parameter distributions for single- and two-phase anhydrite marker bed flow properties for WIPP PA calculations should be based on three sets of data/information: (1) the WIPP-specific, laboratory-generated data presented in this report, (2) WIPP-specific, in situ permeability and threshold pressure test-data, (3) non-WIPP-specific tests performed on analogous materials reported in the literature. The value of the data/information with associated limitations and uncertainties must be considered in the development of distributions for permeability, porosity, and two-phase flow parameters, as outlined below.

- WIPP-specific, laboratory-generated single- and two-phase data:

Value of data/information: measurement of total and effective porosity and liquid and gas permeability under three stress conditions and capillary and threshold pressure on specimens from MB139; control of pore pressure and confining stress; control of saturation; documentation of quality control for all tests.

Sources of uncertainty and limitations: tests performed on small, core-sized specimens; no tests on samples from Zones I or V; cores taken from only three underground locations; all cores taken from MB139.

- WIPP-specific, in situ permeability and threshold pressure test-data:

Value of data/information: tests performed in situ; test performed over full-thickness of marker beds; more than one anhydrite marker bed tested; numerous tests performed at different underground locations; documentation of quality control for all tests.

Sources of uncertainty and limitations: limited number of permeability and threshold pressure tests; limited knowledge of in-situ stress conditions for permeability and threshold pressure conditions; limited knowledge of in-situ saturation conditions; limited knowledge of extent of disturbance to test zone resulting from proximity of excavations.

- Non-WIPP-specific analogous materials:

Value of data/information: available, accessible data published in technical journals and other publications for permeability and porosity.

Sources of uncertainty and limitations: unknown how well analogs represent Salado rock; unknown details regarding test conditions for permeability and threshold pressure tests, including saturation state, test fluids used, stress conditions, and corrections for gas slippage effects; uncertainty in two-phase flow tests, including effects of stress on results and extremely limited data base for two-phase flow tests in low-permeability porous media; no documentation of quality control for any tests.

10.0 REFERENCES

- Amyx, J.W., D.M. Bass, Jr., and R.L. Whiting. 1960. *Petroleum Reservoir Engineering: Physical Properties*. New York, NY: McGraw-Hill, Inc.
- API (American Petroleum Institute). 1956. *Recommended Practice for Determining Permeability of Porous Media*. 3rd ed. API RP 27. Washington, DC: American Petroleum Institute. (Copy on file in the Sandia WIPP Central Files, Sandia National Laboratories, Albuquerque, NM as WPO#8709.)
- API (American Petroleum Institute). 1960. *Recommended Practice for Core-Analysis Procedure*. API RP 40. Washington, DC: American Petroleum Institute. (Copy on file in the Sandia WIPP Central Files, Sandia National Laboratories, Albuquerque, NM as WPO#27179.)
- Basan, P., J.R. Hook, K. Hughes, J. Rathmell, and D.C. Thomas. 1988. "Measuring Porosity, Saturation and Permeability from Cores: An Appreciation of the Difficulties," *The Technical Review* (A Schlumberger Publication). Vol. 36, no. 4, 22-36. (Copy on file in the Sandia WIPP Central Files, Sandia National Laboratories, Albuquerque, NM as WPO#8521.)
- Bass, D.M., Jr. 1987. "Chapter 26 Properties of Reservoir Rocks," *Petroleum Engineering Handbook*. Ed. H.B. Bradley. Richardson, TX: Society of Petroleum Engineers. (Copy of chapter on file in the Sandia WIPP Central Files, Sandia National Laboratories, Albuquerque, NM as WPO#45569.)
- Beauheim, R.L., G.J. Saulnier, Jr., and J.D. Avis. 1991. *Interpretation of Brine-Permeability Tests of the Salado Formation at the Waste Isolation Pilot Plant Site: First Interim Report*. SAND90-0083. Albuquerque, NM: Sandia National Laboratories.
- Beauheim, R.L., R.M. Roberts, T.F. Dale, M.D. Fort, and W.A. Stensrud. 1993. *Hydraulic Testing of Salado Formation Evaporites at the Waste Isolation Pilot Plant Site: Second Interpretive Report*. SAND92-0533. Albuquerque, NM: Sandia National Laboratories.
- Borns, D.J. 1985. *Marker Bed 139: A Study of Drillcore From a Systematic Array*. SAND85-0023. Albuquerque, NM: Sandia National Laboratories.
- Brace, W.F., J.B. Walsh, and W.T. Frangos. 1968. "Hydraulic Properties of Granite Under High Pressure," *Journal of Geophysical Research*. Vol. 73, no. 6, 2225-2236. (Copy on file in the Sandia WIPP Central Files, Sandia National Laboratories, Albuquerque, NM as WPO#45570.)
- Brooks, R.H., and A.T. Corey. 1964. "Hydraulic Properties of Porous Media." Hydrology Paper No. 3. Fort Collins, CO: Colorado State University. (Copy on file in the Sandia WIPP Central Files, Sandia National Laboratories, Albuquerque, NM as WPO#41117.)
- Bush, D.C., and R.E. Jenkins. 1970. "Proper Hydration of Clays for Rock Property Determinations," *Journal of Petroleum Technology*. Vol. 22, no. 7, 800-804. (Copy on file in the Sandia WIPP Central Files, Sandia National Laboratories, Albuquerque, NM as WPO#45572.)

- Christiansen, R.L., and S.M. Howarth. 1995. *Literature Review and Recommendation of Methods for Measuring Relative Permeability of Anhydrite from the Salado Formation at the Waste Isolation Pilot Plant*. SAND93-7074. Albuquerque, NM: Sandia National Laboratories.
- Davies, P.B. 1991. *Evaluation of the Role of Threshold Pressure in Controlling Flow of Waste-Generated Gas into Bedded Salt at the Waste Isolation Pilot Plant*. SAND90-3246. Albuquerque, NM: Sandia National Laboratories.
- Davies, P.B., L.H. Brush, M.A. Molecke, F.T. Mendenhall, and S.W. Webb, eds. 1991. *Waste-Generated Gas at the Waste Isolation Pilot Plant: Papers Presented at the Nuclear Energy Agency Workshop on Gas Generation and Release from Radioactive Waste Repositories*. SAND91-2378. Albuquerque, NM: Sandia National Laboratories.
- Davies, P.B., R.L. Beauchim, and E.D. Gorham. 1992. Appendix A. "Additional Comments on Far-Field Anhydrite Permeability Distribution in 'PA Modeling Using BRAGFLO-1992' 7-8-92 Memo by J. Schreiber," *Preliminary Performance Assessment for the Waste Isolation Pilot Plant, December 1992. Volume 3: Model Parameters*. Sandia WIPP Project. SAND92-0700/3. Albuquerque, NM: Sandia National Laboratories. A-39 through A-45.
- Deal, D.E., and J.B. Case. 1987. *Brine Sampling and Evaluation Program Phase I Report*. DOE-WIPP-87-008. Carlsbad, NM: Westinghouse Electric Corporation. (Copy on file in the Sandia WIPP Central Files, Sandia National Laboratories, Albuquerque, NM as WPO#44308.)
- Fatt, I., and D.H. Davis. 1952. "Technical Note 147. Reduction in Permeability with Overburden Pressure," *Petroleum Transactions, AIME*. Vol. 195, 329. (Copy on file in the Sandia WIPP Central Files, Sandia National Laboratories, Albuquerque, NM as WPO#8627.)
- Fredich, J.T., and D.H. Zeuch. 1996. *Petrographic and X-Ray Diffraction Analyses of Selected Samples from Marker Bed 139 at the Waste Isolation Pilot Plant*. SAND95-1240. Albuquerque, NM: Sandia National Laboratories.
- Freeman, D.L., and D.C. Bush. 1983. "Low-Permeability Laboratory Measurements by Nonsteady-State and Conventional Methods," *Society of Petroleum Engineers Journal*. Vol. 23, no. 6, 928-936. (Copy on file in the Sandia WIPP Central Files, Sandia National Laboratories, Albuquerque, NM as WPO#45575.)
- Freeze, R.A. 1975. "A Stochastic-Conceptual Analysis of One-Dimensional Groundwater Flow in Nonuniform Homogeneous Media," *Water Resources Research*. Vol. 11, no. 5, 725-741. (Copy on file in the Sandia WIPP Central Files, Sandia National Laboratories, Albuquerque, NM as WPO#45948.)
- Gonzales, M.M. 1989. *Compilation and Comparison of Test-Hole Location Surveys in the Vicinity of the Waste Isolation Pilot Plant Site*. SAND88-1065. Albuquerque, NM: Sandia National Laboratories.

- Good, R.J., and R.S. Mikhail. 1981. "The Contact Angle in Mercury Intrusion Porosimetry," *Powder Technology*. Vol. 29, no. 1, 53-62. (Copy on file in the Sandia WIPP Central Files, Sandia National Laboratories, Albuquerque, NM as WPO#45577.)
- Hassler, G.L., and E. Brunner. 1945. "Measurement of Capillary Pressures in Small Core Samples," *Petroleum Transactions, AIME*. Vol. 192, 114-123. (Copy on file in the Sandia WIPP Central Files, Sandia National Laboratories, Albuquerque, NM as WPO#27177.)
- Holcomb, D.J., D.H. Zeuch, K. Morin, R. Hardy, and T.V. Tormey. 1995. *Field and Laboratory Investigations of Coring-Induced Damage in Core Recovered from Marker Bed 139 at the Waste Isolation Pilot Plant Underground Facility*. SAND94-2757. Albuquerque, NM: Sandia National Laboratories.
- Howarth, S.M. 1993. *Conceptual Plan: Two-Phase Flow Laboratory Program for the Waste Isolation Pilot Plant*. SAND93-1197. Albuquerque, NM: Sandia National Laboratories.
- Hsieh, P.A., J.V. Tracy, C.E. Neuzil, J.D. Bredeheft, and S.E. Silliman. 1981. "A Transient Laboratory Method for Determining the Hydraulic Properties of 'Tight' Rocks—I. Theory," *International Journal of Rock Mechanics and Mining Sciences & Geomechanics Abstracts*. Vol. 18, no. 3, 245-252. (Copy on file in the Sandia WIPP Central Files, Sandia National Laboratories, Albuquerque, NM as WPO#45118.)
- Jones, F.O., and W.W. Owens. 1980. "A Laboratory Study of Low-Permeability Gas Sands," *Journal of Petroleum Technology*. Vol. 32, no. 9, 1631-1640. (Copy on file in the Sandia WIPP Central Files, Sandia National Laboratories, Albuquerque, NM as WPO#45579.)
- Keelan, D.K. 1972. "A Critical Review of Core Analysis Techniques," *The Journal of Canadian Petroleum Technology*. Vol. 11, no. 2, 42-55.
- Klinkenberg, L.J. 1941. "The Permeability of Porous Media to Liquids and Gases," *API Drilling and Production Practice*. 200-213. (Copy on file in the Sandia WIPP Central Files, Sandia National Laboratories, Albuquerque, NM as WPO#8556.)
- McLatchie, A.S., R.A. Hemstock, and J.W. Young. 1958. "The Effective Compressibility of Reservoir Rock and Its Effects on Permeability," *Journal of Petroleum Technology*. Vol. 10, 49-51. (Copy on file in the Sandia WIPP Central Files, Sandia National Laboratories, Albuquerque, NM as WPO#45580.)
- Parker, J.C., R.J. Lenhard, and T. Kuppasamy. 1987. "A Parametric Model for Constitutive Properties Governing Multiphase Flow in Porous Media," *Water Resources Research*. Vol. 23, no. 4, 618-624. (Copy on file in the Sandia WIPP Central Files, Sandia National Laboratories, Albuquerque, NM as WPO#41124.)
- Rajan, R.R. 1986. "Theoretically Correct Analytical Solution for Calculating Capillary Pressure-Saturation From Centrifuge Experiments," *Transactions of the SPWLA 27th Annual Logging Symposium, Houston, TX, June 9-13, 1986*. Houston, TX: Society of

Professional Well Log Analysts, Inc. (Copy on file in the Sandia WIPP Central Files, Sandia National Laboratories, Albuquerque, NM as WPO#45949.)

Rudd, N. 1974. "New Techniques for Threshold Pressure Determination in Gas Storage Cap Rock," *Geo-Engineering Laboratories, Inc. Tech Memo No. 6*. Chicago, IL: Institute of Gas Technology. (Copy on file in the Sandia WIPP Central Files, Sandia National Laboratories, Albuquerque, NM as WPO#8622.)

Sandia WIPP Project. 1992. *Preliminary Performance Assessment for the Waste Isolation Pilot Plant, December 1992. Volume 3: Model Parameters*. SAND92-0700/3. Albuquerque, NM: Sandia National Laboratories.

Thomas, L.K., D.L. Katz, and M.R. Tek. 1968. "Threshold Pressure Phenomena in Porous Media," *Society of Petroleum Engineers Journal*. Vol. 8, no. 2, 174-184. (Copy on file in the Sandia WIPP Central Files, Sandia National Laboratories, Albuquerque, NM as WPO#45583.)

Walls, J.D., and J.O. Amaefule. 1985. "Capillary Pressure and Permeability Relationships in Tight Gas Sands," *SPE/DOE Symposium on Low Permeability Gas Reservoirs, Denver, CO, May 19-22, 1985*. SPE/DOE 13879. Dallas, TX: Society of Petroleum Engineers. 293-302.

Warpinski, N.R., and L.W. Teufel. 1992. "Determination of the Effective Stress Law for Permeability and Deformation in Low-Permeability Rocks," *SPE Formation Evaluation*. Vol. 7, no. 2, 123-131.

Appendix A.
Data Report: Rock Physics Associates (Core Laboratories)

The following section includes Appendix A and Appendices A-A through A-C.

Appendix A

Capillary Pressure Measurements in Anhydrite Samples from MB 139

Errata Sheet

Upon review of the "raw" data, the following inconsistencies were found:

Data from sample 3 are not included in the data report because the sample was chipped and it is inconclusive if the "repair" by the laboratory was sufficient.

There are errors in Table 4.1.

- 1) The conversion value used to convert permeability from m^2 to Darcy was in error. The author of the report used the general conversion that a Darcy = $1E-12 m^2$, not the true conversion of Darcy = $9.869E-13 m^2$. The original permeabilities were in m^2 ; thus all the permeability values are off by about 0.1%.
- 2) The permeability of sample 2 at 1450 psi net stress should be 0.000228, not 0.000278 md.
- 3) The permeability of sample 9 at 500 psi net stress should be 0.000476, not 0.000535 md.
- 4) The permeability of sample 16 was unable to be determined in that the Klinkenberg correction slope was negative. Thus no value should have been given.
- 5) The permeability of sample 17 at 500 psi net stress should be 0.000405, not 0.000407 md.

The reported capillary pressure for sample 6 shown in tabulation form on Figure 4.9 is incorrect. The correct data are contained in the text of SAND 94-0472.

The results from Appendix C of this report, *Capillary Pressure Measurements in Anhydrite Samples from MB 139*, are not included in the data report because the data were not qualified by the time of report publication. Appendix A-C data from Sample EX 10-7 5.75-5.9 should not be used because the sample was broken during testing. Errors in Appendix A-C include:

- 1) Second page of Section 1, first line should read "confining pressure" not "confiningressure."
- 2) Second page of Section 1, equation 1, the denominator should read
"A*(P1² - P2²)"
not "A*(P1² * P2²)"
- 3) Basic Rock Properties table, sample EX 10-6 4.50-5.1: the length should be 7.047, not 3.801.

The following modifications should be made to the references on pages A-24 and A-25 in Appendix A.

Ref. No.	Comment
2	copy of Ciftcioglu et al., 1992 on file in SWCF as WPO#45574
3	correct name for second author is "R. Angers"; copy on file in SWCF as WPO#45576
4	the existence of McCullough et al., 1944 could not be verified
5	to Thornton and Marshall, 1947 remove "the" from title; paper is available as Am Inst. of Min & Met Engrs Tech Publ 2126 (1946), 9 pp.
6	correct name for second author is "H.J. Welge"
7	Rose and Bruce, 1949 is published in <i>Petroleum Transactions, AIME</i> , Vol. 186, pp. 127-142; copy on file in SWCF as WPO#45582
8	Calhoun et al., 1949 is published in <i>Petroleum Transactions, AIME</i> , Vol. 186; copy on file in SWCF as WPO#45573
9	complete name of first author is G.L. Hassler Jr.; correct location is <i>Petroleum Transactions</i> ; correct page numbers are 114-123; copy on file in SWCF as WPO#27177
10	to citation for Christiansen the word "Relationships" should be inserted after the word "Pressure" in the title; add: Vol. 7, no. 4
11	to citation for Melrose add: Vol. 29, no. 1
12	to citation for Chen et al. add: pp. 221-228
14	to citation for Purcell add: Vol. 186, pp. 39-48; copy on file in SWCF as WPO#45581
15	correct location for Melrose et al. is pp. 333-343 in <i>Formation Evaluation and Reservoir Geology Proceedings, SPE Annual Technical Conference and Exhibition, Dallas, TX, November 6, 1991</i>
16	correct title for Ward and Morrow paper is "Capillary Pressures and Gas Relative Permeabilities of Low-Permeability Sandstone"; paper presented at the <i>Low Permeability Gas Reservoirs Symposium</i> ; add: pp. 321-334
17	copy of Walls and Howarth, 1993 on file in SWCF as WPO#35253
18	the existence of this Core Laboratories internal document could not be verified
19	in Rajan, 1986 the words "Pressure-Saturation" should replace the words "Pressure Curves" in the paper title; published in <i>Transactions of the SPWLA</i> ; Vol. I, 18 pp.; copy on file in SWCF as WPO#45949
20	to citation for Walls and Amaefule add: pp. 293-302
21	copy of Davies, 1991 on file in SWCF as WPO#26169
22	to Good and Mikhail, 1981 add: Vol. 29, no. 1; copy on file in SWCF as WPO#45577

Final Report



Capillary Pressure Measurements in Anhydrite Samples from MB 139

Prepared By:
Rock Physics Associates
Project # 93-03

Prepared for:

Sandia National Laboratories

August, 1995

Table of Contents

1.0	Introduction	A-8
2.0	Review of Capillary Pressure Measurement Methods	A-9
2.1	Porous Plate Displacement.....	A-9
2.2	Centrifuge Displacement.....	A-11
2.3	Mercury Injection :.....	A-12
2.4	Vapor Desorption.....	A-13
2.5	Choice of Methods for this Project	A-13
3.0	Test Procedures	A-14
3.1	Sample Preparation	A-14
3.2	Porosity and Gas Permeability Measurement	A-15
3.3	Mercury Capillary Pressure Measurements	A-17
3.4	Centrifuge Capillary Pressure Measurements	A-18
3.5	Mineralogical Analysis	A-19
4.0	Results and Discussion.....	A-19
4.1	Porosity and Permeability	A-19
4.2	Capillary Pressure Sample Selection	A-19
4.3	Centrifuge Results.....	A-20
4.4	Mercury Injection Results.....	A-21
4.5	Comparison and Conversion to Air Water System.....	A-21
5.0	Conclusions and Recommendations	A-23
6.0	References	A-24
Appendix A Appendices		
Appendix A-A. Data Report: Rock Physics Associates (Core Laboratories)..... A-67		
Appendix A-B. Data Report: Rock Physics Associates (Core Laboratories)..... A-93		
Appendix A-C. Data Report: Rock Physics Associates (Core Laboratories)..... A-141		

Test Procedures and QA Plan: Capillary Pressure Measurements in Anhydrite

Figures

Figure 2.1: Batch Mode Capillary Pressure Cell	A-10
Figure 2.2: Hydrostatic Overburden Capillary Pressure Cell	A-11
Figure 2.3: Diagram of One Arm of a Multi-Sample Centrifuge Capillary Pressure System	A-12
Figure 3.1: Plug Sample Cutting Sketch	A-15
Figure 4.1: Grain Density Distribution, All Samples.....	A-40
Figure 4.2: Gas Permeability K_1 vs Porosity, All Samples	A-41
Figure 4.3: X ray CT Scans of Samples 5 and 6	A-42
Figure 4.4: X ray CT Scans of Samples 7 and 8	A-43
Figure 4.5: X ray CT Scans of Samples 11 and 12	A-44
Figure 4.6: X ray CT Scans of Samples 13 and 14	A-45
Figure 4.7: X ray CT Scans of Samples 21 and 22	A-46
Figure 4.8: X ray CT Scans of Samples 23 and 24	A-47
Figure 4.9: Centrifuge Capillary Pressure, Sample 6.....	A-48
Figure 4.10: Centrifuge Capillary Pressure, Sample 8.....	A-49
Figure 4.11: Centrifuge Capillary Pressure, Sample 12.....	A-50
Figure 4.12: Centrifuge Capillary Pressure, Sample 14.....	A-51
Figure 4.13: Centrifuge Capillary Pressure, Sample 22.....	A-52
Figure 4.14: Centrifuge Capillary Pressure, Sample 24.....	A-53
Figure 4.15: Mercury Capillary Pressure, Sample 5	A-54
Figure 4.16: Mercury Capillary Pressure, Sample 7	A-55
Figure 4.17: Mercury Capillary Pressure, Sample 11	A-56
Figure 4.18: Mercury Capillary Pressure, Sample 13	A-57
Figure 4.19: Mercury Capillary Pressure, Sample 21	A-58
Figure 4.20: Mercury Capillary Pressure, Sample 23	A-59
Figure 4.21: Air/Water Converted Hg ($\phi = 140$ and 180 deg) and Cent. P_{cap} , Samples 5 and 6	A-60
Figure 4.22: Air/Water Converted Hg ($\phi = 140$ and 180 deg) and Cent. P_{cap} , Samples 7 and 8	A-61
Figure 4.23: Air/Water Converted Hg ($\phi = 140$ and 180 deg) and Cent. P_{cap} , Samples 11 and 12	A-62
Figure 4.24: Air/Water Converted Hg ($\phi = 140$ and 180 deg) and Cent. P_{cap} , Samples 13 and 14	A-63
Figure 4.25: Air/Water Converted Hg ($\phi = 140$ and 180 deg) and Cent. P_{cap} , Samples 21 and 22	A-64
Figure 4.26: Air/Water Converted Hg ($\phi = 140$ and 180 deg) and Cent. P_{cap} , Samples 23 and 24	A-65
Figure 4.27: Equivalent Air-Brine Entry Pressure vs. Perm. for Tight Sands and Anhydrite.....	A-66

Tables

Table 4.1: Porosity and Air Permeability at Three Net Confining Pressures	A-26
Table 4.2: Mercury P_{cap} Data for Sample 5, contact angle 140 deg.	A-28
Table 4.3: Mercury P_{cap} Data for Sample 5, contact angle 180 deg.	A-29
Table 4.4: Mercury P_{cap} Data for Sample 7, contact angle 140 deg.	A-30
Table 4.5: Mercury P_{cap} Data for Sample 7, contact angle 180 deg.	A-31
Table 4.6: Mercury P_{cap} Data for Sample 11, contact angle 140 deg.	A-32
Table 4.7: Mercury P_{cap} Data for Sample 11, contact angle 180 deg.	A-33
Table 4.8: Mercury P_{cap} Data for Sample 13, contact angle 140 deg.	A-34
Table 4.9: Mercury P_{cap} Data for Sample 13, contact angle 180 deg.	A-35
Table 4.10: Mercury P_{cap} Data for Sample 21, contact angle 140 deg.	A-36
Table 4.11: Mercury P_{cap} Data for Sample 21, contact angle 180 deg.	A-37
Table 4.12: Mercury P_{cap} Data for Sample 23, contact angle 140 deg.	A-38
Table 4.13: Mercury P_{cap} Data for Sample 23, contact angle 180 deg.	A-39

Test Procedures and QA Plan: Capillary Pressure Measurements in Anhydrite

1.0 Introduction

The Waste Isolation Pilot Plant (WIPP) is designed to safely contain low-level transuranic radioactive waste. The design relies mainly on the stability and low permeability of the Salado Formation. Interbedded anhydrite layers within the Salado such as Marker Bed (MB) 139 may be more permeable than the surrounding halite and may allow gas generated from the degrading waste to escape from the underground storage rooms. The extent of this gas flow, if any, in response to an applied pressure gradient will be controlled by several factors. These include porosity, intrinsic or absolute permeability, gas-liquid capillary pressure, gas-liquid relative permeability and the degree of interconnectivity of the anhydrite pore system. This report contains the results of a preliminary experimental program to measure the porosity, gas permeability, and capillary pressure of 1 inch diameter by 1 inch long cylindrical samples from MB 139. These tests were conducted as part of the Salado Two-Phase Flow Laboratory Program by a commercial core analysis lab that specializes in testing low permeability rock. Also included is a literature review in the field of capillary pressure.

The capillary pressure tests were carried out on six pairs of samples. The pairs were chosen by a careful screening process that eliminated non-representative or highly heterogeneous samples. The screening process included visual inspection, x-ray imaging for internal irregularities, and measurements of density, porosity, and permeability. One sample from each pair was tested by the mercury injection capillary pressure method and the other was tested by the centrifuge capillary pressure method. These two methods were chosen because they are the most appropriate for low porosity and permeability samples such as the anhydrite. The results from both techniques were reasonably consistent for each pair of samples after the data was converted to an air-brine system. Two features of the data stood out. First, the threshold entry pressures were very low, typically less than 5 psi, and second, the residual wetting phase saturation was less than 30% in all cases. These characteristics would be expected of samples with much higher permeability.

Additional measurements of porosity and gas permeability at multiple confining stresses were performed. These samples were 1.5 inches in diameter and about 1 to 2 inches in length, and the results of these tests are given in Appendix A-C. Because they were not in the original sample set, and were not considered for capillary pressure testing, the results have not been included in the main body of this report. The gas permeability of these samples were not Klinkenberg corrected.

Test Procedures and QA Plan: Capillary Pressure Measurements in Anhydrite

2.0 Review of Capillary Pressure Measurement Methods

The modern literature on capillary pressure measurements can be broadly divided into two groups: 1) material science and 2) oil and gas. The material science publications generally focus on determining pore size distribution of compacted powders, sintered granular materials and ceramics. The method most often used is the high pressure mercury injection technique^{1,2} although the air-water dynamic expulsion method is also reported occasionally³. The major interests in oil and gas are determining water, oil, and gas saturations, relative permeability behavior, and pore size distribution on a variety of different rock types. The methods used are porous plate displacement, centrifuge displacement, mercury injection, and occasionally, vapor desorption. Because the petroleum publications focus on natural materials and include a wide variety of methods, we concentrated on this body of literature. This review is not exhaustive, but rather attempts to highlight important or representative publications. Each of the four primary measurement methods are discussed below, followed by the rationale for selecting the two techniques, mercury injection and centrifuge, that were used in this study.

2.1 Porous Plate Displacement

This method was discussed by McCullough, et al.⁴ and several other early experimenters^{5,6,7,8}. There are two major variations on the method, batch mode porous plate displacement and overburden pressure porous plate displacement. In the batch mode, several samples are placed on a large semi-permeable membrane or capillary plate that can be made of various materials (Figure 2.1). For rock sample testing, the capillary plate material is often porous ceramic, and in soil testing cellulose membranes are used. For drainage cycle testing, the sample is initially fully saturated with the wetting fluid. Each sample is weighed before it goes into the cell, and the density of the wetting and non-wetting fluids are known.

As shown in Figure 2.1, the displacing (non-wetting) fluid fills the upper part of the batch mode cell and the displaced (wetting) fluid fills the lower part of the cell. In this type of test, the non-wetting fluid is often humidified air or nitrogen. Pressure is increased on the non-wetting fluid, and when it exceeds the threshold entry pressure in one or more of the samples, wetting phase fluid begins to flow from the lower part of the cell. The actual volume of this fluid does not matter since there is no way to tell from which sample it came. However, when the fluid flow stops, it signals that all samples are at equilibrium at that pressure and can be removed from the cell for weighing. The saturation in each sample is determined gravimetrically. This process is repeated at higher and higher non-wetting injection pressures until the threshold pressure of the capillary plate is reached. Spontaneous imbibition can be achieved by reducing the injection pressure to zero and

Test Procedures and QA Plan: Capillary Pressure Measurements in Anhydrite

allowing the samples to imbibe the wetting phase fluid. Usually only a small amount of fluid (5% to 10% of pore volume) will spontaneously imbibe.

More recently, porous plate capillary pressure apparatus has been adapted so that overburden or confining pressure can be applied to the sample during testing. In this configuration a sample is jacketed with an elastomeric sleeve around the sides, and two metal end caps are placed on each end of the sample. This assembly is contained within a pressure cell that permits hydrostatic or bi-axial stress to be applied to the sample. The example in Figure 2.2 shows a hydrostatic capillary pressure cell. The semi-permeable membrane or capillary plate is usually mounted on one end of the sample, and the non-wetting phase fluid is injected from the opposite end of the sample. The volume of wetting phase displaced is measured with a precision balance or in a small calibrated glass tube. This arrangement can also be equipped with an oil-wet membrane to permit both forced drainage and imbibition capillary pressure curves.

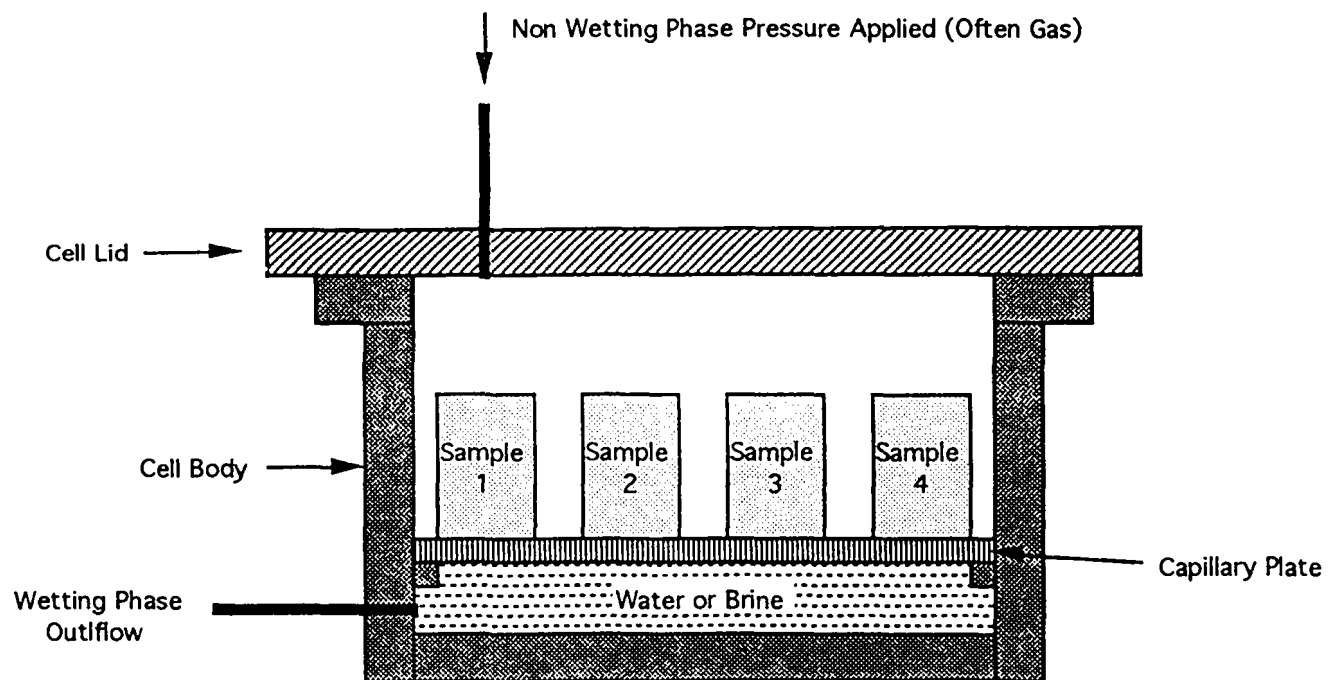


Figure 2.1: Batch Mode Capillary Pressure Cell

Test Procedures and QA Plan: Capillary Pressure Measurements in Anhydrite

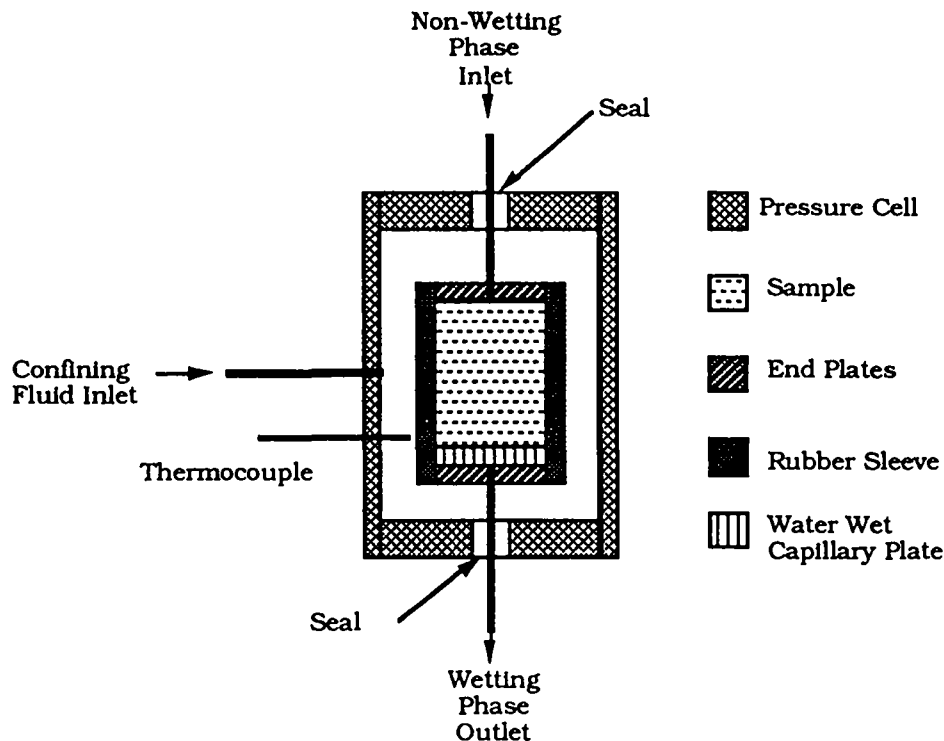


Figure 2.2: Hydrostatic Overburden Capillary Pressure Cell

2.2 Centrifuge Displacement

The centrifuge displacement technique for measuring capillary pressure has been the subject of many studies since first introduced to the petroleum industry by Hassler and Brunner⁹ in 1945. This method involves placing a brine- or oil-saturated sample into a centrifuge rotor and incrementally increasing the rotational speed. A stroboscope device is used to read the volume of fluid that is displaced from the sample at each speed which is collected in a clear plastic calibrated tube (see Figure 2.3). The measured values in centrifuge displacement are centrifugal acceleration (G's) and the average saturation of the sample. The desired results are capillary pressure and the saturation at a specific location on the sample, usually the inflow face.

Converting centrifugal acceleration to pressure is straightforward, but converting average saturation to point saturation is where disagreement sometimes arises. Hassler and Brunner provided a general solution to the problem for a homogeneous sample. Their saturation equation could be solved by successive approximations, thereby achieving any desired degree of accuracy. However, in practice, most people only use the first approximation, because it is mathematically more convenient, and it is often adequate for small sample lengths (where $R_1/R_3 > 0.7$). R_1 and R_3 are the distances from the centrifuge axis to the top end of the sample and to the bottom end of the sample, respectively as shown in Figure 2.3. Therefore, this first approximation has now

Test Procedures and QA Plan: Capillary Pressure Measurements in Anhydrite

become widely known as the "Hassler-Brunner solution." Review of the many responses to and revisions of the Hassler-Brunner approach are presented in several recent articles^{10,11,12}.

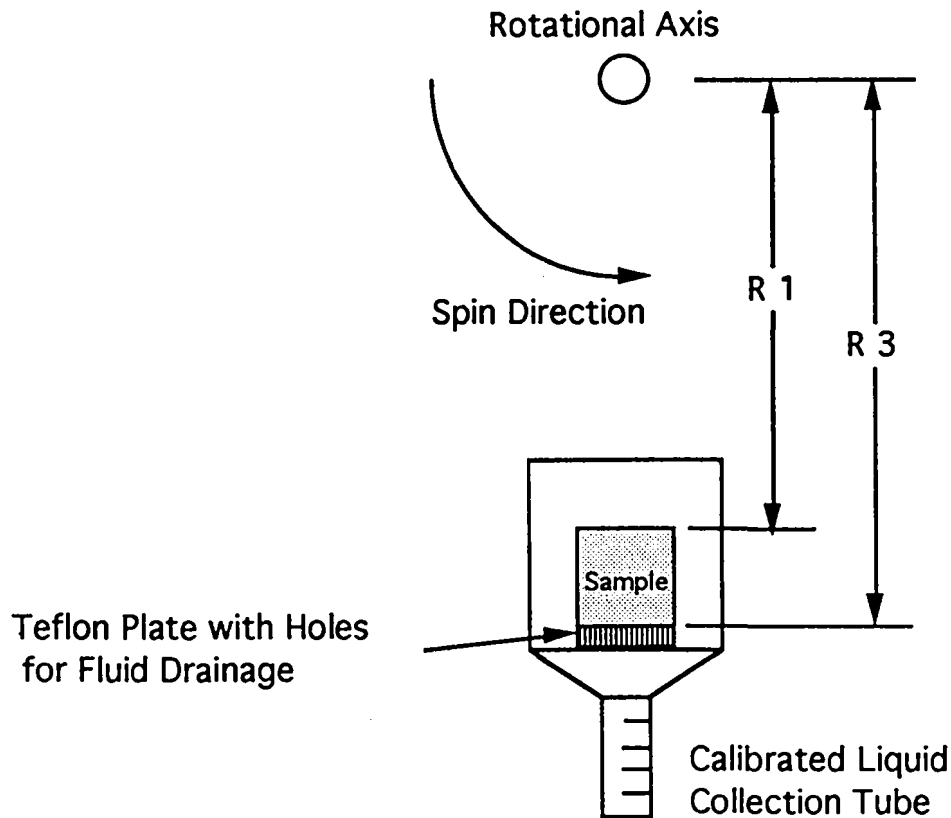


Figure 2.3: Diagram of One Arm of a Multi-Sample Centrifuge Capillary Pressure System

One advantage of the centrifuge method over porous plate methods is that it can be used to develop higher capillary pressures, and therefore results can be obtained at low wetting phase saturations. For example, using a high speed centrifuge with oil as the wetting phase and air as the non-wetting phase, it is possible to measure capillary pressures of 650 psi or more. This is very important for low permeability materials. Another advantage is that the time required for equilibrium is not as long as for porous plate methods. Omoregie¹³ has shown that some porous plate tests require equilibration periods that are greater than 10 times longer than the centrifuge displacement test for the same sample.

2.3 Mercury Injection

The mercury injection method, as applied to rock samples, was first presented by Purcell¹⁴. The method can be used over a wide range of wetting phase saturations, from 100% to less than 10% for some rocks. Because the contact angle of mercury against solid mineral surfaces is about 140 degrees, mercury is the non-wetting phase and air is the wetting phase. A correction factor is used

Test Procedures and QA Plan: Capillary Pressure Measurements in Anhydrite

to apply the air-mercury data to other fluids systems as described in Section 4.5. Current mercury injection instruments can reach up to 50,000 psi mercury pressure.

Equilibrium times are very short for this method because of the high pressures involved, and the method does not depend on displacement of the wetting phase by mass flow through the sample. As a result, mercury injection has been used extensively for characterizing the pore size distribution of sintered powders and ceramics^{1,2}. Mercury injection is intended for samples that will not be seriously affected by drying or evacuation of the pore space. If hydrated clays are present, for example, the sample drying (required for mercury injection) may cause clay damage that would change the pore throat size distribution of the sample. Mercury is very useful for determining the threshold entry pressure of a sample, since the equivalent pressure required to cause mercury to enter an empty pore throat is about 5 times greater than that required for air to displace water.

2.4 Vapor Desorption

Vapor desorption is a method generally used to define the very low wetting phase saturation region of the capillary pressure curve. This portion of the curve is controlled by the smallest pore throat radii. For rock sample testing, the vapor phase is usually water, but nitrogen¹⁵ and other gases can be used. Ward and Morrow¹⁶ describe a typical experiment measuring water vapor desorption isotherms in low permeability sandstones. The method requires saturating a cylindrical rock sample with distilled water. The sample is then placed in a chamber with constant temperature and humidity of 99%. The sample is weighed periodically until its weight stabilizes. The relative humidity is then decreased to values of 98%, 95%, 92%, 90%, 75%, 60%, 40%, and 20%. Based on the weight of the dry sample, water saturation is calculated at each relative humidity. Ward and Morrow show that relative humidity is related to vapor pressure and vapor pressure depends on liquid/gas interface curvature. Therefore capillary pressure at each relative humidity, and water saturation, can be calculated.

2.5 Choice of Methods for this Project

Because of the low porosity and permeability of the Salado anhydrite samples, the methods that best suited testing of these samples are the mercury injection and centrifuge displacement methods. These two methods have a more rapid equilibrium process than the porous plate technique. Also, high threshold entry pressures, are expected, and these methods are the only ones that can be used if the threshold entry pressure is high. The vapor desorption method was not considered because it does not provide data near the 100% wetting phase saturation limit, and water can react with the halite in these samples.

Test Procedures and QA Plan: Capillary Pressure Measurements in Anhydrite

3.0 Test Procedures

The sections below describe the test procedures that were used in this experimental project. For a description of the instrument calibration procedures, please refer to the relevant QA Plan¹⁷ for this project.

3.1 Sample Preparation

The plug samples for these tests came from two six inch diameter whole cores E1X10 and E1X11 provided by Sandia National Laboratories. The cores were drilled downward through the Marker Bed 139 at approximately 90 degrees to the bedding planes. These cores were shipped directly to Marilyn Black, Core Analysis Supervisor, of Core Laboratories in Carrollton, TX. The samples were slabbed (cut) along their length, with the cut approximately 1/3 of the sample diameter from the outer circumference of the core (Figure 3.1). The cutting fluid for slabbing and plug cutting was Isopar, a light refined oil. This fluid was chosen because it can be easily removed from the core by standard drying procedures and because it does not react with halite, as a water based fluid might. After slabbing, both faces of the cores were photographed with white light. See Appendix A-A photographs.

Figure 3.1 shows a sketch of sample cutting locations. Horizontal (with respect to the bedding plane) test plugs were taken from the whole cores at 32 depths, and for vertical sample cutting at 11 depths. Plug sample locations were chosen by Dr. Susan Howarth and Dr. Joel Walls. Slabbed core photos showing the vertical and horizontal plug locations are included in Appendix A. Horizontal plugs 1 inch in diameter were drilled all the way through the whole core. These 5 to 6 inch long plugs were photographed in white light and X-ray scanned. Photographs were also made of the X-ray images and were combined with the white light photos (Appendix A-A). These photos were used to select the segments of the long plugs to use for the 1 inch long test plugs. Two test plugs (A & B) were then cut from each of the horizontal depths and two plugs (C1 and C2) were taken from each of the vertical depths. The end trims were saved for mineralogical analyses (see plug cutting sketch, Figure 3.1). The solid cylindrical plugs were 1 inch in diameter (+/- 0.002") and 1 inch in length (+ 0.002 /- 0.05"). The ends were cut and ground flat and parallel using a diamond face wheel surface grinder. Grinding was done slowly using compressed air flow to keep the cutting surface cool. Flatness of ends were within 0.001" (0.06 degrees) across the ends of the sample. The sides of the sample were straight within 0.02" when rolled across a flat surface plate. Length and diameter of samples were measured with digital calipers to within 0.001".

Test Procedures and QA Plan: Capillary Pressure Measurements in Anhydrite

After cutting and surface grinding, these samples were labeled with a permanent marker and recorded on the sample tracking forms provided by SNL. The samples were dried in a vacuum oven at 104 degrees C until the weight stabilized to within 0.001 gm over a 24 hour period.

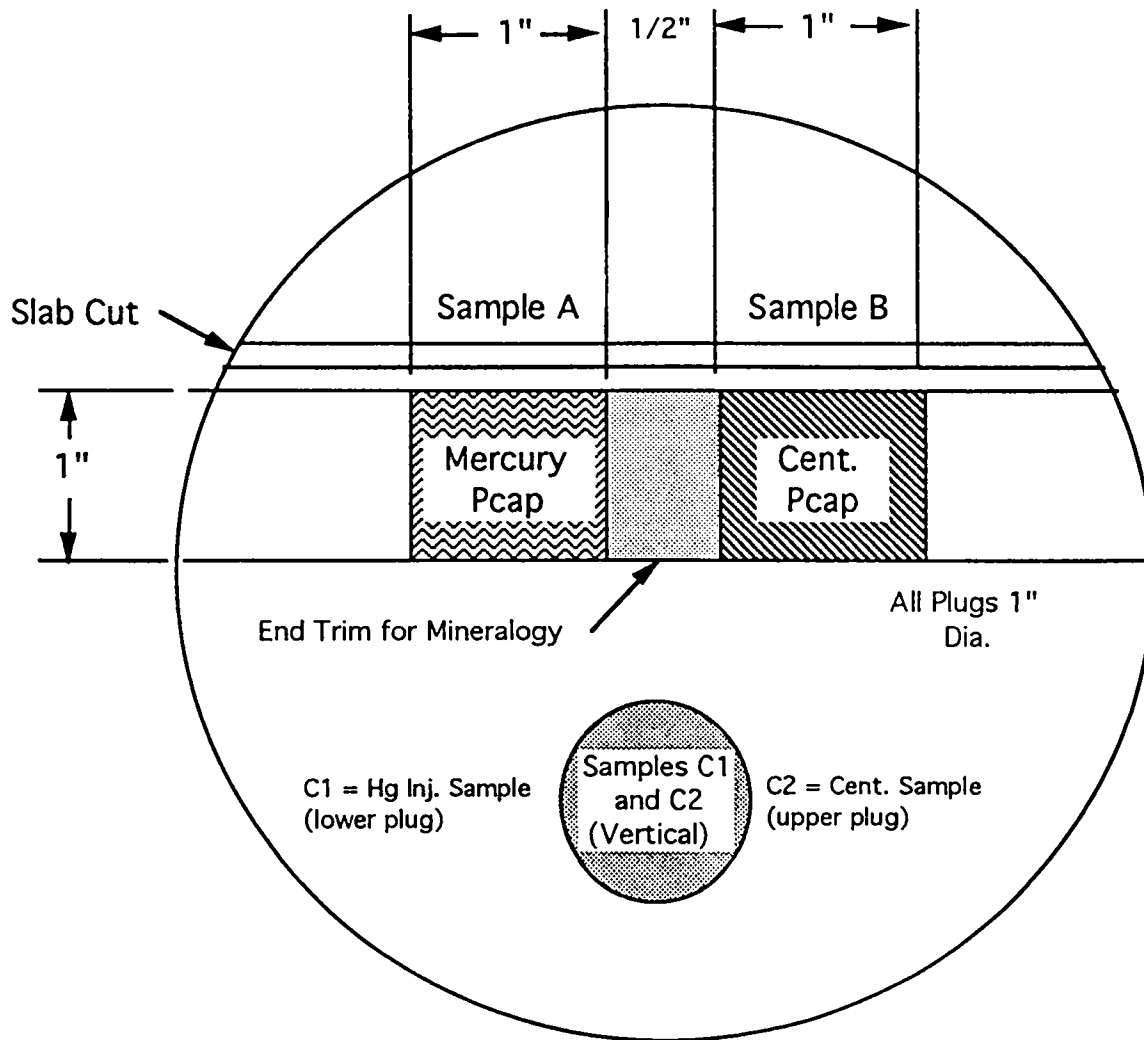


Figure 3.1: Plug Sample Cutting Sketch

3.2 Porosity and Gas Permeability Measurement

Measurement of porosity was done by the pore volume-grain volume method where

$$\text{Porosity} = \text{PV} / (\text{PV} + \text{GV}).$$

1

This is a measurement of the effective porosity, which will not measure pores that are isolated. Since we want to measure the pore space available for fluid flow, this is the correct porosity measurement method. Pore volume data reported on the 1" samples were taken using the Core

Test Procedures and QA Plan: Capillary Pressure Measurements in Anhydrite

Laboratories CMS 300 system which measures direct pore volume by helium expansion. Grain volume data came from the Autoporosimeter system.

The porosity measurements in the CMS-300 are conducted using an initial pore pressure of 200 psig. The pore pressure drops during the test because the gas expands from the pore volume of the rock to a larger volume equal to the pore volume plus a calibrated reference volume. There is no way to know exactly what the final pore pressure will be, so the software for the CMS-300 predicts arbitrarily that the final pressure will be 100 psi. The software then adjusts the P_{ext} to P_{net} (desired) plus 100 psi. After the pore pressure reaches equilibrium and the pore volume is calculated, the CMS-300 software compares the actual final pore pressure to its initial prediction of 100 psi. If the actual final pore pressure differs from the predicted value by more than 25 psi, then the software computes a new pore volume which would have been measured at the actual net stress. It does this by using a pore volume compressibility determined from the actual sample, if the sample was tested at multiple confining stresses. This is an iterative process that is fully described in the CMS-300 manual¹⁸, Chapter 4. If the porosity was measured at only one net stress, the computational algorithm uses a default compressibility of $3 \times 10^{-6} \text{ psi}^{-1}$. The important point is that the difference between the predicted final pore pressure and the actual final pore pressure is usually less than 50 psi, and this difference causes only minor adjustments to the pore volume.

A test to determine the effect of different drying methods on porosity, as called for in the original procedure, was not done. It was determined that in similar tests performed by other labs, there was no difference in porosity with either method. Also, it was determined from petrographic analysis that these samples contained no measurable clay or other hydration sensitive minerals that should be sensitive to drying methodology.

Permeability measurements to air were made in a steady-state system (Extended Range Autopermeameter System) using a constant upstream pressure. Flow rates were determined with a calibrated low range gas flow meter. The measurements were corrected for Klinkenberg slip effects (where possible) and all measurements were done at ambient temperature conditions. This temperature was recorded before each batch of samples was run.

For the steady state gas permeability measurements, net confining stress (P_{net}) reported is defined as

$$P_{net} = P_{ext} - P_{p, ave}$$

2

Test Procedures and QA Plan: Capillary Pressure Measurements in Anhydrite

where P_{ext} is the external hydrostatic pressure applied to the rubber sleeve surrounding the sample. $P_{p, ave}$ is the average pore pressure, or the pressure of the flowing gas inside the sample measured relative to 1 atmosphere (gauge pressure, typical unit = psig). $P_{p,ave}$ is calculated from the average of the inlet and outlet gas pressure. For example, if the upstream pressure is 200 psig and the downstream pressure is 0 psig then the average pore pressure is 100 psig. The system operator, would then adjust the external confining pressure to P_{net} (desired) plus 100 psi to achieve the proper net stress for the test.

The porosity and permeability measurement procedure on the selected horizontal and vertical plugs (A, B, C1 and C2) was as follows;

1. Cool samples to room temperature in a small closed container with desiccant.
2. Weigh each sample on a digital balance to the nearest 0.0001 gm.
3. Measure grain volume in a Boyle's Law expansion cell with helium (helium pycnometer).
4. Place samples in the computer controlled CMS-300 system and measure porosity at the following net confining stresses: 500 psi (3.45 MPa), 870 psi (6.0 MPa), and 1450 psi (10 MPa).
5. Place samples in the steady state system and measure gas permeability at multiple gas injection pressures. For 1 inch diameter samples, use net confining stresses of 500 psi (3.45 MPa), 870 psi (6.0 MPa), and 1450 psi (10 MPa). Compute Klinkenberg-corrected gas permeability. For 1.5" diameter samples, use P_{net} equal to 400 psi (2.76 MPa), 870 psi (6.0 MPa), and 1450 psi (10 MPa) and do not compute Klinkenberg corrected gas permeability.

3.3 Mercury Capillary Pressure Measurements ("A" and "C2" Samples)

This test involved injecting mercury into the pores of six samples under high pressure. The system measures the volume of mercury injected at each pressure from zero to 50,000 psi. The test is destructive to the sample and the samples are disposed of after the test. The tests were carried out by an automated system that records all data on a computer, and data reduction is performed automatically by software provided by the manufacturer. The mercury injection system in use at Core Labs is the 2-sample Micromeritics Autopore II 9220. This is a standard machine for testing porous ceramics, rocks and other materials.

The test procedure followed for the mercury capillary pressure measurements were as follows.

1. Load dry "A" or "C2" samples into sample holder.
2. Check equilibration criteria values in computer set-up screen. It should be set to the longest allowable time (180 sec).

Test Procedures and QA Plan: Capillary Pressure Measurements in Anhydrite

3. Run auto penetrometer mercury injection routine to 50,000 psi.
4. Remove sample and print out results. Perform data reduction using pore volume from CMS-300 at lowest net stress.

3.4 Centrifuge Capillary Pressure Measurements ("B" and "C1" Samples)

This measurement determines the drainage air-oil capillary pressure of six rock sample to pressures up to about 500 psi. Decane was chosen as the wetting phase because it is available in very pure form, it will not react with water soluble minerals in the samples, and it has a well documented surface tension value of 24 dynes/cm at 25 degrees Celsius¹⁶. The samples were first fully saturated with decane, then they were placed in a high speed centrifuge with calibrated collection tubes below each sample. As the speed of the centrifuge was increased, decane was displaced by centrifugal force and collected in the tubes.

The volume in each tube was visually read by the operator using a strobe light synchronized to the speed of the spinning rotor. The collection tubes in this experiment had an original volume of 1 cm³ and were subdivided into 0.025 cm³ divisions, but are readable to 0.01 cm³. Because we had already measured the porosity of these samples, we knew that they had about 0.2 cm³ of pore volume. Therefore to get better volume resolution, small Plexiglas rods whose cross sectional area was about half that of the collection tubes were fabricated. These rods were inserted into the collection tubes as a "ballast volume" to reduce the tube volume by about 50% and improve the volume resolution to about 0.0125/division, readable to 0.005 cm³. Each tube was calibrated with it's ballast volume in place by spinning it with different amounts of kerosene (kerosene density was established by weighing in NIST certified balance), and then weighing the tube to establish a correlation between the visual scale on the tube and the actual volume of fluid.

The measurement procedure was as follows.

1. Saturate "B" and "C1" samples with decane by placing them in a chamber with a working pressure of at least 2000 psi. Evacuate the chamber to less than 100 microns pressure for 24 hours. Degas the decane with vacuum (less than 0.001 atm.) for at least 4 hours. Flood the chamber with the degassed decane and pressure it to 2000 psi. Leave pressure on samples for 24 hours. All centrifuge capillary samples (B and C1 Samples) were saturated together.
2. Measure the density of the degassed decane. Weigh each sample in air and suspended in the decane.
3. Select the smallest volume collection tubes available and partially pre-fill each one to avoid curvature errors at the bottom of the tube. Weigh the samples and load them into the

Test Procedures and QA Plan: Capillary Pressure Measurements in Anhydrite

centrifuge. Begin the capillary pressure measurement procedure (ambient temperature). Expect high entry pressure to gas and very small volume changes. The equilibrium time between speed changes should be at least 48 hours.

4. Remove and immediately weigh the samples. Collect any loose grains in the centrifuge cup and weigh them. Calculate the final decane saturation by gravimetric and volumetric methods. Transmit data to Rock Physics Associates (RPA) for review. After approval from RPA, then go to step 5.
5. Perform data reduction using the standard Hassler-Brunner⁹ method and the alternative Rajan¹⁹ method. Use pore volume from CMS-300 at lowest net stress.

3.5 Mineralogical Analysis

End trims from the ten horizontal sample pairs and five vertical sample pairs were sent to Omni Laboratories in Houston, TX for quantitative X-ray diffraction and thin section point count analysis. This information is presented in Appendix A-B.

4.0 Results and Discussion

4.1 Porosity and Permeability

Porosity of all samples tested is presented in Table 4.1 and ranged from 0.6% to 2.1% at 500 psi net stress. At the next highest net stress (870 psi), porosity measurements could be made on 16 samples. The reduction in porosity from 500 to 870 psi ranged from zero to 12%. Porosity at 1450 psi was only successfully measured on three samples. Porosity, grain density and permeability data for these samples is given in Table 4.1. A plot of the distribution of grain densities is shown in Figure 4.1. Klinkenberg permeability, (K_1) was computed from air permeability measurements at multiple upstream injection pressures. Linear least squares regressions were computed to obtain the slope and intercept of the apparent permeability versus $1/P_{\text{mean}}$. K_1 was rounded to the nearest $\pm 1 \times 10^{-6}$ md. Values of K_1 less than 1×10^{-5} md were not reported. Plots of Klinkenberg permeability (K_1) versus porosity at 500 psi and 870 psi net stress are given in Figure 4.2. The permeability of the samples at 500 psi net stress ranged from about 4×10^{-4} to about 2×10^{-3} millidarcy. The permeability of the samples at 850 psi net stress ranged from about 1×10^{-4} to about 2×10^{-3} millidarcy. The permeability of the samples at 1450 psi net stress ranged from about 5×10^{-5} to about 1×10^{-3} millidarcy.

4.2 Capillary Pressure Sample Selection

To decide which pairs of samples to use for capillary pressure testing, we looked for two major characteristics; (1) adequate permeability and porosity for testing, and (2) reasonable similarity

Test Procedures and QA Plan: Capillary Pressure Measurements in Anhydrite

between the two samples in each pair as evidenced by the x-ray photos, quantitative XRD, porosity, and permeability data. Based on these criteria, S. Howarth and J. Walls selected the six pairs of samples indicated by asterisks in Table 4.1. After choosing these six samples, axial X-ray CT slices were made at two orientations to get a more detailed picture of the distribution of anhydrite (light) and halite (dark) in each sample. These scans were made with a high energy (420 kV) industrial scanner with a resolution of 0.25 mm. The CT slices for the capillary pressure samples are shown in Figures 4.3 to 4.8. We will refer to the different amounts and distributions of the two major minerals in the discussion of capillary pressure results. More importantly though, is that each sample in a pair is similar to the other, and there does not appear to be any physical damage to the samples on the scale detectable with CT scanning.

4.3 Centrifuge Results

The centrifuge air-decane capillary pressure curves are shown in Figures 4.9 through 4.14. The curves were produced using the Hassler-Brunner method. The initial pressure in each plot is 5 psi and the final pressure is 650 psi. This corresponds to centrifuge rotational speeds from 1720 rpm to 17660 rpm. The starting rotational speed was chosen by the Core Labs based on the experimental procedure which expected high entry pressures relative to most oil and gas reservoir rock. Normally the starting speed would be about 300 RPM to correspond to a pressure of about 1 psi. The ending rotational speed is controlled by the limits of the experimental apparatus.

The Hassler-Brunner results are presented because the critical ratio R_1/R_3 (as shown in Figure 2.3) does not exceed 0.7, a requirement for successful application of this method^{9,10,11}. To ensure that errors in this method were small, data reduction was also performed using the Rajan¹⁹ method. The differences between the two in terms of calculated end face saturations were typically less than 1% of pore volume. In these comparisons, the sample pore volume used for data reduction was measured by the CMS-300 at 500 psi net stress, and rounded to the nearest 0.01 cm³. It should be noted that the fluid volume resolution for this system was about +/- 0.005 cm³ or about 2.5% of pore volume.

The oil saturation at the lowest capillary pressure of 5 psi varies from about 85% to 95% for the six samples tested. This means that the entry pressure to oil for all samples was less than 5 psi. Final oil saturations at 650 psi ranged from about 11% to 45%. The general appearance of the curves, with the concave downward shape or "knee" at about 80% to 90% liquid saturation suggests a bi-modal or multi-modal pore size distribution. The relatively low value of the final liquid saturation (for all samples except 14) suggests that the samples do not contain a significant amount of microporosity.

Test Procedures and QA Plan: Capillary Pressure Measurements in Anhydrite

4.4 Mercury Injection Results

Mercury injection capillary pressure curves are shown in Figures 4.15 to 4.20. Pore volume for the mercury injection samples was measured by the CMS-300 at 500 psi net confining stress, consistent with the centrifuge pore volumes. The starting pressure for these tests was about 1.5 psi and the final pressure was about 50,000 psi. This provided a more complete capillary pressure curve from 100% wetting phase saturation to final wetting phase saturations which ranged from about 8% to about 23% for the six samples tested. A similar behavior to the centrifuge results in terms of the downward bend in the curve at higher wetting phase saturations was noted. The relatively low final wetting phase saturation is also similar to the centrifuge results. The entry pressure to mercury was defined for these samples by plotting the volume injected versus the injection pressure. There is a sharp break in the slope of this line corresponding to threshold entry pressure. These mercury injection results, converted to the air/brine system, will be discussed in Section 4.5.

4.5 Comparison and Conversion to Air Water System

Conversion of capillary pressure from one fluid/fluid system to another (i.e. mercury/air to brine/air) is performed using the following equation;

$$P_{c2} = P_{c1} \left(\frac{T_2 \cos \phi_2}{T_1 \cos \phi_1} \right) \quad (3)$$

where;

P_c = capillary pressure,

T = surface tension, and

ϕ = the contact angle at the fluid/solid interface

subscripts 1 and 2 refer to the different fluid systems.

For the fluids used in this study, we used the values shown in Table 4.5.1^{16,21}.

Surface Tension and Contact Angle of Experimental Fluid Systems

Fluid System	T (dynes/cm)	ϕ (degrees)
air/decane	24	0
air/brine	72	0
air/Hg	485	140 (180)

The following example shows how air/decane capillary pressure is converted to air/brine using Equation 3.

$$P_{c \text{ air / brine}} = P_{c \text{ air / decane}} \left(\frac{T_{\text{air/brine}} \cos \phi_{\text{air/brine}}}{T_{\text{air/decane}} \cos \phi_{\text{air/decane}}} \right) \quad (4)$$

Test Procedures and QA Plan: Capillary Pressure Measurements in Anhydrite

$$P_{c \text{ air / brine}} = P_{c \text{ air / decane}} \left(\frac{72 \cos \theta}{24 \cos \theta} \right) = 3 P_{c \text{ air / decane}} \quad (5)$$

This means that to convert air/decane capillary pressures to air/brine we multiply by 3. Similarly, to convert air/Hg to air/brine we divide by 5.16 or 6.74 depending upon whether 140 degrees or 180 degrees respectively is used. The negative sign resulting from the cosine of theta for mercury indicates that the air is the wetting phase and mercury is the non-wetting phase.

Capillary pressure curves for all samples in this project were converted to the air/brine system and are shown in Figures 4.21 through 4.26. The cross-reference between the lab sample numbers used in these figures and the Sandia sample I.D. is in Table 4.1. All capillary pressure samples except 7, 8, 13, and 14 were horizontal plugs. The (A) plots show the comparison using the assumption that theta for air/Hg is 140 degrees, and the (B) plots show the results if 180 degrees is used, as recommended by Good and Mikhail²². The effect of assuming contact angle is 140 versus 180 is relatively small, amounting to a difference in converted air-brine capillary pressure of only about 30%. This data does not strongly support one assumption over the other, but for consistency with most literature on the subject, we will focus on the 140 degree contact angle results in this discussion.

For sample pairs 7-8 and 11-12, the wetting phase saturation at 1000 psi equivalent air brine capillary pressure from centrifuge is substantially lower than from mercury injection. The ending saturation from centrifuge is substantially higher than for mercury in samples pairs 13-14 and 23-24. However, the portion of the curve above 50% wetting phase saturation is of greater interest because it is unlikely that water saturation in the Salado formation *in-situ* would ever be less than 50%. In this region, there is remarkably close agreement between the centrifuge and mercury results for all sample pairs except 13-14. Also, we do not expect the curves to match exactly because there are differences between the two samples in each pair as evidenced by the data in Table 4.1 and the CT scans in Figures 4.3 to 4.8. Note that there is no indication in any of this data that the entry pressure to brine ever exceeds about 15 psi. Tabular data for the mercury injection plots is presented in Tables 4.2 to 4.13. Tabular data for the centrifuge capillary pressure is on the plots (Figures 4.9 to 4.14).

The converted brine entry pressure for the samples is considerably lower than would be expected if the samples were tight sandstones with the same permeability. For example, Figure 4.27 shows a plot of entry pressure versus Klinkenberg (intrinsic) permeability for a group of tight gas sands²⁰, for a compilation of data on oil field rocks²¹, and for the MB 139 anhydrite samples in this project.

Test Procedures and QA Plan: Capillary Pressure Measurements in Anhydrite

types of rock are quite different. The thin section results presented in Appendix B show that porosity in the anhydrite sample is so low as to be all but invisible. Porosity in the tight sandstones ranges from about 5 to 15%, and the low permeability is often caused by clay minerals formed in the pores after deposition. The evaporitic nature of these anhydrite samples would suggest that significant differences from shaly clastics could be expected. Therefore, drawing conclusions about the capillary pressure vs. permeability behavior of the anhydrites from experience with sandstones is not recommended.

5.0 Conclusions and Recommendations

Based on these tests, we find several important results concerning porosity, permeability, and capillary pressure in the MB 139 anhydrite samples tested;

- 1 Porosity ranges from about 0.6 to 2.1 percent and K_a ranges from about 0.026 md to about 0.001 md at 500 psi net stress, as defined by Equation 2.
- 2 Using Hassler-Brunner versus Rajan data reduction methods for the centrifuge end face saturations make no significant difference, probably because the sample lengths were short enough to keep the ratio of R_1/R_3 below 0.7.
- 3 Using a contact angle for air/Hg of 180 degrees, as recommended by Good and Mikhail²², produces converted air/brine capillary pressures that are about 30% lower than if the more commonly assumed angle of 140 degrees is used.
- 4 Mercury and air/brine capillary pressures match fairly well, especially at the higher wetting phase saturations, and the difference in results between 140 degrees or 180 degrees for contact angle in the air/Hg system is negligible. Based on these six samples, we cannot recommend one contact angle value over the other.
- 5 Air/brine threshold entry pressures computed from the six Hg injection samples range from about 1 to 4 psi (.007 to 0.028 Mpa). Air/brine threshold entry pressure from the centrifuge tests could not be determined exactly, but the data shows that for all samples the value is less than 15 psi (0.1 MPa).

We recommend that in future work on capillary pressure of the anhydrite, the experimental systems and procedures should be adjusted to more accurately define the low threshold entry pressure

Test Procedures and QA Plan: Capillary Pressure Measurements in Anhydrite

values. For example, centrifuge tests could be started at a lower centrifuge speed and the Hg injection system could be set to measure the range below 1 psi. Also, it would be useful to test some samples using an overburden system to verify the estimated effect of stress on entry pressure.

6.0 References

- 1 Harbach, F., and H. Nienburg; "Mercury Pressure Porosimetry as an Accessory to the Development of Shaping and Firing Techniques for Dense Ceramic Components," *Ceramic Forum International* v 64 no. 10, Oct., 1987 p 394-397.
- 2 Ciftcioglu, M., D. Smith, and S. Ross; "Sintering Studies on Ordered Monodisperse Silica Compacts - Effect of Consolidation," *Powder Technology*, v 69, No. 2, Feb, 1992, pp 185-193.
- 3 Gelinas, C., and R. Angens; "Improvement of the Dynamic Water Expulsion Method for Pore Size Distribution Measurements," *American Ceramic Society Bulletin*, v. 65, No. 9, Sept. 1986, pp 1297-1300.
- 4 McCullough, J.J., F.W. Albaugh, and P.H. Jones; "Determination of the Interstitial Water Content of Oil and Gas Sand by Laboratory Tests of Core Samples", *API Drilling and Production Practice* (180), 1944.
- 5 Thornton, O.F. and D.L. Marshall; "Estimating Interstitial Water by the Capillary Pressure Method," *Trans. AIME*, Vol. 170, 1947, pp 69-80.
- 6 Bruce, W.A. and H.G. Welge; "Restored State Method for Determination of Oil in Place and Connate Water," *Oil and Gas Journal*, Vol. 46, 1947, p 223.
- 7 Rose, W. and W.A. Bruce; "Evaluation of Capillary Character in Petroleum Reservoir Rock," *Trans. AIME* Vol. 186, 1949, pp 39-48.
- 8 Calhoun, J.C, M. Lewis, and R.C. Newman; "Experiments on the Capillary Properties of Porous Solids"; *Petr. Trans. AIME*, July, 1949, pp 189-196.
- 9 Hassler, G.L. and E. Brunner; "Measurement of Capillary Pressures in Small Core Samples," *Trans., AIME* (192), 1945, p 114
- 10 Christiansen, R.L.; "Geometric Concerns for Accurate Measurement of Capillary Pressure with Centrifuge Methods," *SPE Form. Eval.*, December, 1992, 311-314
- 11 Melrose, J.C.; "Interpretation of Centrifuge Capillary Pressure Data," *The Log Analyst*, Jan.-Feb, 1988, pp 40-47.
- 12 Chen, Zhigang, Huiqing Liu, and Jun Yao; "New Capillary Pressure Models for Parameter Estimation to Interpret Centrifuge Data," SPE paper 24045, presented at the SPE Western Regional Meeting, Bakersfield, CA, March 30- April 1, 1992.
- 13 Omoregie, Z.S., "Factors Affecting the Equivalency of Different Capillary Pressure Measurement Techniques," SPE paper 15384, presented at the SPE Annual Technical Conference, New Orleans, LA, October 5-8, 1986.

Test Procedures and QA Plan: Capillary Pressure Measurements in Anhydrite

- 14 Purcell, W.R., "Capillary Pressures-Their Measurement Using Mercury Injection and the Calculation of Permeability Therefrom"; Petroleum Trans., AIME, Feb, 1949
- 15 Melrose, J.C., J.R. Dixon, and J.E. Mallinson, 1991; "Comparison of Different Techniques for Obtaining Capillary Pressure Data in the Low Saturation Region," SPE 22690 presented at the 66th Annual Technical Conference and Exhibition, Dallas, TX, Oct 6-9, 1991.
- 16 Ward, J.S., and N.R. Morrow; "Capillary Pressure and Gas Relative Permeability of Low Permeability Sandstone," SPE/DOE 13882, presented at the Low Permeability Symposium, Denver, CO, May 19-22, 1985.
- 17 Walls, J.D. and S. Howarth; "Test Procedures and Quality Assurance Plan: Porosity, Permeability and Capillary Pressure Measurements in Anhydrite Samples from the WIPP," Sandia internal report, May 24, 1993.
- 18 Core Laboratories; "Operators Manual for CMS-300", by Core Laboratories Inc., Houston, TX, 1988.
- 19 Rajan, R.R.; "Theoretically Correct Analytical Solution for Calculating Capillary Pressure Curves From Centrifuge Experiments" SPWLA 27th Annual Logging Symposium, Houston, TX, June 9-13, 1986.
- 20 Walls, J.D., and J.O. Amaefule; "Capillary Pressure and Permeability Relationships in Tight Gas Sands", SPE/DOE 13879, presented at the Low Permeability Gas Reservoirs Symposium, Denver, CO, May, 19-22, 1985.
- 21 Davies, Peter B., "Evaluation of the Role of Threshold Pressure in Controlling Flow of Waste Generated Gas into Bedded Salt at the Waste Isolation Pilot Plant," Sandia Report Sand90-3246, UC-721, June, 1991.
- 22 Good, Robert J., and R.S. Mikhail; "The Contact Angle in Mercury Intrusion Porosimetry", Powder Technology, 29, 1981, pp 53-62

Table 4.1: Porosity and Air Permeability at Three Net Confining Stresses

Core Lab ID	Sandia ID	Net Stress psi	Gr. Dens. g/cc	Porosity %	Klinkenberg Perm., md	Cap. Press. Method
1	E1X 10-6 / 4.5A	500	2.637	0.6		
		870				
		1450				
2	E1X 10-6 / 4.5B	500	2.587	0.8	0.000647	
		870		0.7	0.000462	
		1450			0.000278	
3	E1X 10-6 / 5.0A	500	2.489	0.8		
		870				
		1450				
4	E1X 10-6 / 5.0B	500	2.624	0.9	0.001278	
		870		0.9	0.000880	
		1450			0.000646	
5*	E1X 10-6 / 5.25A	500	2.620	0.7	0.000513	Merc. Inject.
		870		0.6	0.000381	
		1450			0.000180	
6*	E1X 10-6 / 5.25B	500	2.617	0.7	0.000581	Centrifuge
		870			0.000297	
		1450			0.000050	
7*	E1X 10-6 / 5.25C1	500	2.953	1.1	0.000948	Merc. Inject.
		870		1.0	0.000549	
		1450				
8*	E1X 10-6 / 5.25C2	500	2.955	1.1	0.000822	Centrifuge
		870		1.0	0.000488	
		1450			0.000138	
9	E1X 10-6 / 5.5A	500	2.848	0.9	0.000535	
		870				
		1450				
10	E1X 10-6 / 5.5B	500	2.943	1.0	0.001083	
		870			0.000176	
		1450				
11*	E1X 10-6 / 5.75A	500	2.888	1.7	0.001804	Merc. Inject.
		870		1.7	0.001559	
		1450		1.6	0.001138	
12*	E1X 10-6 / 5.75B	500	2.923	1.4	0.001364	Centrifuge
		870		1.3	0.001016	
		1450			0.000734	
13*	E1X 10-6 / 5.75C1	500	2.960	1.6	0.001622	Merc. Inject.
		870		1.5	0.000308	
		1450		1.5		
14*	E1X 10-6 / 5.75C2	500	2.946	1.2	0.000611	
		870		1.1	0.000311	
		1450			0.000172	
15	E1X 10-7 / 6.25C1	500	2.962	1.0	0.000594	
		870		0.9	0.000128	
		1450			0.000064	

Table 4.1: Porosity and Air Permeability at Three Net Confining Stresses

(Continued)						
Lab ID	Sandia ID	Net Stress	Gr. Dens.	Porosity	KI	Cap. Press.
		psi	g/cc	%	md	Method
16	E1X 10-7 / 6.25C2	500	2.961	0.6	0.000439	
		870				
		1450				
17	E1X 11-6 / 4.5A	500	2.628	0.8	0.000407	
		870			0.000337	
		1450			0.000101	
18	E1X 11-6 / 4.5B	500	2.630	1.8		
		870				
		1450				
19	E1X 11-6 / 4.75A	500	2.719	0.9	0.000474	
		870			0.000323	
		1450			0.000101	
20	E1X 11-6 / 4.75B	500	2.795	0.9	0.000393	
		870		0.8		
		1450				
21*	E1X 11-6 / 5.0A	500	2.822	1.1	0.000767	Merc. Inject.
		870		1.0	0.000566	
		1450			0.000265	
22*	E1X 11-6 / 5.0B	500	2.690	1.4	0.001482	Centrifuge
		870		1.3	0.000843	
		1450				
23*	E1X 11-6 / 5.25A	500	2.650	2.1	0.001313	Merc. Inject.
		870			0.000585	
		1450				
24*	E1X 11-6 / 5.25B	500	2.674	1.4	0.001515	Centrifuge
		870		1.4	0.000569	
		1450				
25	E1X 11-6 / 5.25C1	500	2.613	0.9	0.001996	
		870		0.8	0.000563	
		1450			0.000293	
26	E1X 11-6 / 5.25C2	500	2.742	1.6	0.002189	
		870			0.000747	
		1450			0.000333	
27	E1X 11-6 / 5.75A	500	2.750	1.6		
		870		1.4		
		1450		1.2		
28	E1X 11-6 / 5.75B	500	2.906			
		870				
		1450				
29	E1X 11-6 / 5.75C1	500	2.959	0.8		
		870				
		1450				
30	E1X 11-6 / 5.75C2	500	2.961	1.0	0.001458	
		870			0.000590	
		1450				

* Indicates capillary pressure sample

TABLE 4.2
MERCURY INJECTION DATA SUMMARY

Sandia National Laboratories
Waste Isolation Pilot Plant
Core: E1X 10-6

Sample Number
File: DAL-93089

5

Contact Angle = 140

Injection Pressure, psia	Mercury Saturation, fraction	1.0-Mercury Saturation, fraction	Other Laboratory Systems		
			Gas-Water, psia	Gas-Oil, psia	Oil-Water, psia
1.5	0.000	1.000	0.30	0.10	0.17
3.0	0.000	1.000	0.58	0.19	0.33
6.0	0.000	1.000	1.2	0.39	0.67
9.0	0.000	1.000	1.7	0.58	1.0
12	0.040	0.960	2.3	0.77	1.3
18	0.040	0.960	3.5	1.2	2.0
25	0.080	0.920	4.8	1.6	2.8
35	0.080	0.920	6.8	2.3	3.9
45	0.120	0.880	8.7	2.9	5.0
55	0.120	0.880	11	3.5	6.1
75	0.120	0.880	14	4.8	8.4
100	0.120	0.880	19	6.5	11
124	0.160	0.840	24	8.0	14
159	0.160	0.840	31	10	18
181	0.160	0.840	35	12	20
200	0.160	0.840	39	13	22
304	0.200	0.800	59	20	34
398	0.200	0.800	77	26	45
499	0.240	0.760	97	32	56
749	0.320	0.680	145	48	84
997	0.400	0.600	193	64	112
1252	0.440	0.560	243	81	140
1603	0.559	0.441	311	104	179
1996	0.599	0.401	387	129	223
2497	0.599	0.401	484	161	279
3489	0.639	0.361	676	225	390
4255	0.639	0.361	825	275	476
4998	0.679	0.321	968	323	559
6973	0.719	0.281	1351	450	780
9965	0.719	0.281	1931	644	1115
12465	0.759	0.241	2416	805	1395
14950	0.839	0.161	2897	966	1673
19920	0.879	0.121	3860	1287	2229
24925	0.879	0.121	4830	1610	2789
29905	0.879	0.121	5795	1932	3346
34908	0.919	0.081	6765	2255	3906
39861	0.919	0.081	7725	2575	4460
44935	0.919	0.081	8708	2903	5028
49759	0.919	0.081	9643	3214	5567

TABLE 4.3
MERCURY INJECTION DATA SUMMARY

Sandia National Laboratories
Waste Isolation Pilot Plant
Core: E1X 10-6

Sample Number 5
File: DAL-93089

Contact Angle = 180

Injection Pressure, psia	Mercury Saturation, fraction	1.0-Mercury Saturation, fraction	Other Laboratory Systems		
			Gas-Water, psia	Gas-Oil, psia	Oil-Water, psia
1.5	0.000	1.000	0.23	0.08	0.13
3.0	0.000	1.000	0.44	0.15	0.26
6.0	0.000	1.000	0.89	0.30	0.51
9.0	0.000	1.000	1.3	0.44	0.77
12	0.040	0.960	1.8	0.59	1.0
18	0.040	0.960	2.7	0.89	1.5
25	0.080	0.920	3.7	1.2	2.1
35	0.080	0.920	5.2	1.7	3.0
45	0.120	0.880	6.7	2.2	3.8
55	0.120	0.880	8.2	2.7	4.7
75	0.120	0.880	11	3.7	6.4
100	0.120	0.880	15	4.9	8.6
124	0.160	0.840	18	6.2	11
159	0.160	0.840	24	7.9	14
181	0.160	0.840	27	9.0	16
200	0.160	0.840	30	9.9	17
304	0.200	0.800	45	15	26
398	0.200	0.800	59	20	34
499	0.240	0.760	74	25	43
749	0.320	0.680	111	37	64
997	0.400	0.600	148	49	85
1252	0.440	0.560	186	62	107
1603	0.559	0.441	238	79	137
1996	0.599	0.401	296	99	171
2497	0.599	0.401	371	124	214
3489	0.639	0.361	518	173	299
4255	0.639	0.361	632	211	365
4998	0.679	0.321	742	247	428
6973	0.719	0.281	1035	345	598
9965	0.719	0.281	1479	493	854
12465	0.759	0.241	1850	617	1068
14950	0.839	0.161	2219	740	1281
19920	0.879	0.121	2957	986	1707
24925	0.879	0.121	3700	1233	2136
29905	0.879	0.121	4440	1480	2563
34908	0.919	0.081	5182	1727	2992
39861	0.919	0.081	5917	1972	3416
44935	0.919	0.081	6671	2224	3851
49759	0.919	0.081	7387	2462	4265

TABLE 4.4
MERCURY INJECTION DATA SUMMARY

Sandia National Laboratories
Waste Isolation Pilot Plant
Core: E1X 10-6

Sample Number 7
File: DAL-93089

Contact Angle = 140

Injection Pressure, psia	Mercury Saturation, fraction	1.0-Mercury Saturation, fraction	Other Laboratory Systems		
			Gas-Water, psia	Gas-Oil, psia	Oil-Water, psia
1.5	0.000	1.000	0.29	0.10	0.17
3.0	0.000	1.000	0.58	0.19	0.34
6.0	0.000	1.000	1.2	0.39	0.67
9.0	0.000	1.000	1.7	0.58	1.0
12	0.026	0.974	2.3	0.77	1.3
18	0.026	0.974	3.5	1.2	2.0
25	0.052	0.948	4.8	1.6	2.8
35	0.078	0.922	6.8	2.3	3.9
45	0.078	0.922	8.7	2.9	5.0
55	0.078	0.922	11	3.6	6.2
75	0.104	0.896	15	4.9	8.4
101	0.104	0.896	20	6.5	11
126	0.130	0.870	24	8.1	14
161	0.130	0.870	31	10	18
179	0.130	0.870	35	12	20
200	0.130	0.870	39	13	22
300	0.156	0.844	58	19	34
402	0.182	0.818	78	26	45
500	0.208	0.792	97	32	56
753	0.234	0.766	146	49	84
1007	0.260	0.740	195	65	113
1246	0.286	0.714	241	80	139
1598	0.338	0.662	310	103	179
1993	0.390	0.610	386	129	223
2495	0.442	0.558	483	161	279
3493	0.494	0.506	677	226	391
4247	0.546	0.454	823	274	475
4978	0.597	0.403	965	322	557
6985	0.649	0.351	1354	451	782
9976	0.701	0.299	1933	644	1116
12443	0.753	0.247	2411	804	1392
14932	0.805	0.195	2894	965	1671
19941	0.857	0.143	3864	1288	2231
24900	0.857	0.143	4825	1608	2786
29876	0.857	0.143	5790	1930	3343
34873	0.883	0.117	6758	2253	3902
39853	0.883	0.117	7723	2574	4459
44917	0.883	0.117	8705	2902	5026
49965	0.883	0.117	9683	3228	5590

TABLE 4.5
MERCURY INJECTION DATA SUMMARY

Sandia National Laboratories
Waste Isolation Pilot Plant
Core: E1X 10-6

Sample Number
File: DAL-93089

7

Contact Angle = 180

Injection Pressure, psia	Mercury Saturation, fraction	1.0-Mercury Saturation, fraction	Other Laboratory Systems		
			Gas-Water, psia	Gas-Oil, psia	Oil-Water, psia
1.5	0.000	1.000	0.23	0.08	0.13
3.0	0.000	1.000	0.45	0.15	0.26
6.0	0.000	1.000	0.89	0.30	0.51
9.0	0.000	1.000	1.3	0.44	0.77
12	0.026	0.974	1.8	0.59	1.0
18	0.026	0.974	2.7	0.89	1.5
25	0.052	0.948	3.7	1.2	2.1
35	0.078	0.922	5.2	1.7	3.0
45	0.078	0.922	6.7	2.2	3.9
55	0.078	0.922	8.2	2.7	4.7
75	0.104	0.896	11	3.7	6.4
101	0.104	0.896	15	5.0	8.6
126	0.130	0.870	19	6.2	11
161	0.130	0.870	24	7.9	14
179	0.130	0.870	27	8.9	15
200	0.130	0.870	30	9.9	17
300	0.156	0.844	45	15	26
402	0.182	0.818	60	20	34
500	0.208	0.792	74	25	43
753	0.234	0.766	112	37	65
1007	0.260	0.740	149	50	86
1246	0.286	0.714	185	62	107
1598	0.338	0.662	237	79	137
1993	0.390	0.610	296	99	171
2495	0.442	0.558	370	123	214
3493	0.494	0.506	519	173	299
4247	0.546	0.454	631	210	364
4978	0.597	0.403	739	246	427
6985	0.649	0.351	1037	346	599
9976	0.701	0.299	1481	494	855
12443	0.753	0.247	1847	616	1067
14932	0.805	0.195	2217	739	1280
19941	0.857	0.143	2960	987	1709
24900	0.857	0.143	3696	1232	2134
29876	0.857	0.143	4435	1478	2561
34873	0.883	0.117	5177	1726	2989
39853	0.883	0.117	5916	1972	3416
44917	0.883	0.117	6668	2223	3850
49965	0.883	0.117	7417	2472	4282

TABLE 4.6
MERCURY INJECTION DATA SUMMARY

Sandia National Laboratories
Waste Isolation Pilot Plant
Core: E1X 10-6

Sample Number
File: DAL-93089

11

Contact Angle = 140

Injection Pressure, psia	Mercury Saturation, fraction	1.0-Mercury Saturation, fraction	Other Laboratory Systems		
			Gas-Water, psia	Gas-Oil, psia	Oil-Water, psia
1.5	0.000	1.000	0.30	0.10	0.17
3.0	0.000	1.000	0.58	0.19	0.33
6.0	0.000	1.000	1.2	0.39	0.67
9.0	0.000	1.000	1.7	0.58	1.0
12	0.000	1.000	2.3	0.77	1.3
18	0.016	0.984	3.5	1.2	2.0
25	0.016	0.984	4.8	1.6	2.8
35	0.032	0.968	6.8	2.3	3.9
45	0.032	0.968	8.7	2.9	5.0
55	0.032	0.968	11	3.6	6.2
75	0.032	0.968	15	4.8	8.4
100	0.032	0.968	19	6.5	11
125	0.032	0.968	24	8.0	14
159	0.048	0.952	31	10	18
181	0.064	0.936	35	12	20
200	0.079	0.921	39	13	22
304	0.143	0.857	59	20	34
398	0.191	0.809	77	26	45
499	0.207	0.793	97	32	56
749	0.271	0.729	145	48	84
997	0.335	0.665	193	64	112
1251	0.382	0.618	242	81	140
1603	0.430	0.570	311	104	179
1995	0.494	0.506	387	129	223
2497	0.590	0.410	484	161	279
3488	0.590	0.410	676	225	390
4254	0.621	0.379	824	275	476
4997	0.637	0.363	968	323	559
6972	0.669	0.331	1351	450	780
9964	0.701	0.299	1931	644	1115
12464	0.717	0.283	2415	805	1395
14949	0.717	0.283	2897	966	1673
19919	0.733	0.267	3860	1287	2229
24924	0.749	0.251	4830	1610	2789
29904	0.765	0.235	5795	1932	3346
34907	0.765	0.235	6765	2255	3906
39860	0.765	0.235	7725	2575	4460
44934	0.765	0.235	8708	2903	5028
49758	0.765	0.235	9643	3214	5567

TABLE 4.7
MERCURY INJECTION DATA SUMMARY

Sandia National Laboratories
Waste Isolation Pilot Plant
Core: E1X 10-6

Sample Number
File: DAL-93089

11

Contact Angle = 180

Injection Pressure, psia	Mercury Saturation, fraction	1.0-Mercury Saturation, fraction	Other Laboratory Systems		
			Gas-Water, psia	Gas-Oil, psia	Oil-Water, psia
1.5	0.000	1.000	0.23	0.08	0.13
3.0	0.000	1.000	0.44	0.15	0.26
6.0	0.000	1.000	0.89	0.30	0.51
9.0	0.000	1.000	1.3	0.44	0.77
12	0.000	1.000	1.8	0.59	1.0
18	0.016	0.984	2.7	0.89	1.5
25	0.016	0.984	3.7	1.2	2.1
35	0.032	0.968	5.2	1.7	3.0
45	0.032	0.968	6.7	2.2	3.9
55	0.032	0.968	8.2	2.7	4.7
75	0.032	0.968	11	3.7	6.4
100	0.032	0.968	15	5.0	8.6
125	0.032	0.968	18	6.2	11
159	0.048	0.952	24	7.9	14
181	0.064	0.936	27	9.0	16
200	0.079	0.921	30	9.9	17
304	0.143	0.857	45	15	26
398	0.191	0.809	59	20	34
499	0.207	0.793	74	25	43
749	0.271	0.729	111	37	64
997	0.335	0.665	148	49	85
1251	0.382	0.618	186	62	107
1603	0.430	0.570	238	79	137
1995	0.494	0.506	296	99	171
2497	0.590	0.410	371	124	214
3488	0.590	0.410	518	173	299
4254	0.621	0.379	632	211	365
4997	0.637	0.363	742	247	428
6972	0.669	0.331	1035	345	598
9964	0.701	0.299	1479	493	854
12464	0.717	0.283	1850	617	1068
14949	0.717	0.283	2219	740	1281
19919	0.733	0.267	2957	986	1707
24924	0.749	0.251	3700	1233	2136
29904	0.765	0.235	4439	1480	2563
34907	0.765	0.235	5182	1727	2992
39860	0.765	0.235	5917	1972	3416
44934	0.765	0.235	6671	2224	3851
49758	0.765	0.235	7387	2462	4265

TABLE 4.8
MERCURY INJECTION DATA SUMMARY

Sandia National Laboratories
Waste Isolation Pilot Plant
Core: E1X 10-6

Sample Number
File: DAL-93089

13

Contact Angle = 140

Injection Pressure, psia	Mercury Saturation, fraction	1.0-Mercury Saturation, fraction	Other Laboratory Systems		
			Gas-Water, psia	Gas-Oil, psia	Oil-Water, psia
1.5	0.000	1.000	0.29	0.10	0.17
3.0	0.000	1.000	0.58	0.19	0.34
6.0	0.018	0.982	1.2	0.39	0.67
9.0	0.036	0.964	1.7	0.58	1.0
12	0.036	0.964	2.3	0.77	1.3
18	0.036	0.964	3.5	1.2	2.0
25	0.073	0.927	4.8	1.6	2.8
35	0.073	0.927	6.8	2.3	3.9
45	0.073	0.927	8.7	2.9	5.0
55	0.091	0.909	11	3.6	6.2
75	0.091	0.909	15	4.8	8.4
100	0.091	0.909	19	6.4	11
125	0.091	0.909	24	8.1	14
160	0.127	0.873	31	10	18
180	0.145	0.855	35	12	20
200	0.145	0.855	39	13	22
300	0.218	0.782	58	19	34
400	0.236	0.764	77	26	45
498	0.254	0.746	96	32	56
746	0.291	0.709	145	48	84
996	0.345	0.655	193	64	111
1246	0.382	0.618	241	80	139
1593	0.418	0.582	309	103	178
1994	0.509	0.491	386	129	223
2490	0.600	0.400	483	161	279
3493	0.600	0.400	677	226	391
4247	0.600	0.400	823	274	475
4991	0.636	0.364	967	322	558
6972	0.672	0.328	1351	450	780
9972	0.708	0.292	1932	644	1116
12476	0.745	0.255	2418	806	1396
14944	0.799	0.201	2896	965	1672
19933	0.799	0.201	3863	1288	2230
24903	0.836	0.164	4826	1609	2786
29899	0.836	0.164	5794	1931	3345
34832	0.836	0.164	6750	2250	3897
39825	0.854	0.146	7718	2573	4456
44921	0.854	0.146	8705	2902	5026
49791	0.854	0.146	9649	3216	5571

TABLE 4.9
MERCURY INJECTION DATA SUMMARY

Sandia National Laboratories
Waste Isolation Pilot Plant
Core: E1X 10-6

Sample Number
File: DAL-93089

13

Contact Angle = 180

Injection Pressure, psia	Mercury Saturation, fraction	1.0-Mercury Saturation, fraction	Other Laboratory Systems		
			Gas-Water, psia	Gas-Oil, psia	Oil-Water, psia
1.5	0.000	1.000	0.23	0.08	0.13
3.0	0.000	1.000	0.45	0.15	0.26
6.0	0.018	0.982	0.89	0.30	0.51
9.0	0.036	0.964	1.3	0.44	0.77
12	0.036	0.964	1.8	0.59	1.0
18	0.036	0.964	2.7	0.89	1.5
25	0.073	0.927	3.7	1.2	2.1
35	0.073	0.927	5.2	1.7	3.0
45	0.073	0.927	6.7	2.2	3.9
55	0.091	0.909	8.2	2.7	4.7
75	0.091	0.909	11	3.7	6.4
100	0.091	0.909	15	4.9	8.5
125	0.091	0.909	19	6.2	11
160	0.127	0.873	24	7.9	14
180	0.145	0.855	27	8.9	15
200	0.145	0.855	30	9.9	17
300	0.218	0.782	44	15	26
400	0.236	0.764	59	20	34
498	0.254	0.746	74	25	43
746	0.291	0.709	111	37	64
996	0.345	0.655	148	49	85
1246	0.382	0.618	185	62	107
1593	0.418	0.582	236	79	137
1994	0.509	0.491	296	99	171
2490	0.600	0.400	370	123	213
3493	0.600	0.400	519	173	299
4247	0.600	0.400	631	210	364
4991	0.636	0.364	741	247	428
6972	0.672	0.328	1035	345	598
9972	0.708	0.292	1480	493	855
12476	0.745	0.255	1852	617	1069
14944	0.799	0.201	2218	739	1281
19933	0.799	0.201	2959	986	1708
24903	0.836	0.164	3697	1232	2134
29899	0.836	0.164	4439	1480	2563
34832	0.836	0.164	5171	1724	2985
39825	0.854	0.146	5912	1971	3413
44921	0.854	0.146	6669	2223	3850
49791	0.854	0.146	7392	2464	4268

TABLE 4.10
MERCURY INJECTION DATA SUMMARY

Sandia National Laboratories
Waste Isolation Pilot Plant
Core: E1X 11-6

Sample Number 21
File: DAL-93089

Contact Angle = 140

Injection Pressure, psia	Mercury Saturation, fraction	1.0-Mercury Saturation, fraction	Other Laboratory Systems		
			Gas-Water, psia	Gas-Oil, psia	Oil-Water, psia
1.5	0.000	1.000	0.29	0.10	0.17
3.0	0.000	1.000	0.58	0.19	0.34
6.0	0.000	1.000	1.2	0.39	0.67
9.0	0.026	0.974	1.7	0.58	1.0
12	0.026	0.974	2.3	0.77	1.3
18	0.051	0.949	3.5	1.2	2.0
25	0.051	0.949	4.8	1.6	2.8
35	0.051	0.949	6.7	2.2	3.9
45	0.051	0.949	8.7	2.9	5.0
55	0.051	0.949	11	3.6	6.2
75	0.051	0.949	15	4.8	8.4
99	0.077	0.923	19	6.4	11
125	0.077	0.923	24	8.1	14
160	0.077	0.923	31	10	18
180	0.077	0.923	35	12	20
200	0.077	0.923	39	13	22
300	0.127	0.873	58	19	34
400	0.178	0.822	78	26	45
498	0.229	0.771	96	32	56
746	0.357	0.643	145	48	84
996	0.433	0.567	193	64	111
1246	0.484	0.516	241	80	139
1593	0.560	0.440	309	103	178
1994	0.662	0.338	386	129	223
2490	0.662	0.338	483	161	279
3494	0.713	0.287	677	226	391
4248	0.738	0.262	823	274	475
4992	0.738	0.262	967	322	558
6972	0.789	0.211	1351	450	780
9972	0.815	0.185	1932	644	1116
12476	0.840	0.160	2418	806	1396
14944	0.866	0.134	2896	965	1672
19933	0.891	0.109	3863	1288	2230
24909	0.891	0.109	4827	1609	2787
29899	0.891	0.109	5794	1931	3345
34832	0.917	0.083	6750	2250	3897
39826	0.917	0.083	7718	2573	4456
44921	0.917	0.083	8705	2902	5026
49791	0.917	0.083	9649	3216	5571

TABLE 4.11
MERCURY INJECTION DATA SUMMARY

Sandia National Laboratories
Waste Isolation Pilot Plant
Core: E1X 11-6

Sample Number
File: DAL-93089

21

Contact Angle = 180

Injection Pressure, psia	Mercury Saturation, fraction	1.0-Mercury Saturation, fraction	Other Laboratory Systems		
			Gas-Water, psia	Gas-Oil, psia	Oil-Water, psia
1.5	0.000	1.000	0.23	0.08	0.13
3.0	0.000	1.000	0.45	0.15	0.26
6.0	0.000	1.000	0.89	0.30	0.51
9.0	0.026	0.974	1.3	0.44	0.77
12	0.026	0.974	1.8	0.59	1.0
18	0.051	0.949	2.7	0.89	1.5
25	0.051	0.949	3.7	1.2	2.1
35	0.051	0.949	5.2	1.7	3.0
45	0.051	0.949	6.7	2.2	3.8
55	0.051	0.949	8.2	2.7	4.7
75	0.051	0.949	11	3.7	6.4
99	0.077	0.923	15	4.9	8.5
125	0.077	0.923	19	6.2	11
160	0.077	0.923	24	7.9	14
180	0.077	0.923	27	8.9	15
200	0.077	0.923	30	9.9	17
300	0.127	0.873	44	15	26
400	0.178	0.822	59	20	34
498	0.229	0.771	74	25	43
746	0.357	0.643	111	37	64
996	0.433	0.567	148	49	85
1246	0.484	0.516	185	62	107
1593	0.560	0.440	236	79	137
1994	0.662	0.338	296	99	171
2490	0.662	0.338	370	123	213
3494	0.713	0.287	519	173	299
4248	0.738	0.262	631	210	364
4992	0.738	0.262	741	247	428
6972	0.789	0.211	1035	345	598
9972	0.815	0.185	1480	493	855
12476	0.840	0.160	1852	617	1069
14944	0.866	0.134	2218	739	1281
19933	0.891	0.109	2959	986	1708
24909	0.891	0.109	3698	1233	2135
29899	0.891	0.109	4439	1480	2563
34832	0.917	0.083	5171	1724	2985
39826	0.917	0.083	5912	1971	3413
44921	0.917	0.083	6669	2223	3850
49791	0.917	0.083	7392	2464	4268

TABLE 4.12
MERCURY INJECTION DATA SUMMARY

Sandia National Laboratories
Waste Isolation Pilot Plant
Core: E1X 11-6

Sample Number
File: DAL-93089

23

Contact Angle = 140

Injection Pressure, psia	Mercury Saturation, fraction	1.0-Mercury Saturation, fraction	Other Laboratory Systems		
			Gas-Water, psia	Gas-Oil, psia	Oil-Water, psia
1.5	0.000	1.000	0.29	0.10	0.17
3.0	0.000	1.000	0.58	0.19	0.34
6.0	0.000	1.000	1.2	0.39	0.67
9.0	0.025	0.975	1.7	0.58	1.0
12	0.025	0.975	2.3	0.77	1.3
18	0.025	0.975	3.5	1.2	2.0
25	0.037	0.963	4.8	1.6	2.8
35	0.062	0.938	6.8	2.3	3.9
45	0.062	0.938	8.7	2.9	5.0
55	0.062	0.938	11	3.6	6.2
75	0.062	0.938	15	4.9	8.4
101	0.075	0.925	20	6.5	11
125	0.075	0.925	24	8.0	14
161	0.087	0.913	31	10	18
179	0.087	0.913	35	12	20
200	0.099	0.901	39	13	22
300	0.124	0.876	58	19	34
401	0.199	0.801	78	26	45
500	0.261	0.739	97	32	56
753	0.385	0.615	146	49	84
1006	0.484	0.516	195	65	113
1245	0.558	0.442	241	80	139
1597	0.658	0.342	309	103	179
1991	0.732	0.268	386	129	223
2493	0.806	0.194	483	161	279
3491	0.868	0.132	677	226	391
4246	0.881	0.119	823	274	475
4976	0.893	0.107	964	321	557
6984	0.893	0.107	1353	451	781
9974	0.893	0.107	1933	644	1116
12442	0.906	0.094	2411	804	1392
14931	0.906	0.094	2894	965	1671
19940	0.906	0.094	3864	1288	2231
24898	0.918	0.082	4825	1608	2786
29874	0.918	0.082	5789	1930	3343
34871	0.918	0.082	6758	2253	3902
39851	0.918	0.082	7723	2574	4459
44916	0.918	0.082	8704	2901	5025
49963	0.918	0.082	9682	3227	5590

TABLE 4.13
MERCURY INJECTION DATA SUMMARY

Sandia National Laboratories
Waste Isolation Pilot Plant
Core: E1X 11-6

Sample Number 23
File: DAL-93089

Contact Angle = 180

Injection Pressure, psia	Mercury Saturation, fraction	1.0-Mercury Saturation, fraction	Other Laboratory Systems		
			Gas-Water, psia	Gas-Oil, psia	Oil-Water, psia
1.5	0.000	1.000	0.23	0.08	0.13
3.0	0.000	1.000	0.45	0.15	0.26
6.0	0.000	1.000	0.89	0.30	0.51
9.0	0.025	0.975	1.3	0.44	0.77
12	0.025	0.975	1.8	0.59	1.0
18	0.025	0.975	2.7	0.89	1.5
25	0.037	0.963	3.7	1.2	2.1
35	0.062	0.938	5.2	1.7	3.0
45	0.062	0.938	6.7	2.2	3.9
55	0.062	0.938	8.2	2.7	4.7
75	0.062	0.938	11	3.7	6.4
101	0.075	0.925	15	5.0	8.6
125	0.075	0.925	18	6.2	11
161	0.087	0.913	24	7.9	14
179	0.087	0.913	27	8.9	15
200	0.099	0.901	30	9.9	17
300	0.124	0.876	45	15	26
401	0.199	0.801	60	20	34
500	0.261	0.739	74	25	43
753	0.385	0.615	112	37	65
1006	0.484	0.516	149	50	86
1245	0.558	0.442	185	62	107
1597	0.658	0.342	237	79	137
1991	0.732	0.268	296	99	171
2493	0.806	0.194	370	123	214
3491	0.868	0.132	518	173	299
4246	0.881	0.119	630	210	364
4976	0.893	0.107	739	246	427
6984	0.893	0.107	1037	346	599
9974	0.893	0.107	1481	494	855
12442	0.906	0.094	1847	616	1066
14931	0.906	0.094	2217	739	1280
19940	0.906	0.094	2960	987	1709
24898	0.918	0.082	3696	1232	2134
29874	0.918	0.082	4435	1478	2561
34871	0.918	0.082	5177	1726	2989
39851	0.918	0.082	5916	1972	3416
44916	0.918	0.082	6668	2223	3850
49963	0.918	0.082	7417	2472	4282

**Figure 4.1: Distribution of Grain Densities
In 1 Inch Diameter Sample Set**

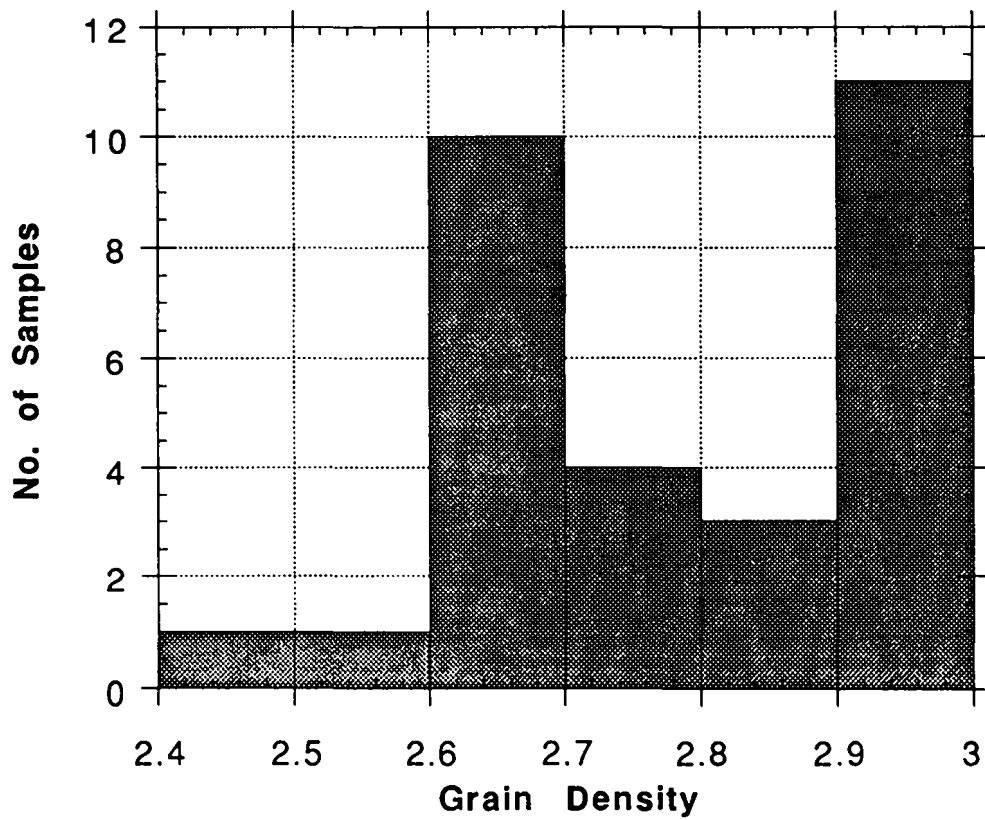


Fig 4.2: Gas Permeability (KI) vs. Porosity, 1" Samples

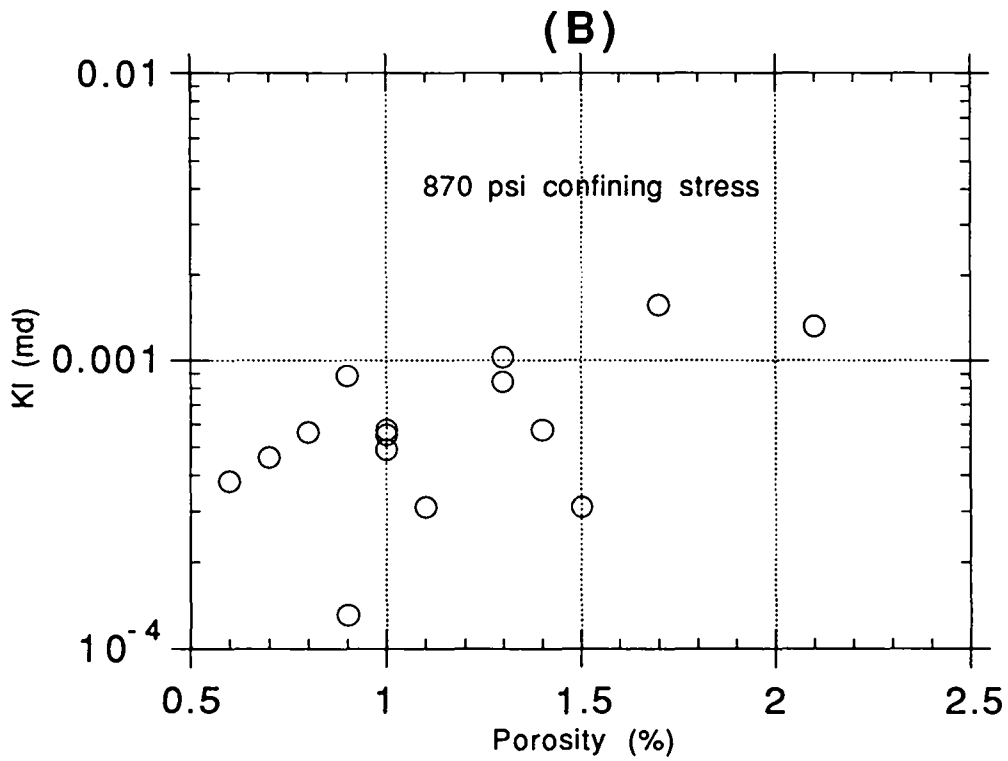
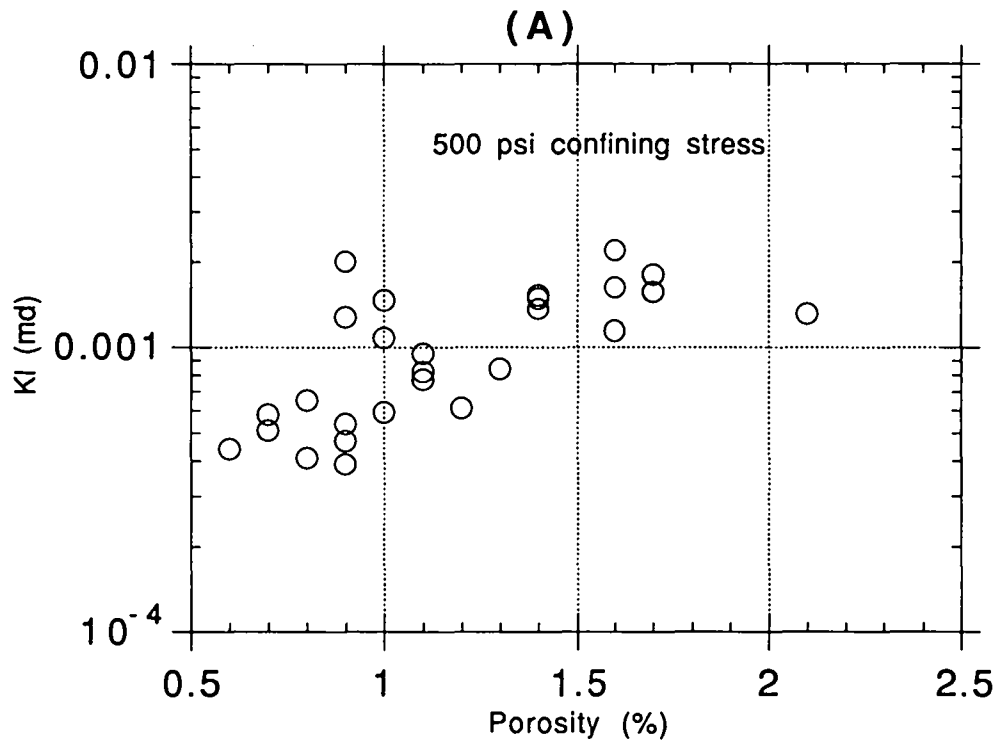


Figure 4.3: CT Scans of Samples 5 and 6

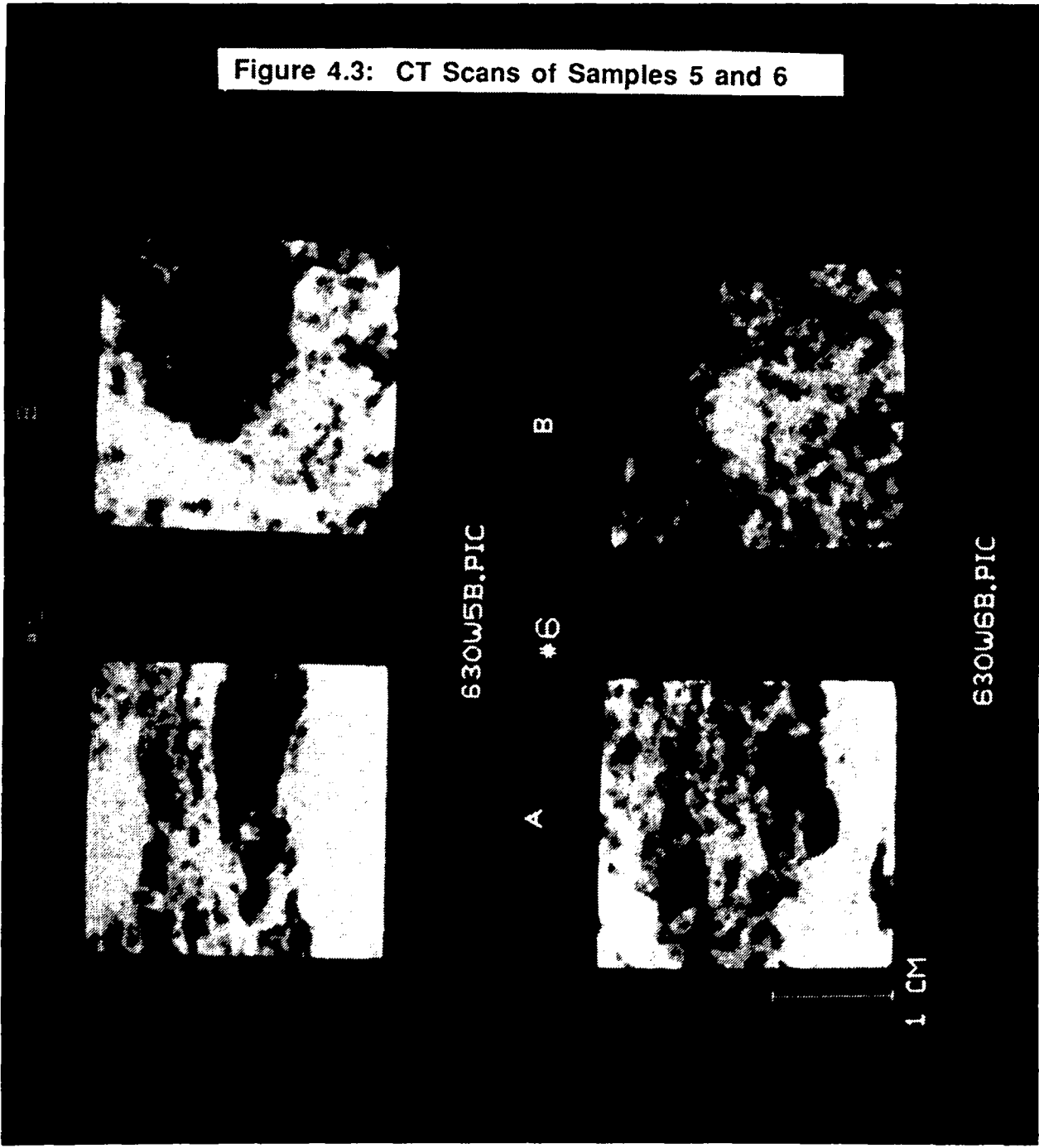


Figure 4.4: CT Scans of Samples 7 and 8

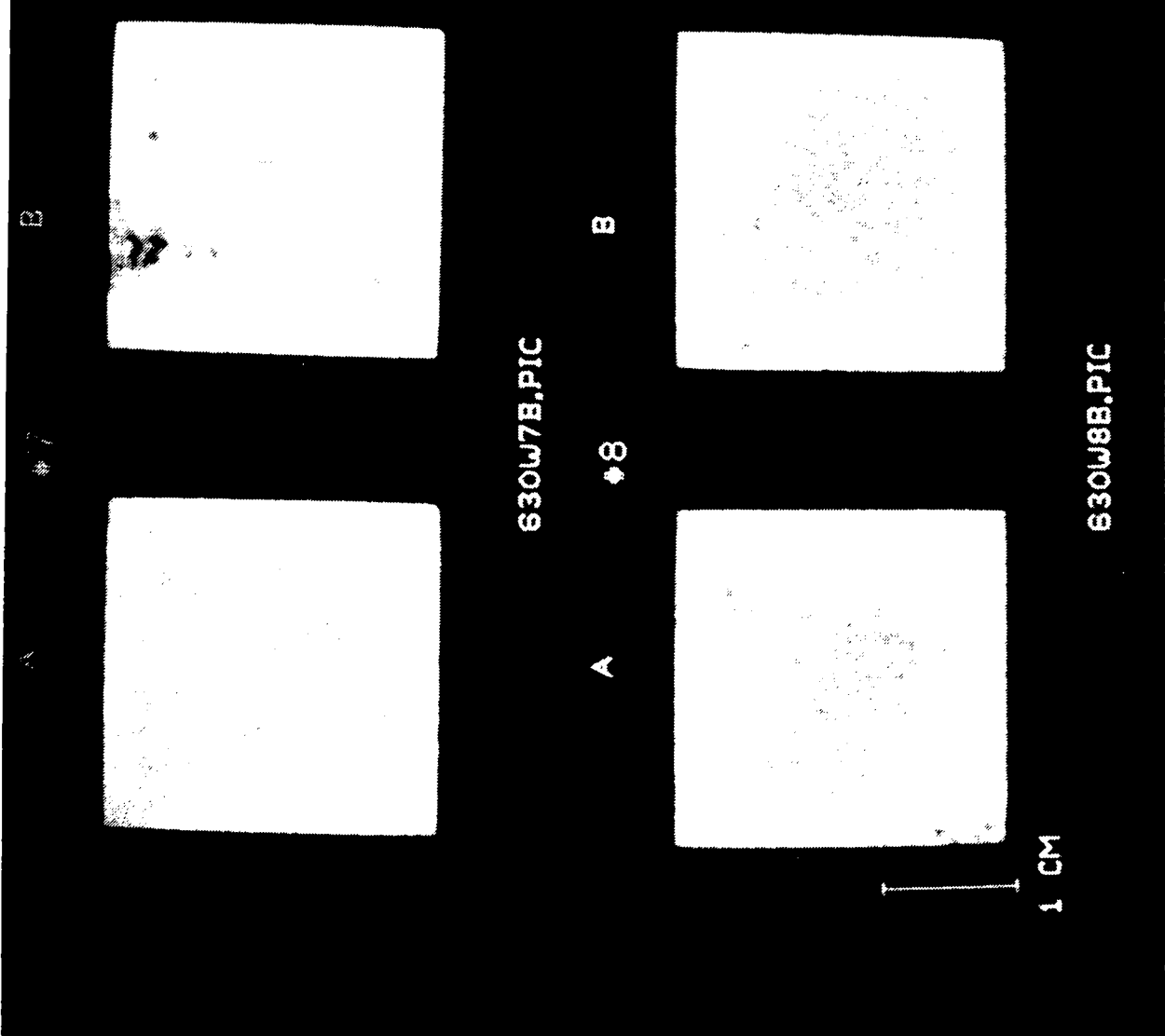


Figure 4.5: CT Scans of Samples 11 and 12

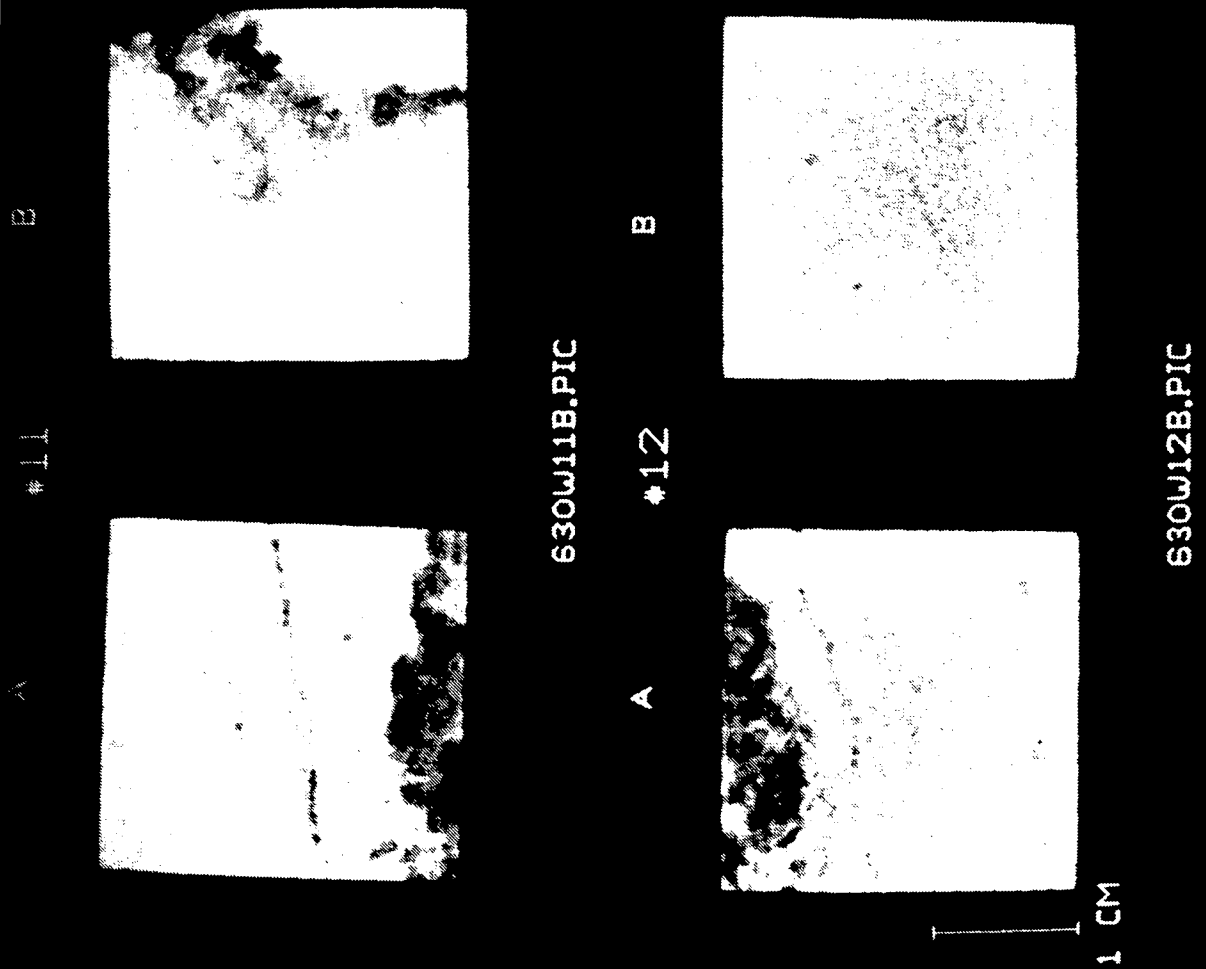


Figure 4.6: CT Scans of Samples 13 and 14

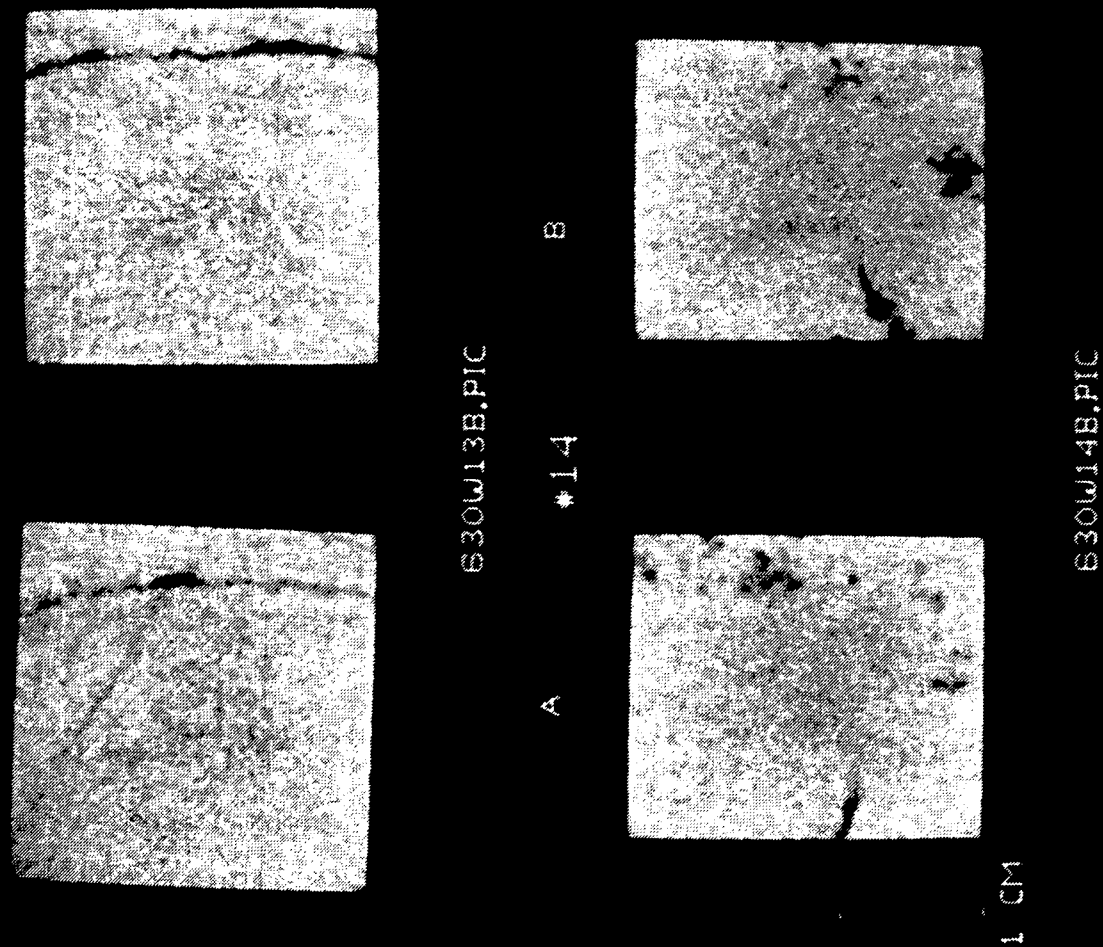


Figure 4.7: CT Scans of Samples 21 and 22

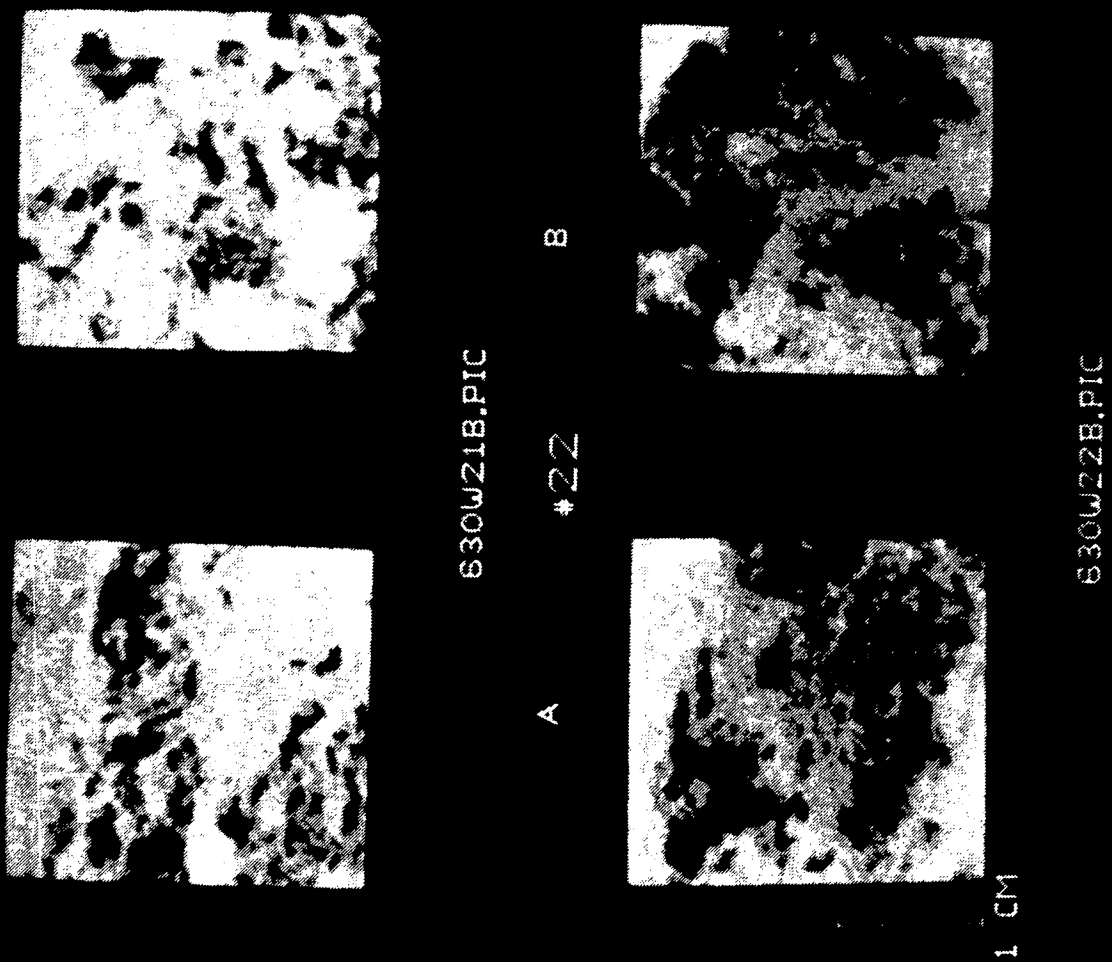


Figure 4.8: CT Scans of Samples 23 and 24

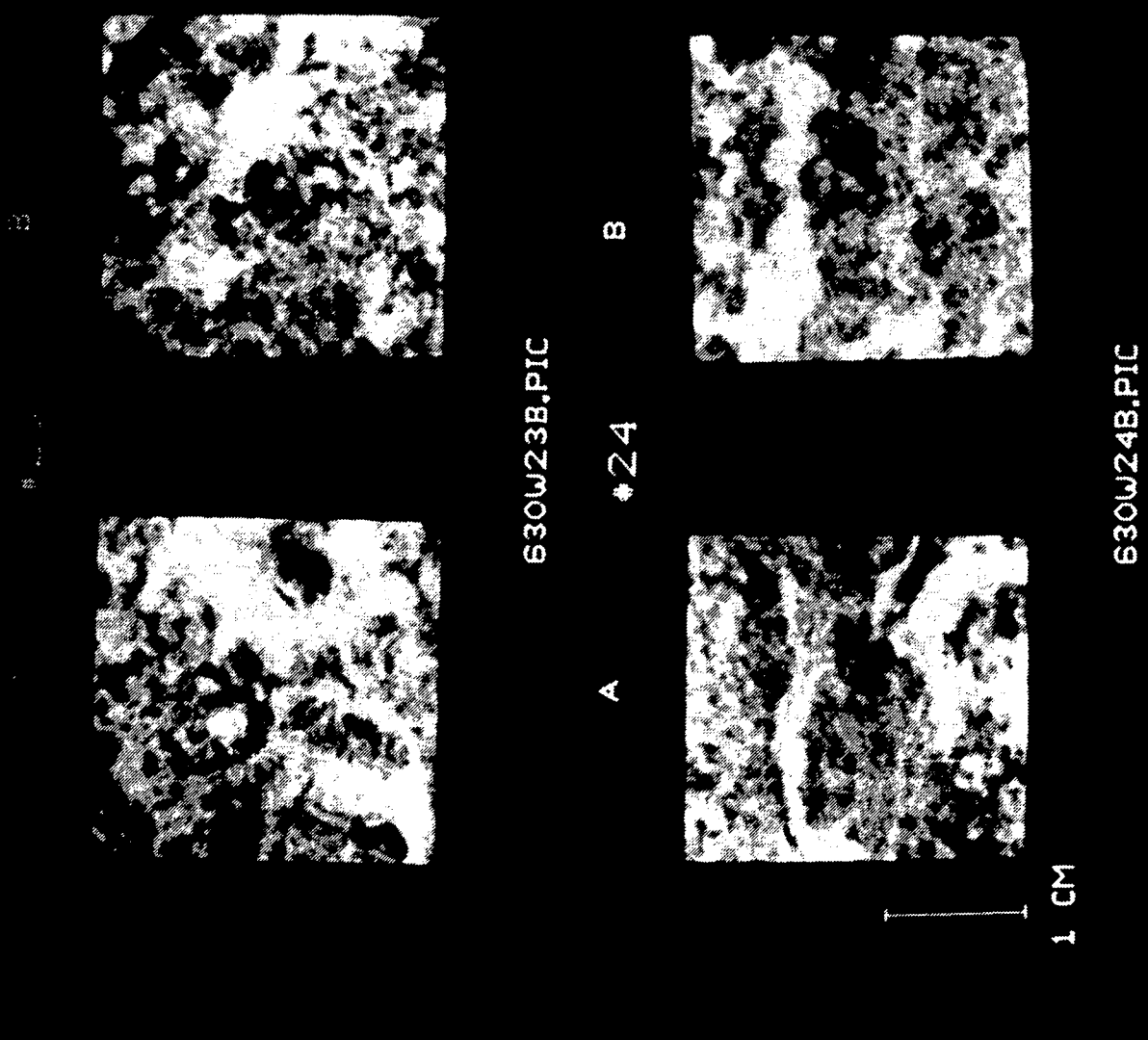


Figure 4.9

GAS-OIL CAPILLARY PRESSURE

Centrifuge Method

Sandia National Laboratories
Waste Isolation Pilot Plant
New Mexico
Core EIX 10-6
Horizontal Plug, B
File: DAL-93089

Sample ID: 6
Initial Oil saturation, fraction: 1.000
Saturant: n-Decane

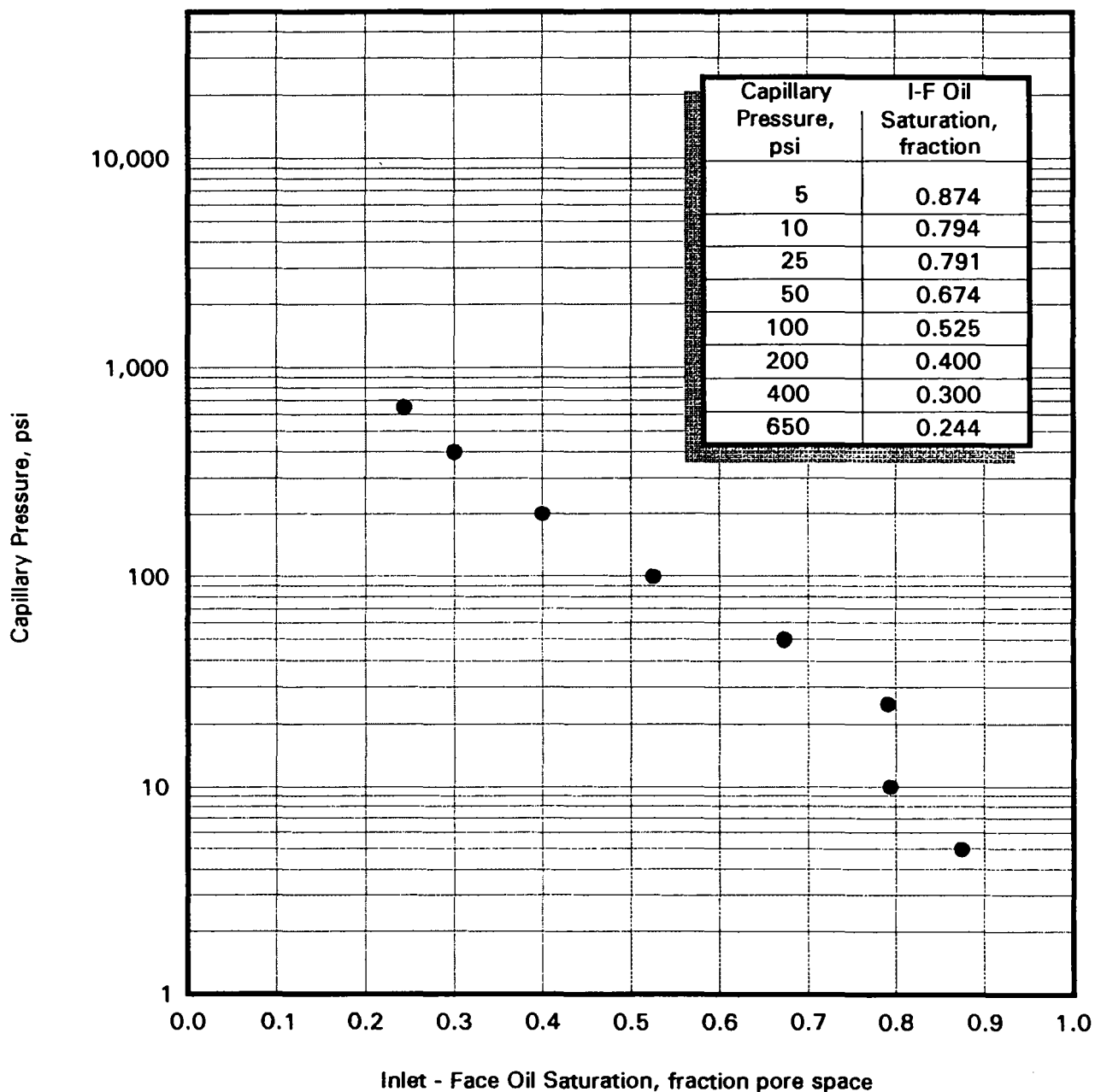


Figure 4.10

GAS-OIL CAPILLARY PRESSURE

Centrifuge Method

Sandia National Laboratories
Waste Isolation Pilot Plant
New Mexico
Core EIX 10-6
Vertical Plug, C2
File: DAL-93089

Sample Number: 8
Initial Oil saturation, fraction: 1.000
Saturant: n-Decane

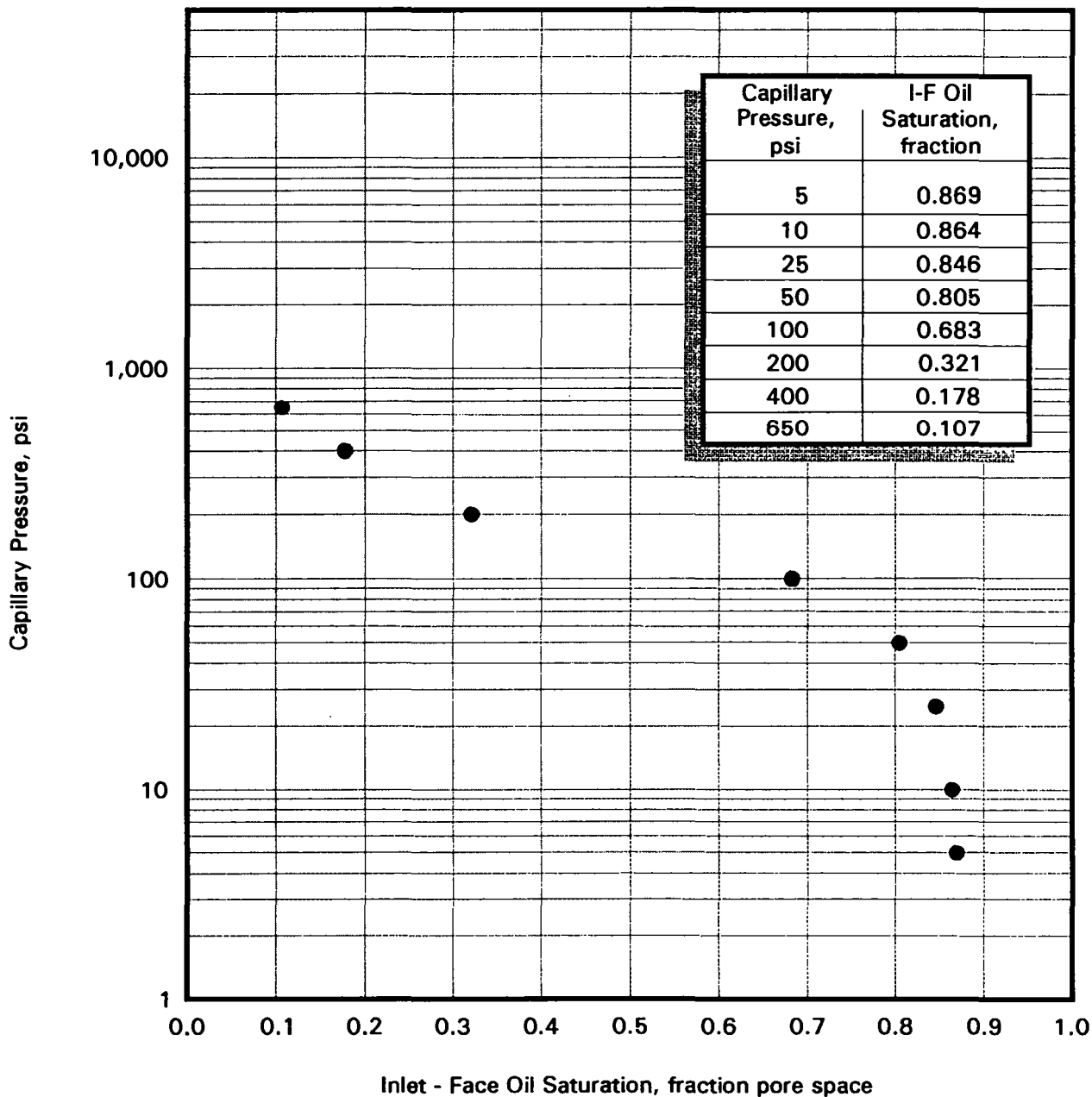


Figure 4.11

GAS-OIL CAPILLARY PRESSURE

Centrifuge Method

Sandia National Laboratories
Waste Isolation Pilot Plant
New Mexico
Core EIX 10-6
Horizontal Plug, B
File: DAL-93089

Sample ID: 12
Initial Oil saturation, fraction: 1.000
Saturant: n-Decane

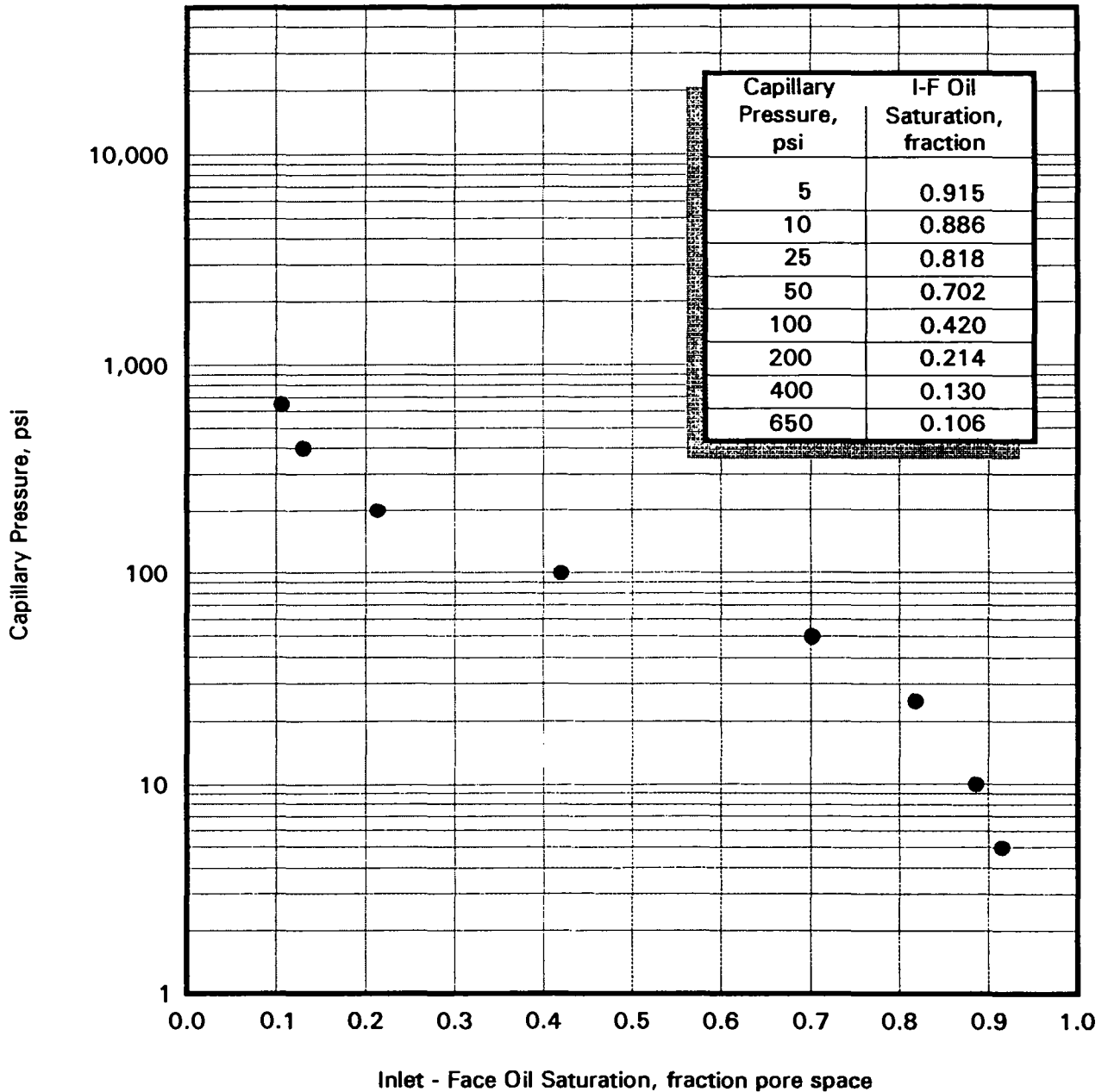


Figure 4.12

GAS-OIL CAPILLARY PRESSURE

Centrifuge Method

Sandia National Laboratories
Waste Isolation Pilot Plant
New Mexico
Core EIX 10-6
Vertical Plug, C2
File: DAL-93089

Sample ID: 14
Initial Oil saturation, fraction: 1.000
Saturant: n-Decane

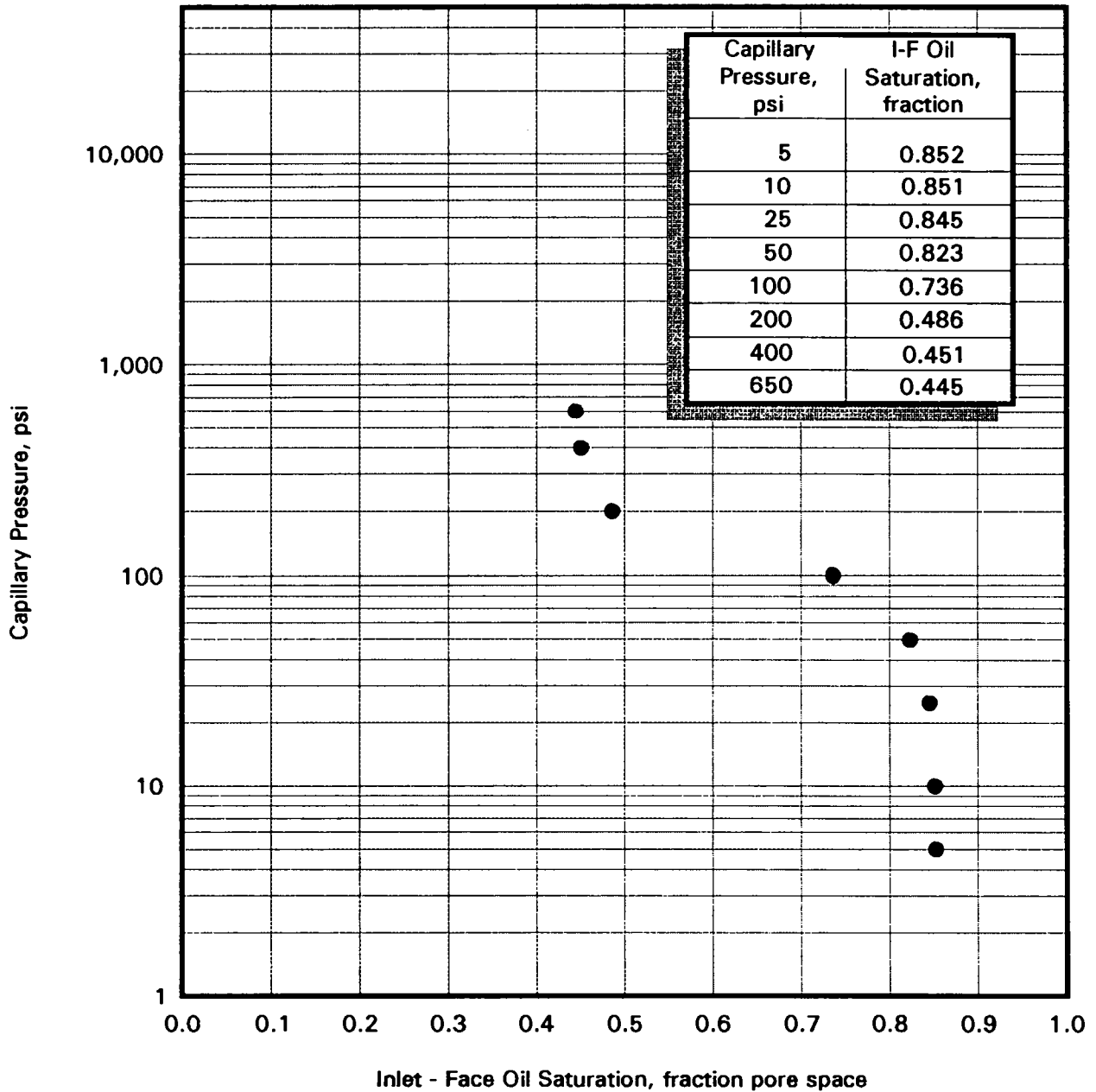


Figure 4.13

GAS-OIL CAPILLARY PRESSURE

Centrifuge Method

Sandia National Laboratories
Waste Isolation Pilot Plant
New Mexico
Core EIX 11-6
Horizontal Plug, B
File: DAL-93089

Sample ID: 22
Initial Oil saturation, fraction: 1.000
Saturant: n-Decane

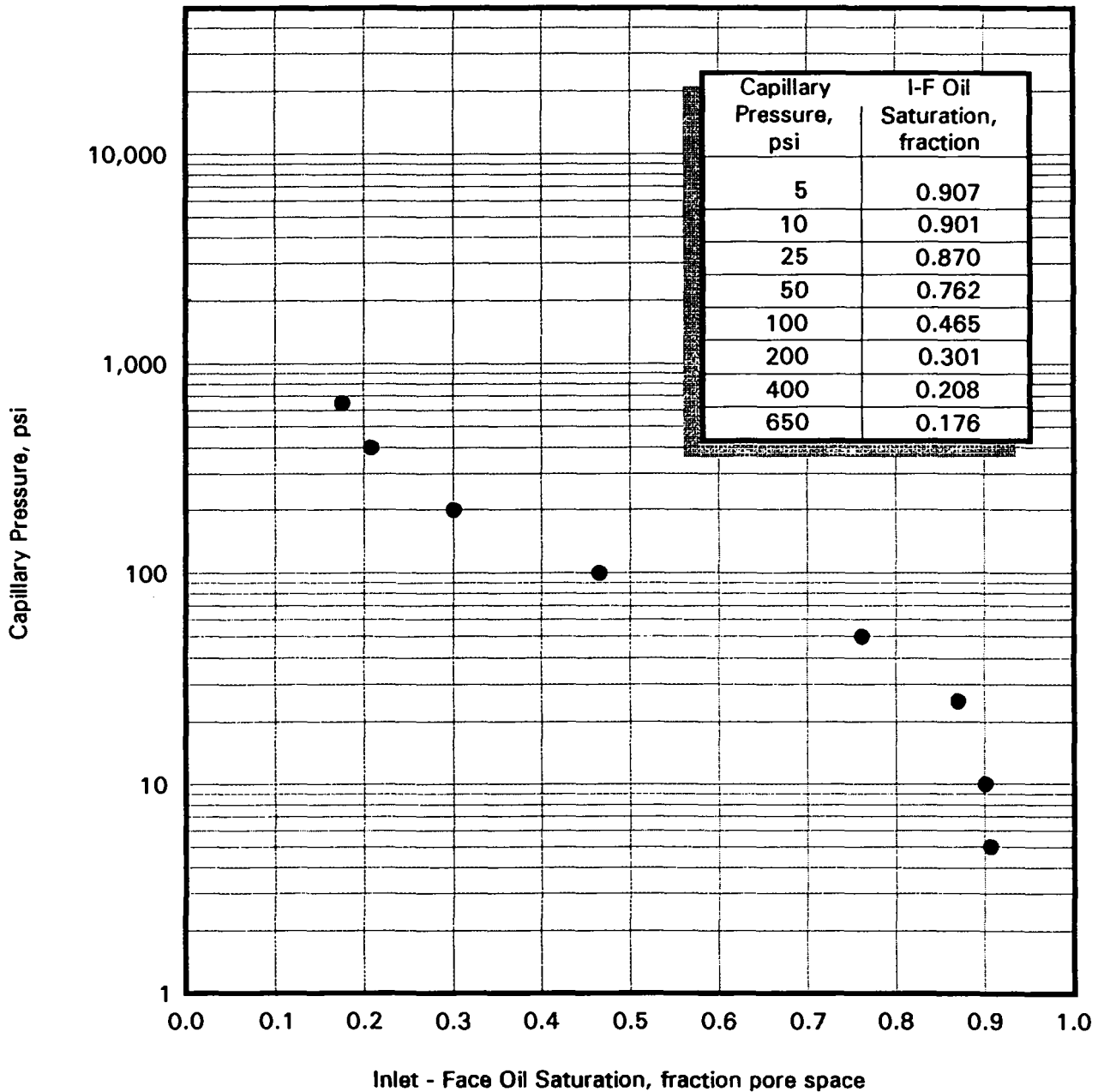


Figure 4.14

GAS-OIL CAPILLARY PRESSURE

Centrifuge Method

Sandia National Laboratories
 Waste Isolation Pilot Plant
 New Mexico
 Core EIX 11-6
 Horizontal Plug, B
 File: DAL-93089

Sample ID: 24
 Initial Oil saturation, fraction: 1.000
 Saturant: n-Decane

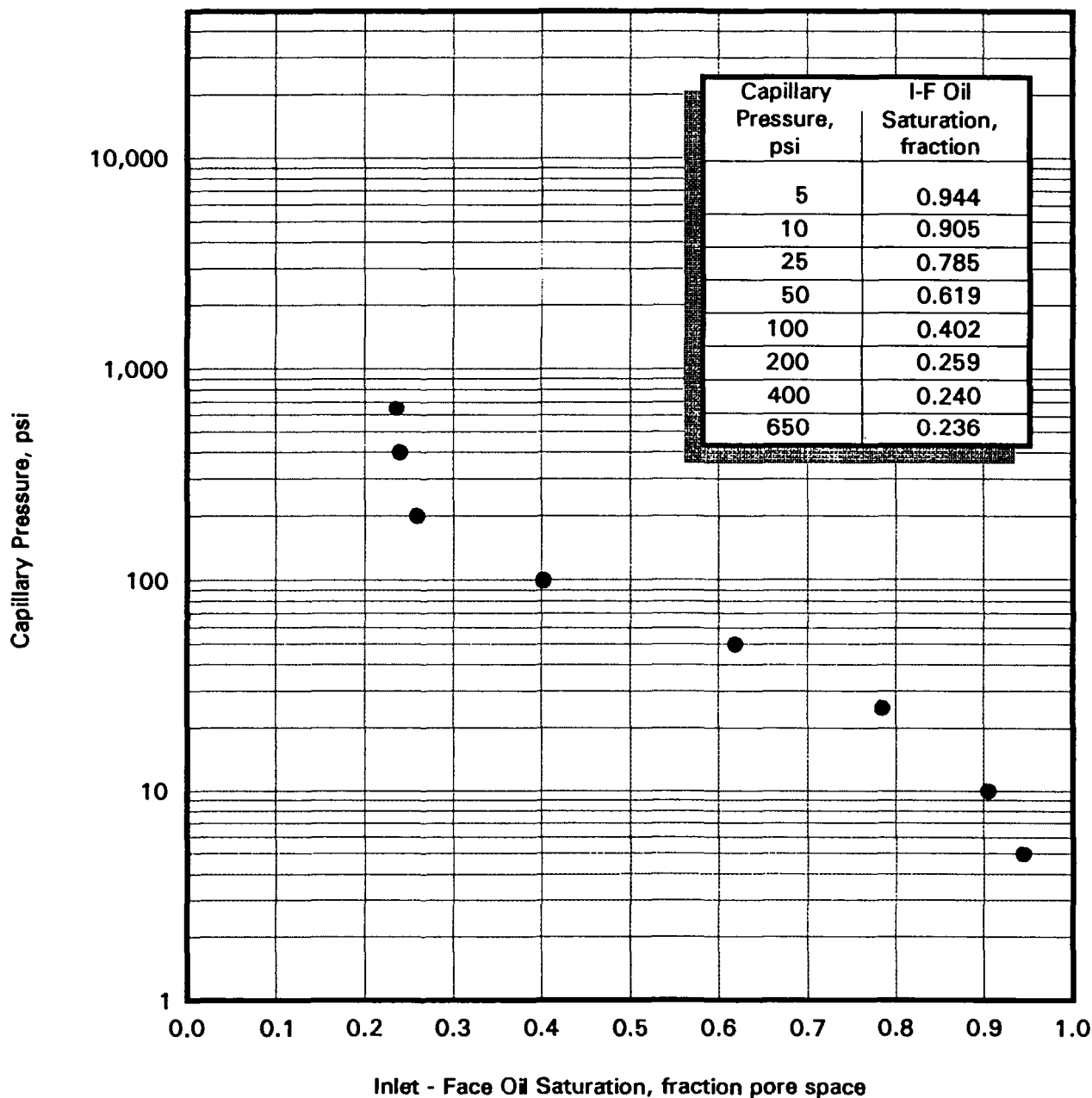


Figure 4.15

MERCURY INJECTION

Sandia National Laboratories
Waste Isolation Pilot Plant
Core: E1X 10-6
File: DAL-93089

Sample Number: 5

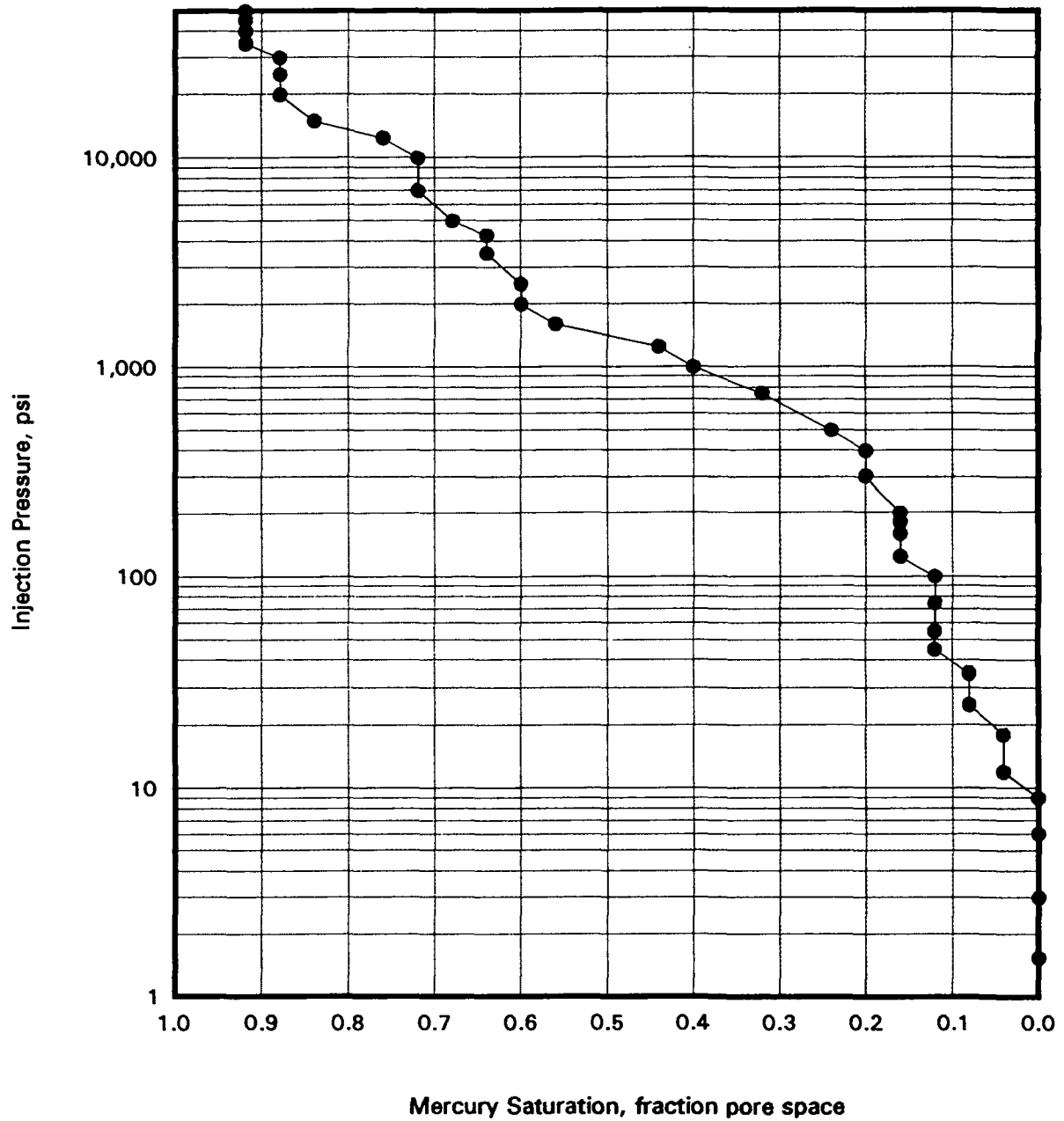


Figure 4.16

MERCURY INJECTION

Sandia National Laboratories
Waste Isolation Pilot Plant
Core: E1X 10-6
File: DAL-93089

Sample Number: 7

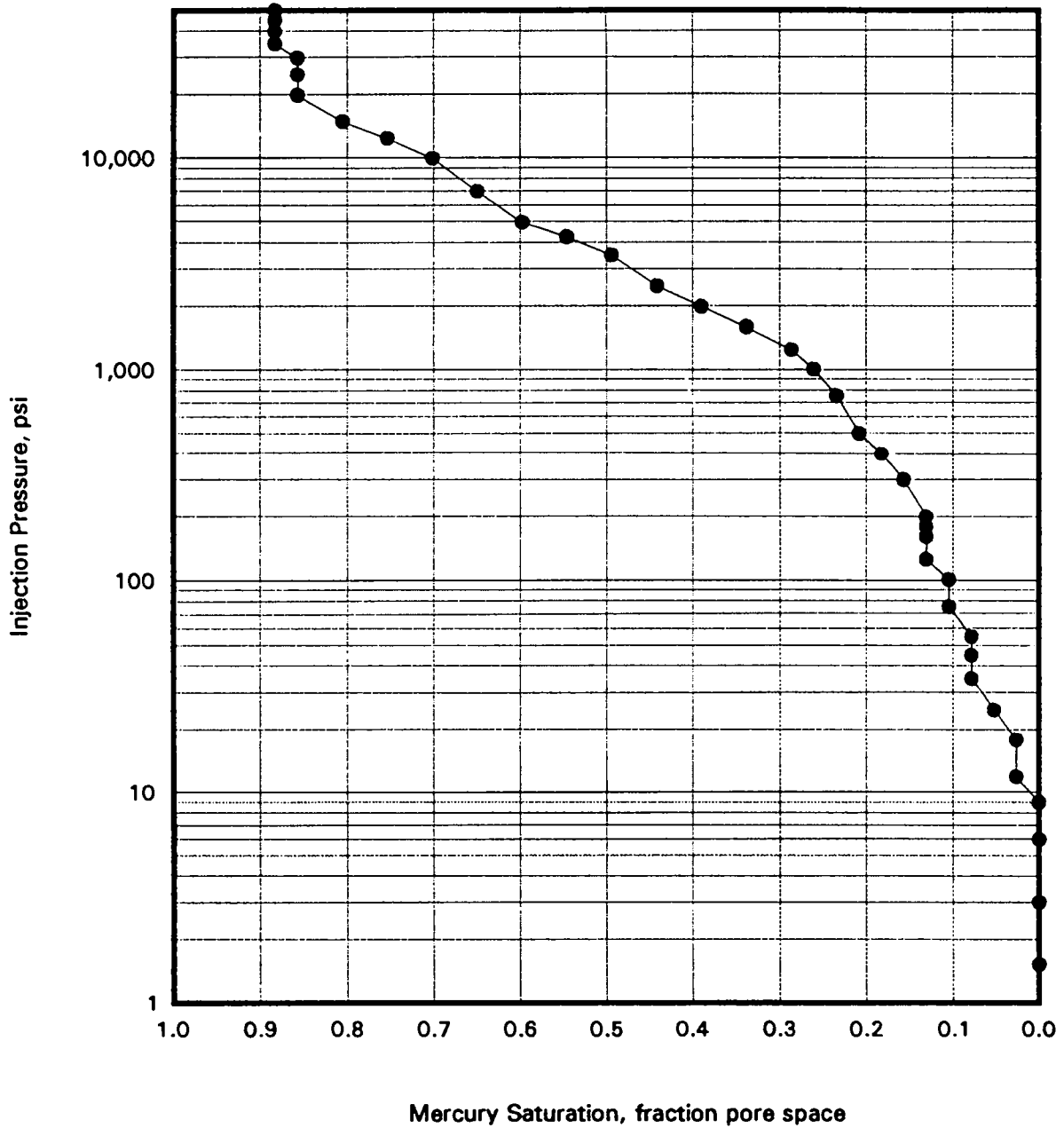


Figure 4.18

MERCURY INJECTION

Sandia National Laboratories
Waste Isolation Pilot Plant
Core: E1X 10-6
File: DAL-93089

Sample Number: 13

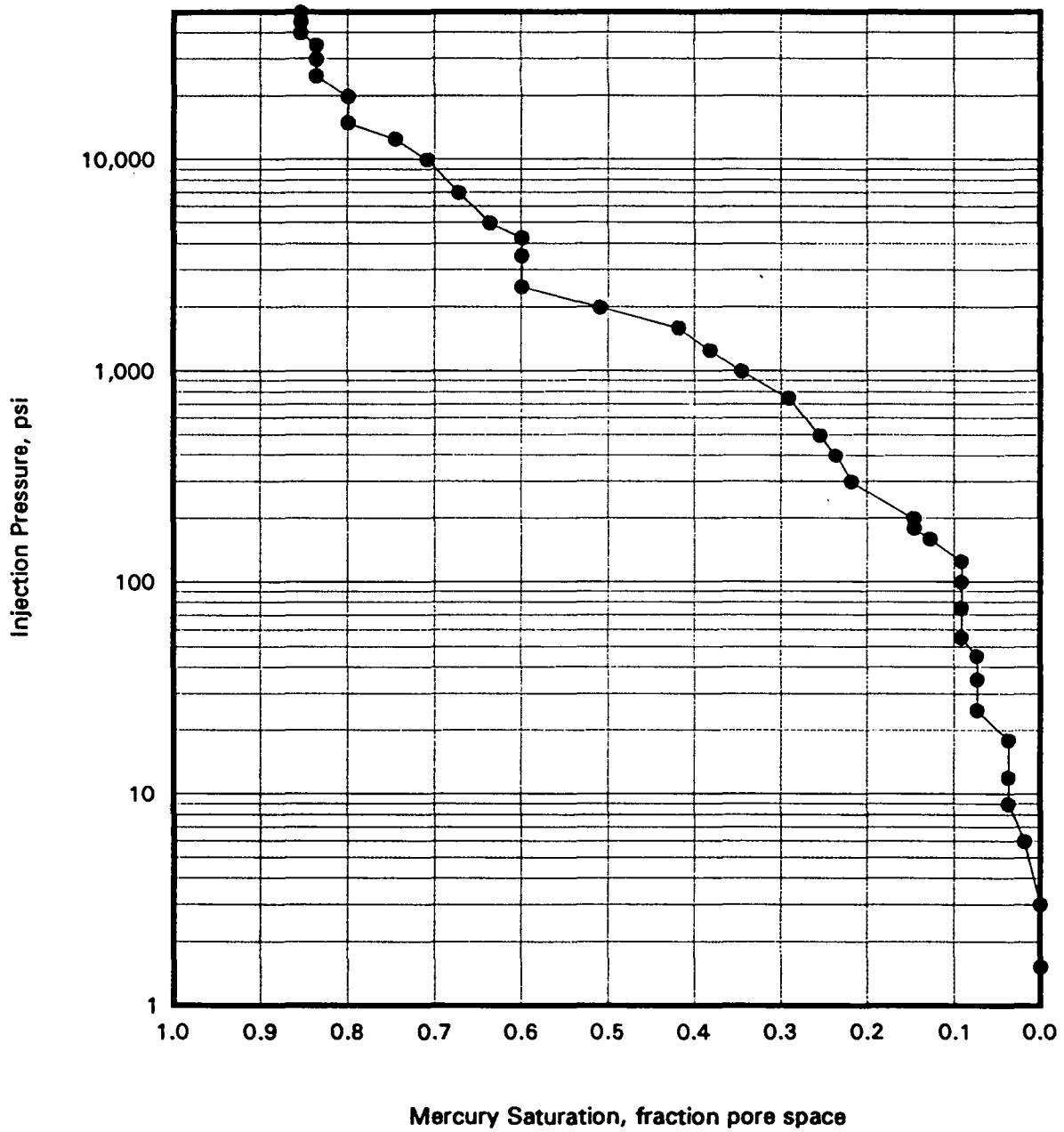


Figure 4.19

MERCURY INJECTION

Sandia National Laboratories
Waste Isolation Pilot Plant
Core: E1X 10-6
File: DAL-93089

Sample Number: 21

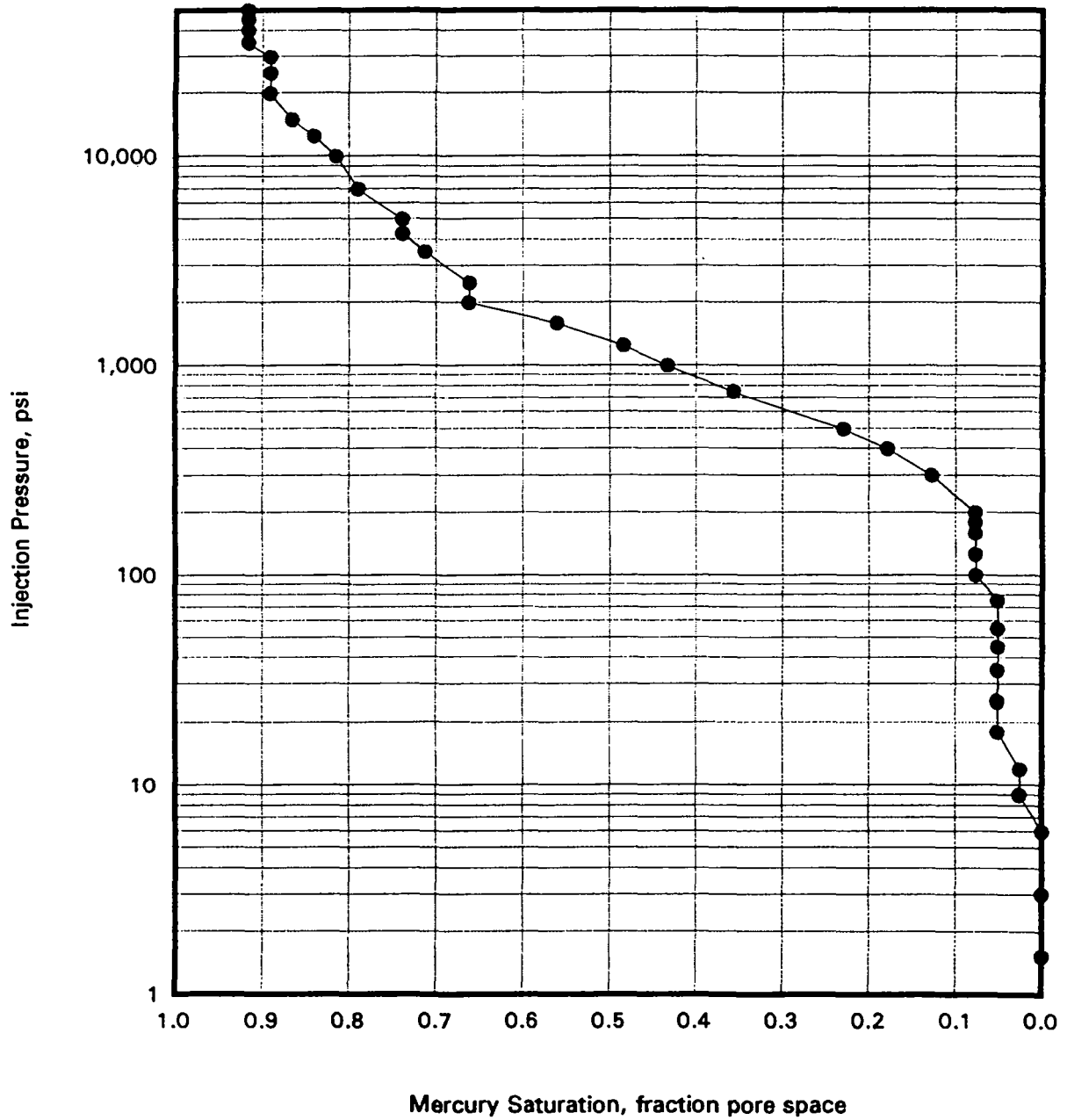


Figure 4.20

MERCURY INJECTION

Sandia National Laboratories
Waste Isolation Pilot Plant
Core: E1X 10-6
File: DAL-93089

Sample Number: 23

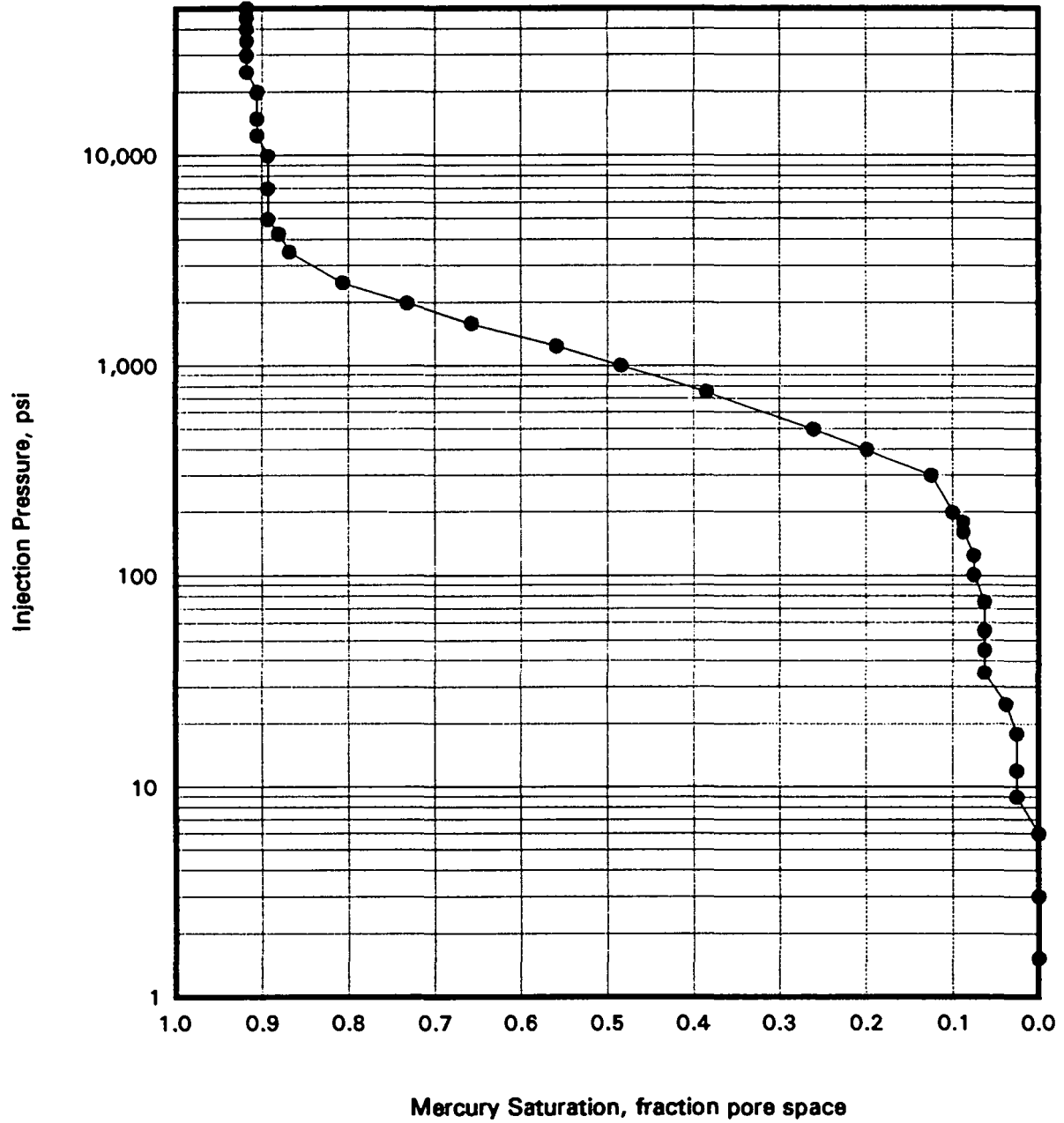


Figure 4.21
 Samples 5 and 6
 Comparison of Converted Hg and Cent. Air/Water Pcap Data

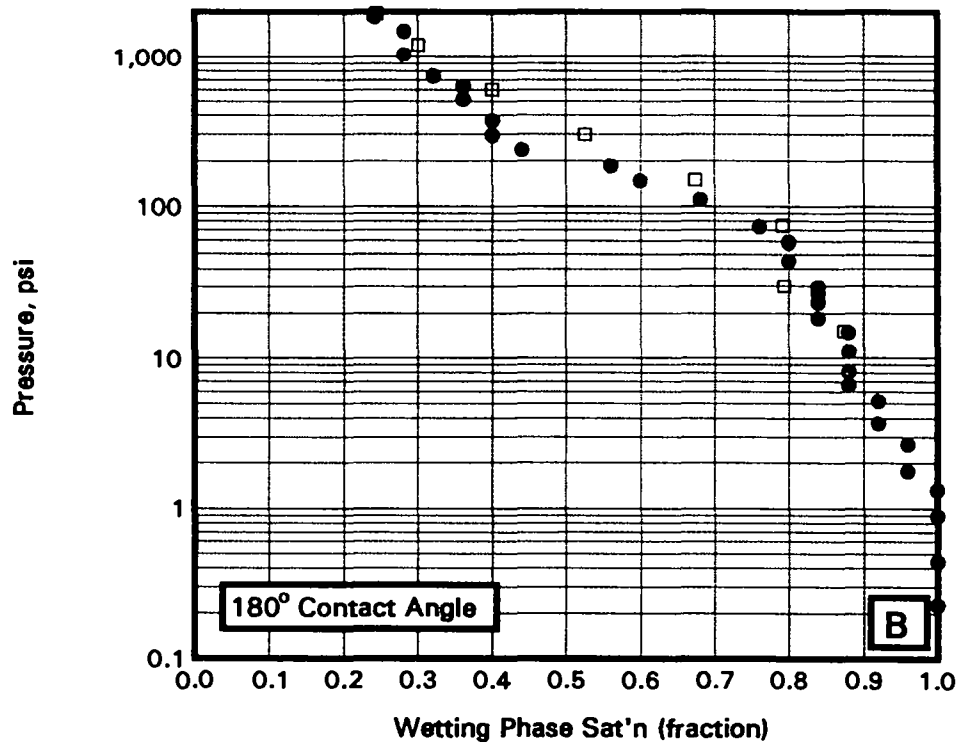
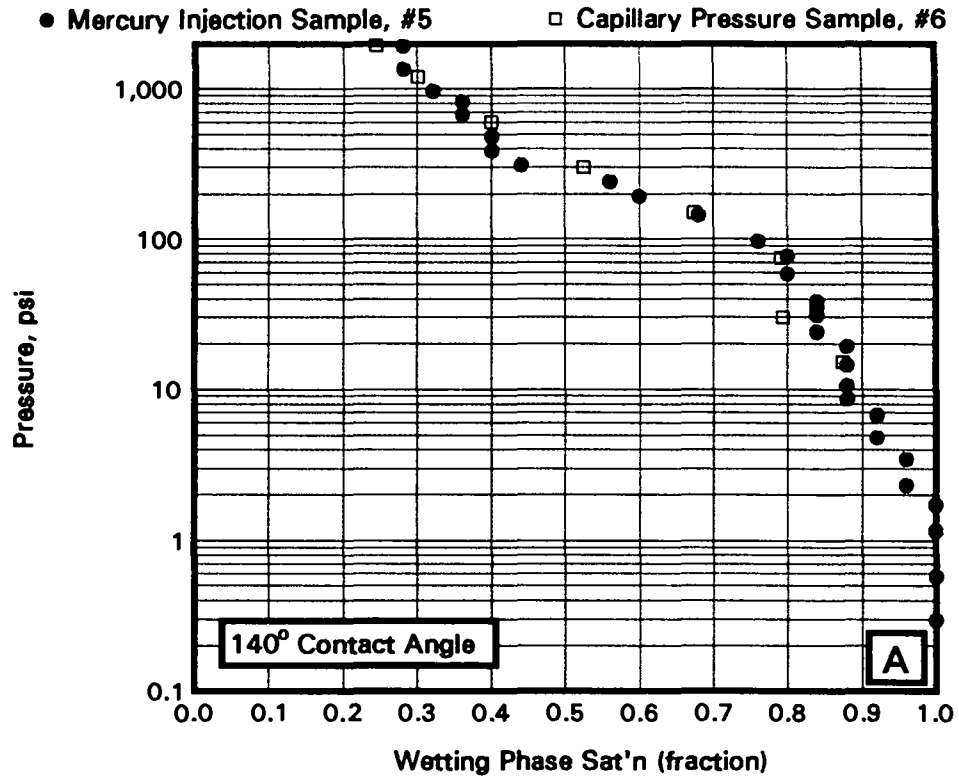


Figure 4.22
 Samples 7 and 8
 Comparison of Converted Hg and Cent. Air/Water Pcap Data

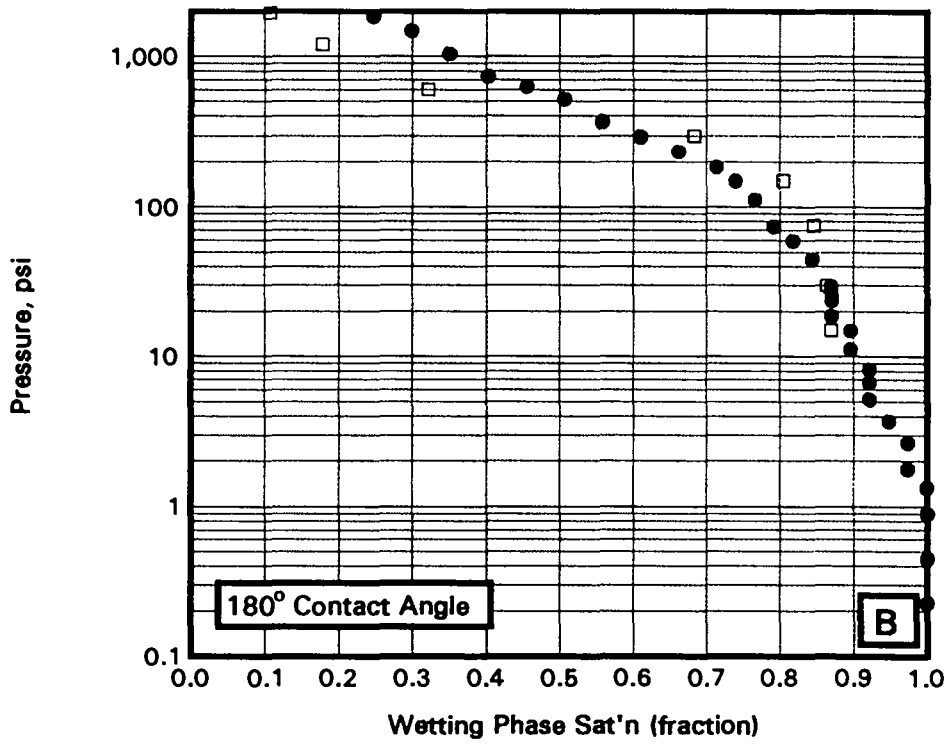
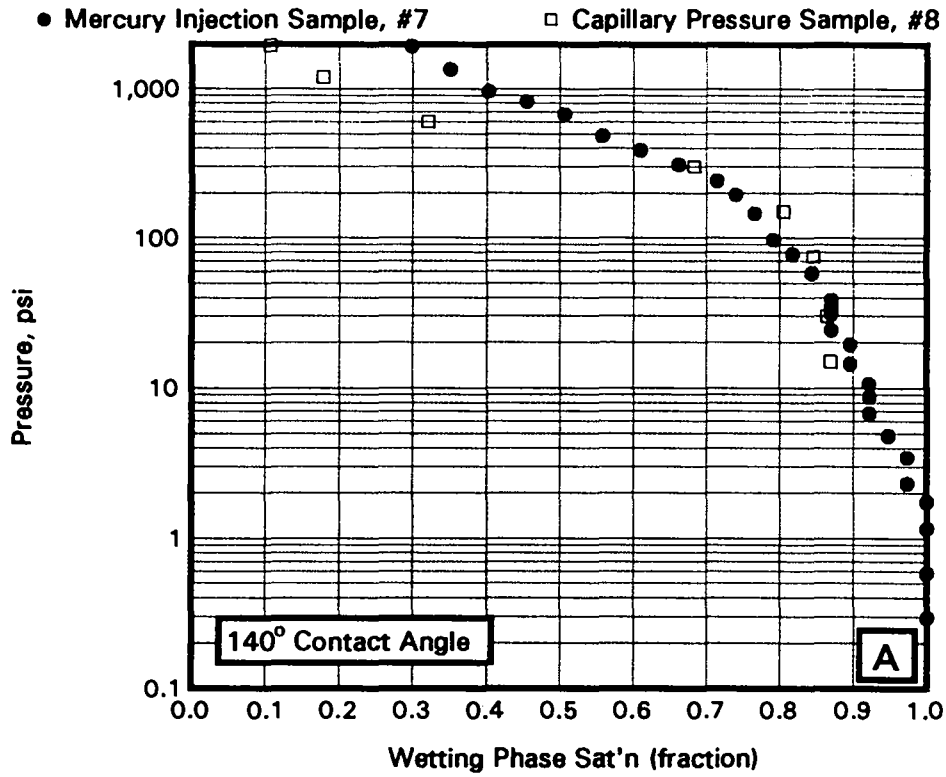


Figure 4.23
 Samples 11 and 12
 Comparison of Converted Hg and Cent. Air/Water Pcap Data

● Mercury Injection Sample, #11 □ Capillary Pressure Sample, #12

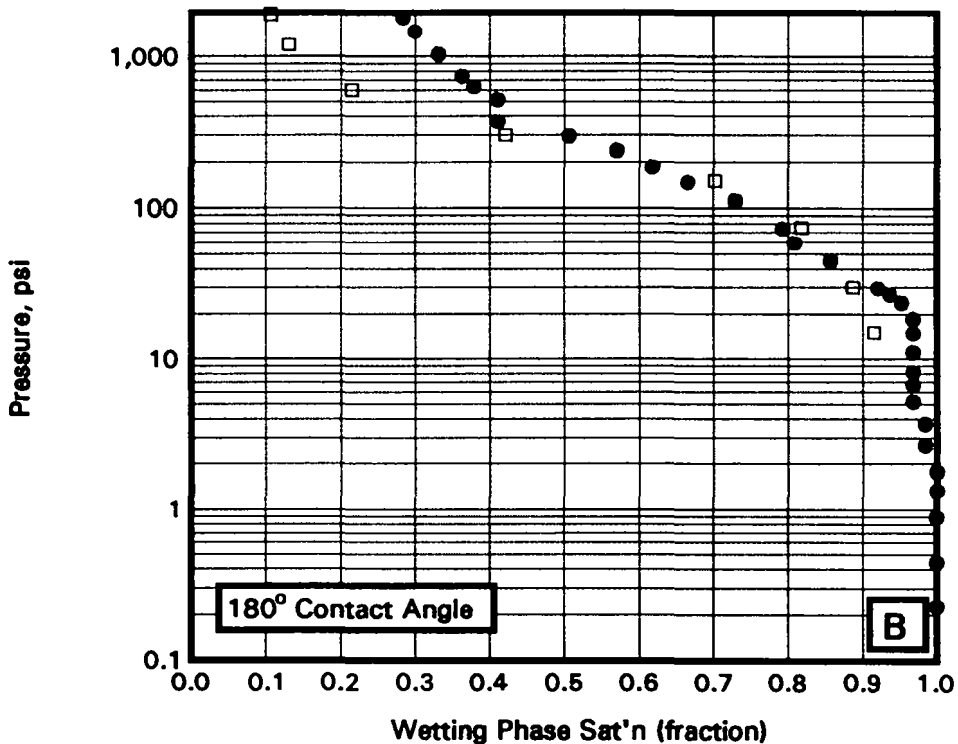
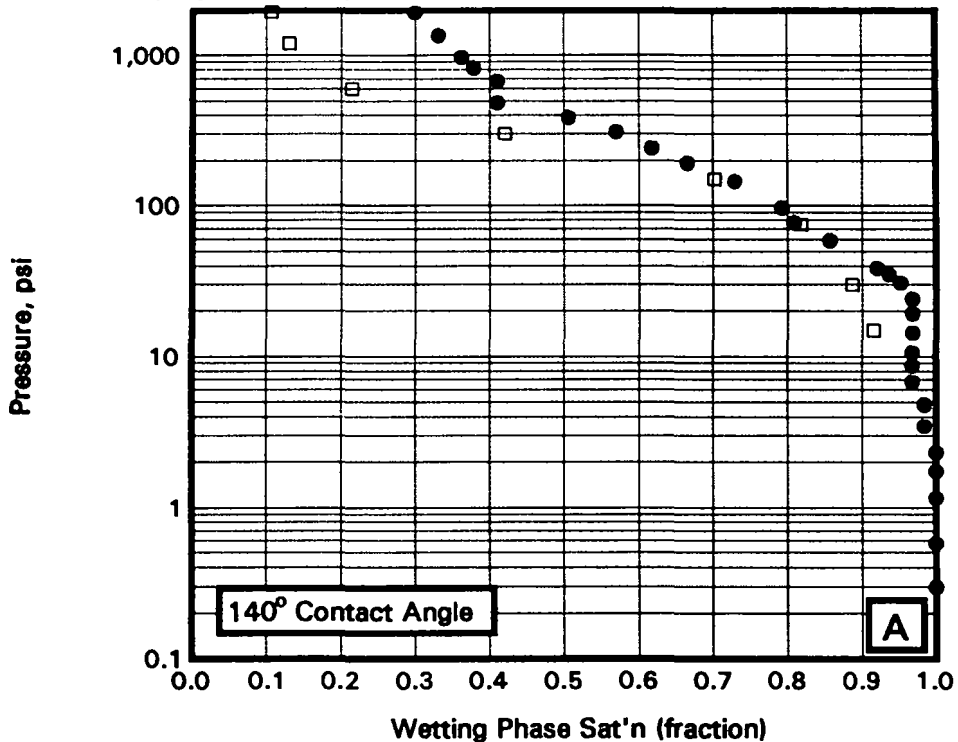


Figure 4.24
 Samples 13 and 14
 Comparison of Converted Hg and Cent. Air/Water Pcap Data

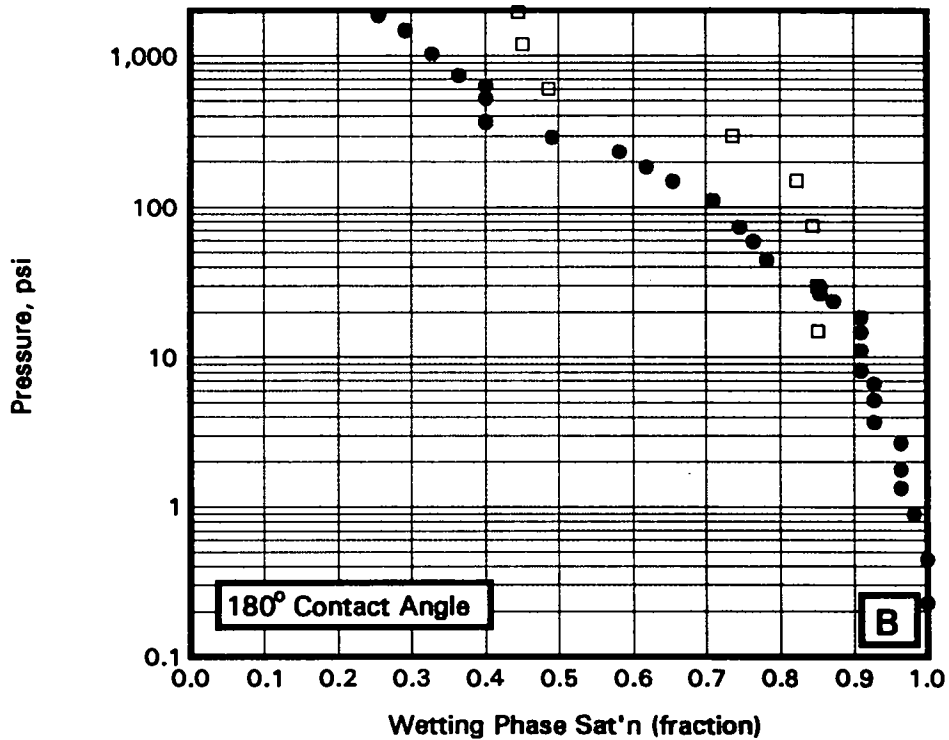
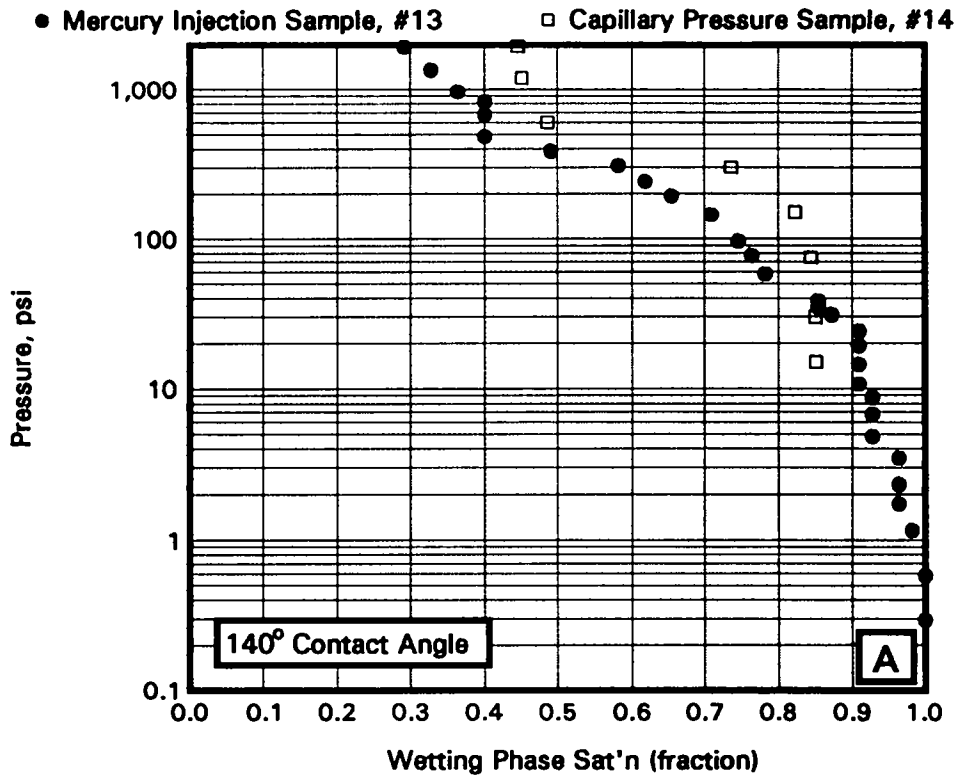


Figure 4.25
 Samples 21 and 22
 Comparison of Converted Hg and Cent. Air/Water Pcap Data

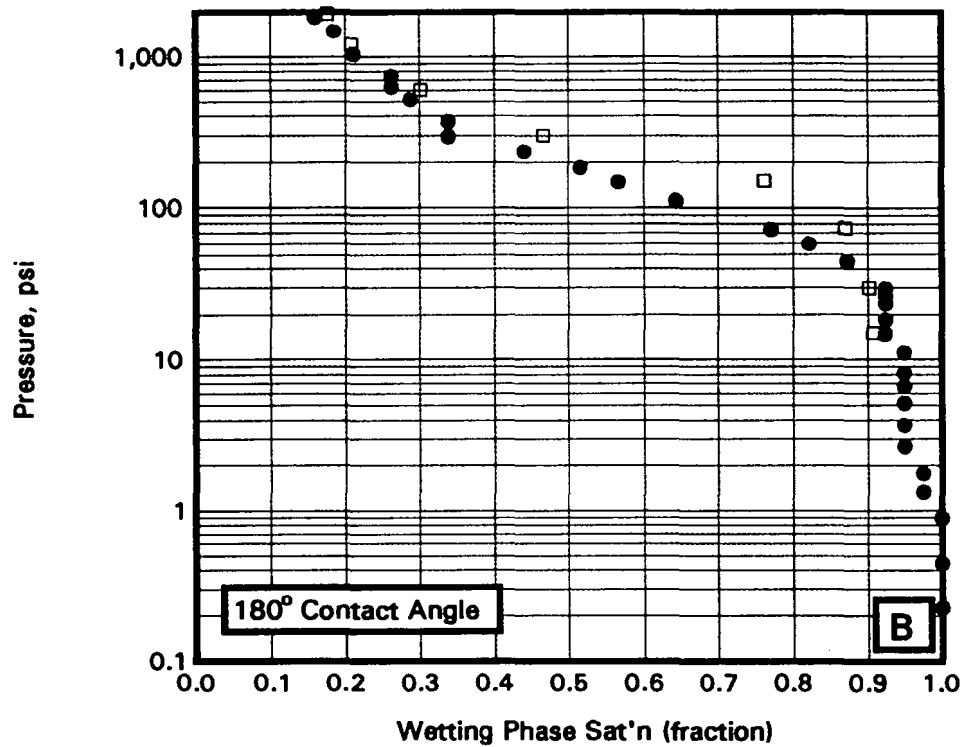
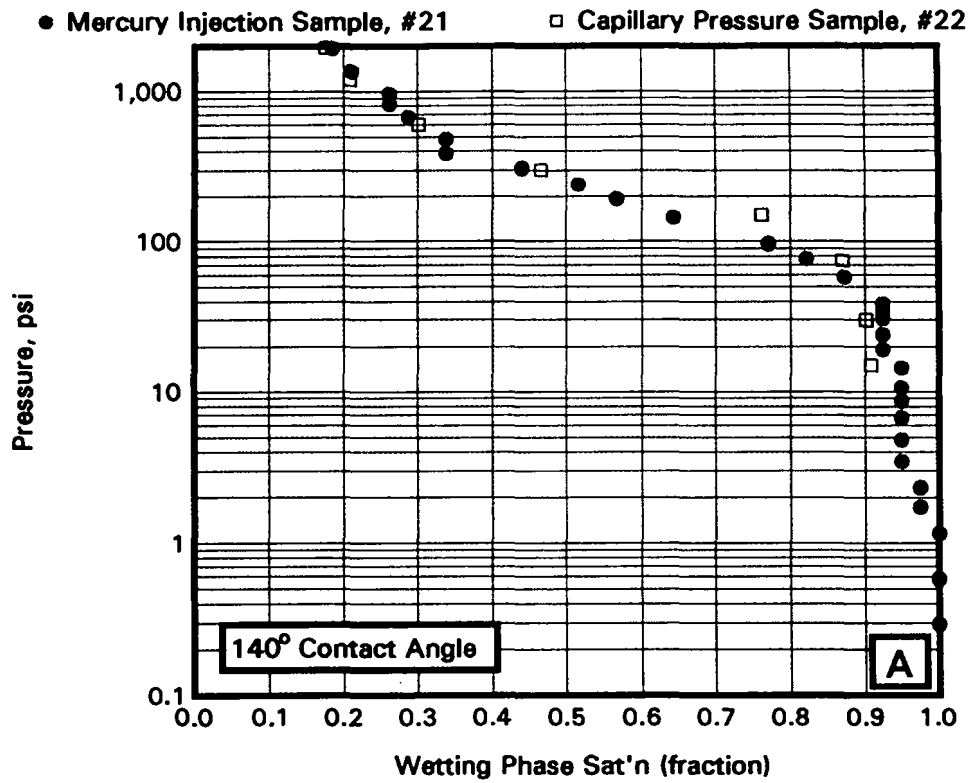


Figure 4.26
 Samples 23 and 24
 Comparison of Converted Hg and Cent. Air/Water Pcap Data

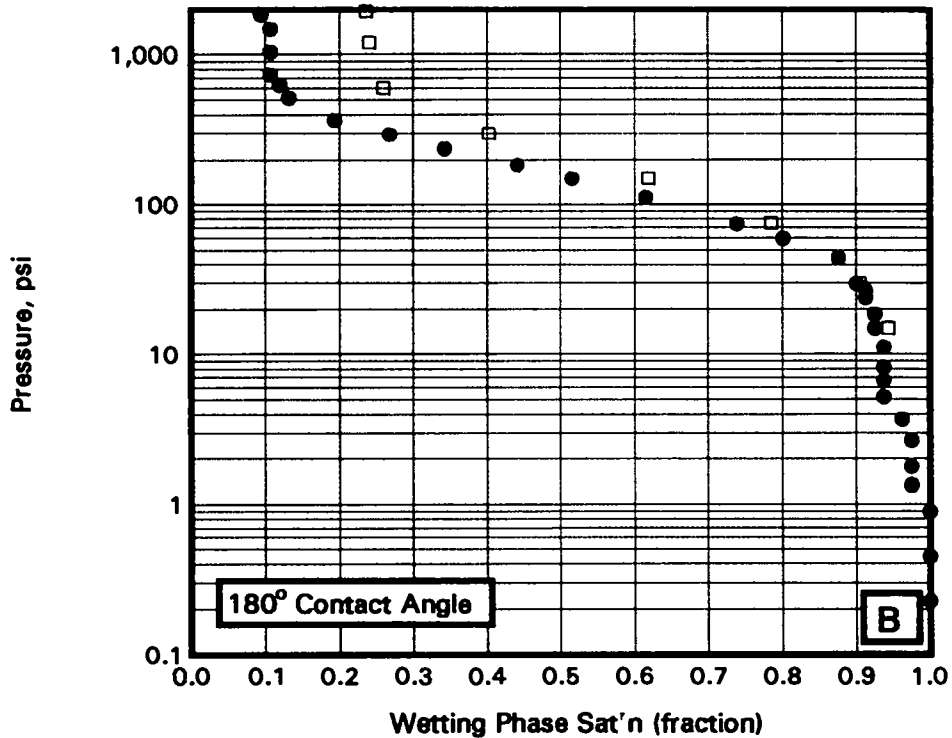
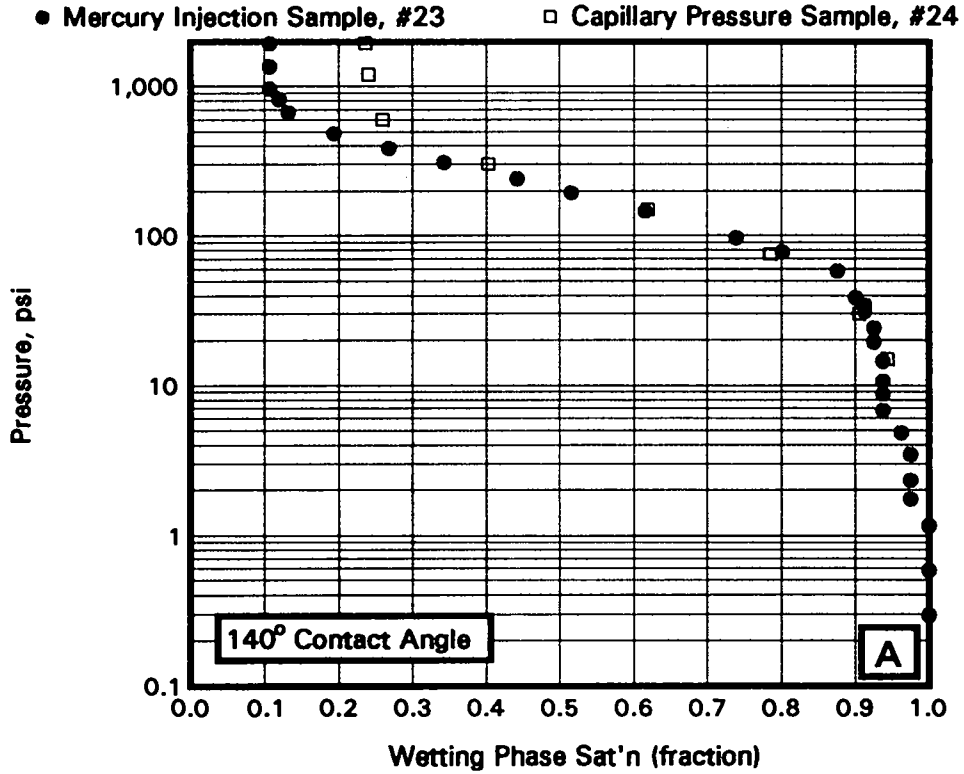
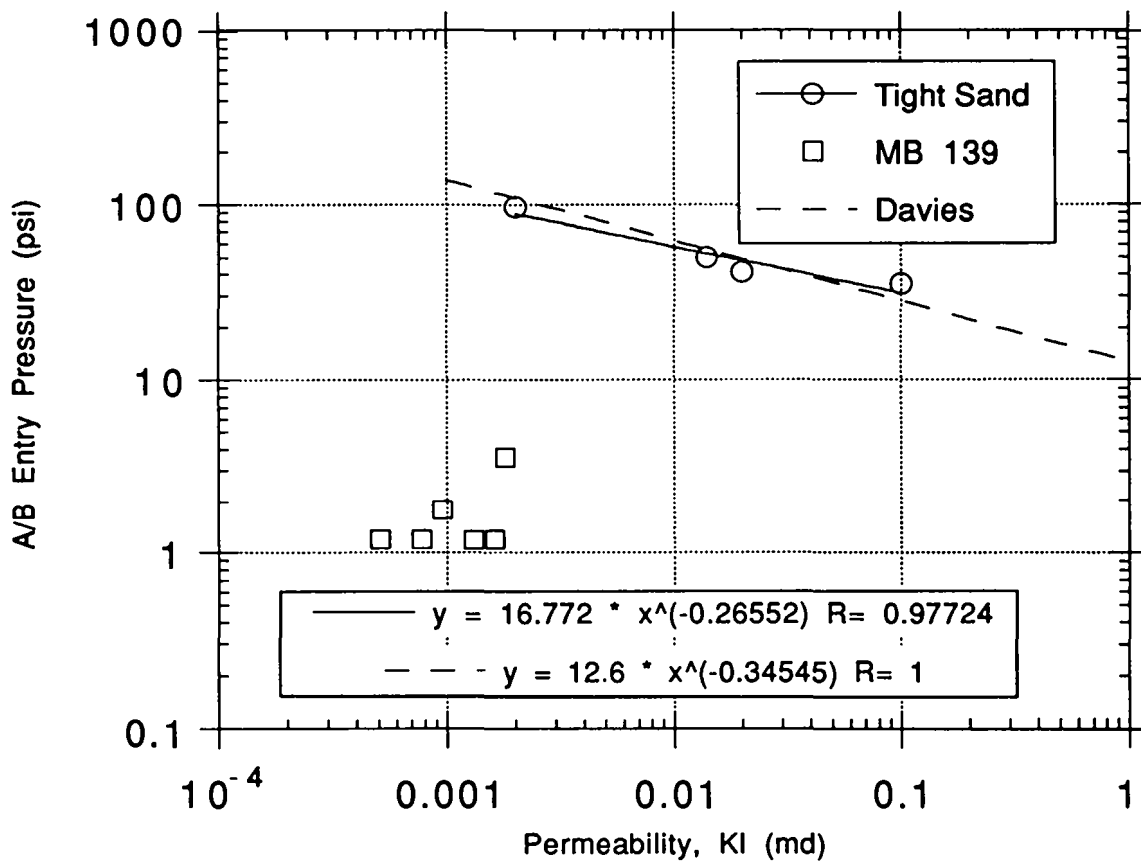
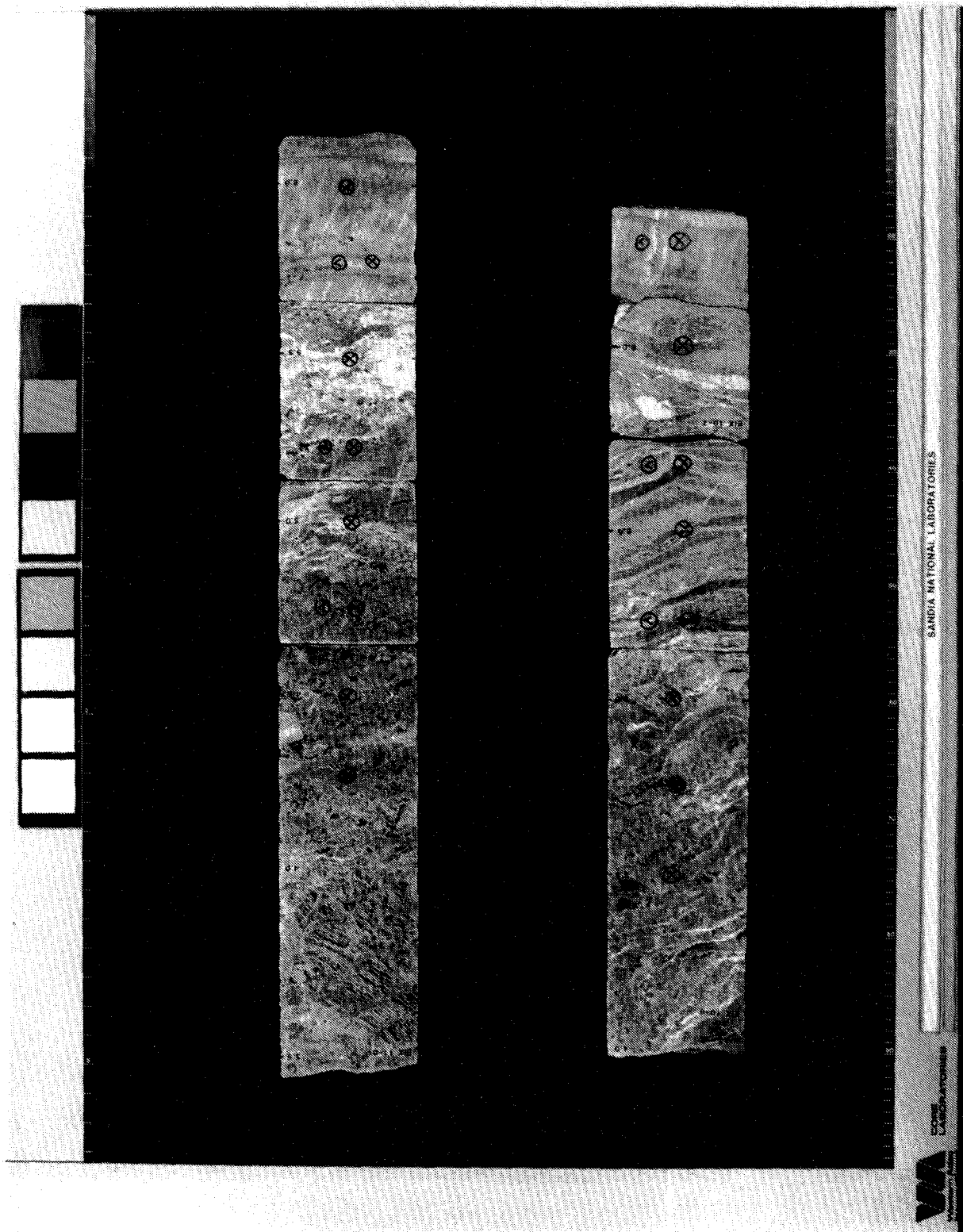


Figure 4.27: Equivalent Air-Brine Entry Pressure vs. Klinkenberg Permeability for Tight Sand Samples (Ref. 19), Davies (Ref. 20) and MB 139



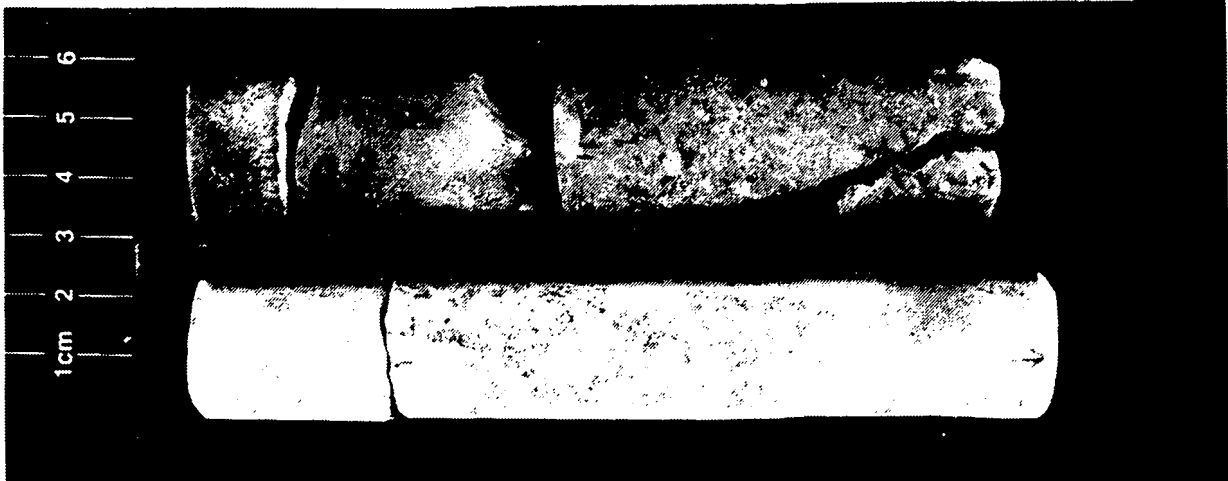
**Appendix A-A.
Appendix A of Appendix A [Data Report: Rock Physics Associates (Core
Laboratories)]**



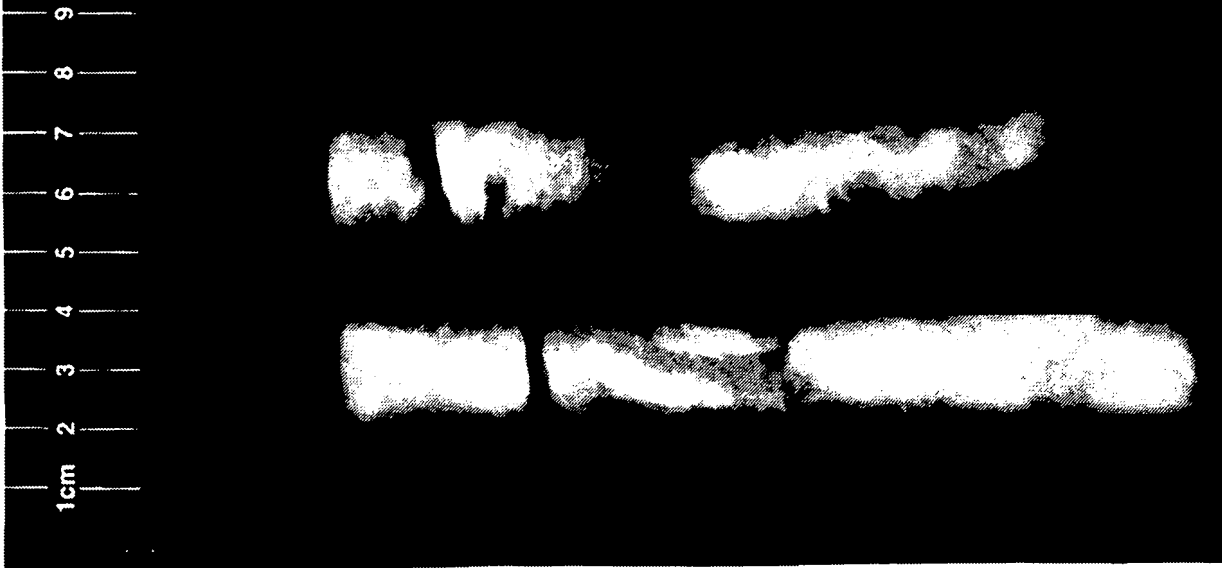


SANDIA
LABORATORIES

SANDIA NATIONAL LABORATORIES



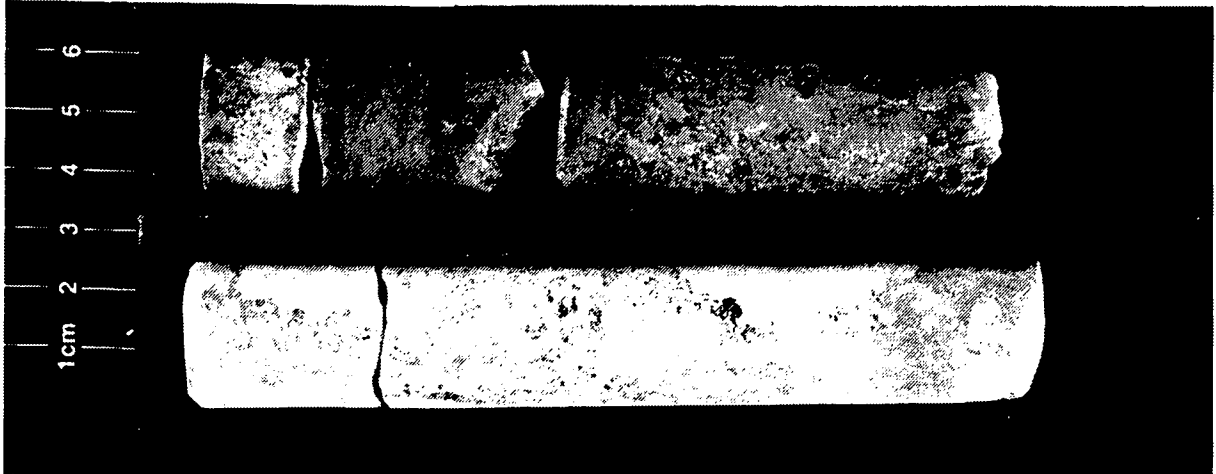
E1X 11 - 6	E1X 11 - 6
HORIZONTAL 4.25 FT.	HORIZONTAL 4.50 FT. 0°





CORE
LABORATORIES

SANDIA NATIONAL LABORATORIES



E1X 11 - 6	E1X 11 - 6
HORIZONTAL 4.25 FT.	HORIZONTAL 4.50 FT. 90°





CORE
LABORATORIES

SANDIA NATIONAL LABORATORIES



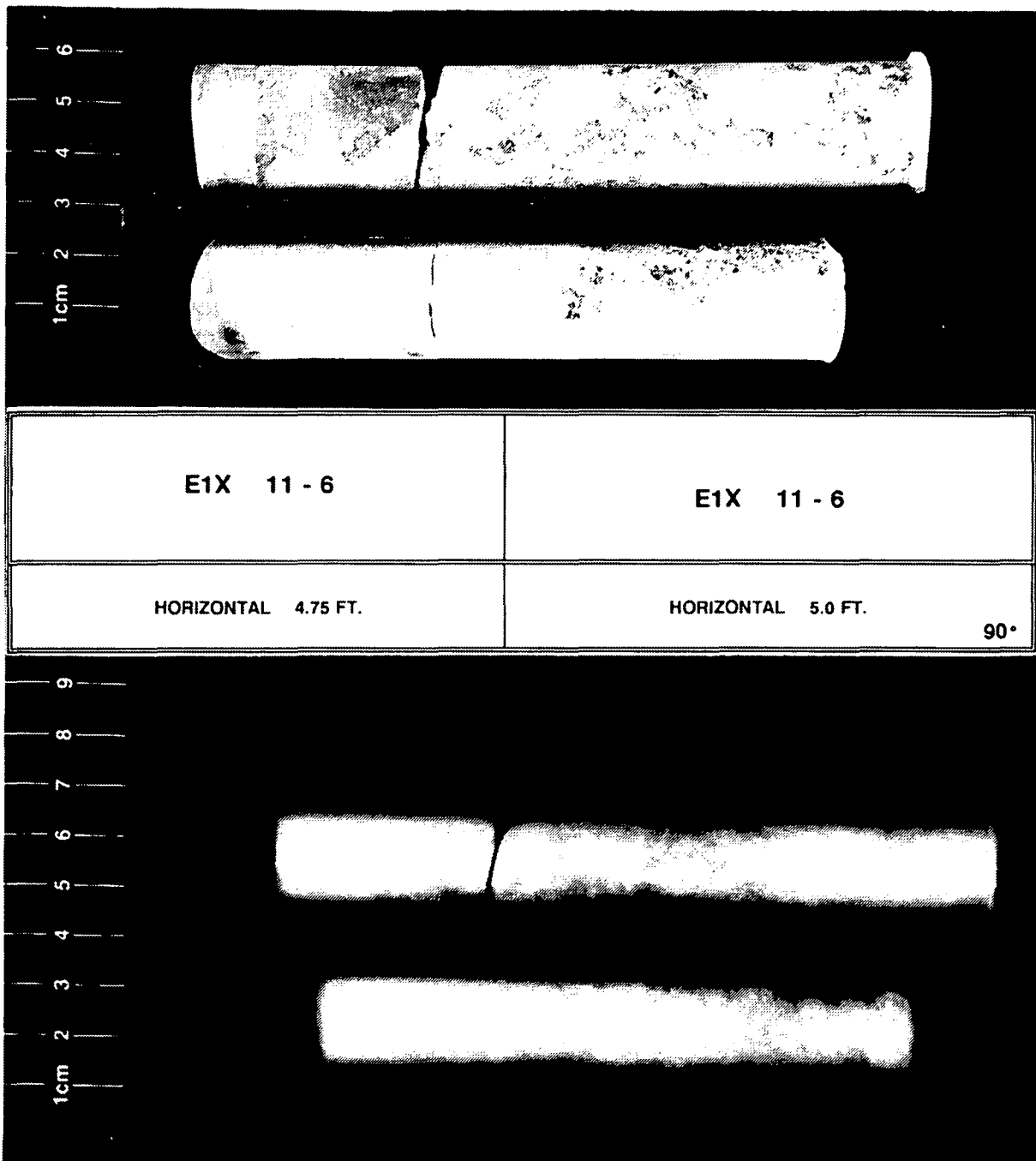
E1X 11 - 6	E1X 11 - 6
HORIZONTAL 4.75 FT.	HORIZONTAL 5.0 FT. 0°





SANDIA
LABORATORIES

SANDIA NATIONAL LABORATORIES



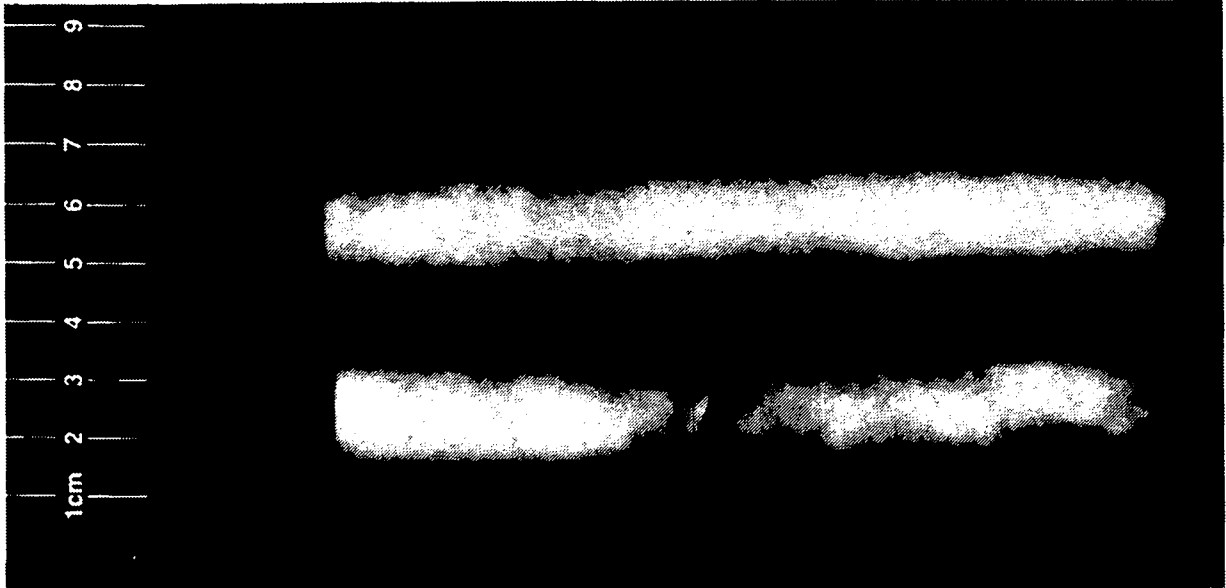


CORE
LABORATORIES

SANDIA NATIONAL LABORATORIES



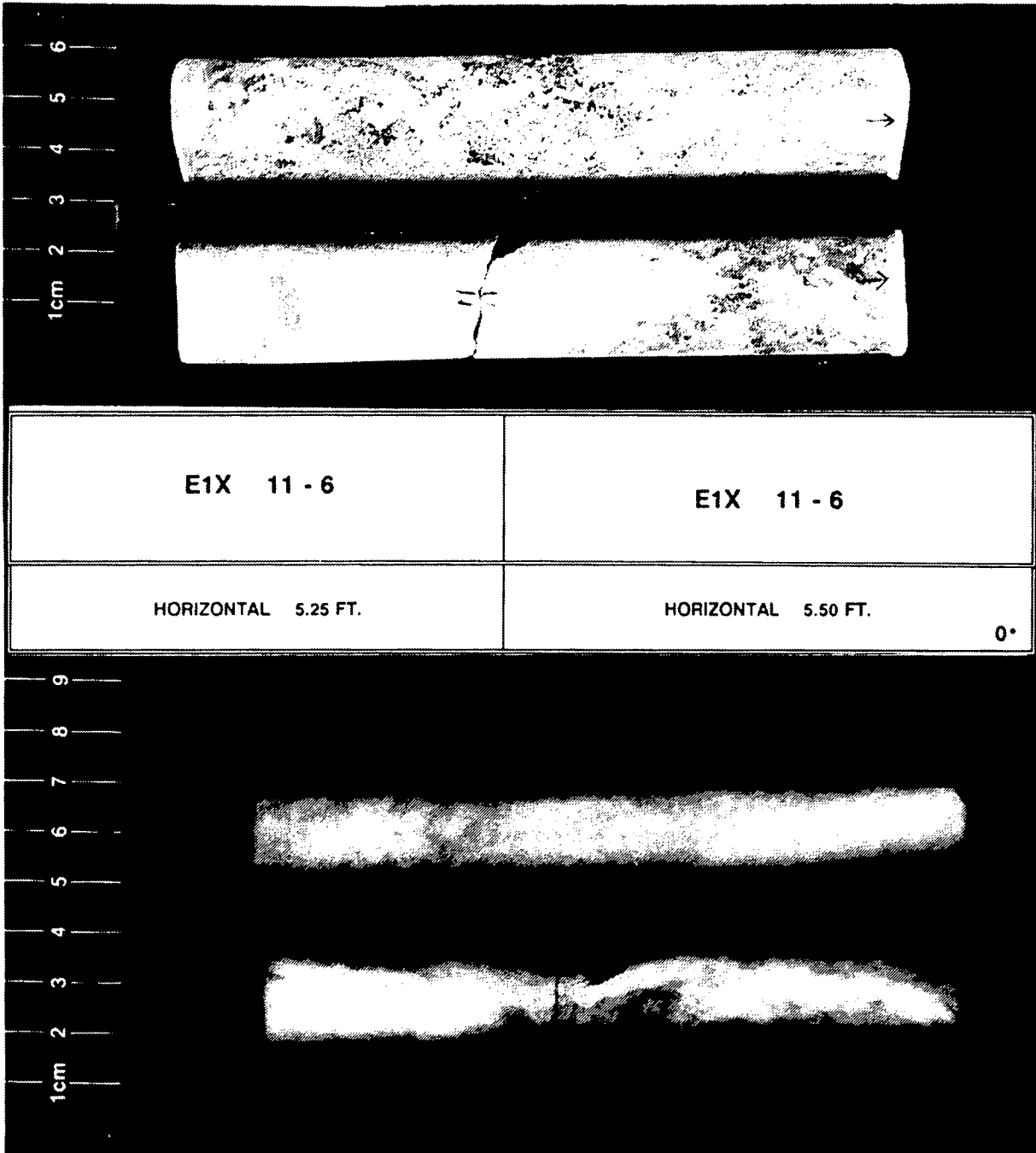
E1X 11 - 6	E1X 11 - 6
HORIZONTAL 5.25 FT.	HORIZONTAL 5.50 FT. 90°





CORE
LABORATORIES

SANDIA NATIONAL LABORATORIES



E1X 11 - 6

E1X 11 - 6

HORIZONTAL 5.25 FT.

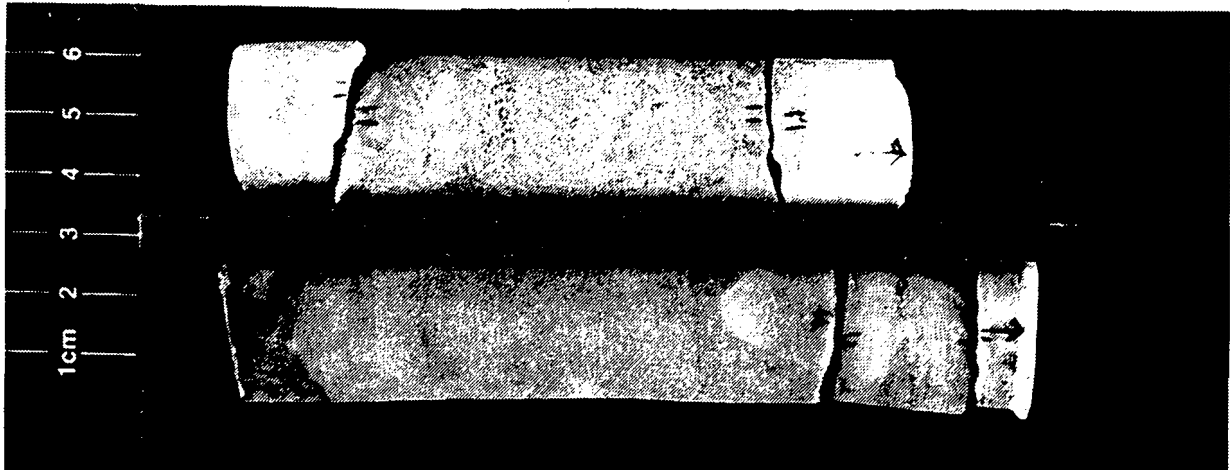
HORIZONTAL 5.50 FT.

0°



CORE
LABORATORIES

SANDIA NATIONAL LABORATORIES



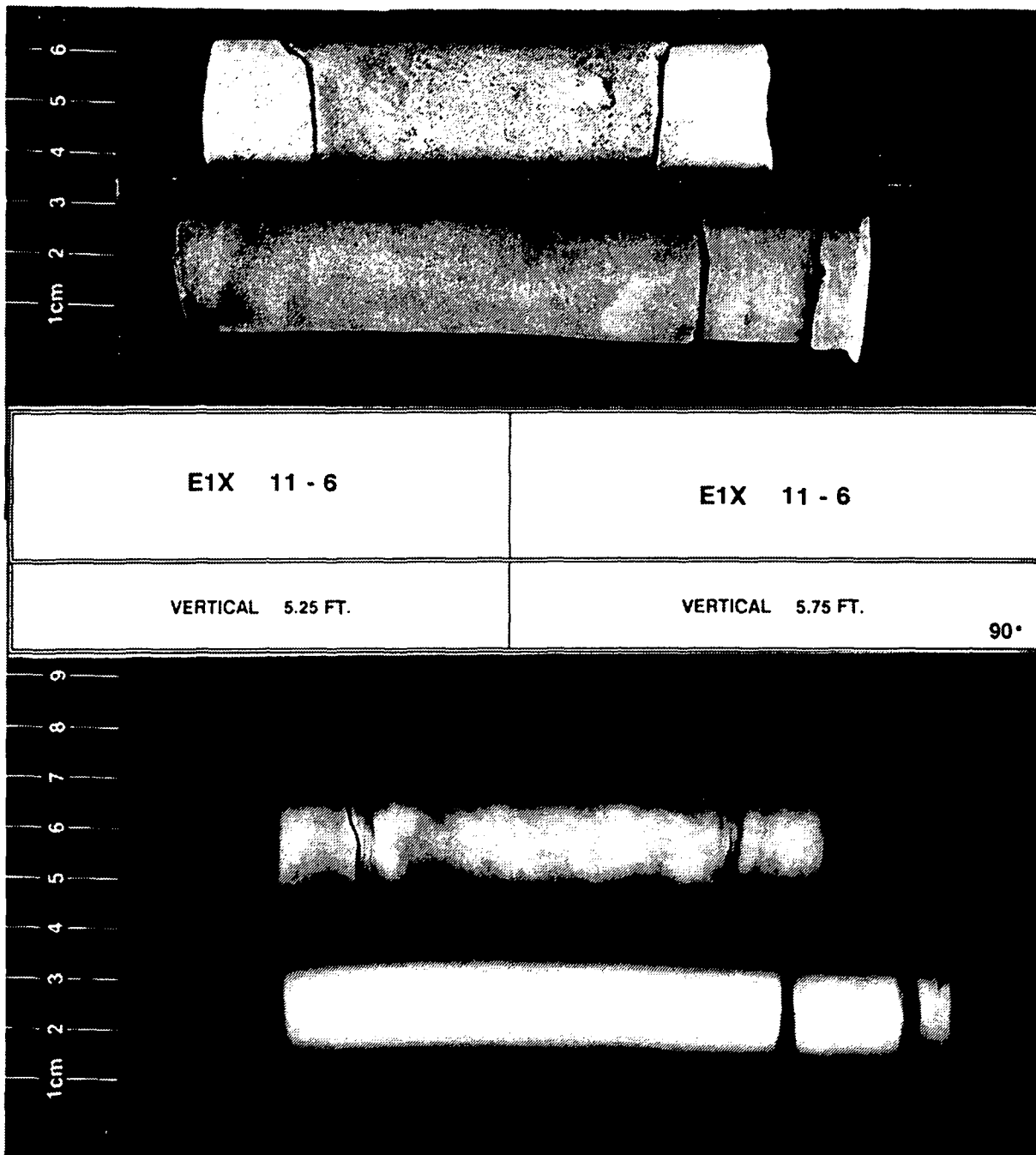
E1X 11 - 6	E1X 11 - 6
VERTICAL 5.25 FT.	VERTICAL 5.75 FT. 0°





CORE
LABORATORIES

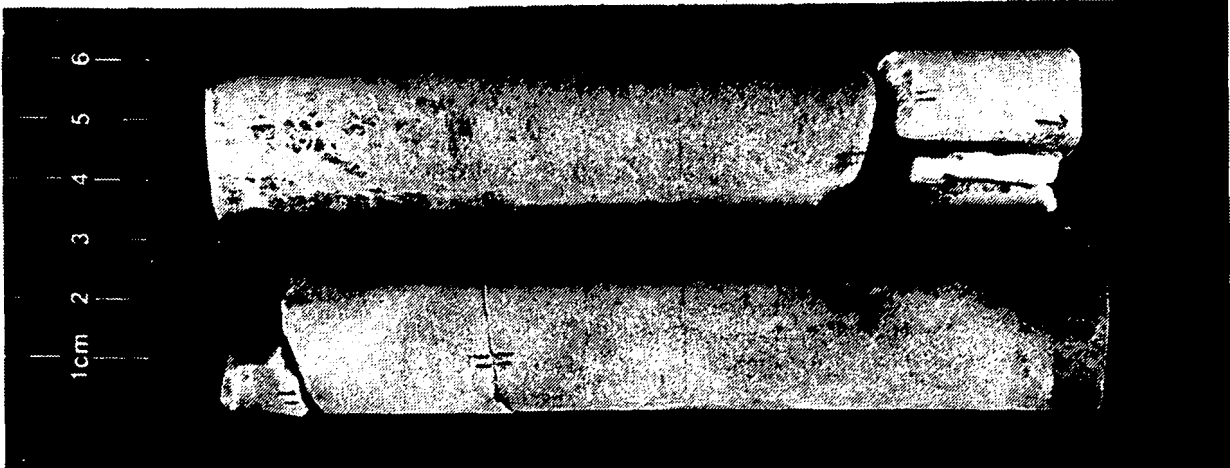
SANDIA NATIONAL LABORATORIES



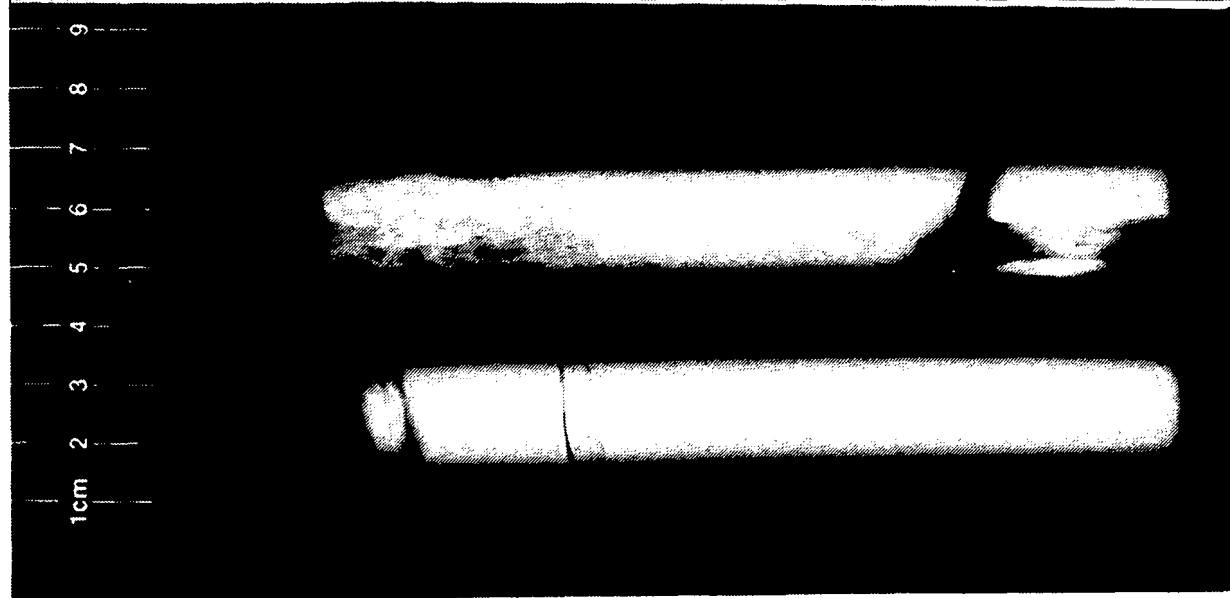


CORE
LABORATORIES

SANDIA NATIONAL LABORATORIES



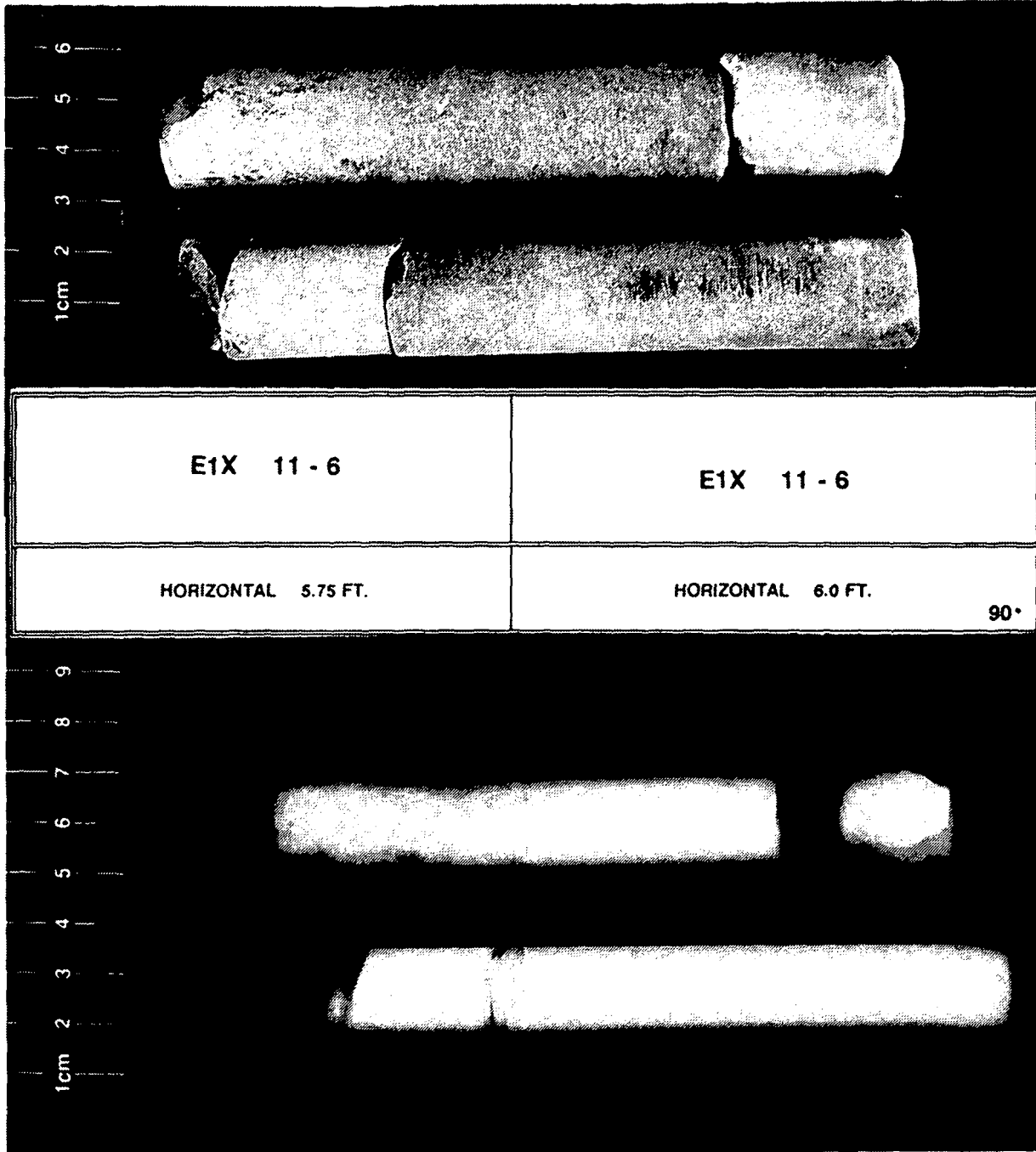
E1X 11 - 6	E1X 11 - 6
HORIZONTAL 5.75 FT.	HORIZONTAL 6.0 FT. 0°





CORE
LABORATORIES

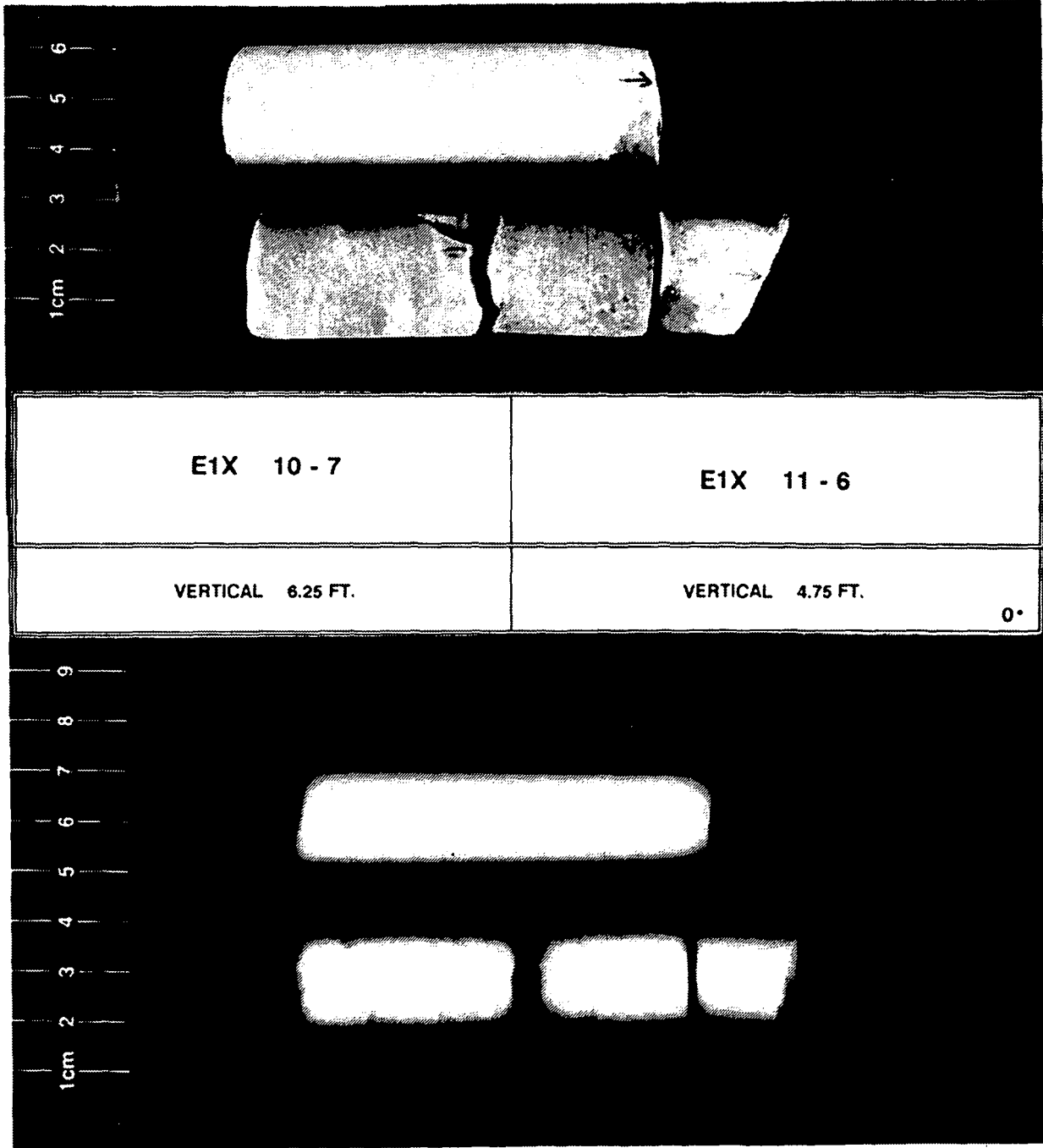
SANDIA NATIONAL LABORATORIES





CORE
LABORATORIES

SANDIA NATIONAL LABORATORIES





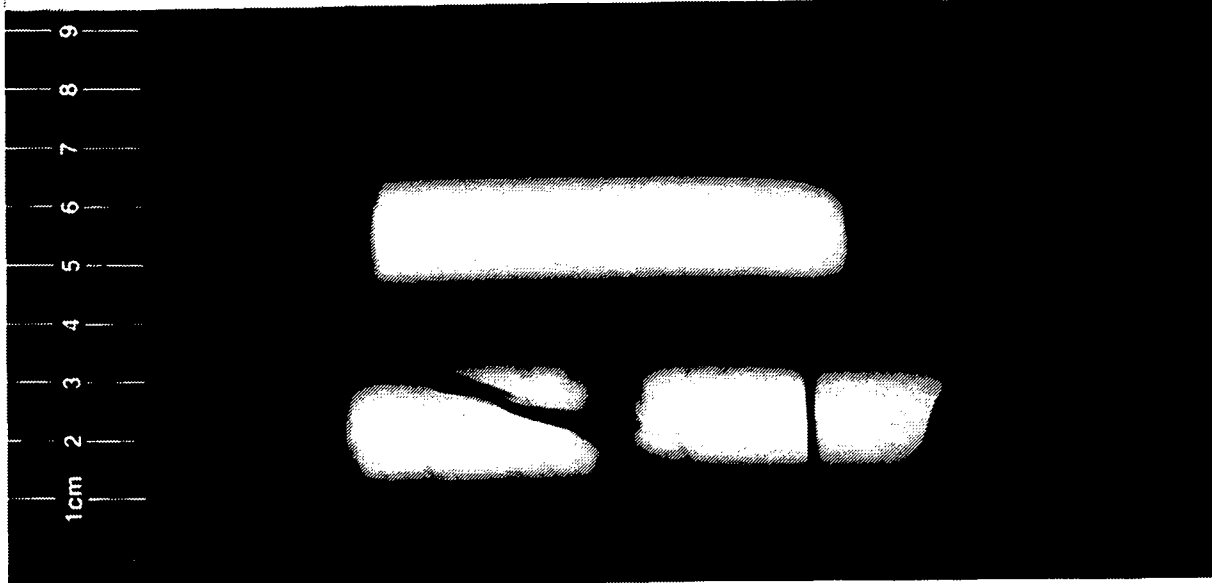
CORE
LABORATORIES

SANDIA NATIONAL LABORATORIES



E1X 10 - 7	E1X 11 - 6
VERTICAL 6.25 FT.	VERTICAL 4.75 FT.

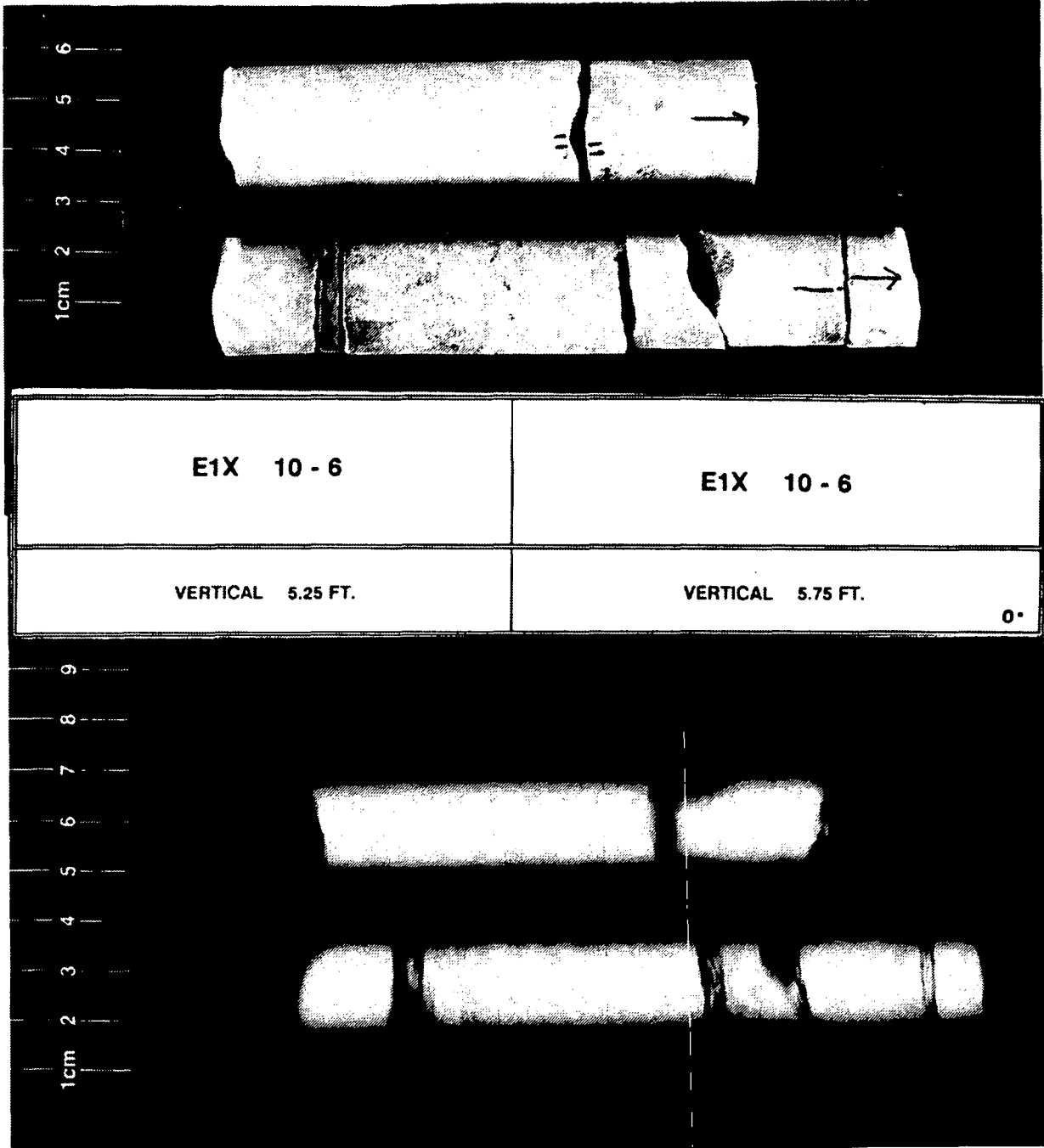
90°





CORE
LABORATORIES

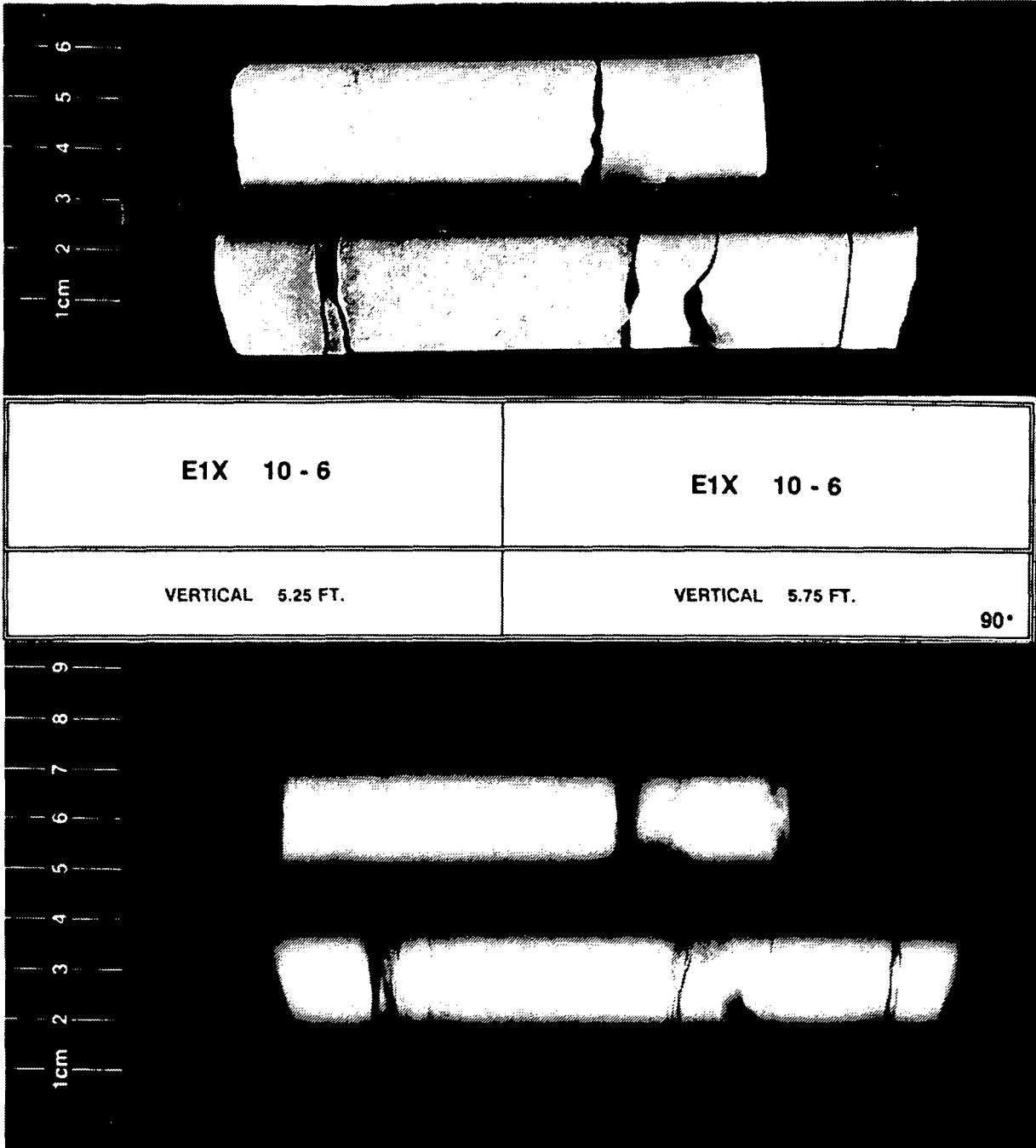
SANDIA NATIONAL LABORATORIES





CORE
LABORATORIES

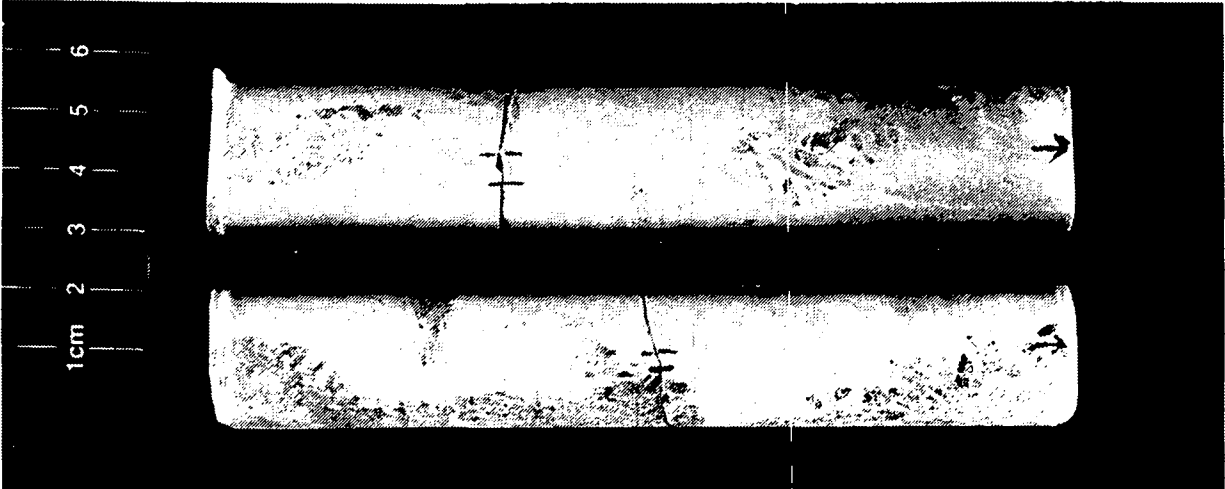
SANDIA NATIONAL LABORATORIES





CORE
LABORATORIES

SANDIA NATIONAL LABORATORIES



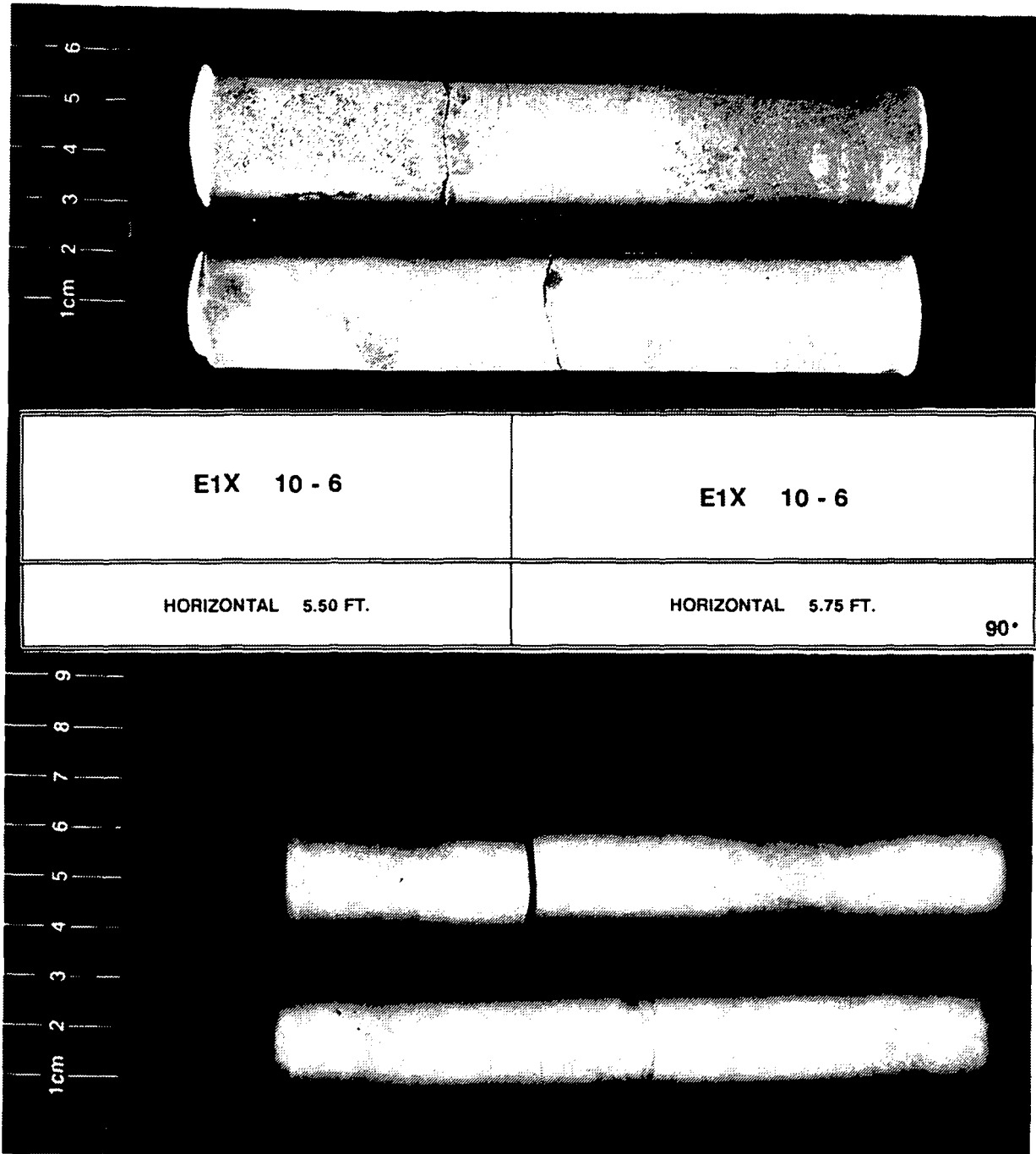
E1X 10 - 6	E1X 10 - 6
HORIZONTAL 5.50 FT.	HORIZONTAL 5.75 FT. 0°





CORE
LABORATORIES

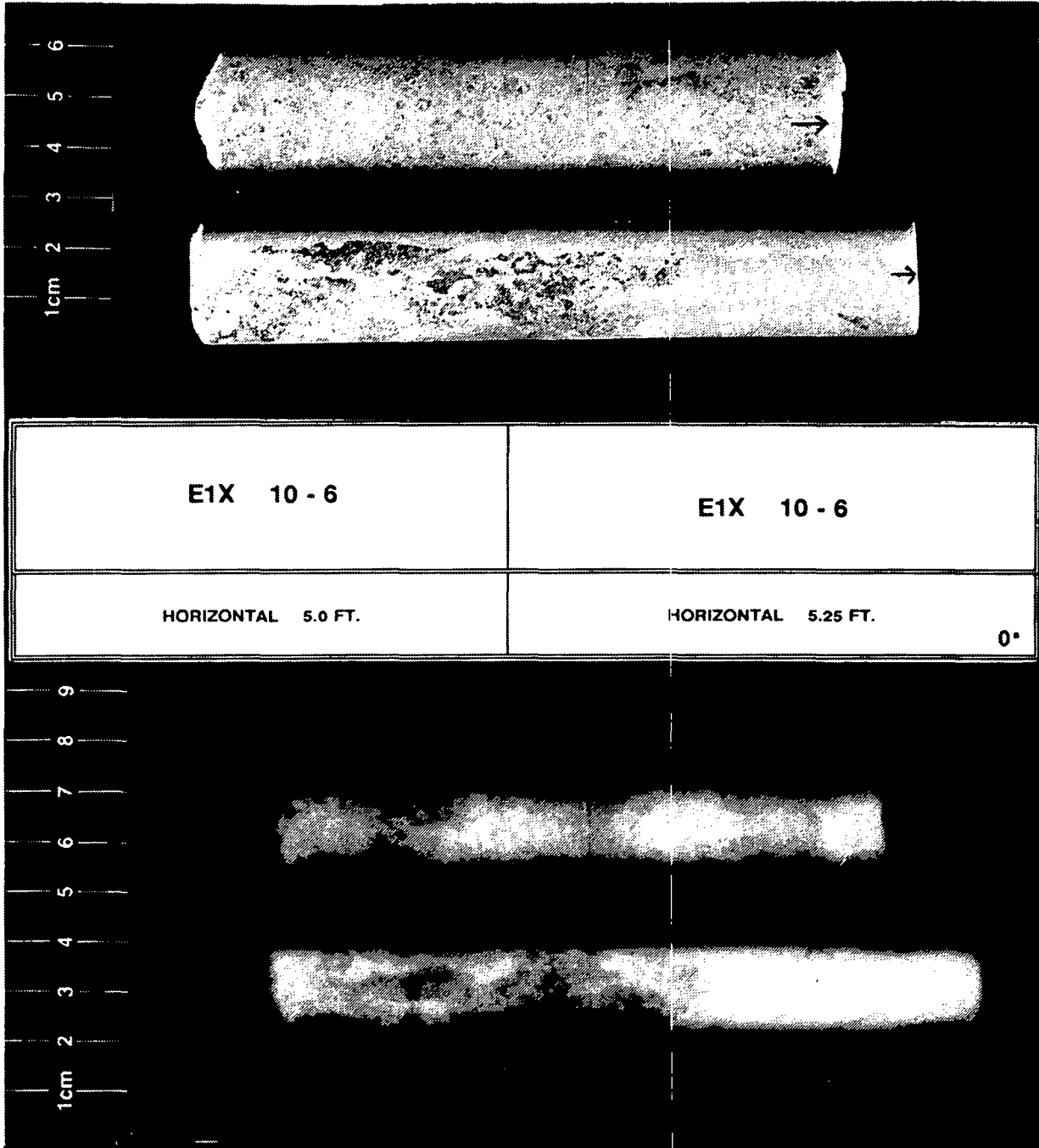
SANDIA NATIONAL LABORATORIES





CORE
LABORATORIES

SANDIA NATIONAL LABORATORIES





CORE
LABORATORIES

SANDIA NATIONAL LABORATORIES



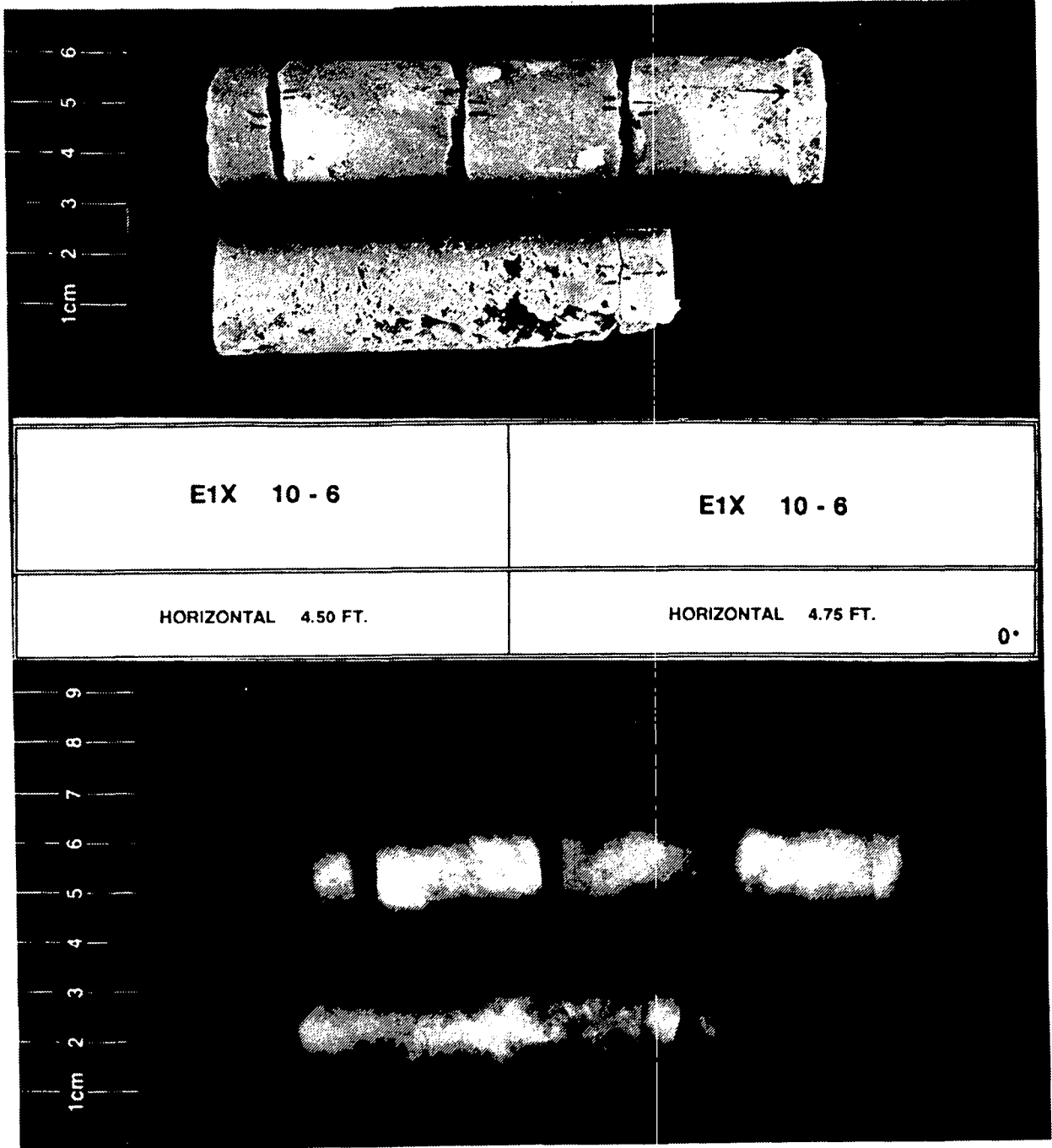
E1X 10 - 6	E1X 10 - 6
HORIZONTAL 5.0 FT.	HORIZONTAL 5.25 FT. 90°





CORE
LABORATORIES

SANDIA NATIONAL LABORATORIES



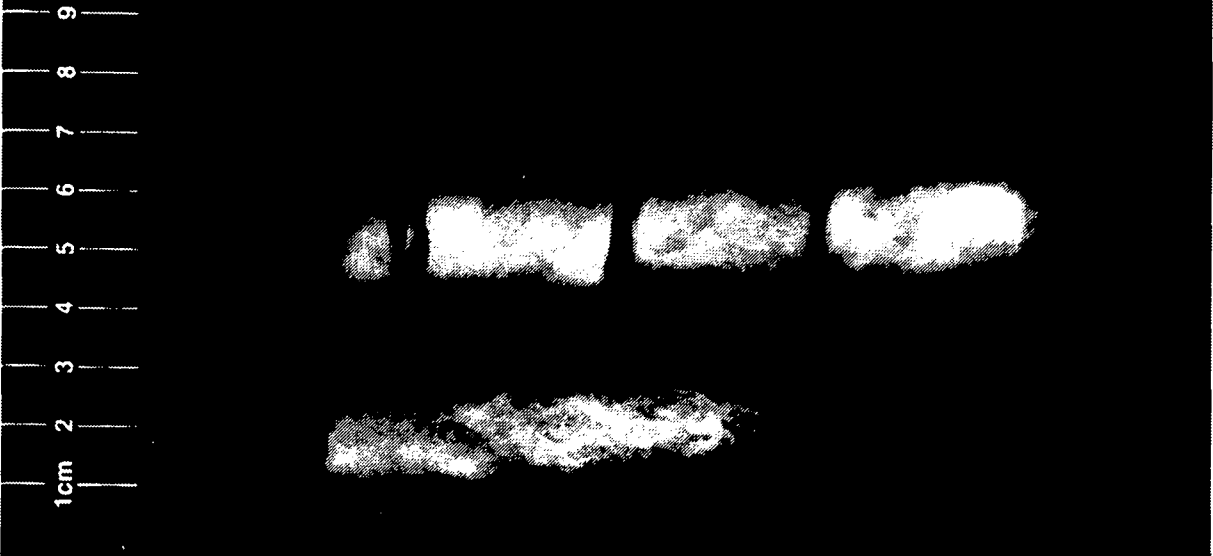


SANDIA
LABORATORIES

SANDIA NATIONAL LABORATORIES



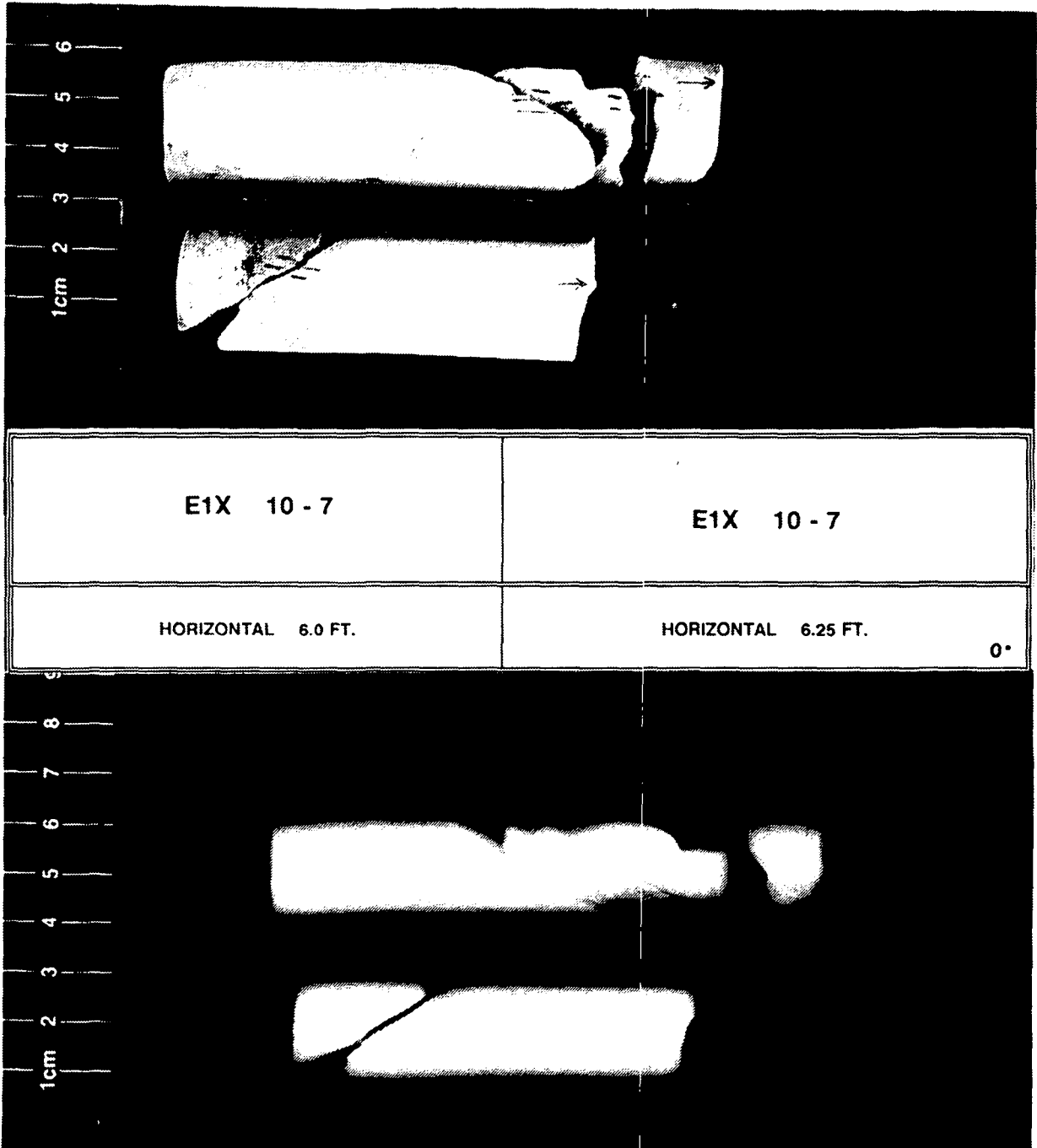
E1X 10 - 6	E1X 10 - 6
HORIZONTAL 4.50 FT.	HORIZONTAL 4.75 FT. 90°





SANDIA
LABORATORIES

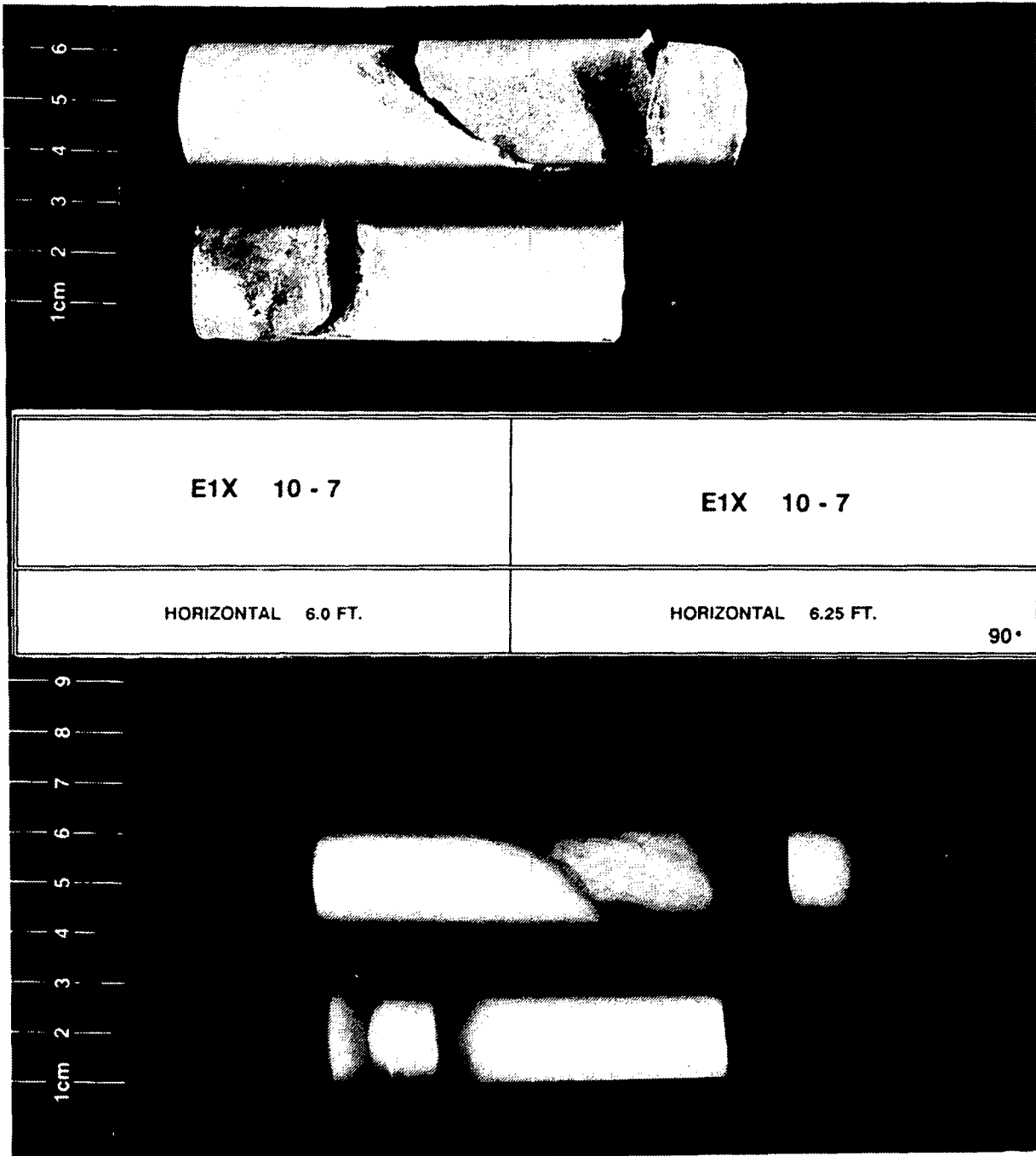
SANDIA NATIONAL LABORATORIES





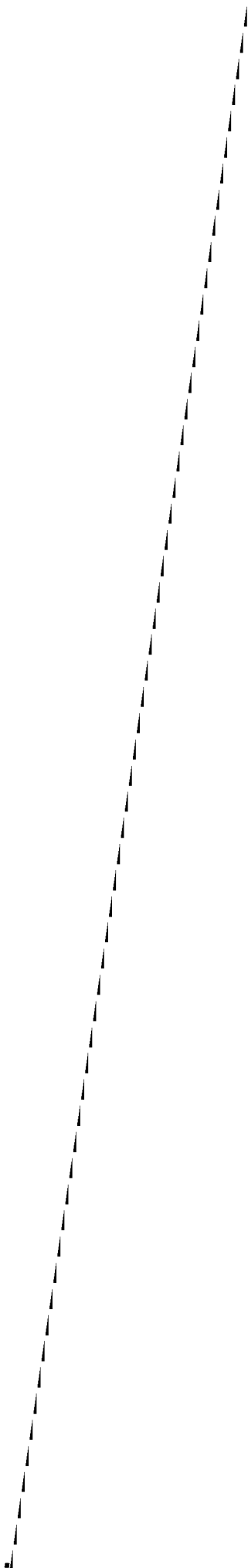
CORE
LABORATORIES

SANDIA NATIONAL LABORATORIES



**Appendix A-B.
Appendix B of Appendix A [Data Report: Rock Physics Associates (Core
Laboratories)]**

**PETROGRAPHIC STUDY
FOR
ROCK PHYSICS ASSOCIATES
WASTE ISOLATION PILOT PLANT**



August 2, 1993

Dr. Joel Walls
Rock Physics Associates
4320 Stevens Creek Boulevard
Suite #282
San Jose, California 95129

SUBJECT: Petrographic Study
Waste Isolation Pilot Plant
File No: G-2016

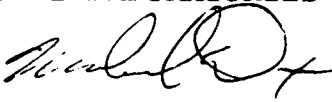
Dear Dr. Walls,

The following final report presents the results of a Petrographic Study, which includes thin section analysis and X-ray diffraction analysis (XRD), performed on fifteen (15) core plug end trim samples from the above referenced well. Included in this report are the analytical data, interpretations of results, and photomicrographs with descriptions. Two (2) copies of this report with photomicrographs are provided, as well as 2 xerox copies.

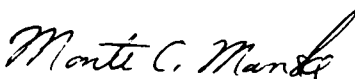
It has been a pleasure to provide this study for Rock Physics Associates. Feel free to contact us if you have any questions concerning this report or if we can be of further service.

Sincerely,

OMNI LABORATORIES



Michael Dixon
Manager, Geologic Services



Monte C. Manske
Senior Geologist

SUMMARY OF PETROGRAPHIC RESULTS

A Petrographic Study was performed on fifteen (15) core plug end trim samples. Included with this Petrographic Study are both thin section analysis and X-ray diffraction (XRD) analysis.

These samples are all evaporitic. Samples consist of a limited mineralogic suite of halite, anhydrite, gypsum, magnesite, and clay. Anhydrite, present in all samples, is the most common mineral. Halite is also very common and occurs in most samples, in some cases nearly as abundant as anhydrite. Magnesite occurs in low amounts in all samples. Gypsum and clay are trace components of most samples. Some iron oxide staining is evident in certain thin sections, but was not quantified.

INTRODUCTION

Thin section petrography and X-ray diffraction (XRD) analyses were performed on 15 core plug end trim samples from the referenced well. Table 1 outlines the sample designations and analyses performed.

TABLE 1
SAMPLE NUMBERS AND PETROGRAPHIC ANALYSES PERFORMED

<u>SAMPLE DESIGNATION (EIX)</u>	<u>SAMPLE # (OMNI)</u>	<u>THIN SECTION (TS)</u>	<u>X-RAY DIFFRACTION (XRD)</u>
10-6 H-4.50'	01	X	X
10-6 H-5.00'	02	X	X
10-6 H-5.25'	03	X	X
10-6 V-5.25'	04	X	X
10-6 H-5.50'	05	X	X
10-6 H-5.75'	06	X	X
10-6 V-5.75'	07	X	X
10-7 V-6.25'	08	X	X
11-6 H-4.50'	09	X	X
11-6 H-4.75'	10	X	X
11-6 H-5.00'	11	X	X
11-6 H-5.25'	12	X	X
11-6 V-5.25'	13	X	X
11-6 H-5.75'	14	X	X
11-6 V-5.75'	15	X	X

The objective of the petrographic analyses was to characterize the lithology and mineralogy in the evaporite interval.

PETROGRAPHIC RESULTS

The following sections briefly characterize the samples with respect to rock fabric, texture, and composition. Specific information on individual samples is provided in the Appendices and Photomicrographs with Captions sections.

Rock Fabric, Texture, and Composition

The samples are massive to "felted", and some show slight subparallel alignment. The principal mineral component, anhydrite (54-99% by weight from XRD), consists of densely packed laths. Areas of anhydrite are commonly separated by semi-circular patches of halite. Halite (trace-46% by weight from XRD) appears isotropic in thin section but is identified by its cubic cleavage, mineral/fluid inclusions, and rare negative crystals. Inclusions in halite are normally undefined dusty clusters. In some cases they are identifiable as magnesite, and occasionally they are aligned in linear aggregates or "trails". Coarser laths of anhydrite, and rare gypsum (0%-trace), occur near the contacts with halite. Magnesite (trace-4% by weight from XRD) is a magnesium carbonate mineral with very high birefringence found associated with both the anhydrite and halite (mainly with anhydrite). It exists as very small, rhombohedral crystals within the rock groundmass. Detrital clay (0%-trace) occurs in stringers in most samples. Crystal size of the anhydrite varies slightly throughout the sample interval. Crystal size is commonly 10-40 microns within the dense portions of the samples, and there is no significant variation between the samples, except in the last sample. Sample EIX 11-6 V-5.75' contains coarser crystals (40-100 microns) throughout. In all samples containing halite, anhydrite crystal size increases dramatically to greater than 500 microns near the halite zones. Coarse gypsum crystals are also present near the halite.

APPENDIX A-B.1

ANALYTICAL PROCEDURES

Sample Preparation

Core plug end trim samples were first separated into two fractions, one for X-ray diffraction analysis and one for thin sectioning. The thin section samples were cut of standard size (to fit a 27 mm by 46 mm glass slide) and thickness (0.03 mm). Samples were cut in oil, or dry whenever possible, to prevent the loss of water soluble phases.

Approximately 4 grams of each X-ray Diffraction sample was first ground in a Brinkmann Retsch MM-2 mortar to attain proper particle size. Samples were then loaded into bulk sample holders for X-ray Diffraction scanning.

Methods

Thin section samples were analyzed on a Nikon polarizing microscope with a Swift automatic point-count attachment stage and box. Three hundred (300) points were counted per thin section, and the percent of each mineral species present was derived. Later, thin section photography was performed with an attached 35 mm camera assembly.

The portions of the samples subjected to X-ray Diffraction analysis were scanned on a Philips XRD unit. The scan range was 2 degrees to 70 degrees two theta. The resultant "patterns" were then analyzed to determine mineralogy.

APPENDIX A-B.2

X-RAY DIFFRACTION DATA

APPENDIX A-B.3

**THIN SECTION POINT-COUNT ANALYSIS
AND
THIN SECTION PHOTOMICROGRAPHS**

**ROCK PHYSICS ASSOCIATES
WASTE ISOLATION PILOT PLANT
Thin Section Modal Analysis**

SAMPLE:	EIX 10-6 H-4.50'	EIX 10-6 H-5.00'	EIX 10-6 H-5.25'	EIX 10-6 V-5.25'
Rock Name:	Evaporite	Evaporite	Evaporite	Evaporite
FRAMEWORK GRAINS				
Quartz	<u>0</u>	<u>0</u>	<u>0</u>	<u>0</u>
Monocrystalline	0	0	0	0
Polycrystalline	0	0	0	0
Feldspar	<u>0</u>	<u>0</u>	<u>0</u>	<u>0</u>
K-feldspar	0	0	0	0
Plagioclase	0	0	0	0
Lithic Fragments	<u>0</u>	<u>0</u>	<u>0</u>	<u>0</u>
Plutonic	0	0	0	0
Volcanic	0	0	0	0
Metamorphic	0	0	0	0
Chert	0	0	0	0
Mudstone	0	0	0	0
Accessory Grains	<u>0</u>	<u>0</u>	<u>0</u>	<u>0</u>
Muscovite	0	0	0	0
Biotite	0	0	0	0
Heavy Minerals	0	0	0	0
ENVIRON. INDICATORS				
Organic Materials	0	0	0	0
Glauconite	0	0	0	0
Calcareous Frag.	0	0	0	0
CLAY MATRIX	tr	tr	tr	tr
AUTHIGENIC CEMENT	<u>100</u>	<u>100</u>	<u>100</u>	<u>100</u>
Clay	0	0	0	0
Quartz Overgrowths	0	0	0	0
Gypsum	tr	tr	tr	tr
Anhydrite	82	72	67	99
Halite	16	26	30	1
Calcite	0	0	0	0
Ankerite	0	0	0	0
Magnesite	2	2	3	tr
Pyrite	0	0	0	0
POROSITY	<u>0</u>	<u>0</u>	<u>0</u>	<u>0</u>
Primary	0	0	0	0
Secondary	0	0	0	0
Microscopic	0	0	0	0
TOTALS	100	100	100	100

**ROCK PHYSICS ASSOCIATES
WASTE ISOLATION PILOT PLANT
Thin Section Modal Analysis**

SAMPLE:	EIX 10-6 H-5.50'	EIX 10-6 H-5.75'	EIX 10-6 V-5.75'	EIX 10-7 V-6.25'
Rock Name:	Evaporite	Evaporite	Evaporite	Evaporite
FRAMEWORK GRAINS				
Quartz	0	0	0	0
Monocrystalline	0	0	0	0
Polycrystalline	0	0	0	0
Feldspar	0	0	0	0
K-feldspar	0	0	0	0
Plagioclase	0	0	0	0
Lithic Fragments	0	0	0	0
Plutonic	0	0	0	0
Volcanic	0	0	0	0
Metamorphic	0	0	0	0
Chert	0	0	0	0
Mudstone	0	0	0	0
Accessory Grains	0	0	0	0
Muscovite	0	0	0	0
Biotite	0	0	0	0
Heavy Minerals	0	0	0	0
ENVIRON. INDICATORS				
Organic Materials	0	0	0	0
Glauconite	0	0	0	0
Calcareous Frag.	0	0	0	0
CLAY MATRIX	tr	tr	tr	tr
AUTHIGENIC CEMENT	<u>100</u>	<u>100</u>	<u>100</u>	<u>100</u>
Clay	0	0	0	0
Quartz Overgrowths	0	0	0	0
Gypsum	tr	0	tr	0
Anhydrite	93	95	82	100
Halite	2	0	15	0
Calcite	0	0	0	0
Ankerite	0	0	0	0
Magnesite	5	5	3	tr
Pyrite	0	0	0	0
POROSITY	0	0	0	0
Primary	0	0	0	0
Secondary	0	0	0	0
Microscopic	0	0	0	0
TOTALS	100	100	100	100

**ROCK PHYSICS ASSOCIATES
WASTE ISOLATION PILOT PLANT
Thin Section Modal Analysis**

SAMPLE:	EIX 11-6 H-4.50'	EIX 11-6 H-4.75'	EIX 11-6 H-5.00'	EIX 11-6 H-5.25'
Rock Name:	Evaporite	Evaporite	Evaporite	Evaporite
FRAMEWORK GRAINS				
Quartz	<u>0</u>	<u>0</u>	<u>0</u>	<u>0</u>
Monocrystalline	0	0	0	0
Polycrystalline	0	0	0	0
Feldspar	<u>0</u>	<u>0</u>	<u>0</u>	<u>0</u>
K-feldspar	0	0	0	0
Plagioclase	0	0	0	0
Lithic Fragments	<u>0</u>	<u>0</u>	<u>0</u>	<u>0</u>
Plutonic	0	0	0	0
Volcanic	0	0	0	0
Metamorphic	0	0	0	0
Chert	0	0	0	0
Mudstone	0	0	0	0
Accessory Grains	<u>0</u>	<u>0</u>	<u>0</u>	<u>0</u>
Muscovite	0	0	0	0
Biotite	0	0	0	0
Heavy Minerals	0	0	0	0
ENVIRON. INDICATORS				
Organic Materials	0	0	0	0
Glaucanite	0	0	0	0
Calcareous Frag.	0	0	0	0
CLAY MATRIX	tr	0	tr	tr
AUTHIGENIC CEMENT	<u>100</u>	<u>100</u>	<u>100</u>	<u>100</u>
Clay	0	0	0	0
Quartz Overgrowths	0	0	0	0
Gypsum	tr	1	tr	tr
Anhydrite	60	71	64	69
Halite	37	26	30	26
Calcite	0	0	0	0
Ankerite	0	0	0	0
Magnesite	3	2	6	5
Pyrite	0	0	0	0
POROSITY	<u>0</u>	<u>0</u>	<u>0</u>	<u>0</u>
Primary	0	0	0	0
Secondary	0	0	0	0
Microscopic	0	0	0	0
TOTALS	100	100	100	100

**ROCK PHYSICS ASSOCIATES
WASTE ISOLATION PILOT PLANT
Thin Section Modal Analysis**

SAMPLE:	EIX 11-6 V-5.25'	EIX 11-6 H-5.75'	EIX 11-6 V-5.75'
Rock Name:	Evaporite	Evaporite	Evaporite
FRAMEWORK GRAINS			
Quartz	0	0	0
Monocrystalline	0	0	0
Polycrystalline	0	0	0
Feldspar	0	0	0
K-feldspar	0	0	0
Plagioclase	0	0	0
Lithic Fragments	0	0	0
Plutonic	0	0	0
Volcanic	0	0	0
Metamorphic	0	0	0
Chert	0	0	0
Mudstone	0	0	0
Accessory Grains	0	0	0
Muscovite	0	0	0
Biotite	0	0	0
Heavy Minerals	0	0	0
ENVIRON. INDICATORS			
Organic Materials	0	0	0
Glauconite	0	0	0
Calcareous Frag.	0	0	0
CLAY MATRIX	tr	tr	0
AUTHIGENIC CEMENT	100	100	100
Clay	0	0	0
Quartz Overgrowths	0	0	0
Gypsum	tr	tr	0
Anhydrite	83	44	100
Halite	12	56	0
Calcite	0	0	0
Ankerite	0	0	0
Magnesite	5	tr	tr
Pyrite	0	0	0
POROSITY	0	0	0
Primary	0	0	0
Secondary	0	0	0
Microscopic	0	0	0
TOTALS	100	100	100

SAMPLE NUMBER: EIX 10-6 H-4.50'

PLATE 1A

This low magnification photomicrograph displays an evaporite rock consisting mainly of anhydrite (tan) and halite (white, center). Anhydrite crystals are generally fine (area of C4) to coarse (H6) near the halite. Magnesite is a patchy carbonate mineral present.

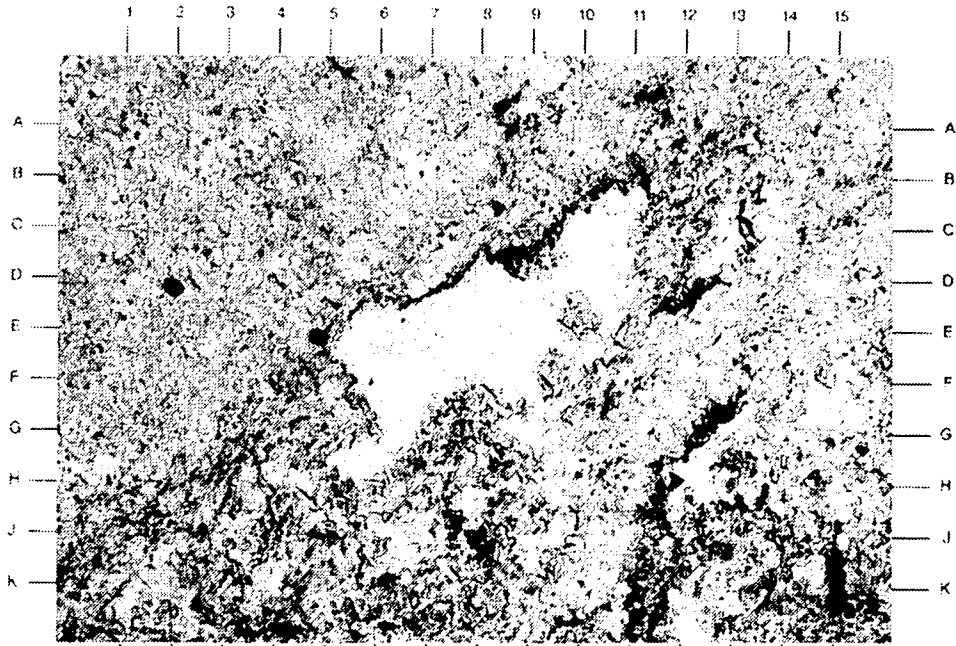
Magnification: 40X

SAMPLE NUMBER: EIX 10-6 H-4.50'

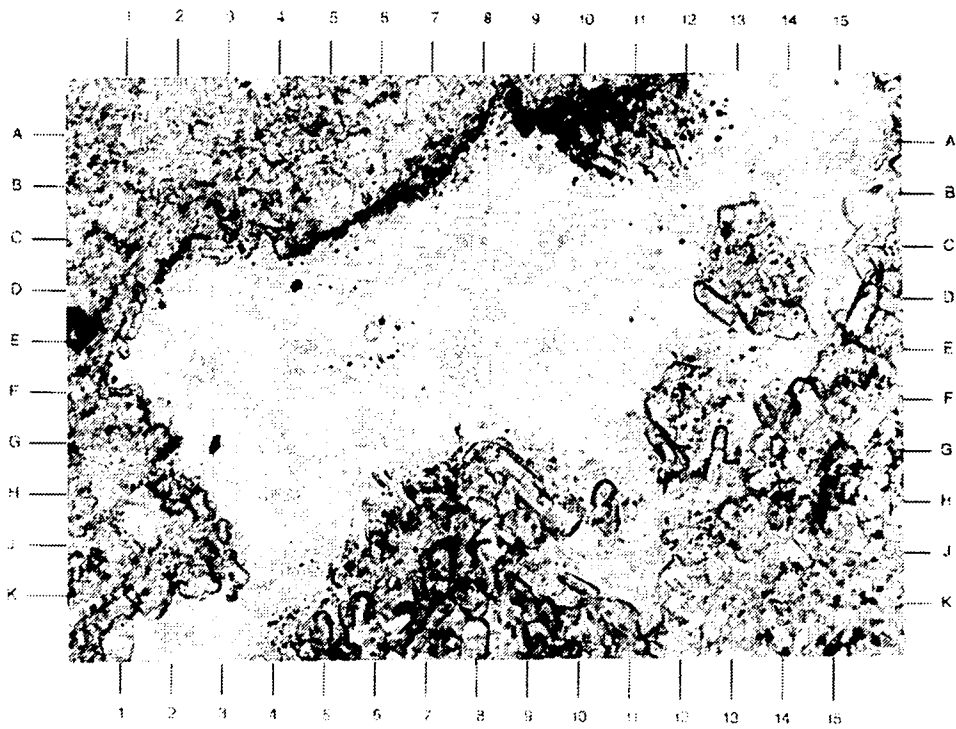
PLATE 1B

The high magnification view documents the relationship of the three main minerals in this sample. Halite (center) appears white, and in this sample shows little evidence of cleavage or inclusions. Tiny rhombs of magnesite (A10) rim the halite/anhydrite contact. Relatively large anhydrite crystal laths (H9) are found bordering the halite.

Magnification: 100X



A



B

SAMPLE NUMBER: EIX 10-6 H-5.00'

PLATE 2A

The low magnification survey view shows a representative section of this evaporite. Halite (white, left of center) is common. Magnesite is found associated with both the halite (G7) and anhydrite (E13). Large anhydrite laths (K7,C5), and occasional gypsum laths, protrude into the halite.

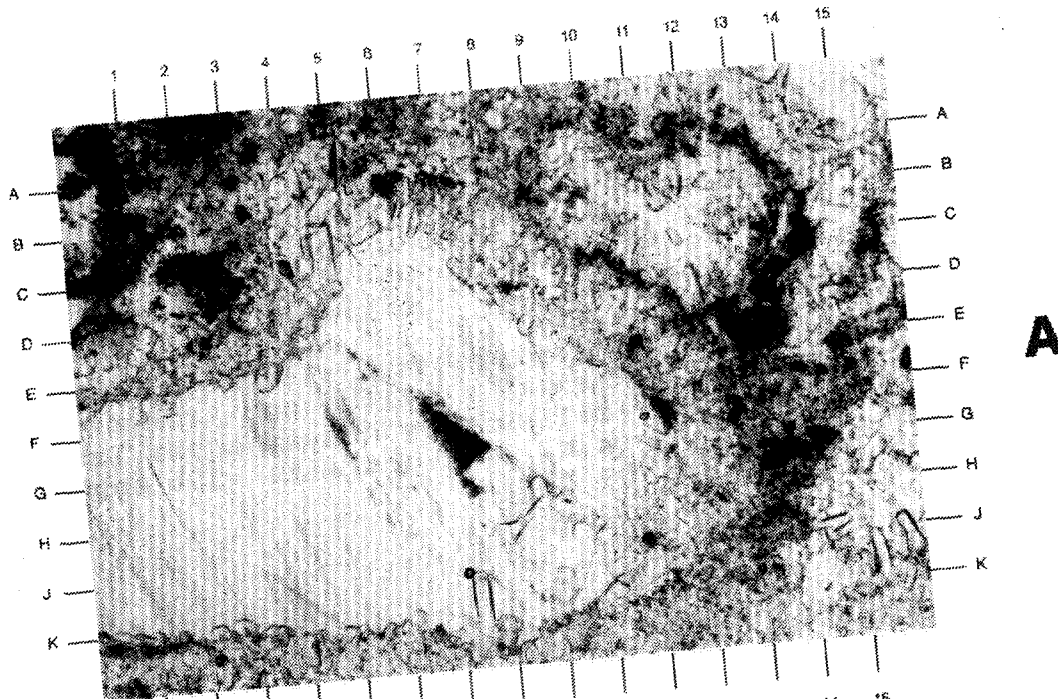
Magnification: 40X

SAMPLE NUMBER: EIX 10-6 H-5.00'

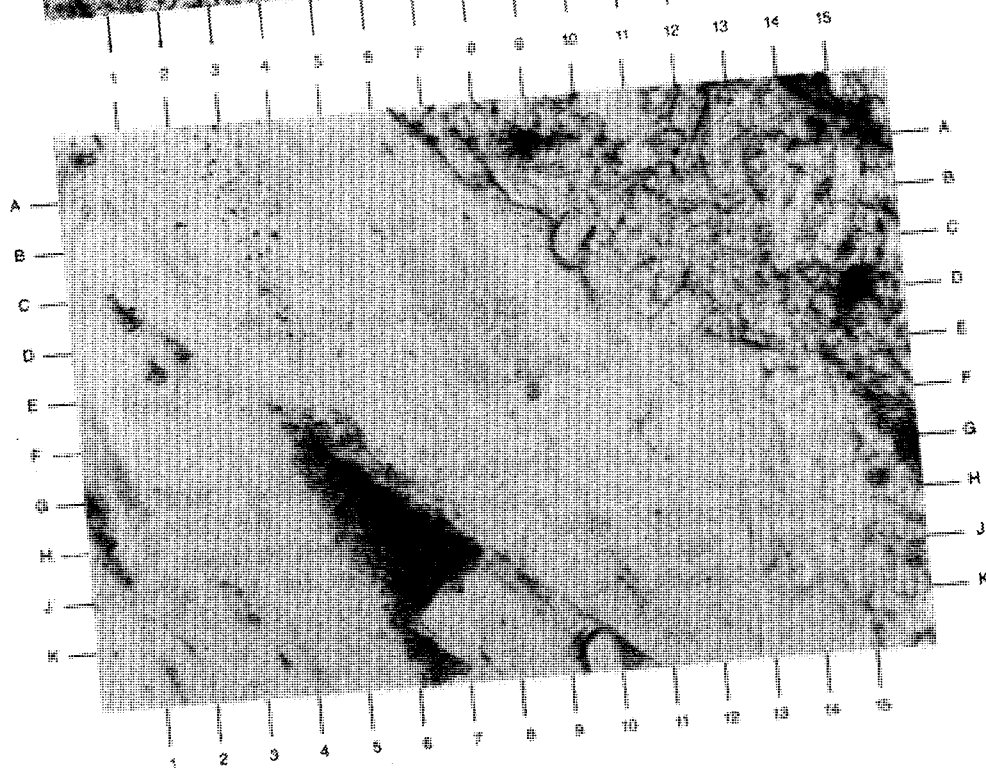
PLATE 2B

The high magnification view demonstrates the interrelationship of all three major mineral phases. Magnesite is composed of small, dark brown, rhombohedral crystals (H6) contained within, in this case, the halite. Halite shows evidence of inclusion zoning (diagonal from A2.5 to D4). Anhydrite is composed of densely-packed, lathlike, bladed crystals (B15,D-E11.5).

Magnification: 100X



A



B

SAMPLE NUMBER: EIX 10-6 H-5.25'

PLATE 3A

The low magnification photomicrograph depicts the complex intergrowth relationship of halite (white) and anhydrite (tan). Original bedding may be defined by clayey zones (subvertical brown streaks at J1,G4). This rock contains 56% anhydrite and 44% halite (weight percent by XRD).

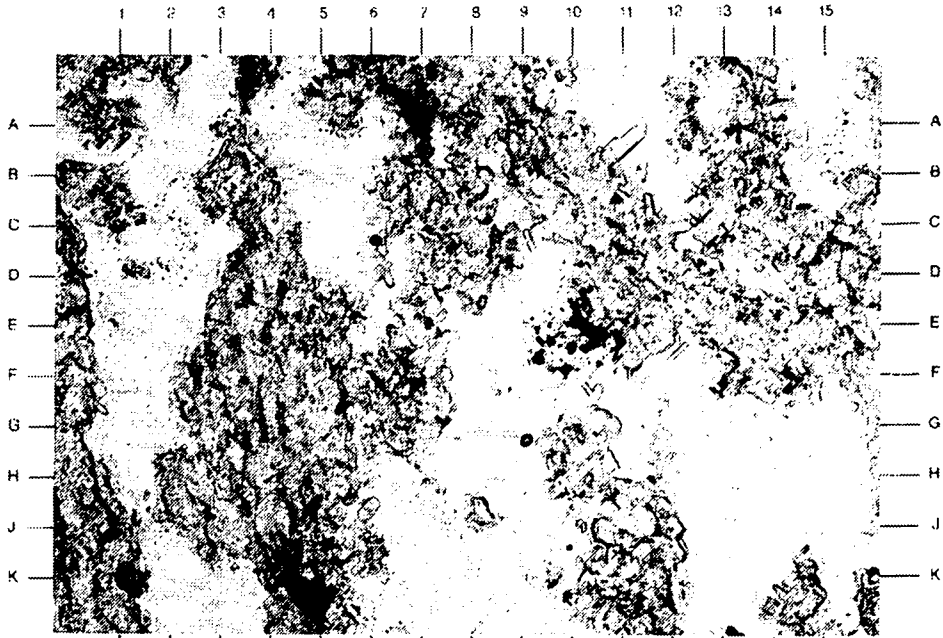
Magnification: 40X

SAMPLE NUMBER: EIX 10-6 H-5.25'

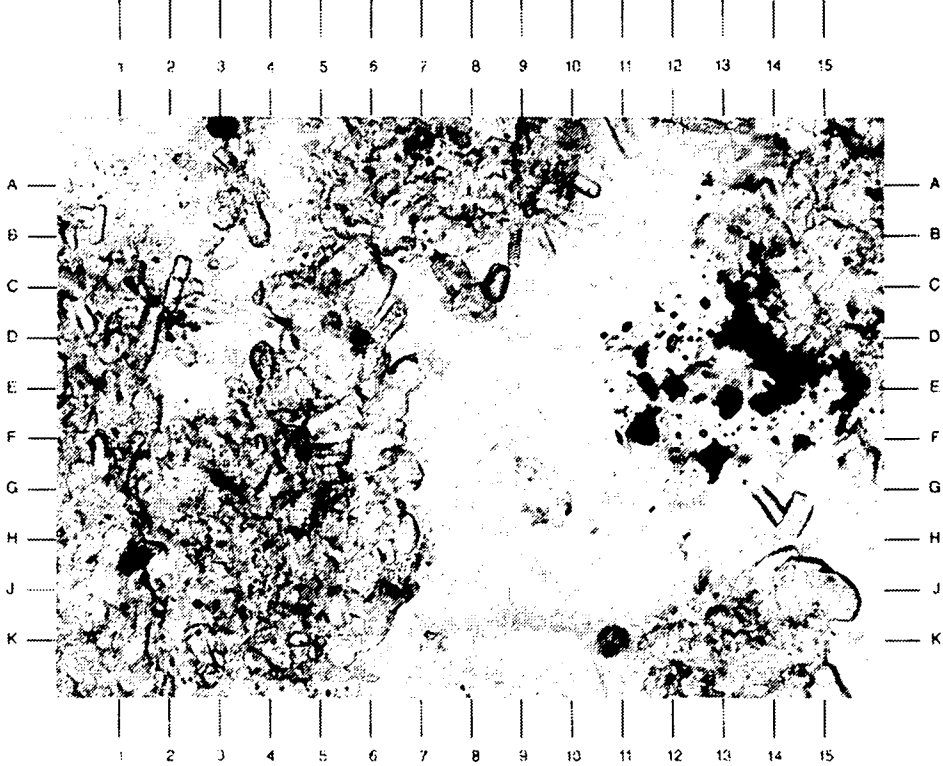
PLATE 3B

In this high magnification photomicrograph, anhydrite laths (B3.5) appear to float in later-forming halite. Magnesite (D13.5) is a trace component that nonetheless occurs with frequency in scattered patches. The halite in this view shows no evidence of zoning or cleavage.

Magnification: 100X



A



B

SAMPLE NUMBER: EIX 10-6 V-5.25'

PLATE 4A

This survey view shows an evaporitic rock composed mainly of anhydrite. Impurities include clay with possible iron oxides (light brown, H1) and magnesite (dark brown, J12.5).

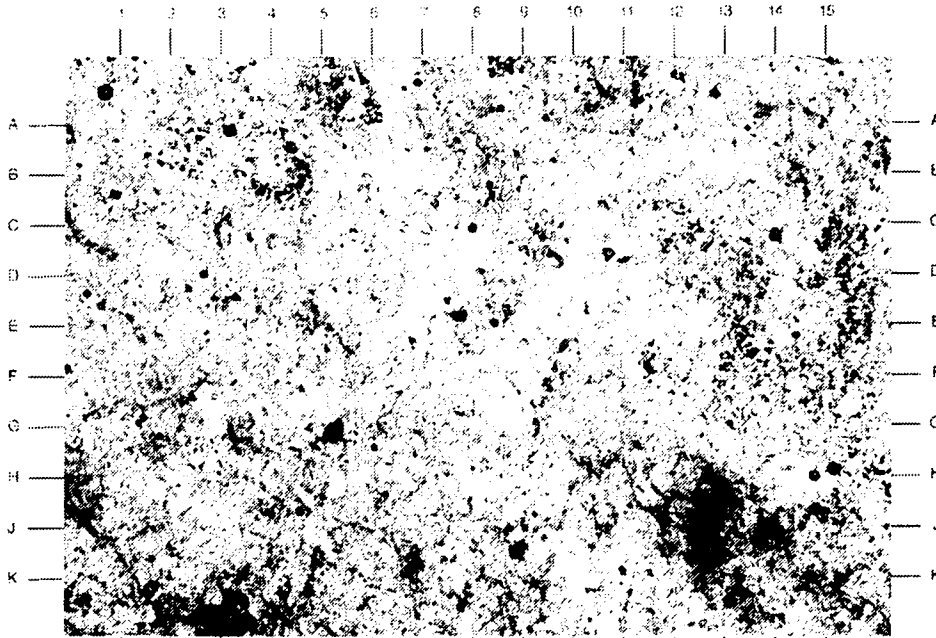
Magnification: 40X

SAMPLE NUMBER: EIX 10-6 V-5.25'

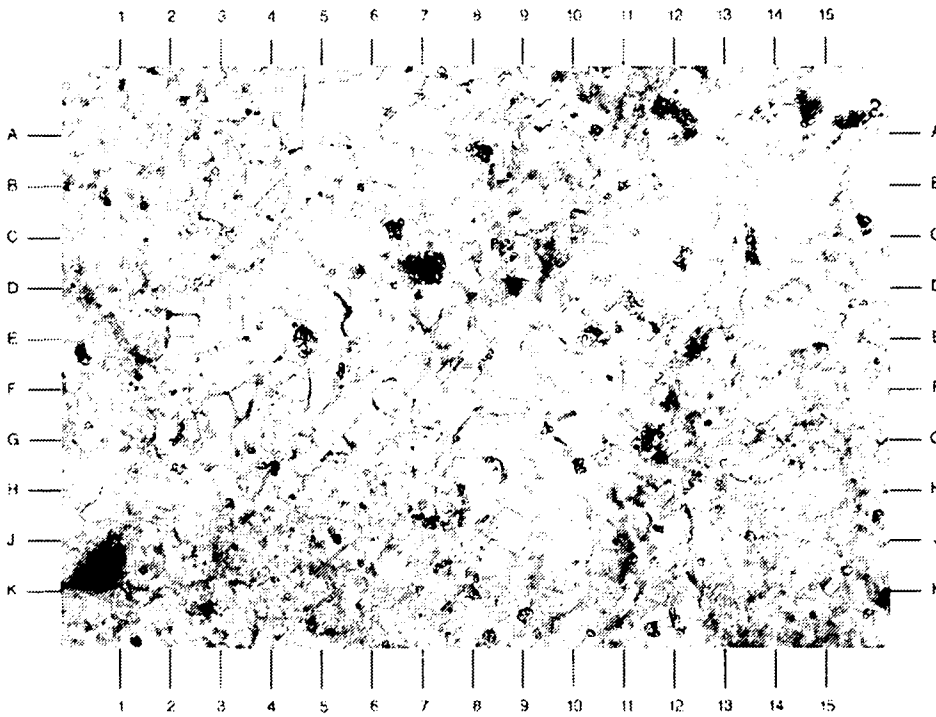
PLATE 4B

This high magnification view depicts the dense intergrowth of individual anhydrite crystals. No visible porosity exists. Magnesite (D7.5) is patchy.

Magnification: 100X



A



B

SAMPLE NUMBER: EIX 10-6 H-5.50'

PLATE 5A

The survey photomicrograph illustrates a massive anhydrite rock. Clay exists in subparallel stringers (left side of photo around D1 and D4). Magnesite occurs in large scattered patches (F10,A12).

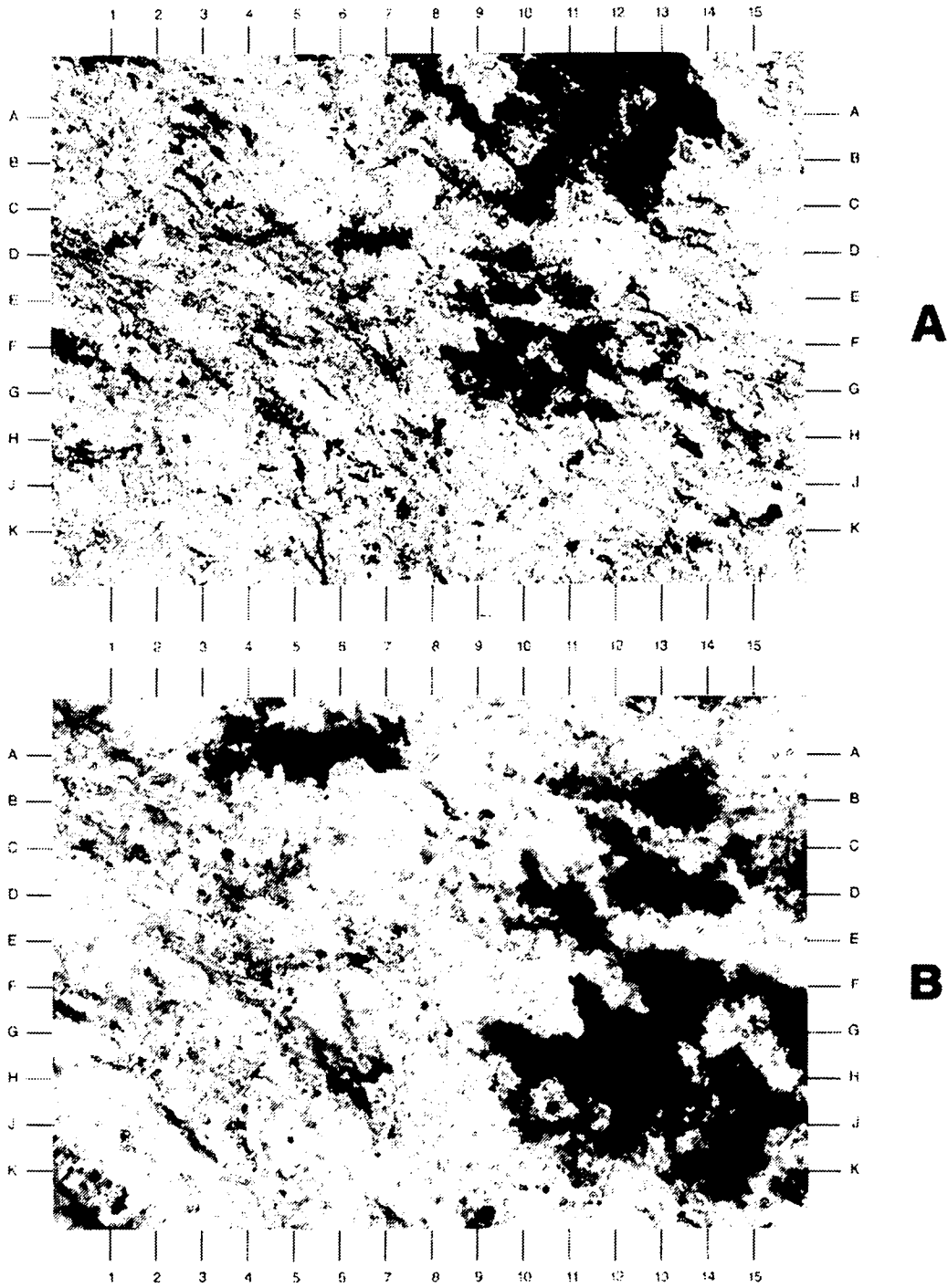
Magnification: 40X

SAMPLE NUMBER: EIX 10-6 H-5.50'

PLATE 5B

The same features are highlighted in the high magnification view. Anhydrite (light) is the main mineral component. Magnesite (H12) is a common accessory mineral made up of tiny individual carbonate rhombs, and is patchy in occurrence. Original depositional orientation is probably defined by clayey zones (around E3).

Magnification: 100X



SAMPLE NUMBER: EIX 10-6 H-5.75'

PLATE 6A

The low magnification photomicrograph displays a fine-grained anhydritic rock with magnesite replacement. Individual laths of anhydrite are interwoven into a felted massive fabric. Clayey streaks (G6.5) trend subparallel. Magnesite (C3) tends to follow this same general orientation.

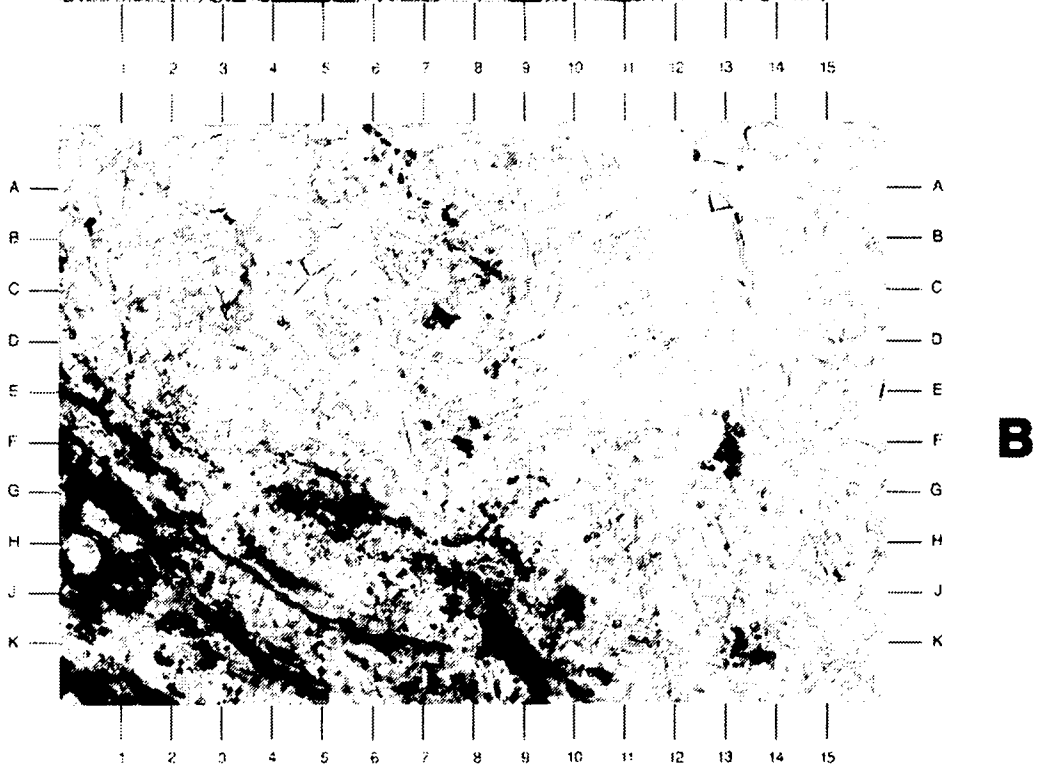
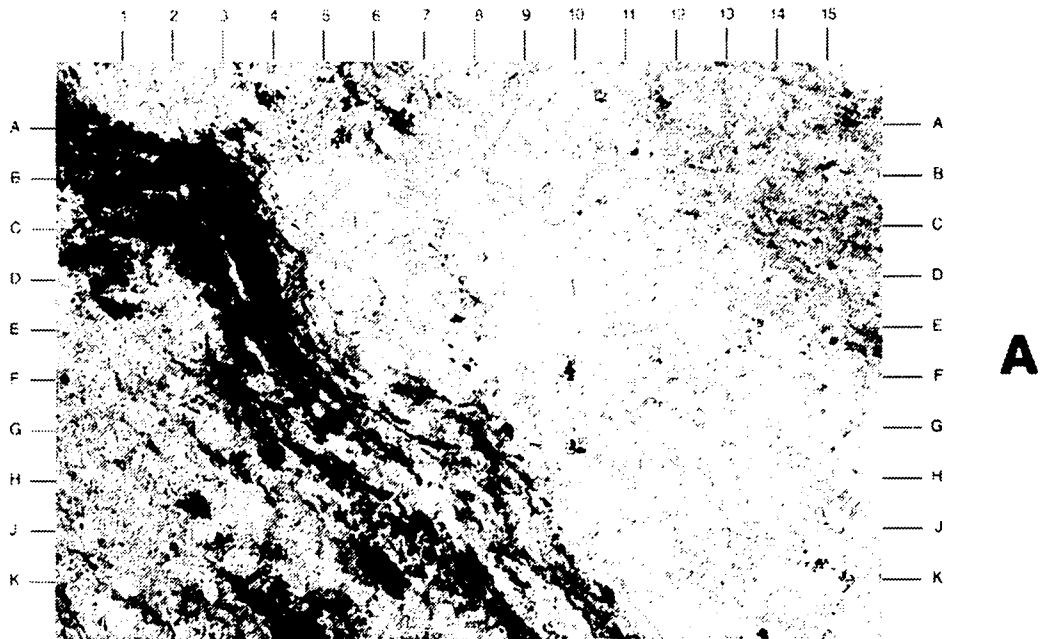
Magnification: 40X

SAMPLE NUMBER: EIX 10-6 H-5.75'

PLATE 6B

This photomicrograph illustrates the fine-grained texture of the anhydrite crystals (area of C5), as well as the relationship of the anhydrite to two other mineral phases. Clay (J5) occurs in stringers, probably along with organic material. Magnesite (G5) is, in the case of this sample, associated with the stringers.

Magnification: 100X



SAMPLE NUMBER: EIX 10-6 V-5.75'

PLATE 7A

The sample depicted in this low magnification photomicrograph actually contains 97% anhydrite and 3% halite, by weight from XRD. However, this field of view shows substantially more halite (white). In some cases the halite is obviously surrounding anhydrite laths (K7.5). Magnesite is associated with both halite and anhydrite. Two large magnesite patches are evident at E5.5 and H12.5. Two stages of anhydrite growth are detected in this sample. The common, massive anhydrite (area of H2) contrasts sharply with the blady anhydrite growing perpendicular to the halite (diagonally across photo from C1 to J5.5).

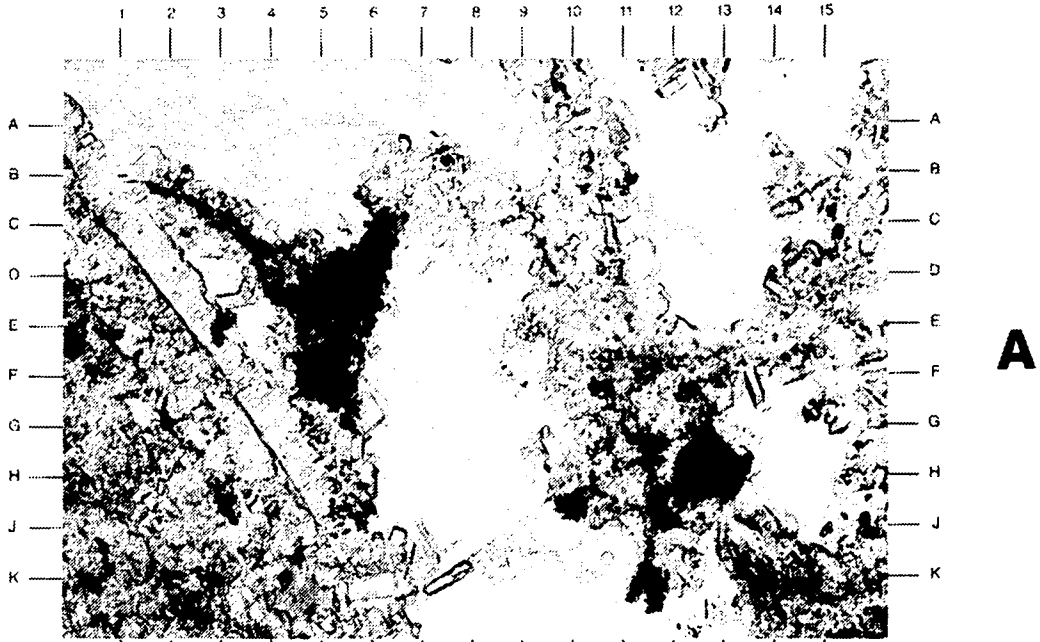
Magnification: 40X

SAMPLE NUMBER: EIX 10-6 V-5.75'

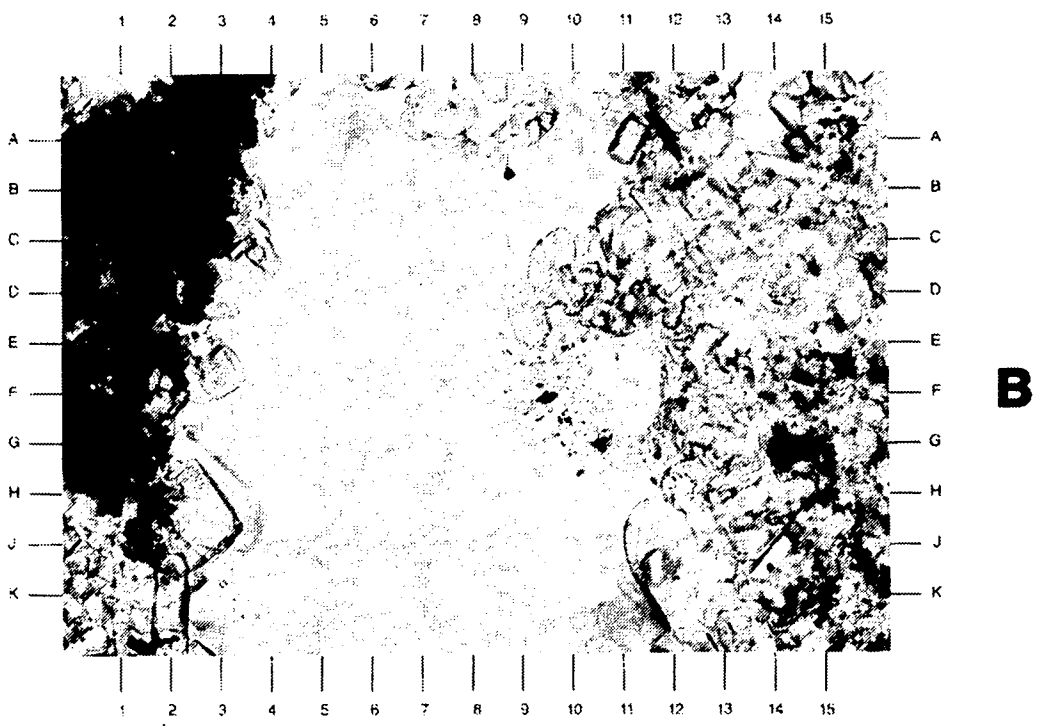
PLATE 7B

The three major mineral components are depicted in this high magnification view. Halite (white) is nearly free of inclusions (some are evident at F10) and obvious cleavage. Magnesite (B2) appears massive but is composed of thousands of individual rhombs. Anhydrite (C11) is coarser near the halite boundary.

Magnification: 100X



A



B

SAMPLE NUMBER: EIX 10-7 V-6.25'

PLATE 8A

The survey photomicrograph depicts massive anhydrite completely void of intercrystalline porosity. Occasional brownish flecks (G12,D9,J5.5) represent clay and magnesite.

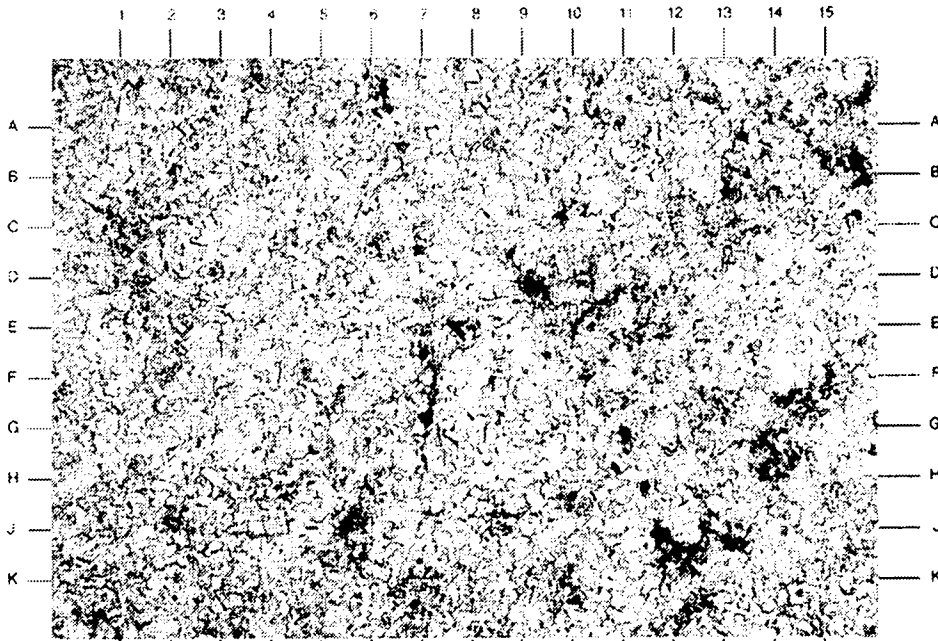
Magnification: 40X

SAMPLE NUMBER: EIX 10-7 V-6.25'

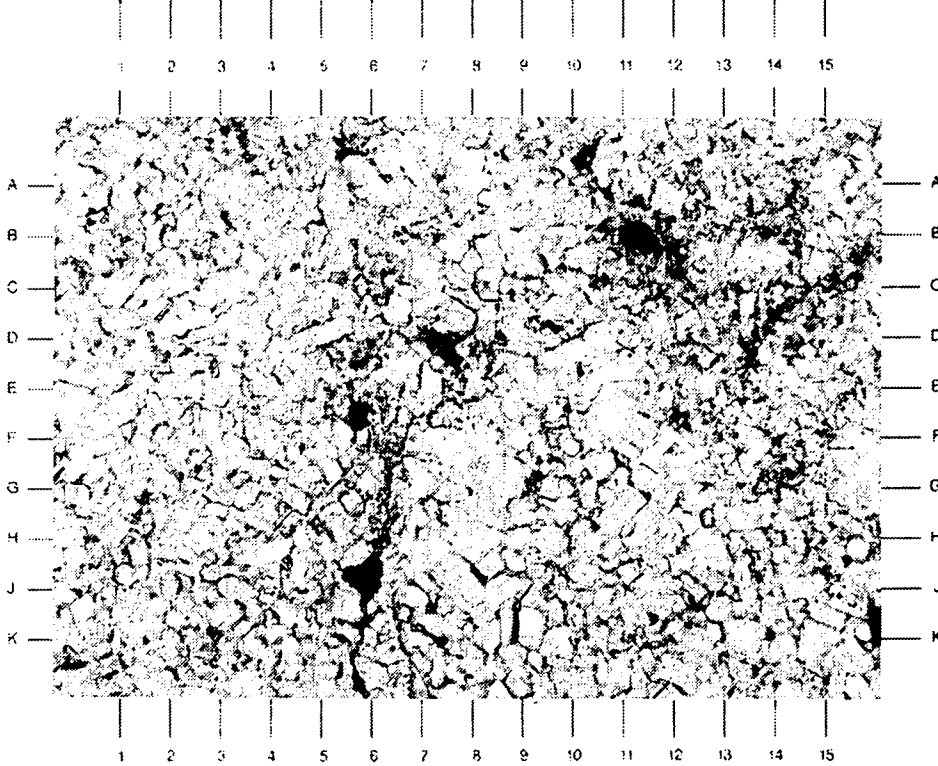
PLATE 8B

The high magnification view demonstrates the complete, dense intergrowth of individual laths of anhydrite (G8). Clay and possible organics exist in faintly defined, narrow zones (D6-K6).

Magnification: 100X



A



B

SAMPLE NUMBER: EIX 11-6 H-4.50'

PLATE 9A

The low magnification photomicrograph demonstrates the mineral associations present in this sequence of evaporites. Clay stringers (C2) occur within the fine anhydrite groundmass. Halite (B12) shows some cleavage (K14) and inclusion zoning (above A15). Iron oxide (D9.5) is unusually common in this sample, and appears to stain anhydrite. Magnesite, in its common cluster form, (K4), occurs sporadically. Some zoning of inclusions (D10,E8) within the halite has occurred.

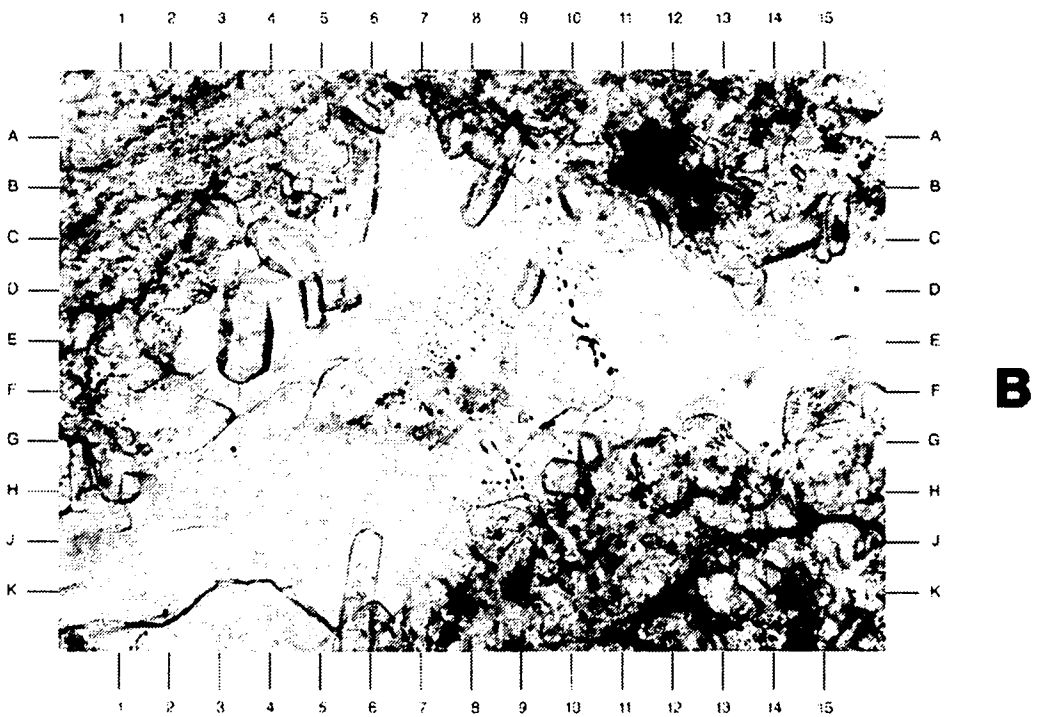
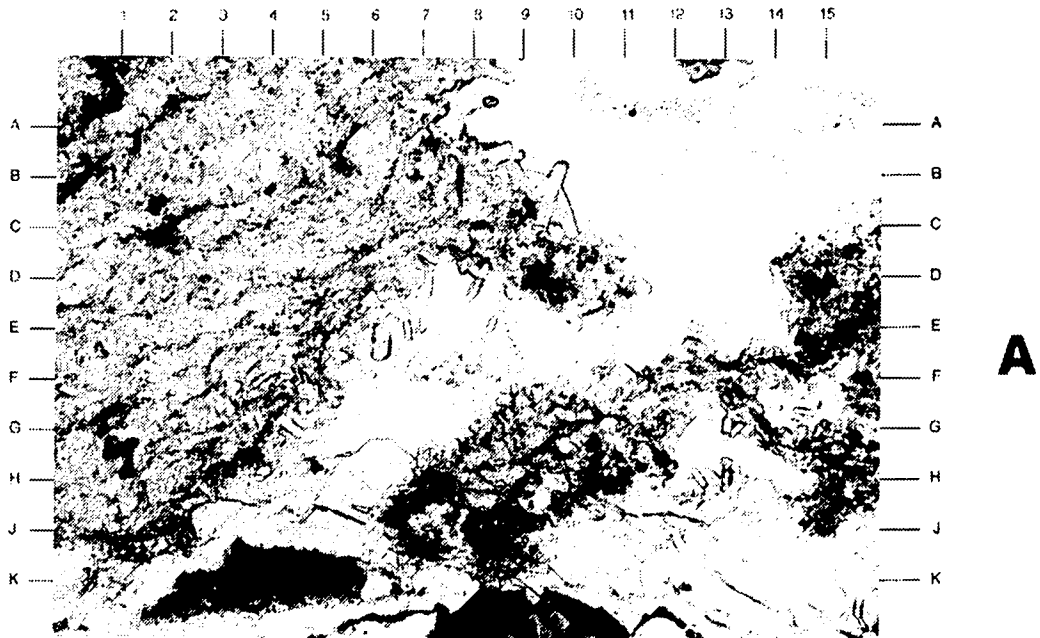
Magnification: 40X

SAMPLE NUMBER: EIX 11-6 H-4.50'

PLATE 9B

The high magnification view demonstrates the nature of the halite. Some zoning of inclusions (D10,E8) has occurred. In other areas, anhydrite crystals (E3.5,B8,K6) are surrounded by later halite.

Magnification: 100X



SAMPLE NUMBER: EIX 11-6 H-4.75'

PLATE 10A

The complex interrelationship of the various evaporite/carbonate mineral phases is evident in this low magnification field of view. Note the irregular borders (H6) between anhydrite (tan) and halite (white). Magnesite (D3) is patchy and irregular.

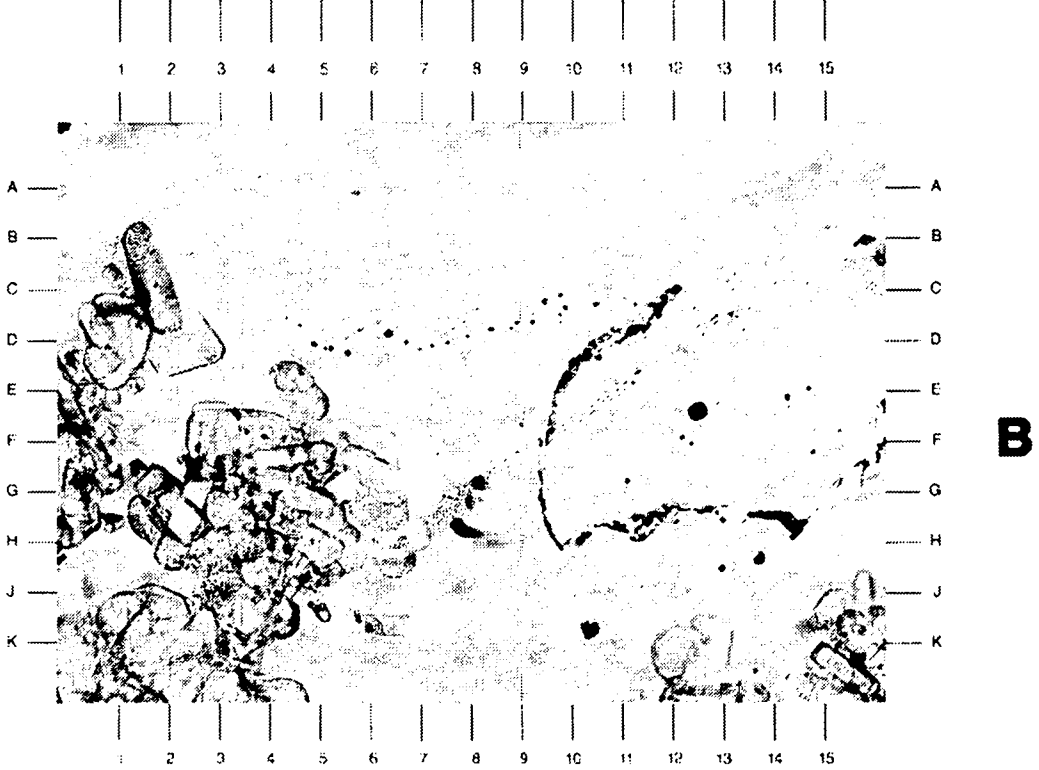
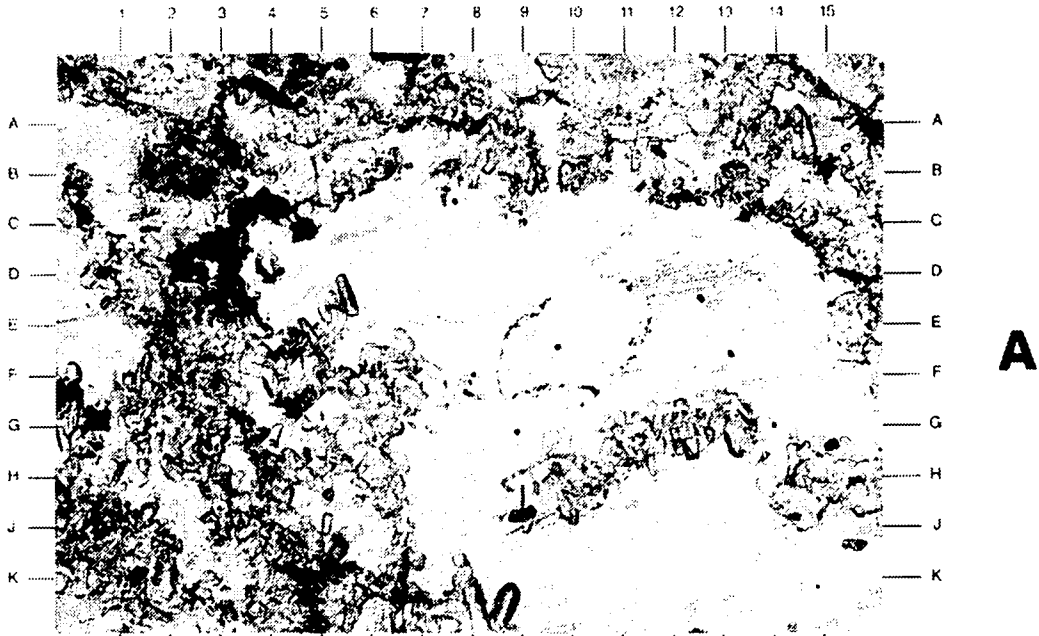
Magnification: 40X

SAMPLE NUMBER: EIX 11-6 H-4.75'

PLATE 10B

The high magnification view shows details of halite in this sample. Some inclusion trails (E11 to G8) are quite regular; others (beak-like area defined by endpoints C12 and H14) are highly irregular. Large anhydrite laths (lower left of photo) are partially surrounded by halite.

Magnification: 100X



SAMPLE NUMBER: EIX 11-6 H-5.00'

PLATE 11A

The low magnification view of this sample shows a more distinct boundary separating halite and anhydrite, than that of the previous sample. The halite/anhydrite contact (E8.5) is also marked by the presence of the carbonate mineral magnesite (J9). Individual crystals within the anhydrite (tan) are small, with the exception of those in one area (G9). The halite is marked by well-defined inclusion zones (across photo at B-C,D,E-F,G,and J).

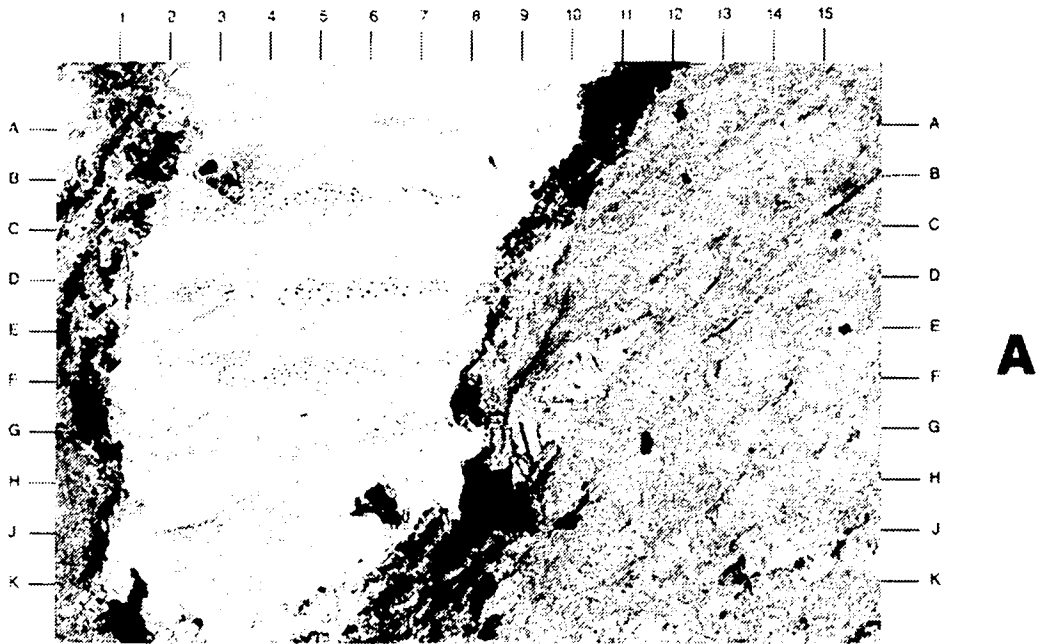
Magnification: 40X

SAMPLE NUMBER: EIX 11-6 H-5.00'

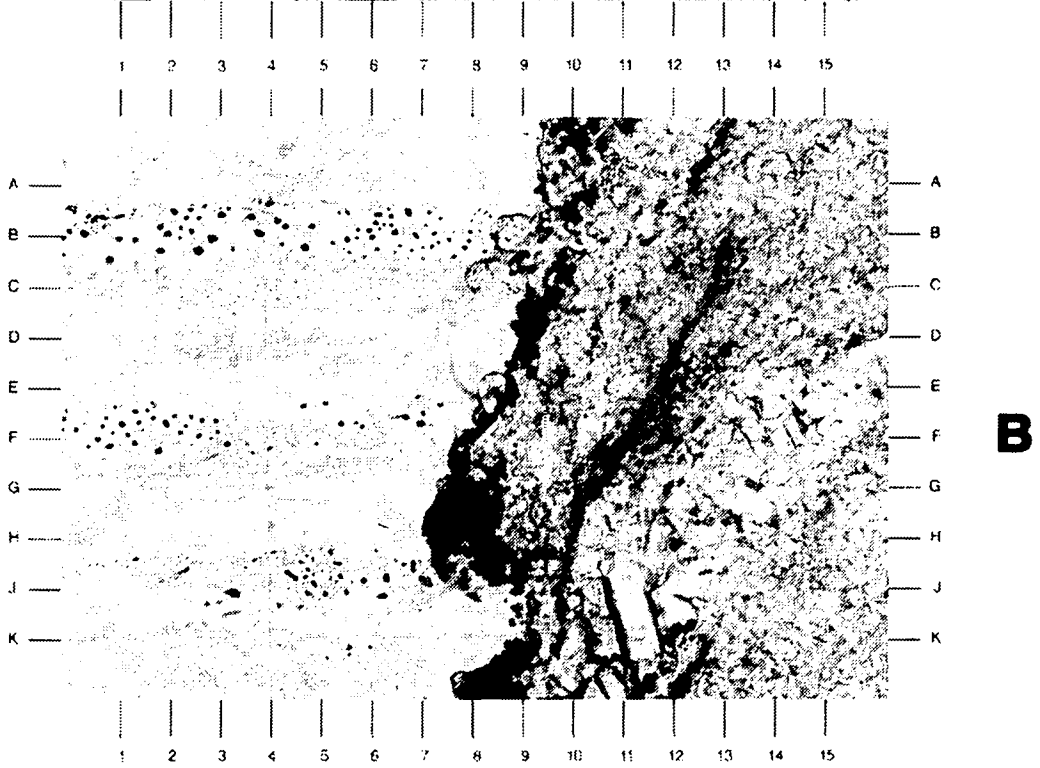
PLATE 11B

The high magnification view of the evaporite shows many of the above features in more detail. Fine-grained anhydrite crystals (C15), coarser anhydrite crystals (F14), and magnesite (H7.5) are clearly noted. Also evident is a clayey streak (diagonally across photo from B13 to K10). The well-defined, parallel, inclusion zones are obvious (B,C,F,J).

Magnification: 100X



A



B

SAMPLE NUMBER: EIX 11-6 H-5.25'

PLATE 12A

This low magnification survey photomicrograph demonstrates the mottled relationship of the two major mineral species present, halite (white) and anhydrite (tan). Magnesite (F3.5) and detrital clay (D-E14) are also present. Most anhydrite laths are very small (area of A-B7); some, however, are much larger (C-D5).

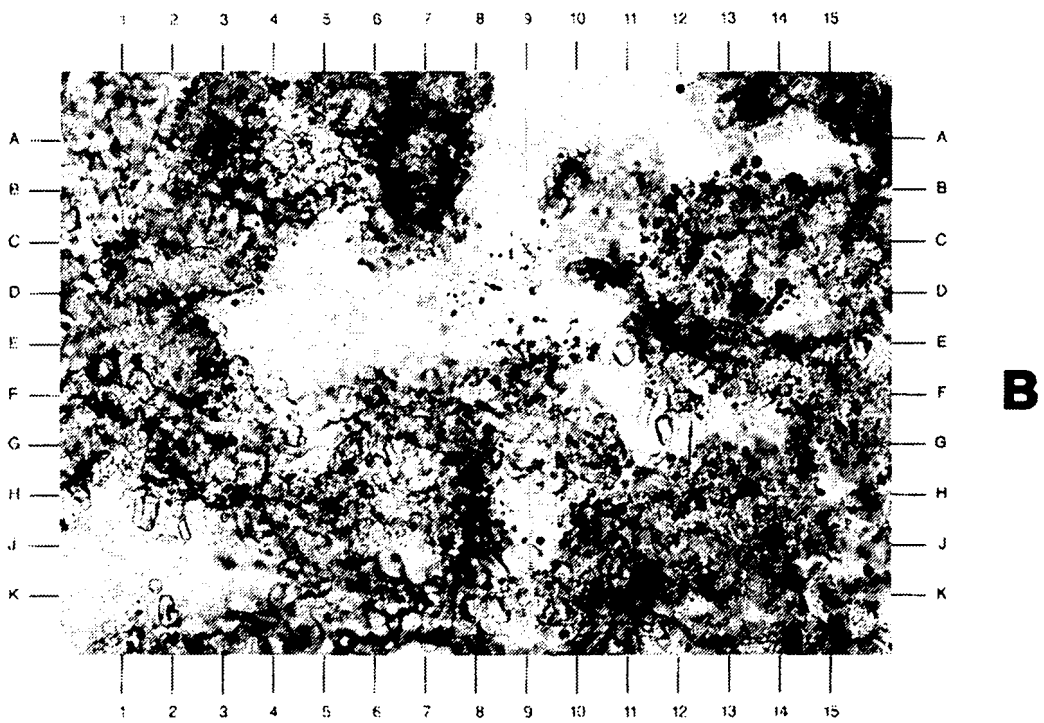
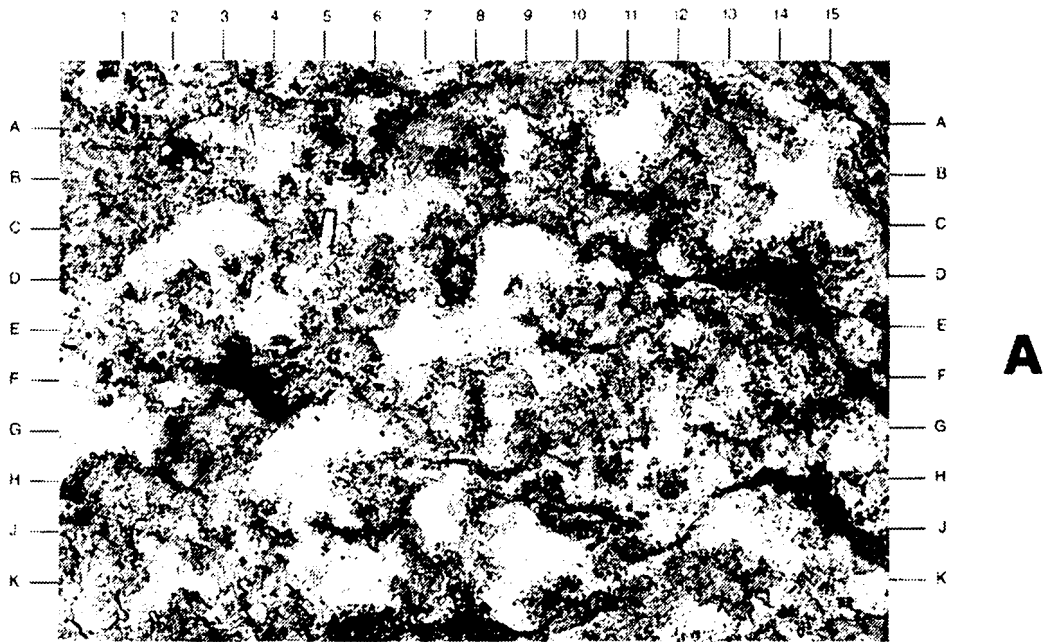
Magnification: 40X

SAMPLE NUMBER: EIX 11-6 H-5.25'

PLATE 12B

The high magnification view of the center of photo "A" demonstrates the complex boundaries present between the halite and anhydrite. The halite in this sample contains dusty inclusions (C-D8.5) with no preferred orientation. Anhydrite laths (G12) are much coarser, where partially surrounded by halite.

Magnification: 100X



SAMPLE NUMBER: EIX 11-6 V-5.25'

PLATE 13A

This survey photomicrograph shows four different minerals present in this evaporite rock. Anhydrite (tan) is massive and fine- (area of D11) to coarse- grained (J7). Halite (white, E7.5) occurs in scattered patches. Magnesite (J2.5) is quite rare, as is detrital clay (above A1) which exists in stringers.

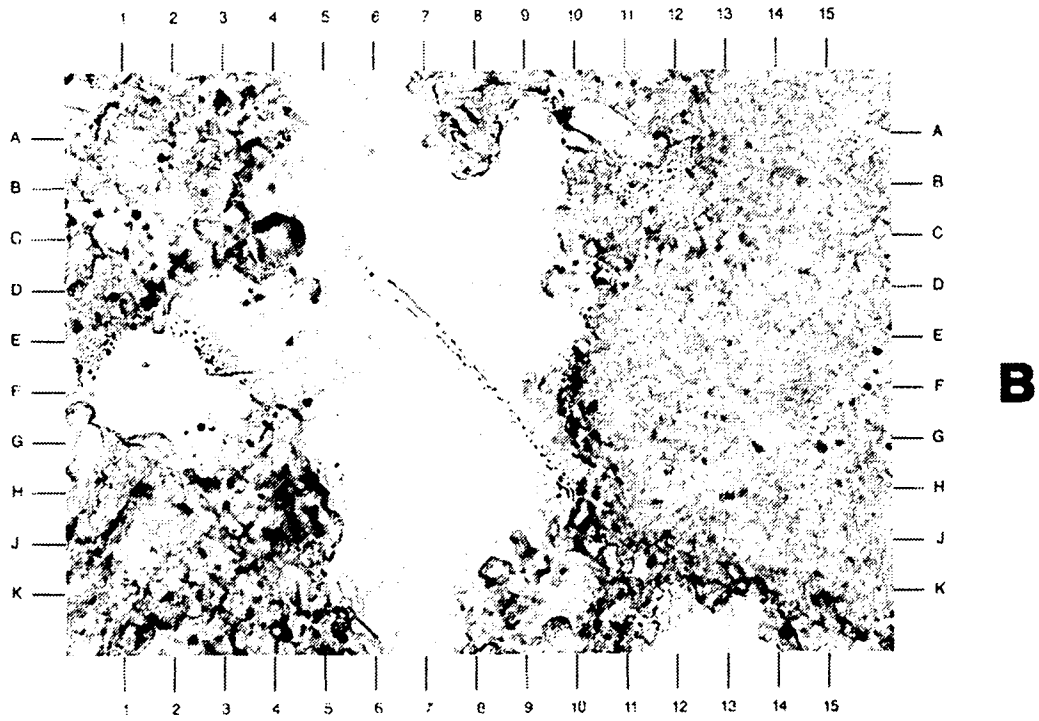
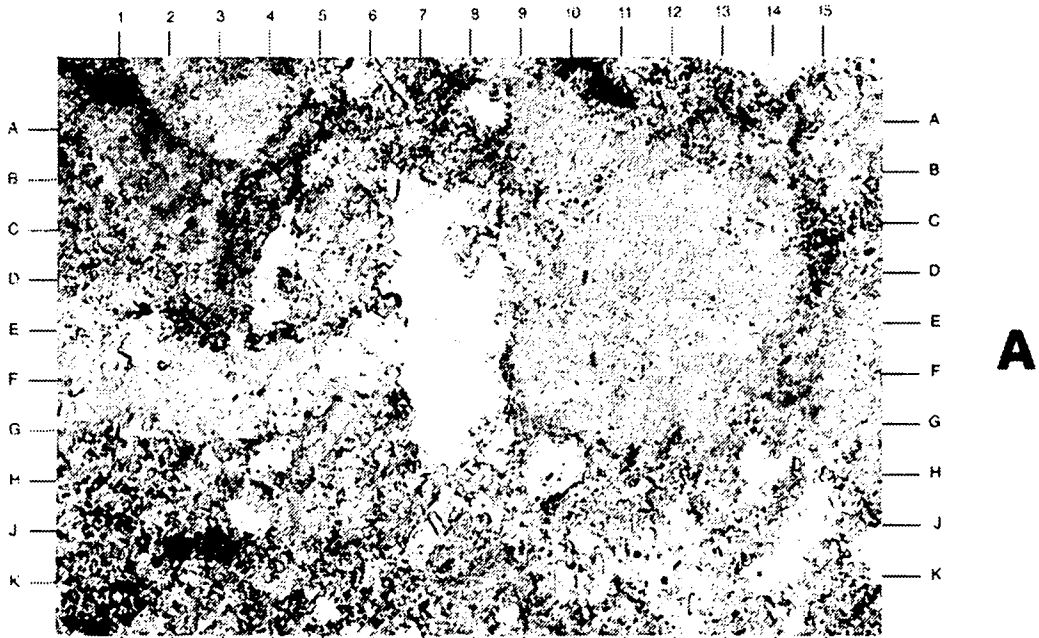
Magnification: 40X

SAMPLE NUMBER: EIX 11-6 V-5.25'

PLATE 13B

This high magnification photomicrograph details an inclusion trail (diagonally from D6 to H10) within the halite. Some iron oxide staining (J4) is present, and is associated with the anhydrite.

Magnification: 100X



SAMPLE NUMBER: EIX 11-6 H-5.75'

PLATE 14A

This low magnification photomicrograph illustrates the mineral associations within this evaporite. Clay and organic material form subparallel stringers (brown, lower left) and are relatively abundant in this sample. Anhydrite (tan) and halite (white) make up the bulk of the rock. Anhydrite is massive and fine-grained, although coarser anhydrite (A13) is found in association with halite. Halite has common unoriented inclusions (D-E14).

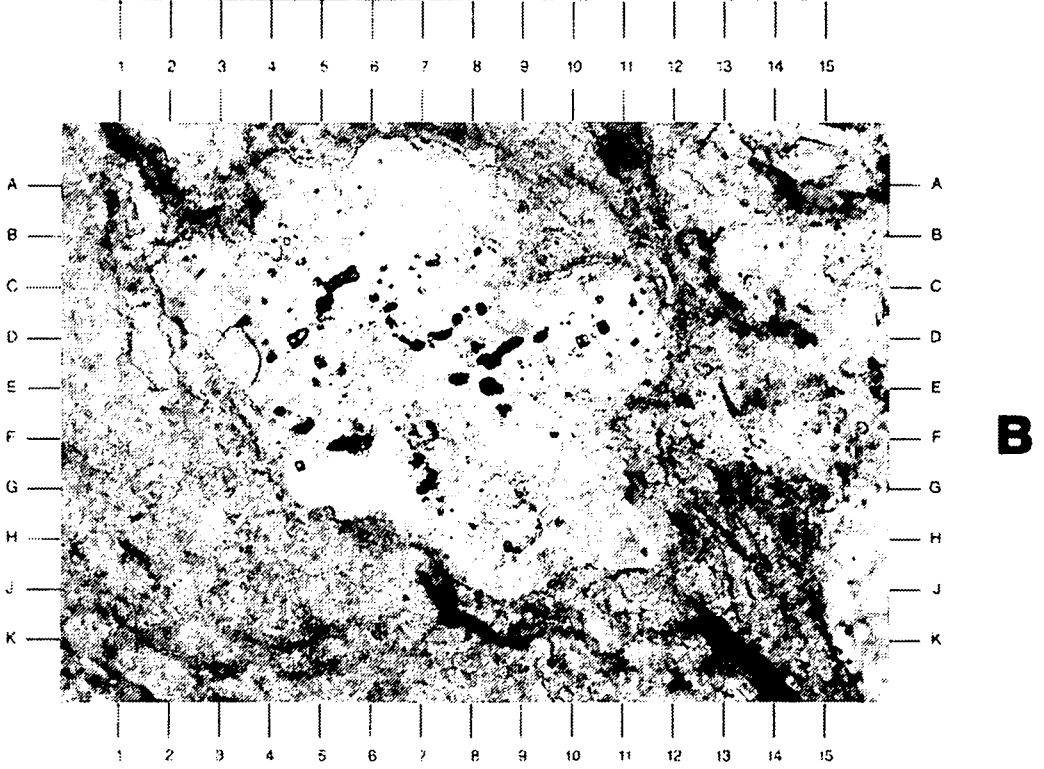
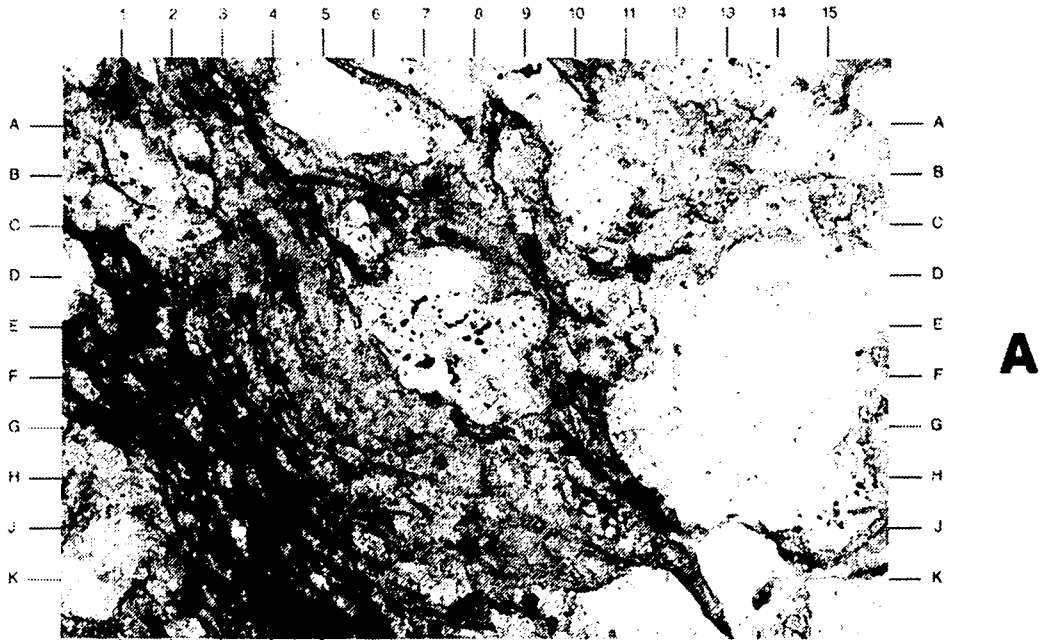
Magnification: 40X

SAMPLE NUMBER: EIX 11-6 H-5.75'

PLATE 14B

This expanded-view photomicrograph of the center of photo "A" illustrates the detail of the dusty inclusions within the halite. Different types of inclusions, including probable magnesite (C5.5) appear randomly scattered. Clay (K8.5, K13) is detrital in origin; some is iron oxide stained (i.e. K8.5).

Magnification: 100X



SAMPLE NUMBER: EIX 11-6 V-5.75'

PLATE 15A

The rock depicted in this low magnification view is a massive anhydrite. An unusual feature of this anhydrite is its coarser-grained texture when compared with that in other samples. Note this coarser crystal size, especially in the upper left and lower right of the photo. Some clay with organics and possible iron oxide (H8,H10,F12,J6) is evident as well.

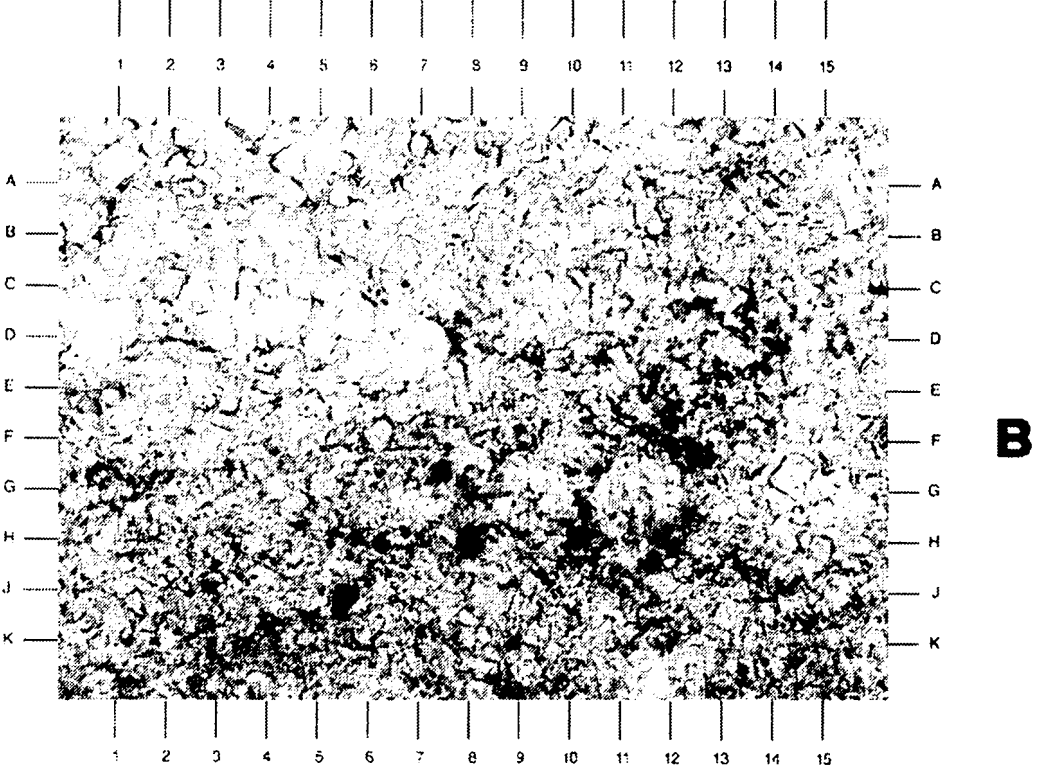
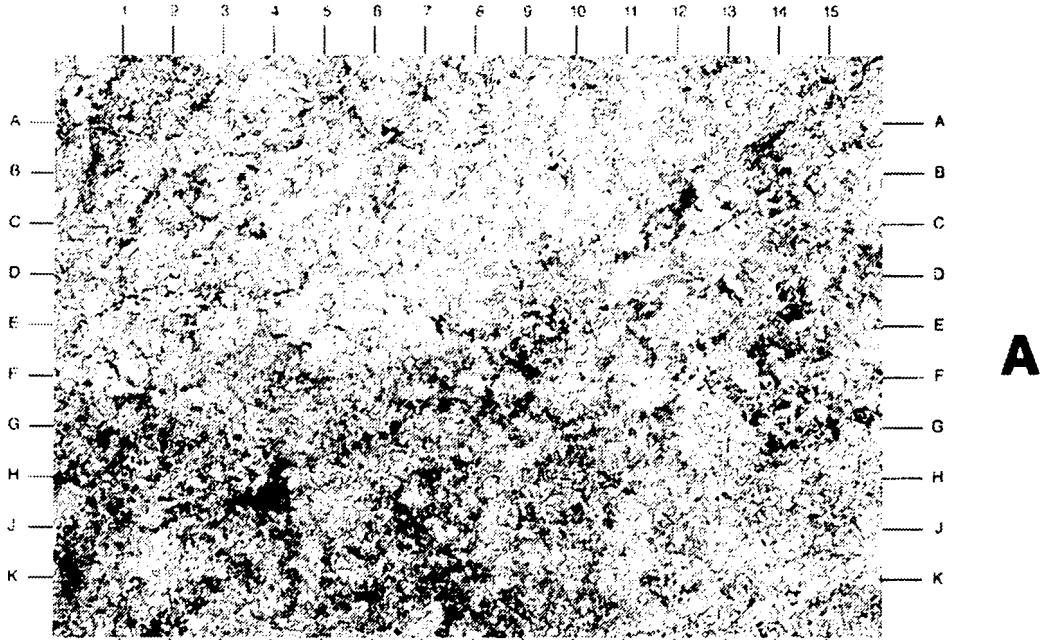
Magnification: 40X

SAMPLE NUMBER: EIX 11-6 V-5.75'

PLATE 15B

The anhydrite crystal size variation is even more evident under high magnification (center of photo "A"). Note the intergrown, almost "feltic" texture of the coarser crystals (area of C5). The finer anhydrite (lower part of photo) shows more iron oxide staining (brown-red). A cluster of magnesite rhombs is visible at F12.

Magnification: 100X



**Appendix A-C.
Appendix C of Appendix A [Data Report: Rock Physics Associates (Core
Laboratories)]**



CORE LABORATORIES

BASIC ROCK PROPERTIES

Waste Isolation Pilot Plant

FINAL REPORT

**PREPARED FOR:
SANDIA NATIONAL LABORATORIES
P.O. Box 5800
Albuquerque, NM 87185**

**PREPARED BY:
CORE LABORATORIES
1875 Monetary Lane
Carrollton, Texas 75006
(214) 466-2673**

**January 24, 1994
File: DAL-93089**

A-143

January 24, 1994

Sandia National Laboratories
P.O. Box 5800
Albuquerque, New Mexico 87185

Attn: Dr. Susan Howarth

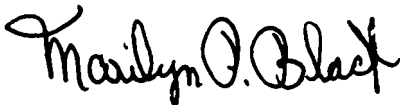
Subject: Basic Rock Properties
Waste Isolation Pilot Plant
File: DAL-93089

Dr. Howarth:

Following are the final results of basic rock properties determinations on selected core material from the subject well. Testing was performed following the procedures dated October 8, 1993 provided by Sandia National Laboratories.

We appreciate the opportunity to have been of service to Sandia National Laboratories. If we may be of further assistance, please telephone (214) 466-2673.

Thank you,



Marilyn P. Black
Supervisor, Petrophysics

TABLE OF CONTENTS

SECTION 1:	Laboratory Procedures	A-147
SECTION 2:	Appendix Calibrations	A-153

Sandia National Laboratories
File: DAL-93089

SECTION 1
LABORATORY PROCEDURES

LABORATORY PROCEDURES

Equipment Calibrations

The calipers used in this study were calibrated against certified gauge blocks traceable to NIST (National Institute of Standards and Technology) standards.

The test balance used for this project reads to 0.0001 grams. The digital balance was calibrated within the last twelve months by an authorized representative of the manufacturer. Prior to this project, the balances were checked against a set of secondary weight standards.

All pressure transducers and the mass flowmeter in the AutoPermeameter™, which was modified to provide extended range values, were calibrated prior to this project. The lower limit of the AutoPermeameter™ was set to 0.0001 millidarcys (md). A standard set of calibrated billets were used to calibrate the helium AutoPorosimeter™ prior to testing.

Calibration documentation is included as an appendix to this report.

Sample Preparation

Eight core plugs, 1.5" in diameter, were drilled using a light refined mineral oil (Isopar-L) as the bit lubricant and coolant. Although the plugs were trimmed to the longest length possible, given sample quality no sample exceeded 1 2/3 inches. Two samples were too chipped for further analysis. The samples were dried to stable weights in a vacuum oven at 220°F, then cooled to room temperature in a small closed container with desiccant prior to basic property determinations.

Basic Properties

The sample dry weights were recorded to the nearest 0.0001 gram. Length and diameter measurements were made using digital calipers. The recorded value of each dimension was determined from an average of 10 caliper measurements. Each sample was placed into a matrix cup and the AutoPorosimeter™ used to inject helium from reference cells of known volume and pressure. Grain volume was determined using Boyle's law of gas expansion. Grain density values were calculated for each sample.

Each sample was then loaded into a hydrostatic coreholder for determination of

permeability to helium and pore volume at 400, 870, and 1450 psi net confining^P pressure. At each pressure, helium was injected into the sample from reference cells of known volume and initial pressure. Pore volume was calculated using Boyle's law. Allowing ample time for the helium in place to exit the sample, the sample was again charged with helium and, using the modified AutoPermeameter™, steady-state permeability values were determined after a 3 to 5 minute stabilization period. Permeability to helium was calculated as follows:

$$K \text{ (md)} = \frac{2000 * 14.696 * P_2 * \mu * Q_a * L}{A * (P_1^2 - P_2^2)} \quad (1)$$

where:

- 2000 = Conversion factor
- 14.696 = Barometric pressure, psi
- μ = Viscosity of helium, 72°F
- Q_a = Flow rate to helium, cc/second
- L = Sample length, cm
- A = Sample area, cm²
- P1 = Upstream pressure, psia
- P2 = Downstream pressure, psia

Basic properties results are presented in tabular format on the following page.

BASIC ROCK PROPERTIES

Extended Range Values

Sample ID	Sample Depth	Net OB, psig	P1, psia	P2, psia	Qa, cc/sec	Area, cm2	Length, cm	Permeability to Helium, md	1/Pm, Atm	Bulk Volume, cc	Grain Volume, cc	Pore Volume, cc	Porosity, percent	Sample Weight, gm	Grain Density, gm/cc
EX 10-5	4.00 - 4.2	400	232	14.651	0.091	11.5	3.568	0.0044625	0.119	40.767	40.376	0.3908	0.96	103.8442	2.572
		870	322.93	14.653	0.07	11.5	3.568	0.0017685	0.087	40.682		0.3061	0.75		
		1450	400.62	14.654	0.051	11.5	3.568	0.0008432	0.071	40.621		0.2449	0.60		
EX 10-6	4.50 - 5.1	400	277.77	14.637	0.065	11.3	3.801 ^{7.047}	0.0023862	0.101	79.967	79.278	0.6889	0.86	213.3797	2.692
		870	276.77	14.637	0.053	11.3	3.801	0.0019487	0.101	79.946		0.6684	0.84		
		1450	373.75	14.641	0.04	11.3	3.801	0.0008042	0.076	79.885		0.6070	0.76		
EX 10-5	4.25 - 4.5	400	226.82	14.386	0.331	11.3	2.054	0.0096913	0.122	23.282	23.098	0.1837	0.79	59.1268	2.560
		870	229.82	14.381	0.182	11.3	2.054	0.0051877	0.120	23.271		0.1726	0.74		
		1450	232.33	14.384	0.095	11.3	2.054	0.0026499	0.119	23.256		0.1576	0.68		
EX 10-7	5.75 - 5.9	400	218.77	14.378	0.244	11.3	4.108	0.0153952	0.126	46.517	44.470	2.0465	4.40	130.0600	2.925
		870	219.03	14.381	0.216	11.3	4.108	0.0135987	0.126	46.436		1.9664	4.23		
		1450	219.53	14.384	0.171	11.3	4.108	0.0107183	0.126	46.419		1.9493	4.20		

A-150

BASIC ROCK PROPERTIES

Extended Range Values

Sample ID	Sample Depth	Net OB, psig	P1, psia	P2, psia	Qa, cc/sec	Area, cm2	Length, cm	Permeability to Helium, md	1/Pm, Atm	Bulk Volume, cc	Grain Volume, cc	Pore Volume, cc	Porosity, percent	Sample Weight, gm	Grain Density, gm/cc
EX 11-5	2.70 - 3.4	400	231.54	14.387	0.116	11.3	2.615	0.0041511	0.120	29.564	29.309	0.2548	0.86	76.3734	2.606
		870	231.09	14.389	0.076	11.3	2.615	0.0027343	0.120	29.507		0.1980	0.67		
		1450	230.94	14.388	0.051	11.3	2.615	0.0018204	0.120	29.503		0.1941	0.66		
EX 11-6	3.80	400	219.78	14.383	0.265	11.3	3.159	0.0127091	0.126	35.8	35.618	0.1817	0.51	90.7512	2.548
		870	216.97	14.383	0.14	11.3	3.159	0.0068903	0.127	35.783		0.1646	0.46		
		1450	217.68	14.385	0.057	11.3	3.159	0.0027974	0.127	35.765		0.1466	0.41		

A-151

Sandia National Laboratories
File: DAL-93089

SECTION 2

**APPENDIX
A-C.1
CALIBRATIONS**

Dec 29,1993 1:27 PM

Description: Calibration of low range flow meter
X-Y Table Size: 41 Active Points: 41

X Variable: Voltage

Xmin: 0.0195	Xmax: 1.67	Xrange: 1.6505
Xmean: 0.5471341463	Xstd: 0.4962067173	Xmedian: 0.403
X@Ymin: 0.02	X@Ymax: 1.67	X@Yrange: 1.65
Xav@Ymax: 1.6275	X@50Y: 0.826376352	Xlt@50Y: 0
Xrt@50Y: 0	X@25Y: 0.44925	X@75Y: 1.43
Xwavemin: 0.0652083333	Xwavemax: 1.6275	Xwaverng: 3.1245833333

Y Variable: Rate, cc's/sec

Ymin: 0.008	Ymax: 0.86	Yrange: 0.852
Ymean: 0.281195122	Ystd: 0.2570742324	Ymedian: 0.206
Y@Xmin: 0.008	Y@Xmax: 0.86	Y@Xrange: 0.852

35 Eqn 64 $y=(a+bx+cx^2)$ $r=0.9999626919$

	Coefficient	Std Error	T(Coef/Err)	95% Confidence Limits	
a	-0.001706727	0.000497417	-3.431179833	-0.002713541	-0.000699914
b	0.5153059743	0.0017051914	302.19832747	0.5118545244	0.5187574241
c	0.0017798469	0.0010476571	1.6988830455	-0.000340699	0.0039003926

Curve-Fit Std Error: 0.001611009953397

Source	Sum of Squares	DF	Mean Square	F
Regr	2.64338782	2	1.32169391	509254
Error	9.86234167e-005	38	2.59535307e-006	
Total	2.64348644	40		

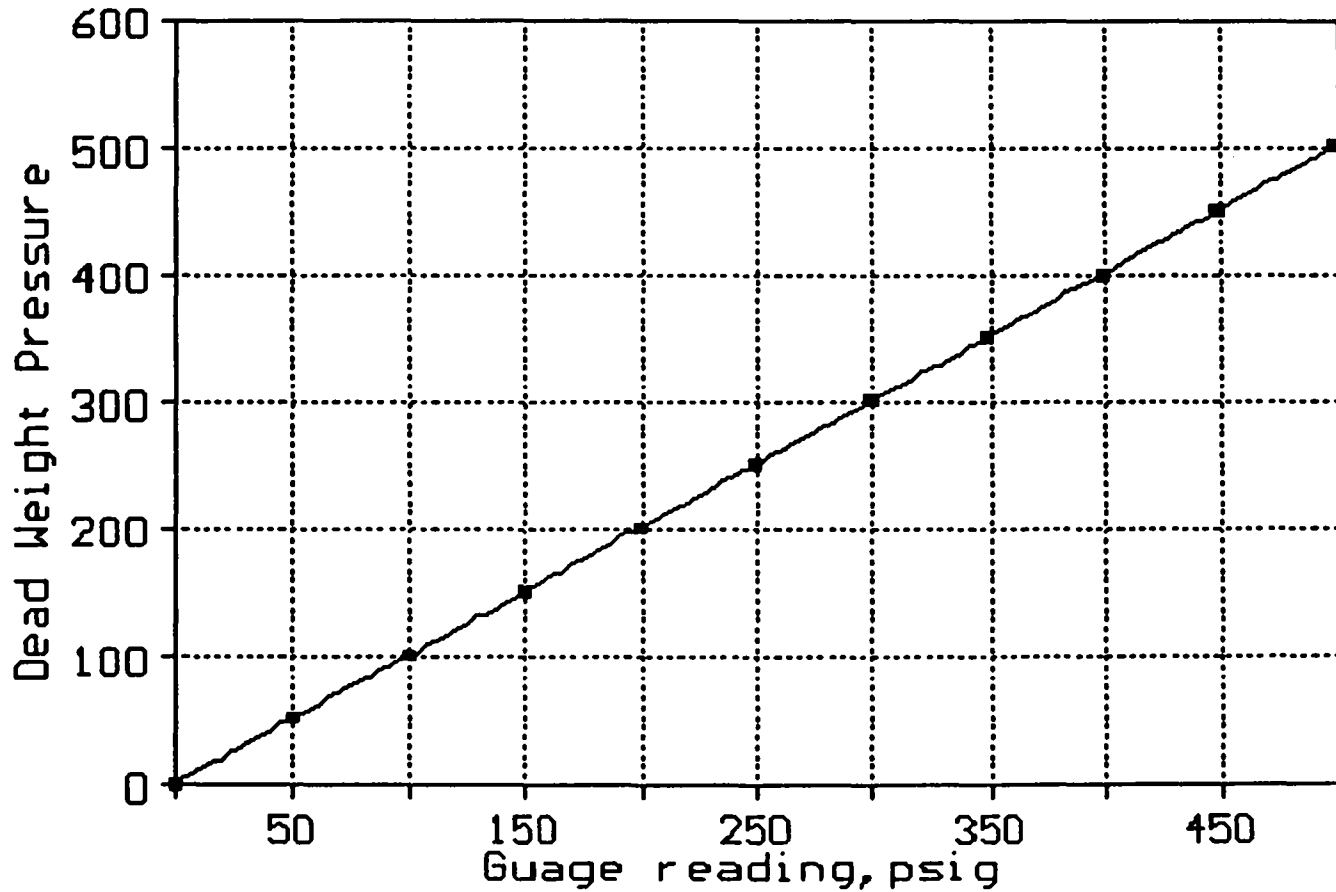
Calibration of low range flow meter

Page 1

#	X-Value	Y-Value	Y-Predict	95% Confidence Intvl	
1	0.0195	0.008	0.00834242	0.00738751	0.00929732
2	0.02	0.008	0.0086001	0.0076465	0.00955371
3	0.046	0.023	0.02200111	0.02111215	0.02289008
4	0.0466	0.023	0.0223104	0.02142286	0.02319794
5	0.0635	0.032	0.03102238	0.03017388	0.03187088
6	0.064	0.032	0.03128015	0.03043276	0.03212753
7	0.0647	0.033	0.03164102	0.0307952	0.03248684
8	0.0793	0.04	0.03916823	0.03835406	0.0399824
9	0.0793	0.039	0.03916823	0.03835406	0.0399824
10	0.0806	0.035	0.0398385	0.03902706	0.04064994
11	0.109	0.054	0.05448277	0.05372716	0.05523838
12	0.11	0.055	0.05499847	0.05424469	0.05575225
13	0.197	0.1	0.09987762	0.09924526	0.10050999
14	0.197	0.099	0.09987762	0.09924526	0.10050999
15	0.1975	0.099	0.10013563	0.09950373	0.10076752
16	0.304	0.156	0.15511078	0.15452336	0.15569819
17	0.308	0.157	0.15717636	0.15658865	0.15776406
18	0.309	0.158	0.15769276	0.15710496	0.15828056
19	0.4	0.206	0.20470044	0.20407954	0.20532134
20	0.402	0.206	0.2057339	0.20511186	0.20635595
21	0.403	0.206	0.20625064	0.20562803	0.20687326
22	0.497	0.256	0.25483998	0.25415483	0.25552513
23	0.497	0.255	0.25483998	0.25415483	0.25552513
24	0.497	0.255	0.25483998	0.25415483	0.25552513
25	0.597	0.307	0.30656529	0.30581209	0.3073185
26	0.597	0.307	0.30656529	0.30581209	0.3073185
27	0.599	0.309	0.30760016	0.30684571	0.30835462
28	0.69	0.357	0.35470178	0.35389731	0.35550625
29	0.692	0.354	0.35573731	0.35493191	0.35654271
30	0.692	0.354	0.35573731	0.35493191	0.35654271
31	0.799	0.412	0.411159	0.41031551	0.4120025
32	0.8005	0.411	0.41193623	0.41109236	0.4127801
33	0.986	0.508	0.50811532	0.50725215	0.50897849
34	0.988	0.51	0.50915296	0.50828978	0.51001614
35	0.991	0.507	0.51070945	0.50984626	0.51157264
36	1.25	0.645	0.64520675	0.64430482	0.64610869
37	1.25	0.645	0.64520675	0.64430482	0.64610869
38	1.61	0.833	0.83254943	0.83106327	0.83403559
39	1.61	0.833	0.83254943	0.83106327	0.83403559
40	1.62	0.842	0.83775998	0.83624546	0.83927451
41	1.67	0.86	0.86381807	0.86215248	0.86548365

Calibration 12/29/93 JAK/R11
500 psi ^{of} Gauge (Heise) Pressure

15 Eqn 64 $y=(at+bx+cx^2)$ $r=0.9999986573$
 $a=-0.29279215$ $b=1.0072454$
 $c=-6.94098186E-006$



Jan 4,1994 10:14 AM

Description: Calibration of low range flow meter

X-Y Table Size: 10 Active Points: 10

X Variable: Voltage

Xmin: 0.0183	Xmax: 0.939	Xrange: 0.9207
Xmean: 0.36466	Xstd: 0.3555943044	Xmedian: 0.2545
X@Ymin: 0.0183	X@Ymax: 0.933	X@Yrange: 0.9147
Xav@Ymax: 0.936	X@50Y: 0.5267812836	Xlt@50Y: 0
Xrt@50Y: 0	X@25Y: 0.2411974498	X@75Y: 0.73375
Xwavemin: 0.0183	Xwavemax: 0.933	Xwaverng: 1.8294

Y Variable: Rate,cc's/sec

Ymin: 0.0042	Ymax: 0.468	Yrange: 0.4638
Ymean: 0.18085	Ystd: 0.1788639784	Ymedian: 0.12675
Y@Xmin: 0.0042	Y@Xmax: 0.468	Y@Xrange: 0.4638

46 Eqn 64 $y=(a+bx+cx^2)$ $r=0.9999476886$

	Coefficient	Std Error	T(Coef/Err)	95% Confidence Limits	
a	-0.00308274	0.0008701821	-3.54263823	-0.005148497	-0.001016983
b	0.507905247	0.005338892	95.133081582	0.4952310549	0.520579439
c	-0.005186764	0.0054385014	-0.953712055	-0.018097423	0.0077238942

Curve-Fit Std Error: 0.001466875254761

Source	Sum of Squares	DF	Mean Square	F
Regr	0.287915843	2	0.143957921	66903.56
Error	1.50620611e-005	7	2.15172301e-006	
Total	0.287930905	9		

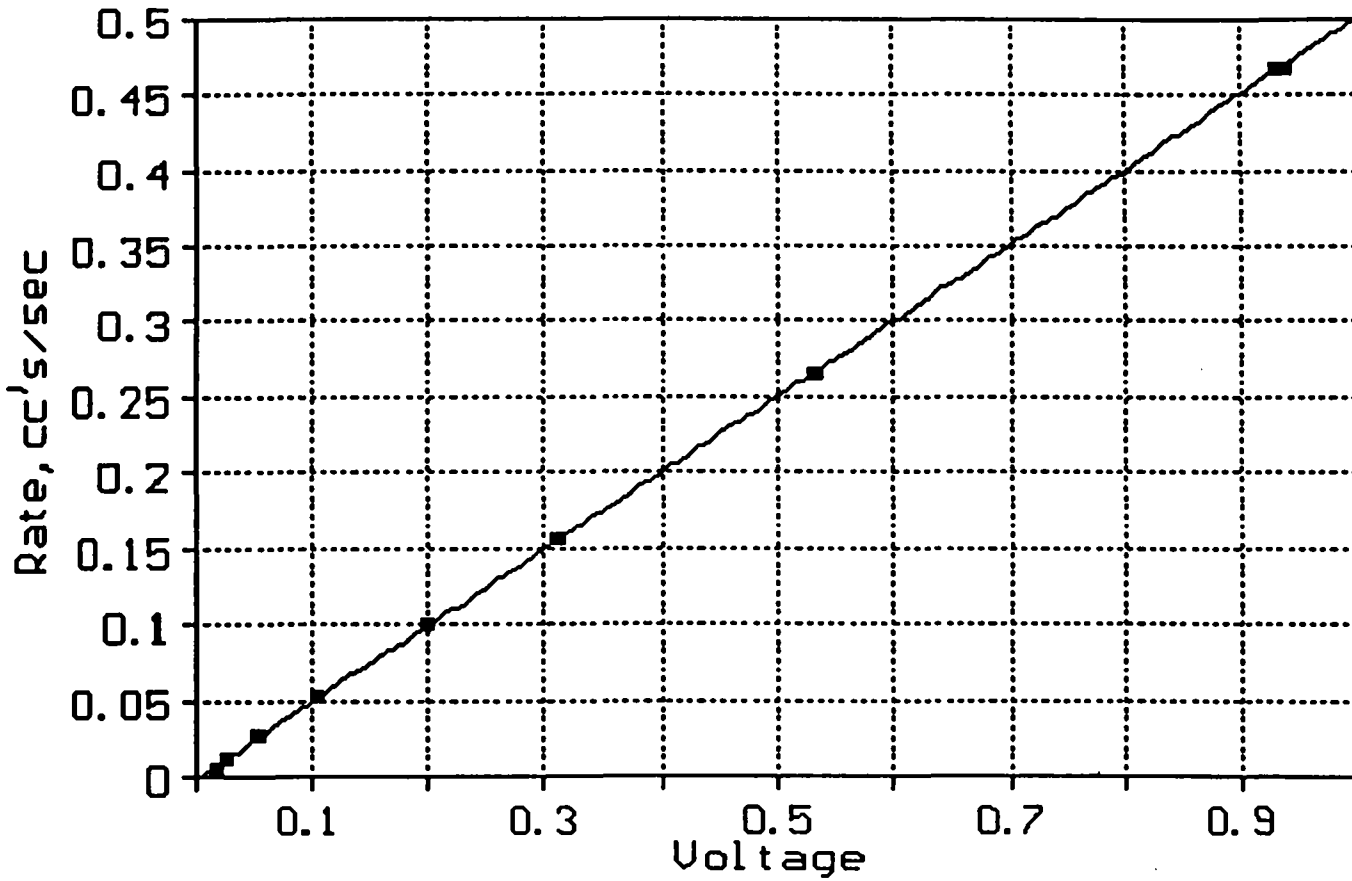
Calibration of low range flow meter

Page 1

#	X-Value	Y-Value	Y-Predict	95% Confidence Intvl	
1	0.0183	0.0042	0.00621019	0.00430902	0.00811136
2	0.0256	0.0096	0.00991623	0.00807568	0.01175679
3	0.0537	0.0254	0.02417681	0.02254044	0.02581319
4	0.105	0.0508	0.05019013	0.04879385	0.05158641
5	0.199	0.0988	0.097785	0.0963985	0.09917151
6	0.31	0.1547	0.15386944	0.15217458	0.1555643
7	0.531	0.265	0.26515248	0.26314924	0.26715572
8	0.532	0.264	0.26565487	0.26365191	0.26765783
9	0.933	0.468	0.46627783	0.46385968	0.46869599
10	0.939	0.468	0.46926701	0.46680086	0.47173316

Calibration of Low Range Flow Meter
11/4/97 Manning

46 Eqn 64 $y=(a+bx+cx^2)$ $r=0.9999476886$
 $a=-0.00308274026$ $b=0.507905247$
 $c=-0.00518676439$



Jan 5,1994 3:40 PM

Description: 500pis Guage Calibration
X-Y Table Size: 11 Active Points: 11

X Variable: Guage reading,psig

Xmin: 0	Xmax: 498.5	Xrange: 498.5
Xmean: 249.09090909	Xstd: 165.20579109	Xmedian: 248.75
X@Ymin: 0	X@Ymax: 498.5	X@Yrange: 498.5
Xav@Ymax: 498.5	X@50Y: 248.75	Xlt@50Y: 0
Xrt@50Y: 0	X@25Y: 124.765625	X@75Y: 373.5
Xwavemin: 0	Xwavemax: 498.5	Xwaverng: 997

Y Variable: Dead Weight Pressure

Ymin: 0	Ymax: 500	Yrange: 500
Ymean: 250	Ystd: 165.83123952	Ymedian: 250
Y@Xmin: 0	Y@Xmax: 500	Y@Xrange: 500

15 Eqn 64 $y=(a+bx+cx^2)$ $r=0.9999986573$

	Coefficient	Std Error	T(Coef/Err)	95% Confidence Limits	
a	-0.29279215	0.1637898374	-1.787608771	-0.671810845	0.0862265447
b	1.0072453999	0.0015277072	659.31835415	1.0037102014	1.0107805985
c	-6.941e-006	2.95099e-006	-2.352084236	-1.377e-005	-1.1222e-007

Curve-Fit Std Error: 0.21483810289

Source	Sum of Squares	DF	Mean Square	F
Regr	274999.631	2	137499.815	2979062
Error	0.369243284	8	0.0461554105	
Total	275000	10		

500pis Guage Calibration
Page 1

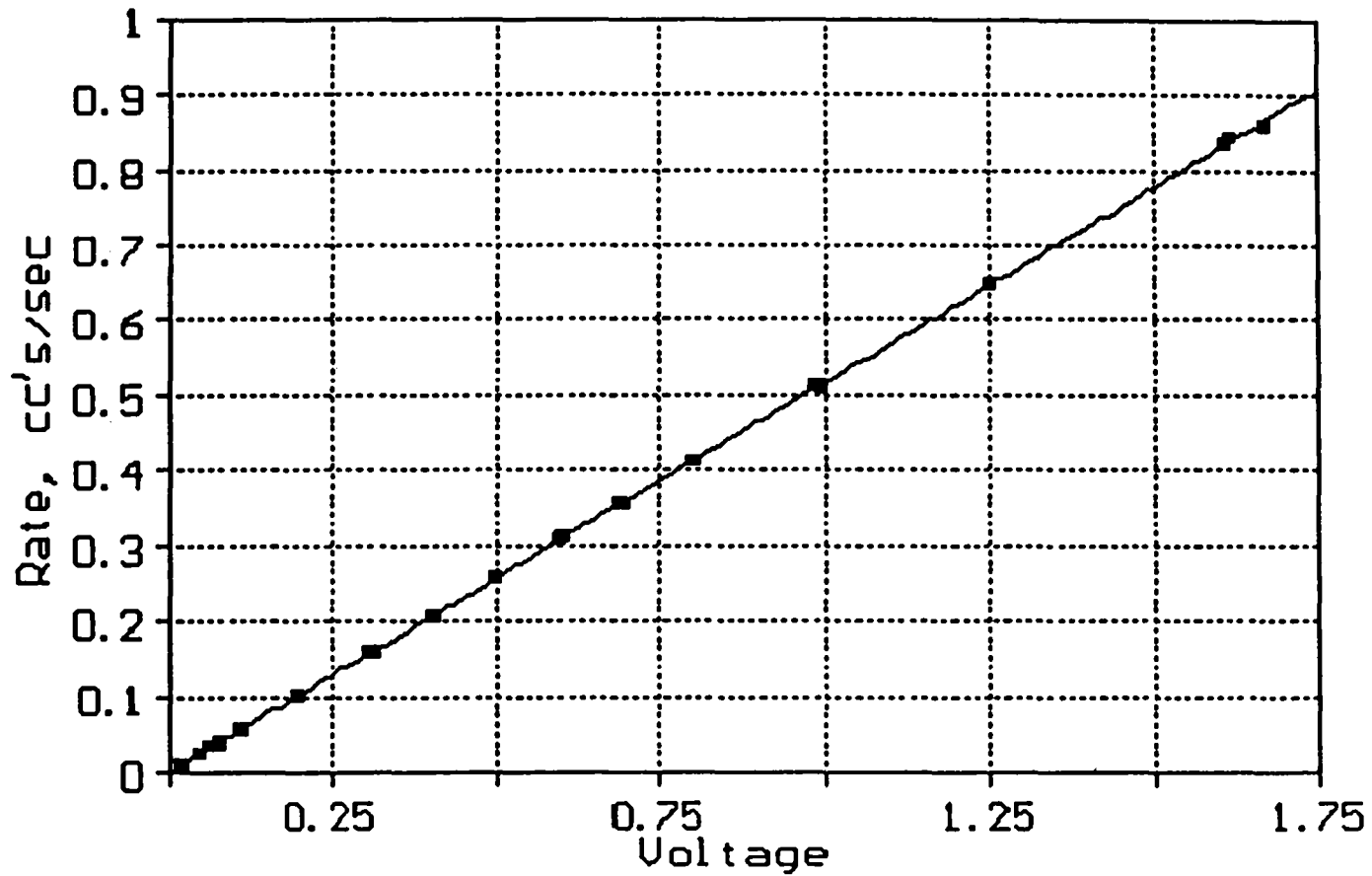
#	X-Value	Y-Value	Y-Predict	95% Confidence Intvl	
1	0	0	-0.2927921	-0.6718108	0.08622654
2	50	50	50.0521254	49.7899743	50.3142765
3	100	100	100.362338	100.155228	100.569448
4	149.5	150	150.135262	149.930963	150.339562
5	199.25	200	200.125293	199.906378	200.344207
6	248.75	250	249.830017	249.603796	250.056238
7	298.5	300	299.751503	299.532283	299.970723
8	348.5	350	349.889232	349.684617	350.093847
9	398.5	400	399.992256	399.784924	400.199588
10	448.5	450	450.060576	449.798295	450.322857
11	498.5	500	500.09419	499.715175	500.473205

Calibration of Low Range Flow Meter (Helium)

1/1/71

Alfredson

35 Eqn 64 $y=(a+bx+cx^2)$ $r=0.9999626919$
 $a=-0.00170672704$ $b=0.515305974$
 $c=0.00177984694$



Jan 6,1994 7:54 AM

Description: Recalibration @ 14.3601 Pb
X-Y Table Size: 6 Active Points: 6

X Variable: Voltage

Xmin: 0.0134	Xmax: 0.221	Xrange: 0.2076
Xmean: 0.0801333333	Xstd: 0.0767259973	Xmedian: 0.05675
X@Ymin: 0.0134	X@Ymax: 0.221	X@Yrange: 0.2076
Xav@Ymax: 0.221	X@50Y: 0.1267811111	Xlt@50Y: 0
Xrt@50Y: 0	X@25Y: 0.0587410639	X@75Y: 0.1913153337
Xwavemin: 0.0134	Xwavemax: 0.221	Xwaverng: 0.4152

Y Variable: Rate, cc's/sec

Ymin: 0.0008	Ymax: 0.1128	Yrange: 0.112
Ymean: 0.03725	Ystd: 0.0410825876	Ymedian: 0.0268
Y@Xmin: 0.0008	Y@Xmax: 0.1128	Y@Xrange: 0.112

53 Eqn 64 $y=(a+bx+cx^2)$ $r=0.9980941858$

	Coefficient	Std Error	T(Coef/Err)	95% Confidence Limits	
a	-0.00574819	0.0023016858	-2.49738265	-0.013018843	0.0015224623
b	0.5389838926	0.0567495106	9.4975954308	0.3597213843	0.718246401
c	-0.016984578	0.2311745348	-0.073470802	-0.747227474	0.7132583175

Curve-Fit Std Error: 0.002315380855453

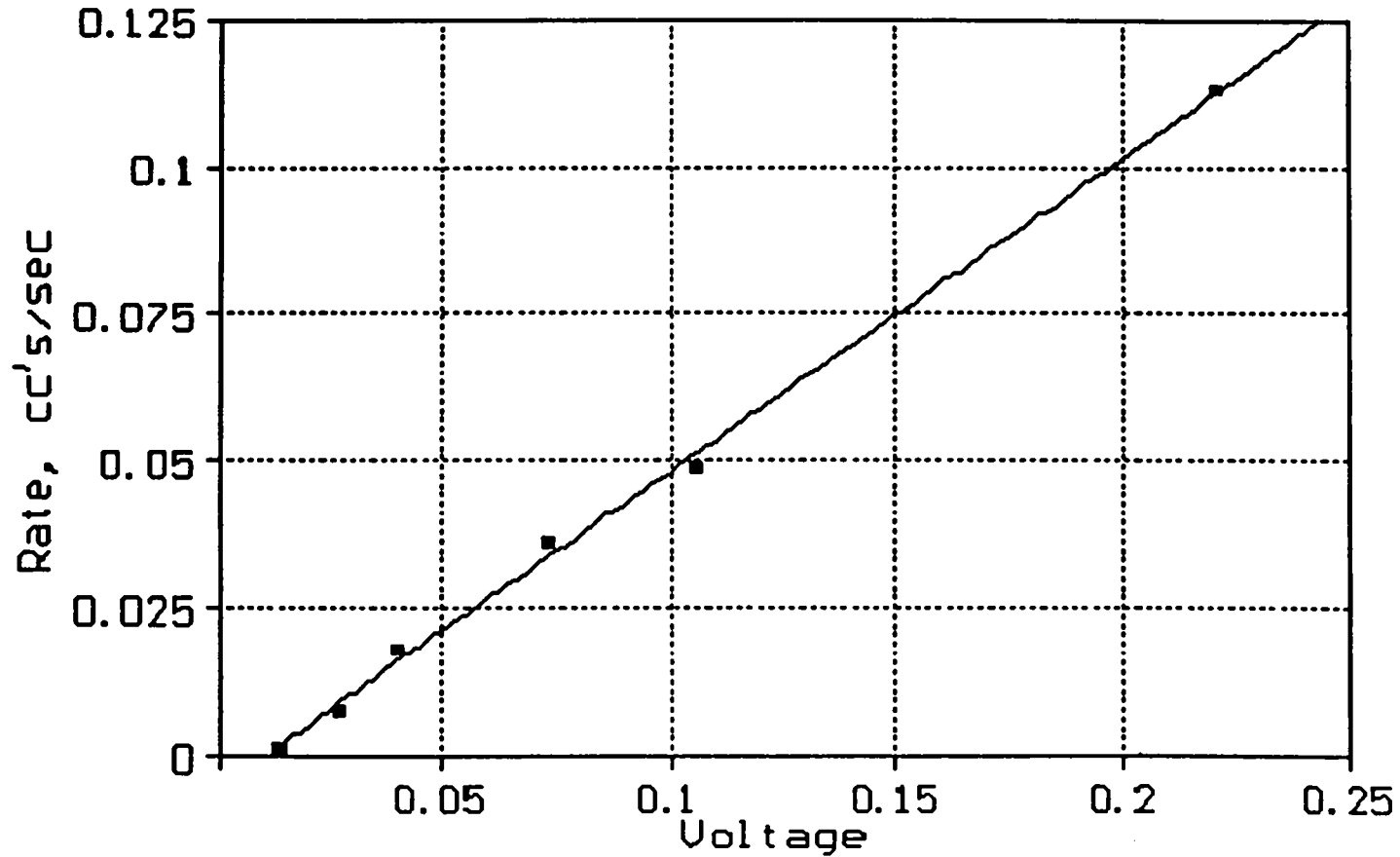
Source	Sum of Squares	DF	Mean Square	F
Regr	0.00842281203	2	0.00421140602	785.5652
Error	1.60829655e-005	3	5.36098851e-006	
Total	0.008438895	5		

Recalibration @ 14.3601 Pb
Page 1

#	X-Value	Y-Value	Y-Predict	95% Confidence Intvl
1	0.0134 .001	0.0008 .001	0.00147114	-0.0039246 0.00686685
2	0.0269 .008	0.0075 .009	0.00873819	0.00468925 0.01278712
3	0.0403 .018	0.0177 .016	0.01594528	0.01250702 0.01938353
4	0.0732 .036	0.0359 .034	0.03361442	0.02926302 0.03796583
5	0.106 .049	0.0488 .051	0.05119326	0.04562369 0.05676284
6	0.221 .113	0.1128 .113	0.11253771	0.10524415 0.11983126

Calibration of Low Range Mass Flow Meter (to Helium)
1/6/94
Morning
Pb = 14.3601
29.2301

53 Eqn 64 $y=(a+bx+cx^2)$ $r=0.9980941858$
 $a=-0.00574819019$ $b=0.538983893$
 $c=-0.0169845785$



1" and 1 1/2" Calibration Ck (Caliper)

DATE: 12/20/93

TECH: JAK

JOB#: 93089

SAMPLE ID	CALIP. BV	HG. BV	WEIGHT	AREA	LENGTH	DIAMETER	PAP
	CC	CC	GMS.	SQCM	CM	CM	DE
10	12.870	0.000	99.837	5.007	<u>2.540</u>	3.540	0.0
20	103.057	0.000	100.520	20.297	<u>3.575</u>	5.080	0.0
10-2	40.868	0.000	103.851	11.455	3.568	3.519	0.0
10-5E	22.295	0.000	59.130	11.343	11.317 2.054	3.501	0.0
10-6	79.991	0.000	213.811	11.351	11.347 7.047	3.501	0.0
10-7	48.490	0.000	130.088	11.518	11.317 3.100	3.738	0.0
11-3	25.600	0.000	76.377	11.342	11.34 2.915	3.930	0.0
11-2	35.851	0.000	90.758	11.350	11.347 3.129	3.501	0.0

5/8

WIPP
UC721 - DISTRIBUTION LIST
SAND94-0472

Federal Agencies

US Department of Energy (4)
Office of Civilian Radioactive Waste Mgmt.
Attn: Deputy Director, RW-2
Acting Director, RW-10
Office of Human Resources & Admin.
Director, RW-30
Office of Program Mgmt. & Integ.
Director, RW-40
Office of Waste Accept., Stor., & Tran.

Forrestal Building
Washington, DC 20585

Attn: Project Director
Yucca Mountain Site Characterization Office
Director, RW-3
Office of Quality Assurance

P.O. Box 30307
Las Vegas, NV 89036-0307

US Department of Energy
Albuquerque Operations Office
Attn: National Atomic Museum Library
P.O. Box 5400
Albuquerque, NM 87185-5400

US Department of Energy
Research & Waste Management Division
Attn: Director
P.O. Box E
Oak Ridge, TN 37831

US Department of Energy (5)
Carlsbad Area Office
Attn: G. Dials
D. Galbraith
M. McFadden
R. Lark
J. A. Mewhinney
P.O. Box 3090
Carlsbad, NM 88221-3090

US Department of Energy
Office of Environmental Restoration and
Waste Management
Attn: M Frei, EM-30
Forrestal Building
Washington, DC 20585-0002

US Department of Energy (3)
Office of Environmental Restoration and
Waste Management
Attn: J. Juri, EM-34, Trevion II
Washington, DC 20585-0002

US Department of Energy
Office of Environmental Restoration and
Waste Management
Attn: S. Schneider, EM-342, Trevion II
Washington, DC 20585-0002

US Department of Energy (2)
Office of Environment, Safety & Health
Attn: C. Borgstrom, EH-25
R. Pelletier, EH-231
Washington, DC 20585

US Department of Energy (2)
Idaho Operations Office
Fuel Processing & Waste Mgmt. Division
785 DOE Place
Idaho Falls, ID 83402

US Environmental Protection Agency (2)
Radiation Protection Programs
Attn: M. Oge
ANR-460
Washington, DC 20460

Boards

Defense Nuclear Facilities Safety Board
Attn: D. Winters
625 Indiana Ave. NW, Suite 700
Washington, DC 20004

Nuclear Waste Technical Review Board (2)
Attn: Chairman
J. L. Cohon
1100 Wilson Blvd., Suite 910
Arlington, VA 22209-2297

State Agencies

Attorney General of New Mexico
P.O. Drawer 1508
Santa Fe, NM 87504-1508

Environmental Evaluation Group (3)
Attn: Library
7007 Wyoming NE
Suite F-2
Albuquerque, NM 87109

NM Environment Department (3)
Secretary of the Environment
Attn: Mark Weidler
1190 St. Francis Drive
Santa Fe, NM 87503-0968

NM Bureau of Mines & Mineral Resources
Socorro, NM 87801

Laboratories/Corporations

Battelle Pacific Northwest Laboratories
Battelle Blvd.
Richland, WA 99352

INTERA, Inc.
Attn: G. A. Freeze
1650 University Blvd. NE, Suite 300
Albuquerque, NM 87102

INTERA, Inc.
Attn: J. F. Pickens
6850 Austin Center Blvd., Suite 300
Austin, TX 78731

Los Alamos National Laboratory
Attn: B. Erdal, INC-12
P.O. Box 1663
Los Alamos, NM 87544

RE/SPEC, Inc.
Attn: A. Robb
4775 Indian School NE, Suite 300
Albuquerque, NM 87110-3927

RE/SPEC, Inc.
Attn: J. L. Ratigan
P. O. Box 725
Rapid City. SD 57709

Tech Repts, Inc. (3)
Attn: J. Chapman (1)
Loretta Robledo (2)
5000 Marble NE, Suite 222
Albuquerque, NM 87110

Westinghouse Electric Corporation (5)
Attn: Library
J. Epstein
J. Lee
B. A. Howard
R. Kehrman
P.O. Box 2078
Carlsbad, NM 88221

S. Cohen & Associates
Attn: Bill Thurber
1355 Beverly Road
McLean, VA 22101

Rock Physics Associates
Attn: J. Walls
4320 Steven Creek Blvd., Ste 282
San Jose, CA 95129

**National Academy of Sciences,
WIPP Panel**

Howard Adler
Oxyrase, Incorporated
7327 Oak Ridge Highway
Knoxville, TN 37931

Tom Kiess
Board of Radioactive Waste Management
GF456
2101 Constitution Ave.
Washington, DC 20418

Rodney C. Ewing
Department of Geology
University of New Mexico
Albuquerque, NM 87131

Charles Fairhurst
Department of Civil and Mineral Engineering
University of Minnesota
500 Pillsbury Dr. SE
Minneapolis, MN 55455-0220

B. John Garrick
PLG Incorporated
4590 MacArthur Blvd., Suite 400
Newport Beach, CA 92660-2027

Leonard F. Konikow
US Geological Survey
431 National Center
Reston, VA 22092

Carl A. Anderson, Director
Board of Radioactive Waste Management
National Research Council
HA 456
2101 Constitution Ave. NW
Washington, DC 20418

Christopher G. Whipple
ICF Kaiser Engineers
1800 Harrison St., 7th Floor
Oakland, CA 94612-3430

John O. Blomeke
720 Clubhouse Way
Knoxville, TN 37909

Sue B. Clark
University of Georgia
Savannah River Ecology Lab
P.O. Drawer E
Aiken, SC 29802

Konrad B. Krauskopf
Department of Geology
Stanford University
Stanford, CA 94305-2115

Della Roy
Pennsylvania State University
217 Materials Research Lab
Hastings Road
University Park, PA 16802

David A. Waite
CH₂ M Hill
P.O. Box 91500
Bellevue, WA 98009-2050

Thomas A. Zordon
Zordan Associates, Inc.
3807 Edinburg Drive
Murrysville, PA 15668

Universities

University of New Mexico
Geology Department
Attn: Library
141 Northrop Hall
Albuquerque, NM 87131

Libraries

Thomas Brannigan Library
Attn: D. Dresp
106 W. Hadley St.
Las Cruces, NM 88001

Government Publications Department
Zimmerman Library
University of New Mexico
Albuquerque, NM 87131

New Mexico Junior College
Pannell Library
Attn: R. Hill
Lovington Highway
Hobbs, NM 88240

New Mexico State Library
Attn: N. McCallan
325 Don Gaspar
Santa Fe, NM 87503

New Mexico Tech
Martin Speere Memorial Library
Campus Street
Socorro, NM 87810

WIPP Public Reading Room
Carlsbad Public Library
101 S. Halagueno St.
Carlsbad, NM 88220

Foreign Addresses

Atomic Energy of Canada, Ltd.
Whiteshell Laboratories
Attn: B. Goodwin
Pinawa, Manitoba, CANADA R0E 1L0

Francois Chenevier (2)
ANDRA
Route de Panorama Robert Schumann
B. P. 38
92266 Fontenay-aux-Roses, Cedex
FRANCE

Claude Sombret
 Centre d'Etudes Nucleaires de la Vallee Rhone
 CEN/VALRHO
 S.D.H.A. B.P. 171
 30205 Bagnols-Sur-Ceze
 FRANCE

Svensk Karnbransleforsorjning AB
 Attn: F. Karlsson
 Project KBS (Karnbranslesakerhet)
 Box 5864
 S-102 48 Stockholm
 SWEDEN

Commissariat a L'Energie Atomique
 Attn: D. Alexandre
 Centre d'Etudes de Cadarache
 13108 Saint Paul Lez Durance Cedex
 FRANCE

Nationale Genossenschaft fur die Lagerung
 Radioaktiver Abfalle (2)
 Attn: S. Vomvoris
 P. Zuidema
 Hardstrasse 73
 CH-5430 Wettingen
 SWITZERLAND

Bundesanstalt fur Geowissenschaften und
 Rohstoffe
 Attn: M. Langer
 Postfach 510 153
 D-30631 Hannover
 GERMANY

AEA Technology
 Attn: J. H. Rees
 D5W/29 Culham Laboratory
 Abington, Oxfordshire OX14 3DB
 UNITED KINGDOM

Bundesministerium fur Forschung und
 Technologie
 Postfach 200 706
 5300 Bonn 2
 GERMANY

AEA Technology
 Attn: W. R. Rodwell
 044/A31 Winfrith Technical Centre
 Dorchester, Dorset DT2 8DH
 UNITED KINGDOM

Institut fur Tieflagerung
 Attn: K. Kuhn
 Theodor-Heuss-Strasse 4
 D-3300 Braunschweig
 GERMANY

AEA Technology
 Attn: J. E. Tinson
 B4244 Harwell Laboratory
 Didcot, Oxfordshire OX11 0RA
 UNITED KINGDOM

Gesellschaft fur Anlagen und Reaktorsicherheit
 (GRS)
 Attn: B. Baltes
 Schwertnergasse 1
 D-50667 Cologne
 GERMANY

Internal

Shingo Tashiro
 Japan Atomic Energy Research Institute
 Tokai-Mura, Ibaraki-Ken, 319-11
 JAPAN

<u>MS</u>	<u>Org.</u>	
1324	6115	P. B. Davies
1324	6115	T. L. Christian-Frear (5)
1324	6115	C. Boney
1324	6115	R. L. Beauheim
1324	6115	S. W. Webb
1320	6831	E. J. Nowak
1322	6121	J. R. Tillerson
1328	6849	D. R. Anderson
1328	6848	H. N. Jow
1335	6801	M. Chu
1335	6801	S. M. Howarth (15)
1341	6832	J. T. Holmes
1395	6800	L. Shephard
1395	6821	M. Marietta
0751	6117	L. S. Costin
0751	6117	N. S. Brodsky
0751	6117	J. T. Fredrich
0751	6117	D. J. Holcomb

Netherlands Energy Research Foundation ECN
 Attn: J. Prij
 3 Westerduinweg
 P.O. Box 1
 1755 ZG Petten
 THE NETHERLANDS

0751	6117	D. H. Zeuch
0705	6116	D. J. Borns
1330	6811	K. Hart (2)
1330	4415	NWM Library (20)
9018	8940-2	Central Technical Files
0899	4414	Technical Library (5)
0619	12690	Review and Approval Desk (2), For DOE/OSTI

SANDIA REPORT

SAND94-0472/2 • UC-721

Unlimited Release

Printed August 1997



TL0006048

**SANDIA NATIONAL
LABORATORIES
TECHNICAL LIBRARY**

Porosity, Single-Phase Permeability, and Capillary Pressure Data from Preliminary Laboratory Experiments on Selected Samples from Marker Bed 139 at the Waste Isolation Pilot Plant

Volume 2 of 3: Appendix B

Susan M. Howarth, Tracy Christian-Frear

Prepared by:
Sandia National Laboratories
Albuquerque, New Mexico 87185 and Livermore, California 94550

Sandia is a multiprogram laboratory operated by Sandia
Corporation, a Lockheed Martin Company, for the United States
Department of Energy under Contract DE-AC04-94AL85000.

Approved for public release; distribution is unlimited.



*299 p., in various
pages*

Issued by Sandia National Laboratories, operated for the United States Department of Energy by Sandia Corporation.

NOTICE: This report was prepared as an account of work sponsored by an agency of the United States Government. Neither the United States Government nor any agency thereof, nor any of their employees, nor any of their contractors, subcontractors, or their employees, makes any warranty, express or implied, or assumes any legal liability or responsibility for the accuracy, completeness, or usefulness of any information, apparatus, product, or process disclosed, or represents that its use would not infringe privately owned rights. Reference herein to any specific commercial product, process, or service by trade name, trademark, manufacturer, or otherwise, does not necessarily constitute or imply its endorsement, recommendation, or favoring by the United States Government, any agency thereof, or any of their contractors or subcontractors. The views and opinions expressed herein do not necessarily state or reflect those of the United States Government, any agency thereof, or any of their contractors.

Printed in the United States of America. This report has been reproduced directly from the best available copy.

Available to DOE and DOE contractors from
Office of Scientific and Technical Information
P.O. Box 62
Oak Ridge, TN 37831

Prices available from (615) 576-8401, FTS 626-8401

Available to the public from
National Technical Information Service
U.S. Department of Commerce
5285 Port Royal Rd
Springfield, VA 22161

NTIS price codes
Printed copy: A13
Microfiche copy: A01

SAND94-0472/2
Unlimited Release
Printed August 1997

Distribution
Category UC-721

**Porosity, Single-Phase Permeability, and Capillary
Pressure Data from Preliminary Laboratory Experiments
on Selected Samples from
Marker Bed 139 at the Waste Isolation Pilot Plant**

Volume 2 of 3: Appendix B

Susan M. Howarth
Tracy Christian-Frear

Geohydrology Department 6115
Sandia National Laboratories
Albuquerque, NM 87185

ABSTRACT

This volume contains the mineralogy, porosity, and permeability results from the Marker Bed 139 specimens evaluated by RE/SPEC, Inc.

Appendix B.
Data Report: RE/SPEC Inc.

The following section includes Appendix B and Appendices B-A through B-J.

Appendix B

Laboratory Measurements of Fluid Transport Properties for Marker Bed 139 Anhydrite from the Waste Isolation Pilot Plant

Errata Sheet

The following data are not included in the data report because the data were not qualified by the time of report publication:

1. Total porosity data on all specimens.
2. Effective porosity data on all specimens.

The liquid permeability data are included in the data report as "scoping only" because the brine dissolved the specimens.

The liquid permeability results for specimen P3X10-6-SP2 are not included in the data report because the gas permeability measurements were unusable (negative slopes for the Klinkenberg correction were reported by RE/SPEC).

One entry in Table 4-8 is in error. The flow rate for the gas inlet pressure at 0.7 MPa and the first 10 MPa confining pressure should be 7.59, not $7.63 \cdot 10^{-8} \text{ m}^3 / \text{s}$.

The following modifications should be made to the reference citations in Appendix B.

Page No.	Change
B-7	in the abstract: Davies et al., 1992 should read Davies et al., 1991
B-17	Brodsky (1990) should read Brodsky and Munson (1991)
B-39	Brodsky (1993) should read Brodsky (1994)
B-58	ANSI/ASME (1986) should read ANSI/ASME (1985)
B-102	Davies et al., 1992 should read Davies et al., 1991
B-103	change ANSI/ASME, 1986 to ANSI/ASME, 1985; copy on file in SWCF as WPO#44996
B-103	change ASTM, 1989 to ASTM, 1992; copy on file in SWCF as WPO#43089
B-103	change ASTM, 1989 to ASTM, 1990; copy on file in SWCF as WPO#43223
B-103	change Brodsky, N.S., 1993 to Brodsky, N.S. 1994; copy on file in SWCF as WPO#10087
B-103	change Brodsky, N.S., 1990 to Brodsky, N.S. and D.E. Munson, 1991; correct title is <i>The Effect of Brine on the Creep of WIPP Salt in Laboratory Tests</i> ; copy on file in SWCF as WPO#26136
B-103	to citation for Chowdiah, 1988 add Vol. 3, no. 4
B-103	copy of Costin and Wawersik, 1980 on file in SWCF as WPO#26748
B-103	in citation for Gilpatrick et al., 1982 the second author is C.G. Baes Jr.; copy on file in SWCF as WPO#45931
B-103	in citation for Davies et al., 1991 the correct name for second author is L.H. Brush; copy on file in SWCF as WPO#25381

Page No.	Change
B-103	copy of Howarth, 1993 on file in SWCF as WPO#21611
B-104	copy of Holcomb and Shields, 1987 on file in SWCF as WPO#26778
B-104	complete author name is C.S. Hurlbut, Jr.; add 18th edition to book title
B-104	in citation for IT Corporation, 1987 add to publication facts: Battelle Memorial Institute; copy on file in SWCF as WPO#45954
B-104	copy of Klinkenberg, 1941 on file in SWCF as WPO#8556
B-104	Stone and Webster, 1983 is available from the NTIS as DE83018265 and on file in SWCF as WPO#46602
B-104	in Stormont and Daemen, 1992 the correct second author's name is J.K.K. Daemen; correct journal title is <i>International Journal of Rock Mechanics and Mining Sciences and Geomechanics Abstracts</i> ; copy on file in SWCF as WPO#45950
B-104	in Sutherland and Cave, 1980 capitalize "Salt" in paper title; correct journal title is <i>International Journal of Rock Mechanics and Mining Sciences and Geomechanics Abstracts</i> ; copy on file in SWCF as WPO#45951
B-104	in citation for Weast, 1974 add 55th edition
B-116	for Chung, 1974 the full journal title is <i>Journal of Applied Crystallography</i> Vol. 7, no. 6; copy on file in SWCF as WPO#45584
B-116	for Davis, 1981 the full journal title is <i>Atmospheric Environment</i> Vol. 15, no. 3; copy on file in SWCF as WPO#45585
B-116	for Davis, 1984 capitalize "Using" in title; full journal title is <i>Advances in X-ray Analysis, Proceedings of the Annual Conference on Applications of X-Ray Analysis</i> , Vol. 27
B-116	for Davis, 1986 the full journal title is <i>Powder Diffraction</i> Vol. 1, no. 3; copy on file in SWCF as WPO#45586
B-116	for Davis, 1988 the full journal title is <i>Advances in X-Ray Analysis, Proceedings of the Annual Conference</i> , Vol. 31
B-116	for Davis and Johnson, 1982 the full journal title is <i>Atmospheric Environment</i> Vol. 16, no 2; copy on file in SWCF as WPO#45587
B-116	for Davis and Johnson, 1987 the full journal title is <i>Advances in X-Ray Analysis, Proceedings of the Annual Conference</i> , Vol. 30
B-116	for Davis et al., 1984 the full journal title is <i>Atmospheric Environment</i> Vol. 18, no 4; copy on file in SWCF as WPO#45588
B-176	the existence of Lab Notebook No. WIPP 04 could not be verified
B-176	the existence of Lab Notebook No. WIPP 02 could not be verified
B-188	copy of ANSI/ASME, 1985 on file in SWCF as WPO#44996
B-196	Holcomb and Shields: no date given; assumed to be 1987; copy on file in SWCF as WPO#26778
B-198	copy of ANSI/ASME, 1985 on file in SWCF as WPO#44996
B-198	Stroup and Senseny, 1987: RSI-0309; copy on file in SWCF as WPO#45638
B-199	Stroup and Senseny, 1987: RSI-0309; copy on file in SWCF as WPO#45638

**LABORATORY MEASUREMENTS OF FLUID TRANSPORT
PROPERTIES FOR MARKER BED 139 ANHYDRITE
FROM THE WASTE ISOLATION PILOT PLANT**

Topical Report RSI-0491

by

Nancy S. Brodsky
RE/SPEC Inc.
P.O. Box 725
Rapid City, South Dakota 57709

prepared for

Sandia National Laboratories
P.O. Box 5800
Albuquerque, NM 87185

January 1994

The content of this report was effective as of January 1994. This report was prepared by RE/SPEC Inc. under Contract No. AA-2020 Amendment 1 with Sandia National Laboratories.

Laboratory Measurements of Fluid Transport Properties for Marker Bed 139 Anhydrite From the Waste Isolation Pilot Plant

N.S. Brodsky
RE/SPEC Inc.
P. O. Box 725
Rapid City, SD 57709-0725

ABSTRACT

Fluid transport properties were measured in the laboratory for specimens of Marker Bed 139 anhydrite from the Waste Isolation Pilot Plant. Measurements included single-phase permeabilities to nitrogen and brine, porosities and mineralogies of materials immediately adjacent to each permeability specimen, and mineralogies of additional specimens taken from near each permeability specimen. An assessment of coring-induced damage was also conducted. The marker bed is non-homogeneous with respect to composition. Specimen mineralogy was characterized and correlations between fluid transport properties and compositional variations were investigated.

Two permeability specimens were taken from the upper and lower sections of borehole P3X11, and a third permeability specimen was taken from the upper/central region of adjacent borehole P3X10. Measurements of permeability to gas and brine were made on each specimen using steady-state flow techniques at confining pressures of 2 MPa, 6 MPa, and 10 MPa. For each value of confining pressure, permeability measurements were made at inlet pore pressures of 0.4 MPa, 0.7 MPa, and 1.0 MPa and at an outlet pore pressure of 0.1 MPa. Gas permeabilities ranged from approximately $1.8 \times 10^{-19} \text{ m}^2$ to $2.5 \times 10^{-17} \text{ m}^2$ and the Klinkenberg-corrected equivalent liquid permeabilities ranged from $1.4 \times 10^{-18} \text{ m}^2$ to $1.6 \times 10^{-17} \text{ m}^2$. Measured brine permeabilities ranged from $4.4 \times 10^{-20} \text{ m}^2$ to $9.7 \times 10^{-17} \text{ m}^2$. Brine permeabilities were higher than gas permeabilities, perhaps because some specimen dissolution occurred during saturation. The laboratory data include the range of permeability values indicated by field measurements, $8 \times 10^{-20} \text{ m}^2$ to $5 \times 10^{-17} \text{ m}^2$ (Davies et. al, 1992). The highest permeabilities were measured in the lowermost section of borehole P3X11, while the lowest permeabilities were measured for the central to upper region of adjacent borehole P3X10. Permeability values do not strongly correlate with any single material characteristic such as porosity, halite content, or anhydrite content; however, these material characteristics may contribute to spatial variations in permeability.

CONTENTS

1.0 INTRODUCTION	B-15
1.1 Background	B-15
1.2 Scope	B-15
1.3 Report Organization	B-18
2.0 SPECIMENS	B-21
2.1 Sample Acquisition	B-21
2.2 Coring and Finishing	B-23
2.3 Drying	B-24
3.0 EXPERIMENTAL METHODS	B-31
3.1 Specimen Characterization	B-31
3.2 Coring-Induced Surface Damage	B-31
3.3 Porosity Measurements	B-32
3.3.1 Effective Porosity	B-32
3.3.2 Total Porosity	B-33
3.4 Brine Production and Saturation	B-34
3.5 Permeability Measurements	B-35
3.5.1 Test Apparatus	B-35
3.5.1.1 LOAD FRAME	B-35
3.5.1.2 INSTRUMENTATION	B-35
3.5.1.3 CONTROL	B-37
3.5.1.4 GAS PERMEABILITY SYSTEM	B-37
3.5.1.5 BRINE PERMEABILITY SYSTEM	B-39
3.5.1.6 SPECIMEN ASSEMBLY	B-39
3.5.1.7 CALIBRATION	B-39
3.5.2 Test Procedure for Permeability Tests	B-42

CONTENTS (Continued)

3.5.3 Data Acquisition and Reduction	B-43
3.5.3.1 DATA ACQUISITION	B-43
3.5.3.2 DATA REDUCTION	B-44
3.5.4 Shakedown Tests for Gas Permeability Measurements	B-45
4.0 TEST RESULTS	B-47
4.1 MB 139 Specimen Characterization	B-47
4.2 Coring-Induced Surface Damage	B-49
4.3 Porosity Measurements	B-58
4.4 Gas Permeability Measurements	B-58
4.5 Brine Permeability Measurements	B-83
5.0 DISCUSSION OF RESULTS	B-89
5.1 Specimen Characterization	B-89
5.2 Porosity	B-89
5.3 Permeability	B-90
6.0 SUMMARY AND CONCLUSIONS	B-101
7.0 REFERENCES	B-103
APPENDIX B.A SOUTH DAKOTA SCHOOL OF MINES AND TECHNOLOGY PETROGRAPHIC ANALYSIS PROCEDURE AND RESULTS	B-105
APPENDIX B.B SOUTH DAKOTA SCHOOL OF MINES AND TECHNOLOGY X-RAY DIFFRACTION PROCEDURE AND RESULTS	B-109
APPENDIX B.C CORE LABORATORIES' EFFECTIVE POROSITY MEASUREMENTS PROCEDURE AND RESULTS	B-150

CONTENTS (Continued)

APPENDIX B.D	DERIVATION OF EQUATION FOR POROSITY CALCULATION BASED ON FLUID DISPLACEMENT MEASUREMENTS	B-167
APPENDIX B.E	BRINE MANUFACTURE	B-173
APPENDIX B.F	ERROR ANALYSES FOR PERMEABILITY MEASUREMENTS	B-185
APPENDIX B.G	FLOW-VERSUS-TIME DATA FOR ALL GAS PERMEABILITY TESTS	B-203
APPENDIX B.H	FLOW RATE-VERSUS-PORE PRESSURE DIFFERENCE ACROSS SPECIMEN FOR GAS PERMEABILITY TESTS	B-237
APPENDIX B.I	FLOW-VERSUS-TIME DATA FOR ALL BRINE PERMEABILITY TESTS	B-251
APPENDIX B.J	FLOW RATE-VERSUS-PORE PRESSURE DIFFERENCE ACROSS SPECIMEN FOR ALL BRINE PERMEABILITY TESTS	B-280

Tables

1-1	Test Matrix for Nitrogen Permeability Tests	B-18
1-2	Test Matrix for Brine Permeability Tests	B-19
2-1	Correlation Between Sample Identification Numbers Used by Sandia National Laboratories and by RE/SPEC Inc	B-21
2-2	Specimen Dimensions	B-23
3-1	Change in Specimen Mass During Saturation Procedure	B-34
3-2	Calibration Specifications	B-42
4-1	Summary of Quantitative Polarized Light Microscopy Analyses of MB 139 Thin Sections	B-48
4-2	Mineralogical Data for MB 139	B-49
4-3	Mineral Compositions of Marker Bed 139 Specimens	B-50
4-4	Results of Effective Porosity and Grain and Bulk Density Measurements on MB 139	B-59

Tables (Continued)

4-5	Porosity, Grain Density, and Bulk Density Measurements by RE/SPEC Inc. and by Core Laboratories	B-60
4-6	Flow Data and Calculated Permeability to Nitrogen for Specimen P3X11-5-2-SP1 .	B-62
4-7	Flow Data and Calculated Permeability to Nitrogen for Specimen P3X10-6-SP2 .	B-63
4-8	Flow Data and Calculated Permeability to Nitrogen for Specimen P3X11-5-3-SP3 .	B-64
4-9	Klinkenberg-Corrected Permeabilities	B-76
4-10	Klinkenberg Constants for MB 139 and Nitrogen Gas at 25°C	B-76
4-11	Flow Data and Permeability to Brine for Marker Bed 139 Specimen SP1	B-85
4-12	Flow Data and Permeability to Brine for Marker Bed 139 Specimen SP2	B-85
4-13	Flow Data and Permeability to Brine for Marker Bed 139 Specimen SP3	B-86

Figures

2-1	Map of WIPP MB 139 anhydrite cores	B-22
2-2	Expanded view of MB 139 anhydrite core showing locations of X-ray diffraction specimen and thin sections for TS1	B-25
2-3	Expanded view of MB 139 anhydrite core showing locations of X-ray diffraction specimen and thin sections for TS2	B-26
2-4	Expanded view of MB 139 anhydrite core showing locations of X-ray diffraction specimen and thin sections for TS3	B-27
2-5	Change in mass during drying at 60°C and 45 percent relative humidity for Specimen P3X11-5-2-SP1. Initial masses are 2.20445 kg, 0.03391 kg, and 0.03745 kg for the permeability specimen and the porosity specimens taken from above (SP1-T) and below (SP1-B) the permeability specimen, respectively	B-28
2-6	Change in mass during drying at 60°C and 45 percent relative humidity for Specimen P3X10-6-SP2. Initial masses are 2.15655 kg, 0.03885 kg, and 0.03367 kg for the permeability specimen and the porosity specimens taken from above (SP2-T) and below (SP2-B) the permeability specimen, respectively	B-29
2-7	Change in mass during drying at 60°C and 45 percent relative humidity for Specimen P3X11-5-3-SP3. Initial masses are 2.17060 kg, 0.03751 kg, and 0.04767 kg for the permeability specimen and the porosity specimens taken from above (SP3-T) and below (SP3-B) the permeability specimen, respectively	B-30
3-1	Load frame used for permeability tests	B-36

Figures (Continued)

3-2	Gas permeability measurement system	B-38
3-3	Liquid permeability apparatus	B-40
3-4	Specimen assembly for permeability tests	B-41
4-1	Average mineral compositions determined using X-ray diffraction for specimens taken from above and below the axes of specimens SP1, SP2, and SP3	B-51
4-2	Mineral compositions for specimens taken from Block TS1. Petrographic analyses were used for Specimens TS1-1, TS1-2, and TS1-3; X-ray diffraction was used for Specimen TS-4	B-52
4-3	Mineral compositions for specimens taken from Block TS2. Petrographic analyses were used for Specimens TS1-1, TS1-2, and TS1-3; X-ray diffraction was used for Specimen TS-4	B-53
4-4	Mineral compositions for specimens taken from Block TS3. Petrographic analyses were used for Specimens TS1-1, TS1-2, and TS1-3; X-ray diffraction was used for Specimen TS-4	B-54
4-5	Average mineral compositions for specimens taken from Blocks TS1, TS2, and TS3 from the upper, middle, and lower sections of the marker bed, respectively	B-55
4-6	Crack occurrence on Specimen P3X11-6/1	B-56
4-7	Crack occurrence on Specimen P3X11-5-3/1	B-57
4-8	Gas volume-versus-time for test on MB 139 anhydrite Specimen P3X11-5-2-SP1 at 2 MPa confining pressure and 1 MPa gas inlet pressure. Symbols represent recorded data points and dashed lines are best fits to linear sections of data	B-61
4-9	Flow rate-versus-gas pressure difference for Specimen P3X11-5-2-SP1 at 2 MPa confining pressure and all gas inlet pressures	B-65
4-10	Permeability as a function of mean reciprocal gas pressure for Specimen P3X11-5-2-SP1 at 2 MPa confining pressure	B-67
4-11	Permeability as a function of mean reciprocal gas pressure for Specimen P3X11-5-2-SP1 at 6 MPa confining pressure	B-68
4-12	Permeability as a function of mean reciprocal gas pressure for Specimen P3X11-5-2-SP1 at 10 MPa confining pressure	B-69
4-13	Permeability as a function of mean reciprocal gas pressure for Specimen P3X10-6-SP2 at 2 MPa confining pressure	B-70
4-14	Permeability as a function of mean reciprocal gas pressure for Specimen P3X10-6-SP2 at 6 MPa confining pressure	B-71
4-15	Permeability as a function of mean reciprocal gas pressure for Specimen P3X10-6-SP2 at 10 MPa confining pressure	B-72

Figures (Continued)

4-16	Permeability as a function of mean reciprocal gas pressure for Specimen P3X11-5-3-SP3 at 2 MPa confining pressure	B-73
4-17	Permeability as a function of mean reciprocal gas pressure for Specimen P3X11-5-3-SP3 at 6 MPa confining pressure	B-74
4-18	Permeability as a function of mean reciprocal gas pressure for Specimen P3X11-5-3-SP3 at 10 MPa confining pressure	B-75
4-19	Change in permeability with increasing effective confining pressure for Specimen P3X10-6-SP2 at an inlet pore pressure of 1.0 MPa	B-77
4-20	Change in permeability with increasing effective confining pressure for Specimen P3X10-6-SP2 at an inlet pore pressure of 0.7 MPa	B-78
4-21	Change in permeability with increasing effective confining pressure for Specimen P3X10-6-SP2 at an inlet pore pressure of 0.4 MPa	B-79
4-22	Change in permeability with increasing mean pore pressure for Specimen P3X10-6-SP2 at a confining pressure of 2 MPa	B-80
4-23	Change in permeability with increasing mean pore pressure for Specimen P3X10-6-SP2 at a confining pressure of 6 MPa	B-81
4-24	Change in permeability with increasing mean pore pressure for Specimen P3X10-6-SP2 at a confining pressure of 10 MPa	B-82
4-25	Change in exit buret level (brine volume)-versus-time for tests on Specimen P3X11-5-2-SP1 at 2 MPa confining pressure and 1 MPa brine inlet pressure. Symbols represent recorded data points and dashed lines are best fits to linear sections of data. The coefficients of variation for the linear least squares fits are given	B-84
4-26	Flow rate-versus-brine pressure difference for Specimen P3X11-5-2-SP1 at 2 MPa confining pressure and all brine inlet pressures	B-87
5-1.	Permeability-versus-confining pressure for all tests. Klinkenberg-corrected values are given for gas permeability tests	B-91
5-2.	Permeability-versus-average anhydrite content of material taken from above and below specimen axes. Only data obtained at 2 MPa confining pressure are shown for Specimens SP1 and SP3	B-93
5-3	Permeability-versus-average anhydrite content of Blocks TS1, TS2, and TS3. Only data obtained at 2 MPa confining pressure are shown for Specimens SP1 and SP3	B-94
5-4	Permeability-versus-average halite content of material taken from above and below specimen axes. Only data obtained at 2 MPa confining pressure are shown for Specimens SP1 and SP3	B-95

Figures (Continued)

- 5-5 Permeability-versus-average halite content of Blocks TS1, TS2, and TS3. Only data obtained at 2 MPa confining pressure are shown for Specimens SP1 and SP3 B-96
- 5-6 Permeability-versus-average effective porosity of specimens taken from above and below axes of permeability specimens. Only data obtained at 2 MPa confining pressure are shown for Specimens SP1 and SP3 B-97
- 5-7 Permeability-versus-total porosity of specimens taken from above axes of permeability specimens. Only data obtained at 2 MPa confining pressure are shown for Specimens SP1 and SP3 B-98
- 5-8 Permeability-versus-depth of origin of each specimen. Only data obtained at 2 MPa confining pressure are shown for Specimens SP1 and SP3 B-99

1.0 INTRODUCTION

1.1 Background

The Department of Energy (DOE) has developed the Waste Isolation Pilot Plant (WIPP) as a research and development facility for the purpose of demonstrating safe management, storage, and disposal of radioactive transuranic (TRU) waste generated by defense programs of the U.S. Government. The WIPP is located in southeastern New Mexico. The underground workings are in the bedded salt of the Salado Formation at a depth of about 660 m. Interbeds of nonsalt materials, principally anhydrite, are also found at the WIPP. Concerns have been raised about the role of gas and brine flow at the WIPP. The Salado salt contains small quantities of brine (0.1 – 1.0 percent by volume) and the interbeds may contain similar amounts. Decomposition of organic wastes and corrosion of metallic wastes and waste canisters may eventually generate gases. The geologic formations of the WIPP will provide the final barrier to radionuclide migration and so the permeability and fluid transport properties of these interbed formations are of great importance in determining the performance of the site for radioactive waste disposal. Of particular concern is the permeability of Marker Bed 139 (MB 139), a 1-m-thick anhydrite layer that underlies the TRU storage rooms at the WIPP. In situ tests show that permeabilities in the anhydrite interbeds are one to two orders of magnitude greater than in the halite. This marker bed may therefore provide a pathway for gas and brine flow.

1.2 Scope

Sandia National Laboratories established the Salado Two-Phase Flow Laboratory Program to measure fluid transport properties for the WIPP and to provide site-specific data to support performance assessment modeling (Howarth, 1993). RE/SPEC Inc. performed scoping activities associated with this program, and this report presents the results of these activities. The scoping activities are divided into three tasks summarized below.

Task 1. Specimen Characterization.

MB 139 is known to have lateral and vertical compositional variations and these may in turn affect fluid transport properties. Detailed characterization of composition can provide correlations between fluid transport properties and composition. X-ray diffraction and petrographic analyses were conducted on three samples that were spaced apart vertically and horizontally within the marker bed. In addition, X-ray diffraction analyses were conducted on material taken from above

and below the axis of each permeability specimen. These data were used to correlate variations in permeability with inhomogeneities in specimen composition.

Task 2. Assessment of Coring-Induced Surface Damage.

One concern that has been raised about laboratory testing is that surface damage produced during coring and finishing will affect laboratory measurements of permeability (Stormont and Daemen, 1992). The extent of surface damage was assessed by impregnating cored specimens with epoxy dye-penetrants and measuring crack densities near the cored surfaces and in the center of the specimens.

Damage, whether it is introduced by coring in the laboratory, or in situ, by deviatoric stresses that form in response to excavation of rooms and shafts at the WIPP, is of concern because it will affect rock permeability. A search of the literature concerning the healing of damage was conducted which did not reveal any studies of fracture healing on anhydrite or within MB 139. The search did, however, reveal a number of studies focusing on fracture healing in salt. The marker bed contains a significant amount of halite, and several studies indicate that halite can fill and perhaps heal fractures in more brittle rocks such as anhydrite. Stone and Webster Engineering Corp (1983) report many observations of salt having filled and healed fractures in adjacent, more brittle rocks, such as fractures and gaps in anhydrite layers at the Cleveland Mine, and fractures in dolomite in the Cleveland and Cayuga Mines.

A laboratory demonstration of crack healing in halite was performed by Costin and Wawarsik (1980) who measured fracture toughness in short rod specimens of salt. Specimens were pieced back together and fracture toughness was remeasured after subjecting specimens to hydrostatic pressures for varied lengths of time at two temperatures. Confining pressure had a more pronounced effect than temperature. Typically, specimens subjected to 10 to 35 MPa regained 70 to 80 percent of their original fracture toughness.

Permeability tests have also been used to assess crack closure and healing. Gilpatrick et al. (1982) measured flow of brine between two optical-quality sodium chloride crystals subjected to 14 MPa confining pressure at temperatures up to 80°C. Permeability decreased as a function of time and this was attributed to deformation by pressure solution. Permeability tests on rock salt have shown that the permeability and porosity of as-received specimens decrease over time at hydrostatic load (Southerland and Cave, 1980, Stormont and Daemen, 1992), implying that damage is introduced during coring but heals at pressure. IT Corp (1987) conducted permeability tests on naturally and artificially fractured rock salt specimens by subjecting them to confining

pressures of 20.6 MPa for up to 8 days. In most cases, the permeabilities of the fractured specimens returned to the same order of magnitude as before fracturing.

The technique of using ultrasonic properties to assess crack closure and healing was applied to rock salt by Brodsky (1990). In that study, compressional wave ultrasonic data were used to assess the extent of crack closure during hydrostatic compression of damaged WIPP salt specimens at 20°C. It was determined that the recovery of ultrasonic velocities depended on pressure and damage level. As expected, the higher the pressure, the greater the velocity recovery during crack closure and healing. It was also found that recovery was more complete in specimens with the least damage and it was concluded that recovery is slower when damage is sufficient to cause changes in the geometry of the crack walls.

Task 3. Determination of Porosity, and Measurements of Gas and Liquid Single-Phase Permeabilities Under Varying Triaxial Stress Conditions.

Sections of MB 139 were taken from two boreholes that were spaced 0.61 m (2 feet) apart in the underground workings at the WIPP. Two boreholes were required to provide a sufficient amount of material. Three cylindrical test specimens with axes parallel to the bedding plane were manufactured from approximately the upper, middle, and lower sections of the marker bed and used for permeability measurements. Specimens from the upper and lower sections of the marker bed were taken from one borehole, while the middle section was taken from the other borehole. Specimens from the upper and middle sections were only 61 mm apart in depth of origin. Pieces of material were taken from directly above and below each specimen axis and used for porosity measurements and for compositional characterization by X-ray diffraction. All permeability and porosity specimens were dried at controlled temperature and relative humidity. Effective (interconnected) porosities were measured by Core Laboratories of Houston, Texas, using a small volume helium porosimeter and then total porosities were measured on the same specimens by RE/SPEC Inc. using gravimetric techniques. Three additional specimens were taken from different sections of the marker bed and characterized using petrographic analysis and X-ray diffraction. Two of these specimens were taken from the upper and lower sections of one borehole, and the third specimen was taken from the upper region of the second borehole.

Gas (nitrogen) and liquid (brine) permeability tests were conducted using the steady-state flow method under the conditions given in Tables 1-1 and 1-2, respectively. Gas permeability tests were conducted first, then the specimens were saturated so that brine permeability tests could be conducted on the same set of specimens. As shown in Tables 1-1 and 1-2, three replicate gas permeability tests and one liquid permeability test were conducted at each test condition for a total of 103 individual permeability determinations. Gas and liquid permeability

tests on each specimen were performed at confining pressures of 2 MPa, 6 MPa, and 10 MPa. At each confining pressure, tests were conducted at three different pore pressure gradients to establish that the relationship between flow rate and pore pressure gradient was linear and that measurements were made in the laminar flow regime. Changes in mean pore pressure can affect gas permeability measurements in a process referred to as “slippage” or the Klinkenberg effect. A Klinkenberg correction was performed for gas permeability tests on each specimen at each value of confining pressure to determine the equivalent liquid permeability.

Table 1-1. Test Matrix for Nitrogen Permeability Tests^(a)

Confining Pressure (MPa)	Gas Inlet Pressure (MPa)	Gas Outlet Pressure (MPa)	Number of Tests		
			Specimen P3X11-5-2-SP1	Specimen P3X10-6-SP2	Specimen P3X11-5-3-SP3
2	1.0 ^(b)	0.1	3	3	3
	0.7	0.1	3	3	3
	0.4	0.1	3	3	3
6	1.0	0.1	3	3	3
	0.7	0.1	3	3	3
	0.4	0.1	3	3	3
10	1.0	0.1	3	3	3
	0.7	0.1	3	3	3
	0.4	0.1	3	3	3

(a) All tests were conducted at 25°C.
(b) Gas inlet pressure = 1.1 MPa for first test on P3X10-6-SP2.

1.3 Report Organization

This report consists of seven chapters, including this introductory chapter, and ten appendices. Chapter 2.0 discusses specimen preparation and drying, the experimental methods are described in Chapter 3.0, and experimental results are given in Chapter 4.0. A discussion of results is given in Chapter 5.0 and the report summary and conclusions are in Chapter 6.0. Cited references are given in Chapter 7.0. Four appendices (B-A, B-B, B-C, B-E) contain procedures and reports for work performed by subcontractors, Appendix B-D contains the derivation of an

Table 1-2. Test Matrix for Brine Permeability Tests^(a)

Confining Pressure (MPa)	Brine Inlet Pressure (MPa)	Brine Outlet Pressure (MPa)	Number of Tests		
			Specimen P3X11-5-2-SP1	Specimen P3X10-6-SP2	Specimen P3X11-5-3-SP3
2	1.0	0.1	2	1	1
	0.7	0.1	1	1	1
	0.4	0.1	1	1	1
6	1.0	0.1	Jacket Leak	1	1
	0.7	0.1		1	1
	0.4	0.1		1	1
10	1.0	0.1		1	1
	0.7	0.1		1	1
	0.4	0.1		1	1

(a) All tests were conducted at 25°C.

equation for determining porosity using gravimetric methods, Appendix B-F contains error analyses, and the remaining appendices (B-G, B-H, B-I, B-J) contain plotted data.

2.0 SPECIMENS

2.1 Sample Acquisition

Sections of MB 139 anhydrite core from two boreholes were shipped from New Mexico to the RE/SPEC Inc. Rapid City location during August of 1992. The first section was marked with identification numbers beginning with P3X11 and the second section with identification numbers beginning with P3X10. The boreholes were 0.61 m (2 feet) apart. The two sample sections are diagrammed in Figure 2-1. Samples P3X11-5 and P3X10-5 each broke into three pieces during shipping. Each of the broken pieces was assigned its original sample number plus a sequential number (i.e., P3X11-5-1, P3X11-5-2, etc.). The locations from which the permeability and porosity specimens were cored are labeled "SP1 4-in core hole," "SP2 4-in core hole," and "SP3 4-in core hole. Labels LC1, LC2, and LC3 designate material used for studies of laboratory coring-induced damage, and labels TS1, TS2, and TS3 designate material used for petrographic thin section and X-ray diffraction analyses.

After core sectioning and labeling of specimens were completed, RE/SPEC Inc. was notified that Sandia National Laboratories had generated a nonconformance report to document mislabeling of these cores. Instead of relabeling all pieces, which could later prove confusing, the matrix shown in Table 2-1 was used to correlate the original and corrected sample identification numbers.

Table 2-1. Correlation Between Sample Identification Numbers Used by Sandia National Laboratories and by RE/SPEC Inc.

Sandia Core Identification Number ^(a)	RE/SPEC Inc. Core Identification Number
P3X10-2	P3X10-5
P3X10-3-1	P3X10-6
P3X10-3-2	P3X10-7
P3X11-3	P3X11-5
P3X11-4	P3X11-6

(a) Corrected sample identification numbers furnished by Janis Trone on March 12, 1993

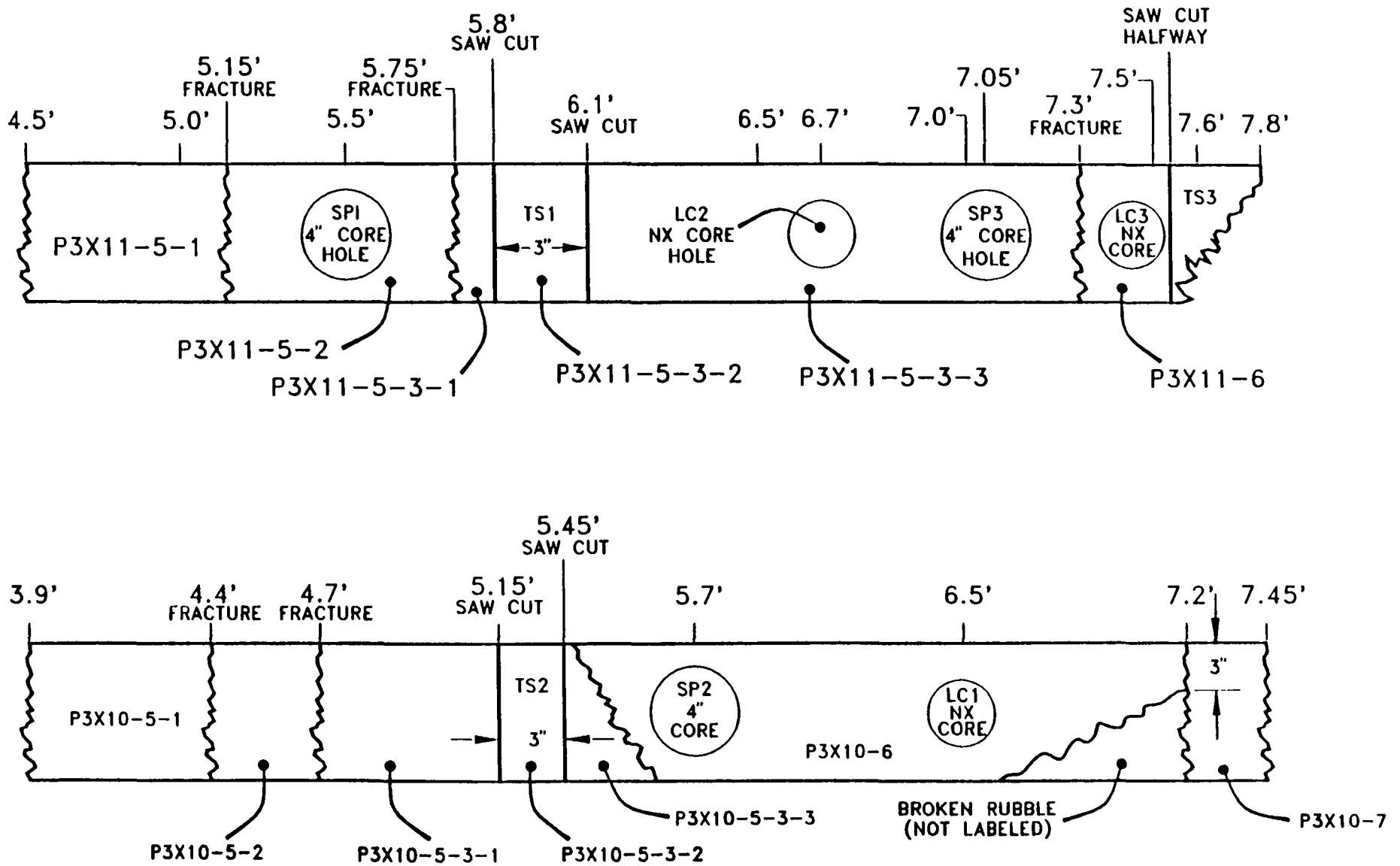


Figure 2-1. Map of WIPP MB 139 anhydrite cores.

Permeability Specimen SP1 had a planar zone of cracks oriented diagonal to the specimen axis. The specimen maintained cohesion across the zone, indicating that the cracks were discontinuous. The zone intersected the specimen surface at about specimen midheight and extended across diagonally, intersecting the other side of the specimen approximately 1 cm from the lower edge.

2.2 Coring and Finishing

Coring was performed according to standard RE/SPEC laboratory procedures. The core was cut dry at a core barrel rotation speed of 1,300 rpm and specimen ends were finished using a lathe. Permeability specimens were cored parallel to the bedding plane of MB 139. Pieces of material were taken from directly above and below each specimen axis and each piece was used for manufacture of a porosity specimen and an X-ray diffraction specimen. The porosity and X-ray diffraction specimens were therefore from the same stratigraphic layers as the permeability specimen. The specimen identification numbers and dimensions of all permeability and porosity test specimens are given in Table 2-2. The same specimens were used for both gas and liquid permeability tests. Specimens P3X11-5-2-SP1, P3X10-6-SP2, and P3X11-5-3-SP3 will be abbreviated in the text as Specimens SP1, SP2, and SP3, respectively. The letters "T" and "B" are appended to permeability specimen identification numbers to denote porosity specimens taken from above and below the permeability specimen axes, respectively.

Table 2-2. Specimen Dimensions

Specimen	Length (m)	Diameter (m)
Permeability Specimens		
P3X11-5-2-SP1	0.10187	0.10145
P3X10-6-SP2	0.10146	0.10147
P3X11-5-3-SP3	0.10141	0.10103
Porosity Specimens		
P3X11-5-2-SP1-T	0.01065	0.03885
P3X11-5-2-SP1-B	0.01178	0.03886
P3X10-6-SP2-T	0.01231	0.03885
P3X10-6-SP2-B	0.01113	0.03885
P3X11-5-3-SP3-T	0.01263	0.03885
P3X11-5-3-SP3-B	0.01508	0.03885

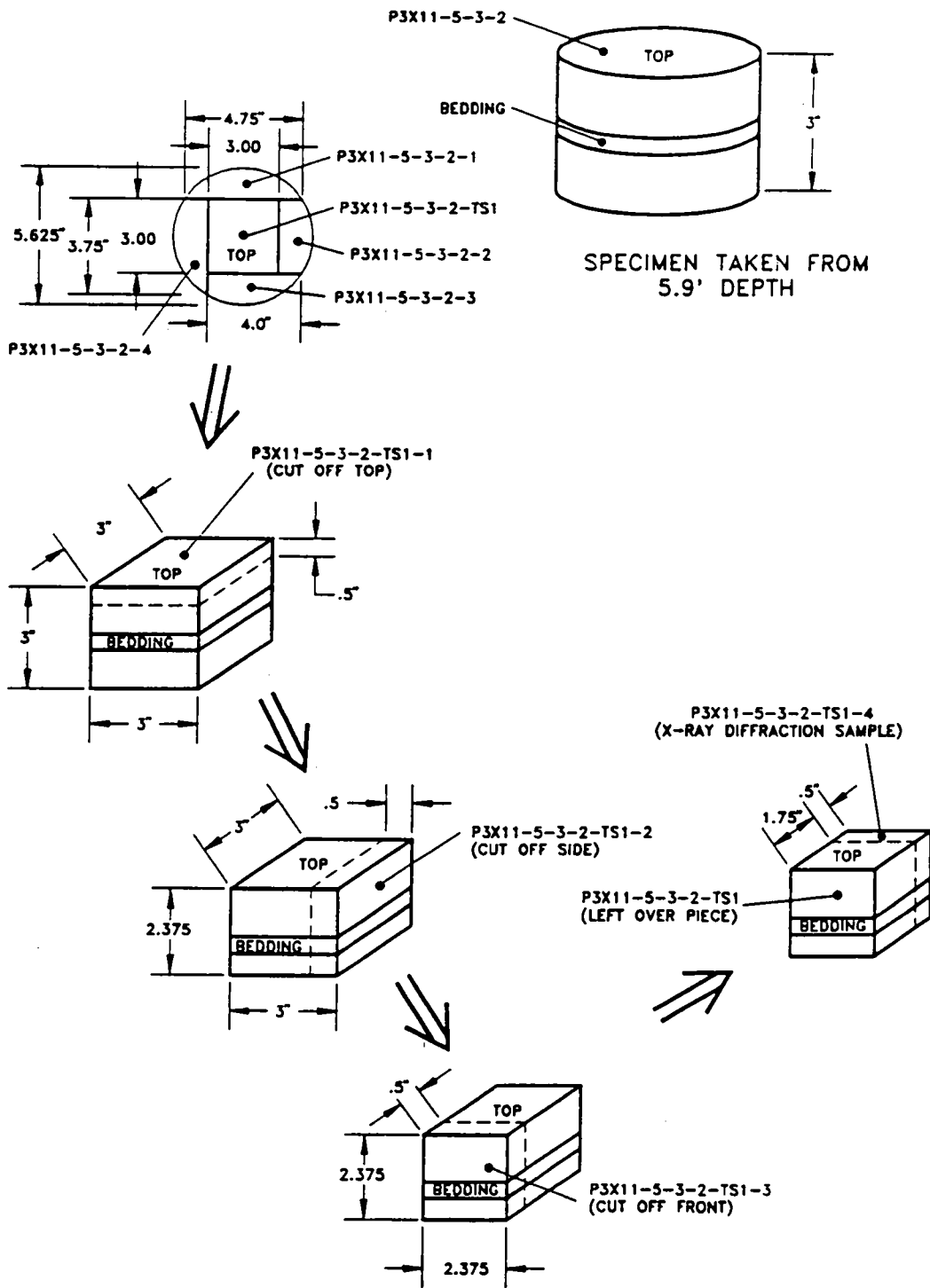
Blocks of material were taken from the locations marked TS1, TS2, and TS3 (see Figure 2-1). Three mutually perpendicular thin sections and an X-ray diffraction specimen were made from each block. The sectioning histories of blocks TS1, TS2, and TS3 are given in Figures 2-2, 2-3, and 2-4, respectively. Thin section specimens P3X11-5-3-2-TS1-1, P3X10-5-3-2-TS2-1, and P3X11-6-TS3-1 (these will be abbreviated in the text as TS1-1, TS2-1, and TS3-1, respectively), were oriented parallel to the bedding plane while the remaining thin sections were perpendicular to the bedding plane and to each other. Specimens TS1-4, TS2-4, and TS3-4 were used for X-ray analyses. These specimens were oriented perpendicular to the bedding plane so that representative samples would be obtained. Additional X-ray diffraction specimens were taken from material above and below the axes of Specimens SP1, SP2, and SP3.

2.3 Drying

All permeability and porosity specimens were dried at 60°C and 45 percent relative humidity to prevent dehydration of clays¹ (Chowdiah, 1988). The changes in mass are given as a function of time in Figures 2-5, 2-6, and 2-7 for Specimens SP1, SP2, and SP3, respectively. The Y-axis for each plot is current mass divided by initial mass. Each figure contains data for a permeability test specimen and for the two 38.9-mm diameter porosity specimens taken from above and below each permeability specimen. Upon initial exposure to humidity, several pieces exhibited an increase in mass. During the first day in the humidity chamber, beads of moisture were observed for a short time on some specimens and so the increase in mass was attributed to moisture absorption. A loss of mass was expected for the first day because a powder, assumed to be salt or rock dust, collected on the bottom of the humidity chamber. This rock dust probably collected on specimens during preparation and then came off in the humidity chamber. The precipitate was cleaned from the chamber and no further accumulations were observed. Specimens were dried until the masses of permeability specimens were constant to within 0.01 g over a one-week period. Each permeability specimen weighed approximately 2,200 g and so a 0.01 g change corresponded to a change in mass of 0.0005 percent.

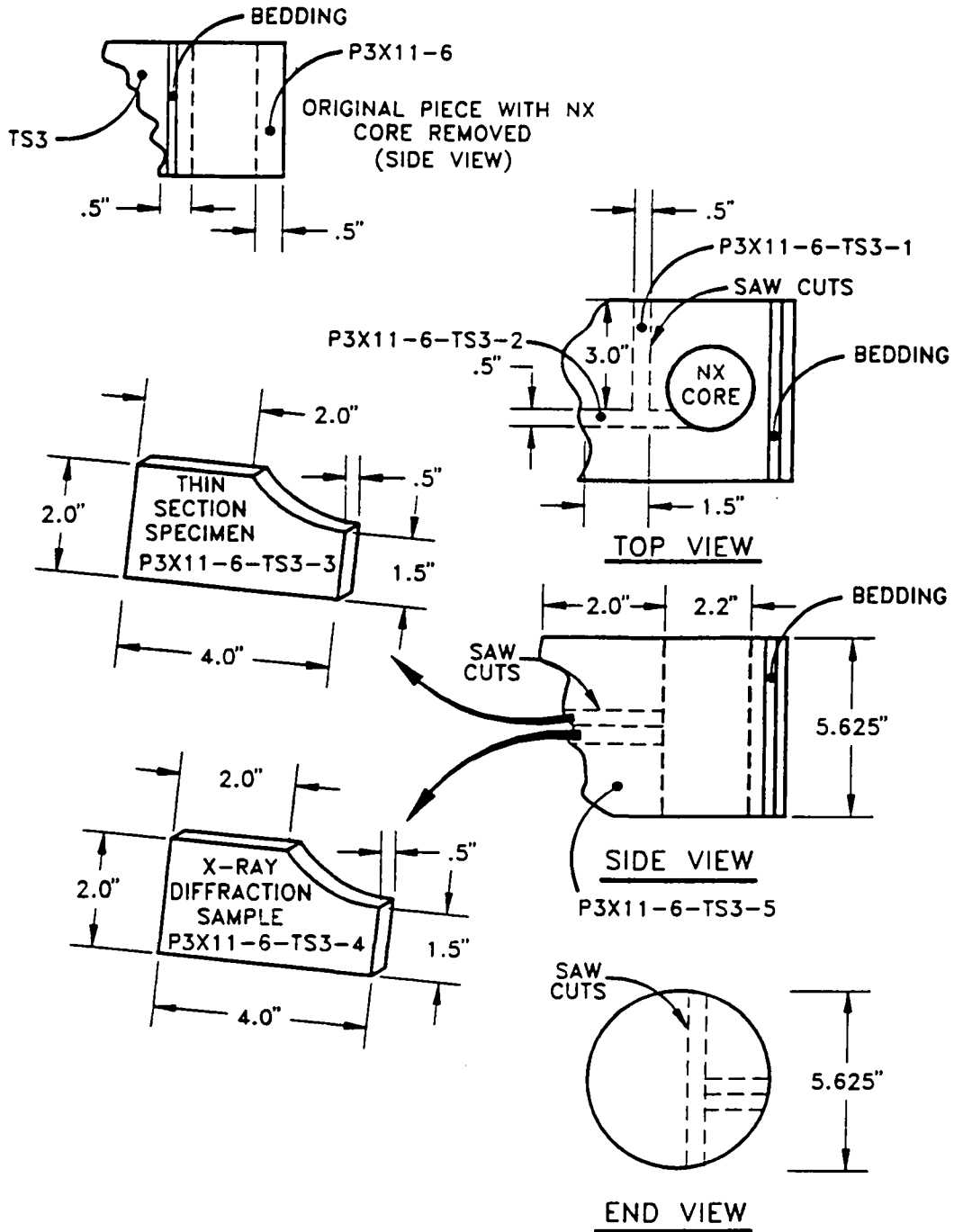
During the setup of Specimen SP3 for permeability testing, the specimen jacket that protected the specimen from the confining fluid was breached, resulting in wetting of the upper specimen surface with silicone oil and a specimen mass gain of 0.3 g. After the specimen was wiped clean with a freon-dampened cloth, its mass returned to its previous value. This specimen was placed back in the humidity chamber to ensure that its mass was stable over a one-week period.

¹ ASTM Standard D4525, "Standard Test Method for Permeability of Rocks by Flowing Air" recommends conditions of 45 percent relative humidity and 63°C for drying specimens that may contain swelling clays.



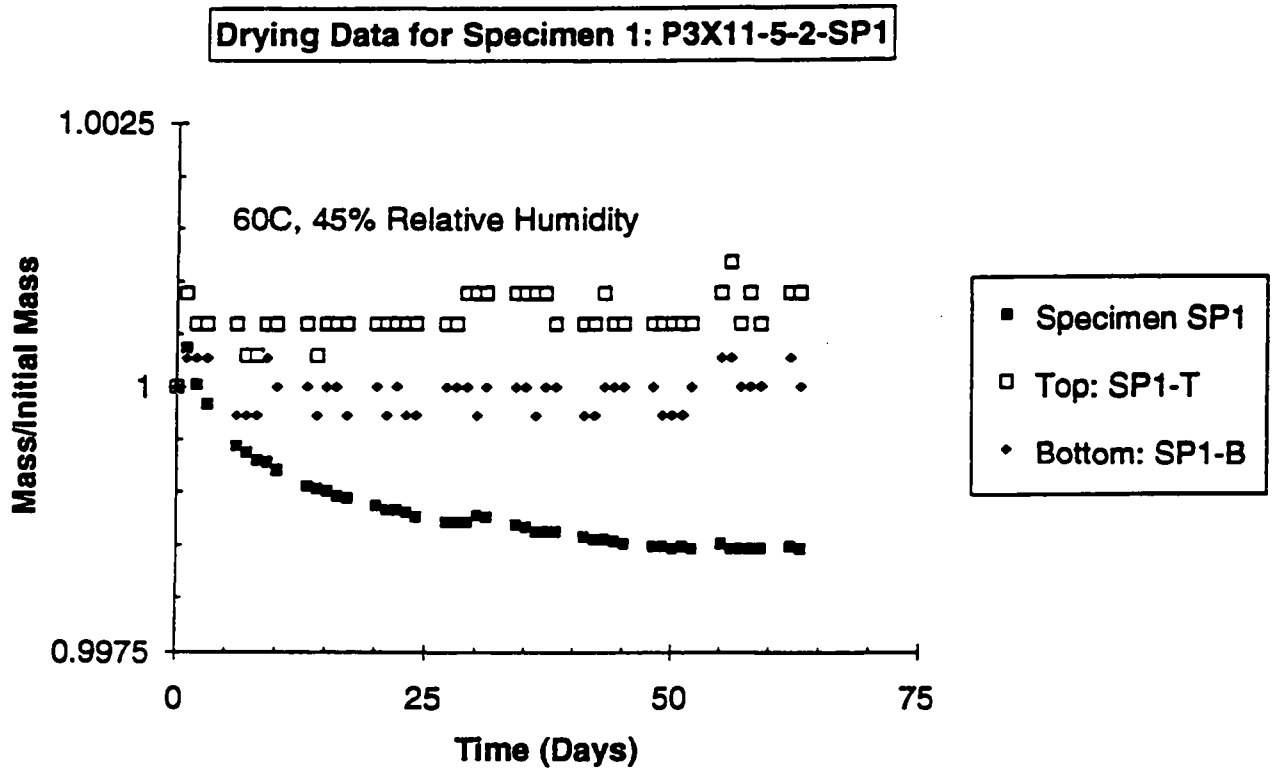
RBI-348-03-011

Figure 2-2. Expanded view of MB 139 anhydrite core showing locations of X-ray diffraction specimen and thin sections for TS1.



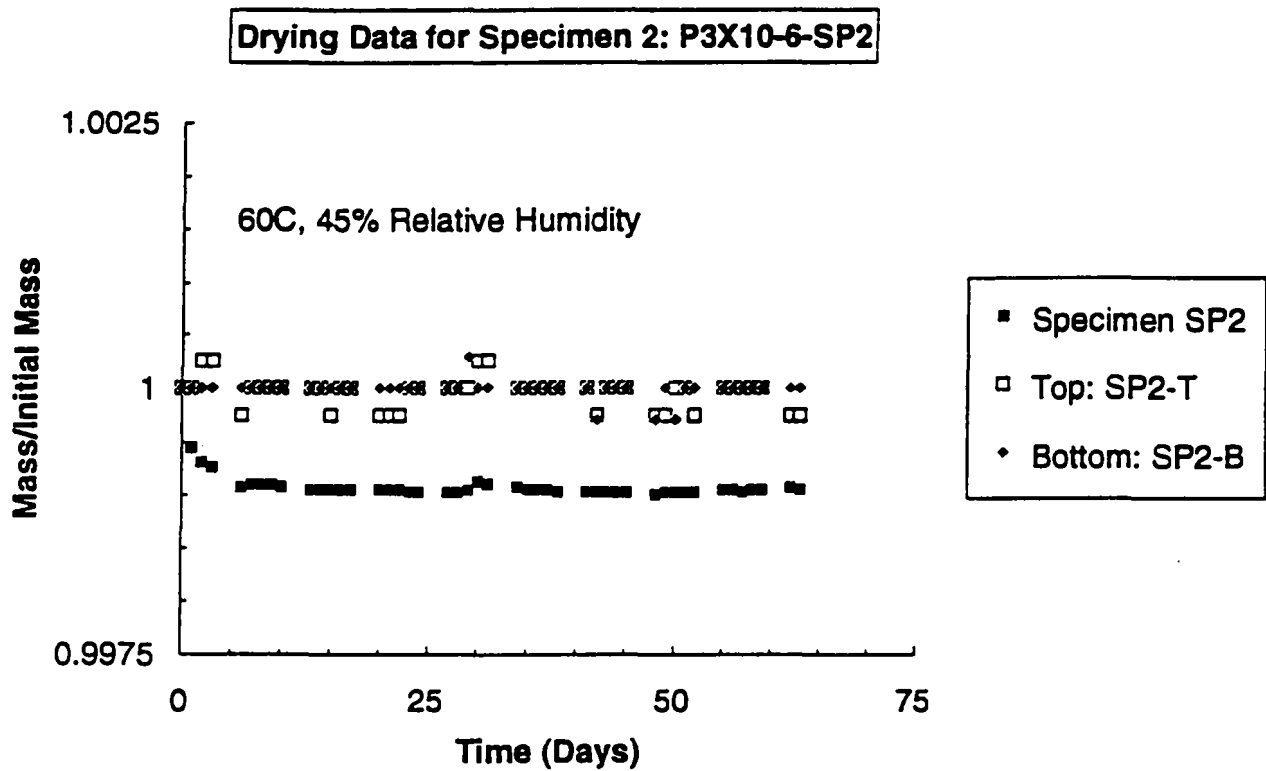
RSI-248-03-009

Figure 2-4. Expanded view of MB 139 anhydrite core showing locations of X-ray diffraction specimen and thin sections for TS3.



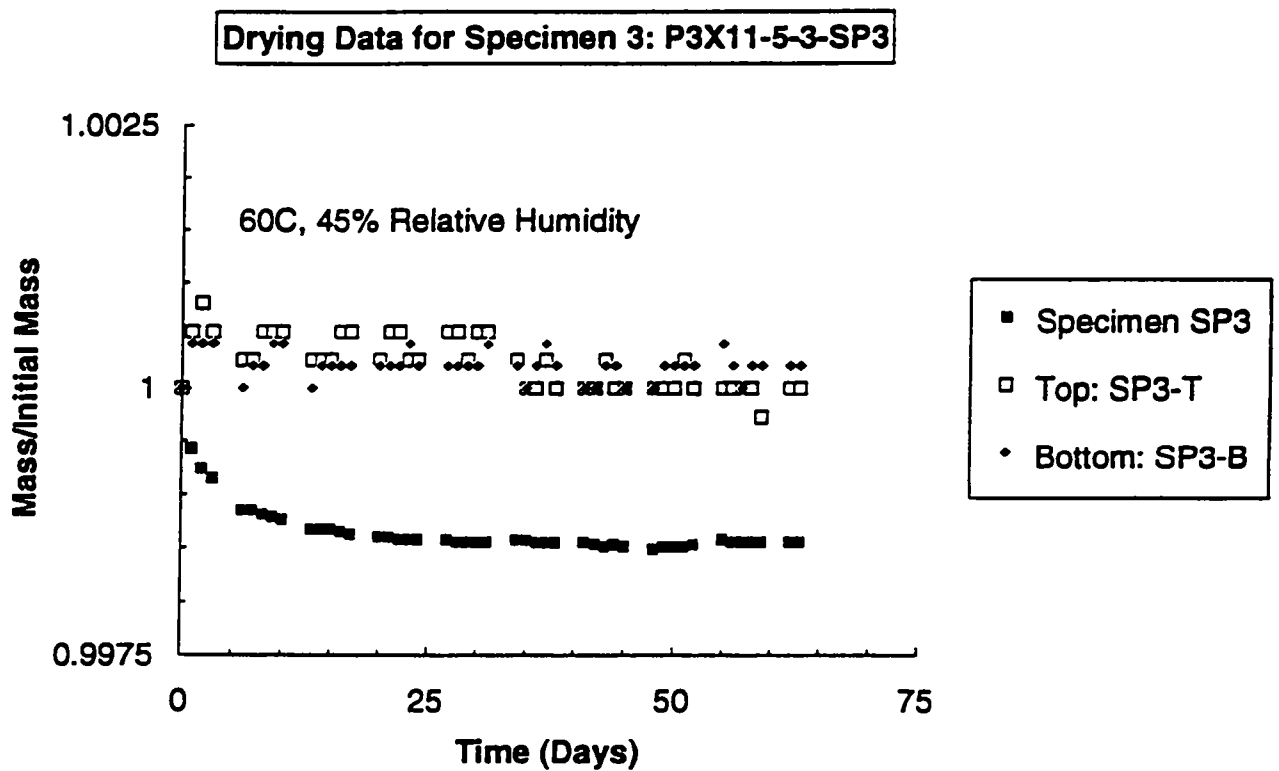
RSI-248-83-022

Figure 2-5. Change in mass during drying at 60°C and 45 percent relative humidity for Specimen P3X11-5-2-SP1. Initial masses are 2.20445 kg, 0.03391 kg, and 0.03745 kg for the permeability specimen and the porosity specimens taken from above (SP1-T) and below (SP1-B) the permeability specimen, respectively.



RSI-248-03-023

Figure 2-6. Change in mass during drying at 60°C and 45 percent relative humidity for Specimen P3X10-6-SP2. Initial masses are 2.15655 kg, 0.03885 kg, and 0.03367 kg for the permeability specimen and the porosity specimens taken from above (SP2-T) and below (SP2-B) the permeability specimen, respectively.



RSI-248-03-024

Figure 2-7. Change in mass during drying at 60°C and 45 percent relative humidity for Specimen P3X11-5-3-SP3. Initial masses are 2.17060 kg, 0.03751 kg, and 0.04767 kg for the permeability specimen and the porosity specimens taken from above (SP3-T) and below (SP3-B) the permeability specimen, respectively.

3.0 EXPERIMENTAL METHODS

3.1 Specimen Characterization

Petrographic analysis and X-ray diffraction were used to determine MB 139 composition. Thin sections and X-ray diffraction samples were manufactured from the TS blocks taken from different sections of the marker bed. Three orthogonal thin sections were made from material at each location. Rectangular blocks approximately 3 inches in length, 2 to 3 inches in width, and 0.5 inches in thickness were roughed out at RE/SPEC Inc. for thin section manufacture and then sent to San Diego Petrographics for final thin section preparation. The X-ray diffraction samples were ground at RE/SPEC Inc. Six additional X-ray diffraction samples were obtained from material taken from above and below the axes of the three permeability specimens. Both types of analyses were performed by the Engineering and Mining Experiment Station at South Dakota School of Mines and Technology in Rapid City, South Dakota. The procedures that were used for petrographic analysis and X-ray diffraction work are given in Appendices B-A and B-B, respectively.

3.2 Coring-Induced Surface Damage

Two specimens were cored for this task. The first specimen, P3X11-6/1 (labeled LC3 NX core in Figure 2-1), was prepared according to standard procedures. The core was cut dry at a core barrel rotation speed of 1,300 rpm. The coring process generally requires less than 10 minutes to produce a 0.1-m-long specimen. The second specimen, P3X11-5-3/1 (labeled LC2 NX core in Figure 2-1), was cored using a slower core barrel advance rate so that the coring process required 23 minutes. The core barrel rotation speed was slowed to 1000 rpm to eliminate the chatter that occurs at this slower advance rate. This procedure was used so that damage induced along the specimen ends using the slower rate could be compared with the standard technique used for the previous core.

The cores were impregnated under vacuum with epoxy containing fluorescent red rhodamine-B dye-penetrant. The vacuum chamber contained two ports; one port was connected to the vacuum pump and the other was valved shut but was connected to a chamber containing a low viscosity epoxy (EPO-TEK 301 with a viscosity of 100 centipoise). The specimen was placed in the chamber and held under a vacuum of 680 mm Hg for 15 minutes. The valve to the epoxy chamber was then opened, allowing the epoxy to be drawn into the specimen. After the epoxy

hardened, the vacuum was removed and the epoxy was permitted to cure overnight. Each core was then sawed in half lengthwise (parallel to the core axis and parallel to bedding) and both halves were polished.

A quantitative analysis of specimens cored at different rates was performed. Each specimen was placed under a petrographic microscope and examined at a magnification of 200X. The microscope's light source was filtered so that the rhodamine-B dye fluoresced under examination. Each specimen was placed on an X-Y microscope stage so that it could be translated by moving the stage relative to a fixed vernier scale. Three lines parallel to the specimen axis were defined for each specimen; these were located along the central specimen axis and 0.5 mm from each edge. The crosshair of the microscope was translated along each line and the locations of all cracks intersected by the crosshair were recorded.

3.3 Porosity Measurements

3.3.1 Effective Porosity

Porosity measurements were conducted on six specimens manufactured from pieces immediately adjacent to the permeability test specimens. Core Laboratories performed effective porosity tests using a helium porosimeter according to the procedure given in Appendix B-C. These specimens were dried at controlled temperature and humidity conditions in the RE/SPEC Inc. laboratory as described in Chapter 2.0. To ensure that no moisture changes occurred during shipping or due to the higher humidity at the Core Laboratories Houston offices, specimen masses were measured at RE/SPEC Inc. before shipping and at Core Laboratories just after receipt and just before testing. Three metal weights were also weighed and shipped to ensure that there were no discrepancies between the outputs of the scales in the two laboratories. The largest difference in the mass measurements for the metal specimens was 0.0018 percent for the 50 g metal weight, indicating that the Core Laboratories and the RE/SPEC scales gave identical values within the accuracy of the measurements. The largest difference in the mass measurements for the anhydrite specimens was 0.0108 g and all but two were less than 0.01 g which is the resolution of the RE/SPEC Inc. scale. This indicates that there was little or no moisture change during shipping and handling.

3.3.2 Total Porosity

Total porosities were measured for the three porosity specimens made from material taken from above each permeability specimen. The procedure that was used followed ASTM D854-83, *Standard Test Method for Specific Gravity of Soils*. Specimens were placed in the humidity chamber at 60°C and 45 percent relative humidity and dried to ensure that masses were constant. The specimens were then ground until all particles passed through a 0.425-mm sieve. Ground specimens were placed in clean, dry, 100-ml flasks of known mass and again dried at 60°C and 45 percent relative humidity to ensure that masses were stable. The masses of the flasks and their contents were then measured. The flasks containing the specimens were then filled with kerosene to the calibration marks and a vacuum was applied to each flask for approximately 5 days until all air was removed. The kerosene levels in the flasks were then adjusted to reach the calibration marks and masses were measured. Each clean flask was also filled to the calibration mark with pure deaerated kerosene and the combined masses were measured. The grain densities and total void volumes were determined using Equation 3-1 which is derived in Appendix B-D.

$$\text{Porosity} = 1 - \left[\frac{\left(\frac{Ms_s}{0.25 \cdot L \cdot \pi \cdot D^2} \right)}{\left(\frac{(Mfk_1 - Mf) \cdot (Mfs_g - Mf)}{(Vf \cdot (Mfs_g - Mf + Mfk_1 - Mfs_g k_2))} \right)} \right] \quad (3-1)$$

where

- Ms_s = Mass of solid specimen before grinding
- L = Specimen length before grinding
- D = Specimen diameter before grinding
- Vf = Volume of flask to calibration mark
- Mf = Mass of flask
- Mfs_g = Mass of flask containing ground specimen
- Mfk_1 = Mass of flask filled with deaerated kerosene to calibration mark
- $Mfs_g k_2$ = Mass of flask containing ground specimen and filled with deaerated kerosene to calibration mark

3.4 Brine Production and Saturation

A standard brine was used for specimen saturation and as the permeant for liquid permeability measurements. Standard brine SB-139-95B was prepared by Twin City Testing of Rapid City, South Dakota, according to directions supplied by Sandia National Laboratories. The specified composition was designed to be 95 percent saturated with respect to the minerals in MB 139. The brine preparation instructions provided by Sandia and the laboratory notes kept by Twin City Testing during brine preparation are given in Appendix B-E. The brine was prepared in two separate batches and the laboratory notes for both are provided.

Permeability specimens were subjected to a saturation procedure after gas permeability measurements had been completed. The masses of three MB 139 specimens were measured and then specimens were submersed in a jar containing 2 gallons of clean brine. It was anticipated that specimen mass would increase while the system was under vacuum until saturation occurred. The specimens were removed from the brine after 4 days and evidence of specimen dissolution was noted. Many grains were loose and sediment had accumulated in the bottom of the jar. Some of the previously machined sharp edges of the specimens were also somewhat rounded. The specimen masses before and after saturation are given in Table 3-1. Although Specimen SP1 shows very little net change, this specimen had undoubtedly absorbed some brine which compensated for the loss of some solid mass. Samples of clean brine and brine used for saturation were sent to Sandia for analysis. The saturation procedure was terminated because of the specimen degradation and it is not known if the specimens achieved saturation.

Table 3-1. Change in Specimen Mass During Saturation Procedure

	Date	Time	Specimen Mass (g)		
			P3X11-5-2-SP1	P3X10-6-SP2	P3X11-5-3-SP3
Before Saturation	8-6-93	16:50	2200.70	2154.15	2163.85
After Saturation	8-10-93	15:20	2199.15	2101.85	2125.35
Net Change			-1.55	-52.3	-38.5

3.5 Permeability Measurements

3.5.1 Test Apparatus

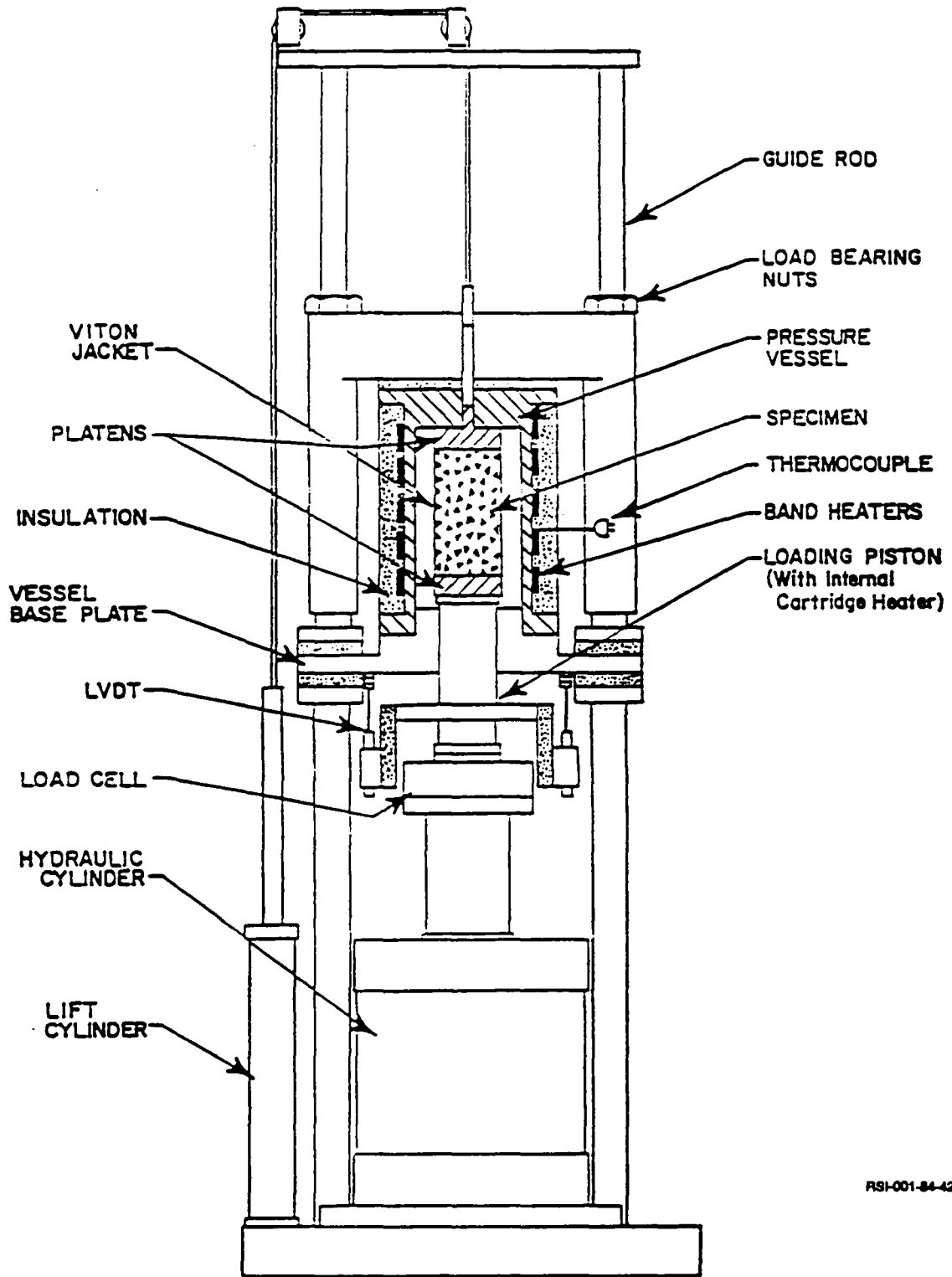
3.5.1.1 LOAD FRAME

Figure 3-1 presents a cross section of a typical load frame used for permeability tests with prominent components labeled for reference. Three test frames were used in this study so that a separate frame could be devoted to each specimen. The frames use single-ended, triaxial pressure vessels. A linear actuator (hydraulic cylinder) bolted to the base of the load frame drives the loading piston, which in turn applies axial compressive force to the specimen. Confining pressure was applied to the jacketed specimens by pressurizing the sealed vessel chamber with silicone oil. A dilatometer system maintained constant confining pressure. The testing machines can apply compressive axial loads up to 1.5 MN and confining pressures up to 70 MPa. The heating system can maintain specimen temperatures up to 200°C.

A control panel houses the accumulators, hydraulic pumps, pressure intensifiers, transducer signal conditioners, temperature controllers, and confining pressure controllers for two adjacent test frames. The panels contain digital meters that display the output of the transducers. The temperature controller gives a digital output of the temperature. Mechanical pressure gages mounted in the panel give readings of oil pressure in the hydraulic cylinder.

3.5.1.2 INSTRUMENTATION

Axial force is measured by a load cell in the load train outside the pressure vessel, while confining pressure is measured by a pressure transducer in the line between the dilatometer and the pressure vessel. Temperature is measured by a thermocouple in the wall of the pressure vessel. The relationship between specimen temperature and that recorded by this thermocouple has been determined by calibration runs at several temperatures spanning the operating range. Two Linear Variable Differential Transformers (LVDTs) mounted outside the pressure vessel monitor displacement of the loading piston relative to the bottom of the pressure vessel and can be used to calculate axial strain of the specimen. Volumetric deformation is measured using a dilatometer. With this technique, volumetric deformation is determined at fixed pressure by first measuring the volume of oil that the dilatometer supplies to the pressure vessel, and then



RSI-001-84-428

Figure 3-1. Load frame used for permeability tests.

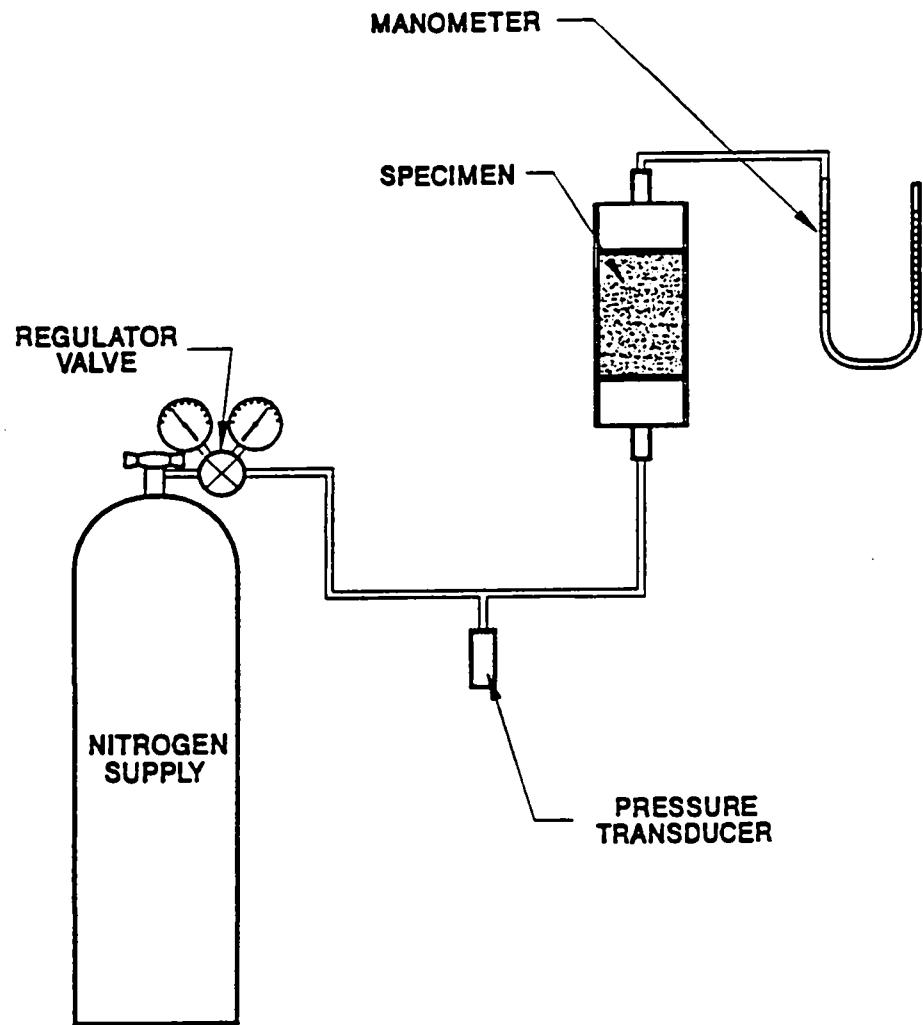
compensating for the axial deformation measured by the LVDTs. A rotary potentiometer or stroke transducer is mounted on the dilatometer shaft to provide a signal proportional to the volume of oil supplied to the pressure vessel.

3.5.1.3 CONTROL

Temperature was maintained at 25°C with a manual set-point controller that regulated power to the band heaters on the vessel. The thermocouple in the pressure vessel wall supplied the feedback signal. Confining pressure was controlled by inputting the pressure transducer signal to a unit that contained two manual set points. These set points were adjusted to maintain the confining pressure constant within 20 kPa. The controller signals the intensifier to advance or retreat, depending upon whether the lower or upper set point has been reached. Axial load was controlled by a Digital Equipment Corporation PDP-11/23 microcomputer. The computer determined the current cross-sectional area of the specimen from the outputs of the deformation transducers and then adjusted the load to maintain constant stress. The deadband on load under computer control was 0.4 kN.

3.5.1.4 GAS PERMEABILITY SYSTEM

The gas permeability measurement system is shown in Figure 3-2. Nitrogen gas pressure was supplied to the lower surface of the specimen by a pressurized gas bottle. The charge pressure was controlled manually with a valve located on the gas bottle and measured by a pressure transducer. A manometer comprising two calibrated burets filled with mineral oil and connected at the base by tubing was used to measure the volume of gas exiting the specimen. As nitrogen filled the left side of the manometer, oil was forced out of the right side and into an overflow reservoir. The position of the gas/oil meniscus on the left side of the manometer was read using the calibrated markings on the buret. Using this system, the gas exit pressure increased over time as the hydraulic head increased, but the pressure increase was very small (less than 0.0045 MPa).



SCALE: NONE

RSI-107-82-019

Figure 3-2. Gas permeability measurement system.

3.5.1.5 BRINE PERMEABILITY SYSTEM

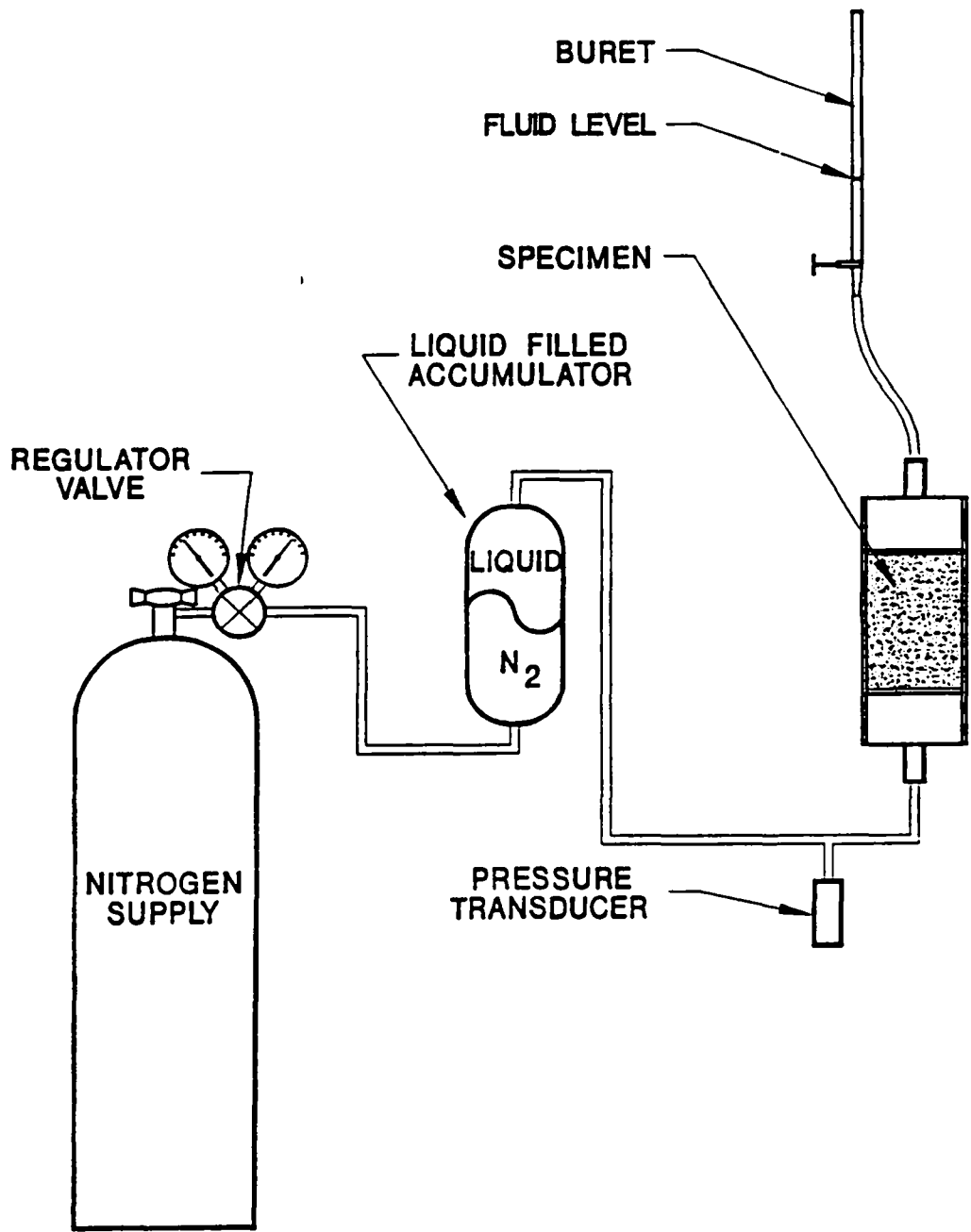
The brine permeability measurement system is shown in Figure 3-3. A nitrogen-driven accumulator supplied pressurized brine to the lower surface of the specimen. The charge pressure (and therefore the pressure drop across the specimen) was regulated manually with a valve located on the nitrogen bottle and was measured by a diaphragm-type pressure transducer in the hydraulic line between the accumulator and the specimen. The pressure drop in the lines between the pressure transducer and the specimen is negligible. Permeant flow through the specimen was captured and measured by a buret attached to the upper end cap of the specimen assembly. Evaporation of the permeant was prevented by placing a thin film of mineral oil on top of the permeant column in the buret (Brodsky, 1993).

3.5.1.6 SPECIMEN ASSEMBLY

The specimen assembly for all permeability tests is shown in Figure 3-4. Permeant entered the system through the lower platen, permeated the specimen, and exited through the upper vent. The spacer extended the length of the specimen assembly so that it could be easily accommodated by the testing machine. Porous felt metal disks were placed along the specimen/platen interfaces to ensure uniform permeant pressure along the specimen's upper and lower surfaces. Two Viton jackets or sleeves were used to protect specimens from the silicone oil used as a confining fluid.

3.5.1.7 CALIBRATION

The transducers used to collect force, pressure, deformation, and temperature data were calibrated using standards traceable to the National Institute of Standards and Technology and documented procedures. Each transducer was calibrated in its normal operating position on the test system so that the signal conditioners, filters, and analog-to-digital converters were included within the end-to-end calibration. Calibration constants were determined for each transducer from a linear, least-squares regression of indicated reading versus standard input. Readings were collected at 20 standard inputs equally spaced over the range of the transducer. These constants were verified immediately before testing began by comparing the predicted response of the transducer using these constants with the standard input applied in ten equally spaced steps over the calibrated range. This verification procedure was performed periodically so that drift or transducer malfunctions would be identified. Table 3-2 gives the range and resolution for these



RSI-187-92-020

Figure 3-3. Liquid permeability apparatus.

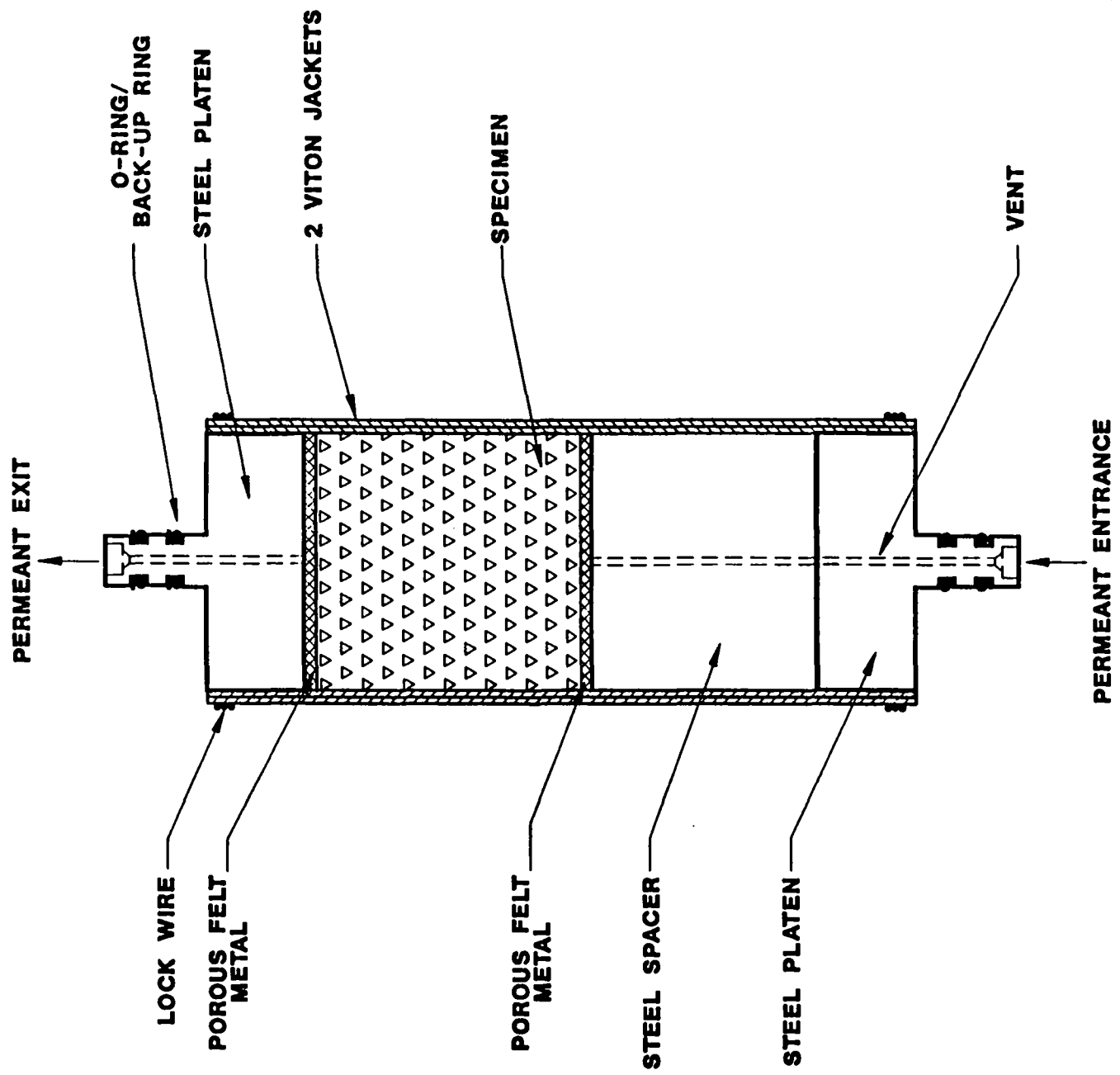


FIG-197-62-109

Figure 3-4. Specimen assembly for permeability tests.

transducers. Prior to testing, verifications showed that the accuracy errors for force and pressure transducers were less than 1 percent of reading and that of thermocouples was $\pm 1^\circ\text{C}$. The accuracy specifications include both nonlinearity and repeatability. The burets used were Class A and are accurate to within 0.1 ml. All transducers were reverified after the completion of testing, and pore pressure and confining pressure transducers were also reverified midway through the testing program (after completion of gas permeability tests). Confining pressure transducers and thermocouples always reverified to within the specifications given above and shown in Table 3-2. Pore pressure transducer errors were within 1.7 percent of target values.

Table 3-2. Calibration Specifications

Measurement	Range	Resolution
Axial Force (kN) ^(a)	0 to 250	0.03 ^(b)
Confining Pressure (MPa) ^(a)	0 to 34.5	0.004 ^(b)
Temperature ($^\circ\text{C}$) ^(c)	0 to 250	0.03 ^(b)
Pore Pressure (MPa) ^(a)	0 to 6.895	0.0008 ^(b)
Permeant Volume at 20 $^\circ\text{C}$ and 0.1 MPa (ml) ^(d)	0 to 50	0.05

(a) Accuracy: 1 percent of reading including nonlinearity and repeatability.
 (b) 14-bit analog-to-digital converter. One bit used for sign.
 (c) Accuracy: $\pm 1^\circ\text{C}$.
 (d) Accuracy: Exit buret calibrated to 0.1 ml.

3.5.2 Test Procedure for Permeability Tests

Assembled specimens were placed in load frames and the pressure vessels were lowered over the specimens. The pressure vessels were then filled with silicone oil, heated to 25 $^\circ\text{C}$, and pressurized to 2 MPa confining pressure. A temperature of 25 $^\circ\text{C}$ was used rather than 20 $^\circ\text{C}$ because heating the pressure vessel facilitates maintaining constant temperature. The temperature and pressure were allowed to stabilize for at least 12 hours. Moisture evaporation from the specimens was prevented during stabilization by closing the lower pore pressure vents and connecting oil traps to the upper vents. (An oil trap comprised flexible tubing that was attached to the upper pore pressure vent at one end and to a buret at the other end. Between the vent and the buret, the tubing was looped so that oil placed in the bottom of the loop was trapped and formed a moisture barrier.) After stabilization, data acquisition was initiated, control of the confining pressure was given to the automatic controller which signaled the dilatometer system to either inject or withdraw oil to maintain the pressure.

Nitrogen pressure was applied to the lower specimen surface for gas permeability measurements or to the brine-filled accumulator for liquid permeability measurements. Permeability was determined by measuring the steady-state flow rate of permeant through the specimen and the pressure drop across the specimen. The pressure drop was controlled throughout the permeability test by manual adjustment. The flow rate was determined manually by monitoring the gas/oil meniscus in the manometer for gas measurements and the in the buret for liquid permeability measurements.

A permeant inlet pressure of 1.0 MPa was used for the first series of permeability tests on each specimen except for the first of three gas permeability measurements for Specimen SP2 which was conducted at an inlet pressure of 1.1 MPa. Outlet pressure was atmospheric (0.1 MPa) and so the pressure drop across the specimen was 0.9 MPa (1.0 MPa for the first measurement on Specimen SP2). Gas permeability measurements proceeded reasonably quickly and so three replicate tests were performed at each test condition. After tests were completed at 1.0 MPa, the inlet pressure was decreased to 0.7 MPa and then to 0.4 MPa for measurements at pore pressure differences of 0.6 and 0.3 MPa, respectively. Confining pressure was then increased to 6 MPa and then to 10 MPa and the sequence of tests at each inlet pressure was repeated for each confining pressure. After each change in confining pressure, the system was allowed to stabilize overnight. After completion of each brine permeability test, the brine that had collected in the exit buret was collected, placed in a sample jar, and sent to Sandia National Laboratory for analysis.

3.5.3 Data Acquisition and Reduction

3.5.3.1 DATA ACQUISITION

A DEC LSI-11/23 microprocessor was used to acquire measurements of time, axial load, confining pressure, volumetric deformation, axial (piston) displacement, and temperature. The computer scanned the data channels at 15-second intervals, logged data at least every 2 hours, and wrote the data to disk on the microprocessor. The logged data were later transmitted to a separate computer for data reduction and analysis. Permeability data included time, pressure drop across the specimen, and the permeant level in the buret. These data were recorded manually and the data acquisition rate depended on the flow rate. For gas permeability tests, data were recorded generally after each 2 ml increment of gas accumulation in a 50 ml buret and so at least 20 data points were used in each permeability determination. For several tests in which gas flow

proceeded slowly, data were collected at approximately even increments of time. Flow rates were slower in the liquid permeability tests and data were recorded at approximately even increments of time.

3.5.3.2 DATA REDUCTION

Permeability to brine was determined from Darcy's law, i.e.,

$$k = \frac{\mu Q L}{A (P_i - P_E)} \quad (3-2)$$

where

- k = Permeability (m^2)
- Q = Flow rate ($m^3 \cdot s^{-1}$)
- P_E = Pressure at exit (MPa)
- μ = Brine viscosity at test temperature (MPa \cdot s)
- L = Specimen Length (m)
- P_i = Pressure at inflow (MPa)
- A = Specimen cross sectional area (m^2)

A value of 1.26 centipoise (1.26×10^{-9} MPa \cdot s) was used for brine viscosity. Flow rates were calculated from the buret level-versus-time data by fitting with a linear least squares regression. The initial readings obtained were not used in the fit if flow rate had not yet stabilized.

Permeability to gas was determined using a modified form of Darcy's law which accounts for changes in gas density with pressure, i.e.,

$$k = \frac{2 \mu L Q_E P_E}{(P_i^2 - P_E^2) A} \quad (3-3)$$

where

- k = Permeability (m^2)
- Q_E = Flow rate at exit ($m^3 \cdot s^{-1}$)
- P_E = Pressure at exit (MPa)
- μ = Viscosity of gas at test temperature (MPa \cdot s)

- L = Specimen Length (m)
 P_i = Pressure at inflow (MPa)
 A = Specimen cross sectional area (m²)

A value of 178 micropoise (1.78×10^{-11} MPa · s) was used for nitrogen viscosity (Weast, 1974). Equation 3-3 was derived from Equation 3-2 using the method given by Holcomb and Shields (1987). The flow rate given in Equation 3-2 is an average rate. Substitution of the ideal gas law,

$$P_{\text{avg}} Q_{\text{avg}} = P_{\text{exit}} Q_{\text{exit}} \quad (3-4)$$

and

$$P_{\text{avg}} = \frac{(P_{\text{inlet}} + P_{\text{exit}})}{2} \quad (3-5)$$

into Equation 3-2 gives Equation 3-3.

For both liquid and gas permeability tests, three values of inlet pressure were used for each confining pressure so that the relationship between flow rate and pressure difference across the specimen could be checked for linearity. A linear relationship implies that flow is laminar. The Klinkenberg correction was also applied to gas permeability data at each confining pressure by plotting permeability versus reciprocal mean pore pressure and fitting a straight line to the data. The permeability axis intercept at a reciprocal mean pressure of zero gives the equivalent liquid permeability value.

3.5.4 Shakedown Tests for Gas Permeability Measurements

Six shakedown tests were performed to evaluate the gas permeability test procedure and equipment. Two of these tests were performed on a solid aluminum specimen and four tests were performed on MB 139 anhydrite. The purpose of testing aluminum was to ensure that there were no gas leaks in the system and that the Viton jacket conformed to the specimen surface and prevented channeling of gas along the specimen/jacket interface. The first test was performed on a solid aluminum specimen at an inlet pore pressure of 0.5 MPa and a confining pressure of 1 MPa, i.e., at an effective confining pressure of 0.5 MPa. This effective confining pressure was less than that used for testing and so any problems with gas channeling along the specimen/jacket interface should have been evident; however, no gas flow was detected. The second test on aluminum contained a flattened aluminum tube inserted between the specimen and jacket that

provided a small pathway for gas flow. Using this specimen configuration a gas flow rate of approximately $3 \text{ ml} \cdot \text{s}^{-1}$ was measured in the manometer. All joints along the gas flow path were inspected for leaks using "Snoop," a commercial gas flow detection fluid and no leaks were detected.

The shakedown tests on MB 139 were run to evaluate the test procedure and to determine rough approximations of gas permeability values so that the appropriate instrumentation would be used for measurements. (Different flow rate detection equipment is required for different ranges of flow rates.) A single specimen was used for all four shakedown tests. The specimen was cored and finished but was not dried. The shakedown testing revealed no problems with the test procedure. The tests did show that flow rates decreased with time for the longer duration tests which was attributed to an equipment malfunction. This problem was eliminated by purchasing and installing new gas pressure regulators for the test systems.

4.0 TEST RESULTS

4.1 MB 139 Specimen Characterization

A total of nine petrographic analyses and nine X-ray diffraction analyses were performed on the marker bed material. The locations from which the specimens were taken were given in Figure 2-1. Specimens SP2 and TS2 were taken from Core P3X10 while SP1, TS1, SP3, and TS3 were taken from Core P3X11. Specimens SP1, SP2, and SP3 were taken from the upper, upper/central, and lower sections of the marker bed, respectively. Blocks TS1, TS2, and TS3 were taken from the central, upper, and lower sections, respectively.

The results of the petrographic analyses are given in Table 4-1. These data are given in terms of volume percent and were converted to weight percentages using the specific gravities in Table 4-2. The X-ray diffraction data were provided in terms of weight percent and are given in Table 4-3 along with the converted petrographic data. The complete reports for optical microscopy and X-ray diffraction analyses as supplied by the South Dakota School of Mines and Technology are given in Appendices A and B, respectively.

The mineral quantities determined by X-ray diffraction for material taken from above and below each permeability specimen were averaged and are plotted in Figure 4-1. Specimen SP1 is notably low in anhydrite and high in polyhalite. The compositions of SP2 and SP3 are more comparable. The compositions of the thin sections and the X-ray diffraction specimens taken from the thin section blocks are shown in Figures 4-2, 4-3, and 4-4 for TS1, TS2, and TS3, respectively. Specimens with identification numbers ending in "-1" and "-4" were originally perpendicular to the bedding plane while the remaining specimens were parallel to bedding. There does not appear to be any systematic difference between specimens of different orientations. The mineral quantities determined for each thin section block were averaged and the bulk compositions of the three thin section blocks are compared in Figure 4-5. Data from block TS2, from the uppermost section of the marker bed are plotted first, then TS1 and TS3 from the central and lower sections, respectively. It is evident that the specimens are primarily anhydrite. Specimens SP3 and TS3, which came from the lowermost section of the marker bed, have larger anhydrite components than do specimens SP1, SP2, TS1, and TS2. Data from blocks TS1, TS2, and TS3 indicate that the upper section of the marker bed (TS2) is enriched in halite. Specimens from the P3X10 borehole (SP2 and TS2), however, generally have more halite than those from the P3X11 borehole, making it difficult to distinguish between vertical and lateral heterogeneities. The average compositions of SP1 and TS1 are different, even though the

Table 4-1. Summary of Quantitative Polarized Light Microscopy Analyses of MB 139 Thin Sections^(a)

Specimen I.D.	Anhydrite (%)	Halite (%)	Polyhalite (%)	Magnesite (%)	Carbon (%)	Total (%)
P3X11-5-3-2-TS1-1	70.4	15.9	9.6	2.0	2.2	100.1
P3X11-5-3-2-TS1-2	45.8	13.4	30.6	9.4	0.8	100.0
P3X11-5-3-2-TS1-3	48.9	26.7	14.9	8.0	1.6	100.1
P3X10-5-3-2-TS2-1	67.8	24.5	0.0	3.5	4.2	100.0
P3X10-5-3-2-TS2-2	43.1	54.8	0.0	0.6	1.6	100.1
P3X10-5-3-2-TS2-3	58.2	37.2	0.0	3.0	1.6	100.0
P3X11-6-TS3-1	95.9	1.4	0.6	0.6	0.2	98.7
P3X11-6-TS3-2	89.9	8.8	0.0	0.0	1.4	100.1
P3X11-6-TS3-3	66.7	31.9	0.0	0.4	1.0	100.0

(a) All values are volume percentages.

specimens were in close proximity in situ. The same is true of SP3 and TS3. These data reflect a high degree of heterogeneity in the marker bed.

Table 4-2. Mineralogical Data for MB 139

Mineral	Composition	Specific Gravity
Anhydrite	CaSO ₄	2.94 ^(a)
Halite	NaCl	2.16 ^(a)
Polyhalite	K ₂ Ca ₂ Mg(SO ₄) ₄ · 2H ₂ O	2.78 ^(a)
Magnesite	MgCO ₃	3.1 ^(a)
Carbonaceous Material	C	1.95 ^(b)

(a) Hurlbut (1971).
(b) The median specific gravity of amorphous carbon (Weast, 1974).

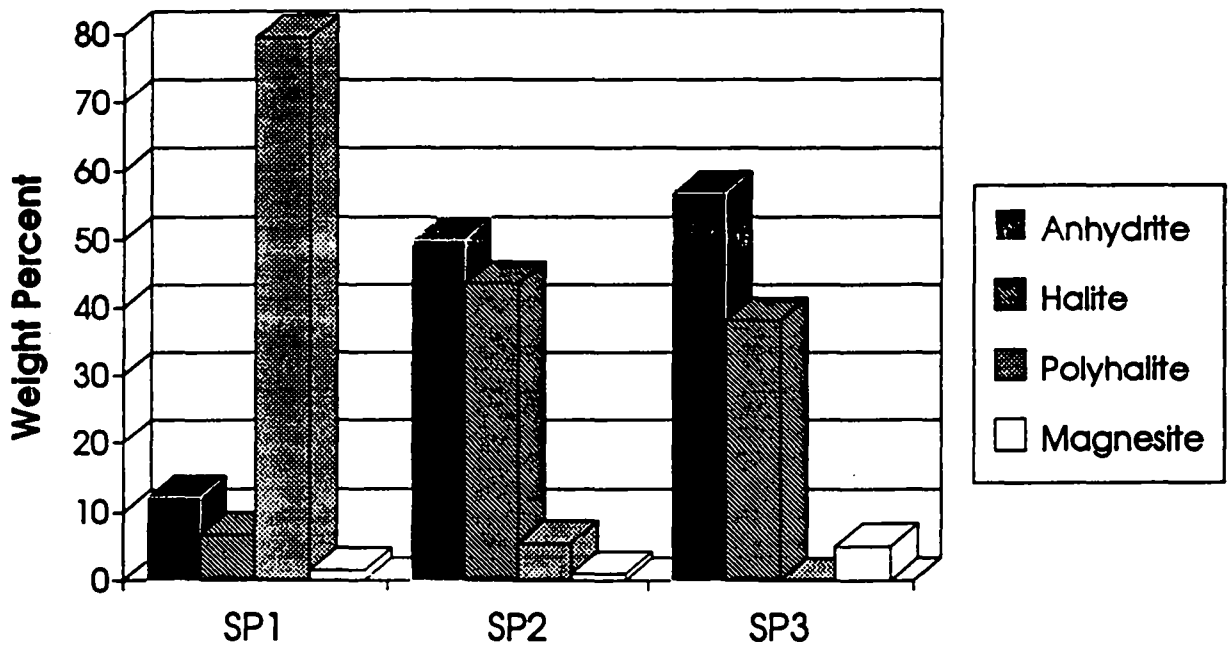
4.2 Coring-Induced Surface Damage

A quantitative analysis of crack occurrence near the surfaces and center axes of specimens cored at different rates was completed using the procedure given in Section 3.2. The data are shown in Figure 4-6 for Specimen P3X11-6/1 which was cored at a standard rate, and in Figure 4-7 for Specimen P3X11-5-3/1 which was cored at the slower rate. The axes of the figures show distance in millimeters from the origin and the outline of each specimen is given. Each crack is represented by an "x," however; some data points lie so close together that they appear to overlay one another. For Specimen P3X11-6/1, an average of approximately 1.4 cracks · cm⁻¹ were detected along the specimen edges while 0.3 cracks · cm⁻¹ were detected along the specimen midsection. For Specimen P3X11-5-3/1, the specimen edges contained an average of 0.1 cracks · cm⁻¹ while no cracks were detected in the midsection.

There were 4 cracks detected along the midsection traverse line for Specimen P3X11-6/1 and no cracks detected along that traverse line for Specimen P3X11-5-3/1. The two traverse lines adjacent to the specimen borders of Specimen P3X11-6/1 contained 8 and 25 cracks, respectively, while for Specimen P3X11-5-3/1 the border traverse lines contained 3 and 0 cracks, respectively. Therefore, there are 2 ± 3 cracks per traverse line for the midsection lines, and 9 ± 11 cracks per traverse line for lines adjacent to specimen borders. These data indicate that higher crack

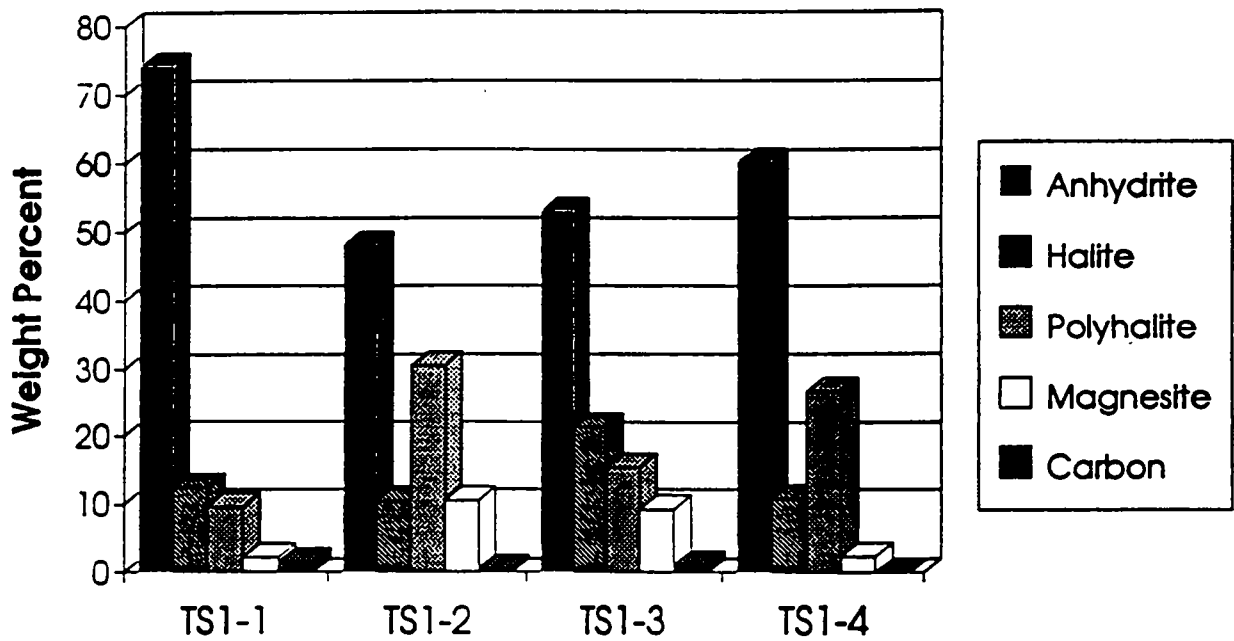
Table 4-3. Mineral Compositions of Marker Bed 139 Specimens^(a)

Specimen I.D	Anhydrite (%)	Halite (%)	Polyhalite (%)	Magnesite (%)	Carbon (%)
P3X11-5-2-SP1T	18.4	10.1	68.8	2.62	(b)
P3X11-5-2-SP1B	6.15	3.36	90.1	0.37	(b)
SP1 Average	12.3	6.7	79.5	1.5	
P3X11-5-3-2-TS1-1	74.3	12.3	9.58	2.23	1.54
P3X11-5-3-2-TS1-2	48.2	10.4	30.5	10.4	0.56
P3X11-5-3-2-TS1-3	53.1	21.3	15.3	9.16	1.15
P3X11-5-3-2-TS1-4	60.3	10.7	26.6	2.34	(b)
TS1 Average	59.0	13.7	20.5	6.04	1.08
P3X10-6-SP2T	55.4	43.5	0	1.13	(b)
P3X10-6-SP2B	44.5	43.6	11.0	0.89	(b)
SP2 Average	50.0	43.5	5.5	1.0	
P3X10-5-3-2-TS2-1	73.5	19.5	0	4.00	3.02
P3X10-5-3-2-TS2-2	50.7	47.3	0	0.74	1.25
P3X10-5-3-2-TS2-3	64.8	30.5	0	3.52	1.18
P3X10-5-3-2-TS2-4	46.8	52.5	0	0.72	(b)
TS2 Average	58.9	37.4	0	2.2	1.3
P3X11-5-3-SP3T	55.2	39.0	0	5.73	(b)
P3X11-5-3-SP3B	58.5	37.2	0	4.32	(b)
SP3 Average	56.9	38.1	0	5.0	
P3X11-6-TS3-1	97.6	1.05	0.58	0.64	0.14
P3X11-6-TS3-2	91.4	6.57	0	1.07	0.94
P3X11-6-TS3-3	73.1	25.7	0	0.46	0.73
P3X11-6-TS3-4	71.8	28.2	0	0	(b)
TS3 Average	83.5	15.4	0.15	0.54	0.60
(a)	All values are weight percentages.				
(b)	Not reported.				



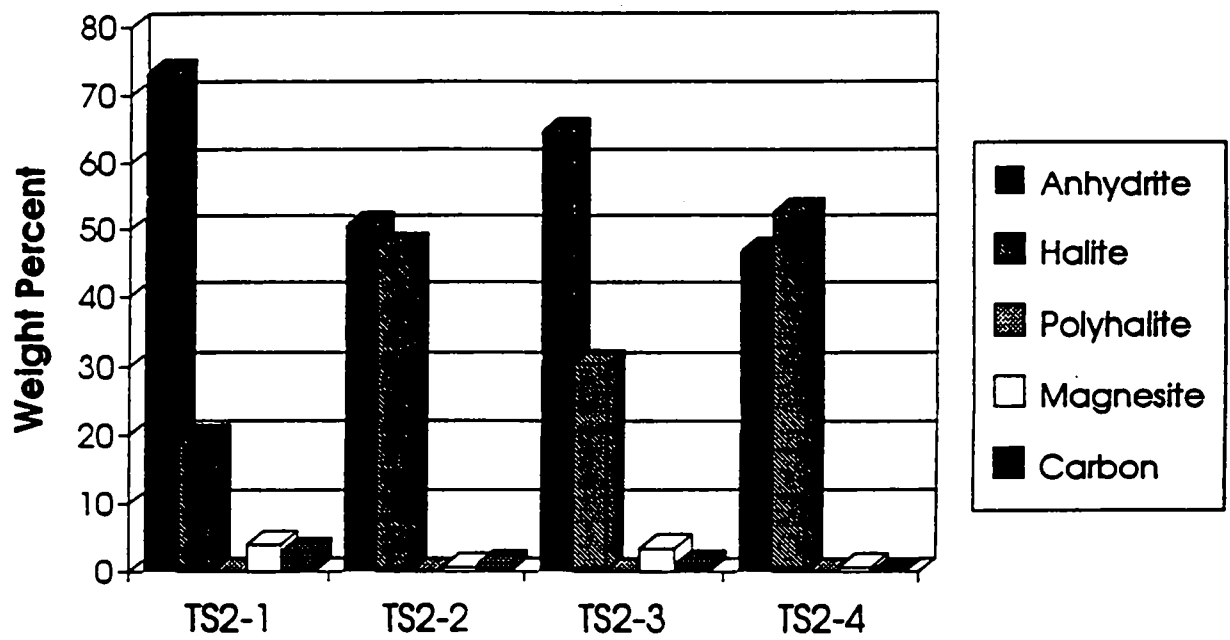
R81-248-04-022

Figure 4-1. Average mineral compositions determined using X-ray diffraction for specimens taken from above and below the axes of specimens SP1, SP2, and SP3.



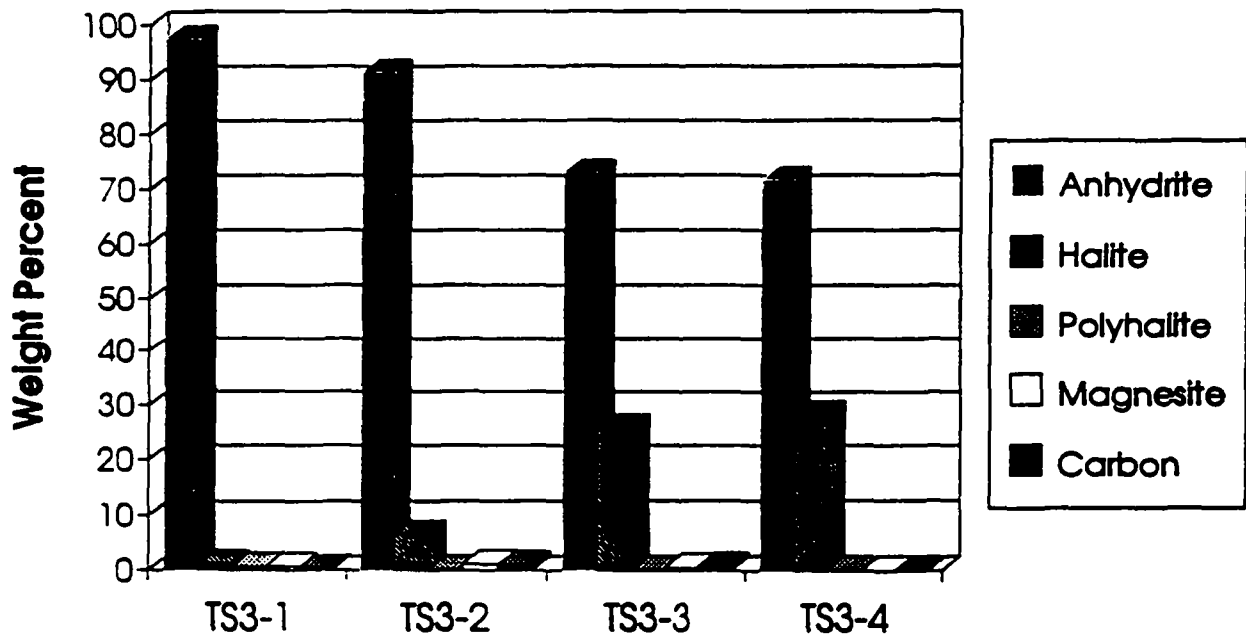
RSI-248-04-023

Figure 4-2. Mineral compositions for specimens taken from Block TS1. Petrographic analyses were used for Specimens TS1-1, TS1-2, and TS1-3; X-ray diffraction was used for Specimen TS1-4.



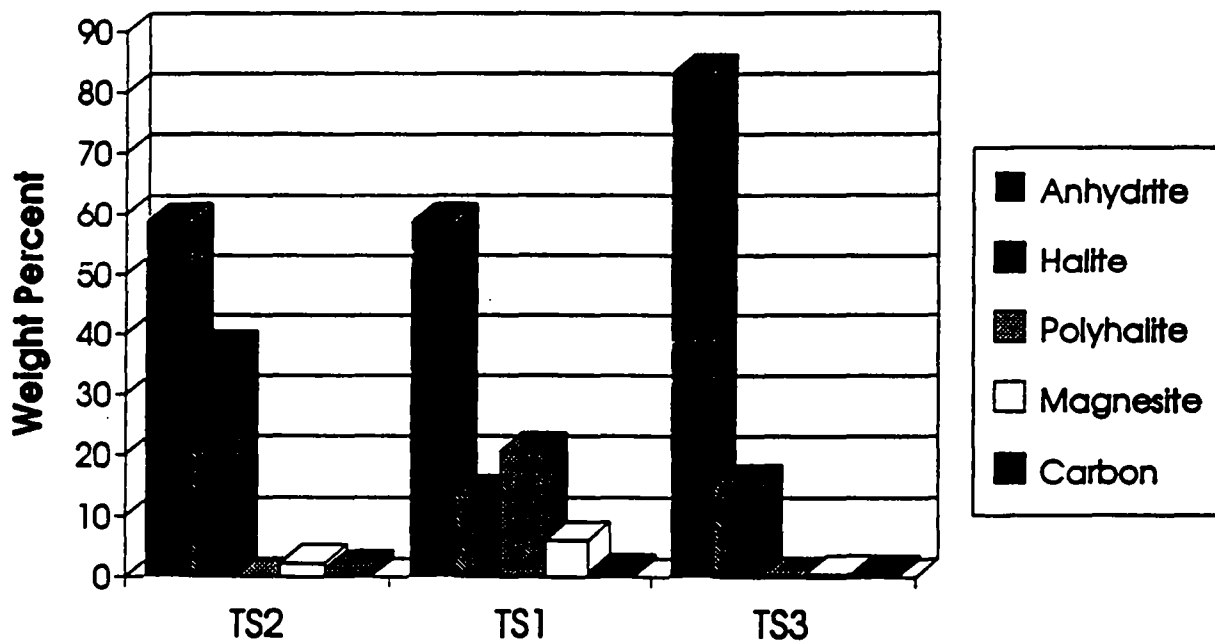
RSI-248-84-024

Figure 4-3. Mineral compositions for specimens taken from Block TS2. Petrographic analyses were used for Specimens TS2-1, TS2-2, and TS2-3; X-ray diffraction was used for Specimen TS2-4.



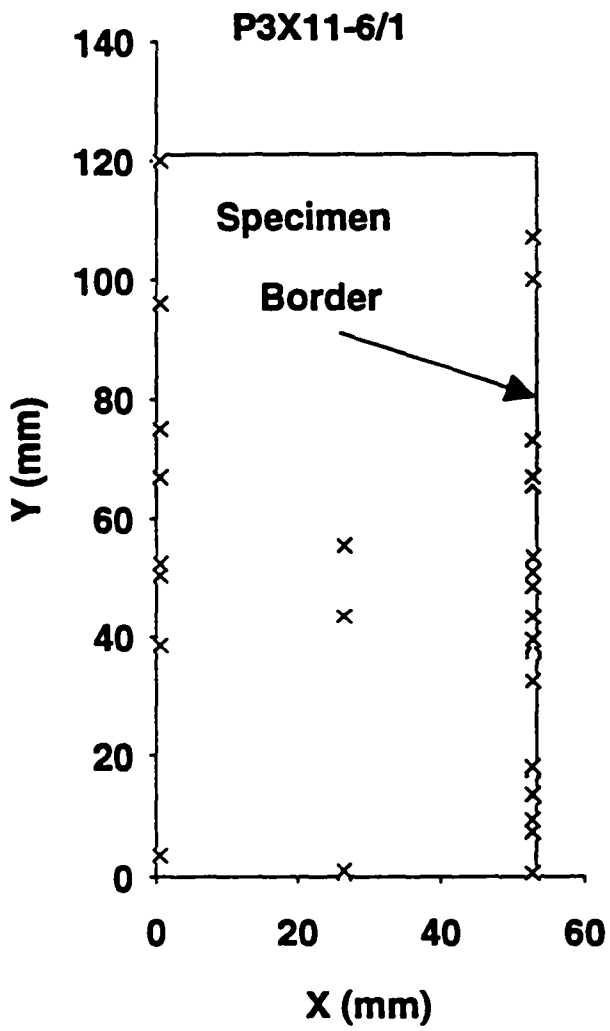
RSI-248-04-025

Figure 4-4. Mineral compositions for specimens taken from Block TS3. Petrographic analyses were used for Specimens TS3-1, TS3-2, and TS3-3; X-ray diffraction was used for Specimen TS3-4.



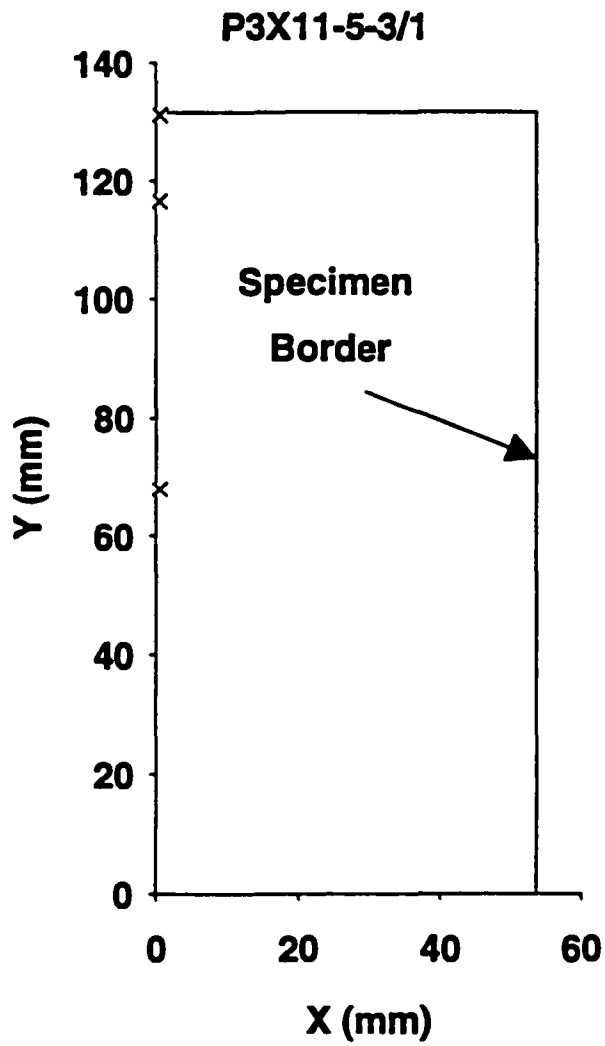
RSI-248-04-026

Figure 4-5. Average mineral compositions for specimens taken from Blocks TS2, TS1, and TS3 from the upper, middle, and lower sections of the marker bed, respectively.



RB1-248-92-023

Figure 4-6. Crack occurrence on Specimen P3X11-6/1.



R31-348-02-024

Figure 4-7. Crack occurrence on Specimen P3X11-5-3/1.

densities are associated with the specimen edges than with the midsection, however; the difference in crack populations is not statistically significant. Slower coring rates may reduce damage; however, differences in crack density between the two specimens may be due to specimen-to-specimen variations.

4.3 Porosity Measurements

Effective porosity and grain and bulk densities were measured for six MB 139 specimens by Core Laboratories using a helium porosimeter and the data are given in Table 4-4. Porosity varied from a low of 1.0 percent to a high of 2.1 percent. The grain densities vary from 2.53 to 2.73 g/cc while the bulk densities vary from 2.51 to 2.68 g/cc. The complete report from Core Laboratories is given in Appendix B-C.

Total porosity was measured for three of the specimens using the method given in Section 3.3.2. The densities and total porosities determined using this method and densities and effective porosities as measured for these specimens by Core Laboratories are given in Table 4-5. In all cases, the total porosities, determined using the fluid displacement technique, were greater than the effective porosities determined by Core Laboratories. In theory, the fluid displacement technique should provide higher values because grains are fractured before the measurement, providing immediate access to the specimen interior. An example of the error calculation, determined using the method given in ANSI/ASME (1986), is given in Section F1 of Appendix B-F. The errors for total porosity measurements are high because the technique relies on measuring small differences in mass among large quantities. Sampling errors were not included in the error analysis. Approximately 20-26 percent of each sample was lost during the grinding and sieving process and this may also contribute to the apparent differences between effective and total porosities.

4.4 Gas Permeability Measurements

Three nitrogen permeability tests were run at each of the test conditions given in Table 1-1. An example of the flow data obtained from each test and the linear least square fitting that was performed to obtain flow rate are given in Figure 4-8. The complete set of figures showing flow data and linear least square fits for all gas permeability tests is given in Appendix B-G. Separate plots are given for each specimen at each confining pressure and gas inlet pressure. Each plot shows the three replicate tests performed at a single set of conditions. The data for Specimens

Table 4-4. Results of Effective Porosity and Grain and Bulk Density Measurements on MB 139^(a)

Specimen I.D.	Porosity (Helium) (%)	Grain Density (g/cc)	Bulk Density (g/cc)	Mass as Sent (RE/SPEC) (g)	Mass as Received (Core Labs) (g)
P3X11-5-2-SP1T	1.7	2.73	2.68	33.94	33.9326
P3X11-5-2-SP1B	2.1	2.73	2.67	37.45	37.4455
P3X10-6-SP2T	1.3	2.69	2.65	38.85	38.8394
P3X10-6-SP2B	1.1	2.57	2.54	33.67	33.6636
P3X11-5-3-SP3T	1.0	2.53	2.51	37.51	37.4992
P3X11-5-3-SP3B	1.8	2.70	2.66	47.68	47.6703

(a) Determined by Core Laboratories, Houston, Texas.

Table 4-5. Porosity, Grain Density, and Bulk Density Measurements by RE/SPEC Inc. and by Core Laboratories

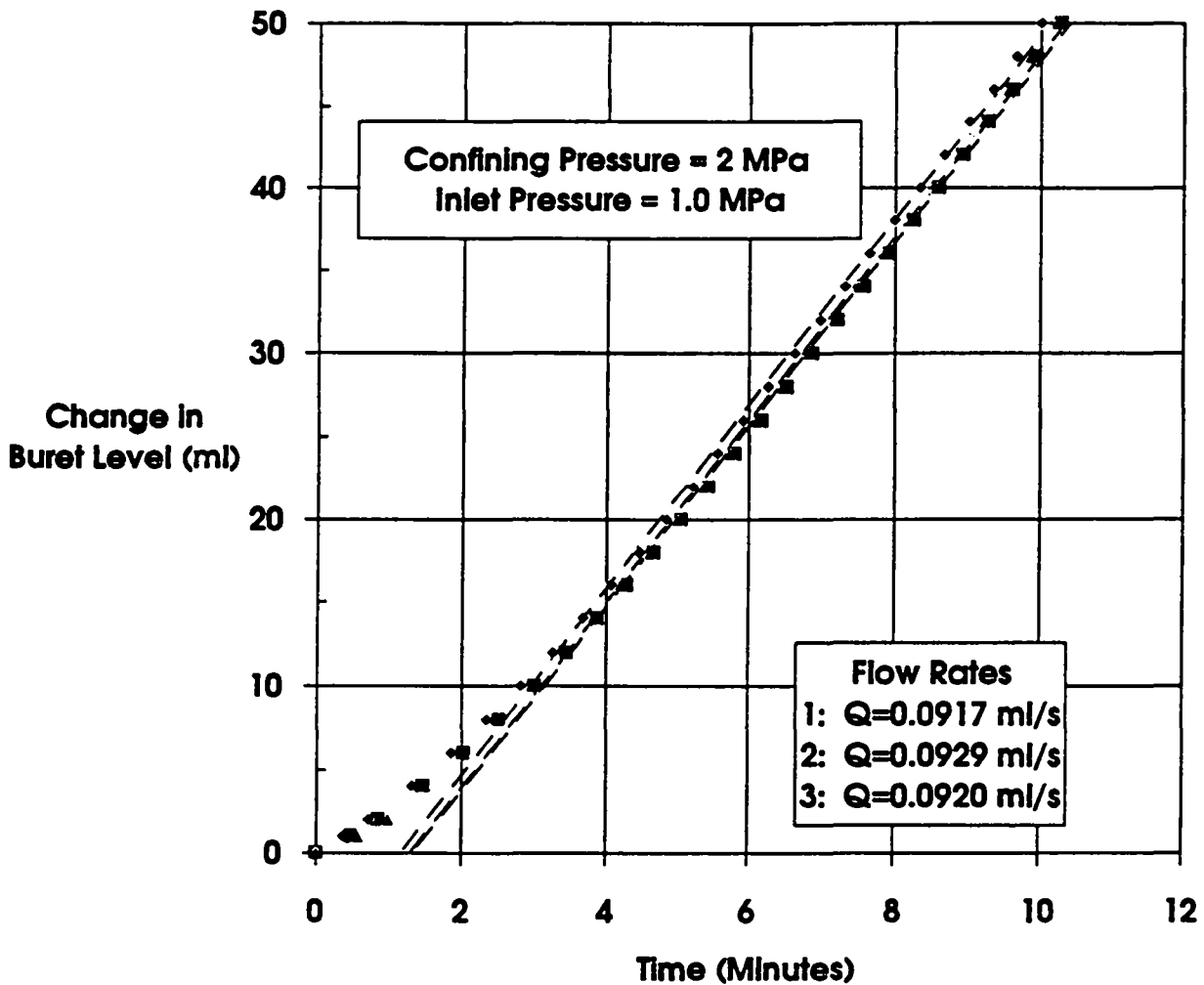
Specimen ID	RE/SPEC Inc. ^(a)			Core Laboratories ^(b)		
	Porosity ^(c) (%)	Grain Density (g/cc)	Bulk Density (g/cc)	Porosity (%)	Grain Density (g/cc)	Bulk Density (g/cc)
P3X11-5-2-SP1T	2.76 ± 0.91	2.76	2.69	1.7	2.73	2.68
P3X10-6-SP2T	2.12 ± 0.79	2.71	2.65	1.3	2.69	2.65
P3X11-5-3-SP3T	2.20 ± 0.81	2.55	2.50	1.0	2.53	2.51

- (a) Measurements of grain density and total porosity were made using a fluid displacement technique. Bulk volume was determined from specimen dimensions.
- (b) Measurements of grain density and effective porosity were made using a small volume helium porosimeter. Bulk volume was determined from a mercury displacement technique.
- (c) Errors bars cover the 95% uncertainty interval; i.e., the interval expected to contain the true value 95% of the time during repeated sampling.

SP1 and SP3 are very reproducible for nominally identical tests. The flow rates determined for SP2 show some scatter but are always reproducible to within a factor of 3 and generally to within a factor of 2 for nominally identical tests. Flow rates are given on each plot in the order in which the three replicate tests were performed. Flow rates and calculated permeabilities are summarized in Table 4-6 through 4-8 for the three specimens, respectively. Error analyses were performed using the method given by ANSI/ASME (1986) and an example error calculation is given in Section F2 of Appendix B-F. The 95 percent uncertainty interval for gas permeability measurements based on experimental uncertainty is approximately ± 6 percent of the measured value.

An example of flow rate plotted versus gas pressure difference across a specimen is given in Figure 4-9 for Specimen SP1 at 2 MPa confining pressure. The plot contains data obtained at the three gas inlet pressures (9 tests). The corresponding data for all gas permeability tests are given in Appendix B-H. The data are not concave towards the pressure axis, showing that flow was not turbulent.

Measurements of gas permeability are complicated by “slippage” or the Klinkenberg effect. Slippage depends upon the mean free path between molecules and results in decreased permeabilities for lower mean free paths. Because gases are compressible, mean free path



RSI-348-94-027

Figure 4-8. Gas volume-versus-time for test on MB 139 anhydrite Specimen P3X11-5-2-SP1 at 2 MPa confining pressure and 1 MPa gas inlet pressure. Symbols represent recorded data points and dashed lines are best fits to linear sections of data.

Table 4-6. Flow Data and Calculated Permeability to Nitrogen for Specimen P3X11-5-2-SP1

Confining Pressure (MPa)	Gas Inlet Pressure = 1.0 MPa ^(a)		Gas Inlet Pressure = 0.7 MPa ^(a)		Gas Inlet Pressure = 0.4 MPa ^(a)	
	Flow Rate (10 ⁻⁸ · m ³ · s ⁻¹)	Permeability (10 ⁻¹⁸ · m ²)	Flow Rate (10 ⁻⁸ · m ³ · s ⁻¹)	Permeability (10 ⁻¹⁸ · m ²)	Flow Rate (10 ⁻⁸ · m ³ · s ⁻¹)	Permeability (10 ⁻¹⁸ · m ²)
2	9.17	4.2	4.89	4.6	1.83	5.5
2	9.29	4.2	4.89	4.6	1.80	5.4
2	9.20	4.2	4.95	4.6	1.76	5.3
6	5.56	2.5	2.93	2.7	1.15	3.4
6	5.56	2.5	2.93	2.7	1.13	3.4
6	5.44	2.5	2.92	2.7	1.14	3.4
10	4.50	2.0	2.33	2.2	0.908	2.7
10	4.40	2.0	2.32	2.2	0.897	2.7
10	4.15	1.9	2.32	2.2	0.898	2.7

(a) Gas outlet pressure = 0.1 MPa for all tests.

Table 4-7. Flow Data and Calculated Permeability to Nitrogen for Specimen P3X10-6-SP2

Confining Pressure (MPa)	Gas Inlet Pressure = 1.0 MPa ^(a)		Gas Inlet Pressure = 0.7 MPa ^(a)		Gas Inlet Pressure = 0.4 MPa ^(a)	
	Flow Rate (10 ⁻⁸ · m ³ · s ⁻¹)	Permeability (10 ⁻¹⁸ · m ²)	Flow Rate (10 ⁻⁸ · m ³ · s ⁻¹)	Permeability (10 ⁻¹⁸ · m ²)	Flow Rate (10 ⁻⁸ · m ³ · s ⁻¹)	Permeability (10 ⁻¹⁸ · m ²)
2	8.96 ^(b)	3.3 ^(b)	3.48	3.2	0.934	2.9
2	9.12	4.1	2.92	2.7	0.746	2.2
2	8.47	3.8	3.14	2.9	0.669	2.0
6	2.70	1.2	1.09	1.0	0.174	0.52
6	2.93	1.3	1.43	1.3	0.167	0.50
6	3.06	1.4	0.610	0.57	0.132	0.39
10	0.927	0.42	0.423	0.39	0.107	0.32
10	0.917	0.41	0.402	0.37	0.0718	0.21
10	1.04	0.47	0.308	0.29	0.0605	0.18

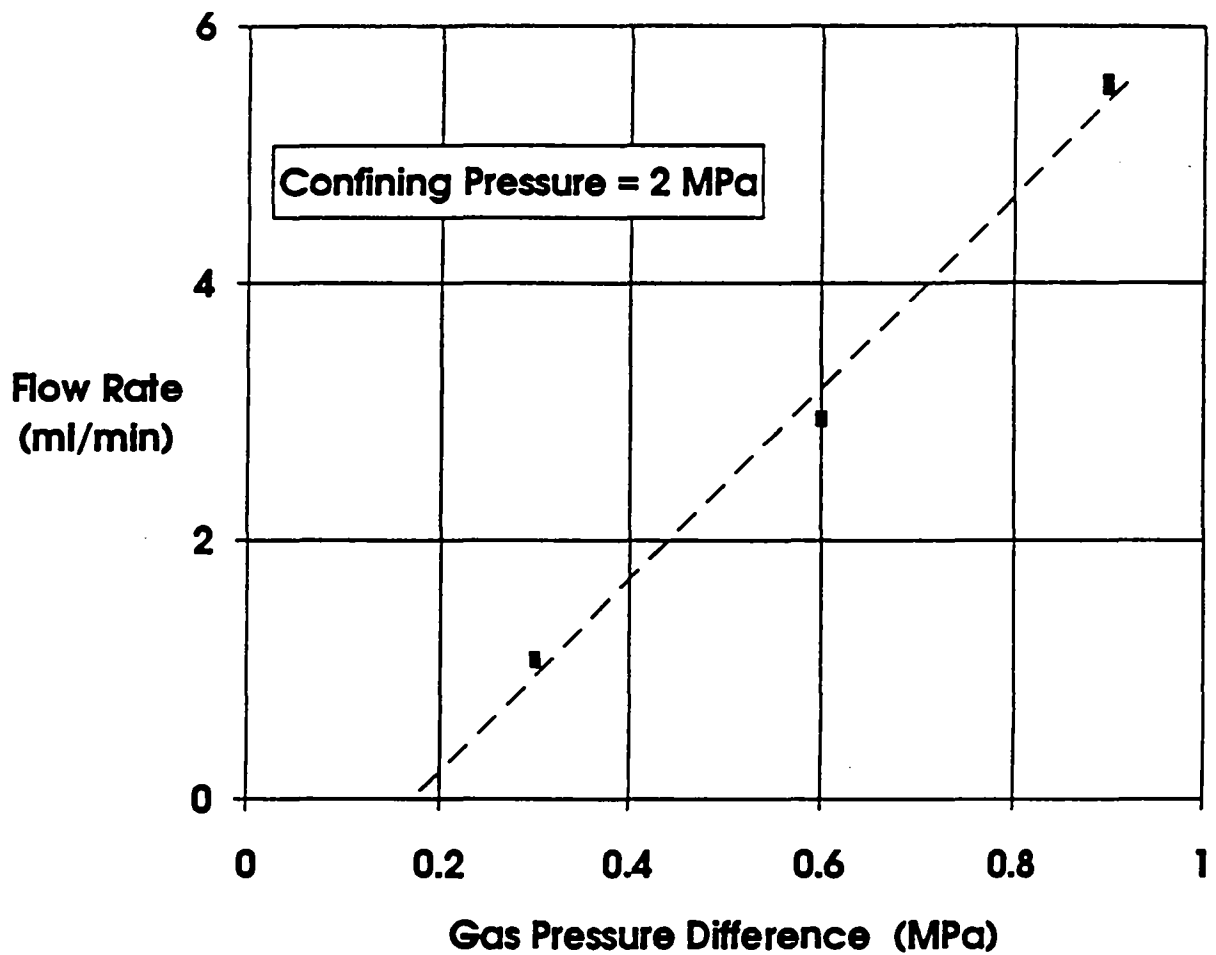
(a) Gas outlet pressure = 0.1 MPa for all tests.

(b) Gas inlet pressure = 1.1 MPa.

Table 4-8. Flow Data and Calculated Permeability to Nitrogen for Specimen P3X11-5-3-SP3

Confining Pressure (MPa)	Gas Inlet Pressure = 1.0 MPa ^(a)		Gas Inlet Pressure = 0.7 MPa ^(a)		Gas Inlet Pressure = 0.4 MPa ^(a)	
	Flow Rate (10 ⁻⁸ · m ³ · s ⁻¹)	Permeability (10 ⁻¹⁸ · m ²)	Flow Rate (10 ⁻⁸ · m ³ · s ⁻¹)	Permeability (10 ⁻¹⁸ · m ²)	Flow Rate (10 ⁻⁸ · m ³ · s ⁻¹)	Permeability (10 ⁻¹⁸ · m ²)
2	44.1	20	23.7	22	8.38	25
2	44.5	20	23.7	22	8.46	25
2	44.3	20	23.7	22	8.49	25
6	24.1	11	12.9	12	4.49	13
6	24.2	11	12.9	12	4.54	14
6	24.1	11	13.0	12	4.52	13
10	14.4	6.5	7.63	7.1	2.80	8.3
10	14.7	6.6	7.59	7.0	2.77	8.2
10	14.5	6.5	7.59	7.1	2.77	8.2

(a) Gas outlet pressure = 0.1 MPa for all tests.



RSI-248-93-085

Figure 4-9. Flow rate-versus-gas pressure difference for Specimen P3X11-5-2-SP1 at 2 MPa confining pressure and all gas inlet pressures.

decreases as mean pore pressure increases and the Klinkenberg effect can become significant. The relation between gas and liquid permeabilities and mean pore pressure for a given material and non-interacting permeants was originally developed by Klinkenberg and is given as (Klinkenberg, 1941):

$$k_L = \frac{k_g}{1 + \frac{b}{p_m}} \quad (4-1)$$

where

k_L = liquid permeability

k_g = gas permeability

p_m = mean pore pressure

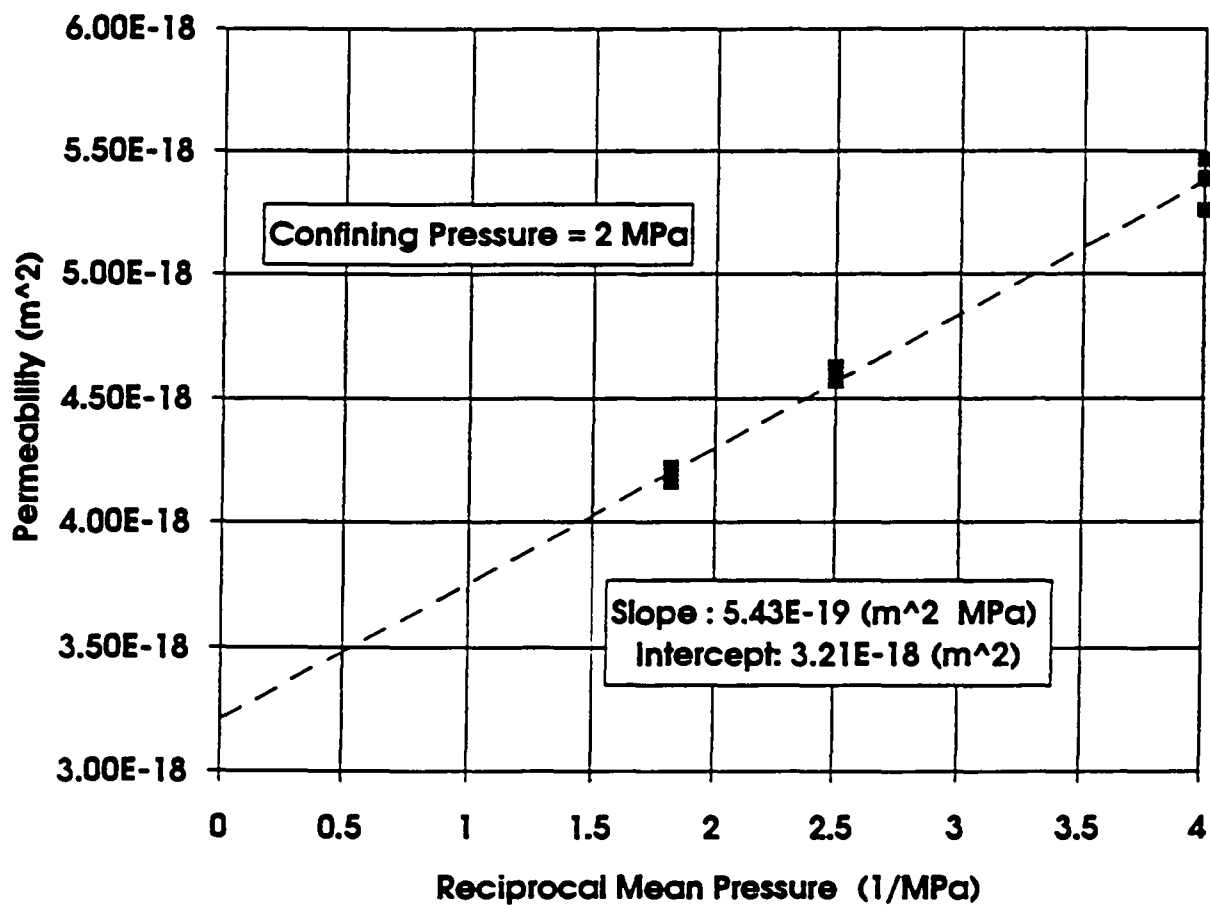
b = Klinkenberg constant for a given gas and material

This equation can be rewritten as

$$k_g = k_L + k_L \left(\frac{b}{p_m} \right) \quad (4-2)$$

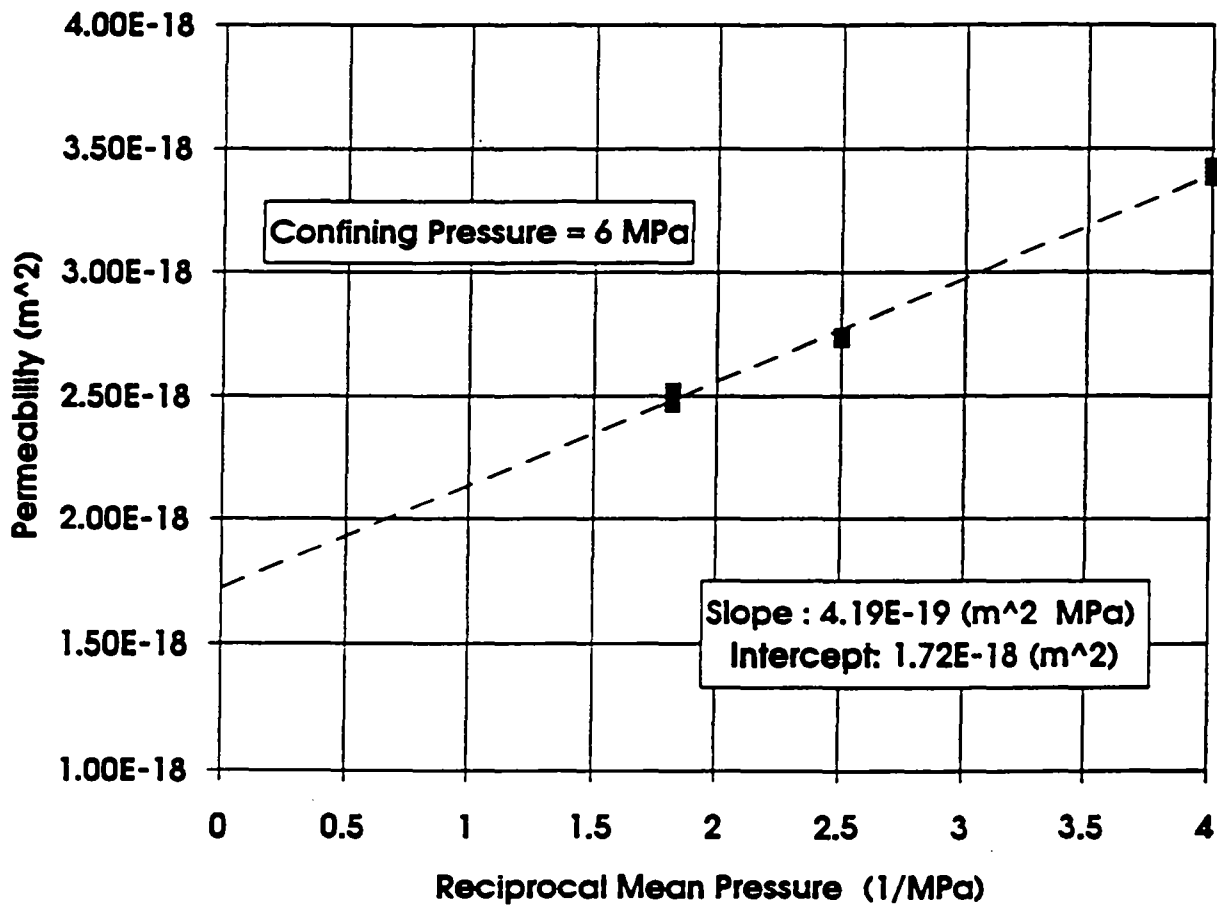
which is the equation of a line in gas permeability versus reciprocal mean pressure coordinates. A plot of gas permeabilities versus reciprocal mean pore pressure should therefore result in a straight line and the intercept at a reciprocal mean pore pressure value of zero provides the equivalent liquid (or Klinkenberg-corrected) permeability.

Permeabilities are plotted as a function of reciprocal mean gas pressure for Specimen SP1 in Figures 4-10 through 4-12 for the three confining pressures, respectively. Data are presented in Figures 4-13 through 4-15 and Figures 4-16 through 4-18 for Specimens SP2 and SP3, respectively. The slopes and intercepts (the Klinkenberg-corrected permeabilities) are given in the figures and the Klinkenberg-corrected permeabilities are also given in Table 4-9. The data obtained for Specimens SP1 and SP3 show the expected positive slope; however, the data for Specimen SP2 (Figures 4-13 through 4-15) show greater scatter and a negative slope at all confining pressures. Although this negative slope is unexpected, the difference between the mean permeability determined at each confining pressure and the value at the intercept is always less than 1 order of magnitude. The intercepts for Specimen SP2 are not given in Table 4-9. These are not true Klinkenberg-corrected permeabilities because of the negative slope of the permeability-versus reciprocal mean pressure curves.



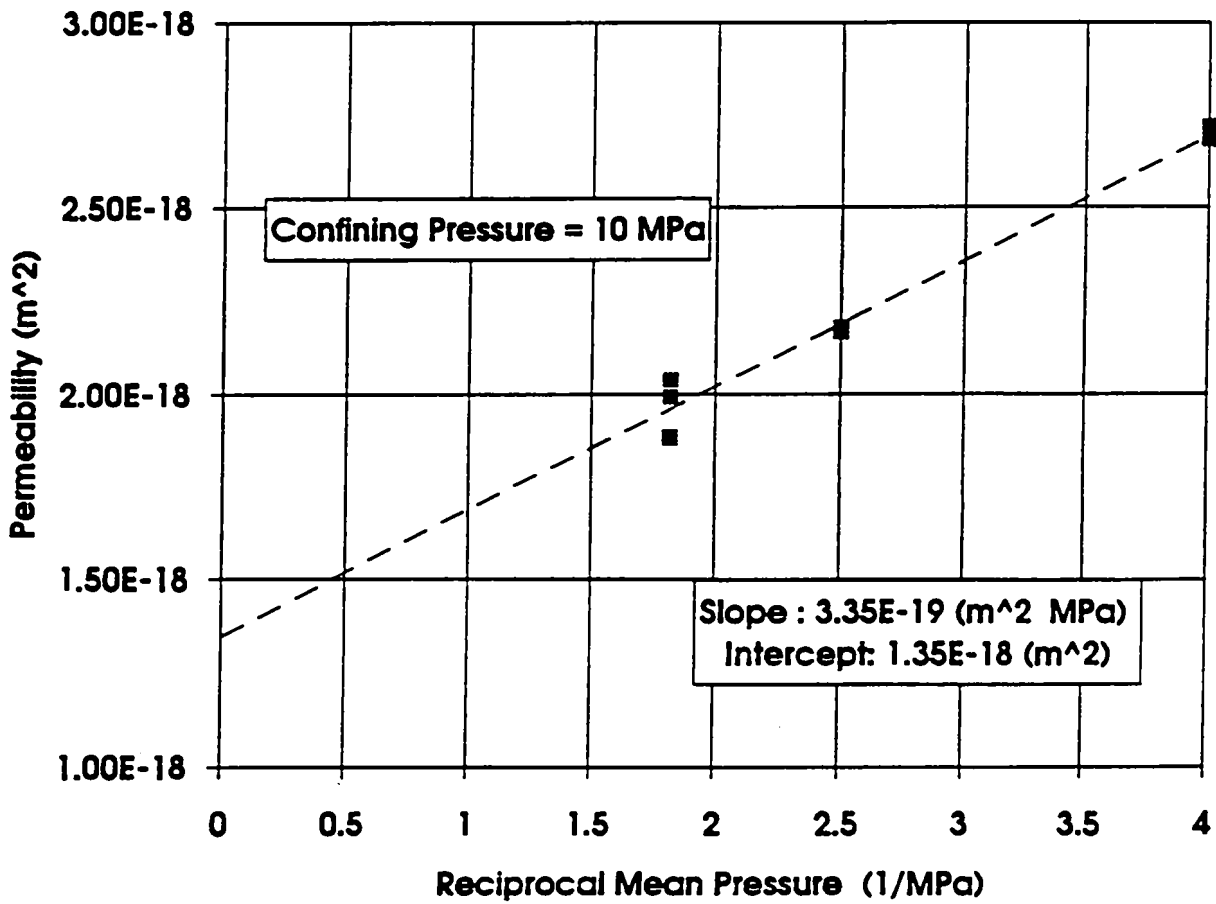
RSI-248-03-04

Figure 4-10. Permeability as a function of mean reciprocal gas pressure for Specimen P3X11-5-2-SP1 at 2 MPa confining pressure.



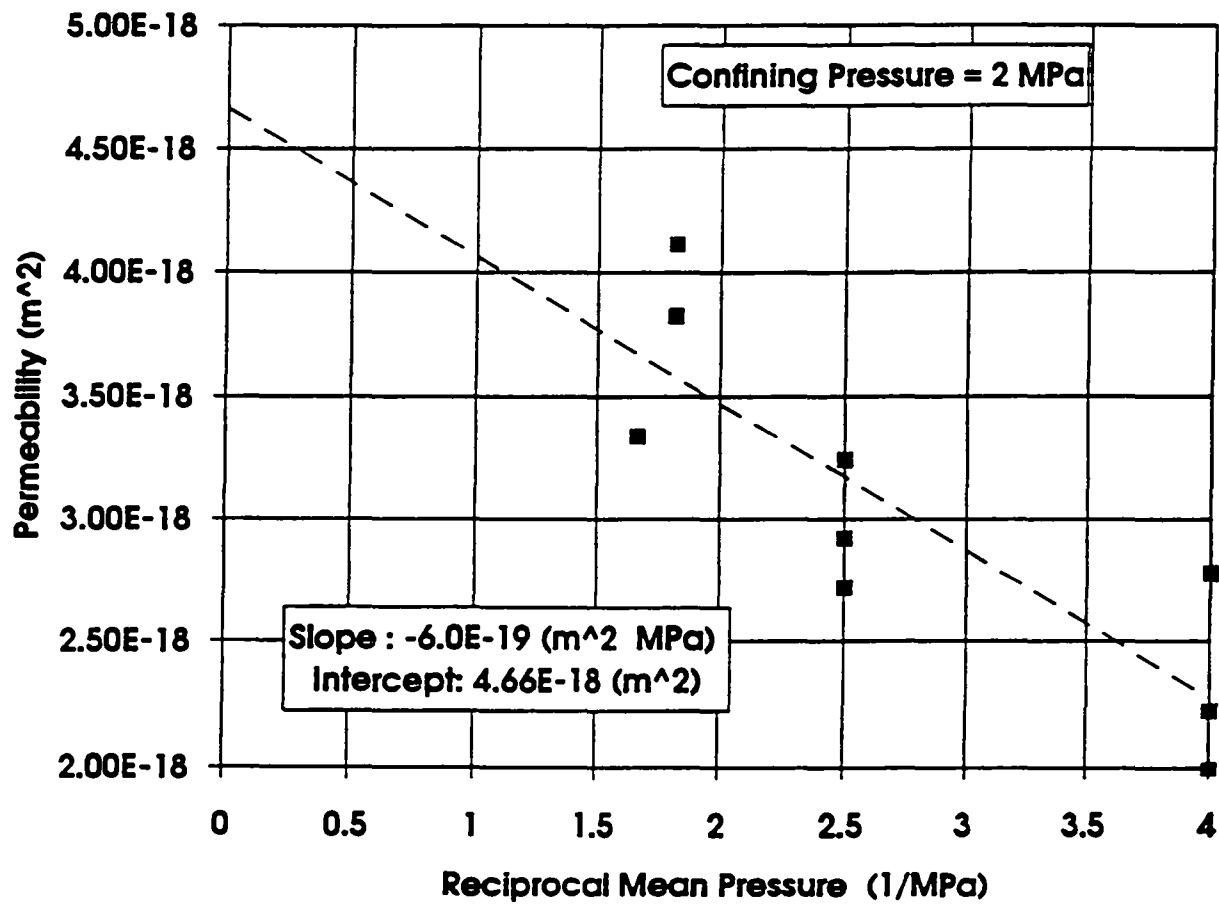
FBI-248-83-06

Figure 4-11. Permeability as a function of mean reciprocal gas pressure for Specimen P3X11-5-2-SP1 at 6 MPa confining pressure.



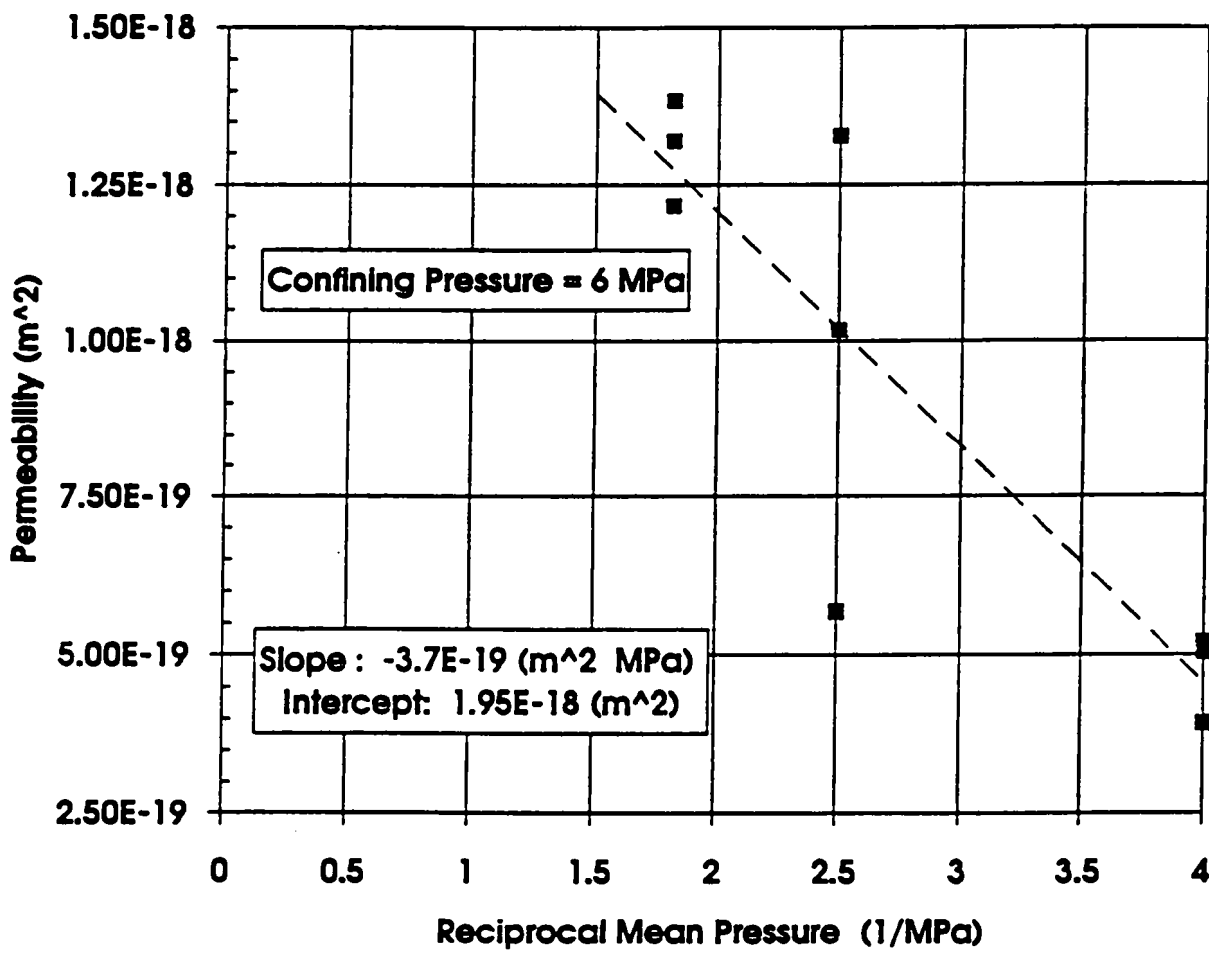
RSI-248-03-06

Figure 4-12. Permeability as a function of mean reciprocal gas pressure for Specimen P3X11-5-2-SP1 at 10 MPa confining pressure.



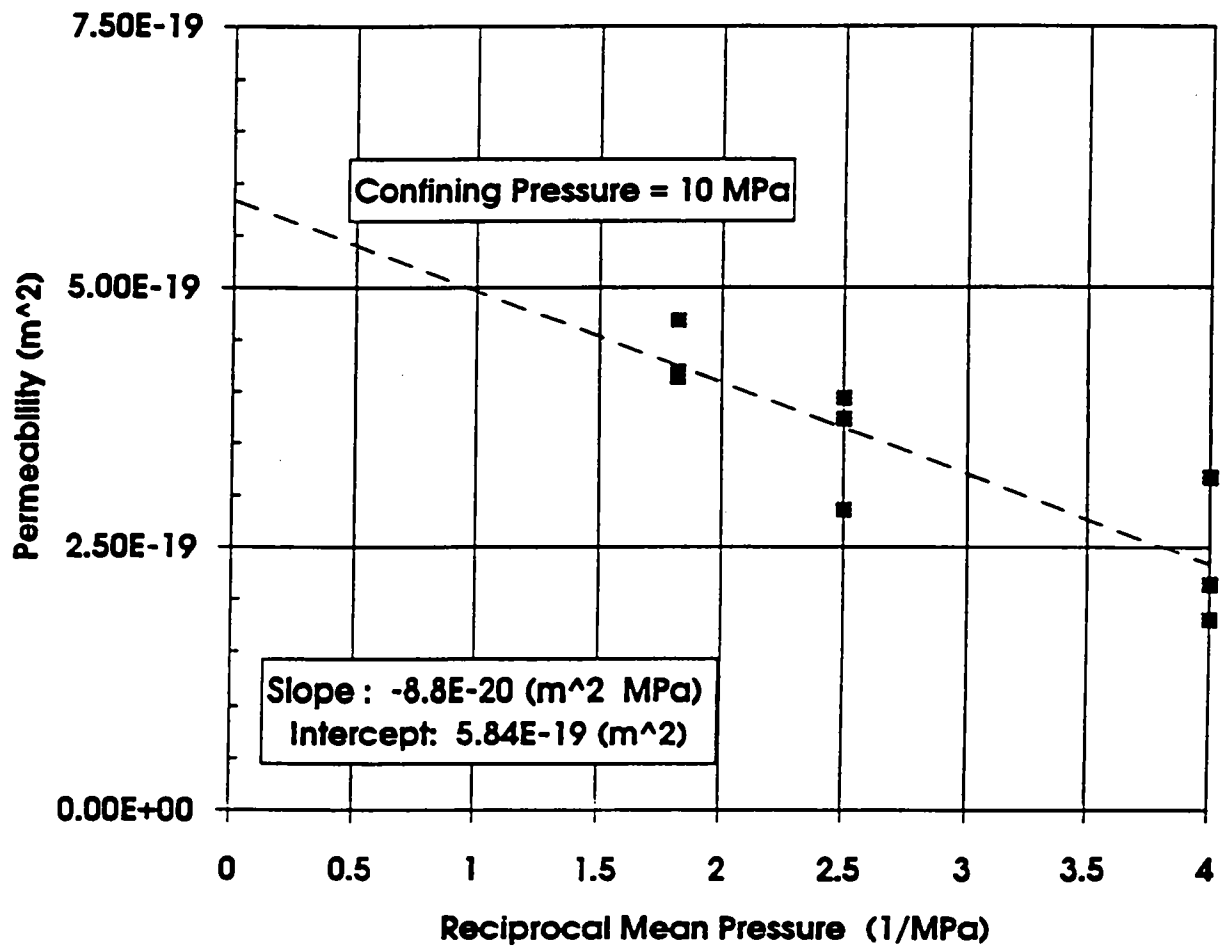
RSI-248-03-07

Figure 4-13. Permeability as a function of mean reciprocal gas pressure for Specimen P3X10-6-SP2 at 2 MPa confining pressure.



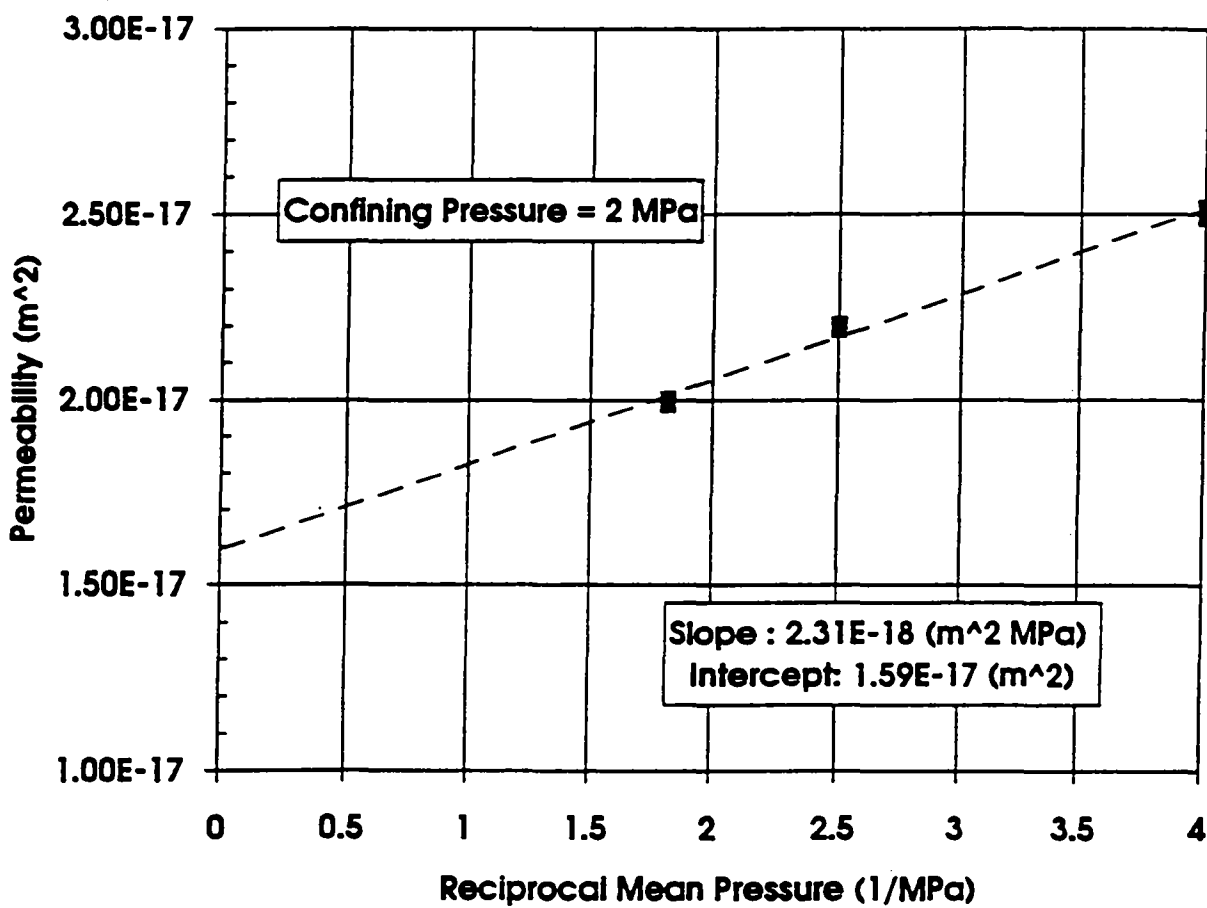
RSI-248-03-08

Figure 4-14. Permeability as a function of mean reciprocal gas pressure for Specimen P3X10-6-SP2 at 6 MPa confining pressure.



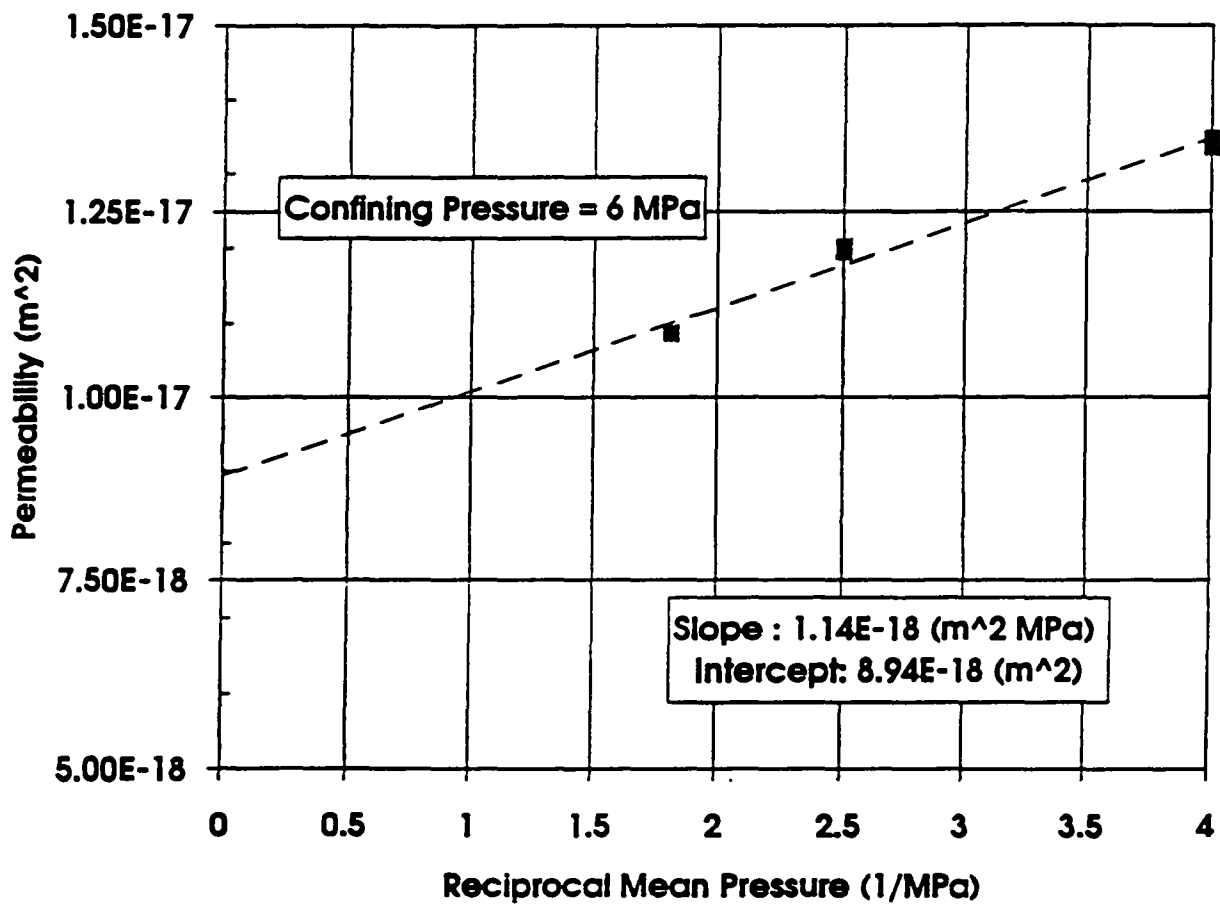
RSI-248-93-00

Figure 4-15. Permeability as a function of mean reciprocal gas pressure for Specimen P3X10-6-SP2 at 10 MPa confining pressure.



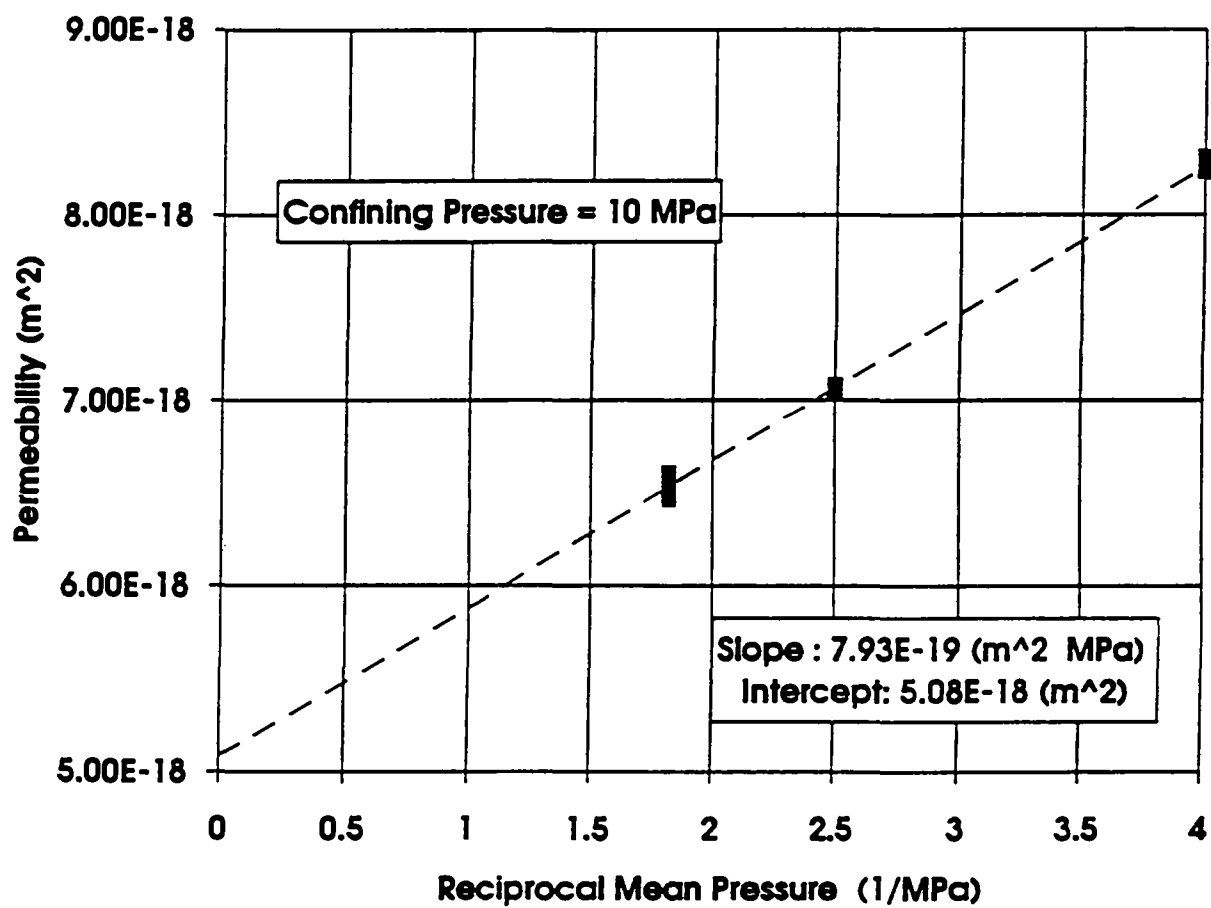
RSI-248-83-100

Figure 4-16. Permeability as a function of mean reciprocal gas pressure for Specimen P3X11-5-3-SP3 at 2 MPa confining pressure.



R81-248-83-101

Figure 4-17. Permeability as a function of mean reciprocal gas pressure for Specimen P3X11-5-3-SP3 at 6 MPa confining pressure.



RSI-248-83-102

Figure 4-18. Permeability as a function of mean reciprocal gas pressure for Specimen P3X11-5-3-SP3 at 10 MPa confining pressure.

Table 4-9. Klinkenberg-Corrected Permeabilities

Confining Pressure (MPa)	Klinkenberg Corrected Permeability	
	P3X11-5-2-SP1 (m ²)	P3X11-5-3-SP3 (m ²)
2	3.2 x 10 ⁻¹⁸	1.6 x 10 ⁻¹⁷
6	1.7 x 10 ⁻¹⁸	8.9 x 10 ⁻¹⁸
10	1.4 x 10 ⁻¹⁸	5.1 x 10 ⁻¹⁸

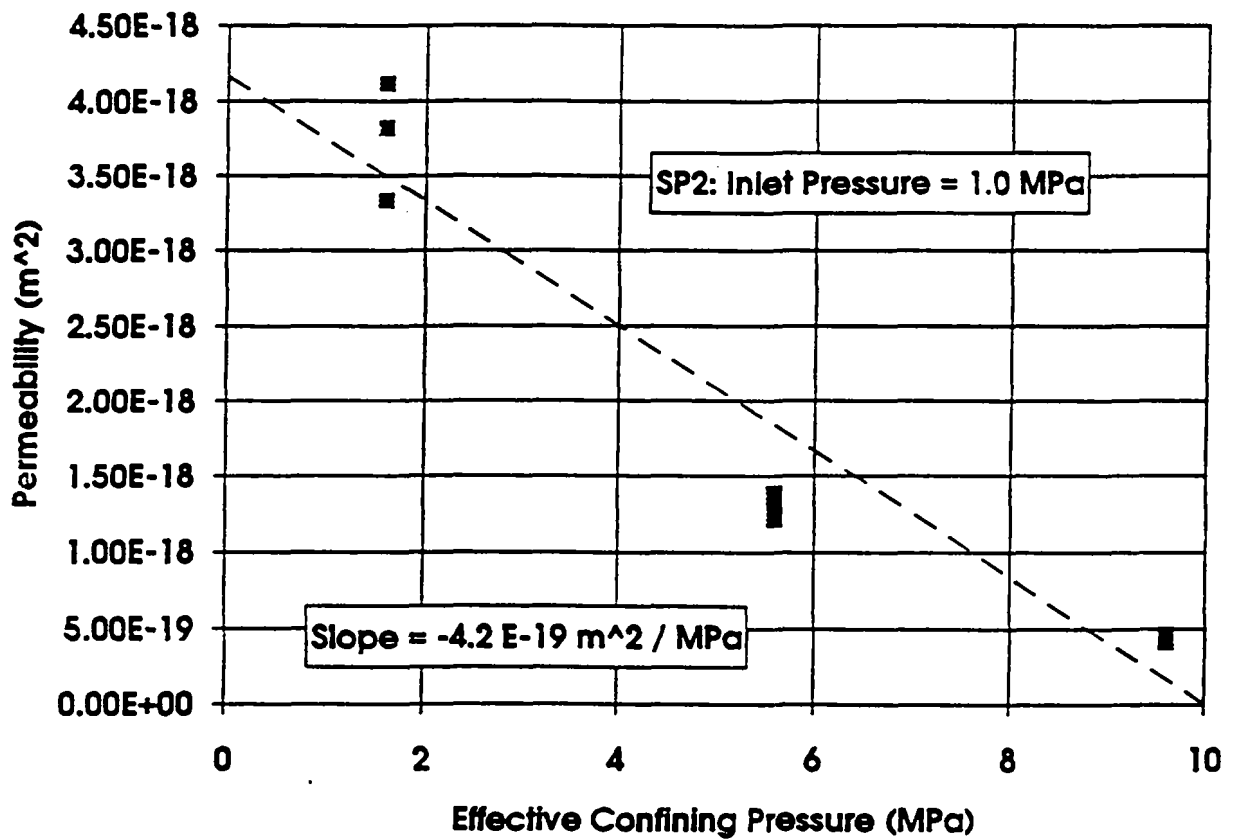
Values of *b*, the Klinkenberg constant for MB 139 and nitrogen gas permeant (Equation 4-2), were calculated for Specimens SP1 and SP3 from the slopes and intercepts of the Klinkenberg plots. These constants are given in Table 4-10.

Table 4-10. Klinkenberg Constants for MB 139 and Nitrogen Gas at 25°C

Confining Pressure (MPa)	Klinkenberg Constant, <i>b</i> (MPa)	
	P3X11-5-2-SP1	P3X11-5-3-SP3
2	0.17	0.15
6	0.24	0.13
10	0.25	0.16

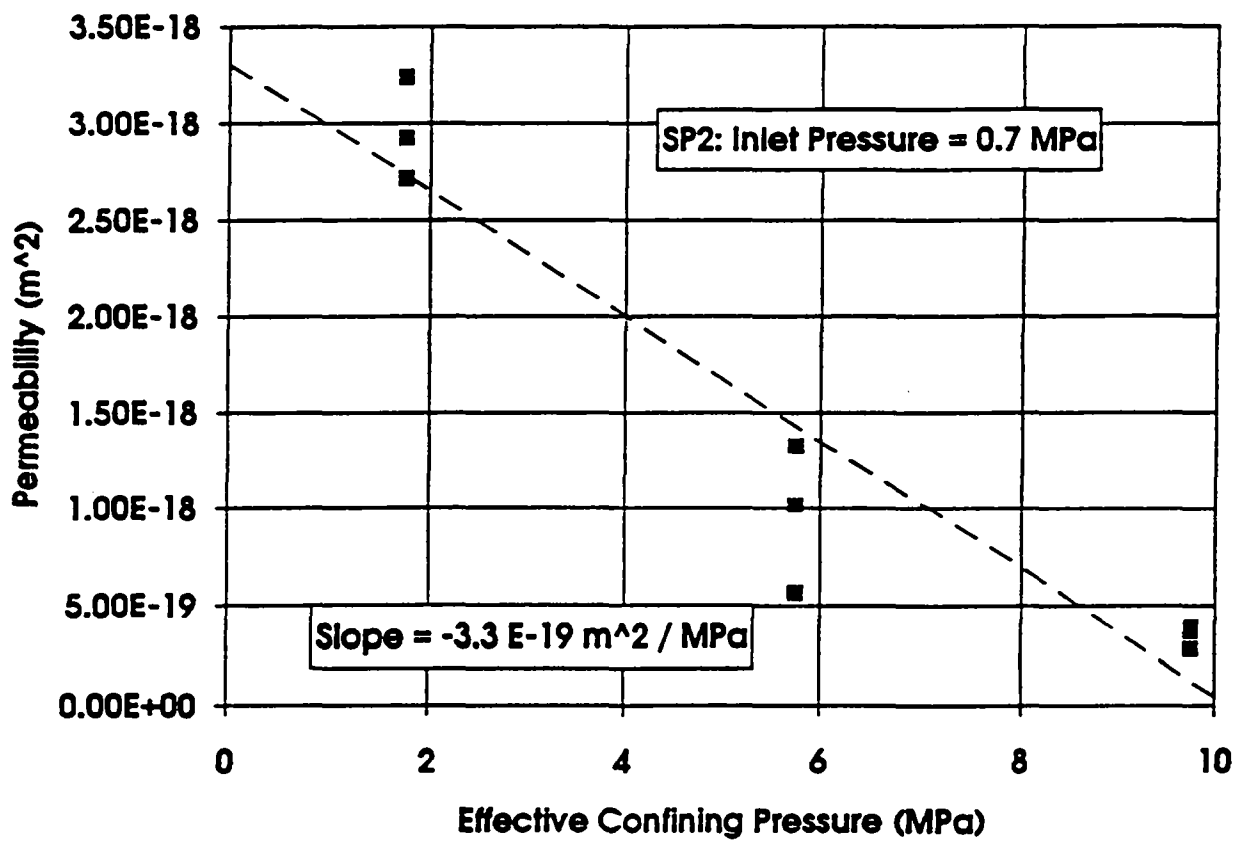
A discussion of the role of effective confining pressure (confining pressure - pore pressure) on permeability measurements may be in part relevant to the observation of negative slopes on the Klinkenberg plots for Specimen SP2. Tables 4-6 through 4-8 show that permeability decreases as confining pressure increases. A decrease in porosity and permeability can be caused by either an increase in confining pressure at constant pore pressure or a decrease in pore pressure at constant confining pressure, as both will result in an increased effective confining pressure. The Klinkenberg effect is of opposite sign and causes permeability to decrease as pore pressure increases. The hypothesis that large effective pressures could negate observations of the Klinkenberg effect was therefore investigated, and the results are described below.

Permeability data for Specimen SP2 are plotted as a function of effective confining pressure in Figures 4-19 through 4-21 for each of the three inlet pore pressures, respectively. The slopes of these plots provide specimen-specific information on the magnitude of the change in



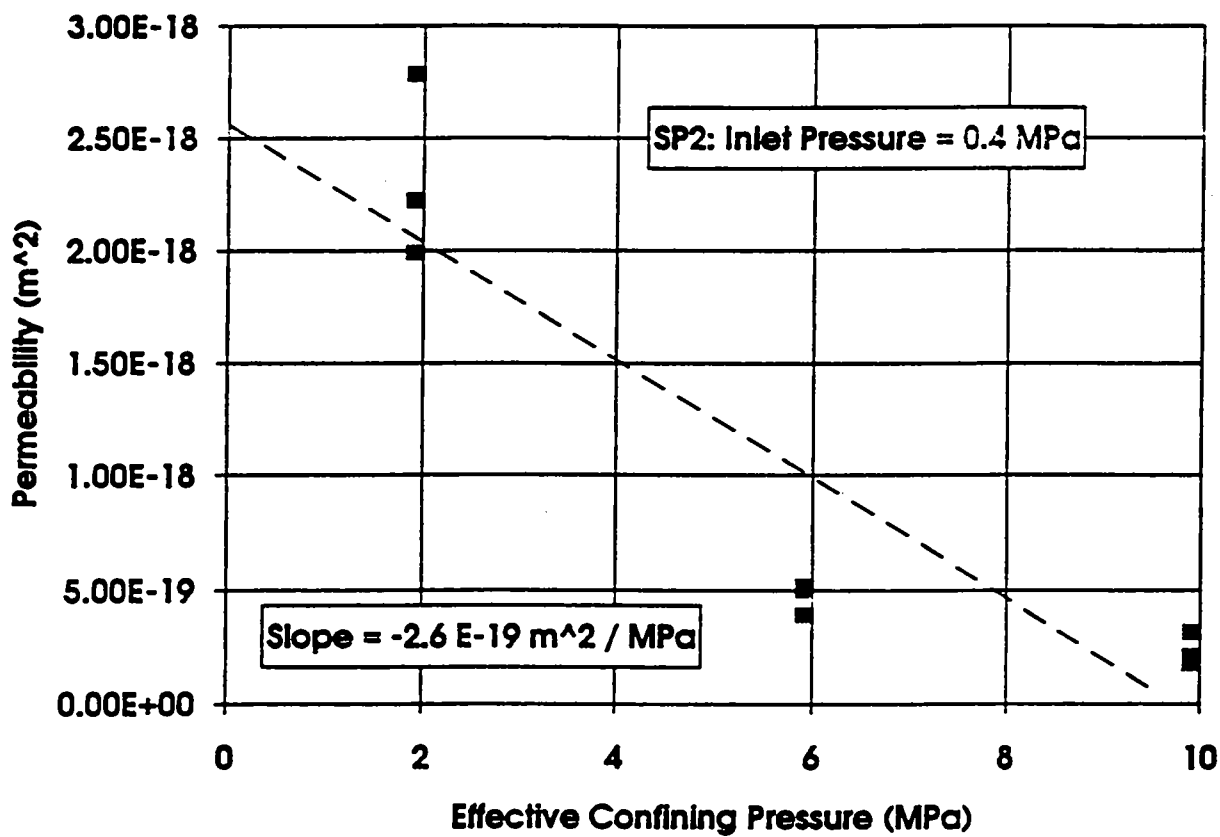
RSI-248-83-115

Figure 4-19. Change in permeability with increasing effective confining pressure for Specimen P3X10-6-SP2 at an inlet pore pressure of 1.0 MPa.



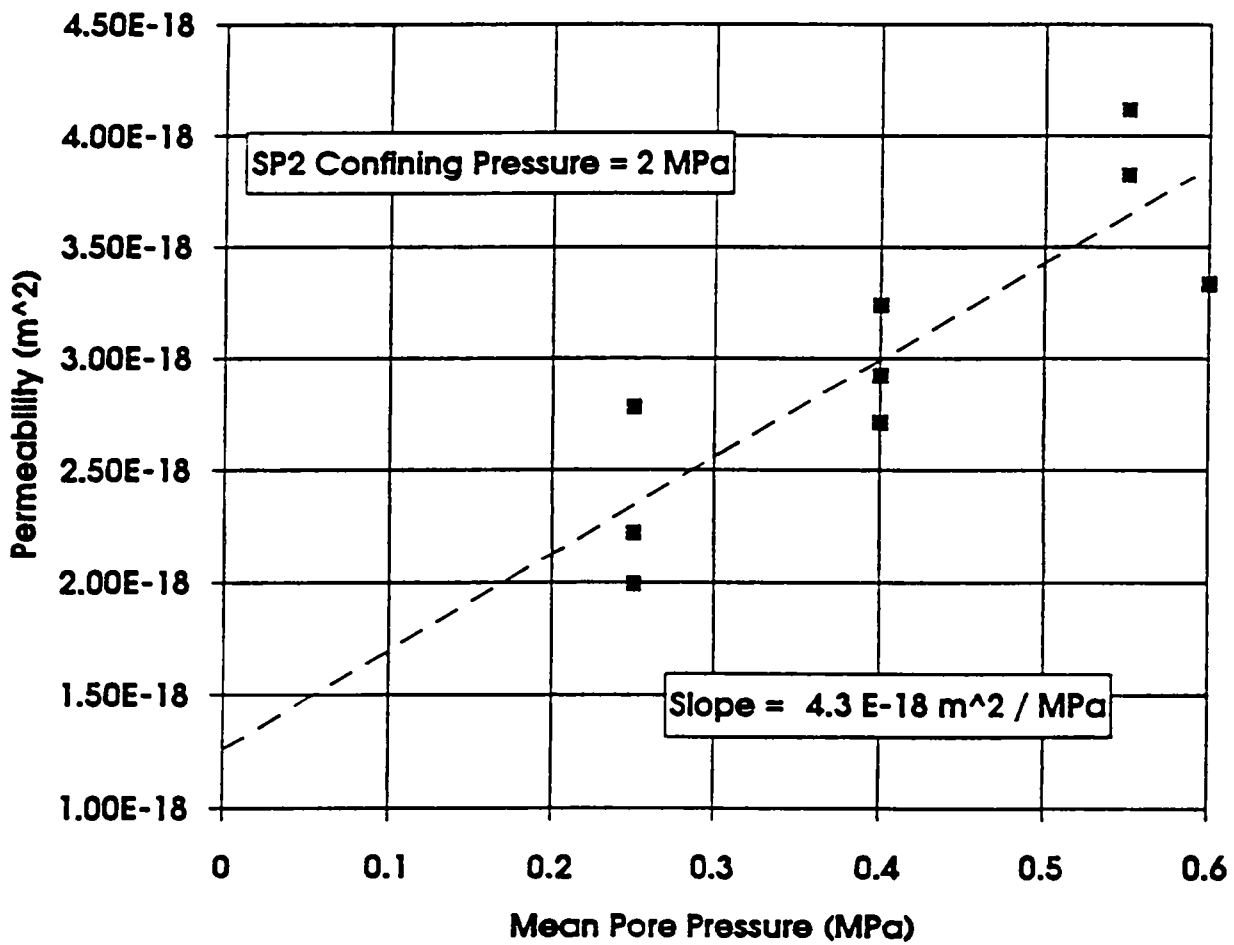
R81-248-03-118

Figure 4-20. Change in permeability with increasing effective confining pressure for Specimen P3X10-6-SP2 at an inlet pore pressure of 0.7 MPa.



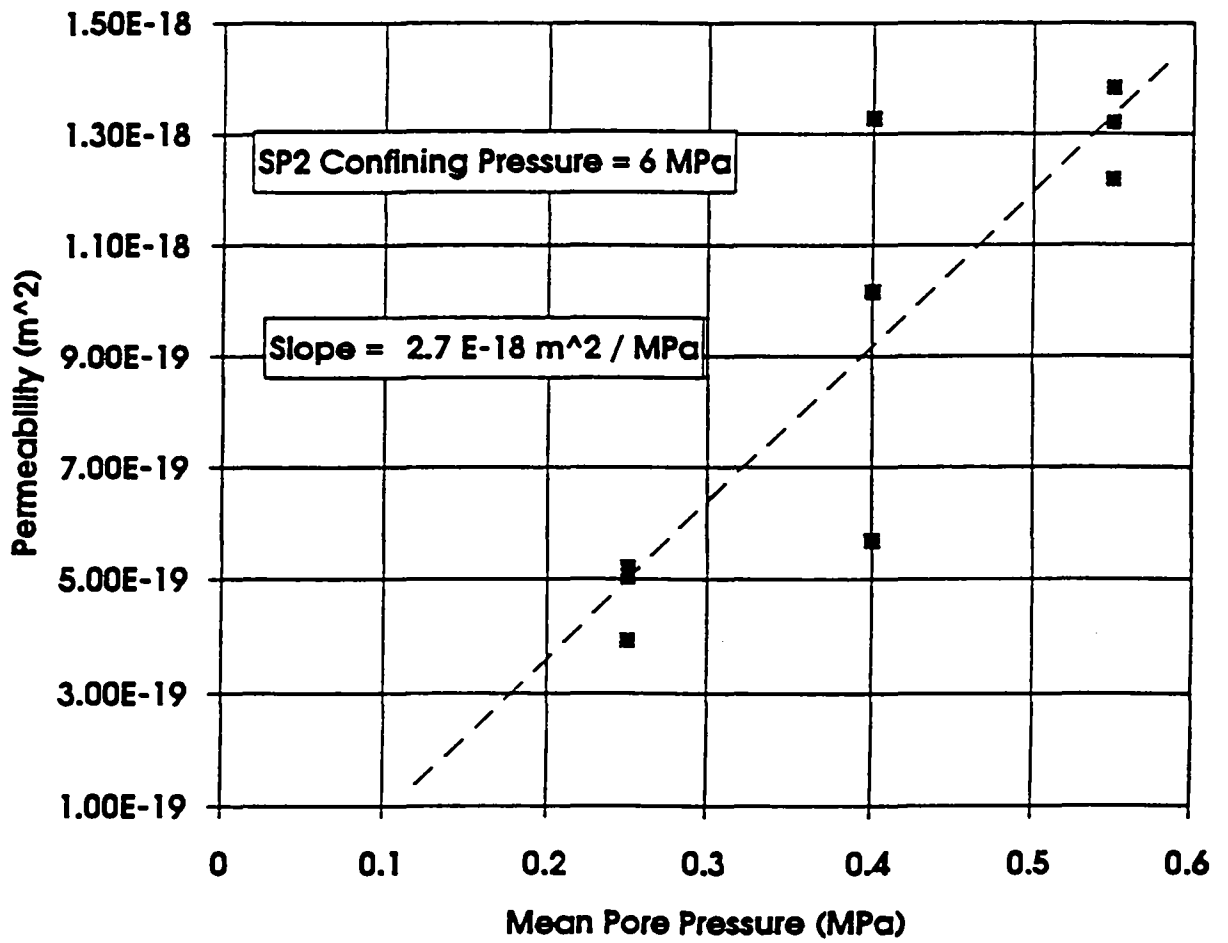
RSI-248-03-117

Figure 4-21. Change in permeability with increasing effective confining pressure for Specimen P3X10-6-SP2 at an inlet pore pressure of 0.4 MPa.



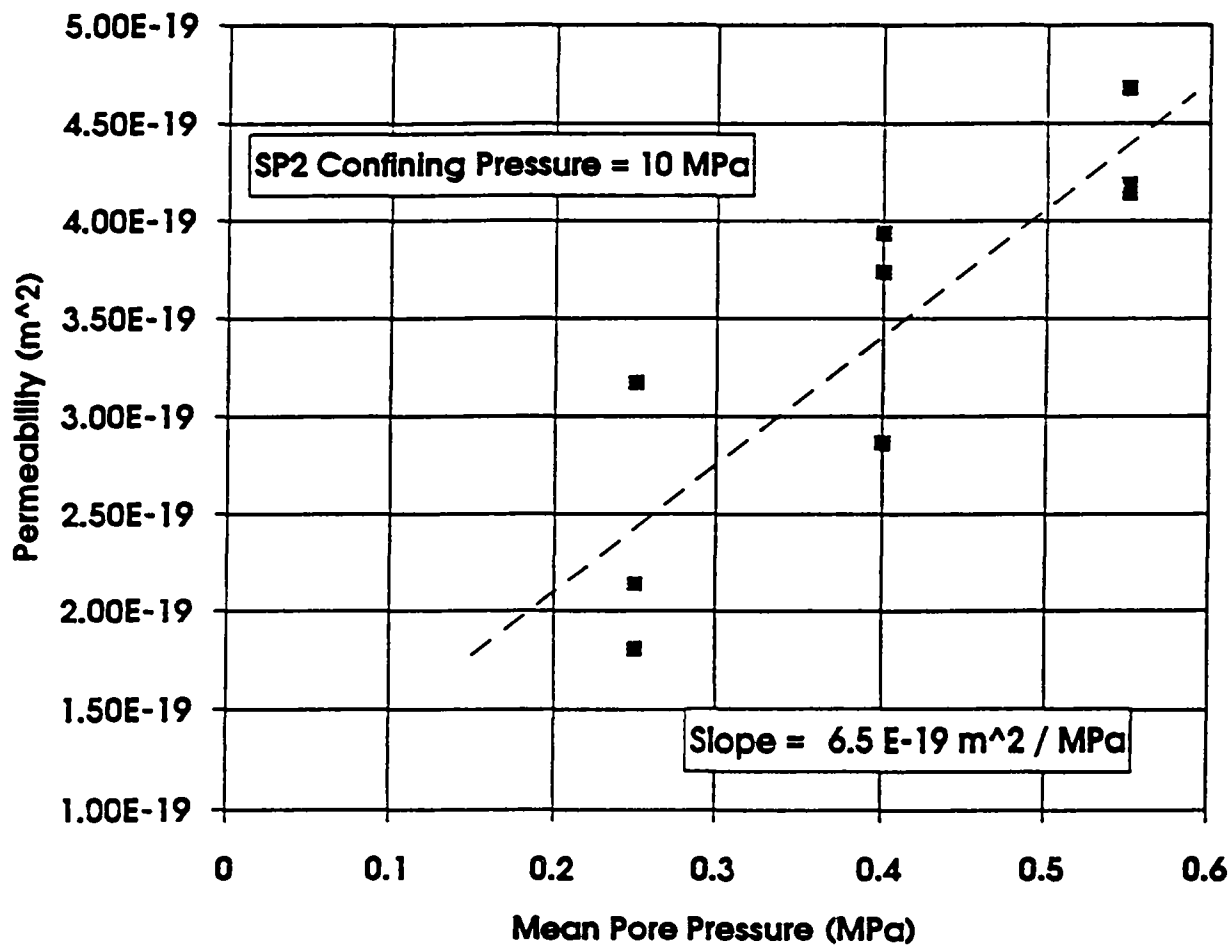
R81-248-03-118

Figure 4-22. Change in permeability with increasing mean pore pressure for Specimen P3X10-6-SP2 at a confining pressure of 2 MPa.



RSI-348-83-119

Figure 4-23. Change in permeability with increasing mean pore pressure for Specimen P3X10-6-SP2 at a confining pressure of 6 MPa.



RSI-348-93-120

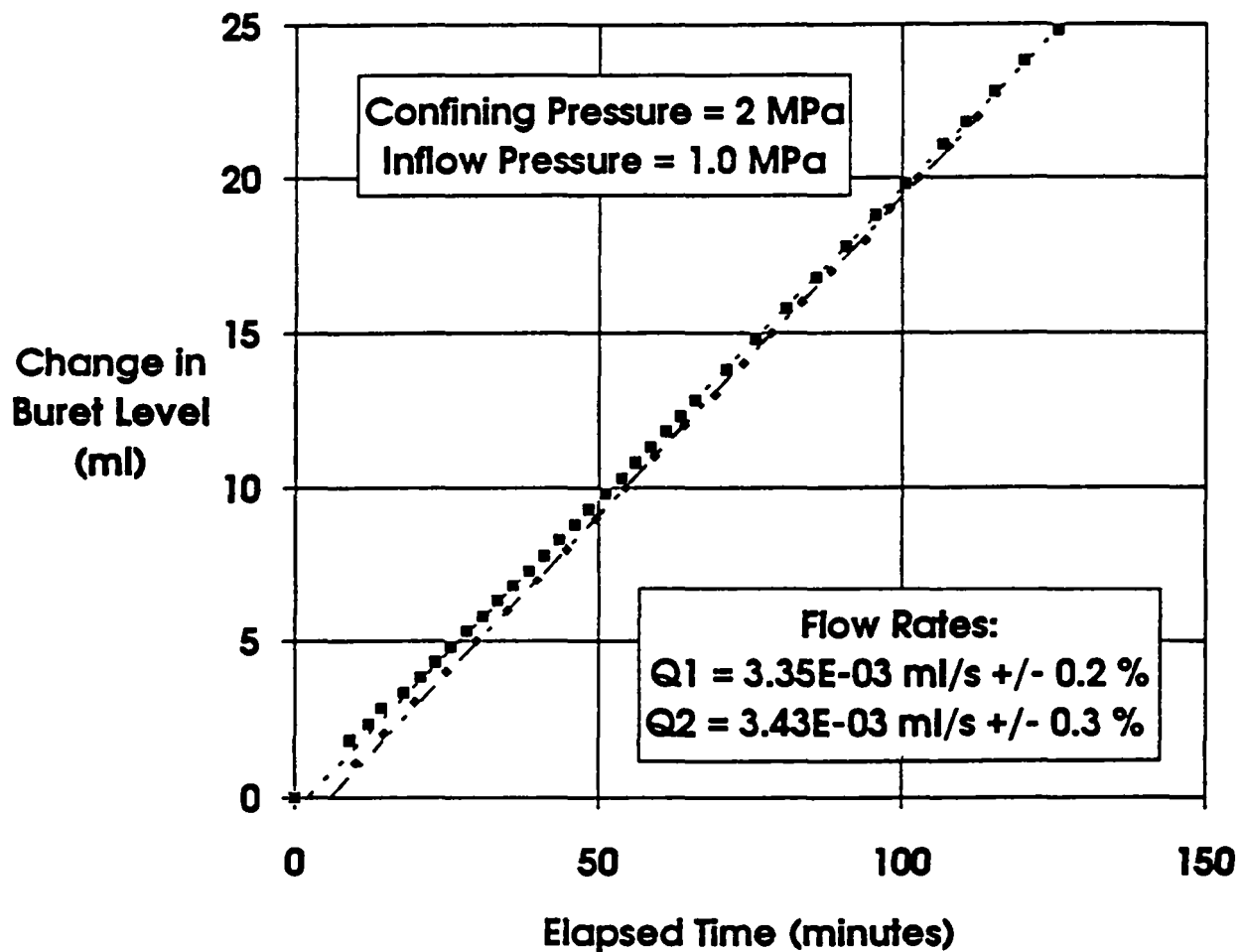
Figure 4-24. Change in permeability with increasing mean pore pressure for Specimen P3X10-6-SP2 at a confining pressure of 10 MPa.

permeability expected for a change in effective confining pressure. The slopes of the plots are $-4.2 \times 10^{-19} \cdot \text{m}^2 \cdot \text{MPa}^{-1}$, $-3.3 \times 10^{-19} \cdot \text{m}^2 \cdot \text{MPa}^{-1}$, and $-2.6 \times 10^{-19} \cdot \text{m}^2 \cdot \text{MPa}^{-1}$, for the three inlet pore pressures, respectively. (The average change in permeability with increasing effective confining pressure is $-3.4 \times 10^{-19} \text{ m}^2 \cdot \text{MPa}^{-1}$.) The changes in permeability observed to accompany changes in mean pore pressure for Specimen SP2 are $4.3 \times 10^{-18} \cdot \text{m}^2 \cdot \text{MPa}^{-1}$, $2.8 \times 10^{-18} \cdot \text{m}^2 \cdot \text{MPa}^{-1}$, and $6.5 \times 10^{-19} \cdot \text{m}^2 \cdot \text{MPa}^{-1}$, as seen in Figures 4-22 through 4-24. The changes in permeability caused by changes in effective confining pressure shown in Figures 4-19 through 4-21 are smaller in magnitude than the changes in permeability observed as a function of mean pore pressure (Figures 4-22 through 4-24). It is therefore unlikely that permeability changes due to effective pressure obscure permeability changes due to the Klinkenberg effect. The reason for the negative slope on Figures 4-13 through 4-15 remains undetermined.

4.5 Brine Permeability Measurements

Liquid permeability tests were run according to the test matrix shown in Table 1-2. An example of the flow data obtained from each test and the linear least square fitting that was performed to obtain flow rate is given in Figure 4-25. The complete set of figures showing flow data and linear least square fits for all brine permeability tests is given in Appendix I. Separate plots are given for each specimen at each confining pressure and gas inlet pressure. Replicate tests were only run at the first set of conditions imposed on Specimen SP1. Because the specimen saturation procedure had to be terminated due to specimen dissolution, the state of specimen saturation was unknown. The replicate test was run to ensure that the specimen had reached saturation and that the flow rate was stable. The replicate tests are shown in Figure 4-25 and are very reproducible in that the slopes differ by only 3 percent. The coefficient of variation for each linear least squares fit is given in the figure. Unfortunately, a jacket leak terminated testing on this specimen before tests could be run at confining pressures of 6 MPa and 10 MPa.

Flow rates and calculated permeabilities are summarized in Tables 4-11 through 4-13 for the three specimens, respectively. An error analysis was performed for the permeability calculation using the method given in ANSI/ASME (1986) and an example is given in Section F3 of Appendix B-F. The 95 percent uncertainty interval based on experimental uncertainties is approximately ± 5 percent. Flow rates are plotted versus brine pressure difference across Specimen SP1 in Figure 4-26 for tests at 2 MPa confining pressure. These data are given for Specimens SP2 and SP3 in Appendix J. None of the data are concave towards the pressure axis, showing that flow was not turbulent.



RSI-248-04-036

Figure 4-25. Change in exit buret level (brine volume)-versus-time for tests on Specimen P3X11-5-2-SP1 at 2 MPa confining pressure and 1 MPa brine inlet pressure. Symbols represent recorded data points and dashed lines are best fits to linear sections of data. The coefficients of variation for the linear least squares fits are given.

Table 4-11. Flow Data and Permeability to Brine for Marker Bed 139 Specimen SP1

Confining Pressure (MPa)	Brine Inlet Pressure ^(a) (MPa)	Specimen P3X11-5-2-SP1	
		Flow Rate (m ³ ·s ⁻¹ × 10 ⁻⁹)	Permeability (m ² × 10 ⁻¹⁷)
2	1.0	3.35	5.9
2	1.0	3.43	6.1
2	0.7	2.02	5.3
2	0.4	0.871	4.6
6	1.0	Test Terminated by Jacket Leak	Test Terminated by Jacket Leak

(a) Brine outlet pressure = 0.1 MPa for all tests.

Table 4-12. Flow Data and Permeability to Brine for Marker Bed 139 Specimen SP2

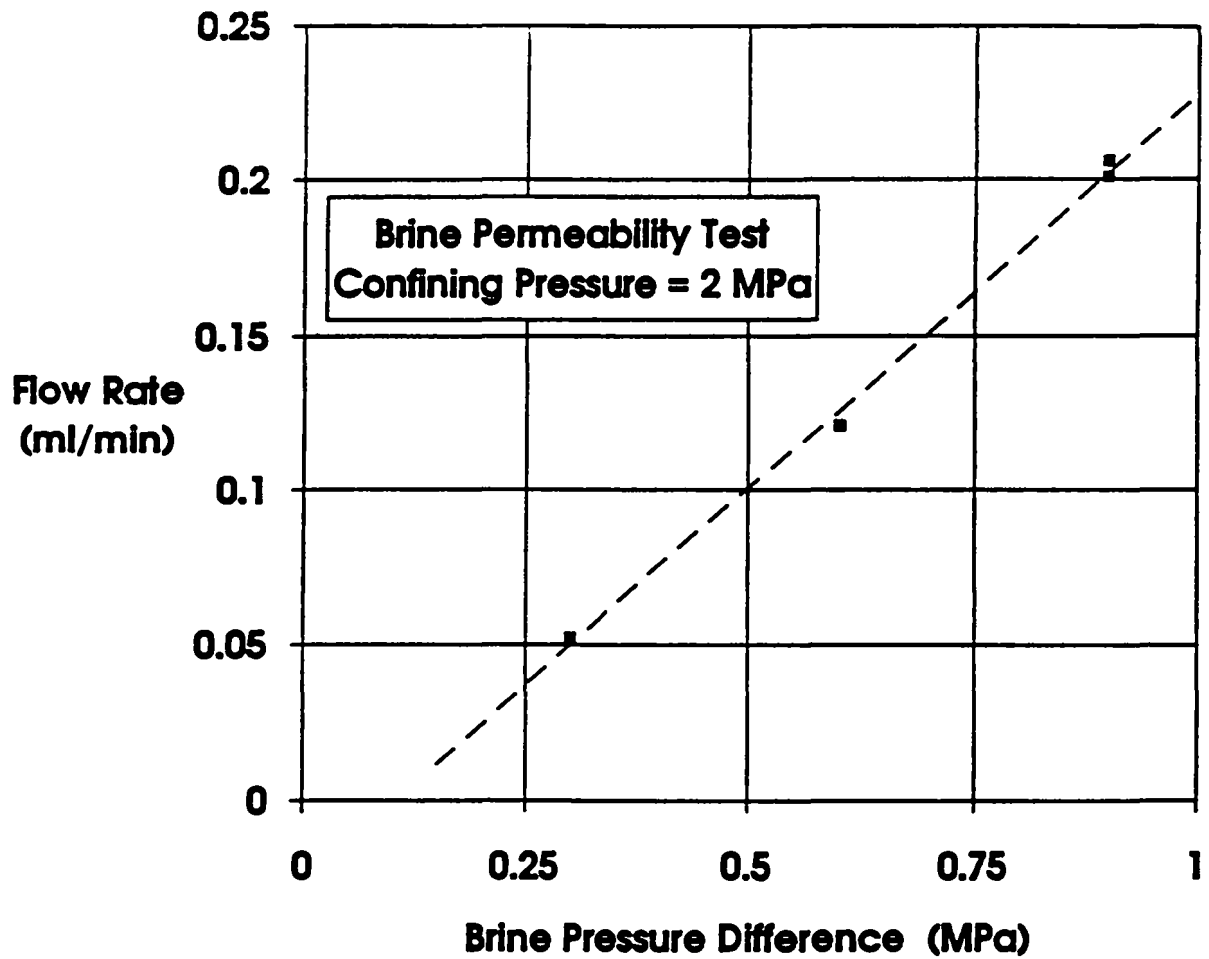
Confining Pressure (MPa)	Brine Inlet Pressure ^(a) (MPa)	Specimen P3X10-6-SP2	
		Flow Rate (m ³ ·s ⁻¹ × 10 ⁻¹¹)	Permeability (m ² × 10 ⁻¹⁹)
2	1.0	5.29	9.3
2	0.7	2.37	6.2
2	0.4	.672	3.5
6	1.0	1.16	2.0
6	0.7	0.519	1.4
6	0.4	0.187	0.98
10	1.0	0.462	0.81
10	0.7	0.233	0.61
10	0.4	0.084	0.44

(a) Brine outlet pressure = 0.1 MPa for all tests.

Table 4-13. Flow Data and Permeability to Brine for Marker Bed 139 Specimen SP3

Confining Pressure (MPa)	Brine Inlet Pressure ^(a) (MPa)	Specimen P3X11-5-3-SP3	
		Flow Rate (m ³ · s ⁻¹ × 10 ⁻⁹)	Permeability (m ² × 10 ⁻¹⁷)
2	1.0	5.54	9.7
2	0.7	2.99	7.9
2	0.4	1.22	6.4
6	1.0	2.61	4.6
6	0.7	1.63	4.3
6	0.4	0.617	3.2
10	1.0	1.56	2.7
10	0.7	0.981	2.6
10	0.4	0.378	2.0

(a) Brine outlet pressure = 0.1 MPa for all tests.



FBI-318-03-110

Figure 4-26. Flow rate-versus-brine pressure difference for Specimen P3X11-5-2-SP1 at 2 MPa confining pressure and all brine inlet pressures.

5.0 DISCUSSION OF RESULTS

5.1 Specimen Characterization

Some vertical and lateral heterogeneity in the marker bed can be inferred from the specimen characterization data. Specimens from the lowermost section of the marker bed, Specimens SP3T and SP3B, and samples from thin section block TS3 are enriched in anhydrite. SP3T and SP3B samples had an average anhydrite content of 57 percent as compared with averages of 12 percent for SP1T and SP1B, and 50 percent for SP2T and SP2B. Specimens from TS3 were 83 percent anhydrite, as compared with 59 percent for both TS1 and TS2. Samples from borehole P3X10 (SP2 and TS2) had the highest halite contents. Specimens SP2T and SP2B had an average halite content of 44 percent, whereas average halite content for Specimens SP1T and SP1B was 7 percent and for Specimens SP3T and SP3B was 38 percent. Specimens from thin section block TS2 averaged 37 percent halite as compared with 14 percent for TS1, and 15 percent for TS3. Comparison of data from the TS blocks shows that the uppermost section of the marker bed, TS2 from P3X10, is enriched in halite; however, it is difficult to distinguish between vertical and lateral heterogeneities in halite content from this data set.

5.2 Porosity

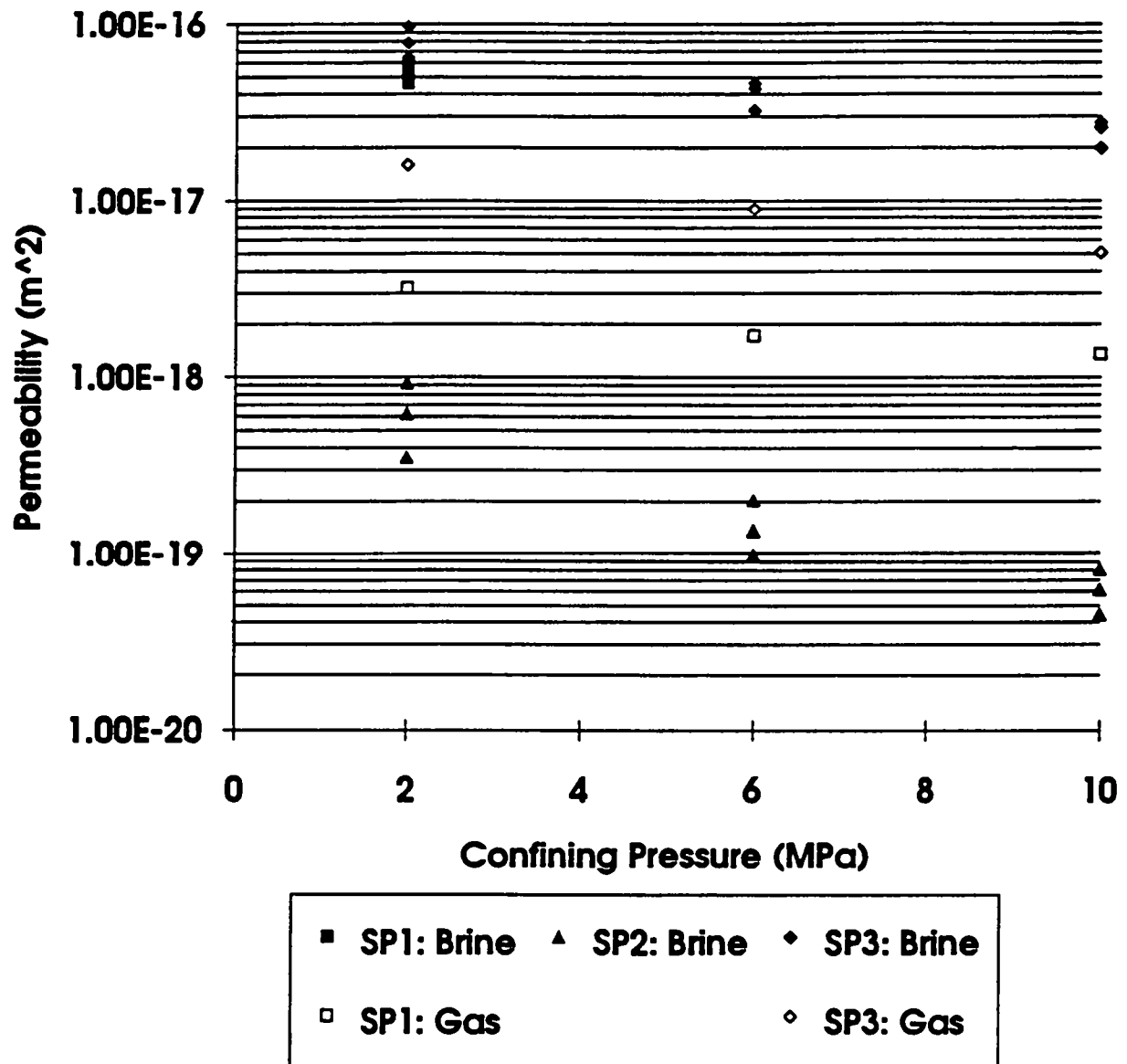
Effective porosity determinations were made for specimens taken from material directly above and below each permeability specimen axis. Because specimen axes were parallel to bedding, the porosity specimens were from the same horizon as each permeability specimen. Total porosities were measured only on the specimens taken from directly above the permeability specimen axis. Effective porosities ranged from a low of 1.0 percent to a high of 2.1 percent and total porosities ranged from 2.1 to 2.8 percent. The porosities of the different sections of the marker bed differ by about 1 percent porosity, which also happens to be the approximate measurement error. Because of the small sample size and large errors, any conclusions about heterogeneity in porosity are tenuous. A discussion of heterogeneity in porosity is included, however, for completeness. The uppermost section of the marker bed has the highest effective and total porosities. It has an average effective porosity of 1.9 percent, while the average effective porosity of the lower section from the same borehole was 1.4 percent. The total porosity for the uppermost section of the marker bed was 2.8 percent, while the lower section from the same borehole had a total porosity of 2.2 percent.

5.3 Permeability

Measured brine permeabilities and Klinkenberg-corrected gas permeabilities are shown in Figure 5-1 as a function of confining pressure. As expected, permeabilities decrease as confining pressure causes interconnected void space to contract. Values of Klinkenberg-corrected gas permeabilities range from $1.4 \times 10^{-18} \cdot \text{m}^2$ to $1.6 \times 10^{-17} \cdot \text{m}^2$ for MB 139 Specimens SP1 and SP3 (there are no Klinkenberg-corrected data for Specimen SP2). Brine permeability values are between $4.4 \times 10^{-20} \cdot \text{m}^2$ and $9.7 \times 10^{-17} \cdot \text{m}^2$ for the specimens tested. These values include the range of permeabilities ($8 \times 10^{-20} \cdot \text{m}^2$ to $5 \times 10^{-17} \cdot \text{m}^2$) inferred from in situ borehole tests (Davies, 1992). Brine permeabilities are higher than equivalent liquid permeabilities, probably because of the dissolution that occurred during the specimen saturation procedure. The brine and equivalent liquid permeabilities generally differ by less than one order of magnitude.

Specimen SP3 had the highest permeability, followed by Specimen SP1 even though Specimen SP1 contained a planar zone of cracks (see Section 2.1). These specimens were taken from the P3X11 borehole of MB 139 while Specimen SP2, with the lowest permeability, was taken from borehole P3X10. The differences in permeability between Specimen SP2 and Specimens SP1 and SP3 may reflect lateral rather than vertical variations in the properties of MB 139, although the two boreholes were only 0.61 m (2 feet) apart.

The test plan that guided this work included both specimen characterization and permeability determinations so that permeability differences could be correlated with differences in rock composition, porosity, and depth of origin. The lowest section of the P3X11 borehole (Specimen SP3) had the highest permeability and also the highest anhydrite content. Permeabilities are plotted versus anhydrite content in Figure 5-2. The anhydrite content given is that of the material taken from above and below the specimen axes. Only brine permeabilities determined at the lowest confining pressure are included in this figure and in Figures 5-3 through 5-8. (A jacket leak terminated brine permeability tests for Specimen SP1 and so only data obtained at comparable conditions on Specimen SP3 are included here.) The gas and brine permeabilities for borehole P3X11 (Specimens SP1 and SP3) appear to increase with anhydrite content. Anhydrite content is also high for the P3X10 specimen (Specimen SP2), however its permeability is low. Permeabilities were replotted versus the average anhydrite contents of specimens from blocks TS1, TS2, and TS3 (Figure 5-3), blocks taken from near Specimens SP1, SP2, and SP3. The composition of each thin section block is the average of four measurements whereas the compositions given in Figure 5-2 are the average of only 2 measurements. Specimen SP2 is now plotted at a much lower anhydrite content. It is possible that a larger sampling of material is required to obtain a representative composition and that once this composition is determined, a



RSI-248-94-028

Figure 5-1. Permeability-versus-confining pressure for all tests. Klinkenberg-corrected values are given for gas permeability tests.

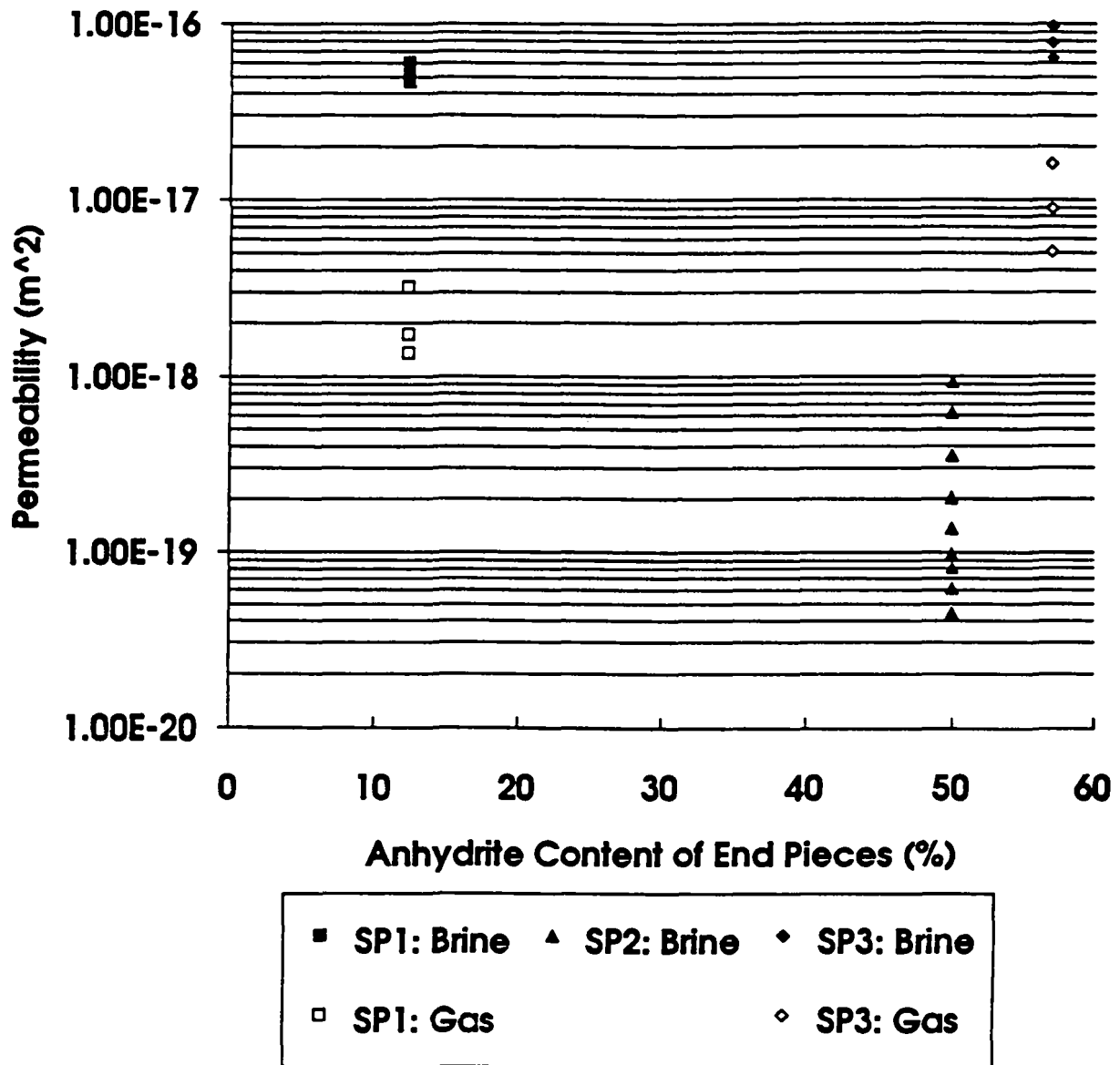
correlation between increasing permeability and increasing anhydrite content becomes more evident.

Specimen SP2 has the lowest permeability and also the highest halite content. Permeabilities are plotted versus halite content in Figure 5-4. The halite content given is that of the material taken from above and below the specimen axes. Surprisingly, the gas and brine permeabilities for borehole P3X11 increase with halite content. The halite content of the P3X10 specimen is very similar to one of the P3X11 specimens (44 percent versus 38 percent), yet its permeability is 2 orders of magnitude lower. Permeabilities were replotted versus the average halite contents of specimens from blocks TS1, TS2, and TS3 (Figure 5-5). The gas and brine permeabilities for borehole P3X11 still increase with halite content; however, with regard to the P3X10 specimen, Figure 5-5 shows the expected correlation between decreasing brine permeability and increasing halite content. It is possible that the larger sampling of material was required to obtain a representative composition. These data may imply that the high halite content in Specimen SP2 contributes to its low permeability.

Permeabilities were examined with respect to effective and total porosities and the data are given in Figures 5-6 and 5-7, respectively. Surprisingly, for the P3X11 specimens, gas and brine permeabilities decrease slightly as porosities increase. It is possible that a larger sampling of material is needed to accurately determine the porosities. The P3X10 specimen has the lowest permeability and lowest porosity, indicating that low porosity may contribute to its low permeability; however, total porosities are similar for this specimen and for one P3X11 specimen, yet they differ in permeability by 2 orders of magnitude.

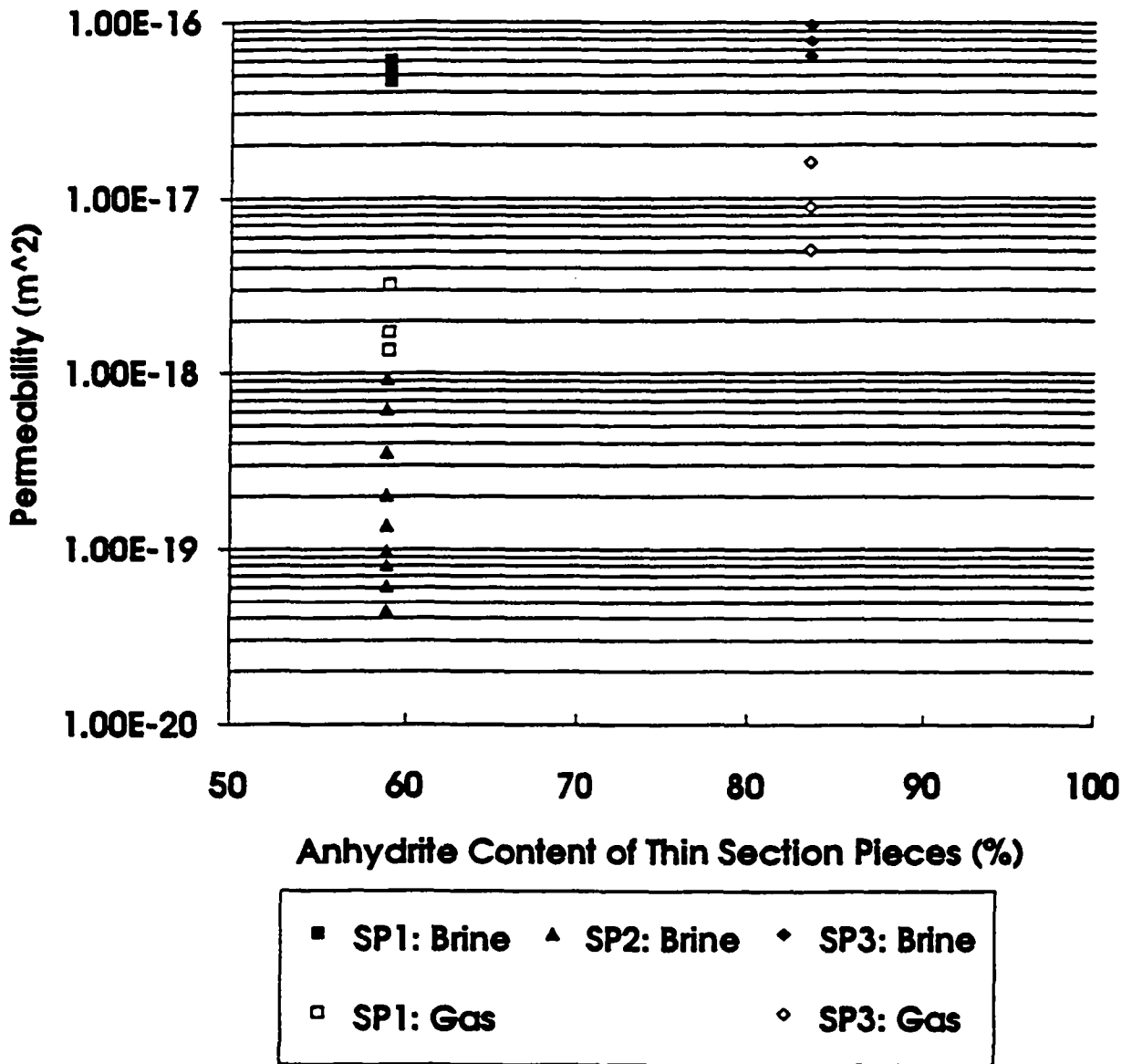
Lastly, permeabilities were viewed with respect to the depth of origin of the specimen and the data are given in Figure 5-8. Gas and brine permeabilities increase with depth for specimens taken from borehole P3X11. The P3X10 specimen and one P3X11 specimen (SP1) were recovered from depths that differ by only 0.061 m, yet brine permeabilities differ by approximately 2 orders of magnitude. The specimen radii were only 0.050 m and so part of both specimens were taken from the same stratigraphic layer.

Permeabilities do not strongly correlate with any single material characteristic such as porosity, halite content, or anhydrite content; however, these material characteristics may contribute to spatial variations in permeability. Fluid flow in rock occurs through the interconnected void space. Heterogeneity of this void space either is not strongly correlated with any single material characteristic measured here, or the data obtained was insufficient in quantity for a correlation to be apparent.



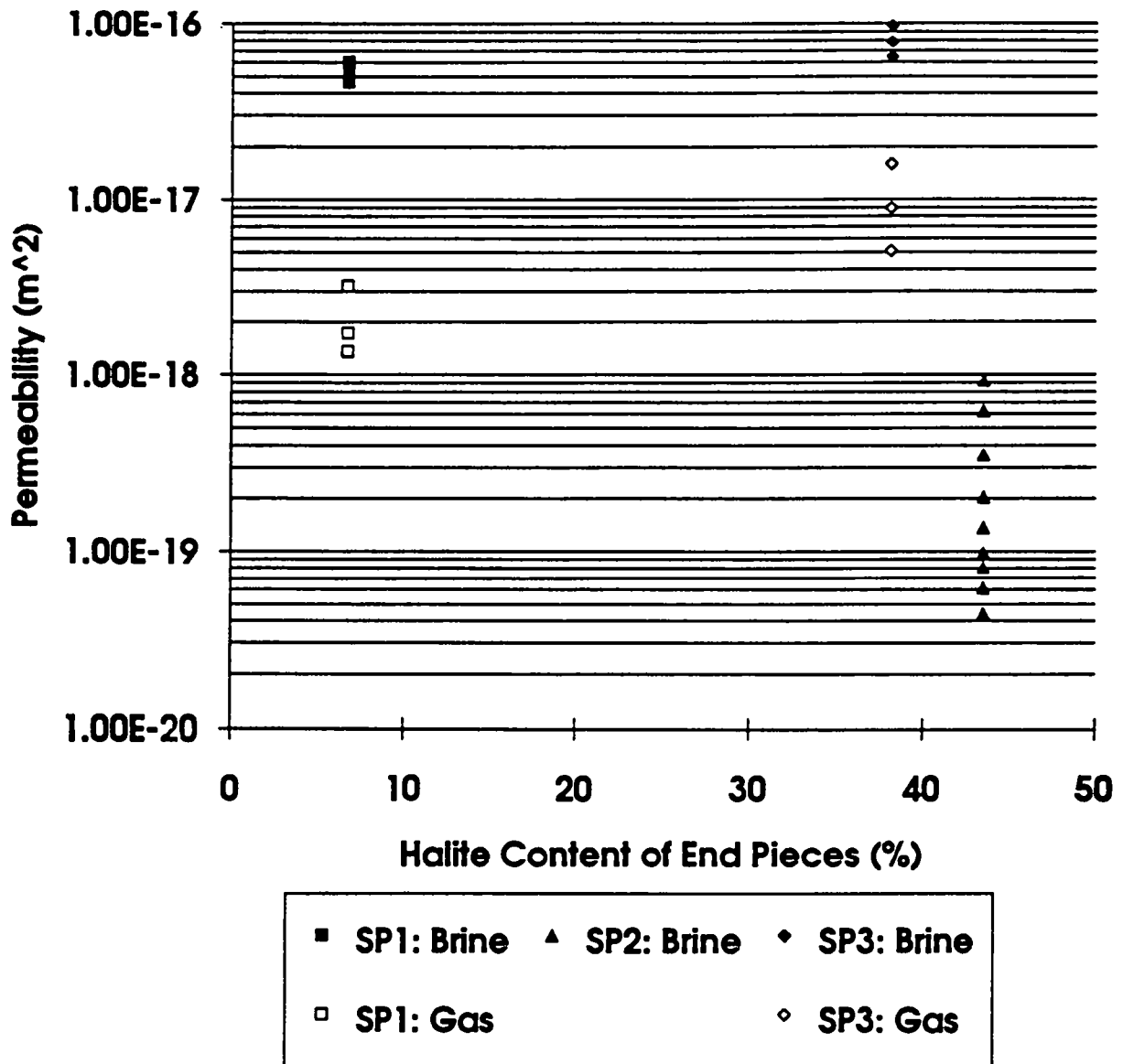
RSI-248-04-029

Figure 5-2. Permeability-versus-average anhydrite content of material taken from above and below specimen axes. Only data obtained at 2 MPa confining pressure are shown for Specimens SP1 and SP3.



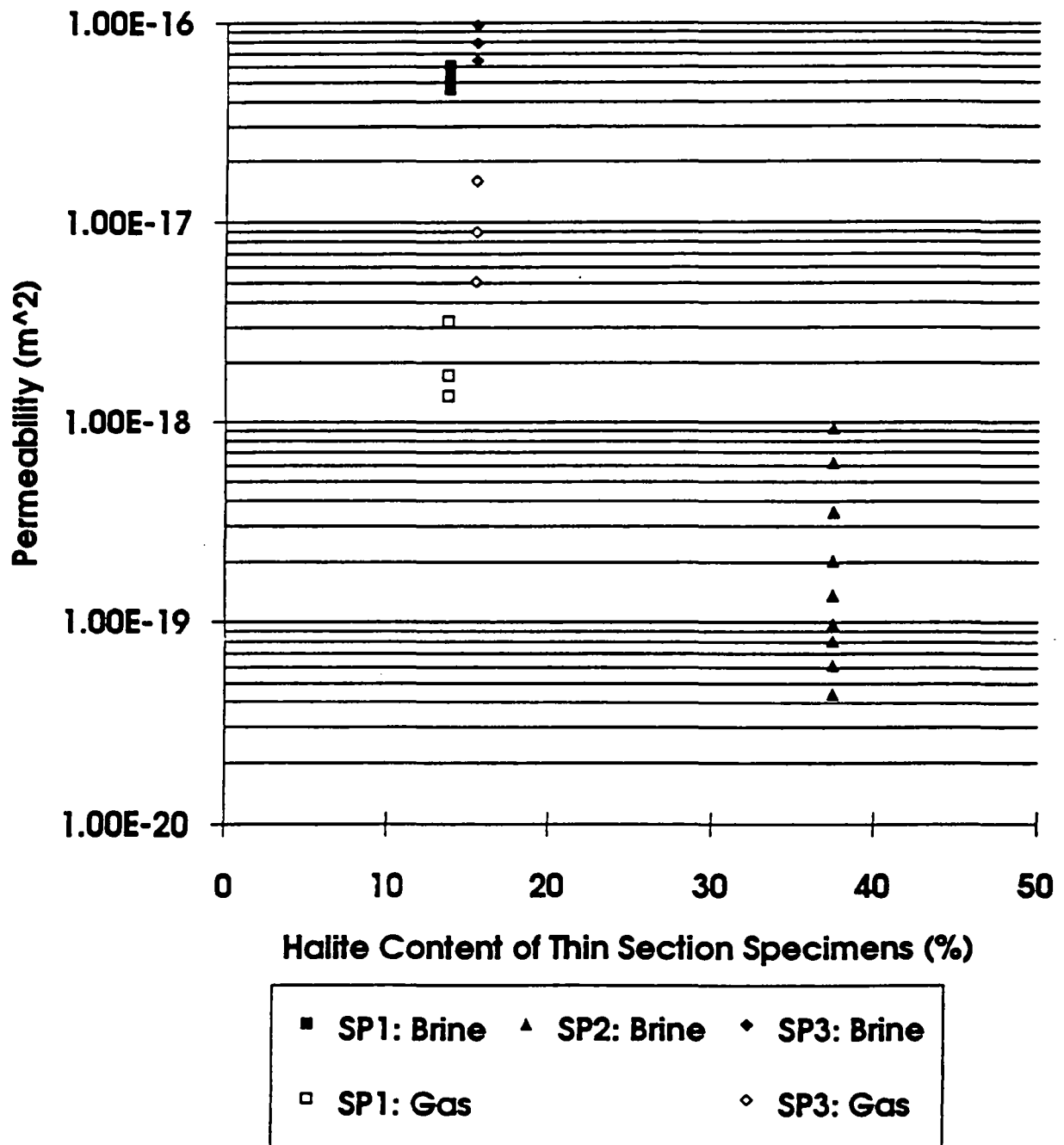
RSI-248-04-030

Figure 5-3. Permeability-versus-average anhydrite content of Blocks TS1, TS2, and TS3. Only data obtained at 2 MPa confining pressure are shown for Specimens SP1 and SP3.



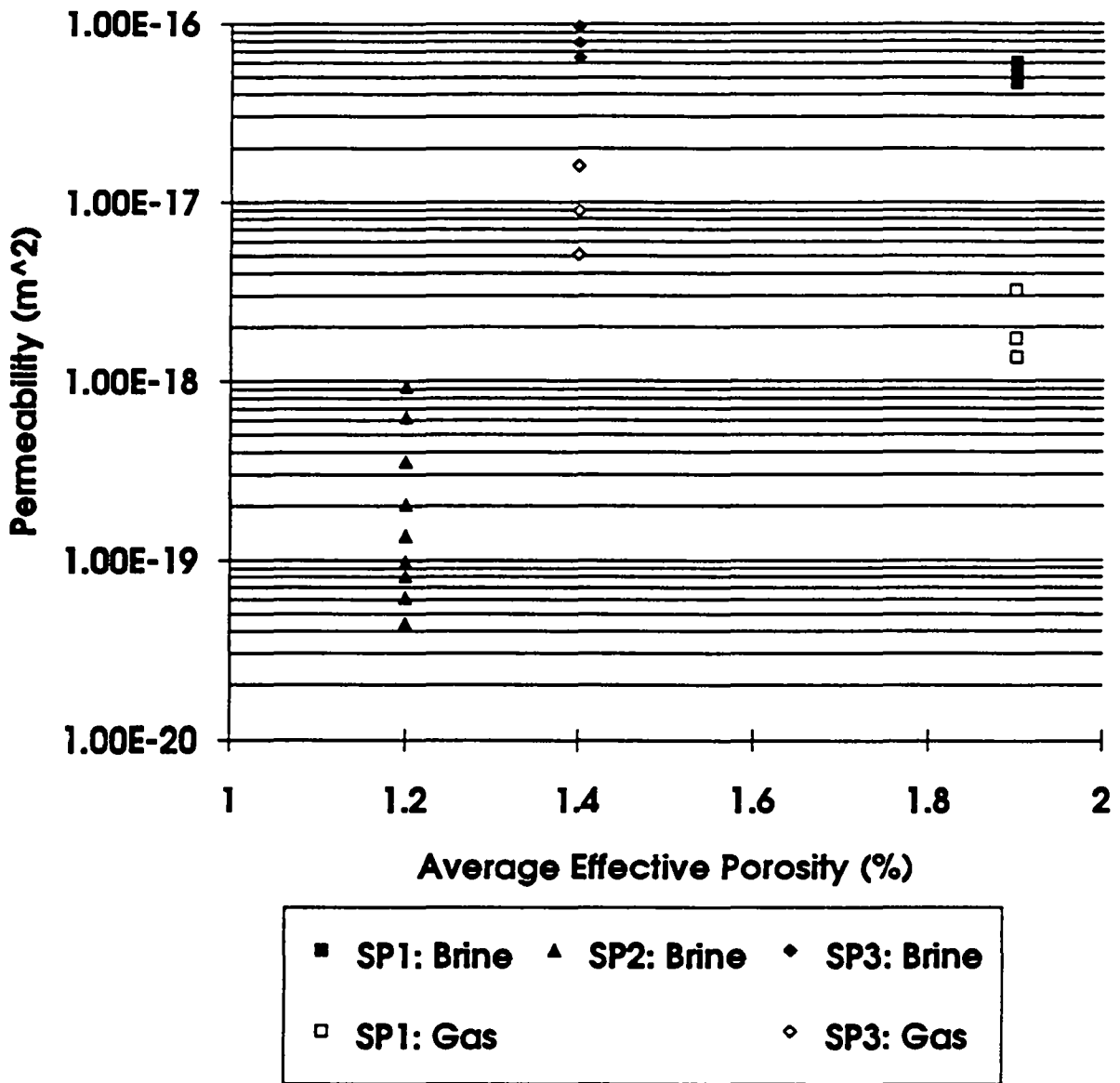
RSI-248-04-031

Figure 5-4. Permeability-versus-average halite content of material taken from above and below specimen axes. Only data obtained at 2 MPa confining pressure are shown for Specimens SP1 and SP3.



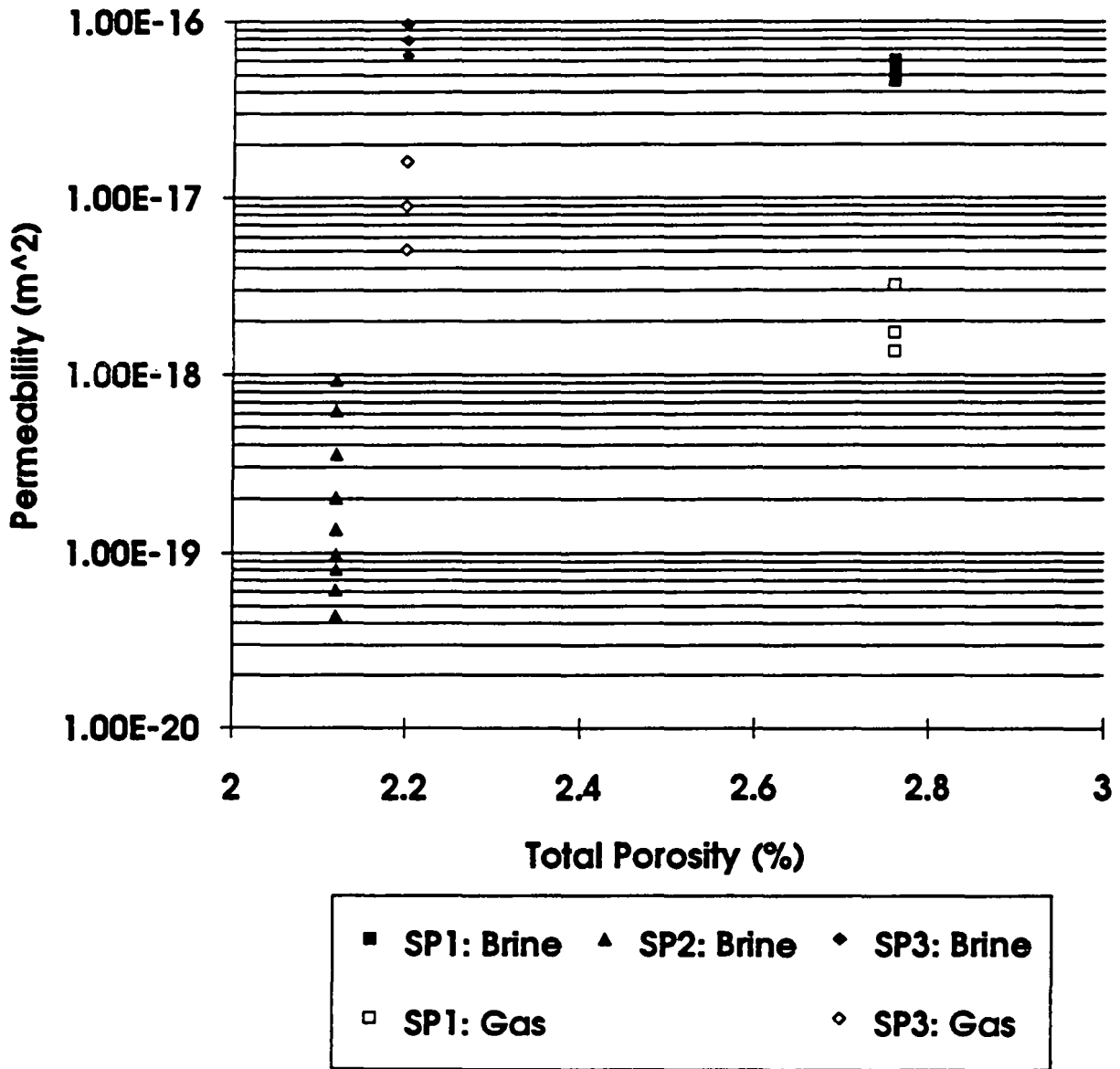
RSI-248-04-035

Figure 5-5. Permeability-versus-average halite content of Blocks TS1, TS2, and TS3. Only data obtained at 2 MPa confining pressure are shown for Specimens SP1 and SP3.



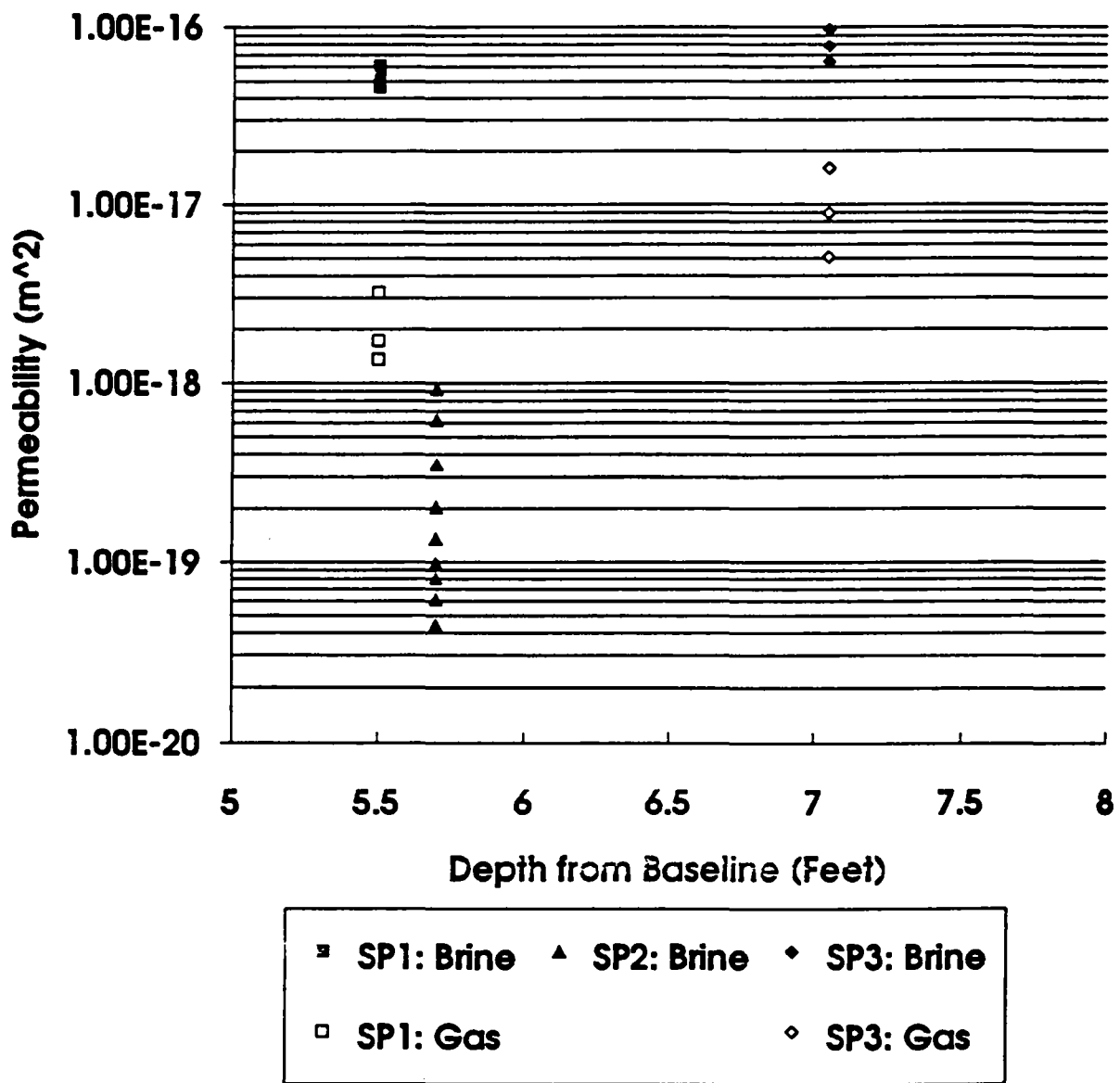
RSI-248-04-032

Figure 5-6. Permeability-versus-average effective porosity of specimens taken from above and below axes of permeability specimens. Only data obtained at 2 MPa confining pressure are shown for Specimens SP1 and SP3.



RSI-248-04-033

Figure 5-7. Permeability-versus-total porosity of specimens taken from above axes of permeability specimens. Only data obtained at 2 MPa confining pressure are shown for Specimens SP1 and SP3.



RBI-248-04-034

Figure 5-8. Permeability-versus-depth of origin of each specimen. Only data obtained at 2 MPa confining pressure are shown for Specimens SP1 and SP3.

6.0 SUMMARY AND CONCLUSIONS

Single-phase brine and nitrogen permeabilities were measured in the laboratory for specimens of Marker Bed 139 taken from the underground workings at the Waste Isolation Pilot Plant. The test plan was designed to provide data to evaluate the causes of spatial variations in permeabilities. Auxiliary measurements therefore included assessment of coring-induced damage, the porosities and mineralogies of materials immediately adjacent to each permeability specimen, and the mineralogies of additional specimens taken from near each permeability specimen. The same specimens were used for both gas and liquid permeability tests to facilitate comparison of results. Two of the three permeability specimens were from the upper and lower sections of borehole P3X11, and these were spaced 0.61 m apart, vertically. The third permeability specimen was from the upper/central region of adjacent borehole P3X10 and its in situ location was 0.06 m below and 0.61 m across from the uppermost specimen from borehole P3X11. Material was taken from immediately above and below the axis of each permeability specimen and used for quantitative analysis by X-ray diffraction and also for measurements of effective and total porosities. Additional blocks of material were taken from near each specimen and these were sectioned for petrographic analysis and for X-ray diffraction studies.

A quantitative analysis of crack occurrence near the surfaces and centers of cored specimens was conducted because coring-induced surface damage, if present, could affect permeability measurements. Although the data indicated that higher crack densities were associated with the specimen edges than with the midsections, the difference in crack densities was not statistically significant.

All permeability and porosity specimens were dried before testing at 60°C and 45 percent relative humidity to prevent dehydration of any clay components. Effective porosities were then measured by Core Laboratories using a helium porosimeter. These specimens were returned to RE/SPEC Inc., dried again at 60°C and 45 percent relative humidity to ensure that moisture contents were stable, and used for measurements of total porosity using gravimetric methods. Effective porosities ranged from 1.0 percent to 2.1 percent while total porosities ranged from 2.1 percent to 2.8 percent. (The errors in porosity measurements are approximately ± 1 percent porosity.) Effective and total porosities were both highest for the uppermost section of the marker bed.

A total of 81 gas permeability and 22 brine permeability measurements were made. Confining pressures of 2 MPa, 6 MPa, and 10 MPa were used and for each value of confining

pressure, permeability measurements were made at inlet pore pressures of 0.4 MPa, 0.7 MPa, and 1.0 MPa and at an outlet pore pressure of 0.1 MPa. One specimen (P3X11-5-2-SP1) experienced a jacket leak during brine permeability measurements and so no data were collected at 6 MPa and 10 MPa confining pressure. The relationship between flow rate and pore pressure difference was checked for linearity at each confining pressure to ensure that the measurements were made in the laminar flow regime. Gas permeability data were corrected for Klinkenberg effects to determine the equivalent liquid permeability at each confining pressure.

Permeabilities to nitrogen and brine each span approximately 2 to 2.5 orders of magnitude. Permeabilities to gas ranged from approximately $1.8 \times 10^{-19} \text{ m}^2$ to $2.5 \times 10^{-17} \text{ m}^2$ and the Klinkenberg-corrected equivalent liquid permeabilities ranged from $1.4 \times 10^{-18} \text{ m}^2$ to $1.6 \times 10^{-17} \text{ m}^2$. Permeabilities to brine ranged from $4.4 \times 10^{-20} \text{ m}^2$ to $9.7 \times 10^{-17} \text{ m}^2$. Permeabilities to brine were higher, perhaps because of some specimen dissolution that occurred during saturation and after completion of the gas permeability tests. The laboratory data include the range of permeability values indicated by field measurements, $8 \times 10^{-20} \text{ m}^2$ to $5 \times 10^{-17} \text{ m}^2$ (Davies et al., 1992).

These data show lateral and vertical variations in permeability for MB 139. The highest permeabilities were measured in the lowermost section of P3X11, while the lowest permeabilities were measured for the central to upper region of adjacent borehole P3X10. The data presented here are limited in extent and additional work must be performed to fully assess the causes of spatial variations in permeability. The specimen with the lowest permeability had the highest halite content and the lowest porosity; however, its porosity and halite content were not substantially different from those of the specimen with the highest permeability. The specimen with the highest permeability also had the highest anhydrite content, however, its anhydrite content did not differ substantially from that of the specimen with the lowest permeability. Permeability values do not strongly correlate with any single material characteristic such as porosity, halite content, or anhydrite content; however, these material characteristics may contribute to spatial variations in permeability. Fluid flow in rock occurs through the interconnected void space. Heterogeneity of this void space either is not strongly correlated with any single material characteristic measured, or the data obtained was insufficient in quantity for a correlation to be apparent.

7.0 REFERENCES

- ANSI/ASME, 1986. *Part 1 Measurement Uncertainty, Instruments and Apparatus*. PTC 19.1-1985. New York, NY: American Society of Mechanical Engineers.
- ASTM. 1989. "Standard Test Method for Specific Gravity of Soils." *Annual Book of ASTM Standards*, Standard D854-83. Vol. 4.08. Philadelphia, PA: ASTM.
- ASTM. 1989. "Standard Test Method for Permeability of Rocks by Flowing Air." *Annual Book of ASTM Standards*, Standard D4525. Vol. 4.08. Philadelphia, PA: ASTM.
- Brodsky, N.S., 1993. *Hydrostatic and Shear Consolidation Tests With Permeability Measurements on Waste Isolation Pilot Plant Crushed Salt*. SAND93-7058. Albuquerque, NM: Sandia National Laboratories.
- Brodsky, N.S., 1990. *The Effect of Brine Injection on the Creep of WIPP Salt During Laboratory Tests*. SAND90-2367. Albuquerque, NM: Sandia National Laboratories.
- Chowdiah, P. 1988. "Influence of Water-Desaturation Technique and Stress on Laboratory Measurement of Hydraulic Properties of Tight Sandstones," *SPE Formation Evaluation*. December, 679-685.
- Costin, L.S., Wawersik, W.R., 1980. *Creep Healing of Fractures in Rock Salt*. SAND80-0392. Albuquerque, NM: Sandia National Laboratories.
- Gilpatrick, L.O., C.G. Baes, A.J. Shor, and C.M. Canonico, 1982. *The Permeability of Salt-Crystal Interfaces to Brine*. ORNL-5874. Oak Ridge, TN: Oak Ridge National Laboratories.
- Davies, P.B., L.G. Brush, M.A. Molecke, F.T. Mendenhall, and S.W. Webb, eds., 1991. *Waste-Generated Gas at the Waste Isolation Pilot Plant: Papers Presented at the Nuclear Energy Agency Workshop on Gas Generation and Release From Radioactive Waste Repositories*. SAND91-2378. Albuquerque, NM: Sandia National Laboratories.
- Howarth, S.M. 1993. *Conceptual Plan: Two-Phase Flow Laboratory Program for the Waste Isolation Pilot Plant*. SAND93-1197. Albuquerque, NM: Sandia National Laboratories.

Holcomb, D.J. and M. Shields, 1987. *Hydrostatic Creep Consolidation of Crushed Salt With Added Water*. SAND87-1990. Albuquerque, NM: Sandia National Laboratories.

Hurlbut, C.S., 1971. *Dana's Manual of Mineralogy*. New York, NY: John Wiley & Sons.

IT Corporation, 1987. *Laboratory Investigation of Crushed Salt Consolidation and Fracture Healing*. BML/ONWI-631. Columbus, OH: Office of Nuclear Waste Isolation.

Klinkenberg, L.J., 1941. "The Permeability of Porous Media to Liquids and Gases," *API Drilling and Production Practice*. 200-213.

Stone and Webster Engineering Corporation, 1983. *Preliminary Assessment of the Healing of Fractures in Salt*. ONWI-363. Columbus, OH: Office of Nuclear Waste Isolation.

Stormont, J.C. and J.J. Daemen, 1992. "Laboratory Study of Gas Permeability Changes in Rock Salt During Deformation," *International Journal of Rock Mechanics Mining Science and Geomechanical Abstracts*. Vol. 29, No. 4, 325-342.

Sutherland, H.J. and S.P. Cave, 1980. "Argon-Gas Permeability of New Mexico Rock salt Under Hydrostatic Compression," *International Journal of Rock Mechanics Mining Science and Geomechanical Abstracts*. Vol. 17, 281-288.

Weast, R.C., ed. 1974. *Handbook of Chemistry and Physics*. Cleveland, OH: CRC Press.

APPENDIX B.A
SOUTH DAKOTA SCHOOL OF MINES AND TECHNOLOGY
PETROGRAPHIC ANALYSIS PROCEDURE AND RESULTS

ENGINEERING AND MINING EXPERIMENT STATION
REPORT OF ANALYSES
Optical Microscopy Laboratory - PLM Section

March 19, 1993

CLIENT: RE/SPEC, Inc.
Rapid City, SD
ATTN: Tom Pfeifle

PROCEDURES: Analysis of thin sections provided by RE/SPEC on 25mm slides. Several correlated with the XRD samples. Analysis was completed by polarizing microscopy at 100X magnification, with 550 m retardation enhancement. Counting was by areal element fraction using a Porton reticle. Six rectangles, each of area 3.256×10^{-4} , of the reticle were used. Three traverses across the section included 10 stops each, for a total of 60 Porton fields per traverse (180 per section). The percentages of table 1 are areal percentages and are equivalent to volume percentages. Because of the similar densities of the components, the percentages are approximately equivalent to weight percentages.

RESULTS:

The components found in these sections are: anhydrite, halite, polyhalite, magnesite, and carbonaceous matter (?). The latter consisted of small but areal significant specks or patches of opaque brown to black material; no orthoscopic or conosopic properties could be obtained from this latter component; it here tentatively identified as carbon. Anhydrite was distinguished by its moderate retardation colors and good crystal shape and cleavage traces. Polyhalite was distinguished by the feathery growth habit and low (gray to first-order yellow) retardation colors. Magnesite occurred as tiny 1-5 m sized equant grains of high relief and retardation color. Halite is transparent but isotropic and could be easily distinguished from all other components; however, some of the halite appeared to have been lost during thin section preparation, leaving holes (also transparent and "isotropic") which are believed to have contained halite. Therefore, obvious holes were included in the halite count. The following table contains the summary of the volume percentages for these samples.

TABLE 1. Summary of Volume Percentages, Evaporite Thin Sections¹

EMES ID	RE/SPEC ID	ANHYD	HALITE	POLYHA	MAGNES	CARBON
923.0854 (0849)	P3X11-5-3-2-TS1-1	70.4 ± 10.2	15.9 ± 2.6	9.6 ± 7.4	2.0 ± 0.06	2.2 ± 1.9
923.0859 (0849)	P3X11-5-3-2-TS1-2	45.8 ± 10.5	13.4 ± 2.3	30.6 ± 6.7	9.4 ± 4.2	0.8 ± 0.6
923.0855 (0849)	P3X11-5-3-2-TS1-3	48.9 ± 12.6	26.7 ± 6.8	14.9 ± 4.4	8.0 ± 3.1	1.6 ± 0.3
923.0852 (0844)	P3X10-5-3-2-TS2-1	67.8 ± 17.6	24.5 ± 19.4	0	3.5 ± 2.5	4.2 ± 0.9
923.0857 (0844)	P3X10-5-3-2-TS2-2	43.1 ± 3.7	54.8 ± 4.1	0	0.6 ± 0.03	1.6 ± 0.7
923.0858 (0844)	P3X10-5-3-2-TS2-3	58.2 ± 3.9	37.2 ± 3.9	0	3.0 ± 0.7	1.6 ± 0.3
923.0856 (0850)	P3X11-6-TS3-1	95.9 ± 3.7	1.4 ± 2.4	0.6 ± 1.1	0.6 ± 0.2	0.2 ± 0.04
923.0851 (0850)	P3 X11-6-TS3-2	89.9 ± 0.8	8.8 ± 1.3	0	0	1.4 ± 0.5
923.0853 (0850)	P3 X11-6-TS3-3	66.7 ± 8.5	31.9 ± 9.3	0	0.4 ± 0.7	1.0 ± 0.2

Values are volume percentages with standard deviations for the three traverse counts given as ± below. XRD samples correlating with optical samples are given in parentheses below EMES ID number.

APPENDIX B.B
SOUTH DAKOTA SCHOOL OF MINES AND TECHNOLOGY
X-RAY DIFFRACTION PROCEDURE AND RESULTS

B.B-1. X-RAY DIFFRACTION PROCEDURES

QUALITY ASSURANCE PROCEDURES - EMES X-RAY DIFFRACTION LABORATORY

Sept. 26, 1992

1. General Aspects

The quality assurance used in the EMES x-ray diffraction laboratory consist of sample custody procedures, sample preparation procedures, and instrument performance checks. In addition, uncertainties in analytical results are estimated using standard variance error propagation of measurement and computational errors in the full quantitative analysis (RIM) method. The XRD Laboratory manager (B.L. Davis) acts as the quality assurance officer for all XRD analytical work.

2. Sample Custody

Samples mailed or otherwise delivered to EMES are logged in according to date received and assigned an identification number. A lab work order is prepared with the i.d. numbers listed and placed with the samples in the lab cabinet. The analyst conducts the analyses in sequence of i.d. number, always maintaining proper labeling and association of filter preparations with the parent samples. Samples are stored for a minimum of 30 days before discarding, but kept longer on request. The custody log book also records date of completion of analysis and date of payment by the client.

3. Instrument Calibration Checks

3.1. X-ray Transmissometer

Weekly transmission measurements are completed on a "Quartz" filter standard. The direct-beam transmissometer attenuation plate, tube power settings, cycle number, maximum open beam intensity, filter transmission ratio, standard deviation, and operator initials and time/date of check are all recorded in the QA calibration log. Adjustments are made to correct misalignment, pulse-height-analyzer settings, or attenuation factors whenever the standard deviation of the filter standard transmission ratio for the 13 cycles exceeds 0.5%

3.2. X-ray Diffractometer

3.2.1. General Instrument alignment - A novaculite standard is scanned weekly at 100 sec/deg rate at 40/20 kV/mA power over the 101 quartz line. Pulse-height-analyzer settings, tube power, detector voltage, integrated intensity, and background integrated intensity are logged for each scan. Minor misalignment generally requires adjustments only to the graphite monochromator, more serious misalignment requires 2:1 settings and sample-height changes; this action has not been required for over 20 years.

3.2.2. Low angle alignment - A special NIST silver behenate low-angle standard has become available during the past several months. This laboratory now has prepared a standard for the Philips diffractometer that is used on all routine projects. The first low-angle adjustment was made on Sept. 19, 1992 which materially improved the sensitivity of large-spacing materials, such as glycolated smectite clays and organic compounds. Low-angle alignment will be checked on a monthly basis.

3.3. Other analytical equipment

This laboratory supports its qualitative and quantitative XRD work with polarizing light microscopy (PLM). While no periodic QA procedure is used here, some optical alignment and stage centering adjustments are made on an "as needed" basis. Electronic balances are checked periodically using standard weight sets and filter specific mass checks on Whatman GF/C 42.5-cm filters (the latter are exceptionally uniform in their composition and weight properties).

4. Analytical Procedures

4.1. General Approach

Detailed operator instructions for x-ray transmission (needed for mass absorption measurements), x-ray diffraction scanning, and data reduction from instrument computers are maintained in the laboratory. Staff have their individual copies as well. The method EMES most often uses for quantitative XRD analysis is the RIM (Reference Intensity Method); calibration curves for light filter loadings of free silica are also used. Where amorphous components are identified, mass absorption measurements (by XRT) alone, or combined with PLM measurements allow complete quantitative analysis of crystalline and amorphous components of the sample.

A flow-diagram schematically illustrating the path of a bulk sample from particle size reduction to final analysis is illustrated in Fig. 1. This particular flow diagram illustrates the procedures for small filters; large filters (8" X 10", for example) are treated similarly except that several filter circles are cut from the large filter and analyzed or ultrasonic stripping of the particles is first completed to concentrate the sample onto a smaller area.

4.2. Procedures for Free Silica (Quartz and Cristobalite)

Our capability currently exists for routine quantitative analysis for α -quartz and α -cristobalite. Tridymite analysis can be completed as well by full RIM analysis, but a calibration curve has not been developed. Quantitative analysis of free silica can be completed by two methods: (1) Full component analysis by the RIM procedures, and (2) thin-layer calibration curve analysis.

4.2.1. Reference Intensity Method (RIM)

For bulk materials the analysis procedure is:

- a. Reduce the sample particles to 10-micron mean diameter or less.
- b. Load the powder onto preweighed Whatman GF/C filters using aerosol (TASC) suspension (Davis, 1986). Take another weighing.
- c. Complete a direct-beam x-ray transmission (XRT) measurement for mass absorption determination ((Davis and Johnson, 1987).
- d. Weigh the sample again to check for losses during XRT analysis.

- e. Cut the filter to 2.5-cm diameter, mount on pedestal and scan by XRD from 3° to 60° 2θ at 40/20 power, CuK α radiation.
- f. Identify components and measure intensities of analytical peaks. Determine overlaps on the component peaks used for analysis. All XRT and XRD data are entered on a RIM analysis log and entered into appropriate computer programs. Output will consists of weight fractions and associated variance errors (Davis, 1981) of all components, calculated mass absorption and density parameters, and a oxide/element table obtained from computer files for each compound found in the analysis.

For ambient filter loads the procedure is:

- a. Cut the filter into 7-cm circles, dry and weigh the circles.
- b. Strip the particles from the circles in a methanol bath using ultrasound.
- c. Dry and weigh the stripped circles. This provides the amount of glass fiber brought down with the particles when accurate tare and load weights of the parent filter are available.
- d. Deposit all or a portion of the methanol suspension onto another filter (Whatman GF/C or Metrical VM-1, depending on sample amount available).
- e. Complete mass absorption analysis by either XRT or by substrate diffraction (depending on filter size and sample amount).
- f. Complete scans and data analysis as in steps d-f for bulk materials.

4.2.2 Calibration procedure.

In this procedure loads must be kept to within $300 \mu\text{gm cm}^{-2}$ on teflon (PTFE) filters in order to eliminate absorption by the sample. The procedure is relatively simple, however.

- a. Weigh a 37-mm PTFE filter and load with aerosol using the TASC system. Reweigh the filter to obtain total mass deposited.
- b. Complete a scan of the novaculite standard at step/dwell conditions matching those of the original scan when the calibration curve was determined.
- c. Complete a full scan and then a scan at $0.25^{\circ} \text{min}^{-1}$ over the quartz and/or cristobalite peaks pertaining to the calibration curve.
- d. Measure the integrated intensities of both quartz/cristobalite peaks and novaculite standard; correct for overlaps on the quartz peaks; adjust the intensities of the analyte peaks, if necessary to match conditions of the original novaculite standard.

- e. Use the calibration curve equation to determine the specific mass of analyte present. Dividing this value by the specific mass from the tared filter and loaded filter weights provides the final weight percent analyte.

Figures 2 and 3 present the calibration curves currently used in this laboratory. Regression lines are shown, and in the case of quartz, subsequent quality control analyses points (+ symbols) indicating continued validity of the curve. For quartz $R = 0.980$ and for cristobalite $R = 0.996$.

The preferred (and least expensive) procedure, where sample amount is sufficient (or ambient filter load is large), is the full RIM procedure. The major drawback to the calibration method is that a full scan of the sample must be completed in order to identify all components for overlap corrections on the quartz or cristobalite peaks, where appropriate. Where ambient filters are analyzed and the loads are light, there may be no choice but to use the calibration method; however, in these cases long scan times are required to obtain a usable pattern for overlap corrections, which leads to considerably higher cost of analysis.

4.3. Lower Limits of Detection

Lower limits of detection are computed for full RIM analyses using relations derived from the "Adiabatic" analysis method of Chung (1974). Procedures for LLD computations have been summarized by Davis (1988). Several approaches are used, depending upon whether reference constants are available and whether the diffraction effects for the analyte are actually seen.

LLD values for quartz or cristobalite are based on the root background intensity criterion use in all counting statistics. It is given by

$$LLD = \frac{6W_i \sqrt{I_b}}{I_j t_i} \quad (1)$$

An estimate of the LLD, even without a measurable peak present, can be given from a 3- σ measurement at the appropriate 2θ position.

Our experience with light ambient aerosol loadings on PTFE filters is that quartz can be detected with $0.25^\circ \text{ min}^{-1}$ scanning to within the 0.05-0.1% by weight range. Even lower values may be obtained with still slower scanning, which then becomes more costly. A study of quartz analysis by the calibration method which contains analytical results in this low weight range was completed by Davis *et al.* (1984).

5. References

The following references provide a reasonably complete documentation of the EMES XRD procedures for quantitative analysis, including sample preparation, mass absorption analysis, detection limits, and error propagation.

Chung, F.H., (1974). Quantitative Interpretation of X-ray Diffraction Patterns of Mixtures - II. Adiabatic Principle of X-ray diffraction Analysis of Mixtures. *J. Appl. Cryst.* 7, 526-531.

Davis, B.L., (1981). A Study of the Errors in X-ray Quantitative Analysis Procedures for Aerosols Collected on Filter Media. *Atm. Environ.* 15, 291-296.

Davis, B.L., (1984). Reference Intensity Quantitative Analysis using Thin-Layer Aerosol Samples. *Adv. X-ray Anal.*, 27, 339-348.

Davis, B.L., (1986). A Tubular Aerosol Suspension Chamber for the Preparation of Powder Samples for X-ray Diffraction Analysis. *Powd. Diff.*, 1, 240-243.

Davis, B.L., (1988). The Estimation of Limits of Detection in RIM Quantitative X-ray Diffraction Analysis. *Adv. X-ray Anal.*, 31, 317-323.

Davis, B.L., and L.R. Johnson (1982). On the Use of Various Filter Substrates for Quantitative Particulate Analysis by X-Ray Diffraction. *Atm. Environ.*, 16, 273-282.

Davis, B.L., and L.R. Johnson, (1987). The Use of Mass Absorption in Quantitative X-ray Diffraction Analysis. *Adv. X-ray Anal.*, 30, 333-342.

Davis, B.L., Johnson, L.R., Stevens, R.K., Courtney, W.J., and D.W. Safriet (1984). The Quartz Content and Elemental Composition of Aerosols from Selected Sites of the EPA Inhalable Particulate Network. *Atm. Environ.*, 18, 771-782.

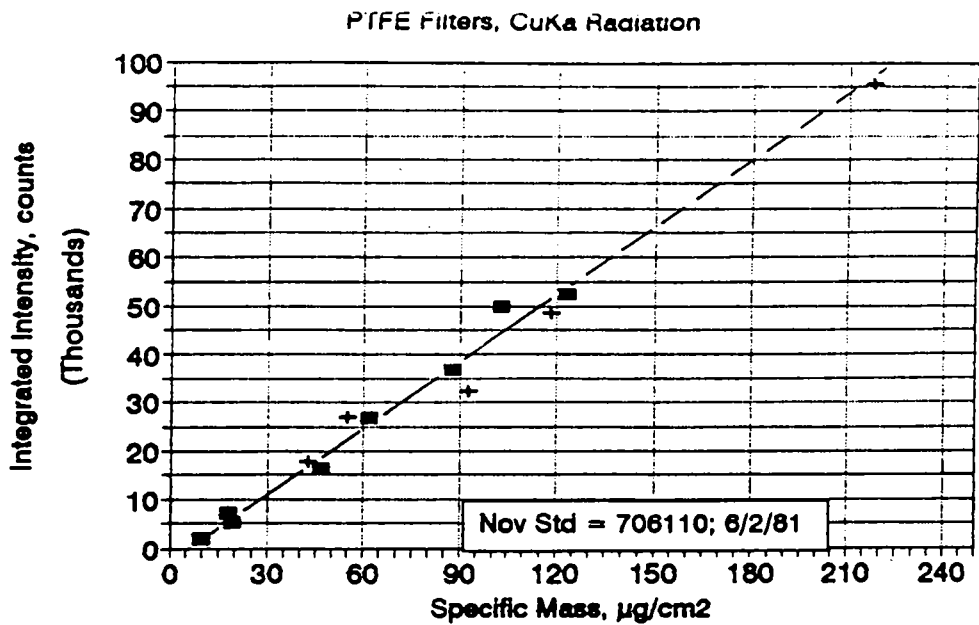


Figure 2

+ Quality Control Ck

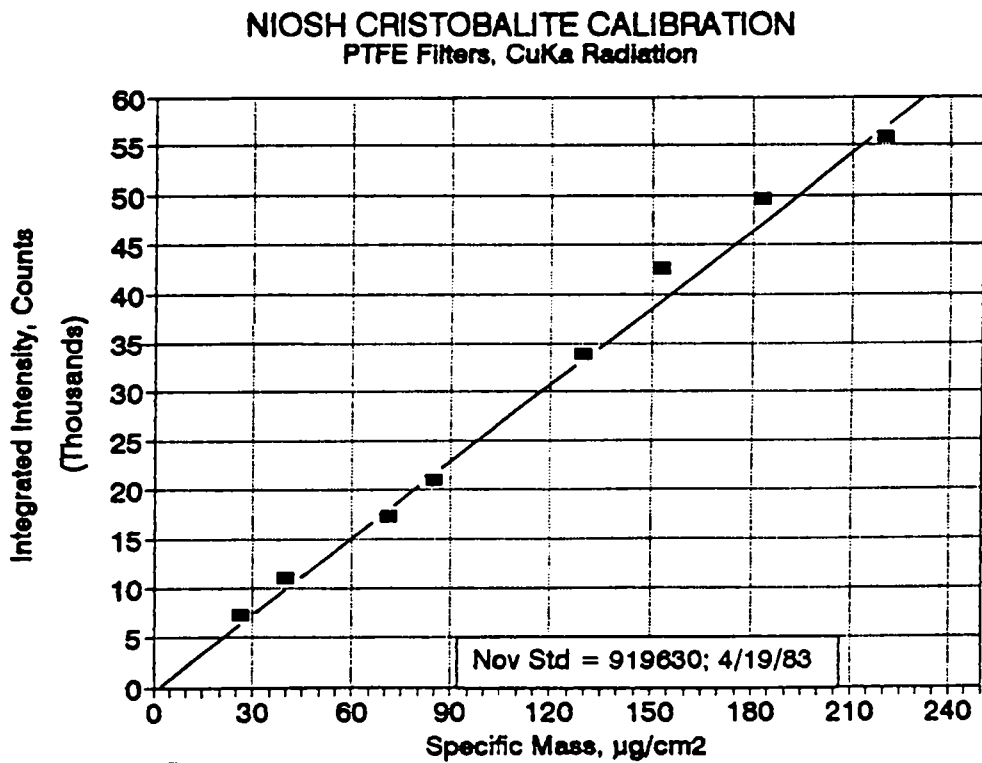


Figure 3

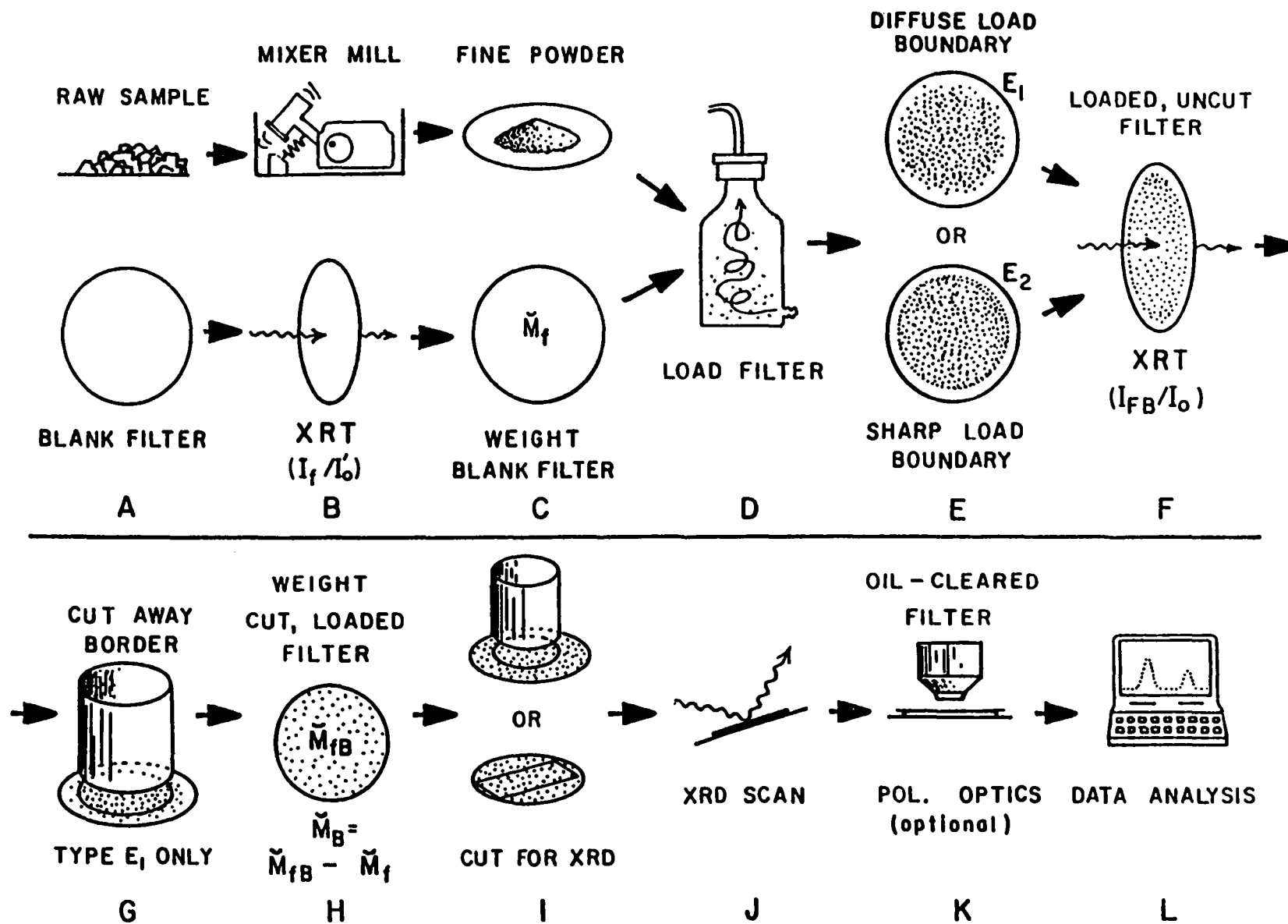


Figure 1 Flow diagram representing the successive steps in sample preparation and analysis. See text for step-by-step explanation.

QUALITY ASSURANCE PROCEDURE - NICOLET/SIEMENS DIFFRACTOMETER
Oct. 20, 1992

1. Background

This Nicolet/Siemens diffractometer has both transmission and diffraction capability. The transmission scanning of the Kentucky gypsum standard will be completed monthly. The brass substrate standard will be completed whenever a Bragg-Brentano scan, or substrate diffraction mass absorption analysis is required. The relative infrequency of these QA scans stems from the greater mechanical alignment stability of this unit compared to the Philips unit. Whenever the scans are completed a plotter dump and integrated intensity of the prime peaks shall be collected and entered into the NICOLET QA file. Logbook entries are to be kept of each QA run as for the Philips QA scans.

2. Transmission Settings

Prime Peaks: Gypsum 020, $2\theta = 11.59^\circ$; $d = 7.63\text{\AA}$
Gypsum 041, $2\theta = 29.11^\circ$; $d = 3.065$

Intervals: 10.50-12.98 $^\circ$ and 27.0-34.00 $^\circ$
35.00-36.00 $^\circ$ in ω

Step: 0.04 $^\circ$ for each interval in 2θ
0.001 $^\circ$ for each interval in ω

Dwell: 4 seconds for all scans

Corrections: $\mu^* = 149.6 \text{ cm}^{-1}$; $T = 0.3\text{mm}$
(correction prompt ans. = yes)

Instrument: $\text{CuK}\alpha_1$, Germanium monochromator, spinner on.
Power = 45 kV; 25 mA
1.0 divergence slit; 0.35 scatter slit
beam stop in place and centered
Counter V. = 9.0; BL = 1.0 v; WW = 6.78 v.
Gain = 32; Damping = 0.4

3. Bragg-Brentano ("Reflection") Settings

Prime Peaks: Brass 110, $2\theta = 42.63^\circ$; $d = 2.121\text{\AA}$
Brass 201, $2\theta = 49.74^\circ$; $d = 1.833\text{\AA}$

Intervals: 41.00-44.00 $^\circ$ and 48.00-51.00 $^\circ$ in 2θ
35.00-36.00 $^\circ$ in ω

Step: 0.04 $^\circ$ for each interval in 2θ
0.001 $^\circ$ for each interval in ω

Dwell: 4 seconds for all scans

Nicolet/Siemens Quality Assurance, p. 2

Correction: No absorption correction

Instrument: CuK α_1 , Germanium monochromator, spinner on.
Power = 45 kV; 25 mA
1.0 divergence slit; 0.35 scatter slit
beam stop removed; Knife stop in place
Counter V. = 9.0; BL = 1.0 v; WW = 6.78 v.
Gain = 32; Damping = 0.4

4. Special Precautions

Handle the standards with care. They must not be dropped or handled by the sample surface in any way. Use the magnet pencil to remove the gypsum standard from the spinner mount. Avoid scratching the brass SDIF reflection stage surface. When scanning the brass stage clean the brass surface with a Q-tip and methanol to remove vaseline.

When integrating the peak intensities place the cross-hair cursor to the left and right of each peak so that the tails are included in the intensity. Label all peaks with d-spacing and peak-height intensity before plotting.

B.B-2. X-RAY DIFFRACTION RESULTS

P3X11-5-3-3-SP3T

EMES0842 RESPEC P3X1 SP3T THIS IS A LEVEL - 1 ANALYSIS
 IFB/IO = .296804 S(IFB/IO) = .002104 IF/IO = .770598
 S(IF/IO) = .003348
 SPEC. FILTER MASS, MF, = .005262
 SPEC. SAMPLE MASS, MB, = .013023
 MEAN PARTICLE RADIUS, RZ, = .0004
 MEAN SAMPLE DENSITY, RHO-Z, = 2.6

No. X-RAY COMPONENTS, N, = 3 No. OF OPTIC COMPONENTS, M, = 0
 No. OF AMORPHOUS COMPONENTS, AM, = 0
 No. OVERLAP SETS, OL, = 0
 NO AMORPHOUS COMPONENTS IN THIS SAMPLE
 FILTER TYPE = 2

COMP- 1	CODE = 28	IPK- 1	= 4921	IBG- 1	= 1008
COMP- 2	CODE = 24	IPK- 2	= 68981	IBG- 2	= 1109
COMP- 3	CODE = 284	IPK- 3	= 3927	IBG- 3	= 1322

NONE NONE SODIUM
 ARE THE ELEMENT NAMES FOR OX FILE CODES 30, 31, AND 32
 FILE REVIEW COMPLETE FOR EMES0842

MUBO(U) = 75.89402 CM2/GM MUBO(C) = 49.88233 CM2/GM
 MUBO = 75.89402 CM2/GM
 WHB = .9192489
 MUFO = 49.52271 MUH = 73.76451 CM2/GM

INTENSITIES, CORRECTED FOR MATRIX AND TRANSPARENCY

IPK- 1 = 5314.051
 IPK- 2 = 79939.68
 IPK- 3 = 3567.678

FINAL INTENSITIES (IPK) CORRECTED FOR OVERLAP

IPK- 1 = 5314.051
 IPK- 2 = 79939.68
 IPK- 3 = 3567.678

EMES0842 RESPEC P3X1 SP3T PAGE 2
PROVISIONAL WEIGHT FRACTIONS AND VARIANCE ERRORS
HALITE

W(I)- 1 = .3902889 +- 5.826536E-02

ANHYDRITE

W(I)- 2 = .5523928 +- 5.477093E-02

MAGNESITE

W(I)- 3 = 5.731841E-02 +- 9.057642E-03

MASS ABSORPTION COEFFICIENTS AND ERRORS

MUC = 73.31308 +- 6.322203 CM2/GM

MUBO = 75.89402 +- 1.410341 CM2/GM

S(MB) = 2.143519E-04 GM/CM2

S(GAMMA) = 8.526044E-03

FINAL WEIGHT FRACTIONS AND VARIANCE ERRORS

HALITE				
W(I)- 1	=	.3902	+ -	.0582
ANHYDRITE				
W(I)- 2	=	.5523	+ -	.0547
MAGNESITE				
W(I)- 3	=	.0573	+ -	8.999999E-03

} 99.98

CALCULATED SAMPLE DENSITY = 2.6 GM/CM3
SAMPLE CRYSTALLINE FRACTION = 1 + - 0

COMPOUND REDUCTION

	OXIDE	ELEMENT
SiO2	= .0029	(.0013)
Al2O3	= .0006	(.0003)
K2O	= .0008	(.0007)
CaO	= .2252	(.161)
Fe2O3	= .0006	(.0004)
MgO	= .0283	(.0171)
H2O	= .0103	(.0011)
CO2	= .0336	(9.099999E-03)
SO3	= .3211	(.1286)
Cl	= ----	(.2311)
SrO	= .0006	(.0005)

ADDITIONAL ELEMENTAL COMPONENTS

Comp-1	NONE	= (0)*
Comp-2	NONE	= (0)*
Comp-3	SODIUM	= (.1477)*

OXIDE TOTAL = .6239 ELEMENT TOTAL = .6994712
* Add these plus any C,F,Cl in ELEMENT TABLE to OXIDE TOTAL
to obtain total weight fraction
RUN COMPLETE FOR SAMPLE EMES0842

EMES0843 RESPEC P3X10-5-3 SP3 THIS IS A LEVEL - 1 ANALYSIS
 IFB/IO = .29479 S(IFB/IO) = .002276 IF/IO = .7725
 S(IF/IO) = .003105
 SPEC. FILTER MASS, MF, = .005217
 SPEC. SAMPLE MASS, MB, = .011852
 MEAN PARTICLE RADIUS, RZ, = .0004
 MEAN SAMPLE DENSITY, RHO-Z, = 2.6

No. X-RAY COMPONENTS, N, = 3 No. OF OPTIC COMPONENTS, M, = 0
 No. OF AMORPHOUS COMPONENTS, AM, = 0
 No. OVERLAP SETS, OL, = 0
 NO AMORPHOUS COMPONENTS IN THIS SAMPLE
 FILTER TYPE = 2

COMP- 1 CODE = 28 IPK- 1 = 4510 IBG- 1 = 835
 COMP- 2 CODE = 24 IPK- 2 = 70260 IBG- 2 = 778
 COMP- 3 CODE = 284 IPK- 3 = 2853 IBG- 3 = 892

NONE NONE SODIUM
 ARE THE ELEMENT NAMES FOR OX FILE CODES 30, 31, AND 32
 FILE REVIEW COMPLETE FOR EMES0843

MUBO(U) = 81.28323 CM2/GM MUBO(C) = 54.14616 CM2/GM
 MUBO = 81.28323 CM2/GM
 WHB = .9119729
 MUFO = 49.47735 MUH = 78.48345 CM2/GM

INTENSITIES, CORRECTED FOR MATRIX AND TRANSPARENCY

IPK- 1 = 4876.995
 IPK- 2 = 81533.86
 IPK- 3 = 2595.764

FINAL INTENSITIES (IPK) CORRECTED FOR OVERLAP

IPK- 1 = 4876.995
 IPK- 2 = 81533.86
 IPK- 3 = 2595.764

EMES0843 RESPEC P3X10-5-3 SP3 PAGE 2
PROVISIONAL WEIGHT FRACTIONS AND VARIANCE ERRORS

HALITE

W(I)- 1 = .3718352 +- 5.736238E-02

ANHYDRITE

W(I)- 2 = .5848726 +- 5.494011E-02

MAGNESITE

W(I)- 3 = 4.329237E-02 +- 6.861721E-03

MASS ABSORPTION COEFFICIENTS AND ERRORS

MUC = 74.20572 +- 6.304063 CM2/GM

MUBO = 81.28323 +- 1.559599 CM2/GM

S(MB) = 2.00615E-04 GM/CM2

S(GAMMA) = 8.704351E-03

FINAL WEIGHT FRACTIONS AND VARIANCE ERRORS

HALITE

W(I)- 1	=	.3718	+-	.0573	} 99.98
ANHYDRITE					
W(I)- 2	=	.5848	+-	.0549	
MAGNESITE					
W(I)- 3	=	.0432	+-	.0068	

CALCULATED SAMPLE DENSITY = 2.62 GM/CM3
 SAMPLE CRYSTALLINE FRACTION = 1 +- 0

COMPOUND REDUCTION

	OXIDE	ELEMENT
SiO2	= .0031	(.0014)
Al2O3	= .0006	(.0003)
K2O	= .0008	(.0006)
CaO	= .2384	(.1703)
Fe2O3	= .0006	(.0004)
MgO	= .0216	(.013)
H2O	= .01	(.0011)
CO2	= .0261	(.0071)
SO3	= .3399	(.1361)
Cl	= ----	(.2202)
SrO	= .0007	(.0005)

ADDITIONAL ELEMENTAL COMPONENTS

Comp-1	NONE	= (0)*
Comp-2	NONE	= (0)*
Comp-3	SODIUM	= (.1408)*

OXIDE TOTAL = .6418 ELEMENT TOTAL = .6925254

* Add these plus any C,F,Cl in ELEMENT TABLE to OXIDE TOTAL to obtain total weight fraction

RUN COMPLETE FOR SAMPLE EMES0843

EMES0844 RESPEC P3X10-5-3-TS2 THIS IS A LEVEL - 1 ANALYSIS
 IFB/IO = .476364 S(IFB/IO) = .002124 IF/IO = .774321
 ϵ (IF/IO) = .003546
 SPEC. FILTER MASS, MF, = .005157
 SPEC. SAMPLE MASS, MB, = .005829
 MEAN PARTICLE RADIUS, RZ, = .0004
 MEAN SAMPLE DENSITY, RHO-Z, = 2.5

No. X-RAY COMPONENTS, N, = 3 No. OF OPTIC COMPONENTS, M, = 0
 No. OF AMORPHOUS COMPONENTS, AM, = 0
 No. OVERLAP SETS, OL, = 0
 NO AMORPHOUS COMPONENTS IN THIS SAMPLE
 FILTER TYPE = 2

COMP- 1	CODE = 28	IPK- 1	= 6600	IBG- 1	= 1554
COMP- 2	CODE = 24	IPK- 2	= 58466	IBG- 2	= 1176
COMP- 3	CODE = 284	IPK- 3	= 489	IBG- 3	= 1261

NONE NONE SODIUM
 ARE THE ELEMENT NAMES FOR OX FILE CODES 30, 31, AND 32
 FILE REVIEW COMPLETE FOR EMES0844

MUBO(U) = 83.34267 CM2/GM MUBO(C) = 69.08415 CM2/GM
 MUBO = 83.34267 CM2/GM
 WHB = .8359386
 MUFO = 49.59643 MUH = 77.80621 CM2/GM

INTENSITIES, CORRECTED FOR MATRIX AND TRANSPARENCY

IPK- 1 = 7604.361
 IPK- 2 = 72084.23
 IPK- 3 = 479.0839

FINAL INTENSITIES (IPK) CORRECTED FOR OVERLAP

IPK- 1 = 7604.361
 IPK- 2 = 72084.23
 IPK- 3 = 479.0839

EMES0844 RESPEC P3X10-5-3-TS2 PAGE 2
PROVISIONAL WEIGHT FRACTIONS AND VARIANCE ERRORS

HALITE

W(I)- 1 = .5247543 +- 6.163265E-02

ANHYDRITE

W(I)- 2 = .4680138 +- 6.094909E-02

MAGNESITE

W(I)- 3 = 7.231909E-03 +- 1.52044E-03

MASS ABSORPTION COEFFICIENTS AND ERRORS

MUC = 75.83946 +- 6.792279 CM2/GM

MUB0 = 83.34267 +- 2.158354 CM2/GM

S(MB) = 1.300237E-04 GM/CM2

S(GAMMA) = 6.391594E-03

EMES0844 RESPEC P3X10-5-3-TS203-19-1993 18:00:46 PAGE 3

FINAL WEIGHT FRACTIONS AND VARIANCE ERRORS

HALITE

W(I)- 1	=	.5247	+-	.0616	} 99.99
ANHYDRITE					
W(I)- 2	=	.468	+-	.0609	
MAGNESITE					
W(I)- 3	=	.0072	+-	.0015	

CALCULATED SAMPLE DENSITY = 2.49 GM/CM3

SAMPLE CRYSTALLINE FRACTION = 1 +- 0

COMPOUND REDUCTION

	OXIDE	ELEMENT
SiO2	= .0025	(.0011)
Al2O3	= .0005	(.0002)
K2O	= .0011	(.0009)
CaO	= .1915	(.1369)
Fe2O3	= .0005	(.0003)
MgO	= .0044	(.0026)
H2O	= .013	(.0014)
CO2	= .0084	(.0023)
SO3	= .2724	(.1091)
Cl	= ----	(.3107)
SrO	= .0005	(.0004)

ADDITIONAL ELEMENTAL COMPONENTS

Comp-1	NONE	= (0)*
Comp-2	NONE	= (0)*
Comp-3	SODIUM	= (.1987)*

OXIDE TOTAL = .4947 ELEMENT TOTAL = .7652856

* Add these plus any C,F,Cl in ELEMENT TABLE to OXIDE TOTAL to obtain total weight fraction

RUN COMPLETE FOR SAMPLE EMES0844

EMES0845 RESPEC P3X10-6-SP2B THIS IS A LEVEL - 1 ANALYSIS
 IFB/IO = .37951 S(IFB/IO) = .002527 IF/IO = .770818
 S(IF/IO) = .001983
 SPEC. FILTER MASS, MF, = .005172
 SPEC. SAMPLE MASS, MB, = .009531
 MEAN PARTICLE RADIUS, RZ, = .0004
 MEAN SAMPLE DENSITY, RHO-Z, = 2.55

No. X-RAY COMPONENTS, N, = 4 No. OF OPTIC COMPONENTS, M, = 0
 No. OF AMORPHOUS COMPONENTS, AM, = 0
 No. OVERLAP SETS, OL, = 2
 NO AMORPHOUS COMPONENTS IN THIS SAMPLE
 FILTER TYPE = 2

COMP- 1	CODE = 28	IPK- 1	= 5859	IBG- 1	= 980
COMP- 2	CODE = 24	IPK- 2	= 59722	IBG- 2	= 670
COMP- 3	CODE = 284	IPK- 3	= 739	IBG- 3	= 969
COMP- 4	CODE = 282	IPK- 4	= 7419	IBG- 4	= 1254

INTENSITY FOR PEAK OF RANK 2 IS TO BE REDUCED BY .06
 OF INTENSITY OF 4 RANKED PEAK
 INTENSITY FOR PEAK OF RANK 3 IS TO BE REDUCED BY .01
 OF INTENSITY OF 4 RANKED PEAK

NONE NONE SODIUM
 ARE THE ELEMENT NAMES FOR OX FILE CODES 30, 31, AND 32
 FILE REVIEW COMPLETE FOR EMES0845

MUBO(U) = 74.34386 CM2/GM MUBO(C) = 55.27669 CM2/GM
 MUBO = 74.34386 CM2/GM
 WHB = .8928337
 MUFO = 50.32928 MUH = 71.77031 CM2/GM

INTENSITIES, CORRECTED FOR MATRIX AND TRANSPARENCY

IPK- 1	= 6479.225
IPK- 2	= 70838.96
IPK- 3	= 689.1416
IPK- 4	= 8008.602

FINAL INTENSITIES (IPK) CORRECTED FOR OVERLAP

IPK- 1	= 6479.225
IPK- 2	= 70358.45
IPK- 3	= 609.0556
IPK- 4	= 8008.602

EMES0845 RESPEC P3X10-6-SP2B PAGE 2
PROVISIONAL WEIGHT FRACTIONS AND VARIANCE ERRORS

HALITE

W(I)- 1 = .4359633 +- 5.941661E-02

ANHYDRITE

W(I)- 2 = .4454184 +- 5.043721E-02

MAGNESITE

W(I)- 3 = 8.964619E-03 +- 1.603963E-03

POLYHALITE

W(I)- 4 = .1096537 +- 1.535986E-02

MASS ABSORPTION COEFFICIENTS AND ERRORS

MUC = 74.99898 +- 6.233814 CM2/GM

MUBO = 74.34386 +- 1.546049 CM2/GM

S(MB) = 1.733964E-04 GM/CM2

S(GAMMA) = 7.138277E-03

FINAL WEIGHT FRACTIONS AND VARIANCE ERRORS

HALITE				
W(I)- 1	=	.4359	+-	.0594
ANHYDRITE				
W(I)- 2	=	.4454	+-	.0504
MAGNESITE				
W(I)- 3	=	.0089	+-	.0016
POLYHALITE				
W(I)- 4	=	.1096	+-	.0153

} 99.98

CALCULATED SAMPLE DENSITY = 2.54 GM/CM3
 SAMPLE CRYSTALLINE FRACTION = 1 +- 0

COMPOUND REDUCTION

	OXIDE	ELEMENT
SiO2	= .0024	(.0011)
Al2O3	= .0004	(.0002)
K2O	= .018	(.015)
CaO	= .2024	(.1447)
Fe2O3	= .0004	(.0003)
MgO	= .0124	(.0075)
H2O	= .0176	(.0019)
CO2	= 8.599999E-03	(.0023)
SO3	= .3173	(.1271)
Cl	= ----	(.2581)
SrO	= .0005	(.0004)

ADDITIONAL ELEMENTAL COMPONENTS

Comp-1	NONE	= (0)*
Comp-2	NONE	= (0)*
Comp-3	SODIUM	= (.165)*

OXIDE TOTAL = .58 ELEMENT TOTAL = .7242136
 * Add these plus any C,F,Cl in ELEMENT TABLE to OXIDE TOTAL
 to obtain total weight fraction
 RUN COMPLETE FOR SAMPLE EMES0845

EMES0846 RESPEC P310X-6-SP2T THIS IS A LEVEL - 1 ANALYSIS
 IFB/IO = .465272 S(IFB/IO) = .00215 IF/IO = .771399
 S(IF/IO) = .001809
 SPEC. FILTER MASS, MF, = .005173
 SPEC. SAMPLE MASS, MB, = .007028
 MEAN PARTICLE RADIUS, RZ, = .0004
 MEAN SAMPLE DENSITY, RHO-Z, = 2.55

No. X-RAY COMPONENTS, N, = 3 No. OF OPTIC COMPONENTS, M, = 0
 No. OF AMORPHOUS COMPONENTS, AM, = 0
 No. OVERLAP SETS, OL, = 0
 NO AMORPHOUS COMPONENTS IN THIS SAMPLE
 FILTER TYPE = 2

COMP- 1	CODE = 28	IPK- 1	= 5545	IBG- 1	= 1247
COMP- 2	CODE = 24	IPK- 2	= 70184	IBG- 2	= 1025
COMP- 3	CODE = 284	IPK- 3	= 778	IBG- 3	= 1187

NONE NONE SODIUM
 ARE THE ELEMENT NAMES FOR OX FILE CODES 30, 31, AND 32
 FILE REVIEW COMPLETE FOR EMES0846

MUSC(U) = 71.93848 CM2/GM MUBO(C) = 58.73722 CM2/GM
 MUBO = 71.93848 CM2/GM
 WHB = .8600098
 MUFO = 50.17389 MUH = 68.89166 CM2/GM

INTENSITIES, CORRECTED FOR MATRIX AND TRANSPARENCY

IPK- 1	= 6359.77
IPK- 2	= 86171.98
IPK- 3	= 757.7855

FINAL INTENSITIES (IPK) CORRECTED FOR OVERLAP

IPK- 1	= 6359.77
IPK- 2	= 86171.98
IPK- 3	= 757.7855

EMES0846 RESPEC P310X-6-SP2T PAGE 2
PROVISIONAL WEIGHT FRACTIONS AND VARIANCE ERRORS
HALITE

W(I)- 1 = .434615 +- 6.070437E-02
ANHYDRITE
W(I)- 2 = .554057 +- 5.988921E-02
MAGNESITE
W(I)- 3 = 1.132811E-02 +- 2.057948E-03

MASS ABSORPTION COEFFICIENTS AND ERRORS

MUC = 75.89401 +- 6.724433 CM2/GM
MUBO = 71.93848 +- 1.648695 CM2/GM
S(MB) = 1.440636E-04 GM/CM2
S(GAMMA) = 5.181955E-03

FINAL WEIGHT FRACTIONS AND VARIANCE ERRORS

HALITE				
W(I)- 1	=	.4346	+ -	.0607
ANHYDRITE				
W(I)- 2	=	.554	+ -	.0598
MAGNESITE				
W(I)- 3	=	.0113	+ -	.002

} 99.99

CALCULATED SAMPLE DENSITY = 2.56 GM/CM3

SAMPLE CRYSTALLINE FRACTION = 1 + - 0

COMPOUND REDUCTION

	OXIDE	ELEMENT
SiO2	= .0029	(.0013)
Al2O3	= .0006	(.0003)
K2O	= .0009	(.0008)
CaO	= .2261	(.1616)
Fe2O3	= .0006	(.0004)
MgO	= .0064	(.0038)
H2O	= .0113	(.0012)
CO2	= .0099	(.0027)
SO3	= .3221	(.129)
Cl	= ----	(.2574)
SrO	= .0006	(.0005)

ADDITIONAL ELEMENTAL COMPONENTS

Comp-1	NONE	= (0)*
Comp-2	NONE	= (0)*
Comp-3	SODIUM	= (.1645)*

OXIDE TOTAL = .5813 ELEMENT TOTAL = .7241158

* Add these plus any C,F,Cl in ELEMENT TABLE to OXIDE TOTAL to obtain total weight fraction

RUN COMPLETE FOR SAMPLE EMES0846

EMES0847 RESPEC P3X11-5-2-SP1b THIS IS A LEVEL - 1 ANALYSIS
 IFB/IO = .410545 S(IFB/IO) = .002242 IF/IO = .77064
 S(IF/IO) = .006611
 SPEC. FILTER MASS, MF, = .005142
 SPEC. SAMPLE MASS, MB, = .008956
 MEAN PARTICLE RADIUS, RZ, = .0004
 MEAN SAMPLE DENSITY, RHO-Z, = 2.75

No. X-RAY COMPONENTS, N, = 4 No. OF OPTIC COMPONENTS, M, = 0
 No. OF AMORPHOUS COMPONENTS, AM, = 0
 No. OVERLAP SETS, OL, = 3
 NO AMORPHOUS COMPONENTS IN THIS SAMPLE
 FILTER TYPE = 2

COMP- 1	CODE = 282	IPK- 1	= 56034	IBG- 1	= 1830
COMP- 2	CODE = 24	IPK- 2	= 10606	IBG- 2	= 1048
COMP- 3	CODE = 27	IPK- 3	= 6714	IBG- 3	= 3121
COMP- 4	CODE = 284	IPK- 4	= 900	IBG- 4	= 1447

INTENSITY FOR PEAK OF RANK 4 IS TO BE REDUCED BY .01
 OF INTENSITY OF 1 RANKED PEAK
 INTENSITY FOR PEAK OF RANK 2 IS TO BE REDUCED BY .06
 OF INTENSITY OF 1 RANKED PEAK
 INTENSITY FOR PEAK OF RANK 3 IS TO BE REDUCED BY .03
 OF INTENSITY OF 2 RANKED PEAK

NONE NONE SODIUM
 ARE THE ELEMENT NAMES FOR OX FILE CODES 30, 31, AND 32
 FILE REVIEW COMPLETE FOR EMES0847

MUBO(U) = 70.34338 CM2/GM MUBO(C) = 54.28053 CM2/GM
 MUBO = 70.34338 CM2/GM
 WHB = .8867326
 MUFO = 50.61736 MUH = 68.10907 CM2/GM

INTENSITIES, CORRECTED FOR MATRIX AND TRANSPARENCY

IPK- 1 = 61183.26
 IPK- 2 = 12716.85
 IPK- 3 = 6523.361
 IPK- 4 = 850.2898

FINAL INTENSITIES (IPK) CORRECTED FOR OVERLAP

IPK- 1 = 61183.26
 IPK- 2 = 9045.854
 IPK- 3 = 6251.986
 IPK- 4 = 238.4572

EMES0847 RESPEC P3X11-5-2-SP18 PAGE 2
 PROVISIONAL WEIGHT FRACTIONS AND VARIANCE ERRORS
 POLYHALITE

W(I)- 1 = .9009456 +- 1.215583E-02

ANHYDRITE

W(I)- 2 = 6.158871E-02 +- 7.763989E-03

HALITE

W(I)- 3 = 3.369105E-02 +- 7.57246E-03

MAGNESITE

W(I)- 4 = 3.774721E-03 +- 6.337309E-04

MASS ABSORPTION COEFFICIENTS AND ERRORS

MUC = 69.1961 +- 6.41779 CM2/GM

MUBO = 70.34338 +- 1.732694 CM2/GM

S(MB) = 1.666558E-04 GM/CM2

S(GAMMA) = 1.016744E-02

FINAL WEIGHT FRACTIONS AND VARIANCE ERRORS

POLYHALITE			
W(I)- 1	=	.9009	+-. .0121
ANHYDRITE			
W(I)- 2	=	.0615	+-. .0077
HALITE			
W(I)- 3	=	.0336	+-. .0075
MAGNESITE			
W(I)- 4	=	.0037	+-. .0006

} 99.97

CALCULATED SAMPLE DENSITY = 2.76 GM/CM3
SAMPLE CRYSTALLINE FRACTION = 1 +- 0

COMPOUND REDUCTION

	OXIDE	ELEMENT
SiO2	= .0003	(.0001)
K2O	= .1408	(.1169)
CaO	= .1928	(.1377)
MgO	= .0621	(.0374)
H2O	= .0547	(.0061)
CO2	= .0022	(.0006)
SO3	= .514	(.2058)
Cl	= ----	(.0199)

ADDITIONAL ELEMENTAL COMPONENTS

Comp-1	NONE	= (0)*
Comp-2	NONE	= (0)*
Comp-3	SODIUM	= (.0127)*

OXIDE TOTAL = .9669 ELEMENT TOTAL = .5377816
* Add these plus any C,F,Cl in ELEMENT TABLE to OXIDE TOTAL
to obtain total weight fraction
RUN COMPLETE FOR SAMPLE EMES0847

EMES0848 RESPEC P3X11-5-2-SP17 THIS IS A LEVEL - 1 ANALYSIS
 IFB/IO = .388932 S(IFB/IO) = .002525 IF/IO = .771763
 S(IF/IO) = .004237
 SPEC. FILTER MASS, MF, = .005181
 SPEC. SAMPLE MASS, MB, = .009851
 MEAN PARTICLE RADIUS, RZ, = .0004
 MEAN SAMPLE DENSITY, RHO-Z, = 2.7

No. X-RAY COMPONENTS, N, = 4 No. OF OPTIC COMPONENTS, M, = 0
 No. OF AMORPHOUS COMPONENTS, AM, = 0
 No. OVERLAP SETS, CL, = 2
 NO AMORPHOUS COMPONENTS IN THIS SAMPLE
 FILTER TYPE = 2

COMP- 1	CODE = 282	IPK- 1	= 41643	IBG- 1	= 1863
COMP- 2	CODE = 24	IPK- 2	= 24220	IBG- 2	= 731
COMP- 3	CODE = 28	IPK- 3	= 1215	IBG- 3	= 1238
COMP- 4	CODE = 284	IPK- 4	= 2189	IBG- 4	= 1910

INTENSITY FOR PEAK OF RANK 2 IS TO BE REDUCED BY .06
 OF INTENSITY OF 1 RANKED PEAK
 INTENSITY FOR PEAK OF RANK 4 IS TO BE REDUCED BY .01
 OF INTENSITY OF 1 RANKED PEAK

NONE NONE SODIUM
 ARE THE ELEMENT NAMES FOR OX FILE CODES 30, 31, AND 32
 FILE REVIEW COMPLETE FOR EMES0848

MUBO(U) = 69.56381 CM2/GM MUBO(C) = 52.26043 CM2/GM
 MUBO = 69.56381 CM2/GM
 WHB = .8959527
 MUFO = 50.00536 MUH = 67.5288 CM2/GM

INTENSITIES, CORRECTED FOR MATRIX AND TRANSPARENCY

IPK- 1 = 45062.32
 IPK- 2 = 26794.08
 IPK- 3 = 1346.838
 IPK- 4 = 2047.132

FINAL INTENSITIES (IPK) CORRECTED FOR OVERLAP

IPK- 1 = 45062.32
 IPK- 2 = 26090.34
 IPK- 3 = 1346.838
 IPK- 4 = 1596.508

EMES0848 RESPEC P3X11-5-2-SP1 PAGE 2
PROVISIONAL WEIGHT FRACTIONS AND VARIANCE ERRORS

POLYHALITE			
W(I)- 1	=	.6883885	+ - 2.940391E-02
ANHYDRITE			
W(I)- 2	=	.184283	+ - 1.944358E-02
HALITE			
W(I)- 3	=	.1011104	+ - 2.242501E-02
MAGNESITE			
W(I)- 4	=	2.621802E-02	+ - 3.845118E-03

MASS ABSORPTION COEFFICIENTS AND ERRORS

MUC	=	69.64076	+ - 5.717682	CM2/GM
MUB0	=	69.56381	+ - 1.519799	CM2/GM
S(MB)	=	1.771482E-04		GM/CM2
S(GAMMA)	=	8.502249E-03		

FINAL WEIGHT FRACTIONS AND VARIANCE ERRORS

POLYHALITE			
W(I)- 1	=	.6883	+ - .0294
ANHYDRITE			
W(I)- 2	=	.1842	+ - .0194
HALITE			
W(I)- 3	=	.1011	+ - .0224
MAGNESITE			
W(I)- 4	=	.0262	+ - .0038

} 99.98

CALCULATED SAMPLE DENSITY = 2.74 GM/CM3
 SAMPLE CRYSTALLINE FRACTION = 1 + - 0

COMPOUND REDUCTION

	OXIDE	ELEMENT
SiO2	= .0009	(.0004)
Al2O3	= .0002	(.0001)
K2O	= .1078	(8.949999E-02)
CaO	= .2031	(.1452)
Fe2O3	= .0002	(.0001)
MgO	= .0588	(.0355)
H2O	= .0439	(.0049)
CO2	= .0146	(.004)
SO3	= .4724	(.1892)
Cl	= ----	(.0598)
SrO	= .0002	(.0001)

ADDITIONAL ELEMENTAL COMPONENTS

Comp-1	NONE	= (0)*
Comp-2	NONE	= (0)*
Comp-3	SODIUM	= (.0382)*

OXIDE TOTAL = .9020999 ELEMENT TOTAL = .5674795
 * Add these plus any C,F,Cl in ELEMENT TABLE to OXIDE TOTAL
 to obtain total weight fraction
 RUN COMPLETE FOR SAMPLE EMES0848

EMES0849 RESPEC P3X11-5-3-2-T THIS IS A LEVEL - 1 ANALYSIS
 IFB/IO = .292076 S(IFB/IO) = .001738 IF/IO = .769349
 S(IF/IO) = .002235
 SPEC. FILTER MASS, MF, = .005197
 SPEC. SAMPLE MASS, MB, = .0129
 MEAN PARTICLE RADIUS, RZ, = .0004
 MEAN SAMPLE DENSITY, RHO-Z, = 2.8

No. X-RAY COMPONENTS, N, = 4 No. OF OPTIC COMPONENTS, M, = 0
 No. OF AMORPHOUS COMPONENTS, AM, = 0
 No. OVERLAP SETS, OL, = 2
 NO AMORPHOUS COMPONENTS IN THIS SAMPLE
 FILTER TYPE = 2

COMP- 1	CODE = 282	IPK- 1	= 15563	IBG- 1	= 1171
COMP- 2	CODE = 24	IPK- 2	= 70226	IBG- 2	= 823
COMP- 3	CODE = 28	IPK- 3	= 1243	IBG- 3	= 1034
COMP- 4	CODE = 284	IPK- 4	= 1662	IBG- 4	= 1231

INTENSITY FOR PEAK OF RANK 2 IS TO BE REDUCED BY .06
 OF INTENSITY OF 1 RANKED PEAK
 INTENSITY FOR PEAK OF RANK 4 IS TO BE REDUCED BY .01
 OF INTENSITY OF 1 RANKED PEAK

NONE NONE SODIUM
 ARE THE ELEMENT NAMES FOR OX FILE CODES 30, 31, AND 32
 FILE REVIEW COMPLETE FOR EMES0849

MUBO(U) = 75.0799 CM2/GM MUBO(C) = 49.89115 CM2/GM
 MUBO = 75.0799 CM2/GM
 WHB = .9185418
 MUFO = 50.45423 MUH = 73.07394 CM2/GM

INTENSITIES, CORRECTED FOR MATRIX AND TRANSPARENCY

IPK- 1 = 16437.12
 IPK- 2 = 81558.69
 IPK- 3 = 1345.202
 IPK- 4 = 1513.302

FINAL INTENSITIES (IPK) CORRECTED FOR OVERLAP

IPK- 1 = 16437.12
 IPK- 2 = 80572.46
 IPK- 3 = 1345.202
 IPK- 4 = 1348.931

EMES0849 RESPEC P3X11-5-3-2-T PAGE 2
PROVISIONAL WEIGHT FRACTIONS AND VARIANCE ERRORS

POLYHALITE

W(I)- 1 = .2661801 +- 2.547559E-02

ANHYDRITE

W(I)- 2 = .6032845 +- .0314958

HALITE

W(I)- 3 = .1070528 +- 2.328252E-02

MAGNESITE

W(I)- 4 = 2.348271E-02 +- 3.392518E-03

MASS ABSORPTION COEFFICIENTS AND ERRORS

MUC = 73.75211 +- 4.297812 CM2/GM

MUBO = 75.0799 +- 1.341273 CM2/GM

S(MB) = 2.129089E-04 GM/CM2

S(GAMMA) = 6.621772E-03

FINAL WEIGHT FRACTIONS AND VARIANCE ERRORS

POLYHALITE			
W(I)- 1	=	.2661	+- .0254
ANHYDRITE			
W(I)- 2	=	.6032	+- .0314
HALITE			
W(I)- 3	=	.107	+- .0232
MAGNESITE			
W(I)- 4	=	.0234	+- .0033

} 99.97

CALCULATED SAMPLE DENSITY = 2.82 GM/CM3
SAMPLE CRYSTALLINE FRACTION = 1 +- 0

COMPOUND REDUCTION

	OXIDE	ELEMENT
SiO2	= .0032	(.0015)
Al2O3	= .0006	(.0003)
K2O	= .0418	(.0347)
CaO	= .2945	(.2104)
Fe2O3	= .0006	(.0004)
MgO	= .0298	(.018)
H2O	= .0201	(.0022)
CO2	= .0136	(.0037)
SO3	= .4913	(.1967)
Cl	= ----	(.0633)
SrO	= .0007	(.0006)

ADDITIONAL ELEMENTAL COMPONENTS

Comp-1	NONE	= (0)*
Comp-2	NONE	= (0)*
Comp-3	SODIUM	= (.0405)*

OXIDE TOTAL = .8961 ELEMENT TOTAL = .5729603
* Add these plus any C,F,Cl in ELEMENT TABLE to OXIDE TOTAL
to obtain total weight fraction
RUN COMPLETE FOR SAMPLE EMES0849

EMES0850 RESPEC P3X11-6-TS3-4 THIS IS A LEVEL - 1 ANALYSIS
IFB/IO = .331338 S(IFB/IO) = .002254 IF/IO = .768025
S(IF/IO) = .002917
SPEC. FILTER MASS, MF, = .005245
SPEC. SAMPLE MASS, MB, = .010438
MEAN PARTICLE RADIUS, RZ, = .0004
MEAN SAMPLE DENSITY, RHO-Z, = 2.7

No. X-RAY COMPONENTS, N, = 2 No. OF OPTIC COMPONENTS, M, = 0
No. OF AMORPHOUS COMPONENTS, AM, = 0
No. OVERLAP SETS, OL, = 0
NO AMORPHOUS COMPONENTS IN THIS SAMPLE
FILTER TYPE = 2

COMP- 1 CODE = 28 IPK- 1 = 3492 IBG- 1 = 832
COMP- 2 CODE = 24 IPK- 2 = 88107 IBG- 2 = 1066

NONE NONE SODIUM
ARE THE ELEMENT NAMES FOR OX FILE CODES 30, 31, AND 32
FILE REVIEW COMPLETE FOR EMES0850

MUBO(U) = 80.54065 CM2/GM MUBO(C) = 56.71294 CM2/GM
MUBO = 80.54065 CM2/GM
WHB = .901226
MUFO = 50.32089 MUH = 77.55573 CM2/GM

INTENSITIES, CORRECTED FOR MATRIX AND TRANSPARENCY

IPK- 1 = 3812.065
IPK- 2 = 103203.4

FINAL INTENSITIES (IPK) CORRECTED FOR OVERLAP

IPK- 1 = 3812.065
IPK- 2 = 103203.4

EMES0850 RESPEC P3X11-6-TS3-4 PAGE 2
PROVISIONAL WEIGHT FRACTIONS AND VARIANCE ERRORS
HALITE

W(I)- 1 = .2819145 +- 5.021604E-02
ANHYDRITE
W(I)- 2 = .7180855 +- 5.021604E-02

MASS ABSORPTION COEFFICIENTS AND ERRORS

MUC = 77.06967 +- 5.799504 CM2/GM
MUBO = 80.54065 +- 1.604231 CM2/GM
S(MB) = 1.840312E-04 GM/CM2
S(GAMMA) = 7.791163E-03

EMES0850 RESPEC P3X11-6-TS3-403-19-1993 18:03:44 PAGE 3

FINAL WEIGHT FRACTIONS AND VARIANCE ERRORS

HALITE

W(I)- 1	=	.2819	+-	.0502	} 99.99
ANHYDRITE					
W(I)- 2	=	.718	+-	.0502	

CALCULATED SAMPLE DENSITY = 2.7 GM/CM3

SAMPLE CRYSTALLINE FRACTION = 1 +- 0

COMPOUND REDUCTION

	OXIDE	ELEMENT
SiO2	= .0038	(.0018)
Al2O3	= .0007	(.0004)
K2O	= .0006	(.0005)
CaO	= .2921	(.2087)
Fe2O3	= .0007	(.0005)
MgO	= .0011	(.0006)
H2O	= 8.499999E-03	(.0009)
CO2	= .0029	(.0008)
SO3	= .417	(.167)
Cl	= ----	(.1669)
SrO	= .0008	(.0007)

ADDITIONAL ELEMENTAL COMPONENTS

Comp-1	NONE	= (0)*
Comp-2	NONE	= (0)*
Comp-3	SODIUM	= (.1067)*

OXIDE TOTAL = .7282 ELEMENT TOTAL = .6561275

* Add these plus any C,F,Cl in ELEMENT TABLE to OXIDE TOTAL
to obtain total weight fraction

RUN COMPLETE FOR SAMPLE EMES0850

APPENDIX B.C
CORE LABORATORIES' EFFECTIVE POROSITY MEASUREMENTS:
PROCEDURE AND RESULTS

B.C-1. EFFECTIVE POROSITY MEASUREMENT PROCEDURE

SAMPLE PREPARATION

1. **PLUG DRYING:** Samples are dried in a convection oven at 240 degrees F. for twelve hours.

PETROPHYSICAL MEASUREMENTS

2. **GRAIN VOLUME:** Direct grain volume measurements are made using a small volume porosimeter. This instrument utilizes the principle of gas expansion as described by Boyle's law. Helium is used as the test gas. The instrument is calibrated daily and test standards are run.

3. **GRAIN DENSITY:** Calculated grain densities are obtained utilizing direct grain volume measurement and clean, dry sample weight. Grain densities are checked against lithology standards.

4. **PLUG DIMENSIONS:** Sample length and diameter are measured using metric calipers.

5. **CMS-300 OPERATIONS:** Plug Samples

A. **PERMEABILITY "k":** Permeability is measured by flowing helium from a reference cell at the selected pressure through the core. The size of the reference cell used is optimized during a pre-test flow through. The chambers available are approximately 2, 9, 56, and 315 cc's. The actual size of each cell is calculated during calibration procedures. The cell combination used varies with each sample. The downstream end of the core is maintained at atmospheric pressure. The upstream pressure decline is monitored in real time, and observed by digital readout and visually displayed in either graphical or tabular form. The difference between the confining stress and the mean pore pressure during flow is the net confining stress. The stress to be used for this project will be supplied by the client.

a).k-air: permeability to air at client specified overburden calculated from time pressure data.

b).k-Klinkenberg: unsteady state equations used with time/pressure data to calculate the Klinkenberg slip corrected permeability at client specified overburden.

B. POROSITY: Pore volume is determined by expansion of helium into the core sample from a known volume source at approximately 240 psig. At pressure equilibrium, Boyle's Law is used to compute pore volume. Porosity is then calculated by using the pore volume from the CMS-300 and the grain volume from the Small Volume Porosimeter.

6. POROSITY: The bulk volume of each sample not run in the CMS-300 will be determined using the DEB unit. This device uses Archimedes' Principle of buoyancy to determine the bulk volume of small samples. A pan of mercury is placed on a calibrated digital scale with the prongs of the apparatus submerged. The scale is zeroed. The sample is then submerged in the mercury to the same reference point. The scale reading is divided by the density of mercury (13.53 gm/cc approx., varies with temperature) to yield the bulk volume. Porosities are calculated using the bulk volume from the DEB and the grain volume from the small volume porosimeter.

Special Instructions for Porosity Measurements of Anhydrite

- (1) Upon receipt, determine the masses of the 6 anhydrite specimens and 3 metric weights using the scale normally used for the porosity measurements. Record these masses on Table 1 under the column heading **As Received** and inform Tom Pfeifle, RE/SPEC, of the results.
- (2) Perform the porosity measurements using the procedure provided.

NOTES: If the measurements of the masses of the specimens performed by Core Laboratories are significantly different from those made by RE/SPEC, the specimens may have to be dried at prescribed temperature and humidity conditions. If no differences in the measurements exist, Step 1 - Plug Drying, can be skipped. Differences of 0.01 grams (after accounting for differences in scale output using the metric weights) are considered significant.

Porosity measurements will be made at ambient pressure only. Overburden pressures should not be simulated.

- (3) Following the porosity measurements, each of the six anhydrite specimens and three metric weights should be weighed. The measurements should be recorded in Table 1 under the column heading **As Sent**.
- (4) Repackage the specimens and metric weights using the sealing procedure followed by RE/SPEC. Return the specimens and metric weights to RE/SPEC along with the results, Table 1, and the core receipt records.

Table 1. Masses of Anhydrite Specimens and Metric Weights

Specimen LD.	RE/SPEC Determined Mass		Core Labs Determined Mass	
	As Sent (g)	As Received (g)	As Received (g)	As Sent (g)
SP1-T				
SP1-B				
SP2-T				
SP2-B				
SP3-T				
SP3-B				
Metric Weight 10 g				
Metric Weight 20 g				
Metric Weight 50 g				
Date				

B.C-2. EFFECTIVE POROSITY MEASUREMENT RESULTS



**RE/SPEC, INC.
ANHYDRITE SAMPLES
CL FILE NO.:57151-17577
FINAL REPORT**

B-158



CORE LABORATORIES

April 27, 1993

RE/SPEC, Inc.
3824 Jet Drive
Rapid City, South Dakota 57701
Attn: Mr. Tom W. Pfeifle

Core Analysis Report
Anhydrite Samples
CL File No. 57151-17577

Dear Mr. Pfeifle:

Six anhydrite samples were received from RE/SPEC, Inc. on April 21, 1993. The samples were analyzed by Core Laboratories personnel as directed by RE/SPEC representatives.

The following documentation includes: petrophysical measurements; a list of Houston laboratory personnel involved in this project; and the resultant data reported in tabular format. The type of equipment used in each procedure is also specified.

Upon completion of analysis, the samples were returned to RE/SPEC via UPS.

We appreciate your business. If we can be of further service, please call.

Very truly yours,

CORE LABORATORIES


Douglas McElroy
Laboratory Coordinator


Michael R. Long
Senior Project Analyst

TABLE OF CONTENTS

SECTION I. PROCEDURES DOCUMENTATION

**SAMPLE PREPARATION
PETROPHYSICAL MEASUREMENTS
SAMPLE DISPOSITION**

SECTION II. TABULAR REPORT

APPENDICES

**APPENDIX A: LIST OF PROJECT ANALYSTS AND PERSONNEL
APPENDIX B: REPORT DISTRIBUTION**

SAMPLE PREPARATION

Upon receipt, the samples were removed from the shipping pouches and inventoried. Each sample was then weighed and the weights recorded to .0001 gram. Three metric weights were received with the samples. These were also weighed to .0001 gram. All weights were recorded on data sheet provided by client.

PETROPHYSICAL MEASUREMENTS

- 1. GRAIN VOLUME:** Direct grain volume measurements were made using a small volume porosimeter. This instrument utilizes the principle of gas expansion as described by Boyle's law. Helium was used as the test gas. The instrument was calibrated daily and test standards were run.
- 2. GRAIN DENSITY:** Calculated grain densities were obtained utilizing direct grain volume measurement and clean, dry sample weight. Grain densities were checked against lithology standards.
- 3. POROSITY:** The bulk volume of each sample was determined using the DEB unit. This device uses Archimedes' principle of buoyancy to determine the bulk volume of small samples. A pan of mercury is placed on a calibrated digital scale with the prongs of the apparatus submerged. The scale is zeroed. The sample is then submerged in the mercury to the same reference point. The scale reading is divided by the density of mercury (13.53 gm/cc approx., varies with temperature) to yield the bulk volume. Porosities were calculated using the bulk volume from the DEB and the grain volume from the small volume porosimeter. T
- 4. BULK DENSITY:** Calculated bulk densities were obtained using the clean, dry sample weight and the Archimedes' bulk volume.
- 5. POST-ANALYSIS WEIGHTS:** Upon completion of all other measurements, samples and metric weights were re-weighed and the results recorded on client data sheet.

SAMPLE DISPOSITION

Upon completion of petrophysical measurements, all samples and metric weights were re-packaged and returned to client.

CORE LABORATORIES

Company : RE/SPEC INC.
 Well : Anhydrite Samples
 Location :
 Co,State :

Field :
 Formation :
 Coring Fluid :
 Elevation :

File No. : 57151-17577
 Date : 22-Apr-1993
 API No. :
 Analysts: Long

C O R E A N A L Y S I S R E S U L T S

SAMPLE NUMBER	POROSITY (HELIUM) %	GRAIN DENSITY gm/cc	BULK DENSITY gm/cc	DESCRIPTION
1	1.7	2.73	2.68	SP1-T
2	2.1	2.73	2.67	SP1-B
3	1.3	2.69	2.65	SP2-T
4	1.1	2.57	2.54	SP2-B
5	1.0	2.53	2.51	SP3-T
6	1.8	2.70	2.66	SP3-B

B-162

APPENDIX A: LIST OF PROJECT ANALYSTS and PERSONNEL

**PETROLEUM SERVICES MANAGER
LABORATORY COORDINATOR
SENIOR PROJECT ANALYST
TECHNICAL SALES REPRESENTATIVE**

**FEDERICA M. MANNI
DOUG McELROY
MICHAEL R. LONG
TOM SWISHER**

APPENDIX B: REPORT DISTRIBUTION

**RE/SPEC, INC.
ANHYDRITE SAMPLES
CL FILE NO.:57151-17577**

3 cc

**Mr. Tom F. Pfeifle
RE/SPEC, Inc.
3824 Jet Drive
Rapid City, South Dakota 57701**

Table 1. Masses of Anhydrite Specimens and Metric Weights

Specimen I.D.	RE/SPEC Determined Mass		Core Labs Determined Mass	
	As Sent (g)	As Received (g)	As Received (g)	As Sent (g)
SP1-T	33.94	33.94	33.9326	33.9433
SP1-B	37.45	37.45	37.4455	37.4558
SP2-T	38.85	38.84	38.8394	38.8421
SP2-B	33.67	33.66	33.6636	33.6670
SP3-T	37.51	37.49	37.4992	37.4970
SP3-B	47.68	47.67	47.6703	47.6696
Metric Weight 10 g	10.00	10.00	9.9999	10.0000
Metric Weight 20 g	20.00	20.00	19.9998	20.0002
Metric Weight 50 g	50.00	50.00	49.9991	50.0000
Date	4-15-93	5-7-93	4-22-93	4-25-93

APPENDIX B.D
DERIVATION OF EQUATION FOR POROSITY CALCULATION BASED
ON FLUID DISPLACEMENT MEASUREMENTS

Attachment 1

Derivation of Equation for Porosity Using Fluid Displacement Measurements

The equation to be derived is porosity given in terms of the quantities measured using the fluid displacement technique:

$$\text{Porosity} = 1 - \left[\frac{\left(\frac{M_{s_1}}{0.25 \cdot L \cdot \pi \cdot D^2} \right)}{\left(\frac{(M_{fk_1} - M_f) \cdot (M_{fs_g} - M_f)}{(V_f \cdot (M_{fs_g} - M_f + M_{fk_1} - M_{fs_gk_2}))} \right)} \right] \quad (1)$$

where the measured quantities are

- M_{s_1} = Mass of solid specimen before grinding
- L = Specimen length before grinding
- D = Specimen diameter before grinding
- V_f = Volume of flask to calibration mark
- M_f = Mass of flask
- M_{fs_g} = Mass of flask containing ground specimen
- M_{fk_1} = Mass of flask filled with deaerated kerosene to calibration mark
- $M_{fs_gk_2}$ = Mass of flask containing ground specimen and filled with deaerated kerosene to calibration mark

Let

- M_{k_1} = Mass of kerosene required to fill empty flask
- M_{k_2} = Mass of kerosene required to fill the flask containing the ground specimen
- M_{s_g} = Mass of ground specimen
- ρ_b = Bulk density of solid specimen
- ρ_g = Grain density
- ρ_k = Kerosene density
- V_g = Grain volume of solid specimen
- V_b = Bulk volume of solid specimen
- V_{s_g} = Volume of ground specimen

It follows from these defined quantities that

$$V_{s_g} = \frac{Mk_1 - Mk_2}{\rho_k} \quad (2)$$

$$Ms_g = Mfs_g - Mf \quad (3)$$

$$\rho_k = \frac{Mfk_1 - Mf}{Vf} \quad (4)$$

$$\rho_b = \frac{Ms_g}{0.25 \cdot \pi \cdot L \cdot D^2} \quad (5)$$

$$\rho_g = \frac{Ms_g}{Vg} = \frac{Ms_g}{V_{s_g}} \quad (6)$$

The derivation begins with

$$\text{Porosity} = \frac{\text{Bulk Specimen Volume} - \text{Grain Volume}}{\text{Bulk Specimen Volume}} \quad (7)$$

or

$$P = \frac{Vb - Vg}{Vb} \quad (8)$$

Multiply and divide by Ms_g to obtain

$$P = 1 - \frac{Ms_g \cdot Vg}{Ms_g \cdot Vb} = 1 - \frac{\rho_b}{\rho_g} \quad (9)$$

Substitute Equation 6 into Equation 9 to obtain

$$P = 1 - \frac{\rho_b \cdot V_{s_g}}{M_{s_g}} \quad (10)$$

Expressions for M_{s_g} , and ρ_b are given in Equations 3 and 5. An expression is needed for V_{s_g} in terms of the quantities directly measured using the fluid displacement technique. Begin with Equation 2:

$$V_{s_g} = \frac{Mk_1 - Mk_2}{\rho_k}$$

Add and subtract Mf from the right hand side numerator to obtain

$$V_{s_g} = \frac{Mfk_1 - Mfk_2}{\rho_k} \quad (11)$$

Add and subtract M_{s_g} from the right hand side numerator to obtain

$$V_{s_g} = \frac{Mfk_1 - Mf_{s_g}k_2 + M_{s_g}}{\rho_k} \quad (12)$$

Substituting expressions for M_{s_g} , ρ_k , ρ_b , and V_{s_g} (Equations 3 through 5 and Equation 12) into Equation 10 completes the derivation of Equation 1.

APPENDIX B.E
BRINE MANUFACTURE

**B.E-1. PROCEDURE SUPPLIED BY
SANDIA NATIONAL LABORATORIES**

Date: 07 June 1993
To: Susan Howarth, 6119
Karen Robinson
From: Karen Robinson, 6119
Subject: Preparation of Standard Brine SB-139-95B

SUMMARY

This memo describes the preparation of the standard brine SB-139-95B. I am giving quite a bit of detail in case you want to use this to generate a brine-preparation procedure for future use. In brief, I prepared 1 liter of brine, adjusted the pH to ~6.1 with HCl, and split the brine into two 500-mL lots. You sent one bottle to Chem Nuclear Geotech for analysis; the other bottle is being stored in 823/2079.

RECIPE

Craig Novak supplied a recipe for an average QPB brine, a brine expected to be saturated with respect to the minerals in Marker Bed 139. The brine described here is slightly undersaturated and contains 95% of the salts recommended by Craig.

Table 1a shows the "95%" recipe and the amounts of salts actually weighed out. Table 1b shows the calculated composition based on the "95%" recipe and the calculated composition based on the amounts of salts actually weighed out.

PROCEDURE

Detailed notes about the preparation are in my lab notebook (Lab Notebook No. WIPP 04, pp.21-23); those notes are summarized in Attachment 1.

Reagents

Reagent grade salts were used. All salts were used "as is" from the bottle (that is, they were not dried in the lab oven).

Deionized water from the Barnstead Nanopure A deionizer was used.

Standard pH buffer solutions were prepared from pHydriion buffer capsules.

Trace-metal grade hydrochloric acid was used to adjust the pH.

Equipment

Reagents were weighed out using the Mettler AE163 balance. The balance was calibrated before use with the internal calibration weight. The calibration was checked with selected standard weights. Details can be found in the balance log book (Lab Notebook No. WIPP 02, p. 25).

Glassware included a 1000-mL class-A volumetric flask and a powder funnel.

Plasticware included weighing boats, 500-mL polyethylene bottles, various plastic beakers, and a teflon stirring rod.

Other equipment included a Thermolyne Nuova 7 stir plate; a magnetic stir bar and stir-bar retriever; and a Sentron model 2001 pH system (meter and probe).

Preparation

In brief, the required amounts of salts were dissolved in deionized water in the volumetric flask; dissolution was speeded by using the magnetic stirrer. The volume was adjusted to 1000 mL in the volumetric flask. The pH was then adjusted by adding ~4 mL of HCl. The solution was then transferred to two 500-mL polyethylene bottles. The step-by-step details are in Attachment 1.

Note that although the final volume of the solution was ~1004 mL (after the pH was adjusted), I used a volume of 1000 mL to calculate the concentrations of the solutes.

WORK REMAINING

As we discussed, I will also prepare one liter of the "saturated" recipe. This work has been delayed somewhat because there wasn't enough NaCl in the lab. More was ordered and has recently arrived. I expect to have the brine prepared and the memo documenting its preparation written by Friday, June 18.

\karen\misc\sbs-139-b.1

copy to: 6119 C. F. Novak
6119 K. L. Robinson

TABLE 1a: Recipes -- Amounts of Salts Needed and Weighed Out

Salt	Amount needed for 1 liter of "95%" soln (grams)	Amount weighed out for SB-139-95B (grams)
NaHCO ₃	0.00127	*
CaCl ₂ · 2H ₂ O	1.2156	1.2144
MgSO ₄	18.9250	18.9238
MgCl ₂ · 6H ₂ O	124.076	124.0775
KCl	30.7753	30.7727
NaCl	193.8998	193.8973
Na ₂ B ₄ O ₇	6.6523	6.6519
NaBr	1.7819	1.7837

* Don't have appropriate equipment to accurately measure 0.00127 g of a salt.

Table 1b: Brine Compositions -- Target and Calculated

Species	Calc'd Comp. "95%" Recipe (mg/L)	Calc'd Comp SB-139-95B* (mg/L)
HCO ₃	0.922	**
Cl	176106	176100
SO ₄	15103	15100
Na	78198	78200
K	16141	16140
Ca	331	330
Mg	18657	18660
B	1430	1430
Br	1384	1390

* Concentrations rounded to nearest 10 mg/L.

** Probably equilibrated with atmosphere.

ATTACHMENT 1: Preparation of SB-139-95B

- 04/30/93: Put ~200 mL deionized water and small magnetic stir bar into 1000-mL volumetric flask.
Weighed Na₂B₄O₇; transferred quantitatively to vol. flask.
Began stirring. Stirred for ~3 hrs. Left standing over weekend.
Weighed other salts (CaCl₂·2H₂O, MgCl₂·6H₂O, KCl, NaCl, MgSO₄, NaBr) into plastic beakers. Covered with parafilm.
- 05/03/93: Resumed stirring.
Quantitatively transferred chloride salts (CaCl₂·2H₂O, MgCl₂·2H₂O, KCl, NaCl) to vol. flask.
Added deionized water to fill flask ~two-thirds.
Stirred ~2 hrs.
Quantitatively transferred remaining salts (MgSO₄, NaBr) to vol. flask.
Continued stirring. At end of work day turned off stirrer and left to stand overnight.
- 05/04/93: Removed stir bar with magnetic stir-bar retriever. Rinsed with deionized water, adding all rinse water to flask.
Diluted with deionized water to volume and inverted to mix thoroughly.
Calibrated pH system with standard buffers 7 and 4. Checked calibration with standard buffer 6.4.
Measured initial pH of solution as 7.0.
Alternately added aliquots of HCl, mixed the solution by inverting the vol. flask, and checked the pH of the solution. After ~4 mL of HCl were added (in 6 unequal increments) the pH of the solution was 6.14.
The final volume of the solution was ~1004 mL. Note that concentrations of solutes were calculated using a volume of 1000 mL. The solution was transferred to two 500-mL polyethylene bottles. One was given to S. Howarth for shipping to ChemNuclear Geotech for chemical analysis. The other is currently stored in 823/2079.

B.E-2. LABORATORY NOTES SUPPLIED BY TWIN CITY TESTING

August 3, 1993

2821 Plant Street
P.O. Box 6703, 57709-6703
Rapid City, South Dakota 57702-0335
Chemistry (605) 341-7284
Engineering/Environmental (605) 348-5850
Fax: (605) 341-0868

640 West Main
Lead. South Dakota 57754
(605) 584-2007
Fax: (303) 584-2007

RE/SPEC

Attn: Nancy S. Bradsky, Ph.D.
3824 Jet Drive
Rapid City, SD 57709

Preparation of Brine Solution

7/30/93: Weigh all salts into glass beakers and covered with plastic film. Set up large stirrer and 5 gallon vessel added 2000 ml of deionized water to vessel and started stirrer. Salts were quantitatively added in the following order: $MgCl_2 \cdot 6H_2O$, NaCl, KCl, $CaCl_2 \cdot 2H_2O$, $NaHCO_3$, $MgSO_4 \cdot 7H_2O$, Na_2B_4O , NaBr. Added deionized water to approximately 16 liters total volume. Covered and allowed to stir over the weekend.

8/2/93: Stopped stirrer and allowed to stand for three hours. Salts were not fully dissolved. Resumed stirring and added 2000 ml deionized water. Allowed to stir overnight.

8/3/93: Stopped stirrer. Diluted to final volume of 19 liters (5 gallons) by transferring solution to 19-1000 ml vol. flasks. Deionized water was added to make up deficient volume. Vol. flasks were then emptied back into 5 gallon vessel for mixing and pH adjustment. Calibrated pH meter with standard buffers 7 and 4. Initial pH of the solution measured 7.50. Added aliquots of conc. HCl to a pH of 5.96, added aliquots of 10N NaOH to a final pH of 6.16. Volume of conc. HCl added was 54 ml. Volume of 10N NaOH added was 7 ml. Final volume of solution was 19061 ml. Solution was transferred to five 1 gallon polyethylene bottles.

Amounts of Salts Needed and Weighed

<u>Salt</u>	<u>Amount Needed for 19 liters of Brine, grams</u>	<u>Amount weighed, grams</u>
NaHCO ₃	0.0241	0.0242
CaCl ₂ ·7H ₂ O	23.0964	23.0965
*MgSO ₄ ·7H ₂ O	735.623	735.620
MgCl ₂ ·6H ₂ O	2357.444	2357.4450
KCl	584.731	584.7308
NaCl	3684.0962	3684.0962
Na ₂ B ₄ O	126.3937	126.3939
NaBr	33.8561	33.8563

* Recipe for brine solution called for MgSO₄ - MgSO₄·7H₂O was used and the weight adjusted to allow for H₂O present.

September 3, 1993

RE/SPEC

Attn: Nancy S. Brodsky, Ph.D.
3824 Jet Drive
Rapid City, SD 57709

Preparation of Brine Solution

8/30/93: Weigh all salts into glass beakers and covered with plastic film. Set up large stirrer and 5 gallon vessel added 2000 ml of deionized water to vessel and started stirrer. Salts were quantitatively added in the following order: $MgCl_2 \cdot 6H_2O$, NaCl, KCl, $CaCl_2 \cdot 2H_2O$, $NaHCO_3$, $MgSO_4 \cdot 7H_2O$, $Na_2B_4O_{10}$, NaBr. Added deionized water to approximately 16 liters total volume. Covered and allowed to stir.

9/3/93: Stopped stirrer and allowed to stand for three hours. All salts were dissolved. Diluted solution to final volume of 19 liters (5 gallons) by transferring to 19 -1000 ml vol. flasks. Deionized water was added to make up deficient volume. Vol. flasks were then emptied back into 5 gallon vessel for mixing and pH adjustment. Calibrated pH meter with standard buffers 7 and 4. Initial pH of the solution measured 7.50. Added aliquots of conc. HCl to a pH of 6.18. Volume of conc. HCl added was 48.5 ml. Solution was transferred to five (5) one (1) gallon polyethylene bottles.

Amounts of Salts Needed and Weighed

<u>Salt</u>	<u>Amount Needed for 19 liters of Brine, grams</u>	<u>Amount weighed, grams</u>
NaHCO ₃	0.0241	0.0242
CaCl ₂ ·7H ₂ O	23.0964	23.0963
*MgSO ₄ ·7H ₂ O	735.623	735.623
MgCl ₂ ·6H ₂ O	2357.444	2357.4440
KCl	584.731	584.7311
NaCl	3684.0962	3684.0962
Na ₂ B ₄ O ₁₀	126.3937	126.3939
NaBr	33.8561	33.8561

* Recipe for brine solution called for MgSO₄ - MgSO₄·7H₂O was used and the weight adjusted to allow for H₂O present.

APPENDIX B.F
ERROR ANALYSES

B.F-1. ERROR ANALYSIS FOR TOTAL POROSITY MEASUREMENTS

Attachment 2

CALCULATION OF ERRORS FOR TOTAL POROSITY MEASUREMENTS.

Application: Contract 248b calculation of total porosity using fluid displacement technique. Used ANSIVASME PTC 19.1-1985. "Part I Measurement Uncertainty ; Instruments and Apparatus".

Mathcad file: Syntax:

- := User is defining a value or function
- = Mathcad is returning a calculated value
- units such as "length" and "mass" are returned by mathcad.

SPECIMEN P3X11-5-2-SP1-T

Input Values:

$M_{ss} := .03394 \cdot \text{kg}$	Bulk mass of specimen, before grinding
$L := 0.4192 \cdot 0.0254 \cdot \text{m}$	Specimen length, before grinding
$D := 1.5297 \cdot 0.0254 \cdot \text{m}$	Specimen diameter, before grinding
$M_{fk} := .12297 \cdot \text{kg}$	Mass of flask with kerosene to cal. mark
$M_f := 0.04301 \cdot \text{kg}$	Mass of flask alone
$V_f := .0001 \cdot \text{m}^3$	Volume of flask to cal. mark
$M_{gsf} := .06998 \cdot \text{kg}$	Mass of ground specimen in flask
$M_{fsk} := .14214 \cdot \text{kg}$	Mass of flask with ground specimen and kerosene to calibration mark

$$\text{Porosity} := 1 - \frac{\frac{M_{ss}}{0.25 \cdot L \cdot \pi \cdot D^2}}{\frac{(M_{fk} - M_f) \cdot (M_{gsf} - M_f)}{V_f \cdot (M_{gsf} - M_f + M_{fk} - M_{fsk})}} \quad \text{Porosity} = 0.02764$$

$$\begin{aligned} \text{vol} &:= 0.25 \cdot \pi \cdot L \cdot D^2 & \text{vol} &= 1.26248 \cdot 10^{-5} \cdot \text{length}^3 \\ \text{blkden} &:= \frac{M_{ss}}{\text{vol}} & \text{blkden} &= 2688.35737 \cdot \text{mass} \cdot \text{length}^{-3} \end{aligned}$$

Calculate Sensitivity Factors, Sx

Define sensitivity factors for each input parameter:

$$SM_{ss} := \frac{d}{dM_{ss}} \left[\frac{\frac{-M_{ss}}{0.25 \cdot \pi \cdot L \cdot D^2}}{\frac{(M_{fk} - M_f) \cdot (M_{gsf} - M_f)}{V_f \cdot (M_{gsf} - M_f + M_{fk} - M_{fsk})}} + 1 \right]$$

$$S_L := \frac{d}{dL} \left[\frac{\frac{-M_{ss}}{0.25 \cdot \pi \cdot L \cdot D^2}}{\frac{(M_{fk} - M_f) \cdot (M_{gsf} - M_f)}{V_f \cdot (M_{gsf} - M_f + M_{fk} - M_{fsk})}} + 1 \right]$$

$$S_D := \frac{d}{dD} \left[\frac{\frac{-M_{ss}}{0.25 \cdot \pi \cdot L \cdot D^2}}{\frac{(M_{fk} - M_f) \cdot (M_{gsf} - M_f)}{V_f \cdot (M_{gsf} - M_f + M_{fk} - M_{fsk})}} + 1 \right]$$

$$SM_{fk} := \frac{d}{dM_{fk}} \left[\left[\frac{\frac{-M_{ss}}{0.25 \cdot \pi \cdot L \cdot D^2}}{\frac{(M_{fk} - M_f) \cdot (M_{gsf} - M_f)}{V_f \cdot (M_{gsf} - M_f + M_{fk} - M_{fsk})}} + 1 \right] \right]$$

$$SM_f := \frac{d}{dM_f} \left[\left[\frac{\frac{-M_{ss}}{0.25 \cdot \pi \cdot L \cdot D^2}}{\frac{(M_{fk} - M_f) \cdot (M_{gsf} - M_f)}{V_f \cdot (M_{gsf} - M_f + M_{fk} - M_{fsk})}} + 1 \right] \right]$$

$$SV_f := \frac{d}{dV_f} \left[\left[\frac{\frac{-M_{ss}}{0.25 \cdot \pi \cdot L \cdot D^2}}{\frac{(M_{fk} - M_f) \cdot (M_{gsf} - M_f)}{V_f \cdot (M_{gsf} - M_f + M_{fk} - M_{fsk})}} + 1 \right] \right]$$

$$SM_{gsf} := \frac{d}{dM_{gsf}} \left[\left[\frac{\frac{-M_{ss}}{0.25 \cdot \pi \cdot L \cdot D^2}}{\frac{(M_{fk} - M_f) \cdot (M_{gsf} - M_f)}{V_f \cdot (M_{gsf} - M_f + M_{fk} - M_{fsk})}} + 1 \right] \right]$$

$$SM_{fsk} := \frac{d}{dM_{fsk}} \left[\left[\frac{\frac{-M_{ss}}{0.25 \cdot \pi \cdot L \cdot D^2}}{\frac{(M_{fk} - M_f) \cdot (M_{gsf} - M_f)}{V_f \cdot (M_{gsf} - M_f + M_{fk} - M_{fsk})}} + 1 \right] \right]$$

Summary of Sensitivity Factors, List of Returned Values:

$$SM_{ss} = -28.64943 \cdot \text{mass}^{-1}$$

$$SM_{gsf} = -88.5978 \cdot \text{mass}^{-1}$$

$$SM_f = 76.43194 \cdot \text{mass}^{-1}$$

$$SM_{fk} = -112.45597 \cdot \text{mass}^{-1}$$

$$SL = 91.29315 \cdot \text{length}^{-1}$$

$$SV_f = -9723.61758 \cdot \text{length}^{-1}$$

$$SD = 50.0475 \cdot \text{length}^{-1}$$

$$SM_{fsk} = 124.66176 \cdot \text{mass}^{-1}$$

List Errors Associated With Each Input Parameter

$me := 0.5 \cdot 10^{-5} \cdot \text{kg}$ Maximum error in mass measurement, scale. Applicable to Mss, Mf, Mfk, Mgsf, Mfsk

$fe := 5 \cdot 10^{-8} \cdot \text{m}^3 \frac{Mfk - Mf}{Vf}$ Max. error in mass measurement due to 0.05 ml imprecision in filling flask to calibration mark with kerosene. Applicable to Mfk, Mgsf, Mfsk
 $fe = 0.00004 \cdot \text{mass}$

$le := 0.0012 \cdot 0.0254 \cdot \text{m}$ Maximum error in specimen length (total indicated runnout). Applicable to L

$de := .0004 \cdot 0.0254 \cdot \text{m}$ Maximum error in specimen diameter (total indicated runnout). Applicable to D.

$ve := 1 \cdot 10^{-7} \cdot \text{m}^3$ Maximum error in flask volume (1/10 ml). Applicable to Vf.

CALCULATE UNCERTAINTIES

BIAS LIMIT = B

$$B := \sqrt{(me)^2 \cdot (SMss^2 + SMf^2) + (le \cdot SL)^2 + (de \cdot SD)^2 + (ve \cdot SVf)^2 + (SMfk^2 + SMfsk^2 + SMgsf^2) \cdot (fe + me)^2}$$

$B = 0.00906$

Root sum of squares uncertainty = URss:

$URss := \sqrt{B^2}$ $URss = 0.00906$

For Reference: Full equation for URss is

$URss = \text{sqrt}(B^2 + (t \cdot S)^2)$

where S is the precision error and t is an index found in statistics charts. The t index decreases with increasing degrees of freedom. All calibration error are bias errors. Errors that can be reduced with repeated measurements are precision errors.

Relative error, as a percent of porosity:

Porosity = 0.02764 $Rel_Err_pcnt := \frac{100 \cdot URss}{Porosity}$ $Rel_Err_pcnt = 32.76848$

B.F-2. ERROR ANALYSIS FOR GAS PERMEABILITY MEASUREMENTS

CALCULATION OF ERRORS FOR GAS PERMEABILITY MEASUREMENTS.

Application: Contract 248b calculation of gas permeability.

Used ANSI/ASME PTC 19.1-1985. "Part I Measurement
Uncertainty ; Instruments and Apparatus".

Mathcad file: Syntax:

:= User is defining a value or function

= Mathcad is returning a calculated value

units such as "length" and "mass" are returned by mathcad.

Definitions:

$$N := \frac{\text{kg} \cdot \text{m}}{\text{sec}^2}$$

$$\text{MPa} := \frac{10^6 \cdot N}{\text{m}^2}$$

GENERIC SPECIMEN

Input Values:

$$Q := \frac{20 \cdot 10^{-6} \cdot \text{m}^3}{86400 \cdot \text{sec}}$$

Flow rate

$$L := 0.1 \cdot \text{m}$$

Specimen length

$$D := 0.1 \cdot \text{m}$$

Specimen diameter

$$P_e := 0.1 \cdot \text{MPa}$$

Exit pore pressure

$$P_{in} := 0.4 \cdot \text{MPa}$$

Inlet pore pressure (low value gives worst case error)

$$u := 1.78 \cdot 10^{-11} \cdot \text{MPa} \cdot \text{sec}$$

Viscosity of nitrogen gas

$$A := 0.25 \cdot \pi \cdot D^2$$

$$\text{Perm} := \frac{2 \cdot Q \cdot P_e \cdot u \cdot L}{(P_{in}^2 - P_e^2) \cdot A}$$

$$\text{Perm} = 6.995 \cdot 10^{-20} \cdot \text{length}^2$$

Calculate Sensitivity Factors, Sx

Define sensitivity factors for each input parameter:

$$SQ := \frac{d}{dQ} \frac{2 \cdot Q \cdot Pe \cdot u \cdot L}{(Pin^2 - Pe^2) \cdot A}$$

$$SQ = 3.0218 \cdot 10^{-10} \cdot \text{length}^{-1} \cdot \text{time}$$

$$SPe := \frac{d}{dPe} \frac{2 \cdot Q \cdot Pe \cdot u \cdot L}{(Pin^2 - Pe^2) \cdot A}$$

$$SPe = 7.9276 \cdot 10^{-25} \cdot \text{mass}^{-1} \cdot \text{length}^3 \cdot \text{time}^2$$

$$SPin := \frac{d}{dPin} \frac{2 \cdot Q \cdot Pe \cdot u \cdot L}{(Pin^2 - Pe^2) \cdot A}$$

$$SPin = -3.7306 \cdot 10^{-25} \cdot \text{mass}^{-1} \cdot \text{length}^3 \cdot \text{time}^2$$

$$Su := \frac{d}{du} \frac{2 \cdot Q \cdot Pe \cdot u \cdot L}{(Pin^2 - Pe^2) \cdot A}$$

$$Su = 3.9298 \cdot 10^{-15} \cdot \text{mass}^{-1} \cdot \text{length}^3 \cdot \text{time}$$

$$SL := \frac{d}{dL} \frac{2 \cdot Q \cdot Pe \cdot u \cdot L}{(Pin^2 - Pe^2) \cdot A}$$

$$SL = 6.995 \cdot 10^{-19} \cdot \text{length}$$

$$SD := \frac{d}{dL} \frac{2 \cdot Q \cdot Pe \cdot u \cdot L}{(Pin^2 - Pe^2) \cdot (0.25 \cdot \pi \cdot D^2)}$$

$$SD = 6.995 \cdot 10^{-19} \cdot \text{length}$$

Summary of Relative Sensitivity Factors:

$$SQr := SQ \cdot \frac{Q}{Perm}$$

$$SLr := SL \cdot \frac{L}{Perm}$$

$$SQr = 1$$

$$SPer := SPe \cdot \frac{Pe}{Perm}$$

$$SDr := SD \cdot \frac{D}{Perm}$$

$$SLr = 1$$

$$SDr = 1$$

$$SPinr := SPin \cdot \frac{Pin}{Perm}$$

$$SPer = 1.1333$$

$$SPinr = -2.1333$$

$$Sur := Su \cdot \frac{u}{Perm}$$

$$Sur = 1$$

List Errors Associated With Each Input Parameter

$P_{err} := 0.01 \cdot P_e$	Errors in pore pressures; taken from transducer reverification data
$P_{inerr} := 0.01 \cdot MPa$	
$Q_{err} := Q \cdot 0.02$	Maximum error in flow rate - taken from errors to linear least square fits to data.
$L_{err} := 0.0005 \cdot 0.0254 \cdot m$	Measurement errors in specimen dimensions
$D_{err} := 0.005 \cdot 0.0254 \cdot m$	
$u_{err} := \frac{.07}{6} \cdot u$	Holcomb and Shields report that argon changes 7 percent over a 6 MPa pressure change. The maximum pressure change across the specimen here is 1.0 MPa. Therefore an error of 7/6 percent is used.

CALCULATE UNCERTAINTIES

B is the bias limit:

$$B := \sqrt{(SP_{in} \cdot P_{inerr})^2 + (SP_e \cdot P_{err})^2 + (SQ \cdot Q_{err})^2 + (SL \cdot L_{err})^2 + (SD \cdot D_{err})^2 + (Su \cdot u_{err})^2}$$

$$B = 4.1445 \cdot 10^{-21} \cdot \text{length}^2$$

Root sum of squares uncertainty = URss:

$$UR_{ss} := \sqrt{B^2}$$

$$UR_{ss} = 4.1445 \cdot 10^{-21} \cdot \text{length}^2$$

For Reference: Full equation for URss is

$$UR_{ss} = \sqrt{B^2 + (t \cdot S)^2}$$

where S is the precision error and t is an index found in statistics charts. The t index decreases with increasing degrees of freedom. All calibration error are bias errors. Errors that can be reduced with repeated measurements are precision errors.

Relative error, as a percent of porosity:

$$Perm = 6.995 \cdot 10^{-20} \cdot \text{length}^2$$

$$Rel_Err_pcnt := \frac{100 \cdot UR_{ss}}{Perm}$$

$$Rel_Err_pcnt = 5.9251$$

B.F-3. ERROR ANALYSIS FOR BRINE PERMEABILITY MEASUREMENTS

CALCULATION OF ERRORS FOR BRINE PERMEABILITY MEASUREMENTS.

Application: Contract 248b calculation of gas permeability.

Used ANSI/ASME PTC 19.1-1985. "Part I Measurement Uncertainty ; Instruments and Apparatus".

Mathcad file: Syntax:

:= User is defining a value or function

= Mathcad is returning a calculated value

units such as "length" and "mass" are returned by mathcad.

Definitions:

$$N := \frac{\text{kg} \cdot \text{m}}{\text{sec}^2}$$

$$\text{MPa} := \frac{10^6 \cdot N}{\text{m}^2}$$

GENERIC SPECIMEN

Input Values:

$$Q := 1 \cdot 10^{-9} \frac{\text{m}^3}{\text{sec}}$$

Flow rate

$$L := 0.1015 \cdot \text{m}$$

Specimen length

$$D := 0.1015 \cdot \text{m}$$

Specimen diameter

$$P_g := 0.3 \cdot \text{MPa}$$

Inlet gage pore pressure

$$u := 1.26 \cdot 10^{-9} \cdot \text{MPa} \cdot \text{sec}$$

Viscosity of brine (Stroup and Senseny, 1987) - no data for MB 139 brine recipe.

Where

$$A := 0.25 \cdot \pi \cdot D^2$$

Specimen cross-sectional area

$$P_e := 0.1 \cdot \text{MPa}$$

Exit pore pressure

$$P_{in} := P_g + P_e$$

$$\text{Perm} := \frac{Q \cdot u \cdot L}{(P_{in} - P_e) \cdot A}$$

$$\text{Perm} = 5.2686 \cdot 10^{-17} \cdot \text{length}^2$$

$$\text{Perm} := \frac{Q \cdot u \cdot L}{(P_g) \cdot A}$$

$$\text{Perm} = 5.2686 \cdot 10^{-17} \cdot \text{length}^2$$

CALCULATION OF ERRORS FOR BRINE PERMEABILITY MEASUREMENTS.

Application: Contract 248b calculation of gas permeability.
Used ANSI/ASME PTC 19.1-1985. "Part I Measurement
Uncertainty ; Instruments and Apparatus".

Mathcad file: Syntax:

- := User is defining a value or function
 - = Mathcad is returning a calculated value
- units such as "length" and "mass" are returned by mathcad.

Definitions:

$$N := \frac{\text{kg} \cdot \text{m}}{\text{sec}^2}$$

$$\text{MPa} := \frac{10^6 \cdot N}{\text{m}^2}$$

GENERIC SPECIMEN

Input Values:

$$Q := 1 \cdot 10^{-9} \frac{\text{m}^3}{\text{sec}}$$

Flow rate

$$L := 0.1015 \cdot \text{m}$$

Specimen length

$$D := 0.1015 \cdot \text{m}$$

Specimen diameter

$$P_g := 0.3 \cdot \text{MPa}$$

Inlet gage pore pressure

$$u := 1.26 \cdot 10^{-9} \cdot \text{MPa} \cdot \text{sec}$$

Viscosity of brine (Stroup and Senseny, 1987) - no
data for MB 139 brine recipe.

Where

$$A := 0.25 \cdot \pi \cdot D^2$$

Specimen cross-sectional area

$$P_e := 0.1 \cdot \text{MPa}$$

Exit pore pressure

$$P_{in} := P_g + P_e$$

$$\text{Perm} := \frac{Q \cdot u \cdot L}{(P_{in} - P_e) \cdot A}$$

$$\text{Perm} = 5.2686 \cdot 10^{-17} \cdot \text{length}^2$$

$$\text{Perm} := \frac{Q \cdot u \cdot L}{(P_g) \cdot A}$$

$$\text{Perm} = 5.2686 \cdot 10^{-17} \cdot \text{length}^2$$

Calculate Sensitivity Factors, Sx

Define sensitivity factors for each input parameter:

$$SQ := \frac{d}{dQ} \frac{Q \cdot u \cdot L}{(Pg) \cdot A}$$

$$SQ = 5.2686 \cdot 10^{-8} \cdot \text{length}^{-1} \cdot \text{time}$$

$$SPg := \frac{d}{dPg} \frac{Q \cdot u \cdot L}{(Pg) \cdot A}$$

$$SPg = -1.7562 \cdot 10^{-22} \cdot \text{mass}^{-1} \cdot \text{length}^3 \cdot \text{time}^2$$

$$Su := \frac{d}{du} \frac{Q \cdot u \cdot L}{(Pg) \cdot A}$$

$$Su = 4.1814 \cdot 10^{-14} \cdot \text{mass}^{-1} \cdot \text{length}^3 \cdot \text{time}$$

$$SL := \frac{d}{dL} \frac{Q \cdot u \cdot L}{(Pg) \cdot A}$$

$$SL = 5.1907 \cdot 10^{-16} \cdot \text{length}$$

$$SD := \frac{d}{dL} \frac{Q \cdot u \cdot L}{(Pg) \cdot (0.25 \cdot \pi \cdot D^2)}$$

$$SD = 5.1907 \cdot 10^{-16} \cdot \text{length}$$

Summary of Relative Sensitivity Factors:

$$SQr := SQ \cdot \frac{Q}{\text{Perm}}$$

$$SQr = 1$$

$$SPgr := SPg \cdot \frac{Pg}{\text{Perm}}$$

$$SPgr = -1$$

$$Sur := Su \cdot \frac{u}{\text{Perm}}$$

$$Sur = 1$$

$$SLr := SL \cdot \frac{L}{\text{Perm}}$$

$$SLr = 1$$

$$SDr := SD \cdot \frac{D}{\text{Perm}}$$

$$SDr = 1$$

List Errors Associated With Each Input Parameter

$P_{gerr} := 0.01 \cdot \text{MPa}$	Maximum error in pore pressure gage reading; taken from transducer reverification data
$Q_{err} := 0.03 \cdot Q$	Maximum error in flow rate (3%) - taken from standard error in linear fit to data.
$L_{err} := 0.0005 \cdot 0.0254 \cdot \text{m}$ $D_{err} := 0.005 \cdot 0.0254 \cdot \text{m}$	Measurement errors in specimen dimensions
$u_{err} := 0.01 \cdot 10^{-9} \cdot \text{MPa} \cdot \text{sec}$	Used precision of reported viscosity.

CALCULATE UNCERTAINTIES

B is the bias limit:

$$B := \sqrt{(SPg \cdot P_{gerr})^2 + (SQ \cdot Q_{err})^2 + (SL \cdot L_{err})^2 + (SD \cdot D_{err})^2 + (Su \cdot u_{err})^2}$$

$$B = 2.4003 \cdot 10^{-18} \cdot \text{length}^2$$

Root sum of squares uncertainty = URss:

$$UR_{ss} := \sqrt{B^2}$$

$$UR_{ss} = 2.4003 \cdot 10^{-18} \cdot \text{length}^2$$

For Reference: Full equation for URss is

$$UR_{ss} = \sqrt{B^2 + (t \cdot S)^2}$$

where S is the precision error and t is an index found in statistics charts. The t index decreases with increasing degrees of freedom. All calibration error are bias errors. Errors that can be reduced with repeated measurements are precision errors.

Relative error, as a percent of permeability:

$$\text{Perm} = 5.2686 \cdot 10^{-17} \cdot \text{length}^2 \quad \text{Rel_Err_pcnt} := \frac{100 \cdot UR_{ss}}{\text{Perm}}$$

$$\text{Rel_Err_pcnt} = 4.556$$

APPENDIX B.G
FLOW-VERSUS-TIME DATA FOR ALL GAS
PERMEABILITY TESTS

Figures

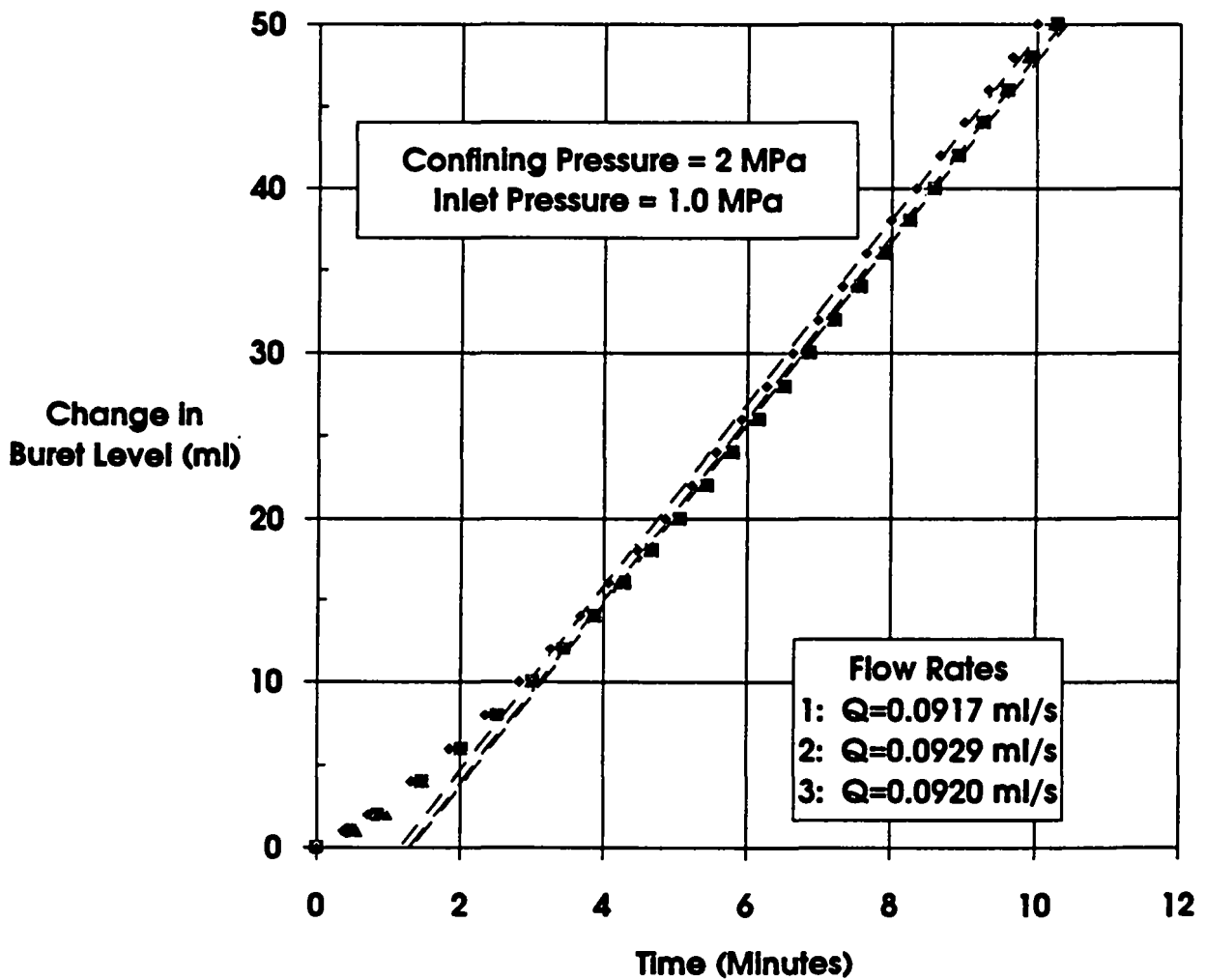
- G-1 Gas volume-versus-time for tests on Specimen P3X11-5-2-SP1 at 2 MPa confining pressure and 1.0 MPa gas inlet pressure. Symbols represent recorded data points and dashed lines are best fits to linear sections of data B-209
- G-2 Gas volume-versus-time for tests on Specimen P3X11-5-2-SP1 at 2 MPa confining pressure and 0.7 MPa gas inlet pressure. Symbols represent recorded data points and dashed lines are best fits to linear sections of data B-210
- G-3 Gas volume-versus-time for tests on Specimen P3X11-5-2-SP1 at 2 MPa confining pressure and 0.4 MPa gas inlet pressure. Symbols represent recorded data points and dashed lines are best fits to linear sections of data B-211
- G-4 Gas volume-versus-time for tests on Specimen P3X11-5-2-SP1 at 6 MPa confining pressure and 1.0 MPa gas inlet pressure. Symbols represent recorded data points and dashed lines are best fits to linear sections of data B-212
- G-5 Gas volume-versus-time for tests on Specimen P3X11-5-2-SP1 at 6 MPa confining pressure and 0.7 MPa gas inlet pressure. Symbols represent recorded data points and dashed lines are best fits to linear sections of data B-213
- G-6 Gas volume-versus-time for tests on Specimen P3X11-5-2-SP1 at 6 MPa confining pressure and 0.4 MPa gas inlet pressure. Symbols represent recorded data points and dashed lines are best fits to linear sections of data B-214
- G-7 Gas volume-versus-time for tests on Specimen P3X11-5-2-SP1 at 10 MPa confining pressure and 1.0 MPa gas inlet pressure. Symbols represent recorded data points and dashed lines are best fits to linear sections of data B-215
- G-8 Gas volume-versus-time for tests on Specimen P3X11-5-2-SP1 at 10 MPa confining pressure and 0.7 MPa gas inlet pressure. Symbols represent recorded data points and dashed lines are best fits to linear sections of data B-216
- G-9 Gas volume-versus-time for tests on Specimen P3X11-5-2-SP1 at 10 MPa confining pressure and 0.4 MPa gas inlet pressure. Symbols represent recorded data points and dashed lines are best fits to linear sections of data B-217
- G-10 Gas volume-versus-time for tests on Specimen P3X10-6-SP2 at 2 MPa confining pressure and 1.0 MPa gas inlet pressure. Symbols represent recorded data points and dashed lines are best fits to linear sections of data B-218
- G-11 Gas volume-versus-time for tests on Specimen P3X10-6-SP2 at 2 MPa confining pressure and 0.7 MPa gas inlet pressure. Symbols represent recorded data points and dashed lines are best fits to linear sections of data B-219

Figures (Continued)

- G-12 Gas volume-versus-time for tests on Specimen P3X10-6-SP2 at 2 MPa confining pressure and 0.4 MPa gas inlet pressure. Symbols represent recorded data points and dashed lines are best fits to linear sections of data B-220
- G-13 Gas volume-versus-time for tests on Specimen P3X10-6-SP2 at 6 MPa confining pressure and 1.0 MPa gas inlet pressure. Symbols represent recorded data points and dashed lines are best fits to linear sections of data B-221
- G-14 Gas volume-versus-time for tests on Specimen P3X10-6-SP2 at 6 MPa confining pressure and 0.7 MPa gas inlet pressure. Symbols represent recorded data points and dashed lines are best fits to linear sections of data B-222
- G-15 Gas volume-versus-time for tests on Specimen P3X10-6-SP2 at 6 MPa confining pressure and 0.4 MPa gas inlet pressure. Symbols represent recorded data points and dashed lines are best fits to linear sections of data B-223
- G-16 Gas volume-versus-time for tests on Specimen P3X10-6-SP2 at 10 MPa confining pressure and 1.0 MPa gas inlet pressure. Symbols represent recorded data points and dashed lines are best fits to linear sections of data B-224
- G-17 Gas volume-versus-time for tests on Specimen P3X10-6-SP2 at 10 MPa confining pressure and 0.7 MPa gas inlet pressure. Symbols represent recorded data points and dashed lines are best fits to linear sections of data B-225
- G-18 Gas volume-versus-time for tests on Specimen P3X10-6-SP2 at 10 MPa confining pressure and 0.4 MPa gas inlet pressure. Symbols represent recorded data points and dashed lines are best fits to linear sections of data B-226
- G-19 Gas volume-versus-time for tests on Specimen P3X11-5-3-SP3 at 2 MPa confining pressure and 1.0 MPa gas inlet pressure. Symbols represent recorded data points and dashed lines are best fits to linear sections of data B-227
- G-20 Gas volume-versus-time for tests on Specimen P3X11-5-3-SP3 at 2 MPa confining pressure and 0.7 MPa gas inlet pressure. Symbols represent recorded data points and dashed lines are best fits to linear sections of data B-228
- G-21 Gas volume-versus-time for tests on Specimen P3X11-5-3-SP3 at 2 MPa confining pressure and 0.4 MPa gas inlet pressure. Symbols represent recorded data points and dashed lines are best fits to linear sections of data B-229
- G-22 Gas volume-versus-time for tests on Specimen P3X11-5-3-SP3 at 6 MPa confining pressure and 1.0 MPa gas inlet pressure. Symbols represent recorded data points and dashed lines are best fits to linear sections of data B-230

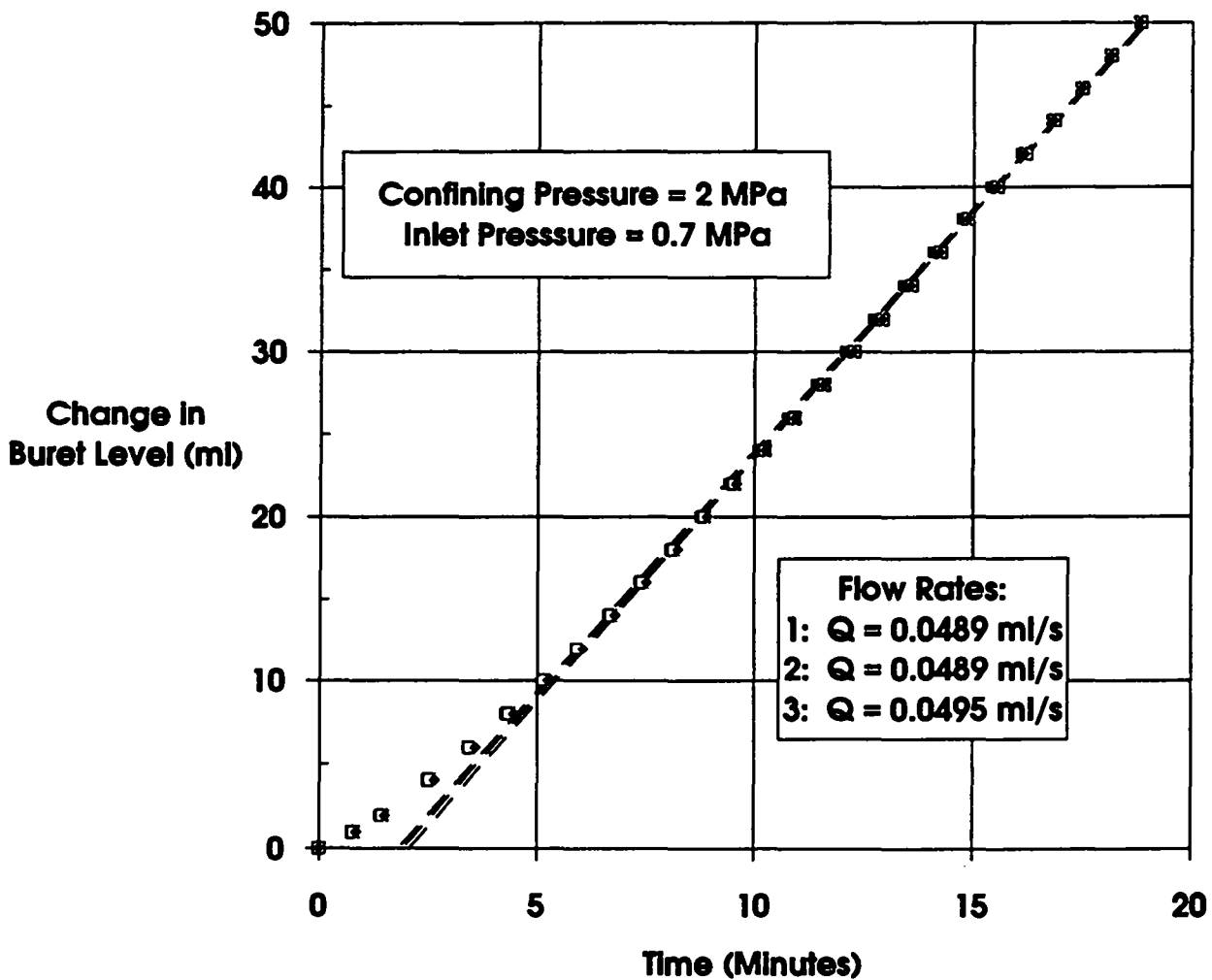
Figures (Continued)

- G-23** Gas volume-versus-time for tests on Specimen P3X11-5-3-SP3 at 6 MPa confining pressure and 0.7 MPa gas inlet pressure. Symbols represent recorded data points and dashed lines are best fits to linear sections of data B-231
- G-24** Gas volume-versus-time for tests on Specimen P3X11-5-3-SP3 at 6 MPa confining pressure and 0.4 MPa gas inlet pressure. Symbols represent recorded data points and dashed lines are best fits to linear sections of data B-232
- G-25** Gas volume-versus-time for tests on Specimen P3X11-5-3-SP3 at 10 MPa confining pressure and 1.0 MPa gas inlet pressure. Symbols represent recorded data points and dashed lines are best fits to linear sections of data B-233
- G-26** Gas volume-versus-time for tests on Specimen P3X11-5-3-SP3 at 10 MPa confining pressure and 0.7 MPa gas inlet pressure. Symbols represent recorded data points and dashed lines are best fits to linear sections of data B-234
- G-27** Gas volume-versus-time for tests on Specimen P3X11-5-3-SP3 at 10 MPa confining pressure and 0.4 MPa gas inlet pressure. Symbols represent recorded data points and dashed lines are best fits to linear sections of data B-235



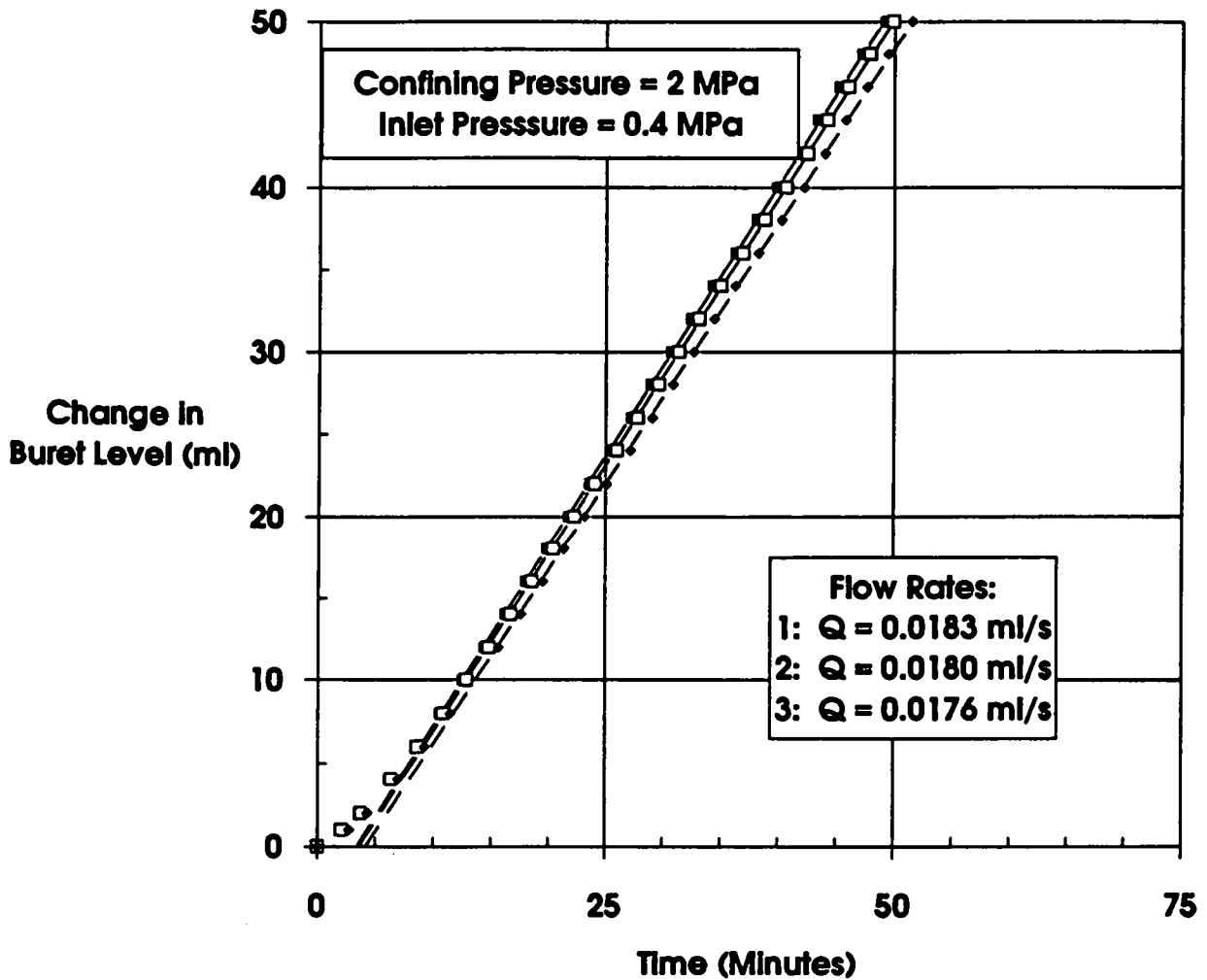
RSI-248-03-068

Figure G-1. Gas volume-versus-time for tests on Specimen P3X11-5-2-SP1 at 2 MPa confining pressure and 1.0 MPa gas inlet pressure. Symbols represent recorded data points and dashed lines are best fits to linear sections of data.



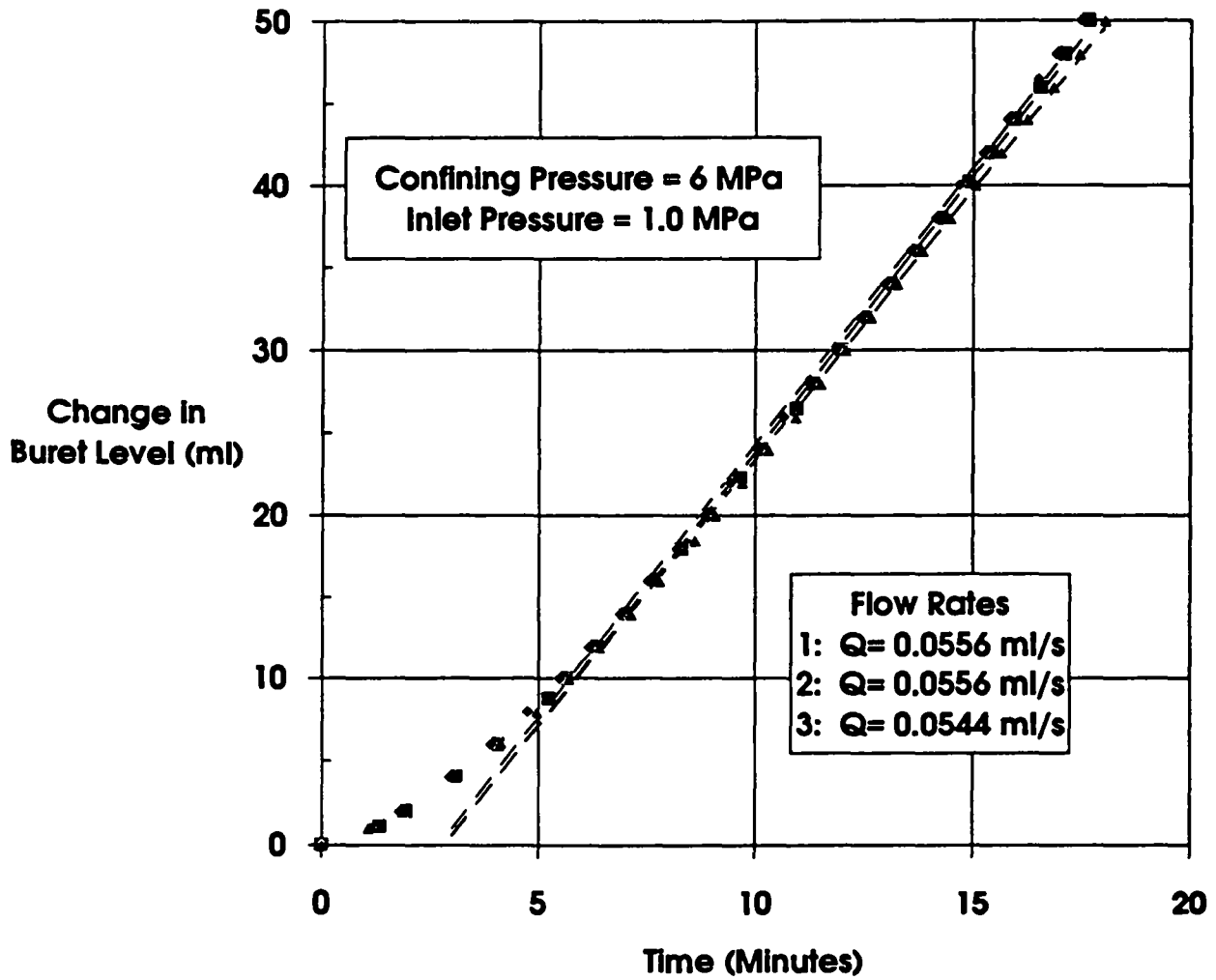
RSI-248-03-060

Figure G-2. Gas volume-versus-time for tests on Specimen P3X11-5-2-SP1 at 2 MPa confining pressure and 0.7 MPa gas inlet pressure. Symbols represent recorded data points and dashed lines are best fits to linear sections of data.



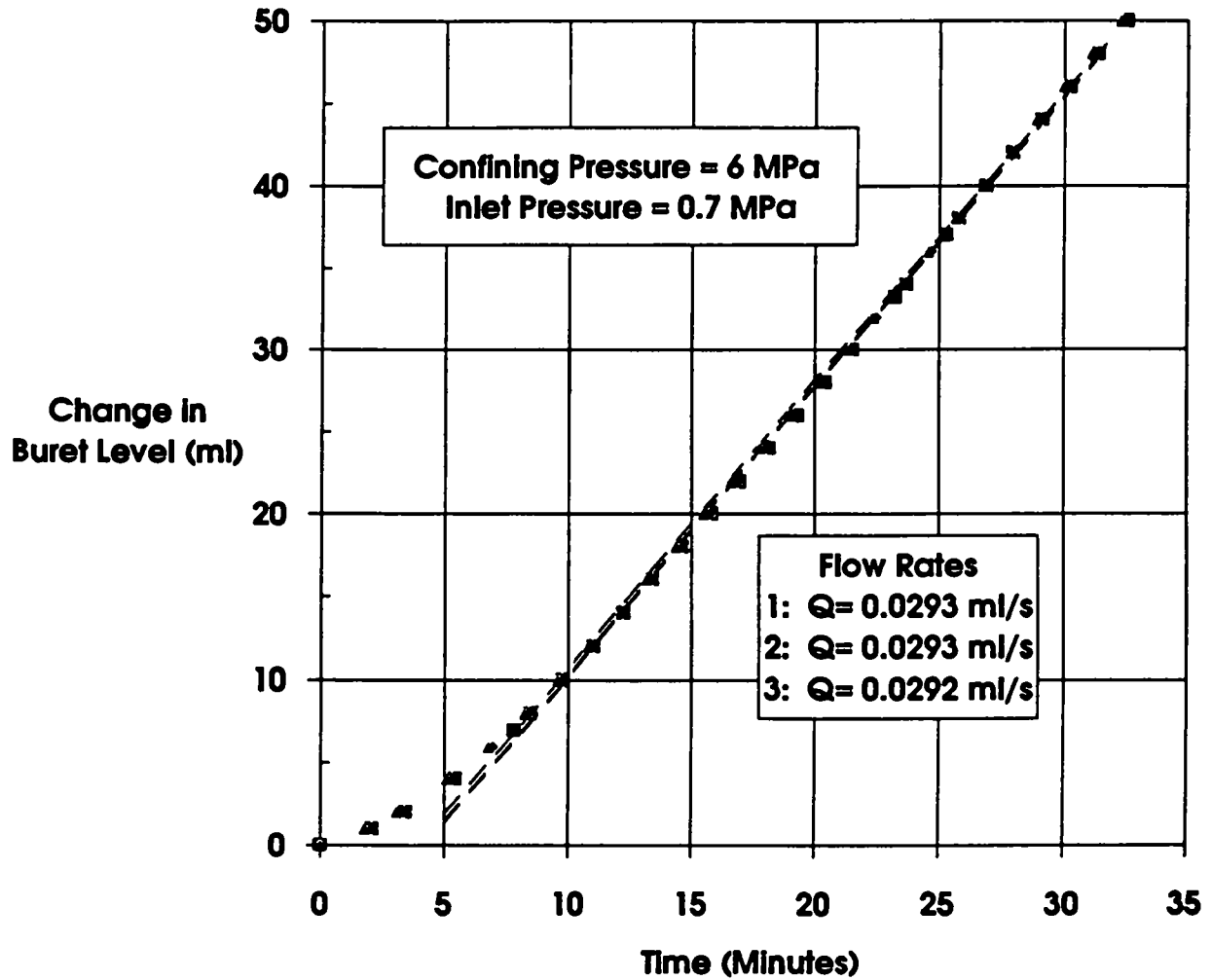
RSI-248-03-080

Figure G-3. Gas volume-versus-time for tests on Specimen P3X11-5-2-SP1 at 2 MPa confining pressure and 0.4 MPa gas inlet pressure. Symbols represent recorded data points and dashed lines are best fits to linear sections of data.



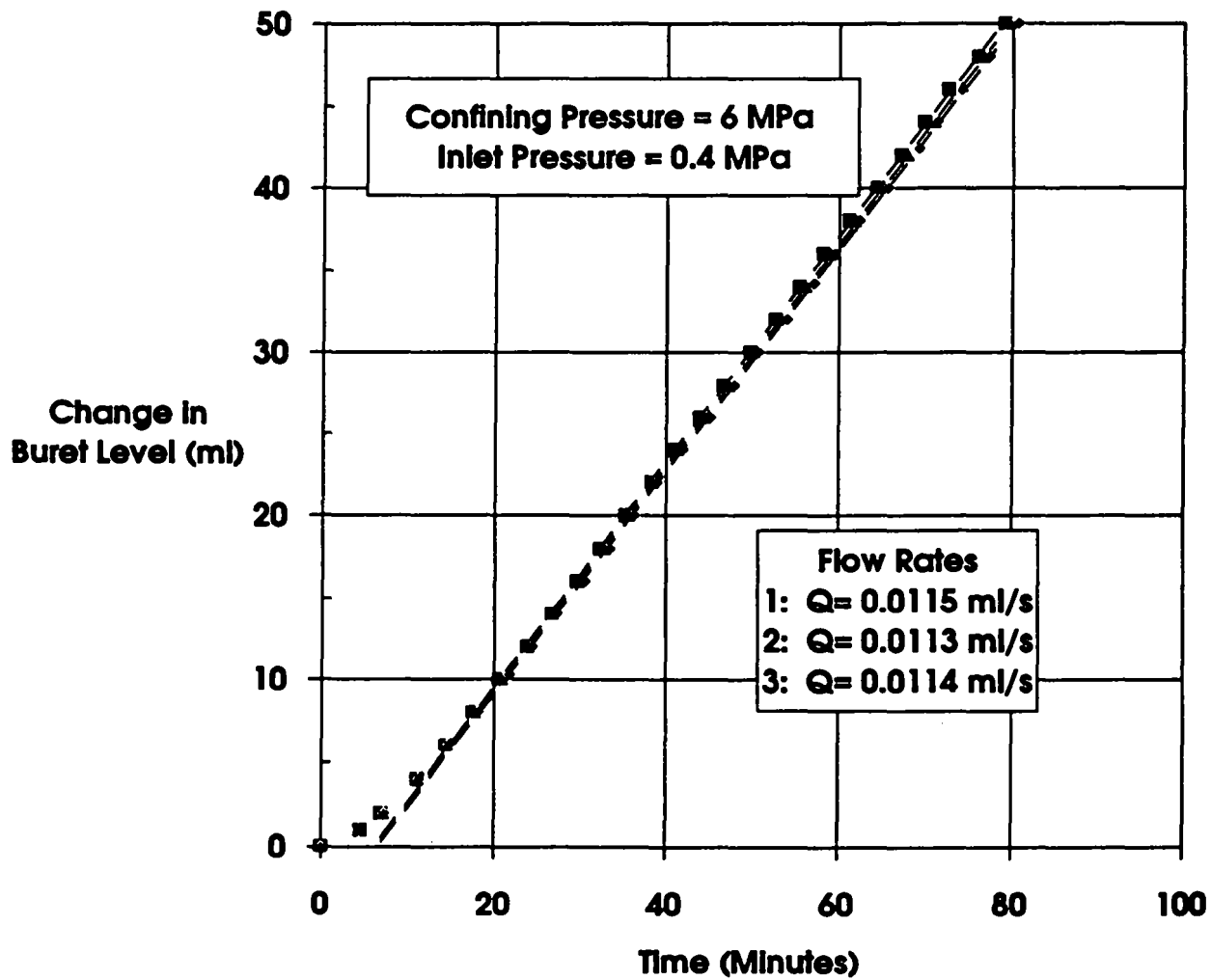
RSI-248-03-001

Figure G-4. Gas volume-versus-time for tests on Specimen P3X11-5-2-SP1 at 6 MPa confining pressure and 1.0 MPa gas inlet pressure. Symbols represent recorded data points and dashed lines are best fits to linear sections of data.



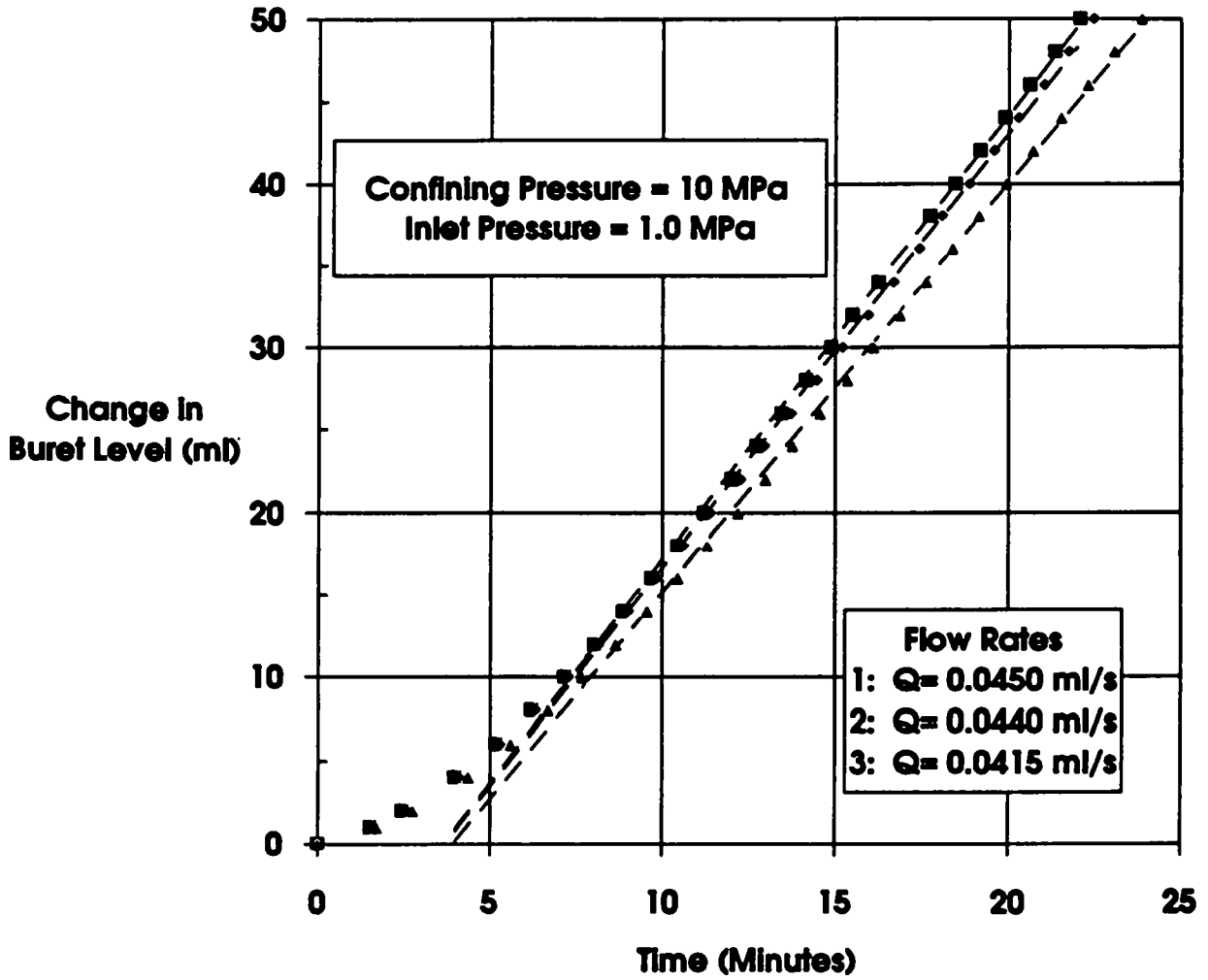
RSI-248-93-062

Figure G-5. Gas volume-versus-time for tests on Specimen P3X11-5-2-SP1 at 6 MPa confining pressure and 0.7 MPa gas inlet pressure. Symbols represent recorded data points and dashed lines are best fits to linear sections of data.



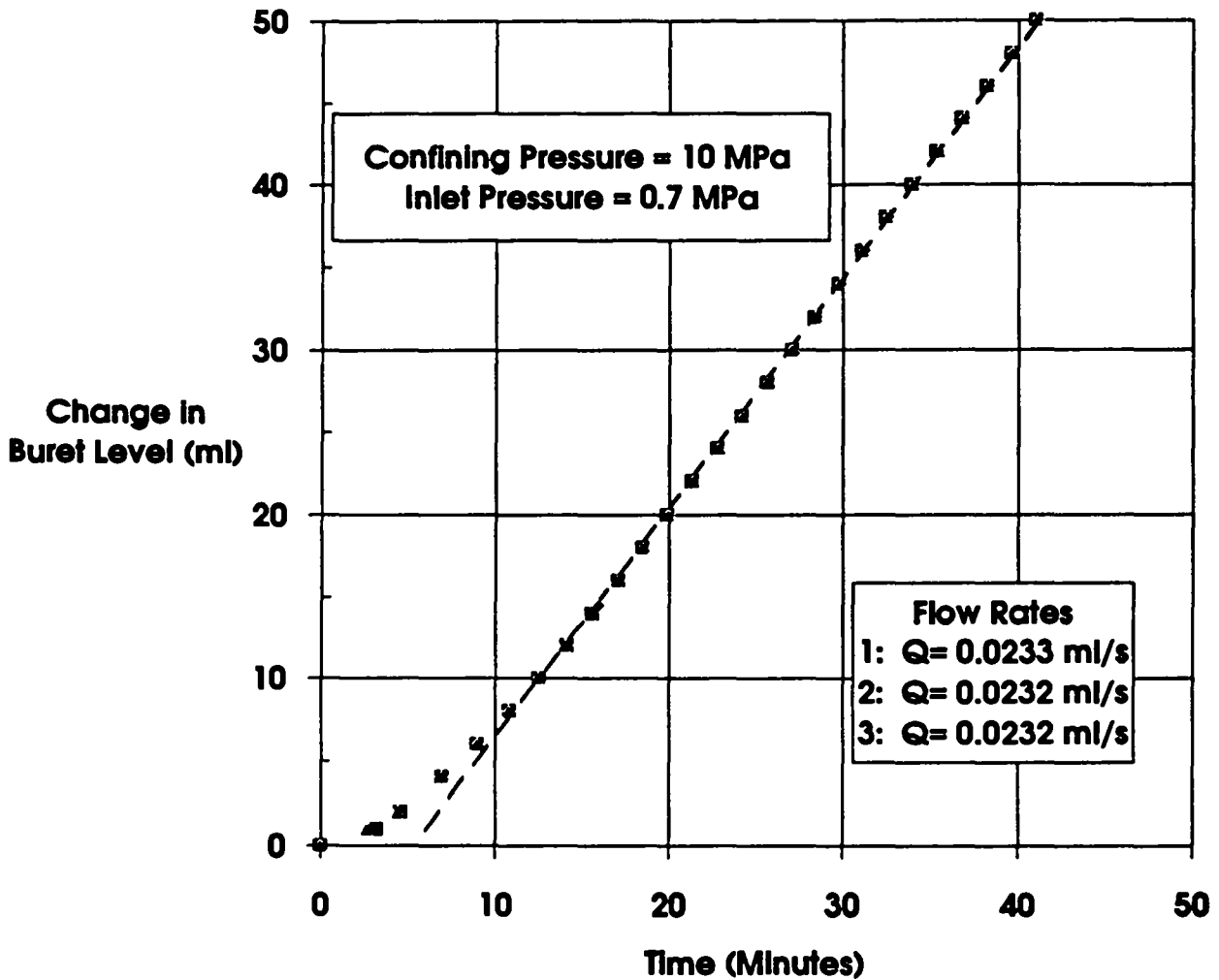
FB1-245-00-003

Figure G-6. Gas volume-versus-time for tests on Specimen P3X11-5-2-SP1 at 6 MPa confining pressure and 0.4 MPa gas inlet pressure. Symbols represent recorded data points and dashed lines are best fits to linear sections of data.



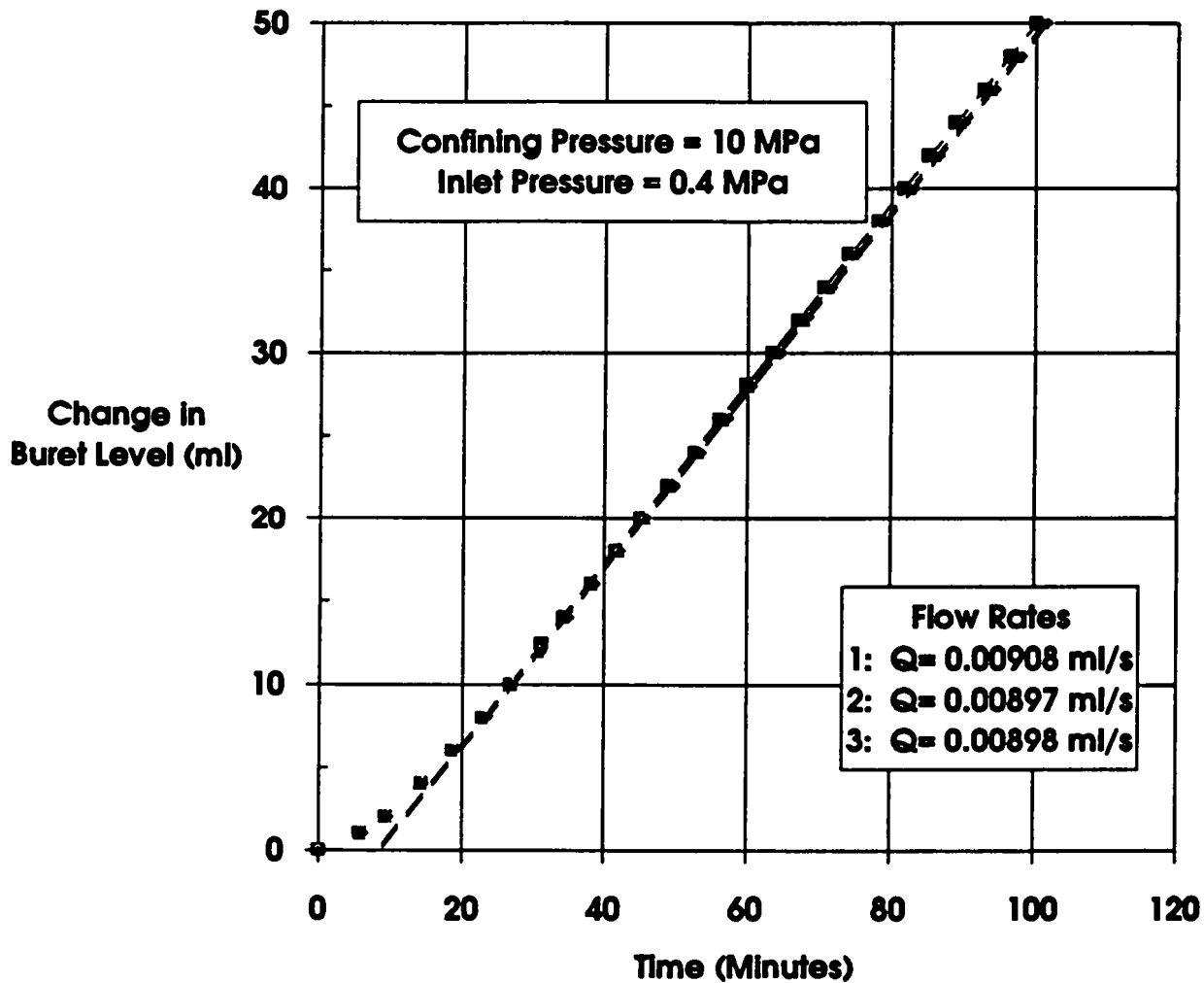
FBI-345-03-004

Figure G-7. Gas volume-versus-time for tests on Specimen P3X11-5-2-SP1 at 10 MPa confining pressure and 1.0 MPa gas inlet pressure. Symbols represent recorded data points and dashed lines are best fits to linear sections of data.



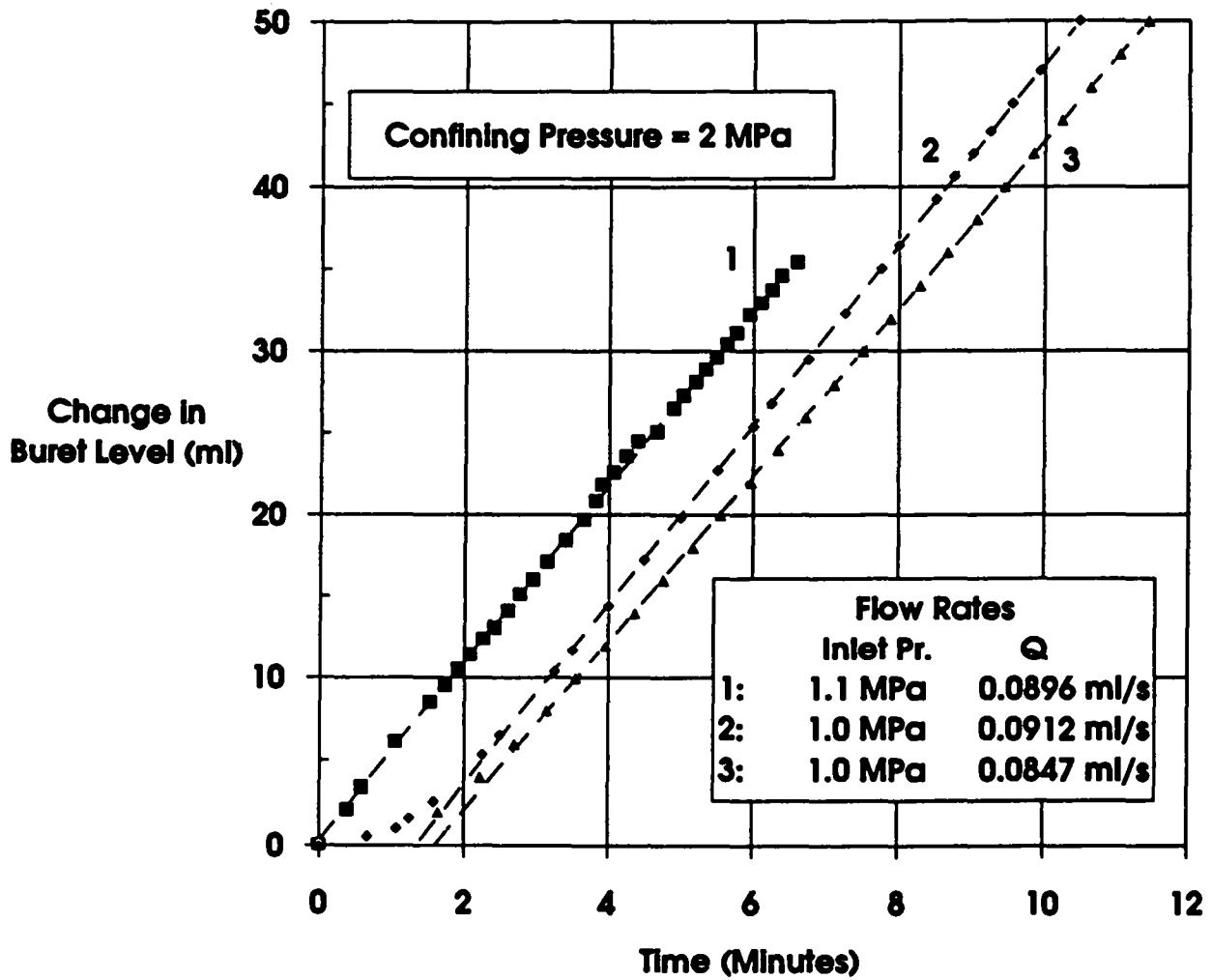
RSI-248-03-065

Figure G-8. Gas volume-versus-time for tests on Specimen P3X11-5-2-SP1 at 10 MPa confining pressure and 0.7 MPa gas inlet pressure. Symbols represent recorded data points and dashed lines are best fits to linear sections of data.



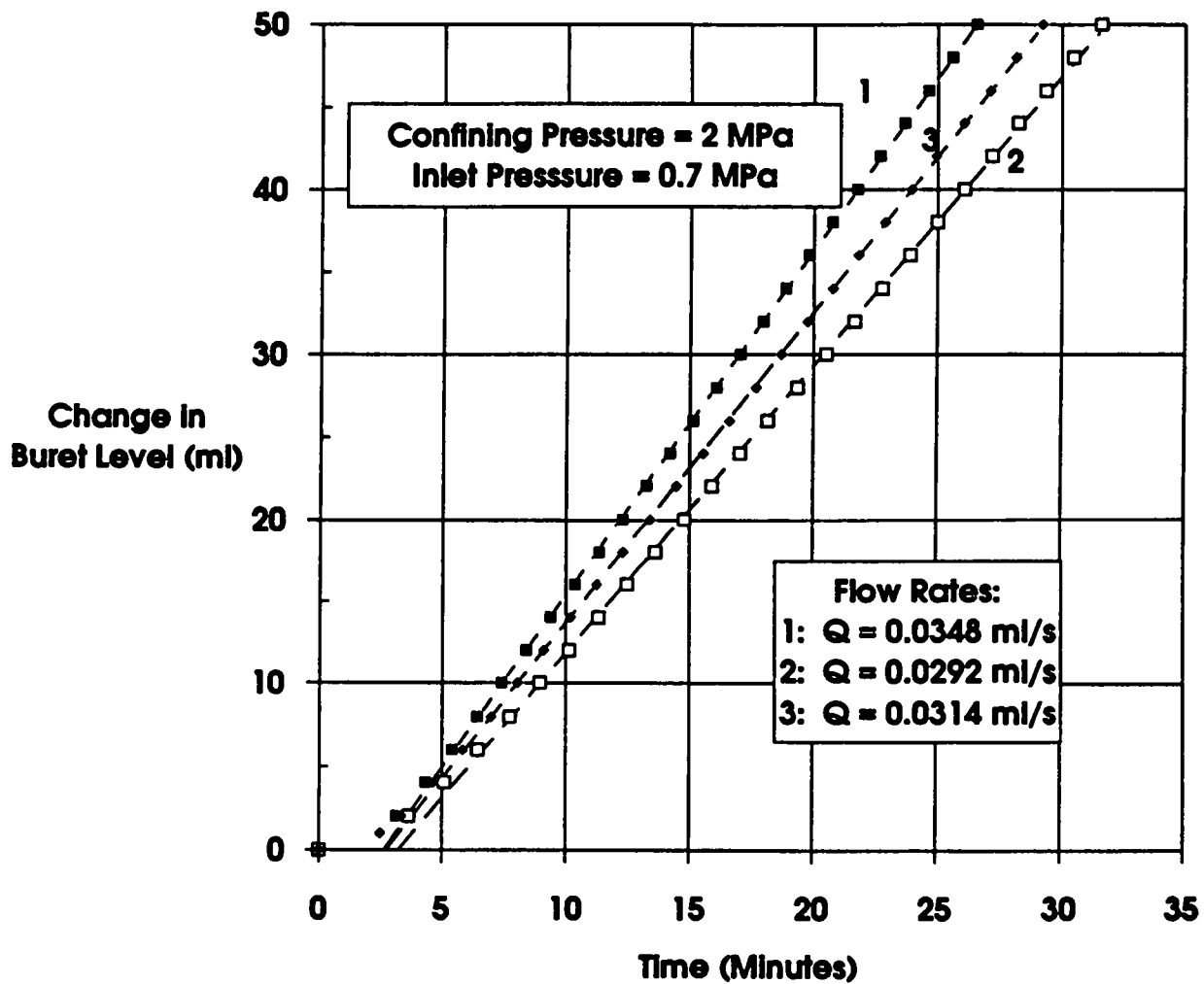
R81-248-03-008

Figure G-9. Gas volume-versus-time for tests on Specimen P3X11-5-2-SP1 at 10 MPa confining pressure and 0.4 MPa gas inlet pressure. Symbols represent recorded data points and dashed lines are best fits to linear sections of data.



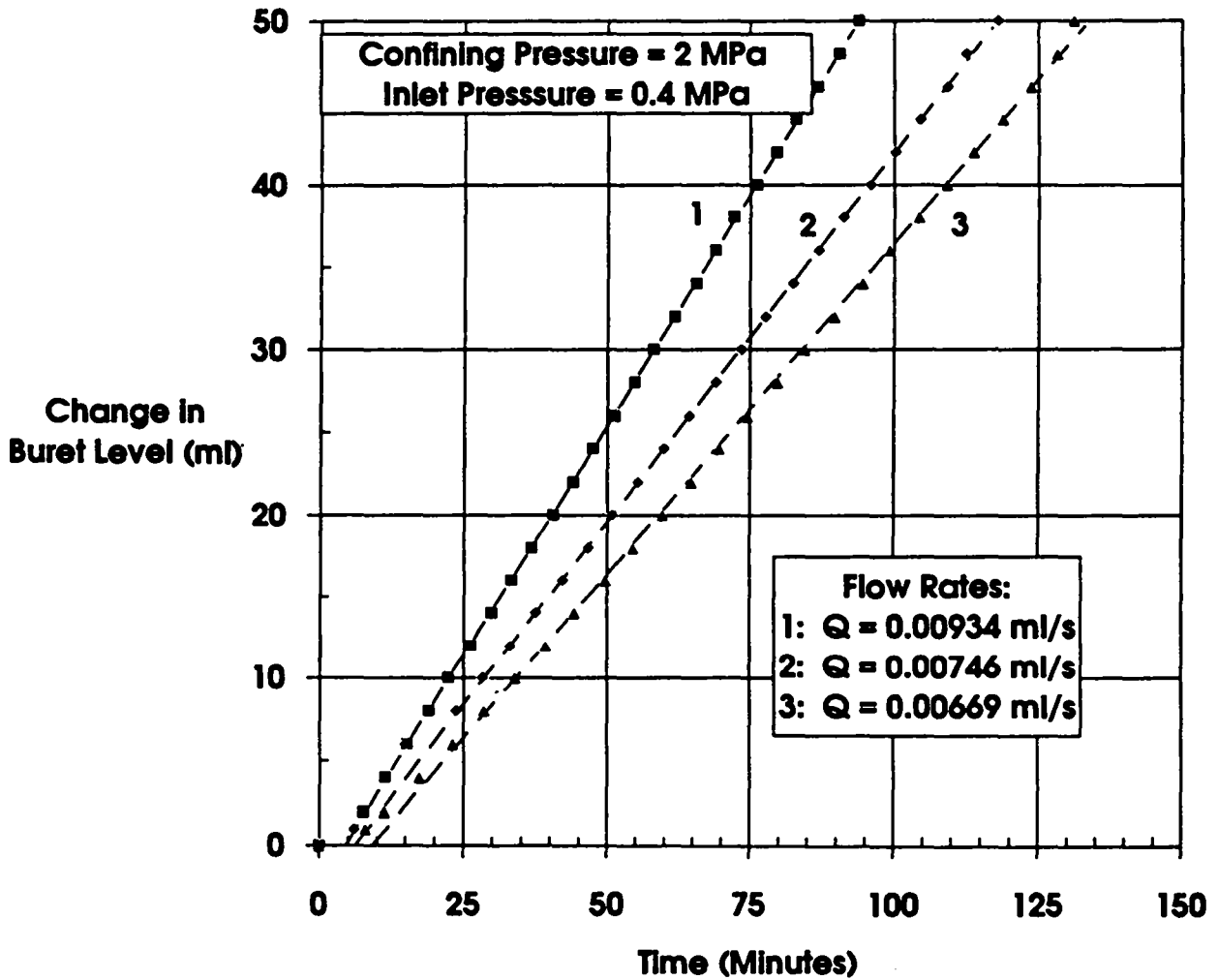
RSI-248-83-087

Figure G-10. Gas volume-versus-time for tests on Specimen P3X10-6-SP2 at 2 MPa confining pressure and 1.0 MPa gas inlet pressure. Symbols represent recorded data points and dashed lines are best fits to linear sections of data.



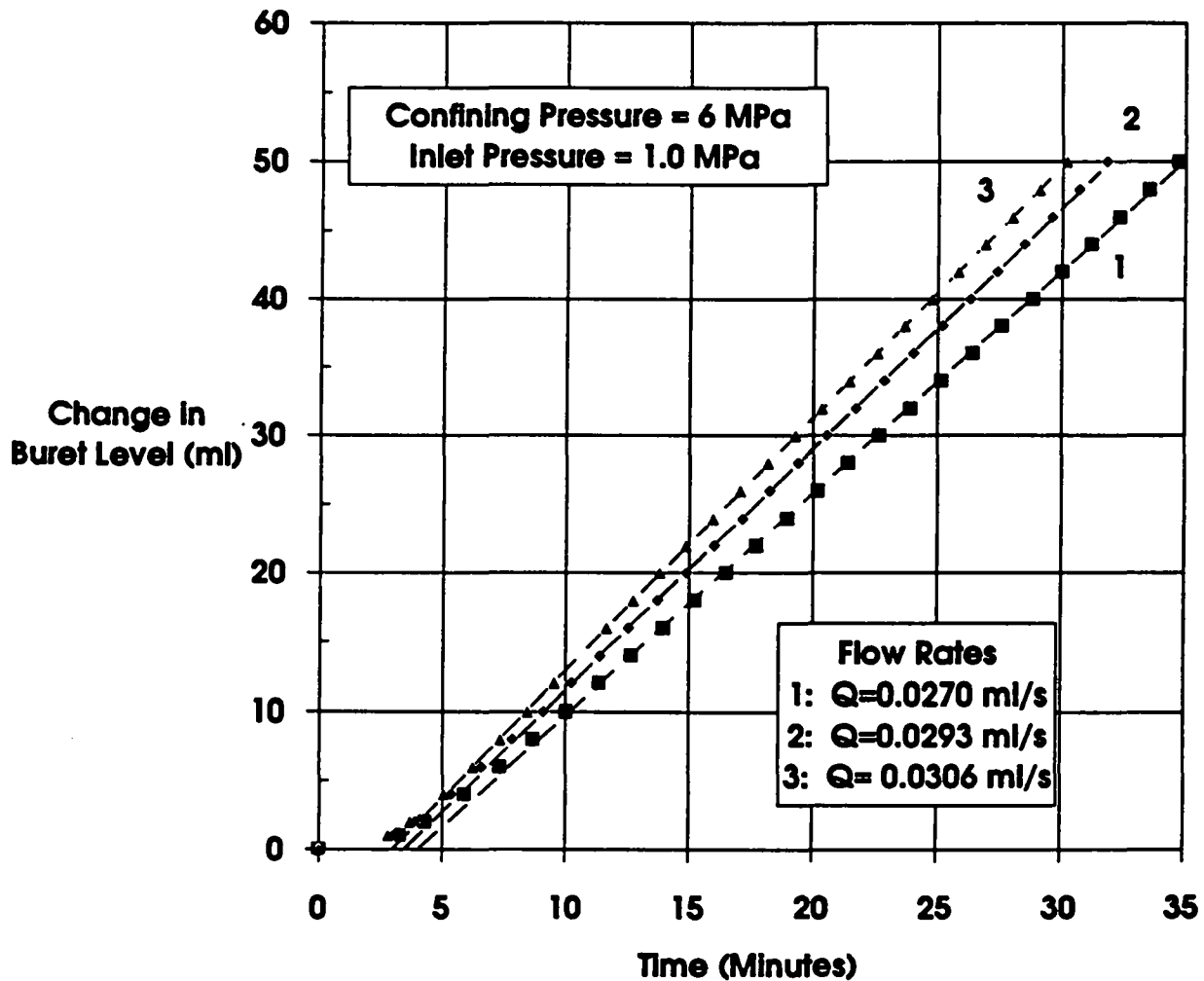
RSI-348-03-008

Figure G-11. Gas volume-versus-time for tests on Specimen P3X10-6-SP2 at 2 MPa confining pressure and 0.7 MPa gas inlet pressure. Symbols represent recorded data points and dashed lines are best fits to linear sections of data.



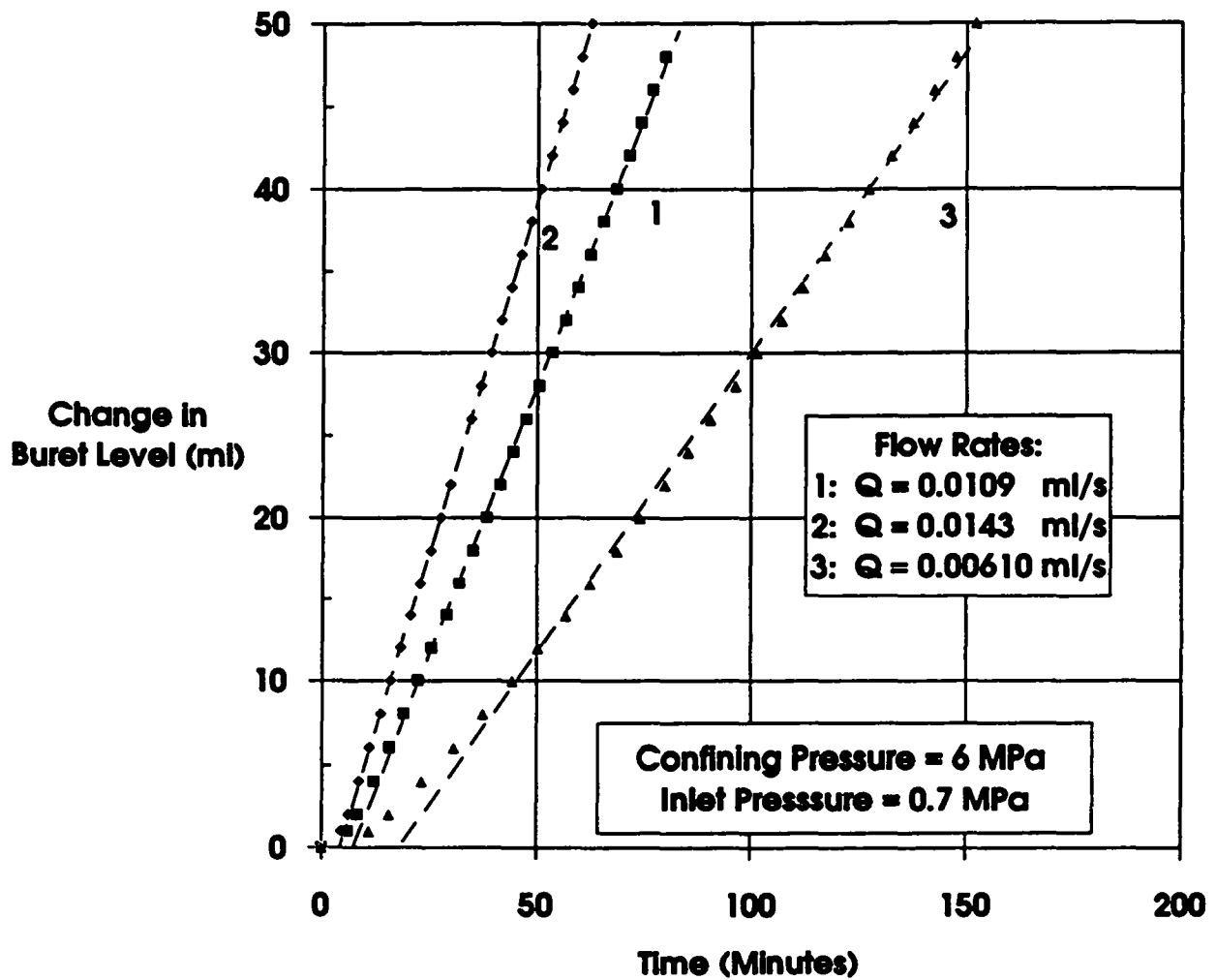
FB1-248-03-000

Figure G-12. Gas volume-versus-time for tests on Specimen P3X10-6-SP2 at 2 MPa confining pressure and 0.4 MPa gas inlet pressure. Symbols represent recorded data points and dashed lines are best fits to linear sections of data.



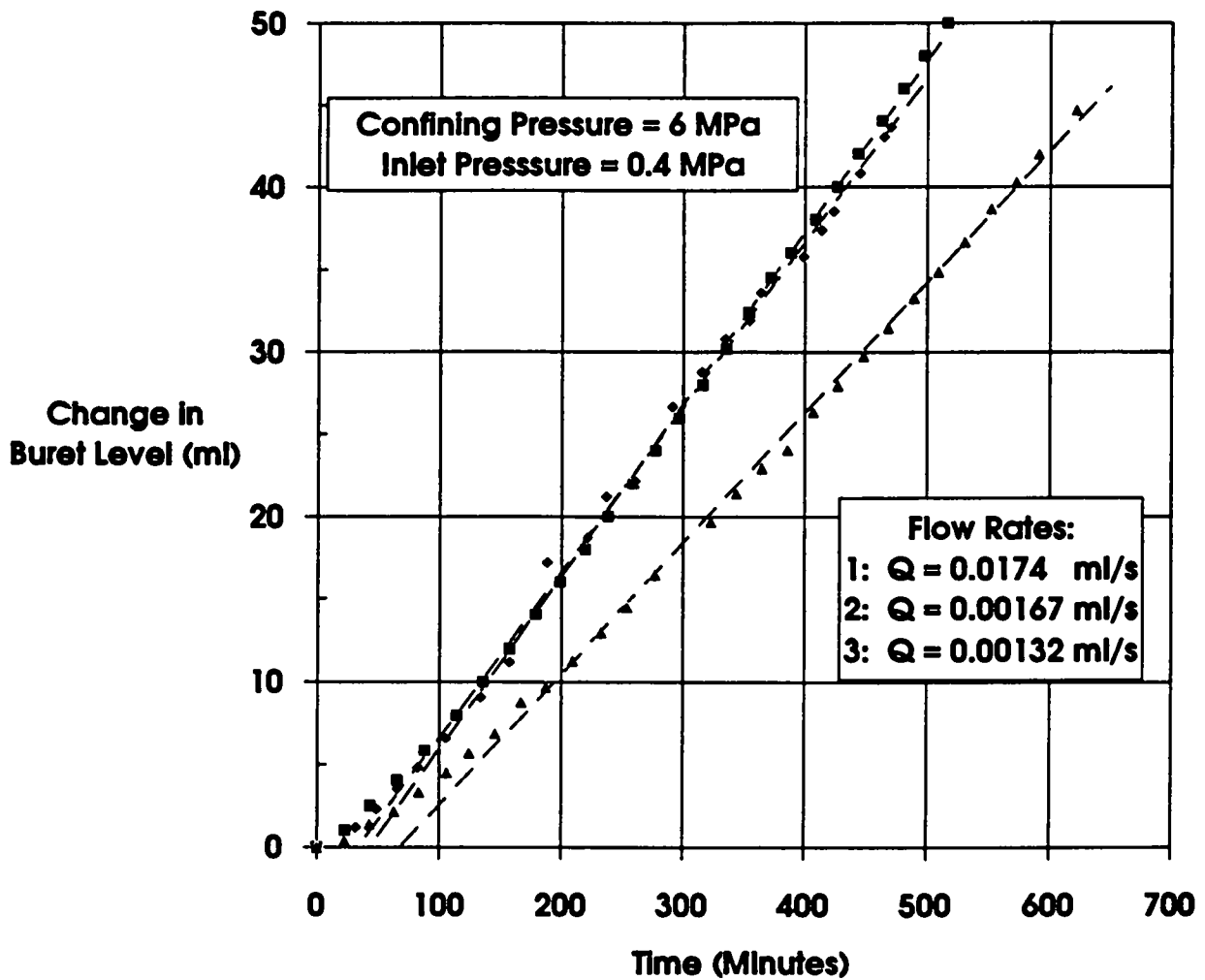
R81-248-03-070

Figure G-13. Gas volume-versus-time for tests on Specimen P3X10-6-SP2 at 6 MPa confining pressure and 1.0 MPa gas inlet pressure. Symbols represent recorded data points and dashed lines are best fits to linear sections of data.



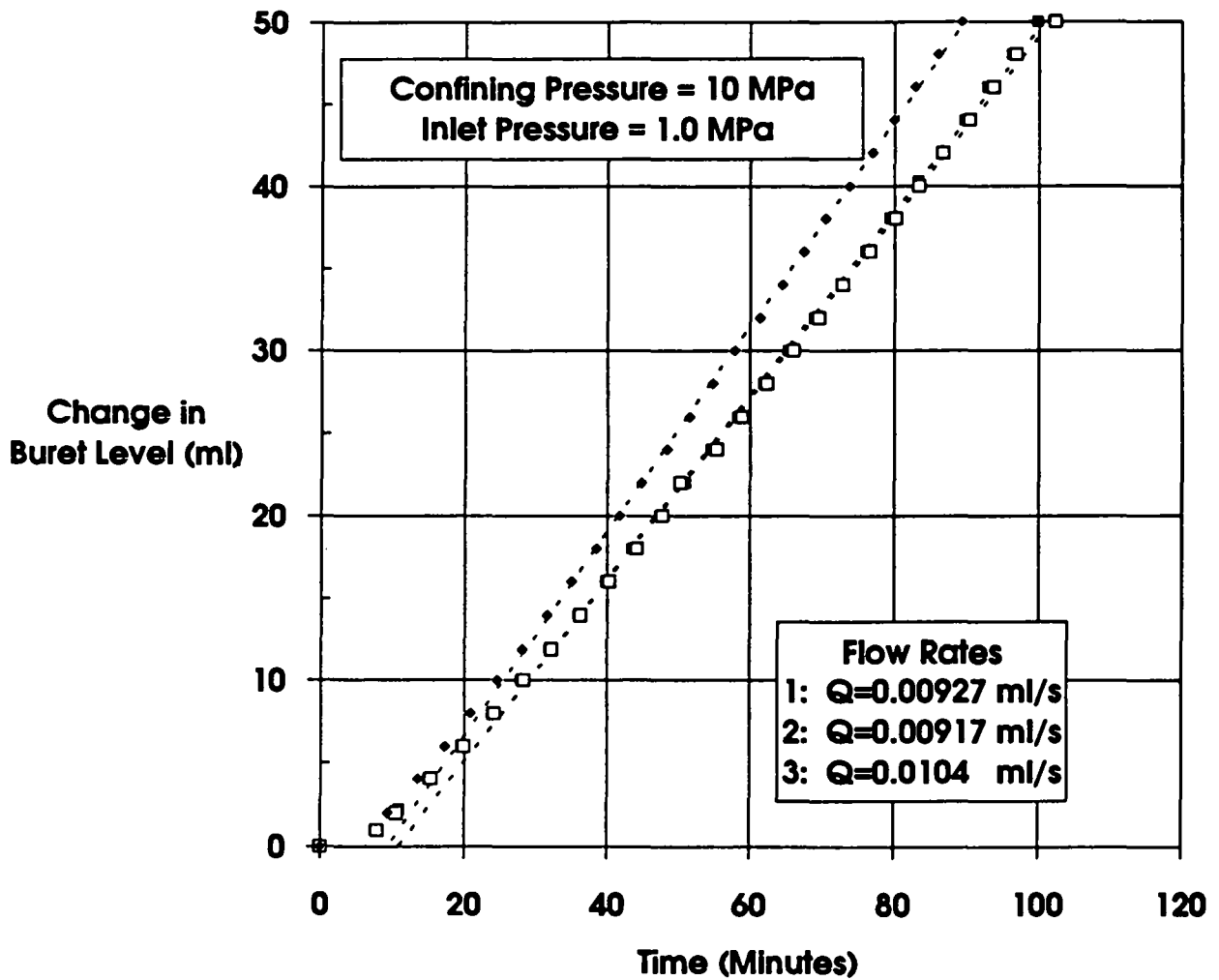
R81-248-83-071

Figure G-14. Gas volume-versus-time for tests on Specimen P3X10-6-SP2 at 6 MPa confining pressure and 0.7 MPa gas inlet pressure. Symbols represent recorded data points and dashed lines are best fits to linear sections of data.



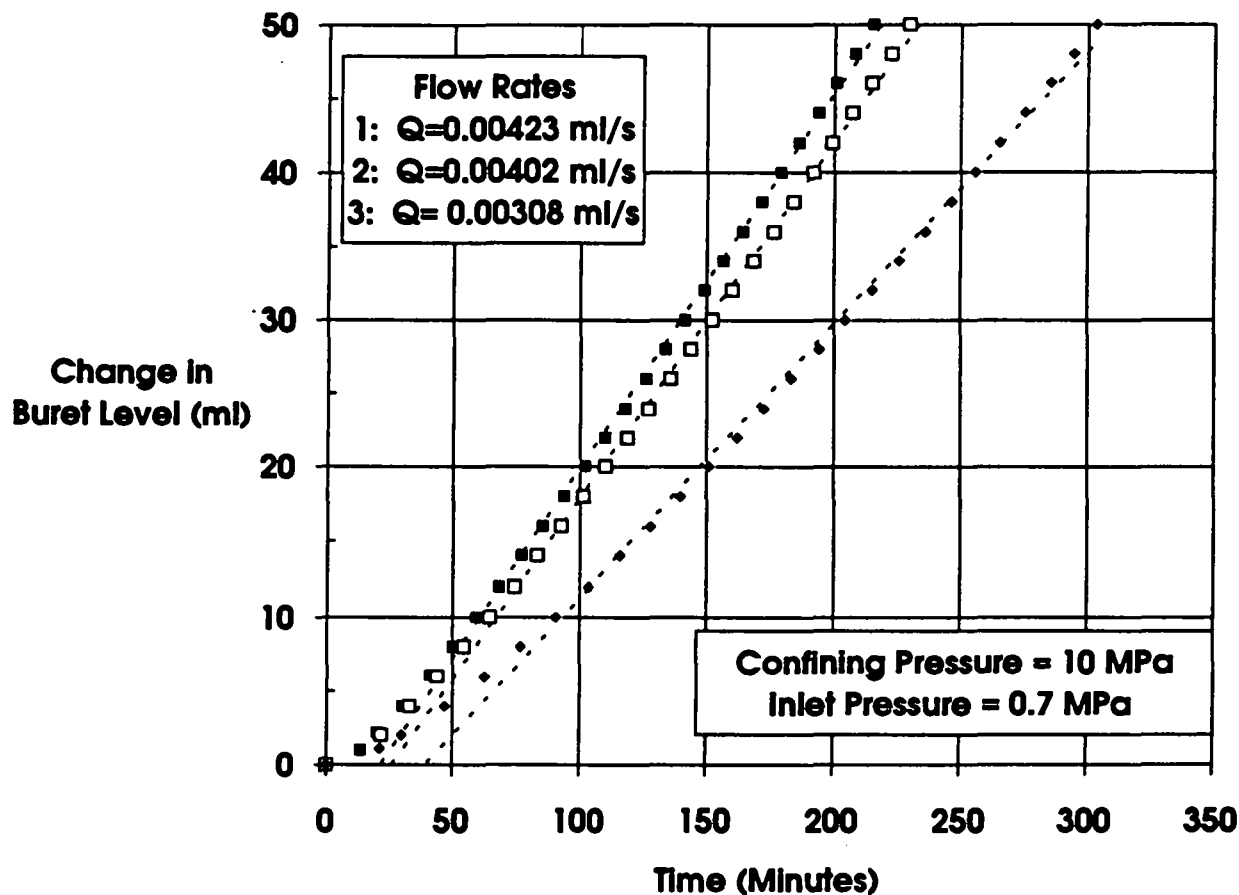
RBI-248-03-072

Figure G-15. Gas volume-versus-time for tests on Specimen P3X10-6-SP2 at 6 MPa confining pressure and 0.4 MPa gas inlet pressure. Symbols represent recorded data points and dashed lines are best fits to linear sections of data.



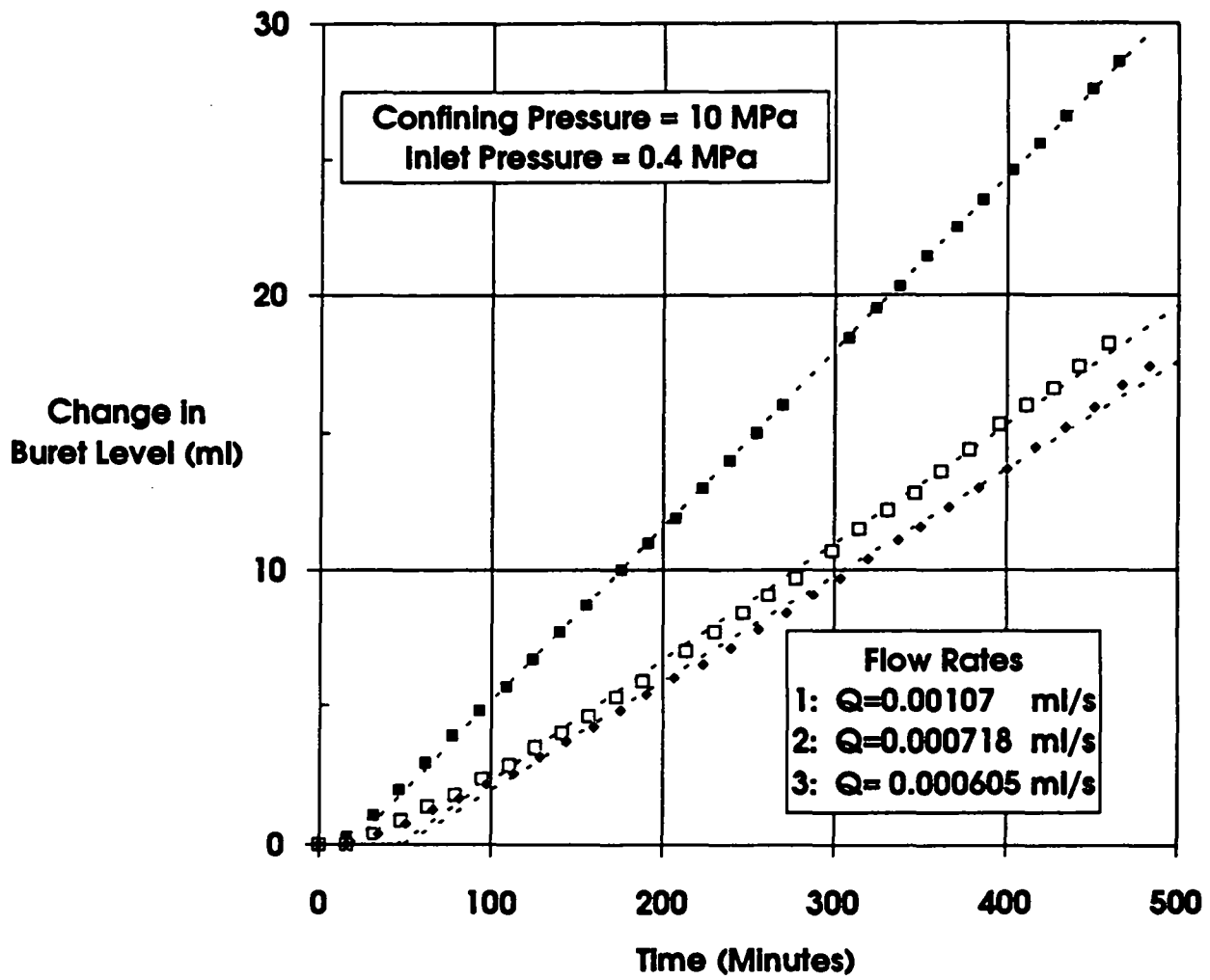
FBI-248-83-073

Figure G-16. Gas volume-versus-time for tests on Specimen P3X10-6-SP2 at 10 MPa confining pressure and 1.0 MPa gas inlet pressure. Symbols represent recorded data points and dashed lines are best fits to linear sections of data.



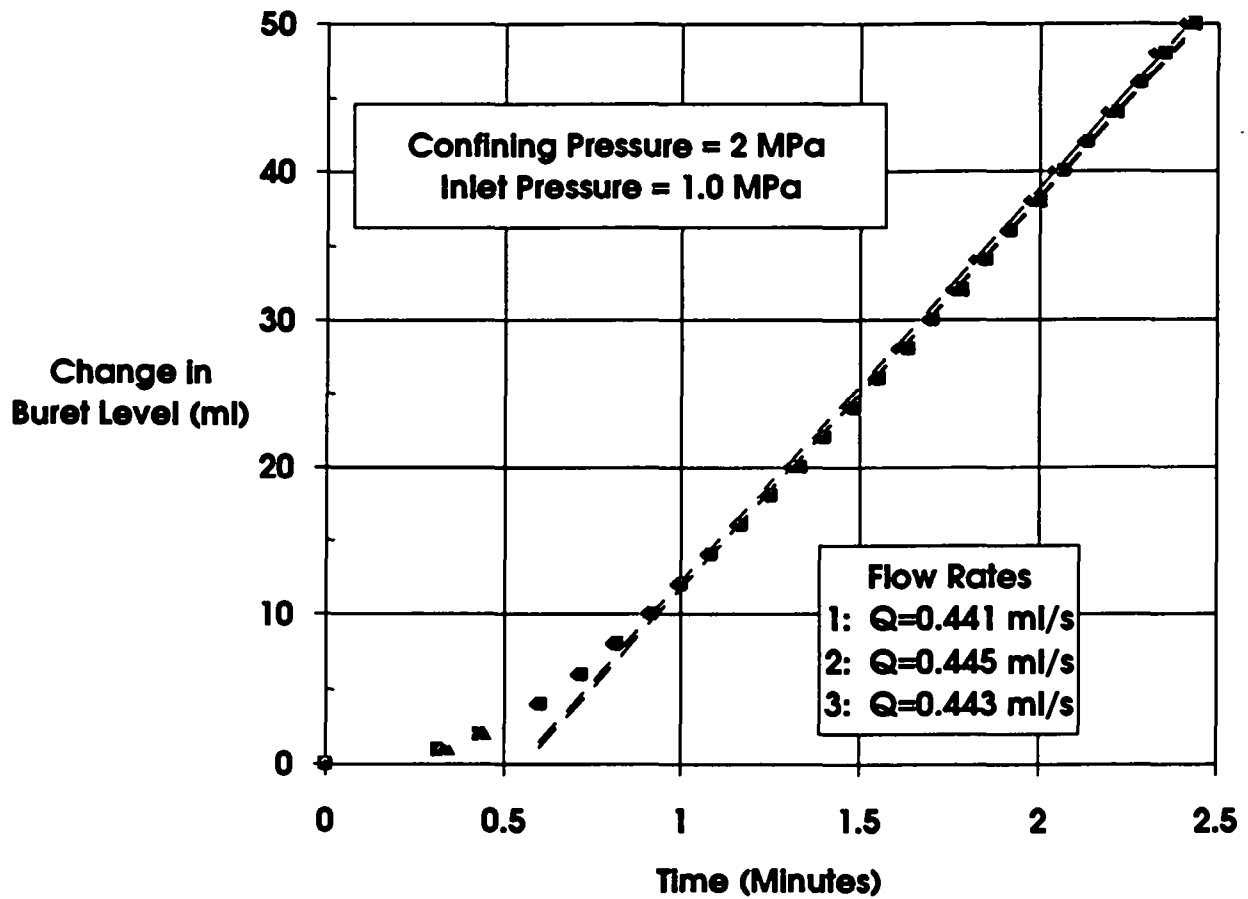
RBI-248-83-074

Figure G-17. Gas volume-versus-time for tests on Specimen P3X10-6-SP2 at 10 MPa confining pressure and 0.7 MPa gas inlet pressure. Symbols represent recorded data points and dashed lines are best fits to linear sections of data.



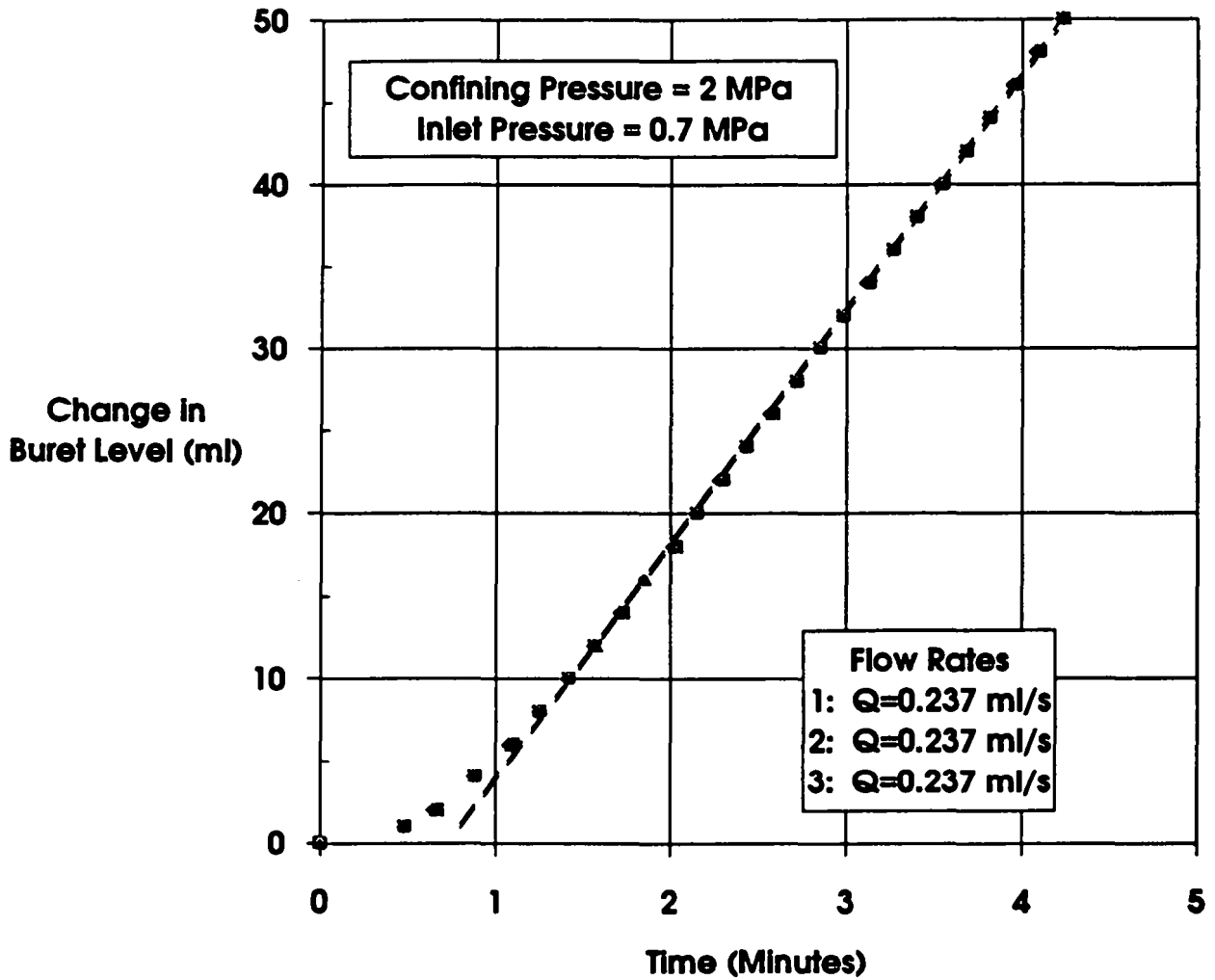
PSI-248-03-075

Figure G-18. Gas volume-versus-time for tests on Specimen P3X10-6-SP2 at 10 MPa confining pressure and 0.4 MPa gas inlet pressure. Symbols represent recorded data points and dashed lines are best fits to linear sections of data.



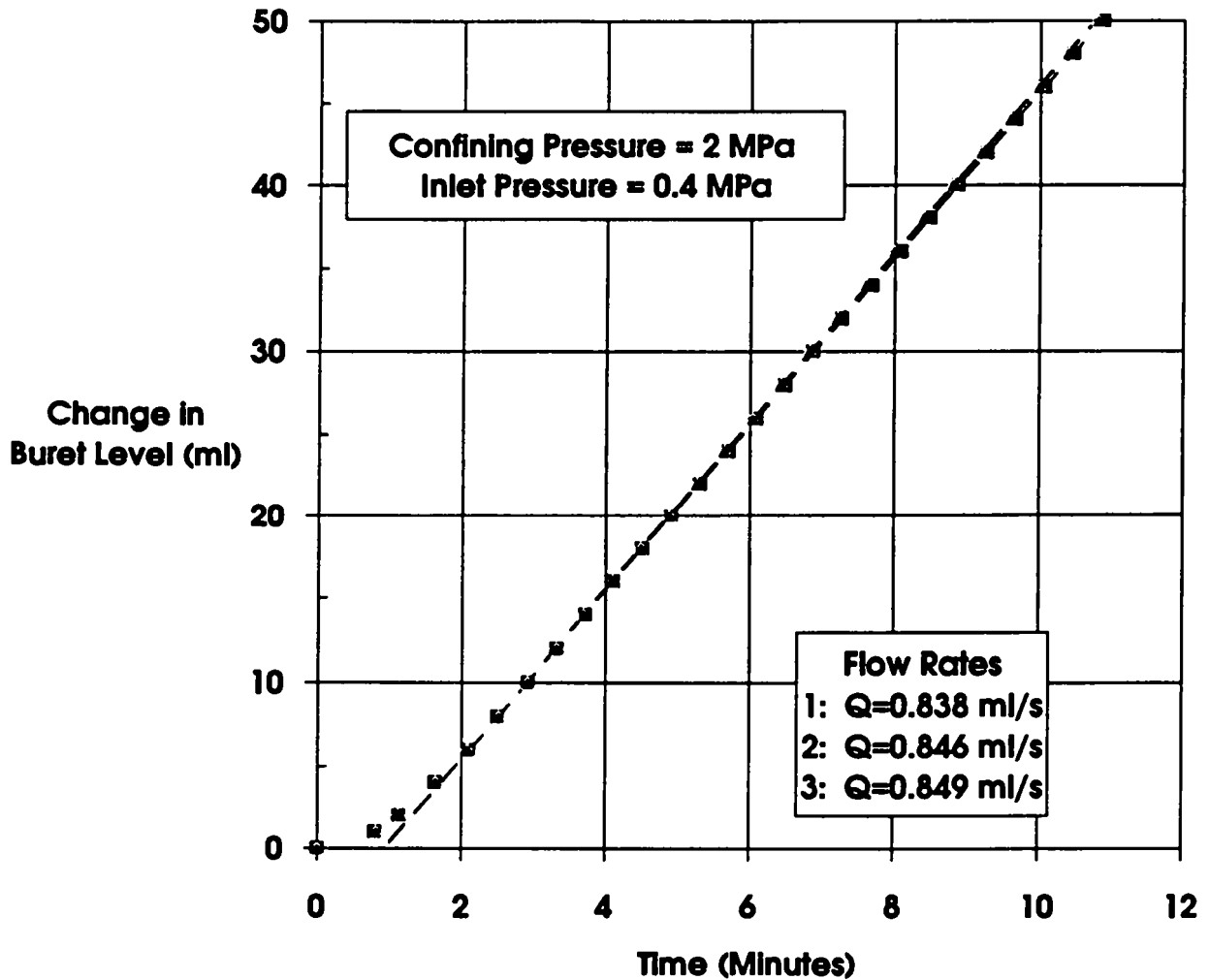
RSI-348-83-076

Figure G-19. Gas volume-versus-time for tests on Specimen P3X11-5-3-SP3 at 2 MPa confining pressure and 1.0 MPa gas inlet pressure. Symbols represent recorded data points and dashed lines are best fits to linear sections of data.



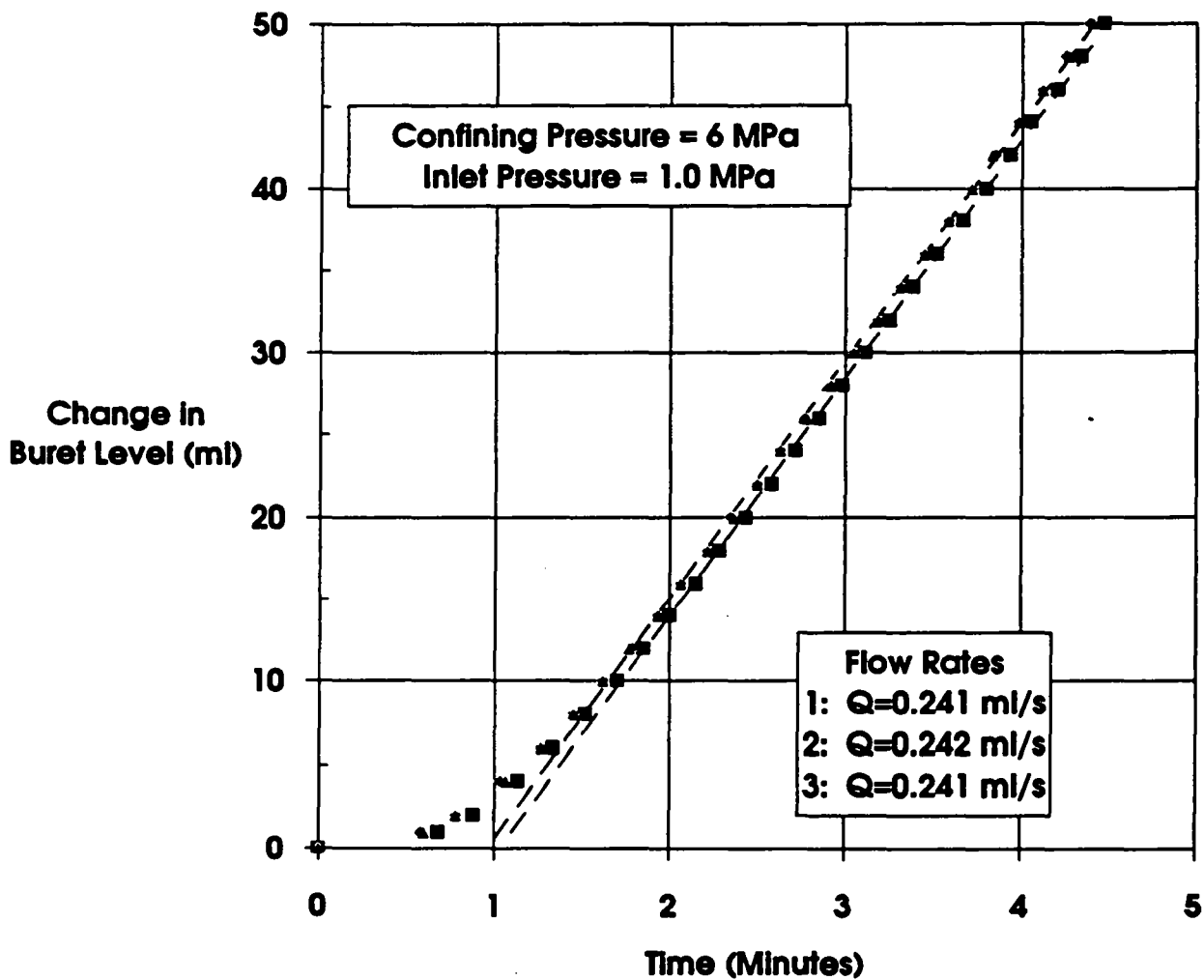
R81-248-03-077

Figure G-20. Gas volume-versus-time for tests on Specimen P3X11-5-3-SP3 at 2 MPa confining pressure and 0.7 MPa gas inlet pressure. Symbols represent recorded data points and dashed lines are best fits to linear sections of data.



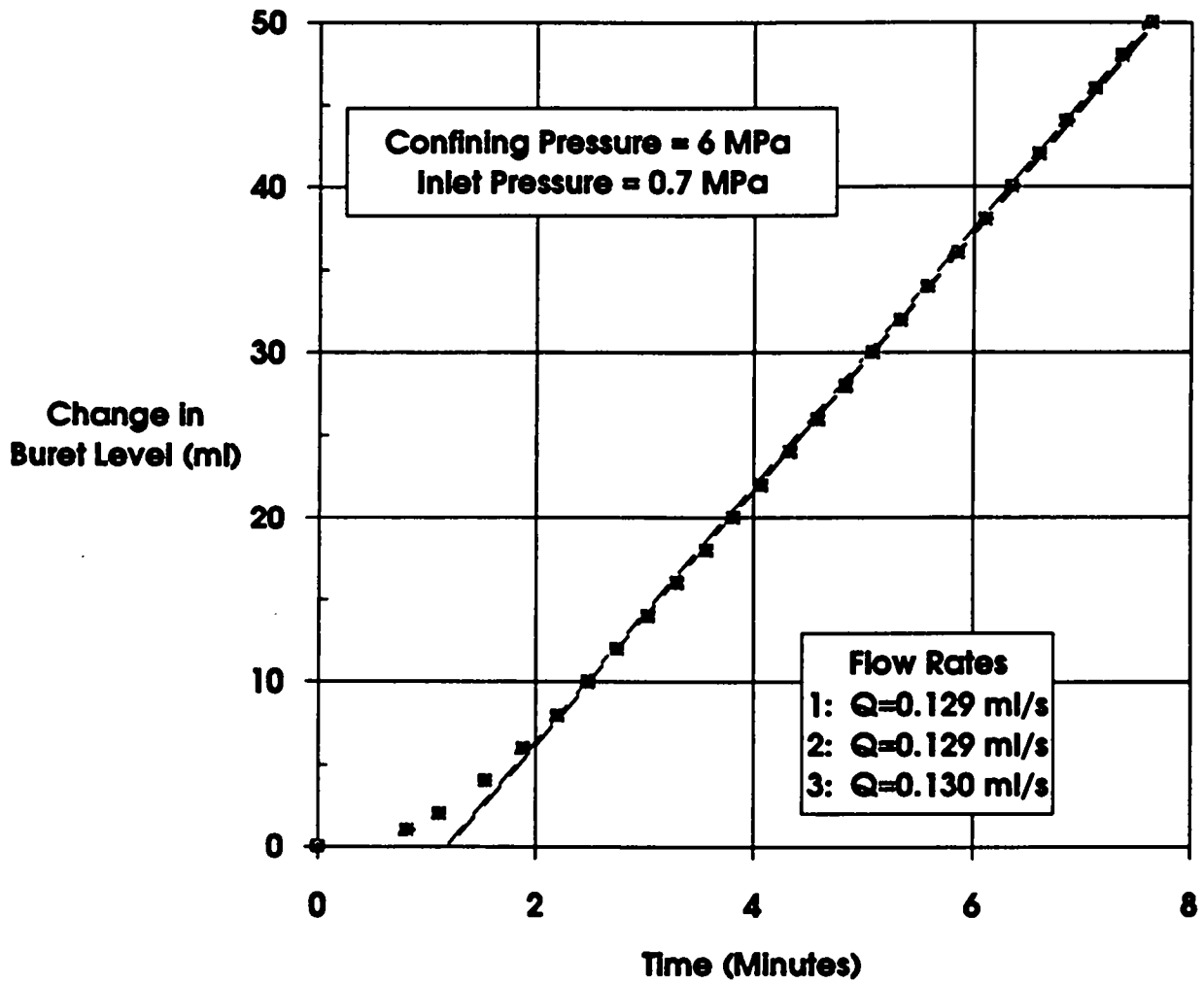
FBI-248-03-078

Figure G-21. Gas volume-versus-time for tests on Specimen P3X11-5-3-SP3 at 2 MPa confining pressure and 0.4 MPa gas inlet pressure. Symbols represent recorded data points and dashed lines are best fits to linear sections of data.



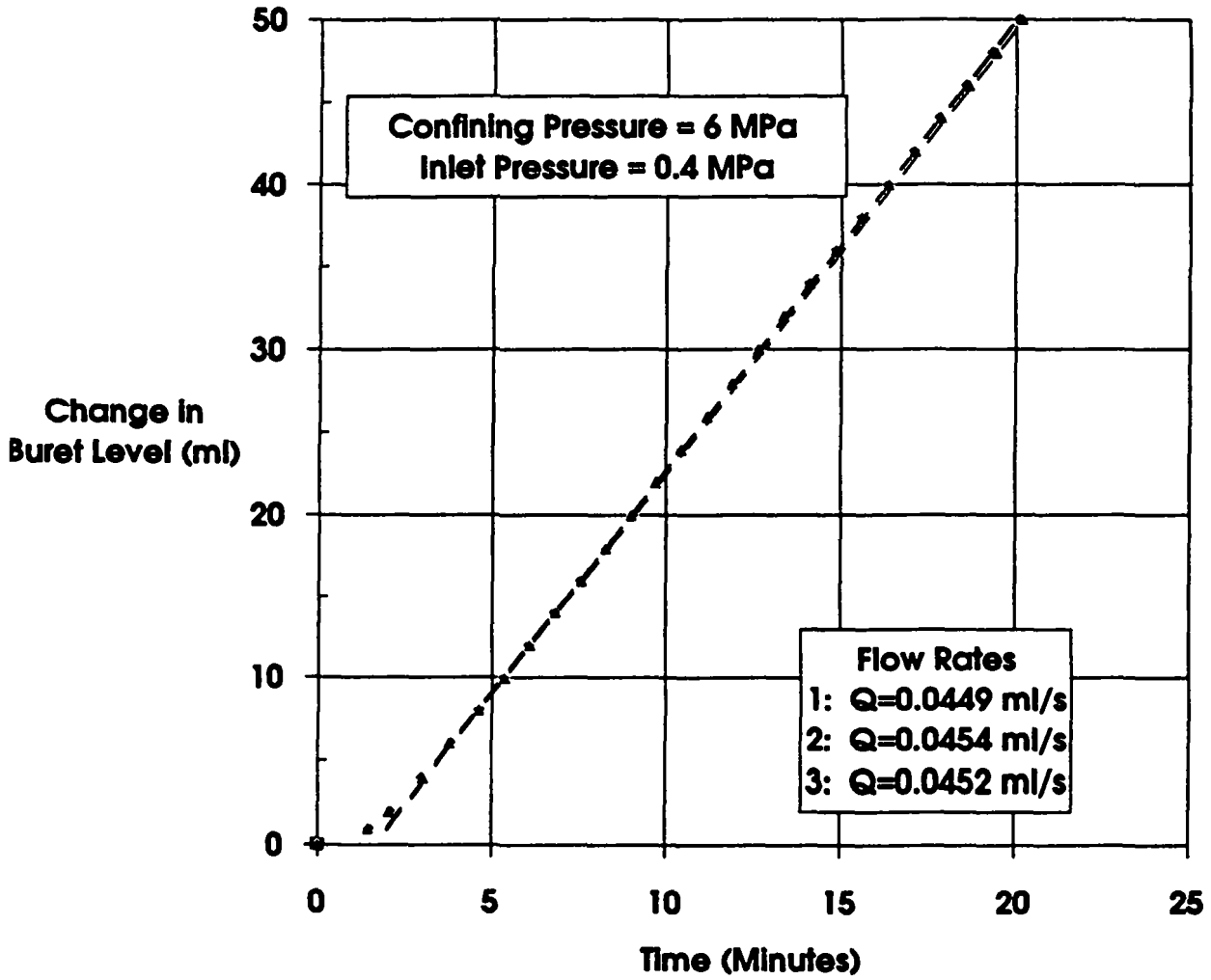
R81-248-83-079

Figure G-22. Gas volume-versus-time for tests on Specimen P3X11-5-3-SP3 at 6 MPa confining pressure and 1.0 MPa gas inlet pressure. Symbols represent recorded data points and dashed lines are best fits to linear sections of data.



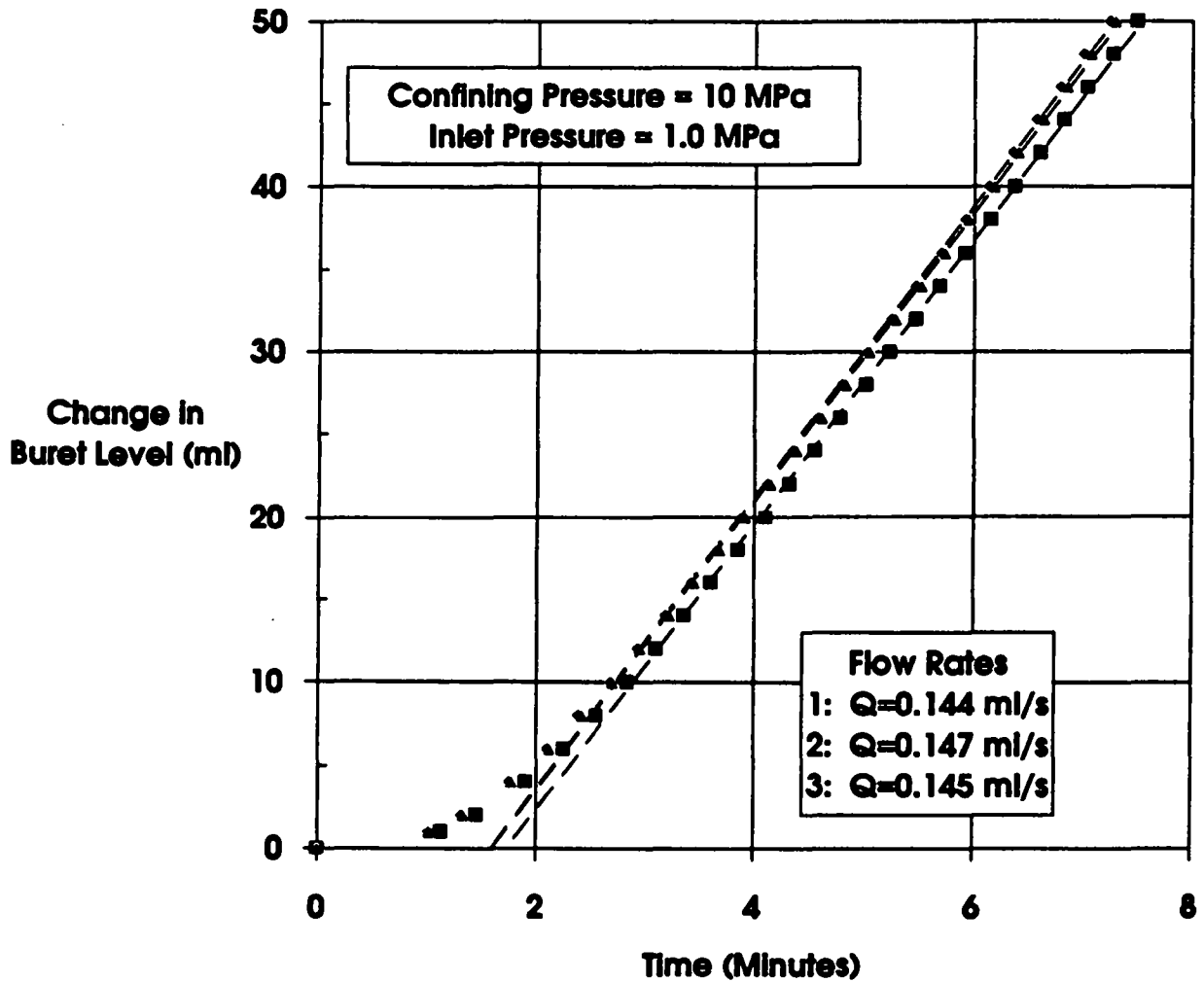
R81-248-03-080

Figure G-23. Gas volume-versus-time for tests on Specimen P3X11-5-3-SP3 at 6 MPa confining pressure and 0.7 MPa gas inlet pressure. Symbols represent recorded data points and dashed lines are best fits to linear sections of data.



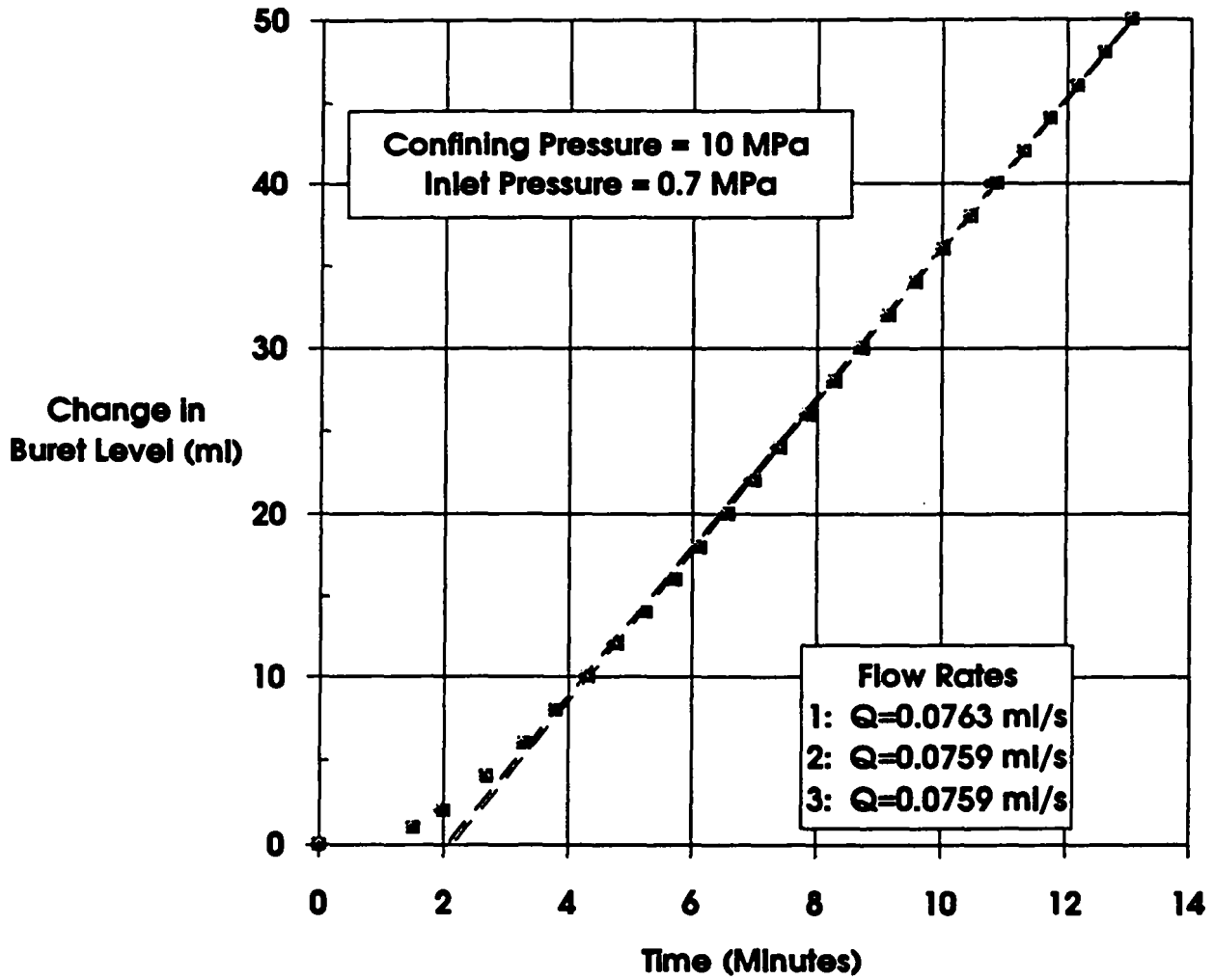
RSI-248-03-081

Figure G-24. Gas volume-versus-time for tests on Specimen P3X11-5-3-SP3 at 6 MPa confining pressure and 0.4 MPa gas inlet pressure. Symbols represent recorded data points and dashed lines are best fits to linear sections of data.



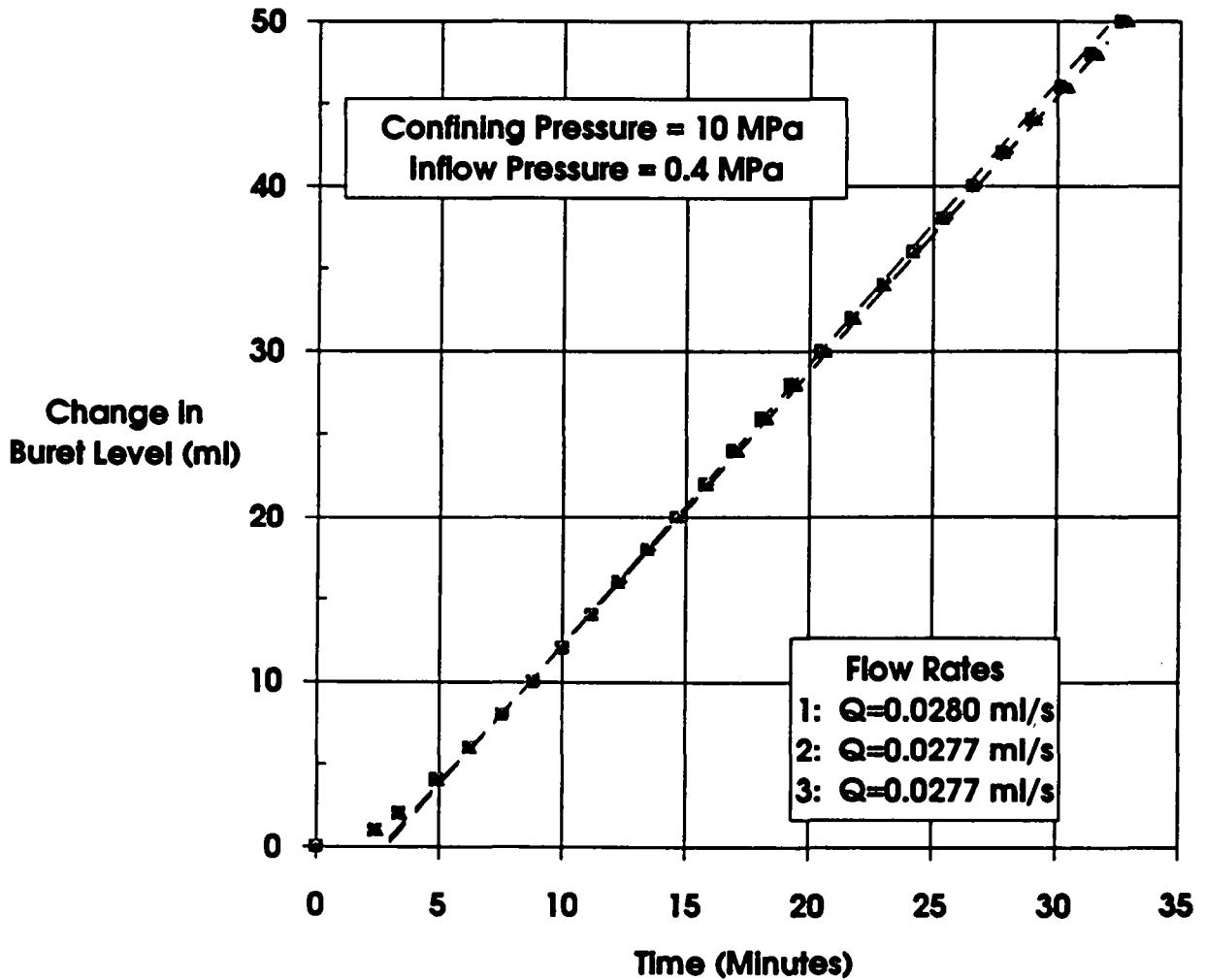
R81-248-80-082

Figure G-25. Gas volume-versus-time for tests on Specimen P3X11-5-3-SP3 at 10 MPa confining pressure and 1.0 MPa gas inlet pressure. Symbols represent recorded data points and dashed lines are best fits to linear sections of data.



FSI-248-63-083

Figure G-26. Gas volume-versus-time for tests on Specimen P3X11-5-3-SP3 at 10 MPa confining pressure and 0.7 MPa gas inlet pressure. Symbols represent recorded data points and dashed lines are best fits to linear sections of data.



R81-248-03-084

Figure G-27. Gas volume-versus-time for tests on Specimen P3X11-5-3-SP3 at 10 MPa confining pressure and 0.4 MPa gas inlet pressure. Symbols represent recorded data points and dashed lines are best fits to linear sections of data.

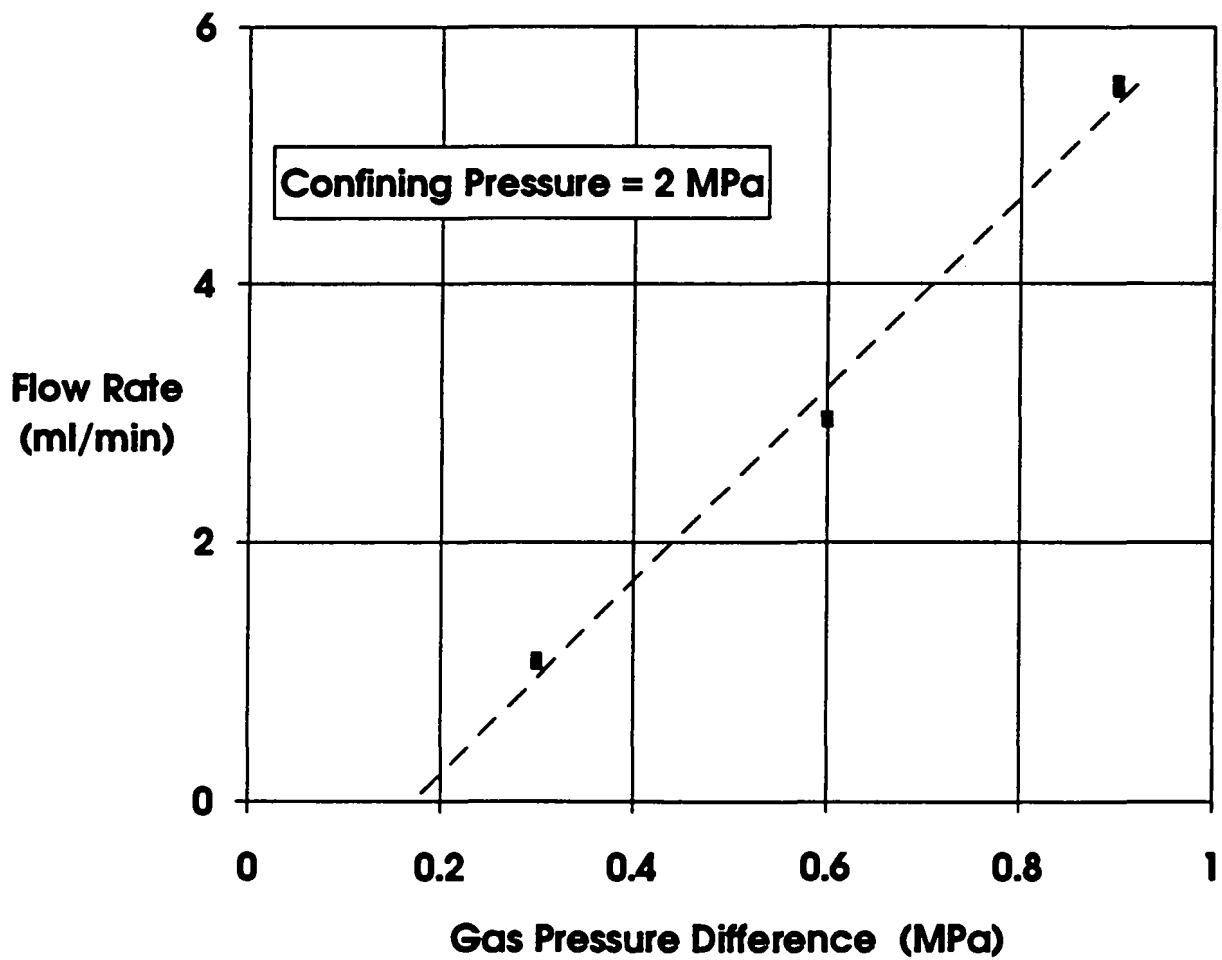
B-236

**APPENDIX B.H. FLOW RATE-VERSUS-PORE PRESSURE DIFFERENCE
ACROSS SPECIMEN FOR GAS PERMEABILITY TESTS**

B-238

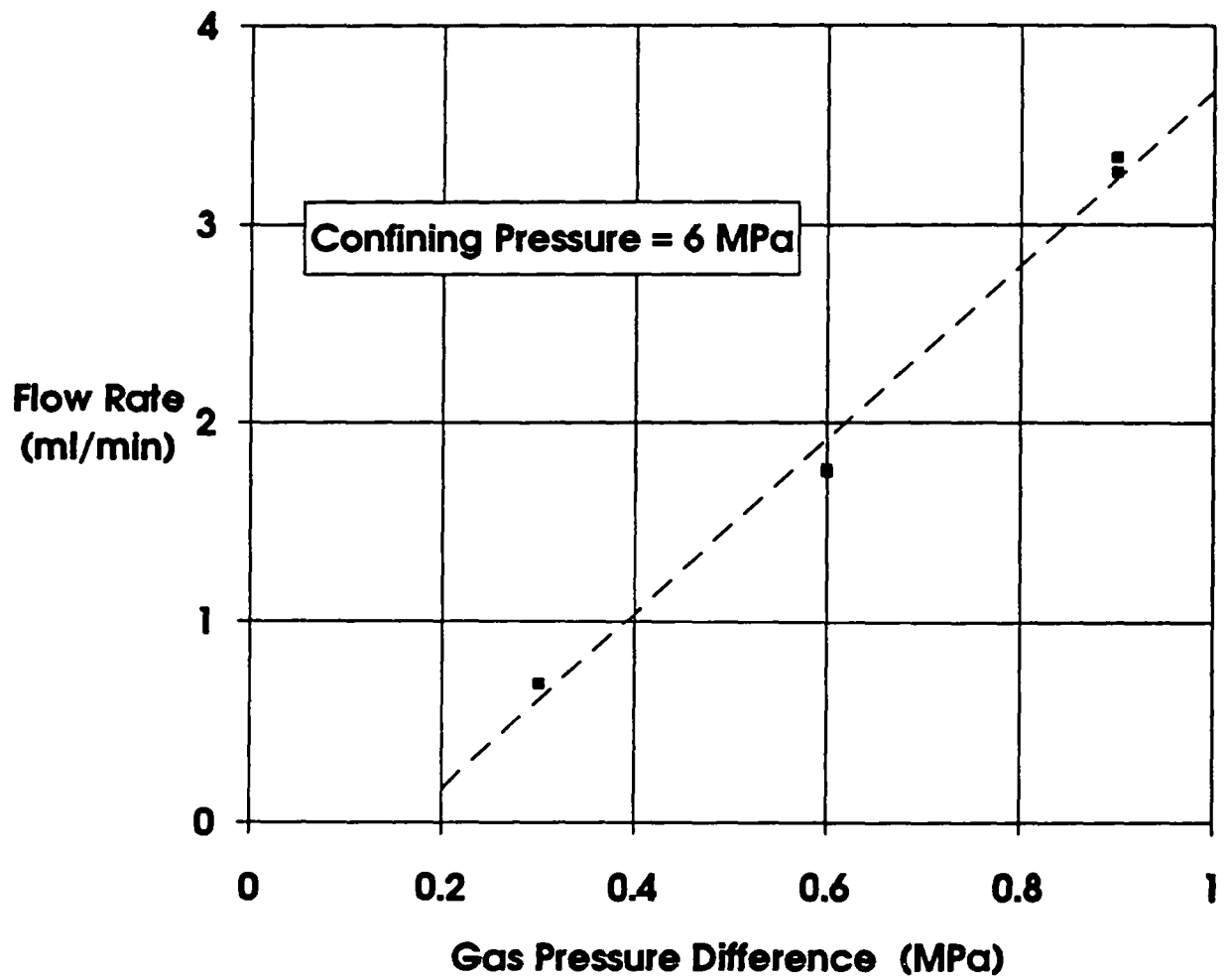
Figures

H-1.	Flow rate-versus-gas pressure difference difference for Specimen P3X11-5-2-SP1 at 2 MPa confining pressure and all gas inlet perssures.	B-241
H-2.	Flow rate-versus-gas pressure difference difference for Specimen P3X11-5-2-SP1 at 6 MPa confining pressure and all gas inlet perssures.	B-242
H-3.	Flow rate-versus-gas pressure difference difference for Specimen P3X11-5-2-SP1 at 10 MPa confining pressure and all gas inlet perssures.	B-243
H-4.	Flow rate-versus-gas pressure difference difference for Specimen P3X10-6-SP2 at 2 MPa confining pressure and all gas inlet perssures.	B-244
H-5.	Flow rate-versus-gas pressure difference difference for Specimen P3X10-6-SP2 at 6 MPa confining pressure and all gas inlet perssures.	B-245
H-6.	Flow rate-versus-gas pressure difference difference for Specimen P3X10-6-SP2 at 10 MPa confining pressure and all gas inlet perssures.	B-246
H-7.	Flow rate-versus-gas pressure difference difference for Specimen P3X11-5-3-SP3 at 2 MPa confining pressure and all gas inlet perssures.	B-247
H-8.	Flow rate-versus-gas pressure difference difference for Specimen P3X11-5-3-SP3 at 6 MPa confining pressure and all gas inlet perssures.	B-248
H-9.	Flow rate-versus-gas pressure difference difference for Specimen P3X11-5-3-SP3 at 10 MPa confining pressure and all gas inlet perssures.	B-249



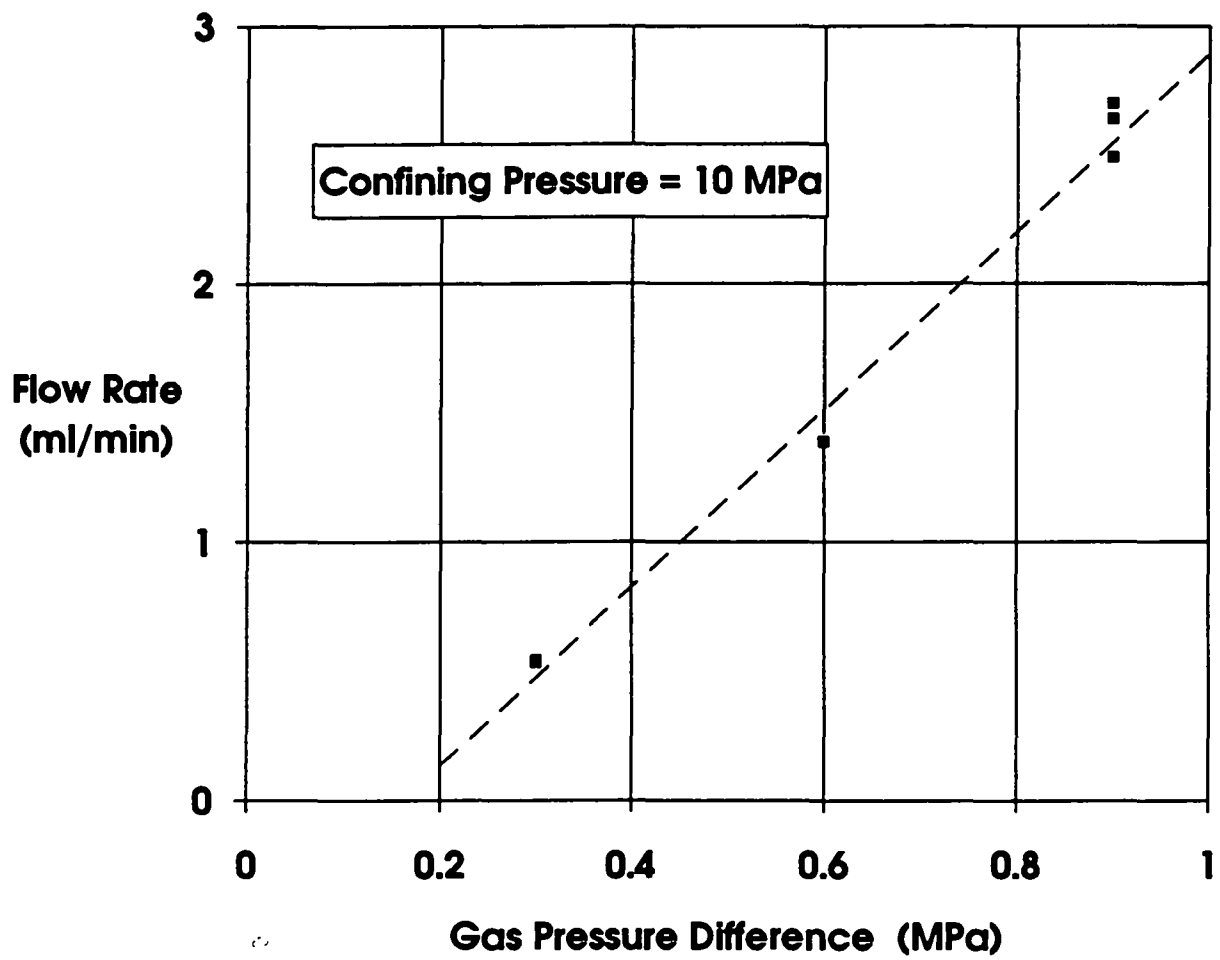
RSI-248-83-085

Figure H-1. Flow rate-versus-gas pressure difference difference for Specimen P3X11-5-2-SP1 at 2 MPa confining pressure and all gas inlet pressures.



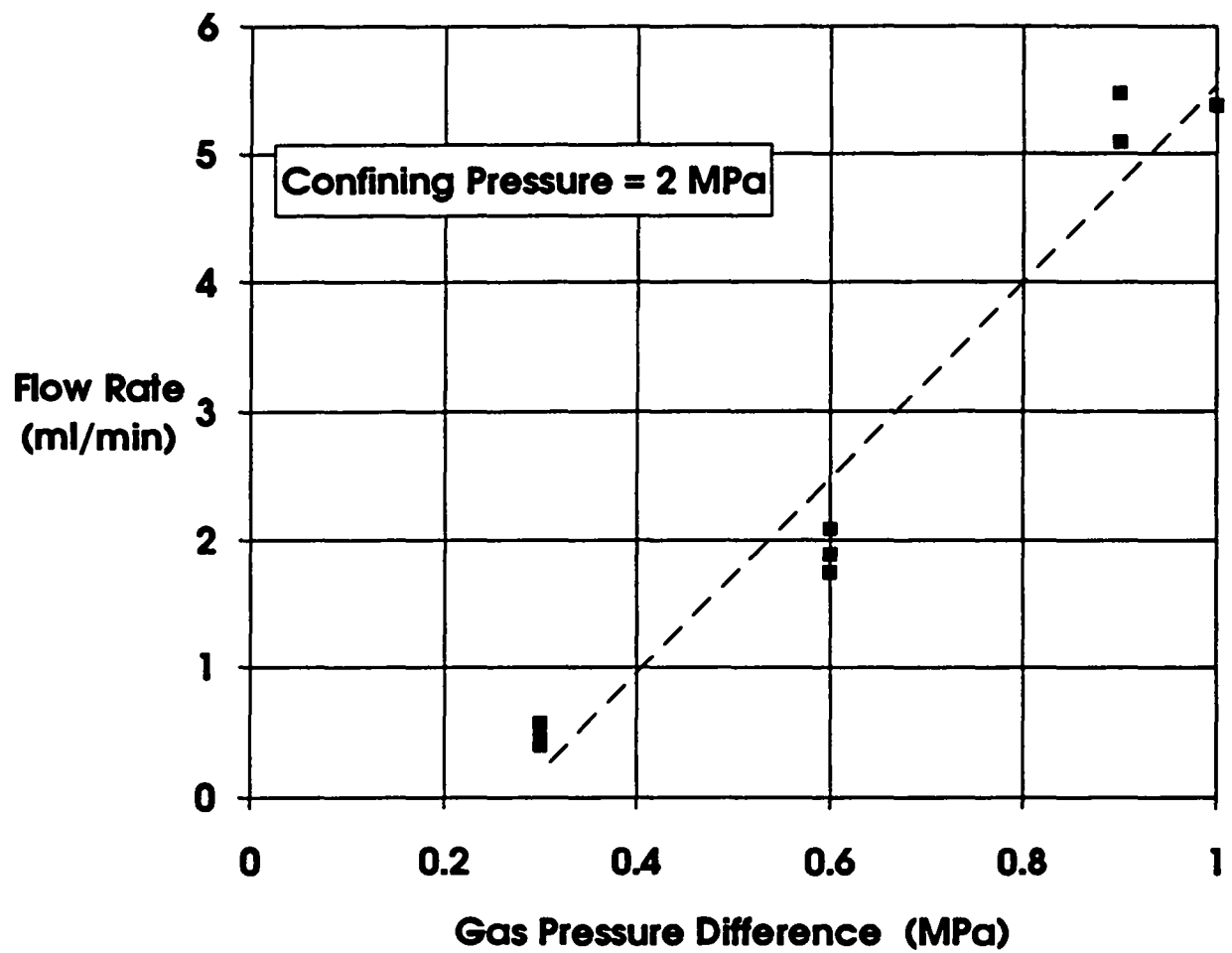
RSI-248-93-086

Figure H-2. Flow rate-versus-gas pressure difference difference for Specimen P3X11-5-2-SP1 at 6 MPa confining pressure and all gas inlet pressures.



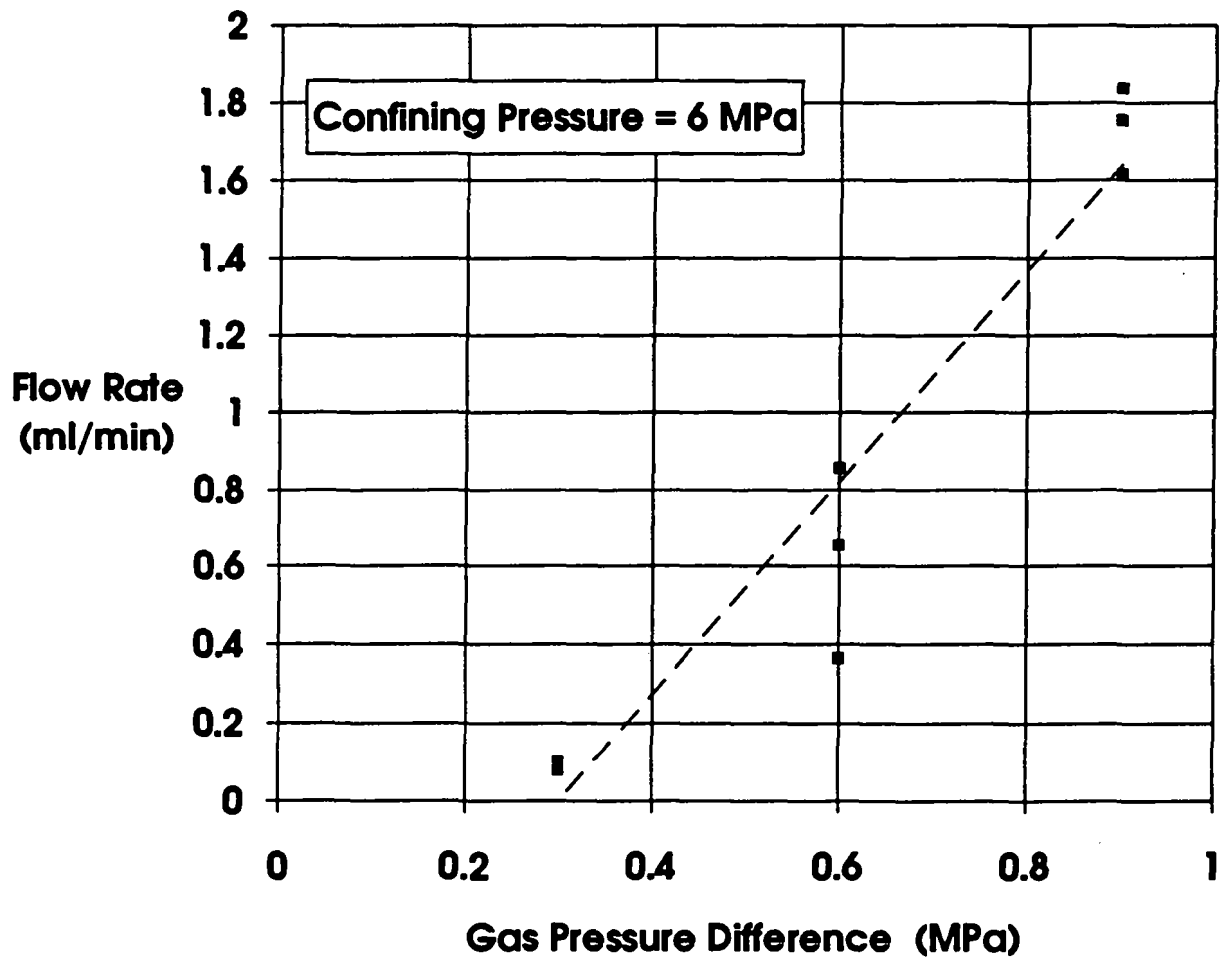
R81-248-83-087

Figure H-3. Flow rate-versus-gas pressure difference difference for Specimen P3X11-5-2-SP1 at 10 MPa confining pressure and all gas inlet pressures.



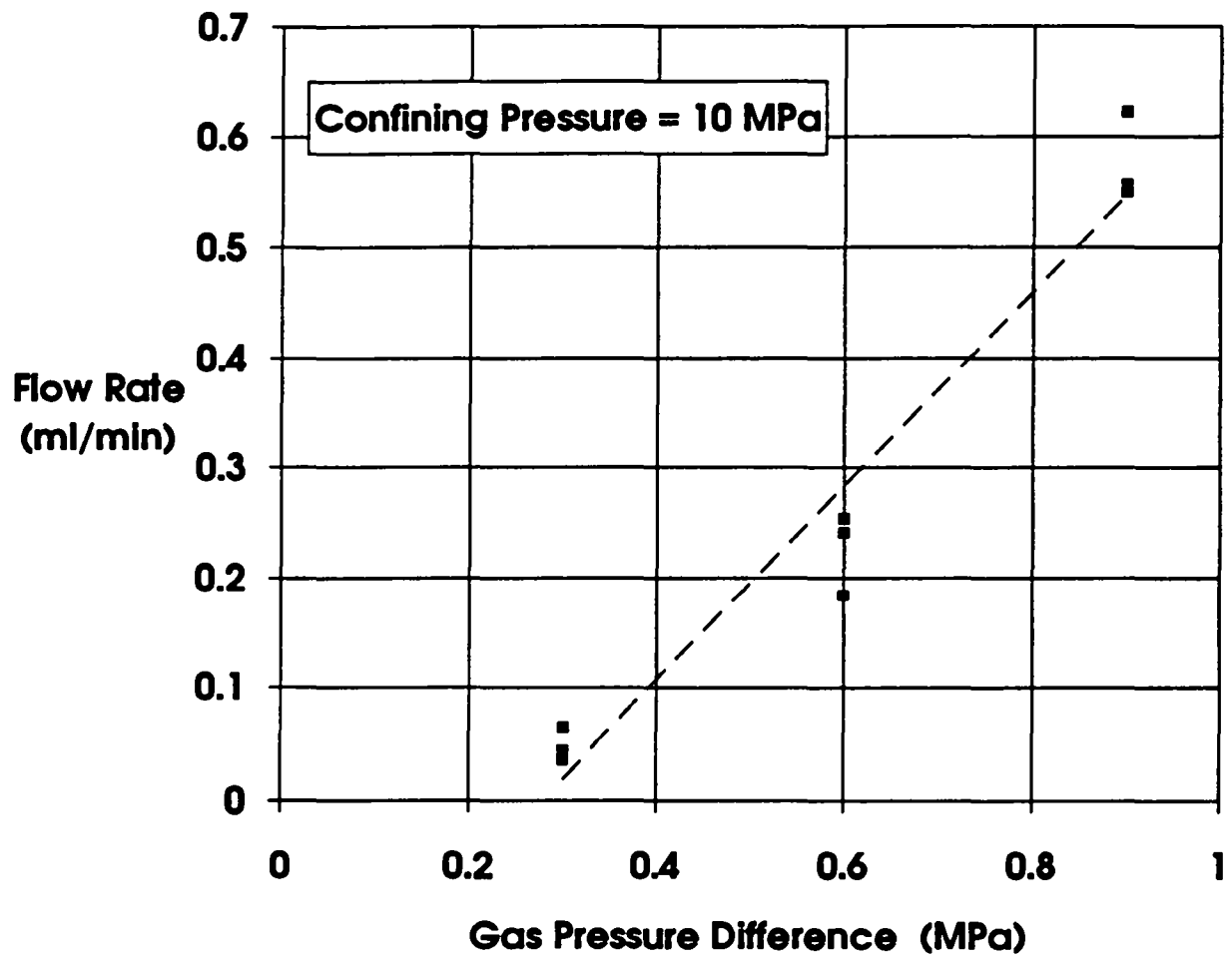
RSI-248-83-088

Figure H-4. Flow rate-versus-gas pressure difference difference for Specimen P3X10-6-SP2 at 2 MPa confining pressure and all gas inlet pressures.



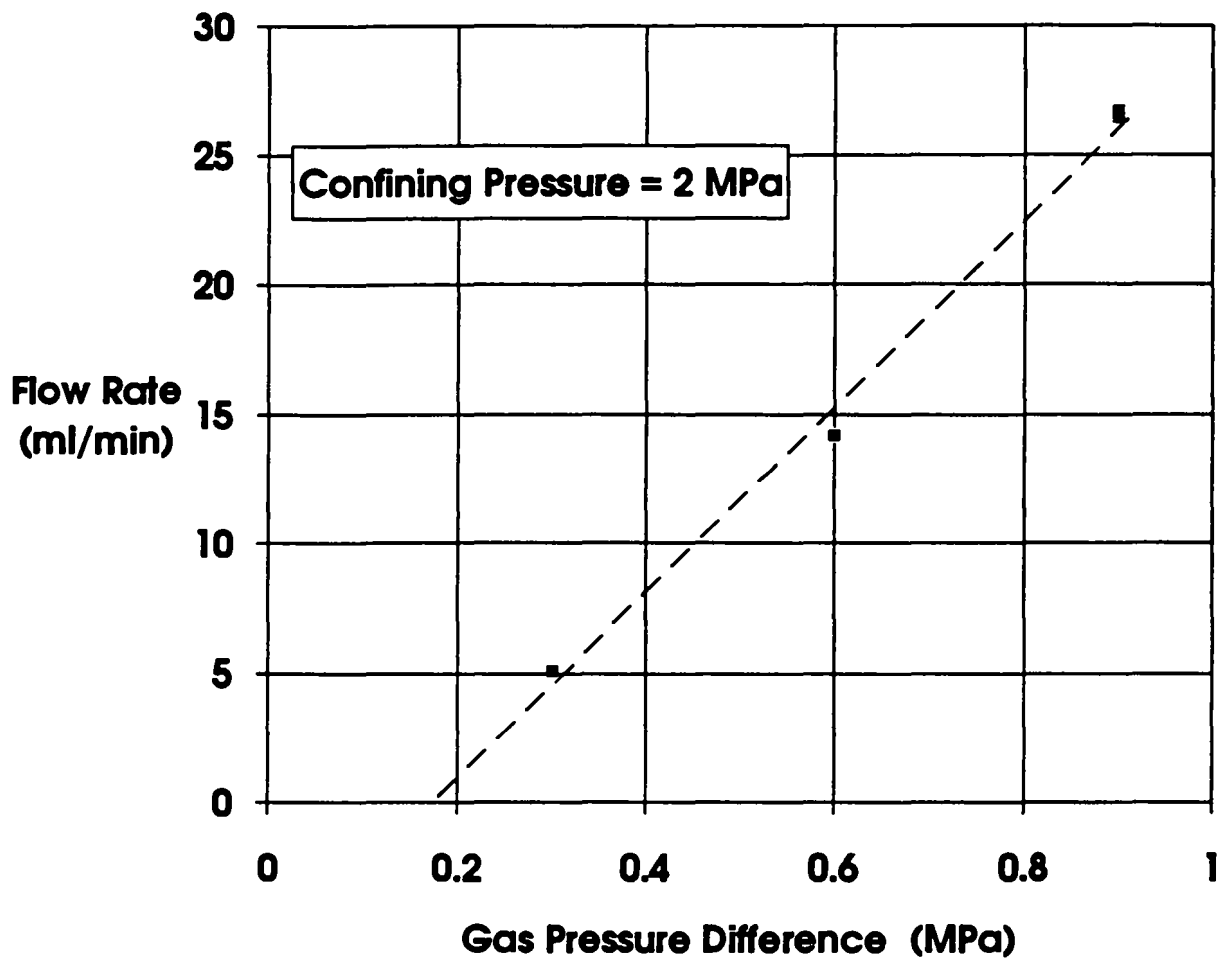
RSI-248-93-080

Figure H-5. Flow rate-versus-gas pressure difference difference for Specimen P3X10-6-SP2 at 6 MPa confining pressure and all gas inlet pressures.



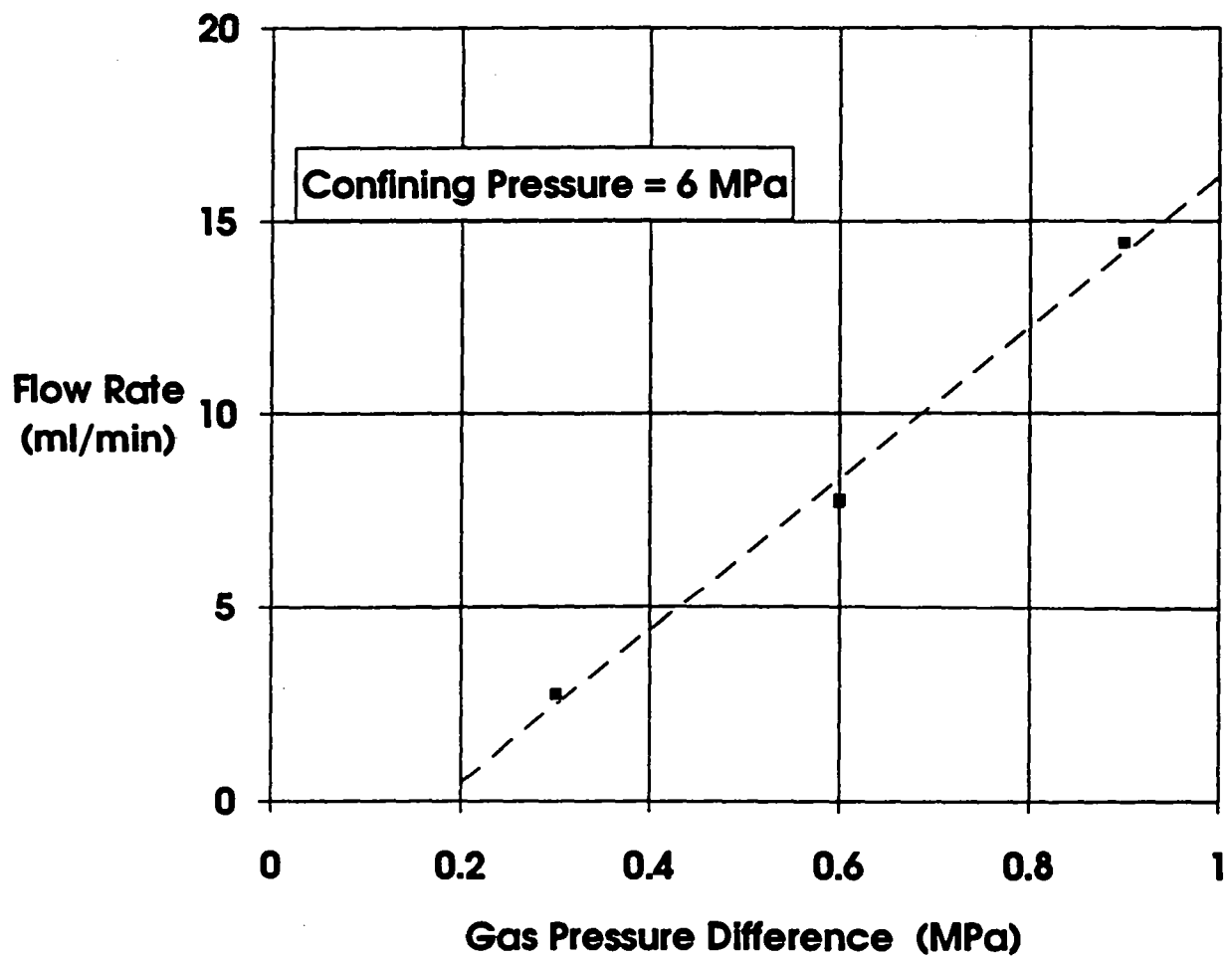
FR-348-63-080

Figure H-6. Flow rate-versus-gas pressure difference difference for Specimen P3X10-6-SP2 at 10 MPa confining pressure and all gas inlet pressures.



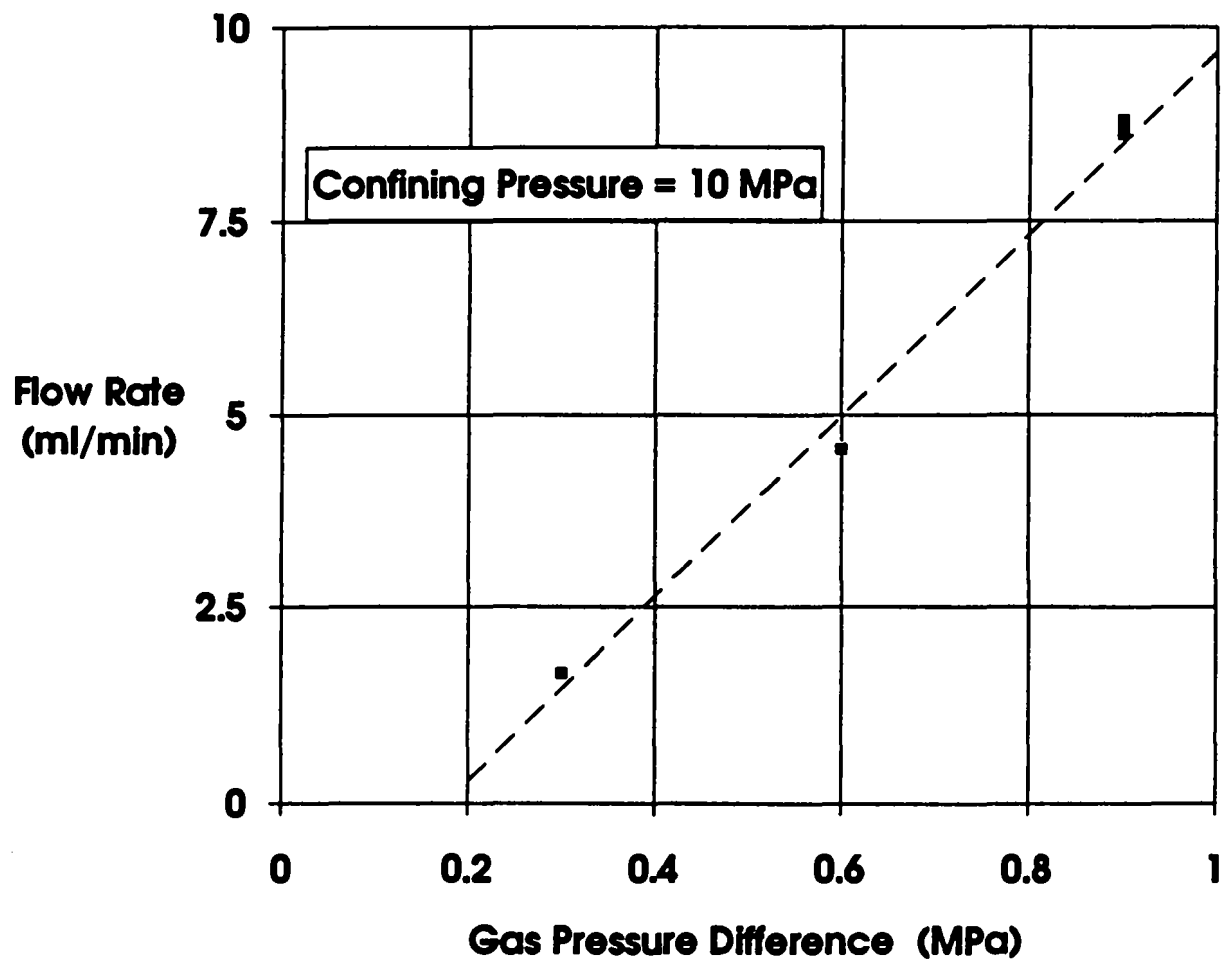
FBI-248-83-081

Figure H-7. Flow rate-versus-gas pressure difference difference for Specimen P3X11-5-3-SP3 at 2 MPa confining pressure and all gas inlet pressures.



RSI-248-03-082

Figure H-8. Flow rate-versus-gas pressure difference difference for Specimen P3X11-5-3-SP3 at 6 MPa confining pressure and all gas inlet pressures.



RSI-248-83-003

Figure H-9. Flow rate-versus-gas pressure difference difference for Specimen P3X11-5-3-SP3 at 10 MPa confining pressure and all gas inlet pressures.

APPENDIX B.I
FLOW-VERSUS-TIME DATA FOR ALL BRINE
PERMEABILITY TESTS

Figures

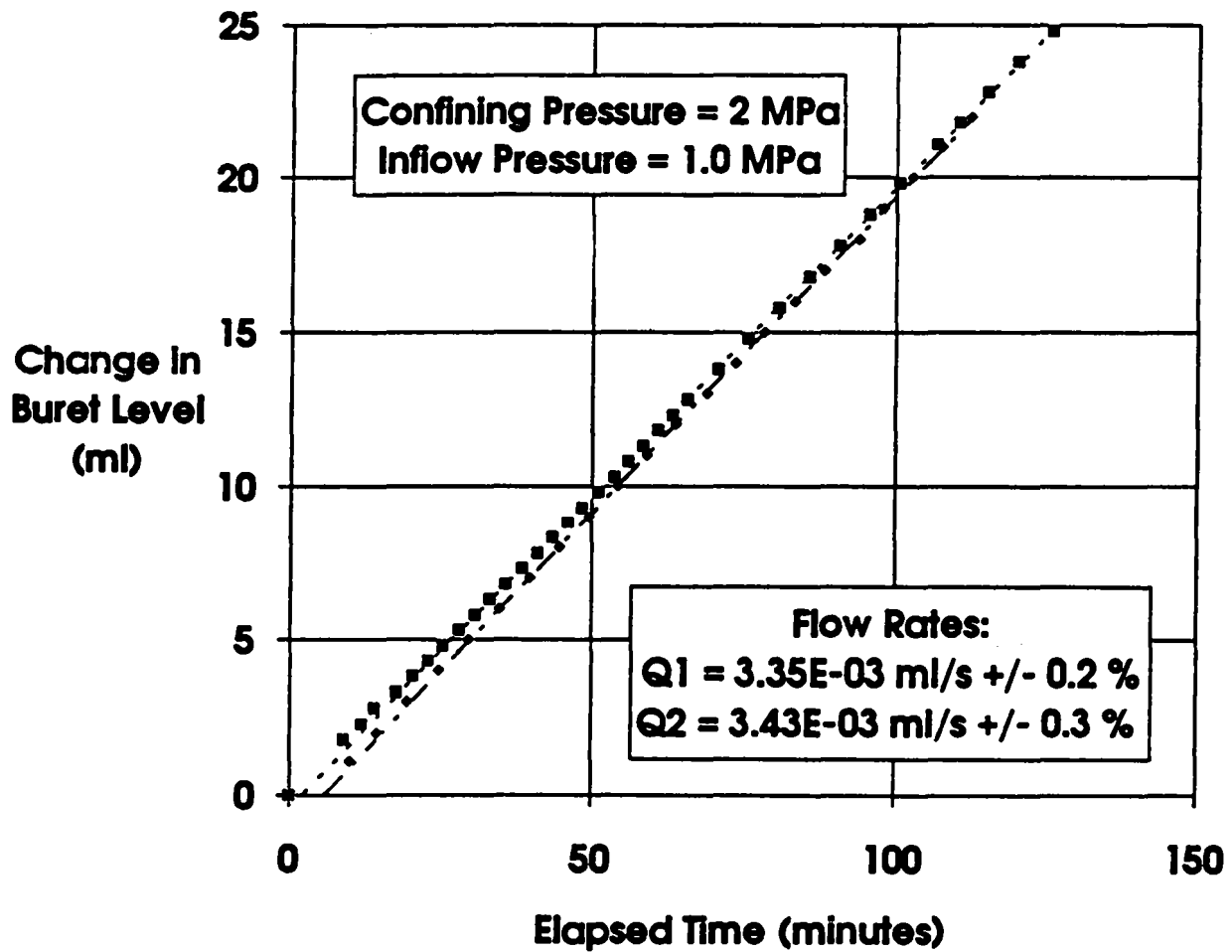
- I-1 Change in exit buret level (brine volume)-versus-time for tests on Specimen P3X11-5-2-SP1 at 2 MPa confining pressure and 1.0 MPa brine inlet pressure. Symbols are recorded data points; dashed lines are best fits to linear sections of data. Coefficient of variation for linear least square fit is given B-257
- I-2 Change in exit buret level (brine volume)-versus-time for tests on Specimen P3X11-5-2-SP1 at 2 MPa confining pressure and 0.7 MPa brine inlet pressure. Symbols are recorded data points; dashed lines are best fits to linear sections of data. Coefficient of variation for linear least square fit is given B-258
- I-3 Change in exit buret level (brine volume)-versus-time for tests on Specimen P3X11-5-2-SP1 at 2 MPa confining pressure and 0.4 MPa brine inlet pressure. Symbols are recorded data points; dashed lines are best fits to linear sections of data. Coefficient of variation for linear least square fit is given B-259
- I-4 Change in exit buret level (brine volume)-versus-time for tests on Specimen P3X10-6-SP2 at 2 MPa confining pressure and 1.0 MPa brine inlet pressure. Symbols are recorded data points; dashed lines are best fits to linear sections of data. Coefficient of variation for linear least square fit is given B-260
- I-5 Change in exit buret level (brine volume)-versus-time for tests on Specimen P3X10-6-SP2 at 2 MPa confining pressure and 0.7 MPa brine inlet pressure. Symbols are recorded data points; dashed lines are best fits to linear sections of data. Coefficient of variation for linear least square fit is given B-261
- I-6 Change in exit buret level (brine volume)-versus-time for tests on Specimen P3X10-6-SP2 at 2 MPa confining pressure and 0.4 MPa brine inlet pressure. Symbols are recorded data points; dashed lines are best fits to linear sections of data. Coefficient of variation for linear least square fit is given B-262
- I-7 Change in exit buret level (brine volume)-versus-time for tests on Specimen P3X10-6-SP2 at 6 MPa confining pressure and 1.0 MPa brine inlet pressure. Symbols are recorded data points; dashed lines are best fits to linear sections of data. Coefficient of variation for linear least square fit is given B-263
- I-8 Change in exit buret level (brine volume)-versus-time for tests on Specimen P3X10-6-SP2 at 6 MPa confining pressure and 0.7 MPa brine inlet pressure. Symbols are recorded data points; dashed lines are best fits to linear sections of data. Coefficient of variation for linear least square fit is given B-264

Figures (continued)

- I-9 Change in exit buret level (brine volume)-versus-time for tests on Specimen P3X10-6-SP2 at 6 MPa confining pressure and 0.4 MPa brine inlet pressure. Symbols are recorded data points; dashed lines are best fits to linear sections of data. Coefficient of variation for linear least square fit is given B-265
- I-10 Change in exit buret level (brine volume)-versus-time for tests on Specimen P3X10-6-SP2 at 10 MPa confining pressure and 1.0 MPa brine inlet pressure. Symbols are recorded data points; dashed lines are best fits to linear sections of data. Coefficient of variation for linear least square fit is given B-266
- I-11 Change in exit buret level (brine volume)-versus-time for tests on Specimen P3X10-6-SP2 at 10 MPa confining pressure and 0.7 MPa brine inlet pressure. Symbols are recorded data points; dashed lines are best fits to linear sections of data. Coefficient of variation for linear least square fit is given B-267
- I-12 Change in exit buret level (brine volume)-versus-time for tests on Specimen P3X10-6-SP2 at 10 MPa confining pressure and 0.4 MPa brine inlet pressure. Symbols are recorded data points; dashed lines are best fits to linear sections of data. Coefficient of variation for linear least square fit is given B-268
- I-13 Change in exit buret level (brine volume)-versus-time for tests on Specimen P3X11-5-3-SP3 at 2 MPa confining pressure and 1.0 MPa brine inlet pressure. Symbols are recorded data points; dashed lines are best fits to linear sections of data. Coefficient of variation for linear least square fit is given B-269
- I-14 Change in exit buret level (brine volume)-versus-time for tests on Specimen P3X11-5-3-SP3 at 2 MPa confining pressure and 0.7 MPa brine inlet pressure. Symbols are recorded data points; dashed lines are best fits to linear sections of data. Coefficient of variation for linear least square fit is given B-270
- I-15 Change in exit buret level (brine volume)-versus-time for tests on Specimen P3X11-5-3-SP3 at 2 MPa confining pressure and 0.4 MPa brine inlet pressure. Symbols are recorded data points; dashed lines are best fits to linear sections of data. Coefficient of variation for linear least square fit is given B-271
- I-16 Change in exit buret level (brine volume)-versus-time for tests on Specimen P3X11-5-3-SP3 at 6 MPa confining pressure and 1.0 MPa brine inlet pressure. Symbols are recorded data points; dashed lines are best fits to linear sections of data. Coefficient of variation for linear least square fit is given B-272

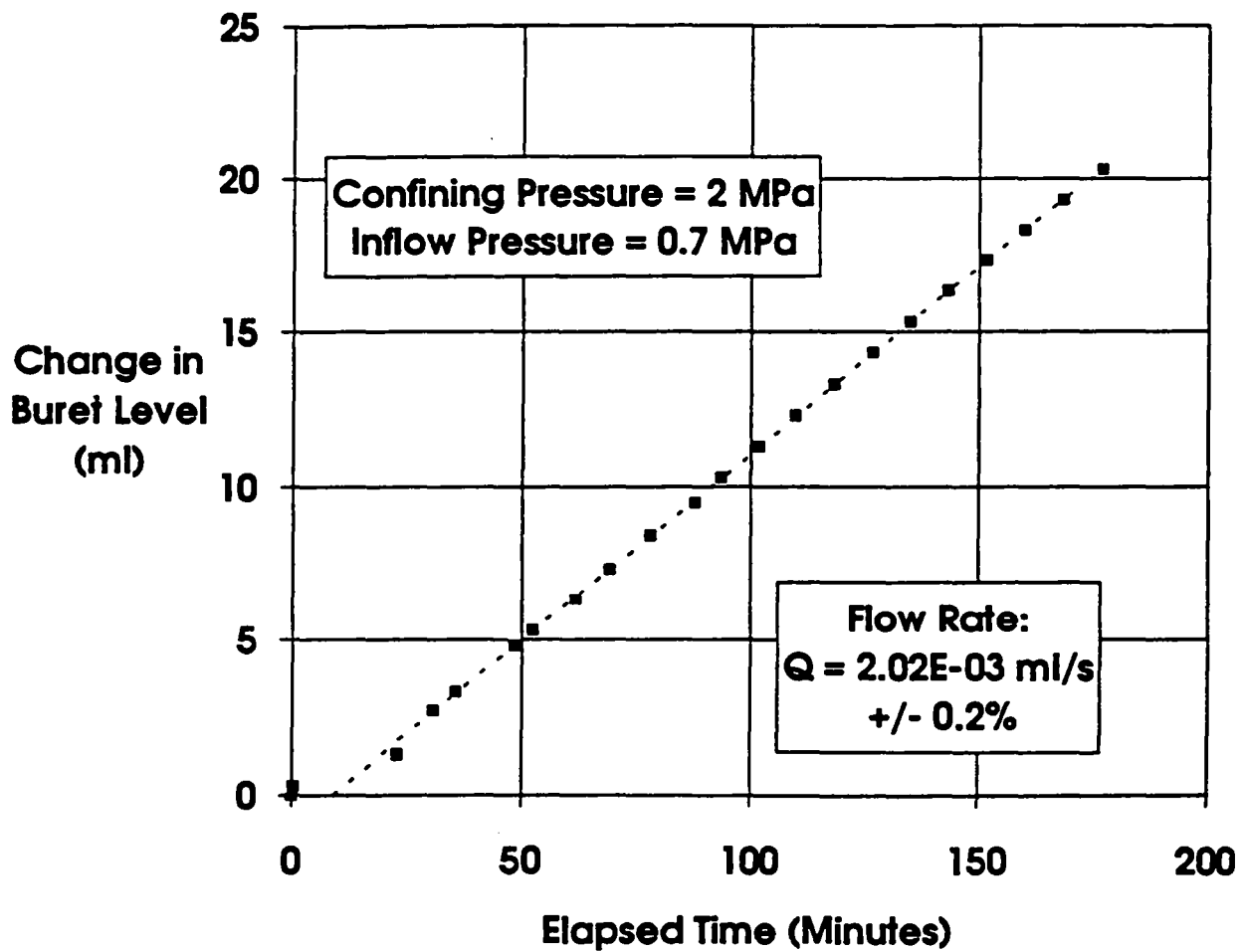
Figures (continued)

- I-17 Change in exit buret level (brine volume)-versus-time for tests on Specimen P3X11-5-3-SP3 at 6 MPa confining pressure and 0.7 MPa brine inlet pressure. Symbols are recorded data points; dashed lines are best fits to linear sections of data. Coefficient of variation for linear least square fit is given B-273
- I-18 Change in exit buret level (brine volume)-versus-time for tests on Specimen P3X11-5-3-SP3 at 6 MPa confining pressure and 0.4 MPa brine inlet pressure. Symbols are recorded data points; dashed lines are best fits to linear sections of data. Coefficient of variation for linear least square fit is given B-274
- I-19 Change in exit buret level (brine volume)-versus-time for tests on Specimen P3X11-5-3-SP3 at 10 MPa confining pressure and 1.0 MPa brine inlet pressure. Symbols are recorded data points; dashed lines are best fits to linear sections of data. Coefficient of variation for linear least square fit is given B-275
- I-20 Change in exit buret level (brine volume)-versus-time for tests on Specimen P3X11-5-3-SP3 at 10 MPa confining pressure and 0.7 MPa brine inlet pressure. Symbols are recorded data points; dashed lines are best fits to linear sections of data. Coefficient of variation for linear least square fit is given B-276
- I-21 Change in exit buret level (brine volume)-versus-time for tests on Specimen P3X11-5-3-SP3 at 10 MPa confining pressure and 0.4 MPa brine inlet pressure. Symbols are recorded data points; dashed lines are best fits to linear sections of data. Coefficient of variation for linear least square fit is given B-277



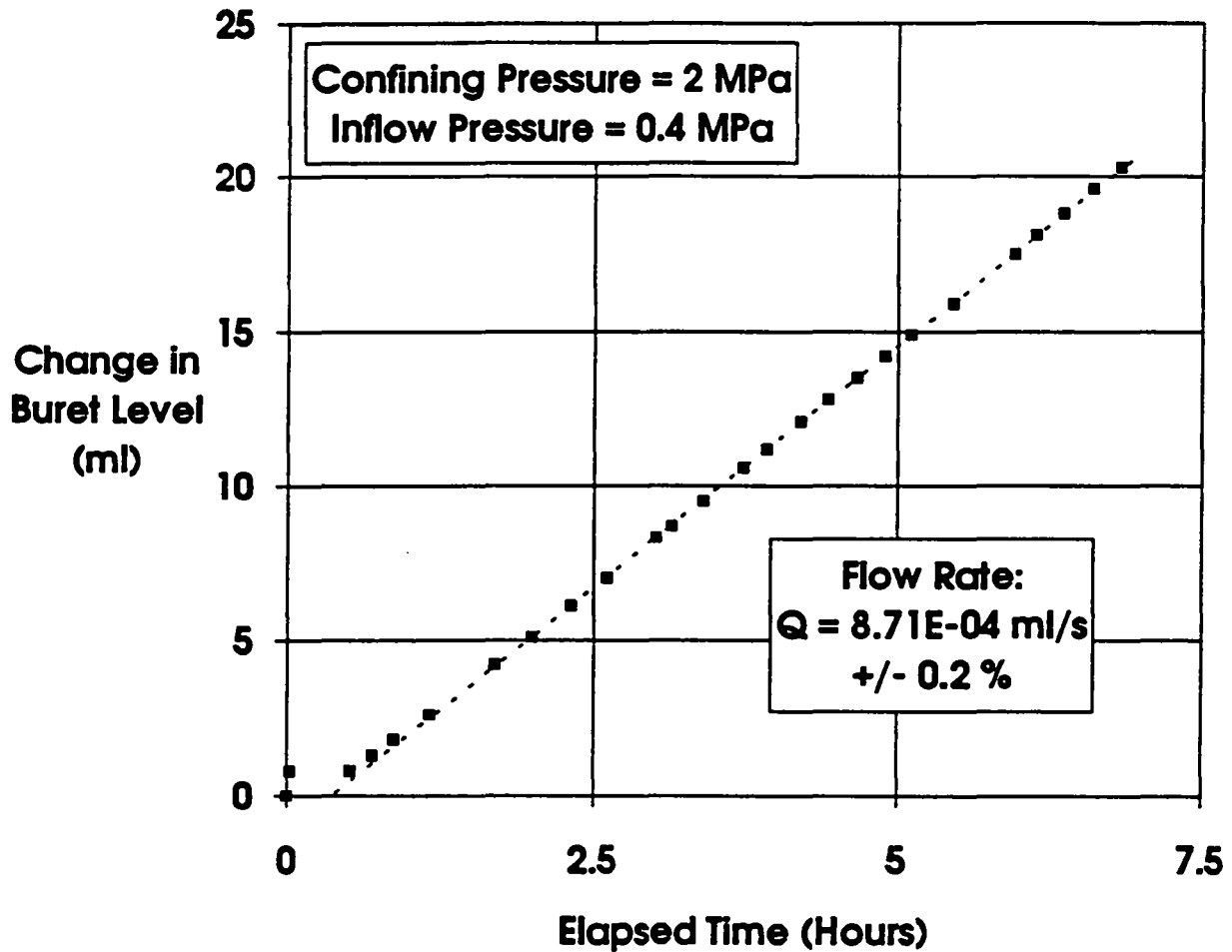
P31-348-04-001

Figure I-1. Change in exit buret level (brine volume)-versus-time for tests on Specimen P3X11-5-2-SP1 at 2 MPa confining pressure and 1.0 MPa brine inlet pressure. Symbols are recorded data points; dashed lines are best fits to linear sections of data. Coefficient of variation for linear least square fits are given.



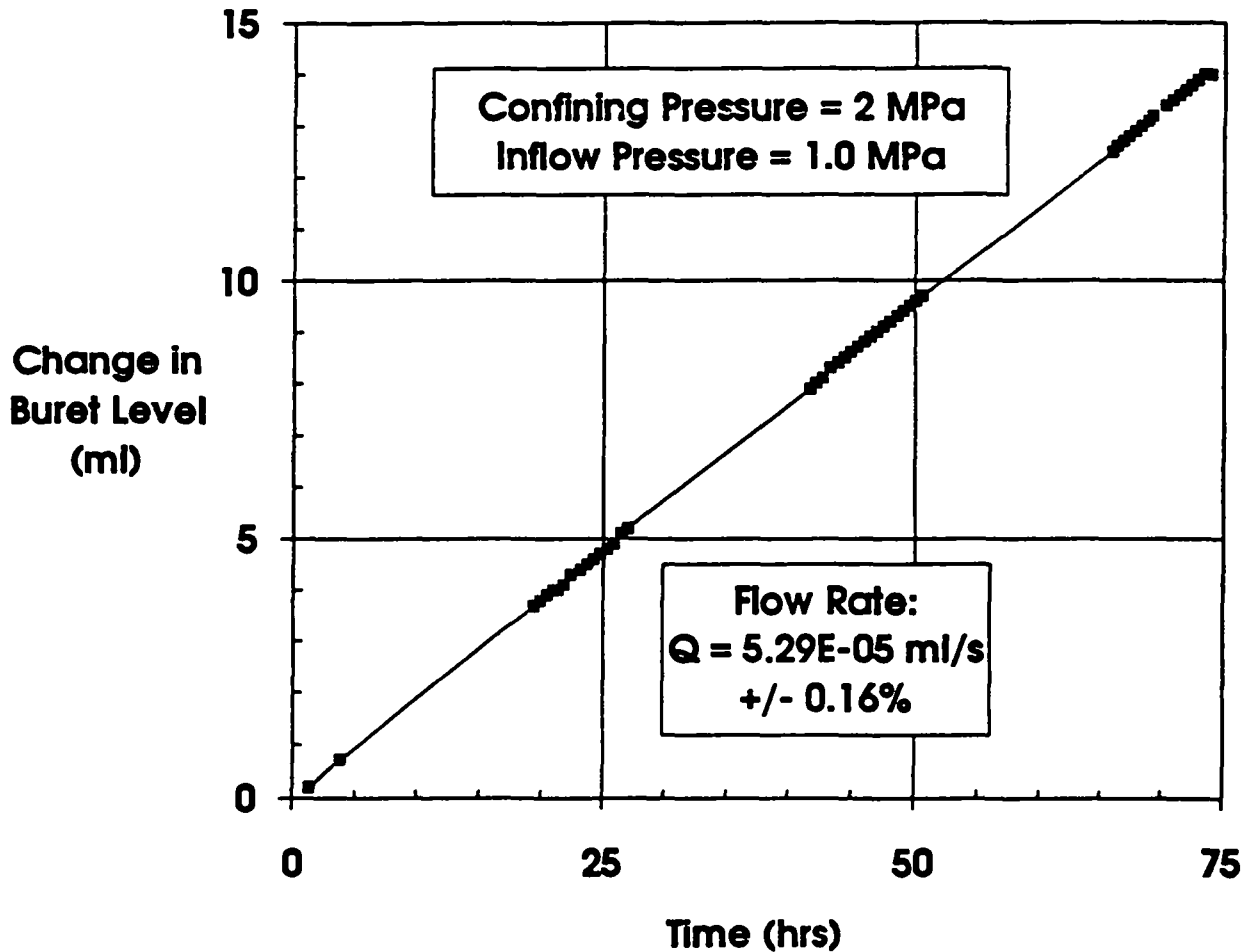
R81-348-04-002

Figure I-2. Change in exit buret level (brine volume)-versus-time for tests on Specimen P3X11-5-2-SP1 at 2 MPa confining pressure and 0.7 MPa brine inlet pressure. Symbols are recorded data points; dashed lines are best fits to linear sections of data. Coefficient of variation for linear least square fits are given.



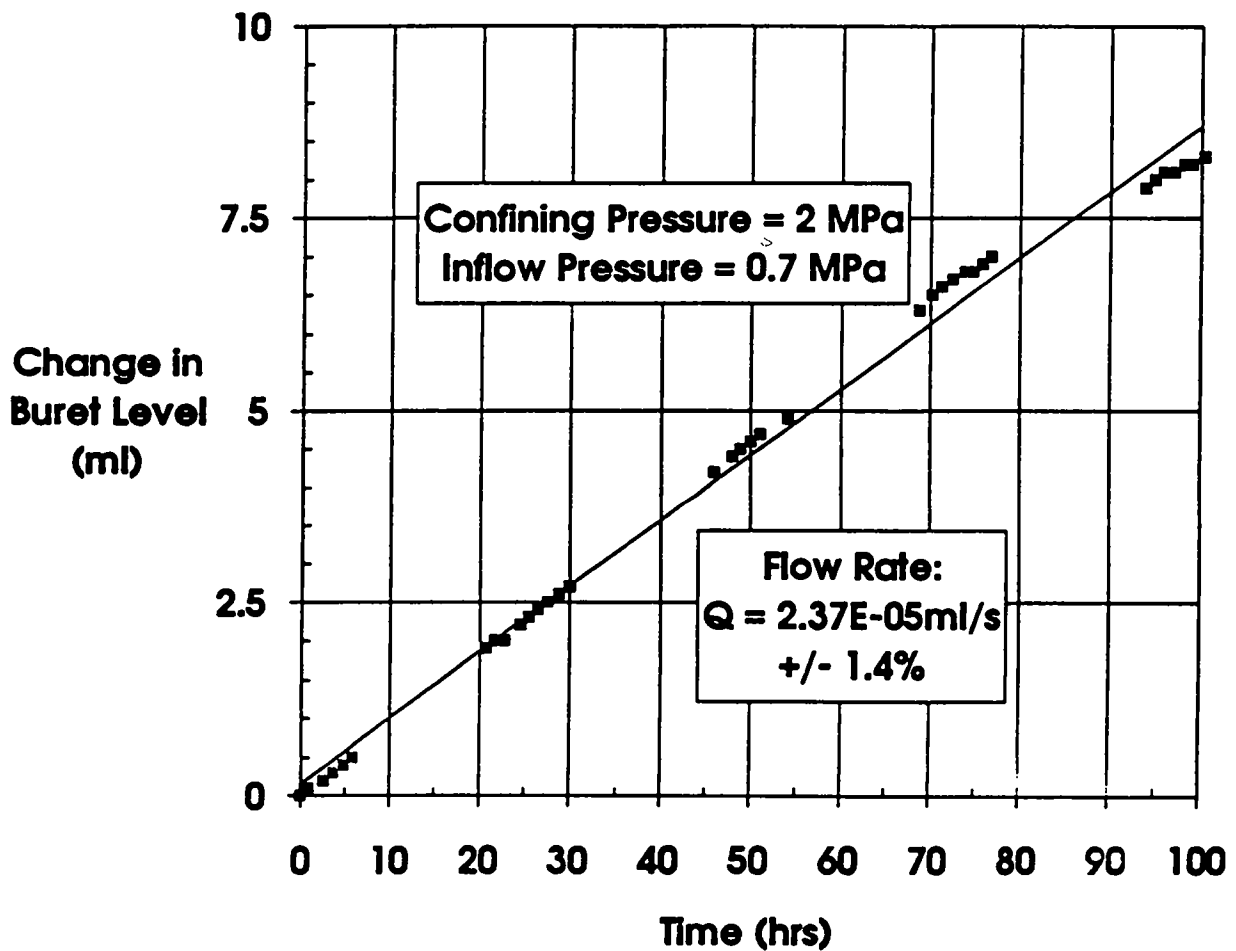
RSI-248-04-003

Figure I-3. Change in exit buret level (brine volume)-versus-time for tests on Specimen P3X11-5-2-SP1 at 2 MPa confining pressure and 0.4 MPa brine inlet pressure. Symbols are recorded data points; dashed lines are best fits to linear sections of data. Coefficient of variation for linear least square fits are given.



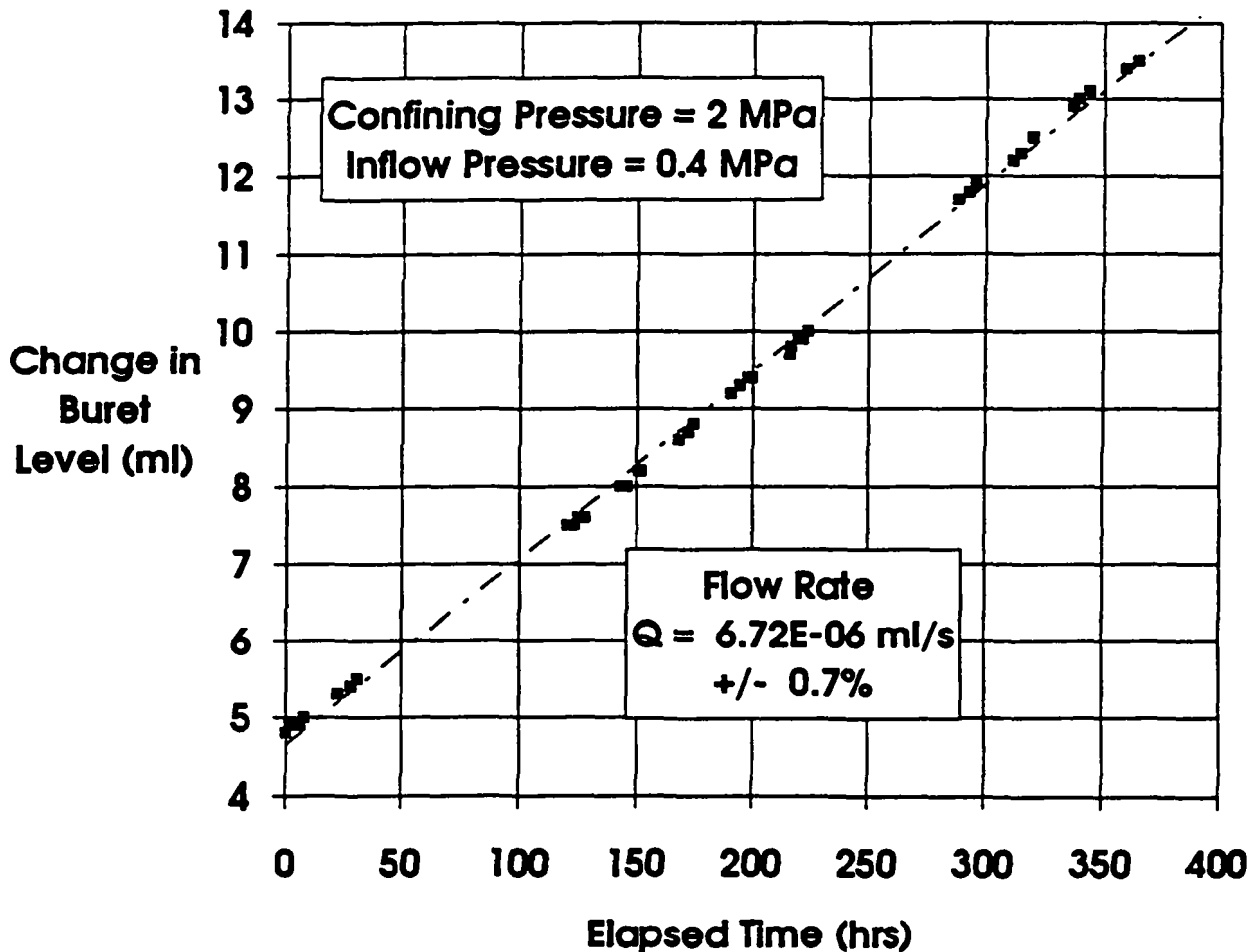
RSI-248-04-004

Figure I-4. Change in exit buret level (brine volume)-versus-time for tests on Specimen P3X10-6-SP2 at 2 MPa confining pressure and 1.0 MPa brine inlet pressure. Symbols are recorded data points; dashed lines are best fits to linear sections of data. Coefficient of variation for linear least square fits are given.



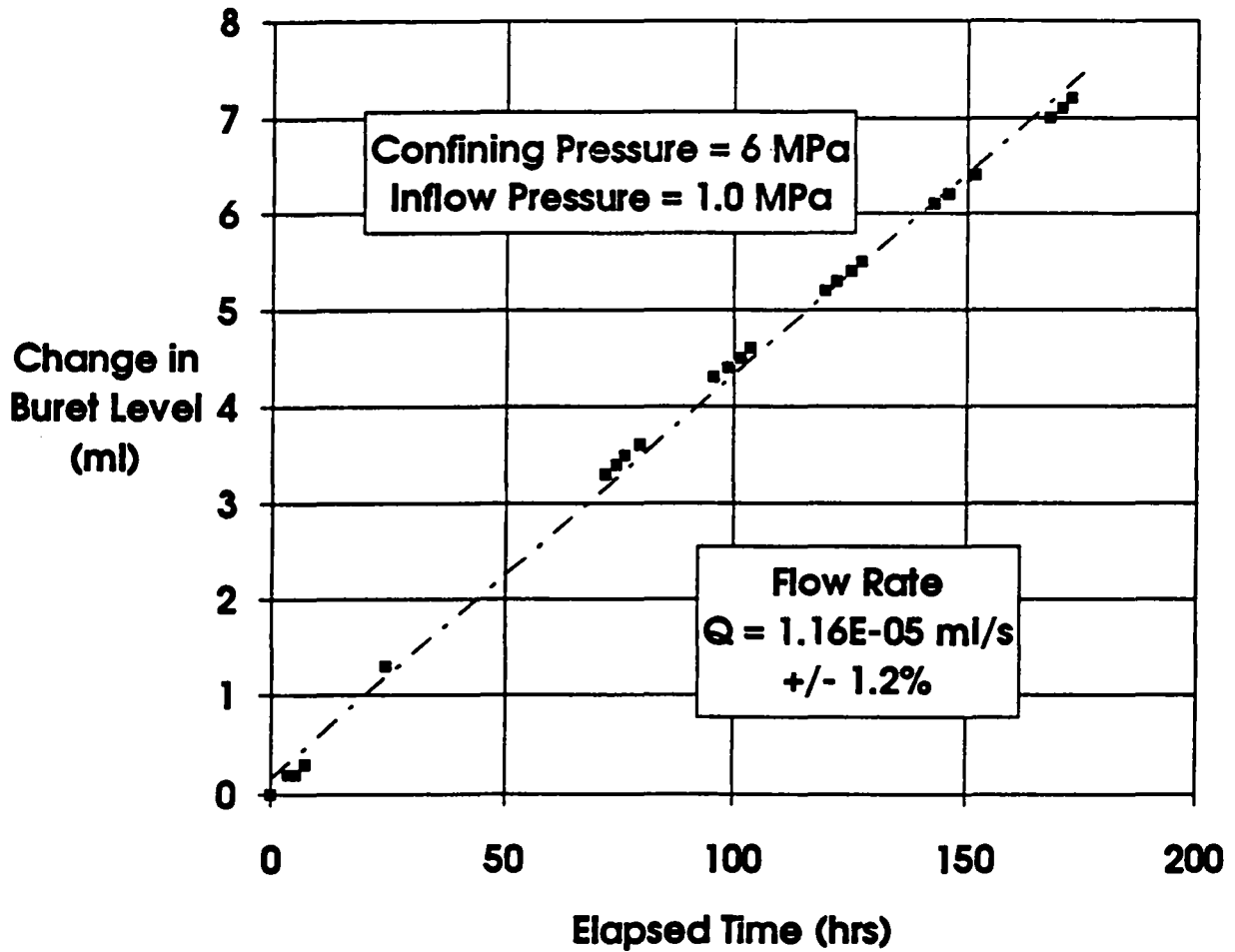
FSI-248-84-006

Figure I-5. Change in exit buret level (brine volume)-versus-time for tests on Specimen P3X10-6-SP2 at 2 MPa confining pressure and 0.7 MPa brine inlet pressure. Symbols are recorded data points; dashed lines are best fits to linear sections of data. Coefficient of variation for linear least square fits are given.



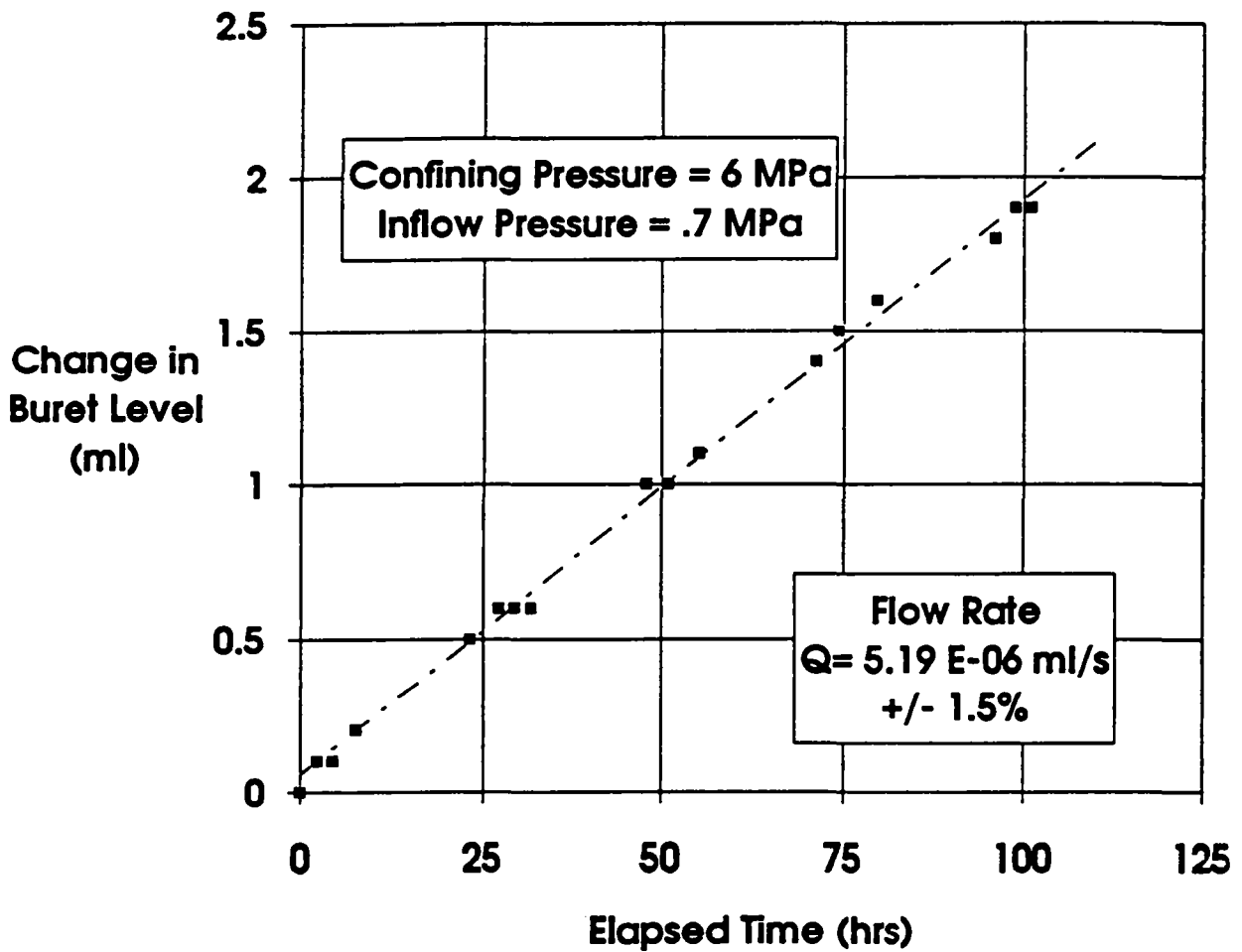
RSI-248-94-008

Figure I-6. Change in exit buret level (brine volume)-versus-time for tests on Specimen P3X10-6-SP2 at 2 MPa confining pressure and 0.4 MPa brine inlet pressure. Symbols are recorded data points; dashed lines are best fits to linear sections of data. Coefficient of variation for linear least square fits are given.



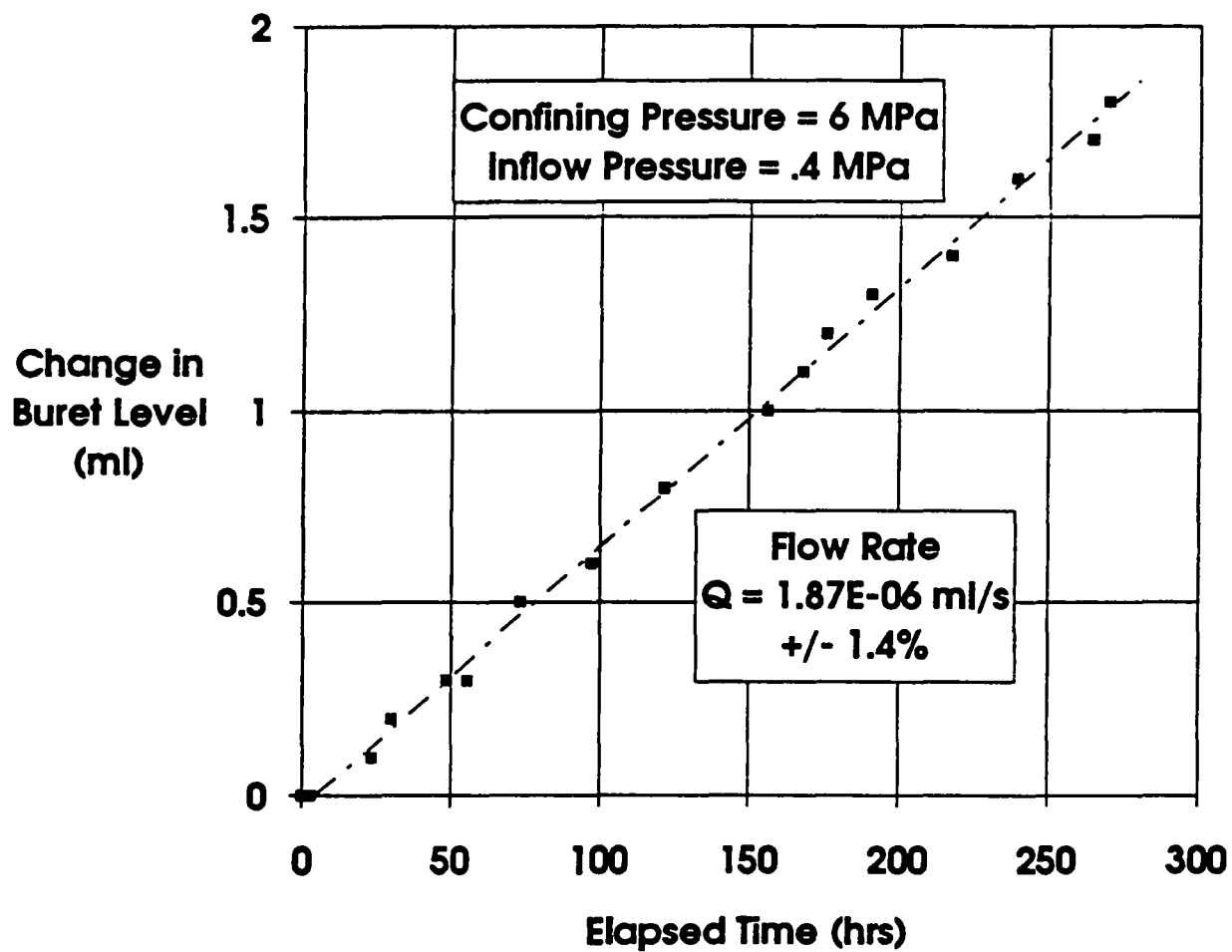
RSI-248-04-007

Figure I-7. Change in exit buret level (brine volume)-versus-time for tests on Specimen P3X10-6-SP2 at 6 MPa confining pressure and 1.0 MPa brine inlet pressure. Symbols are recorded data points; dashed lines are best fits to linear sections of data. Coefficient of variation for linear least square fits are given.



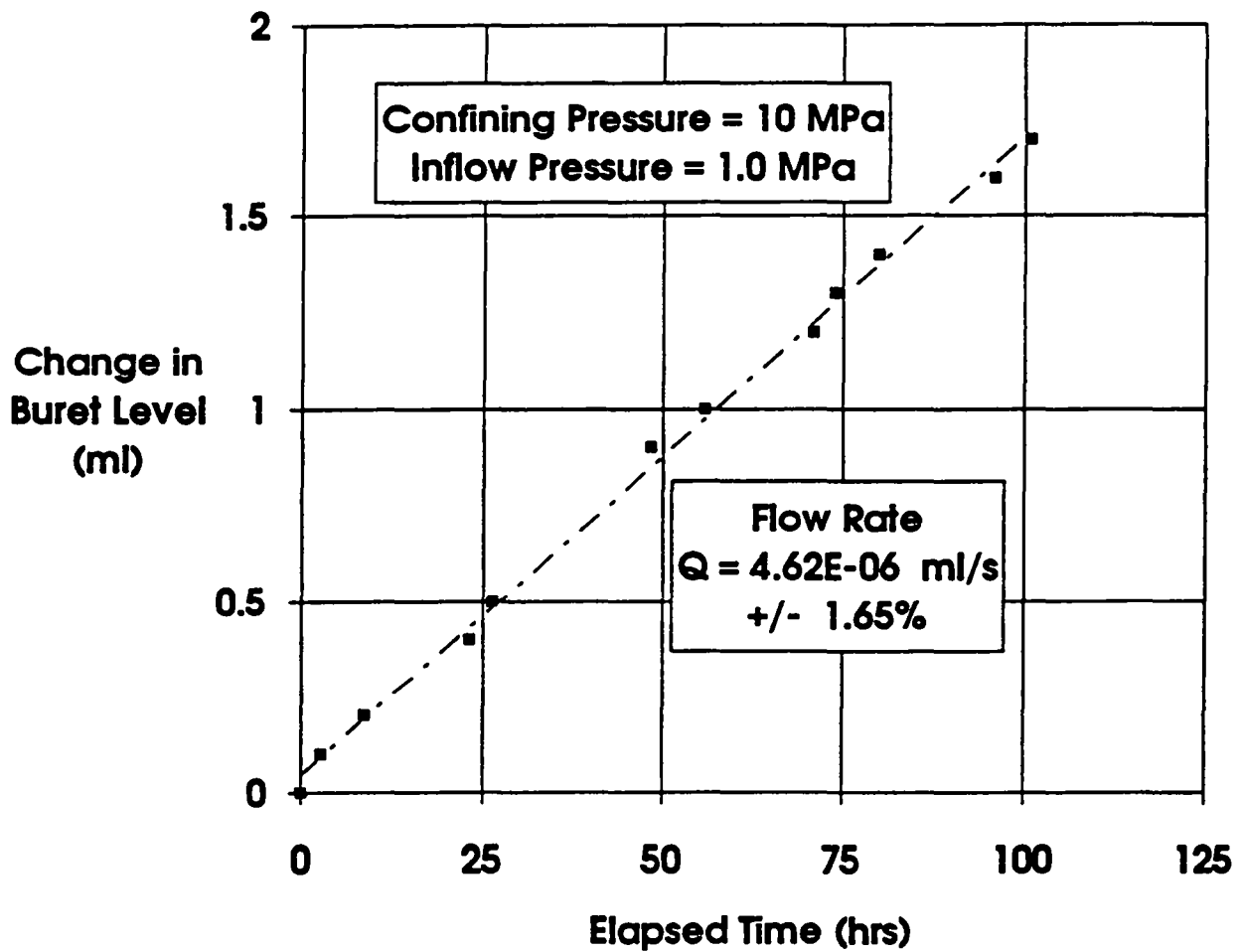
RSI-248-04-008

Figure I-8. Change in exit buret level (brine volume)-versus-time for tests on Specimen P3X10-6-SP2 at 6 MPa confining pressure and 0.7 MPa brine inlet pressure. Symbols are recorded data points; dashed lines are best fits to linear sections of data. Coefficient of variation for linear least square fits are given.



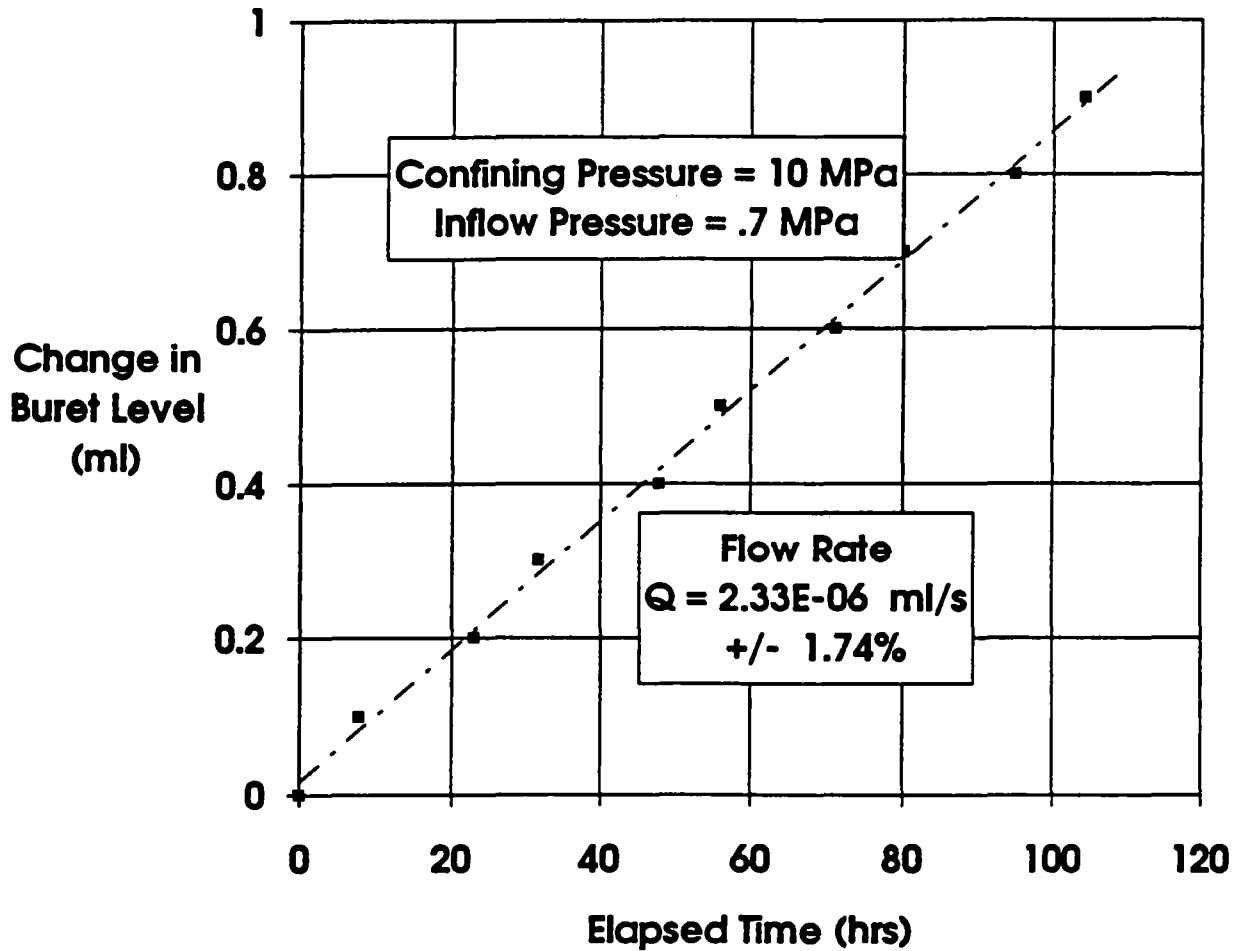
RSI-248-94-009

Figure I-9. Change in exit buret level (brine volume)-versus-time for tests on Specimen P3X10-6-SP2 at 6 MPa confining pressure and 0.4 MPa brine inlet pressure. Symbols are recorded data points; dashed lines are best fits to linear sections of data. Coefficient of variation for linear least square fits are given.



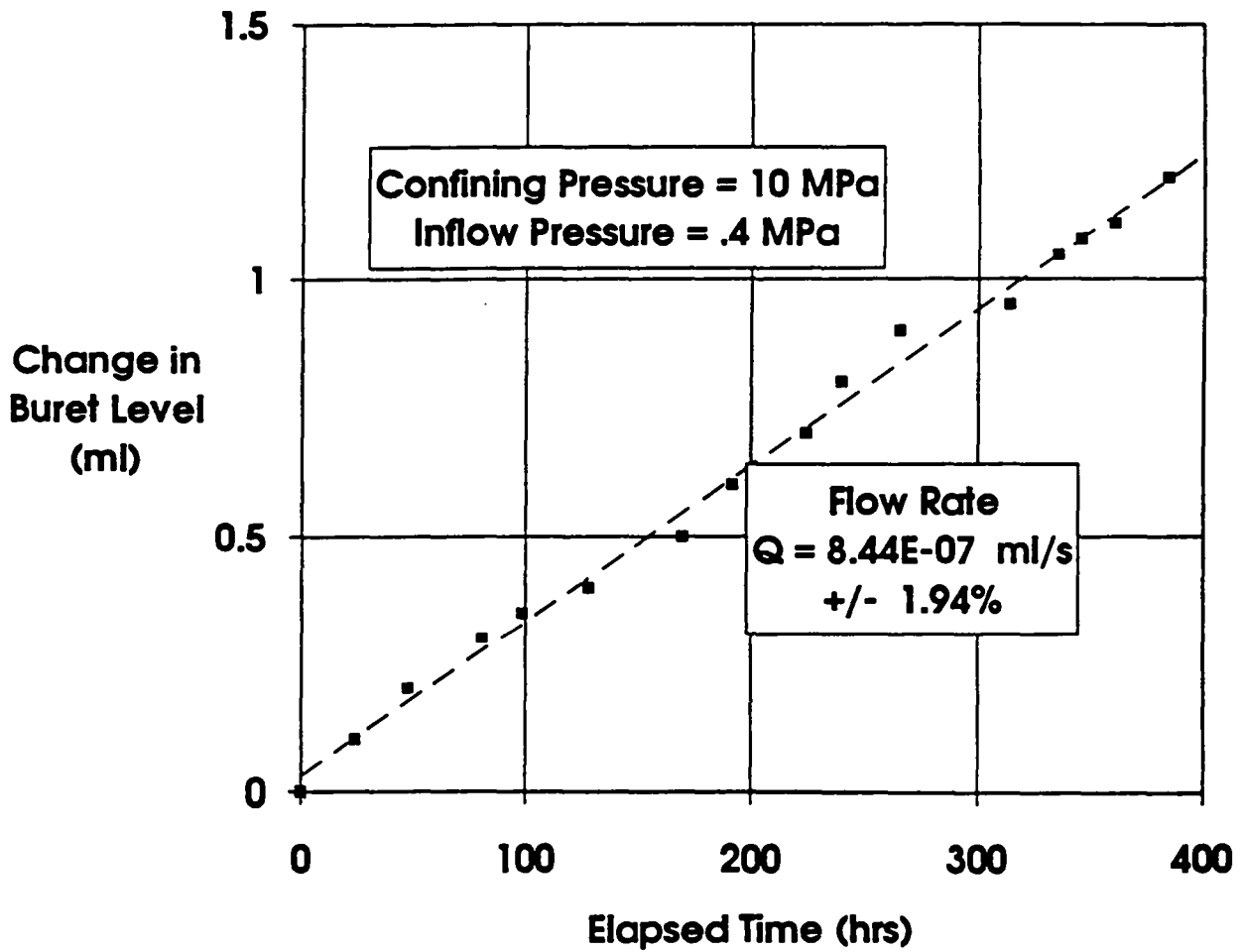
R81-248-04-010

Figure I-10. Change in exit buret level (brine volume)-versus-time for tests on Specimen P3X10-6-SP2 at 10 MPa confining pressure and 1.0 MPa brine inlet pressure. Symbols are recorded data points; dashed lines are best fits to linear sections of data. Coefficient of variation for linear least square fits are given.



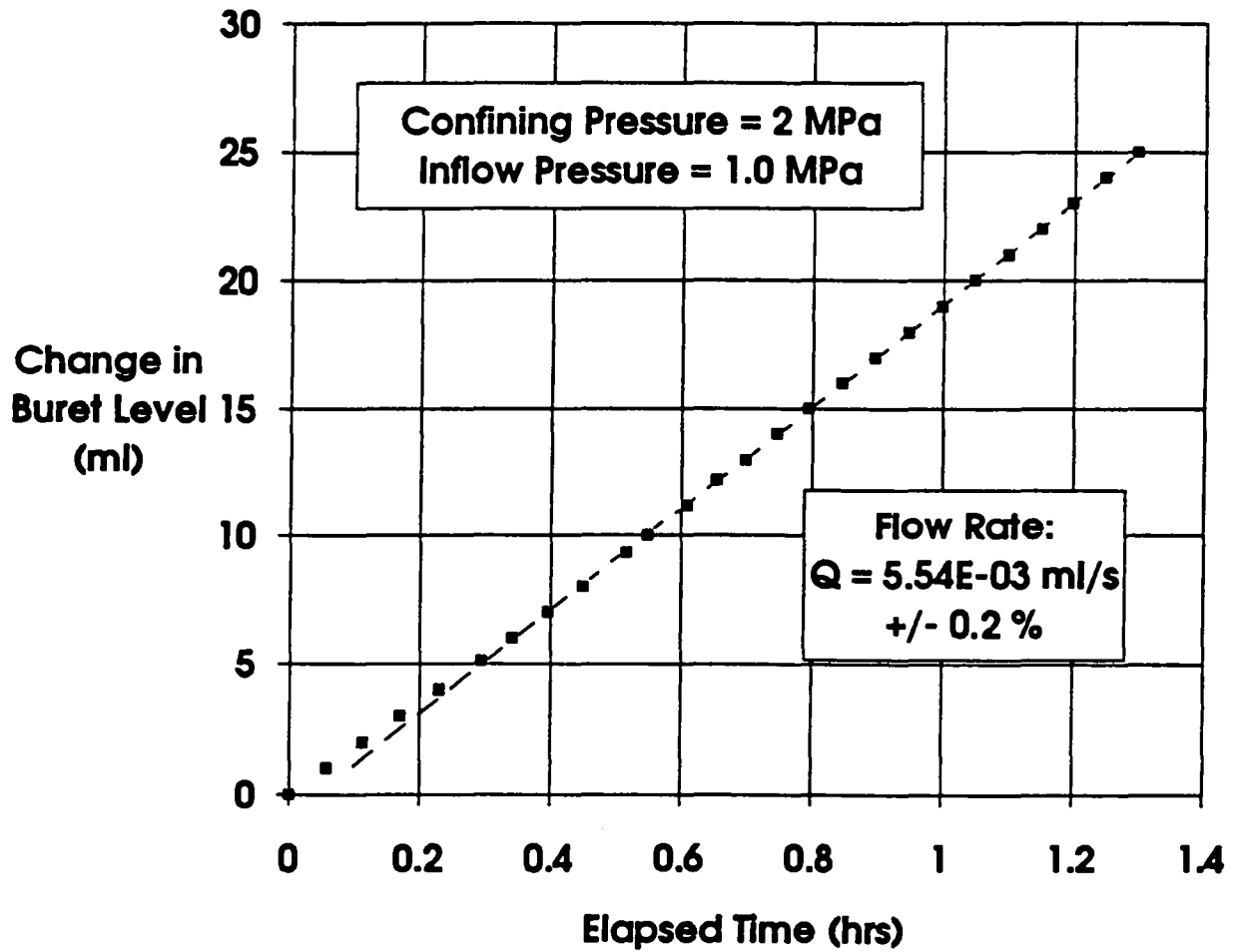
RSI-248-04-011

Figure I-11. Change in exit buret level (brine volume)-versus-time for tests on Specimen P3X10-6-SP2 at 10 MPa confining pressure and 0.7 MPa brine inlet pressure. Symbols are recorded data points; dashed lines are best fits to linear sections of data. Coefficient of variation for linear least square fits are given.



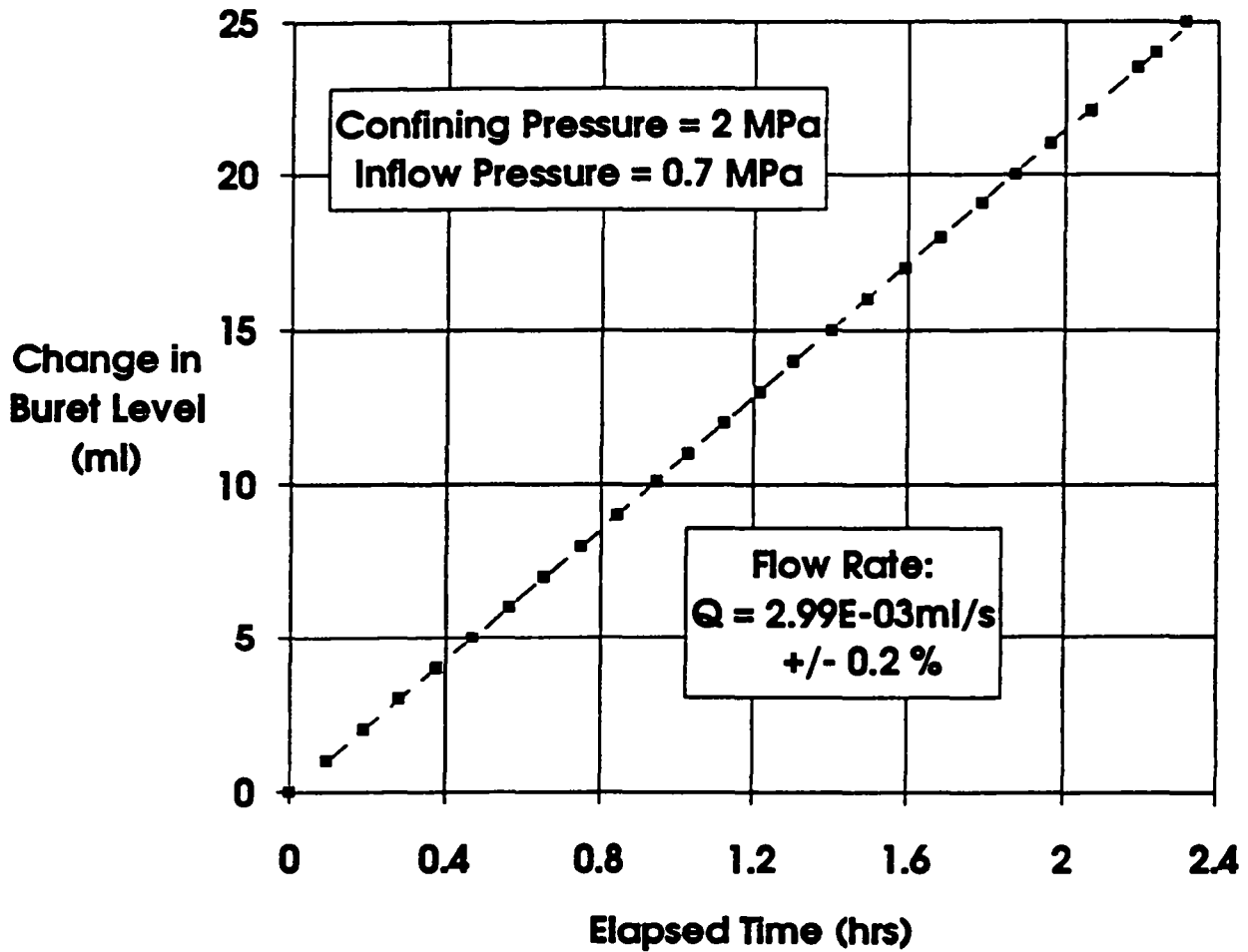
RSI-248-04-012

Figure I-12. Change in exit buret level (brine volume)-versus-time for tests on Specimen P3X10-6-SP2 at 10 MPa confining pressure and 0.4 MPa brine inlet pressure. Symbols are recorded data points; dashed lines are best fits to linear sections of data. Coefficient of variation for linear least square fits are given.



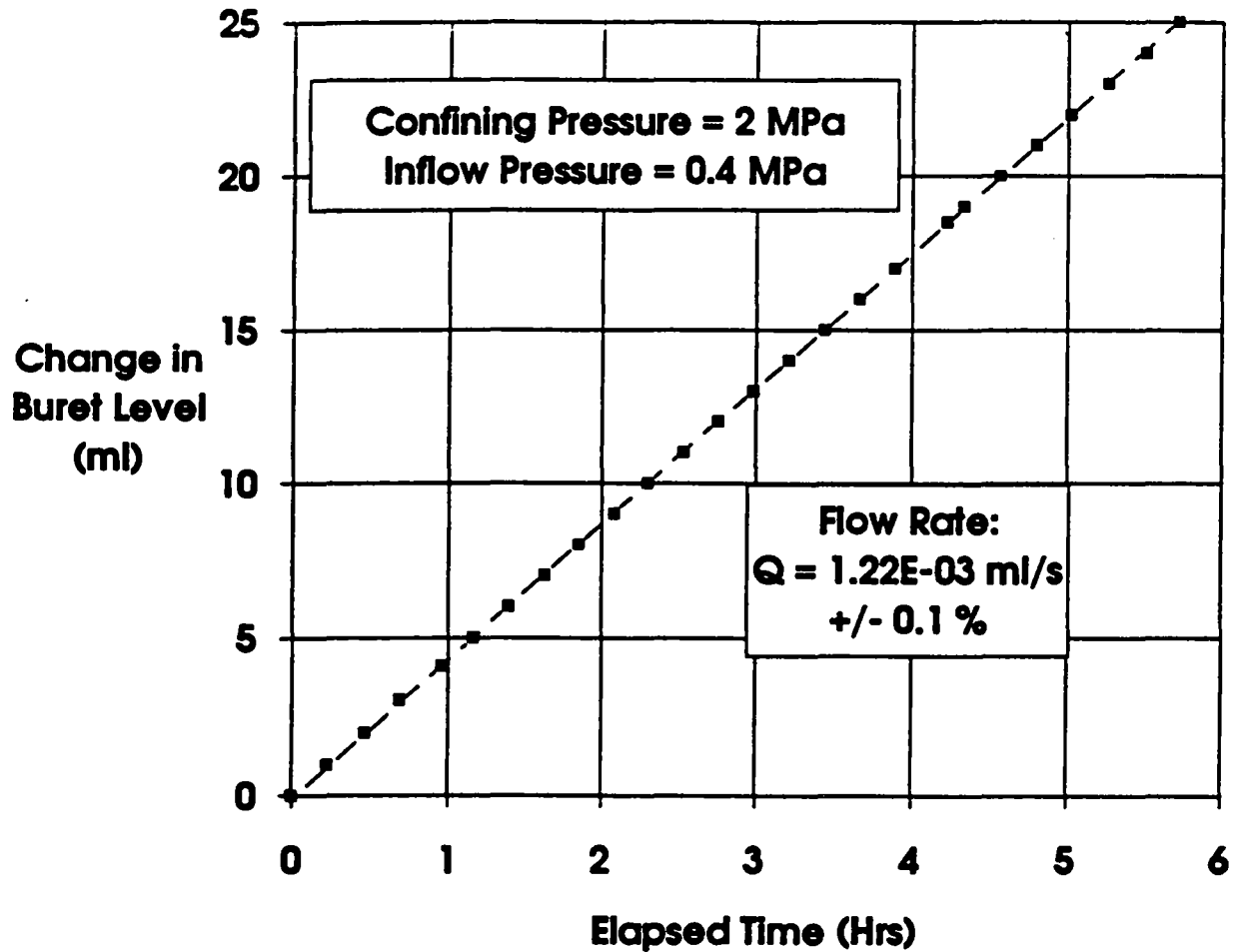
RSI-248-04-013

Figure I-13. Change in exit buret level (brine volume)-versus-time for tests on Specimen P3X11-5-3-SP3 at 2 MPa confining pressure and 1.0 MPa brine inlet pressure. Symbols are recorded data points; dashed lines are best fits to linear sections of data. Coefficient of variation for linear least square fits are given.



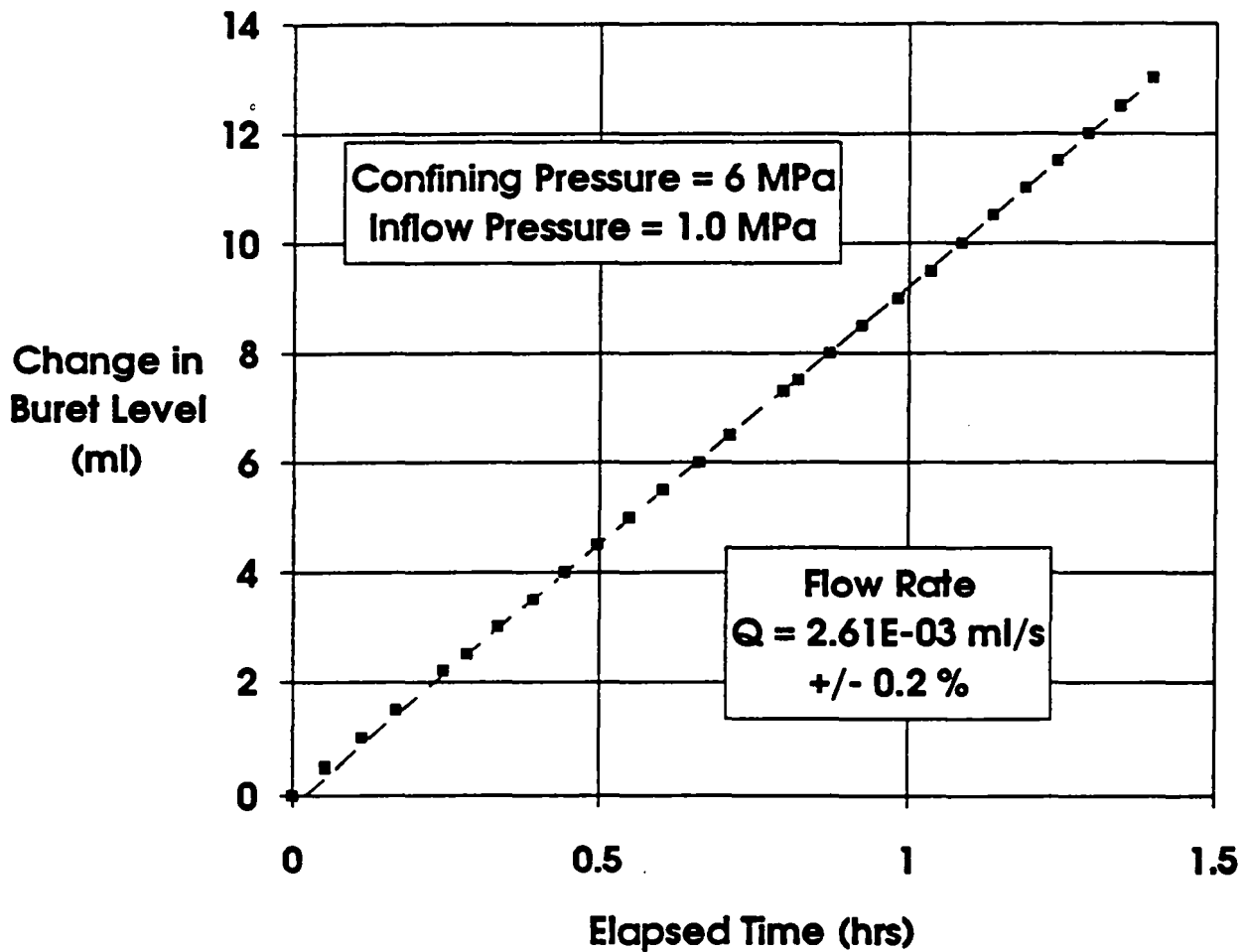
RSI-248-04-014

Figure I-14. Change in exit buret level (brine volume)-versus-time for tests on Specimen P3X11-5-3-SP3 at 2 MPa confining pressure and 0.7 MPa brine inlet pressure. Symbols are recorded data points; dashed lines are best fits to linear sections of data. Coefficient of variation for linear least square fits are given.



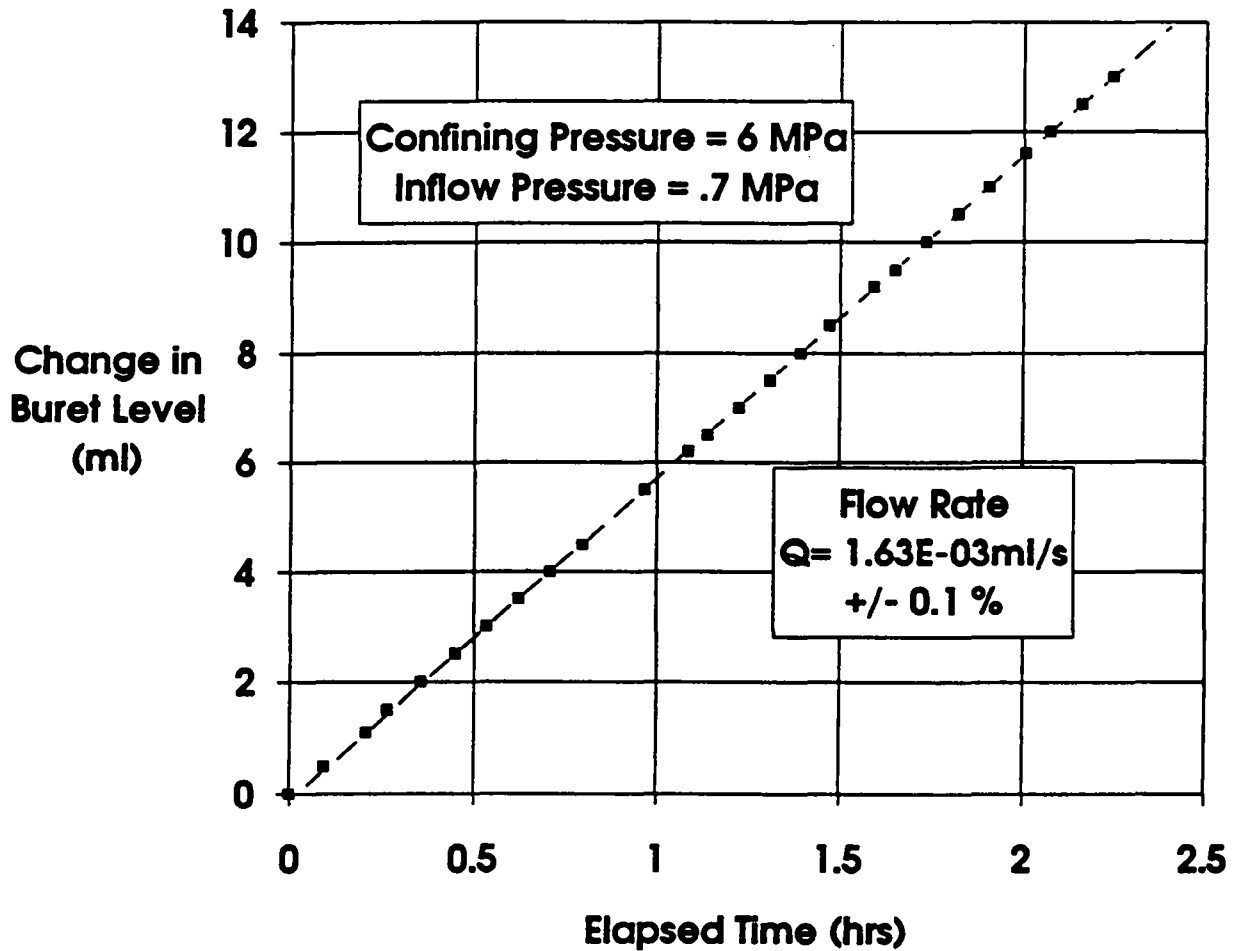
R31-348-04-015

Figure I-15. Change in exit buret level (brine volume)-versus-time for tests on Specimen P3X11-5-3-SP3 at 2 MPa confining pressure and 0.4 MPa brine inlet pressure. Symbols are recorded data points; dashed lines are best fits to linear sections of data. Coefficient of variation for linear least square fits are given.



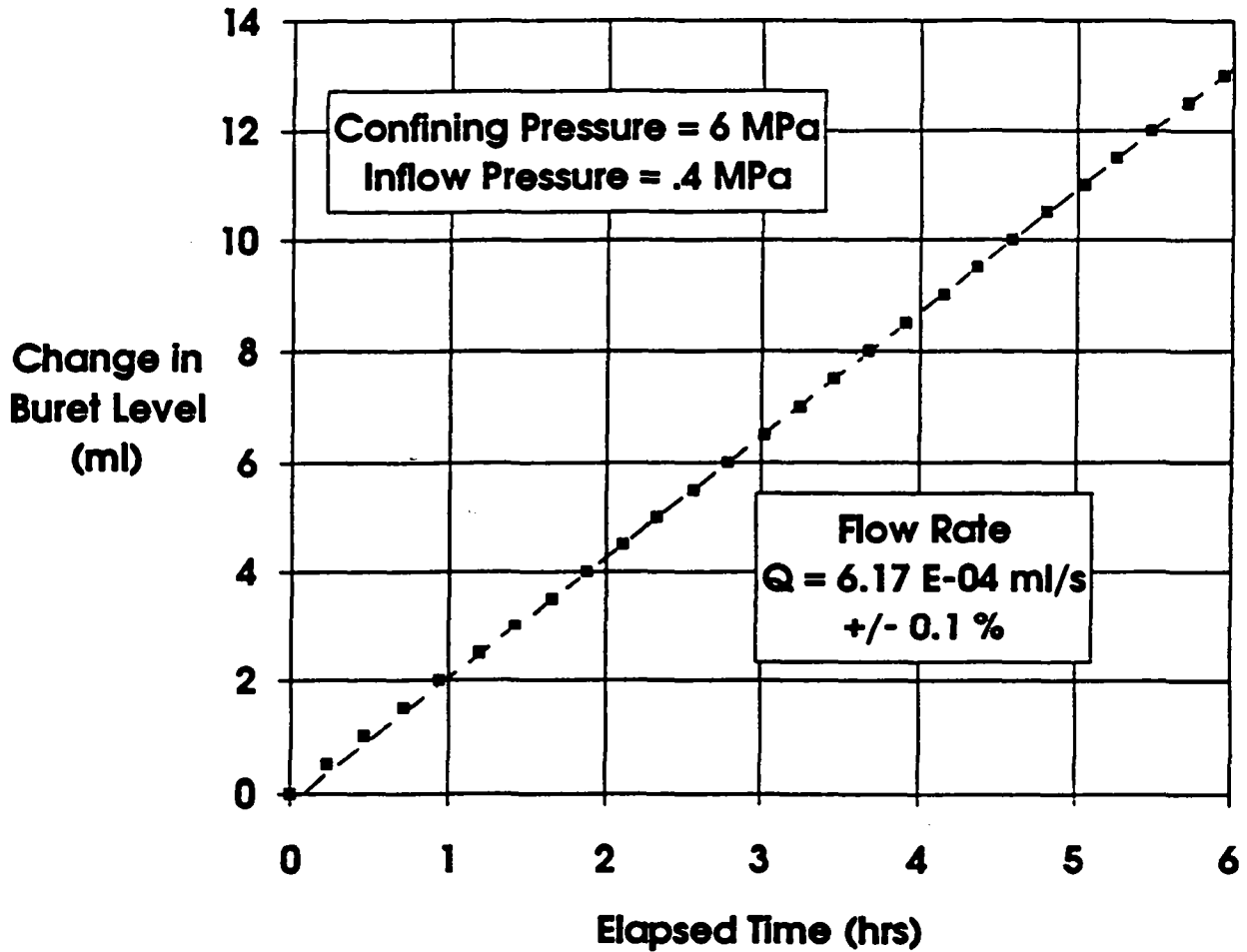
RSI-248-04-018

Figure I-16. Change in exit buret level (brine volume)-versus-time for tests on Specimen P3X11-5-3-SP3 at 6 MPa confining pressure and 1.0 MPa brine inlet pressure. Symbols are recorded data points; dashed lines are best fits to linear sections of data. Coefficient of variation for linear least square fits are given.



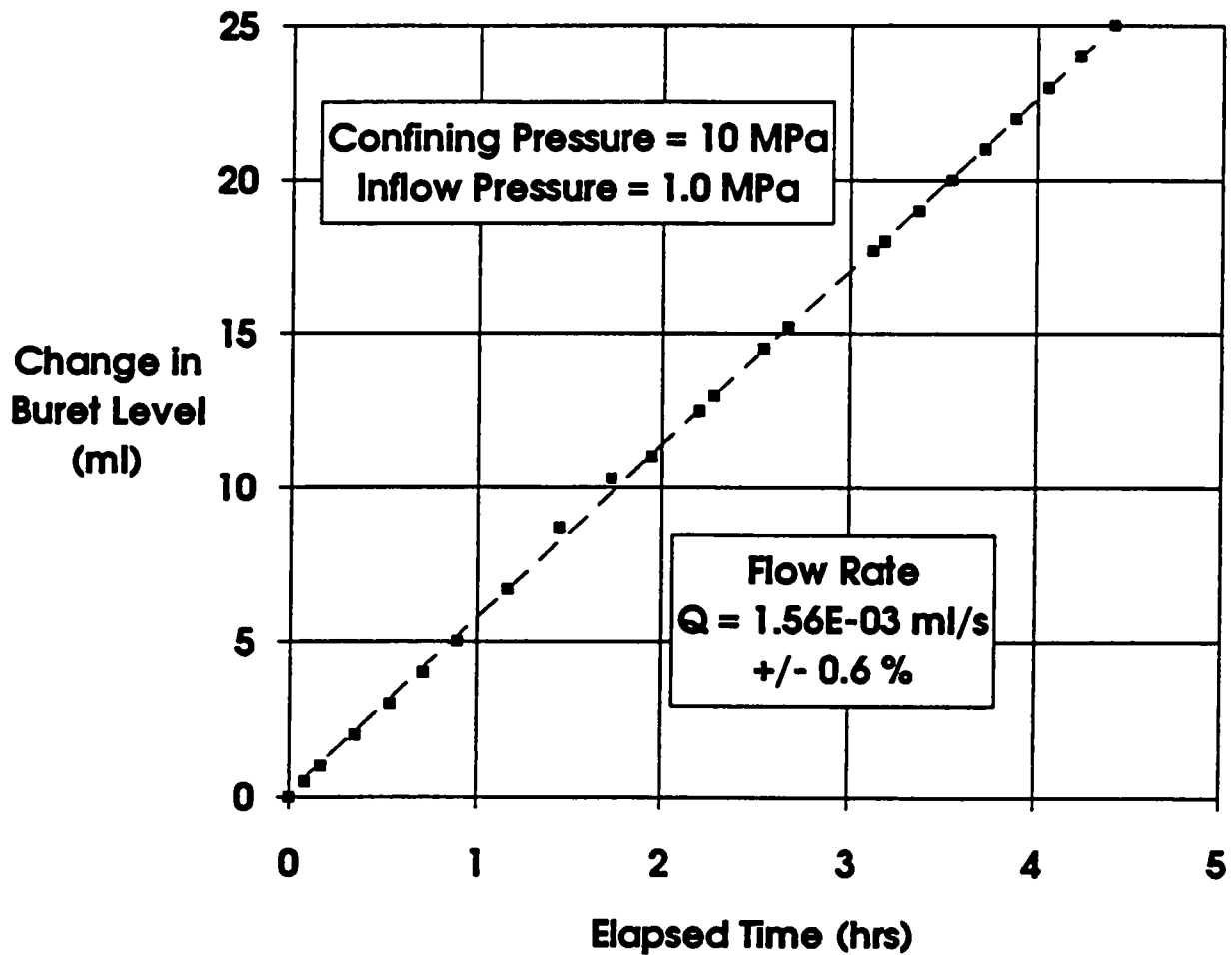
FBI-248-04-017

Figure I-17. Change in exit buret level (brine volume)-versus-time for tests on Specimen P3X11-5-3-SP3 at 6 MPa confining pressure and 0.7 MPa brine inlet pressure. Symbols are recorded data points; dashed lines are best fits to linear sections of data. Coefficient of variation for linear least square fits are given.



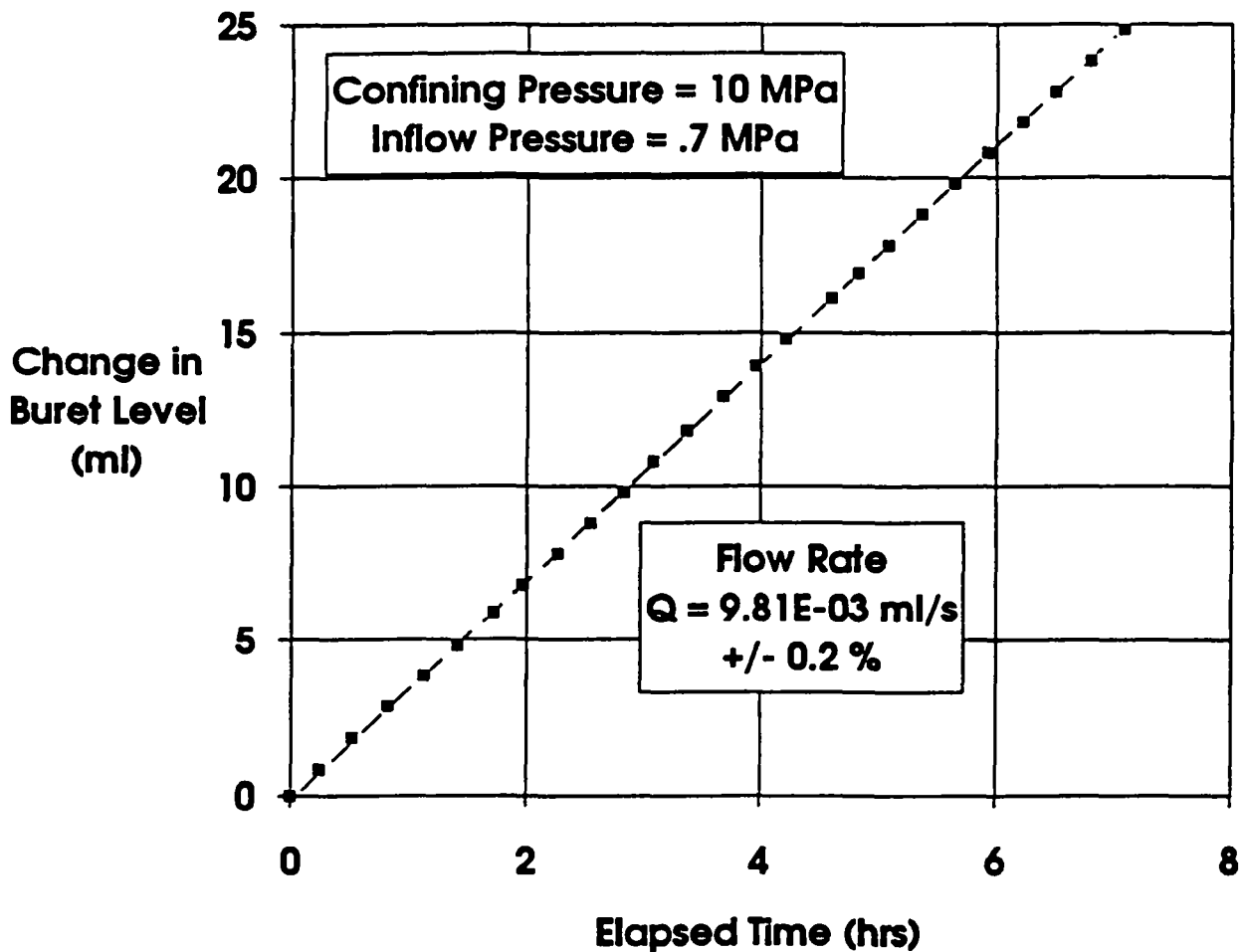
FBI-348-04-018

Figure I-18. Change in exit buret level (brine volume)-versus-time for tests on Specimen P3X11-5-3-SP3 at 6 MPa confining pressure and 0.4 MPa brine inlet pressure. Symbols are recorded data points; dashed lines are best fits to linear sections of data. Coefficient of variation for linear least square fits are given.



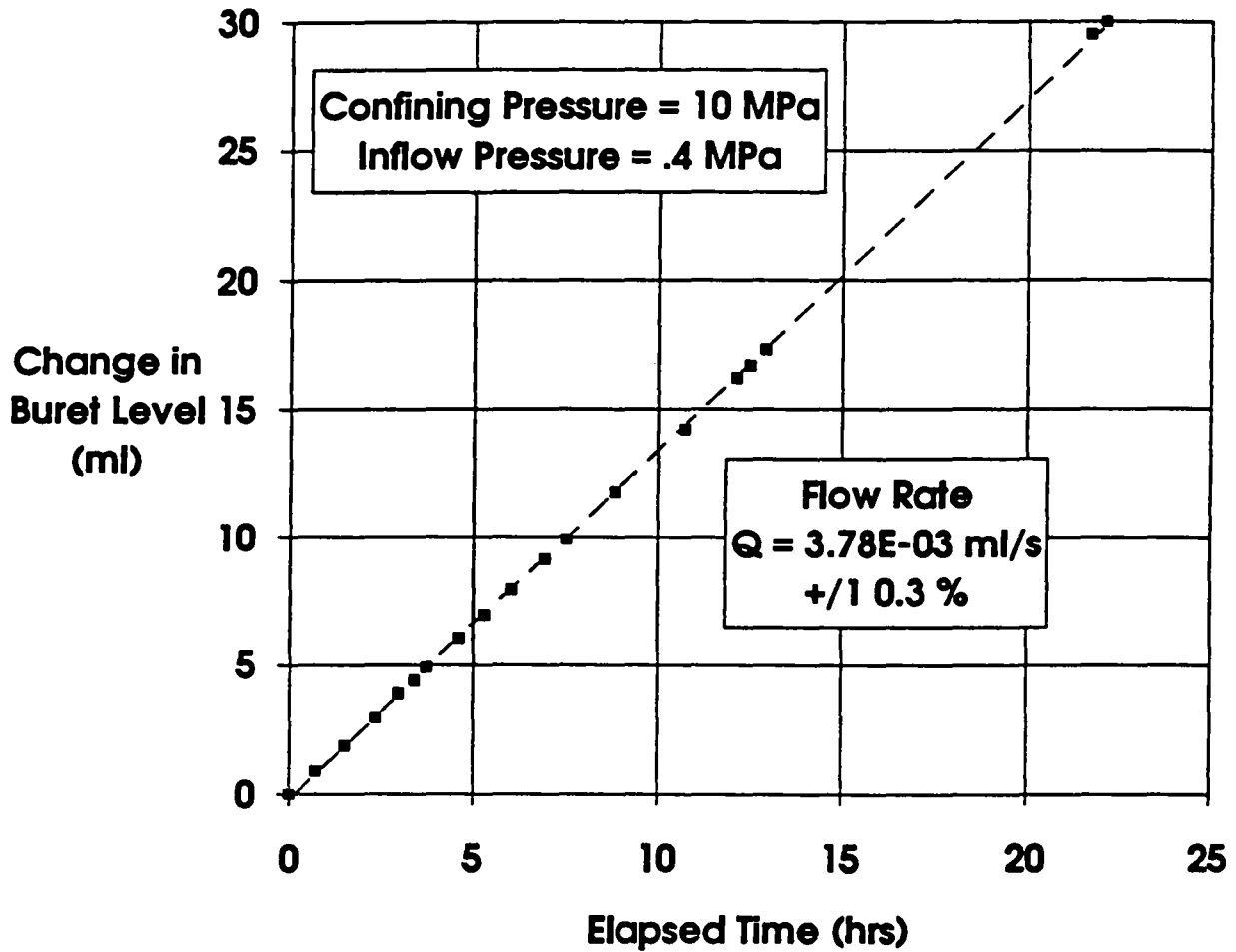
RSI-248-04-019

Figure I-19. Change in exit buret level (brine volume)-versus-time for tests on Specimen P3X11-5-3-SP3 at 10 MPa confining pressure and 1.0 MPa brine inlet pressure. Symbols are recorded data points; dashed lines are best fits to linear sections of data. Coefficient of variation for linear least square fits are given.



RSI-248-04-020

Figure I-20. Change in exit buret level (brine volume)-versus-time for tests on Specimen P3X11-5-3-SP3 at 10 MPa confining pressure and 0.7 MPa brine inlet pressure. Symbols are recorded data points; dashed lines are best fits to linear sections of data. Coefficient of variation for linear least square fits are given.



RSI-248-04-021

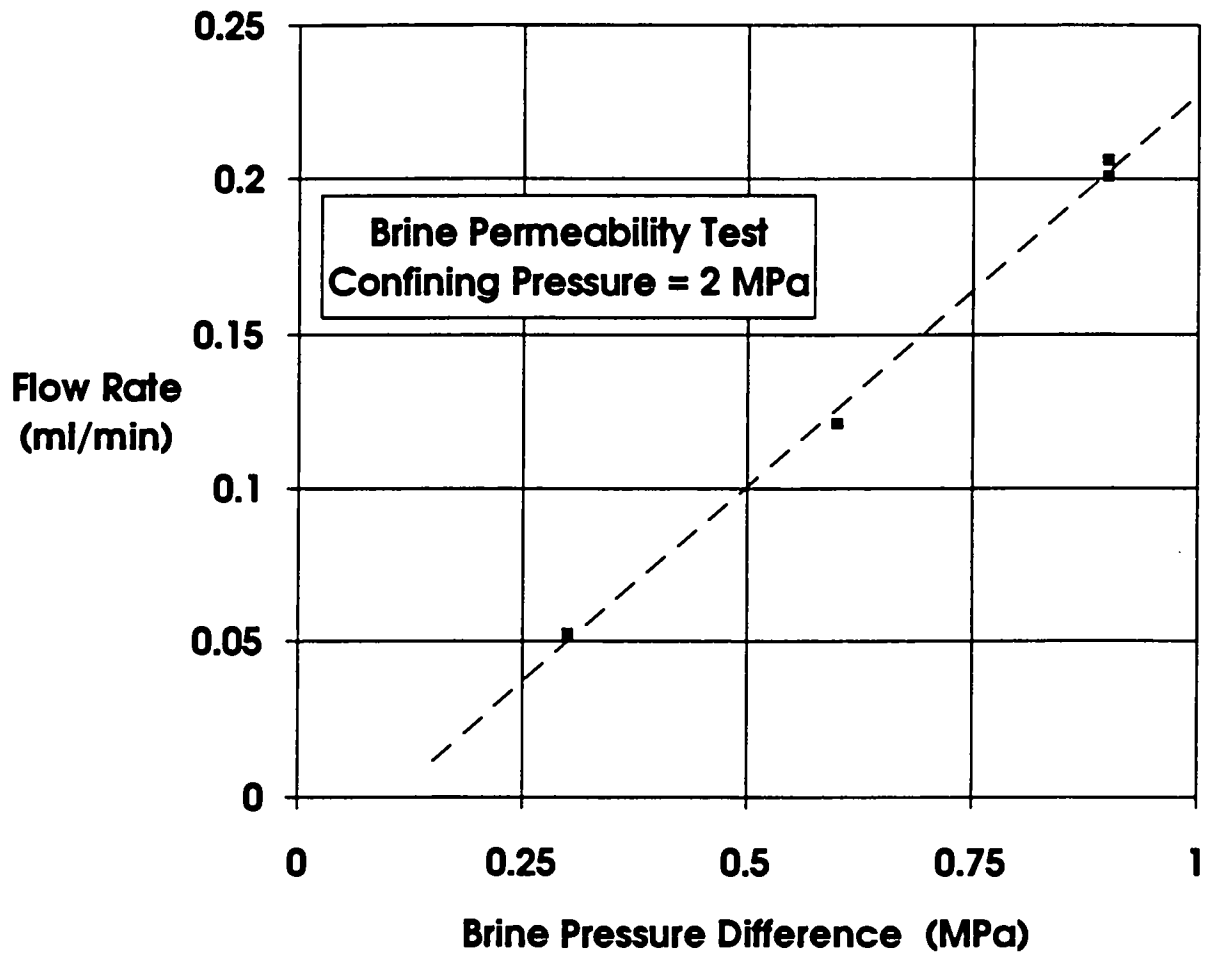
Figure I-21. Change in exit buret level (brine volume)-versus-time for tests on Specimen P3X11-5-3-SP3 at 10 MPa confining pressure and 0.4 MPa brine inlet pressure. Symbols are recorded data points; dashed lines are best fits to linear sections of data. Coefficient of variation for linear least square fits are given.

APPENDIX B.J
FLOW RATE-VERSUS-PORE PRESSURE DIFFERENCE
ACROSS SPECIMEN FOR ALL BRINE PERMEABILITY TESTS

Figures

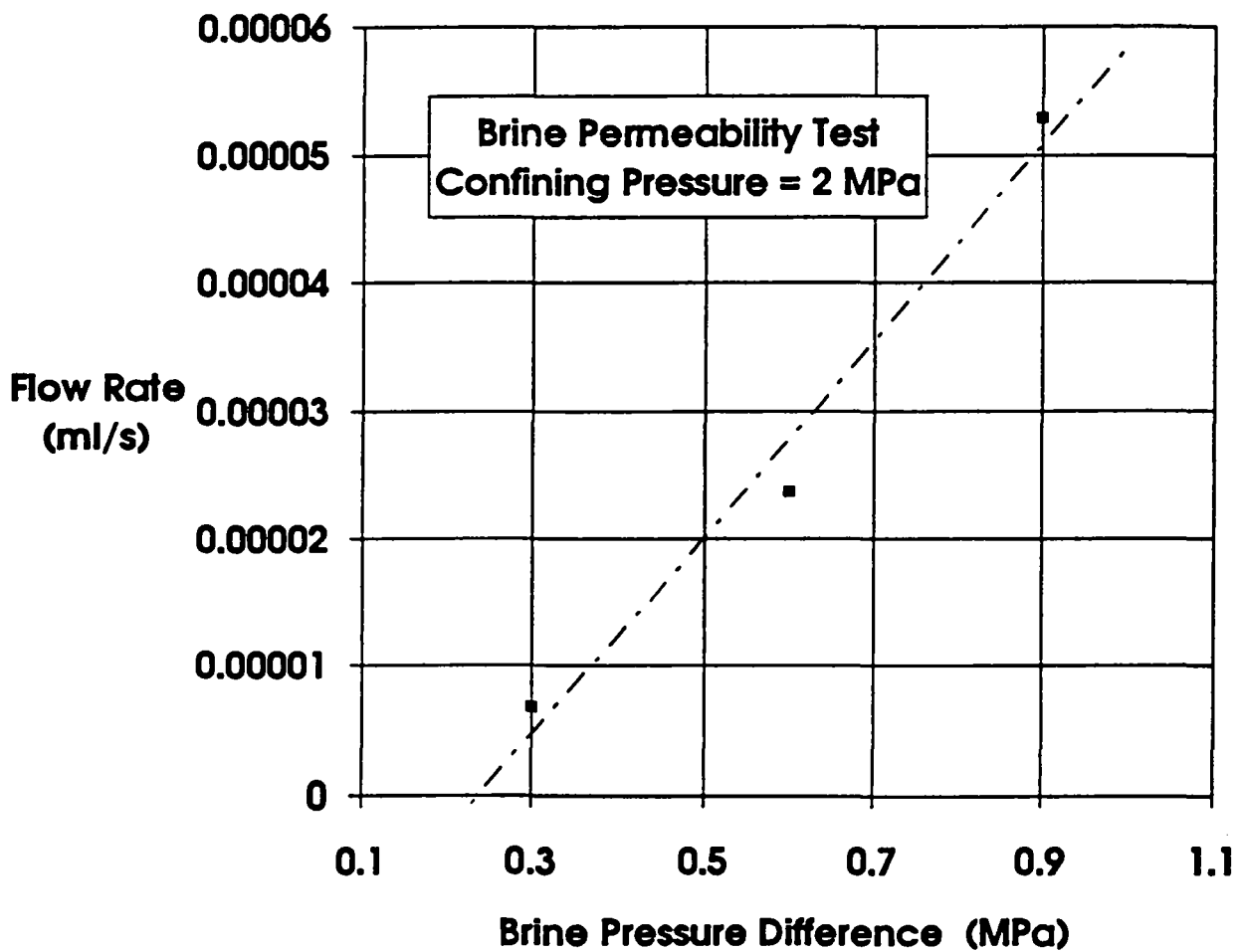
J-1 Flow rate-versus-brine pressure difference for Specimen P3X11-5-2-SP1 at 2 MPa confining pressure and all brine inlet pressures	B-283
J-2 Flow rate-versus-brine pressure difference for Specimen P3X10-6-SP2 at 2 MPa confining pressure and all brine inlet pressures	B-284
J-3 Flow rate-versus-brine pressure difference for Specimen P3X10-6-SP2 at 6 MPa confining pressure and all brine inlet pressures	B-285
J-4 Flow rate-versus-brine pressure difference for Specimen P3X10-6-SP2 at 10 MPa confining pressure and all brine inlet pressures	B-286
J-5 Flow rate-versus-brine pressure difference for Specimen P3X11-5-3-SP3 at 2 MPa confining pressure and all brine inlet pressures	B-287
J-6 Flow rate-versus-brine pressure difference for Specimen P3X11-5-3-SP3 at 6 MPa confining pressure and all brine inlet pressures	B-288
J-7 Flow rate-versus-brine pressure difference for Specimen P3X11-5-3-SP3 at 10 MPa confining pressure and all brine inlet pressures	B-289

B-282



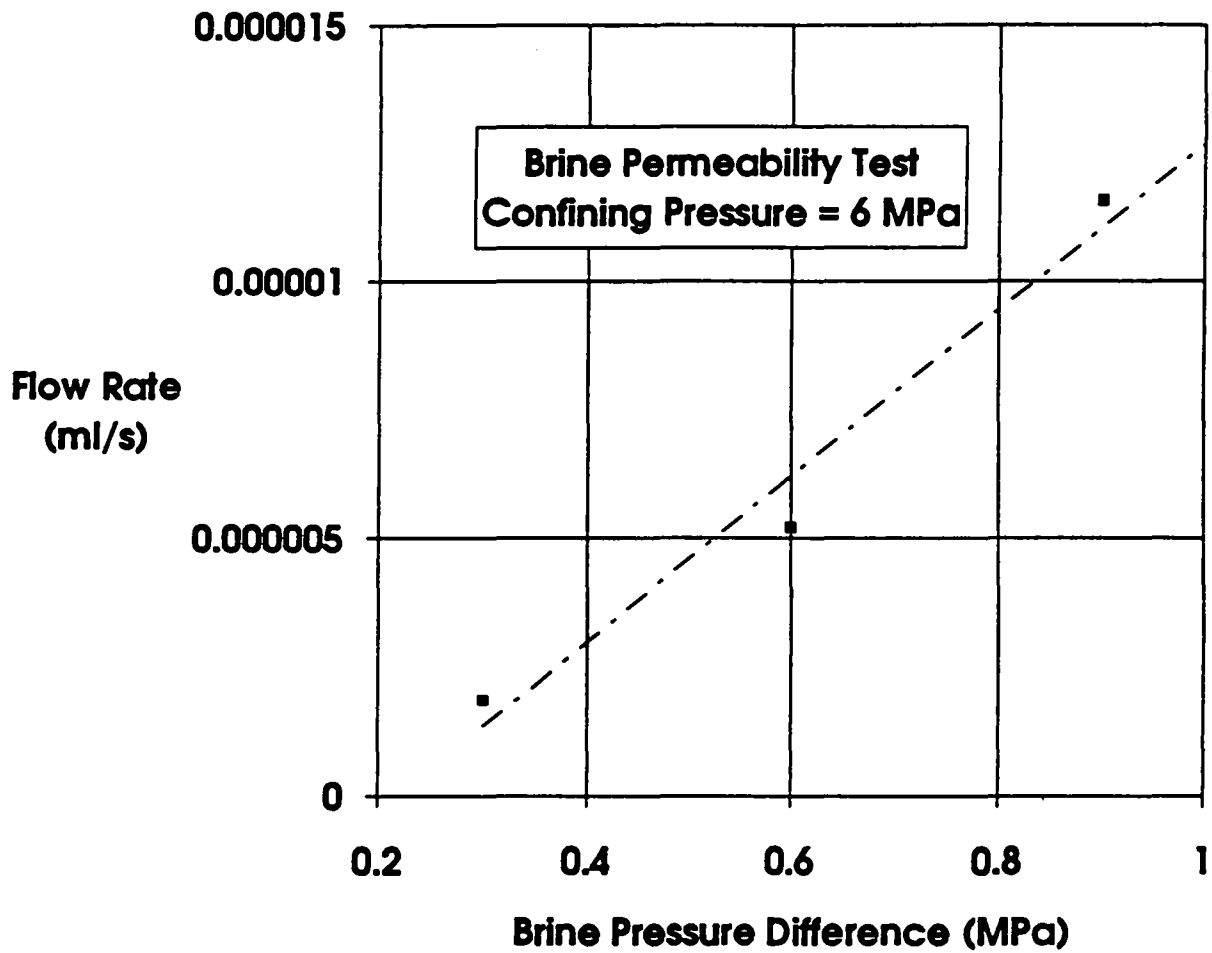
RSI-248-03-110

Figure J-1. Flow rate-versus-brine pressure difference for Specimen P3X11-5-2-SP1 at 2 MPa confining pressure and all brine inlet pressures.



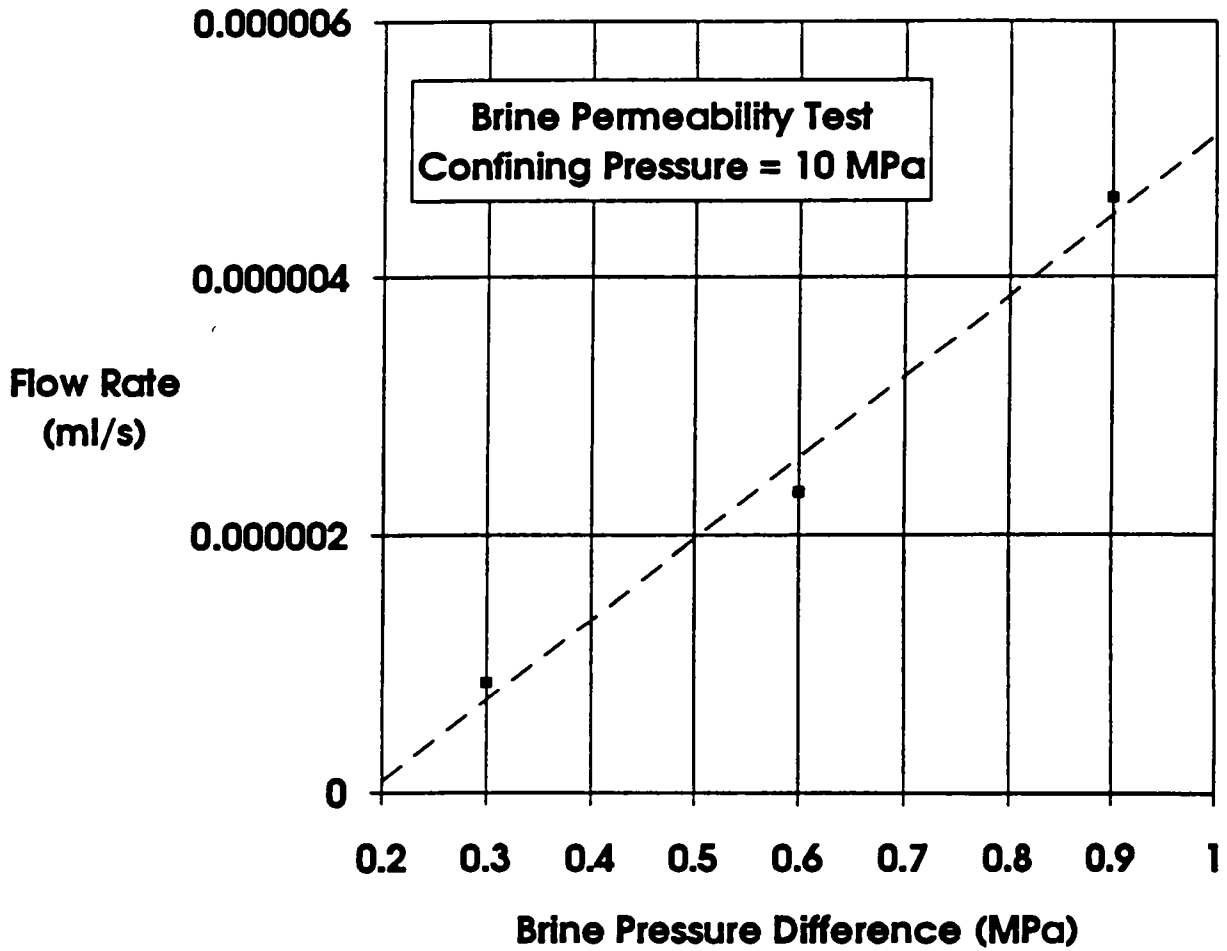
R81-348-04-037

Figure J-2. Flow rate-versus-brine pressure difference for Specimen P3X10-6-SP2 at 2 MPa confining pressure and all brine inlet pressures.



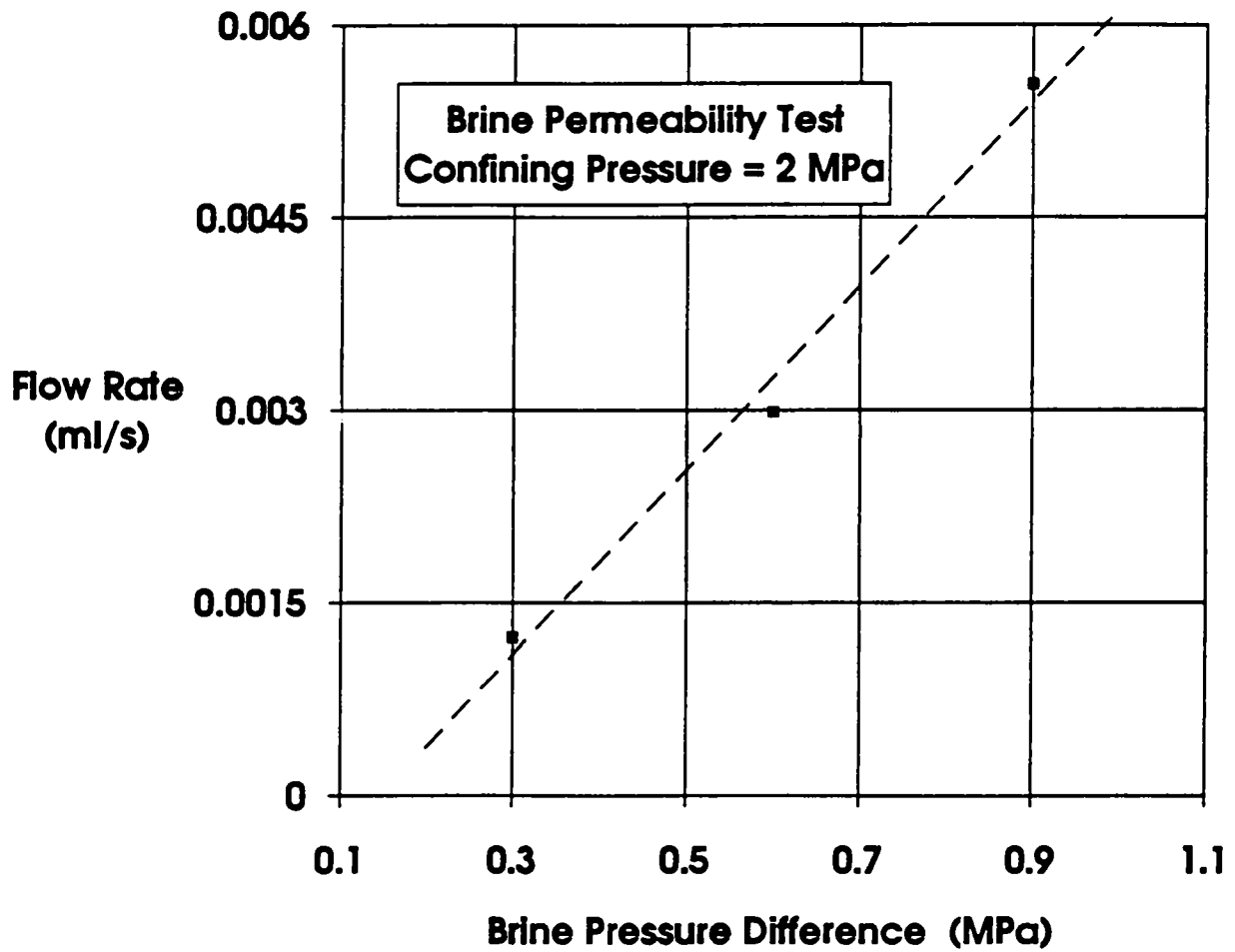
FBI-248-04-038

Figure J-3. Flow rate-versus-brine pressure difference for Specimen P3X10-6-SP2 at 6 MPa confining pressure and all brine inlet pressures.



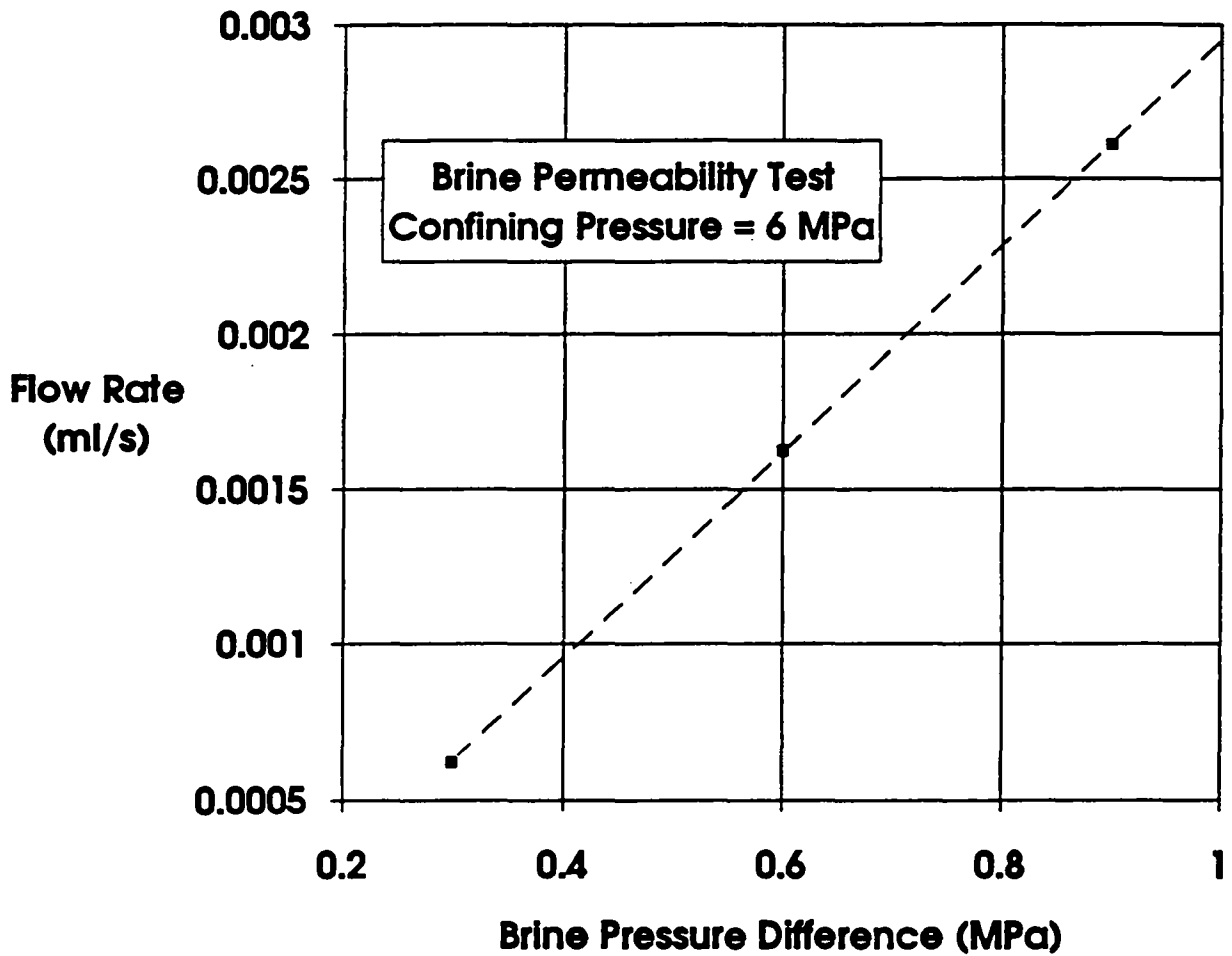
RBI-248-84-038

Figure J-4. Flow rate-versus-brine pressure difference for Specimen P3X10-6-SP2 at 10 MPa confining pressure and all brine inlet pressures.



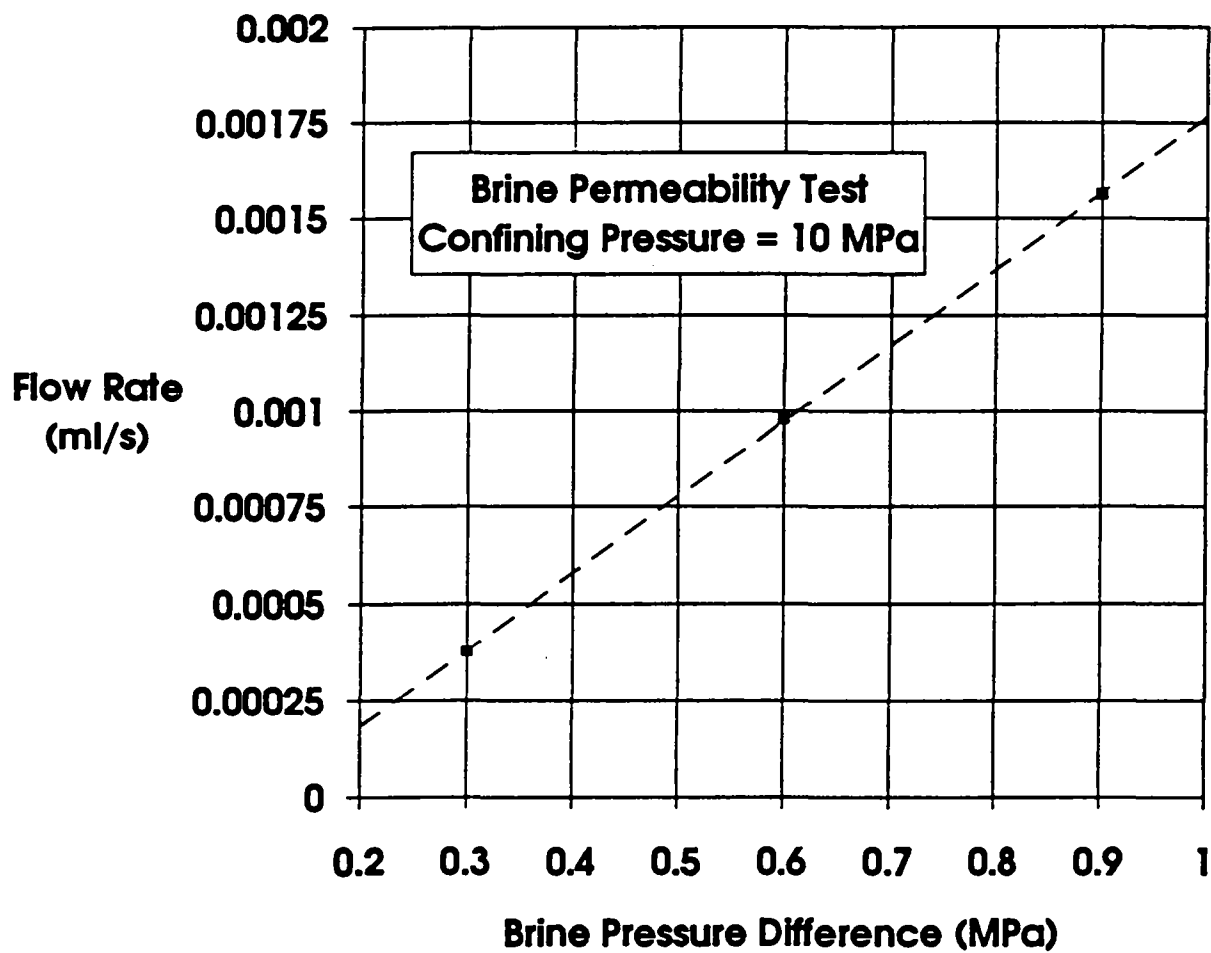
RSI-248-04-040

Figure J-5. Flow rate-versus-brine pressure difference for Specimen P3X11-5-3-SP3 at 2 MPa confining pressure and all brine inlet pressures.



R81-248-04-041

Figure J-6. Flow rate-versus-brine pressure difference for Specimen P3X11-5-3-SP3 at 6 MPa confining pressure and all brine inlet pressures.



RSI-248-04-042

Figure J-7. Flow rate-versus-brine pressure difference for Specimen P3X11-5-3-SP3 at 10 MPa confining pressure and all brine inlet pressures.

WIPP
UC721 - DISTRIBUTION LIST
SAND94-0472

Federal Agencies

US Department of Energy (4)
Office of Civilian Radioactive Waste Mgmt.
Attn: Deputy Director, RW-2
Acting Director, RW-10
Office of Human Resources & Admin.
Director, RW-30
Office of Program Mgmt. & Integ.
Director, RW-40
Office of Waste Accept., Stor., & Tran.
Forrestal Building
Washington, DC 20585

Attn: Project Director
Yucca Mountain Site Characterization Office
Director, RW-3
Office of Quality Assurance
P.O. Box 30307
Las Vegas, NV 89036-0307

US Department of Energy
Albuquerque Operations Office
Attn: National Atomic Museum Library
P.O. Box 5400
Albuquerque, NM 87185-5400

US Department of Energy
Research & Waste Management Division
Attn: Director
P.O. Box E
Oak Ridge, TN 37831

US Department of Energy (5)
Carlsbad Area Office
Attn: G. Dials
D. Galbraith
M. McFadden
R. Lark
J. A. Mewhinney
P.O. Box 3090
Carlsbad, NM 88221-3090

US Department of Energy
Office of Environmental Restoration and
Waste Management
Attn: M Frei, EM-30
Forrestal Building
Washington, DC 20585-0002

US Department of Energy (3)
Office of Environmental Restoration and
Waste Management
Attn: J. Juri, EM-34, Trevion II
Washington, DC 20585-0002

US Department of Energy
Office of Environmental Restoration and
Waste Management
Attn: S. Schneider, EM-342, Trevion II
Washington, DC 20585-0002

US Department of Energy (2)
Office of Environment, Safety & Health
Attn: C. Borgstrom, EH-25
R. Pelletier, EH-231
Washington, DC 20585

US Department of Energy (2)
Idaho Operations Office
Fuel Processing & Waste Mgmt. Division
785 DOE Place
Idaho Falls, ID 83402

US Environmental Protection Agency (2)
Radiation Protection Programs
Attn: M. Oge
ANR-460
Washington, DC 20460

Boards

Defense Nuclear Facilities Safety Board
Attn: D. Winters
625 Indiana Ave. NW, Suite 700
Washington, DC 20004

Nuclear Waste Technical Review Board (2)
Attn: Chairman
J. L. Cohon
1100 Wilson Blvd., Suite 910
Arlington, VA 22209-2297

State Agencies

Attorney General of New Mexico
P.O. Drawer 1508
Santa Fe, NM 87504-1508

Environmental Evaluation Group (3)
Attn: Library
7007 Wyoming NE
Suite F-2
Albuquerque, NM 87109

NM Environment Department (3)
Secretary of the Environment
Attn: Mark Weidler
1190 St. Francis Drive
Santa Fe, NM 87503-0968

NM Bureau of Mines & Mineral Resources
Socorro, NM 87801

Laboratories/Corporations

Battelle Pacific Northwest Laboratories
Battelle Blvd.
Richland, WA 99352

INTERA, Inc.
Attn: G. A. Freeze
1650 University Blvd. NE, Suite 300
Albuquerque, NM 87102

INTERA, Inc.
Attn: J. F. Pickens
6850 Austin Center Blvd., Suite 300
Austin, TX 78731

Los Alamos National Laboratory
Attn: B. Erdal, INC-12
P.O. Box 1663
Los Alamos, NM 87544

RE/SPEC, Inc.
Attn: A. Robb
4775 Indian School NE, Suite 300
Albuquerque, NM 87110-3927

RE/SPEC, Inc.
Attn: J. L. Ratigan
P. O. Box 725
Rapid City, SD 57709

Tech Reps, Inc. (3)
Attn: J. Chapman (1)
Loretta Robledo (2)
5000 Marble NE, Suite 222
Albuquerque, NM 87110

Westinghouse Electric Corporation (5)
Attn: Library
J. Epstein
J. Lee
B. A. Howard
R. Kehrman
P.O. Box 2078
Carlsbad, NM 88221

S. Cohen & Associates
Attn: Bill Thurber
1355 Beverly Road
McLean, VA 22101

Rock Physics Associates
Attn: J. Walls
4320 Steven Creek Blvd., Ste 282
San Jose, CA 95129

National Academy of Sciences, WIPP Panel

Howard Adler
Oxyrase, Incorporated
7327 Oak Ridge Highway
Knoxville, TN 37931

Tom Kiess
Board of Radioactive Waste Management
GF456
2101 Constitution Ave.
Washington, DC 20418

Rodney C. Ewing
Department of Geology
University of New Mexico
Albuquerque, NM 87131

Charles Fairhurst
Department of Civil and Mineral Engineering
University of Minnesota
500 Pillsbury Dr. SE
Minneapolis, MN 55455-0220

B. John Garrick
PLG Incorporated
4590 MacArthur Blvd., Suite 400
Newport Beach, CA 92660-2027

Leonard F. Konikow
US Geological Survey
431 National Center
Reston, VA 22092

Carl A. Anderson, Director
Board of Radioactive Waste Management
National Research Council
HA 456
2101 Constitution Ave. NW
Washington, DC 20418

Christopher G. Whipple
ICF Kaiser Engineers
1800 Harrison St., 7th Floor
Oakland, CA 94612-3430

John O. Blomeke
720 Clubhouse Way
Knoxville, TN 37909

Sue B. Clark
University of Georgia
Savannah River Ecology Lab
P.O. Drawer E
Aiken, SC 29802

Konrad B. Krauskopf
Department of Geology
Stanford University
Stanford, CA 94305-2115

Della Roy
Pennsylvania State University
217 Materials Research Lab
Hastings Road
University Park, PA 16802

David A. Waite
CH₂ M Hill
P.O. Box 91500
Bellevue, WA 98009-2050

Thomas A. Zordon
Zordan Associates, Inc.
3807 Edinburg Drive
Murrysville, PA 15668

Universities

University of New Mexico
Geology Department
Attn: Library
141 Northrop Hall
Albuquerque, NM 87131

Libraries

Thomas Brannigan Library
Attn: D. Dresp
106 W. Hadley St.
Las Cruces, NM 88001

Government Publications Department
Zimmerman Library
University of New Mexico
Albuquerque, NM 87131

New Mexico Junior College
Pannell Library
Attn: R. Hill
Lovington Highway
Hobbs, NM 88240

New Mexico State Library
Attn: N. McCallan
325 Don Gaspar
Santa Fe, NM 87503

New Mexico Tech
Martin Speere Memorial Library
Campus Street
Socorro, NM 87810

WIPP Public Reading Room
Carlsbad Public Library
101 S. Halagueno St.
Carlsbad, NM 88220

Foreign Addresses

Atomic Energy of Canada, Ltd.
Whiteshell Laboratories
Attn: B. Goodwin
Pinawa, Manitoba, CANADA R0E 1L0

Francois Chenevier (2)
ANDRA
Route de Panorama Robert Schumann
B. P. 38
92266 Fontenay-aux-Roses, Cedex
FRANCE

Claude Sombret
Centre d'Etudes Nucleaires de la Vallee Rhone
CEN/VALRHO
S.D.H.A. B.P. 171
30205 Bagnols-Sur-Ceze
FRANCE

Commissariat a L'Energie Atomique
Attn: D. Alexandre
Centre d'Etudes de Cadarache
13108 Saint Paul Lez Durance Cedex
FRANCE

Bundesanstalt fur Geowissenschaften und
Rohstoffe
Attn: M. Langer
Postfach 510 153
D-30631 Hannover
GERMANY

Bundesministerium fur Forschung und
Technologie
Postfach 200 706
5300 Bonn 2
GERMANY

Institut fur Tieflagerung
Attn: K. Kuhn
Theodor-Heuss-Strasse 4
D-3300 Braunschweig
GERMANY

Gesellschaft fur Anlagen und Reaktorsicherheit
(GRS)
Attn: B. Baltes
Schwertnergasse 1
D-50667 Cologne
GERMANY

Shingo Tashiro
Japan Atomic Energy Research Institute
Tokai-Mura, Ibaraki-Ken, 319-11
JAPAN

Netherlands Energy Research Foundation ECN
Attn: J. Prij
3 Westerduinweg
P.O. Box 1
1755 ZG Petten
THE NETHERLANDS

Svensk Karnbransleforsorjning AB
Attn: F. Karlsson
Project KBS (Karnbranslesakerhet)
Box 5864
S-102 48 Stockholm
SWEDEN

Nationale Genossenschaft fur die Lagerung
Radioaktiver Abfalle (2)
Attn: S. Vomvoris
P. Zuidema
Hardstrasse 73
CH-5430 Wettingen
SWITZERLAND

AEA Technology
Attn: J. H. Rees
D5W/29 Culham Laboratory
Abington, Oxfordshire OX14 3DB
UNITED KINGDOM

AEA Technology
Attn: W. R. Rodwell
044/A31 Winfrith Technical Centre
Dorchester, Dorset DT2 8DH
UNITED KINGDOM

AEA Technology
Attn: J. E. Tinson
B4244 Harwell Laboratory
Didcot, Oxfordshire OX11 0RA
UNITED KINGDOM

Internal

<u>MS</u>	<u>Org.</u>	
1324	6115	P. B. Davies
1324	6115	T. L. Christian-Frear (5)
1324	6115	C. Boney
1324	6115	R. L. Beauheim
1324	6115	S. W. Webb
1320	6831	E. J. Nowak
1322	6121	J. R. Tillerson
1328	6849	D. R. Anderson
1328	6848	H. N. Jow
1335	6801	M. Chu
1335	6801	S. M. Howarth (15)
1341	6832	J. T. Holmes
1395	6800	L. Shephard
1395	6821	M. Marietta
0751	6117	L. S. Costin
0751	6117	N. S. Brodsky
0751	6117	J. T. Fredrich
0751	6117	D. J. Holcomb

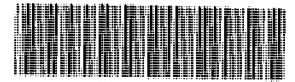
0751	6117	D. H. Zeuch
0705	6116	D. J. Borns
1330	6811	K. Hart (2)
1330	4415	NWM Library (20)
9018	8940-2	Central Technical Files
0899	4414	Technical Library (5)
0619	12690	Review and Approval Desk (2), For DOE/OSTI

SANDIA REPORT

SAND94-0472/3 • UC-721

Unlimited Release

Printed August 1997



TL0006050

**SANDIA NATIONAL
LABORATORIES
TECHNICAL LIBRARY**

Porosity, Single-Phase Permeability, and Capillary Pressure Data from Preliminary Laboratory Experiments on Selected Samples from Marker Bed 139 at the Waste Isolation Pilot Plant

Volume 3 of 3: Appendices C, D, E, and F

Susan M. Howarth, Tracy Christian-Frear

Prepared by
Sandia National Laboratories
Albuquerque, New Mexico 87185 and Livermore, California 94550

Sandia is a multiprogram laboratory operated by Sandia
Corporation, a Lockheed Martin Company, for the United States
Department of Energy under Contract DE-AC04-94AL85000.

Approved for public release; distribution is unlimited.

**Sandia National Laboratories**

301 p, in
various pagings

Issued by Sandia National Laboratories, operated for the United States Department of Energy by Sandia Corporation.

NOTICE: This report was prepared as an account of work sponsored by an agency of the United States Government. Neither the United States Government nor any agency thereof, nor any of their employees, nor any of their contractors, subcontractors, or their employees, makes any warranty, express or implied, or assumes any legal liability or responsibility for the accuracy, completeness, or usefulness of any information, apparatus, product, or process disclosed, or represents that its use would not infringe privately owned rights. Reference herein to any specific commercial product, process, or service by trade name, trademark, manufacturer, or otherwise, does not necessarily constitute or imply its endorsement, recommendation, or favoring by the United States Government, any agency thereof, or any of their contractors or subcontractors. The views and opinions expressed herein do not necessarily state or reflect those of the United States Government, any agency thereof, or any of their contractors.

Printed in the United States of America. This report has been reproduced directly from the best available copy.

Available to DOE and DOE contractors from
Office of Scientific and Technical Information
P.O. Box 62
Oak Ridge, TN 37831

Prices available from (615) 576-8401, FTS 626-8401

Available to the public from
National Technical Information Service
U.S. Department of Commerce
5285 Port Royal Rd
Springfield, VA 22161

NTIS price codes
Printed copy: A14
Microfiche copy: A01

SAND94-0472/3
Unlimited Release
Printed August 1997

Distribution
Category UC-721

**Porosity, Single-Phase Permeability, and Capillary
Pressure Data from Preliminary Laboratory Experiments
on Selected Samples from
Marker Bed 139 at the Waste Isolation Pilot Plant**

Volume 3 of 3: Appendices C, D, E and F

Susan M. Howarth
Tracy Christian-Frear

Geohydrology Department 6115
Sandia National Laboratories
Albuquerque, NM 87185

ABSTRACT

This volume contains the mineralogy, porosity, and permeability results from the Marker Bed 139 specimens evaluated by TerraTek, Inc. This volume also documents the brine recipe used by RE/SPEC, Inc., the parameter package submitted to Performance Assessment based on all the data, and a memo on the mixed Brooks and Corey two-phase characteristic curves.

Appendix C.
Data Report: TerraTek Inc.

The following appendix section includes Appendix C and Appendices C-A through C-E.

Appendix C

Characterization of MB139 at WIPP

Errata Sheet

Total porosity data for sample EP2 is not included in the data report because the mass loss during crushing was excessive.

The liquid permeability data are included in the data report as "scoping only" because the saturation data (Table 8) were characterized as scoping only in the laboratory notebooks.

The following errors in the Appendix, *Characterization of MB139 at WIPP*, are noted:

1. Table 3: Sample designations should not have a "-" separating the letters from the numerals (e.g., PX-1 should be PX1).
2. Table 4: Rows 8 and 9 of the data indicate PX4 should be PX3.
3. Table 6: Sample B's grain volume ($V_{g\text{ eff}}$) should be 773.00, not 723.00 cc.
4. Table 6: Sample E's effective porosity (ϕ_{eff}) should be 1.45, not 1.55%.

The following modifications should be made to the references on page C-82 in Appendix C.

Ref. No.	Comment
1	copy of Davies, 1991 on file in SWCF as WPO#26169
2	authors are A.M. Petrovic, J.E. Siebert, and P.E. Rieke; journal title is <i>Soil Science Society of America Journal</i> Vol. 46, no. 3; copy on file in SWCF as WPO#42627
3	authors are P.K. Hunt, P. Engler, and C. Bajsarowicz; journal title is <i>Journal of Petroleum Technology</i> Vol. 40, no. 9; copy on file in SWCF as WPO#45565
4	authors are G.O. Brown, M.L. Stone, and J.E. Gazin; journal title is <i>Water Resources Research</i> Vol. 29, no. 2; copy on file in SWCF as WPO#42086
5	authors are R.A. Johns, J.S. Steude, L.M. Castanier, and P.V. Roberts; journal title is <i>Journal of Geophysical Research</i> Vol. 98, no. B2; copy on file in SWCF as WPO#40567
6	the existence of Vinegar and Hill could not be verified (company confidential document); cited on p. C-14.
7	the publication date for this ISRM method is 1981
8	correct publisher of Taylor, 1982 is University Science Books, Mill Valley, CA
9	the publisher location for <i>Handbook of Chemistry and Physics</i> is Boca Raton, FL

The following modifications should be made to the references in Appendix C-A: Procedures.

Page No.	Change
C-86	reference 1: existence of Operator's Manual 961036 could not be verified
C-87	reference 2: publisher location is Swarthmore, PA
C-87	reference 4: correct name of second author is R.C. Reynolds, Jr.
C-91	reference 9: cited pages are on file in SWCF
C-91	reference 10: cited pages are on file in SWCF

CHARACTERIZATION OF MARKER BED 139 AT WIPP

**Final Report
Contract AD-3656**

**Nancy S. Davis, Org. 7216
Sandia Contracting Representative**

Submitted to:

**Sandia National Laboratories
P.O Box 5800
Albuquerque, NM 87185-5800**

**Attention: Dr. Susan Howarth, Org. 6115
Sandia Delegated Representative**

Submitted by:

**Joanne T. Fredrich
Principal Investigator**

**TERRATEK, INC.
University Research Park
400 Wakara Way
Salt Lake City, Utah 84108**

**TR94-20
December, 1993**

Table of Contents

1.0 Introduction	C-11
2.0 Core Receipt and Inspection	C-11
3.0 X-Ray CT Non-Destructive Core Analysis	C-14
3.1 Application of a Second Generation CT Scanner	C-14
3.2 Exploratory Application of a Third Generation CT Scanner	C-23
4.0 Sample Preparation	C-30
5.0 XRD Analyses	C-34
6.0 Petrography	C-36
6.1 Overview	C-37
6.2 Petrographic Descriptions	C-38
6.2.1 Sample PX1.	C-38
6.2.2 Sample PX2.	C-39
6.2.3 Sample PX3.	C-39
6.2.4 Sample PX4.	C-39
6.2.5 Sample PX5.	C-40
6.2.6 Sample PX6.	C-40
7.0 Effective Porosity, Total Porosity, and Saturation	C-71
8.0 Single Phase Permeability	C-74
8.1 Gas Single-Phase Permeability	C-74
8.2 Liquid Single-Phase Permeability	C-74
9.0 Summary and Recommendations	C-80
10.0 References	C-82
APPENDIX C-A: Procedures	C-83
A.1 X-Ray Computerized Tomography	C-84
A.1.1 Background.	C-84
A.1.2 TerraTek's CT Facility.	C-84
A.1.3 Operating Procedures.	C-85
A.1.4 Imaging of fluid flow through cores.	C-86
A.2 X-Ray Diffraction (XRD) Analyses	C-87
A.3 Petrographic Analyses	C-87
A.4 Porosity Measurement	C-88

A.4.1	Gas porosimetry.	C-91
A.4.2	Bulk volume.	C-91
A.4.3	Powdering for measurement of total porosity.	C-91
A.5	Liquid Saturation	C-92
A.6	Gas Single-Phase Permeability	C-92
A.7	Liquid Single-Phase Permeability	C-93
A.8	Calibration Facilities and Instrumentation	C-93
APPENDIX C-B:	Index of CT Cross-sectional Images from Whole Core Scan (E1X-08) . .	C-97
APPENDIX C-C:	Drying History of Samples A-F & EP1-8	C-99
APPENDIX C-D:	Gas Permeability Spreadsheets	C-105
APPENDIX C-E:	Liquid Permeability Spreadsheets	C-179

List of Tables

Table 1.	Sample Identification	C-30
Table 2.	Drying Times	C-35
Table 3.	XRD Semi-Quantitative Mineralogic Analyses	C-35
Table 4.	Modal Analyses	C-36
Table 5.	Grain Size, Sorting, and Porosity from 300-Point Count	C-37
Table 6.	Bulk Volume, Effective Grain Volume, and Effective Porosity	C-72
Table 7.	Bulk Density, Grain Density, and Total Porosity	C-73
Table 8.	Liquid (OMS) Saturation	C-73
Table 9.	Single Phase Gas Permeability	C-75
Table 9.	Single Phase Gas Permeability (continued)	C-76
Table 9.	Single Phase Gas Permeability (continued)	C-77
Table 10.	Single Phase Klinkenberg Gas Permeability	C-78
Table 11.	Single Phase Liquid Permeability vs Calculated Klinkenberg Permeability . . .	C-79
Table B1.	Index of CT Images for E1X08	C-98

List of Figures

Figure 1.	As-received MB139 Core E1X07	C-12
Figure 2.	As-received MB139 Core E1X08	C-13
Figure 3.	Representative cross-sectional images of E1X08-3.	C-15
Figure 4.	Representative cross-sectional images of E1X08-4.	C-16
Figure 5.	Representative cross-sectional images of E1X08-5.	C-17
Figure 6.	Representative cross-sectional images of E1X08-6.	C-18
Figure 7a.	Longitudinal reconstruction of E1X08-4 (3.55-4.13 feet).	C-19
Figure 7b.	Longitudinal reconstruction of E1X08-4 (4.14-4.72 feet).	C-20
Figure 7c.	Longitudinal reconstruction of E1X08-4 (4.73-5.33 feet).	C-21
Figure 7d.	Longitudinal reconstruction of E1X08-4 (5.34-5.94 feet).	C-22
Figure 8.	Examples of coring-induced damage as evidenced by CT cross-sectional images in tuff cores from the tunnel beds in Rainer Mesa, Nevada Test Site. (Images furnished with permission of Dr. B.L. Ristvet, Defense Nuclear Agency).	C-24
Figure 9.	CT cross-sectional images from E1X08-4 showing linear features of comparatively low density. Such features, possibly pre-existing healed fractures, were very rare in the E1X08 images.	C-25
Figure 10a.	Raw image from E1X08-5 (salt) acquired with a third-generation Philips 60/TX CT scanner. Beam-hardening, as evidenced by the bright ring on the sample perimeter, is present.	C-26
Figure 10b.	Image shown in Figure 10a following post-processing with CORESCAN™ to eliminate beam-hardening artifacts.	C-27
Figure 11a.	Raw image from E1X08-4 (anhydrite with mudrock) acquired with a third-generation Philips 60/TX CT scanner. Beam-hardening, as evidenced by the bright ring on the sample perimeter, is present.	C-28

Figure 11b.	Image shown in Figure 11a following post-processing with CORESCAN™ to eliminate beam-hardening artifacts.	C-29
Figure 12.	Experimental program.	C-31
Figure 13.	Documentation of sample preparation from core E1X08-4.	C-32
Figure 14.	Documentation of sample preparation from core E1X07-4.	C-33
Figure 15.	Schematic illustrating PX sample preparation. Thin sections were prepared parallel to O1-O3. O1 is horizontal (parallel to bedding) and O2 and O3 are vertical and mutually perpendicular. XRD analyses were conducted on half of the O2 split.	C-34
Figure 16.	Grain size histogram for PX1	C-41
Figure 17.	Grain size histogram for PX2	C-44
Figure 18.	Grain size histogram for PX3	C-47
Figure 19.	Grain size histogram for PX4	C-50
Figure 20.	Grain size histogram for PX5	C-53
Figure 21.	Grain size histogram for PX6	C-56
Figure A1a.	Documentation of thin section preparation from PX samples from core E1X08-4.	C-89
Figure A1b.	Documentation of thin section preparation from PX samples from core E1X07-4.	C-90
Figure A2.	Schematic of experimental system for gas permeability measurement.	C-94
Figure A3.	Schematic of experimental system for liquid permeability measurement.	C-95

1.0 Introduction

The Waste Isolation Pilot Plant (WIPP) is the U.S. Department of Energy's planned repository for transuranic waste generated by defense programs. The WIPP is located 660 m underground in the Salado Formation which consists of thick halite with interbeds of minerals such as clay and anhydrite. The polycrystalline Salado salt contains 0.1 to 1% brine in intragranular fluid inclusions and as an intergranular pore fluid. The anhydrite interbed layers are expected to contain similar quantities. Quantification of the amount of brine, and its mobility and flow rate are critical for accurate assessment of the long-term performance of the repository. Field tests indicate that the permeability of the Salado anhydrite interbeds is 1 to 2 orders of magnitude greater than that of the halite intervals and sensitivity analyses show that the anhydrite beds would be the favored path for fluid flow [1].

The effort described here focused on characterization of the anhydrite bed known as Marker Bed 139 (MB139) which occurs beneath the planned waste-storage rooms. Laboratory investigations were performed on two cores from MB139 to (1) characterize the lithology and mineralogy; (2) determine total and effective porosity; (3) measure maximum achievable liquid saturation; (3) determine single-phase (both gas and liquid) permeability under varying stress conditions; and (4) explore the use of X-ray computerized axial tomography (CT) for identification and characterization of natural and coring-induced fractures and for tracking fluid flow through cores.

2.0 Core Receipt and Inspection

Two core samples identified as E1X07 and E1X08 were received at TerraTek on November 23, 1992. The core containers were photographed immediately upon receipt and opened for examination on November 25, 1992. The core pieces were sheathed individually in saran wrap, packed in bubble wrap, and sealed in 8" diameter PVC tubes. The first tube contained three 5½" diameter cores with identification and length as follows: E1X07-3 (3'8" to 4'); E1X07-4 (4' to 6'2"); and E1X07-5 (6'2" to 7'5"). The second tube contained four 5½" diameter cores with identification and length as follows: E1X08-3 (2'8" to 3'6"); E1X08-4 (3'6" to 6'); E1X08-5 (6' to 6'4"); and E1X08-6 (6'4" to 7'4½"). Photographs were taken to document conditions during each stage of unwrapping and the cores were noted to be in good condition (Figures 1 and 2).

Bedding was approximately perpendicular to the core axis. Significant lithologic discontinuities were apparent at each of the break points (Figures 1 and 2). Both the upper and lower core pieces from E1X07 and E1X08 (E1X07-3 and E1X07-5; E1X08-3 and E1X08-6) were identified as halite and thus not considered to be part of the marker bed. The lower portion of the marker bed in both cores (-5.8 to 6.2 feet for E1X07; -6.0 to 6.3 feet for E1X08) was identified as mudrock. The remaining material was identified as anhydrite mixed with mudrock. Core E1X08 was separated into two pieces (identified as E1X08-4 and E1X08-5) at the interface between the mixed anhydrite/mudrock and mudrock zones. Core E1X07 contained no throughgoing fissure at this lithologic discontinuity; however, some partial separation along the bedding plane was apparent along a portion of the circumference (Figure 1).

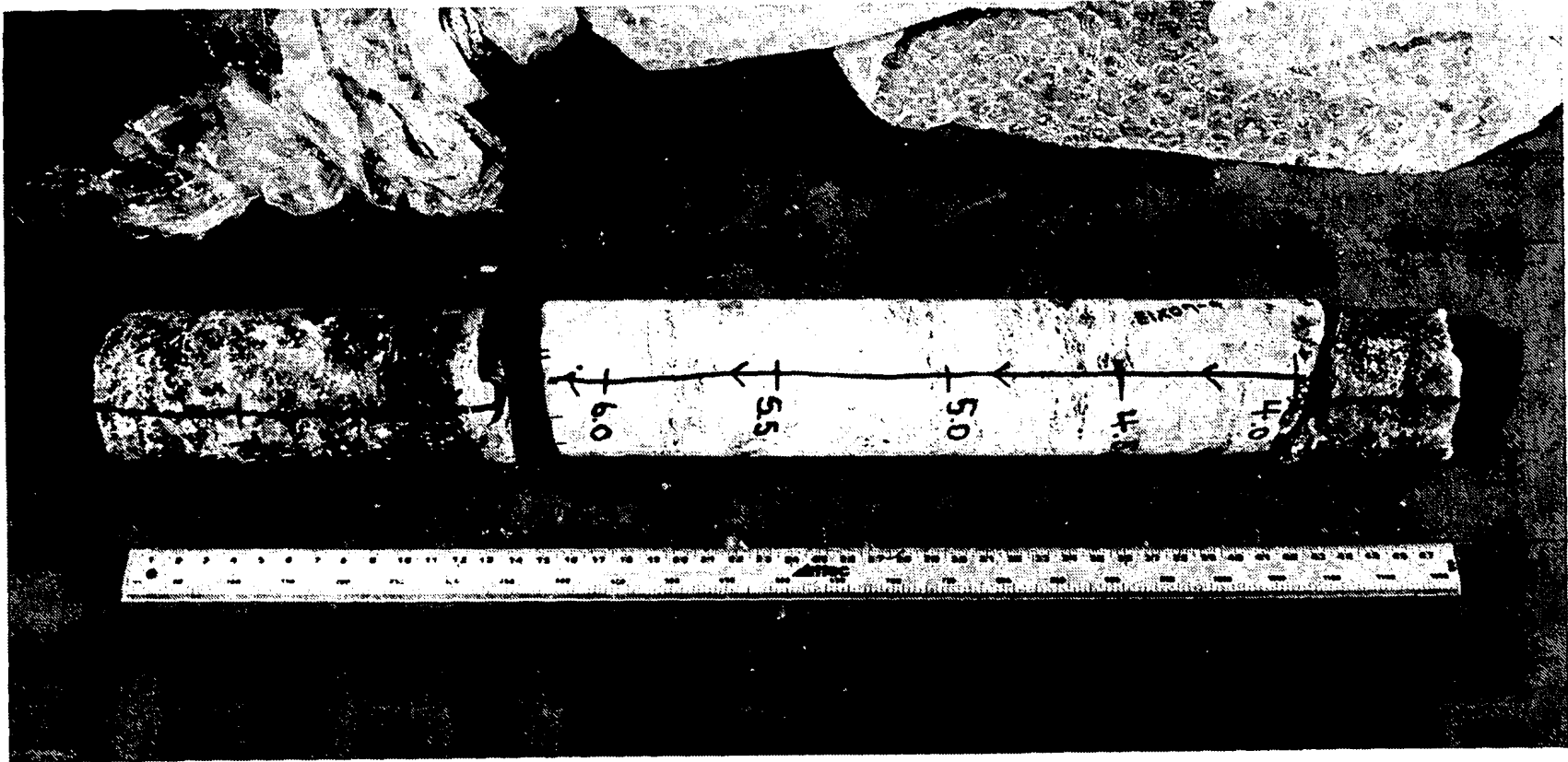


Figure 1. As-received MB 139 Core E1X07.

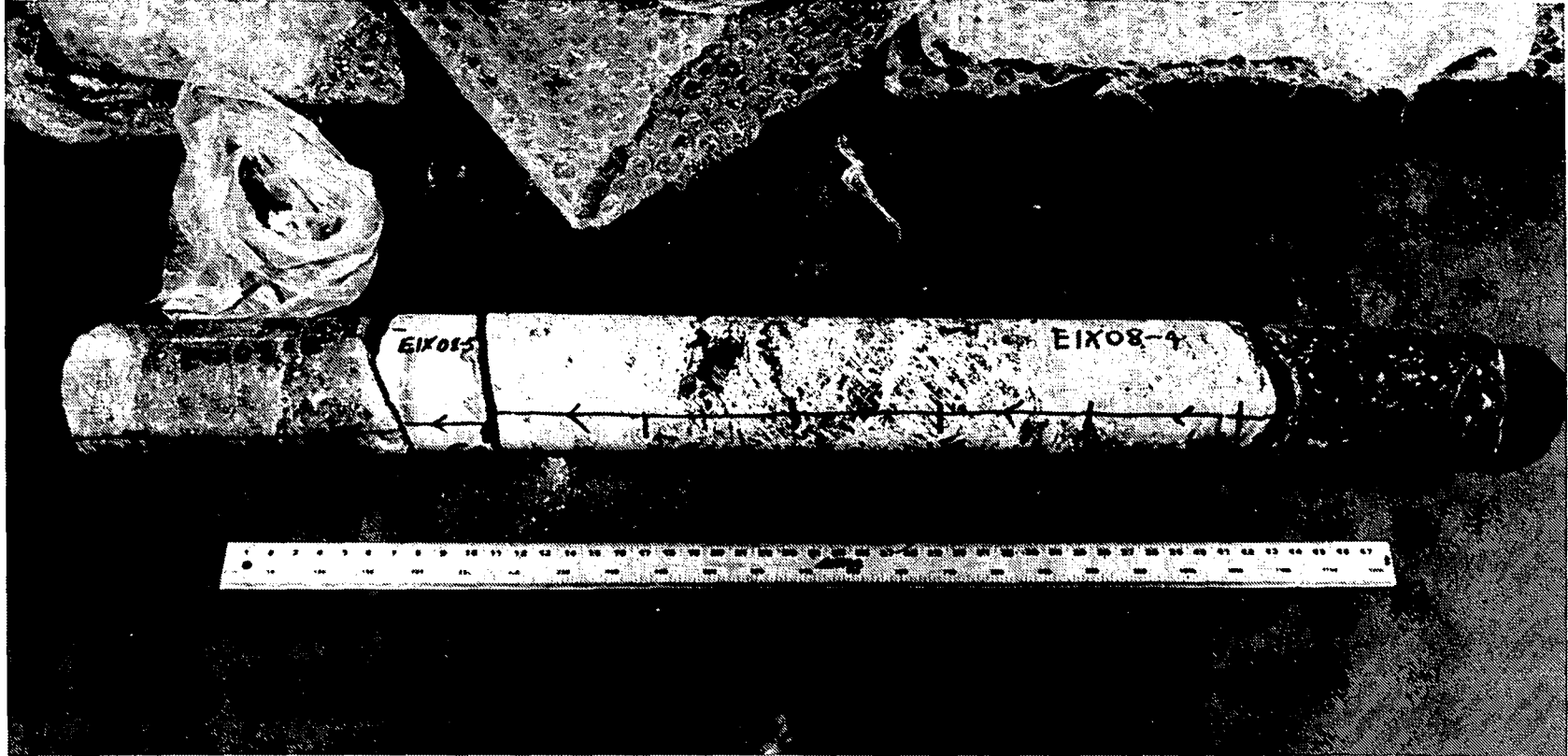


Figure 2. As-received MB 139 Core EIX08.

3.0 X-Ray CT Non-Destructive Core Analysis

3.1 Application of a Second Generation CT Scanner

A whole core x-ray computerized tomography (CT) scan was performed on core E1X08 in its as-received condition to investigate the applicability of CT for the identification of natural and coring-induced fractures. The four core pieces (E1X08-3, E1X08-4, E1X08-5, E1X08-6; previously identified as halite, anhydrite with mudrock, mudrock, and halite, respectively) were scanned continuously in TerraTek's Second Generation CT Facility using a beam width of 3 mm and energy of 120 KV (see Appendix A for facility description and operating procedures).

Representative cross-sectional images from each of the core pieces are shown in Figures 3-6 (see Appendix B for an index of cross-sectional images with respect to depth). A vertical reconstruction through core E1X08-4, which traverses the bulk of MB139, is shown in Figure 7. The images from the two cores identified as halite (E1X08-3 and E1X08-6) are of acceptable quality (Figures 3 and 6); however, the images from cores E1X08-4 and E1X08-5 contain severe beam-hardening artifacts (Figures 4 and 5), as evidenced by apparent concentric increases in density.

"Beam hardening" is a term used to describe the selective filtration of the lower energy component of the x-ray beam which occurs as the beam penetrates the sample. Beam-hardening causes the effective energy of the x-ray beam to increase as the beam penetrates the sample; this leads to an artificially high CT number on the sample circumference, which implies an artificially high density. Beam-hardening is a well known characteristic of all x-ray CT scanners since they employ polychromatic x-ray sources [2-5]; however, its effect is usually small for standard geologic cores (i.e., NX- or HQ- size) with low-to-medium densities (i.e., oil/gas reservoir rock).

In second-generation CT scanners such as TerraTek's Ohio Nuclear DeltaScan 100, beam-hardening corrections may be performed using either (1) single energy pre-reconstruction corrections or (2) by "pre-filtering" the x-ray beam to absorb the low-energy portion prior to penetration of the sample [6]. TerraTek's CT facility employs the first technique. A fused quartz sample with a nominal diameter of four inches and density of 2.20 g/cc is scanned and an algorithm which is part of the DeltaScan 100's programming is used to calculate non-linear coefficients which are later used in the DeltaScan's reconstruction algorithm to perform beam-hardening corrections during scanning of the test specimen.

The severe beam hardening which occurred during CT scanning of Core E1X08 was apparently caused by (1) the very large diameter of the core (6 inch); and (2) the relatively high density of the material ($\rho_{\text{anhydrite}} = 2.9\text{-}3.0 \text{ g/cc}$). The standard beam-hardening correction procedure was therefore inadequate. Attempts to "pre-filter" the x-ray beam by either encasing the core in a hollow aluminum tube (with a nominal wall thickness of $\frac{1}{8}$ inch) or by placing thin aluminum shields (nominally $\frac{3}{8}$ inch) over the x-ray source did not yield significant improvements. Generation of the non-linear coefficients by scanning a 5 inch diameter aluminum sample with a density of 2.70 g/cc also did not yield significant improvements.

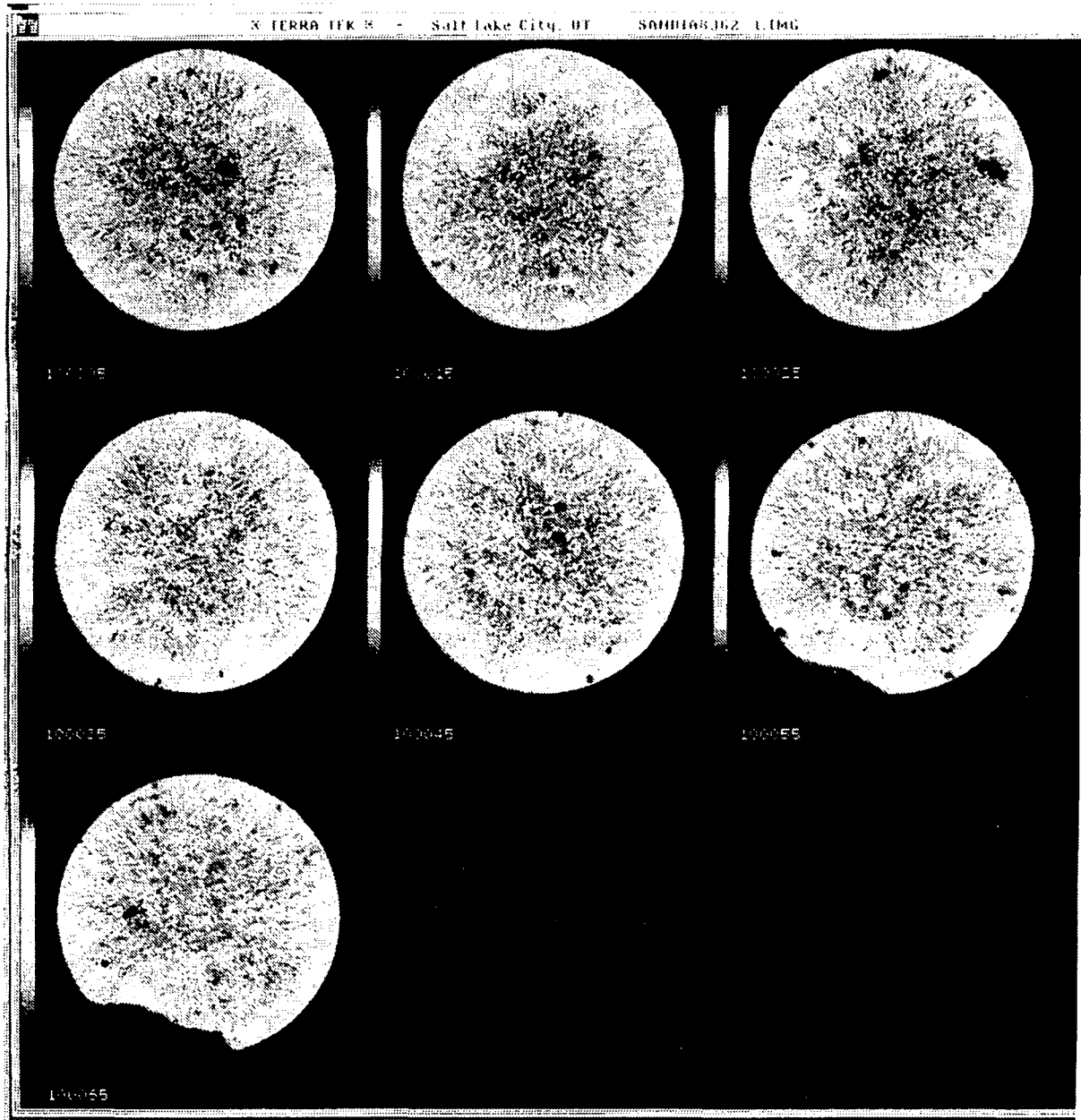


Figure 3. Representative cross-sectional images of EIX08-3.

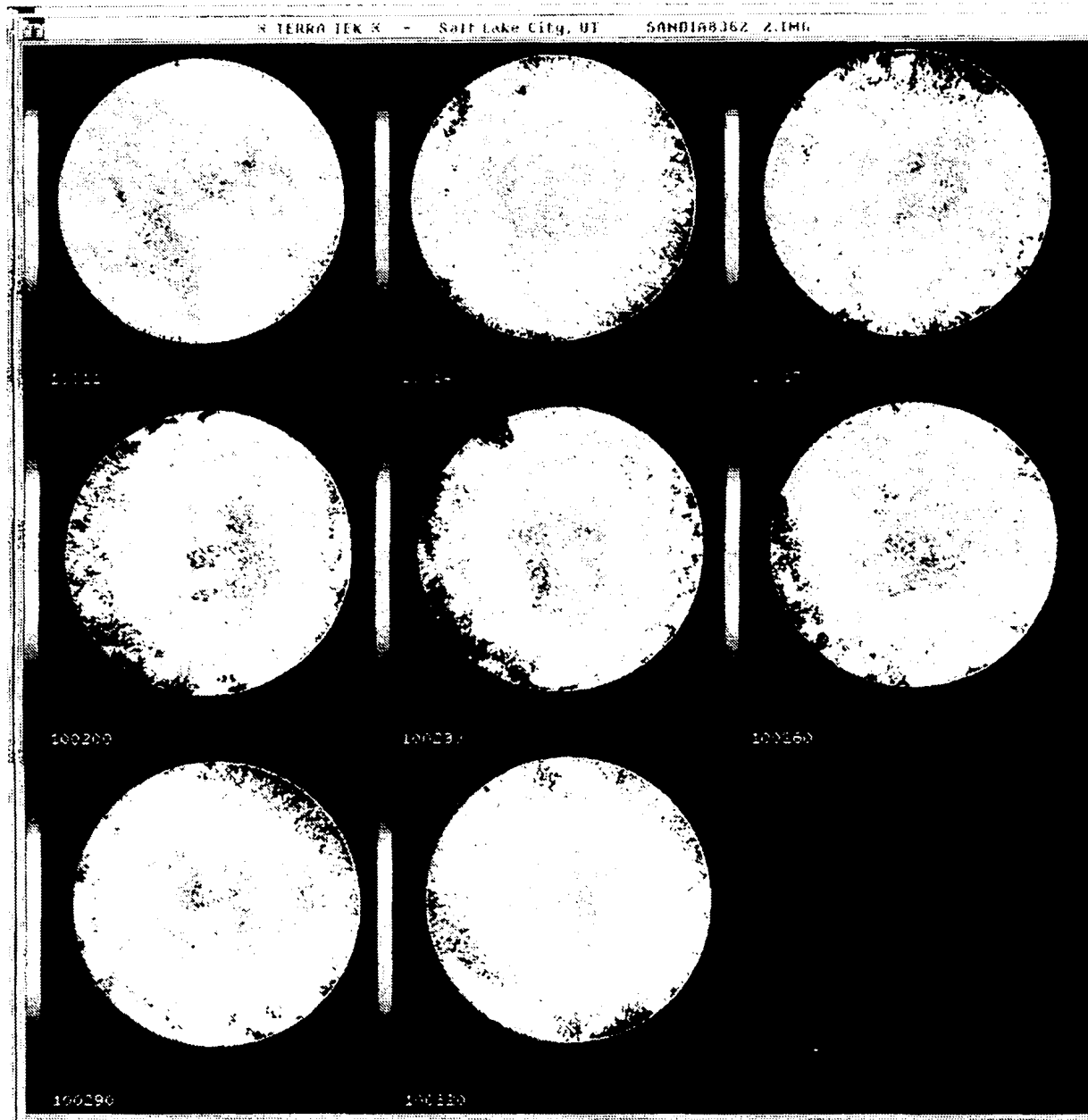


Figure 4. Representative cross-sectional images of E1X08-4.

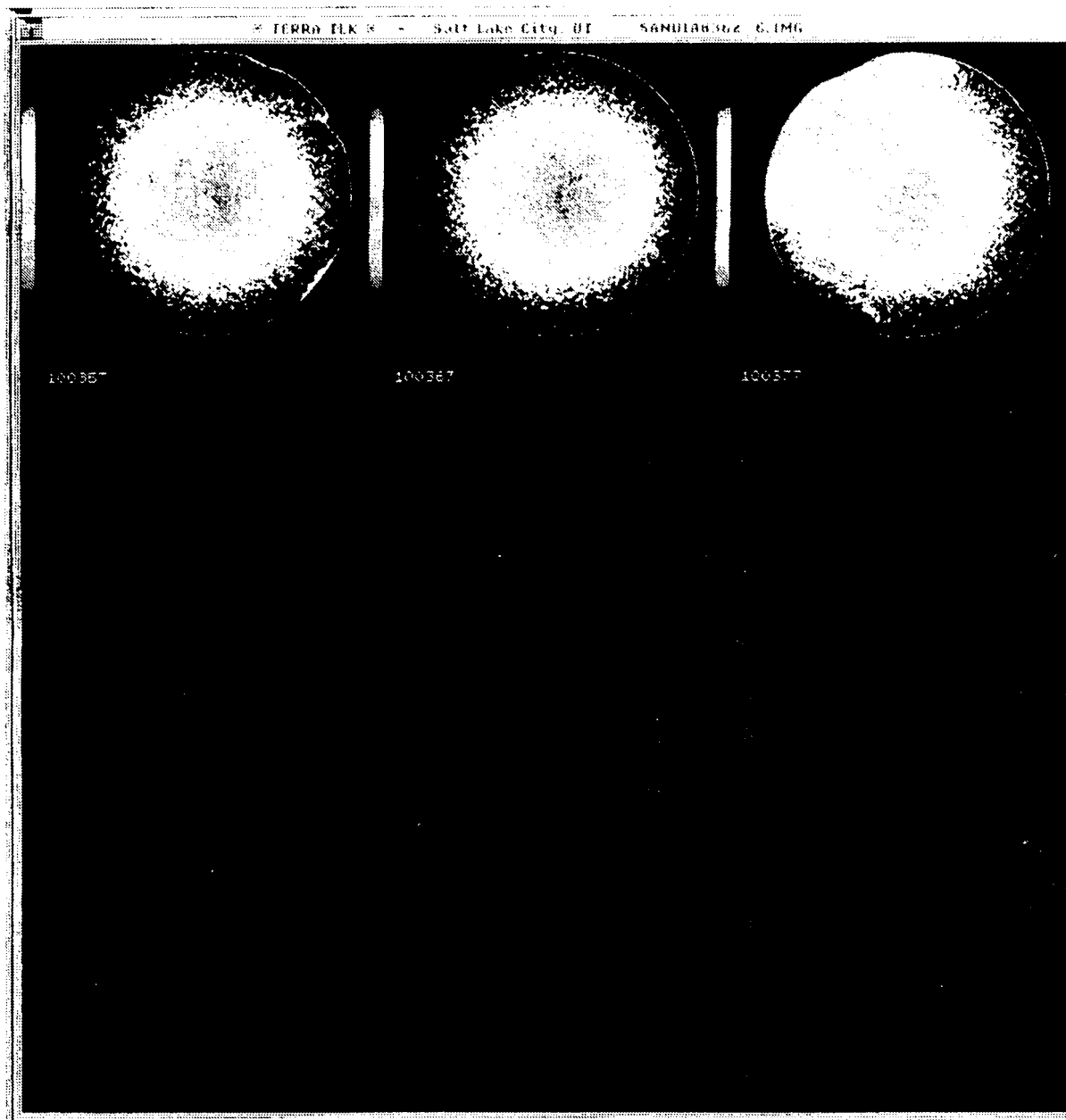


Figure 5. Representative cross-sectional images of E1X08-5.

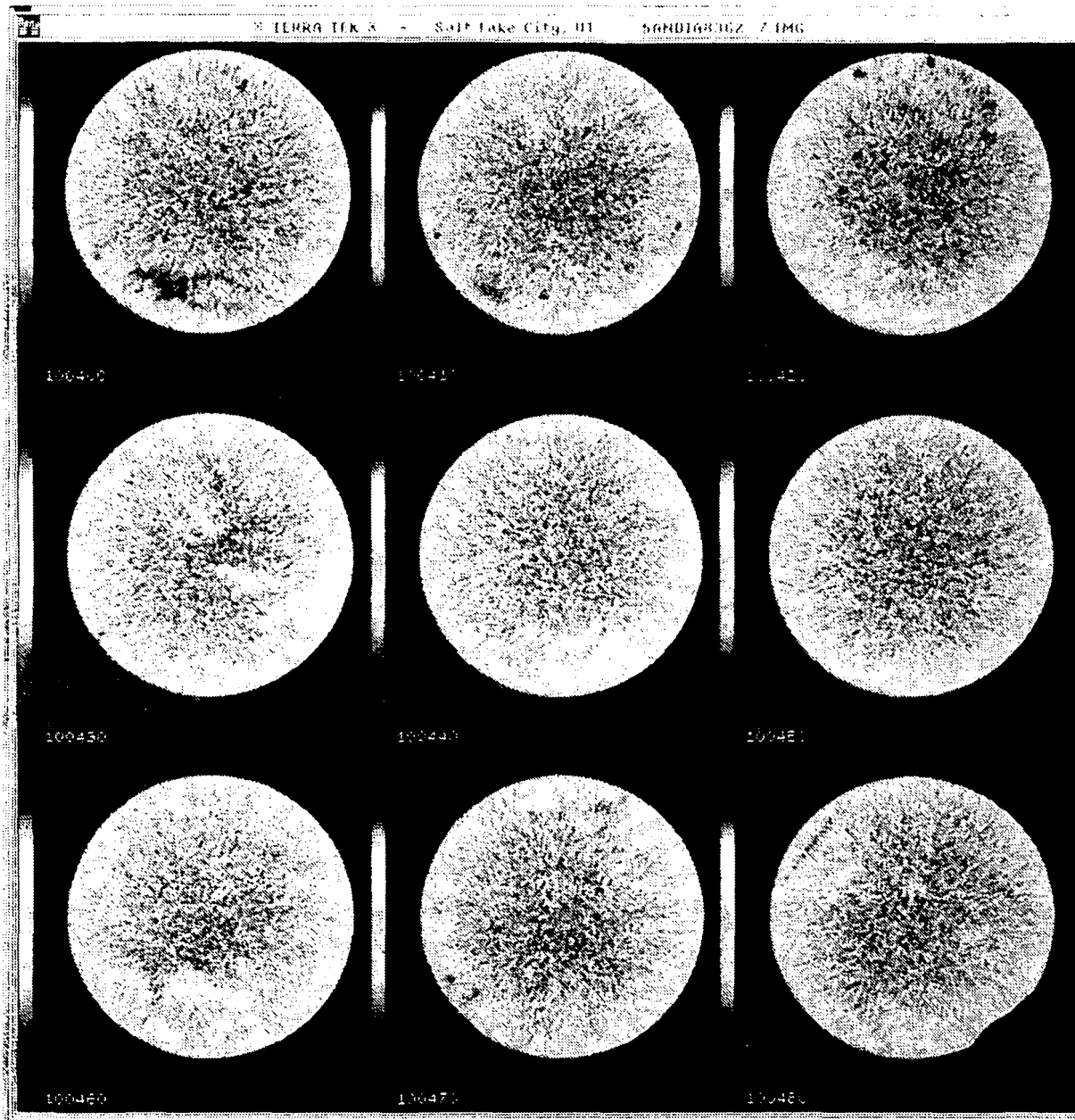


Figure 6. Representative cross-sectional images of E1X08-6.

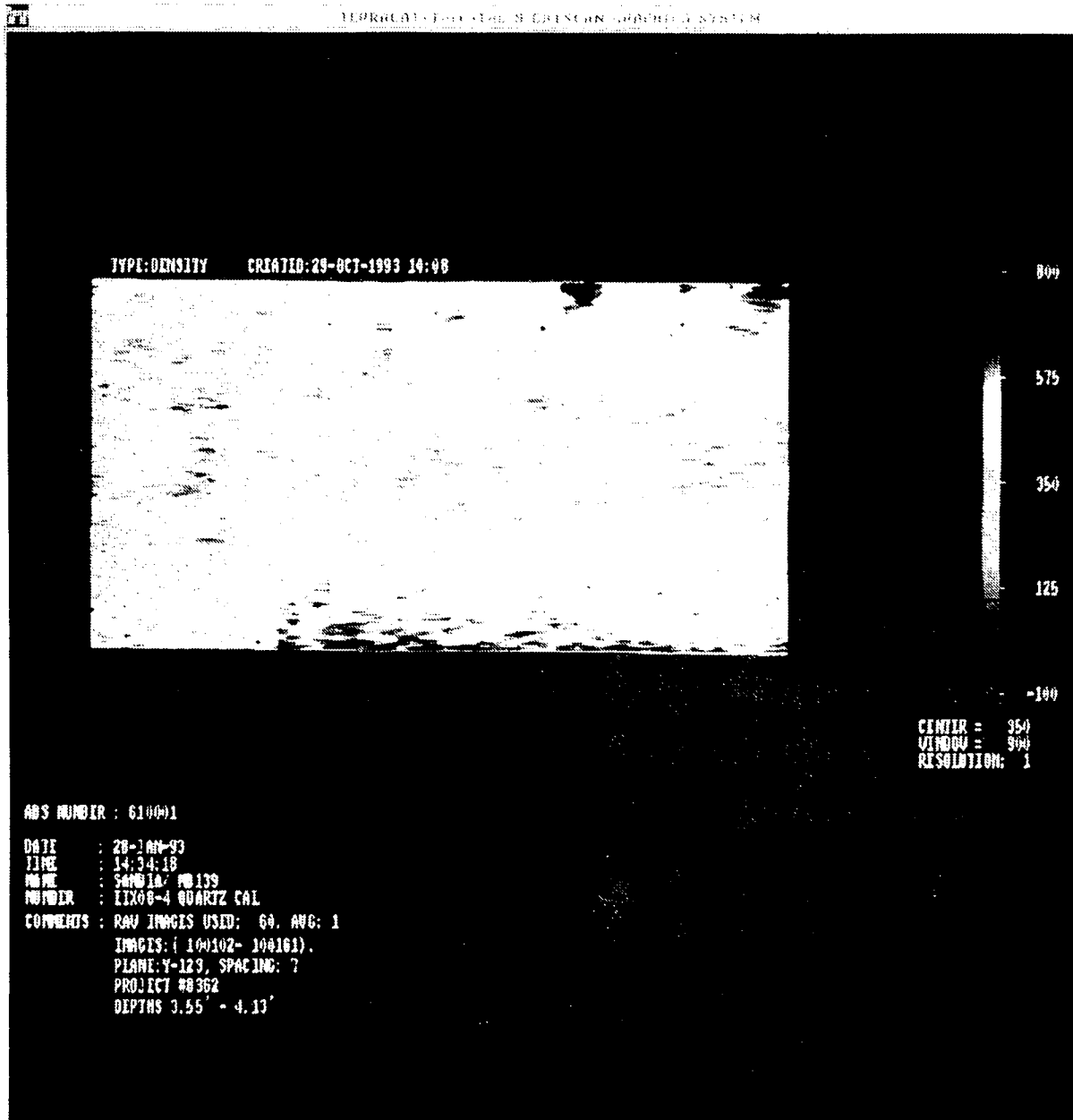


Figure 7a. Longitudinal reconstruction of E1X08-4 (3.55-4.13 feet).

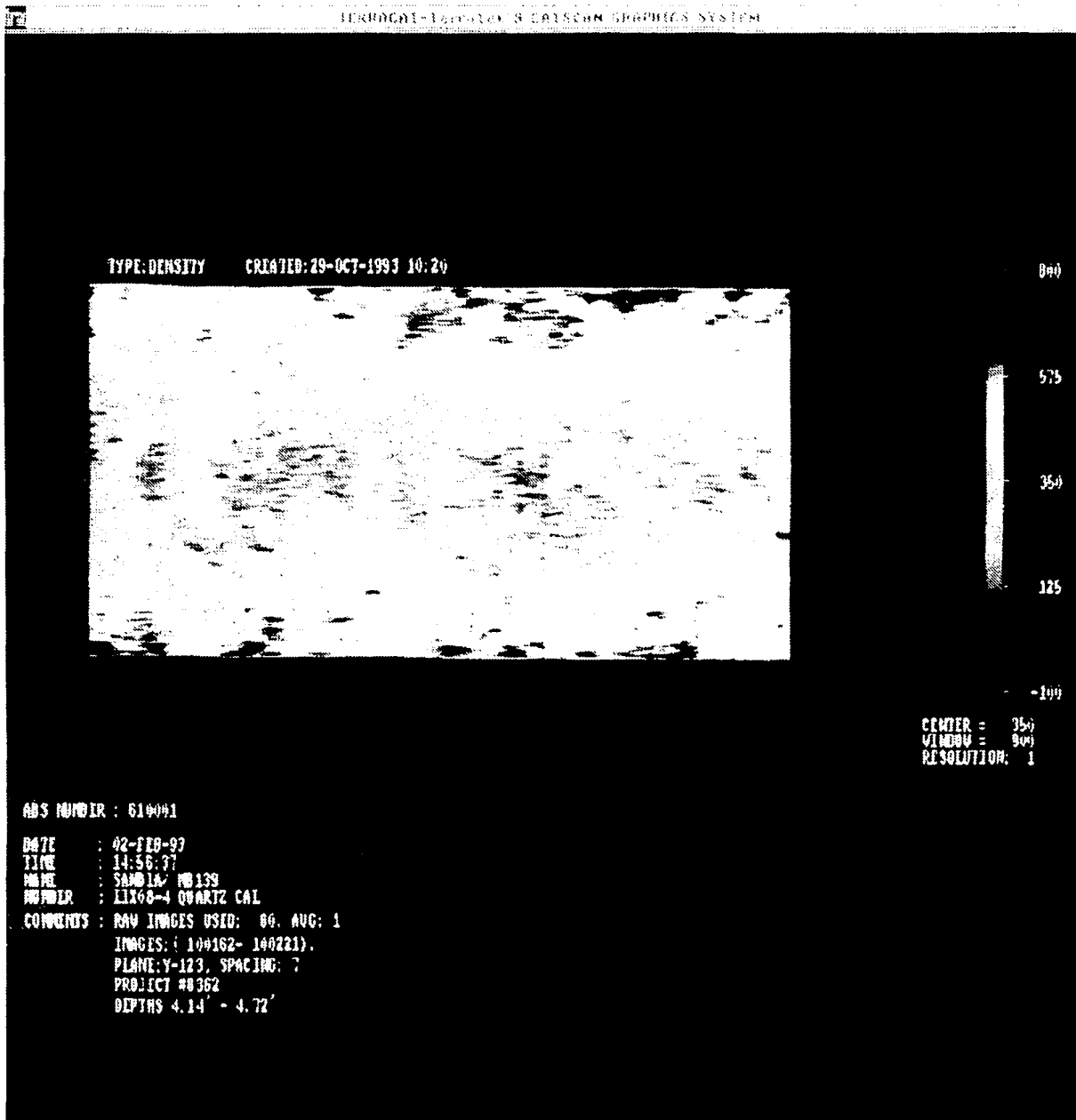


Figure 7b. Longitudinal reconstruction of EIX08-4 (4.14-4.72 feet).



Figure 7c. Longitudinal reconstruction of EIX08-4 (4.73-5.33 feet).

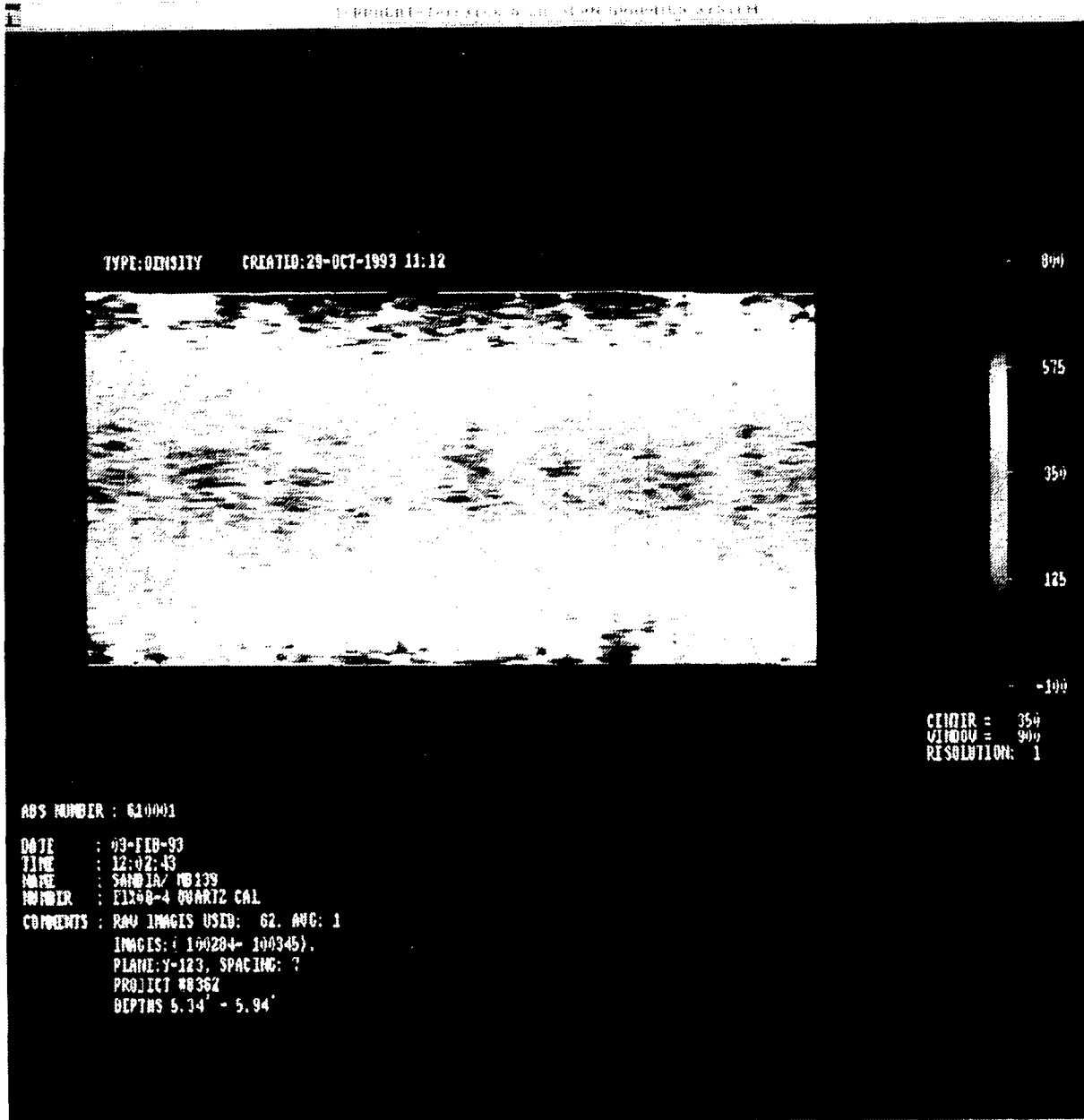


Figure 7d. Longitudinal reconstruction of EIX08-4 (5.34-5.94 feet).

A number of observations may nevertheless be made. First, there is no evidence for substantial coring-induced damage (in the form of circumferential fractures around the core perimeter) in core E1X08 (Figures 3-7). Figure 8 shows several examples where CT scans have successfully identified coring-induced damage in HQ-sized (2¼ inch diameter) core from the tunnel beds in Rainer Mesa, Nevada Test Site (images furnished with permission of Dr. B.L. Ristvet, Defense Nuclear Agency). Furthermore, the occasional chips which occur along the core axis of E1X08 do not appear to be marked by damage zones extending into the intact core. (Note that sample E1X08-5 (6.0 to 6.4 ft), which is classified as mudrock, ultimately fractured into several pieces during handling. The sample broke along what was possibly either a pre-existing healed fracture or bedding plane which may have been unduly stressed during either coring, shipping, and/or handling.) Second, the two whole-core pieces identified as halite, E1X08-3 (2.7 to 3.5 ft) and E1X08-6 (6.3 to 7.4 ft) appear to be very homogeneous both laterally and vertically (Figures 3 and 6). These two core pieces appear to be of substantially lower density than either E1X08-4 (anhydrite/mudrock) and E1X08-5 (mudrock). Third, core piece E1X08-5 (6.0 to 6.4 ft), classified as mudrock, appears to be the densest portion of core E1X08 overall (Figure 5). Images from this core exhibit the grossest beam-hardening. This core piece appears to be remarkably homogeneous both laterally and vertically in the upper section; however, the lower interval exhibits substantial lateral and vertical heterogeneity. Finally, core piece E1X08-4 (3.6 to 6.0 ft) exhibits substantial lateral and cross-sectional heterogeneity across the entire core length (Figure 7). The 5.5 to 6.0 ft interval appears to be highest, and the 3.6 to 3.7 ft interval lowest, in overall density. Narrow linear features of comparatively low density which appear in a few images at both the top and bottom of the core (Figure 9) may be healed fractures.

3.2 Exploratory Application of a Third Generation CT Scanner

Midway through the contract performance period, TerraTek acquired a more advanced third generation Philips 60/TX CT scanner. Advantages of the Philips scanner include a higher maximum operating voltage (140 KV vs 120 KV for the DeltaScan 100) and current (250 mA versus 25 mA for the DeltaScan 100) for the x-ray tube. TerraTek at this time also completed development of a new software package which includes a capability to perform automatic numerical correction for beam-hardening artifacts. Several scans were performed through intact pieces of cores E1X08-5 (halite) and E1X08-4 (anhydrite mixed with mudrock) to investigate whether the more powerful scanner would yield high quality images of very large, dense samples such as the MB139 cores.

The raw images from E1X08-5 and E1X08-4 are shown in Figures 10a and 11a, and the images following processing with CORESCAN™ to correct for beam-hardening are shown in Figures 10b and 11b. The images obtained with the Philips 60/TX scanner are excellent, and many details such as scattered low density inclusions and occasional pockets of a higher density mineral are visible in the halite core (Figure 10b). Similarly, the images from the E1X08-4 (Figure 11b) suggest two dominant mineral phases, possibly anhydrite and halite.

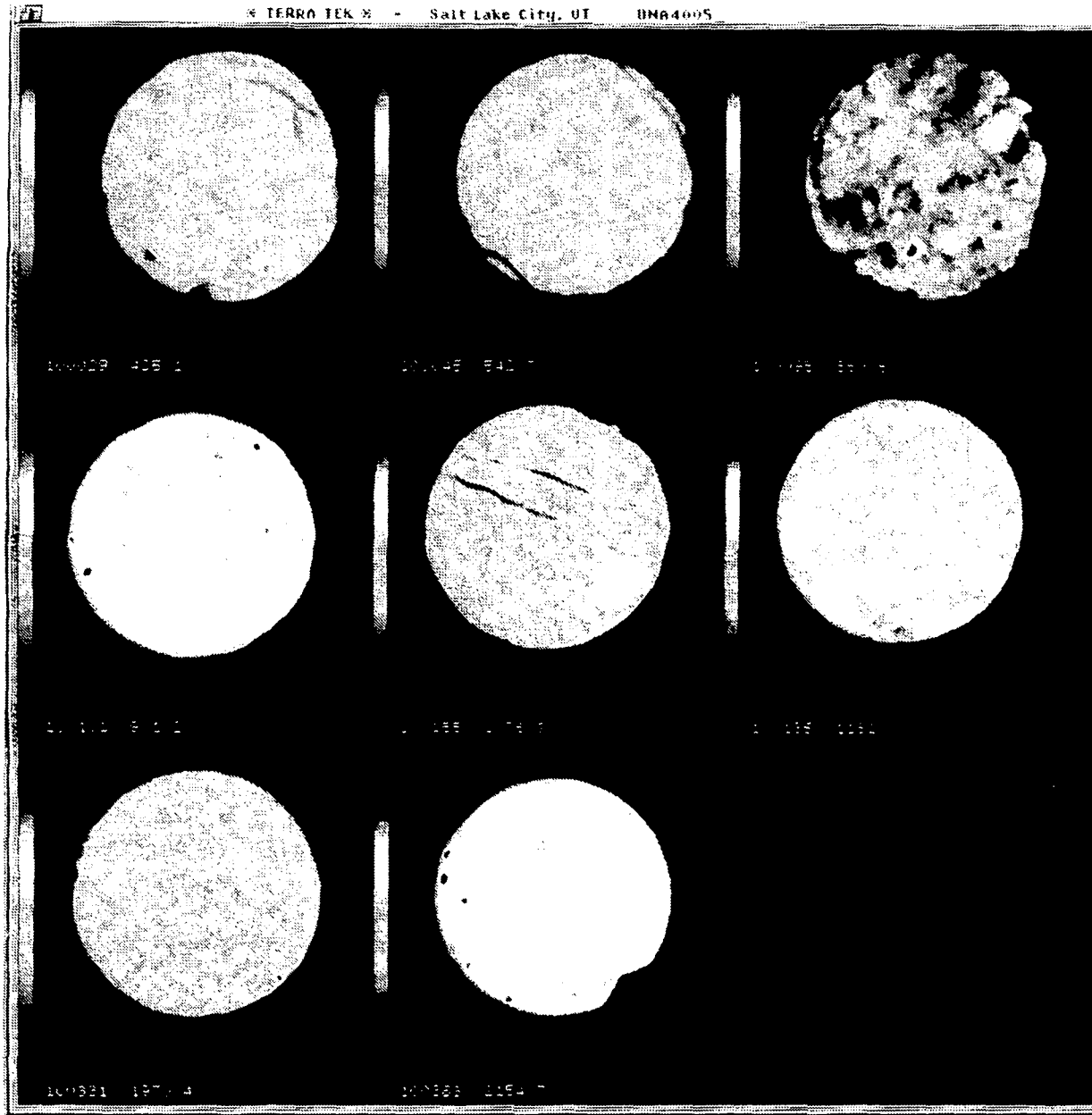


Figure 8. Examples of coring-induced damage as evidenced by CT cross-sectional images in tuff cores from the tunnel beds in Rainer Mesa, Nevada Test Site. (Images furnished with permission of Dr. B.L. Ristvet, Defense Nuclear Agency).

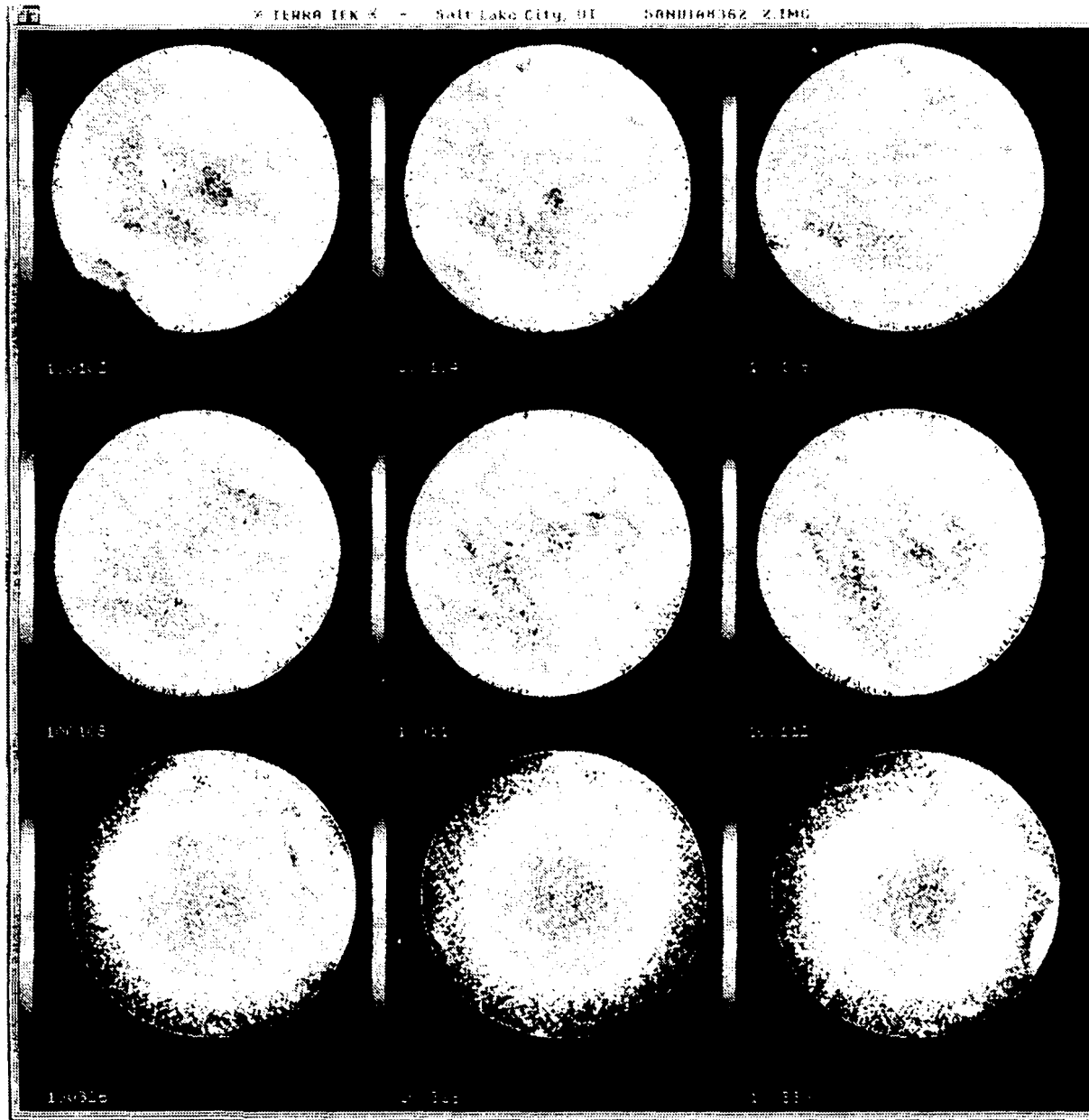


Figure 9. CT cross-sectional images from E1X08-4 showing linear features of comparatively low density. Such features, possibly pre-existing healed fractures, were very rare in the E1X08 images.

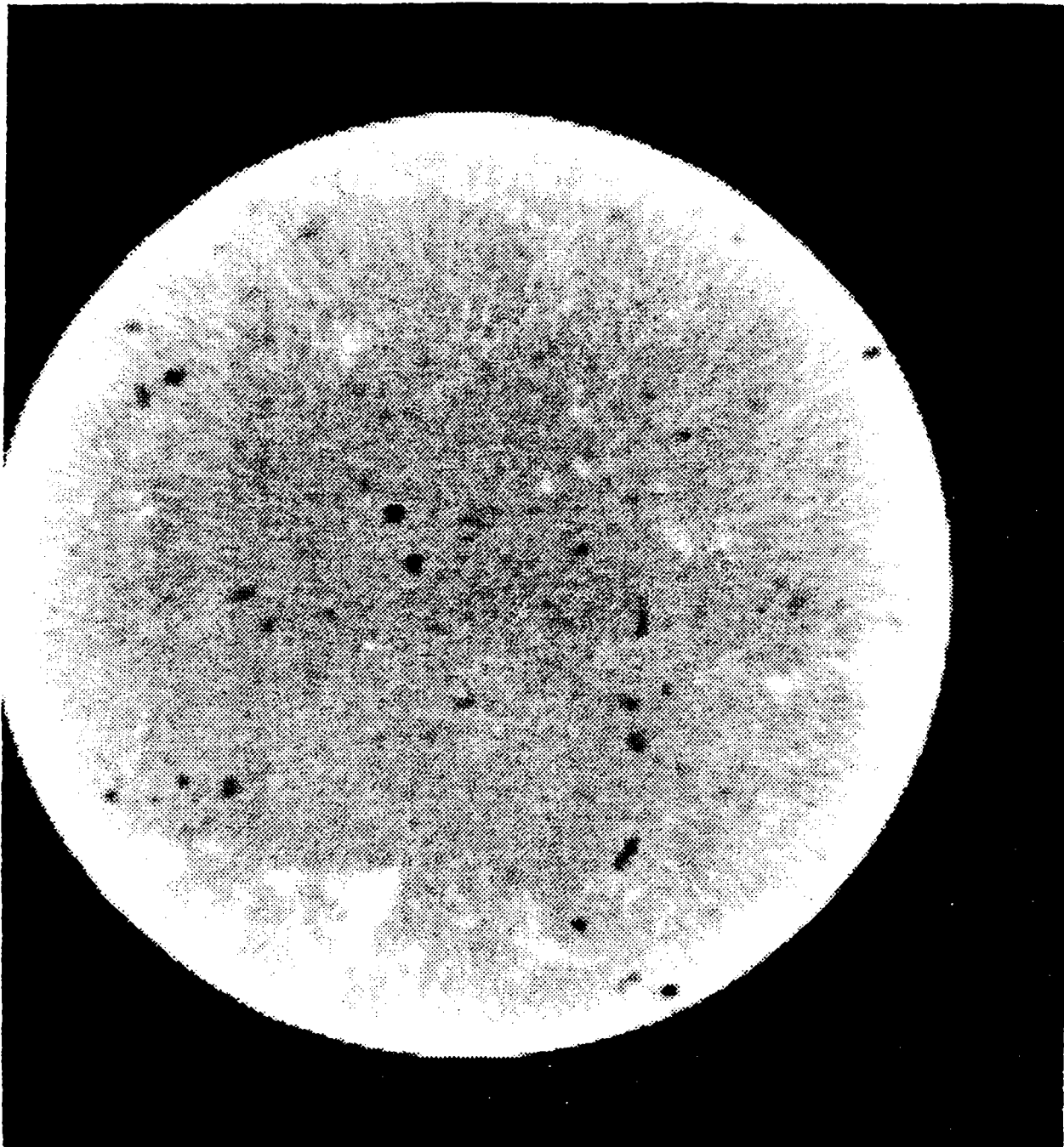


Figure 10a. Raw image from E1X08-5 (halite) acquired with a third-generation Philips 60/TX CT scanner. Beam-hardening, as evidenced by the bright ring on the sample perimeter, is present.

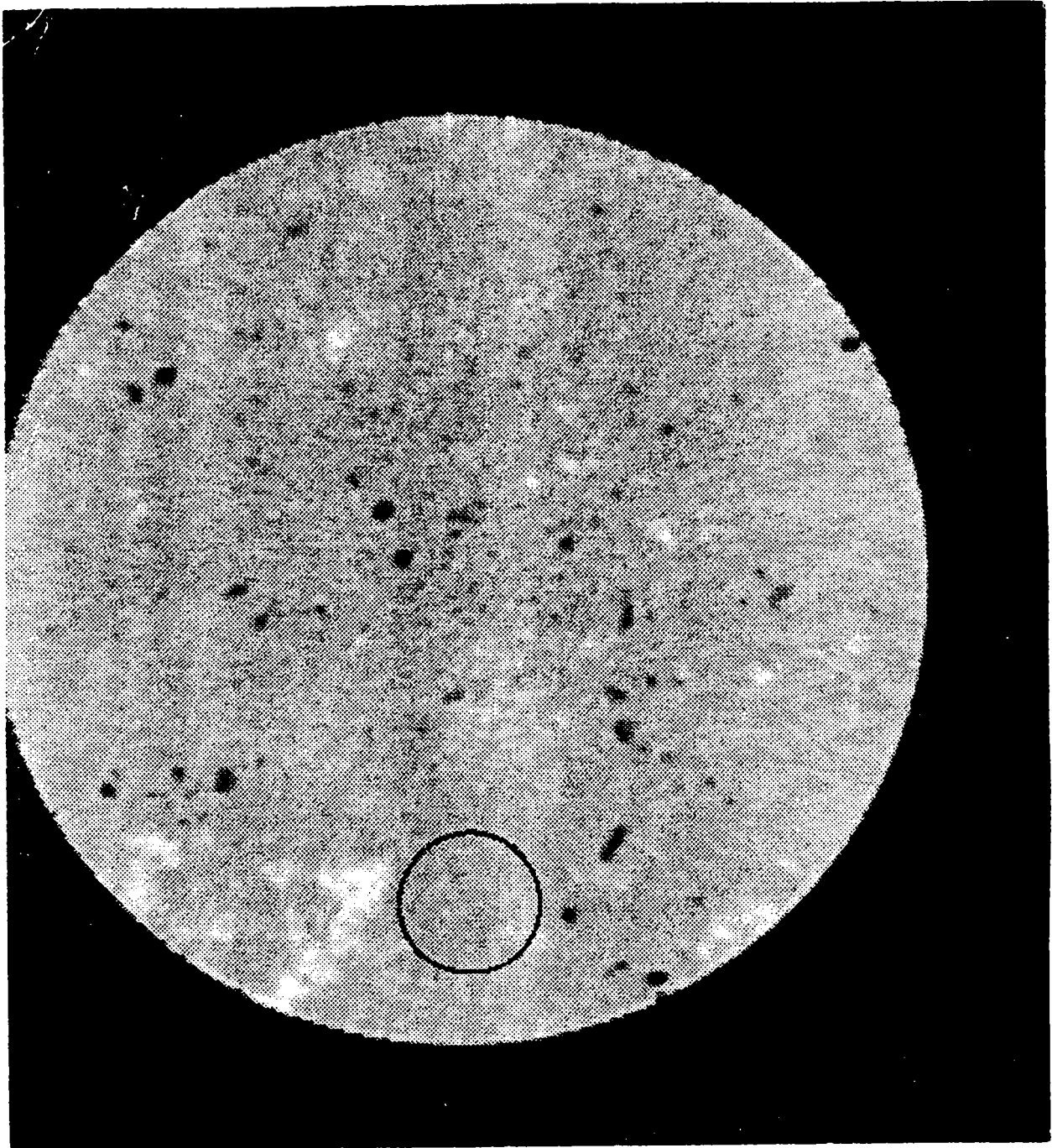


Figure 10b. Image shown in Figure 10a following post-processing with CORESCAN™ to eliminate beam-hardening artifacts.

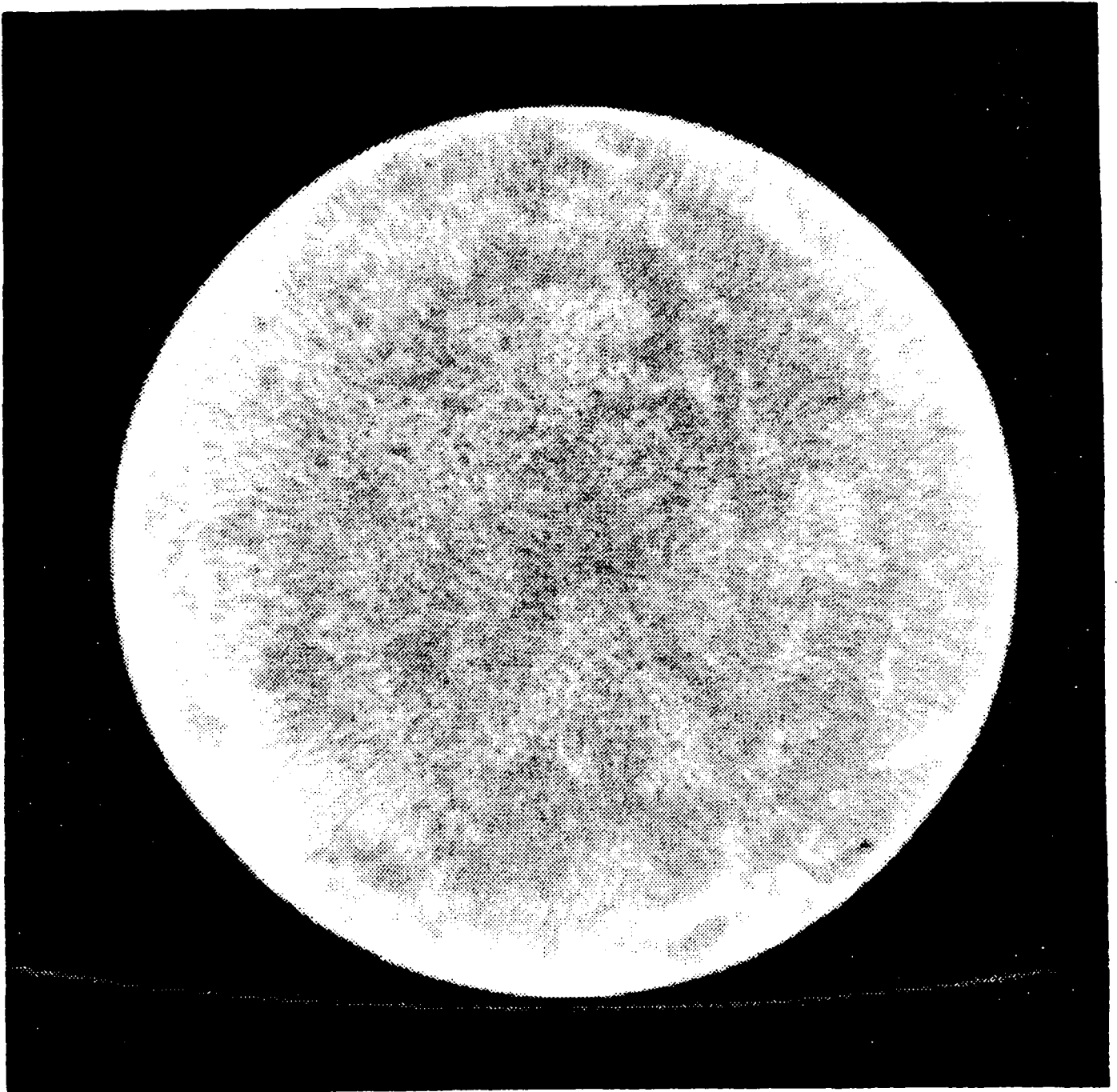


Figure 11a. Raw image from E1X08-4 (anhydrite with mudrock) acquired with a third-generation Philips 60/TX CT scanner. Beam-hardening, as evidenced by the bright ring on the sample perimeter, is present.

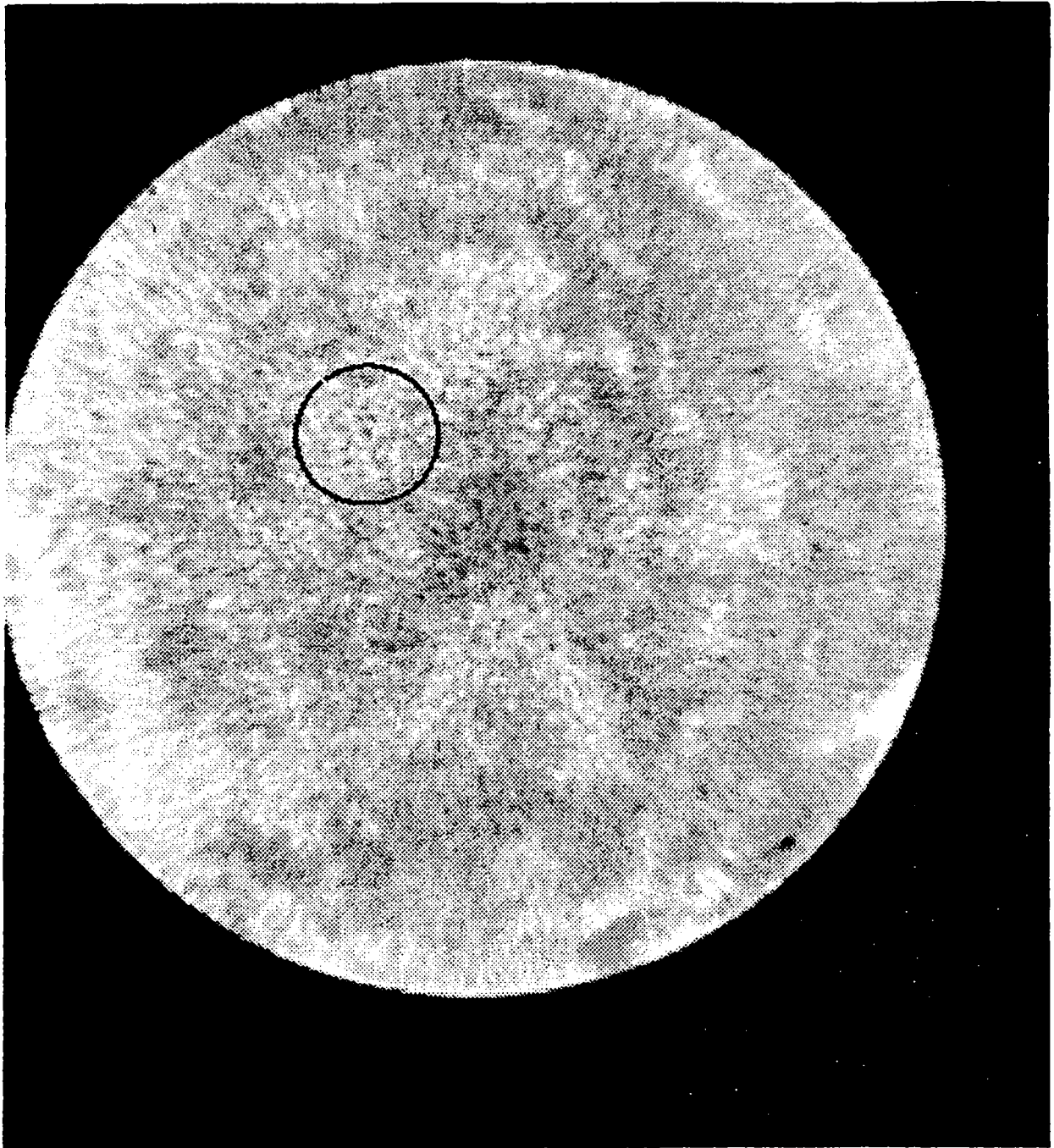


Figure 11b. Image shown in Figure 11a following post-processing with CORESCAN™ to eliminate beam-hardening artifacts.

4.0 Sample Preparation

Sample preparation focused on core intervals E1X07-4 and E1X08-4. MB139 was considered to include core interval E1X08-5; however, this section was too small for complete characterization. A total of six four-inch diameter samples (hereafter referred to as A-F) and fourteen two-inch diameter samples (hereafter referred to as EP1-8 and PX1-6) were diamond-cored from E1X08-4 and E1X07-4 in an orientation perpendicular to the original core axis. The samples were located such that complete characterization would be performed on three separate intervals of each of the MB139 cores. The experimental program is detailed in Figure 12. The identification of each sample is documented in Figures 13 and 14 and cataloged in Table 1.

Table 1. Sample Identification

Sample	Core	Depth (feet)
A	E1X08	3.63-4.00
B	E1X08	4.47-4.84
C	E1X08	5.34-5.71
D	E1X07	4.14-4.50
E	E1X07	4.64-5.00
F	E1X07	5.19-5.56
EP1	E1X08	3.50-3.63
EP2	E1X08	4.33-4.47
EP3	E1X08	5.05-5.19
EP4	E1X08	5.85-6.00
EP5	E1X07	4.00-4.14
EP6	E1X07	4.50-4.64
EP7	E1X07	5.00-5.14
EP8	E1X07	5.59-5.73
PX1	E1X08	4.00-4.14
PX2	E1X08	4.86-5.00
PX3	E1X08	5.71-5.85
PX4	E1X07	4.00-4.14
PX5	E1X07	5.00-5.14
PX6	E1X07	5.73-5.87

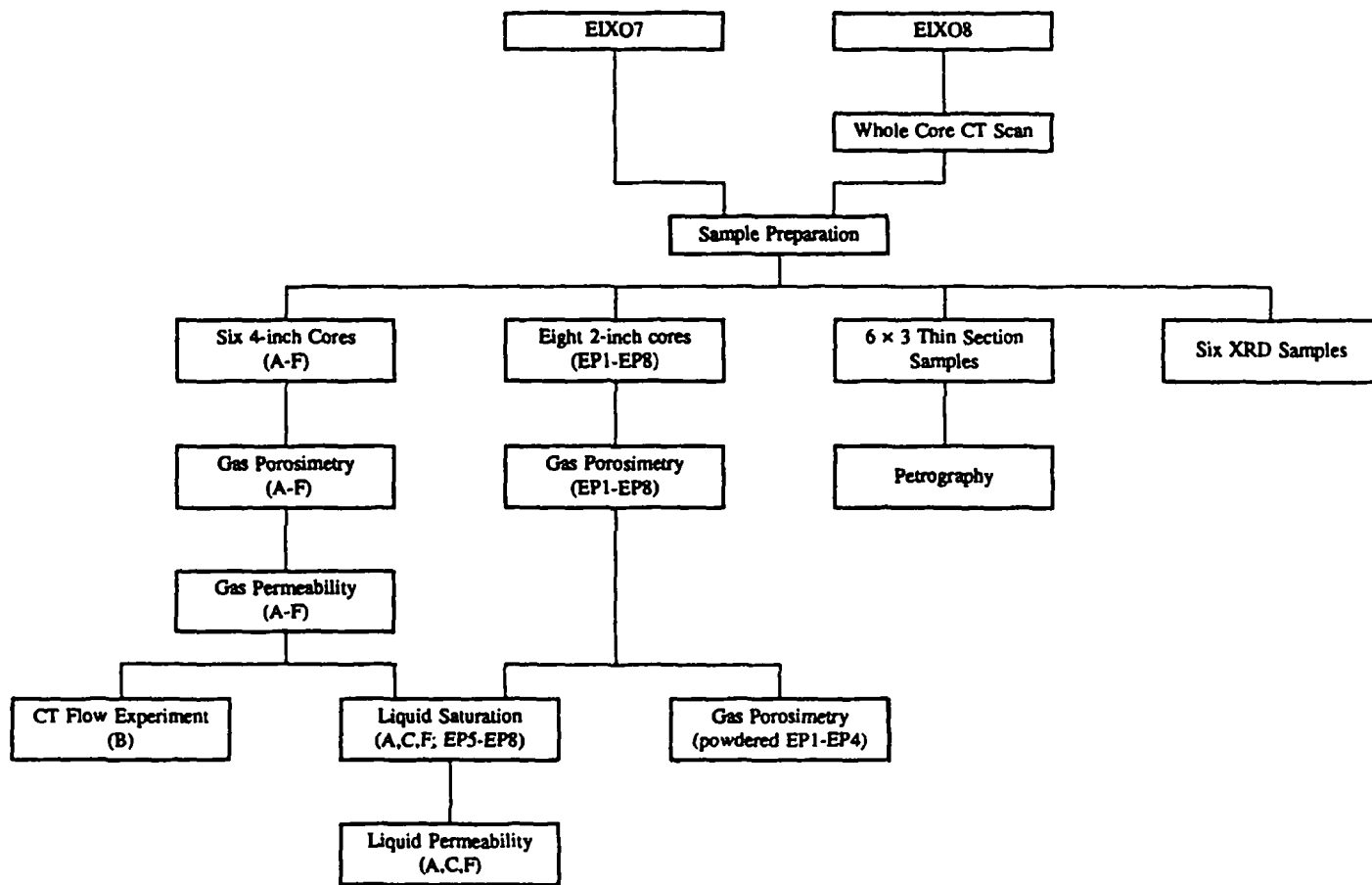


Figure 12. Experimental program.

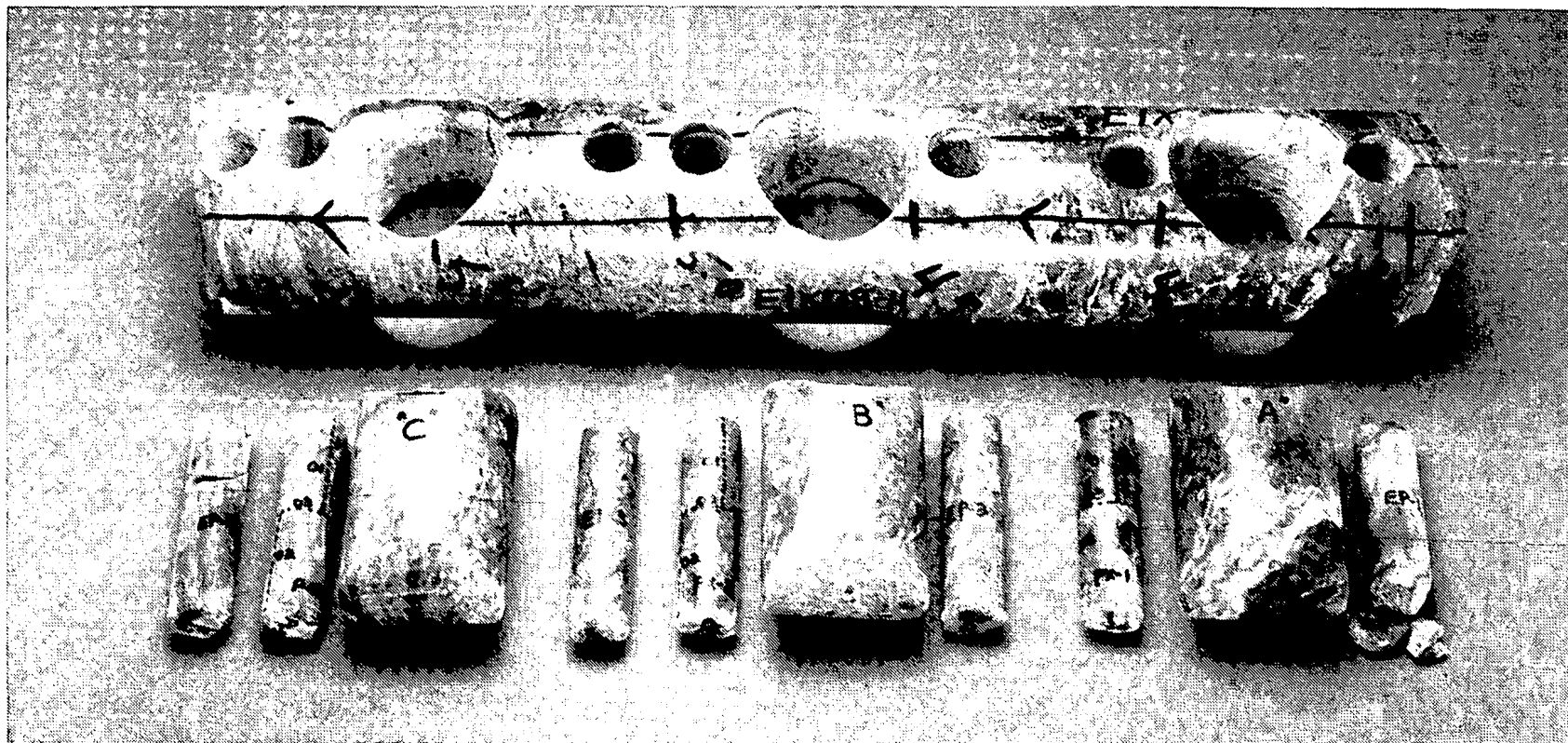


Figure 13. Documentation of sample preparation from core E1X08-4.



Figure 14. Documentation of sample preparation from core E1X07-4.

The ends of the six four-inch samples were cut with a diamond saw and endground flat and parallel. The ends of eight of the two-inch samples (EP1-8) were cut approximately perpendicular to the core axis with a diamond saw. The remaining six two-inch cores (PX1-6) were cut with a diamond saw into several pieces for petrographic study and X-Ray Diffraction (XRD) analysis (Figure 15, also see Figure A1 Appendix C-A). To avoid any possible reaction with water-sensitive minerals, odorless mineral spirits (OMS) were used as a coolant during diamond-coring and end-grinding. Petrographic samples were vacuum-impregnated with a blue-dye epoxy and used to prepare oversized (approximately $2 \times 1\frac{1}{2}$ inch) thin ($30\mu\text{m}$) sections by an outside agent.

Samples A-F and EP1-8 were dried to constant mass in a constant-humidity oven. Criteria for weight stabilization exceeded ISRM recommendations [7], which define stability as successive mass determinations (4 hr intervals) differing by less than 0.1% of the sample mass. The MB139 samples were dried until no observable systematic mass change occurred. Temperature ranged from approximately $55\text{-}66^\circ\text{C}$ and approximate relative humidity varied from 44-54% over the more than 2500 hours required to dry all samples. Total drying times are listed in Table 2 and the drying histories are shown graphically (Appendix C-C) (note that samples were initially removed from the oven after the ISRM criteria [7] were satisfied (at ~200 hours) and then returned to the oven after analysis of the mass measurements suggested that complete drying had not yet been achieved).

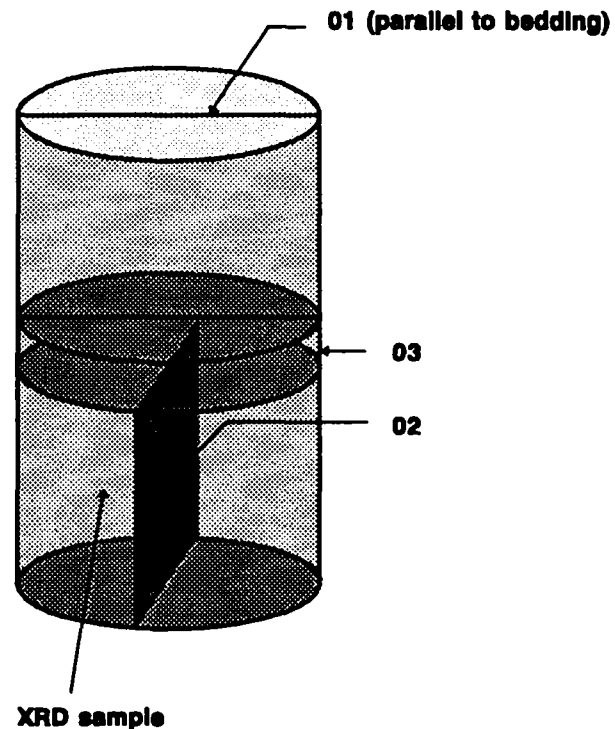


Figure 15. Schematic illustrating PX sample preparation. Thin sections were prepared parallel to O1-O3. O1 is horizontal (parallel to bedding) and O2 and O3 are vertical and mutually perpendicular. XRD analyses were conducted on half of the O2 split.

5.0 XRD Analyses

XRD analyses for determination of semi-quantitative mineralogy were performed on samples PX1-3 from E1X08-4 and PX4-6 from E1X07-4 and are reported in Table 3.

Table 2. Drying Times

Sample	Time (hours)
A	1546
B	366
C	918
D	2532
E	558
F	1787
EP1	918
EP2	366
EP3	366
EP4	366
EP5	918
EP6	918
EP7	558
EP8	366

Table 3. XRD Semi-Quantitative Mineralogic Analyses

Sample	Anhydrite (wt%)	Halite (wt%)	Ferroan Dolomite*† (wt%)	Polyhalite†‡ (wt%)	Aragonite (wt%)	Quartz (wt%)
PX-1	70	30	trace	trace	—	—
PX-2	32	68	—	—	—	—
PX-3	98	2	—	—	—	—
PX-4	7	23	≈30	≈28	12	trace‡
PX-5	62	38	—	—	—	—
PX-6	81	19	—	—	—	—

* Or another cation-disordered Ca-Mg-Fe carbonate. May be well crystalline.

§ No standards available for quantification. Accuracy estimated at ±20%.

† $K_2Ca_2Mg(SO_4)_4 \cdot 2H_2O$. According to Dana's System of Mineralogy, the salmon-pink color of samples containing this mineral may be due to finely divided inclusions of iron oxide.

‡ Tentative identification.

6.0 Petrography

Petrographic analyses, including a 300-point count for mineral identification and grain (crystal) size measurement, were conducted on eighteen thin sections (see Figure 15 for schematic of the three mutually perpendicular sections prepared from each PX sample and Appendix C-D for documentation of thin-section preparation). Point count data are given in Tables 4 and 5 and histograms of grain size distribution are shown in Figures 16-21. Micrographs illustrating the characteristic mineralogy and texture of each PX sample are shown in Plates 1 to 6.

Table 4. Modal Analyses

Sample	Anhydrite (vol%)	Halite (vol%)	Carbonate* (vol%)	Polyhalite (vol%)	Pyrite (vol%)
PX1-O1	6	<1	5	87	1
PX1-O2	67	20	6	7	—
PX1-O3	33	2	7	56	1
PX2-O1	62	37	2	—	—
PX2-O2	48	51	2	—	—
PX2-O3	67	30	4	—	—
PX3-O1	80	3	16	—	—
PX4-O2	87	1	12	—	—
PX4-O3	86	2	10	—	1
PX4-O1	50	44	1	5	—
PX4-O2	20	12	13	55	—
PX4-O3	27	14	3	57	—
PX5-O1	66	26	9	—	—
PX5-O2	79	18	3	—	—
PX5-O3	75	21	4	—	—
PX6-O1	82	17	<1	—	<1
PX6-O2	81	16	3	—	—
PX6-O3	92	4	4	—	—

* Unidentified very finely crystalline carbonate, possibly dolomite.

6.1 Overview

The dominant minerals in MB 139 are anhydrite, halite, and polyhalite; small amounts of very finely crystalline carbonate (tentatively identified as dolomite) are also present (typically about 5 vol%). The distribution of the major mineral phases, as the marker bed is traversed both laterally and vertically, is highly variable.

Anhydrite is typically finely crystalline, although textural alterations are observed when it is closely associated with halite or polyhalite. Anhydrite adjacent to and within halite crystals is coarser, whereas anhydrite intergrown with polyhalite tends to occur as elongate, tabular crystals. Halite crystals and nodules are usually impure, containing anhydrite and/or carbonate inclusions. Halite occurs as nodules, up to 2-3 cm in diameter, which likely grew displacively in the sediment within anhydrite laminae. Halite also fills space between intergrown polyhalite and

Table 5. Grain Size, Sorting, and Porosity from 300-Point Count

Sample	Median Grain Size (μm)	Sorting (ϕ)	Porosity (%)
PX1-O1	15	0.98	—
PX1-O2	23.5	2.00	—
PX1-O3	20	0.91	—
PX2-O1	66	2.06	—
PX2-O2	64	1.96	—
PX2-O3	39	2.15	—
PX3-O1	16.5	0.85	<1
PX3-O2	13.5	0.83	—
PX3-O3	12.5	0.92	—
PX4-O1	128	1.91	—
PX4-O2	26	1.54	—
PX4-O3	38	1.34	—
PX5-O1	64	1.80	—
PX5-O2	45	2.02	—
PX5-O3	62.5	1.86	—
PX6-O1	17	1.51	—
PX6-O2	17	1.56	—
PX6-O3	16	1.02	—

anhydrite structures. Polyhalite, which dominates specific areas of samples PX1 and PX4 but is absent in the other samples, occurs as narrow, needle-like crystals which form spherulitic to pseudocross-like structures (see Plates 1 and 4). Finely crystalline ($< 8 \mu\text{m}$ grain size) carbonate is a minor phase in all samples and occurs in scattered patches and as thin wisps, which commonly define bedding. This material, which appears dolomitic, is typically microporous, as evidenced by a light blue color in thin section. Very minor pyrite and possible clay minerals are observed in some thin sections, but always constitute $\leq 1\%$ of the bulk composition.

Total porosity in all six samples appears very low ($\leq 2\%$) and poorly connected when observed in 2-D. Microporosity associated with carbonate minerals is the most commonly observed porosity type. Fractures, at angles between 45° and 90° to bedding and with apparent apertures ranging from 10 to $30 \mu\text{m}$, are present in several samples. (Note that since thin sections were prepared at ambient conditions, in situ apertures are probably lower.) A number of bedding parallel fractures (with apertures up to tens of microns) are also observed. High-angle fractures are commonly confined to individual laminae and often terminate at the interface between laminae. Several healed fractures (sometimes filled by anhydrite) were observed.

6.2 Petrographic Descriptions (see Figure 15 for sample locations)

6.2.1 Sample PX1. Mineral distribution varies significantly amongst the three sections. O1 and O3 are dominated by polyhalite, but contain lesser amounts of halite, anhydrite, carbonate (dolomite?), and pyrite. O2 is dominated by anhydrite and halite; polyhalite is present in only a small area of the section.

Polyhalite generally occurs as small spherulites composed of tiny, radiating, needle-like crystals which are intergrown to form a tightly interlocked crystal network. Singular elongate and tabular anhydrite crystals are commonly scattered throughout the polyhalite. Anhydrite is also intergrown with polyhalite in the outer portions of spherulites. Finely crystalline carbonate, probably dolomite, is also intergrown with anhydrite and polyhalite in the outer portions of spherulites. Finely crystalline carbonate also fills spaces between spherulites and occurs in somewhat randomly distributed patches. Halite fills areas between spherulites. Minor pyrite is scattered throughout these areas.

Most of section O2 and one edge of section O3 are dominated by anhydrite and halite. Anhydrite is generally finely crystalline, except when it is located adjacent to halite crystals where an increase in crystal size is apparent. Halite within anhydrite forms irregular nodules which appear to be aligned along bedding planes, which are very irregular. Finely crystalline carbonate material in these areas occurs in small randomly distributed patches and as thin wisps (which define bedding). Some carbonate patches exhibit a somewhat peloidal texture.

Minor microporosity is apparent within some of the finely crystalline carbonate patches and is most abundant in O3, which contains more finely crystalline carbonate than O2 or O1. Both open and healed fractures, with apertures of $10\text{-}30 \mu\text{m}$, are present in anhydrite laminae in O2.

6.2.2 Sample PX2. All sections are very similar and dominated by intergrown anhydrite and halite with minor finely crystalline carbonate. Halite crystals are very large, particularly in O2, and range up to several centimeters in diameter. Note that such large crystals cannot be measured concurrently with the fine-grained material, and histograms constructed for these three sections (Figures 17a-c) are for "matrix" only. Anhydrite ranges from fine to medium crystalline and is generally coarser than in most of the other PX samples. Anhydrite crystals adjacent to halite are typically coarser than those residing in the fine-grained matrix. Carbonate material is finely crystalline and occurs as scattered patches, and in O3 as thin wisps which define bedding. Bedding is not apparent in O1 or O2.

Minor microporosity is seen within patches of finely crystalline carbonate. Several narrow fractures are present on one edge of O3. These fractures are partially within halite crystals and parallel to cleavage. Note that their proximity to the sample edge may suggest a relationship to sample preparation.

6.2.3 Sample PX3. PX3 is dominated by finely crystalline anhydrite which occurs in thin irregular laminae in all sections. Anhydrite appears more finely crystalline in this sample than in any of the other samples: this may be due to the low abundance of halite given the previously noted observation that anhydrite associated with halite is commonly more coarsely crystalline. Finely crystalline carbonate material is second in abundance, occurring in thin wisps along bedding planes and as irregular patches in the anhydrite matrix. Halite is least abundant and forms small irregular nodules within certain anhydrite laminae in O2 and O3, and in the central portion of O1.

Bedding in all three samples is defined by thin, finely crystalline carbonate laminae and appears oriented at about 30° to the core axis in O2. Several thin fractures (partings) parallel to bedding were observed.

Minor microporosity is present within the finely crystalline carbonate material in all sections. Fractures, oriented at about 45° to bedding and with somewhat irregular traces, are present on one end of O1. O3 contains a healed, very narrow fracture which appears confined to several laminae and is oriented at about 80° to vertical.

6.2.4 Sample PX4. PX4 is composed of intergrown polyhalite, halite, anhydrite, and finely crystalline carbonate. Polyhalite occurs as needle-like crystals in spherulitic to pseudo-cross type structures. Elongate anhydrite crystals are intergrown in the outer portions of the spherulites and halite fills space between spherulites. Polyhalite spherulites, containing very little halite or anhydrite, dominate portions of O2 and O3. Anhydrite, in addition to being intergrown with polyhalite, also occurs as equant crystals in the matrix. Finely crystalline carbonate material, which is most abundant in O2, occurs in scattered patches and as thin wisps, which may define bedding. Crystal size is highly variable, and the high sorting (2.94 phi) found for O1 reflects the abundance of elongate crystals.

Only hints of bedding are observed in the PX4 sections. The irregular interface between mixed mineralogy and the polyhalite-dominated areas may represent bedding. Thin wisps of finely crystalline carbonate may define bedding in O2.

Very little porosity, consisting of minor microporosity associated with finely crystalline carbonate, was observed in the PX4 sections.

6.2.5 Sample PX5. PX5 is dominated by admixed anhydrite and halite. Anhydrite occurs as both individual laminae and combined with halite in other laminae. Grains are fine to medium crystalline and appear much coarser than in the underlying sample PX6. As observed previously, anhydrite in close association with halite is usually more coarsely crystalline than in laminae containing only anhydrite. Halite forms nodules within specific laminae in O2 and O3, but appears somewhat randomly oriented in O1 (O1, which is parallel to bedding, may possibly have been prepared from a lamination rich in halite). Carbonate material is finely crystalline and occurs as scattered patches and wisps parallel to laminae.

Bedding is easily recognizable in O2 and O3, but less distinct in thin section O1. Wisps of carbonate material commonly define bedding in this PX sample.

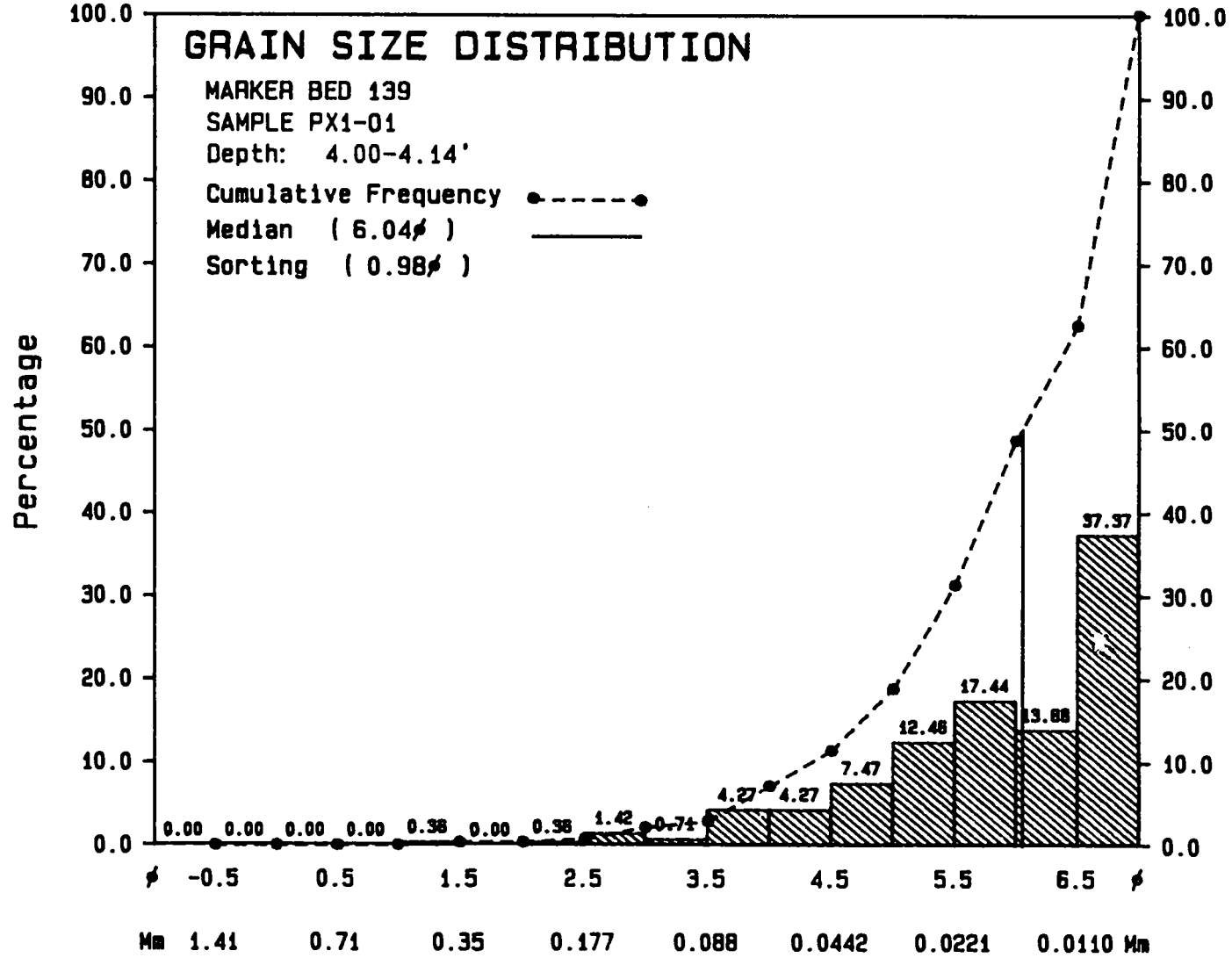
Minor microporosity is present within the finely crystalline carbonate material. One high-angle (to bedding) fracture was observed in an anhydrite lamination in O2. Total porosity appears quite low.

6.2.6 Sample PX6. Sample PX6 is characterized by bedded to laminated anhydrite containing nodular halite. Halite nodules are relatively impure and contain abundant anhydrite inclusions, which may indicate displacive growth in an anhydrite mush prior to lithification. Anhydrite is finely crystalline, except where closely associated with halite. Minor finely crystalline carbonate occurs as wisps parallel to laminations. Minor clay may also be present along some bedding planes. Scattered pyrite framboids were observed in O1.

Bedding is best developed in this sample, although somewhat wavy and discontinuous. Local bedding appears oriented at about 20° to the long dimension (vertical) of thin section P2-O2. Some laminae contain exclusively anhydrite, whereas others contain a mixture of anhydrite and halite. Growth of halite nodules has disrupted some of the original depositional texture.

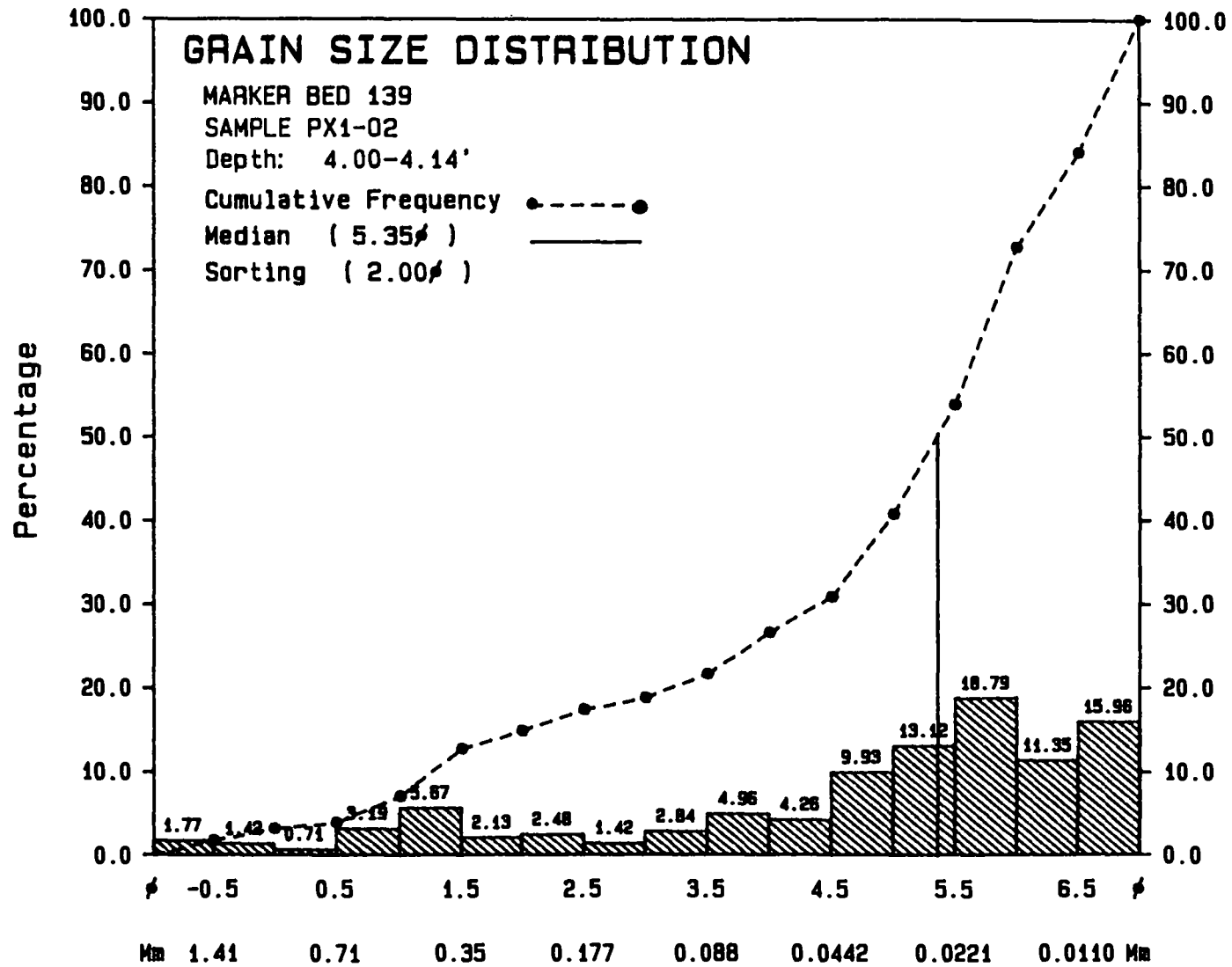
Total porosity appears low. Microporosity associated with finely crystalline carbonate wisps and patches is most common. Several narrow fractures oriented between 70° and 90° to bedding and with apertures less than 20 µm are present in O2 and O3. Bedding-parallel fractures are present in O2.

FIGURE 16A. GRAIN/CRYSTAL SIZE HISTOGRAM FOR SAMPLE PX1-01.



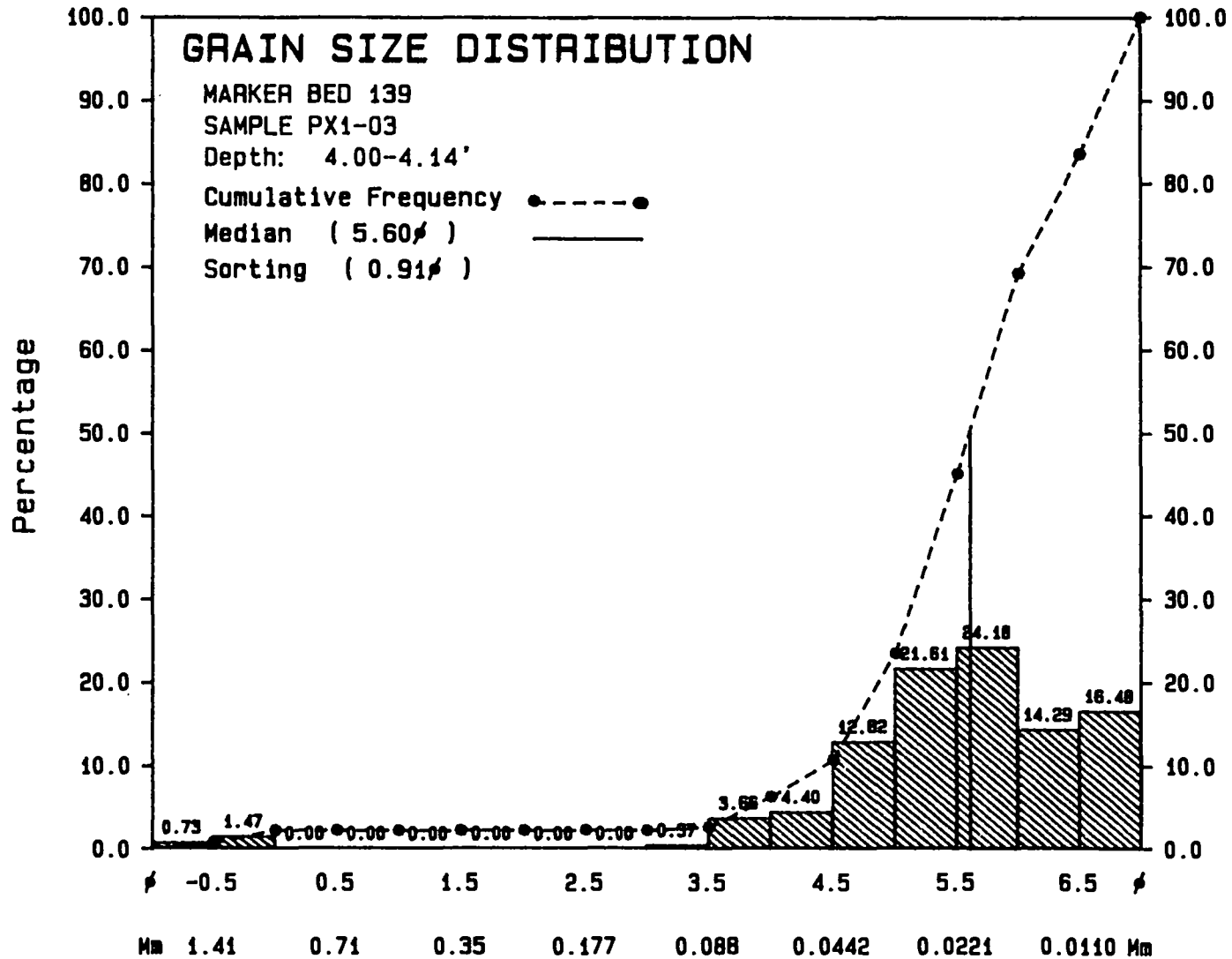
C-41

FIGURE 16B. GRAIN/CRYSTAL SIZE HISTOGRAM FOR SAMPLE PX1-02.



C-42

FIGURE 16C. GRAIN/CRYSTAL SIZE HISTOGRAM FOR SAMPLE PX1-03.



C-43

FIGURE 17A. GRAIN/CRYSTAL SIZE HISTOGRAM FOR SAMPLE PX2-01.

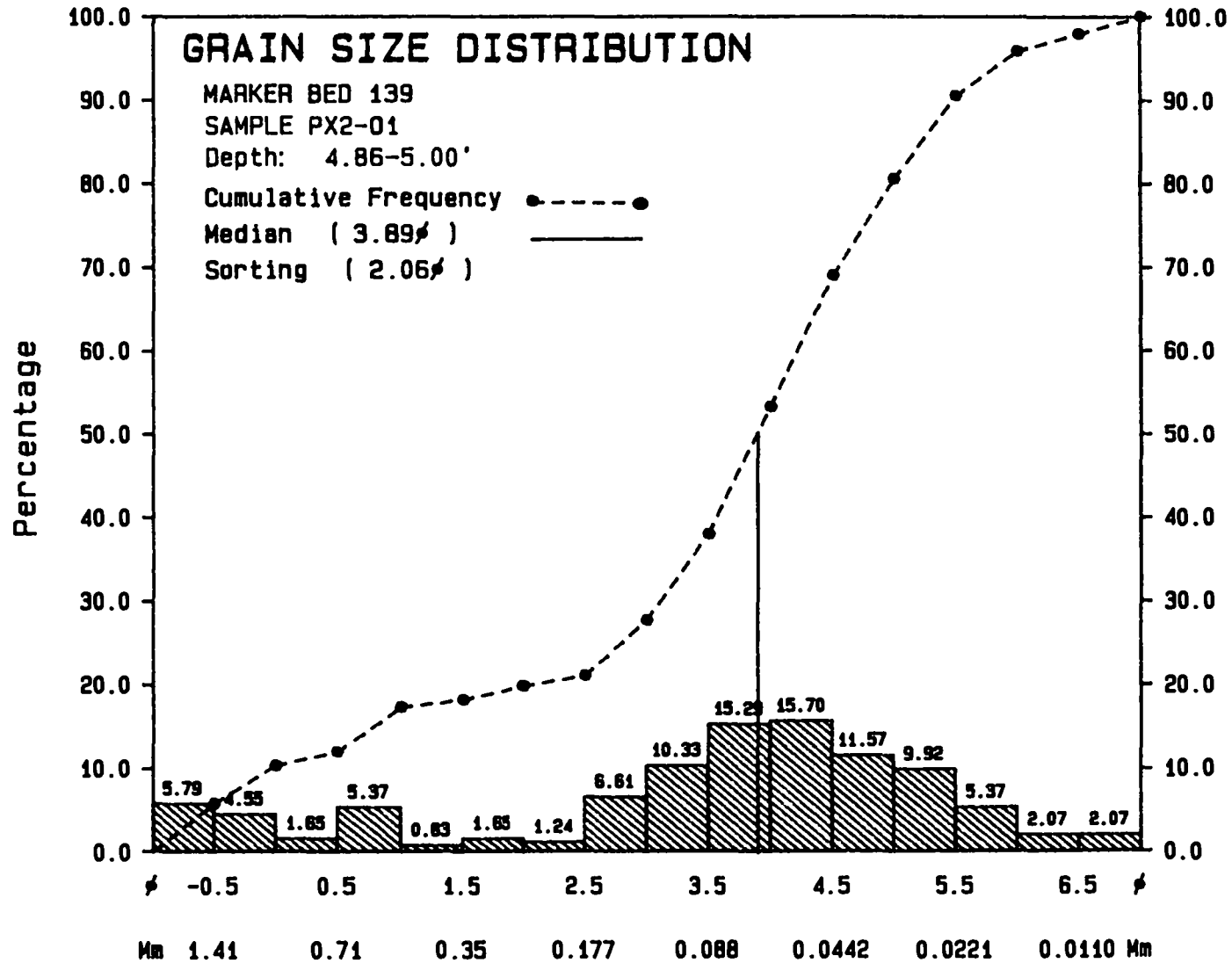
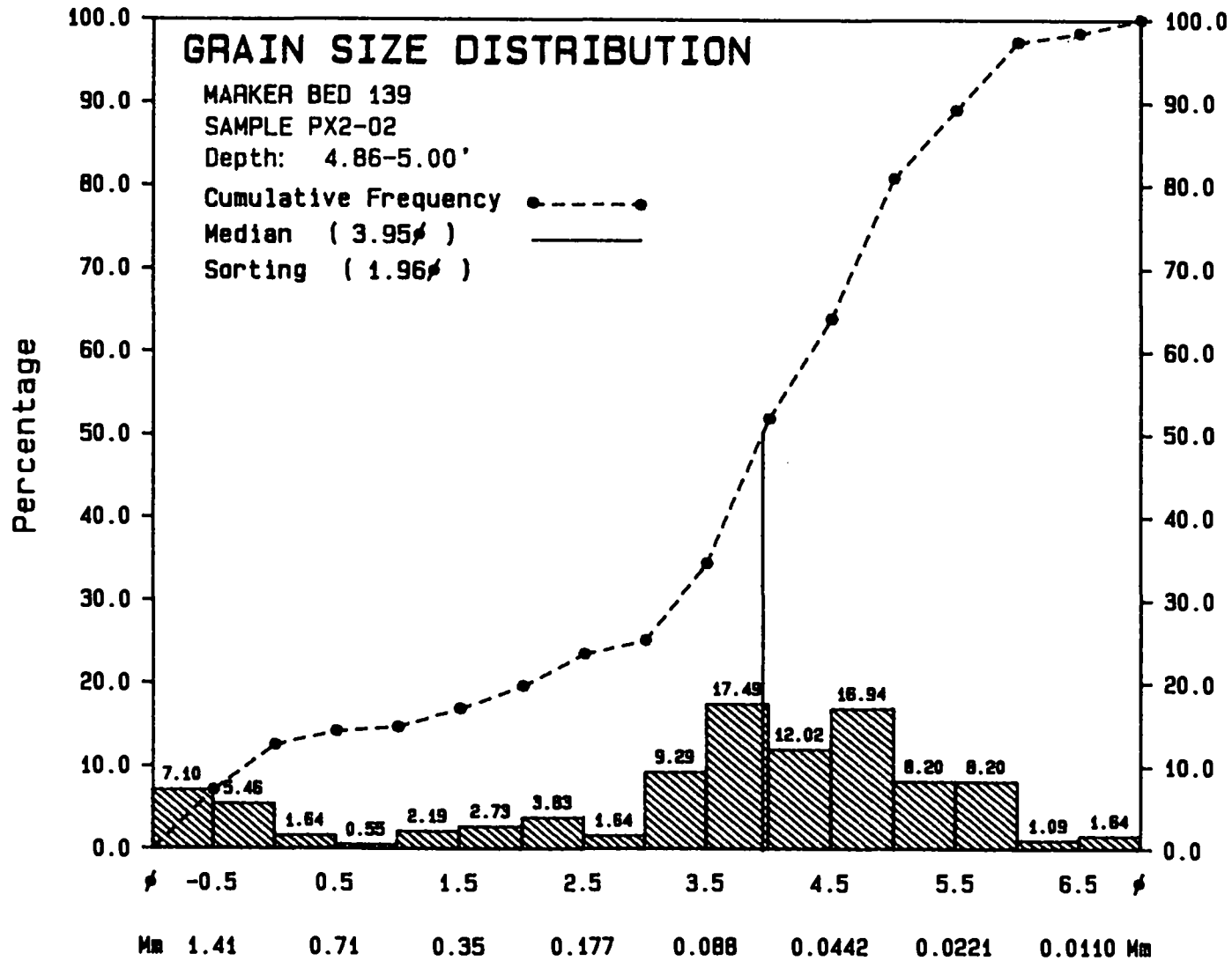
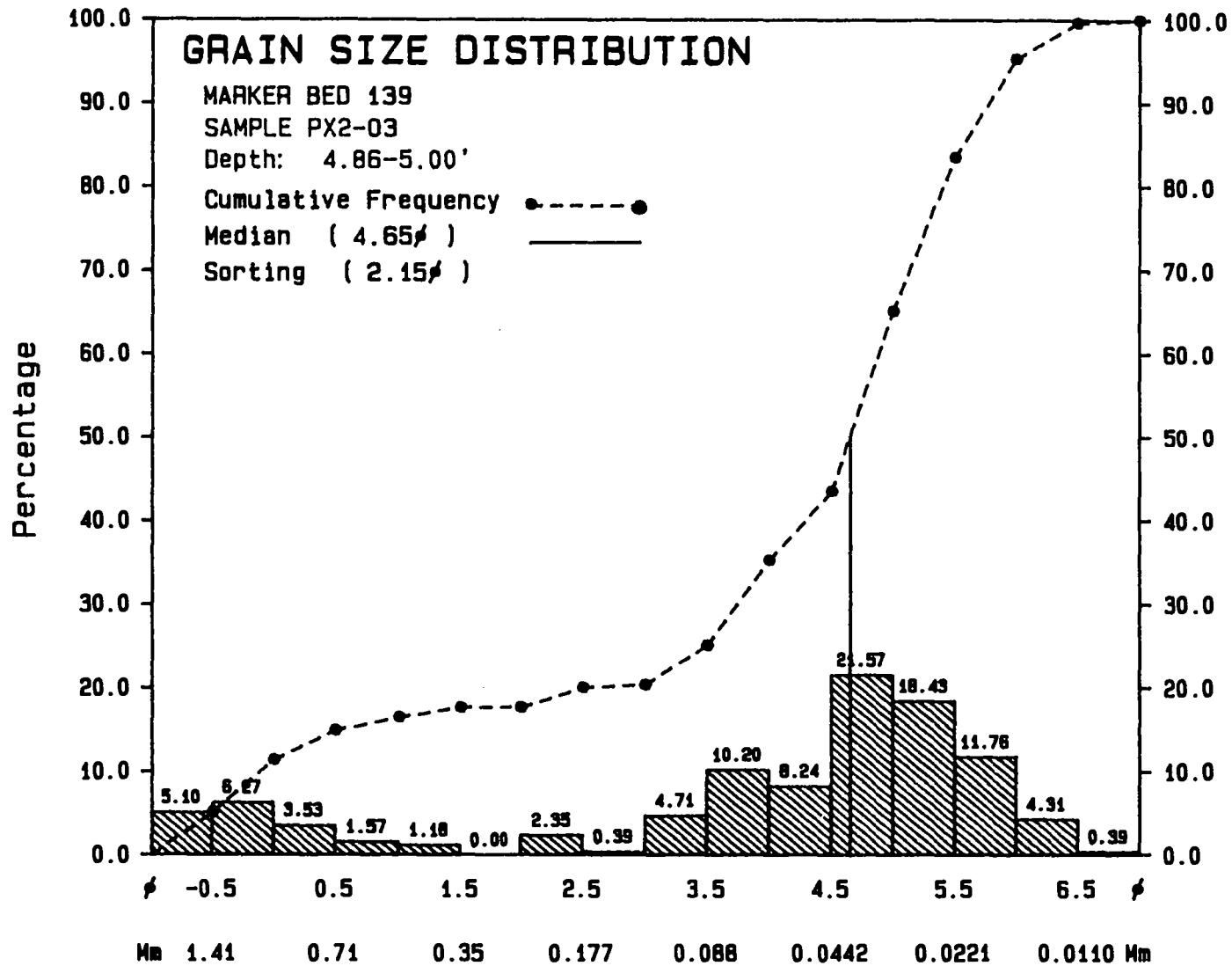


FIGURE 17B. GRAIN/CRYSTAL SIZE HISTOGRAM FOR SAMPLE PX2-02.



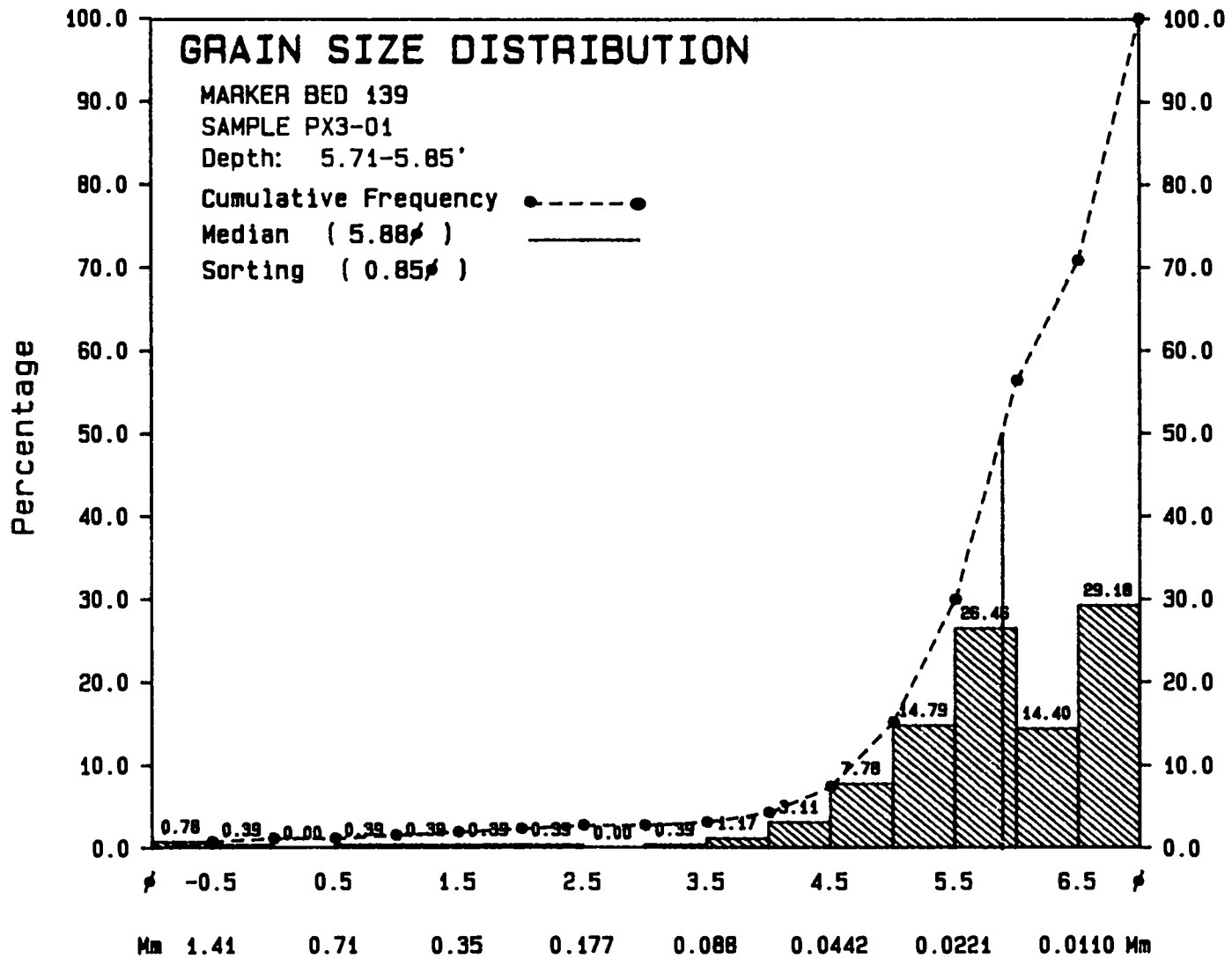
C-45

FIGURE 17C. GRAIN/CRYSTAL SIZE HISTOGRAM OF SAMPLE PX2-03.



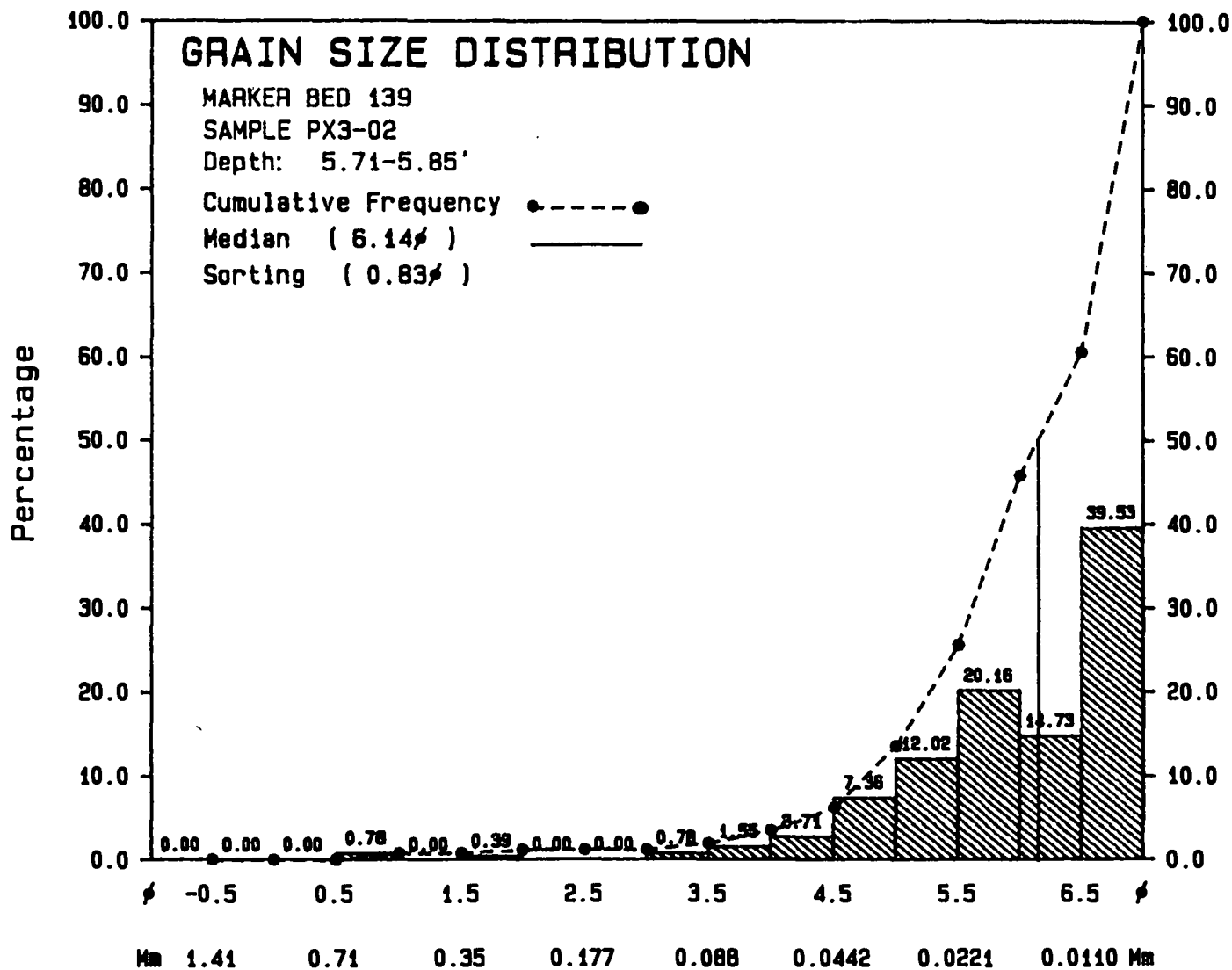
C-46

FIGURE 18A. GRAIN/CRYSTAL SIZE HISTOGRAM FOR SAMPLE PX3-01.



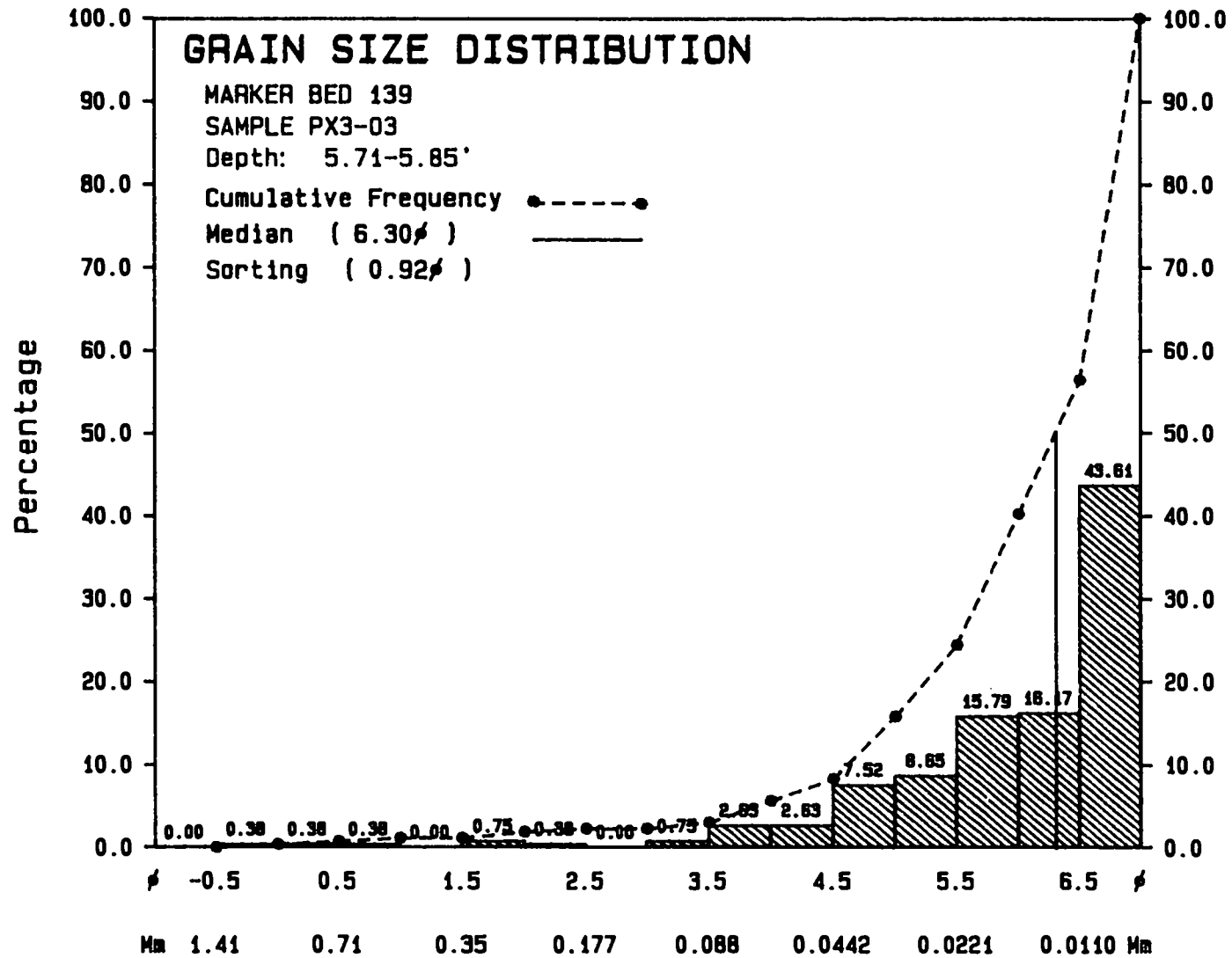
C-47

FIGURE 188. GRAIN/CRYSTAL SIZE HISTOGRAM OF SAMPLE PX3-02.



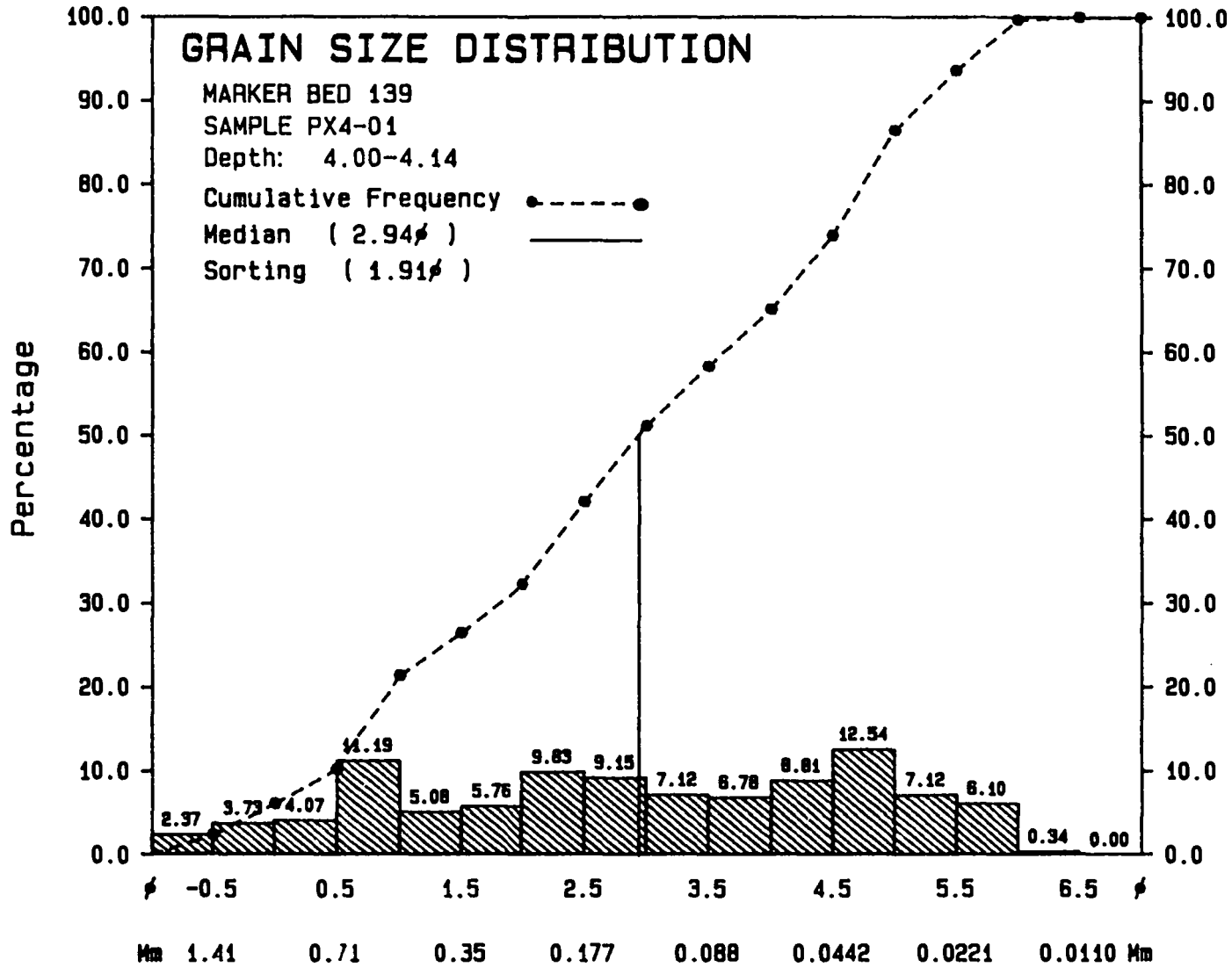
C-48

FIGURE 18C. GRAIN/CRYSTAL SIZE HISTOGRAM OF SAMPLE PX3-03.



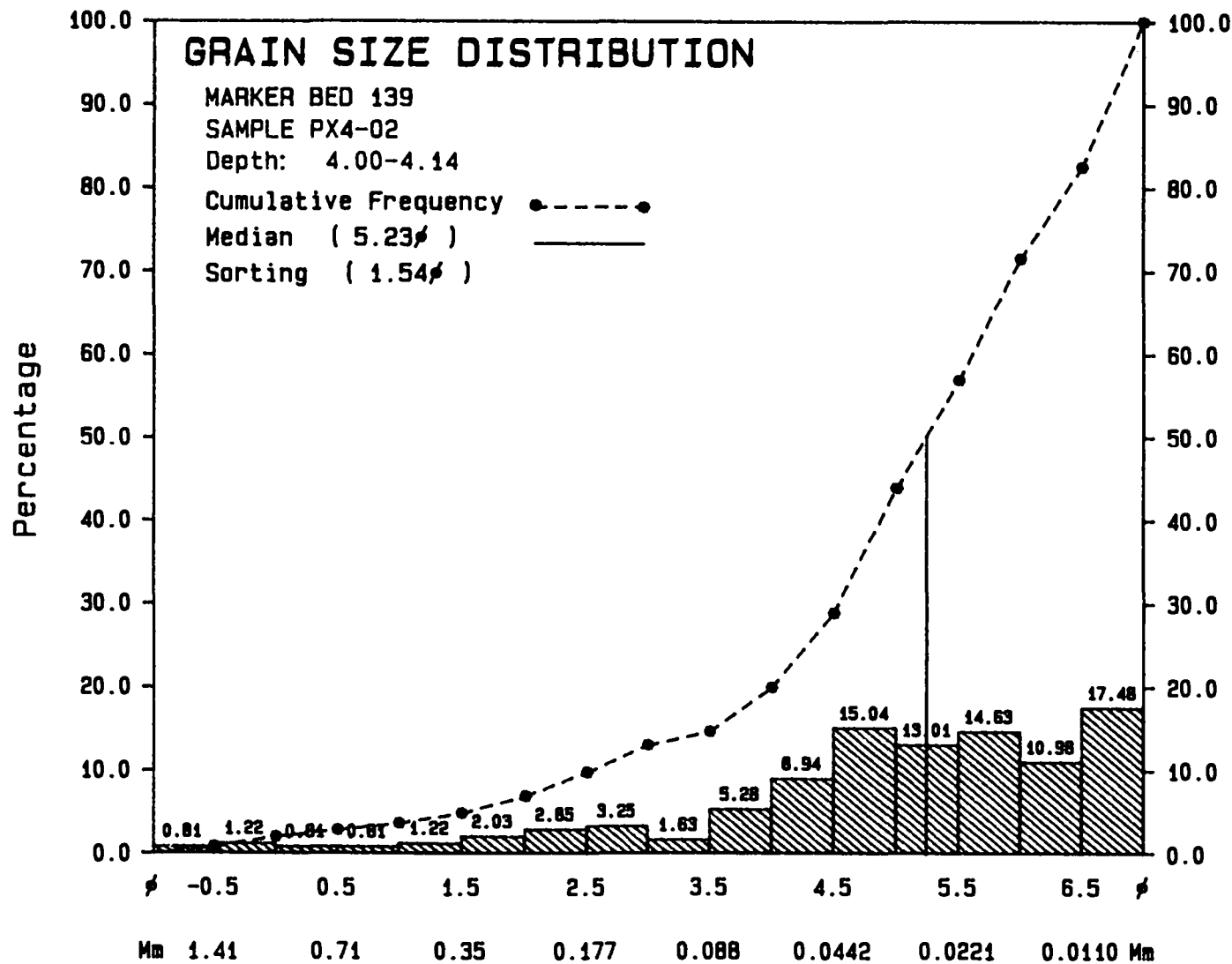
C-49

FIGURE 19A. GRAIN/CRYSTAL SIZE HISTOGRAM FOR SAMPLE PX4-01.



C-50

FIGURE 198. GRAIN/CRYSTAL SIZE HISTOGRAM FOR SAMPLE PX4-02.



C-51

FIGURE 19C. GRAIN/CRYSTAL SIZE HISTOGRAM FOR SAMPLE PX4-03.

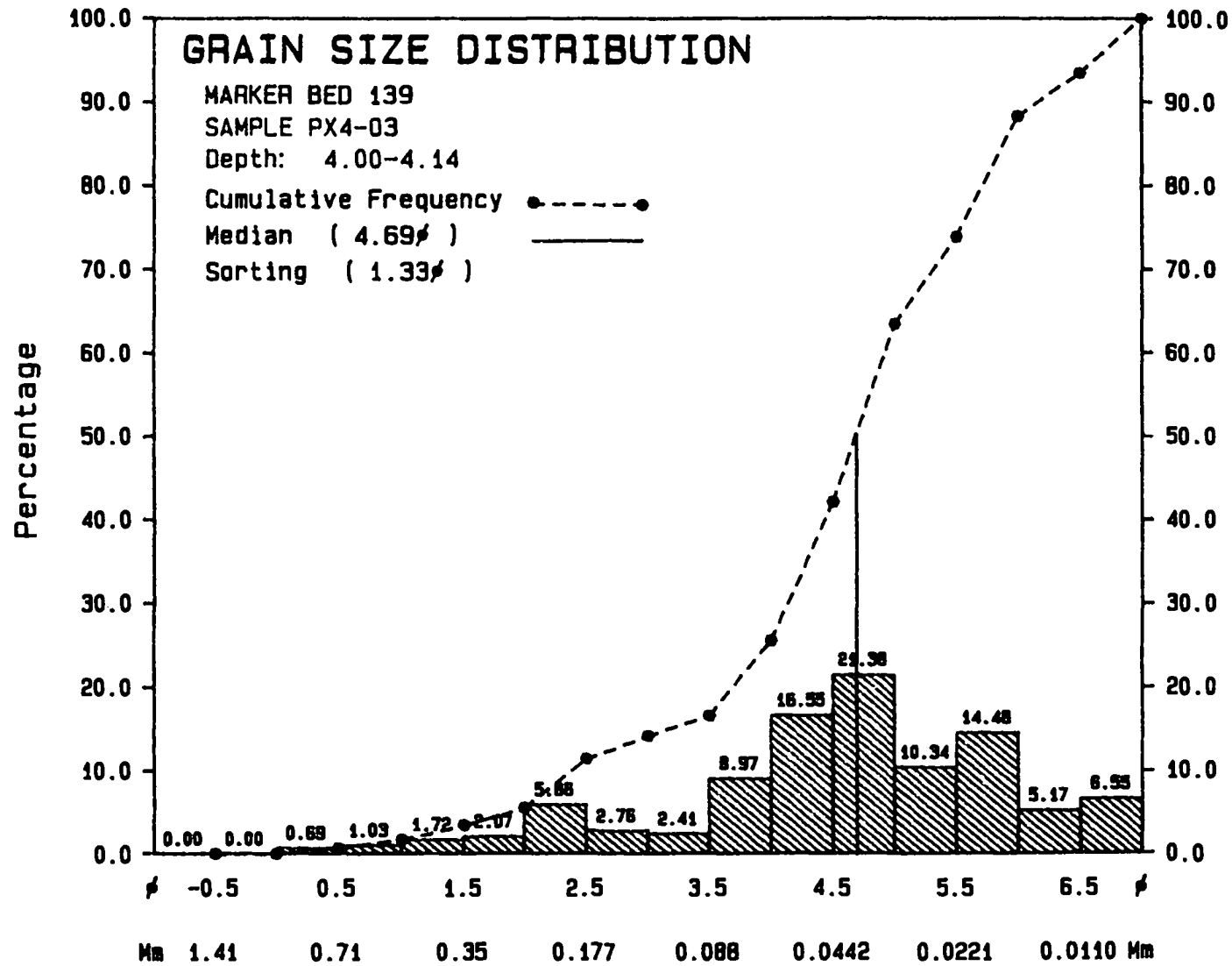


FIGURE 20A. GRAIN/CRYSTAL SIZE HISTOGRAM FOR SAMPLE PX5-01.

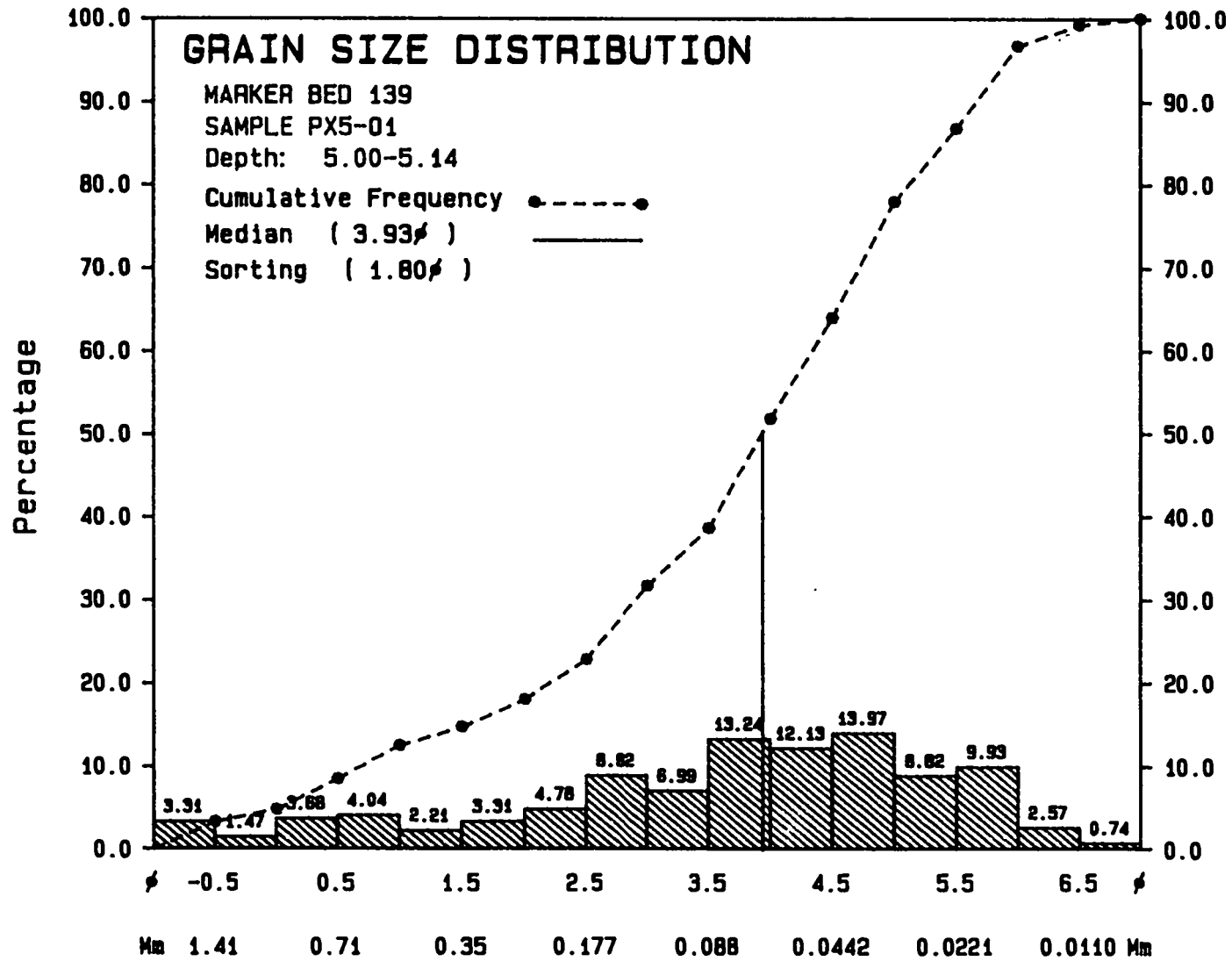


FIGURE 20B. GRAIN/CRYSTAL SIZE HISTOGRAM FOR SAMPLE PX5-02.

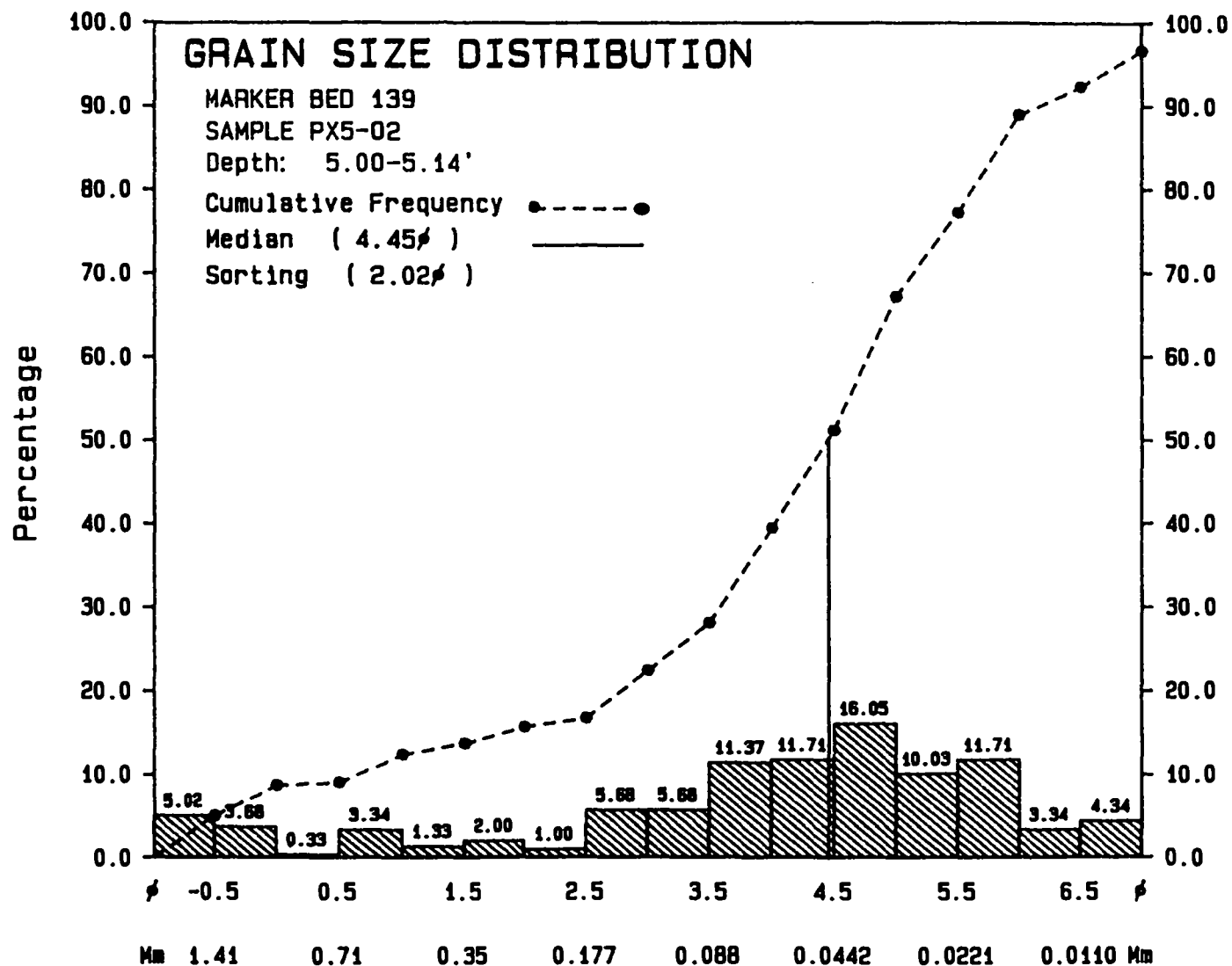


FIGURE 20C. GRAIN/CRYSTAL SIZE HISTOGRAM FOR SAMPLE PX5-03.

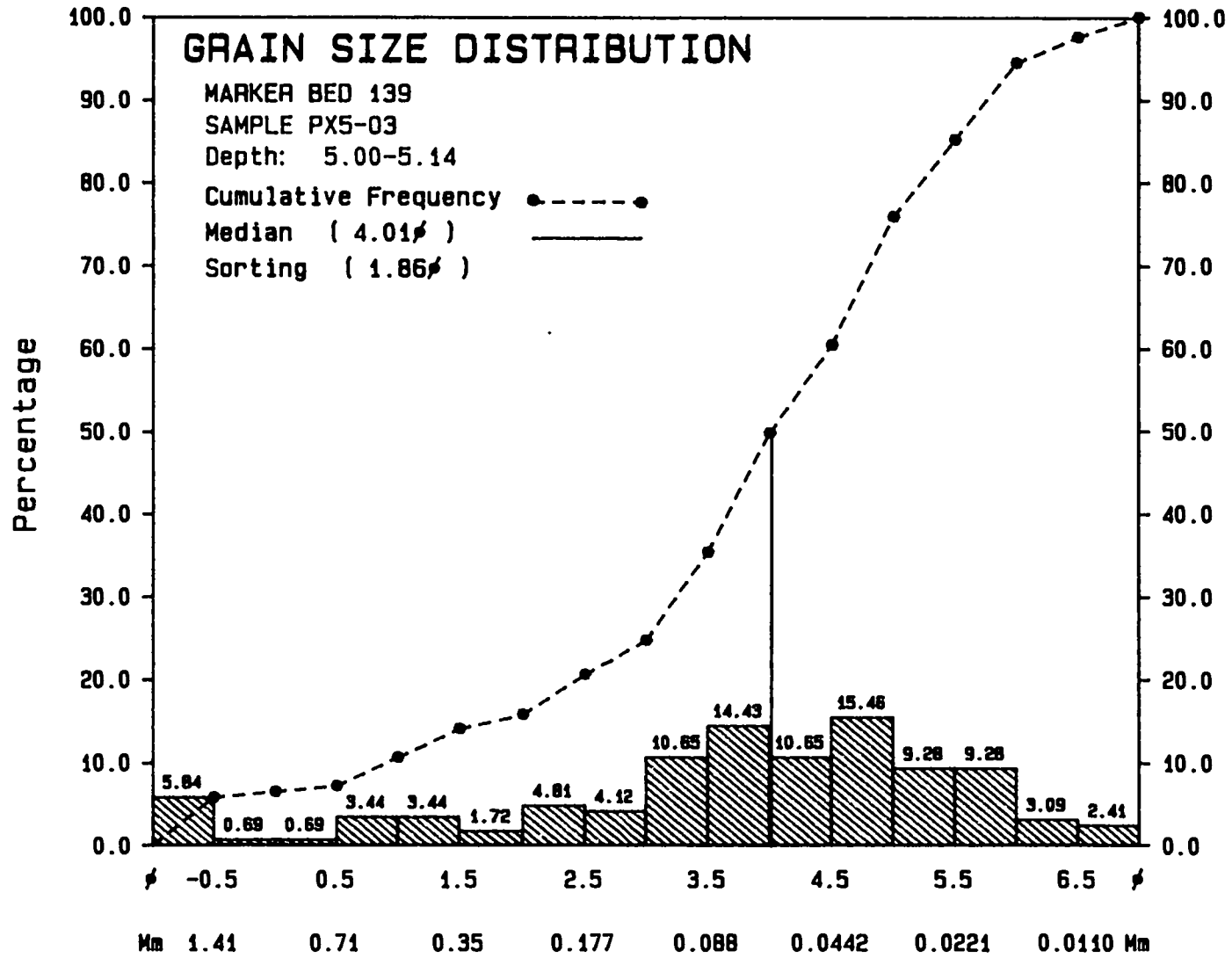
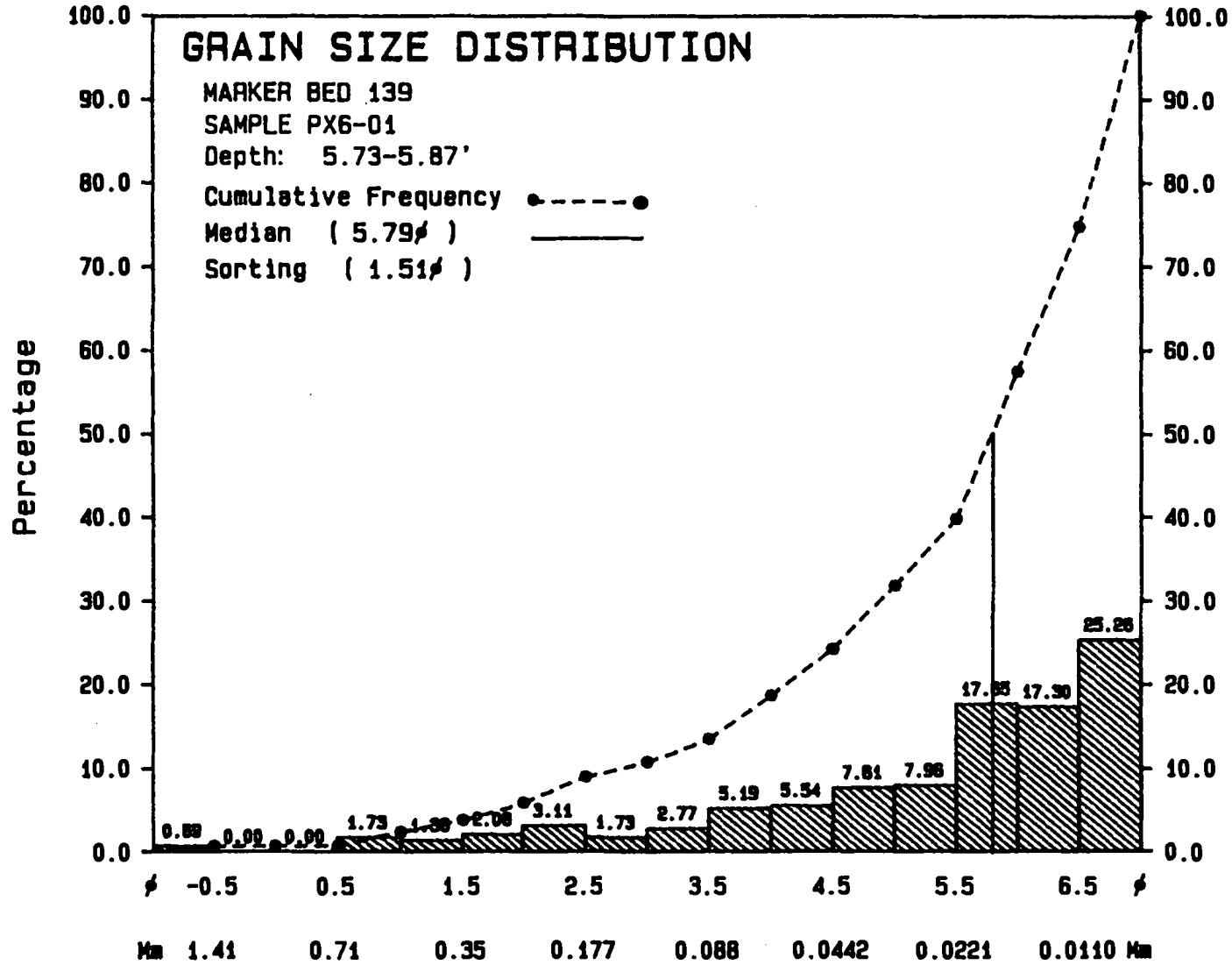
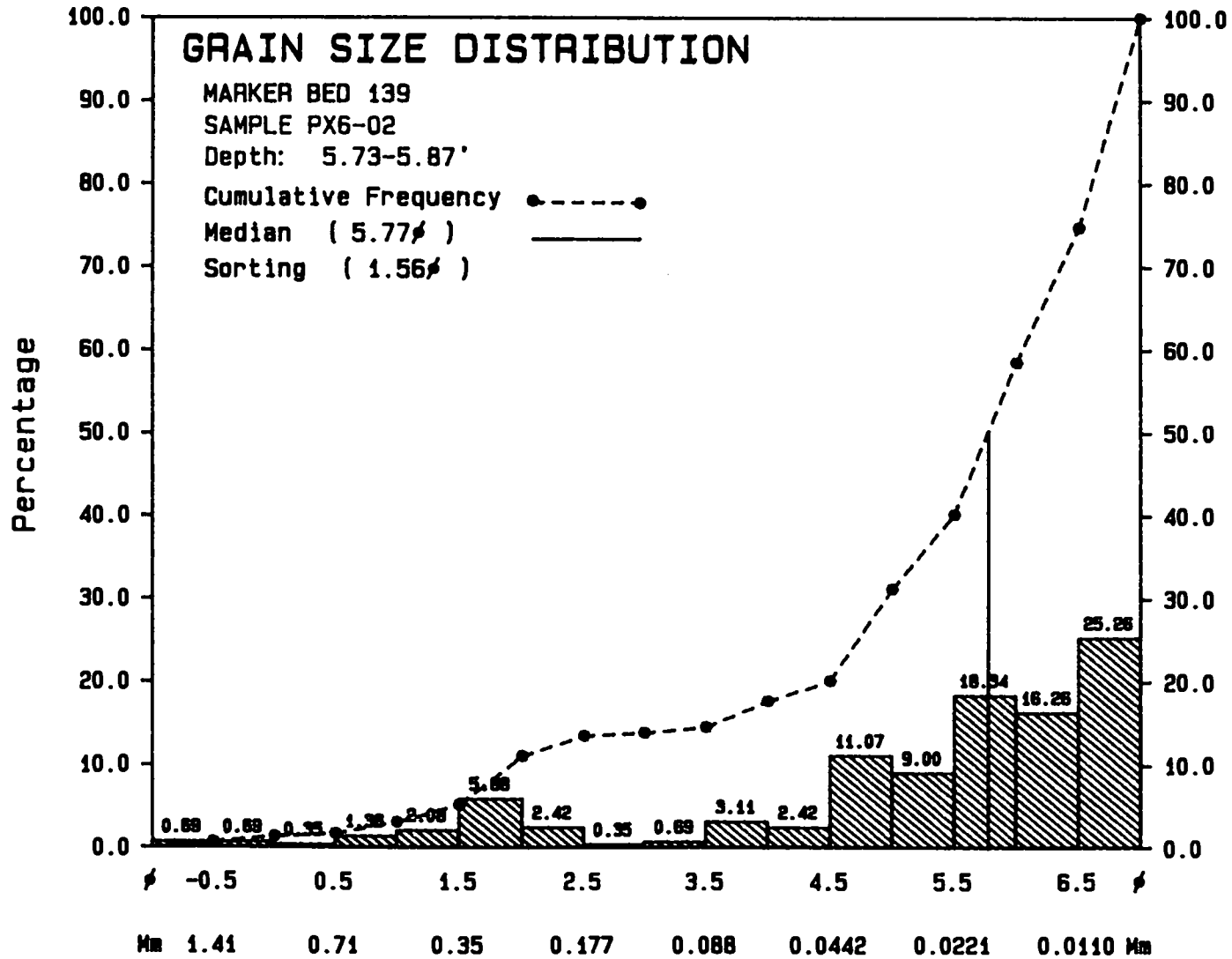


FIGURE 21A. GRAIN/CRYSTAL SIZE HISTOGRAM FOR SAMPLE PX6-01.



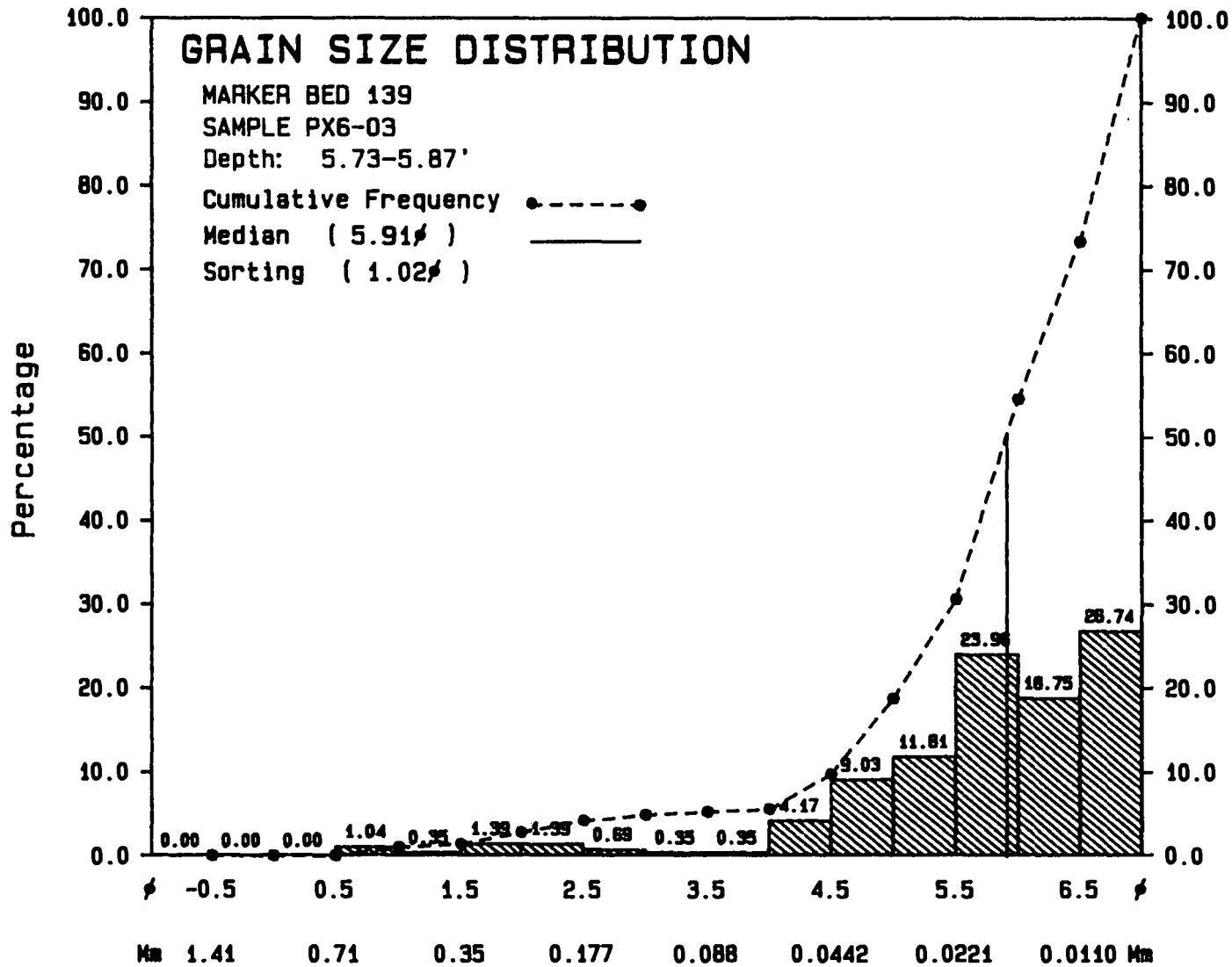
C-56

FIGURE 21B. GRAIN/CRYSTAL SIZE HISTOGRAM FOR SAMPLE PX6-02.



C-57

FIGURE 21C. GRAIN/CRYSTAL SIZE HISTOGRAM FOR SAMPLE PX6-03.



C-58

Plate 1
Sample PX1

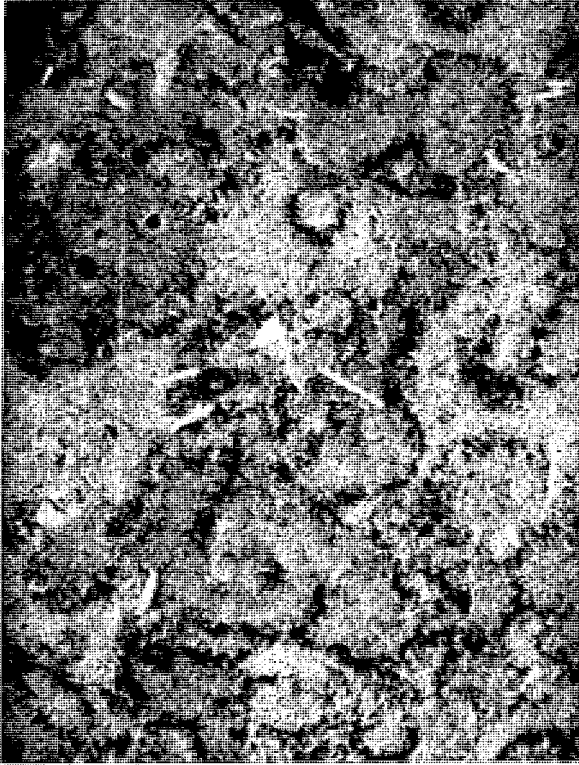
- A. **General view of thin section PX1-O1 showing intergrown polyhalite spherulites. Each spherulite is composed of tiny, radiating, needle-like crystals. Elongate tabular crystals scattered throughout the view are anhydrite. Finely crystalline carbonate (dolomite?) is also present and appears as dark patches. Plane-polarized light. (40×)**

- B. **Low magnification view of an open fracture in thin section PX1-O2. This fracture dips at approximately 45° and extends across one corner of the thin section. Anhydrite is the dominant mineral in this portion of the sample. Minor halite (white patches) is also present. Plane-polarized light. (20×)**

- C. **View of the interface between polyhalite and anhydrite in thin section PX1-O2. The upper portion of the photomicrograph is dominated by anhydrite whereas the lower portion contains more abundant polyhalite. Black patches represent halite (isotropic under crossed nicols). Finely crystalline carbonate (dolomite?) occurs in irregular brownish patches throughout the central portion of the view. Crossed-nicols. (20×)**

- D. **Overview of thin section PX1-O3 showing abundant polyhalite. Minor amounts of finely crystalline carbonate (dolomite?) are also present. Iron staining (reddish brown color) is present in the lower portion of the view. Plane-polarized light. (40×)**

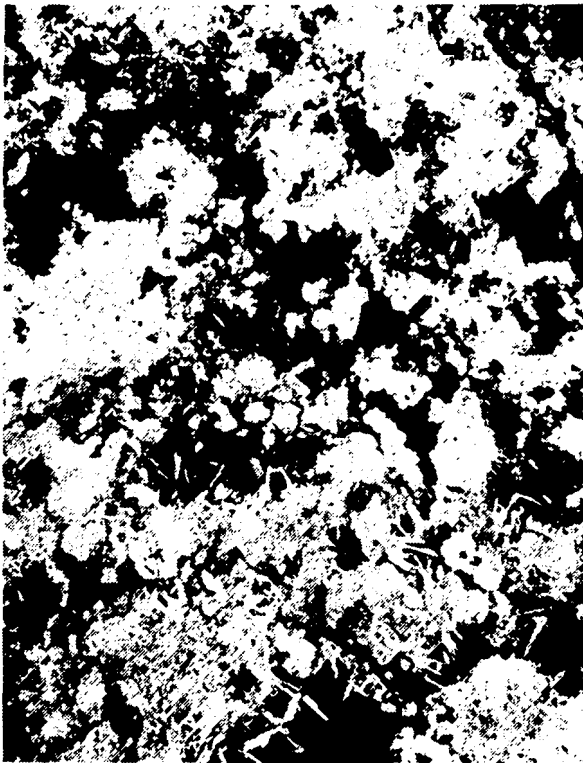
Plate 1



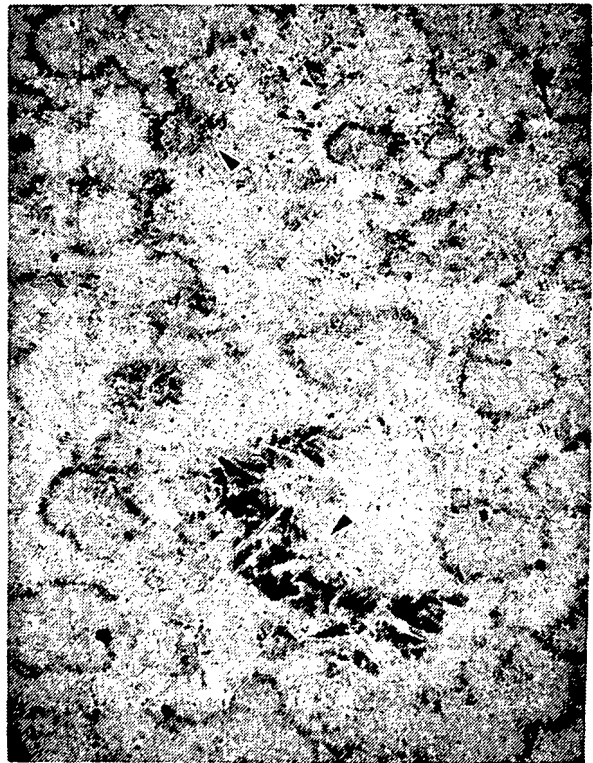
A



B



C



D

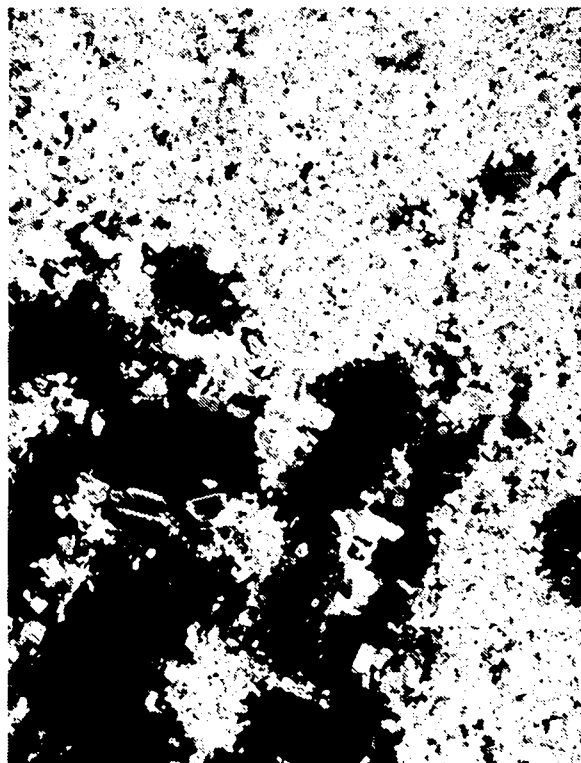
Plate 2
Sample PX2

- A. Low magnification view of thin section PX2-O1 showing large halite crystals (lower left) surrounded by more finely crystalline anhydrite. Minor carbonate (dolomite?) appears as dark brown patches within both halite and anhydrite. Many of the halite crystals in this sample are too large to photograph. Plane-polarized light. (20×)
- B. Same view as the previous photomicrograph more clearly showing halite distribution. Significant variation in anhydrite crystal size is also evident. Note high birefringence which is characteristic of anhydrite. Halite is isotropic and appears black. Crossed-nicols. (20×)
- C. Low magnification view of thin section PX2-O2 showing large halite crystals with minor anhydrite around crystal edges and as inclusions. Halite crystals in this thin section are larger than in the other two thin sections from this sample. Crossed-nicols. (20×)
- D. Overview of thin section PX2-O3 showing fractures developed along cleavage planes in relatively large halite crystals. Note fluid inclusion trains along fractures, indicating earlier fractures which have healed. Plane-polarized light. (40×)

Plate 2



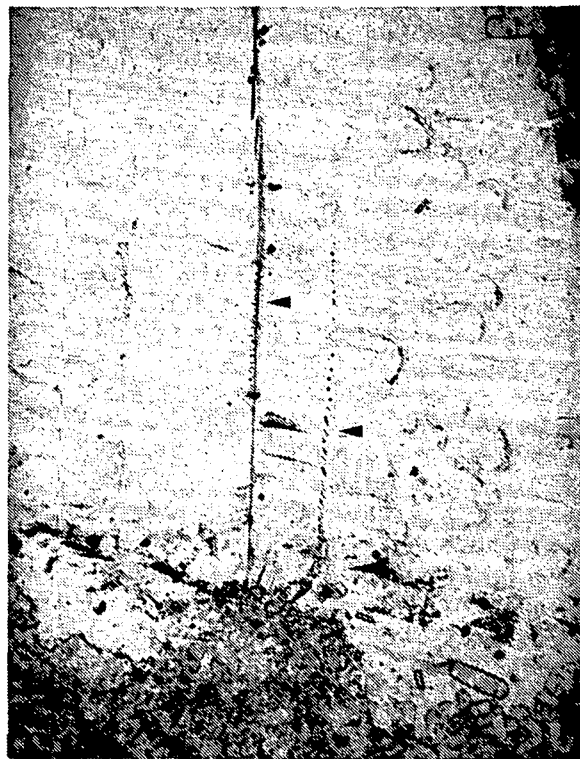
A



B



C

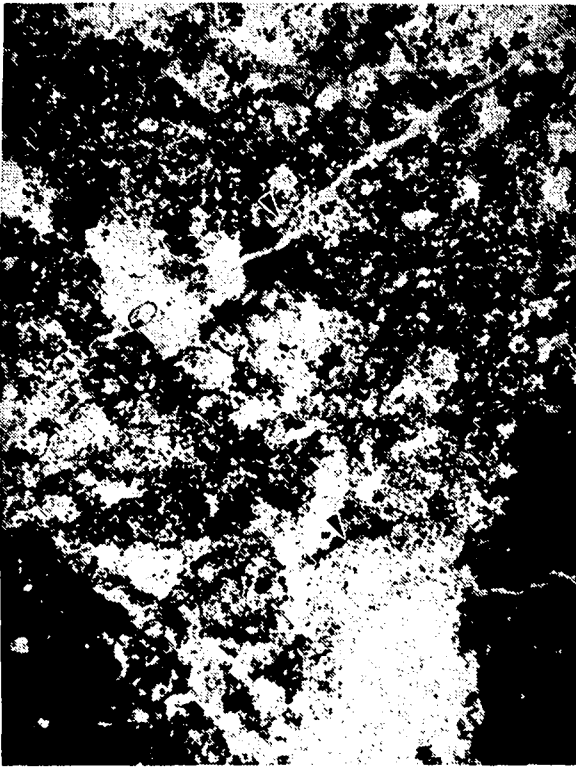


D

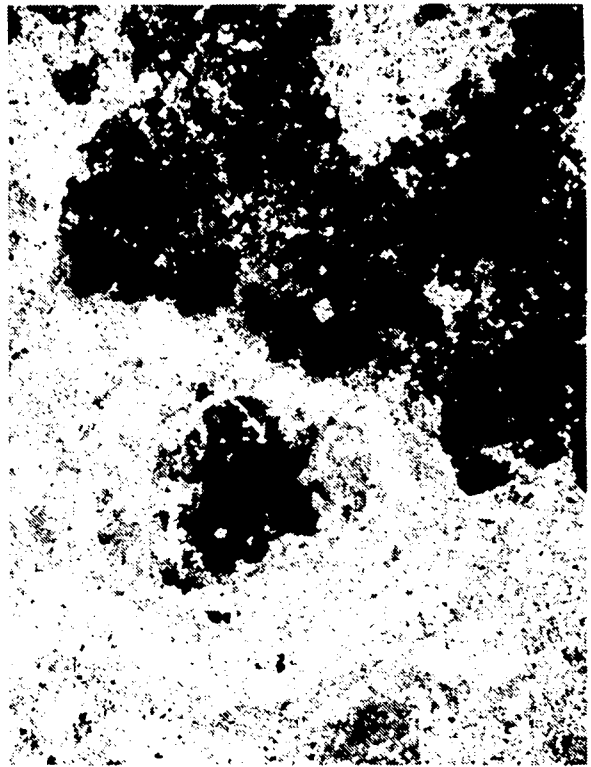
Plate 3
Sample PX3

- A. Overview of thin section PX3-O1 showing low angle fractures in a matrix composed of anhydrite, carbonate (dolomite?), and halite. Plane-polarized light. (40×)
- B. Low magnification view of thin section PX3-O1 showing the distribution of various mineral components. Halite appears black and forms nodules in the upper portion of the view. Anhydrite and carbonate (dolomite?) occur as inclusions in halite and comprise most of the matrix. Note variation in crystal size. Crossed-nicols. (20×)
- C. Overview of thin section PX3-O2 showing interlaminated halite, anhydrite, and carbonate (dolomite?). Halite appears black and occurs in much larger crystals than either anhydrite or dolomite. Crossed-nicols. (40×)
- D. Low magnification view of thin section PX3-O3 showing irregular anhydrite (white) and carbonate (dolomite?) (dark) laminae. The fracture running from left to right through the central portion of the view is generally parallel to laminations. Plane-polarized light. (20×)

Plate 3



A



B



C



D

Plate 4
Sample PX4

- A. Low magnification view of thin section PX4-O1 showing intergrown halite, polyhalite, and anhydrite. Halite appears white under plane light. Polyhalite along with anhydrite forms relatively large radiating structures. Anhydrite also dominates the matrix between halite and polyhalite crystals. Plane-polarized light. (20x)
- B. More detailed view of thin section PX4-O1. Isotropic halite appears black. Anhydrite occurs as small equant crystals around halite nodules and as elongate needles intergrown with polyhalite. Central portions of the cross-like structures are composed primarily of polyhalite. Crossed-nicols. (40x)
- C. Overview of thin section PX4-O2 showing abundant fibrous polyhalite. Small halite patches (black) are also present on the left side of the view. Minor anhydrite is also present. This thin section is dominated by polyhalite. Crossed-nicols. (40x)
- D. View of intergrown halite, polyhalite, and anhydrite characteristic of thin section PX4-O3. Anhydrite appears in shades of red, yellow, and blue. Note crystal size variation in anhydrite. Polyhalite occurs as needle-like crystals in the central portions of radiating structures. Halite (black) fills space between the other minerals. Crossed-nicols. (40x)

Plate 4



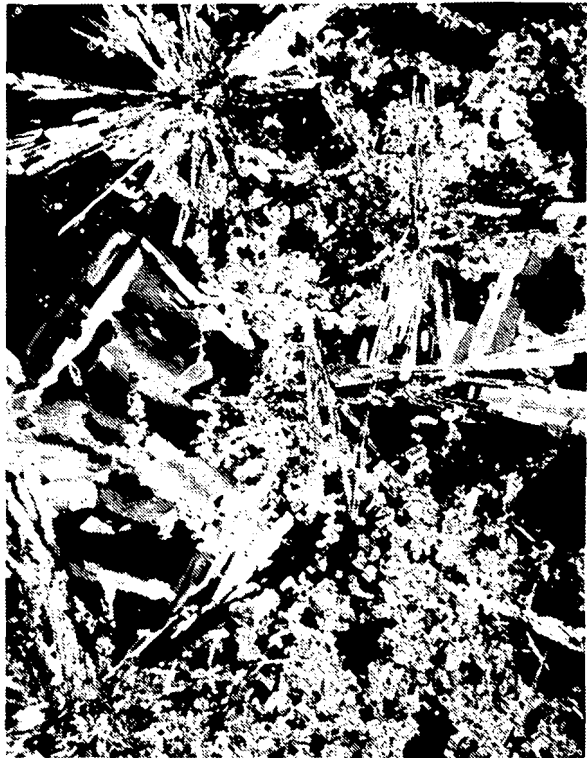
A



B



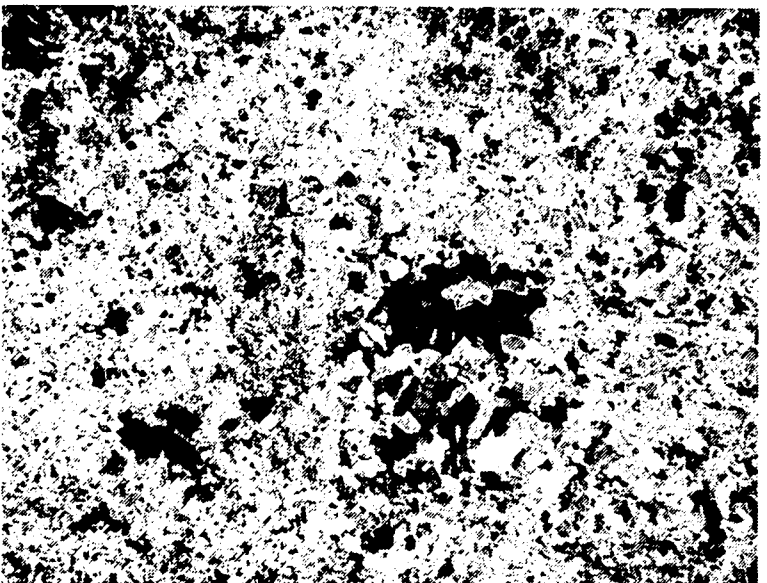
C



D

Plate 5
Sample PX5

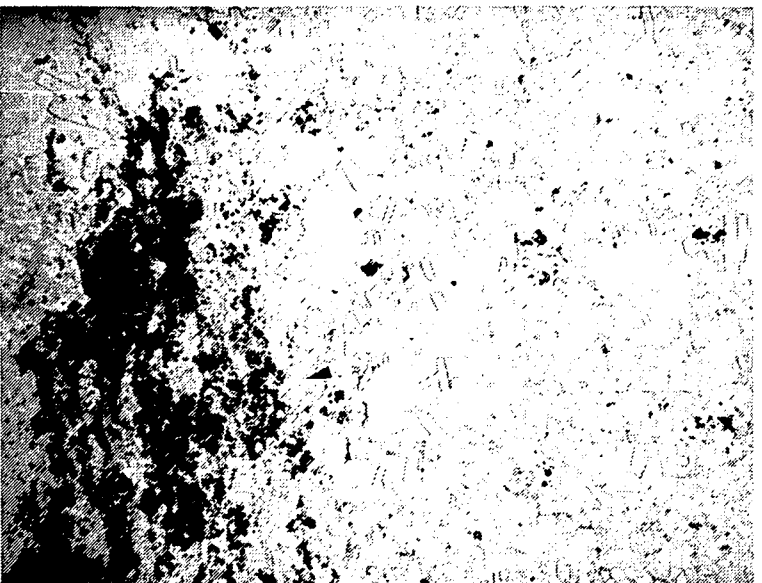
- A. Low magnification view of relatively coarsely crystalline anhydrite with minor halite. Anhydrite in this sample appears coarser than in the overlying or underlying sample. Minor carbonate (dolomite?) appears dark in the lower left. Crossed-nicols. (20×)
- B. Low magnification view of high-angle fractures in thin section PX5-O2. Fractures are near vertical and commonly terminate at the interface between different minerals. Anhydrite and halite are the dominant mineral constituents. Minor carbonate (dolomite?), which appears as small dark patches, is scattered throughout. Plane-polarized light. (20×)
- C. Overview showing the distribution of mineral components in thin section PX5-O3. Halite and anhydrite dominate the upper portion of the view. Many anhydrite crystals appear tabular in this view. Halite fills space between anhydrite crystals. Finely crystalline carbonate, probably dolomite, appears dark and is most abundant in the lower portion of the view. Plane-polarized light. (40×)
- D. Same view as the previous photomicrograph showing mineral distribution. Crossed-nicols. (40×)



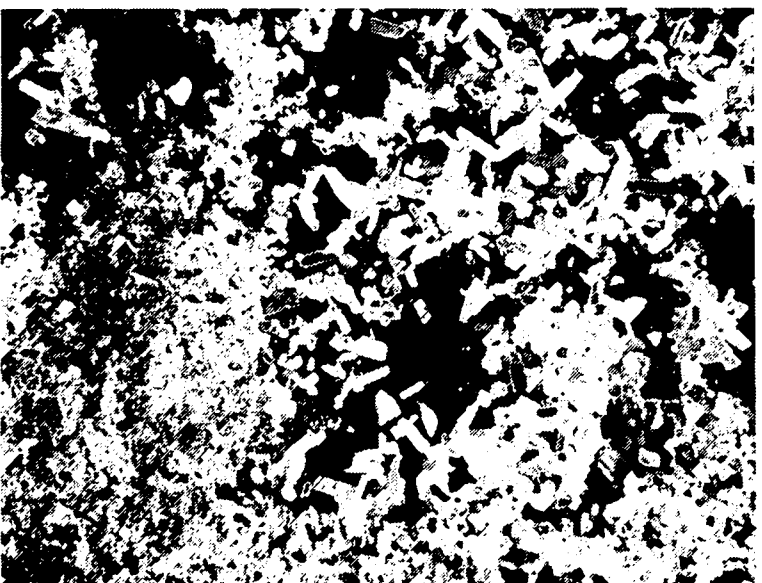
A



B



C

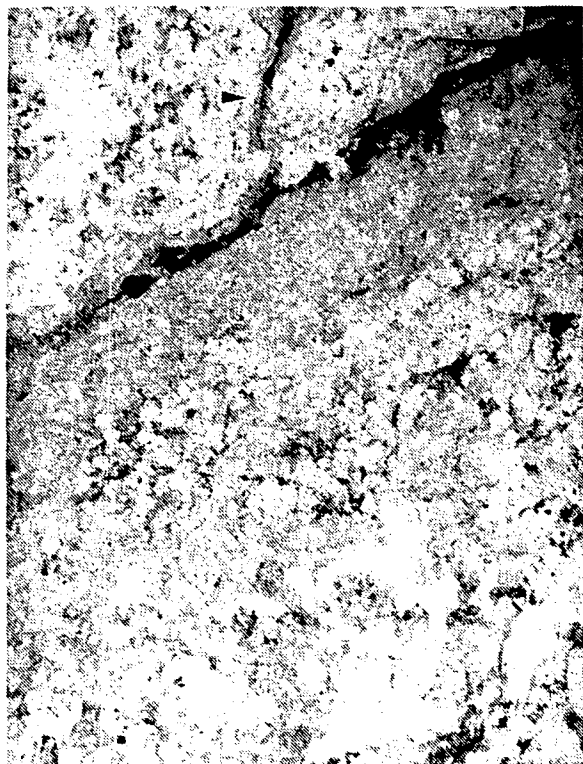


D

Plate 6
Sample PX6

- A. Low magnification view of thin section PX6-O1. A narrow high-angle fracture (arrow) in the upper portion of the view terminates at a thin carbonate lamination. Intergrown anhydrite and halite dominate the matrix. Minor pyrite (black patches) is seen in the carbonate lamination in the upper portion of the view. Plane-polarized light. (20×)
- B. Low magnification view showing a near vertical fracture in thin section PX6-O2. A fracture oriented subparallel to bedding is also seen in the upper portion of the view. Some laminae in this sample are dominated by anhydrite, whereas others contain both anhydrite and halite. Crossed-nicols. (20×)
- C. Overview of a lamination containing both halite and anhydrite in thin section PX6-O2. Anhydrite around halite crystals appears more coarsely crystalline than in the matrix away from halite nodules. Crossed-nicols. (40×)
- D. Overview of a healed fracture (arrow) in thin section PX6-O3. This fracture is primarily filled by anhydrite, but a very narrow aperture is present in the center. Anhydrite dominates the matrix. This fracture also appears parallel to narrow open fractures in other portions of the thin section. Plane-polarized light. (40×)

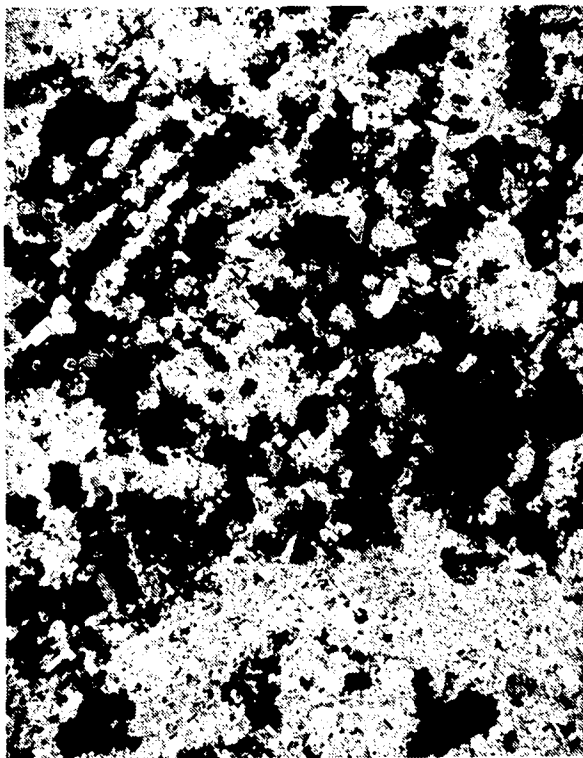
Plate 6



A



B



C



D

7.0 Effective Porosity, Total Porosity, and Saturation

The bulk volumes V_b of the intact samples (A-F and EP1-8) were determined from the volume of fluid displaced when the samples were immersed in water (see Appendix C-A). Samples were first coated with wax to prevent the water from penetrating the sample and the data were corrected for the amount of fluid volume displaced by the wax. (Note that for several samples (A-C, F, and EP4-8) which were later saturated with Odorless Mineral Spirits (OMS), V_b was remeasured by directly submerging the saturated sample in OMS and measuring the mass of fluid displaced. These measurements are believed to be more accurate than the waxed measurements (since they do not require a correction for the amount of fluid displaced by the wax); however, these data are not used in subsequent calculations since they were not available for all samples. We simply make note of the fact that the two sets of measurements for the seven samples all agreed to within 0.30%.)

Boyle's law helium gas porosimetry was used to determine the effective grain volume $V_{g\text{ eff}}$ of the intact samples A-F and EP1-EP8 (Appendix C-A). Data are reported in Table 6, where the effective (i.e. interconnected) porosity ϕ_{eff} is defined by

$$\phi_{\text{eff}} = 1 - \frac{V_{g\text{ eff}}}{V_{\text{bulk}}} \quad (1)$$

Samples EP4-8 were subsequently powdered for determination of total porosity (see Appendix C-A). Because mass is not fully conserved during the (initially violent) powdering process, data are normalized with respect to mass to obtain the bulk density ρ_b (for the intact sample) and the (true) grain density ρ_g for the powdered sample. Data are reported in Table 7, where the total porosity ϕ is defined by

$$\phi = 1 - \frac{\rho_b}{\rho_g} \quad (2)$$

The largest difference between the effective and total porosity for the four samples on which both measurements were performed is 0.2%; however, no discrepancy may be formally identified since the two measurements for all samples agree within the experimental errors. Note that the data for sample EP2 suggests that the total porosity may be somewhat *less* than the effective porosity (again, the two measurements technically agree within the experimental errors). Sample EP2 experienced the largest loss of material loss during the powdering process (19 g, or 8% of the original sample mass). It is likely that this loss of 8 wt% of the original sample is the cause for the slight discrepancy between the measurement of effective versus total porosity for EP2. This inference is consistent with the pervasive heterogeneity which characterizes the MB 139 samples (e.g., Figures 13 and 14 and Section 9).

Samples EP4-8 and samples A, C, and F were vacuum saturated with a non-reactive fluid (odorless mineral spirits) for determination of maximum achievable saturation (Appendix C-A).

Table 6. Bulk Volume, Effective Grain Volume, and Effective Porosity*

Sample	V_b (cc)	$V_{g\text{eff}}$ (cc)	$\phi_{g\text{eff}}$ (%)
A	822.84±4.94	807.47±3.23	1.87±0.71
B	776.83±4.66	723.00±3.09	0.49±0.72
C	819.62±4.92	811.31±3.25	1.01±0.71
D	803.84±4.82	798.00±3.19	0.73±0.72
E	843.08±5.06	829.98±3.32	1.55±0.71
F	815.25±4.89	807.09±3.23	1.00±0.71
EP1	83.47±0.50	82.39±0.21	1.29±0.64
EP2	84.39±0.51	83.75±0.21	0.75±0.64
EP3	83.54±0.50	83.19±0.21	0.42±0.64
EP4	83.35±0.50	82.01±0.21	1.60±0.64
EP5	84.85±0.51	83.22±0.21	1.92±0.64
EP6	84.04±0.50	81.74±0.20	2.73±0.63
EP7	83.73±0.50	83.27±0.21	0.55±0.64
EP8	84.52±0.51	83.19±0.21	1.57±0.64

* Quoted uncertainties are derived from formal propagation of random and systematic errors [8]. Sources for systematic error in V_b include pressure transducer accuracy, porosimeter calibration (two constants), and random error is calculated from duplicate measurements. Error in V_b is estimated at 0.6%, based upon comparison of waxed-buoyant measurements with those determined from direct OMS buoyant measurements (see text) and includes an allowance for systematic errors in OMS measurements due to accuracy of digital balances and uncertainty in density of OMS (which was measured directly).

for procedures). Data are reported in Table 8. Calculated saturations for the four smaller samples (EP5-8) are in excess of 100%; however, the associated uncertainties are substantial. The largest source of error, which is not readily quantifiable, apparently results from the moisture-sensitivity of the samples. The samples were moisture-equilibrated in a constant temperature and humidity oven at conditions (60°C, 45% R.H.) which deviated substantially from the ambient conditions. The four EP samples were all found to have experienced some weight gain during the period following the gas porosimetry measurement of effective grain volume and prior to the liquid saturation, even though the samples were plastic-wrapped and stored in ziploc bags during the interim. An additional complication is the change in pore volume, due to a loss of absorbed and/or adsorbed water, which probably occurred during the evacuation process preceding liquid saturation. It is believed that the resultant changes in pore volume, while small in the absolute sense are nevertheless significant relative to the very small pore volume of the EP samples, and the cause of the calculated unphysical (>100%) saturations. Additional support for this hypothesis is offered by the observed inverse relationship between over-saturation and

Table 7. Bulk Density, Grain Density, and Total Porosity*

Sample	ρ_b (g/cc)	ρ_g (g/cc)	ϕ (%)	$M_{original}^\dagger$ (%)
EP1	2.530±0.006	2.566±0.005	1.40±0.30	98
EP2	2.643±0.006	2.658±0.005	0.56±0.29	92
EP3	2.574±0.006	2.585±0.005	0.43±0.30	98
EP4	2.836±0.006	2.882±0.005	1.60±0.49	94

* Quoted uncertainties are derived from formal propagation of random and systematic errors [8]. Error in mass determination includes random errors derived from duplicate measurements and systematic errors due to balance accuracy. Sources for systematic error in V_g include pressure transducer accuracy, porosimeter calibration (two constants), and random error calculated from duplicate measurements. Error in V_b is based upon comparison of waxed-buoyant measurements with those determined from direct OMS buoyant measurements (see text) and includes an allowance for systematic errors in OMS measurements due to accuracy of digital balances and uncertainty in density of OMS (which was measured directly).

† Percentage of original sample mass used for determination of total porosity. (Reduction is due to material losses which occur during the powdering process.)

Table 8. Liquid (OMS) Saturation*

Sample	m_s (g)	m_d (g)	V_b (cc)	$V_{g,eff}$ (cc)	S
EP5	220.998±0.002	219.596±0.002	84.85±0.51	83.22±0.21	1.2±0.3
EP6	222.678±0.004	220.796±0.002	84.04±0.50	81.74±0.20	1.1±0.2
EP7	234.143±0.003	233.502±0.002	83.73±0.50	83.27±0.21	1.9±1.2
EP8	230.016±0.005	228.722±0.002	84.52±0.51	83.19±0.21	1.3±0.4
A	2151.88±0.04	2140.18±0.04	822.84±4.94	807.47±3.23	1.0±0.4
C	2214.84±0.04	2208.66±0.04	819.62±4.92	811.31±3.25	1.0±0.7
F	2333.49±0.04	2327.39±0.04	815.25±4.89	807.09±3.23	1.0±0.7

* Quoted uncertainties are derived from formal propagation of random and systematic errors [8]. Sources for systematic error in m_s and m_d include digital balance accuracy and random error (for m_s) is calculated from duplicate measurements. The density of the saturant (OMS) was measured directly with a calibrated pycnometer and digital balance and is 0.753±0.011 g/cc. Error in fluid density includes uncertainty caused by small temperature fluctuations. Sources for systematic error in $V_{g,eff}$ include pressure transducer accuracy, porosimeter calibration (two constants), and random error calculated from duplicate measurements. Error in V_b is estimated at 0.6%, based upon comparison of waxed-buoyant measurements with those determined from direct OMS buoyant measurements (see text) and includes an allowance for systematic errors in OMS measurements due to accuracy of digital balances and uncertainty in density of OMS (which was measured directly).

pore volume. (Note that for consistency, the "dry" mass used in the saturation calculation is that determined at the time of the effective porosity measurement. Although it is known that the "dry" mass immediately prior to saturation differs, it would be inconsistent to apply this data since the porosity to go along with this second "dry" state is unknown.)

8.0 Single Phase Permeability

8.1 Gas Single-Phase Permeability

Single-phase gas (nitrogen) permeabilities were measured for samples A-F at three effective stress conditions (2, 6, and 10 MPa) using the steady state technique (see Appendix C-A for a schematic of the experimental assembly and procedures). Apparent gas permeabilities k_g were measured at four different mean pore pressures at each effective stress condition (Table 9) and used to calculate Klinkenberg (a.k.a. equivalent liquid) permeabilities k_w (Table 10). (Raw data are compiled in Appendix C-D).

8.2 Liquid Single-Phase Permeability

Single-phase liquid permeabilities k_l were measured at three effective stress conditions (2, 6, and 10 MPa) using the steady state technique (see Appendix C-A for a schematic of the experimental assembly and procedures) for samples A, C, and F (see Section 7.0 and Table 8 above for saturation data). The calculated permeabilities are reported in Table 11. (Raw data are included in Appendix C-E).

The measurements of liquid permeability agree well with the calculated Klinkenberg permeabilities. The differences for seven out of the nine data sets fall within the experimental errors, although the liquid permeabilities do appear, on average, to be systematically lower than the extrapolated Klinkenberg permeabilities.

Table 9. Single Phase Gas Permeability*

Sample	$P_{c\ off}$ (MPa)	$P_{p\ mean}$ (MPa)	k_g (μ Da)
A	2	0.2725	12.3 \pm 0.2
		0.3405	11.6 \pm 0.2
		0.4090	11.0 \pm 0.2
		0.4779	10.6 \pm 0.2
	6	0.2728	8.88 \pm 0.14
		0.3397	8.40 \pm 0.13
		0.4105	7.82 \pm 0.12
		0.4787	7.56 \pm 0.12
	10	0.2716	7.29 \pm 0.11
		0.3421	6.84 \pm 0.11
		0.4100	6.55 \pm 0.10
		0.4795	6.31 \pm 0.10
B	2	0.2797	19.8 \pm 0.3
		0.3475	18.5 \pm 0.3
		0.4176	17.5 \pm 0.3
		0.4881	16.8 \pm 0.3
	6	0.2758	13.2 \pm 0.2
		0.3464	12.1 \pm 0.2
		0.4166	11.3 \pm 0.2
		0.4878	10.7 \pm 0.2
	10	0.2755	8.23 \pm 0.13
		0.3452	7.54 \pm 0.11
		0.4159	7.02 \pm 0.11
		0.4867	6.69 \pm 0.10

* Quoted uncertainties are derived from formal propagation of random and systematic errors [8]. Sources for systematic error in k_g include pressure transducer accuracy (differential, gauge, and barometric), accuracy of flow rate measurement (volume and time), caliper accuracy, and uncertainty in temperature measurements. Random error included in flow rate error is calculated from 4 duplicate measurements. Gas viscosity is 0.0176 cp [9].

Table 9. Single Phase Gas Permeability* (continued)

Sample	$P_{c, eff}$ (MPa)	$P_{p, mean}$ (MPa)	k_g (μ Da)
C	2	0.2871	7.84 \pm 0.12
		0.3559	7.26 \pm 0.11
		0.4224	6.81 \pm 0.10
		0.4940	6.50 \pm 0.10
	6	0.3337	5.41 \pm 0.08
		0.3552	4.86 \pm 0.07
		0.4236	4.49 \pm 0.07
		0.4787	4.25 \pm 0.07
	10	0.3361	4.09 \pm 0.06
		0.3545	3.67 \pm 0.06
		0.4248	3.41 \pm 0.05
		0.4940	3.21 \pm 0.05
D	2	0.4686	0.275 \pm 0.014
		0.5453	0.261 \pm 0.013
		0.6224	0.238 \pm 0.012
		0.6787	0.239 \pm 0.012
	6	0.4743	0.127 \pm 0.007
		0.5439	0.120 \pm 0.006
		0.6142	0.113 \pm 0.006
		0.6875	0.106 \pm 0.005
	10	0.4743	0.088 \pm 0.004
		0.5431	0.083 \pm 0.004
		0.6111	0.080 \pm 0.005
		0.6856	0.078 \pm 0.004

* Quoted uncertainties are derived from formal propagation of random and systematic errors [8]. Sources for systematic error in k_g include pressure transducer accuracy (differential, gauge, and barometric), accuracy of flow rate measurement (volume and time), caliper accuracy, and uncertainty in temperature measurements. Random error included in flow rate error is calculated from 4 duplicate measurements. Gas viscosity is 0.0176 cp [9].

Table 9. Single Phase Gas Permeability* (continued)

Sample	$P_{c, eff}$ (MPa)	$P_{p, mean}$ (MPa)	k_g (μ Da)
E	2	0.1023	1168 \pm 19
		0.1711	1054 \pm 17
		0.2401	997 \pm 16
		0.3086	927 \pm 15
	6	0.1192	497 \pm 8
		0.1980	426 \pm 7
		0.2660	398 \pm 6
		0.3345	382 \pm 6
	10	0.1290	292 \pm 5
		0.1968	253 \pm 4
		0.2671	218 \pm 4
		0.3342	208 \pm 3
F	2	0.4510	1.77 \pm 0.03
		0.5233	1.69 \pm 0.02
		0.5908	1.62 \pm 0.02
		0.6581	1.57 \pm 0.02
	6	0.4524	1.23 \pm 0.02
		0.5193	1.15 \pm 0.02
		0.5921	1.11 \pm 0.02
		0.6597	1.06 \pm 0.02
	10	0.4525	1.06 \pm 0.016
		0.5176	0.99 \pm 0.01
		0.5911	0.95 \pm 0.01
		0.6636	0.91 \pm 0.01

* Quoted uncertainties are derived from formal propagation of random and systematic errors [8]. Sources for systematic error in k_g include pressure transducer accuracy (differential, gauge, and barometric), accuracy of flow rate measurement (volume and time), caliper accuracy, and uncertainty in temperature measurements. Random error included in flow rate error is calculated from 4 duplicate measurements. Gas viscosity is 0.0176 cp [9].

Table 10. Calculated Klinkenberg Permeability

Sample	$P_{c,eff}$ (MPa)	k_{∞} (μ Da)
A	2	8.36 \pm 0.12
	6	5.76 \pm 0.20
	10	5.05 \pm 0.03
B	2	12.76 \pm 0.09
	6	7.50 \pm 0.12
	10	4.67 \pm 0.04
C	2	4.63 \pm 0.06
	6	2.63 \pm 0.03
	10	2.01 \pm 0.02
D	2	0.147 \pm 0.019
	6	0.060 \pm 0.004
	10	0.055 \pm 0.008
E	2	836 \pm 28
	6	307 \pm 19
	10	155 \pm 8
F	2	1.13 \pm 0.02
	6	0.70 \pm 0.03
	10	0.58 \pm 0.01

Table 11. Single Phase Liquid Permeability* vs Calculated Klinkenberg Permeability

Sample	$P_{c,eff}$ (MPa)	k_l (μ Da)	k_w (μ Da)
A	2	6.75 \pm 1.36	8.36 \pm 0.12
	6	5.76 \pm 0.65	5.76 \pm 0.20
	10	5.37 \pm 0.60	5.05 \pm 0.03
C	2	3.66 \pm 0.40	4.63 \pm 0.06
	6	2.43 \pm 0.27	2.63 \pm 0.03
	10	1.83 \pm 0.20	2.01 \pm 0.02
F	2	1.06 \pm 0.12	1.13 \pm 0.02
	6	0.62 \pm 0.07	0.70 \pm 0.03
	10	0.52 \pm 0.06	0.58 \pm 0.01

* Quoted uncertainties are derived from formal propagation of random and systematic errors [8]. Sources for systematic error in k_l include differential pressure transducer accuracy, accuracy of flow rate measurement (volume and time), caliper accuracy, and uncertainty in fluid viscosity. Random error is calculated from at least 5 duplicate measurements. Experimental measurement of OMS viscosity is 1.29 cp with an assumed maximum uncertainty of 10%.

9.0 Summary and Recommendations

The laboratory investigations demonstrate that Marker Bed 139 is characterized by significant and pervasive heterogeneity. Remarkable heterogeneity occurs as the marker bed is traversed vertically, and some variability is also apparent as the marker bed is traversed laterally. Mineralogy varies dramatically, and although porosity is typically $-0.5-3.0\%$, permeability varies by approximately four orders of magnitude (e.g., from tenths of microdarcies to hundreds of microdarcies at an effective pressure of 2 MPa).

Attempts to use a second-generation x-ray CT scanner to identify natural and coring-induced fractures were unsuccessful, due to the large diameter of the core material (6 inches) and high bulk density (close to 3 g/cc). Several attempts to compensate and/or correct for pronounced image artifacts caused by excessive beam-hardening were unsuccessful. However, preliminary scoping tests which were performed with a more powerful and advanced third-generation CT scanner (acquired midway through the contract performance period) yielded promising results. Thus, with the newer CT technology it may be possible to perform highly detailed non-destructive lithologic evaluations. Also, fractures with apertures on the order of tenths of millimeters should be resolvable with the more advanced scanner.

The marker bed exhibits four distinct mineralogic zones. The upper portion is rich in polyhalite, which is manifested by a conspicuous salmon-pink color. Halite and anhydrite are also major mineral phases in this section, as are dolomite and aragonite. The central region contains both anhydrite and halite, which occur in varying proportions and account for nearly all of the solid phase. The lower portion of this central region is dominated by anhydrite with markedly smaller (<20%) amounts of halite. The very bottom of the marker bed is significantly more fine-grained than the rest of the marker bed; unfortunately, this section is limited in length (4-5") and thus no samples for detailed testing were prepared from this region. CT scans, however, indicate that this region is the densest part of the entire marker bed. Thus, this region may contain nearly 100% anhydrite, or possibly small amounts of very dense impurities such as pyrite (which was identified in thin-section).

The petrographic studies corroborate the general observations above and, moreover, indicate that marked heterogeneity can exist at even the cm scale. For example, the volumetric percentage of various minerals may vary by as much as 20 to 30% for samples prepared from locations separated by only two or three centimeters. The modal analyses based on 300-point counts consistently suggest the occurrence of several vol% (and sometimes as much as 16 vol%) of a carbonate phase, tentatively identified as dolomite, in each of the eighteen thin sections examined. Although the XRD analyses are recognized as only semi-quantitative in nature, the apparent absence of carbonate in four of the six samples tested is conspicuous. Although it is possible that the carbonate material is present only locally, it is more likely that the XRD analyses fail to identify carbonate in the MB139 samples because of variations in crystallinity and possibly mg/fe/ca cation ratios (as compared to the reference standards used to calibrate the diffractometer). Thus, depending upon the level of investigations to be performed in the future, it may be worthwhile to restrict further XRD analyses to a single institution and to invest in the development of a set of standards specific to the WIPP.

Measurements of effective and total porosity consistently indicate that the bulk porosity of the marker bed is quite low, and varies from 0.4% to 2.7%. The measurements of effective versus total porosity agree within the experimental errors. Permeability, however, varies by approximately four orders of magnitude (e.g., from tenths of microdarcies to hundreds of microdarcies at an effective pressure of 2 MPa). A permeability on the order of millidarcies was measured for one sample at an effective stress of 2 MPa and may represent fracture permeability. The other extreme is embodied by a single sample with a permeability on the order of tenths of microdarcies (i.e., hundreds of nanodarcies) at an effective stress of 2 MPa. Four other samples are characterized by permeabilities on the order of microdarcies. The measurements of liquid permeability agree well with calculated Klinkenberg (a.k.a equivalent liquid) permeabilities. The differences for seven out of the nine data sets fall within the experimental errors, although the liquid permeabilities do appear, on average, to be systematically lower than the extrapolated Klinkenberg permeabilities.

Calculations of achievable saturation suggest that complete saturation is probably attained by routine vacuum saturation; however, the experimental errors are significant given the excessively small pore volumes of the samples. Interpretation is further complicated by possible changes in pore volume caused by the apparent adsorption and/or absorption of moisture from the atmosphere which occurred while samples were between various parts of the testing program. Although very small in the absolute sense, the hypothesized changes in pore volume are significant in the relative sense. Thus, it may be advisable to either equilibrate samples to local atmospheric conditions or else make provisions to acquire a constant temperature and constant humidity oven dedicated exclusively to the test program.

10.0 References

1. Davies, P. B., Evaluation of the role of threshold pressure in controlling flow of waste-generated gas into bedded salt at the Waste Isolation Pilot Plant, SAND90-3246, Sandia National Laboratories, Albuquerque, New Mexico, 1991.
2. A. M. Petrovic et al., Soil bulk density analysis in three dimensions by computed tomographic scanning, *Am. J. Soil Sci. Soc.*, v. 46, p. 445-450, 1982.
3. P. K. Hunt et al., Computed tomography as a core analysis tool: Applications, instrument evaluation, and image improvement techniques, *J. Pet. Tech.*, 1203-1210, (Sept.) 1988.
4. Brown et al., Accuracy of gamma ray computerized tomography in porous media, *Water Resour. Res.*, 29, 479-486, 1993.
5. Johns et al., Nondestructive measurements of fracture aperture in crystalline rock cores using x ray computed tomography, *J. Geophys. Res.*, 98, 1889-1900, 1993.
6. H. J. Vinegar & G. E. Hill, Beam-hardening corrections on the DeltaScan 100 CT Scanner, Report No. BRC-2044, Shell Development Company, Houston, 1988 (Company Confidential).
7. Rock Characterization, Testing, and Monitoring: ISRM Suggested Methods, E. T. Brown (Ed.), 211 p., Pergamon Press, New York.
8. J. R. Taylor, An Introduction to Error Analysis: The Study of Uncertainties in Physical Measurements, Oxford University Press, 1982.
9. Handbook of Chemistry and Physics, 66th ed., CRC Press, Inc., Florida, 1985.

APPENDIX C-A: Procedures

A.1 X-Ray Computerized Tomography

A.1.1 Background. Computerized tomography (CT) is a non-destructive technique for the evaluation of the internal structure of a material. Imaging technology is based on the analysis of the attenuation of x-rays as they pass through a material. This attenuation is due to scattering and adsorption and is characterized by Beer's law:

$$I = I_0 e^{-\alpha x} \quad (3)$$

where I_0 and I are the incident and attenuated x-ray intensity, x is the thickness of the material, and α is the linear attenuation coefficient.

The attenuation of the x-rays is dependant on photoelectric adsorption and Compton scattering. Photoelectric adsorption is dependent on the electron density or the effective atomic number of the material and is a predominant term at x-ray energies below 100 kV. Compton scattering is dependent on the density of the material and becomes a more predominant term at energy levels above 100 kV. Thus, the attenuation coefficient for a material depends upon both the density and effective atomic number of the material as well as the energy level of the x-ray:

$$\alpha = \rho \left(a + \frac{bZ^{3.8}}{E^{3.2}} \right) \quad (4)$$

where ρ is the mass density of the material, Z is the effective atomic number, E is the x-ray energy level, a is the Klein-Nishina coefficient, and b is a constant. At high energy levels, and for materials with similar chemical composition, differences in the effective atomic number are small. Differences in attenuation are thus due primarily to differences in mass density.

A.1.2 TerraTek's CT Facility. At the start of the performance period for this contract, TerraTek's CT facility employed an Ohio Nuclear DeltaScan 100. The DeltaScan 100 is a second generation medical CT imaging machine and TerraTek's scanner was originally built in 1980 for use as a head scanner. No hardware modifications were made to the scanner for use as a material imager. When a test sample is inserted in the scanner, an x-ray source and detector are passed in parallel planes past the sample (called a traverse). The tube and detector are then rotated through a specified number of degrees and another traverse occurs. This is repeated through a 180-degree rotation. A cross-sectional image of the test sample can then be generated by dividing the sample up into small discrete elements (or pixels) and solving a set of linear equations. The linear attenuation coefficient for each element can be determined through reconstruction algorithms intrinsic to the scanner's computer.

The x-ray beam is collimated into three fan shaped beams which are attenuated as they pass through the sample. The width of the beam, which determines the volume of material (voxel) for which linear attenuation coefficients are calculated, can be adjusted from 3 to 10 mm. The attenuated x-rays are measured by three detectors with measurements recorded every 3° in a 180° rotation. Each image requires two minutes to complete the 60 scans. The maximum diameter of a sample is limited to 305 mm. However, with large samples resolution is decreased since

the pixel array is fixed at 256×256 . Also, for some materials the maximum diameter must be reduced to insure successful X-ray penetration.

The data array is composed of CT numbers which are defined as normalized attenuation coefficients for the material being scanned. Cross-sectional images may reveal the presence of open fractures, filled fractures, vugs, and mineral inclusions. Broken or crushed sections of core can be identified before the sample is removed from its packaging, aluminum casing, or rubber sleeves. Vertical reconstructions are built from a series of cross-sectional images. Six contiguous rows or columns (in either the x or y direction) of data elements for each cross section in the series are averaged. For discontinuous scanning, the image is completed by interpolating between scans. The resultant image represents the core as it would appear if it were slabbed through the x or y plane as defined above. The software utilized to process the CT data is Shell Development Company's CATPIX programming, which was licensed to TerraTek in 1987. Although modifications were made to the graphics display software, no modifications were made to the fundamental algorithms used to process the data.

During the performance period for this contract, TerraTek constructed a new, more advanced CT facility employing a third generation Philips 60/TX CT scanner. The Philips 60/TX provides significantly greater resolution and imaging capabilities and TerraTek has since discontinued use of its original second generation CT facility. TerraTek has also developed a software for advanced CT analysis which provides automatic numerical correction for beam-hardening, density and atomic number determination, and many other features. The C++ software is implemented on a Sun SparcStation 10 and marketed under the name CORESCAN™. The new CT facility was used only for exploratory (scoping) work under the present contract, and the operating procedures described below refer to the DeltaScan 100.

A.1.3 Operating Procedures. The scan tube was mounted on to a table designed by Shell Development Company which provides positioning control of the sample to within 0.002 inch. Positions were measured by an Acu-Rite III scale assembly which is mounted onto the table and the scanning sequence (consisting of the number of scans, the distance which the scan table moves between scans, and the feed rate) were programmed into an Aerotech Unidex IIIa Motion Controller. The position of the first scan was indicated by a fixed light source. The gantry system and data acquisition were controlled by a VAX PDP 11/04 computer system. Scan data acquired with the VAX PDP 11/04 was transferred to magnetic tape, and then to a Microvax II GPX color graphics work station.

The data array generated by the scanner is composed of CT numbers which are defined as normalized attenuation coefficients for the material being scanned. CT numbers are defined as follows:

$$CT\# = K \frac{\mu_{PIX} - \mu_{PHA}}{\mu_{PHA}} \quad (5)$$

where μ_{PIX} is the attenuation coefficient of the pixel being measured, μ_{PHA} is the attenuation coefficient of the "phantom" used to generate the non-linear coefficients for the back projection

algorithm, and K is a constant. The phantom used for calibration depends upon the material to be scanned. For example, for medical scanning of human subjects, a phantom filled with distilled, deionized water is used to calibrate the CT number scale so that the CT number of water equals zero. For scanning of geologic materials, TerraTek uses a 4.17 inch diameter fused quartz standard. The fused quartz standard is mounted on a platform so that the standard extends beyond the platform into the plane of the CT scan traverse; essentially, the quartz standard is suspended in air. The nonlinear coefficients are generated by software which is part of the Ohio Nuclear DeltaScan 100 programming such that the CT number of the fused quartz standard is equal to zero.

Consistency is maintained by scanning a second 0.978 inch diameter fused quartz standard in the scan tube immediately after the nonlinear coefficients are obtained. The average CT number of this standard is calculated based upon a Region of Interest (ROI) equal to approximately 80% of the sample diameter (to avoid any data distortion at the circumference of the standard). This standard is then scanned before each programmed sequence of scans and the average CT number is compared to the initial CT value obtained for the standard. Any variance can be corrected for using another routine in the DeltaScan 100 programming.

The manufacturer's general operating procedures¹ for the CT Scanner were adhered to during use.

A.1.4 Imaging of fluid flow through cores. Dynamic flow tests may be performed in which a non-reactive highly attenuating liquid is injected into a core sample and scanned as the fluid front penetrates the sample. A common dopants is sodium iodide. For flow tests which are conducted under elevated hydrostatic pressures, grooved end plugs and mesh screens are mounted on each end of the sample to insure that flow is homogeneous across the sample end faces. The sample and end plugs are then jacketed in a viton sleeve and pressure taps are located at each end of the sample. The pressure taps are connected to a differential pressure transducer and the pressure difference between the upstream and downstream ends is recorded on an X-Y plotter. The sample assembly is then placed in an aluminum pressure vessel and mounted in the scanner.

Before beginning fluid flow, the sample is scanned under hydrostatic stress conditions to establish the initial test condition. This condition is assumed to represent zero saturation. Once the initial conditions have been established, fluid flow begins at a constant rate until a stable differential pressure is achieved. Scanning can be performed intermittently to investigate saturation phenomena such as fingering. Under steady-state flow, the core can be scanned continuously to establish saturation profiling and liquid content distribution. A series of cross-sectional images at steady-state can be displayed perpendicular to the axis of the core and pore fluid imbibition can be identified by variations in the color assignments. The saturation for each location can also be determined along the length of the core.

¹Operator's Manual Delta Scan 100 Series Brain Scanner, Manual No. 961036 Revision B, Technicare Corporation, Ohio, 1980.

A.2 X-Ray Diffraction (XRD) Analyses

XRD analyses were performed by the University Of Utah Research Institute in accordance with guidelines provided in reference texts.^{2,3,4} In preparation for bulk XRD analysis, an approximately 50 gram sample was crushed to <18 mesh (<1 mm) and thoroughly homogenized to ensure that the portion to be analyzed was representative of the whole sample. A one gram split of the crushed sample was then ground in acetone in an agate mortar to <325 mesh (<45 μm). The powdered split was then completely mixed by rolling it on weighing paper. The powder was then x-rayed at $2^\circ 2\theta$ per minute from 10 - $65^\circ 2\theta$ and $1^\circ 2\theta$ per minute from 2 - $10^\circ 2\theta$ using a Phillips XRG-3100 diffractometer.⁵ A quartz standard⁶ was x-rayed at the completion of each sample to monitor drift in x-ray intensity. Diagnostic peaks of minerals identified on the resulting diffractograms were rescanned on duplicate samples. Approximate weight percentages of mineral phases were determined by comparing diagnostic peak intensities with those generated by standard pure phases mixed in various known proportions. Results are reported in weight percent and are the average of three duplicate samples. Variables that can effect calculation of the proportion of each mineral phase in a sample include: matrix absorption, peak overlap, crystallinity and crystal size, amorphous or organic content, absorption factors, chemical substitution, preparation techniques, and detection limits. Although many of these variables can be controlled, some cannot; hence, the results of XRD analysis are semi-quantitative.

A.3 Petrographic Analyses

Petrography was conducted with a Leitz Laborlux 12 Pol polarizing microscope equipped with objectives of $2.5\times$ (0.08 numerical aperture (NA)), $6.3\times$ (0.2 NA), $25\times$ (0.55 NA), and $40\times$ (0.70 NA). Eye pieces were $10\times$, yielding possible magnifications $25\times$, $63\times$, $250\times$, and $400\times$. Photomicrographs were taken with a Nikon Labophot-pol polarizing microscope equipped with objectives of $2\times$ (0.08 NA), $4\times$ (0.2 NA), $10\times$ (0.50 NA), and $20\times$ (0.04 NA). Eye pieces were $10\times$, yielding possible magnifications of $20\times$, $40\times$, $100\times$, and $200\times$. The camera system was a Nikon UFX automatic system with a Nikon FX-35A camera body.

²*Methods & Practices in X-Ray Powder Diffraction*, R. Jenkins (Ed.), JCPDS— International Centre for Diffraction Data, 1986.

³Starkey, H. C., P. D. Blackmon, and P. L. Hauff, The routine mineralogical analysis of clay-bearing samples, *U.S. Geol. Surv. Bull.* 1563, 32p., 1984.

⁴Moore, D. M., and R. C. Reynolds, *X-ray Diffraction and the Identification and Analysis of Clay Minerals*, Oxford University Press, 332p., New York, 1989.

⁵The UURI maintains a service contract with Philips Electronic Instruments which includes two preventive maintenance checks per year.

⁶The quartz standard was supplied as part of the standard stock package when the XRD machine was purchased from Philips Electronic Instruments.

Three mutually perpendicular thin sections were prepared from each PX sample (Figure A1). Sections were mounted on a Leitz #553428 mechanical stage for point count analysis (300 points). Grain/crystal size was measured using a micrometer reticle in the eyepiece which was calibrated to a Zeiss 5+100/100 calibration plate. Size determinations are accurate to approximately 10 μm . Imaging problems necessarily arise with objects whose dimensions are less than the thickness of the thin section.

Minerals were identified using standard petrographic techniques, such as appearance, extinction, birefringence, cleavage, crystal habit, pleochroism, and interference, following reference texts.⁷ Textural parameters follow Blatt et al.⁸ Sample composition and grain/crystal size were determined by point counts of 300 discrete points. Spacing between points was approximately 0.9 mm for the most commonly used objective. As the mechanical stage was moved to each point the object under the cross hairs was identified and diameter (defined as the longest axis for non-spherical objects) was measured for grains and crystals using the micrometer in the eyepiece. Histograms of grain size distribution were constructed using software developed by TerraTek.

A.4 Porosity Measurement

Gas porosimetry was used to determine the bulk ("effective") grain volume $V_{g\text{ eff}}$ of intact samples and the "total" grain volume V_g of powdered samples. The bulk volume V_b of intact samples was calculated from the fluid volume displaced by the submerged test sample (Archimedes principle). Masses of intact or powdered samples are determined with electronic balances. These data were used to calculate the interconnected ("effective") porosity ϕ_{eff} and total porosity ϕ :

$$\phi_{\text{eff}} = 1 - \frac{V_{g\text{ eff}}}{V_b} \quad (6)$$

$$\phi = 1 - \frac{\rho_b}{\rho_s} \quad (7)$$

where the bulk density ρ_b and grain density ρ_s are given by

$$\rho_b = \frac{m_d}{V_b} \quad (8)$$

⁷Deer, W. A., R. A. Howie, and J. Zussman, *An Introduction to the Rock Forming Minerals*, Longmans, Green, and Co., Ltd., London, 1966.

⁸Blatt, H., G. Middleton, and R. Murray, *Origin of Sedimentary Rocks*, Prentice Hall, Inc., New Jersey, 1980.

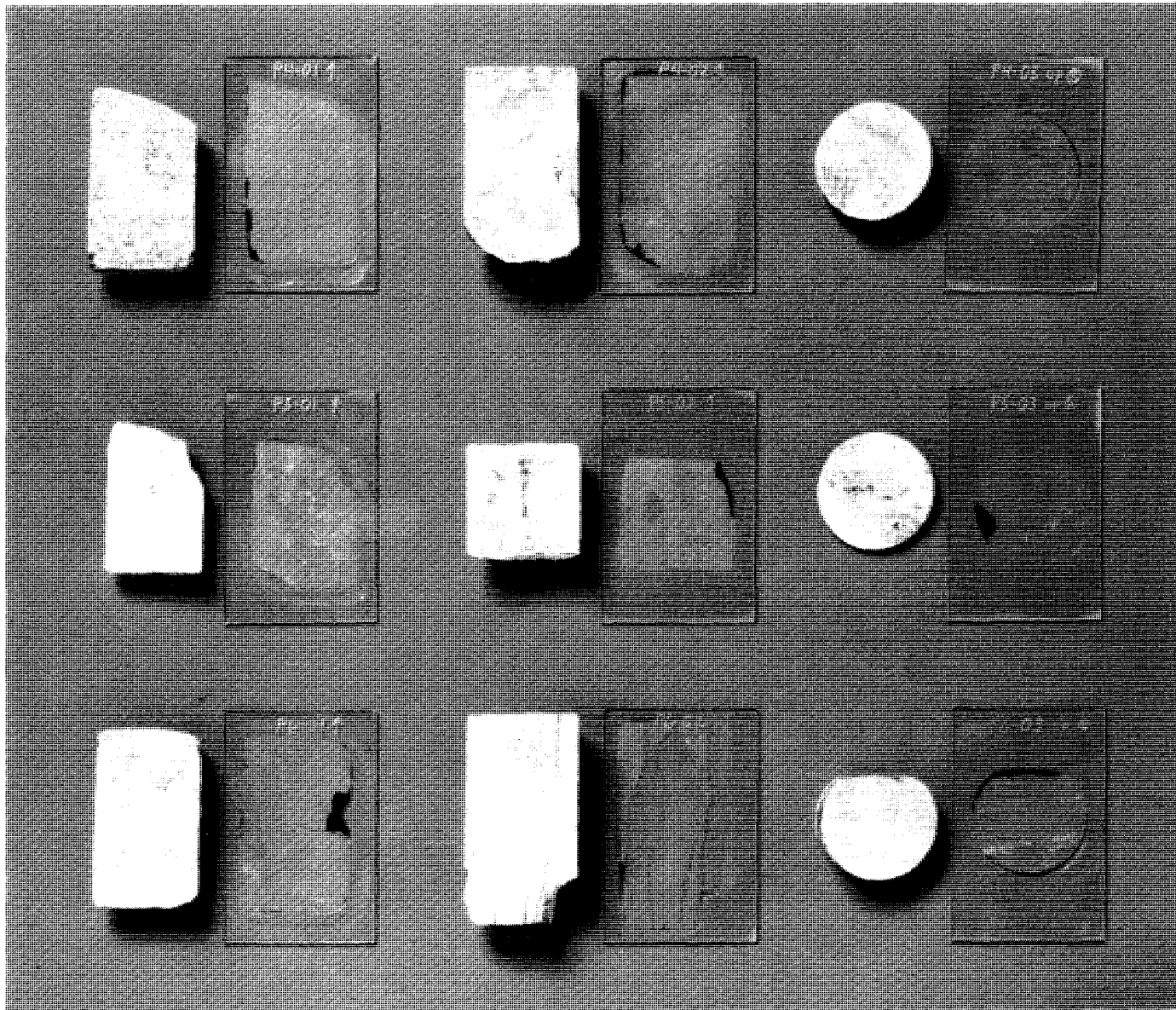


Figure A1a. Documentation of thin section preparation from PX samples from core E1X08-4.

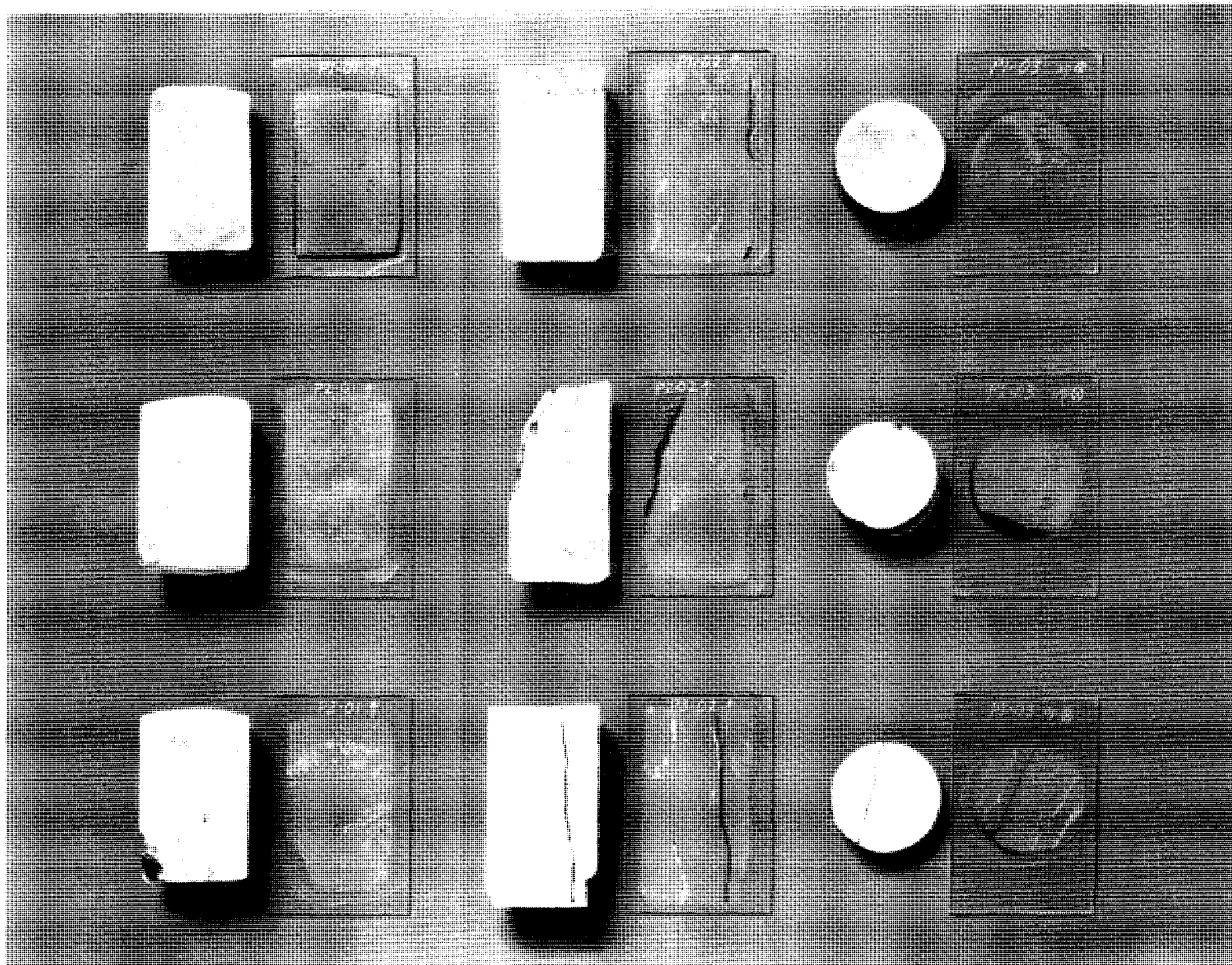


Figure A1b. Documentation of this section preparation from PX samples from core E1X08-4.

$$\rho_g = \frac{m_d}{V_g} \quad (9)$$

and m_d is the mass of either the dry intact or dry powdered sample. Note that because mass is not fully conserved during the powdering of the sample for determination of total porosity, the ratio of bulk and grain density is used to calculate porosity rather than the ratio of bulk and grain volumes.

A.4.1 Gas porosimetry. Gas porosimetry is based on Boyle's law which holds that for an ideal gas at constant temperature the volume of the gas will vary inversely with pressure:

$$\frac{P_1}{P_2} = \frac{V_2}{V_1} \quad (10)$$

where P_1 is the initial pressure in the initial volume V_1 and P_2 is the final pressure in the final volume V_2 . Calibration of TerraTek's custom-made gas expansion porosimeter was performed using a series of steel billets of known volume. A linear regression was performed to determine the relationship between the measured ratio P_1/P_2 and the sample volume. The measured pressure ratio with the sample in the porosimeter was then used to determine the grain volume $V_{g\text{ eff}}$ of the sample. Two duplicate runs were performed.

A.4.2 Bulk volume. Bulk volume was calculated from the fluid volume displaced when the test sample was submerged in fluid (Archimedes' principle).⁹ The volume of fluid displaced, which is equal to the sample bulk volume, is given by the difference between the weight in air and the buoyant weight divided by the temperature corrected density of the fluid. Samples were coated with wax so that fluid could not penetrate the sample (measurements were corrected for the volume of the wax). (Alternatively, saturated samples may be immersed directly.) The weight measurements are performed with appropriately ranged electronic balances. Temperature of the immersion fluid was measured to 0.1°C immediately following the weight measurements using a thermometer. As a check, the bulk volume of regularly shaped samples was also measured with calipers.¹⁰

A.4.3 Powdering for measurement of total porosity. Samples were crushed and pulverized to 350 mesh (approximately <46 microns) using a shatter box and then dried in a humidity-controlled oven for an additional 24 hours to drive off any adsorbed water the powder may have imbibed (e.g. from atmospheric humidity) during the pulverizing process. Following the second drying period, the powder was allowed to reach ambient temperature in a vacuum chamber.

⁹Rock Characterization, Testing, & Monitoring: ISRM Suggested Methods, E. T. Brown (Ed.), 211p., Pergamon Press, New York. Procedures for water displacement method for determination of bulk volume of solid and porous samples are outlined on p. 82.

¹⁰Rock Characterization, Testing, & Monitoring: ISRM Suggested Methods, E. T. Brown (Ed.), 211p., Pergamon Press, New York. Procedure for determination of bulk volume using the caliper method is given on p. 82.

A.5 Liquid Saturation

Cores were vacuum saturated with a non-reactive liquid, odorless mineral spirits (OMS). Samples were first subjected to vacuum, flooded with CO₂ (to facilitate displacement of any residual air), re-evacuated, and then flooded with OMS while under vacuum. Mass of the samples was measured using an appropriately ranged digital mass balances prior to and following saturation. The saturation S of the samples is given by:

$$S = \frac{\rho_s - \rho_d}{\phi_{eff} \rho_f} = \frac{\frac{(m_s - m_d)}{V_b}}{\frac{V_{\phi_{eff}} \rho_f}{V_b}} = \frac{m_s - m_d}{V_{\phi_{eff}} \rho_f} \quad (11)$$

where ρ_s and ρ_d are the saturated and dry bulk densities, m_s and m_d are the saturated and dry masses, ϕ_{eff} is the effective porosity, $V_{\phi_{eff}}$ is the effective pore volume, ρ_f is the density of the pore fluid, and V_b is the bulk volume. Density of the saturating fluid was measured directly using a calibrated precision pycnometer and appropriately ranged digital balance.

A.6 Gas Single-Phase Permeability

Gas single-phase permeability was measured under hydrostatic confining pressures using the steady-state flow method (Figure A2). The pore fluid was nitrogen gas and samples were jacketed in viton tubing (70 durometer) to prevent bypassing of the sample by the fluid.

Because of the compressibility of gases, the differential form of Darcy's law must be integrated using the condition appropriate for gas flow (i.e. at constant temperature and steady state the product (pressure \times velocity) is constant throughout the sample) to determine the permeability k_g . The gas permeability k_g was calculated from the following equation¹¹:

$$k_g = -\frac{Q_2}{A} \left(\frac{2P_2 L}{P_2^2 - P_1^2} \right) \mu = v_2 \left(\frac{P_2}{P_m} \right) \left(\frac{L}{\Delta P} \right) \mu \quad (12)$$

where $v_2 = Q_2/A$, and Q_2 is the volumetric flow rate (or "discharge") at the downstream end, A is the cross-sectional area of the sample, P_1 and P_2 are the gas pressures at the upstream and downstream reservoirs, μ is the gas viscosity, L is the length of the sample in the macroscopic flow direction, and $P_m = 1/2(P_1 + P_2)$.

Gas permeability varies with the pressure of the gas due to the so-called "slip" effect. The "Klinkenberg permeability" k_{∞} (a.k.a. equivalent liquid permeability) was calculated from the following relation²:

¹¹e.g., Dullien, F. A. L., *Porous Media— Fluid Transport and Pore Structure*, 2nd ed., Academic Press, New York, 1992.

$$\frac{v_2 P_2 L \mu}{\Delta P P_m} = k_w \left(1 + \frac{b}{P_m} \right) \quad (13)$$

where b is a constant characteristic of both the gas and porous medium and the permeability. The left hand side of equation 5 was plotted against $1/P_m$ and a straight line was fit to the data; the slope of the line is bk_w and the intercept is k_w .

Mean pore pressures were minimized, but sufficient to cause fluid flow along the sample length. Measurements were made at four different mean pore pressures (increments of approximately 0.07 MPa) to allow for accurate determination of the Klinkenberg permeability. Measurements were repeated four times at each mean pore pressure.

Pressure drops across the core were chosen such that laminar flow was favored. Analysis to verify the existence of Darcian (i.e., laminar viscous) flow was performed for verification. The analysis followed standard industry practice of relating the difference of the squared upstream and downstream pressures ($P_1^2 - P_2^2$) to the basis flow rate Q_{basis} ¹². A strong linear correlation ($R > 0.99$) is evidence of laminar viscous flow.

A.7 Liquid Single-Phase Permeability

Liquid permeabilities were measured for saturated samples at hydrostatic confining pressures using the steady state technique (Figure A3). Permeability k_i is calculated using Darcy's law:

$$Q = \left(\frac{k_i A}{\mu} \right) \left(\frac{\Delta P}{L} \right) \quad (14)$$

where Q is the volumetric flow rate (or "discharge"), A is the cross-sectional area of the sample, L is the length of the sample in the macroscopic flow direction, $\Delta P = P_1 - P_2$ is the hydrostatic pressure drop across the sample length, and μ is the viscosity of the fluid.

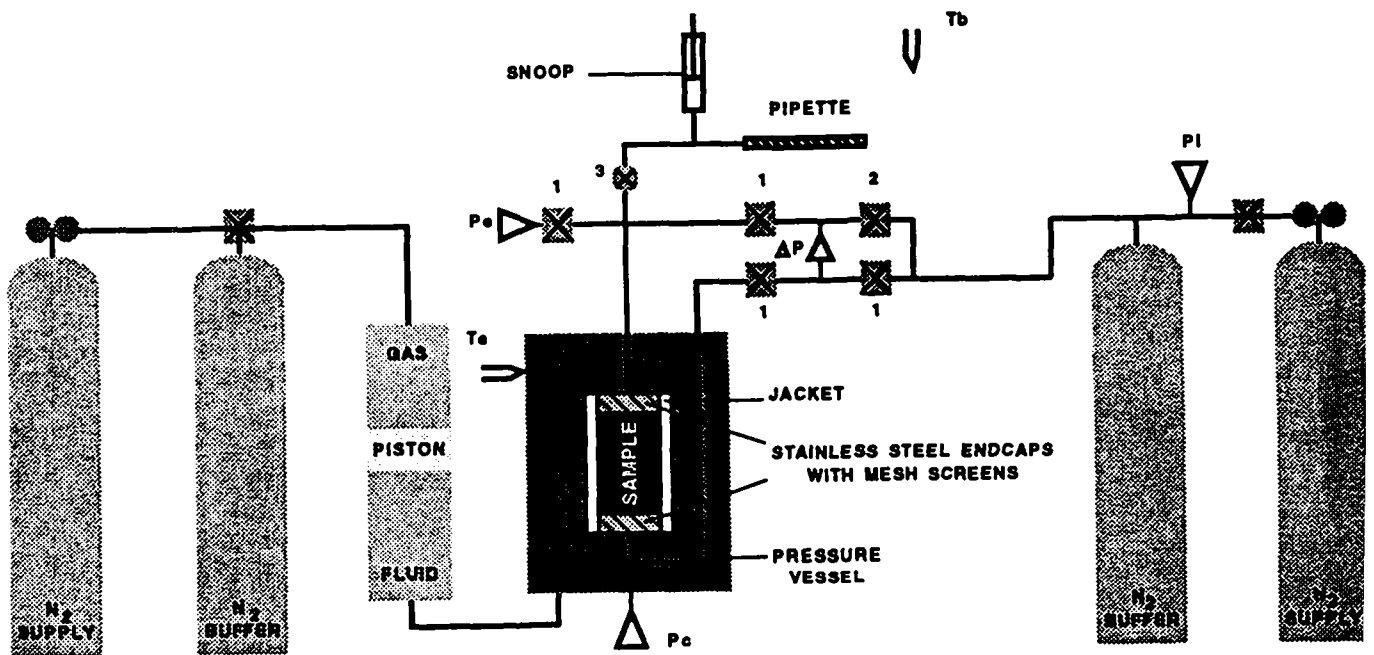
Pressure drops across the core were chosen such that laminar flow was assured. The fluid pressure differential was minimized, but sufficient to cause fluid flow along the sample length. Flow measurements were performed at least 5 times.

A.8 Calibration Facilities and Instrumentation

TerraTek operates a calibration lab used to support the various testing groups within the company. The lab maintains calibration standards for force, pressure, mass, displacement, temperature, and voltage. These standards are wholly owned by the Company and are traceable

¹²e.g., *Handbook of Natural Gas Engineering*, D. L. Katz et al., McGraw-Hill Book Company, New York, 1959.

GAS PERMEAMETER

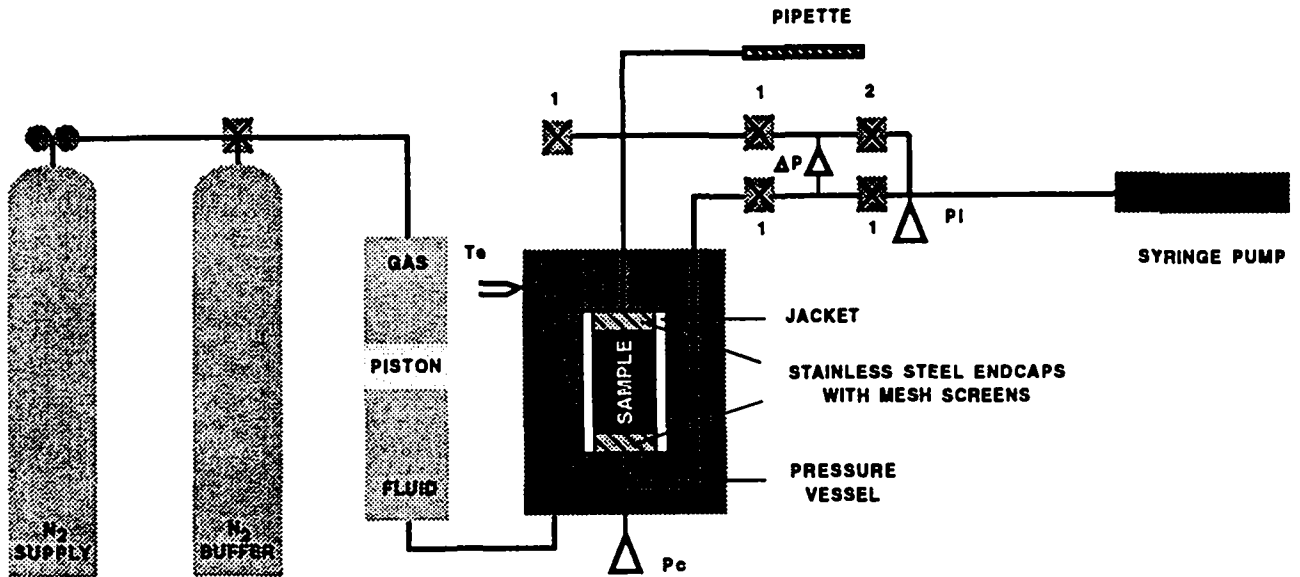


N_2 = NITROGEN GAS
 (STANDARD 304 CU. FT. BOTTLES)
 SNOOP = LEAK DETECTION SOAP SOLUTION

PI = INJECTION PRESSURE TRANSDUCER	1 = ISOLATION VALVE
Pe = EXIT PRESSURE TRANSDUCER	2 = "SHORTING" VALVE (ISOLATES INJECTION LINE FROM EXIT LINE)
Pc = CONFINING PRESSURE TRANSDUCER	3 = MICRO-METERING VALVE
ΔP = DIFFERENTIAL PRESSURE TRANSDUCER	
Te = VESSEL TEMPERATURE (FLOW)	
Tb = ROOM TEMPERATURE (BASIS)	

Figure A2. Schematic of experimental system for gas permeability measurement.

LIQUID PERMEAMETER



N₂ = NITROGEN GAS
 (STANDARD 304 CU. FT. BOTTLES)

PI = INJECTION PRESSURE TRANSDUCER

1 = ISOLATION VALVE

P_c = CONFINING PRESSURE TRANSDUCER

2 = "SHORTING" VALVE (ISOLATES
 INJECTION LINE FROM EXIT LINE)

ΔP = DIFFERENTIAL PRESSURE TRANSDUCER

3 = MICRO-METERING VALVE

T_c = VESSEL TEMPERATURE (FLOW)

Figure A3. Schematic of experimental system for liquid permeability measurement.

to the National Institute of Standards and Technology. Calibration records consisting of certificates, data sheets, reports, and calibration schedules are maintained.

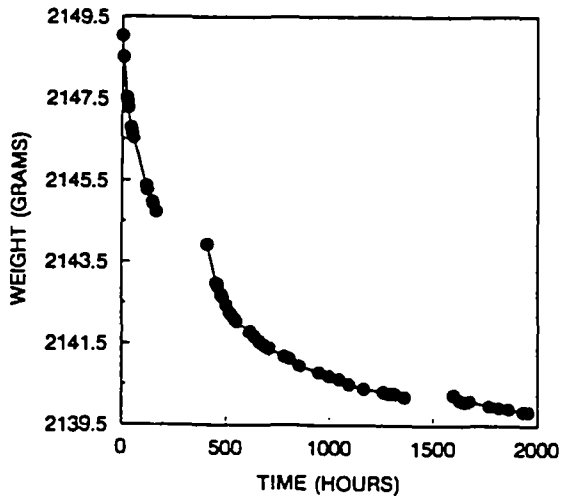
**APPENDIX C-B: Index of CT Cross-sectional Images from
Whole Core Scan (E1X-08)**

Table B1. Index of CT Images for E1X08

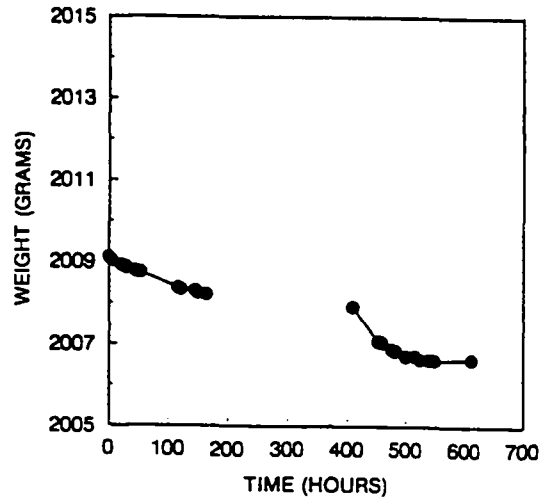
Image No.	Depth (feet)
100005	2.706
100015	2.805
100025	2.903
100035	3.002
100045	3.100
100055	3.198
100065	3.297
100110	3.686
100140	3.981
100170	4.277
100200	4.572
100230	4.867
100260	5.163
100290	5.458
100320	5.753
100357	6.029
100367	6.128
100377	6.226
100400	6.452
100410	6.551
100420	6.649
100430	6.747
100440	6.846
100450	6.944
100460	7.043
100470	7.141
100480	7.240

APPENDIX C-C: Drying History of Samples A-F & EP1-8

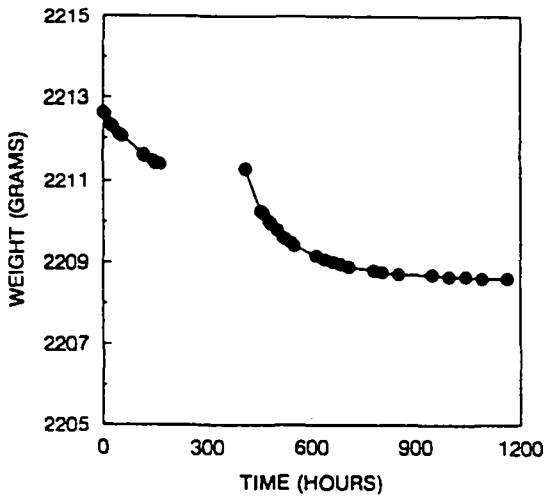
SAMPLE "A"



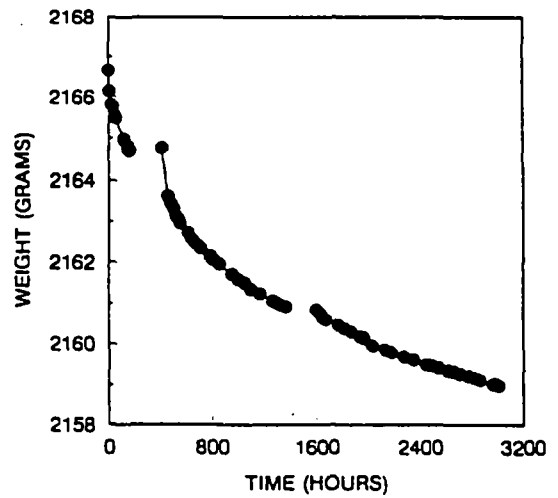
SAMPLE "B"

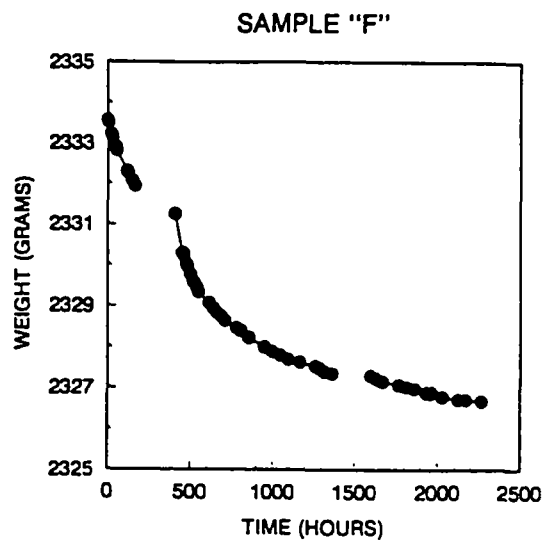
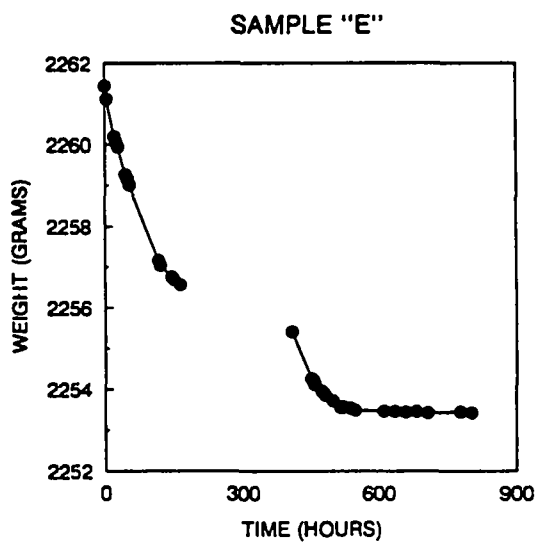


SAMPLE "C"

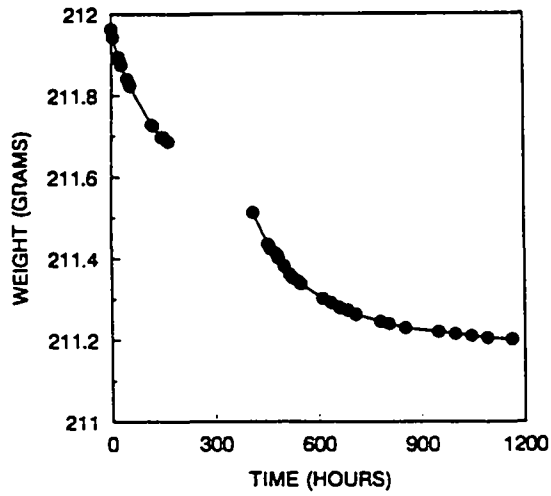


SAMPLE "D"

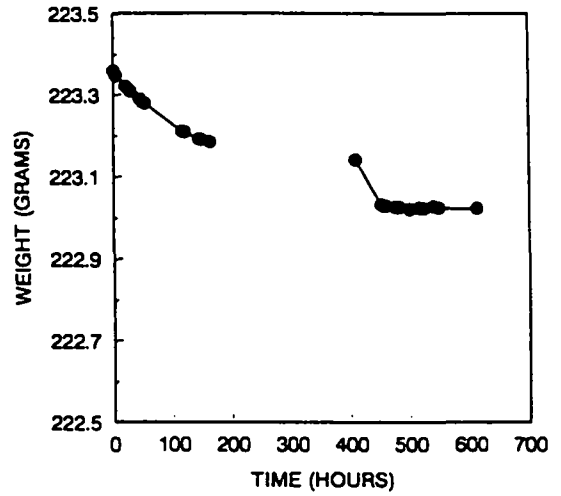




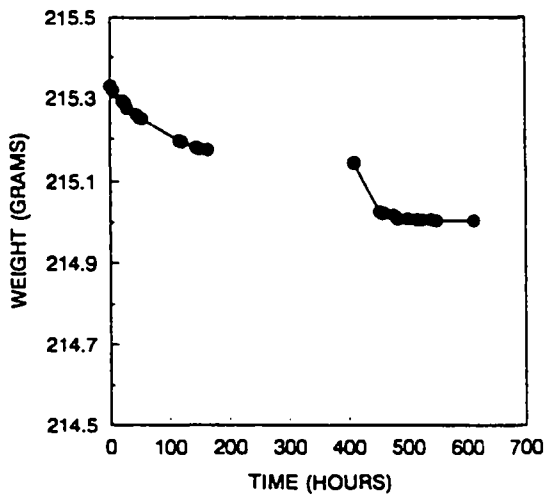
SAMPLE "EP1"



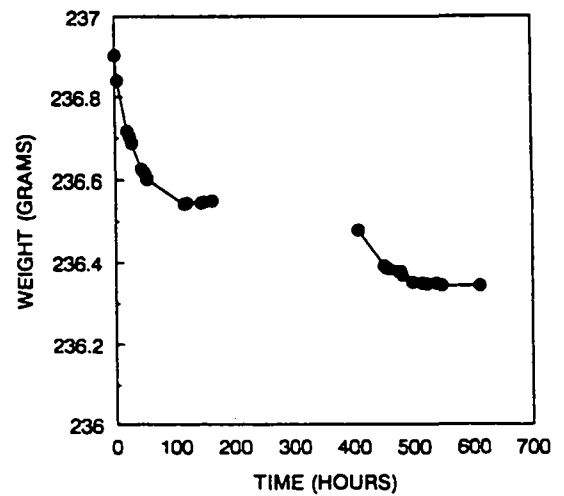
SAMPLE "EP2"

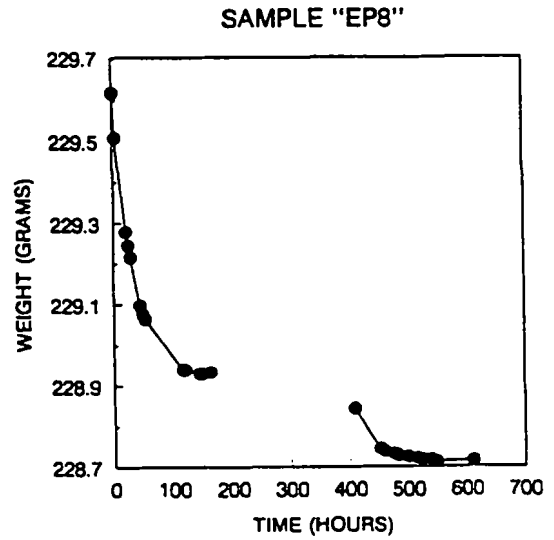
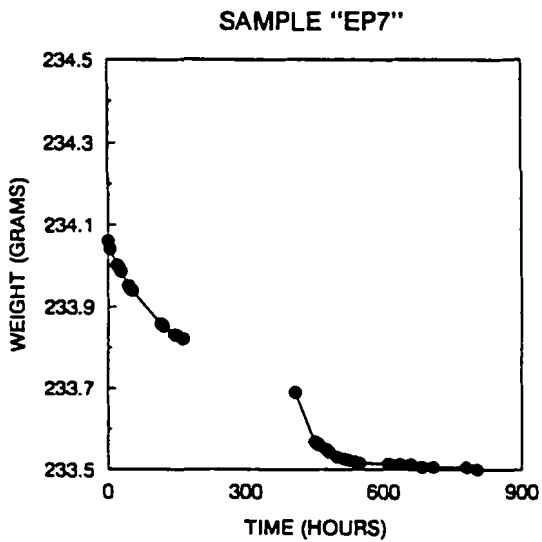
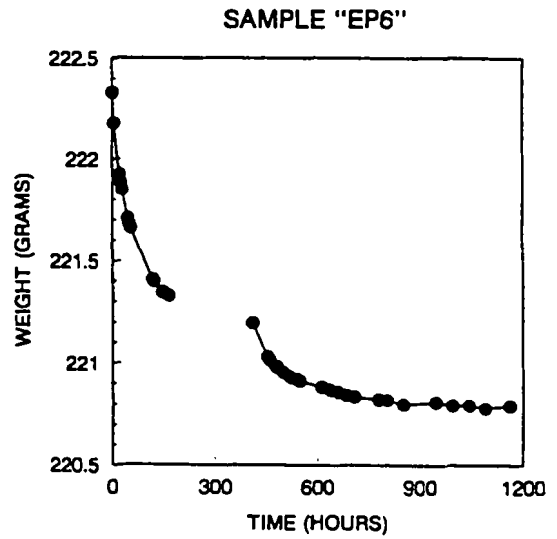
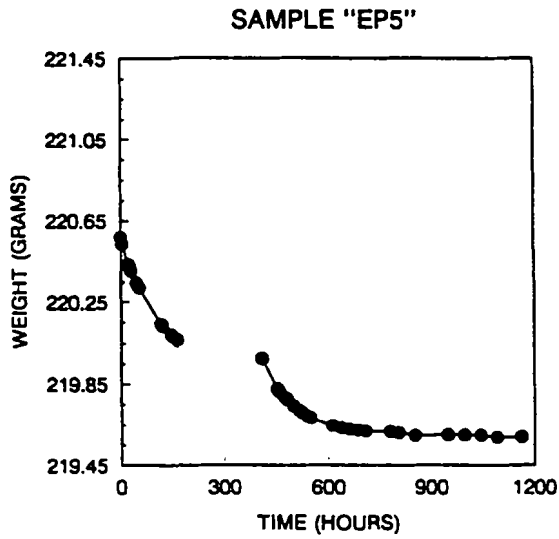


SAMPLE "EP3"



SAMPLE "EP4"





APPENDIX C-D: Gas Permeability Spreadsheets

Steady State Gas Permeability Data

Project #:	8362	Net Effective Stress:	2 MPa	290.1 psid	Gas:	N2		
Sample #:	A	Length:	10.117 cm		gas deviation z factors:	ze =	1.0000	zb = 1.0000
Stress Level #:	1	Diameter:	10.170 cm		Viscosity:	0.0176 cp		
Regime #:	1	Area:	81.233 cm ²					
Pressure Data Filename:	8362AG.S1B							
XDCR calibration factors:	Pc =	222.869 psig/volt	PI =	55.4417 psig/volt	ΔP =	11.0272 psid/volt	Pe =	5.5211 psig/volt

Date	Time of Day	File Time (min)	Regime #	Pb Barometric Pressure	Pc Confining Pressure	PI Inlet Pressure	ΔP Differential Pressure	Pm Mean Pore Pressure Pe*ΔP/2	Pe Exit Pressure	Te Flow Temp (°C)	Tb Ambient Temp (°C)	Qb Flow Rate @Pb&Tb (ml/sec)	
26 May 93	12:51	108	AS1R1a	12.33 psia	1.423 volts	0.870 volts	3.874 volts		1.057 volts	23	22	0.05232	
26 May 93	12:54	108	AS1R1b	12.33 psia	1.423 volts	0.870 volts	3.874 volts		1.057 volts	23	22	0.05232	
26 May 93	12:56	113	AS1R1c	12.33 psia	1.423 volts	0.870 volts	3.874 volts		1.057 volts	23	22	0.05219	
26 May 93	12:58	113	AS1R1d	12.33 psia	1.423 volts	0.870 volts	3.874 volts		1.057 volts	23	22	0.05229	
AVERAGES			AS1R1										
					GAUGE	GAUGE	DIFFERENTIAL	GAUGE	GAUGE	(°C)	(°C)		
					1.423 volts	0.870 volts	3.874 volts		1.057 volts				
					317.1 psig	48.23 psig	42.72 psid	27.20 psig	5.836 psig	23	22		
					21.58 atm	3.282 atm	2.907 atm	1.851 atm	0.3971 atm				
					2.187 Mpa	0.3326 Mpa	0.2945 Mpa	0.1875 Mpa	0.04024 Mpa				
			ABSOLUTE	ABSOLUTE	ABSOLUTE	DIFFERENTIAL	ABSOLUTE	ABSOLUTE	(°K)	(°K)	(ml/sec)		
			12.33 psia	329.5 psia	60.56 psia	42.72 psid	39.53 psia	18.17 psia					
			0.8390 atm	22.42 atm	4.121 atm	2.907 atm	2.690 atm	1.236 atm	296	295	0.05228		
			0.08501 Mpa	2.272 Mpa	0.4176 Mpa	0.2945 Mpa	0.2725 Mpa	0.1252 Mpa					

C-106

Apparent gas permeability: $K_a = (v_e \cdot P_e \cdot u \cdot L) / (P_m \cdot \Delta P)$

Boyle's Law: $V_e = (P_b / P_e) \cdot (T_e / T_b) \cdot (z_e / z_b) \cdot V_b$
 $Q_e = (P_b / P_e) \cdot (T_e / T_b) \cdot (z_e / z_b) \cdot Q_b$

$v_e = Q_e / A = (P_b / P_e) \cdot (T_e / T_b) \cdot (z_e / z_b) \cdot (Q_b / A)$

Parameter	Traditional Units	SI Units
u = gas viscosity	0.0176 cp	* 1.0E-3 Pa*sec/cp 1.760E-05 Pa*sec
L = sample length	10.117 cm	* 1.0E-2 m/cm 1.012E-01 m
A = sample circular cross sectional area	81.233 cm ²	* 1.0E-4 m ² /cm ² 8.123E-03 m ²
Pb = flow measurement basis pressure (absolute)	0.8390 atm	* 1.013E+5 Pa/atm 8.499E+04 Pa
ΔP = pressure drop across sample length	2.907 atm	* 1.013E+5 Pa/atm 2.945E+05 Pa
Pm = mean pore pressure (absolute)	2.690 atm	* 1.013E+5 Pa/atm 2.725E+05 Pa
Pe = exit pressure (absolute)	1.236 atm	* 1.013E+5 Pa/atm 1.252E+05 Pa
Te = sample temperature (absolute)	296 °K	296 °K
Tb = flow measurement basis temperature (absolute)	295 °K	295 °K
ze = gas deviation factor at Pe and Te	1.0000	1.0000
zb = gas deviation factor at Pb and Te	1.0000	1.0000
Qb = flow rate at base conditions	0.05228 cm ³ /s	* 1.0E-6 m ³ /cm ³ 5.228E-08 m ³ /s
ve = flow velocity at sample exit end	4.383E-04 cm/s	* 1.0E-2 m/cm 4.383E-06 m/s
	Ka = 1.23E-05 d	* 9.872E-13 m ² /d 1.22E-17 m ²
	Ka = 1.23E-02 md	1.22E-13 cm ²
	Ka = 1.23E+01 μd	

Steady State Gas Permeability Data

Project #:	8362	Net Effective Stress:	2 Mpa	290.1 psid	Gas:	N2		
Sample #:	A	Length:	10.117 cm		gas deviation z factors:	ze =	1.0000	zb = 1.0000
Stress Level #:	1	Diameter:	10.170 cm		Viscosity:	0.0176 cp		
Regime #:	2	Area:	81.233 cm ²					
Pressure Data Filename:	8362AG.S1B							
XDCR calibration factors:	Pc =	222.869 psig/volt	PI =	55.4417 psig/volt	ΔP =	11.0272 psid/volt	Pe =	5.5211 psig/volt

Date	Time of Day	File Time (min)	Regime #	Pb Barometric Pressure	Pc Confining Pressure	PI Inlet Pressure	ΔP Differential Pressure	Pm Mean Pore Pressure Pe+ΔP/2	Pe Exit Pressure	Te Flow Temp (°C)	Tb Ambient Temp (°C)	Qb Flow Rate @Pb&Tb (ml/sec)
26 May 93	15:41	278	AS1R2a	12.30 psia	1.465 volts	1.045 volts	3.851 volts		2.871 volts	23	23	0.06131
26 May 93	15:45	283	AS1R2b	12.30 psia	1.465 volts	1.045 volts	3.851 volts		2.871 volts	23	23	0.06122
26 May 93	15:48	283	AS1R2c	12.30 psia	1.466 volts	1.045 volts	3.851 volts		2.872 volts	23	23	0.06125
26 May 93	15:50	288	AS1R2d	12.30 psia	1.466 volts	1.045 volts	3.851 volts		2.872 volts	23	23	0.06133
AVERAGES			AS1R2									
					GUAGE	GUAGE	DIFFERENTIAL	GUAGE	GUAGE	(°C)	(°C)	
					1.466 volts	1.045 volts	3.851 volts		2.872 volts			
					326.6 psig	57.94 psig	42.47 psid	37.09 psig	15.854 psig	23	23	
					22.22 atm	3.942 atm	2.890 atm	2.524 atm	1.0788 atm			
					2.252 Mpa	0.3995 Mpa	0.2928 Mpa	0.2557 Mpa	0.10931 Mpa			
				ABSOLUTE	ABSOLUTE	DIFFERENTIAL	ABSOLUTE	ABSOLUTE	(°K)	(°K)	(ml/sec)	
				12.3 psia	338.9 psia	70.24 psia	42.47 psid	49.39 psia	28.15 psia			
				0.8370 atm	23.06 atm	4.779 atm	2.890 atm	3.361 atm	1.916 atm	296	296	0.06128
				0.08481 Mpa	2.337 Mpa	0.4843 Mpa	0.2928 Mpa	0.3405 Mpa	0.1941 Mpa			

Apparent gas permeability: $K_a = (v_e \cdot P_e \cdot u \cdot L) / (P_m \cdot \Delta P)$

Boyle's Law:

$$v_e = (P_b / P_e) \cdot (T_e / T_b) \cdot (z_e / z_b) \cdot v_b$$

$$Q_e = (P_b / P_e) \cdot (T_e / T_b) \cdot (z_e / z_b) \cdot Q_b$$

$$v_e = Q_e / A = (P_b / P_e) \cdot (T_e / T_b) \cdot (z_e / z_b) \cdot (Q_b / A)$$

Parameter	Traditional Units	SI Units
μ - gas viscosity	0.0176 cp	* 1.0E-3 Pa*sec/cp 1.760E-05 Pa*sec
L - sample length	10.117 cm	* 1.0E-2 m/cm 1.012E-01 m
A - sample circular cross sectional area	81.233 cm ²	* 1.0E-4 m ² /cm ² 8.123E-03 m ²
Pb - flow measurement basis pressure (absolute)	0.8370 atm	* 1.013E+5 Pa/atm 8.478E+04 Pa
ΔP - pressure drop across sample length	2.890 atm	* 1.013E+5 Pa/atm 2.927E+05 Pa
Pm - mean pore pressure (absolute)	3.361 atm	* 1.013E+5 Pa/atm 3.404E+05 Pa
Pe - exit pressure (absolute)	1.916 atm	* 1.013E+5 Pa/atm 1.941E+05 Pa
Te - sample temperature (absolute)	296 °K	296 °K
Tb - flow measurement basis temperature (absolute)	296 °K	296 °K
ze - gas deviation factor at Pe and Te	1.0000	1.0000
zb - gas deviation factor at Pb and Te	1.0000	1.0000
Qb - flow rate at base conditions	0.06128 cm ³ /s	* 1.0E-6 m ³ /cm ³ 6.128E-08 m ³ /s
ve - flow velocity at sample exit end	3.296E-04 cm/s	* 1.0E-2 m/cm 3.296E-06 m/s
	Ka =	1.16E-05 d * 9.872E-13 m ² /d 1.14E-17 m ²
	Ka =	1.16E-02 md 1.14E-13 cm ²
	Ka =	1.16E+01 μd

C-107

Steady State Gas Permeability Data

Project #: 8362	Net Effective Stress: 2 Mpa 290.1 psid	Gas: N2
Sample #: A	Length: 10.117 cm	gas deviation z factors: ze = 1.0000 zb = 1.0000
Stress Level #: 1	Diameter: 10.170 cm	Viscosity: 0.0176 cp
Regime #: 3	Area: 81.233 cm ²	
Pressure Data Filename: 8362AG.S1B		
XDCR calibration factors:	Pc = 222.869 psig/volt Pi = 55.4417 psig/volt ΔP = 11.0272 psid/volt	Pe = 5.5211 psig/volt

Date	Time of Day	File Time (min)	Regime #	Pb Barometric Pressure	Pc Confining Pressure	Pi Inlet Pressure	ΔP Differential Pressure	Pm Mean Pore Pressure Pe+ΔP/2	Pe Exit Pressure	Te Flow Temp (°C)	Tb Ambient Temp (°C)	Qb Flow Rate @Pb&Tb (ml/sec)	
27 May 93	10:51	1428	AS1R3a	12.30 psia	1.512 volts	1.228 volts	3.904 volts		4.618 volts	23	22	0.07055	
27 May 93	10:54	1428	AS1R3b	12.30 psia	1.512 volts	1.228 volts	3.905 volts		4.618 volts	23	22	0.07050	
27 May 93	10:57	1433	AS1R3c	12.30 psia	1.512 volts	1.228 volts	3.905 volts		4.618 volts	23	22	0.07053	
27 May 93	10:59	1433	AS1R3d	12.30 psia	1.512 volts	1.228 volts	3.905 volts		4.618 volts	23	22	0.07056	
AVERAGES				AS1R3	GUAGE		DIFFERENTIAL	GUAGE		(°C)	(°C)		
			1.512 volts		1.228 volts	3.905 volts			4.618 volts				
			337.0 psig		68.08 psig	43.06 psid			25.496 psig	23	22		
			22.93 atm		4.633 atm	2.930 atm			1.7349 atm				
			2.323 Mpa		0.4694 Mpa	0.2969 Mpa			0.17579 Mpa				
					ABSOLUTE		DIFFERENTIAL	ABSOLUTE		ABSOLUTE	(°K)	(°K)	(ml/sec)
			12.3 psia		349.3 psia	80.38 psia			37.80 psia				
			0.8370 atm		23.77 atm	5.470 atm			2.572 atm	296	295	0.07053	
		0.08481 Mpa	2.408 Mpa	0.5542 Mpa			0.2606 Mpa						

C-108

Apparent gas permeability: $K_a = (v_e \cdot P_e \cdot u \cdot L) / (P_m \cdot \Delta P)$

Boyle's Law: $V_e = (P_b / P_e) \cdot (T_e / T_b) \cdot (z_e / z_b) \cdot V_b$
 $Q_e = (P_b / P_e) \cdot (T_e / T_b) \cdot (z_e / z_b) \cdot Q_b$

$v_e = Q_e / A = (P_b / P_e) \cdot (T_e / T_b) \cdot (z_e / z_b) \cdot (Q_b / A)$

Parameter	Traditional Units	SI Units
μ = gas viscosity	0.0176 cp	* 1.0E-3 Pa*sec/cp 1.760E-05 Pa*sec
L = sample length	10.117 cm	* 1.0E-2 m/cm 1.012E-01 m
A = sample circular cross sectional area	81.233 cm ²	* 1.0E-4 m ² /cm ² 8.123E-03 m ²
Pb = flow measurement basis pressure (absolute)	0.8370 atm	* 1.013E+5 Pa/atm 8.478E+04 Pa
ΔP = pressure drop across sample length	2.930 atm	* 1.013E+5 Pa/atm 2.968E+05 Pa
Pm = mean pore pressure (absolute)	4.037 atm	* 1.013E+5 Pa/atm 4.089E+05 Pa
Pe = exit pressure (absolute)	2.572 atm	* 1.013E+5 Pa/atm 2.605E+05 Pa
Te = sample temperature (absolute)	296 °K	296 °K
Tb = flow measurement basis temperature (absolute)	295 °K	295 °K
ze = gas deviation factor at Pe and Te	1.0000	1.0000
zb = gas deviation factor at Pb and Te	1.0000	1.0000
Qb = flow rate at base conditions	0.07053 cm ³ /s	* 1.0E-6 m ³ /cm ³ 7.053E-08 m ³ /s
ve = flow velocity at sample exit end	2.835E-04 cm/s	* 1.0E-2 m/cm 2.835E-06 m/s
	Ka = 1.10E-05 d	* 9.872E-13 m ² /d 1.08E-17 m ²
	Ka = 1.10E-02 md	1.08E-13 cm ²
	Ka = 1.10E+01 μd	

Steady State Gas Permeability Data

Project #:	8362	Net Effective Stress:	2 Mpa	290.1 psid	Gas:	N2		
Sample #:	A	Length:	10.117 cm		gas deviation z factors:	ze = 1.0000	zb = 1.0000	
Stress Level #:	1	Diameter:	10.170 cm		Viscosity:	0.0176 cp		
Regime #:	4	Area:	81.233 cm ²					
Pressure Data Filename:	8362AG.S1B							
XDCR calibration factors:	Pc = 222.869 psig/volt	P1 = 55.4417 psig/volt	ΔP = 11.0272 psid/volt	Pe = 5.5211 psig/volt				

Date	Time of Day	File Time (min)	Regime #	Pb Barometric Pressure	Pc Confining Pressure	P1 Inlet Pressure	ΔP Differential Pressure	Pm Mean Pore Pressure Pe*ΔP/2	Pe Exit Pressure	Te Flow Temp (°C)	Tb Ambient Temp (°C)	Qb Flow Rate @Pb&Tb (ml/sec)
27 May 93	14:50	1668	AS1R4a	12.29 psia	1.558 volts	1.409 volts	3.920 volts		6.415 volts	23	23	0.08047
27 May 93	14:53	1668	AS1R4b	12.29 psia	1.558 volts	1.409 volts	3.920 volts		6.415 volts	23	23	0.08060
27 May 93	14:55	1673	AS1R4c	12.29 psia	1.559 volts	1.409 volts	3.920 volts		6.414 volts	23	23	0.08053
27 May 93	14:57	1673	AS1R4d	12.29 psia	1.559 volts	1.409 volts	3.920 volts		6.414 volts	23	23	0.08053
AVERAGES			AS1R4									
					GUAGE	GUAGE	DIFFERENTIAL	GUAGE	GUAGE	(°C)	(°C)	
					1.559 volts	1.409 volts	3.920 volts	57.03 psig	35.415 psig	23	23	
					347.3 psig	78.12 psig	43.23 psid	2.941 atm	3.881 atm	2.4098 atm		
					23.64 atm	5.316 atm	2.941 atm	0.3932 Mpa	0.24418 Mpa			
					2.395 Mpa	0.5386 Mpa	0.2980 Mpa	ABSOLUTE	ABSOLUTE	(°K)	(°K)	(ml/sec)
					12.29 psia	359.6 psia	90.41 psia	43.23 psid	69.32 psia	47.71 psia		
	0.8363 atm	24.47 atm	6.152 atm	2.941 atm	4.717 atm	3.246 atm	296	296	0.08053			
		0.08474 Mpa	2.480 Mpa	0.6233 Mpa	0.2980 Mpa	0.4779 Mpa	0.3289 Mpa					

C-109

Apparent gas permeability: $K_a = (v_e \cdot P_e \cdot u \cdot L) / (P_m \cdot \Delta P)$

Boyle's Law:

$$v_e = (P_b / P_e) \cdot (T_e / T_b) \cdot (z_e / z_b) \cdot v_b$$

$$Q_e = (P_b / P_e) \cdot (T_e / T_b) \cdot (z_e / z_b) \cdot Q_b$$

$$v_e = Q_e / A = (P_b / P_e) \cdot (T_e / T_b) \cdot (z_e / z_b) \cdot (Q_b / A)$$

Parameter	Traditional Units	SI Units
μ = gas viscosity	0.0176 cp	* 1.0E-3 Pa*sec/cp 1.760E-05 Pa*sec
L = sample length	10.117 cm	* 1.0E-2 m/cm 1.012E-01 m
A = sample circular cross sectional area	81.233 cm ²	* 1.0E-4 m ² /cm ² 8.123E-03 m ²
Pb = flow measurement basis pressure (absolute)	0.8363 atm	* 1.013E+5 Pa/atm 8.472E+04 Pa
ΔP = pressure drop across sample length	2.941 atm	* 1.013E+5 Pa/atm 2.980E+05 Pa
Pm = mean pore pressure (absolute)	4.717 atm	* 1.013E+5 Pa/atm 4.778E+05 Pa
Pe = exit pressure (absolute)	3.246 atm	* 1.013E+5 Pa/atm 3.288E+05 Pa
Te = sample temperature (absolute)	296 °K	296 °K
Tb = flow measurement basis temperature (absolute)	296 °K	296 °K
ze = gas deviation factor at Pe and Te	1.0000	1.0000
zb = gas deviation factor at Pb and Te	1.0000	1.0000
Qb = flow rate at base conditions	0.08053 cm ³ /s	* 1.0E-6 m ³ /cm ³ 8.053E-08 m ³ /s
ve = flow velocity at sample exit end	2.554E-04 cm/s	* 1.0E-2 m/cm 2.554E-06 m/s
	Ka = 1.06E-05 d	* 9.872E-13 m ² /d 1.05E-17 m ²
	Ka = 1.06E-02 md	1.05E-13 cm ²
	Ka = 1.06E+01 μd	

Steady State Gas Permeability Data

Project #: 8362	Net Effective Stress: 6 Mpa 870.2 psid	Gas: N2
Sample #: A	Length: 10.117 cm	gas deviation z factors: ze = 1.0000 zb = 1.0000
Stress Level #: 2	Diameter: 10.170 cm	Viscosity: 0.0176 cp
Regime #: 1	Area: 81.233 cm ²	
Pressure Data Filename: 8362AG.S2A		
XDCR calibration factors: Pc = 222.869 psig/volt P1 = 55.4417 psig/volt ΔP = 11.0272 psid/volt Pe = 5.5211 psig/volt		

Date	Time of Day	File Time (min)	Regime #	Pb Barometric Pressure	Pc Confining Pressure	P1 Inlet Pressure	ΔP Differential Pressure	Pm Mean Pore Pressure Pe*ΔP/2	Pe Exit Pressure	Te Flow Temp (°C)	Tb Ambient Temp (°C)	Qb Flow Rate @Pb&Tb (ml/sec)
28 May 93	12:17	272	AS2R1a	12.32 psia	4.027 volts	0.866 volts	3.833 volts		1.107 volts	23	23	0.03740
28 May 93	12:20	277	AS2R1b	12.32 psia	4.027 volts	0.866 volts	3.833 volts		1.107 volts	23	23	0.03745
28 May 93	12:23	277	AS2R1c	12.32 psia	4.027 volts	0.866 volts	3.833 volts		1.107 volts	23	23	0.03739
28 May 93	12:25	282	AS2R1d	12.32 psia	4.027 volts	0.866 volts	3.833 volts		1.107 volts	23	23	0.03743
AVERAGES			AS2R1									
				GAUGE	GAUGE	DIFFERENTIAL	GAUGE	GAUGE	(°C)	(°C)		
				4.027 volts	0.866 volts	3.833 volts		1.107 volts				
				897.5 psig	48.01 psig	42.27 psid	27.25 psig	6.112 psig	23	23		
				61.07 atm	3.267 atm	2.876 atm	1.854 atm	0.4159 atm				
				6.188 Mpa	0.3310 Mpa	0.2914 Mpa	0.1879 Mpa	0.04214 Mpa				
				ABSOLUTE	ABSOLUTE	ABSOLUTE	DIFFERENTIAL	ABSOLUTE	ABSOLUTE	(°K)	(°K)	(ml/sec)
		12.32 psia	909.8 psia	60.33 psia	42.27 psid	39.57 psia	18.43 psia					
		0.8383 atm	61.91 atm	4.105 atm	2.876 atm	2.692 atm	1.254 atm	296	296	0.03742		
		0.08494 Mpa	6.273 Mpa	0.4160 Mpa	0.2914 Mpa	0.2728 Mpa	0.1271 Mpa					

Apparent gas permeability: $K_a = (v_e \cdot P_e \cdot u \cdot L) / (P_m \cdot \Delta P)$

Boyle's Law:

$$v_e = (P_b / P_e) \cdot (T_e / T_b) \cdot (z_e / z_b) \cdot v_b$$

$$Q_e = (P_b / P_e) \cdot (T_e / T_b) \cdot (z_e / z_b) \cdot Q_b$$

$$v_e = Q_e / A \cdot (P_b / P_e) \cdot (T_e / T_b) \cdot (z_e / z_b) \cdot (Q_b / A)$$

Parameter	Traditional Units	SI Units
μ = gas viscosity	0.0176 cp	* 1.0E-3 Pa*sec/cp 1.760E-05 Pa*sec
L = sample length	10.117 cm	* 1.0E-2 m/cm 1.012E-01 m
A = sample circular cross sectional area	81.233 cm ²	* 1.0E-4 m ² /cm ² 8.123E-03 m ²
Pb = flow measurement basis pressure (absolute)	0.8383 atm	* 1.013E+5 Pa/atm 8.492E+04 Pa
ΔP = pressure drop across sample length	2.876 atm	* 1.013E+5 Pa/atm 2.913E+05 Pa
Pm = mean pore pressure (absolute)	2.692 atm	* 1.013E+5 Pa/atm 2.727E+05 Pa
Pe = exit pressure (absolute)	1.254 atm	* 1.013E+5 Pa/atm 1.271E+05 Pa
Te = sample temperature (absolute)	296 °K	296 °K
Tb = flow measurement basis temperature (absolute)	296 °K	296 °K
ze = gas deviation factor at Pe and Te	1.0000	1.0000
zb = gas deviation factor at Pb and Te	1.0000	1.0000
Qb = flow rate at base conditions	0.03742 cm ³ /s	* 1.0E-6 m ³ /cm ³ 3.742E-08 m ³ /s
ve = flow velocity at sample exit end	3.079E-04 cm/s	* 1.0E-2 m/cm 3.079E-06 m/s
	Ka = 8.88E-06 d	* 9.872E-13 m ² /d 8.77E-18 m ²
	Ka = 8.88E-03 md	8.77E-14 cm ²
	Ka = 8.88E+00 μd	

C-110

Steady State Gas Permeability Data

Project #:	8362	Net Effective Stress:	6 Mpa	870.2 psid	Gas:	N2		
Sample #:	A	Length:	10.117 cm		gas deviation z factors:	ze = 1.0000	zb = 1.0000	
Stress Level #:	2	Diameter:	10.170 cm		Viscosity:	0.0176 cp		
Regime #:	2	Area:	81.233 cm ²					
Pressure Data Filename:	8362AG.S2A							
XDCR calibration factors:	Pc = 222.869 psig/volt	PI = 55.4417 psig/volt	AP = 11.0272 psid/volt	Pe = 5.5211 psig/volt				

Date	Time of Day	File Time (min)	Regime #	Pb Barometric Pressure	Pc Confining Pressure	P1 Inlet Pressure	ΔP Differential Pressure	Pm Mean Pore Pressure Pe+ΔP/2	Pe Exit Pressure	Te Flow Temp (°C)	Tb Ambient Temp (°C)	Qb Flow Rate @Pb&Tb (ml/sec)
28 May 93	14:34	407	AS2R2a	12.30 psia	4.071 volts	1.040 volts	3.829 volts		2.871 volts	23	23	0.04414
28 May 93	14:37	412	AS2R2b	12.30 psia	4.071 volts	1.040 volts	3.829 volts		2.871 volts	23	23	0.04410
28 May 93	14:39	412	AS2R2c	12.30 psia	4.071 volts	1.040 volts	3.829 volts		2.871 volts	23	23	0.04411
28 May 93	14:47	422	AS2R2d	12.30 psia	4.071 volts	1.040 volts	3.830 volts		2.870 volts	23	23	0.04403
AVERAGES												

C-111

Apparent gas permeability: $K_a = (v_e \cdot P_e \cdot u \cdot L) / (P_m \cdot \Delta P)$

Boyle's Law: $v_e = (P_b / P_e) \cdot (T_e / T_b) \cdot (z_e / z_b) \cdot v_b$
 $Q_e = (P_b / P_e) \cdot (T_e / T_b) \cdot (z_e / z_b) \cdot Q_b$

$v_e = Q_e / A = (P_b / P_e) \cdot (T_e / T_b) \cdot (z_e / z_b) \cdot (Q_b / A)$

Parameter	Traditional Units	SI Units
μ = gas viscosity	0.0176 cp	• 1.0E-3 Pa*sec/cp 1.760E-05 Pa*sec
L = sample length	10.117 cm	• 1.0E-2 m/cm 1.012E-01 m
A = sample circular cross sectional area	81.233 cm ²	• 1.0E-4 m ² /cm ² 8.123E-03 m ²
Pb = flow measurement basis pressure (absolute)	0.8370 atm	• 1.013E+5 Pa/atm 8.478E+04 Pa
ΔP = pressure drop across sample length	2.873 atm	• 1.013E+5 Pa/atm 2.911E+05 Pa
Pm = mean pore pressure (absolute)	3.352 atm	• 1.013E+5 Pa/atm 3.396E+05 Pa
Pe = exit pressure (absolute)	1.915 atm	• 1.013E+5 Pa/atm 1.940E+05 Pa
Te = sample temperature (absolute)	296 °K	296 °K
Tb = flow measurement basis temperature (absolute)	296 °K	296 °K
ze = gas deviation factor at Pe and Te	1.0000	1.0000
zb = gas deviation factor at Pb and Te	1.0000	1.0000
Qb = flow rate at base conditions	0.04409 cm ³ /s	• 1.0E-6 m ³ /cm ³ 4.409E-08 m ³ /s
ve = flow velocity at sample exit end	2.372E-04 cm/s	• 1.0E-2 m/cm 2.372E-06 m/s
	Ka = 8.40E-06 d	• 9.872E-13 m ² /d 8.29E-18 m ²
	Ka = 8.40E-03 md	8.29E-14 cm ²
	Ka = 8.40E+00 μd	

Steady State Gas Permeability Data

Project #:	8362	Net Effective Stress:	6 Mpa	870.2 psid	Gas:	N2		
Sample #:	A	Length:	10.117 cm		gas deviation z factors:	ze = 1.0000	zb = 1.0000	
Stress Level #:	2	Diameter:	10.170 cm		Viscosity:	0.0176 cp		
Regime #:	3	Area:	81.233 cm ²					
Pressure Data Filename:	8362AG.S2A							
XDCR calibration factors:	Pc = 222.869 psig/volt	Pi = 55.4417 psig/volt	ΔP = 11.0272 psid/volt	Pe = 5.5211 psig/volt				

Date	Time of Day	File Time (min)	Regime #	Pb Barometric Pressure	Pc Confining Pressure	Pi Inlet Pressure	ΔP Differential Pressure	Pm Mean Pore Pressure Pe*ΔP/2	Pe Exit Pressure	Te Flow Temp (°C)	Tb Ambient Temp (°C)	Qb Flow Rate @Pb&Tb (ml/sec)	
01 Jun 93	13:27	6102	AS2R3a	12.32 psia	4.116 volts	1.225 volts	3.841 volts		4.716 volts	23	22	0.04952	
01 Jun 93	13:32	6107	AS2R3b	12.32 psia	4.116 volts	1.225 volts	3.841 volts		4.716 volts	23	22	0.04948	
01 Jun 93	13:34	6107	AS2R3c	12.32 psia	4.116 volts	1.225 volts	3.841 volts		4.715 volts	23	22	0.04962	
01 Jun 93	13:37	6112	AS2R3d	12.32 psia	4.116 volts	1.225 volts	3.841 volts		4.715 volts	23	22	0.04954	
AVERAGES			AS2R3										
					GUAGE	GUAGE	DIFFERENTIAL	GUAGE	GUAGE		(°C)	(°C)	
					4.116 volts	1.225 volts	3.841 volts		4.716 volts		23	22	
					917.3 psig	67.92 psig	42.36 psid	47.21 psig	26.035 psig				
					62.42 atm	4.621 atm	2.882 atm	3.213 atm	1.7716 atm				
					6.325 Mpa	0.4683 Mpa	0.2920 Mpa	0.3255 Mpa	0.17950 Mpa				
			ABSOLUTE	ABSOLUTE	ABSOLUTE	DIFFERENTIAL	ABSOLUTE	ABSOLUTE		(°K)	(°K)	(ml/sec)	
			12.32 psia	929.6 psia	80.24 psia	42.36 psid	59.53 psia	38.35 psia					
			0.8383 atm	63.26 atm	5.460 atm	2.882 atm	4.051 atm	2.610 atm		296	295	0.04954	
			0.08494 Mpa	6.410 Mpa	0.5532 Mpa	0.2920 Mpa	0.4105 Mpa	0.2644 Mpa					

C-112

Apparent gas permeability: $K_a = (v_e \cdot P_e \cdot u \cdot L) / (P_m \cdot \Delta P)$

Boyle's Law: $v_e = (P_b / P_e) \cdot (T_e / T_b) \cdot (z_e / z_b) \cdot v_b$
 $Q_e = (P_b / P_e) \cdot (T_e / T_b) \cdot (z_e / z_b) \cdot Q_b$

$v_e = Q_e / A = (P_b / P_e) \cdot (T_e / T_b) \cdot (z_e / z_b) \cdot (Q_b / A)$

Parameter	Traditional Units	SI Units
μ = gas viscosity	0.0176 cp	* 1.0E-3 Pa*sec/cp 1.760E-05 Pa*sec
L = sample length	10.117 cm	* 1.0E-2 m/cm 1.012E-01 m
A = sample circular cross sectional area	81.233 cm ²	* 1.0E-4 m ² /cm ² 8.123E-03 m ²
Pb = flow measurement basis pressure (absolute)	0.8383 atm	* 1.013E+5 Pa/atm 8.492E+04 Pa
ΔP = pressure drop across sample length	2.882 atm	* 1.013E+5 Pa/atm 2.920E+05 Pa
Pm = mean pore pressure (absolute)	4.051 atm	* 1.013E+5 Pa/atm 4.104E+05 Pa
Pe = exit pressure (absolute)	2.610 atm	* 1.013E+5 Pa/atm 2.644E+05 Pa
Te = sample temperature (absolute)	296 °K	296 °K
Tb = flow measurement basis temperature (absolute)	295 °K	295 °K
ze = gas deviation factor at Pe and Te	1.0000	1.0000
zb = gas deviation factor at Pb and Te	1.0000	1.0000
Qb = flow rate at base conditions	0.04954 cm ³ /s	* 1.0E-6 m ³ /cm ³ 4.954E-08 m ³ /s
ve = flow velocity at sample exit end	1.966E-04 cm/s	* 1.0E-2 m/cm 1.966E-06 m/s
	Ka = 7.82E-06 d	* 9.872E-13 m ² /d 7.72E-18 m ²
	Ka = 7.82E-03 md	7.72E-14 cm ²
	Ka = 7.82E+00 μd	

Steady State Gas Permeability Data

Project #:	8362	Net Effective Stress:	6 Mpa	870.2 psid	Gas:	N2		
Sample #:	A	Length:	10.117 cm		gas deviation z factors:	ze =	1.0000	zb = 1.0000
Stress Level #:	2	Diameter:	10.170 cm		Viscosity:	0.0176 cp		
Regime #:	4	Area:	81.233 cm ²					
Pressure Data Filename:	8362AG.S2A							
XDCR calibration factors:	Pc =	222.869 psig/volt	Pi =	55.4417 psig/volt	ΔP =	11.0272 psid/volt	Pe =	5.5211 psig/volt

Date	Time of Day	File Time (min)	Regime #	Pb Barometric Pressure	Pc Confining Pressure	Pi Inlet Pressure	ΔP Differential Pressure	Pm Mean Pore Pressure Pe+ΔP/2	Pe Exit Pressure	Te Flow Temp (°C)	Tb Ambient Temp (°C)	Qb Flow Rate @Pb&Tb (ml/sec)
02 Jun 93	13:14	7527	AS2R4a	12.21 psia	4.160 volts	1.407 volts	3.874 volts		6.496 volts	23	22	0.05676
02 Jun 93	13:17	7532	AS2R4b	12.21 psia	4.160 volts	1.407 volts	3.874 volts		6.496 volts	23	22	0.05679
02 Jun 93	13:19	7532	AS2R4c	12.21 psia	4.160 volts	1.407 volts	3.874 volts		6.496 volts	23	22	0.05683
02 Jun 93	13:21	7537	AS2R4d	12.21 psia	4.160 volts	1.407 volts	3.875 volts		6.496 volts	23	22	0.05682
AVERAGES			AS2R4									
				GUAGE	GUAGE	DIFFERENTIAL	GUAGE	GUAGE	(°C)	(°C)		
				4.160 volts	1.407 volts	3.874 volts		6.496 volts				
				927.1 psig	78.01 psig	42.72 psid	57.23 psig	35.865 psig	23	22		
				63.09 atm	5.308 atm	2.907 atm	3.894 atm	2.4405 atm				
				6.392 Mpa	0.5378 Mpa	0.2946 Mpa	0.3946 Mpa	0.24728 Mpa				
				ABSOLUTE	ABSOLUTE	ABSOLUTE	DIFFERENTIAL	ABSOLUTE	ABSOLUTE	(°K)	(°K)	(ml/sec)
12.21 psia	939.3 psia	90.22 psia	42.72 psid	69.44 psia	48.08 psia							
0.8308 atm	63.92 atm	6.139 atm	2.907 atm	4.725 atm	3.271 atm	296	295	0.05680				
0.08419 Mpa	6.477 Mpa	0.6220 Mpa	0.2946 Mpa	0.4787 Mpa	0.3315 Mpa							

C-113

Apparent gas permeability: $K_a = (v_e \cdot P_e \cdot u \cdot L) / (P_m \cdot \Delta P)$

Boyle's Law: $V_e = (P_b/P_e) \cdot (T_e/T_b) \cdot (z_e/z_b) \cdot V_b$
 $Q_e = (P_b/P_e) \cdot (T_e/T_b) \cdot (z_e/z_b) \cdot Q_b$

$v_e = Q_e/A = (P_b/P_e) \cdot (T_e/T_b) \cdot (z_e/z_b) \cdot (Q_b/A)$

Parameter	Traditional Units	SI Units
μ = gas viscosity	0.0176 cp	* 1.0E-3 Pa*sec/cp 1.760E-05 Pa*sec
L = sample length	10.117 cm	* 1.0E-2 m/cm 1.012E-01 m
A = sample circular cross sectional area	81.233 cm ²	* 1.0E-4 m ² /cm ² 8.123E-03 m ²
Pb = flow measurement basis pressure (absolute)	0.8308 atm	* 1.013E+5 Pa/atm 8.416E+04 Pa
ΔP = pressure drop across sample length	2.907 atm	* 1.013E+5 Pa/atm 2.945E+05 Pa
Pm = mean pore pressure (absolute)	4.725 atm	* 1.013E+5 Pa/atm 4.786E+05 Pa
Pe = exit pressure (absolute)	3.271 atm	* 1.013E+5 Pa/atm 3.314E+05 Pa
Te = sample temperature (absolute)	296 °K	296 °K
Tb = flow measurement basis temperature (absolute)	295 °K	295 °K
ze = gas deviation factor at Pe and Te	1.0000	1.0000
zb = gas deviation factor at Pb and Te	1.0000	1.0000
Qb = flow rate at base conditions	0.05680 cm ³ /s	* 1.0E-6 m ³ /cm ³ 5.680E-08 m ³ /s
ve = flow velocity at sample exit end	1.782E-04 cm/s	* 1.0E-2 m/cm 1.782E-06 m/s
	Ka =	* 7.56E-06 d 7.46E-18 m ²
	Ka =	7.56E-03 md 7.46E-14 cm ²
	Ka =	7.56E+00 μd

Steady State Gas Permeability Data

Project #:	8362	Net Effective Stress:	10 Mpa	1450.4 psid	Gas:	N2						
Sample #:	A	Length:	10.117 cm		gas deviation z factors:	ze =	1.0000	zb =	1.0000			
Stress Level #:	3	Diameter:	10.170 cm		Viscosity:	0.0176 cp						
Regime #:	1	Area:	81.233 cm ²									
Pressure Data Filename:	8362AG.S3A											
XDCR calibration factors:	Pc =	222.869	psig/volt	Pi =	55.4417	psig/volt	ΔP =	11.0272	psid/volt	Pe =	5.5211	psig/volt

Date	Time of Day	File Time (min)	Regime #	Pb Barometric Pressure	Pc Confining Pressure	Pi Inlet Pressure	ΔP Differential Pressure	Pm Mean Pore Pressure Pe*ΔP/2	Pe Exit Pressure	Te Flow Temp (°C)	Tb Ambient Temp (°C)	Qb Flow Rate @Pb&Tb (ml/sec)
03 Jun 93	09:28	1085	AS3R1a	12.30 psia	6.629 volts	0.866 volts	3.853 volts		1.059 volts	23	21	0.03065
03 Jun 93	09:33	1090	AS3R1b	12.30 psia	6.629 volts	0.866 volts	3.853 volts		1.058 volts	23	21	0.03056
03 Jun 93	09:35	1090	AS3R1c	12.30 psia	6.629 volts	0.866 volts	3.853 volts		1.058 volts	23	21	0.03057
03 Jun 93	09:38	1095	AS3R1d	12.30 psia	6.629 volts	0.866 volts	3.853 volts		1.058 volts	23	21	0.03062
AVERAGES			AS3R1									
					GAUGE	GAUGE	DIFFERENTIAL	GAUGE	GAUGE	(°C)	(°C)	
					6.629 volts	0.866 volts	3.853 volts		1.058 volts			
					1477.4 psig	48.01 psig	42.49 psid	27.09 psig	5.843 psig	23	21	
					100.53 atm	3.267 atm	2.891 atm	1.843 atm	0.3976 atm			
					10.186 Mpa	0.3310 Mpa	0.2929 Mpa	0.1868 Mpa	0.04028 Mpa			
					ABSOLUTE	ABSOLUTE	ABSOLUTE	DIFFERENTIAL	ABSOLUTE	ABSOLUTE	(°K)	(°K)
			12.3 psia	1489.7 psia	60.31 psia	42.49 psid	39.39 psia	18.14 psia				
			0.8370 atm	101.37 atm	4.104 atm	2.891 atm	2.680 atm	1.235 atm	296	294	0.03060	
			0.08481 Mpa	10.271 Mpa	0.4158 Mpa	0.2929 Mpa	0.2716 Mpa	0.1251 Mpa				

C-114

Apparent gas permeability: $K_a = (v_e \cdot P_e \cdot u \cdot L) / (P_m \cdot \Delta P)$

Boyle's Law: $V_e = (P_b / P_e) \cdot (T_e / T_b) \cdot (z_e / z_b) \cdot V_b$
 $Q_e = (P_b / P_e) \cdot (T_e / T_b) \cdot (z_e / z_b) \cdot Q_b$

$v_e = Q_e / A = (P_b / P_e) \cdot (T_e / T_b) \cdot (z_e / z_b) \cdot (Q_b / A)$

Parameter	Traditional Units	SI Units
μ = gas viscosity	0.0176 cp	* 1.0E-3 Pa*sec/cp 1.760E-05 Pa*sec
L = sample length	10.117 cm	* 1.0E-2 m/cm 1.012E-01 m
A = sample circular cross sectional area	81.233 cm ²	* 1.0E-4 m ² /cm ² 8.123E-03 m ²
Pb = flow measurement basis pressure (absolute)	0.8370 atm	* 1.013E+5 Pa/atm 8.478E+04 Pa
ΔP = pressure drop across sample length	2.891 atm	* 1.013E+5 Pa/atm 2.929E+05 Pa
Pm = mean pore pressure (absolute)	2.680 atm	* 1.013E+5 Pa/atm 2.715E+05 Pa
Pe = exit pressure (absolute)	1.235 atm	* 1.013E+5 Pa/atm 1.251E+05 Pa
Te = sample temperature (absolute)	296 °K	296 °K
Tb = flow measurement basis temperature (absolute)	294 °K	294 °K
ze = gas deviation factor at Pe and Te	1.0000	1.0000
zb = gas deviation factor at Pb and Te	1.0000	1.0000
Qb = flow rate at base conditions	0.03060 cm ³ /s	* 1.0E-6 m ³ /cm ³ 3.060E-08 m ³ /s
ve = flow velocity at sample exit end	2.571E-04 cm/s	* 1.0E-2 m/cm 2.571E-06 m/s
	Ka =	* 7.29E-06 d 7.20E-18 m ²
	Ka =	* 7.29E-03 md 7.20E-14 cm ²
	Ka =	* 7.29E+00 μd

Steady State Gas Permeability Data

Project #: 8362	Net Effective Stress: 10 Mpa 1450.4 psid	Gas: N2
Sample #: A	Length: 10.117 cm	gas deviation z factors: ze = 1.0000 zb = 1.0000
Stress Level #: 3	Diameter: 10.170 cm	Viscosity: 0.0176 cp
Regime #: 2	Area: 81.233 cm ²	
Pressure Data Filename: 8362AG.S3A		
XDCR calibration factors:	Pc = 222.869 psig/volt P1 = 55.4417 psig/volt ΔP = 11.0272 psid/volt	Pe = 5.5211 psig/volt

Date	Time of Day	File Time (min)	Regime #	Pb Barometric Pressure	Pc Confining Pressure	P1 Inlet Pressure	ΔP Differential Pressure	Pm Mean Pore Pressure Pe+ΔP/2	Pe Exit Pressure	Te Flow Temp (°C)	Tb Ambient Temp (°C)	Qb Flow Rate @Pb&Tb (ml/sec)	
03 Jun 93	14:15	1372	AS3R2a	12.32 psia	6.674 volts	1.047 volts	3.820 volts		2.939 volts	23	22	0.03577	
03 Jun 93	14:19	1372	AS3R2b	12.32 psia	6.674 volts	1.047 volts	3.821 volts		2.939 volts	23	22	0.03584	
03 Jun 93	14:21	1377	AS3R2c	12.32 psia	6.674 volts	1.047 volts	3.821 volts		2.939 volts	23	22	0.03595	
03 Jun 93	14:24	1377	AS3R2d	12.32 psia	6.674 volts	1.047 volts	3.821 volts		2.939 volts	23	22	0.03599	
03 Jun 93	14:26	1382	AS3R2e	12.32 psia	6.674 volts	1.047 volts	3.821 volts		2.938 volts	23	22	0.03601	
AVERAGES			AS3R2										
					GUAGE	GUAGE	DIFFERENTIAL	GUAGE	GUAGE		(°C)	(°C)	
					6.674 volts	1.047 volts	3.821 volts	37.29 psig	16.225 psig	23	22		
					1487.4 psig	58.05 psig	42.13 psid	2.538 atm	1.1041 atm				
					101.21 atm	3.950 atm	2.867 atm	0.2571 Mpa	0.11187 Mpa				
					10.255 Mpa	0.4002 Mpa	0.2905 Mpa	0.2571 Mpa	0.11187 Mpa				
			ABSOLUTE	ABSOLUTE	ABSOLUTE	DIFFERENTIAL	ABSOLUTE	ABSOLUTE		(°K)	(°K)	(ml/sec)	
			12.32 psia	1499.7 psia	70.37 psia	42.13 psid	49.61 psia	28.55 psia					
			0.8383 atm	102.05 atm	4.788 atm	2.867 atm	3.376 atm	1.942 atm	296	295	0.03589		
			0.08494 Mpa	10.340 Mpa	0.4852 Mpa	0.2905 Mpa	0.3421 Mpa	0.1968 Mpa					

Apparent gas permeability: $K_a = (v_e \cdot P_e \cdot u \cdot L) / (P_m \cdot \Delta P)$

Boyle's Law: $v_e = (P_b / P_e) \cdot (T_e / T_b) \cdot (z_e / z_b) \cdot v_b$
 $Q_e = (P_b / P_e) \cdot (T_e / T_b) \cdot (z_e / z_b) \cdot Q_b$

$v_e = Q_e / A = (P_b / P_e) \cdot (T_e / T_b) \cdot (z_e / z_b) \cdot (Q_b / A)$

Parameter	Traditional Units	SI Units
μ = gas viscosity	0.0176 cp	* 1.0E-3 Pa*sec/cp 1.760E-05 Pa*sec
L = sample length	10.117 cm	* 1.0E-2 m/cm 1.012E-01 m
A = sample circular cross sectional area	81.233 cm ²	* 1.0E-4 m ² /cm ² 8.123E-03 m ²
Pb = flow measurement basis pressure (absolute)	0.8383 atm	* 1.013E+5 Pa/atm 8.492E+04 Pa
ΔP = pressure drop across sample length	2.867 atm	* 1.013E+5 Pa/atm 2.904E+05 Pa
Pm = mean pore pressure (absolute)	3.376 atm	* 1.013E+5 Pa/atm 3.420E+05 Pa
Pe = exit pressure (absolute)	1.942 atm	* 1.013E+5 Pa/atm 1.968E+05 Pa
Te = sample temperature (absolute)	296 °K	296 °K
Tb = flow measurement basis temperature (absolute)	295 °K	295 °K
ze = gas deviation factor at Pe and Te	1.0000	1.0000
zb = gas deviation factor at Pb and Te	1.0000	1.0000
Qb = flow rate at base conditions	0.03589 cm ³ /s	* 1.0E-6 m ³ /cm ³ 3.589E-08 m ³ /s
ve = flow velocity at sample exit end	1.913E-04 cm/s	* 1.0E-2 m/cm 1.913E-06 m/s
	Ka = 6.84E-06 d	* 9.872E-13 m ² /d 6.75E-18 m ²
	Ka = 6.84E-03 md	6.75E-14 cm ²
	Ka = 6.84E+00 μd	

C-115

Steady State Gas Permeability Data

Project #: 8362	Net Effective Stress: 10 Mpa 1450.4 psid	Gas: N2
Sample #: A	Length: 10.117 cm	gas deviation z factors: ze = 1.0000 zb = 1.0000
Stress Level #: 3	Diameter: 10.170 cm	Viscosity: 0.0176 cp
Regime #: 3	Area: 81.233 cm ²	
Pressure Data Filename: B362AG.S3A		
XDCR calibration factors: Pc = 222.869 psig/volt Pi = 55.4417 psig/volt ΔP = 11.0272 psid/volt Pe = 5.5211 psig/volt		

Date	Time of Day	File Time (min)	Regime #	Pb Barometric Pressure	Pc Confining Pressure	Pi Inlet Pressure	ΔP Differential Pressure	Pm Mean Pore Pressure Pe*ΔP/2	Pe Exit Pressure	Te Flow Temp (°C)	Tb Ambient Temp (°C)	Qb Flow Rate ●Pb&Tb (ml/sec)	
04 Jun 93	09:31	2527	AS3R3a	12.29 psia	6.719 volts	1.229 volts	3.879 volts		4.669 volts	23	21	0.04180	
04 Jun 93	09:39	2532	AS3R3b	12.29 psia	6.719 volts	1.229 volts	3.880 volts		4.669 volts	23	21	0.04169	
04 Jun 93	09:43	2537	AS3R3c	12.29 psia	6.719 volts	1.229 volts	3.879 volts		4.670 volts	23	21	0.04179	
04 Jun 93	09:46	2542	AS3R3d	12.29 psia	6.719 volts	1.229 volts	3.879 volts		4.670 volts	23	21	0.04180	
AVERAGES			AS3R3										
					GUAGE	GUAGE	DIFFERENTIAL	GUAGE	GUAGE		(°C)	(°C)	
					6.719 volts	1.229 volts	3.879 volts	47.17 psig	25.781 psig	23	21		
					1497.5 psig	68.14 psig	42.78 psid	3.210 atm	1.7543 atm				
					101.90 atm	4.636 atm	2.911 atm	0.3252 Mpa	0.17775 Mpa				
					10.325 Mpa	0.4698 Mpa	0.2949 Mpa	0.3252 Mpa	0.17775 Mpa				
			ABSOLUTE	ABSOLUTE	ABSOLUTE	DIFFERENTIAL	ABSOLUTE	ABSOLUTE		(°K)	(°K)	(ml/sec)	
			12.29 psia	1509.7 psia	80.43 psia	42.78 psid	59.46 psia	38.07 psia					
			0.8363 atm	102.73 atm	5.473 atm	2.911 atm	4.046 atm	2.591 atm	296	294	0.04177		
			0.08474 Mpa	10.409 Mpa	0.5545 Mpa	0.2949 Mpa	0.4100 Mpa	0.2625 Mpa					

Apparent gas permeability: $K_a = (v_e \cdot P_e \cdot u \cdot L) / (P_m \cdot \Delta P)$

Boyle's Law: $v_e = (P_b / P_e) \cdot (T_e / T_b) \cdot (z_e / z_b) \cdot v_b$
 $Q_e = (P_b / P_e) \cdot (T_e / T_b) \cdot (z_e / z_b) \cdot Q_b$

$v_e = Q_e / A = (P_b / P_e) \cdot (T_e / T_b) \cdot (z_e / z_b) \cdot (Q_b / A)$

Parameter	Traditional Units	SI Units
μ = gas viscosity	0.0176 cp	* 1.0E-3 Pa*sec/cp 1.760E-05 Pa*sec
L = sample length	10.117 cm	* 1.0E-2 m/cm 1.012E-01 m
A = sample circular cross sectional area	81.233 cm ²	* 1.0E-4 m ² /cm ² 8.123E-03 m ²
Pb = flow measurement basis pressure (absolute)	0.8363 atm	* 1.013E+5 Pa/atm 8.472E+04 Pa
ΔP = pressure drop across sample length	2.911 atm	* 1.013E+5 Pa/atm 2.949E+05 Pa
Pm = mean pore pressure (absolute)	4.046 atm	* 1.013E+5 Pa/atm 4.099E+05 Pa
Pe = exit pressure (absolute)	2.591 atm	* 1.013E+5 Pa/atm 2.624E+05 Pa
Te = sample temperature (absolute)	296 °K	296 °K
Tb = flow measurement basis temperature (absolute)	294 °K	294 °K
ze = gas deviation factor at Pe and Te	1.0000	1.0000
zb = gas deviation factor at Pb and Te	1.0000	1.0000
Qb = flow rate at base conditions	0.04177 cm ³ /s	* 1.0E-6 m ³ /cm ³ 4.177E-08 m ³ /s
ve = flow velocity at sample exit end	1.671E-04 cm/s	* 1.0E-2 m/cm 1.671E-06 m/s
	Ka = 6.55E-06 d	* 9.872E-13 m ² /d 6.46E-18 m ²
	Ka = 6.55E-03 md	6.46E-14 cm ²
	Ka = 6.55E+00 ud	

C-116

Steady State Gas Permeability Data

Project #:	8362	Net Effective Stress:	10 Mpa	1450.4 psid	Gas:	N2						
Sample #:	A	Length:	10.117 cm		gas deviation z factors:	ze =	1.0000	zb =	1.0000			
Stress Level #:	3	Diameter:	10.170 cm		Viscosity:	0.0176 cp						
Regime #:	4	Area:	81.233 cm ²									
Pressure Data Filename:	8362AG.S3A											
XDCR calibration factors:	Pc =	222.869	psig/volt	Pi =	55.4417	psig/volt	ΔP =	11.0272	psid/volt	Pe =	5.5211	psig/volt

Date	Time of Day	File Time (min)	Regime #	Pb Barometric Pressure	Pc Confining Pressure	Pi Inlet Pressure	ΔP Differential Pressure	Pm Mean Pore Pressure Pe-ΔP/2	Pe Exit Pressure	Te Flow Temp (°C)	Tb Ambient Temp (°C)	Qb Flow Rate ●Pb&Tb (ml/sec)
04 Jun 93	16:35	2952	AS3R4a	12.23 psia	6.764 volts	1.407 volts	3.857 volts		6.530 volts	23	22	0.04725
04 Jun 93	16:37	2952	AS3R4b	12.23 psia	6.764 volts	1.407 volts	3.857 volts		6.530 volts	23	22	0.04723
04 Jun 93	16:39	2957	AS3R4c	12.23 psia	6.764 volts	1.407 volts	3.857 volts		6.530 volts	23	22	0.04720
04 Jun 93	16:42	2957	AS3R4d	12.23 psia	6.764 volts	1.407 volts	3.857 volts		6.530 volts	23	22	0.04728
AVERAGES												
				GUAGE	GUAGE	DIFFERENTIAL	GUAGE	GUAGE		(°C)	(°C)	
				6.764 volts	1.407 volts	3.857 volts	6.530 volts	6.530 volts		23	22	
				1507.5 psig	78.01 psig	42.53 psid	57.32 psig	36.053 psig				
				102.58 atm	5.308 atm	2.894 atm	3.900 atm	2.4532 atm				
				10.394 Mpa	0.5378 Mpa	0.2932 Mpa	0.3952 Mpa	0.24858 Mpa				
				ABSOLUTE	ABSOLUTE	ABSOLUTE	DIFFERENTIAL	ABSOLUTE	ABSOLUTE		(°K)	(°K)
			12.23 psia	1519.7 psia	90.24 psia	42.53 psid	69.55 psia	48.28 psia				
			0.8322 atm	103.41 atm	6.140 atm	2.894 atm	4.732 atm	3.285 atm		296	295	0.04724
			0.08432 Mpa	10.478 Mpa	0.6222 Mpa	0.2932 Mpa	0.4795 Mpa	0.3329 Mpa				

C-117

Apparent gas permeability: $K_a = (v_e \cdot P_e \cdot u \cdot L) / (P_m \cdot \Delta P)$

Boyle's Law: $V_e = (P_b / P_e) \cdot (T_e / T_b) \cdot (z_e / z_b) \cdot V_b$
 $Q_e = (P_b / P_e) \cdot (T_e / T_b) \cdot (z_e / z_b) \cdot Q_b$

$v_e = Q_e / A = (P_b / P_e) \cdot (T_e / T_b) \cdot (z_e / z_b) \cdot (Q_b / A)$

Parameter	Traditional Units	SI Units
μ = gas viscosity	0.0176 cp	* 1.0E-3 Pa*sec/cp 1.760E-05 Pa*sec
L = sample length	10.117 cm	* 1.0E-2 m/cm 1.012E-01 m
A = sample circular cross sectional area	81.233 cm ²	* 1.0E-4 m ² /cm ² 8.123E-03 m ²
Pb = flow measurement basis pressure (absolute)	0.8322 atm	* 1.013E+5 Pa/atm 8.430E+04 Pa
ΔP = pressure drop across sample length	2.894 atm	* 1.013E+5 Pa/atm 2.932E+05 Pa
Pm = mean pore pressure (absolute)	4.732 atm	* 1.013E+5 Pa/atm 4.794E+05 Pa
Pe = exit pressure (absolute)	3.285 atm	* 1.013E+5 Pa/atm 3.328E+05 Pa
Te = sample temperature (absolute)	296 °K	296 °K
Tb = flow measurement basis temperature (absolute)	295 °K	295 °K
ze = gas deviation factor at Pe and Te	1.0000	1.0000
zb = gas deviation factor at Pb and Te	1.0000	1.0000
Qb = flow rate at base conditions	0.04724 cm ³ /s	* 1.0E-6 m ³ /cm ³ 4.724E-08 m ³ /s
ve = flow velocity at sample exit end	1.478E-04 cm/s	* 1.0E-2 m/cm 1.478E-06 m/s
	Ka = 6.31E-06 d	* 9.872E-13 m ² /d 6.23E-18 m ²
	Ka = 6.31E-03 md	6.23E-14 cm ²
	Ka = 6.31E+00 μd	

Steady State Gas Permeability Data

Project #:	8362	Net Effective Stress:	2 Mpa	290.1 psig	Gas:	N2		
Sample #:	B	Length:	9.557 cm		gas deviation z factors:	ze =	1.0000	zb = 1.0000
Stress Level #:	1	Diameter:	10.171 cm		Viscosity:	0.0176 cp		
Regime #:	1	Area:	81.249 cm ²					
Pressure Data Filename:	8362BG.S1B							
XDCR calibration factors:	Pc =	222.869 psig/volt	Pl =	55.4417 psig/volt	ΔP =	11.0272 psid/volt	Pe =	5.5211 psig/volt

Date	Time of Day	File Time (min)	Regime #	Pb Barometric Pressure	Pc Confining Pressure	Pl Inlet Pressure	ΔP Differential Pressure	Pm Mean Pore Pressure Pe+ΔP/2	Pe Exit Pressure	Te Flow Temp (°C)	Tb Ambient Temp (°C)	Qb Flow Rate @Pb&Tb (ml/sec)	
31 Mar 93	11:52	188	BS1R1a	12.39 psia	1.433 volts	0.901 volts	4.009 volts		1.100 volts	25	21	0.09272	
31 Mar 93	11:54	193	BS1R1b	12.39 psia	1.431 volts	0.901 volts	4.009 volts		1.100 volts	25	22	0.09407	
31 Mar 93	11:56	193	BS1R1c	12.39 psia	1.429 volts	0.901 volts	4.009 volts		1.100 volts	25	22	0.09274	
31 Mar 93	11:59	198	BS1R1d	12.39 psia	1.428 volts	0.901 volts	4.009 volts		1.100 volts	25	22	0.09259	
AVERAGES			BS1R1										
				GUAGE	GUAGE	DIFFERENTIAL	GUAGE	GUAGE	(°C)	(°C)			
				1.430 volts	0.901 volts	4.009 volts		1.100 volts					
				318.8 psig	49.95 psig	44.21 psid	28.18 psig	6.073 psig		25	22		
				21.69 atm	3.399 atm	3.008 atm	1.917 atm	0.4133 atm					
				2.198 Mpa	0.3444 Mpa	0.3048 Mpa	0.1943 Mpa	0.04187 Mpa					
				ABSOLUTE	ABSOLUTE	DIFFERENTIAL	ABSOLUTE	ABSOLUTE	(°K)	(°K)	(ml/sec)		
				12.39 psia	331.1 psia	62.34 psia	44.21 psid	40.57 psia	18.46 psia				
		0.8431 atm	22.53 atm	4.242 atm	3.008 atm	2.760 atm	1.256 atm	298	295	0.09303			
		0.08543 Mpa	2.283 Mpa	0.4298 Mpa	0.3048 Mpa	0.2797 Mpa	0.1273 Mpa						

C-118

Apparent gas permeability: $K_a = (v_e \cdot P_e \cdot u \cdot L) / (P_m \cdot \Delta P)$

Boyle's Law: $V_e = (P_b / P_e) \cdot (T_e / T_b) \cdot (z_e / z_b) \cdot V_b$
 $Q_e = (P_b / P_e) \cdot (T_e / T_b) \cdot (z_e / z_b) \cdot Q_b$

$v_e = Q_e / A = (P_b / P_e) \cdot (T_e / T_b) \cdot (z_e / z_b) \cdot (Q_b / A)$

Parameter	Traditional Units	SI Units
μ = gas viscosity	0.0176 cp	* 1.0E-3 Pa*sec/cp 1.760E-05 Pa*sec
L = sample length	9.557 cm	* 1.0E-2 m/cm 9.557E-02 m
A = sample circular cross sectional area	81.249 cm ²	* 1.0E-4 m ² /cm ² 8.125E-03 m ²
Pb = flow measurement basis pressure (absolute)	0.8431 atm	* 1.013E+5 Pa/atm 8.540E+04 Pa
ΔP = pressure drop across sample length	3.008 atm	* 1.013E+5 Pa/atm 3.047E+05 Pa
Pm = mean pore pressure (absolute)	2.760 atm	* 1.013E+5 Pa/atm 2.796E+05 Pa
Pe = exit pressure (absolute)	1.256 atm	* 1.013E+5 Pa/atm 1.273E+05 Pa
Te = sample temperature (absolute)	298 °K	298 °K
Tb = flow measurement basis temperature (absolute)	295 °K	295 °K
ze = gas deviation factor at Pe and Te	1.0000	1.0000
zb = gas deviation factor at Pb and Te	1.0000	1.0000
Qb = flow rate at base conditions	0.09303 cm ³ /s	* 1.0E-6 m ³ /cm ³ 9.303E-08 m ³ /s
ve = flow velocity at sample exit end	7.769E-04 cm/s	* 1.0E-2 m/cm 7.769E-06 m/s
	Ka =	* 9.872E-13 m ² /d 1.95E-17 m ²
	Ka =	0.0198 md 1.95E-13 cm ²
	Ka =	19.8 μd

Steady State Gas Permeability Data

Project #:	8362	Net Effective Stress:	2 Mpa	290.1 psig	Gas:	N2		
Sample #:	B	Length:	9.557 cm		gas deviation z factors:	ze = 1.0000	zb = 1.0000	
Stress Level #:	1	Diameter:	10.171 cm		Viscosity:	0.0176 cp		
Regime #:	2	Area:	81.249 cm ²					
Pressure Data Filename:	8362BG.S1B							
XDCR calibration factors:	Pc =	222.869 psig/volt	Pi =	55.4417 psig/volt	ΔP =	11.0272 psid/volt	Pe =	5.5211 psig/volt

Date	Time of Day	File Time (min)	Regime #	Pb Barometric Pressure	Pc Confining Pressure	Pi Inlet Pressure	ΔP Differential Pressure	Pm Mean Pore Pressure Pe+ΔP/2	Pe Exit Pressure	Te Flow Temp (°C)	Tb Ambient Temp (°C)	Qb Flow Rate @Pb&Tb (ml/sec)
31 Mar 93	14:19	338	BS1R2a	12.37 psia	1.476 volts	1.251 volts	5.778 volts		1.118 volts	25	22	0.15462
31 Mar 93	14:23	343	BS1R2b	12.37 psia	1.470 volts	1.251 volts	5.778 volts		1.118 volts	25	22	0.15668
31 Mar 93	14:25	343	BS1R2c	12.37 psia	1.474 volts	1.251 volts	5.777 volts		1.118 volts	25	22	0.15729
31 Mar 93	14:29	348	BS1R2d	12.37 psia	1.473 volts	1.251 volts	5.777 volts		1.119 volts	25	22	0.15613
AVERAGES			BS1R2	GUAGE	GUAGE	DIFFERENTIAL	GUAGE	GUAGE	(°C)	(°C)		
				1.473 volts	1.251 volts	5.778 volts		1.118 volts				
				328.3 psig	69.36 psig	63.71 psid	38.03 psig	6.174 psig	25	22		
				22.34 atm	4.719 atm	4.335 atm	2.588 atm	0.4201 atm				
				2.264 Mpa	0.4782 Mpa	0.4393 Mpa	0.2622 Mpa	0.04257 Mpa				
				ABSOLUTE	ABSOLUTE	ABSOLUTE	DIFFERENTIAL	ABSOLUTE	ABSOLUTE	(°K)	(°K)	(ml/sec)
				12.37 psia	340.7 psia	81.73 psia	63.71 psid	50.40 psia	18.54 psia			
0.8417 atm	23.18 atm	5.561 atm	4.335 atm	3.429 atm	1.262 atm	298	295	0.15618				
0.08529 Mpa	2.349 Mpa	0.5635 Mpa	0.4393 Mpa	0.3475 Mpa	0.1279 Mpa							

C-119

Apparent gas permeability: $K_a = (v_e \cdot P_e \cdot u \cdot L) / (P_m \cdot \Delta P)$

Boyle's Law: $v_e = (P_b / P_e) \cdot (T_e / T_b) \cdot (z_e / z_b) \cdot v_b$
 $Q_e = (P_b / P_e) \cdot (T_e / T_b) \cdot (z_e / z_b) \cdot Q_b$

$v_e = Q_e / A = (P_b / P_e) \cdot (T_e / T_b) \cdot (z_e / z_b) \cdot (Q_b / A)$

Parameter	Traditional Units	SI Units
μ = gas viscosity	0.0176 cp	* 1.0E-3 Pa*sec/cp 1.760E-05 Pa*sec
L = sample length	9.557 cm	* 1.0E-2 m/cm 9.557E-02 m
A = sample circular cross sectional area	81.249 cm ²	* 1.0E-4 m ² /cm ² 8.125E-03 m ²
Pb = flow measurement basis pressure (absolute)	0.8417 atm	* 1.013E+5 Pa/atm 8.527E+04 Pa
ΔP = pressure drop across sample length	4.335 atm	* 1.013E+5 Pa/atm 4.392E+05 Pa
Pm = mean pore pressure (absolute)	3.429 atm	* 1.013E+5 Pa/atm 3.474E+05 Pa
Pe = exit pressure (absolute)	1.262 atm	* 1.013E+5 Pa/atm 1.278E+05 Pa
Te = sample temperature (absolute)	298 °K	298 °K
Tb = flow measurement basis temperature (absolute)	295 °K	295 °K
ze = gas deviation factor at Pe and Te	1.0000	1.0000
zb = gas deviation factor at Pb and Te	1.0000	1.0000
Qb = flow rate at base conditions	0.15618 cm ³ /s	* 1.0E-6 m ³ /cm ³ 1.562E-07 m ³ /s
ve = flow velocity at sample exit end	1.295E-03 cm/s	* 1.0E-2 m/cm 1.295E-05 m/s
	Ka =	1.85E-05 d * 9.872E-13 m ² /d 1.83E-17 m ²
	Ka =	0.0185 md 1.83E-13 cm ²
	Ka =	18.5 μd

Steady State Gas Permeability Data

Project #:	8362	Net Effective Stress:	2 Mpa	290.1 psig	Gas:	N2			
Sample #:	B	Length:	9.557 cm		gas deviation z factors:	ze =	1.0000	zb =	1.0000
Stress Level #:	1	Diameter:	10.171 cm		Viscosity:	0.0176 cp			
Regime #:	3	Area:	81.249 cm ²						
Pressure Data Filename:	8362BG.S1B								
XDCR calibration factors:	Pc =	222.869 psig/volt	Pl =	55.4417 psig/volt	ΔP =	11.0272 psid/volt	Pe =	5.5211 psig/volt	

Date	Time of Day	File Time (min)	Regime #	Pb Barometric Pressure	Pc Confining Pressure	Pl Inlet Pressure	ΔP Differential Pressure	Pm Mean Pore Pressure Pe+ΔP/2	Pe Exit Pressure	Te Flow Temp (°C)	Tb Ambient Temp (°C)	Qb Flow Rate @Pb&Tb (ml/sec)	
31 Mar 93	16:23	463	BS1R3a	12.37 psia	1.516 volts	1.600 volts	7.461 volts		1.279 volts	25	22	0.22910	
31 Mar 93	16:27	463	BS1R3b	12.37 psia	1.517 volts	1.600 volts	7.460 volts		1.279 volts	25	22	0.23135	
31 Mar 93	16:29	468	BS1R3c	12.37 psia	1.517 volts	1.599 volts	7.460 volts		1.279 volts	25	22	0.22949	
31 Mar 93	16:31	468	BS1R3d	12.37 psia	1.518 volts	1.599 volts	7.459 volts		1.279 volts	25	22	0.22805	
AVERAGES			BS1R3										
				GAUGE	GAUGE	DIFFERENTIAL	GAUGE	GAUGE			(°C)	(°C)	
				1.517 volts	1.600 volts	7.460 volts	1.279 volts						
				338.1 psig	88.68 psig	82.26 psid	48.19 psig	7.061 psig			25	22	
				23.01 atm	6.034 atm	5.598 atm	3.279 atm	0.4805 atm					
				2.331 Mpa	0.6114 Mpa	0.5672 Mpa	0.3323 Mpa	0.04869 Mpa					
			ABSOLUTE	ABSOLUTE	ABSOLUTE	DIFFERENTIAL	ABSOLUTE	ABSOLUTE		(°K)	(°K)	(ml/sec)	
			12.37 psia	350.5 psia	101.05 psia	82.26 psid	60.56 psia	19.43 psia					
			0.8417 atm	23.85 atm	6.876 atm	5.598 atm	4.121 atm	1.322 atm		298	295	0.22950	
			0.08529 Mpa	2.416 Mpa	0.6967 Mpa	0.5672 Mpa	0.4176 Mpa	0.1340 Mpa					

Apparent gas permeability: $K_a = (v_e \cdot P_e \cdot u \cdot L) / (P_m \cdot \Delta P)$

Boyle's Law: $V_e = (P_b / P_e) \cdot (T_e / T_b) \cdot (z_e / z_b) \cdot V_b$
 $Q_e = (P_b / P_e) \cdot (T_e / T_b) \cdot (z_e / z_b) \cdot Q_b$

$v_e = Q_e / A = (P_b / P_e) \cdot (T_e / T_b) \cdot (z_e / z_b) \cdot (Q_b / A)$

Parameter	Traditional Units	SI Units
u = gas viscosity	0.0176 cp	• 1.0E-3 Pa*sec/cp 1.760E-05 Pa*sec
L = sample length	9.557 cm	• 1.0E-2 m/cm 9.557E-02 m
A = sample circular cross sectional area	81.249 cm ²	• 1.0E-4 m ² /cm ² 8.125E-03 m ²
Pb = flow measurement basis pressure (absolute)	0.8417 atm	• 1.013E+5 Pa/atm 8.527E+04 Pa
ΔP = pressure drop across sample length	5.598 atm	• 1.013E+5 Pa/atm 5.670E+05 Pa
Pm = mean pore pressure (absolute)	4.121 atm	• 1.013E+5 Pa/atm 4.175E+05 Pa
Pe = exit pressure (absolute)	1.322 atm	• 1.013E+5 Pa/atm 1.339E+05 Pa
Te = sample temperature (absolute)	298 °K	298 °K
Tb = flow measurement basis temperature (absolute)	295 °K	295 °K
ze = gas deviation factor at Pe and Te	1.0000	1.0000
zb = gas deviation factor at Pb and Te	1.0000	1.0000
Qb = flow rate at base conditions	0.22950 cm ³ /s	• 1.0E-6 m ³ /cm ³ 2.295E-07 m ³ /s
ve = flow velocity at sample exit end	1.816E-03 cm/s	• 1.0E-2 m/cm 1.816E-05 m/s
	Ka =	• 9.872E-13 m ² /d 1.73E-17 m ²
	Ka =	0.0175 md 1.73E-13 cm ²
	Ka =	17.5 μd

C-120

Steady State Gas Permeability Data

Project #:	8362	Net Effective Stress:	2 Mpa	290.1 psig	Gas:	N2		
Sample #:	B	Length:	9.557 cm		gas deviation z factors:	ze = 1.0000	zb = 1.0000	
Stress Level #:	1	Diameter:	10.171 cm		Viscosity:	0.0176 cp		
Regime #:	4	Area:	81.249 cm ²					
Pressure Data Filename:	8362BG.S1B							
XDCR calibration factors:	Pc =	222.869 psig/volt	Pl =	55.4417 psig/volt	ΔP =	11.0272 psid/volt	Pe =	5.5211 psig/volt

Date	Time of Day	File Time (min)	Regime #	Pb Barometric Pressure	Pc Confining Pressure	Pl Inlet Pressure	ΔP Differential Pressure	Pm Mean Pore Pressure Pe+ΔP/2	Pe Exit Pressure	Te Flow Temp (°C)	Tb Ambient Temp (°C)	Qb Flow Rate @Pb&Tb (ml/sec)
01 Apr 93	09:20	1480	BS1R4a	12.28 psia	1.569 volts	1.947 volts	9.099 volts		1.514 volts	25	21	0.31721
01 Apr 93	09:23	1480	BS1R4b	12.28 psia	1.570 volts	1.947 volts	9.097 volts		1.514 volts	25	22	0.31422
01 Apr 93	09:25	1485	BS1R4c	12.28 psia	1.570 volts	1.947 volts	9.097 volts		1.514 volts	25	22	0.31496
01 Apr 93	09:27	1485	BS1R4d	12.28 psia	1.568 volts	1.946 volts	9.096 volts		1.514 volts	25	22	0.31671
AVERAGES			BS1R4									
				GAUGE	GAUGE	DIFFERENTIAL	GAUGE	GAUGE	(°C)	(°C)		
				1.569 volts	1.947 volts	9.097 volts	58.52 psig	1.514 volts	25	22		
				349.7 psig	107.93 psig	100.32 psid	8.359 psig					
				23.80 atm	7.344 atm	6.826 atm	0.5688 atm					
				2.411 Mpa	0.7442 Mpa	0.6917 Mpa	0.05763 Mpa					
			ABSOLUTE	ABSOLUTE	ABSOLUTE	DIFFERENTIAL	ABSOLUTE	ABSOLUTE	(°K)	(°K)	(ml/sec)	
			12.28 psia	362.0 psia	120.21 psia	100.32 psid	70.80 psia	20.64 psia	298	295	0.31577	
			0.8356 atm	24.63 atm	8.180 atm	6.826 atm	4.817 atm	1.404 atm				
			0.08467 Mpa	2.496 Mpa	0.8288 Mpa	0.6917 Mpa	0.4881 Mpa	0.1423 Mpa				

C-121

Apparent gas permeability: $K_a = (v_e \cdot P_e \cdot u \cdot L) / (P_m \cdot \Delta P)$

Boyle's Law: $V_e = (P_b / P_e) \cdot (T_e / T_b) \cdot (z_e / z_b) \cdot V_b$
 $Q_e = (P_b / P_e) \cdot (T_e / T_b) \cdot (z_e / z_b) \cdot Q_b$

$v_e = Q_e / A = (P_b / P_e) \cdot (T_e / T_b) \cdot (z_e / z_b) \cdot (Q_b / A)$

Parameter	Traditional Units	SI Units
μ = gas viscosity	0.0176 cp	* 1.0E-3 Pa*sec/cp 1.760E-05 Pa*sec
L = sample length	9.557 cm	* 1.0E-2 m/cm 9.557E-02 m
A = sample circular cross sectional area	81.249 cm ²	* 1.0E-4 m ² /cm ² 8.125E-03 m ²
Pb = flow measurement basis pressure (absolute)	0.8356 atm	* 1.013E+5 Pa/atm 8.465E+04 Pa
ΔP = pressure drop across sample length	6.826 atm	* 1.013E+5 Pa/atm 6.915E+05 Pa
Pm = mean pore pressure (absolute)	4.817 atm	* 1.013E+5 Pa/atm 4.880E+05 Pa
Pe = exit pressure (absolute)	1.404 atm	* 1.013E+5 Pa/atm 1.423E+05 Pa
Te = sample temperature (absolute)	298 °K	298 °K
Tb = flow measurement basis temperature (absolute)	295 °K	295 °K
ze = gas deviation factor at Pe and Te	1.0000	1.0000
zb = gas deviation factor at Pb and Te	1.0000	1.0000
Qb = flow rate at base conditions	0.31577 cm ³ /s	* 1.0E-6 m ³ /cm ³ 3.158E-07 m ³ /s
ve = flow velocity at sample exit end	2.338E-03 cm/s	* 1.0E-2 m/cm 2.338E-05 m/s
	Ka =	* 9.872E-13 m ² /d 1.66E-17 m ²
	Ka =	0.0168 md 1.66E-13 cm ²
	Ka =	16.8 μd

Steady State Gas Permeability Data

Project #: 8362	Net Effective Stress: 6 Mpa 870.2 psig	Gas: N2
Sample #: B	Length: 9.557 cm	gas deviation z factors: ze = 1.0000 zb = 1.0000
Stress Level #: 2	Diameter: 10.171 cm	Viscosity: 0.0176 cp
Regime #: 2	Area: 81.249 cm ²	
Pressure Data Filename: 8362BG.S2A		
XDCR calibration factors: Pc = 222.869 psig/volt Pi = 55.4417 psig/volt ΔP = 11.0272 psid/volt Pe = 5.5211 psig/volt		

Date	Time of Day	File Time (min)	Regime #	Pb Barometric Pressure	Pc Confining Pressure	Pi Inlet Pressure	ΔP Differential Pressure	Pm Mean Pore Pressure Pe-ΔP/2	Pe Exit Pressure	Te Flow Temp (°C)	Tb Ambient Temp (°C)	Qb Flow Rate @Pb&Tb (ml/sec)	
01 Apr 93	16:24	272	BS2R2a	12.21 psia	4.072 volts	1.251 volts	5.800 volts		1.097 volts	25	22	0.10411	
01 Apr 93	16:28	277	BS2R2b	12.21 psia	4.064 volts	1.251 volts	5.800 volts		1.098 volts	25	22	0.10400	
01 Apr 93	16:30	277	BS2R2c	12.21 psia	4.063 volts	1.251 volts	5.799 volts		1.098 volts	25	22	0.10349	
01 Apr 93	16:31	282	BS2R2d	12.21 psia	4.061 volts	1.251 volts	5.799 volts		1.098 volts	25	22	0.10360	
AVERAGES					GUAGE	GUAGE	DIFFERENTIAL	GUAGE	GUAGE	(°C)	(°C)		
					4.065 volts	1.251 volts	5.800 volts		1.098 volts				
					906.0 psig	69.36 psig	63.95 psid	38.04 psig	6.061 psig		25	22	
					61.65 atm	4.719 atm	4.352 atm	2.588 atm	0.4124 atm				
					6.246 Mpa	0.4782 Mpa	0.4409 Mpa	0.2623 Mpa	0.04179 Mpa				
				ABSOLUTE	ABSOLUTE	ABSOLUTE	DIFFERENTIAL	ABSOLUTE	ABSOLUTE	(°K)	(°K)	(ml/sec)	
					12.21 psia	918.2 psia	81.57 psia	63.95 psid	50.25 psia	18.27 psia			
				0.8308 atm	62.48 atm	5.550 atm	4.352 atm	3.419 atm	1.243 atm	298	295	0.10380	
				0.08419 Mpa	6.331 Mpa	0.5624 Mpa	0.4409 Mpa	0.3464 Mpa	0.1260 Mpa				

C-123

Apparent gas permeability: $K_a = (v_e \cdot P_e \cdot u \cdot L) / (P_m \cdot \Delta P)$

Boyle's Law: $v_e = (P_b / P_e) \cdot (T_e / T_b) \cdot (z_e / z_b) \cdot v_b$
 $Q_e = (P_b / P_e) \cdot (T_e / T_b) \cdot (z_e / z_b) \cdot Q_b$

$v_e = Q_e / A = (P_b / P_e) \cdot (T_e / T_b) \cdot (z_e / z_b) \cdot (Q_b / A)$

Parameter	Traditional Units	SI Units
μ = gas viscosity	0.0176 cp	• 1.0E-3 Pa*sec/cp 1.760E-05 Pa*sec
L = sample length	9.557 cm	• 1.0E-2 m/cm 9.557E-02 m
A = sample circular cross sectional area	81.249 cm ²	• 1.0E-4 m ² /cm ² 8.125E-03 m ²
Pb = flow measurement basis pressure (absolute)	0.8308 atm	• 1.013E+5 Pa/atm 8.416E+04 Pa
ΔP = pressure drop across sample length	4.352 atm	• 1.013E+5 Pa/atm 4.408E+05 Pa
Pm = mean pore pressure (absolute)	3.419 atm	• 1.013E+5 Pa/atm 3.464E+05 Pa
Pe = exit pressure (absolute)	1.243 atm	• 1.013E+5 Pa/atm 1.259E+05 Pa
Te = sample temperature (absolute)	298 °K	298 °K
Tb = flow measurement basis temperature (absolute)	295 °K	295 °K
ze = gas deviation factor at Pe and Te	1.0000	1.0000
zb = gas deviation factor at Pb and Te	1.0000	1.0000
Qb = flow rate at base conditions	0.10380 cm ³ /s	• 1.0E-6 m ³ /cm ³ 1.038E-07 m ³ /s
ve = flow velocity at sample exit end	8.625E-04 cm/s	• 1.0E-2 m/cm 8.625E-06 m/s
	Ka = 1.21E-05 d	• 9.872E-13 m ² /d 1.20E-17 m ²
	Ka = 0.0121 md	1.20E-13 cm ²
	Ka = 12.1 μd	

Steady State Gas Permeability Data

Project #:	8362	Net Effective Stress:	6 Mpa	870.2 psig	Gas:	N2		
Sample #:	B	Length:	9.557 cm		gas deviation z factors:	ze = 1.0000	zb = 1.0000	
Stress Level #:	2	Diameter:	10.171 cm		Viscosity:	0.0176 cp		
Regime #:	3	Area:	81.249 cm ²					
Pressure Data Filename:	8362BG.S2A							
XDCR calibration factors:	Pc =	222.869 psig/volt	PI =	55.4417 psig/volt	ΔP =	11.0272 psid/volt	Pe =	5.5211 psig/volt

Date	Time of Day	File Time (min)	Regime #	Pb Barometric Pressure	Pc Confining Pressure	PI Inlet Pressure	ΔP Differential Pressure	Pm Mean Pore Pressure Pe-ΔP/2	Pe Exit Pressure	Te Flow Temp (°C)	Tb Ambient Temp (°C)	Qb Flow Rate @Pb&Tb (ml/sec)
02 Apr 93	08:40	1253	BS2R3a	12.31 psia	4.120 volts	1.601 volts	7.475 volts		1.248 volts	25	21	0.14744
02 Apr 93	08:42	1253	BS2R3b	12.31 psia	4.113 volts	1.601 volts	7.475 volts		1.250 volts	25	21	0.14782
02 Apr 93	08:44	1253	BS2R3c	12.31 psia	4.115 volts	1.601 volts	7.474 volts		1.250 volts	25	21	0.14782
02 Apr 93	08:46	1258	BS2R3d	12.31 psia	4.117 volts	1.601 volts	7.474 volts		1.251 volts	25	21	0.14804
AVERAGES			BS2R3									
				GUAGE	GUAGE	DIFFERENTIAL	GUAGE	GUAGE	(°C)	(°C)		
				4.116 volts	1.601 volts	7.475 volts		1.250 volts				
				917.4 psig	88.76 psig	82.42 psid	48.11 psig	6.900 psig	25	21		
				62.42 atm	6.040 atm	5.609 atm	3.274 atm	0.4695 atm				
				6.325 Mpa	0.6120 Mpa	0.5683 Mpa	0.3317 Mpa	0.04757 Mpa				
				ABSOLUTE	ABSOLUTE	ABSOLUTE	DIFFERENTIAL	ABSOLUTE	ABSOLUTE	(°K)	(°K)	(ml/sec)
				12.31 psia	929.7 psia	101.07 psia	82.42 psid	60.42 psia	19.21 psia	298	294	0.14778
0.8376 atm	63.26 atm	6.878 atm	5.609 atm	4.111 atm	1.307 atm							
0.08487 Mpa	6.410 Mpa	0.6969 Mpa	0.5683 Mpa	0.4166 Mpa	0.1324 Mpa							

C-124

Apparent gas permeability: $K_a = (v_e \cdot P_e \cdot u \cdot L) / (P_m \cdot \Delta P)$

Boyle's Law: $V_e = (P_b / P_e) \cdot (T_e / T_b) \cdot (z_e / z_b) \cdot V_b$
 $Q_e = (P_b / P_e) \cdot (T_e / T_b) \cdot (z_e / z_b) \cdot Q_b$

$v_e = Q_e / A = (P_b / P_e) \cdot (T_e / T_b) \cdot (z_e / z_b) \cdot (Q_b / A)$

Parameter	Traditional Units	SI Units
μ = gas viscosity	0.0176 cp	• 1.0E-3 Pa*sec/cp 1.760E-05 Pa*sec
L = sample length	9.557 cm	• 1.0E-2 m/cm 9.557E-02 m
A = sample circular cross sectional area	81.249 cm ²	• 1.0E-4 m ² /cm ² 8.125E-03 m ²
Pb = flow measurement basis pressure (absolute)	0.8376 atm	• 1.013E+5 Pa/atm 8.485E+04 Pa
ΔP = pressure drop across sample length	5.609 atm	• 1.013E+5 Pa/atm 5.681E+05 Pa
Pm = mean pore pressure (absolute)	4.111 atm	• 1.013E+5 Pa/atm 4.165E+05 Pa
Pe = exit pressure (absolute)	1.307 atm	• 1.013E+5 Pa/atm 1.324E+05 Pa
Te = sample temperature (absolute)	298 °K	298 °K
Tb = flow measurement basis temperature (absolute)	294 °K	294 °K
ze = gas deviation factor at Pe and Te	1.0000	1.0000
zb = gas deviation factor at Pb and Te	1.0000	1.0000
Qb = flow rate at base conditions	0.14778 cm ³ /s	• 1.0E-6 m ³ /cm ³ 1.478E-07 m ³ /s
ve = flow velocity at sample exit end	1.181E-03 cm/s	• 1.0E-2 m/cm 1.181E-05 m/s
	Ka = 1.13E-05 d	• 9.872E-13 m ² /d 1.11E-17 m ²
	Ka = 0.0113 md	1.11E-13 cm ²
	Ka = 11.3 μd	

Steady State Gas Permeability Data

Project #:	8362	Net Effective Stress:	6 Mpa	870.2 psig	Gas:	N2		
Sample #:	B	Length:	9.557 cm		gas deviation z factors:	ze = 1.0000	zb = 1.0000	
Stress Level #:	2	Diameter:	10.171 cm		Viscosity:	0.0176 cp		
Regime #:	4	Area:	81.249 cm ²					
Pressure Data Filename:	8362BG.S2A							
XDCR calibration factors:	Pc = 222.869 psig/volt	PI = 55.4417 psig/volt	ΔP = 11.0272 psid/volt	Pe = 5.5211 psig/volt				

Date	Time of Day	File Time (min)	Regime #	Pb Barometric Pressure	Pc Confining Pressure	PI Inlet Pressure	ΔP Differential Pressure	Pm Mean Pore Pressure Pe*ΔP/2	Pe Exit Pressure	Te Flow Temp (°C)	Tb Ambient Temp (°C)	Qb Flow Rate @Pb&Tb (ml/sec)
02 Apr 93	14:31	1602	BS2R4a	12.32 psia	4.167 volts	1.951 volts	9.144 volts		1.451 volts	25	22	0.20243
02 Apr 93	14:33	1602	BS2R4b	12.32 psia	4.170 volts	1.950 volts	9.143 volts		1.451 volts	25	22	0.20222
02 Apr 93	14:35	1607	BS2R4c	12.32 psia	4.168 volts	1.950 volts	9.143 volts		1.451 volts	25	22	0.20121
02 Apr 93	14:37	1607	BS2R4d	12.32 psia	4.168 volts	1.950 volts	9.143 volts		1.451 volts	25	22	0.20161
AVERAGES			BS2R4									
					GUAGE	GUAGE	DIFFERENTIAL	GUAGE	GUAGE	(°C)	(°C)	
					4.168 volts	1.950 volts	9.143 volts		1.451 volts			
					929.0 psig	108.13 psig	100.82 psid	58.42 psig	8.011 psig	25	22	
					63.21 atm	7.357 atm	6.861 atm	3.975 atm	0.5451 atm			
					6.405 Mpa	0.7455 Mpa	0.6952 Mpa	0.4028 Mpa	0.05523 Mpa			
				ABSOLUTE	ABSOLUTE	DIFFERENTIAL	ABSOLUTE	ABSOLUTE	(°K)	(°K)	(ml/sec)	
				12.32 psia	941.3 psia	120.45 psia	100.82 psid	70.74 psia	20.33 psia			
				0.8383 atm	64.05 atm	8.196 atm	6.861 atm	4.814 atm	1.383 atm	298	295	0.20187
				0.08494 Mpa	6.490 Mpa	0.8304 Mpa	0.6952 Mpa	0.4878 Mpa	0.1402 Mpa			

C-125

Apparent gas permeability: $K_a = (v_e * P_e * u * L) / (P_m * \Delta P)$

Boyle's Law: $v_e = (P_b / P_e) * (T_e / T_b) * (z_e / z_b) * v_b$
 $Q_e = (P_b / P_e) * (T_e / T_b) * (z_e / z_b) * Q_b$

$v_e = Q_e / A = (P_b / P_e) * (T_e / T_b) * (z_e / z_b) * (Q_b / A)$

Parameter	Traditional Units	SI Units
μ = gas viscosity	0.0176 cp	* 1.0E-3 Pa*sec/cp 1.760E-05 Pa*sec
L = sample length	9.557 cm	* 1.0E-2 m/cm 9.557E-02 m
A = sample circular cross sectional area	81.249 cm ²	* 1.0E-4 m ² /cm ² 8.125E-03 m ²
Pb = flow measurement basis pressure (absolute)	0.8383 atm	* 1.013E+5 Pa/atm 8.492E+04 Pa
ΔP = pressure drop across sample length	6.861 atm	* 1.013E+5 Pa/atm 6.950E+05 Pa
Pm = mean pore pressure (absolute)	4.814 atm	* 1.013E+5 Pa/atm 4.876E+05 Pa
Pe = exit pressure (absolute)	1.383 atm	* 1.013E+5 Pa/atm 1.401E+05 Pa
Te = sample temperature (absolute)	298 °K	298 °K
Tb = flow measurement basis temperature (absolute)	295 °K	295 °K
ze = gas deviation factor at Pe and Te	1.0000	1.0000
zb = gas deviation factor at Pb and Te	1.0000	1.0000
Qb = flow rate at base conditions	0.20187 cm ³ /s	* 1.0E-6 m ³ /cm ³ 2.019E-07 m ³ /s
ve = flow velocity at sample exit end	1.521E-03 cm/s	* 1.0E-2 m/cm 1.521E-05 m/s
	Ka = 1.07E-05 d	* 9.872E-13 m ² /d 1.06E-17 m ²
	Ka = 0.0107 md	1.06E-13 cm ²
	Ka = 10.7 μd	

Steady State Gas Permeability Data

Project #: 8362	Net Effective Stress: 10 Mpa 1450.4 psig	Gas: N2
Sample #: B	Length: 9.557 cm	gas deviation z factors: ze = 1.0000 zb = 1.0000
Stress Level #: 3	Diameter: 10.171 cm	Viscosity: 0.0176 cp
Regime #: 1	Area: 81.249 cm ²	
Pressure Data Filename: 8362BG.S3A		
XDCR calibration factors: Pc = 222.869 psig/volt P1 = 55.4417 psig/volt ΔP = 11.0272 psid/volt Pe = 5.5211 psig/volt		

Date	Time of Day	File Time (min)	Regime #	Pb Barometric Pressure	Pc Confining Pressure	P1 Inlet Pressure	ΔP Differential Pressure	Pm Mean Pore Pressure Pe*ΔP/2	Pe Exit Pressure	Te Flow Temp (°C)	Tb Ambient Temp (°C)	Qb Flow Rate @Pb&Tb (ml/sec)
05 Apr 93	13:18	4159	BS3R1a	12.23 psia	6.630 volts	0.907 volts	4.132 volts		0.896 volts	25	22	0.03985
05 Apr 93	13:20	4164	BS3R1b	12.23 psia	6.634 volts	0.907 volts	4.132 volts		0.896 volts	25	22	0.03982
05 Apr 93	13:23	4164	BS3R1c	12.23 psia	6.633 volts	0.907 volts	4.132 volts		0.896 volts	25	22	0.03990
05 Apr 93	13:26	4169	BS3R1d	12.23 psia	6.631 volts	0.907 volts	4.132 volts		0.896 volts	25	22	0.03984
AVERAGES			BS3R1									
					GUAGE	GUAGE	DIFFERENTIAL	GUAGE	GUAGE	(°C)	(°C)	
					6.632 volts	0.907 volts	4.132 volts		0.896 volts			
					1478.1 psig	50.29 psig	45.56 psid	27.73 psig	4.947 psig	25	22	
					100.58 atm	3.422 atm	3.100 atm	1.887 atm	0.3366 atm			
					10.191 Mpa	0.3467 Mpa	0.3142 Mpa	0.1912 Mpa	0.03411 Mpa			
			ABSOLUTE	ABSOLUTE	ABSOLUTE	DIFFERENTIAL	ABSOLUTE	ABSOLUTE	(°K)	(°K)	(ml/sec)	
			12.23 psia	1490.3 psia	62.52 psia	45.56 psid	39.96 psia	17.18 psia				
			0.8322 atm	101.41 atm	4.254 atm	3.100 atm	2.719 atm	1.169 atm	298	295	0.03985	
			0.08432 Mpa	10.275 Mpa	0.4310 Mpa	0.3142 Mpa	0.2755 Mpa	0.1184 Mpa				

C-126

Apparent gas permeability: $K_a = (v_e \cdot P_e \cdot u \cdot L) / (P_m \cdot \Delta P)$

Boyle's Law: $V_e = (P_b/P_e) \cdot (T_e/T_b) \cdot (z_e/z_b) \cdot V_b$
 $Q_e = (P_b/P_e) \cdot (T_e/T_b) \cdot (z_e/z_b) \cdot Q_b$

$v_e = Q_e/A = (P_b/P_e) \cdot (T_e/T_b) \cdot (z_e/z_b) \cdot (Q_b/A)$

Parameter	Traditional Units	SI Units
u = gas viscosity	0.0176 cp	* 1.0E-3 Pa*sec/cp 1.760E-05 Pa*sec
L = sample length	9.557 cm	* 1.0E-2 m/cm 9.557E-02 m
A = sample circular cross sectional area	81.249 cm ²	* 1.0E-4 m ² /cm ² 8.125E-03 m ²
Pb = flow measurement basis pressure (absolute)	0.8322 atm	* 1.013E+5 Pa/atm 8.430E+04 Pa
ΔP = pressure drop across sample length	3.100 atm	* 1.013E+5 Pa/atm 3.141E+05 Pa
Pm = mean pore pressure (absolute)	2.719 atm	* 1.013E+5 Pa/atm 2.754E+05 Pa
Pe = exit pressure (absolute)	1.169 atm	* 1.013E+5 Pa/atm 1.184E+05 Pa
Te = sample temperature (absolute)	298 °K	298 °K
Tb = flow measurement basis temperature (absolute)	295 °K	295 °K
ze = gas deviation factor at Pe and Te	1.0000	1.0000
zb = gas deviation factor at Pb and Te	1.0000	1.0000
Qb = flow rate at base conditions	0.03985 cm ³ /s	* 1.0E-6 m ³ /cm ³ 3.985E-08 m ³ /s
ve = flow velocity at sample exit end	3.528E-04 cm/s	* 1.0E-2 m/cm 3.528E-06 m/s
	Ka = 8.23E-06 d	* 9.872E-13 m ² /d 8.12E-18 m ²
	Ka = 0.0082 md	8.12E-14 cm ²
	Ka = 8.23 μd	

Steady State Gas Permeability Data

Project #:	8362	Net Effective Stress:	10 Mpa	1450.4 psig	Gas:	N2		
Sample #:	B	Length:	9.557 cm		gas deviation z factors:	ze = 1.0000	zb = 1.0000	
Stress Level #:	3	Diameter:	10.171 cm		Viscosity:	0.0176 cp		
Regime #:	2	Area:	81.249 cm ²					
Pressure Data Filename:	8362BG.S3A							
XDCR calibration factors:	Pc = 222.869 psig/volt	Pl = 55.4417 psig/volt	AP = 11.0272 psid/volt	Pe = 5.5211 psig/volt				

Date	Time of Day	File Time (min)	Regime #	Pb Barometric Pressure	Pc Confining Pressure	Pl Inlet Pressure	AP Differential Pressure	Pm Mean Pore Pressure Pe+AP/2	Pe Exit Pressure	Te Flow Temp (°C)	Tb Ambient Temp (°C)	Qb Flow Rate @Pb&Tb (ml/sec)	
05 Apr 93	16:04	4324	BS3R2a	12.21 psia	6.661 volts	1.252 volts	5.791 volts		1.073 volts	25	22	0.06445	
05 Apr 93	16:07	4329	BS3R2b	12.21 psia	6.682 volts	1.252 volts	5.790 volts		1.074 volts	25	22	0.06401	
05 Apr 93	16:10	4334	BS3R2c	12.21 psia	6.690 volts	1.252 volts	5.790 volts		1.073 volts	25	22	0.06430	
05 Apr 93	16:15	4339	BS3R2d	12.21 psia	6.695 volts	1.252 volts	5.791 volts		1.073 volts	25	22	0.06430	
AVERAGES			BS3R2		GUAGE	GUAGE	DIFFERENTIAL	GUAGE	GUAGE	(°C)	(°C)		
					6.682 volts	1.252 volts	5.791 volts		1.073 volts				
					1489.2 psig	69.41 psig	63.85 psid	37.85 psig	5.926 psig	25	22		
					101.33 atm	4.723 atm	4.345 atm	2.576 atm	0.4032 atm				
					10.268 Mpa	0.4786 Mpa	0.4403 Mpa	0.2610 Mpa	0.04086 Mpa				
					ABSOLUTE	ABSOLUTE	ABSOLUTE	DIFFERENTIAL	ABSOLUTE	ABSOLUTE	(°K)	(°K)	(ml/sec)
					12.21 psia	1501.4 psia	81.62 psia	63.85 psid	50.06 psia	18.14 psia			
			0.8308 atm	102.17 atm	5.554 atm	4.345 atm	3.407 atm	1.234 atm	298	295	0.06427		
			0.08419 Mpa	10.352 Mpa	0.5628 Mpa	0.4403 Mpa	0.3452 Mpa	0.1250 Mpa					

C-127

Apparent gas permeability: $K_a = (v_e \cdot P_e \cdot u \cdot L) / (P_m \cdot \Delta P)$

Boyle's Law: $V_e = (P_b / P_e) \cdot (T_e / T_b) \cdot (z_e / z_b) \cdot V_b$
 $Q_e = (P_b / P_e) \cdot (T_e / T_b) \cdot (z_e / z_b) \cdot Q_b$

$v_e = Q_e / A = (P_b / P_e) \cdot (T_e / T_b) \cdot (z_e / z_b) \cdot (Q_b / A)$

Parameter	Traditional Units	SI Units
μ = gas viscosity	0.0176 cp	* 1.0E-3 Pa*sec/cp 1.760E-05 Pa*sec
L = sample length	9.557 cm	* 1.0E-2 m/cm 9.557E-02 m
A = sample circular cross sectional area	81.249 cm ²	* 1.0E-4 m ² /cm ² 8.125E-03 m ²
Pb = flow measurement basis pressure (absolute)	0.8308 atm	* 1.013E+5 Pa/atm 8.416E+04 Pa
ΔP = pressure drop across sample length	4.345 atm	* 1.013E+5 Pa/atm 4.401E+05 Pa
Pm = mean pore pressure (absolute)	3.407 atm	* 1.013E+5 Pa/atm 3.451E+05 Pa
Pe = exit pressure (absolute)	1.234 atm	* 1.013E+5 Pa/atm 1.250E+05 Pa
Te = sample temperature (absolute)	298 °K	298 °K
Tb = flow measurement basis temperature (absolute)	295 °K	295 °K
ze = gas deviation factor at Pe and Te	1.0000	1.0000
zb = gas deviation factor at Pb and Te	1.0000	1.0000
Qb = flow rate at base conditions	0.06427 cm ³ /s	* 1.0E-6 m ³ /cm ³ 6.427E-08 m ³ /s
ve = flow velocity at sample exit end	5.379E-04 cm/s	* 1.0E-2 m/cm 5.379E-06 m/s
	Ka = 7.54E-06 d	* 9.872E-13 m ² /d 7.45E-18 m ²
	Ka = 0.00754 md	7.45E-14 cm ²
	Ka = 7.54 μ d	

Steady State Gas Permeability Data

Project #: 8362	Net Effective Stress: 10 Mpa	1450.4 psig	Gas: N2
Sample #: B	Length: 9.557 cm		gas deviation z factors: ze = 1.0000 zb = 1.0000
Stress Level #: 3	Diameter: 10.171 cm		Viscosity: 0.0176 cp
Regime #: 3	Area: 81.249 cm ²		
Pressure Data Filename: 8362BG.S3A			
XDCR calibration factors: Pc = 222.869 psig/volt	Pl = 55.4417 psig/volt	ΔP = 11.0272 psid/volt	Pe = 5.5211 psig/volt

Date	Time of Day	File Time (min)	Regime #	Pb Barometric Pressure	Pc Confining Pressure	Pl Inlet Pressure	ΔP Differential Pressure	Pm Mean Pore Pressure Pe+ΔP/2	Pe Exit Pressure	Te Flow Temp (°C)	Tb Ambient Temp (°C)	Qb Flow Rate @Pb&Tb (ml/sec)	
06 Apr 93	10:17	5419	BS3R3a	12.27 psia	6.737 volts	1.602 volts	7.460 volts		1.253 volts	25	22	0.09236	
06 Apr 93	10:21	5424	BS3R3b	12.27 psia	6.735 volts	1.602 volts	7.460 volts		1.253 volts	25	22	0.09234	
06 Apr 93	10:24	5424	BS3R3c	12.27 psia	6.736 volts	1.602 volts	7.460 volts		1.253 volts	25	22	0.09236	
06 Apr 93	10:26	5429	BS3R3d	12.27 psia	6.735 volts	1.602 volts	7.460 volts		1.253 volts	25	22	0.09227	
AVERAGES			BS3R3										
					GUAGE	GUAGE	DIFFERENTIAL	GUAGE	GUAGE		(°C)	(°C)	
					6.736 volts	1.602 volts	7.460 volts		1.253 volts		25	22	
					1501.2 psig	88.82 psig	82.26 psid	48.05 psig	6.918 psig				
					102.15 atm	6.044 atm	5.598 atm	3.270 atm	0.4707 atm				
					10.350 Mpa	0.6124 Mpa	0.5672 Mpa	0.3313 Mpa	0.04770 Mpa				
			ABSOLUTE	ABSOLUTE	ABSOLUTE	DIFFERENTIAL	ABSOLUTE	ABSOLUTE		(°K)	(°K)	(ml/sec)	
			12.27 psia	1513.5 psia	101.09 psia	82.26 psid	60.32 psia	19.19 psia		298	295	0.09233	
			0.8349 atm	102.98 atm	6.879 atm	5.598 atm	4.104 atm	1.306 atm					
			0.08460 Mpa	10.435 Mpa	0.6970 Mpa	0.5672 Mpa	0.4159 Mpa	0.1323 Mpa					

Apparent gas permeability: $K_a = (v_e \cdot P_e \cdot u \cdot L) / (P_m \cdot \Delta P)$

Boyle's Law: $v_e = (P_b / P_e) \cdot (T_e / T_b) \cdot (z_e / z_b) \cdot v_b$
 $Q_e = (P_b / P_e) \cdot (T_e / T_b) \cdot (z_e / z_b) \cdot Q_b$

$v_e = Q_e / A = (P_b / P_e) \cdot (T_e / T_b) \cdot (z_e / z_b) \cdot (Q_b / A)$

Parameter	Traditional Units	SI Units
μ = gas viscosity	0.0176 cp	* 1.0E-3 Pa*sec/cp 1.760E-05 Pa*sec
L = sample length	9.557 cm	* 1.0E-2 m/cm 9.557E-02 m
A = sample circular cross sectional area	81.249 cm ²	* 1.0E-4 m ² /cm ² 8.125E-03 m ²
Pb = flow measurement basis pressure (absolute)	0.8349 atm	* 1.013E+5 Pa/atm 8.458E+04 Pa
ΔP = pressure drop across sample length	5.598 atm	* 1.013E+5 Pa/atm 5.670E+05 Pa
Pm = mean pore pressure (absolute)	4.104 atm	* 1.013E+5 Pa/atm 4.158E+05 Pa
Pe = exit pressure (absolute)	1.306 atm	* 1.013E+5 Pa/atm 1.323E+05 Pa
Te = sample temperature (absolute)	298 °K	298 °K
Tb = flow measurement basis temperature (absolute)	295 °K	295 °K
ze = gas deviation factor at Pe and Te	1.0000	1.0000
zb = gas deviation factor at Pb and Te	1.0000	1.0000
Qb = flow rate at base conditions	0.09233 cm ³ /s	* 1.0E-6 m ³ /cm ³ 9.233E-08 m ³ /s
ve = flow velocity at sample exit end	7.341E-04 cm/s	* 1.0E-2 m/cm 7.341E-06 m/s
	Ka = 7.02E-06 d	* 9.872E-13 m ² /d 6.93E-18 m ²
	Ka = 0.00702 md	6.93E-14 cm ²
	Ka = 7.02 μd	

C-128

Steady State Gas Permeability Data

Project #:	8362	Net Effective Stress:	10 Mpa	1450.4 psig	Gas:	N2		
Sample #:	B	Length:	9.557 cm		gas deviation z factors:	ze = 1.0000	zb = 1.0000	
Stress Level #:	3	Diameter:	10.171 cm		Viscosity:	0.0176 cp		
Regime #:	4	Area:	81.249 cm ²					
Pressure Data Filename:	8362BG.S3A							
XDCR calibration factors:	Pc = 222.869 psig/volt	Pi = 55.4417 psig/volt	ΔP = 11.0272 psid/volt	Pe = 5.5211 psig/volt				

Date	Time of Day	File Time (min)	Regime #	Pb Barometric Pressure	Pc Confining Pressure	Pi Inlet Pressure	ΔP Differential Pressure	Pm Mean Pore Pressure Pe+ΔP/2	Pe Exit Pressure	Te Flow Temp (°C)	Tb Ambient Temp (°C)	Qb Flow Rate @Pb&Tb (ml/sec)	
06 Apr 93	13:39	5619	BS3R4a	12.28 psia	6.776 volts	1.950 volts	9.122 volts		1.451 volts	25	22	0.12571	
06 Apr 93	13:42	5624	BS3R4b	12.28 psia	6.780 volts	1.950 volts	9.122 volts		1.451 volts	25	22	0.12590	
06 Apr 93	13:44	5624	BS3R4c	12.28 psia	6.777 volts	1.950 volts	9.122 volts		1.451 volts	25	22	0.12598	
06 Apr 93	13:46	5629	BS3R4d	12.28 psia	6.776 volts	1.950 volts	9.122 volts		1.451 volts	25	22	0.12571	
AVERAGES			BS3R4										
					GUAGE	GUAGE	DIFFERENTIAL	GUAGE	GUAGE	(°C)	(°C)		
					6.777 volts	1.950 volts	9.122 volts		1.451 volts				
					1510.4 psig	108.11 psig	100.59 psid	58.31 psig	8.011 psig	25	22		
					102.78 atm	7.357 atm	6.845 atm	3.967 atm	0.5451 atm				
					10.414 Mpa	0.7454 Mpa	0.6935 Mpa	0.4020 Mpa	0.05523 Mpa				
			ABSOLUTE	ABSOLUTE	ABSOLUTE	DIFFERENTIAL	ABSOLUTE	ABSOLUTE	(°K)	(°K)	(ml/sec)		
			12.28 psia	1522.7 psia	120.39 psia	100.59 psid	70.59 psia	20.29 psia					
			0.8356 atm	103.61 atm	8.192 atm	6.845 atm	4.803 atm	1.381 atm	298	295	0.12583		
			0.08467 Mpa	10.499 Mpa	0.8301 Mpa	0.6935 Mpa	0.4867 Mpa	0.1399 Mpa					

C-129

Apparent gas permeability: $K_a = (v_e \cdot P_e \cdot u \cdot L) / (P_m \cdot \Delta P)$

Boyle's Law: $v_e = (P_b / P_e) \cdot (T_e / T_b) \cdot (z_e / z_b) \cdot v_b$
 $Q_e = (P_b / P_e) \cdot (T_e / T_b) \cdot (z_e / z_b) \cdot Q_b$

$v_e = Q_e / A = (P_b / P_e) \cdot (T_e / T_b) \cdot (z_e / z_b) \cdot (Q_b / A)$

Parameter	Traditional Units	SI Units
μ = gas viscosity	0.0176 cp	• 1.0E-3 Pa*sec/cp 1.760E-05 Pa*sec
L = sample length	9.557 cm	• 1.0E-2 m/cm 9.557E-02 m
A = sample circular cross sectional area	81.249 cm ²	• 1.0E-4 m ² /cm ² 8.125E-03 m ²
Pb = flow measurement basis pressure (absolute)	0.8356 atm	• 1.013E+5 Pa/atm 8.465E+04 Pa
ΔP = pressure drop across sample length	6.845 atm	• 1.013E+5 Pa/atm 6.934E+05 Pa
Pm = mean pore pressure (absolute)	4.803 atm	• 1.013E+5 Pa/atm 4.866E+05 Pa
Pe = exit pressure (absolute)	1.381 atm	• 1.013E+5 Pa/atm 1.399E+05 Pa
Te = sample temperature (absolute)	298 °K	298 °K
Tb = flow measurement basis temperature (absolute)	295 °K	295 °K
ze = gas deviation factor at Pe and Te	1.0000	1.0000
zb = gas deviation factor at Pb and Te	1.0000	1.0000
Qb = flow rate at base conditions	0.12583 cm ³ /s	• 1.0E-6 m ³ /cm ³ 1.258E-07 m ³ /s
ve = flow velocity at sample exit end	9.468E-04 cm/s	• 1.0E-2 m/cm 9.468E-06 m/s
	Ka = 6.69E-06 d	• 9.872E-13 m ² /d 6.60E-18 m ²
	Ka = 0.00669 md	6.60E-14 cm ²
	Ka = 6.69 μd	

Steady State Gas Permeability Data

Project #:	8362	Net Effective Stress:	2 Mpa	290.1 psid	Gas:	N2		
Sample #:	C	Length:	10.043 cm		gas deviation z factors:	ze = 1.0000	zb = 1.0000	
Stress Level #:	1	Diameter:	10.168 cm		Viscosity:	0.0176 cp		
Regime #:	1	Area:	81.201 cm ²					
Pressure Data Filename:	8362CG.S1B							
XDCR calibration factors:	Pc = 222.869 psig/volt	PI = 55.4417 psig/volt	ΔP = 11.0272 psid/volt	Pe = 5.5211 psig/volt				

Date	Time of Day	File Time (min)	Regime #	Pb Barometric Pressure	Pc Confining Pressure	PI Inlet Pressure	ΔP Differential Pressure	Pm Mean Pore Pressure Pe+ΔP/2	Pe Exit Pressure	Te Flow Temp (°C)	Tb Ambient Temp (°C)	Qb Flow Rate @Pb&Tb (ml/sec)	
27 Apr 93	13:40	266	CS1R1a	12.36 psia	1.434 volts	0.962 volts	4.416 volts		0.893 volts	23	23	0.04023	
27 Apr 93	13:45	271	CS1R1b	12.36 psia	1.434 volts	0.963 volts	4.415 volts		0.894 volts	23	23	0.04023	
27 Apr 93	13:49	271	CS1R1c	12.36 psia	1.434 volts	0.963 volts	4.415 volts		0.896 volts	23	23	0.04007	
27 Apr 93	13:52	276	CS1R1d	12.36 psia	1.434 volts	0.963 volts	4.415 volts		0.897 volts	23	23	0.04025	
AVERAGES			CS1R1										
					GAUGE	GAUGE	DIFFERENTIAL	GAUGE	GAUGE	(°C)	(°C)		
					1.434 volts	0.963 volts	4.415 volts		0.895 volts				
					319.6 psig	53.38 psig	48.69 psid	29.29 psig	4.941 psig	23	23		
					21.75 atm	3.632 atm	3.313 atm	1.993 atm	0.3362 atm				
				2.204 Mpa	0.3680 Mpa	0.3357 Mpa	0.2019 Mpa	0.03407 Mpa					
				ABSOLUTE	ABSOLUTE	ABSOLUTE	DIFFERENTIAL	ABSOLUTE	ABSOLUTE	(°K)	(°K)	(ml/sec)	
				12.36 psia	332.0 psia	65.74 psia	48.69 psid	41.65 psia	17.30 psia				
				0.8410 atm	22.59 atm	4.473 atm	3.313 atm	2.834 atm	1.177 atm	296	296	0.04020	
				0.08522 Mpa	2.289 Mpa	0.4532 Mpa	0.3357 Mpa	0.2871 Mpa	0.1193 Mpa				

C-130

Apparent gas permeability: $K_a = (v_e \cdot P_e \cdot u \cdot L) / (P_m \cdot \Delta P)$

Boyle's Law: $V_e = (P_b/P_e) \cdot (T_e/T_b) \cdot (z_e/z_b) \cdot V_b$
 $Q_e = (P_b/P_e) \cdot (T_e/T_b) \cdot (z_e/z_b) \cdot Q_b$

$v_e = Q_e/A = (P_b/P_e) \cdot (T_e/T_b) \cdot (z_e/z_b) \cdot (Q_b/A)$

Parameter	Traditional Units	SI Units
μ = gas viscosity	0.0176 cp	* 1.0E-3 Pa*sec/cp 1.760E-05 Pa*sec
L = sample length	10.043 cm	* 1.0E-2 m/cm 1.004E-01 m
A = sample circular cross sectional area	81.201 cm ²	* 1.0E-4 m ² /cm ² 8.120E-03 m ²
Pb = flow measurement basis pressure (absolute)	0.8410 atm	* 1.013E+5 Pa/atm 8.520E+04 Pa
ΔP = pressure drop across sample length	3.313 atm	* 1.013E+5 Pa/atm 3.356E+05 Pa
Pm = mean pore pressure (absolute)	2.834 atm	* 1.013E+5 Pa/atm 2.871E+05 Pa
Pe = exit pressure (absolute)	1.177 atm	* 1.013E+5 Pa/atm 1.193E+05 Pa
Te = sample temperature (absolute)	296 °K	296 °K
Tb = flow measurement basis temperature (absolute)	296 °K	296 °K
ze = gas deviation factor at Pe and Te	1.0000	1.0000
zb = gas deviation factor at Pb and Te	1.0000	1.0000
Qb = flow rate at base conditions	0.04020 cm ³ /s	* 1.0E-6 m ³ /cm ³ 4.020E-08 m ³ /s
ve = flow velocity at sample exit end	3.536E-04 cm/s	* 1.0E-2 m/cm 3.536E-06 m/s
	Ka = 7.84E-06 d	* 9.872E-13 m ² /d 7.74E-18 m ²
	Ka = 7.84E-03 md	7.74E-14 cm ²
	Ka = 7.84E+00 μd	

Steady State Gas Permeability Data

Project #: 8362	Net Effective Stress: 2 Mpa 290.1 psid	Gas: N2
Sample #: C	Length: 10.043 cm	gas deviation z factors: ze = 1.0000 zb = 1.0000
Stress Level #: 1	Diameter: 10.168 cm	Viscosity: 0.0176 cp
Regime #: 2	Area: 81.201 cm ²	
Pressure Data Filename: 8362CG.S1B		
XDCR calibration factors:	Pc = 222.869 psig/volt P1 = 55.4417 psig/volt ΔP = 11.0272 psid/volt	Pe = 5.5211 psig/volt

Date	Time of Day	File Time (min)	Regime #	Pb Barometric Pressure	Pc Confining Pressure	P1 Inlet Pressure	ΔP Differential Pressure	Pm Mean Pore Pressure Pe+ΔP/2	Pe Exit Pressure	Te Flow Temp (°C)	Tb Ambient Temp (°C)	Qb Flow Rate @Pb&Tb (ml/sec)
27 Apr 93	16:45	451	CS1R2a	12.34 psia	1.477 volts	1.138 volts	4.375 volts		2.745 volts	23	23	0.04577
27 Apr 93	16:47	451	CS1R2b	12.34 psia	1.478 volts	1.138 volts	4.375 volts		2.745 volts	23	23	0.04583
27 Apr 93	16:50	456	CS1R2c	12.34 psia	1.478 volts	1.138 volts	4.375 volts		2.745 volts	23	23	0.04571
27 Apr 93	16:50	461	CS1R2d	12.34 psia	1.478 volts	1.138 volts	4.375 volts		2.743 volts	23	23	0.04579
27 Apr 93	17:01	466	CS1R2d	12.34 psia	1.479 volts	1.138 volts	4.375 volts		2.743 volts	23	23	0.04568
AVERAGES			CS1R2									
					GAUGE	GAUGE	DIFFERENTIAL	GAUGE	GAUGE			
					1.478 volts	1.138 volts	4.375 volts		2.744 volts			
					329.4 psig	63.09 psig	48.24 psid	39.27 psig	15.151 psig	23	23	
					22.41 atm	4.293 atm	3.283 atm	2.672 atm	1.0310 atm			
					2.271 Mpa	0.4350 Mpa	0.3326 Mpa	0.2708 Mpa	0.10446 Mpa			
					ABSOLUTE	ABSOLUTE	ABSOLUTE	DIFFERENTIAL	ABSOLUTE	ABSOLUTE		
			12.34 psia	341.7 psia	75.43 psia	48.24 psid	51.61 psia	27.49 psia				
			0.8397 atm	23.25 atm	5.133 atm	3.283 atm	3.512 atm	1.871 atm	296	296	0.04578	
			0.08508 Mpa	2.356 Mpa	0.5201 Mpa	0.3326 Mpa	0.3559 Mpa	0.1895 Mpa				

Apparent gas permeability: $K_a = (v_e \cdot P_e \cdot u \cdot L) / (P_m \cdot \Delta P)$

Boyle's Law: $V_e = (P_b / P_e) \cdot (T_e / T_b) \cdot (z_e / z_b) \cdot V_b$
 $Q_e = (P_b / P_e) \cdot (T_e / T_b) \cdot (z_e / z_b) \cdot Q_b$

$v_e = Q_e / A = (P_b / P_e) \cdot (T_e / T_b) \cdot (z_e / z_b) \cdot (Q_b / A)$

Parameter	Traditional Units	SI Units
μ = gas viscosity	0.0176 cp	* 1.0E-3 Pa*sec/cp 1.760E-05 Pa*sec
L = sample length	10.043 cm	* 1.0E-2 m/cm 1.004E-01 m
A = sample circular cross sectional area	81.201 cm ²	* 1.0E-4 m ² /cm ² 8.120E-03 m ²
Pb = flow measurement basis pressure (absolute)	0.8397 atm	* 1.013E+5 Pa/atm 8.506E+04 Pa
ΔP = pressure drop across sample length	3.283 atm	* 1.013E+5 Pa/atm 3.325E+05 Pa
Pm = mean pore pressure (absolute)	3.512 atm	* 1.013E+5 Pa/atm 3.558E+05 Pa
Pe = exit pressure (absolute)	1.871 atm	* 1.013E+5 Pa/atm 1.895E+05 Pa
Te = sample temperature (absolute)	296 °K	296 °K
Tb = flow measurement basis temperature (absolute)	296 °K	296 °K
ze = gas deviation factor at Pe and Te	1.0000	1.0000
zb = gas deviation factor at Pb and Te	1.0000	1.0000
Qb = flow rate at base conditions	0.04578 cm ³ /s	* 1.0E-6 m ³ /cm ³ 4.578E-08 m ³ /s
ve = flow velocity at sample exit end	2.531E-04 cm/s	* 1.0E-2 m/cm 2.531E-06 m/s
	Ka = 7.26E-06 d	* 9.872E-13 m ² /d 7.16E-18 m ²
	Ka = 7.26E-03 md	7.16E-14 cm ²
	Ka = 7.26E+00 μd	

C-131

Steady State Gas Permeability Data

Project #: 8362	Net Effective Stress: 2 Mpa 290.1 psid	Gas: N2
Sample #: C	Length: 10.043 cm	gas deviation z factors: ze = 1.0000 zb = 1.0000
Stress Level #: 1	Diameter: 10.168 cm	Viscosity: 0.0176 cp
Regime #: 4	Area: 81.201 cm ²	
Pressure Data Filename: 8362CG.S1B		
XDCR calibration factors: Pc = 222.869 psig/volt Pi = 55.4417 psig/volt ΔP = 11.0272 psid/volt Pe = 5.5211 psig/volt		

Date	Time of Day	File Time (min)	Regime #	Pb Barometric Pressure	Pc Confining Pressure	Pi Inlet Pressure	ΔP Differential Pressure	Pm Mean Pore Pressure Pe*ΔP/2	Pe Exit Pressure	Te Flow Temp (°C)	Tb Ambient Temp (°C)	Qb Flow Rate @Pb&Tb (ml/sec)
28 Apr 93	14:15	1741	CS1R4a	12.42 psia	1.566 volts	1.506 volts	4.477 volts		6.259 volts	23	23	0.05789
28 Apr 93	14:17	1741	CS1R4b	12.42 psia	1.566 volts	1.506 volts	4.477 volts		6.258 volts	23	23	0.05798
28 Apr 93	14:20	1746	CS1R4c	12.42 psia	1.566 volts	1.506 volts	4.478 volts		6.257 volts	23	23	0.05784
28 Apr 93	14:23	1746	CS1R4d	12.42 psia	1.566 volts	1.506 volts	4.478 volts		6.256 volts	23	23	0.05785
AVERAGES			CS1R4									
					GAUGE	GAUGE	DIFFERENTIAL	GAUGE	GAUGE	(°C)	(°C)	
					1.566 volts	1.506 volts	4.478 volts	59.24 psig	34.548 psig	23	23	
					349.0 psig	83.50 psig	49.37 psid	4.031 atm	2.3509 atm			
					23.75 atm	5.681 atm	3.360 atm	0.4084 Mpa	0.23820 Mpa			
					2.406 Mpa	0.5757 Mpa	0.3404 Mpa	ABSOLUTE	ABSOLUTE	(°K)	(°K)	(ml/sec)
					12.42 psia	361.4 psia	95.92 psia	49.37 psid	71.66 psia	46.97 psia	296	296
			0.8451 atm	24.59 atm	6.527 atm	3.360 atm	4.876 atm	3.196 atm				
			0.08563 Mpa	2.492 Mpa	0.6613 Mpa	0.3404 Mpa	0.4940 Mpa	0.3238 Mpa				

C-133

Apparent gas permeability: $K_a = (v_e \cdot P_e \cdot u \cdot L) / (P_m \cdot \Delta P)$

Boyle's Law: $v_e = (P_b / P_e) \cdot (T_e / T_b) \cdot (z_e / z_b) \cdot v_b$
 $Q_e = (P_b / P_e) \cdot (T_e / T_b) \cdot (z_e / z_b) \cdot Q_b$

$v_e = Q_e / A = (P_b / P_e) \cdot (T_e / T_b) \cdot (z_e / z_b) \cdot (Q_b / A)$

Parameter	Traditional Units	SI Units
μ = gas viscosity	0.0176 cp	* 1.0E-3 Pa*sec/cp 1.760E-05 Pa*sec
L = sample length	10.043 cm	* 1.0E-2 m/cm 1.004E-01 m
A = sample circular cross sectional area	81.201 cm ²	* 1.0E-4 m ² /cm ² 8.120E-03 m ²
Pb = flow measurement basis pressure (absolute)	0.8451 atm	* 1.013E+5 Pa/atm 8.561E+04 Pa
ΔP = pressure drop across sample length	3.360 atm	* 1.013E+5 Pa/atm 3.403E+05 Pa
Pm = mean pore pressure (absolute)	4.876 atm	* 1.013E+5 Pa/atm 4.939E+05 Pa
Pe = exit pressure (absolute)	3.196 atm	* 1.013E+5 Pa/atm 3.238E+05 Pa
Te = sample temperature (absolute)	296 °K	296 °K
Tb = flow measurement basis temperature (absolute)	296 °K	296 °K
ze = gas deviation factor at Pe and Te	1.0000	1.0000
zb = gas deviation factor at Pb and Te	1.0000	1.0000
Qb = flow rate at base conditions	0.05789 cm ³ /s	* 1.0E-6 m ³ /cm ³ 5.789E-08 m ³ /s
ve = flow velocity at sample exit end	1.885E-04 cm/s	* 1.0E-2 m/cm 1.885E-06 m/s
	Ka = 6.50E-06 d	* 9.872E-13 m ² /d 6.42E-18 m ²
	Ka = 6.50E-03 md	6.42E-14 cm ²
	Ka = 6.50E+00 μd	

Steady State Gas Permeability Data

Project #:	8362	Net Effective Stress:	6 Mpa	870.2 psid	Gas:	N2	
Sample #:	C	Length:	10.043 cm		gas deviation z factors:	ze = 1.0000	zb = 1.0000
Stress Level #:	2	Diameter:	10.168 cm		Viscosity:	0.0176 cp	
Regime #:	1	Area:	81.201 cm ²				
Pressure Data Filename:	8362CG.S2A						
XDCR calibration factors:	Pc = 222.869 psig/volt	Pl = 55.4417 psig/volt	ΔP = 11.0272 psid/volt	Pe = 5.5211 psig/volt			

Date	Time of Day	File Time (min)	Regime #	Pb Barometric Pressure	Pc Confining Pressure	Pl Inlet Pressure	ΔP Differential Pressure	Pm Mean Pore Pressure Pe*ΔP/2	Pe Exit Pressure	Te Flow Temp (°C)	Tb Ambient Temp (°C)	Qb Flow Rate @Pb&Tb (ml/sec)	
29 Apr 93	16:26	255	CS2R1a	12.34 psia	4.036 volts	0.956 volts	4.388 volts		0.897 volts	23	23	0.02748	
29 Apr 93	16:30	260	CS2R1b	12.34 psia	4.036 volts	0.956 volts	4.389 volts		0.897 volts	23	23	0.02747	
29 Apr 93	16:34	265	CS2R1c	12.34 psia	4.036 volts	0.956 volts	4.389 volts		0.896 volts	23	23	0.02755	
29 Apr 93	16:38	265	CS2R1d	12.34 psia	4.036 volts	0.956 volts	4.389 volts		0.896 volts	23	23	0.02750	
AVERAGES			CS2R1										
					GUAGE	GUAGE	DIFFERENTIAL	GUAGE	GUAGE	(°C)	(°C)		
					4.036 volts	0.956 volts	4.389 volts		0.897 volts				
					899.5 psig	53.00 psig	48.40 psid	29.15 psig	4.950 psig	23	23		
					61.21 atm	3.607 atm	3.293 atm	1.983 atm	0.3368 atm				
					6.202 Mpa	0.3654 Mpa	0.3337 Mpa	0.2010 Mpa	0.03413 Mpa				
			ABSOLUTE	ABSOLUTE	ABSOLUTE	DIFFERENTIAL	ABSOLUTE	ABSOLUTE	(°K)	(°K)	(ml/sec)		
			12.34 psia	911.8 psia	65.34 psia	48.40 psid	41.49 psia	17.29 psia					
			0.8397 atm	62.05 atm	4.446 atm	3.293 atm	2.823 atm	1.176 atm	296	296	0.02750		
			0.08508 Mpa	6.287 Mpa	0.4505 Mpa	0.3337 Mpa	0.2860 Mpa	0.1192 Mpa					

C-134

Apparent gas permeability: $K_a = (v_e \cdot P_e \cdot u \cdot L) / (P_m \cdot \Delta P)$

Boyle's Law: $V_e = (P_b / P_e) \cdot (T_e / T_b) \cdot (z_e / z_b) \cdot V_b$

$Q_e = (P_b / P_e) \cdot (T_e / T_b) \cdot (z_e / z_b) \cdot Q_b$

$v_e = Q_e / A = (P_b / P_e) \cdot (T_e / T_b) \cdot (z_e / z_b) \cdot (Q_b / A)$

Parameter	Traditional Units	SI Units
μ = gas viscosity	0.0176 cp	* 1.0E-3 Pa*sec/cp 1.760E-05 Pa*sec
L = sample length	10.043 cm	* 1.0E-2 m/cm 1.004E-01 m
A = sample circular cross sectional area	81.201 cm ²	* 1.0E-4 m ² /cm ² 8.120E-03 m ²
Pb = flow measurement basis pressure (absolute)	0.8397 atm	* 1.013E+5 Pa/atm 8.506E+04 Pa
ΔP = pressure drop across sample length	3.293 atm	* 1.013E+5 Pa/atm 3.336E+05 Pa
Pm = mean pore pressure (absolute)	2.823 atm	* 1.013E+5 Pa/atm 2.860E+05 Pa
Pe = exit pressure (absolute)	1.176 atm	* 1.013E+5 Pa/atm 1.192E+05 Pa
Te = sample temperature (absolute)	296 °K	296 °K
Tb = flow measurement basis temperature (absolute)	296 °K	296 °K
ze = gas deviation factor at Pe and Te	1.0000	1.0000
zb = gas deviation factor at Pb and Te	1.0000	1.0000
Qb = flow rate at base conditions	0.02750 cm ³ /s	* 1.0E-6 m ³ /cm ³ 2.750E-08 m ³ /s
ve = flow velocity at sample exit end	2.417E-04 cm/s	* 1.0E-2 m/cm 2.417E-06 m/s
	Ka = 5.41E-06 d	* 9.872E-13 m ² /d 5.34E-18 m ²
	Ka = 5.41E-03 md	5.34E-14 cm ²
	Ka = 5.41E+00 μd	

Steady State Gas Permeability Data

Project #:	8362	Net Effective Stress:	6 Mpa	870.2 psid	Gas:	N2		
Sample #:	C	Length:	10.043 cm		gas deviation z factors:	ze = 1.0000	zb = 1.0000	
Stress Level #:	2	Diameter:	10.168 cm		Viscosity:	0.0176 cp		
Regime #:	2	Area:	81.201 cm ²					
Pressure Data Filename:	8362CG.S2A							
XDCR calibration factors:	Pc =	222.869 psig/volt	PI =	55.4417 psig/volt	ΔP =	11.0272 psid/volt	Pe =	5.5211 psig/volt

Date	Time of Day	File Time (min)	Regime #	Pb Barometric Pressure	Pc Confining Pressure	PI Inlet Pressure	ΔP Differential Pressure	Pm Mean Pore Pressure Pe+ΔP/2	Pe Exit Pressure	Te Flow Temp (°C)	Tb Ambient Temp (°C)	Qb Flow Rate @Pb&Tb (ml/sec)
30 Apr 93	12:42	1470	CS2R2a	12.33 psia	4.080 volts	1.133 volts	4.367 volts		2.733 volts	23	22	0.03043
30 Apr 93	12:45	1475	CS2R2b	12.33 psia	4.080 volts	1.134 volts	4.366 volts		2.737 volts	23	22	0.03040
30 Apr 93	12:48	1475	CS2R2c	12.33 psia	4.080 volts	1.134 volts	4.365 volts		2.738 volts	23	22	0.03040
30 Apr 93	12:52	1480	CS2R2d	12.33 psia	4.080 volts	1.134 volts	4.365 volts		2.739 volts	23	22	0.03046
AVERAGES			CS2R2									
				GAUGE	GAUGE	DIFFERENTIAL	GAUGE	GAUGE	(°C)	(°C)		
				4.080 volts	1.134 volts	4.366 volts	2.737 volts					
				909.3 psig	62.86 psig	48.14 psid	39.18 psig	15.110 psig	23	22		
				61.87 atm	4.277 atm	3.276 atm	2.666 atm	1.0282 atm				
				6.269 Mpa	0.4334 Mpa	0.3319 Mpa	0.2701 Mpa	0.10418 Mpa				
				ABSOLUTE	ABSOLUTE	ABSOLUTE	DIFFERENTIAL	ABSOLUTE	ABSOLUTE	(°K)	(°K)	(ml/sec)
12.33 psia	921.6 psia	75.19 psia	48.14 psid	51.51 psia	27.44 psia							
0.8390 atm	62.71 atm	5.116 atm	3.276 atm	3.505 atm	1.867 atm	296	295	0.03042				
0.08501 Mpa	6.354 Mpa	0.5184 Mpa	0.3319 Mpa	0.3552 Mpa	0.1892 Mpa							

Apparent gas permeability: $K_a = (v_e \cdot P_e \cdot u) / (P_m \cdot \Delta P)$

Boyle's Law: $V_e = (P_b/P_e) \cdot (T_e/T_b) \cdot (z_e/z_b) \cdot V_b$
 $Q_e = (P_b/P_e) \cdot (T_e/T_b) \cdot (z_e/z_b) \cdot Q_b$

$v_e = Q_e/A = (P_b/P_e) \cdot (T_e/T_b) \cdot (z_e/z_b) \cdot (Q_b/A)$

Parameter	Traditional Units	SI Units
μ = gas viscosity	0.0176 cp	* 1.0E-3 Pa*sec/cp 1.760E-05 Pa*sec
L = sample length	10.043 cm	* 1.0E-2 m/cm 1.004E-01 m
A = sample circular cross sectional area	81.201 cm ²	* 1.0E-4 m ² /cm ² 8.120E-03 m ²
Pb = flow measurement basis pressure (absolute)	0.8390 atm	* 1.013E+5 Pa/atm 8.499E+04 Pa
ΔP = pressure drop across sample length	3.276 atm	* 1.013E+5 Pa/atm 3.318E+05 Pa
Pm = mean pore pressure (absolute)	3.505 atm	* 1.013E+5 Pa/atm 3.551E+05 Pa
Pe = exit pressure (absolute)	1.867 atm	* 1.013E+5 Pa/atm 1.891E+05 Pa
Te = sample temperature (absolute)	296 °K	296 °K
Tb = flow measurement basis temperature (absolute)	295 °K	295 °K
ze = gas deviation factor at Pe and Te	1.0000	1.0000
zb = gas deviation factor at Pb and Te	1.0000	1.0000
Qb = flow rate at base conditions	0.03042 cm ³ /s	* 1.0E-6 m ³ /cm ³ 3.042E-08 m ³ /s
ve = flow velocity at sample exit end	1.689E-04 cm/s	* 1.0E-2 m/cm 1.689E-06 m/s
	Ka = 4.86E-06 d	* 9.872E-13 m ² /d 4.79E-18 m ²
	Ka = 4.86E-03 md	4.79E-14 cm ²
	Ka = 4.86E+00 μd	

C-135

Steady State Gas Permeability Data

Project #: 8362	Net Effective Stress: 6 Mpa 870.2 psid	Gas: N2
Sample #: C	Length: 10.043 cm	gas deviation z factors: ze = 1.0000 zb = 1.0000
Stress Level #: 2	Diameter: 10.168 cm	Viscosity: 0.0176 cp
Regime #: 3	Area: 81.201 cm ²	
Pressure Data Filename: 8362CG.S2A		
XDCR calibration factors:	Pc = 222.869 psig/volt P1 = 55.4417 psig/volt ΔP = 11.0272 psid/volt	Pe = 5.5211 psig/volt

Date	Time of Day	File Time (min)	Regime #	Pb Barometric Pressure	Pc Confining Pressure	P1 Inlet Pressure	ΔP Differential Pressure	Pm Mean Pore Pressure Pe+ΔP/2	Pe Exit Pressure	Te Flow Temp (°C)	Tb Ambient Temp (°C)	Qb Flow Rate @Pb&Tb (ml/sec)
03 May 93	12:11	5756	CS2R3a	12.20 psia	4.124 volts	1.316 volts	4.420 volts		4.504 volts	23	23	0.03438
03 May 93	12:15	5761	CS2R3b	12.20 psia	4.124 volts	1.316 volts	4.420 volts		4.503 volts	23	23	0.03440
03 May 93	12:18	5765	CS2R3c	12.20 psia	4.124 volts	1.316 volts	4.421 volts		4.503 volts	23	23	0.03447
03 May 93	12:21	5770	CS2R3d	12.20 psia	4.124 volts	1.316 volts	4.422 volts		4.503 volts	23	23	0.03447
AVERAGES			CS2R3									
					GUAGE	GUAGE	DIFFERENTIAL	GUAGE	GUAGE	(°C)	(°C)	
					4.124 volts	1.316 volts	4.421 volts	49.24 psig	4.503 volts			
					919.1 psig	72.96 psig	48.75 psid	24.863 psig		23	23	
					62.54 atm	4.965 atm	3.317 atm	1.6918 atm				
					6.337 Mpa	0.5031 Mpa	0.3361 Mpa	0.3395 Mpa	0.17142 Mpa			
					ABSOLUTE	ABSOLUTE	ABSOLUTE	DIFFERENTIAL	ABSOLUTE	ABSOLUTE	(°K)	(°K)
			12.2 psia	931.3 psia	85.16 psia	48.75 psid	61.44 psia	37.06 psia				
			0.8302 atm	63.37 atm	5.795 atm	3.317 atm	4.181 atm	2.522 atm	296	296	0.03443	
			0.08412 Mpa	6.421 Mpa	0.5872 Mpa	0.3361 Mpa	0.4236 Mpa	0.2555 Mpa				

C-136

Apparent gas permeability: $K_a = (v_e \cdot P_e \cdot u \cdot L) / (P_m \cdot \Delta P)$

Boyle's Law: $v_e = (P_b / P_e) \cdot (T_e / T_b) \cdot (z_e / z_b) \cdot v_b$
 $Q_e = (P_b / P_e) \cdot (T_e / T_b) \cdot (z_e / z_b) \cdot Q_b$

$v_e = Q_e / A = (P_b / P_e) \cdot (T_e / T_b) \cdot (z_e / z_b) \cdot (Q_b / A)$

Parameter	Traditional Units	SI Units
u = gas viscosity	0.0176 cp	* 1.0E-3 Pa*sec/cp 1.760E-05 Pa*sec
L = sample length	10.043 cm	* 1.0E-2 m/cm 1.004E-01 m
A = sample circular cross sectional area	81.201 cm ²	* 1.0E-4 m ² /cm ² 8.120E-03 m ²
Pb = flow measurement basis pressure (absolute)	0.8302 atm	* 1.013E+5 Pa/atm 8.409E+04 Pa
ΔP = pressure drop across sample length	3.317 atm	* 1.013E+5 Pa/atm 3.360E+05 Pa
Pm = mean pore pressure (absolute)	4.181 atm	* 1.013E+5 Pa/atm 4.235E+05 Pa
Pe = exit pressure (absolute)	2.522 atm	* 1.013E+5 Pa/atm 2.555E+05 Pa
Te = sample temperature (absolute)	296 °K	296 °K
Tb = flow measurement basis temperature (absolute)	296 °K	296 °K
ze = gas deviation factor at Pe and Te	1.0000	1.0000
zb = gas deviation factor at Pb and Te	1.0000	1.0000
Qb = flow rate at base conditions	0.03443 cm ³ /s	* 1.0E-6 m ³ /cm ³ 3.443E-08 m ³ /s
ve = flow velocity at sample exit end	1.396E-04 cm/s	* 1.0E-2 m/cm 1.396E-06 m/s
	Ka = 4.49E-06 d	* 9.872E-13 m ² /d 4.43E-18 m ²
	Ka = 4.49E-03 md	4.43E-14 cm ²
	Ka = 4.49E+00 μd	

Steady State Gas Permeability Data

Project #:	8362	Net Effective Stress:	6 Mpa	870.2 psid	Gas:	N2		
Sample #:	C	Length:	10.043 cm		gas deviation z factors:	ze = 1.0000	zb = 1.0000	
Stress Level #:	2	Diameter:	10.168 cm		Viscosity:	0.0176 cp		
Regime #:	4	Area:	81.201 cm ²					
Pressure Data Filename:	8362CG.S2A							
XDCR calibration factors:	Pc =	222.869 psig/volt	Pi =	55.4417 psig/volt	ΔP =	11.0272 psid/volt	Pe =	5.5211 psig/volt

Date	Time of Day	File Time (min)	Regime #	Pb Barometric Pressure	Pc Confining Pressure	Pi Inlet Pressure	ΔP Differential Pressure	Pm Mean Pore Pressure Pe+ΔP/2	Pe Exit Pressure	Te Flow Temp (°C)	Tb Ambient Temp (°C)	Qb Flow Rate @Pb&Tb (ml/sec)	
03 May 93	16:29	6015	CS2R4a	12.12 psia	4.169 volts	1.498 volts	4.431 volts		6.338 volts	23	23	0.03828	
03 May 93	16:32	6020	CS2R4b	12.12 psia	4.169 volts	1.498 volts	4.432 volts		6.338 volts	23	23	0.03846	
03 May 93	16:35	6025	CS2R4c	12.12 psia	4.169 volts	1.498 volts	4.432 volts		6.338 volts	23	23	0.03843	
03 May 93	16:41	6030	CS2R4d	12.12 psia	4.169 volts	1.498 volts	4.433 volts		6.337 volts	23	23	0.03827	
03 May 93	16:44	6035	CS2R4e	12.12 psia	4.169 volts	1.498 volts	4.434 volts		6.336 volts	23	23	0.03842	
AVERAGES			CS2R4		GUAGE	GUAGE	DIFFERENTIAL	GUAGE	GUAGE	(°C)	(°C)		
					4.169 volts	1.498 volts	4.432 volts		6.337 volts				
					929.1 psig	83.05 psig	48.88 psid		59.43 psig	34.989 psig	23	23	
					63.22 atm	5.651 atm	3.326 atm		4.044 atm	2.3809 atm			
					6.406 Mpa	0.5726 Mpa	0.3370 Mpa		0.4097 Mpa	0.24124 Mpa			
					ABSOLUTE	ABSOLUTE	ABSOLUTE	DIFFERENTIAL	ABSOLUTE	ABSOLUTE	(°K)	(°K)	(ml/sec)
					12.12 psia	941.3 psia	95.17 psia	48.88 psid	71.55 psia	47.11 psia			
			0.8247 atm	64.05 atm	6.476 atm	3.326 atm	4.869 atm	3.206 atm	296	296	0.03836		
			0.08356 Mpa	6.490 Mpa	0.6562 Mpa	0.3370 Mpa	0.4933 Mpa	0.3248 Mpa					

C-137

Apparent gas permeability: $K_a = (v_e \cdot P_e \cdot u \cdot L) / (P_m \cdot \Delta P)$

Boyle's Law: $v_e = (P_b / P_e) \cdot (T_e / T_b) \cdot (z_e / z_b) \cdot v_b$
 $Q_e = (P_b / P_e) \cdot (T_e / T_b) \cdot (z_e / z_b) \cdot Q_b$

$v_e = Q_e / A = (P_b / P_e) \cdot (T_e / T_b) \cdot (z_e / z_b) \cdot (Q_b / A)$

Parameter	Traditional Units	SI Units
μ = gas viscosity	0.0176 cp	* 1.0E-3 Pa*sec/cp 1.760E-05 Pa*sec
L = sample length	10.043 cm	* 1.0E-2 m/cm 1.004E-01 m
A = sample circular cross sectional area	81.201 cm ²	* 1.0E-4 m ² /cm ² 8.120E-03 m ²
Pb = flow measurement basis pressure (absolute)	0.8247 atm	* 1.013E+5 Pa/atm 8.354E+04 Pa
ΔP = pressure drop across sample length	3.326 atm	* 1.013E+5 Pa/atm 3.369E+05 Pa
Pm = mean pore pressure (absolute)	4.869 atm	* 1.013E+5 Pa/atm 4.932E+05 Pa
Pe = exit pressure (absolute)	3.206 atm	* 1.013E+5 Pa/atm 3.247E+05 Pa
Te = sample temperature (absolute)	296 °K	296 °K
Tb = flow measurement basis temperature (absolute)	296 °K	296 °K
ze = gas deviation factor at Pe and Te	1.0000	1.0000
zb = gas deviation factor at Pb and Te	1.0000	1.0000
Qb = flow rate at base conditions	0.03836 cm ³ /s	* 1.0E-6 m ³ /cm ³ 3.836E-08 m ³ /s
ve = flow velocity at sample exit end	1.215E-04 cm/s	* 1.0E-2 m/cm 1.215E-06 m/s
	Ka =	4.25E-06 d * 9.872E-13 m ² /d 4.20E-18 m ²
	Ka =	4.25E-03 md 4.20E-14 cm ²
	Ka =	4.25E+00 μd

Steady State Gas Permeability Data

Project #:	8362	Net Effective Stress:	10 Mpa	1450.4 psid	Gas:	N2						
Sample #:	C	Length:	10.043 cm		gas deviation z factors:	ze =	1.0000	zb =	1.0000			
Stress Level #:	3	Diameter:	10.168 cm		Viscosity:	0.0176 cp						
Regime #:	1	Area:	81.201 cm ²									
Pressure Data Filename:	8362CG.S3A											
XDCR calibration factors:	Pc =	222.869	psig/volt	PI =	55.4417	psig/volt	ΔP =	11.0272	psid/volt	Pe =	5.5211	psig/volt

Date	Time of Day	File Time (min)	Regime #	Pb Barometric Pressure	Pc Confining Pressure	PI Inlet Pressure	ΔP Differential Pressure	Pm Mean Pore Pressure Pe+ΔP/2	Pe Exit Pressure	Te Flow Temp (°C)	Tb Ambient Temp (°C)	Qb Flow Rate @Pb&Tb (ml/sec)
04 May 93	17:19	350	CS3R1a	12.20 psia	6.638 volts	0.957 volts	4.420 volts		0.876 volts	23	22	0.02110
04 May 93	17:25	355	CS3R1b	12.20 psia	6.638 volts	0.957 volts	4.420 volts		0.875 volts	23	22	0.02108
04 May 93	17:29	355	CS3R1c	12.20 psia	6.638 volts	0.957 volts	4.420 volts		0.875 volts	23	22	0.02104
04 May 93	17:34	360	CS3R1d	12.20 psia	6.638 volts	0.957 volts	4.420 volts		0.875 volts	23	22	0.02105
AVERAGES					GUAGE	GUAGE	DIFFERENTIAL	GUAGE	GUAGE	(°C)	(°C)	
					6.638 volts	0.957 volts	4.420 volts		0.875 volts			
					1479.4 psig	53.06 psig	48.74 psid	29.20 psig	4.832 psig	23	22	
					100.67 atm	3.610 atm	3.317 atm	1.987 atm	0.3288 atm			
					10.200 Mpa	0.3658 Mpa	0.3361 Mpa	0.2013 Mpa	0.03332 Mpa			
					ABSOLUTE	ABSOLUTE	ABSOLUTE	DIFFERENTIAL	ABSOLUTE	ABSOLUTE	(°K)	(°K)
				12.2 psia	1491.6 psia	65.26 psia	48.74 psid	41.40 psia	17.03 psia			
				0.8302 atm	101.50 atm	4.441 atm	3.317 atm	2.817 atm	1.159 atm	296	295	0.02107
				0.08412 Mpa	10.284 Mpa	0.4499 Mpa	0.3361 Mpa	0.2855 Mpa	0.1174 Mpa			

C-138

Apparent gas permeability: $K_a = (v_e \cdot P_e \cdot u \cdot L) / (P_m \cdot \Delta P)$

Boyle's Law: $V_e = (P_b / P_e) \cdot (T_e / T_b) \cdot (z_e / z_b) \cdot V_b$
 $Q_e = (P_b / P_e) \cdot (T_e / T_b) \cdot (z_e / z_b) \cdot Q_b$

$v_e = Q_e / A = (P_b / P_e) \cdot (T_e / T_b) \cdot (z_e / z_b) \cdot (Q_b / A)$

Parameter	Traditional Units	SI Units
μ = gas viscosity	0.0176 cp	* 1.0E-3 Pa*sec/cp 1.760E-05 Pa*sec
L = sample length	10.043 cm	* 1.0E-2 m/cm 1.004E-01 m
A = sample circular cross sectional area	81.201 cm ²	* 1.0E-4 m ² /cm ² 8.120E-03 m ²
Pb = flow measurement basis pressure (absolute)	0.8302 atm	* 1.013E+5 Pa/atm 8.409E+04 Pa
ΔP = pressure drop across sample length	3.317 atm	* 1.013E+5 Pa/atm 3.360E+04 Pa
Pm = mean pore pressure (absolute)	2.817 atm	* 1.013E+5 Pa/atm 2.854E+05 Pa
Pe = exit pressure (absolute)	1.159 atm	* 1.013E+5 Pa/atm 1.174E+05 Pa
Te = sample temperature (absolute)	296 °K	296 °K
Tb = flow measurement basis temperature (absolute)	295 °K	295 °K
ze = gas deviation factor at Pe and Te	1.0000	1.0000
zb = gas deviation factor at Pb and Te	1.0000	1.0000
Qb = flow rate at base conditions	0.02107 cm ³ /s	* 1.0E-6 m ³ /cm ³ 2.107E-08 m ³ /s
ve = flow velocity at sample exit end	1.865E-04 cm/s	* 1.0E-2 m/cm 1.865E-06 m/s
	Ka =	4.09E-06 d
	Ka =	4.09E-03 md
	Ka =	4.09E+00 μd

Steady State Gas Permeability Data

Project #:	8362	Net Effective Stress:	10 Mpa	1450.4 psid	Gas:	N2		
Sample #:	C	Length:	10.043 cm		gas deviation z factors:	ze = 1.0000	zb = 1.0000	
Stress Level #:	3	Diameter:	10.168 cm		Viscosity:	0.0176 cp		
Regime #:	2	Area:	81.201 cm ²					
Pressure Data Filename:	8362CG.S3A							
XDCR calibration factors:	Pc = 222.869 psig/volt	Pi = 55.4417 psig/volt	ΔP = 11.0272 psid/volt	Pe = 5.5211 psig/volt				

Date	Time of Day	File Time (min)	Regime #	Pb Barometric Pressure	Pc Confining Pressure	Pi Inlet Pressure	ΔP Differential Pressure	Pm Mean Pore Pressure Pe+ΔP/2	Pe Exit Pressure	Te Flow Temp (°C)	Tb Ambient Temp (°C)	Qb Flow Rate @Pb&Tb (ml/sec)
05 May 93	13:04	1535	CS3R2a	12.28 psia	6.683 volts	1.138 volts	4.434 volts		2.660 volts	23	21	0.02341
05 May 93	13:10	1540	CS3R2b	12.28 psia	6.683 volts	1.138 volts	4.434 volts		2.660 volts	23	21	0.02325
05 May 93	13:15	1545	CS3R2c	12.28 psia	6.683 volts	1.138 volts	4.434 volts		2.660 volts	23	21	0.02329
05 May 93	13:20	1550	CS3R2d	12.28 psia	6.683 volts	1.138 volts	4.434 volts		2.660 volts	23	21	0.02340
05 May 93	13:25	1555	CS3R2e	12.28 psia	6.683 volts	1.138 volts	4.434 volts		2.660 volts	23	21	0.02330
AVERAGES			CS3R2		GUAGE	GUAGE	DIFFERENTIAL	GUAGE	GUAGE	(°C)	(°C)	
					6.683 volts	1.138 volts	4.434 volts		2.660 volts			
					1489.4 psig	63.09 psig	48.89 psid	39.13 psig	14.686 psig	23	21	
					101.35 atm	4.293 atm	3.327 atm	2.663 atm	0.9993 atm			
					10.269 Mpa	0.4350 Mpa	0.3371 Mpa	0.2698 Mpa	0.10126 Mpa			
					ABSOLUTE	ABSOLUTE	ABSOLUTE	DIFFERENTIAL	ABSOLUTE	ABSOLUTE	(°K)	(°K)
				12.28 psia	1501.7 psia	75.37 psia	48.89 psid	51.41 psia	26.97 psia			
				0.8356 atm	102.19 atm	5.129 atm	3.327 atm	3.498 atm	1.835 atm	296	294	0.02334
				0.08467 Mpa	10.354 Mpa	0.5197 Mpa	0.3371 Mpa	0.3545 Mpa	0.1859 Mpa			

C-139

Apparent gas permeability: $K_a = (v_e \cdot P_e \cdot u \cdot L) / (P_m \cdot \Delta P)$

Boyle's Law: $V_e = (P_b/P_e) \cdot (T_e/T_b) \cdot (z_e/z_b) \cdot V_b$
 $Q_e = (P_b/P_e) \cdot (T_e/T_b) \cdot (z_e/z_b) \cdot Q_b$

$v_e = Q_e/A = (P_b/P_e) \cdot (T_e/T_b) \cdot (z_e/z_b) \cdot (Q_b/A)$

Parameter	Traditional Units	SI Units
μ = gas viscosity	0.0176 cp	* 1.0E-3 Pa*sec/cp 1.760E-05 Pa*sec
L = sample length	10.043 cm	* 1.0E-2 m/cm 1.004E-01 m
A = sample circular cross sectional area	81.201 cm ²	* 1.0E-4 m ² /cm ² 8.120E-03 m ²
Pb = flow measurement basis pressure (absolute)	0.8356 atm	* 1.013E+5 Pa/atm 8.465E+04 Pa
ΔP = pressure drop across sample length	3.327 atm	* 1.013E+5 Pa/atm 3.370E+05 Pa
Pm = mean pore pressure (absolute)	3.498 atm	* 1.013E+5 Pa/atm 3.544E+05 Pa
Pe = exit pressure (absolute)	1.835 atm	* 1.013E+5 Pa/atm 1.859E+05 Pa
Te = sample temperature (absolute)	296 °K	296 °K
Tb = flow measurement basis temperature (absolute)	294 °K	294 °K
ze = gas deviation factor at Pe and Te	1.0000	1.0000
zb = gas deviation factor at Pb and Te	1.0000	1.0000
Qb = flow rate at base conditions	0.02334 cm ³ /s	* 1.0E-6 m ³ /cm ³ 2.334E-08 m ³ /s
ve = flow velocity at sample exit end	1.318E-04 cm/s	* 1.0E-2 m/cm 1.318E-06 m/s
	Ka = 3.67E-06 d	* 9.872E-13 m ² /d 3.62E-18 m ²
	Ka = 3.67E-03 md	3.62E-14 cm ²
	Ka = 3.67E+00 μd	

Steady State Gas Permeability Data

Project #: 8362	Net Effective Stress: 10 Mpa 1450.4 psid	Gas: N2
Sample #: C	Length: 10.043 cm	gas deviation z factors: ze = 1.0000 zb = 1.0000
Stress Level #: 3	Diameter: 10.168 cm	Viscosity: 0.0176 cp
Regime #: 3	Area: 81.201 cm ²	
Pressure Data Filename: 8362CG.S3A		
XDCR calibration factors: Pc = 222.869 psig/volt	Pi = 55.4417 psig/volt	ΔP = 11.0272 psid/volt Pe = 5.5211 psig/volt

Date	Time of Day	File Time (min)	Regime #	Pb Barometric Pressure	Pc Confining Pressure	Pi Inlet Pressure	ΔP Differential Pressure	Pm Mean Pore Pressure Pe*ΔP/2	Pe Exit Pressure	Te Flow Temp (°C)	Tb Ambient Temp (°C)	Qb Flow Rate @Pb&Tb (ml/sec)	
05 May 93	16:56	1765	CS3R3a	12.29 psia	6.728 volts	1.316 volts	4.390 volts		4.549 volts	23	22	0.02584	
05 May 93	17:00	1770	CS3R3b	12.29 psia	6.728 volts	1.316 volts	4.390 volts		4.550 volts	23	22	0.02579	
05 May 93	17:04	1770	CS3R3c	12.29 psia	6.728 volts	1.316 volts	4.390 volts		4.550 volts	23	22	0.02574	
05 May 93	17:04	1775	CS3R3d	12.29 psia	6.728 volts	1.316 volts	4.390 volts		4.550 volts	23	22	0.02571	
05 May 93	17:13	1780	CS3R3e	12.29 psia	6.728 volts	1.316 volts	4.390 volts		4.550 volts	23	22	0.02579	
AVERAGES			CS3R3		GUAGE	GUAGE	DIFFERENTIAL	GUAGE	GUAGE	(°C)	(°C)		
					6.728 volts	1.316 volts	4.390 volts		4.550 volts				
					1499.5 psig	72.96 psig	48.41 psid		49.32 psig	25.120 psig	23	22	
					102.03 atm	4.965 atm	3.294 atm		3.356 atm	1.7093 atm			
					10.338 Mpa	0.5031 Mpa	0.3338 Mpa		0.3401 Mpa	0.17320 Mpa			
					ABSOLUTE	ABSOLUTE	ABSOLUTE	DIFFERENTIAL	ABSOLUTE	ABSOLUTE	(°K)	(°K)	(ml/sec)
						12.29 psia	1511.8 psia	85.25 psia	48.41 psid	61.61 psia	37.41 psia		
				0.8363 atm	102.87 atm	5.801 atm	3.294 atm	4.193 atm	2.546 atm	296	295	0.02577	
				0.08474 Mpa	10.423 Mpa	0.5878 Mpa	0.3338 Mpa	0.4248 Mpa	0.2579 Mpa				

C-140

Apparent gas permeability: $K_a = (v_e \cdot P_e \cdot u \cdot L) / (P_m \cdot \Delta P)$

Boyle's Law: $V_e = (P_b / P_e) \cdot (T_e / T_b) \cdot (z_e / z_b) \cdot V_b$
 $Q_e = (P_b / P_e) \cdot (T_e / T_b) \cdot (z_e / z_b) \cdot Q_b$

$v_e = Q_e / A = (P_b / P_e) \cdot (T_e / T_b) \cdot (z_e / z_b) \cdot (Q_b / A)$

Parameter	Traditional Units	SI Units
μ = gas viscosity	0.0176 cp	* 1.0E-3 Pa*sec/cp 1.760E-05 Pa*sec
L = sample length	10.043 cm	* 1.0E-2 m/cm 1.004E-01 m
A = sample circular cross sectional area	81.201 cm ²	* 1.0E-4 m ² /cm ² 8.120E-03 m ²
Pb = flow measurement basis pressure (absolute)	0.8363 atm	* 1.013E+5 Pa/atm 8.472E+04 Pa
ΔP = pressure drop across sample length	3.294 atm	* 1.013E+5 Pa/atm 3.337E+05 Pa
Pm = mean pore pressure (absolute)	4.193 atm	* 1.013E+5 Pa/atm 4.247E+05 Pa
Pe = exit pressure (absolute)	2.546 atm	* 1.013E+5 Pa/atm 2.579E+05 Pa
Te = sample temperature (absolute)	296 °K	296 °K
Tb = flow measurement basis temperature (absolute)	295 °K	295 °K
ze = gas deviation factor at Pe and Te	1.0000	1.0000
zb = gas deviation factor at Pb and Te	1.0000	1.0000
Qb = flow rate at base conditions	0.02577 cm ³ /s	* 1.0E-6 m ³ /cm ³ 2.577E-08 m ³ /s
ve = flow velocity at sample exit end	1.046E-04 cm/s	* 1.0E-2 m/cm 1.046E-06 m/s
	Ka = 3.41E-06 d	* 9.872E-13 m ² /d 3.36E-18 m ²
	Ka = 3.41E-03 md	3.36E-14 cm ²
	Ka = 3.41E+00 μd	

Steady State Gas Permeability Data

Project #: 8362	Net Effective Stress: 10 Mpa	1450.4 psid	Gas: N2
Sample #: C	Length: 10.043 cm		gas deviation z factors: ze = 1.0000 zb = 1.0000
Stress Level #: 3	Diameter: 10.168 cm		Viscosity: 0.0176 cp
Regime #: 4	Area: 81.201 cm ²		
Pressure Data Filename: 8362CG.S3A			
XDCR calibration factors: Pc = 222.869 psig/volt Pi = 55.4417 psig/volt ΔP = 11.0272 psid/volt Pe = 5.5211 psig/volt			

Date	Time of Day	File Time (min)	Regime #	Pb Barometric Pressure	Pc Confining Pressure	Pi Inlet Pressure	ΔP Differential Pressure	Pm Mean Pore Pressure Pe+ΔP/2	Pe Exit Pressure	Te Flow Temp (°C)	Tb Ambient Temp (°C)	Qb Flow Rate @Pb&Tb (ml/sec)	
06 May 93	14:34	3060	CS3R4a	12.29 psia	6.772 volts	1.499 volts	4.422 volts		6.335 volts	23	22	0.02838	
06 May 93	14:38	3065	CS3R4b	12.29 psia	6.772 volts	1.499 volts	4.422 volts		6.335 volts	23	22	0.02854	
06 May 93	14:43	3070	CS3R4c	12.29 psia	6.772 volts	1.499 volts	4.422 volts		6.336 volts	23	22	0.02851	
06 May 93	14:48	3075	CS3R4d	12.29 psia	6.772 volts	1.499 volts	4.422 volts		6.336 volts	23	22	0.02842	
06 May 93	14:53	3080	CS3R4e	12.29 psia	6.772 volts	1.499 volts	4.422 volts		6.335 volts	23	22	0.02848	
AVERAGES			CS3R4										
					GAUGE	GAUGE	DIFFERENTIAL	GAUGE	GAUGE	(°C)	(°C)		
					6.772 volts	1.499 volts	4.422 volts		6.335 volts				
					1509.3 psig	83.11 psig	48.76 psid	59.36 psig	34.978 psig	23	22		
					102.70 atm	5.655 atm	3.318 atm	4.039 atm	2.3801 atm				
					10.406 Mpa	0.5730 Mpa	0.3362 Mpa	0.4093 Mpa	0.24117 Mpa				
			ABSOLUTE	ABSOLUTE	ABSOLUTE	DIFFERENTIAL	ABSOLUTE	ABSOLUTE	(°K)	(°K)	(ml/sec)		
			12.29 psia	1521.6 psia	95.40 psia	48.76 psid	71.65 psia	47.27 psia					
			0.8363 atm	103.54 atm	6.491 atm	3.318 atm	4.875 atm	3.216 atm	296	295	0.02846		
			0.08474 Mpa	10.491 Mpa	0.6577 Mpa	0.3362 Mpa	0.4940 Mpa	0.3259 Mpa					

C-141

Apparent gas permeability: $K_a = (v_e \cdot P_e \cdot u \cdot L) / (P_m \cdot \Delta P)$

Boyle's Law: $v_e = (P_b / P_e) \cdot (T_e / T_b) \cdot (z_e / z_b) \cdot v_b$
 $Q_e = (P_b / P_e) \cdot (T_e / T_b) \cdot (z_e / z_b) \cdot Q_b$

$v_e = Q_e / A = (P_b / P_e) \cdot (T_e / T_b) \cdot (z_e / z_b) \cdot (Q_b / A)$

Parameter	Traditional Units	SI Units
μ = gas viscosity	0.0176 cp	* 1.0E-3 Pa*sec/cp 1.760E-05 Pa*sec
L = sample length	10.043 cm	* 1.0E-2 m/cm 1.004E-01 m
A = sample circular cross sectional area	81.201 cm ²	* 1.0E-4 m ² /cm ² 8.120E-03 m ²
Pb = flow measurement basis pressure (absolute)	0.8363 atm	* 1.013E+5 Pa/atm 8.472E+04 Pa
ΔP = pressure drop across sample length	3.318 atm	* 1.013E+5 Pa/atm 3.361E+05 Pa
Pm = mean pore pressure (absolute)	4.875 atm	* 1.013E+5 Pa/atm 4.939E+05 Pa
Pe = exit pressure (absolute)	3.216 atm	* 1.013E+5 Pa/atm 3.258E+05 Pa
Te = sample temperature (absolute)	296 °K	296 °K
Tb = flow measurement basis temperature (absolute)	295 °K	295 °K
ze = gas deviation factor at Pe and Te	1.0000	1.0000
zb = gas deviation factor at Pb and Te	1.0000	1.0000
Qb = flow rate at base conditions	0.02846 cm ³ /s	* 1.0E-6 m ³ /cm ³ 2.846E-08 m ³ /s
ve = flow velocity at sample exit end	9.144E-05 cm/s	* 1.0E-2 m/cm 9.144E-07 m/s
	Ka = 3.21E-06 d	* 9.872E-13 m ² /d 3.17E-18 m ²
	Ka = 3.21E-03 md	3.17E-14 cm ²
	Ka = 3.21E+00 μd	

Steady State Gas Permeability Data

Project #:	8362	Target Net Eff. Stress:	2 Mpa	290.1 psid	Gas:	N2		
Sample #:	D	Length:	9.886 cm		gas deviation z factors:	ze =	1.0000	zb = 1.0000
Stress Level #:	1	Diameter:	10.168 cm		Viscosity:	0.0176 cp		
Regime #:	1	Area:	81.201 cm ²					
Pressure Data Filename:	8362DG.S1A							
XDCR calibration factors:	Pc =	222.869 psig/volt	Pi =	55.4417 psig/volt	ΔP =	11.0272 psid/volt	Pe =	5.5211 psig/volt

Date	Time of Day	File Time (min)	Regime #	Pb Barometric Pressure	Pc Confining Pressure	Pi Inlet Pressure	ΔP Differential Pressure	Pm Mean Pore Pressure Pe-ΔP/2	Pe Exit Pressure	Te Flow Temp (°C)	Tb Ambient Temp (°C)	Qb Flow Rate @Pb&Tb (ml/sec)	
12 Jul 93	07:38	4174	DS1R1a	12.29 psia	1.534 volts	1.904 volts	9.176 volts		0.919 volts	23	22	0.004849	
12 Jul 93	07:43	4179	DS1R1b	12.29 psia	1.534 volts	1.904 volts	9.176 volts		0.919 volts	23	22	0.004889	
12 Jul 93	07:47	4184	DS1R1c	12.29 psia	1.534 volts	1.904 volts	9.176 volts		0.919 volts	23	22	0.004904	
12 Jul 93	07:54	4191	DS1R1d	12.29 psia	1.535 volts	1.904 volts	9.176 volts		0.919 volts	23	22	0.004848	
12 Jul 93	07:58	4196	DS1R1e	12.29 psia	1.535 volts	1.904 volts	9.178 volts		0.919 volts	23	22	0.004866	
AVERAGES			DS1R1		GAUGE	GAUGE	DIFFERENTIAL	GAUGE	GAUGE	(°C)	(°C)		
					1.534 volts	1.904 volts	9.176 volts		0.919 volts				
					342.0 psig	105.56 psig	101.19 psid	55.67 psig	5.074 psig		23	22	
					23.27 atm	7.183 atm	6.886 atm	3.788 atm	0.3453 atm				
					2.358 Mpa	0.7278 Mpa	0.6977 Mpa	0.3838 Mpa	0.03498 Mpa				
					ABSOLUTE	ABSOLUTE	ABSOLUTE	DIFFERENTIAL	ABSOLUTE	ABSOLUTE	(°K)	(°K)	(ml/sec)
						12.29 psia	354.3 psia	117.85 psia	101.19 psid	67.96 psia	17.36 psia		
				0.8363 atm	24.11 atm	8.019 atm	6.886 atm	4.624 atm	1.182 atm	296	295	0.00487	
				0.08474 Mpa	2.443 Mpa	0.8126 Mpa	0.6977 Mpa	0.4686 Mpa	0.1197 Mpa				

C-142

Apparent gas permeability: $K_a = (v_e \cdot P_e \cdot u \cdot L) / (P_m \cdot \Delta P)$

Boyle's Law: $V_e = (P_b / P_e) \cdot (T_e / T_b) \cdot (z_e / z_b) \cdot V_b$
 $Q_e = (P_b / P_e) \cdot (T_e / T_b) \cdot (z_e / z_b) \cdot Q_b$

$v_e = Q_e / A = (P_b / P_e) \cdot (T_e / T_b) \cdot (z_e / z_b) \cdot (Q_b / A)$

Parameter	Traditional Units	SI Units
u = gas viscosity	0.0176 cp	* 1.0E-3 Pa*sec/cp 1.760E-05 Pa*sec
L = sample length	9.886 cm	* 1.0E-2 m/cm 9.886E-02 m
A = sample circular cross sectional area	81.201 cm ²	* 1.0E-4 m ² /cm ² 8.120E-03 m ²
Pb = flow measurement basis pressure (absolute)	0.8363 atm	* 1.013E+5 Pa/atm 8.472E+04 Pa
ΔP = pressure drop across sample length	6.886 atm	* 1.013E+5 Pa/atm 6.975E+05 Pa
Pm = mean pore pressure (absolute)	4.624 atm	* 1.013E+5 Pa/atm 4.604E+05 Pa
Pe = exit pressure (absolute)	1.182 atm	* 1.013E+5 Pa/atm 1.197E+05 Pa
Te = sample temperature (absolute)	296 °K	296 °K
Tb = flow measurement basis temperature (absolute)	295 °K	295 °K
ze = gas deviation factor at Pe and Te	1.0000	1.0000
zb = gas deviation factor at Pb and Te	1.0000	1.0000
Qb = flow rate at base conditions	0.00487 cm ³ /s	* 1.0E-6 m ³ /cm ³ 4.873E-09 m ³ /s
ve = flow velocity at sample exit end	4.262E-05 cm/s	* 1.0E-2 m/cm 4.262E-07 m/s
	Ka =	2.75E-07 d
	Ka =	2.75E-04 md
	Ka =	2.75E-01 μd
Pc - Pm = Actual N.E.S.	286.3 psid	1.97 MPa

Steady State Gas Permeability Data

Project #:	8362	Target Net Eff. Stress:	2 Mpa	290.1 psid	Gas:	N2						
Sample #:	D	Length:	9.886 cm		gas deviation z factors:	ze =	1.0000	zb =	1.0000			
Stress Level #:	1	Diameter:	10.168 cm		Viscosity:	0.0176 cp						
Regime #:	2	Area:	81.201 cm ²									
Pressure Data Filename:	8362DG.S1A											
XDCR calibration factors:	Pc =	222.869	psig/volt	Pi =	55.4417	psig/volt	ΔP =	11.0272	psid/volt	Pe =	5.5211	psig/volt

Date	Time of Day	File Time (min)	Regime #	Pb Barometric Pressure	Pc Confining Pressure	Pi Inlet Pressure	ΔP Differential Pressure	Pm Mean Pore Pressure Pe*ΔP/2	Pe Exit Pressure	Te Flow Temp (°C)	Tb Ambient Temp (°C)	Qb Flow Rate @Pb&Tb (ml/sec)
12 Jul 93	12:44	4476	DS1R2a	12.32 psia	1.598 volts	2.102 volts	9.155 volts		2.950 volts	23	23	0.005378
12 Jul 93	12:47	4481	DS1R2b	12.32 psia	1.598 volts	2.102 volts	9.155 volts		2.950 volts	23	23	0.005387
12 Jul 93	12:51	4486	DS1R2c	12.32 psia	1.598 volts	2.102 volts	9.155 volts		2.950 volts	23	23	0.005362
12 Jul 93	12:55	4491	DS1R2d	12.32 psia	1.598 volts	2.102 volts	9.156 volts		2.950 volts	23	23	0.005371
12 Jul 93	13:01	4496	DS1R2e	12.32 psia	1.598 volts	2.102 volts	9.156 volts		2.950 volts	23	23	0.005358
AVERAGES			DS1R2		GAUGE	GAUGE	DIFFERENTIAL	GAUGE	GAUGE	(°C)	(°C)	
					1.598 volts	2.102 volts	9.155 volts		2.950 volts			
					356.1 psig	116.54 psig	100.96 psid	66.77 psig	16.287 psig	23	23	
					24.23 atm	7.930 atm	6.870 atm	4.543 atm	1.1083 atm			
					2.456 Mpa	0.8035 Mpa	0.6961 Mpa	0.4603 Mpa	0.11230 Mpa			
					ABSOLUTE	ABSOLUTE	DIFFERENTIAL	ABSOLUTE	ABSOLUTE	(°K)	(°K)	
					12.32 psia	368.5 psia	128.86 psia	100.96 psia	79.09 psia	28.61 psia	296	296
			0.8383 atm	25.07 atm	8.768 atm	6.870 atm	5.381 atm	1.947 atm				
			0.08494 Mpa	2.540 Mpa	0.8884 Mpa	0.6961 Mpa	0.5453 Mpa	0.1972 Mpa				

C-143

Apparent gas permeability: $K_a = (v_e \cdot P_e \cdot u \cdot L) / (P_m \cdot \Delta P)$

Boyle's Law: $v_e = (P_b / P_e) \cdot (T_e / T_b) \cdot (z_e / z_b) \cdot v_b$
 $Q_e = (P_b / P_e) \cdot (T_e / T_b) \cdot (z_e / z_b) \cdot Q_b$

$v_e = Q_e / A = (P_b / P_e) \cdot (T_e / T_b) \cdot (z_e / z_b) \cdot (Q_b / A)$

Parameter	Traditional Units	SI Units
μ = gas viscosity	0.0176 cp	* 1.0E-3 Pa*sec/cp 1.760E-05 Pa*sec
L = sample length	9.886 cm	* 1.0E-2 m/cm 9.886E-02 m
A = sample circular cross sectional area	81.201 cm ²	* 1.0E-4 m ² /cm ² 8.120E-03 m ²
Pb = flow measurement basis pressure (absolute)	0.8383 atm	* 1.013E+5 Pa/atm 8.492E+04 Pa
ΔP = pressure drop across sample length	6.870 atm	* 1.013E+5 Pa/atm 6.959E+05 Pa
Pm = mean pore pressure (absolute)	5.381 atm	* 1.013E+5 Pa/atm 5.451E+05 Pa
Pe = exit pressure (absolute)	1.947 atm	* 1.013E+5 Pa/atm 1.972E+05 Pa
Te = sample temperature (absolute)	296 °K	296 °K
Tb = flow measurement basis temperature (absolute)	296 °K	296 °K
ze = gas deviation factor at Pe and Te	1.0000	1.0000
zb = gas deviation factor at Pb and Te	1.0000	1.0000
Qb = flow rate at base conditions	0.00537 cm ³ /s	* 1.0E-6 m ³ /cm ³ 5.374E-09 m ³ /s
ve = flow velocity at sample exit end	2.850E-05 cm/s	* 1.0E-2 m/cm 2.850E-07 m/s
	Ka =	2.61E-07 d * 9.872E-13 m ² /d 2.58E-19 m ²
	Ka =	2.61E-04 md 2.58E-15 cm ²
	Ka =	2.61E-01 μd
Pc - Pm = Actual N.E.S.	289.4 psid	2.00 MPa

Steady State Gas Permeability Data

Project #:	8362	Target Net Eff. Stress:	2 Mpa	290.1 psid	Gas:	N2						
Sample #:	D	Length:	9.886 cm		gas deviation z factors:	ze =	1.0000	zb =	1.0000			
Stress Level #:	1	Diameter:	10.168 cm		Viscosity:	0.0176 cp						
Regime #:	3	Area:	81.201 cm ²									
Pressure Data Filename:	8362DG.S1A											
XDCR calibration factors:	Pc =	222.869	psig/volt	Pl =	55.4417	psig/volt	ΔP =	11.0272	psid/volt	Pe =	5.5211	psig/volt

Date	Time of Day	File Time (min)	Regime #	Pb Barometric Pressure	Pc Confining Pressure	Pl Inlet Pressure	ΔP Differential Pressure	Pm Mean Pore Pressure Pe*ΔP/2	Pe Exit Pressure	Te Flow Temp (°C)	Tb Ambient Temp (°C)	Qb Flow Rate @Pb&Tb (ml/sec)	
12 Jul 93	17:05	4738	DS1R3a	12.29 psia	1.646 volts	2.277 volts	9.160 volts		4.720 volts	23	23	0.005750	
12 Jul 93	17:09	4743	DS1R3b	12.29 psia	1.646 volts	2.277 volts	9.160 volts		4.720 volts	23	23	0.005742	
12 Jul 93	17:13	4748	DS1R3c	12.29 psia	1.645 volts	2.277 volts	9.590 volts		4.720 volts	23	23	0.005760	
12 Jul 93	17:16	4753	DS1R3d	12.29 psia	1.645 volts	2.277 volts	9.590 volts		4.720 volts	23	23	0.005767	
12 Jul 93	17:19	4758	DS1R3e	12.29 psia	1.645 volts	2.277 volts	9.590 volts		4.720 volts	23	23	0.005764	
AVERAGES			DS1R3		GUAGE	GUAGE	DIFFERENTIAL	GUAGE	GUAGE	(°C)	(°C)		
					1.645 volts	2.277 volts	9.418 volts		4.720 volts				
					366.7 psig	126.24 psig	103.85 psid		77.99 psig	26.060 psig	23	23	
					24.95 atm	8.590 atm	7.067 atm		5.307 atm	1.7732 atm			
					2.528 Mpa	0.8704 Mpa	0.7160 Mpa		0.5377 Mpa	0.17967 Mpa			
					ABSOLUTE	ABSOLUTE	ABSOLUTE	DIFFERENTIAL	ABSOLUTE	ABSOLUTE	(°K)	(°K)	(ml/sec)
					12.29 psia	379.0 psia	138.53 psia	103.85 psid	90.28 psia	38.35 psia			
			0.8363 atm	25.79 atm	9.426 atm	7.067 atm	6.143 atm	2.610 atm	296	296	0.00575		
			0.08474 Mpa	2.613 Mpa	0.9551 Mpa	0.7160 Mpa	0.6224 Mpa	0.2644 Mpa					

C-144

Apparent gas permeability: $K_a = (v_e \cdot P_e \cdot u \cdot L) / (P_m \cdot \Delta P)$

Boyle's Law: $v_e = (P_b / P_e) \cdot (T_e / T_b) \cdot (z_e / z_b) \cdot v_b$
 $Q_e = (P_b / P_e) \cdot (T_e / T_b) \cdot (z_e / z_b) \cdot Q_b$

$v_e = Q_e / A = (P_b / P_e) \cdot (T_e / T_b) \cdot (z_e / z_b) \cdot (Q_b / A)$

Parameter	Traditional Units	SI Units
μ = gas viscosity	0.0176 cp	* 1.0E-3 Pa*sec/cp 1.760E-05 Pa*sec
L = sample length	9.886 cm	* 1.0E-2 m/cm 9.886E-02 m
A = sample circular cross sectional area	81.201 cm ²	* 1.0E-4 m ² /cm ² 8.120E-03 m ²
Pb = flow measurement basis pressure (absolute)	0.8363 atm	* 1.013E+5 Pa/atm 8.472E+04 Pa
ΔP = pressure drop across sample length	7.067 atm	* 1.013E+5 Pa/atm 7.159E+05 Pa
Pm = mean pore pressure (absolute)	6.143 atm	* 1.013E+5 Pa/atm 6.223E+05 Pa
Pe = exit pressure (absolute)	2.610 atm	* 1.013E+5 Pa/atm 2.643E+05 Pa
Te = sample temperature (absolute)	296 °K	296 °K
Tb = flow measurement basis temperature (absolute)	296 °K	296 °K
ze = gas deviation factor at Pe and Te	1.0000	1.0000
zb = gas deviation factor at Pb and Te	1.0000	1.0000
Qb = flow rate at base conditions	0.00575 cm ³ /s	* 1.0E-6 m ³ /cm ³ 5.755E-09 m ³ /s
ve = flow velocity at sample exit end	2.271E-05 cm/s	* 1.0E-2 m/cm 2.271E-07 m/s
	Ka =	2.38E-07 d * 9.872E-13 m ² /d 2.34E-19 m ²
	Ka =	2.38E-04 md 2.34E-15 cm ²
	Ka =	2.38E-01 μd
Pc - Pm = Actual N.E.S.	288.7 psid	1.99 MPa

Steady State Gas Permeability Data

Project #: 8362	Target Net Eff. Stress: 2 Mpa	290.1 psid	Gas: N2
Sample #: D	Length: 9.886 cm		gas deviation z factors: ze = 1.0000 zb = 1.0000
Stress Level #: 1	Diameter: 10.168 cm		Viscosity: 0.0176 cp
Regime #: 4	Area: 81.201 cm ²		
Pressure Data Filename: 8362DG.S1A			
XDCR calibration factors: Pc = 222.869 psig/volt P1 = 55.4417 psig/volt ΔP = 11.0272 psid/volt Pe = 5.5211 psig/volt			

Date	Time of Day	File Time (min)	Regime #	Pb Barometric Pressure	Pc Confining Pressure	P1 Inlet Pressure	ΔP Differential Pressure	Pm Mean Pore Pressure Pe+ΔP/2	Pe Exit Pressure	Te Flow Temp (°C)	Tb Ambient Temp (°C)	Qb Flow Rate @Pb&Tb (ml/sec)	
13 Jul 93	07:41	5613	DS1R4a	12.33 psia	1.678 volts	2.449 volts	9.158 volts		6.451 volts	23	21	0.006108	
13 Jul 93	07:44	5618	DS1R4b	12.33 psia	1.678 volts	2.449 volts	9.158 volts		6.451 volts	23	21	0.006070	
13 Jul 93	07:47	5623	DS1R4c	12.33 psia	1.678 volts	2.449 volts	9.159 volts		6.450 volts	23	21	0.006066	
13 Jul 93	07:50	5628	DS1R4d	12.33 psia	1.678 volts	2.449 volts	9.159 volts		6.450 volts	23	21	0.006107	
13 Jul 93	07:53	5633	DS1R4e	12.33 psia	1.678 volts	2.449 volts	9.158 volts		6.450 volts	23	21	0.006111	
AVERAGES			DS1R4		GUAGE	GUAGE	DIFFERENTIAL	GUAGE	GUAGE	(°C)	(°C)		
					1.678 volts	2.449 volts	9.158 volts	86.11 psig	35.613 psig	23	21		
					374.0 psig	135.78 psig	100.99 psid	5.859 atm	2.4233 atm				
					25.45 atm	9.239 atm	6.872 atm	0.5937 Mpa	0.24555 Mpa				
					2.578 Mpa	0.9361 Mpa	0.6963 Mpa						
					ABSOLUTE	ABSOLUTE	ABSOLUTE	ABSOLUTE	ABSOLUTE	ABSOLUTE	(°K)	(°K)	(ml/sec)
					12.33 psia	386.3 psia	148.11 psia	100.99 psid	98.44 psia	47.94 psia	296	294	0.00609
			0.8390 atm	26.29 atm	10.078 atm	6.872 atm	6.698 atm	3.262 atm					
			0.08501 Mpa	2.663 Mpa	1.0212 Mpa	0.6963 Mpa	0.6787 Mpa	0.3306 Mpa					

C-145

Apparent gas permeability: $K_a = (v_e \cdot P_e \cdot u \cdot L) / (P_m \cdot \Delta P)$

Boyle's Law: $v_e = (P_b / P_e) \cdot (T_e / T_b) \cdot (z_e / z_b) \cdot v_b$
 $Q_e = (P_b / P_e) \cdot (T_e / T_b) \cdot (z_e / z_b) \cdot Q_b$

$v_e = Q_e / A = (P_b / P_e) \cdot (T_e / T_b) \cdot (z_e / z_b) \cdot (Q_b / A)$

Parameter	Traditional Units	SI Units
μ = gas viscosity	0.0176 cp	* 1.0E-3 Pa*sec/cp 1.760E-05 Pa*sec
L = sample length	9.886 cm	* 1.0E-2 m/cm 9.886E-02 m
A = sample circular cross sectional area	81.201 cm ²	* 1.0E-4 m ² /cm ² 8.120E-03 m ²
Pb = flow measurement basis pressure (absolute)	0.8390 atm	* 1.013E+5 Pa/atm 8.499E+04 Pa
ΔP = pressure drop across sample length	6.872 atm	* 1.013E+5 Pa/atm 6.961E+05 Pa
Pm = mean pore pressure (absolute)	6.698 atm	* 1.013E+5 Pa/atm 6.785E+05 Pa
Pe = exit pressure (absolute)	3.262 atm	* 1.013E+5 Pa/atm 3.305E+05 Pa
Te = sample temperature (absolute)	296 °K	296 °K
Tb = flow measurement basis temperature (absolute)	294 °K	294 °K
ze = gas deviation factor at Pe and Te	1.0000	1.0000
zb = gas deviation factor at Pb and Te	1.0000	1.0000
Qb = flow rate at base conditions	0.00609 cm ³ /s	* 1.0E-6 m ³ /cm ³ 6.088E-09 m ³ /s
ve = flow velocity at sample exit end	1.941E-05 cm/s	* 1.0E-2 m/cm 1.941E-07 m/s
	Ka = 2.39E-07 d	* 9.872E-13 m ² /d 2.36E-19 m ²
	Ka = 2.39E-04 md	2.36E-15 cm ²
	Ka = 2.39E-01 μd	
Pc - Pm = Actual N.E.S.	287.9 psid	1.98 MPa

Steady State Gas Permeability Data

Project #:	8362	Target Net Eff. Stress:	6 Mpa	870.2 psid	Gas:	N2						
Sample #:	D	Length:	9.886 cm		gas deviation z factors:	ze =	1.0000	zb =	1.0000			
Stress Level #:	2	Diameter:	10.168 cm		Viscosity:	0.0176 cp						
Regime #:	1	Area:	81.201 cm ²									
Pressure Data Filename:	8362DG.S2A											
XDCR calibration factors:	Pc =	222.869	psig/volt	PI =	55.4417	psig/volt	ΔP =	11.0272	psid/volt	Pe =	5.5211	psig/volt

Date	Time of Day	File Time (min)	Regime #	Pb Barometric Pressure	Pc Confining Pressure	PI Inlet Pressure	ΔP Differential Pressure	Pm Mean Pore Pressure Pe+ΔP/2	Pe Exit Pressure	Te Flow Temp (°C)	Tb Ambient Temp (°C)	Qb Flow Rate @Pb&Tb (ml/sec)
15 Jul 93	14:47	1353	DS2R1a	12.30 psia	4.158 volts	1.918 volts	9.165 volts		1.078 volts	23	23	0.002292
15 Jul 93	14:51	1358	DS2R1b	12.30 psia	4.158 volts	1.918 volts	9.165 volts		1.078 volts	23	23	0.002289
15 Jul 93	14:56	1363	DS2R1c	12.30 psia	4.158 volts	1.918 volts	9.164 volts		1.079 volts	23	23	0.002281
15 Jul 93	15:01	1368	DS2R1d	12.30 psia	4.158 volts	1.918 volts	9.164 volts		1.080 volts	23	23	0.002275
15 Jul 93	15:06	1373	DS2R1e	12.30 psia	4.158 volts	1.918 volts	9.164 volts		1.081 volts	23	23	0.002287
AVERAGES					GUAGE	GUAGE	DIFFERENTIAL	GUAGE	GUAGE	(°C)	(°C)	
					4.158 volts	1.918 volts	9.164 volts		1.079 volts			
					926.7 psig	106.34 psig	101.06 psid	56.49 psig	5.958 psig	23	23	
					63.06 atm	7.236 atm	6.877 atm	3.844 atm	0.4054 atm			
					6.389 Mpa	0.7332 Mpa	0.6968 Mpa	0.3895 Mpa	0.04108 Mpa			
				ABSOLUTE	ABSOLUTE	ABSOLUTE	DIFFERENTIAL	ABSOLUTE	ABSOLUTE	(°K)	(°K)	(ml/sec)
					12.3 psia	939.0 psia	118.64 psia	101.06 psid	68.79 psia	18.26 psia		
				0.8370 atm	63.89 atm	8.073 atm	6.877 atm	4.681 atm	1.242 atm	296	296	0.00228
				0.08481 Mpa	6.474 Mpa	0.8180 Mpa	0.6968 Mpa	0.4743 Mpa	0.1259 Mpa			

C-146

Apparent gas permeability: $K_a = (v_e \cdot P_e \cdot u \cdot L) / (P_m \cdot \Delta P)$

Boyle's Law: $v_e = (P_b / P_e) \cdot (T_e / T_b) \cdot (z_e / z_b) \cdot v_b$

$Q_e = (P_b / P_e) \cdot (T_e / T_b) \cdot (z_e / z_b) \cdot Q_b$

$v_e = Q_e / A = (P_b / P_e) \cdot (T_e / T_b) \cdot (z_e / z_b) \cdot (Q_b / A)$

Parameter	Traditional Units	SI Units
μ = gas viscosity	0.0176 cp	* 1.0E-3 Pa*sec/cp 1.760E-05 Pa*sec
L = sample length	9.886 cm	* 1.0E-2 m/cm 9.886E-02 m
A = sample circular cross sectional area	81.201 cm ²	* 1.0E-4 m ² /cm ² 8.120E-03 m ²
Pb = flow measurement basis pressure (absolute)	0.8370 atm	* 1.013E+5 Pa/atm 8.478E+04 Pa
ΔP = pressure drop across sample length	6.877 atm	* 1.013E+5 Pa/atm 6.966E+05 Pa
Pm = mean pore pressure (absolute)	4.681 atm	* 1.013E+5 Pa/atm 4.742E+05 Pa
Pe = exit pressure (absolute)	1.242 atm	* 1.013E+5 Pa/atm 1.259E+05 Pa
Te = sample temperature (absolute)	296 °K	296 °K
Tb = flow measurement basis temperature (absolute)	296 °K	296 °K
ze = gas deviation factor at Pe and Te	1.0000	1.0000
zb = gas deviation factor at Pb and Te	1.0000	1.0000
Qb = flow rate at base conditions	0.00228 cm ³ /s	* 1.0E-6 m ³ /cm ³ 2.284E-09 m ³ /s
ve = flow velocity at sample exit end	1.895E-05 cm/s	* 1.0E-2 m/cm 1.895E-07 m/s
Ka =	1.27E-07 d	* 9.872E-13 m ² /d 1.26E-19 m ²
Ka =	1.27E-04 md	1.26E-15 cm ²
Ka =	1.27E-01 μd	
Pc - Pm = Actual N.E.S.	870.2 psid	6.00 MPa

Steady State Gas Permeability Data

Project #:	8362	Target Net Eff. Stress:	6 Mpa	870.2 psid	Gas:	N2						
Sample #:	D	Length:	9.886 cm		gas deviation z factors:	ze =	1.0000	zb =	1.0000			
Stress Level #:	2	Diameter:	10.168 cm		Viscosity:	0.0176 cp						
Regime #:	2	Area:	81.201 cm ²									
Pressure Data Filename:	8362DG.S2A											
XDCR calibration factors:	Pc =	222.869	psig/volt	Pi =	55.4417	psig/volt	ΔP =	11.0272	psid/volt	Pe =	5.5211	psig/volt

Date	Time of Day	File Time (min)	Regime #	Pb Barometric Pressure	Pc Confining Pressure	Pi Inlet Pressure	ΔP Differential Pressure	Pm Mean Pore Pressure Pe*ΔP/2	Pe Exit Pressure	Te Flow Temp (°C)	Tb Ambient Temp (°C)	Qb Flow Rate @Pb&Tb (ml/sec)	
16 Jul 93	13:47	2735	DS2R2a	12.36 psia	4.203 volts	2.095 volts	9.129 volts		2.931 volts	23	23	0.002449	
16 Jul 93	13:52	2740	DS2R2b	12.36 psia	4.203 volts	2.095 volts	9.131 volts		2.931 volts	23	23	0.002424	
16 Jul 93	13:57	2745	DS2R2c	12.36 psia	4.203 volts	2.095 volts	9.132 volts		2.931 volts	23	23	0.002444	
16 Jul 93	14:01	2750	DS2R2d	12.36 psia	4.203 volts	2.096 volts	9.132 volts		2.931 volts	23	23	0.002460	
16 Jul 93	14:06	2755	DS2R2e	12.36 psia	4.203 volts	2.096 volts	9.133 volts		2.932 volts	23	23	0.002442	
AVERAGES			DS2R2		GUAGE	GUAGE	DIFFERENTIAL	GUAGE	GUAGE	(°C)	(°C)		
					4.203 volts	2.095 volts	9.131 volts		2.931 volts				
					936.7 psig	116.17 psig	100.69 psid	66.53 psig	16.183 psig	23	23		
					63.74 atm	7.905 atm	6.852 atm	4.527 atm	1.1012 atm				
					6.458 Mpa	0.8010 Mpa	0.6943 Mpa	0.4587 Mpa	0.11158 Mpa				
					ABSOLUTE	ABSOLUTE	ABSOLUTE	DIFFERENTIAL	ABSOLUTE	ABSOLUTE	(°K)	(°K)	(ml/sec)
					12.36 psia	949.1 psia	128.53 psia	100.69 psid	78.89 psia	28.54 psia	296	296	0.00244
	0.8410 atm	64.58 atm	8.746 atm	6.852 atm	5.368 atm	1.942 atm							
	0.08522 Mpa	6.544 Mpa	0.8862 Mpa	0.6943 Mpa	0.5439 Mpa	0.1968 Mpa							

Apparent gas permeability: $K_a = (v_e \cdot P_e \cdot u \cdot L) / (P_m \cdot \Delta P)$

Boyle's Law: $v_e = (P_b / P_e) \cdot (T_e / T_b) \cdot (z_e / z_b) \cdot v_b$
 $Q_e = (P_b / P_e) \cdot (T_e / T_b) \cdot (z_e / z_b) \cdot Q_b$

$v_e = Q_e / A = (P_b / P_e) \cdot (T_e / T_b) \cdot (z_e / z_b) \cdot (Q_b / A)$

Parameter	Traditional Units	SI Units
μ = gas viscosity	0.0176 cp	* 1.0E-3 Pa*sec/cp 1.760E-05 Pa*sec
L = sample length	9.886 cm	* 1.0E-2 m/cm 9.886E-02 m
A = sample circular cross sectional area	81.201 cm ²	* 1.0E-4 m ² /cm ² 8.120E-03 m ²
Pb = flow measurement basis pressure (absolute)	0.8410 atm	* 1.013E+5 Pa/atm 8.520E+04 Pa
ΔP = pressure drop across sample length	6.852 atm	* 1.013E+5 Pa/atm 6.941E+05 Pa
Pm = mean pore pressure (absolute)	5.368 atm	* 1.013E+5 Pa/atm 5.438E+05 Pa
Pe = exit pressure (absolute)	1.942 atm	* 1.013E+5 Pa/atm 1.968E+05 Pa
Te = sample temperature (absolute)	296 °K	296 °K
Tb = flow measurement basis temperature (absolute)	296 °K	296 °K
ze = gas deviation factor at Pe and Te	1.0000	1.0000
zb = gas deviation factor at Pb and Te	1.0000	1.0000
Qb = flow rate at base conditions	0.00244 cm ³ /s	* 1.0E-6 m ³ /cm ³ 2.444E-09 m ³ /s
ve = flow velocity at sample exit end	1.303E-05 cm/s	* 1.0E-2 m/cm 1.303E-07 m/s
	Ka = 1.20E-07 d	* 9.872E-13 m ² /d 1.18E-19 m ²
	Ka = 1.20E-04 md	1.18E-15 cm ²
	Ka = 1.20E-01 μd	
Pc - Pm = Actual N.E.S.	870.2 psid	6.00 MPa

C-147

Steady State Gas Permeability Data

Project #:	8362	Target Net Eff. Stress:	6 Mpa	870.2 psid	Gas:	N2		
Sample #:	0	Length:	9.886 cm		gas deviation z factors:	ze = 1.0000	zb = 1.0000	
Stress Level #:	2	Diameter:	10.168 cm		Viscosity:	0.0176 cp		
Regime #:	3	Area:	81.201 cm ²					
Pressure Data Filename:	8362DG.S2A							
XDCR calibration factors:	Pc = 222.869 psig/volt	Pi = 55.4417 psig/volt	ΔP = 11.0272 psid/volt	Pe = 5.5211 psig/volt				

Date	Time of Day	File Time (min)	Regime #	Pb Barometric Pressure	Pc Confining Pressure	Pi Inlet Pressure	ΔP Differential Pressure	Pm Mean Pore Pressure Pe*ΔP/2	Pe Exit Pressure	Te Flow Temp (°C)	Tb Ambient Temp (°C)	Qb Flow Rate @Pb&Tb (ml/sec)	
17 Jul 93	14:20	4208	DS2R3a	12.35 psia	4.248 volts	2.270 volts	9.050 volts		4.859 volts	23	23	0.002590	
17 Jul 93	14:25	4213	DS2R3b	12.35 psia	4.249 volts	2.271 volts	9.051 volts		4.859 volts	23	23	0.002603	
17 Jul 93	14:29	4213	DS2R3c	12.35 psia	4.249 volts	2.271 volts	9.052 volts		4.859 volts	23	23	0.002565	
17 Jul 93	14:33	4218	DS2R3d	12.35 psia	4.249 volts	2.271 volts	9.054 volts		4.859 volts	23	23	0.002562	
17 Jul 93	14:37	4223	DS2R3e	12.35 psia	4.249 volts	2.271 volts	9.054 volts		4.859 volts	23	23	0.002574	
AVERAGES			DS2R3										
					GUAGE	GUAGE	DIFFERENTIAL	GUAGE	GUAGE	(°C)	(°C)		
					4.249 volts	2.271 volts	9.052 volts	76.74 psig	4.859 volts	23	23		
					946.9 psig	125.90 psig	99.82 psid	5.222 atm	26.827 psig				
					64.43 atm	8.567 atm	6.792 atm	1.8255 atm					
					6.529 Mpa	0.8680 Mpa	0.6882 Mpa	0.5291 Mpa	0.18497 Mpa				
			ABSOLUTE	ABSOLUTE	ABSOLUTE	DIFFERENTIAL	ABSOLUTE	ABSOLUTE	(°K)	(°K)	(ml/sec)		
			12.35 psia	959.3 psia	138.25 psia	99.82 psid	89.09 psia	39.18 psia					
			0.8404 atm	65.27 atm	9.407 atm	6.792 atm	6.062 atm	2.666 atm	296	296	0.00258		
			0.08515 Mpa	6.614 Mpa	0.9532 Mpa	0.6882 Mpa	0.6142 Mpa	0.2701 Mpa					

C-148

Apparent gas permeability: $K_a = (v_e \cdot P_e \cdot u \cdot L) / (P_m \cdot \Delta P)$

Boyle's Law: $V_e = (P_b / P_e) \cdot (T_e / T_b) \cdot (z_e / z_b) \cdot V_b$

$Q_e = (P_b / P_e) \cdot (T_e / T_b) \cdot (z_e / z_b) \cdot Q_b$

$v_e = Q_e / A \cdot (P_b / P_e) \cdot (T_e / T_b) \cdot (z_e / z_b) \cdot (Q_b / A)$

Parameter	Traditional Units	SI Units
μ = gas viscosity	0.0176 cp	* 1.0E-3 Pa*sec/cp 1.760E-05 Pa*sec
L = sample length	9.886 cm	* 1.0E-2 m/cm 9.886E-02 m
A = sample circular cross sectional area	81.201 cm ²	* 1.0E-4 m ² /cm ² 8.120E-03 m ²
Pb = flow measurement basis pressure (absolute)	0.8404 atm	* 1.013E+5 Pa/atm 8.513E+04 Pa
ΔP = pressure drop across sample length	6.792 atm	* 1.013E+5 Pa/atm 6.881E+05 Pa
Pm = mean pore pressure (absolute)	6.062 atm	* 1.013E+5 Pa/atm 6.141E+05 Pa
Pe = exit pressure (absolute)	2.666 atm	* 1.013E+5 Pa/atm 2.700E+05 Pa
Te = sample temperature (absolute)	296 °K	296 °K
Tb = flow measurement basis temperature (absolute)	296 °K	296 °K
ze = gas deviation factor at Pe and Te	1.0000	1.0000
zb = gas deviation factor at Pb and Te	1.0000	1.0000
Qb = flow rate at base conditions	0.00258 cm ³ /s	* 1.0E-6 m ³ /cm ³ 2.580E-09 m ³ /s
ve = flow velocity at sample exit end	1.002E-05 cm/s	* 1.0E-2 m/cm 1.002E-07 m/s
	Ka = 1.13E-07 d	* 9.872E-13 m ² /d 1.11E-19 m ²
	Ka = 1.13E-04 md	1.11E-15 cm ²
	Ka = 1.13E-01 μd	
Pc - Pm = Actual N.E.S.	870.2 psid	6.00 MPa

Steady State Gas Permeability Data

Project #: 8362	Target Net Eff. Stress: 6 Mpa	870.2 psid	Gas: N2
Sample #: D	Length: 9.886 cm		gas deviation z factors: ze = 1.0000 zb = 1.0000
Stress Level #: 2	Diameter: 10.168 cm		Viscosity: 0.0176 cp
Regime #: 4	Area: 81.201 cm ²		
Pressure Data Filename: 8362DG.S2A			
XDCR calibration factors: Pc = 222.869 psig/volt Pi = 55.4417 psig/volt ΔP = 11.0272 psid/volt Pe = 5.5211 psig/volt			

Date	Time of Day	File Time (min)	Regime #	Pb Barometric Pressure	Pc Confining Pressure	Pi Inlet Pressure	ΔP Differential Pressure	Pm Mean Pore Pressure Pe*ΔP/2	Pe Exit Pressure	Te Flow Temp (°C)	Tb Ambient Temp (°C)	Qb Flow Rate @Pb&Tb (ml/sec)
19 Jul 93	17:37	7285	DS2R4a	12.32 psia	4.297 volts	2.454 volts	8.982 volts		6.859 volts	23	23	0.002709
19 Jul 93	17:41	7290	DS2R4b	12.32 psia	4.297 volts	2.454 volts	8.983 volts		6.858 volts	23	23	0.002700
19 Jul 93	17:45	7295	DS2R4c	12.32 psia	4.297 volts	2.454 volts	8.982 volts		6.858 volts	23	23	0.002684
19 Jul 93	17:49	7295	DS2R4d	12.32 psia	4.297 volts	2.454 volts	8.983 volts		6.858 volts	23	23	0.002684
19 Jul 93	17:53	7300	DS2R4e	12.32 psia	4.297 volts	2.454 volts	8.983 volts		6.858 volts	23	23	0.002677
AVERAGES			DS2R4		GAUGE	GAUGE	DIFFERENTIAL	GAUGE	GAUGE	(°C)	(°C)	
					4.297 volts	2.454 volts	8.983 volts	87.39 psig	6.858 volts			
					957.7 psig	136.05 psig	99.05 psid	37.865 psig		23	23	
					65.17 atm	9.258 atm	6.740 atm	2.5765 atm				
					6.603 Mpa	0.9381 Mpa	0.6829 Mpa	0.26107 Mpa				
					ABSOLUTE	ABSOLUTE	DIFFERENTIAL	ABSOLUTE	ABSOLUTE	(°K)	(°K)	
					12.32 psia	970.0 psia	148.37 psia	99.05 psid	99.71 psia	50.18 psia		
			0.8383 atm	66.00 atm	10.096 atm	6.740 atm	6.785 atm	3.415 atm	296	296	0.00269	
			0.08494 Mpa	6.688 Mpa	1.0230 Mpa	0.6829 Mpa	0.6875 Mpa	0.3460 Mpa				

C-149

Apparent gas permeability: $K_a = (v_e \cdot P_e \cdot u \cdot L) / (P_m \cdot \Delta P)$

Boyle's Law: $v_e = (P_b / P_e) \cdot (T_e / T_b) \cdot (z_e / z_b) \cdot v_b$
 $Q_e = (P_b / P_e) \cdot (T_e / T_b) \cdot (z_e / z_b) \cdot Q_b$

$v_e = Q_e / A = (P_b / P_e) \cdot (T_e / T_b) \cdot (z_e / z_b) \cdot (Q_b / A)$

Parameter	Traditional Units	SI Units
μ = gas viscosity	0.0176 cp	* 1.0E-3 Pa*sec/cp 1.760E-05 Pa*sec
L = sample length	9.886 cm	* 1.0E-2 m/cm 9.886E-02 m
A = sample circular cross sectional area	81.201 cm ²	* 1.0E-4 m ² /cm ² 8.120E-03 m ²
Pb = flow measurement basis pressure (absolute)	0.8383 atm	* 1.013E+5 Pa/atm 8.492E+04 Pa
ΔP = pressure drop across sample length	6.740 atm	* 1.013E+5 Pa/atm 6.828E+05 Pa
Pm = mean pore pressure (absolute)	6.785 atm	* 1.013E+5 Pa/atm 6.873E+05 Pa
Pe = exit pressure (absolute)	3.415 atm	* 1.013E+5 Pa/atm 3.459E+05 Pa
Te = sample temperature (absolute)	296 °K	296 °K
Tb = flow measurement basis temperature (absolute)	296 °K	296 °K
ze = gas deviation factor at Pe and Te	1.0000	1.0000
zb = gas deviation factor at Pb and Te	1.0000	1.0000
Qb = flow rate at base conditions	0.00269 cm ³ /s	* 1.0E-6 m ³ /cm ³ 2.694E-09 m ³ /s
ve = flow velocity at sample exit end	8.146E-06 cm/s	* 1.0E-2 m/cm 8.146E-08 m/s
	Ka = 1.06E-07 d	* 9.872E-13 m ² /d 1.04E-19 m ²
	Ka = 1.06E-04 md	1.04E-15 cm ²
	Ka = 1.06E-01 μd	
Pc - Pm = Actual N.E.S.	870.3 psid	6.00 MPa

Steady State Gas Permeability Data

Project #:	8362	Target Net Eff. Stress:	10 Mpa	1450.4 psid	Gas:	N2		
Sample #:	D	Length:	9.886 cm		gas deviation z factors:	ze = 1.0000	zb = 1.0000	
Stress Level #:	3	Diameter:	10.168 cm		Viscosity:	0.0176 cp		
Regime #:	4'	Area:	81.201 cm ²					
Pressure Data Filename:	8362DG.S3A							
XDCR calibration factors:	Pc =	222.869 psig/volt	PI =	55.4417 psig/volt	ΔP =	11.0272 psid/volt	Pe =	5.5211 psig/volt

Date	Time of Day	File Time (min)	Regime #	Pb Barometric Pressure	Pc Confining Pressure	Pi Inlet Pressure	ΔP Differential Pressure	Pm Mean Pore Pressure Pe+ΔP/2	Pe Exit Pressure	Te Flow Temp (°C)	Tb Ambient Temp (°C)	Qb Flow Rate @Pb&Tb (ml/sec)	
27 Jul 93	14:36	10262	DS3R4'a	12.40 psia	6.898 volts	2.460 volts	9.088 volts		6.687 volts	23	23	0.002014	
27 Jul 93	14:41	10267	DS3R4'b	12.40 psia	6.898 volts	2.460 volts	9.087 volts		6.689 volts	23	23	0.001987	
27 Jul 93	14:46	10272	DS3R4'c	12.40 psia	6.898 volts	2.460 volts	9.088 volts		6.688 volts	23	23	0.001970	
27 Jul 93	14:52	10277	DS3R4'd	12.40 psia	6.898 volts	2.460 volts	9.089 volts		6.688 volts	23	23	0.001979	
27 Jul 93	14:57	10282	DS3R4'e	12.40 psia	6.898 volts	2.460 volts	9.089 volts		6.688 volts	23	23	0.001993	
AVERAGES			DS3R4'		GUAGE	GUAGE	DIFFERENTIAL	GUAGE	GUAGE	(°C)	(°C)		
					6.898 volts	2.460 volts	9.088 volts		6.688 volts				
					1537.4 psig	136.39 psig	100.22 psid	87.03 psig	36.925 psig		23	23	
					104.61 atm	9.281 atm	6.819 atm	5.922 atm	2.5126 atm				
					10.600 Mpa	0.9404 Mpa	0.6910 Mpa	0.6001 Mpa	0.25459 Mpa				
					ABSOLUTE	ABSOLUTE	DIFFERENTIAL	ABSOLUTE	ABSOLUTE	(°K)	(°K)		
					12.4 psia	1549.8 psia	148.79 psia	100.22 psid	99.43 psia	49.33 psia			
			0.8438 atm	105.45 atm	10.124 atm	6.819 atm	6.766 atm	3.356 atm		296	296	0.00199	
			0.08550 Mpa	10.685 Mpa	1.0258 Mpa	0.6910 Mpa	0.6856 Mpa	0.3401 Mpa					

Apparent gas permeability: $K_a = (v_e \cdot P_e \cdot u \cdot L) / (P_m \cdot \Delta P)$

Boyle's Law: $V_e = (P_b / P_e) \cdot (T_e / T_b) \cdot (z_e / z_b) \cdot V_b$

$Q_e = (P_b / P_e) \cdot (T_e / T_b) \cdot (z_e / z_b) \cdot Q_b$

$v_e = Q_e / A = (P_b / P_e) \cdot (T_e / T_b) \cdot (z_e / z_b) \cdot (Q_b / A)$

Parameter	Traditional Units	SI Units
μ = gas viscosity	0.0176 cp	* 1.0E-3 Pa*sec/cp 1.760E-05 Pa*sec
L = sample length	9.886 cm	* 1.0E-2 m/cm 9.886E-02 m
A = sample circular cross sectional area	81.201 cm ²	* 1.0E-4 m ² /cm ² 8.120E-03 m ²
Pb = flow measurement basis pressure (absolute)	0.8438 atm	* 1.013E+5 Pa/atm 8.547E+04 Pa
ΔP = pressure drop across sample length	6.819 atm	* 1.013E+5 Pa/atm 6.908E+05 Pa
Pm = mean pore pressure (absolute)	6.766 atm	* 1.013E+5 Pa/atm 6.854E+05 Pa
Pe = exit pressure (absolute)	3.356 atm	* 1.013E+5 Pa/atm 3.400E+05 Pa
Te = sample temperature (absolute)	296 °K	296 °K
Tb = flow measurement basis temperature (absolute)	296 °K	296 °K
ze = gas deviation factor at Pe and Te	1.0000	1.0000
zb = gas deviation factor at Pb and Te	1.0000	1.0000
Qb = flow rate at base conditions	0.00199 cm ³ /s	* 1.0E-6 m ³ /cm ³ 1.987E-09 m ³ /s
ve = flow velocity at sample exit end	6.152E-06 cm/s	* 1.0E-2 m/cm 6.152E-08 m/s
	Ka =	7.79E-08 d * 9.872E-13 m ² /d 7.69E-20 m ²
	Ka =	7.79E-05 md 7.69E-16 cm ²
	Ka =	7.79E-02 μd
Pc - Pm = Actual N.E.S.	1450.3 psid	10.00 MPa

C-150

Steady State Gas Permeability Data

Project #:	8362	Target Net Eff. Stress:	10 Mpa	1450.4 psid	Gas:	N2						
Sample #:	D	Length:	9.886 cm		gas deviation z factors:	ze =	1.0000	zb =	1.0000			
Stress Level #:	3	Diameter:	10.168 cm		Viscosity:	0.0176 cp						
Regime #:	3'	Area:	81.201 cm ²									
Pressure Data Filename:	8362DG.S3A											
XDCR calibration factors:	Pc =	222.869	psig/volt	Pi =	55.4417	psig/volt	ΔP =	11.0272	psid/volt	Pe =	5.5211	psig/volt

Date	Time of Day	File Time (min)	Regime #	Pb Barometric Pressure	Pc Confining Pressure	Pi Inlet Pressure	ΔP Differential Pressure	Pm Mean Pore Pressure Pe·ΔP/2	Pe Exit Pressure	Te Flow Temp (°C)	Tb Ambient Temp (°C)	Qb Flow Rate @Pb&Tb (ml/sec)
28 Jul 93	08:47	11353	DS3R3'a	12.38 psia	6.849 volts	2.270 volts	9.136 volts		4.686 volts	23	22	0.001837
28 Jul 93	08:53	11358	DS3R3'b	12.38 psia	6.849 volts	2.270 volts	9.137 volts		4.687 volts	23	22	0.001822
28 Jul 93	08:58	11363	DS3R3'c	12.38 psia	6.849 volts	2.270 volts	9.137 volts		4.687 volts	23	22	0.001828
28 Jul 93	09:04	11368	DS3R3'd	12.38 psia	6.849 volts	2.270 volts	9.138 volts		4.687 volts	23	22	0.001847
28 Jul 93	09:10	11373	DS3R3'e	12.38 psia	6.849 volts	2.270 volts	9.139 volts		4.688 volts	23	22	0.001831
AVERAGES			DS3R3'		GUAGE	GUAGE	DIFFERENTIAL	GUAGE	GUAGE	(°C)	(°C)	
					6.849 volts	2.270 volts	9.137 volts		4.687 volts			
					1526.4 psig	125.85 psig	100.76 psid	76.26 psig	25.877 psig	23	22	
					103.87 atm	8.564 atm	6.856 atm	5.189 atm	1.7608 atm			
					10.524 Mpa	0.8677 Mpa	0.6947 Mpa	0.5258 Mpa	0.17842 Mpa			
					ABSOLUTE	ABSOLUTE	ABSOLUTE	DIFFERENTIAL	ABSOLUTE	ABSOLUTE	(°K)	(°K)
				12.38 psia	1538.8 psia	138.23 psia	100.76 psid	88.64 psia	38.26 psia			
				0.8424 atm	104.71 atm	9.406 atm	6.856 atm	6.031 atm	2.603 atm	296	295	0.00183
				0.08536 Mpa	10.610 Mpa	0.9531 Mpa	0.6947 Mpa	0.6111 Mpa	0.2638 Mpa			

Apparent gas permeability: $K_a = (v_e \cdot P_e \cdot u \cdot L) / (P_m \cdot \Delta P)$

Boyle's Law: $v_e = (P_b/P_e) \cdot (T_e/T_b) \cdot (z_e/z_b) \cdot v_b$
 $Q_e = (P_b/P_e) \cdot (T_e/T_b) \cdot (z_e/z_b) \cdot Q_b$

$v_e = Q_e/A = (P_b/P_e) \cdot (T_e/T_b) \cdot (z_e/z_b) \cdot (Q_b/A)$

Parameter	Traditional Units	SI Units
μ = gas viscosity	0.0176 cp	* 1.0E-3 Pa·sec/cp 1.760E-05 Pa·sec
L = sample length	9.886 cm	* 1.0E-2 m/cm 9.886E-02 m
A = sample circular cross sectional area	81.201 cm ²	* 1.0E-4 m ² /cm ² 8.120E-03 m ²
Pb = flow measurement basis pressure (absolute)	0.8424 atm	* 1.013E+5 Pa/atm 8.534E+04 Pa
ΔP = pressure drop across sample length	6.856 atm	* 1.013E+5 Pa/atm 6.945E+05 Pa
Pm = mean pore pressure (absolute)	6.031 atm	* 1.013E+5 Pa/atm 6.110E+05 Pa
Pe = exit pressure (absolute)	2.603 atm	* 1.013E+5 Pa/atm 2.637E+05 Pa
Te = sample temperature (absolute)	296 °K	296 °K
Tb = flow measurement basis temperature (absolute)	295 °K	295 °K
ze = gas deviation factor at Pe and Te	1.0000	1.0000
zb = gas deviation factor at Pb and Te	1.0000	1.0000
Qb = flow rate at base conditions	0.00183 cm ³ /s	* 1.0E-6 m ³ /cm ³ 1.833E-09 m ³ /s
ve = flow velocity at sample exit end	7.330E-06 cm/s	* 1.0E-2 m/cm 7.330E-08 m/s
	Ka =	8.03E-08 d * 9.872E-13 m ² /d 7.93E-20 m ²
	Ka =	8.03E-05 md 7.93E-16 cm ²
	Ka =	8.03E-02 μd
Pc - Pm = Actual N.E.S.	1450.2 psid	10.00 MPa

C-151

Steady State Gas Permeability Data

Project #:	8362	Target Net Eff. Stress:	10 Mpa	1450.4 psid	Gas:	N2					
Sample #:	D	Length:	9.886 cm		gas deviation z factors:	ze =	1.0000	zb = 1.0000			
Stress Level #:	3	Diameter:	10.168 cm		Viscosity:	0.0176 cp					
Regime #:	2'	Area:	81.201 cm ²								
Pressure Data Filename:	8362DG.S3A										
XDCR calibration factors:	Pc =	222.869	psig/volt	Pl =	55.4417	psig/volt	ΔP =	11.0272 psid/volt	Pe =	5.5211	psig/volt

Date	Time of Day	File Time (min)	Regime #	Pb Barometric Pressure	Pc Confining Pressure	Pl Inlet Pressure	ΔP Differential Pressure	Pm Mean Pore Pressure Pe+ΔP/2	Pe Exit Pressure	Te Flow Temp (°C)	Tb Ambient Temp (°C)	Qb Flow Rate @Pb&Tb (ml/sec)
29 Jul 93	10:54	12917	DS3R2'a	12.38 psia	6.805 volts	2.097 volts	9.176 volts		2.860 volts	23	23	0.001712
29 Jul 93	11:00	12922	DS3R2'b	12.38 psia	6.805 volts	2.097 volts	9.175 volts		2.860 volts	23	23	0.001704
29 Jul 93	11:05	12932	DS3R2'c	12.38 psia	6.805 volts	2.097 volts	9.176 volts		2.860 volts	23	23	0.001699
29 Jul 93	11:11	12937	DS3R2'd	12.38 psia	6.805 volts	2.097 volts	9.177 volts		2.860 volts	23	23	0.001699
29 Jul 93	11:21	12947	DS3R2'e	12.38 psia	6.805 volts	2.098 volts	9.177 volts		2.861 volts	23	23	0.001704
AVERAGES			DS3R2'									
				GUAGE	GUAGE	DIFFERENTIAL	GUAGE	GUAGE	(°C)	(°C)		
				6.805 volts	2.097 volts	9.176 volts	2.860 volts					
				1516.6 psig	116.27 psig	101.19 psid	66.39 psig	15.791 psig	23	23		
				103.20 atm	7.912 atm	6.885 atm	4.517 atm	1.0745 atm				
				10.457 Mpa	0.8017 Mpa	0.6977 Mpa	0.4577 Mpa	0.10888 Mpa				
				ABSOLUTE	ABSOLUTE	ABSOLUTE	ABSOLUTE	ABSOLUTE	(°K)	(°K)	(ml/sec)	
		12.38 psia	1529.0 psia	128.65 psia	101.19 psid	78.77 psia	28.17 psia					
		0.8424 atm	104.04 atm	8.754 atm	6.885 atm	5.360 atm	1.917 atm	296	296	0.001704		
		0.08536 Mpa	10.542 Mpa	0.8870 Mpa	0.6977 Mpa	0.5431 Mpa	0.1942 Mpa					

Apparent gas permeability: $K_a = (v_e \cdot P_e \cdot u \cdot L) / (P_m \cdot \Delta P)$

Boyle's Law: $v_e = (P_b / P_e) \cdot (T_e / T_b) \cdot (z_e / z_b) \cdot v_b$
 $Q_e = (P_b / P_e) \cdot (T_e / T_b) \cdot (z_e / z_b) \cdot Q_b$

$v_e = Q_e / A = (P_b / P_e) \cdot (T_e / T_b) \cdot (z_e / z_b) \cdot (Q_b / A)$

Parameter	Traditional Units	SI Units
μ = gas viscosity	0.0176 cp	* 1.0E-3 Pa*sec/cp 1.760E-05 Pa*sec
L = sample length	9.886 cm	* 1.0E-2 m/cm 9.886E-02 m
A = sample circular cross sectional area	81.201 cm ²	* 1.0E-4 m ² /cm ² 8.120E-03 m ²
Pb = flow measurement basis pressure (absolute)	0.8424 atm	* 1.013E+5 Pa/atm 8.534E+04 Pa
ΔP = pressure drop across sample length	6.885 atm	* 1.013E+5 Pa/atm 6.975E+05 Pa
Pm = mean pore pressure (absolute)	5.360 atm	* 1.013E+5 Pa/atm 5.429E+05 Pa
Pe = exit pressure (absolute)	1.917 atm	* 1.013E+5 Pa/atm 1.942E+05 Pa
Te = sample temperature (absolute)	296 °K	296 °K
Tb = flow measurement basis temperature (absolute)	296 °K	296 °K
ze = gas deviation factor at Pe and Te	1.0000	1.0000
zb = gas deviation factor at Pb and Te	1.0000	1.0000
Qb = flow rate at base conditions	0.00170 cm ³ /s	* 1.0E-6 m ³ /cm ³ 1.704E-09 m ³ /s
ve = flow velocity at sample exit end	9.220E-06 cm/s	* 1.0E-2 m/cm 9.220E-08 m/s
	Ka =	8.33E-08 d * 9.872E-13 m ² /d 8.23E-20 m ²
	Ka =	8.33E-05 md 8.23E-16 cm ²
	Ka =	8.33E-02 μd
Pc - Pm = Actual N.E.S.	1450.2 psid	10.00 MPa

C-152

Steady State Gas Permeability Data

Project #: 0362	Target Net Eff. Stress: 10 Mpa 1450.4 psid	Gas: N2
Sample #: D	Length: 9.886 cm	gas deviation z factors: ze = 1.0000 zb = 1.0000
Stress Level #: 3	Diameter: 10.168 cm	Viscosity: 0.0176 cp
Regime #: 1'	Area: 81.201 cm ²	
Pressure Data Filename: 8362DG.S3A		
XDCR calibration factors: Pc = 222.869 psig/volt Pi = 55.4417 psig/volt ΔP = 11.0272 psid/volt Pe = 5.5211 psig/volt		

Date	Time of Day	File Time (min)	Regime #	Pb Barometric Pressure	Pc Confining Pressure	Pi Inlet Pressure	ΔP Differential Pressure	Pm Mean Pore Pressure Pe*ΔP/2	Pe Exit Pressure	Te Flow Temp (°C)	Tb Ambient Temp (°C)	Qb Flow Rate @Pb&Tb (ml/sec)
30 Jul 93	15:31	14637	DS3R1'a	12.42 psia	6.758 volts	1.918 volts	9.174 volts		1.048 volts	23	23	0.001578
30 Jul 93	15:37	14642	DS3R1'b	12.42 psia	6.758 volts	1.918 volts	9.174 volts		1.048 volts	23	23	0.001568
30 Jul 93	15:56	14662	DS3R1'c	12.42 psia	6.758 volts	1.918 volts	9.175 volts		1.049 volts	23	23	0.001553
30 Jul 93	16:10	14677	DS3R1'd	12.42 psia	6.758 volts	1.918 volts	9.175 volts		1.050 volts	23	23	0.001544
30 Jul 93	16:16	14682	DS3R1'e	12.42 psia	6.758 volts	1.918 volts	9.175 volts		1.050 volts	23	23	0.001548
AVERAGES					GAUGE	GAUGE	DIFFERENTIAL	GAUGE	GAUGE	(°C)	(°C)	
					6.758 volts	1.918 volts	9.175 volts		1.049 volts			
					1506.1 psig	106.34 psig	101.17 psid	56.38 psig	5.792 psig	23	23	
					102.49 atm	7.236 atm	6.884 atm	3.836 atm	0.3941 atm			
					10.385 Mpa	0.7332 Mpa	0.6975 Mpa	0.3887 Mpa	0.03993 Mpa			
				ABSOLUTE	ABSOLUTE	ABSOLUTE	DIFFERENTIAL	ABSOLUTE	ABSOLUTE	(°K)	(°K)	(ml/sec)
					12.42 psia	1518.6 psia	118.76 psia	101.17 psid	68.80 psia	18.21 psia		
				0.8451 atm	103.33 atm	8.081 atm	6.884 atm	4.681 atm	1.239 atm	296	296	0.001561
				0.08563 Mpa	10.470 Mpa	0.8188 Mpa	0.6975 Mpa	0.4743 Mpa	0.1256 Mpa			

C-153

Apparent gas permeability: $K_a = (v_e \cdot P_e \cdot u \cdot L) / (P_m \cdot \Delta P)$

Boyle's Law: $v_e = (P_b / P_e) \cdot (T_e / T_b) \cdot (z_e / z_b) \cdot v_b$
 $Q_e = (P_b / P_e) \cdot (T_e / T_b) \cdot (z_e / z_b) \cdot Q_b$

$v_e = Q_e / A = (P_b / P_e) \cdot (T_e / T_b) \cdot (z_e / z_b) \cdot (Q_b / A)$

Parameter	Traditional Units	SI Units
μ = gas viscosity	0.0176 cp	• 1.0E-3 Pa*sec/cp 1.760E-05 Pa*sec
L = sample length	9.886 cm	• 1.0E-2 m/cm 9.886E-02 m
A = sample circular cross sectional area	81.201 cm ²	• 1.0E-4 m ² /cm ² 8.120E-03 m ²
Pb = flow measurement basis pressure (absolute)	0.8451 atm	• 1.013E+5 Pa/atm 8.561E+04 Pa
ΔP = pressure drop across sample length	6.884 atm	• 1.013E+5 Pa/atm 6.974E+05 Pa
Pm = mean pore pressure (absolute)	4.681 atm	• 1.013E+5 Pa/atm 4.742E+05 Pa
Pe = exit pressure (absolute)	1.239 atm	• 1.013E+5 Pa/atm 1.255E+05 Pa
Te = sample temperature (absolute)	296 °K	296 °K
Tb = flow measurement basis temperature (absolute)	296 °K	296 °K
ze = gas deviation factor at Pe and Te	1.0000	1.0000
zb = gas deviation factor at Pb and Te	1.0000	1.0000
Qb = flow rate at base conditions	0.00156 cm ³ /s	• 1.0E-6 m ³ /cm ³ 1.561E-09 m ³ /s
ve = flow velocity at sample exit end	1.311E-05 cm/s	• 1.0E-2 m/cm 1.311E-07 m/s
	Ka = 8.77E-08 d	• 9.872E-13 m ² /d 8.66E-20 m ²
	Ka = 8.77E-05 md	8.66E-16 cm ²
	Ka = 8.77E-02 μd	
Pc - Pm = Actual N.E.S.	1449.8 psid	10.00 MPa

Steady State Gas Permeability Data

Project #:	8362	Net Effective Stress:	2 Mpa	290.1 psig	Gas:	N2			
Sample #:	E	Length:	10.358 cm		gas deviation z factors:	ze =	1.0000	zb =	1.0000
Stress Level #:	1	Diameter:	10.175 cm		Viscosity:	0.0176 cp			
Regime #:	1	Area:	81.313 cm ²						
Pressure Data Filename:	8362EG.S1B								
XDCR calibration factors:	Pc =	222.869 psig/volt	PI =	5.4862 psig/volt	ΔP =	1.6591 psid/volt	Pe =	5.5211 psig/volt	

Date	Time of Day	File Time (min)	Regime #	Pb Barometric Pressure	Pc Confining Pressure	PI Inlet Pressure	ΔP Differential Pressure	Pm Mean Pore Pressure Pe*ΔP/2	Pe Exit Pressure	Te Flow Temp (°C)	Tb Ambient Temp (°C)	Qb Flow Rate @Pb&Tb (ml/sec)
16 Apr 93	11:32	1454	ES1R1a	12.32 psia	1.314 volts	0.729 volts	1.857 volts		0.178 volts	23	22	0.13136
16 Apr 93	11:36	1459	ES1R1b	12.32 psia	1.313 volts	0.729 volts	1.857 volts		0.178 volts	23	22	0.13098
16 Apr 93	11:39	1459	ES1R1c	12.32 psia	1.312 volts	0.729 volts	1.856 volts		0.178 volts	23	22	0.13119
16 Apr 93	11:42	1464	ES1R1d	12.32 psia	1.311 volts	0.729 volts	1.856 volts		0.178 volts	23	22	0.13106
AVERAGES			ES1R1									
					GAUGE	GAUGE	DIFFERENTIAL	GAUGE	GAUGE	(°C)	(°C)	
					1.313 volts	0.729 volts	1.857 volts	2.523 psig	0.178 volts	23	22	
					292.5 psig	4.00 psig	3.080 psid	0.1717 atm	0.06687 atm			
					19.90 atm	0.272 atm	0.2096 atm	0.01739 Mpa	0.006776 Mpa			
					2.017 Mpa	0.0276 Mpa	0.02124 Mpa	0.01739 Mpa	0.006776 Mpa			
				ABSOLUTE	ABSOLUTE	ABSOLUTE	DIFFERENTIAL	ABSOLUTE	ABSOLUTE	(°K)	(°K)	(ml/sec)
				12.32 psia	304.8 psia	16.32 psia	3.080 psid	14.84 psia	13.30 psia			
				0.8383 atm	20.74 atm	1.110 atm	0.2096 atm	1.010 atm	0.9052 atm	296	295	0.13115
				0.08494 Mpa	2.102 Mpa	0.1125 Mpa	0.02124 Mpa	0.1023 Mpa	0.09172 Mpa			

C-154

Apparent gas permeability: $K_a = (v_e \cdot P_e \cdot u \cdot L) / (P_m \cdot \Delta P)$

Boyle's Law: $V_e = (P_b / P_e) \cdot (T_e / T_b) \cdot (z_e / z_b) \cdot V_b$

$Q_e = (P_b / P_e) \cdot (T_e / T_b) \cdot (z_e / z_b) \cdot Q_b$

$v_e = Q_e / A = (P_b / P_e) \cdot (T_e / T_b) \cdot (z_e / z_b) \cdot (Q_b / A)$

Parameter	Traditional Units	SI Units
μ = gas viscosity	0.0176 cp	* 1.0E-3 Pa*sec/cp 1.760E-05 Pa*sec
L = sample length	10.358 cm	* 1.0E-2 m/cm 1.036E-01 m
A = sample circular cross sectional area	81.313 cm ²	* 1.0E-4 m ² /cm ² 8.131E-03 m ²
Pb = flow measurement basis pressure (absolute)	0.8383 atm	* 1.013E+5 Pa/atm 8.492E+04 Pa
ΔP = pressure drop across sample length	0.210 atm	* 1.013E+5 Pa/atm 2.123E+04 Pa
Pm = mean pore pressure (absolute)	1.010 atm	* 1.013E+5 Pa/atm 1.023E+05 Pa
Pe = exit pressure (absolute)	0.905 atm	* 1.013E+5 Pa/atm 9.170E+04 Pa
Te = sample temperature (absolute)	296 °K	296 °K
Tb = flow measurement basis temperature (absolute)	295 °K	295 °K
ze = gas deviation factor at Pe and Te	1.0000	1.0000
zb = gas deviation factor at Pb and Te	1.0000	1.0000
Qb = flow rate at base conditions	0.13115 cm ³ /s	* 1.0E-6 m ³ /cm ³ 1.311E-07 m ³ /s
ve = flow velocity at sample exit end	1.499E-03 cm/s	* 1.0E-2 m/cm 1.499E-05 m/s
	Ka =	1.17E-03 d * 9.872E-13 m ² /d 1.15E-15 m ²
	Ka =	1.17 md 1.15E-11 cm ²
	Ka =	1168 μd

Steady State Gas Permeability Data

Project #:	8362	Net Effective Stress:	2 Mpa	290.1 psig	Gas:	N2			
Sample #:	E	Length:	10.358 cm		gas deviation z factors:	ze =	1.0000	zb =	1.0000
Stress Level #:	1	Diameter:	10.175 cm		Viscosity:	0.0176 cp			
Regime #:	2	Area:	81.313 cm ²						
Pressure Data Filename:	8362EG.S1B								
XDCR calibration factors:	Pc =	222.869 psig/volt	P1 =	5.4862 psig/volt	ΔP =	1.6591 psid/volt	Pe =	5.5211 psig/volt	

Date	Time of Day	File Time (min)	Regime #	Pb Barometric Pressure	Pc Confining Pressure	P1 Inlet Pressure	ΔP Differential Pressure	Pm Mean Pore Pressure Pe+ΔP/2	Pe Exit Pressure	Te Flow Temp (°C)	Tb Ambient Temp (°C)	Qb Flow Rate @Pb&Tb (ml/sec)	
16 Apr 93	14:15	1618	ES1R2a	12.32 psia	1.355 volts	2.552 volts	1.895 volts		1.979 volts	23	23	0.20356	
16 Apr 93	14:18	1618	ES1R2b	12.32 psia	1.355 volts	2.552 volts	1.894 volts		1.978 volts	23	23	0.20274	
16 Apr 93	14:19	1623	ES1R2c	12.32 psia	1.355 volts	2.552 volts	1.895 volts		1.978 volts	23	23	0.20202	
16 Apr 93	14:22	1623	ES1R2d	12.32 psia	1.354 volts	2.551 volts	1.894 volts		1.977 volts	23	23	0.20192	
16 Apr 93	14:23	1628	ES1R2e	12.32 psia	1.353 volts	2.551 volts	1.894 volts		1.977 volts	23	23	0.20202	
AVERAGES			ES1R2										
					GAUGE	GAUGE	DIFFERENTIAL	GAUGE	GAUGE	(°C)	(°C)		
					1.354 volts	2.552 volts	1.894 volts						
					301.9 psig	14.00 psig	3.143 psid	12.491 psig	10.9196 psig		23	23	
					20.54 atm	0.953 atm	0.2139 atm	0.8500 atm	0.74303 atm				
					2.081 Mpa	0.0965 Mpa	0.02167 Mpa	0.08612 Mpa	0.075288 Mpa				
					ABSOLUTE	ABSOLUTE	DIFFERENTIAL	ABSOLUTE	ABSOLUTE	(°K)	(°K)	(ml/sec)	
			12.32 psia	314.2 psia	26.32 psia	3.143 psid	24.81 psia	23.24 psia					
			0.8383 atm	21.38 atm	1.791 atm	0.2139 atm	1.688 atm	1.5814 atm		296	296	0.20256	
			0.08494 Mpa	2.166 Mpa	0.1815 Mpa	0.02167 Mpa	0.1711 Mpa	0.16023 Mpa					

C-155

Apparent gas permeability: $K_a = (v_e \cdot P_e \cdot u \cdot L) / (P_m \cdot \Delta P)$

Boyle's Law: $v_e = (P_b / P_e) \cdot (T_e / T_b) \cdot (z_e / z_b) \cdot v_b$
 $Q_e = (P_b / P_e) \cdot (T_e / T_b) \cdot (z_e / z_b) \cdot Q_b$

$v_e = Q_e / A = (P_b / P_e) \cdot (T_e / T_b) \cdot (z_e / z_b) \cdot (Q_b / A)$

Parameter	Traditional Units	SI Units
μ = gas viscosity	0.0176 cp	* 1.0E-3 Pa*sec/cp 1.760E-05 Pa*sec
L = sample length	10.358 cm	* 1.0E-2 m/cm 1.036E-01 m
A = sample circular cross sectional area	81.313 cm ²	* 1.0E-4 m ² /cm ² 8.131E-03 m ²
Pb = flow measurement basis pressure (absolute)	0.8383 atm	* 1.013E+5 Pa/atm 8.492E+04 Pa
ΔP = pressure drop across sample length	0.2139 atm	* 1.013E+5 Pa/atm 2.166E+04 Pa
Pm = mean pore pressure (absolute)	1.688 atm	* 1.013E+5 Pa/atm 1.710E+05 Pa
Pe = exit pressure (absolute)	1.581 atm	* 1.013E+5 Pa/atm 1.602E+05 Pa
Te = sample temperature (absolute)	296 °K	296 °K
Tb = flow measurement basis temperature (absolute)	296 °K	296 °K
ze = gas deviation factor at Pe and Te	1.0000	1.0000
zb = gas deviation factor at Pb and Te	1.0000	1.0000
Qb = flow rate at base conditions	0.20256 cm ³ /s	* 1.0E-6 m ³ /cm ³ 2.026E-07 m ³ /s
ve = flow velocity at sample exit end	1.321E-03 cm/s	* 1.0E-2 m/cm 1.321E-05 m/s
	Ka =	1.05E-03 d * 9.872E-13 m ² /d 1.04E-15 m ²
	Ka =	1.05 md 1.04E-11 cm ²
	Ka =	1054 μd

Steady State Gas Permeability Data

Project #:	0362	Net Effective Stress:	2 Mpa	290.1 psig	Gas:	N2		
Sample #:	E	Length:	10.358 cm		gas deviation z factors:	ze = 1.0000	zb = 1.0000	
Stress Level #:	1	Diameter:	10.175 cm		Viscosity:	0.0176 cp		
Regime #:	3	Area:	81.313 cm ²					
Pressure Data Filename:	0362EG.S1B							
XDCR calibration factors:	Pc =	222.869 psig/volt	Pl =	5.4862 psig/volt	ΔP =	1.6591 psid/volt	Pe =	5.5211 psig/volt

Date	Time of Day	File Time (min)	Regime #	Pb Barometric Pressure	Pc Confining Pressure	Pl Inlet Pressure	ΔP Differential Pressure	Pm Mean Pore Pressure Pe+ΔP/2	Pe Exit Pressure	Te Flow Temp (°C)	Tb Ambient Temp (°C)	Qb Flow Rate @Pb&Tb (ml/sec)	
16 Apr 93	16:30	1753	ES1R3a	12.32 psia	1.405 volts	4.377 volts	1.867 volts		3.796 volts	23	23	0.26508	
16 Apr 93	16:34	1753	ES1R3b	12.32 psia	1.405 volts	4.376 volts	1.866 volts		3.794 volts	23	23	0.26438	
16 Apr 93	16:36	1758	ES1R3c	12.32 psia	1.405 volts	4.377 volts	1.869 volts		3.794 volts	23	23	0.26438	
16 Apr 93	16:37	1758	ES1R3d	12.32 psia	1.404 volts	4.377 volts	1.868 volts		3.795 volts	23	23	0.26560	
AVERAGES			ES1R3										
					GUAGE	GUAGE	DIFFERENTIAL	GUAGE	GUAGE	(°C)	(°C)		
					1.405 volts	4.377 volts	1.868 volts		3.795 volts				
					313.1 psig	24.01 psig	3.098 psid	22.500 psig	20.9512 psig	23	23		
					21.30 atm	1.634 atm	0.2108 atm	1.5311 atm	1.42564 atm				
					2.159 Mpa	0.1656 Mpa	0.02136 Mpa	0.15513 Mpa	0.144453 Mpa				
			ABSOLUTE	ABSOLUTE	ABSOLUTE	DIFFERENTIAL	ABSOLUTE	ABSOLUTE	(°K)	(°K)	(ml/sec)		
			12.32 psia	325.4 psia	36.33 psia	3.098 psid	34.82 psia	33.27 psia					
			0.8383 atm	22.14 atm	2.472 atm	0.2108 atm	2.369 atm	2.2640 atm	296	296	0.26486		
			0.08494 Mpa	2.244 Mpa	0.2505 Mpa	0.02136 Mpa	0.2401 Mpa	0.22940 Mpa					

Apparent gas permeability: $K_a = (v_e \cdot P_e \cdot u \cdot L) / (P_m \cdot \Delta P)$

Boyle's Law: $V_e = (P_b / P_e) \cdot (T_e / T_b) \cdot (z_e / z_b) \cdot V_b$
 $Q_e = (P_b / P_e) \cdot (T_e / T_b) \cdot (z_e / z_b) \cdot Q_b$

$v_e = Q_e / A \cdot (P_b / P_e) \cdot (T_e / T_b) \cdot (z_e / z_b) \cdot (Q_b / A)$

Parameter	Traditional Units	SI Units
μ = gas viscosity	0.0176 cp	* 1.0E-3 Pa*sec/cp 1.760E-05 Pa*sec
L = sample length	10.358 cm	* 1.0E-2 m/cm 1.036E-01 m
A = sample circular cross sectional area	81.313 cm ²	* 1.0E-4 m ² /cm ² 8.131E-03 m ²
Pb = flow measurement basis pressure (absolute)	0.8383 atm	* 1.013E+5 Pa/atm 8.492E+04 Pa
ΔP = pressure drop across sample length	0.2108 atm	* 1.013E+5 Pa/atm 2.136E+04 Pa
Pm = mean pore pressure (absolute)	2.369 atm	* 1.013E+5 Pa/atm 2.400E+05 Pa
Pe = exit pressure (absolute)	2.264 atm	* 1.013E+5 Pa/atm 2.293E+05 Pa
Te = sample temperature (absolute)	296 °K	296 °K
Tb = flow measurement basis temperature (absolute)	296 °K	296 °K
ze = gas deviation factor at Pe and Te	1.0000	1.0000
zb = gas deviation factor at Pb and Te	1.0000	1.0000
Qb = flow rate at base conditions	0.26486 cm ³ /s	* 1.0E-6 m ³ /cm ³ 2.649E-07 m ³ /s
ve = flow velocity at sample exit end	1.206E-03 cm/s	* 1.0E-2 m/cm 1.206E-05 m/s
	Ka = 9.97E-04 d	* 9.872E-13 m ² /d 9.84E-16 m ²
	Ka = 1.00 md	9.84E-12 cm ²
	Ka = 997 μd	

C-156

Steady State Gas Permeability Data

Project #:	8362	Net Effective Stress:	2 Mpa	290.1 psig	Gas:	N2			
Sample #:	E	Length:	10.358 cm		gas deviation z factors:	ze =	1.0000	zb =	1.0000
Stress Level #:	1	Diameter:	10.175 cm		Viscosity:	0.0176 cp			
Regime #:	4	Area:	81.313 cm ²						
Pressure Data Filename:	8362EG.S1B								
XDCR calibration factors:	Pc =	222.869 psig/volt	PI =	5.4862 psig/volt	ΔP =	1.6591 psid/volt	Pe =	5.5211 psig/volt	

Date	Time of Day	File Time (min)	Regime #	Pb Barometric Pressure	Pc Confining Pressure	PI Inlet Pressure	ΔP Differential Pressure	Pm Mean Pore Pressure Pe+ΔP/2	Pe Exit Pressure	Te Flow Temp (°C)	Tb Ambient Temp (°C)	Qb Flow Rate @Pb&Tb (ml/sec)	
19 Apr 93	14:45	5968	ES1R4a	12.38 psia	1.447 volts	6.196 volts	1.792 volts		5.595 volts	23	23	0.30303	
19 Apr 93	14:48	5968	ES1R4b	12.38 psia	1.446 volts	6.197 volts	1.794 volts		5.596 volts	23	23	0.30326	
19 Apr 93	14:51	5973	ES1R4c	12.38 psia	1.446 volts	6.197 volts	1.794 volts		5.595 volts	23	23	0.30211	
19 Apr 93	14:53	5973	ES1R4d	12.38 psia	1.444 volts	6.197 volts	1.794 volts		5.595 volts	23	23	0.30234	
AVERAGES			ES1R4										
				GUAGE	GUAGE	DIFFERENTIAL	GUAGE	GUAGE			(°C)	(°C)	
				1.446 volts	6.197 volts	1.794 volts		5.595 volts					
				322.2 psig	34.00 psig	2.976 psid	32.380 psig	30.8919 psig		23	23		
				21.93 atm	2.313 atm	0.2025 atm	2.2033 atm	2.10206 atm					
				2.222 Mpa	0.2344 Mpa	0.02052 Mpa	0.22325 Mpa	0.212992 Mpa					
		ABSOLUTE	ABSOLUTE	ABSOLUTE	DIFFERENTIAL	ABSOLUTE	ABSOLUTE			(°K)	(°K)	(ml/sec)	
		12.38 psia	334.6 psia	46.38 psia	2.976 psid	44.76 psia	43.27 psia						
		0.8424 atm	22.77 atm	3.156 atm	0.2025 atm	3.046 atm	2.9445 atm		296	296		0.30269	
		0.08536 Mpa	2.307 Mpa	0.3198 Mpa	0.02052 Mpa	0.3086 Mpa	0.29835 Mpa						

C-157

Apparent gas permeability: $K_a = (v_e \cdot P_e \cdot u \cdot L) / (P_m \cdot \Delta P)$

Boyle's Law: $v_e = (P_b / P_e) \cdot (T_e / T_b) \cdot (z_e / z_b) \cdot v_b$
 $Q_e = (P_b / P_e) \cdot (T_e / T_b) \cdot (z_e / z_b) \cdot Q_b$

$v_e = Q_e / A \cdot (P_b / P_e) \cdot (T_e / T_b) \cdot (z_e / z_b) \cdot (Q_b / A)$

Parameter	Traditional Units	SI Units
μ = gas viscosity	0.0176 cp	* 1.0E-3 Pa*sec/cp 1.760E-05 Pa*sec
L = sample length	10.358 cm	* 1.0E-2 m/cm 1.036E-01 m
A = sample circular cross sectional area	81.313 cm ²	* 1.0E-4 m ² /cm ² 8.131E-03 m ²
Pb = flow measurement basis pressure (absolute)	0.8424 atm	* 1.013E+5 Pa/atm 8.534E+04 Pa
ΔP = pressure drop across sample length	0.2025 atm	* 1.013E+5 Pa/atm 2.051E+04 Pa
Pm = mean pore pressure (absolute)	3.046 atm	* 1.013E+5 Pa/atm 3.085E+05 Pa
Pe = exit pressure (absolute)	2.944 atm	* 1.013E+5 Pa/atm 2.983E+05 Pa
Te = sample temperature (absolute)	296 °K	296 °K
Tb = flow measurement basis temperature (absolute)	296 °K	296 °K
ze = gas deviation factor at Pe and Te	1.0000	1.0000
zb = gas deviation factor at Pb and Te	1.0000	1.0000
Qb = flow rate at base conditions	0.30269 cm ³ /s	* 1.0E-6 m ³ /cm ³ 3.027E-07 m ³ /s
ve = flow velocity at sample exit end	1.065E-03 cm/s	* 1.0E-2 m/cm 1.065E-05 m/s
	Ka =	9.27E-04 d * 9.872E-13 m ² /d 9.15E-16 m ²
	Ka =	0.927 md 9.15E-12 cm ²
	Ka =	927 μd

Steady State Gas Permeability Data

Project #:	8362	Net Effective Stress:	6 Mpa	870.2 psig	Gas:	N2		
Sample #:	E	Length:	10.358 cm		gas deviation z factors:	ze = 1.0000	zb = 1.0000	
Stress Level #:	2	Diameter:	10.175 cm		Viscosity:	0.0176 cp		
Regime #:	2	Area:	81.313 cm ²					
Pressure Data Filename:	8362EG.S2A							
XDCR calibration factors:	Pc = 222.869 psig/volt	P1 = 5.4862 psig/volt	ΔP = 1.6591 psid/volt	Pe = 5.5211 psig/volt				

Date	Time of Day	File Time (min)	Regime #	Pb Barometric Pressure	Pc Confining Pressure	P1 Inlet Pressure	ΔP Differential Pressure	Pm Mean Pore Pressure Pe+ΔP/2	Pe Exit Pressure	Te Flow Temp (°C)	Tb Ambient Temp (°C)	Qb Flow Rate @Pb&Tb (ml/sec)
21 Apr 93	10:26	1462	ES2R2a	12.36 psia	3.974 volts	3.265 volts	1.891 volts		2.678 volts	23	23	0.09443
21 Apr 93	10:28	1462	ES2R2b	12.36 psia	3.975 volts	3.265 volts	1.890 volts		2.678 volts	23	23	0.09434
21 Apr 93	10:30	1462	ES2R2c	12.36 psia	3.982 volts	3.265 volts	1.890 volts		2.678 volts	23	23	0.09421
21 Apr 93	10:32	1468	ES2R2d	12.36 psia	3.980 volts	3.266 volts	1.890 volts		2.679 volts	23	23	0.09383
21 Apr 93	10:34	1468	ES2R2e	12.36 psia	3.985 volts	3.266 volts	1.890 volts		2.679 volts	23	23	0.09416
AVERAGES			ES2R2									
					GAUGE	GAUGE	DIFFERENTIAL	GAUGE	GAUGE	(°C)	(°C)	
					3.979 volts	3.265 volts	1.890 volts		2.678 volts			
					886.8 psig	17.91 psig	3.14 psid	16.36 psig	14.788 psig	23	23	
					60.35 atm	1.219 atm	0.213 atm	1.113 atm	1.0062 atm			
					6.115 Mpa	0.1235 Mpa	0.0216 Mpa	0.1128 Mpa	0.10196 Mpa			
					ABSOLUTE	ABSOLUTE	ABSOLUTE	DIFFERENTIAL	ABSOLUTE	ABSOLUTE	(°K)	(°K)
			12.36 psia	899.2 psia	30.27 psia	3.14 psid	28.72 psia	27.15 psia				
			0.8410 atm	61.19 atm	2.060 atm	0.213 atm	1.954 atm	1.847 atm	296	296	0.09420	
			0.08522 Mpa	6.200 Mpa	0.2087 Mpa	0.0216 Mpa	0.1980 Mpa	0.1872 Mpa				

C-159

Apparent gas permeability: $K_a = (v_e \cdot P_e \cdot u \cdot L) / (P_m \cdot \Delta P)$

Boyle's Law: $v_e = (P_b / P_e) \cdot (T_e / T_b) \cdot (z_e / z_b) \cdot v_b$
 $Q_e = (P_b / P_e) \cdot (T_e / T_b) \cdot (z_e / z_b) \cdot Q_b$

$v_e = Q_e / A = (P_b / P_e) \cdot (T_e / T_b) \cdot (z_e / z_b) \cdot (Q_b / A)$

Parameter	Traditional Units	SI Units
μ = gas viscosity	0.0176 cp	* 1.0E-3 Pa*sec/cp 1.760E-05 Pa*sec
L = sample length	10.358 cm	* 1.0E-2 m/cm 1.036E-01 m
A = sample circular cross sectional area	81.313 cm ²	* 1.0E-4 m ² /cm ² 8.131E-03 m ²
Pb = flow measurement basis pressure (absolute)	0.8410 atm	* 1.013E+5 Pa/atm 8.520E+04 Pa
ΔP = pressure drop across sample length	0.213 atm	* 1.013E+5 Pa/atm 2.162E+04 Pa
Pm = mean pore pressure (absolute)	1.954 atm	* 1.013E+5 Pa/atm 1.979E+05 Pa
Pe = exit pressure (absolute)	1.847 atm	* 1.013E+5 Pa/atm 1.871E+05 Pa
Te = sample temperature (absolute)	296 °K	296 °K
Tb = flow measurement basis temperature (absolute)	296 °K	296 °K
ze = gas deviation factor at Pe and Te	1.0000	1.0000
zb = gas deviation factor at Pb and Te	1.0000	1.0000
Qb = flow rate at base conditions	0.09420 cm ³ /s	* 1.0E-6 m ³ /cm ³ 9.420E-08 m ³ /s
ve = flow velocity at sample exit end	5.275E-04 cm/s	* 1.0E-2 m/cm 5.275E-06 m/s
	Ka = 4.26E-04 d	* 9.872E-13 m ² /d 4.21E-16 m ²
	Ka = 4.26E-01 md	4.21E-12 cm ²
	Ka = 4.26E+02 μd	

Steady State Gas Permeability Data

Project #:	8362	Net Effective Stress:	6 Mpa	870.2 psig	Gas:	N2		
Sample #:	E	Length:	10.358 cm		gas deviation z factors:	ze = 1.0000	zb = 1.0000	
Stress Level #:	2	Diameter:	10.175 cm		Viscosity:	0.0176 cp		
Regime #:	3	Area:	81.313 cm ²					
Pressure Data Filename:	8362EG.S2A							
XDCR calibration factors:	Pc = 222.869 psig/volt	Pi = 5.4862 psig/volt	ΔP = 1.6591 psid/volt	Pe = 5.5211 psig/volt				

Date	Time of Day	File Time (min)	Regime #	Pb Barometric Pressure	Pc Confining Pressure	Pi Inlet Pressure	ΔP Differential Pressure	Pm Mean Pore Pressure Pe*ΔP/2	Pe Exit Pressure	Te Flow Temp (°C)	Tb Ambient Temp (°C)	Qb Flow Rate @Pb&Tb (ml/sec)	
21 Apr 93	14:42	1716	ES2R3a	12.35 psia	4.022 volts	5.078 volts	1.911 volts		4.463 volts	23	23	0.11980	
21 Apr 93	14:44	1716	ES2R3b	12.35 psia	4.023 volts	5.078 volts	1.912 volts		4.463 volts	23	23	0.11958	
21 Apr 93	14:46	1721	ES2R3c	12.35 psia	4.023 volts	5.078 volts	1.912 volts		4.462 volts	23	23	0.11930	
21 Apr 93	14:47	1721	ES2R3d	12.35 psia	4.023 volts	5.077 volts	1.912 volts		4.462 volts	23	23	0.11965	
21 Apr 93	14:49	1726	ES2R3e	12.35 psia	4.023 volts	5.077 volts	1.911 volts		4.462 volts	23	23	0.11947	
AVERAGES			ES2R3		GUAGE	GUAGE	DIFFERENTIAL	GUAGE	GUAGE	(°C)	(°C)		
					4.023 volts	5.078 volts	1.912 volts		4.462 volts				
					896.6 psig	27.86 psig	3.17 psid		26.22 psig	24.637 psig	23	23	
					61.01 atm	1.896 atm	0.216 atm		1.784 atm	1.6765 atm			
					6.182 Mpa	0.1921 Mpa	0.0219 Mpa		0.1808 Mpa	0.16987 Mpa			
					ABSOLUTE	ABSOLUTE	ABSOLUTE	DIFFERENTIAL	ABSOLUTE	ABSOLUTE	(°K)	(°K)	(ml/sec)
						12.35 psia	908.9 psia	40.21 psia	3.17 psid	38.57 psia	36.99 psia	296	296
				0.8404 atm	61.85 atm	2.736 atm	0.216 atm	2.625 atm	2.517 atm				
				0.08515 Mpa	6.267 Mpa	0.2772 Mpa	0.0219 Mpa	0.2660 Mpa	0.2550 Mpa				

C-160

Apparent gas permeability: $K_a = (v_e \cdot P_e \cdot u \cdot L) / (P_m \cdot \Delta P)$

Boyle's Law: $v_e = (P_b / P_e) \cdot (T_e / T_b) \cdot (z_e / z_b) \cdot v_b$
 $Q_e = (P_b / P_e) \cdot (T_e / T_b) \cdot (z_e / z_b) \cdot Q_b$

$v_e = Q_e / A = (P_b / P_e) \cdot (T_e / T_b) \cdot (z_e / z_b) \cdot (Q_b / A)$

Parameter	Traditional Units	SI Units
μ = gas viscosity	0.0176 cp	* 1.0E-3 Pa*sec/cp 1.760E-05 Pa*sec
L = sample length	10.358 cm	* 1.0E-2 m/cm 1.036E-01 m
A = sample circular cross sectional area	81.313 cm ²	* 1.0E-4 m ² /cm ² 8.131E-03 m ²
Pb = flow measurement basis pressure (absolute)	0.8404 atm	* 1.013E+5 Pa/atm 8.513E+04 Pa
ΔP = pressure drop across sample length	0.216 atm	* 1.013E+5 Pa/atm 2.186E+04 Pa
Pm = mean pore pressure (absolute)	2.625 atm	* 1.013E+5 Pa/atm 2.659E+05 Pa
Pe = exit pressure (absolute)	2.517 atm	* 1.013E+5 Pa/atm 2.550E+05 Pa
Te = sample temperature (absolute)	296 °K	296 °K
Tb = flow measurement basis temperature (absolute)	296 °K	296 °K
ze = gas deviation factor at Pe and Te	1.0000	1.0000
zb = gas deviation factor at Pb and Te	1.0000	1.0000
Qb = flow rate at base conditions	0.11958 cm ³ /s	* 1.0E-6 m ³ /cm ³ 1.196E-07 m ³ /s
ve = flow velocity at sample exit end	4.910E-04 cm/s	* 1.0E-2 m/cm 4.910E-06 m/s
	Ka = 3.98E-04 d	* 9.872E-13 m ² /d 3.93E-16 m ²
	Ka = 3.98E-01 md	3.93E-12 cm ²
	Ka = 3.98E+02 μd	

Steady State Gas Permeability Data

Project #:	8362	Net Effective Stress:	6 Mpa	870.2 psig	Gas:	N2		
Sample #:	E	Length:	10.358 cm		gas deviation z factors:	ze = 1.0000	zb = 1.0000	
Stress Level #:	2	Diameter:	10.175 cm		Viscosity:	0.0176 cp		
Regime #:	4	Area:	81.313 cm ²					
Pressure Data Filename:	8362EG.S2A							
XDCR calibration factors:	Pc =	222.869 psig/volt	P1 =	5.4862 psig/volt	ΔP =	1.6591 psid/volt	Pe =	5.5211 psig/volt

Date	Time of Day	File Time (min)	Regime #	Pb Barometric Pressure	Pc Confining Pressure	P1 Inlet Pressure	ΔP Differential Pressure	Pm Mean Pore Pressure Pe*ΔP/2	Pe Exit Pressure	Te Flow Temp (°C)	Tb Ambient Temp (°C)	Qb Flow Rate @Pb&Tb (ml/sec)
21 Apr 93	17:01	1716	ES2R4a	12.34 psia	4.068 volts	6.918 volts	1.982 volts		6.255 volts	23	23	0.14981
21 Apr 93	17:03	1716	ES2R4b	12.34 psia	4.068 volts	6.917 volts	1.985 volts		6.254 volts	23	23	0.15021
21 Apr 93	17:05	1721	ES2R4c	12.34 psia	4.068 volts	6.917 volts	1.985 volts		6.253 volts	23	23	0.15032
21 Apr 93	17:07	1721	ES2R4d	12.34 psia	4.068 volts	6.916 volts	1.985 volts		6.253 volts	23	23	0.15026
AVERAGES			ES2R4									
					GAUGE	GAUGE	DIFFERENTIAL	GAUGE	GAUGE	(°C)	(°C)	
					4.068 volts	6.917 volts	1.984 volts	36.17 psig	6.254 volts			
					906.6 psig	37.95 psig	3.29 psid	34.528 psig		23	23	
					61.69 atm	2.582 atm	0.224 atm	2.461 atm	2.3495 atm			
					6.251 Mpa	0.2616 Mpa	0.0227 Mpa	0.2494 Mpa	0.23806 Mpa			
					ABSOLUTE	ABSOLUTE	ABSOLUTE	DIFFERENTIAL	ABSOLUTE	ABSOLUTE	(°K)	(°K)
			12.34 psia	919.0 psia	50.29 psia	3.29 psid	48.51 psia	46.87 psia				
			0.8397 atm	62.53 atm	3.422 atm	0.224 atm	3.301 atm	3.189 atm	296	296	0.15015	
			0.08508 Mpa	6.336 Mpa	0.3467 Mpa	0.0227 Mpa	0.3345 Mpa	0.3231 Mpa				

C-161

Apparent gas permeability: $K_a = (v_e \cdot P_e \cdot u \cdot L) / (P_m \cdot \Delta P)$

Boyle's Law: $V_e = (P_b / P_e) \cdot (T_e / T_b) \cdot (z_e / z_b) \cdot V_b$
 $Q_e = (P_b / P_e) \cdot (T_e / T_b) \cdot (z_e / z_b) \cdot Q_b$

$v_e = Q_e / A \cdot (P_b / P_e) \cdot (T_e / T_b) \cdot (z_e / z_b) \cdot (Q_b / A)$

Parameter	Traditional Units	SI Units
μ = gas viscosity	0.0176 cp	* 1.0E-3 Pa*sec/cp 1.760E-05 Pa*sec
L = sample length	10.358 cm	* 1.0E-2 m/cm 1.036E-01 m
A = sample circular cross sectional area	81.313 cm ²	* 1.0E-4 m ² /cm ² 8.131E-03 m ²
Pb = flow measurement basis pressure (absolute)	0.8397 atm	* 1.013E+5 Pa/atm 8.506E+04 Pa
ΔP = pressure drop across sample length	0.224 atm	* 1.013E+5 Pa/atm 2.269E+04 Pa
Pm = mean pore pressure (absolute)	3.301 atm	* 1.013E+5 Pa/atm 3.344E+05 Pa
Pe = exit pressure (absolute)	3.189 atm	* 1.013E+5 Pa/atm 3.231E+05 Pa
Te = sample temperature (absolute)	296 °K	296 °K
Tb = flow measurement basis temperature (absolute)	296 °K	296 °K
ze = gas deviation factor at Pe and Te	1.0000	1.0000
zb = gas deviation factor at Pb and Te	1.0000	1.0000
Qb = flow rate at base conditions	0.15015 cm ³ /s	* 1.0E-6 m ³ /cm ³ 1.502E-07 m ³ /s
ve = flow velocity at sample exit end	4.862E-04 cm/s	* 1.0E-2 m/cm 4.862E-06 m/s
	Ka =	* 9.872E-13 m ² /d 3.77E-16 m ²
	Ka =	3.82E-01 md 3.77E-12 cm ²
	Ka =	3.82E+02 ud

Steady State Gas Permeability Data

Project #:	8362	Net Effective Stress:	10 Mpa	1450.4 psig	Gas:	N2						
Sample #:	E	Length:	10.358 cm		gas deviation z factors:	ze =	1.0000	zb =	1.0000			
Stress Level #:	3	Diameter:	10.175 cm		Viscosity:	0.0176 cp						
Regime #:	1	Area:	81.313 cm ²									
Pressure Data Filename:	8362EG.S3A											
XDCR calibration factors:	Pc =	222.869	psig/volt	PI =	5.4862	psig/volt	ΔP =	1.6591	psid/volt	Pe =	5.5211	psig/volt

Date	Time of Day	File Time (min)	Regime #	Pb Barometric Pressure	Pc Confining Pressure	PI Inlet Pressure	ΔP Differential Pressure	Pm Mean Pore Pressure Pe+ΔP/2	Pe Exit Pressure	Te Flow Temp (°C)	Tb Ambient Temp (°C)	Qb Flow Rate @Pb&Tb (ml/sec)			
22 Apr 93	14:17	308	ES3R1a	12.20 psia	6.537 volts	1.497 volts	2.038 volts		0.872 volts	23	23	0.04611			
22 Apr 93	14:21	313	ES3R1b	12.20 psia	6.536 volts	1.498 volts	2.042 volts		0.871 volts	23	23	0.04595			
22 Apr 93	14:26	318	ES3R1c	12.20 psia	6.537 volts	1.498 volts	2.043 volts		0.871 volts	23	23	0.04615			
22 Apr 93	14:30	323	ES3R1d	12.20 psia	6.537 volts	1.498 volts	2.044 volts		0.870 volts	23	23	0.04579			
22 Apr 93	14:33	323	ES3R1e	12.20 psia	6.536 volts	1.499 volts	2.045 volts		0.871 volts	23	23	0.04575			
AVERAGES			ES3R1	GUAGE		GUAGE		DIFFERENTIAL	GUAGE		GUAGE	(°C)	(°C)		
				6.537 volts		1.498 volts		2.042 volts	6.50 psig		4.809 psig	23	23		
				1456.8 psig		8.22 psig		3.39 psid	0.443 atm		0.3272 atm				
				99.13 atm		0.559 atm		0.231 atm	0.0448 Mpa		0.03316 Mpa				
				10.044 Mpa		0.0567 Mpa		0.0234 Mpa	0.0448 Mpa		0.03316 Mpa				
				ABSOLUTE		ABSOLUTE		DIFFERENTIAL	ABSOLUTE		ABSOLUTE		(°K)	(°K)	(ml/sec)
				12.2 psia		1469.0 psia		20.42 psia	3.39 psid		18.70 psia		17.01 psia		
0.8302 atm		99.96 atm		1.389 atm	0.231 atm		1.273 atm		1.157 atm	296	296	0.04600			
0.08412 Mpa		10.128 Mpa		0.1408 Mpa	0.0234 Mpa		0.1290 Mpa		0.1173 Mpa						

C-162

Apparent gas permeability: $K_a = (v_e \cdot P_e \cdot u \cdot L) / (P_m \cdot \Delta P)$

Boyle's Law: $V_e = (P_b/P_e) \cdot (T_e/T_b) \cdot (z_e/z_b) \cdot V_b$
 $Q_e = (P_b/P_e) \cdot (T_e/T_b) \cdot (z_e/z_b) \cdot Q_b$

$v_e = Q_e/A = (P_b/P_e) \cdot (T_e/T_b) \cdot (z_e/z_b) \cdot (Q_b/A)$

Parameter	Traditional Units	SI Units
μ = gas viscosity	0.0176 cp	* 1.0E-3 Pa*sec/cp 1.760E-05 Pa*sec
L = sample length	10.358 cm	* 1.0E-2 m/cm 1.036E-01 m
A = sample circular cross sectional area	81.313 cm ²	* 1.0E-4 m ² /cm ² 8.131E-03 m ²
Pb = flow measurement basis pressure (absolute)	0.8302 atm	* 1.013E+5 Pa/atm 8.409E+04 Pa
ΔP = pressure drop across sample length	0.231 atm	* 1.013E+5 Pa/atm 2.336E+04 Pa
Pm = mean pore pressure (absolute)	1.273 atm	* 1.013E+5 Pa/atm 1.289E+05 Pa
Pe = exit pressure (absolute)	1.157 atm	* 1.013E+5 Pa/atm 1.172E+05 Pa
Te = sample temperature (absolute)	296 °K	296 °K
Tb = flow measurement basis temperature (absolute)	296 °K	296 °K
ze = gas deviation factor at Pe and Te	1.0000	1.0000
zb = gas deviation factor at Pb and Te	1.0000	1.0000
Qb = flow rate at base conditions	0.04600 cm ³ /s	* 1.0E-6 m ³ /cm ³ 4.600E-08 m ³ /s
ve = flow velocity at sample exit end	4.058E-04 cm/s	* 1.0E-2 m/cm 4.058E-06 m/s
	Ka =	2.92E-04 d * 9.872E-13 m ² /d 2.88E-16 m ²
	Ka =	2.92E-01 md 2.88E-12 cm ²
	Ka =	2.92E+02 μd

Steady State Gas Permeability Data

Project #: 8362	Net Effective Stress: 10 Mpa 1450.4 psig	Gas: N2
Sample #: E	Length: 10.358 cm	gas deviation z factors: ze = 1.0000 zb = 1.0000
Stress Level #: 3	Diameter: 10.175 cm	Viscosity: 0.0176 cp
Regime #: 2	Area: 81.313 cm ²	
Pressure Data Filename: 8362EG.S3A		
XDCR calibration factors: Pc = 222.869 psig/volt Pi = 5.4862 psig/volt AP = 1.6591 psid/volt Pe = 5.5211 psig/volt		

Date	Time of Day	File Time (min)	Regime #	Pb Barometric Pressure	Pc Confining Pressure	Pi Inlet Pressure	ΔP Differential Pressure	Pm Mean Pore Pressure Pe+ΔP/2	Pe Exit Pressure	Te Flow Temp (°C)	Tb Ambient Temp (°C)	Qb Flow Rate @Pb&Tb (ml/sec)
22 Apr 93	16:57	468	ES3R2a	12.21 psia	6.582 volts	3.274 volts	1.920 volts		2.671 volts	23	23	0.05722
22 Apr 93	17:00	473	ES3R2b	12.21 psia	6.581 volts	3.274 volts	1.921 volts		2.670 volts	23	23	0.05741
22 Apr 93	17:03	473	ES3R2c	12.21 psia	6.581 volts	3.274 volts	1.922 volts		2.670 volts	23	23	0.05727
22 Apr 93	17:06	478	ES3R2d	12.21 psia	6.581 volts	3.274 volts	1.924 volts		2.669 volts	23	23	0.05731
AVERAGES			ES3R2									
					GAUGE	GAUGE	DIFFERENTIAL	GAUGE	GAUGE	(°C)	(°C)	
					6.581 volts	3.274 volts	1.922 volts	16.34 psig	2.670 volts	23	23	
					1466.8 psig	17.96 psig	3.19 psid	1.112 atm	14.741 psig			
					99.81 atm	1.222 atm	0.217 atm	0.10164 Mpa	1.0031 atm			
					10.113 Mpa	0.1238 Mpa	0.0220 Mpa	0.1126 Mpa	0.10164 Mpa			
					ABSOLUTE	ABSOLUTE	ABSOLUTE	DIFFERENTIAL	ABSOLUTE	ABSOLUTE	(°K)	(°K)
			12.21 psia	1479.0 psia	30.17 psia	3.19 psid	28.55 psia	26.95 psia	296	296	0.05730	
			0.8308 atm	100.64 atm	2.053 atm	0.217 atm	1.942 atm	1.834 atm				
			0.08419 Mpa	10.197 Mpa	0.2080 Mpa	0.0220 Mpa	0.1968 Mpa	0.1858 Mpa				

C-163

Apparent gas permeability: $K_a = (v_e \cdot P_e \cdot u \cdot L) / (P_m \cdot \Delta P)$

Boyle's Law: $v_e = (P_b / P_e) \cdot (T_e / T_b) \cdot (z_e / z_b) \cdot v_b$

$Q_e = (P_b / P_e) \cdot (T_e / T_b) \cdot (z_e / z_b) \cdot Q_b$

$v_e = Q_e / A = (P_b / P_e) \cdot (T_e / T_b) \cdot (z_e / z_b) \cdot (Q_b / A)$

Parameter	Traditional Units	SI Units
μ = gas viscosity	0.0176 cp	* 1.0E-3 Pa*sec/cp 1.760E-05 Pa*sec
L = sample length	10.358 cm	* 1.0E-2 m/cm 1.036E-01 m
A = sample circular cross sectional area	81.313 cm ²	* 1.0E-4 m ² /cm ² 8.131E-03 m ²
Pb = flow measurement basis pressure (absolute)	0.8308 atm	* 1.013E+5 Pa/atm 8.416E+04 Pa
ΔP = pressure drop across sample length	0.217 atm	* 1.013E+5 Pa/atm 2.198E+04 Pa
Pm = mean pore pressure (absolute)	1.942 atm	* 1.013E+5 Pa/atm 1.968E+05 Pa
Pe = exit pressure (absolute)	1.834 atm	* 1.013E+5 Pa/atm 1.858E+05 Pa
Te = sample temperature (absolute)	296 °K	296 °K
Tb = flow measurement basis temperature (absolute)	296 °K	296 °K
ze = gas deviation factor at Pe and Te	1.0000	1.0000
zb = gas deviation factor at Pb and Te	1.0000	1.0000
Qb = flow rate at base conditions	0.05730 cm ³ /s	* 1.0E-6 m ³ /cm ³ 5.730E-08 m ³ /s
ve = flow velocity at sample exit end	3.193E-04 cm/s	* 1.0E-2 m/cm 3.193E-06 m/s
	Ka = 2.53E-04 d	* 9.872E-13 m ² /d 2.50E-16 m ²
	Ka = 2.53E-01 md	2.50E-12 cm ²
	Ka = 2.53E+02 μd	

Steady State Gas Permeability Data

Project #: 8362	Net Effective Stress: 10 Mpa 1450.4 psid	Gas: N2
Sample #: E	Length: 10.358 cm	gas deviation z factors: ze = 1.0000 zb = 1.0000
Stress Level #: 3	Diameter: 10.175 cm	Viscosity: 0.0176 cp
Regime #: 3	Area: 81.313 cm ²	
Pressure Data Filename: 8362EG.S3A		
XDCR calibration factors:	Pc = 222.869 psig/volt Pi = 5.4862 psig/volt ΔP = 1.6591 psid/volt	Pe = 5.5211 psig/volt

Date	Time of Day	File Time (min)	Regime #	Pb Barometric Pressure	Pc Confining Pressure	Pi Inlet Pressure	ΔP Differential Pressure	Pm Mean Pore Pressure Pe+ΔP/2	Pe Exit Pressure	Te Flow Temp (°C)	Tb Ambient Temp (°C)	Qb Flow Rate @Pb&Tb (ml/sec)	
23 Apr 93	10:55	1547	ES3R3a	12.29 psia	6.630 volts	5.118 volts	1.947 volts		4.497 volts	22	23	0.06744	
23 Apr 93	10:57	1552	ES3R3b	12.29 psia	6.631 volts	5.118 volts	1.947 volts		4.497 volts	22	23	0.06749	
23 Apr 93	11:00	1552	ES3R3c	12.29 psia	6.631 volts	5.118 volts	1.948 volts		4.497 volts	22	23	0.06762	
23 Apr 93	11:03	1557	ES3R3d	12.29 psia	6.631 volts	5.119 volts	1.948 volts		4.497 volts	22	23	0.06758	
AVERAGES			ES3R3										
					GAUGE	GAUGE	DIFFERENTIAL	GAUGE	GAUGE		(°C)	(°C)	
					6.631 volts	5.118 volts	1.948 volts		4.497 volts				
					1477.8 psig	28.08 psig	3.23 psid	26.44 psig	24.828 psig		22	23	
					100.56 atm	1.911 atm	0.220 atm	1.799 atm	1.6895 atm				
					10.189 Mpa	0.1936 Mpa	0.0223 Mpa	0.1823 Mpa	0.17119 Mpa				
			ABSOLUTE	ABSOLUTE	DIFFERENTIAL	ABSOLUTE	ABSOLUTE		(°K)	(°K)	(ml/sec)		
			12.29 psia	1490.1 psia	40.37 psia	3.23 psid	38.73 psia	37.12 psia					
			0.8363 atm	101.39 atm	2.747 atm	0.220 atm	2.636 atm	2.526 atm	295	296	0.06753		
			0.08474 Mpa	10.274 Mpa	0.2783 Mpa	0.0223 Mpa	0.2671 Mpa	0.2559 Mpa					

C-164

Apparent gas permeability: $K_a = (v_e \cdot P_e \cdot u \cdot L) / (P_m \cdot \Delta P)$

Boyle's Law: $v_e = (P_b / P_e) \cdot (T_e / T_b) \cdot (z_e / z_b) \cdot Q_b$
 $Q_e = (P_b / P_e) \cdot (T_e / T_b) \cdot (z_e / z_b) \cdot Q_b$

$v_e = Q_e / A = (P_b / P_e) \cdot (T_e / T_b) \cdot (z_e / z_b) \cdot (Q_b / A)$

Parameter	Traditional Units	SI Units
μ = gas viscosity	0.0176 cp	* 1.0E-3 Pa*sec/cp 1.760E-05 Pa*sec
L = sample length	10.358 cm	* 1.0E-2 m/cm 1.036E-01 m
A = sample circular cross sectional area	81.313 cm ²	* 1.0E-4 m ² /cm ² 8.131E-03 m ²
Pb = flow measurement basis pressure (absolute)	0.8363 atm	* 1.013E+5 Pa/atm 8.472E+04 Pa
ΔP = pressure drop across sample length	0.220 atm	* 1.013E+5 Pa/atm 2.227E+04 Pa
Pm = mean pore pressure (absolute)	2.636 atm	* 1.013E+5 Pa/atm 2.670E+05 Pa
Pe = exit pressure (absolute)	2.526 atm	* 1.013E+5 Pa/atm 2.559E+05 Pa
Te = sample temperature (absolute)	295 °K	295 °K
Tb = flow measurement basis temperature (absolute)	296 °K	296 °K
ze = gas deviation factor at Pe and Te	1.0000	1.0000
zb = gas deviation factor at Pb and Te	1.0000	1.0000
Qb = flow rate at base conditions	0.06753 cm ³ /s	* 1.0E-6 m ³ /cm ³ 6.753E-08 m ³ /s
ve = flow velocity at sample exit end	2.741E-04 cm/s	* 1.0E-2 m/cm 2.741E-06 m/s
	Ka = 2.18E-04 d	* 9.872E-13 m ² /d 2.15E-16 m ²
	Ka = 2.18E-01 md	2.15E-12 cm ²
	Ka = 2.18E+02 μd	

Steady State Gas Permeability Data

Project #:	8362	Net Effective Stress:	10 Mpa	1450.4 psid	Gas:	N2						
Sample #:	E	Length:	10.358 cm		gas deviation z factors:	ze =	1.0000	zb =	1.0000			
Stress Level #:	3	Diameter:	10.175 cm		Viscosity:	0.0176 cp						
Regime #:	4	Area:	81.313 cm ²									
Pressure Data Filename:	8362EG.S3A											
XDCR calibration factors:	Pc =	222.869	psig/volt	Pi =	5.4862	psig/volt	ΔP =	1.6591	psid/volt	Pe =	5.5211	psig/volt

Date	Time of Day	File Time (min)	Regime #	Pb Barometric Pressure	Pc Confining Pressure	Pi Inlet Pressure	ΔP Differential Pressure	Pm Mean Pore Pressure Pe*ΔP/2	Pe Exit Pressure	Te Flow Temp (°C)	Tb Ambient Temp (°C)	Qb Flow Rate @Pb&Tb (ml/sec)		
23 Apr 93	15:04	1793	ES3R4a	12.25 psia	6.673 volts	6.916 volts	1.932 volts		6.270 volts	23	23	0.08035		
23 Apr 93	15:07	1798	ES3R4b	12.25 psia	6.673 volts	6.916 volts	1.933 volts		6.269 volts	23	23	0.08029		
23 Apr 93	15:10	1803	ES3R4c	12.25 psia	6.673 volts	6.916 volts	1.934 volts		6.269 volts	23	23	0.08014		
23 Apr 93	15:12	1803	ES3R4d	12.25 psia	6.673 volts	6.916 volts	1.934 volts		6.269 volts	23	23	0.08040		
AVERAGES			ES3R4	GUAGE		GUAGE		DIFFERENTIAL	GUAGE		(°C)	(°C)		
				6.673 volts		6.916 volts		1.933 volts	6.269 volts					
				1487.2 psig		37.94 psig		3.21 psid	36.22 psig		34.613 psig	23	23	
				101.20 atm		2.582 atm		0.218 atm	2.464 atm		2.3553 atm			
				10.254 Mpa		0.2616 Mpa		0.0221 Mpa	0.2497 Mpa		0.23865 Mpa			
				ABSOLUTE		ABSOLUTE		DIFFERENTIAL	ABSOLUTE		ABSOLUTE		(°K)	(°K)
12.25 psia		1499.5 psia		3.21 psid	48.47 psia		46.86 psia							
0.8336 atm		102.03 atm		0.218 atm	3.298 atm		3.189 atm		296	296	0.08030			
0.08446 Mpa		10.338 Mpa		0.3461 Mpa	0.3342 Mpa		0.3231 Mpa							

C-165

Apparent gas permeability: $K_a = (v_e \cdot P_e \cdot u \cdot L) / (P_m \cdot \Delta P)$

Boyle's Law: $v_e = (P_b / P_e) \cdot (T_e / T_b) \cdot (z_e / z_b) \cdot v_b$
 $Q_e = (P_b / P_e) \cdot (T_e / T_b) \cdot (z_e / z_b) \cdot Q_b$

$v_e = Q_e / A = (P_b / P_e) \cdot (T_e / T_b) \cdot (z_e / z_b) \cdot (Q_b / A)$

Parameter	Traditional Units	SI Units
μ = gas viscosity	0.0176 cp	* 1.0E-3 Pa*sec/cp 1.760E-05 Pa*sec
L = sample length	10.358 cm	* 1.0E-2 m/cm 1.036E-01 m
A = sample circular cross sectional area	81.313 cm ²	* 1.0E-4 m ² /cm ² 8.131E-03 m ²
Pb = flow measurement basis pressure (absolute)	0.8336 atm	* 1.013E+5 Pa/atm 8.444E+04 Pa
ΔP = pressure drop across sample length	0.218 atm	* 1.013E+5 Pa/atm 2.211E+04 Pa
Pm = mean pore pressure (absolute)	3.298 atm	* 1.013E+5 Pa/atm 3.341E+05 Pa
Pe = exit pressure (absolute)	3.189 atm	* 1.013E+5 Pa/atm 3.230E+05 Pa
Te = sample temperature (absolute)	296 °K	296 °K
Tb = flow measurement basis temperature (absolute)	296 °K	296 °K
ze = gas deviation factor at Pe and Te	1.0000	1.0000
zb = gas deviation factor at Pb and Te	1.0000	1.0000
Qb = flow rate at base conditions	0.08030 cm ³ /s	* 1.0E-6 m ³ /cm ³ 8.030E-08 m ³ /s
ve = flow velocity at sample exit end	2.581E-04 cm/s	* 1.0E-2 m/cm 2.581E-06 m/s
	Ka =	2.08E-04 d * 9.872E-13 m ² /d 2.06E-16 m ²
	Ka =	2.08E-01 md 2.06E-12 cm ²
	Ka =	2.08E+02 μd

Steady State Gas Permeability Data

Project #: 8362	Net Effective Stress: 2 Mpa 290.1 psid	Gas: N2
Sample #: F	Length: 10.029 cm	gas deviation z factors: ze = 1.0000 zb = 1.0000
Stress Level #: 1	Diameter: 10.170 cm	Viscosity: 0.0176 cp
Regime #: 1	Area: 81.233 cm ²	
Pressure Data Filename: 8362FG.S1A		
XDCR calibration factors:	Pc = 222.869 psig/volt P1 = 55.4417 psig/volt ΔP = 11.0272 psid/volt Pe = 5.5211 psig/volt	

Date	Time of Day	File Time (min)	Regime #	Pb Barometric Pressure	Pc Confining Pressure	P1 Inlet Pressure	ΔP Differential Pressure	Pm Mean Pore Pressure Pe*ΔP/2	Pe Exit Pressure	Te Flow Temp (°C)	Tb Ambient Temp (°C)	Qb Flow Rate @Pb&Tb (ml/sec)		
08 Jun 93	08:01	990	FS1R1a	12.33 psia	1.539 volts	1.797 volts	8.550 volts		1.074 volts	23	21	0.02758		
08 Jun 93	08:06	995	FS1R1b	12.33 psia	1.539 volts	1.797 volts	8.551 volts		1.074 volts	23	21	0.02759		
08 Jun 93	08:10	1000	FS1R1c	12.33 psia	1.539 volts	1.797 volts	8.551 volts		1.074 volts	23	21	0.02757		
08 Jun 93	08:14	1005	FS1R1d	12.33 psia	1.539 volts	1.797 volts	8.552 volts		1.073 volts	23	21	0.02760		
AVERAGES			FS1R1											
					GAUGE	GAUGE	DIFFERENTIAL	GAUGE	GAUGE	(°C)	(°C)			
					1.539 volts	1.797 volts	8.551 volts	53.08 psig	1.074 volts			23	21	
					343.0 psig	99.63 psig	94.29 psid	0.3659 Mpa	5.928 psig					
					23.34 atm	6.779 atm	6.416 atm	0.3612 atm	0.4034 atm					
					2.365 Mpa	0.6869 Mpa	0.6501 Mpa	0.3659 Mpa	0.04087 Mpa					
			ABSOLUTE	ABSOLUTE	ABSOLUTE	DIFFERENTIAL	ABSOLUTE	ABSOLUTE	(°K)	(°K)				
			12.33 psia	355.3 psia	111.96 psia	94.29 psid	65.41 psia	18.26 psia						
			0.8390 atm	24.18 atm	7.618 atm	6.416 atm	4.451 atm	1.242 atm			296	294	0.02759	
			0.08501 Mpa	2.450 Mpa	0.7719 Mpa	0.6501 Mpa	0.4510 Mpa	0.1259 Mpa						

C-166

Apparent gas permeability: $K_a = (v_e \cdot P_e \cdot u \cdot L) / (P_m \cdot \Delta P)$

Boyle's Law: $v_e = (P_b / P_e) \cdot (T_e / T_b) \cdot (z_e / z_b) \cdot v_b$
 $Q_e = (P_b / P_e) \cdot (T_e / T_b) \cdot (z_e / z_b) \cdot Q_b$

$v_e = Q_e / A = (P_b / P_e) \cdot (T_e / T_b) \cdot (z_e / z_b) \cdot (Q_b / A)$

Parameter	Traditional Units	SI Units
μ = gas viscosity	0.0176 cp	* 1.0E-3 Pa*sec/cp 1.760E-05 Pa*sec
L = sample length	10.029 cm	* 1.0E-2 m/cm 1.003E-01 m
A = sample circular cross sectional area	81.233 cm ²	* 1.0E-4 m ² /cm ² 8.123E-03 m ²
Pb = flow measurement basis pressure (absolute)	0.8390 atm	* 1.013E+5 Pa/atm 8.499E+04 Pa
ΔP = pressure drop across sample length	6.416 atm	* 1.013E+5 Pa/atm 6.500E+04 Pa
Pm = mean pore pressure (absolute)	4.451 atm	* 1.013E+5 Pa/atm 4.508E+05 Pa
Pe = exit pressure (absolute)	1.242 atm	* 1.013E+5 Pa/atm 1.259E+05 Pa
Te = sample temperature (absolute)	296 °K	296 °K
Tb = flow measurement basis temperature (absolute)	294 °K	294 °K
ze = gas deviation factor at Pe and Te	1.0000	1.0000
zb = gas deviation factor at Pb and Te	1.0000	1.0000
Qb = flow rate at base conditions	0.02759 cm ³ /s	* 1.0E-6 m ³ /cm ³ 2.759E-08 m ³ /s
ve = flow velocity at sample exit end	2.309E-04 cm/s	* 1.0E-2 m/cm 2.309E-06 m/s
	Ka = 1.77E-06 d	* 9.872E-13 m ² /d 1.75E-10 m ²
	Ka = 1.77E-03 md	1.75E-14 cm ²
	Ka = 1.77E+00 μd	

Steady State Gas Permeability Data

Project #:	8362	Net Effective Stress:	2 Mpa	290.1 psid	Gas:	N2			
Sample #:	F	Length:	10.029 cm		gas deviation z factors:	ze =	1.0000	zb =	1.0000
Stress Level #:	1	Diameter:	10.170 cm		Viscosity:	0.0176 cp			
Regime #:	2	Area:	81.233 cm ²						
Pressure Data Filename:	8362FG.S1A								
XDCR calibration factors:	Pc =	222.869 psig/volt	PI =	55.4417 psig/volt	ΔP =	11.0272 psid/volt	Pe =	5.5211 psig/volt	

Date	Time of Day	File Time (min)	Regime #	Pb Barometric Pressure	Pc Confining Pressure	P1 Inlet Pressure	ΔP Differential Pressure	Pm Mean Pore Pressure Pe*ΔP/2	Pe Exit Pressure	Te Flow Temp (°C)	Tb Ambient Temp (°C)	Qb Flow Rate @Pb&Tb (ml/sec)	
08 Jun 93	11:52	1226	FS1R2a	12.35 psia	1.584 volts	1.985 volts	8.549 volts		2.971 volts	23	21	0.03051	
08 Jun 93	11:56	1226	FS1R2b	12.35 psia	1.584 volts	1.985 volts	8.550 volts		2.971 volts	23	21	0.03048	
08 Jun 93	12:00	1231	FS1R2c	12.35 psia	1.584 volts	1.985 volts	8.550 volts		2.971 volts	23	21	0.03040	
08 Jun 93	12:04	1231	FS1R2d	12.35 psia	1.584 volts	1.985 volts	8.550 volts		2.971 volts	23	21	0.03041	
AVERAGES			FS1R2										

C-167

Apparent gas permeability: $K_a = (v_e \cdot P_e \cdot u \cdot L) / (P_m \cdot \Delta P)$

Boyle's Law: $v_e = (P_b / P_e) \cdot (T_e / T_b) \cdot (z_e / z_b) \cdot v_b$
 $Q_e = (P_b / P_e) \cdot (T_e / T_b) \cdot (z_e / z_b) \cdot Q_b$

$v_e = Q_e / A = (P_b / P_e) \cdot (T_e / T_b) \cdot (z_e / z_b) \cdot (Q_b / A)$

Parameter	Traditional Units	SI Units
u = gas viscosity	0.0176 cp	* 1.0E-3 Pa*sec/cp 1.760E-05 Pa*sec
L = sample length	10.029 cm	* 1.0E-2 m/cm 1.003E-01 m
A = sample circular cross sectional area	81.233 cm ²	* 1.0E-4 m ² /cm ² 8.123E-03 m ²
Pb = flow measurement basis pressure (absolute)	0.8404 atm	* 1.013E+5 Pa/atm 8.513E+04 Pa
ΔP = pressure drop across sample length	6.415 atm	* 1.013E+5 Pa/atm 6.499E+05 Pa
Pm = mean pore pressure (absolute)	5.164 atm	* 1.013E+5 Pa/atm 5.231E+05 Pa
Pe = exit pressure (absolute)	1.957 atm	* 1.013E+5 Pa/atm 1.982E+05 Pa
Te = sample temperature (absolute)	296 °K	296 °K
Tb = flow measurement basis temperature (absolute)	294 °K	294 °K
ze = gas deviation factor at Pe and Te	1.0000	1.0000
zb = gas deviation factor at Pb and Te	1.0000	1.0000
Qb = flow rate at base conditions	0.03045 cm ³ /s	* 1.0E-6 m ³ /cm ³ 3.045E-08 m ³ /s
ve = flow velocity at sample exit end	1.621E-04 cm/s	* 1.0E-2 m/cm 1.621E-06 m/s
	Ka =	1.69E-06 d * 9.872E-13 m ² /d 1.67E-18 m ²
	Ka =	1.69E-03 md 1.67E-14 cm ²
	Ka =	1.69E+00 ud

Steady State Gas Permeability Data

Project #:	8362	Net Effective Stress:	2 Mpa	290.1 psid	Gas:	N2		
Sample #:	F	Length:	10.029 cm		gas deviation z factors:	ze = 1.0000	zb = 1.0000	
Stress Level #:	1	Diameter:	10.170 cm		Viscosity:	0.0176 cp		
Regime #:	3	Area:	81.233 cm ²					
Pressure Data Filename:	8362FG.S1B							
XDCR calibration factors:	Pc = 222.869 psig/volt	Pi = 55.4417 psig/volt	ΔP = 11.0272 psid/volt	Pe = 5.5211 psig/volt				

Date	Time of Day	File Time (min)	Regime #	Pb Barometric Pressure	Pc Confining Pressure	Pi Inlet Pressure	ΔP Differential Pressure	Pm Mean Pore Pressure Pe+ΔP/2	Pe Exit Pressure	Te Flow Temp (°C)	Tb Ambient Temp (°C)	Qb Flow Rate @Pb&Tb (ml/sec)
08 Jun 93	16:36	140	FS1R3a	12.35 psia	1.629 volts	2.166 volts	8.601 volts		4.695 volts	23	22	0.03333
08 Jun 93	16:42	145	FS1R3b	12.35 psia	1.629 volts	2.166 volts	8.601 volts		4.695 volts	23	22	0.03327
08 Jun 93	16:46	150	FS1R3c	12.35 psia	1.629 volts	2.166 volts	8.601 volts		4.694 volts	23	22	0.03329
08 Jun 93	16:49	155	FS1R3d	12.35 psia	1.629 volts	2.166 volts	8.601 volts		4.695 volts	23	22	0.03332
AVERAGES			FS1R3									
					GUAGE	GUAGE	DIFFERENTIAL	GUAGE	GUAGE	(°C)	(°C)	
					1.629 volts	2.166 volts	8.601 volts		4.695 volts			
					363.1 psig	120.09 psig	94.84 psid	73.34 psig	25.920 psig	23	22	
					24.70 atm	8.171 atm	6.454 atm	4.991 atm	1.7638 atm			
					2.503 Mpa	0.8280 Mpa	0.6539 Mpa	0.5057 Mpa	0.17871 Mpa			
				ABSOLUTE	ABSOLUTE	ABSOLUTE	DIFFERENTIAL	ABSOLUTE	ABSOLUTE	(°K)	(°K)	(ml/sec)
				12.35 psia	375.4 psia	132.44 psia	94.84 psid	85.69 psia	38.27 psia			
				0.8404 atm	25.54 atm	9.012 atm	6.454 atm	5.831 atm	2.604 atm	296	295	0.03330
				0.08515 Mpa	2.588 Mpa	0.9131 Mpa	0.6539 Mpa	0.5908 Mpa	0.2639 Mpa			

C-168

Apparent gas permeability: $K_a = (v_e \cdot P_e \cdot u \cdot L) / (P_m \cdot \Delta P)$

Boyle's Law: $V_e = (P_b/P_e) \cdot (T_e/T_b) \cdot (z_e/z_b) \cdot V_b$
 $Q_e = (P_b/P_e) \cdot (T_e/T_b) \cdot (z_e/z_b) \cdot Q_b$

$v_e = Q_e/A = (P_b/P_e) \cdot (T_e/T_b) \cdot (z_e/z_b) \cdot (Q_b/A)$

Parameter	Traditional Units	SI Units
μ = gas viscosity	0.0176 cp	* 1.0E-3 Pa*sec/cp 1.760E-05 Pa*sec
L = sample length	10.029 cm	* 1.0E-2 m/cm 1.003E-01 m
A = sample circular cross sectional area	81.233 cm ²	* 1.0E-4 m ² /cm ² 8.123E-03 m ²
Pb = flow measurement basis pressure (absolute)	0.8404 atm	* 1.013E+5 Pa/atm 8.513E+04 Pa
ΔP = pressure drop across sample length	6.454 atm	* 1.013E+5 Pa/atm 6.538E+05 Pa
Pm = mean pore pressure (absolute)	5.831 atm	* 1.013E+5 Pa/atm 5.907E+05 Pa
Pe = exit pressure (absolute)	2.604 atm	* 1.013E+5 Pa/atm 2.638E+05 Pa
Te = sample temperature (absolute)	296 °K	296 °K
Tb = flow measurement basis temperature (absolute)	295 °K	295 °K
ze = gas deviation factor at Pe and Te	1.0000	1.0000
zb = gas deviation factor at Pb and Te	1.0000	1.0000
Qb = flow rate at base conditions	0.03330 cm ³ /s	* 1.0E-6 m ³ /cm ³ 3.330E-08 m ³ /s
ve = flow velocity at sample exit end	1.327E-04 cm/s	* 1.0E-2 m/cm 1.327E-06 m/s
	Ka = 1.62E-06 d	* 9.872E-13 m ² /d 1.60E-18 m ²
	Ka = 1.62E-03 md	1.60E-14 cm ²
	Ka = 1.62E+00 μd	

Steady State Gas Permeability Data

Project #: 8362	Net Effective Stress: 2 Mpa 290.1 psid	Gas: N2
Sample #: F	Length: 10.029 cm	gas deviation z factors: ze = 1.0000 zb = 1.0000
Stress Level #: 1	Diameter: 10.170 cm	Viscosity: 0.0176 cp
Regime #: 4	Area: 81.233 cm ²	
Pressure Data Filename: 8362FG.S1B		
XDCR calibration factors: Pc = 222.869 psig/volt Pi = 55.4417 psig/volt ΔP = 11.0272 psid/volt Pe = 5.5211 psig/volt		

Date	Time of Day	File Time (min)	Regime #	Pb Barometric Pressure	Pc Confining Pressure	Pi Inlet Pressure	ΔP Differential Pressure	Pm Mean Pore Pressure Pe-ΔP/2	Pe Exit Pressure	Te Flow Temp (°C)	Tb Ambient Temp (°C)	Qb Flow Rate @Pb&Tb (ml/sec)	
09 Jun 93	09:09	1132	FS1R4a	12.39 psia	1.674 volts	2.333 volts	8.509 volts		6.545 volts	23	21	0.03535	
09 Jun 93	09:11	1137	FS1R4b	12.39 psia	1.674 volts	2.333 volts	8.509 volts		6.546 volts	23	21	0.03532	
09 Jun 93	09:14	1132	FS1R4c	12.39 psia	1.674 volts	2.333 volts	8.510 volts		6.546 volts	23	21	0.03532	
09 Jun 93	09:18	1142	FS1R4d	12.39 psia	1.674 volts	2.333 volts	8.511 volts		6.547 volts	23	21	0.03539	
AVERAGES			FS1R4										
					GAUGE	GAUGE	DIFFERENTIAL	GAUGE	GAUGE		(°C)	(°C)	
					1.674 volts	2.333 volts	8.510 volts		6.546 volts				
					373.1 psig	129.35 psig	93.84 psid	83.06 psig	36.141 psig		23	21	
					25.39 atm	8.801 atm	6.385 atm	5.652 atm	2.4592 atm				
					2.572 Mpa	0.8918 Mpa	0.6470 Mpa	0.5727 Mpa	0.24918 Mpa				
			ABSOLUTE	ABSOLUTE	ABSOLUTE	DIFFERENTIAL	ABSOLUTE	ABSOLUTE		(°K)	(°K)	(ml/sec)	
			12.39 psia	385.5 psia	141.74 psia	93.84 psid	95.45 psia	48.53 psia					
			0.8431 atm	26.23 atm	9.644 atm	6.385 atm	6.495 atm	3.302 atm		296	294	0.03535	
			0.08543 Mpa	2.658 Mpa	0.9772 Mpa	0.6470 Mpa	0.6581 Mpa	0.3346 Mpa					

C-169

Apparent gas permeability: $K_a = (v_e \cdot P_e \cdot u \cdot L) / (P_m \cdot \Delta P)$

Boyle's Law: $V_e = (P_b / P_e) \cdot (T_e / T_b) \cdot (z_e / z_b) \cdot V_b$
 $Q_e = (P_b / P_e) \cdot (T_e / T_b) \cdot (z_e / z_b) \cdot Q_b$

$v_e = Q_e / A = (P_b / P_e) \cdot (T_e / T_b) \cdot (z_e / z_b) \cdot (Q_b / A)$

Parameter	Traditional Units	SI Units
μ = gas viscosity	0.0176 cp	* 1.0E-3 Pa*sec/cp 1.760E-05 Pa*sec
L = sample length	10.029 cm	* 1.0E-2 m/cm 1.003E-01 m
A = sample circular cross sectional area	81.233 cm ²	* 1.0E-4 m ² /cm ² 8.123E-03 m ²
Pb = flow measurement basis pressure (absolute)	0.8431 atm	* 1.013E+5 Pa/atm 8.540E+04 Pa
ΔP = pressure drop across sample length	6.385 atm	* 1.013E+5 Pa/atm 6.468E+05 Pa
Pm = mean pore pressure (absolute)	6.495 atm	* 1.013E+5 Pa/atm 6.579E+05 Pa
Pe = exit pressure (absolute)	3.302 atm	* 1.013E+5 Pa/atm 3.345E+05 Pa
Te = sample temperature (absolute)	296 °K	296 °K
Tb = flow measurement basis temperature (absolute)	294 °K	294 °K
ze = gas deviation factor at Pe and Te	1.0000	1.0000
zb = gas deviation factor at Pb and Te	1.0000	1.0000
Qb = flow rate at base conditions	0.03535 cm ³ /s	* 1.0E-6 m ³ /cm ³ 3.535E-08 m ³ /s
ve = flow velocity at sample exit end	1.118E-04 cm/s	* 1.0E-2 m/cm 1.118E-06 m/s
	Ka = 1.57E-06 d	* 9.872E-13 m ² /d 1.55E-18 m ²
	Ka = 1.57E-03 md	1.55E-14 cm ²
	Ka = 1.57E+00 μd	

Steady State Gas Permeability Data

Project #: 8362	Net Effective Stress: 6 Mpa 870.2 psid	Gas: N2
Sample #: F	Length: 10.029 cm	gas deviation z factors: ze = 1.0000 zb = 1.0000
Stress Level #: 2	Diameter: 10.170 cm	Viscosity: 0.0176 cp
Regime #: 1	Area: 81.233 cm ²	
Pressure Data Filename: 8362FG.S2A		
XDCR calibration factors:	Pc = 222.869 psig/volt Pi = 55.4417 psig/volt ΔP = 11.0272 psid/volt Pe = 5.5211 psig/volt	

Date	Time of Day	File Time (min)	Regime #	Pb Barometric Pressure	Pc Confining Pressure	Pi Inlet Pressure	ΔP Differential Pressure	Pm Mean Pore Pressure Pe-ΔP/2	Pe Exit Pressure	Te Flow Temp (°C)	Tb Ambient Temp (°C)	Qb Flow Rate @Pb&Tb (ml/sec)	
09 Jun 93	15:20	230	FS2R1a	12.37 psia	4.142 volts	1.806 volts	8.612 volts		1.044 volts	23	22	0.01939	
09 Jun 93	15:25	235	FS2R1b	12.37 psia	4.142 volts	1.806 volts	8.613 volts		1.044 volts	23	22	0.01935	
09 Jun 93	15:33	240	FS2R1c	12.37 psia	4.142 volts	1.806 volts	8.613 volts		1.044 volts	23	22	0.01939	
09 Jun 93	15:38	245	FS2R1d	12.37 psia	4.142 volts	1.806 volts	8.613 volts		1.044 volts	23	22	0.01934	
AVERAGES			FS2R1										
					GAUGE	GAUGE	DIFFERENTIAL	GAUGE	GAUGE		(°C)	(°C)	
					4.142 volts	1.806 volts	8.613 volts	53.25 psig	1.044 volts		23	22	
					923.1 psig	100.13 psig	94.97 psid	3.624 atm	5.764 psig				
					62.81 atm	6.813 atm	6.463 atm	0.3922 atm					
					6.365 Mpa	0.6904 Mpa	0.6548 Mpa	0.03974 Mpa					
			ABSOLUTE	ABSOLUTE	ABSOLUTE	DIFFERENTIAL	ABSOLUTE	ABSOLUTE		(°K)	(°K)	(ml/sec)	
			12.37 psia	935.5 psia	112.50 psia	94.97 psid	65.62 psia	18.13 psia					
			0.8417 atm	63.66 atm	7.655 atm	6.463 atm	4.465 atm	1.234 atm		296	295	0.01937	
			0.08529 Mpa	6.450 Mpa	0.7756 Mpa	0.6548 Mpa	0.4524 Mpa	0.1250 Mpa					

Apparent gas permeability: $K_a = (v_e \cdot P_e \cdot u \cdot L) / (P_m \cdot \Delta P)$

Boyle's Law: $v_e = (P_b / P_e) \cdot (T_e / T_b) \cdot (z_e / z_b) \cdot v_b$
 $Q_e = (P_b / P_e) \cdot (T_e / T_b) \cdot (z_e / z_b) \cdot Q_b$

$v_e = Q_e / A = (P_b / P_e) \cdot (T_e / T_b) \cdot (z_e / z_b) \cdot (Q_b / A)$

Parameter	Traditional Units	SI Units
μ = gas viscosity	0.0176 cp	* 1.0E-3 Pa*sec/cp 1.760E-05 Pa*sec
L = sample length	10.029 cm	* 1.0E-2 m/cm 1.003E-01 m
A = sample circular cross sectional area	81.233 cm ²	* 1.0E-4 m ² /cm ² 8.123E-03 m ²
Pb = flow measurement basis pressure (absolute)	0.8417 atm	* 1.013E+5 Pa/atm 8.527E+04 Pa
ΔP = pressure drop across sample length	6.463 atm	* 1.013E+5 Pa/atm 6.547E+05 Pa
Pm = mean pore pressure (absolute)	4.465 atm	* 1.013E+5 Pa/atm 4.523E+05 Pa
Pe = exit pressure (absolute)	1.234 atm	* 1.013E+5 Pa/atm 1.250E+05 Pa
Te = sample temperature (absolute)	296 °K	296 °K
Tb = flow measurement basis temperature (absolute)	295 °K	295 °K
ze = gas deviation factor at Pe and Te	1.0000	1.0000
zb = gas deviation factor at Pb and Te	1.0000	1.0000
Qb = flow rate at base conditions	0.01937 cm ³ /s	* 1.0E-6 m ³ /cm ³ 1.937E-08 m ³ /s
ve = flow velocity at sample exit end	1.632E-04 cm/s	* 1.0E-2 m/cm 1.632E-06 m/s
	Ka = 1.23E-06 d	* 9.872E-13 m ² /d 1.22E-18 m ²
	Ka = 1.23E-03 md	1.22E-14 cm ²
	Ka = 1.23E+00 μd	

C-170

Steady State Gas Permeability Data

Project #:	8362	Net Effective Stress:	6 Mpa	870.2 psid	Gas:	N2			
Sample #:	F	Length:	10.029 cm		gas deviation z factors:	ze =	1.0000	zb =	1.0000
Stress Level #:	2	Diameter:	10.170 cm		Viscosity:	0.0176 cp			
Regime #:	2	Area:	81.233 cm ²						
Pressure Data Filename:	8362FG.S2A								
XDCR calibration factors:	Pc =	222.869 psig/volt	P1 =	55.4417 psig/volt	ΔP =	11.0272 psid/volt	Pe =	5.5211 psig/volt	

Date	Time of Day	File Time (min)	Regime #	Pb Barometric Pressure	Pc Confining Pressure	P1 Inlet Pressure	ΔP Differential Pressure	Pm Mean Pore Pressure Pe·ΔP/2	Pe Exit Pressure	Te Flow Temp (°C)	Tb Ambient Temp (°C)	Qb Flow Rate @Pb&Tb (ml/sec)
10 Jun 93	09:38	1325	FS2R2a	12.37 psia	4.187 volts	1.986 volts	8.664 volts		2.748 volts	23	22	0.02084
10 Jun 93	09:45	1335	FS2R2b	12.37 psia	4.187 volts	1.987 volts	8.666 volts		2.748 volts	23	22	0.02094
10 Jun 93	09:49	1340	FS2R2c	12.37 psia	4.187 volts	1.987 volts	8.666 volts		2.749 volts	23	22	0.02098
10 Jun 93	09:54	1340	FS2R2d	12.37 psia	4.187 volts	1.987 volts	8.666 volts		2.749 volts	23	22	0.02091
10 Jun 93	10:00	1345	FS2R2e	12.37 psia	4.187 volts	1.987 volts	8.667 volts		2.749 volts	23	22	0.02092
AVERAGES			FS2R2		GAUGE	GAUGE	DIFFERENTIAL	GAUGE	GAUGE	(°C)	(°C)	
				4.187 volts	1.987 volts	8.666 volts	2.749 volts					
				933.2 psig	110.15 psig	95.56 psid	62.96 psig	15.175 psig	23	22		
				63.50 atm	7.495 atm	6.502 atm	4.284 atm	1.0326 atm				
				6.434 Mpa	0.7595 Mpa	0.6589 Mpa	0.4341 Mpa	0.10463 Mpa				
				ABSOLUTE	ABSOLUTE	ABSOLUTE	ABSOLUTE	ABSOLUTE	(°K)	(°K)	(ml/sec)	
				12.37 psia	945.5 psia	122.52 psia	95.56 psid	75.33 psia	27.55 psia			
		0.8417 atm	64.34 atm	8.337 atm	6.502 atm	5.126 atm	1.874 atm	296	295	0.02092		
		0.08529 Mpa	6.519 Mpa	0.8448 Mpa	0.6589 Mpa	0.5193 Mpa	0.1899 Mpa					

C-171

Apparent gas permeability: $K_a = (v_e \cdot P_e \cdot u \cdot L) / (P_m \cdot \Delta P)$

Boyle's Law: $V_e = (P_b / P_e) \cdot (T_e / T_b) \cdot (z_e / z_b) \cdot V_b$
 $Q_e = (P_b / P_e) \cdot (T_e / T_b) \cdot (z_e / z_b) \cdot Q_b$

$v_e = Q_e / A = (P_b / P_e) \cdot (T_e / T_b) \cdot (z_e / z_b) \cdot (Q_b / A)$

Parameter	Traditional Units	SI Units
μ = gas viscosity	0.0176 cp	* 1.0E-3 Pa·sec/cp 1.760E-05 Pa·sec
L = sample length	10.029 cm	* 1.0E-2 m/cm 1.003E-01 m
A = sample circular cross sectional area	81.233 cm ²	* 1.0E-4 m ² /cm ² 8.123E-03 m ²
Pb = flow measurement basis pressure (absolute)	0.8417 atm	* 1.013E+5 Pa/atm 8.527E+04 Pa
ΔP = pressure drop across sample length	6.502 atm	* 1.013E+5 Pa/atm 6.587E+05 Pa
Pm = mean pore pressure (absolute)	5.126 atm	* 1.013E+5 Pa/atm 5.192E+05 Pa
Pe = exit pressure (absolute)	1.874 atm	* 1.013E+5 Pa/atm 1.899E+05 Pa
Te = sample temperature (absolute)	296 °K	296 °K
Tb = flow measurement basis temperature (absolute)	295 °K	295 °K
ze = gas deviation factor at Pe and Te	1.0000	1.0000
zb = gas deviation factor at Pb and Te	1.0000	1.0000
Qb = flow rate at base conditions	0.02092 cm ³ /s	* 1.0E-6 m ³ /cm ³ 2.092E-08 m ³ /s
ve = flow velocity at sample exit end	1.160E-04 cm/s	* 1.0E-2 m/cm 1.160E-06 m/s
	Ka =	1.15E-06 d * 9.872E-13 m ² /d 1.14E-18 m ²
	Ka =	1.15E-03 md 1.14E-14 cm ²
	Ka =	1.15E+00 μd

Steady State Gas Permeability Data

Project #:	8362	Net Effective Stress:	6 Mpa	870.2 psid	Gas:	N2						
Sample #:	F	Length:	10.029 cm		gas deviation z factors:	ze =	1.0000	zb =	1.0000			
Stress Level #:	2	Diameter:	10.170 cm		Viscosity:	0.0176 cp						
Regime #:	4	Area:	81.233 cm ²									
Pressure Data Filename:	8362FG.S2A											
XDCR calibration factors:	Pc =	222.869	psig/volt	PI =	55.4417	psig/volt	ΔP =	11.0272	psid/volt	Pe =	5.5211	psig/volt

Date	Time of Day	File Time (min)	Regime #	Pb Barometric Pressure	Pc Confining Pressure	Pi Inlet Pressure	ΔP Differential Pressure	Pm Mean Pore Pressure Pe+ΔP/2	Pe Exit Pressure	Te Flow Temp (°C)	Tb Ambient Temp (°C)	Qb Flow Rate @Pb&Tb (ml/sec)			
11 Jun 93	08:57	2725	FS2R4a	12.31 psia	4.277 volts	2.338 volts	8.530 volts		6.581 volts	23	22	0.02422			
11 Jun 93	09:01	2730	FS2R4b	12.31 psia	4.277 volts	2.338 volts	8.530 volts		6.581 volts	23	22	0.02425			
11 Jun 93	09:05	2735	FS2R4c	12.31 psia	4.277 volts	2.338 volts	8.530 volts		6.581 volts	23	22	0.02422			
11 Jun 93	09:09	2740	FS2R4d	12.31 psia	4.277 volts	2.338 volts	8.530 volts		6.582 volts	23	22	0.02423			
AVERAGES			FS2R4	GUAGE		GUAGE		DIFFERENTIAL	GUAGE		GUAGE	(°C)	(°C)		
				4.277 volts	2.338 volts	8.530 volts	6.581 volts	23	22						
				953.2 psig	129.62 psig	94.06 psid	83.37 psig	36.336 psig	23	22					
				64.86 atm	8.820 atm	6.401 atm	5.673 atm	2.4725 atm							
				6.572 Mpa	0.8937 Mpa	0.6485 Mpa	0.5748 Mpa	0.25053 Mpa							
				ABSOLUTE		ABSOLUTE		DIFFERENTIAL	ABSOLUTE		ABSOLUTE		(°K)	(°K)	(ml/sec)
				12.31 psia	965.5 psia	141.93 psia	94.06 psid	95.68 psia	48.65 psia	296	295	0.02423			
0.8376 atm	65.70 atm	9.658 atm	6.401 atm	6.510 atm	3.310 atm										
0.08487 Mpa	6.657 Mpa	0.9786 Mpa	0.6485 Mpa	0.6597 Mpa	0.3354 Mpa										

C-173

Apparent gas permeability: $K_a = (v_e \cdot P_e \cdot u \cdot L) / (P_m \cdot \Delta P)$

Boyle's Law: $V_e = (P_b / P_e) \cdot (T_e / T_b) \cdot (z_e / z_b) \cdot V_b$
 $Q_e = (P_b / P_e) \cdot (T_e / T_b) \cdot (z_e / z_b) \cdot Q_b$

$v_e = Q_e / A = (P_b / P_e) \cdot (T_e / T_b) \cdot (z_e / z_b) \cdot (Q_b / A)$

Parameter	Traditional Units	SI Units
u = gas viscosity	0.0176 cp	* 1.0E-3 Pa*sec/cp 1.760E-05 Pa*sec
L = sample length	10.029 cm	* 1.0E-2 m/cm 1.003E-01 m
A = sample circular cross sectional area	81.233 cm ²	* 1.0E-4 m ² /cm ² 8.123E-03 m ²
Pb = flow measurement basis pressure (absolute)	0.8376 atm	* 1.013E+5 Pa/atm 8.485E+04 Pa
ΔP = pressure drop across sample length	6.401 atm	* 1.013E+5 Pa/atm 6.484E+05 Pa
Pm = mean pore pressure (absolute)	6.510 atm	* 1.013E+5 Pa/atm 6.595E+05 Pa
Pe = exit pressure (absolute)	3.310 atm	* 1.013E+5 Pa/atm 3.353E+05 Pa
Te = sample temperature (absolute)	296 °K	296 °K
Tb = flow measurement basis temperature (absolute)	295 °K	295 °K
ze = gas deviation factor at Pe and Te	1.0000	1.0000
zb = gas deviation factor at Pb and Te	1.0000	1.0000
Qb = flow rate at base conditions	0.02423 cm ³ /s	* 1.0E-6 m ³ /cm ³ 2.423E-08 m ³ /s
ve = flow velocity at sample exit end	7.573E-05 cm/s	* 1.0E-2 m/cm 7.573E-07 m/s
	Ka =	* 9.872E-13 m ² /d 1.05E-18 m ²
	Ka =	1.06E-03 md 1.05E-14 cm ²
	Ka =	1.06E+00 μd

Steady State Gas Permeability Data

Project #:	8362	Net Effective Stress:	10 Mpa	1450.4 psid	Gas:	N2		
Sample #:	F	Length:	10.029 cm		gas deviation z factors:	ze = 1.0000	zb = 1.0000	
Stress Level #:	3	Diameter:	10.170 cm		Viscosity:	0.0176 cp		
Regime #:	1	Area:	81.233 cm ²					
Pressure Data Filename:	8362FG.S3A							
XDCR calibration factors:	Pc = 222.869 psig/volt	Pl = 55.4417 psig/volt	AP = 11.0272 psid/volt	Pe = 5.5211 psig/volt				

Date	Time of Day	File Time (min)	Regime #	Pb Barometric Pressure	Pc Confining Pressure	Pl Inlet Pressure	AP Differential Pressure	Pm Mean Pore Pressure Pe+AP/2	Pe Exit Pressure	Te Flow Temp (°C)	Tb Ambient Temp (°C)	Qb Flow Rate @Pb&Tb (ml/sec)	
11 Jun 93	15:48	387	FS3R1a	12.27 psia	6.746 volts	1.809 volts	8.631 volts		1.044 volts	23	23	0.01690	
11 Jun 93	15:53	392	FS3R1b	12.27 psia	6.747 volts	1.809 volts	8.631 volts		1.044 volts	23	23	0.01696	
11 Jun 93	15:58	397	FS3R1c	12.27 psia	6.747 volts	1.809 volts	8.632 volts		1.044 volts	23	23	0.01695	
11 Jun 93	16:03	402	FS3R1d	12.27 psia	6.747 volts	1.809 volts	8.633 volts		1.043 volts	23	23	0.01692	
AVERAGES			FS3R1		GUAGE	GUAGE	DIFFERENTIAL	GUAGE	GUAGE	(°C)	(°C)		
					6.747 volts	1.809 volts	8.632 volts		1.044 volts				
					1503.6 psig	100.29 psig	95.18 psid	53.35 psig	5.763 psig	23	23		
					102.32 atm	6.825 atm	6.477 atm	3.631 atm	0.3921 atm				
					10.367 Mpa	0.6915 Mpa	0.6563 Mpa	0.3679 Mpa	0.03973 Mpa				
					ABSOLUTE	ABSOLUTE	ABSOLUTE	DIFFERENTIAL	ABSOLUTE	ABSOLUTE	(°K)	(°K)	(ml/sec)
					12.27 psia	1515.9 psia	112.56 psia	95.18 psid	65.62 psia	18.03 psia			
			0.8349 atm	103.15 atm	7.660 atm	6.477 atm	4.465 atm	1.227 atm	296	296	0.01693		
			0.08460 Mpa	10.452 Mpa	0.7761 Mpa	0.6563 Mpa	0.4525 Mpa	0.1243 Mpa					

C-174

Apparent gas permeability: $K_a = (v_e \cdot P_e \cdot u \cdot L) / (P_m \cdot \Delta P)$

Boyle's Law: $v_e = (P_b / P_e) \cdot (T_e / T_b) \cdot (z_e / z_b) \cdot v_b$

$Q_e = (P_b / P_e) \cdot (T_e / T_b) \cdot (z_e / z_b) \cdot Q_b$

$v_e = Q_e / A = (P_b / P_e) \cdot (T_e / T_b) \cdot (z_e / z_b) \cdot (Q_b / A)$

Parameter	Traditional Units	SI Units
μ = gas viscosity	0.0176 cp	* 1.0E-3 Pa*sec/cp 1.760E-05 Pa*sec
L = sample length	10.029 cm	* 1.0E-2 m/cm 1.003E-01 m
A = sample circular cross sectional area	81.233 cm ²	* 1.0E-4 m ² /cm ² 8.123E-03 m ²
Pb = flow measurement basis pressure (absolute)	0.8349 atm	* 1.013E+5 Pa/atm 8.458E+04 Pa
AP = pressure drop across sample length	6.477 atm	* 1.013E+5 Pa/atm 6.561E+05 Pa
Pm = mean pore pressure (absolute)	4.465 atm	* 1.013E+5 Pa/atm 4.524E+05 Pa
Pe = exit pressure (absolute)	1.227 atm	* 1.013E+5 Pa/atm 1.243E+05 Pa
Te = sample temperature (absolute)	296 °K	296 °K
Tb = flow measurement basis temperature (absolute)	296 °K	296 °K
ze = gas deviation factor at Pe and Te	1.0000	1.0000
zb = gas deviation factor at Pb and Te	1.0000	1.0000
Qb = flow rate at base conditions	0.01693 cm ³ /s	* 1.0E-6 m ³ /cm ³ 1.693E-08 m ³ /s
ve = flow velocity at sample exit end	1.418E-04 cm/s	* 1.0E-2 m/cm 1.418E-06 m/s
	Ka = 1.06E-06 d	* 9.872E-13 m ² /d 1.05E-18 m ²
	Ka = 1.06E-03 md	1.05E-14 cm ²
	Ka = 1.06E+00 ud	

Steady State Gas Permeability Data

Project #:	8362	Net Effective Stress:	10 Mpa	1450.4 psid	Gas:	N2						
Sample #:	F	Length:	10.029 cm		gas deviation z factors:	ze =	1.0000	zb =	1.0000			
Stress Level #:	3	Diameter:	10.170 cm		Viscosity:	0.0176 cp						
Regime #:	2	Area:	81.233 cm ²									
Pressure Data Filename:	8362FG.S3A											
XDCR calibration factors:	Pc =	222.869	psig/volt	PI =	55.4417	psig/volt	ΔP =	11.0272	psid/volt	Pe =	5.5211	psig/volt

Date	Time of Day	File Time (min)	Regime #	Pb Barometric Pressure	Pc Confining Pressure	P1 Inlet Pressure	ΔP Differential Pressure	Pm Mean Pore Pressure Pe+ΔP/2	Pe Exit Pressure	Te Flow Temp (°C)	Tb Ambient Temp (°C)	Qb Flow Rate @Pb&Tb (ml/sec)
14 Jun 93	09:29	4330	FS3R2a	12.40 psia	6.791 volts	1.986 volts	8.670 volts		2.719 volts	23	22	0.01790
14 Jun 93	09:33	4335	FS3R2b	12.40 psia	6.790 volts	1.986 volts	8.670 volts		2.720 volts	23	22	0.01791
14 Jun 93	09:39	4340	FS3R2c	12.40 psia	6.790 volts	1.986 volts	8.610 volts		2.721 volts	23	22	0.01785
14 Jun 93	09:44	4345	FS3R2d	12.40 psia	6.790 volts	1.986 volts	8.620 volts		2.721 volts	23	22	0.01792
AVERAGES			FS3R2									
				GUAGE	GUAGE	DIFFERENTIAL	GUAGE	GUAGE	(°C)	(°C)		
				6.790 volts	1.986 volts	8.643 volts		2.720 volts				
				1513.3 psig	110.11 psig	95.30 psid	62.67 psig	15.019 psig		23	22	
				102.98 atm	7.492 atm	6.485 atm	4.264 atm	1.0220 atm				
				10.434 Mpa	0.7592 Mpa	0.6571 Mpa	0.4321 Mpa	0.10355 Mpa				
				ABSOLUTE	ABSOLUTE	DIFFERENTIAL	ABSOLUTE	ABSOLUTE	ABSOLUTE	(°K)	(°K)	(ml/sec)
		12.4 psia	1525.7 psia	122.51 psia	95.30 psid	75.07 psia	27.42 psia					
		0.8438 atm	103.82 atm	8.336 atm	6.485 atm	5.108 atm	1.866 atm	296	295	0.01789		
		0.08550 Mpa	10.520 Mpa	0.8447 Mpa	0.6571 Mpa	0.5176 Mpa	0.1890 Mpa					

C-175

Apparent gas permeability: $K_a = (v_e \cdot P_e \cdot u \cdot L) / (P_m \cdot \Delta P)$

Boyle's Law: $V_e = (P_b / P_e) \cdot (T_e / T_b) \cdot (z_e / z_b) \cdot V_b$
 $Q_e = (P_b / P_e) \cdot (T_e / T_b) \cdot (z_e / z_b) \cdot Q_b$

$v_e = Q_e / A = (P_b / P_e) \cdot (T_e / T_b) \cdot (z_e / z_b) \cdot (Q_b / A)$

Parameter	Traditional Units	SI Units
μ = gas viscosity	0.0176 cp	* 1.0E-3 Pa*sec/cp 1.760E-05 Pa*sec
L = sample length	10.029 cm	* 1.0E-2 m/cm 1.003E-01 m
A = sample circular cross sectional area	81.233 cm ²	* 1.0E-4 m ² /cm ² 8.123E-03 m ²
Pb = flow measurement basis pressure (absolute)	0.8438 atm	* 1.013E+5 Pa/atm 8.547E+04 Pa
ΔP = pressure drop across sample length	6.485 atm	* 1.013E+5 Pa/atm 6.569E+05 Pa
Pm = mean pore pressure (absolute)	5.108 atm	* 1.013E+5 Pa/atm 5.175E+05 Pa
Pe = exit pressure (absolute)	1.866 atm	* 1.013E+5 Pa/atm 1.890E+05 Pa
Te = sample temperature (absolute)	296 °K	296 °K
Tb = flow measurement basis temperature (absolute)	295 °K	295 °K
ze = gas deviation factor at Pe and Te	1.0000	1.0000
zb = gas deviation factor at Pb and Te	1.0000	1.0000
Qb = flow rate at base conditions	0.01789 cm ³ /s	* 1.0E-6 m ³ /cm ³ 1.789E-08 m ³ /s
ve = flow velocity at sample exit end	9.996E-05 cm/s	* 1.0E-2 m/cm 9.996E-07 m/s
	Ka =	9.94E-07 d * 9.872E-13 m ² /d 9.81E-19 m ²
	Ka =	9.94E-04 md 9.81E-15 cm ²
	Ka =	9.94E-01 μd

Steady State Gas Permeability Data

Project #:	8362	Net Effective Stress:	10 Mpa	1450.4 psid	Gas:	N2			
Sample #:	F	Length:	10.029 cm		gas deviation z factors:	ze =	1.0000	zb =	1.0000
Stress Level #:	3	Diameter:	10.170 cm		Viscosity:	0.0176 cp			
Regime #:	3	Area:	81.233 cm ²						
Pressure Data Filename:	8362FG.S3A								
XDCR calibration factors:	Pc =	222.869 psig/volt	Pl =	55.4417 psig/volt	ΔP =	11.0272 psid/volt	Pe =	5.5211 psig/volt	

Date	Time of Day	File Time (min)	Regime #	Pb Barometric Pressure	Pc Confining Pressure	Pl Inlet Pressure	ΔP Differential Pressure	Pm Mean Pore Pressure Pe*ΔP/2	Pe Exit Pressure	Te Flow Temp (°C)	Tb Ambient Temp (°C)	Qb Flow Rate @Pb&Tb (ml/sec)	
14 Jun 93	16:17	4737	FS3R3a	12.34 psia	6.835 volts	2.172 volts	8.644 volts		4.662 volts	23	23	0.01961	
14 Jun 93	16:21	4742	FS3R3b	12.34 psia	6.834 volts	2.172 volts	8.644 volts		4.661 volts	23	23	0.01960	
14 Jun 93	16:26	4747	FS3R3c	12.34 psia	6.834 volts	2.172 volts	8.644 volts		4.661 volts	23	23	0.01959	
14 Jun 93	16:31	4752	FS3R3d	12.34 psia	6.835 volts	2.172 volts	8.645 volts		4.661 volts	23	23	0.01959	
AVERAGES			FS3R3										
					GAUGE	GAUGE	DIFFERENTIAL	GAUGE	GAUGE		(°C)	(°C)	
					6.835 volts	2.172 volts	8.644 volts		4.661 volts				
					1523.2 psig	120.42 psig	95.32 psid	73.40 psig	25.735 psig		23	23	
					103.65 atm	8.194 atm	6.486 atm	4.994 atm	1.7512 atm				
					10.502 Mpa	0.8303 Mpa	0.6572 Mpa	0.5060 Mpa	0.17744 Mpa				
			ABSOLUTE	ABSOLUTE	DIFFERENTIAL	ABSOLUTE	ABSOLUTE		(°K)	(°K)	(ml/sec)		
			12.34 psia	1535.5 psia	132.76 psia	95.32 psid	85.74 psia	38.08 psia					
			0.8397 atm	104.49 atm	9.034 atm	6.486 atm	5.834 atm	2.591 atm		296	296	0.01960	
			0.08508 Mpa	10.587 Mpa	0.9153 Mpa	0.6572 Mpa	0.5911 Mpa	0.2625 Mpa					

C-176

Apparent gas permeability: $K_a = (v_e \cdot P_e \cdot u \cdot L) / (P_m \cdot \Delta P)$

Boyle's Law: $V_e = (P_b / P_e) \cdot (T_e / T_b) \cdot (z_e / z_b) \cdot V_b$

$Q_e = (P_b / P_e) \cdot (T_e / T_b) \cdot (z_e / z_b) \cdot Q_b$

$v_e = Q_e / A = (P_b / P_e) \cdot (T_e / T_b) \cdot (z_e / z_b) \cdot (Q_b / A)$

Parameter	Traditional Units	SI Units
μ - gas viscosity	0.0176 cp	* 1.0E-3 Pa*sec/cp 1.760E-05 Pa*sec
L - sample length	10.029 cm	* 1.0E-2 m/cm 1.003E-01 m
A - sample circular cross sectional area	81.233 cm ²	* 1.0E-4 m ² /cm ² 8.123E-03 m ²
Pb - flow measurement basis pressure (absolute)	0.8397 atm	* 1.013E+5 Pa/atm 8.506E+04 Pa
ΔP - pressure drop across sample length	6.486 atm	* 1.013E+5 Pa/atm 6.571E+05 Pa
Pm - mean pore pressure (absolute)	5.834 atm	* 1.013E+5 Pa/atm 5.910E+05 Pa
Pe - exit pressure (absolute)	2.591 atm	* 1.013E+5 Pa/atm 2.625E+05 Pa
Te - sample temperature (absolute)	296 °K	296 °K
Tb - flow measurement basis temperature (absolute)	296 °K	296 °K
ze - gas deviation factor at Pe and Te	1.0000	1.0000
zb - gas deviation factor at Pb and Te	1.0000	1.0000
Qb - flow rate at base conditions	0.01960 cm ³ /s	* 1.0E-6 m ³ /cm ³ 1.960E-08 m ³ /s
ve - flow velocity at sample exit end	7.818E-05 cm/s	* 1.0E-2 m/cm 7.818E-07 m/s
	Ka = 9.45E-07 d	* 9.872E-13 m ² /d 9.33E-19 m ²
	Ka = 9.45E-04 md	9.33E-15 cm ²
	Ka = 9.45E-01 μd	

Steady State Gas Permeability Data

Project #:	8362	Net Effective Stress:	10 Mpa	1450.4 psid	Gas:	N2		
Sample #:	F	Length:	10.029 cm		gas deviation z factors:	ze =	1.0000	zb = 1.0000
Stress Level #:	3	Diameter:	10.170 cm		Viscosity:	0.0176 cp		
Regime #:	4	Area:	81.233 cm ²					
Pressure Data Filename:	8362FG.S3A							
XDCR calibration factors:	Pc =	222.869 psig/volt	Pi =	55.4417 psig/volt	ΔP =	11.0272 psid/volt	Pe =	5.5211 psig/volt

Date	Time of Day	File Time (min)	Regime #	Pb Barometric Pressure	Pc Confining Pressure	Pi Inlet Pressure	ΔP Differential Pressure	Pm Mean Pore Pressure Pe+ΔP/2	Pe Exit Pressure	Te Flow Temp (°C)	Tb Ambient Temp (°C)	Qb Flow Rate @Pb&Tb (ml/sec)
15 Jun 93	12:47	5967	FS3R4a	12.30 psia	6.883 volts	2.337 volts	8.406 volts		6.808 volts	23	23	0.02060
15 Jun 93	12:51	5972	FS3R4b	12.30 psia	6.884 volts	2.337 volts	8.407 volts		6.808 volts	23	23	0.02062
15 Jun 93	12:56	5977	FS3R4c	12.30 psia	6.884 volts	2.338 volts	8.408 volts		6.809 volts	23	23	0.02062
15 Jun 93	13:01	5982	FS3R4d	12.30 psia	6.883 volts	2.338 volts	8.408 volts		6.809 volts	23	23	0.02060
AVERAGES					GAUGE	GAUGE	DIFFERENTIAL	GAUGE	GAUGE	(°C)	(°C)	
					6.884 volts	2.338 volts	8.407 volts		6.809 volts			
					1534.1 psig	129.59 psig	92.71 psid	83.94 psig	37.590 psig	23	23	
					104.39 atm	8.818 atm	6.308 atm	5.712 atm	2.5579 atm			
					10.577 Mpa	0.8935 Mpa	0.6392 Mpa	0.5788 Mpa	0.25918 Mpa			
					ABSOLUTE	ABSOLUTE	DIFFERENTIAL	ABSOLUTE	ABSOLUTE	(°K)	(°K)	(ml/sec)
					12.3 psia	1546.4 psia	141.89 psia	92.71 psid	96.24 psia	49.89 psia	296	296
				0.8370 atm	105.23 atm	9.655 atm	6.308 atm	6.549 atm	3.395 atm			
				0.08481 Mpa	10.662 Mpa	0.9783 Mpa	0.6392 Mpa	0.6636 Mpa	0.3440 Mpa			

C-177

Apparent gas permeability: $K_a = (v_e \cdot P_e \cdot u \cdot L) / (P_m \cdot \Delta P)$

Boyle's Law: $v_e = (P_b / P_e) \cdot (T_e / T_b) \cdot (z_e / z_b) \cdot v_b$
 $Q_e = (P_b / P_e) \cdot (T_e / T_b) \cdot (z_e / z_b) \cdot Q_b$

$v_e = Q_e / A \cdot (P_b / P_e) \cdot (T_e / T_b) \cdot (z_e / z_b) \cdot (Q_b / A)$

Parameter	Traditional Units	SI Units
μ = gas viscosity	0.0176 cp	* 1.0E-3 Pa*sec/cp 1.760E-05 Pa*sec
L = sample length	10.029 cm	* 1.0E-2 m/cm 1.003E-01 m
A = sample circular cross sectional area	81.233 cm ²	* 1.0E-4 m ² /cm ² 8.123E-03 m ²
Pb = flow measurement basis pressure (absolute)	0.8370 atm	* 1.013E+5 Pa/atm 8.478E+04 Pa
ΔP = pressure drop across sample length	6.308 atm	* 1.013E+5 Pa/atm 6.390E+05 Pa
Pm = mean pore pressure (absolute)	6.549 atm	* 1.013E+5 Pa/atm 6.634E+05 Pa
Pe = exit pressure (absolute)	3.395 atm	* 1.013E+5 Pa/atm 3.439E+05 Pa
Te = sample temperature (absolute)	296 °K	296 °K
Tb = flow measurement basis temperature (absolute)	296 °K	296 °K
ze = gas deviation factor at Pe and Te	1.0000	1.0000
zb = gas deviation factor at Pb and Te	1.0000	1.0000
Qb = flow rate at base conditions	0.02061 cm ³ /s	* 1.0E-6 m ³ /cm ³ 2.061E-08 m ³ /s
ve = flow velocity at sample exit end	6.255E-05 cm/s	* 1.0E-2 m/cm 6.255E-07 m/s
	Ka =	9.07E-07 d * 9.872E-13 m ² /d 8.96E-19 m ²
	Ka =	9.07E-04 md 8.96E-15 cm ²
	Ka =	9.07E-01 μd

APPENDIX C-E: Liquid Permeability Spreadsheets

Steady State Liquid Permeability Data			
Project #:	8362	Target Eff.Stress:	2 Mpa 290.1 psid
Sample #:	A	Length:	10.117 cm
Stress Level #:	1	Diameter:	10.170 cm
		Area:	81.233 cm ²
Pressure Data Filename:	8362AL.S1B		
XDCR calibration factors:	Pc =	222.869 psig/volt	ΔP = 11.0272 psid/volt

All measurements made at room temperature of ~23 °C and with 0 psig back pressure

Date	Time of Day	Regime #	Pc Confining Pressure			ΔP Differential Pressure			Pm Mean Pore Pressure		Effective Stress		Volume Increment	Elapsed Time	Q Flow Rate	K Permeability	
			volts	psig	MPa	volts	psid	MPa	psig	MPa	psid	MPa				μd	m ²
16 Aug 93	12:15	AS1a	1.406	313.4	2.160	4.066	44.84	0.3091	22.42	0.1546	290.9	2.006	0.03	250.42	1.1980E-04	6.31	6.23E-18
16 Aug 93	12:21	AS1b	1.402	312.5	2.154	4.047	44.63	0.3077	22.31	0.1538	290.1	2.001	0.03	241.35	1.2430E-04	6.58	6.49E-18
16 Aug 93	14:31	AS1c	1.398	311.6	2.148	3.896	42.96	0.2962	21.48	0.1481	290.1	2.000	0.03	253.38	1.1840E-04	6.51	6.42E-18
16 Aug 93	14:38	AS1d	1.398	311.6	2.148	3.891	42.91	0.2958	21.45	0.1479	290.1	2.000	0.03	232.92	1.2880E-04	7.09	7.00E-18
16 Aug 93	14:47	AS1e	1.398	311.6	2.148	3.922	43.25	0.2982	21.62	0.1491	289.9	1.999	0.03	228.83	1.3110E-04	7.16	7.07E-18
16 Aug 93	14:50	AS1f	1.398	311.6	2.148	3.926	43.29	0.2985	21.65	0.1492	289.9	1.999	0.03	228.66	1.3120E-04	7.16	7.06E-18
16 Aug 93	14:54	AS1g	1.400	312.0	2.151	3.918	43.20	0.2979	21.60	0.1489	290.4	2.002	0.03	227.10	1.3210E-04	7.22	7.13E-18
16 Aug 93	15:02	AS1h	1.400	312.0	2.151	3.910	43.12	0.2973	21.56	0.1486	290.5	2.003	0.03	268.58	1.1170E-04	6.12	6.04E-18
16 Aug 93	15:04	AS1i	1.400	312.0	2.151	3.912	43.14	0.2974	21.57	0.1487	290.4	2.003	0.03	248.96	1.2050E-04	6.60	6.51E-18
AVERAGES		AS1		312.0	2.151		43.48	0.2998	21.74	0.1499	290.3	2.001			1.2421E-04	6.75	6.66E-18

Darcy's law: $K = (Q \cdot \mu \cdot L) / (\Delta P \cdot A)$

Parameter	Traditional Units	SI Units
Q = volumetric flow rate across A	1.242E-04 cm ³ /s	• 1.0E-6 m ³ /cm ³ 1.242E-10 m ³ /s
μ = fluid viscosity	1.29 cp	• 1.0E-3 Pa*sec/cp 1.29E-03 Pa*sec
L = sample length	10.117 cm	• 1.0E-2 m/cm 1.012E-01 m
ΔP = pressure drop across sample length	2.959 atm	• 1.013E+5 Pa/atm 2.997E+05 Pa
A = sample circular cross sectional area	81.233 cm ²	• 1.0E-4 m ² /cm ² 8.123E-03 m ²
K = specific permeability	6.74E-06 d	6.66E-18 m ²
	6.74E-03 md	
	6.74E+00 μd	

C-180

Steady State Liquid Permeability Data			
Project #:	8362	Target Eff.Stress:	6 Mpa 870.2 psid
Sample #:	A	Length:	10.117 cm
Stress Level #:	2	Diameter:	10.170 cm
		Area:	81.233 cm ²
Pressure Data Filename:	8362AL.S2A		
XDCR calibration factors:	Pc = 222.869 psig/volt	ΔP = 11.0272 psid/volt	

All measurements made at room temperature of ~23 °C and with 0 psig back pressure

Date	Time of Day	Regime #	Pc Confining Pressure			ΔP Differential Pressure			Pm Mean Pore Pressure		Effective Stress		Volume Increment	Elapsed Time	Q Flow Rate	K Permeability	
			volts	psig	MPa	volts	psid	MPa	psig	MPa	psid	MPa				μd	m ²
19 Aug 93	13:24	AS2a	4.007	893.0	6.157	4.094	45.15	0.3113	22.57	0.1556	870.5	6.002	0.10	951.27	1.0512E-04	5.50	5.43E-18
19 Aug 93	13:46	AS2b	4.007	893.0	6.157	4.114	45.37	0.3128	22.68	0.1564	870.4	6.001	0.06	553.56	1.0839E-04	5.64	5.57E-18
19 Aug 93	14:19	AS2c	4.007	893.0	6.157	4.087	45.07	0.3107	22.53	0.1554	870.5	6.002	0.07	671.94	1.0418E-04	5.46	5.39E-18
19 Aug 93	14:51	AS2d	4.007	893.0	6.157	4.047	44.63	0.3077	22.31	0.1538	870.7	6.003	0.10	854.49	1.1703E-04	6.19	6.11E-18
19 Aug 93	15:19	AS2e	4.007	893.0	6.157	4.016	44.29	0.3053	22.14	0.1527	870.9	6.005	0.10	890.20	1.1233E-04	5.99	5.91E-18
AVERAGES		AS2		893.0	6.157		44.90	0.3096	22.45	0.1548	870.6	6.002			1.0941E-04	5.76	5.68E-18

Darcy's law: $K = (Q \cdot \mu \cdot L) / (\Delta P \cdot A)$

Parameter	Traditional Units	SI Units
Q = volumetric flow rate across A	1.094E-04 cm ³ /s	• 1.0E-6 m ³ /cm ³ 1.094E-10 m ³ /s
μ = fluid viscosity	1.29 cp	• 1.0E-3 Pa*sec/cp 1.29E-03 Pa*sec
L = sample length	10.117 cm	• 1.0E-2 m/cm 1.012E-01 m
ΔP = pressure drop across sample length	3.055 atm	• 1.013E+5 Pa/atm 3.095E+05 Pa
A = sample circular cross sectional area	81.233 cm ²	• 1.0E-4 m ² /cm ² 8.123E-03 m ²
K = specific permeability	5.75E-06 d	5.68E-18 m ²
	5.75E-03 md	
	5.75E+00 μd	

C-181

Steady State Liquid Permeability Data					
Project #:	8362	Target Eff. Stress:	10 Mpa 1450.4 psid	Fluid:	Odorless Mineral Spirit
Sample #:	A	Length:	10.117 cm		
Stress Level #:	3	Diameter:	10.170 cm	Viscosity	1.29 cp @ 23 °C
		Area:	81.233 cm ²		
Pressure Data Filename:	8362AL.S3A				
XDCR calibration factors:	Pc =	222.869 psig/volt	ΔP =	11.0272 psid/volt	

All measurements made at room temperature of ~23 °C and with 0 psig back pressure

Date	Time of Day	Regime #	Pc Confining Pressure			ΔP Differential Pressure			Pm Mean Pore Pressure ΔP/2		Effective Stress Pc-Pm		Volume Increment ml	Elapsed Time sec	Q Flow Rate ml/sec	K Permeability	
			volts	psig	MPa	volts	psid	MPa	psig	MPa	psid	MPa				μd	m ²
20 Aug 93	14:25	AS3a	6.602	1471.4	10.145	3.780	41.68	0.2874	20.84	0.1437	1450.5	10.001	0.08	874.99	9.1430E-05	5.18	5.11E-18
20 Aug 93	14:57	AS3b	6.604	1471.8	10.148	3.764	41.51	0.2862	20.75	0.1431	1451.1	10.005	0.10	1033.84	9.6727E-05	5.50	5.43E-18
20 Aug 93	15:48	AS3c	6.602	1471.4	10.145	3.743	41.27	0.2846	20.64	0.1423	1450.7	10.003	0.08	892.20	8.9666E-05	5.13	5.06E-18
20 Aug 93	16:18	AS3d	6.602	1471.4	10.145	3.715	40.97	0.2825	20.48	0.1412	1450.9	10.004	0.10	1052.49	9.5013E-05	5.48	5.41E-18
20 Aug 93	17:13	AS3e	6.600	1470.9	10.142	3.668	40.45	0.2789	20.22	0.1394	1450.7	10.002	0.09	948.18	9.4919E-05	5.54	5.47E-18
AVERAGES		AS3		1471.4	10.145		41.18	0.2839	20.59	0.1419	1450.8	10.003			9.3551E-05	5.37	5.30E-18

Darcy's law: $K = (Q \cdot \mu \cdot L) / (\Delta P \cdot A)$

Parameter	Traditional Units	SI Units
Q = volumetric flow rate across A	9.355E-05 cm ³ /s	• 1.0E-6 m ³ /cm ³ 9.355E-11 m ³ /s
μ = fluid viscosity	1.29 cp	• 1.0E-3 Pa*sec/cp 1.29E-03 Pa*sec
L = sample length	10.117 cm	• 1.0E-2 m/cm 1.012E-01 m
ΔP = pressure drop across sample length	2.802 atm	• 1.013E+5 Pa/atm 2.838E+05 Pa
A = sample circular cross sectional area	81.233 cm ²	• 1.0E-4 m ² /cm ² 8.123E-03 m ²
K = specific permeability	5.36E-06 d	5.30E-18 m ²
	5.36E-03 md	
	5.36E+00 ud	

Steady State Liquid Permeability Data			
Project #:	8362	Target Eff.Stress:	2 Mpa 290.1 psid
Sample #:	C	Length:	10.043 cm
Stress Level #:	1	Diameter:	10.168 cm
		Area:	81.201 cm ²
Pressure Data Filename:	8362CL.S1B		
XDCR calibration factors:	Pc = 222.869 psig/volt	ΔP = 11.0272 psid/volt	

All measurements made at room temperature of ~23 °C and with 0 psig back pressure

Date	Time of Day	Regime #	Pc Confining Pressure			ΔP Differential Pressure			Pm Mean Pore Pressure ΔP/2		Effective Stress Pc-Pm		Volume Increment ml	Elapsed Time sec	Q Flow Rate ml/sec	K Permeability	
			volts	psig	MPa	volts	psid	MPa	psig	MPa	psid	MPa				μd	m ²
28 Aug 93	14:22	CS1a	1.430	318.7	2.197	5.303	58.48	0.4032	29.24	0.2016	289.5	1.996	0.09	968.22	9.2954E-05	3.73	3.68E-18
28 Aug 93	14:49	CS1b	1.431	318.9	2.199	5.311	58.57	0.4038	29.28	0.2019	289.6	1.997	0.10	1090.49	9.1702E-05	3.67	3.62E-18
28 Aug 93	15:24	CS1c	1.437	320.3	2.208	5.191	57.24	0.3947	28.62	0.1973	291.6	2.011	0.09	1007.17	8.9359E-05	3.66	3.61E-18
28 Aug 93	15:58	CS1d	1.432	319.1	2.200	5.033	55.50	0.3827	27.75	0.1913	291.4	2.009	0.09	1065.45	8.4471E-05	3.57	3.52E-18
28 Aug 93	16:36	CS1e	1.429	318.5	2.196	4.792	52.84	0.3643	26.42	0.1822	292.1	2.014	0.09	1095.34	8.2166E-05	3.65	3.60E-18
AVERAGES		CS1		319.1	2.200		56.53	0.3897	28.26	0.1949	290.8	2.005			8.8131E-05	3.65	3.61E-18

Darcy's law: $K = (Q \cdot \mu \cdot L) / (\Delta P \cdot A)$

Parameter	Traditional Units	SI Units
Q = volumetric flow rate accross A	8.813E-05 cm ³ /s	• 1.0E-6 m ³ /cm ³ 8.813E-11 m ³ /s
μ = fluid viscosity	1.29 cp	• 1.0E-3 Pa*sec/cp 1.29E-03 Pa*sec
L = sample length	10.043 cm	• 1.0E-2 m/cm 1.004E-01 m
ΔP = pressure drop across sample length	3.846 atm	• 1.013E+5 Pa/atm 3.896E+05 Pa
A = sample circular cross sectional area	81.201 cm ²	• 1.0E-4 m ² /cm ² 8.120E-03 m ²
K = specific permeability	3.66E-06 d	3.61E-18 m ²
	3.66E-03 md	
	3.66E+00 μd	

C-183

Steady State Liquid Permeability Data			
Project #:	8362	Target Eff.Stress:	6 Mpa 870.2 psid
Sample #:	C	Length:	10.043 cm
Stress Level #:	2	Diameter:	10.168 cm
		Area:	81.201 cm ²
Pressure Data Filename:	8362CL.S2A		
XDCR calibration factors:	Pc = 222.869 psig/volt	ΔP = 11.0272 psid/volt	Fluid: Odorless Mineral Spirit
		Viscosity	1.29 cp @ 23 °C

All measurements made at room temperature of ~23 °C and with 0 psig back pressure

Date	Time of Day	Regime #	Pc Confining Pressure			ΔP Differential Pressure			Pm Mean Pore Pressure ΔP/2		Effective Stress Pc-Pm		Volume Increment ml	Elapsed Time sec	Q Flow Rate ml/sec	K Permeability	
			volts	psig	MPa	volts	psid	MPa	psig	MPa	psid	MPa				μd	m ²
29 Aug 93	15:07	CS2a	4.017	895.3	6.173	4.611	50.85	0.3506	25.42	0.1753	869.8	5.997	0.06	1141.38	5.2568E-05	2.42	2.39E-18
29 Aug 93	16:01	CS2b	4.017	895.3	6.173	4.568	50.37	0.3473	25.19	0.1737	870.1	5.999	0.08	1561.78	5.1224E-05	2.38	2.35E-18
29 Aug 93	17:11	CS2c	4.017	895.3	6.173	4.539	50.05	0.3451	25.03	0.1725	870.2	6.000	0.10	1900.76	5.2611E-05	2.46	2.43E-18
30 Aug 93	16:43	CS2d	4.019	895.7	6.176	4.704	51.87	0.3576	25.94	0.1788	869.8	5.997	0.06	1128.34	5.3175E-05	2.40	2.37E-18
30 Aug 93	17:08	CS2e	4.020	895.9	6.177	4.728	52.14	0.3595	26.07	0.1797	869.9	5.998	0.06	1093.75	5.4857E-05	2.47	2.44E-18
AVERAGES		CS2		895.5	6.174		51.06	0.3520	25.53	0.1760	870.0	5.998			5.2887E-05	2.43	2.40E-18

Darcy's law: $K = (Q \cdot \mu \cdot L) / (\Delta P \cdot A)$

Parameter	Traditional Units	SI Units
Q = volumetric flow rate across A	5.289E-05 cm ³ /s	• 1.0E-6 m ³ /cm ³ 5.289E-11 m ³ /s
μ = fluid viscosity	1.29 cp	• 1.0E-3 Pa*sec/cp 1.29E-03 Pa*sec
L = sample length	10.043 cm	• 1.0E-2 m/cm 1.004E-01 m
ΔP = pressure drop across sample length	3.474 atm	• 1.013E+5 Pa/atm 3.519E+05 Pa
A = sample circular cross sectional area	81.201 cm ²	* 1.0E-4 m ² /cm ² 8.120E-03 m ²
K = specific permeability	2.43E-06 d	2.40E-18 m ²
	2.43E-03 md	
	2.43E+00 μd	

C-184

Steady State Liquid Permeability Data			
Project #:	8362	Target Eff. Stress:	10 Mpa 1450.4 psid
Sample #:	C	Length:	10.043 cm
Stress Level #:	3	Diameter:	10.168 cm
		Area:	81.201 cm ²
Pressure Data Filename:	8362CL.S3A		
XDCR calibration factors:	Pc = 222.869 psig/volt	AP =	11.0272 psid/volt

All measurements made at room temperature of ~23 °C and with 0 psig back pressure

Date	Time of Day	Regime #	Pc Confining Pressure			ΔP Differential Pressure			Pm Mean Pore Pressure		Effective Stress		Volume Increment	Elapsed Time	Q Flow Rate	K Permeability	
			volts	psig	MPa	volts	psid	MPa	psig	MPa	psid	MPa				ml	sec
01 Sep 93	15:50	CS3a	6.623	1476.1	10.177	4.626	51.01	0.3517	25.51	0.1759	1450.6	10.001	0.08	1968.85	4.0633E-05	1.87	1.84E-18
01 Sep 93	16:25	CS3b	6.624	1476.3	10.179	4.571	50.41	0.3475	25.20	0.1738	1451.1	10.005	0.10	2460.06	4.0649E-05	1.89	1.87E-18
01 Sep 93	17:22	CS3c	6.620	1475.4	10.172	4.537	50.03	0.3449	25.02	0.1725	1450.4	10.000	0.08	2073.88	3.8575E-05	1.81	1.78E-18
01 Sep 93	17:59	CS3d	6.621	1475.6	10.174	4.502	49.64	0.3423	24.82	0.1711	1450.8	10.003	0.08	2080.34	3.8455E-05	1.82	1.79E-18
01 Sep 93	18:40	CS3e	6.618	1474.9	10.169	4.473	49.32	0.3401	24.66	0.1700	1450.3	9.999	0.08	2133.20	3.7502E-05	1.78	1.76E-18
AVERAGES		CS3		1475.7	10.174		50.08	0.3453	25.04	0.1727	1450.6	10.002			3.9163E-05	1.83	1.81E-18

Darcy's law: $K = (Q \cdot \mu \cdot L) / (\Delta P \cdot A)$

Parameter	Traditional Units	SI Units
Q = volumetric flow rate across A	3.916E-05 cm ³ /s	• 1.0E-6 m ³ /cm ³ 3.916E-11 m ³ /s
μ = fluid viscosity	1.29 cp	* 1.0E-3 Pa*sec/cp 1.29E-03 Pa*sec
L = sample length	10.043 cm	* 1.0E-2 m/cm 1.004E-01 m
ΔP = pressure drop across sample length	3.408 atm	* 1.013E+5 Pa/atm 3.452E+05 Pa
A = sample circular cross sectional area	81.201 cm ²	* 1.0E-4 m ² /cm ² 8.120E-03 m ²
K = specific permeability	1.83E-06 d	1.81E-18 m ²
	1.83E-03 md	
	1.83E+00 μd	

Steady State Liquid Permeability Data			
Project #:	8362	Target Eff.Stress:	2 Mpa 290.1 psid
Sample #:	F	Length:	10.029 cm
Stress Level #:	1	Diameter:	10.170 cm
		Area:	81.233 cm ²
Pressure Data Filename:	8362FL.S1B		
XDCR calibration factors:	Pc = 222.663 psig/volt	ΔP = 11.0303 psid/volt	Fluid: Odorless Mineral Spirit
			Viscosity 1.29 cp @ 23 °C

All measurements made at room temperature of ~23 °C and with 0 psig back pressure

Date	Time of Day	Regime #	Pc Confining Pressure			ΔP Differential Pressure			Pm Mean Pore Pressure ΔP/2		Effective Stress Pc-Pm		Volume Increment ml	Elapsed Time sec	Q Flow Rate ml/sec	K Permeability	
			volts	psig	MPa	volts	psid	MPa	psig	MPa	psid	MPa				μd	m ²
14 Oct 93	13:05	FS1a	1.510	336.2	2.318	8.462	93.34	0.6435	46.67	0.3218	289.6	1.996	0.10	2268.77	4.4077E-05	1.11	1.09E-18
14 Oct 93	13:51	FS1b	1.522	338.9	2.337	8.469	93.42	0.6441	46.71	0.3220	292.2	2.015	0.10	2227.37	4.4896E-05	1.12	1.11E-18
14 Oct 93	14:47	FS1c	1.513	336.9	2.323	8.430	92.99	0.6411	46.49	0.3206	290.4	2.002	0.10	2481.42	4.0300E-05	1.01	1.00E-18
14 Oct 93	16:28	FS1d	1.508	335.8	2.315	8.376	92.39	0.6370	46.19	0.3185	289.6	1.997	0.10	2419.16	4.1337E-05	1.05	1.03E-18
14 Oct 93	17:13	FS1e	1.511	336.4	2.320	8.344	92.04	0.6346	46.02	0.3173	290.4	2.002	0.10	2459.29	4.0662E-05	1.03	1.02E-18
AVERAGES		FS1		336.8	2.322		92.83	0.6401	46.42	0.3200	290.4	2.002			4.2254E-05	1.07	1.05E-18

Darcy's law: $K = (Q \cdot \mu \cdot L) / (\Delta P \cdot A)$

Parameter	Traditional Units	SI Units
Q = volumetric flow rate across A	4.225E-05 cm ³ /s	• 1.0E-6 m ³ /cm ³ 4.225E-11 m ³ /s
μ = fluid viscosity	1.29 cp	• 1.0E-3 Pa*sec/cp 1.29E-03 Pa*sec
L = sample length	10.029 cm	• 1.0E-2 m/cm 1.003E-01 m
ΔP = pressure drop across sample length	6.317 atm	• 1.013E+5 Pa/atm 6.399E+05 Pa
A = sample circular cross sectional area	81.233 cm ²	• 1.0E-4 m ² /cm ² 8.123E-03 m ²
K = specific permeability	1.07E-06 d	1.05E-18 m ²
	1.07E-03 md	
	1.07E+00 μd	

C-186

Steady State Liquid Permeability Data			
Project #:	8362	Target Eff. Stress:	6 Mpa 870.2 psid
Sample #:	F	Length:	10.029 cm
Stress Level #:	2	Diameter:	10.170 cm
		Area:	81.233 cm ²
Pressure Data Filename:	8362FL.S2A		
XDCR calibration factors:	Pc =	222.663 psig/volt	ΔP = 11.0303 psid/volt

All measurements made at room temperature of ~23 °C and with 0 psig back pressure

Date	Time of Day	Regime #	Pc Confining Pressure			ΔP Differential Pressure			Pm Mean Pore Pressure		Effective Stress		Volume Increment	Elapsed Time	Q Flow Rate	K Permeability	
			volts	psig	MPa	volts	psid	MPa	psig	MPa	psid	MPa				μd	m ²
16 Oct 93	11:59	FS2a	4.119	917.1	6.324	8.367	92.29	0.6363	46.15	0.3182	871.0	6.005	0.09	3705.41	2.4289E-05	0.616	6.08E-19
16 Oct 93	13:05	FS2b	4.121	917.6	6.327	8.551	94.32	0.6503	47.16	0.3252	870.4	6.001	0.08	3230.25	2.4766E-05	0.615	6.07E-19
16 Oct 93	14:02	FS2c	4.123	918.0	6.330	8.564	94.46	0.6513	47.23	0.3257	870.8	6.004	0.09	3557.91	2.5296E-05	0.627	6.19E-19
16 Oct 93	15:05	FS2d	4.124	918.3	6.331	8.560	94.42	0.6510	47.21	0.3255	871.1	6.006	0.07	2719.19	2.5743E-05	0.638	6.30E-19
16 Oct 93	15:55	FS2e	4.123	918.0	6.330	8.552	94.33	0.6504	47.17	0.3252	870.9	6.004	0.06	2392.26	2.5081E-05	0.622	6.14E-19
16 Oct 93	16:39	FS2f	4.121	917.6	6.327	8.549	94.30	0.6502	47.15	0.3251	870.4	6.002	0.06	2406.01	2.4938E-05	0.619	6.11E-19
AVERAGES		FS2		917.8	6.328		94.02	0.6482	47.01	0.3241	870.8	6.004			2.5019E-05	0.623	6.15E-19

Darcy's law: $K = (Q \cdot \mu \cdot L) / (\Delta P \cdot A)$

Parameter	Traditional Units	SI Units
Q = volumetric flow rate across A	2.502E-05 cm ³ /s	• 1.0E-6 m ³ /cm ³ 2.502E-11 m ³ /s
μ = fluid viscosity	1.29 cp	• 1.0E-3 Pa*sec/cp 1.29E-03 Pa*sec
L = sample length	10.029 cm	• 1.0E-2 m/cm 1.003E-01 m
ΔP = pressure drop across sample length	6.398 atm	• 1.013E+5 Pa/atm 6.481E+05 Pa
A = sample circular cross sectional area	81.233 cm ²	• 1.0E-4 m ² /cm ² 8.123E-03 m ²
K = specific permeability	6.23E-07 d	6.15E-19 m ²
	6.23E-04 md	
	6.23E-01 μd	

C-187

Steady State Liquid Permeability Data			
Project #:	8362	Target Eff.Stress:	10 Mpa 1450.4 psid
Sample #:	F	Length:	10.029 cm
Stress Level #:	3	Diameter:	10.170 cm
		Area:	81.233 cm ²
Pressure Data Filename:	8362FL.S3A		
XDCR calibration factors:	Pc = 222.663 psig/volt	ΔP =	11.0303 psid/volt

All measurements made at room temperature of ~23 °C and with 0 psig back pressure

Date	Time of Day	Regime #	Pc Confining Pressure			ΔP Differential Pressure			Pm Mean Pore Pressure		Effective Stress		Volume Increment	Elapsed Time	Q Flow Rate	K Permeability	
			volts	psig	MPa	volts	psid	MPa	psig	MPa	psid	MPa				ml	sec
18 Oct 93	13:49	FS3a	6.729	1498.3	10.330	8.551	94.32	0.6503	47.16	0.3252	1451.1	10.005	0.05	2326.95	2.1487E-05	0.533	5.26E-19
18 Oct 93	14:37	FS3b	6.725	1497.4	10.324	8.575	94.58	0.6521	47.29	0.3261	1450.1	9.998	0.08	3757.42	2.1291E-05	0.527	5.20E-19
18 Oct 93	15:44	FS3c	6.729	1498.3	10.330	8.588	94.73	0.6531	47.36	0.3266	1450.9	10.004	0.06	2863.16	2.0956E-05	0.518	5.11E-19
18 Oct 93	16:37	FS3d	6.727	1497.9	10.327	8.592	94.77	0.6534	47.39	0.3267	1450.5	10.001	0.04	1947.66	2.0537E-05	0.507	5.01E-19
19 Oct 93	10:39	FS3e	6.726	1497.6	10.326	8.556	94.38	0.6507	47.19	0.3253	1450.4	10.000	0.08	3976.81	2.0117E-05	0.499	4.93E-19
19 Oct 93	12:05	FS3f	6.732	1499.0	10.335	8.556	94.38	0.6507	47.19	0.3253	1451.8	10.010	0.09	4270.68	2.1074E-05	0.523	5.16E-19
19 Oct 93	13:34	FS3g	6.726	1497.6	10.326	8.576	94.60	0.6522	47.30	0.3261	1450.3	10.000	0.07	3222.61	2.1722E-05	0.537	5.31E-19
AVERAGES		FS3		1498.0	10.328		94.54	0.6518	47.27	0.3259	1450.7	10.003			2.1026E-05	0.521	5.14E-19

Darcy's law: $K = (Q \cdot \mu \cdot L) / (\Delta P \cdot A)$

Parameter	Traditional Units	SI Units
Q = volumetric flow rate across A	2.103E-05 cm ³ /s	* 1.0E-6 m ³ /cm ³ 2.103E-11 m ³ /s
μ = fluid viscosity	1.29 cp	* 1.0E-3 Pa*sec/cp 1.29E-03 Pa*sec
L = sample length	10.029 cm	* 1.0E-2 m/cm 1.003E-01 m
ΔP = pressure drop across sample length	6.433 atm	* 1.013E+5 Pa/atm 6.516E+05 Pa
A = sample circular cross sectional area	81.233 cm ²	* 1.0E-4 m ² /cm ² 8.123E-03 m ²
K = specific permeability	5.21E-07 d	5.14E-19 m ²
	5.21E-04 md	
	5.21E-01 μd	

C-188

Appendix D.
Marker Bed 139 Brine Recipe Documentation

The following information is provided as Appendix D of this document.

Appendix D

Marker Bed 139 Brine Recipe Documentation

Errata Sheet

The following modifications should be made to the reference citations in Appendix D.

Page No.	Change
D-3	the existence of Lab Notebook No. WIPP 04 could not be verified
D-4	the existence of Lab Notebook No. WIPP 02 could not be verified
D-10	the existence of Lab Notebook No. WIPP 04 could not be verified
D-10	the existence of Lab Notebook No. WIPP 02 could not be verified
D-14	the existence of Lab Notebook No. WIPP 04 could not be verified
D-14	the existence of Lab Notebook No. WIPP 02 could not be verified
D-29	the existence of the Chem-Nuclear Geotech reports could not be verified
D-29	Felmy and Weare, 1986 is in Vol. 50, no. 12; copy on file in SWCF as WPO#30421
D-29	copy of Finley et al., 1992 on file in SWCF as WPO#26222
D-30	Harvie and Weare, 1980 is in Vol. 44, no. 7; copy on file in SWCF as WPO#30423
D-30	in Harvie et al, 1984 "Strengths" is plural in the title; paper is in Vol. 48, no. 4; copy on file in SWCF as WPO#30422
D-30	copy of Krumhansl et al., 1991 on file in SWCF as WPO#27786
D-30	copy of McCaffrey et al., 1987 on file in SWCF as WPO#42577
D-30	the existence of the UNC Geotech Analytical Laboratory report could not be verified

Date: 27 March 1993
To: Craig Novak, 6119; and Susan Howarth, 6119
Karen Robinson
From: Karen Robinson, 6119
Subject: Status Report on the Preparation of Standard Brines SB-139-A and SB-139-95A

SUMMARY

In February, I prepared 100-ml batches of two synthetic brines. SB-139-A has a composition close to that of an "average" QPB brine and is expected to be saturated with respect to the minerals in Marker Bed 139. SB-139-95A is expected to be slightly undersaturated because the element concentrations are about 95% of those in the first brine. I have calculated the probable compositions of those brines based on the masses of salts used.

I have not yet measured the pH of either brine, but expect to do so by the first week of April. I have not yet confirmed the compositions of the brines by chemical analyses; I hope this will be done in early April.

In the following paragraphs I give some details about the recipes, my procedure, problem areas and recommendations, and what remains to be done.

RECIPES

Craig Novak supplied a recipe for an average QPB brine. Table 1a shows his recipe (amounts of salts needed for 1 liter of brine) as well as the amounts needed for 100 mL of brine (saturated) and the amounts needed for 100 mL of "95%" brine. Table 1b shows the average QPB composition (target composition), the calculated composition based on the "saturated" recipe, and the calculated composition based on the "95%" recipe.

Table 2a shows the masses of salts used (weighed out) for the two brines. Table 2b shows the calculated compositions of those two brines based on the masses of salts used.

PROCEDURE

Detailed notes about my procedure are in my lab notebook (Lab Notebook No. WIPP 04, pp.6-12).

Reagents

Reagent grade salts were used. Some of these (magnesium sulfate, sodium chloride, sodium bromide, and sodium tetraborate) had been dried in the lab oven at 110°C and stored in a desiccator (by S. Yeh or J. Kelly). Others (calcium chloride dihydrate, magnesium chloride hexahydrate, and potassium chloride) were used "as is" from the bottle.

Deionized water from the Barnstead Nanopure A deionizer was used.

Equipment

Reagents were weighed out using the Mettler AE163 balance. The balance was calibrated before use with the internal calibration weight. The calibration was checked with selected standard weights. Details can be found in the balance log book (Lab Notebook No. WIPP 02, p. 24).

Glassware included a 100-mL class-A volumetric flask, glass beakers, and watchglasses.

Plasticware included weighing boats, 125-mL polyethylene bottles, a small plastic funnel, and a teflon stirring rod (which also served as a boiling stick when solutions were heated).

Other equipment included a Thermolyne Nuova 7 stir plate; a Bransonic Ultrasonic bath; a Nalgene hand-operated vacuum pump; a Nalgene filter holder with receiver (Nalge Cat. No. 300-4000); Whatman filter paper (grade 41, size 4.7 cm).

Preparation

In brief, the required amounts of salts were dissolved in deionized water, the volume was adjusted to 100mL in the volumetric flask, and the solution was filtered and transferred to a polyethylene bottle for storage. The step-by-step details for each solution are in Attachment 1.

In practice, preparing saturated and near-saturated solutions is somewhat challenging. Problem areas are discussed below.

PROBLEM AREAS/RECOMMENDATIONS

To prepare a standard solution, one usually dissolves the salt (or salts) in deionized water in a beaker and keeps the volume less than (perhaps half or three-quarters of) the final desired volume. This concentrated solution is then allowed to cool (if necessary) and is transferred quantitatively to the appropriate size volumetric flask. This won't work with a saturated solution. One ends up trying to quantitatively transfer the solution plus the undissolved stuff (a kind of wet slush). Under these conditions it is difficult to be certain that everything was rinsed out of the beaker.

Alternatively, one can put the dry salts directly into the volumetric, add water (a little less than the final desired amount), shake the flask occasionally (to speed mixing), and wait patiently for the salts to dissolve. The problem encountered with the 100-mL volumetric flask was that because of the narrow neck, the salts wouldn't flow freely into the flask; more than 100 mL of water were needed to get all the salts into the flask!

Another problem I noted was that after the volumetric flask was inverted to mix the contents, the brine didn't drain cleanly from the stopper or the neck of the flask. Droplets clung to the neck and eventually salt precipitated out. (The amounts were small and apparently immediately redissolved when the flask was shaken or inverted to mix the contents.) Also, droplets clung to the ground glass stopper, which had to be left ajar to avoid being "cemented" in place.

Recommendation

Attachment 2 gives the procedure that I would try next, if I were asked to prepare another batch.

WORK REMAINING

I still need to measure the pH of the solutions and adjust them to ~6.1 if necessary. I also need to confirm the brine compositions by chemical analysis.

Measurement/Adjustment of pH

I plan to use the Sentron Model 2001 pH System to check the pH of the samples. With this system I can use as little as one drop of solution. This will both conserve the solution and reduce the chance of contamination. If necessary, I'll use reagent grade HCl and NaOH to adjust the pH to ~6.1.

Chemical Analyses

Cations (B, Ca, K, Mg, and Na) will be determined by ICP-MS by Jeff Reich (1824). Anions (Br, Cl, SO₄, and perhaps HCO₃) will be determined by ion chromatography by John Kelly (6119). Fred will pay for the ICP-MS analyses. I will need to dilute the samples to the appropriate concentration ranges for these analyses.

With both of these analytical techniques, the time-consuming (and therefore expensive) part of the procedure is the instrument set-up and calibration. For efficiency, therefore, these brines will be run along with a number of Fred Gelbard's Culebra brines.

I need to do the following: 1) calculate dilutions factors for the SB-139 brines and for Fred's Culebra brines, 2) meet with John to select some of Fred's brines based on the Cl and SO₄ results (John has both the brines and the data), 3) check with Fred to see if he agrees with our selections, 4) check with Jeff Reich to find out when he can do the cation analyses, 5) dilute the samples for cation analyses the morning they will be run, 6) find out when John will be running the IC again, 7) dilute the SB-139 samples for anion analyses.

\karen\misc\sb-139-a.1

copy to: 6119 K. L. Robinson

TABLE 1a: Recipes -- Amounts of Salts Needed

Salt	Amount needed for 1 liter of "saturated" soln (grams)	Amount needed for 100 mL of "saturated" soln (grams)	Amount needed for 100 mL of "95%" solution (grams)
NaHCO ₃	0.00133547	0.000134	0.000127
CaCl ₂ ·2H ₂ O	1.27954	0.12795	0.12156
MgSO ₄	19.92105	1.99210	1.89250
MgCl ₂ ·6H ₂ O	130.606	13.0606	12.4076
KCl	32.395	3.2395	3.0775
NaCl	204.105	20.4105	19.3900
Na ₂ B ₄ O ₇	7.0024	0.70024	0.66523
NaBr	1.87565	0.18756	0.17819

Table 1b: Brine Compositions -- Target and Calculated

Species	Target Comp. Average QPB (mg/L)	Calc'd Comp. "Sat'd" Recipe (mg/L)	Calc'd Comp. "95%" Recipe (mg/L)
HC03	0.970	0.970	0.922
Cl	192171	185391	176121
S04	15898	15898	15103
Na	82315	82315	78199
K	16990	16990	16141
Ca	348.8	348.8	331.4
Mg	19641	19641	18659
B	1505	1505	1430
Br	1457	1457	1384

TABLE 2a: Actual Amounts of Salts Used (Weighed Out)

Salt	Amount used for 100 mL of "saturated" soln (grams)	Amount used for 100 mL of "95%" solution (grams)
NaHCO ₃	0*	0*
CaCl ₂ ·2H ₂ O	0.1284	0.1218
MgSO ₄	1.9921	1.8907
MgCl ₂ ·6H ₂ O	13.0605	12.4072
KCl	3.2412	3.0783
NaCl	20.4109	19.3903
Na ₂ B ₄ O ₇	0.7027	0.66574
NaBr	0.1875	0.1789

* don't have appropriate equipment to accurately measure 0.00013 g of a salt.

Table 2b: Calculated Brine Compositions*

Species	SB-139-A ("Sat'd" Recipe) (mg/L)	SB-139-95A ("95%" Recipe) (mg/L)
HCO ₃	-**	-**
Cl	185390	176120
SO ₄	15890	15080
Na	82320	78200
K	17000	16140
Ca	350	330
Mg	19640	18660
B	1510	1430
Br	1460	1390

* concentrations rounded to nearest 10 mg/L.

** probably equilibrated with atmosphere.

ATTACHMENT 1: Preparation of SB-139-A and SB-139-95A (aka "Dear Diary")

Preparation of SB-139-A

- 02/04/93: Weighed Na₂B₄O₇. Transferred quantitatively to 150 mL beaker with DI water; adjusted volume to ~50 mL; placed in ultrasonic bath ~30 min.
- 02/05/93: Na₂B₄O₇ dissolved overnight. Transferred solution to 100-mL vol. flask. Weighed other salts (CaCl₂·2H₂O, MgCl₂·6H₂O, KCl, NaBr, MgSO₄, NaCl) and transferred to vol. flask. Salts wouldn't dissolve (flask too full to mix and volume >100 mL), so transferred contents of flask to 250-mL beaker and adjusted volume to ~200 mL. Covered with evaporating watchglass and heated gently to dissolve salts. Salts dissolved in ~30 min. Removed watchglass and continued heating to reduce volume. Left covered overnight (not on hot plate).
- 02/08/93: Continued evaporating, uncovered, on hot plate. Reduced volume to ~100 mL. Removed from heat; rinsed walls of beaker with a few mLs of DI water. Left covered overnight.
- 02/09/93: Continued evaporating, uncovered, on hot plate. Reduced volume to ~75 mL (solution plus precipitates). Removed from heat; rinsed walls of beaker with a few mLs of DI water. Left to cool, covered. Transferred contents of beaker to 100-mL vol. flask. A thin cloudy residue remained in the bottom of the beaker. (It wouldn't rinse out, but scrubbed out easily with Alconox and a bottle brush.) Diluted contents of vol. flask to ~99 mL. Left stoppered overnight.
- 02/10/93: Significant quantity of undissolved salt in flask. Inverted several times to mix. Added DI water to within ~2 mm of mark on flask.
- 02/16/93: Salts appeared dissolved but solution was cloudy. Diluted to mark. Inverted to mix. Cleaned 125-mL poly. bottle by soaking in DI water for ~3 hrs. Left to air-dry overnight.
- 02/17/93: Filtered solution through Whatman 41 filter paper. Transferred to clean, dry poly. bottle. Labelled "SB-139-A"; dated 2/17/93.

Preparation of SB-139-95A

- 02/17/93: Weighed Na₂B₄O₇. Transferred quantitatively to 150 mL beaker with DI water; adjusted volume to ~50 mL. Left covered with watch glass.
- 02/18/93: Na₂B₄O₇ dissolved overnight. Weighed other salts (CaCl₂·2H₂O, MgCl₂·6H₂O, KCl, NaBr, MgSO₄, NaCl) and transferred to beaker with Na₂B₄O₇ solution. Put on hot plate to reduce volume to ~80 mL. Rinsed beaker walls with a few mL of DI water. Left covered overnight (not on hot plate).
- 02/19/93: Transferred contents of beaker to 100-mL vol. flask. (Spilled a few mL of the final rinse water -- shouldn't measurably affect final concentrations.) Diluted almost to mark (~5 mm below line). Shook to mix.
- 02/22/93: Small amount of salt remained undissolved. Added a little more DI water.
- 02/23/93: Everything dissolved. Diluted to mark. Mixed. Filtered through Whatman 41 filter paper. Transferred to clean, dry poly. bottle. Labelled "SB-139-95A"; dated 2/23/93.

ATTACHMENT 2: Recommendation

If I were to prepare another batch I would try the following:

- Prepare a larger batch (500 mL or 1 L). This allows the use of a flask with a wider neck.
- Be sure the volumetric flask is clean and dry.
- Transfer the salts to the flask. Use a powder funnel (wide stem) and, if needed, a teflon stirring rod. Save the weighing containers (boats or whatever the salts were in) but don't rinse them yet.
- After all the salts have been transferred (except for the small amounts of residue in the weighing containers), rinse the stirring rod, then the weighing containers, and finally the funnel with deionized water. All rinse water should go into the flask. This ensures that the salts were transferred quantitatively.
- Add deionized water to the flask to just below the neck. Mix the contents by gently swirling the flask (don't invert to mix). Wait patiently for salts to dissolve, swirling occasionally (every half-hour or so during the day).
- When no more salts appear to dissolve (probably after a day or two), add deionized water to within 1 or 2 cm of the mark on the neck of the flask. Mix by tipping the flask. Avoid allowing the solution to touch the stopper. The stopper will not drain completely and is likely to get "cemented" in place by tiny salt crystals.
- Eventually, everything should dissolve (this could take several days). At this point, adjust to the final volume with deionized water, mix the solution thoroughly by inverting the flask, and transfer the solution immediately to a clean, dry plastic bottle.

If this doesn't work, I have some other ideas to try.

Date: 07 June 1993
To: Susan Howarth, 6119
Karen Robinson
From: Karen Robinson, 6119
Subject: Preparation of Standard Brine SB-139-95B

SUMMARY

This memo describes the preparation of the standard brine SB-139-95B. I am giving quite a bit of detail in case you want to use this to generate a brine-preparation procedure for future use. In brief, I prepared 1 liter of brine, adjusted the pH to ~6.1 with HCl, and split the brine into two 500-mL lots. You sent one bottle to Chem Nuclear Geotech for analysis; the other bottle is being stored in 823/2079.

RECIPE

Craig Novak supplied a recipe for an average QPB brine, a brine expected to be saturated with respect to the minerals in Marker Bed 139. The brine described here is slightly undersaturated and contains 95% of the salts recommended by Craig.

Table 1a shows the "95%" recipe and the amounts of salts actually weighed out. Table 1b shows the calculated composition based on the "95%" recipe and the calculated composition based on the amounts of salts actually weighed out.

PROCEDURE

Detailed notes about the preparation are in my lab notebook (Lab Notebook No. WIPP 04, pp.21-23); those notes are summarized in Attachment 1.

Reagents

Reagent grade salts were used. All salts were used "as is" from the bottle (that is, they were not dried in the lab oven).

Deionized water from the Barnstead Nanopure A deionizer was used.

Standard pH buffer solutions were prepared from pHDrion buffer capsules.

Trace-metal grade hydrochloric acid was used to adjust the pH.

Equipment

Reagents were weighed out using the Mettler AE163 balance. The balance was calibrated before use with the internal calibration weight. The calibration was checked with selected standard weights. Details can be found in the balance log book (Lab Notebook No. WIPP 02, p. 25).

Glassware included a 1000-mL class-A volumetric flask and a powder funnel.

Plasticware included weighing boats, 500-mL polyethylene bottles, various plastic beakers, and a teflon stirring rod.

Other equipment included a Thermolyne Nuova 7 stir plate; a magnetic stir bar and stir-bar retriever; and a Sentron model 2001 pH system (meter and probe).

Preparation

In brief, the required amounts of salts were dissolved in deionized water in the volumetric flask; dissolution was speeded by using the magnetic stirrer. The volume was adjusted to 1000 mL in the volumetric flask. The pH was then adjusted by adding ~4 mL of HCl. The solution was then transferred to two 500-mL polyethylene bottles. The step-by-step details are in Attachment 1.

Note that although the final volume of the solution was ~1004 mL (after the pH was adjusted), I used a volume of 1000 mL to calculate the concentrations of the solutes.

WORK REMAINING

As we discussed, I will also prepare one liter of the "saturated" recipe. This work has been delayed somewhat because there wasn't enough NaCl in the lab. More was ordered and has recently arrived. I expect to have the brine prepared and the memo documenting its preparation written by Friday, June 18.

\karen\misc\s-b-139-b.1

copy to: 6119 C. F. Novak
6119 K. L. Robinson

TABLE 1a: Recipes -- Amounts of Salts Needed and Weighed Out

Salt	Amount needed for 1 liter of "95%" soln (grams)	Amount weighed out for SB-139-95B (grams)
NaHCO ₃	0.00127	*
CaCl ₂ ·2H ₂ O	1.2156	1.2144
MgSO ₄	18.9250	18.9238
MgCl ₂ ·6H ₂ O	124.076	124.0775
KCl	30.7753	30.7727
NaCl	193.8998	193.8973
Na ₂ B ₄ O ₇	6.6523	6.6519
NaBr	1.7819	1.7837

* Don't have appropriate equipment to accurately measure 0.00127 g of a salt.

Table 1b: Brine Compositions -- Target and Calculated

Species	Calc'd Comp. "95%" Recipe (mg/L)	Calc'd Comp SB-139-95B* (mg/L)
HCO ₃	0.922	**
Cl	176106	176100
SO ₄	15103	15100
Na	78198	78200
K	16141	16140
Ca	331	330
Mg	18657	18660
B	1430	1430
Br	1384	1390

* Concentrations rounded to nearest 10 mg/L.

** Probably equilibrated with atmosphere.

ATTACHMENT 1: Preparation of SB-139-95B

- 04/30/93: Put ~200 mL deionized water and small magnetic stir bar into 1000-mL volumetric flask.
Weighed Na₂B₄O₇; transferred quantitatively to vol. flask.
Began stirring. Stirred for ~3 hrs. Left standing over weekend.
Weighed other salts (CaCl₂·2H₂O, MgCl₂·6H₂O, KCl, NaCl, MgSO₄, NaBr) into plastic beakers. Covered with parafilm.
- 05/03/93: Resumed stirring.
Quantitatively transferred chloride salts (CaCl₂·2H₂O, MgCl₂·2H₂O, KCl, NaCl) to vol. flask.
Added deionized water to fill flask ~two-thirds.
Stirred ~2 hrs.
Quantitatively transferred remaining salts (MgSO₄, NaBr) to vol. flask.
Continued stirring. At end of work day turned off stirrer and left to stand overnight.
- 05/04/93: Removed stir bar with magnetic stir-bar retriever. Rinsed with deionized water, adding all rinse water to flask.
Diluted with deionized water to volume and inverted to mix thoroughly.
Calibrated pH system with standard buffers 7 and 4. Checked calibration with standard buffer 6.4.
Measured initial pH of solution as 7.0.
Alternately added aliquots of HCl, mixed the solution by inverting the vol. flask, and checked the pH of the solution. After ~4 mL of HCl were added (in 6 unequal increments) the pH of the solution was 6.14.
The final volume of the solution was ~1004 mL. Note that concentrations of solutes were calculated using a volume of 1000 mL. The solution was transferred to two 500-mL polyethylene bottles. One was given to S. Howarth for shipping to ChemNuclear Geotech for chemical analysis. The other is currently stored in 823/2079.

Date: 18 June 1993
To: Susan Howarth, 6119
From: *Karen Robinson*
Karen Robinson, 6119
Subject: Preparation of Standard Brine SB-139-B

SUMMARY

This memo describes the preparation of the standard brine SB-139-B. I am giving quite a bit of detail in case you want to use this to generate a brine-preparation procedure for future use. In brief, I prepared 1 liter of brine, adjusted the pH to ~6.1 with HCl, and split the brine into two 500-mL lots. I am giving one bottle to you for possible shipment to Chem Nuclear Geotech for analysis; the other bottle is being stored in 823/2079.

RECIPE

Craig Novak supplied a recipe for an average QPB brine, a brine expected to be saturated with respect to the minerals in Marker Bed 139.

Table 1a shows his recipe ("saturated solution") and the amounts of salts actually weighed out. Table 1b shows the calculated composition based on the recipe and the calculated composition based on the amounts of salts actually weighed out.

PROCEDURE

Detailed notes about the preparation are in my lab notebook (Lab Notebook No. WIPP 04, pp.26-27 & 34); those notes are summarized in Attachment 1.

Reagents

Reagent grade salts were used. All salts were used "as is" from the bottle (that is, they were not dried in the lab oven).

Deionized water from the Barnstead Nanopure A deionizer was used.

Standard pH buffer solutions were prepared from pHydrion buffer capsules.

Trace-metal grade hydrochloric acid was used to adjust the pH.

Equipment

Reagents were weighed out using the Mettler AE163 balance. The balance was calibrated before use with the internal calibration weight. The calibration was checked with selected standard weights. Details can be found in the balance log book (Lab Notebook No. WIPP 02, p. 25).

Glassware included a 1000-mL class-A volumetric flask and a powder funnel.

Plasticware included weighing boats, 500-mL polyethylene bottles, various plastic beakers, and a teflon stirring rod.

Other equipment included a Thermolyne Nuova 7 stir plate; a magnetic stir bar and stir-bar retriever; an adjustable Finnpiette (1-5 mL), and a Sentron model 2001 pH system (meter and probe).

Preparation

In brief, the required amounts of salts were dissolved in deionized water in the volumetric flask; dissolution was speeded by using the magnetic stirrer. The volume was adjusted to 1000 mL in the volumetric flask. The pH was then adjusted by adding ~4 mL of HCl. The solution was then transferred to two 500-mL polyethylene bottles. The step-by-step details are in Attachment 1.

Note that although the final volume of the solution was ~1004 mL (after the pH was adjusted), I used a volume of 1000 mL to calculate the concentrations of the solutes. Also, I ignored the HCl in calculating the chloride concentration.

\karen\misc\s-b-139-b.2

copy to: 6119 C. F. Novak
6119 K. L. Robinson

TABLE 1a: Recipes -- Amounts of Salts Needed and Weighed Out

Salt	Amount needed for 1 liter of "sat'd" soln (grams)	Amount weighed out for SB-139-B (grams)
NaHCO ₃	0.00134	*
CaCl ₂ ·2H ₂ O	1.27954	1.2790
MgSO ₄	19.92105	19.9259
MgCl ₂ ·6H ₂ O	130.606	130.6083
KCl	32.395	32.3960
NaCl	204.105	203.1150
Na ₂ B ₄ O ₇	7.0024	7.0018
NaBr	1.87565	1.8745

* Don't have appropriate equipment to accurately measure 0.00013 g of a salt.

Table 1b: Brine Compositions -- Target and Calculated

Species	Calc'd Comp. "Sat'd" Recipe (mg/L)	Calc'd Comp SB-139-B* (mg/L)
HCO ₃	0.970	**
Cl	185391	184770
SO ₄	15898	15900
Na	82315	81920
K	16990	16990
Ca	349	350
Mg	19641	19640
B	1505	1500
Br	1457	1460

* Concentrations rounded to nearest 10 mg/L.

** Probably equilibrated with atmosphere.

ATTACHMENT 1: Preparation of SB-139-B

- 05/21/93: Put ~200 mL deionized water and small magnetic stir bar into 1000-mL volumetric flask.
Discovered shortage of salts (NaCl, possibly KCl) in lab. Postponed further work until they arrive. Covered vol. flask.
- 06/10/93: Weighed Na₂B₄O₇; transferred quantitatively to vol. flask.
Began stirring. Stirred for ~3 hrs. Left standing over night.
Weighed other salts (CaCl₂·2H₂O, MgCl₂·6H₂O, KCl, NaCl, MgSO₄, NaBr) into plastic beakers. Covered with parafilm.
- 06/11/93: Resumed stirring.
Quantitatively transferred chloride salts (CaCl₂·2H₂O, MgCl₂·2H₂O, KCl, NaCl) to vol. flask.
Added deionized water to fill flask ~two-thirds.
Stirred ~1 hr. Let sit over weekend.
- 06/14/93: Resumed stirring.
Quantitatively transferred remaining salts (MgSO₄, NaBr) to vol. flask. Added deionized water until base of flask was almost full.
Continued stirring. At end of work day turned off stirrer and left to stand overnight.
- 06/15/93: Continued stirring. Let sit overnight.
- 06/16/93: Continued stirring. Left stirring overnight.
- 06/17/93: Stopped stirring.
Removed stir bar with magnetic stir-bar retriever. Rinsed with deionized water, adding all rinse water to flask.
Diluted with deionized water to volume and inverted to mix thoroughly.
- 06/18/93: Calibrated pH system with standard buffers 7 and 4. Checked calibration with standard buffer 6.4.
Measured initial pH of solution as 7.04.
Added 4.0 mL of trace-metal grade HCl, mixed the solution by inverting the vol. flask several times, and checked the pH of the solution. The final pH of the solution was 6.15.
The final volume of the solution was ~1004 mL. Note that concentrations of solutes were calculated using a volume of 1000 mL.
The solution was transferred to two 500-mL polyethylene bottles. One was given to S. Howarth for possible shipment to ChemNuclear Geotech for chemical analysis. The other is currently stored in 823/2079.



Sandia National Laboratories

MANAGED BY MARTIN MARIETTA CORPORATION
FOR THE U. S. DEPARTMENT OF ENERGY

P. O. BOX 5800
ALBUQUERQUE, NEW MEXICO 87185-1320

date: 26 April 1994

to: Susan M. Howarth, Dept. 6115, MS 1324, 848-0676

from: Craig F. Novak, Dept. 6119, MS 1320, 848-0619

subject: Formulation and Recipe for a "Standard" Marker Bed 139 Brine

A standard brine with little or no potential to dissolve rock from Marker Bed 139 was needed for flow experiments. This memo documents the process used to develop a composition for this standard brine, which will be given the name SB-139-B.

The brines collected in the QPB boreholes in the Q-access drift (Finley et al., 1992) are believed to represent brines from Marker Bed 139. If this is indeed the case, these brine compositions should be in equilibrium with the solids in the marker bed, and thus should not dissolve marker bed material. Chemical analyses of 20 brine samples from these boreholes are available, collected between October 1989 and July 1992. Discussion of these and other Salado brine samples can be found in the memo "Evaluation of Chemical Analysis Data of Brine Samples from the Small Scale Brine Inflow Experiments," by Novak, dated 17 June 1993; modified 26 July 1993. The results of the analyses are listed in Table 1, along with an arithmetic average of the element concentrations, in mM and mg/L. This average concentration was used by K.L. Robinson to develop a recipe from which to synthesize SB-139-Brine. Although it cannot be guaranteed that this brine will not cause dissolution of MB139 material, this is a reasonable brine composition for simulating brine from Marker Bed 139.

Reference

Finley, S.J., D.J. Hanson, and R. Parsons. 1992. *Small-Scale Brine Inflow Experiments—Data Report Through 6/6/91*. SAND91-1956. Albuquerque, New Mexico: Sandia National Laboratories.

Table 1. Concentrations used to determine “standard” MB139 composition.

Borehole	Collection Date	Analysis Report*	B, mM	Br, mM	Ca, mM	Cl, mM	K, mM	Mg, mM	Na, mM	SO4, mM
QPB 01	16-Aug-90	UNC3	138	18.1	7.53	5501	426	776	3463	160
QPB 01	20-Sep-90	UNC3	144	18.8	7.88	5614	448	817	3554	166
QPB 02	4-Oct-89	UNC2	139	18.5	7.93	5571	431	813	3596	166
QPB 02	13-Dec-89	UNC1	149	18.8	9.43	5529	453	866	3676	177
QPB 02	20-Jul-90	UNC3	144	18.8	7.83	5472	453	842	3493	165
QPB 02	16-Aug-90	UNC3	145	18.7	7.98	5444	458	819	3443	164
QPB 02	20-Sep-90	UNC3	144	18.6	10.17	5585	436	825	3637	166
QPB 03	16-Jan-90	UNC1	96	13.1	12.64	5487	312	611	4148	133
QPB 03	20-Jul-90	UNC3	140	18.6	7.78	5557	453	842	3633	169
QPB 03	16-Aug-90	UNC3	141	18.6	7.88	5416	460	809	3391	164
QPB 03	20-Sep-90	UNC3	146	18.6	7.68	5529	435	825	3493	165
QPB 04	27-Apr-90	UNC2	130	17.5	9.88	5501	399	767	3650	171
QPB 04	20-Jul-90	UNC3	143	18.6	7.58	5416	472	823	3435	165
QPB 04	16-Aug-90	UNC3	140	18.5	8.83	5501	451	821	3596	168
QPB 04	20-Sep-90	UNC3	144	18.6	11.17	5642	431	821	3639	169
QPB 05	27-Apr-90	UNC2	132	17.4	9.53	5529	409	784	3678	177
QPB 05	15-Jun-90	UNC2	137	18.2	8.03	5501	416	813	3537	164
QPB 05	20-Jul-90	UNC3	140	18.5	8.88	5585	451	821	3554	170
QPB 05	16-Aug-90	UNC3	146	18.8	7.83	5501	427	825	3430	165
QPB 05	20-Sep-90	UNC3	147	18.5	7.81	5360	460	823	3428	164
average, mM			139	18.2	8.71	5512	434	807	3574	165
average, mg/L			1505	1453	349	195419	16971	19618	82159	15888

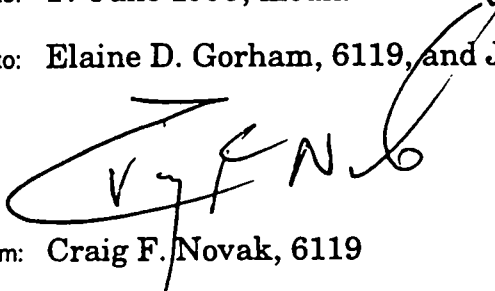
Sandia National Laboratories

Albuquerque, New Mexico 87185

date: 17 June 1993, modified 26 July 1993

to: Elaine D. Gorham, 6119, and J. Foesch, 6119

from: Craig F. Novak, 6119

A handwritten signature in black ink, appearing to read 'C. F. Novak', is written over the 'from:' line. The signature is stylized and somewhat cursive.

subject: Evaluation of Chemical Analysis Data of Brine Samples from the Small Scale Brine Inflow Experiments

Summary

This memorandum documents the chemical compositions of 51 Salado brine samples collected as part of the Small Scale Brine Inflow Experiments. The compositions were examined for trends with time, location, and borehole size, but few trends were found. Most of the observed variations in compositions can be explained by the hypothesis of equilibrium evaporation during brine accumulation. Brine compositions are consistent with published data from previous studies of Salado Formation brines.

Introduction

Salado brine samples have been collected as part of the Small-Scale Brine Inflow Experiments (SSBIE), which were intended to provide some understanding of brine flow and transport mechanisms within the Salado Formation. Some of these brine samples have been analyzed for major chemical constituents under the supposition that transport information might be gleaned from the brine compositions. This memorandum examines the chemical analysis data of these brines to determine what can and cannot be learned about Salado transport from

these chemical data. This memorandum does not examine brine inflow rates or borehole humidity data, and considers these quantities only peripherally as they impact interpretation of brine composition data. Comments and conclusions within this memorandum pertain only to the chemical component of the SSBIE, and have no implications for the strictly flow-related portion of these experiments.

The stratigraphic locations and orientations of the SSBIE boreholes are given in Figure 1. Ten boreholes are located in Room D in the north (experimental) end of the facility. Among the Room D boreholes, no brine has accumulated in DBT16 or DBT17. Brine has been withdrawn from all other Room D boreholes, including the nominally 4" diameter vertical boreholes DBT10, DBT11, DBT12, DBT13, DBT14, and DBT15, and from the vertical boreholes DBT31 and DBT32, which were nominally 4" in diameter when drilled, but were later enlarged to nominally 36" in diameter (Finley et al., 1992). Two subhorizontal boreholes from which brine has been sampled are located in the L4 drift, the nominally 4" diameter L4B01 and the nominally 36" diameter L4X01. Five boreholes are located in the Q-access drift approximately halfway between the Air Intake Shaft and the entrance to Room Q. Brine has been collected from all five of these nominally 2" diameter vertical boreholes numbered QPB01, QPB02, QPB03, QPB04, and QPB05. Details about borehole drilling history, brine sampling procedures, and brine inflow rates through 6 June 1991 can be found in Finley et al. (1992).

The stratigraphic units that the boreholes intersect are shown in Figure 1. The large diameter boreholes DBT31 and DBT 32 pass through several halite and argillaceous halite units, while the large borehole L4X01 is entirely within an argillaceous halite unit. The mineralogy of the Salado near the waste facility horizon is examined by Stein (1985), who in particular examined the residues remaining when the NaCl(s) in bulk halite samples was removed by dissolution. One conclusion in this report is "The non-NaCl components of halite [in the Salado Formation]...in the immediate vicinity (e.g., 100 vertical feet) of the WIPP facility horizon...consist[s] of quartz, anhydrite, gypsum, magnesite, polyhalite, and clays, with traces of...other minerals" (p. 20, Stein, 1985). The presence of these accessory minerals is an important consideration in understanding the measured chemical compositions of brines from the SSBIE, as discussed below.

Selected brine samples were submitted for chemical analysis, as reported in UNC Geotech Analytical Laboratory (1990), Chem-Nuclear Geotech Analytical Laboratory (1990), and Chem-Nuclear Geotech Analytical Laboratory (1991). Table 1 gives a summary of these chemical analyses, along with sample collection and analysis dates.

Analyzed Brine Compositions

The composition data from Table 1 are plotted versus bromide concentration in Figure 2, with open symbols denoting small (2" and 4") diameter boreholes and filled symbols denoting large (36") diameter boreholes. Bromide concentration was chosen as the abscissa because dissolved bromide has been shown to act conservatively during seawater evaporation until the bromide concentration is approximately 90 times greater than that in seawater, i.e., up to bromide concentrations of about 65 to 70 mM (McCaffrey et al., 1987). (Conservative behavior in this case means that bromide is not lost from the aqueous phase by precipitation but merely becomes more concentrated in solution as water is removed from the brine.) Because none of the measured bromide concentrations from the SSBIE exceeds 40 mM, it is reasonable to assume that bromide behaved conservatively when Salado brines were formed.

The concentrations of chloride, magnesium, potassium, sulfate, and boron (Figure 2) increase linearly as the bromide concentration increases, while the concentrations of sodium and calcium decrease linearly as the bromide concentration increases. This suggests that the brines are in chemical equilibrium with respect to halite, $\text{NaCl}(s)$, because chemical thermodynamics indicates that the product of the activities ("effective" concentrations) of Na^+ and Cl^- will be constant when in equilibrium with halite. A similar argument holds for Ca^{2+} and SO_4^{2-} and equilibrium with anhydrite, $\text{CaSO}_4(s)$. The presence of both these minerals in the map units that the boreholes intersect supports this suggestion. However, this trend is defined primarily by the data from the large diameter boreholes.

Much less concentration variation is seen when considering only the small diameter boreholes, i.e., the open symbols in Figure 2. This is emphasized by "zooming in" on the concentration ranges that represent all the 2" and 4" diameter

boreholes, as is done in Figure 3. On this expanded scale, the compositions of the Room D small boreholes seem to form a cluster distinct from the Q-access and Room L small boreholes. In this representation, most of the element concentrations in the small diameter boreholes seem to form a linear trend over a very narrow (17-21 mM) bromide concentration range.

Close examination of the potassium and magnesium concentrations in the small diameter boreholes, Figure 3, shows that the Q-access and L4B01 data cluster around bromide concentrations of 17 to 19 mM (with one outlying point at 13 mM), while the Room D data span the range from 19 to 21 mM bromide. The concentrations of most, if not all, other elements exhibit small but distinct differences between the Q-access/L4B01 and Room D populations. It is unlikely that these differences are caused by systematic sampling or analytical errors because samples from most locations were analyzed in the same batches.

In previous analyses of brine composition from the Salado (Stein and Krumhansl, 1988), data were presented in graphical form as Na/Cl mass ratio versus K/Mg mass ratio; the SSBIE data from the small diameter boreholes are plotted thus in Figure 4. In this representation, the samples from the Room D small diameter boreholes cluster tightly in an apparently distinct population from the Q-access and L4B01 samples. The brine compositions from the small diameter boreholes seem to fall into two populations, one for the small DBT boreholes, and one for the small L4 and QPB boreholes. The sodium to chloride mass ratios are approximately the same for all the small boreholes, but the Room D samples are deficient in potassium and enriched in magnesium relative to the L4B01 and Q-access samples, as can be seen from Figure 3. However, the differences in the magnesium to potassium ratios observed for Room D and Room L4/Q-access are likely to be unimportant with regard to the solubility and migration behavior of actinides in Salado brines.

Figure 5 presents Na/Cl versus K/Mg mass ratios for all SSBIE samples, including analyses for brines from large diameter boreholes. Samples from the large diameter boreholes do not cluster with the small boreholes. Some of the brine analyses from the large DBT boreholes fall near the small borehole population, but others do not, generally being depleted in sodium relative to chloride. One of the analyses from the large L4X01 borehole appears to be depleted in sodium relative to

chloride, but the other three L4X01 samples also have lower potassium to magnesium ratios, and appear on Figure 5 to look more similar to the large DBT borehole samples.

The accuracies of the chemical analyses summarized in Table 1 were not reported. However, it is worthwhile to consider approximate "error bars" on these data to determine whether the two data clusters in Figure 5 merge into one population when uncertainties are included. Assume one is interested in the ratio $R=x/y$, where the quantities x and y have associated $\pm a\%$ and $\pm b\%$ uncertainties, respectively. The associated ranges in values for x and y yield as uncertainty bounds on R the smallest ratio $R_s = \frac{(1-a)}{(1+b)} R$ and the largest ratio $R_l = \frac{(1+a)}{(1-b)} R$. If a and b are both 5%, then $R_s/R = 0.90$ and $R_l/R = 1.10$, giving about a 10% error bar on the final ratio. (A value of 5% may be conservative; if $a = b = 10\%$, the error on the final ratio will be about 20%.) When this 5% error is included with the data (Figure 6), the brines still appear to fall into two distinct populations. The trends described above remain clearly distinguishable even after considering the possible magnitude of errors associated with sampling handling and analysis.

Effects of Evaporation on Brine Compositions

There are several reasons to suspect that water evaporation from the brine may have occurred while brine was accumulating in the boreholes. Figure 2 shows that concentrations in brines from the large diameter boreholes increase linearly with bromide concentration, while concentrations from the small diameter boreholes cluster at the low concentration end of this correlation. When bromide is assumed to behave conservatively during evaporation, this suggests that the brines were concentrated by evaporation in the large diameter boreholes.

The seals for the large boreholes also suggest evaporation may be occurring, as presented in the attached memorandum from Jim Foesch. The L4X01 borehole is closed with a brattice cloth seal that is considered to provide poor isolation of the gas phase within the L4X01 borehole. Humidity measurements within L4X01 and within Room L4 are correlated, suggesting that gas can flow out of and into the borehole as pressure changes within the drift. The DBT31 and DBT32 boreholes

are sealed in a different manner from L4X01, using a 90 cm flange with a rubber gasket. This arrangement provides a better seal than for L4X01, but the seal is still not as good as those on the small diameter boreholes. Thus, loss of water vapor through exchange with the atmosphere is plausible for the L4X01 borehole and the large DBT boreholes.

The total void volume within boreholes relative to brine sample size provides a further suggestion that evaporation may be more important in the large boreholes. Table 2 shows the diameters and lengths of the SSBIE boreholes, along with calculated internal volumes (assuming cylindrical boreholes) and the mass of water needed to bring the air within the borehole to a relative humidity of 75%, the relative humidity approximately in equilibrium with Salado brines. As shown, the mass of water necessary to reach 75% relative humidity is about 1 gram for L4B01 and the small DBT boreholes, and about 0.1 gram for the Q-access boreholes, while it is on the order of 70 grams for DBT31, DBT32, and L4X01. A comparison of these masses of water to the mass of water in the brine samples is given in Table 3. This calculation assumed that about three quarters of the brine mass was H₂O, estimated by assuming a brine density of 1200 g/liter and 300 g/liter total dissolved solids. As Table 3 shows, only for the large diameter boreholes is the mass of water in the air a significant fraction of the mass of water in the collected brine. This means that, if all boreholes were perfectly sealed, and contained dry air (relative humidity 0%) at the start of a test interval, and all water in the air came from brine evaporation, the evaporation would affect the brine compositions only in the large diameter boreholes.

Evaporation Path Modeling

Equilibrium evaporation path modeling was performed to determine whether the hypothesis of water evaporation was consistent with the brine composition data. Three average brines, called $\overline{\text{DBT}}$, $\overline{\text{QPB}}$, and $\overline{\text{L4B01}}$, were defined as the arithmetic average of all samples for every small diameter borehole in a given room or drift. The equilibrium evaporation paths of these brines were calculated with the PHRQPITZ code (Plummer et al., 1988), using the Pitzer specific ion interaction approach and the data set of Felmy and Weare (1986) and Harvie et al. (1984).

Using this code, the three average brines were sequentially evaporated to the following endpoints:

- (1) halite, NaCl(s) , saturation;
- (2) anhydrite, $\text{CaSO}_4\text{(s)}$, saturation in equilibrium with halite;
- (3) polyhalite, $\text{K}_2\text{MgCa}_2\text{(SO}_4)_4 \cdot 2\text{H}_2\text{O(s)}$, saturation in equilibrium with halite and anhydrite; and
- (4) sylvite, KCl(s) , saturation in equilibrium with halite and polyhalite, but not anhydrite.

Anhydrite equilibrium was not maintained in step 4 because more anhydrite would have needed to dissolve than had precipitated in the evaporation sequence. The modeling assumed a closed system, i.e., the model did not allow $\text{CO}_2\text{(g)}$ to dissolve or exsolve. The final solution for the average L4 brine was slightly oversaturated with respect to a borate mineral that has not been observed near the repository horizon in the Salado. The calculated evaporation paths are plotted versus bromide concentration along with the measured concentrations for the large boreholes in Figure 7; three evaporation lines are shown for each element because the three average brine compositions are slightly different.

A comparison of the modeling results with composition data is shown in Figure 7, where the lines represent calculated evaporation paths for the three average brines, the solid squares represent data from the large DBT boreholes, and the filled circles represent data from the large L4 borehole. For all elements except total inorganic carbon (TIC), the calculated evaporation paths of the average brines agree very well with the observed compositions from the large boreholes, indicating that the hypothesis of water evaporation within boreholes is consistent with the data. Calculated evaporation paths are similar for the three different average brines.

The agreement between evaporation path modeling and the data points on Figure 7 provides partial verification and validation of both the chemical model (Felmy and Weare, 1986; Harvie et al., 1984; Harvie and Weare, 1980), and the PHRQPITZ implementation of this chemical model. The SSBIE brines are complex, highly concentrated chemical systems, and are independent from the data used to parameterize the chemical model. Nonetheless, excellent agreement

between the model and data was achieved through straightforward analysis. This provides additional confidence that the methods used above can successfully describe the geochemical behavior of brine constituents in evaporite environments such as the Salado Formation.

The lack of agreement between the modeled and measured TIC data could be attributed to numerous causes. Carbon dioxide may have been lost during brine accumulation while water was evaporating. This explanation is consistent with the lower values measured in the large diameter boreholes relative to the TIC concentrations predicted by the model. Other possible explanations include CO₂(g) outgassing during sample storage and handling, and errors or uncertainty in pH measurement.

Compositional Trends over Multiple Samples from the Same Borehole

As shown in Table 1, several different brine samples from each of the boreholes were chemically analyzed. The samples were withdrawn at different times to determine whether composition is a function of sampling date. This section examines the data for such variation for the eight boreholes from which three or more brine samples were analyzed. These small diameter boreholes include four from the Q-access drift, and four from Room D. Because the compositional variation of the nominally 36" diameter boreholes was explained above, the 36" borehole data are not discussed here. The time spans represented by data for the boreholes with multiple samples range from five to thirty months. With so few samples, it would be difficult to define temporal trends. However, some regular variation in compositions might become apparent.

Plots of these data for the Room D and Q-access boreholes are given in Figures 8 and 9, respectively. The data were reduced by calculating the average element concentrations for all samples from each borehole, and normalizing individual sample concentrations with respect to this average. This method of data reduction allows direct comparison of the magnitude of compositional variations among different elements. As shown in Figure 8 for boreholes DBT10, DBT11, DBT12, and DBT13, concentrations of all elements except boron and calcium vary by less than ~5% from the borehole average. Boron varies by up to ~10% in DBT12,

and calcium varies by up to ~20%. Figure 9 shows similar plots for QPB02, QPB03, QPB04, and QPB05. Here there is more variation from the average, particularly seen in one QPB03 sample taken on 16 January 1990. However, if this data point is discounted, the variations appear about the same as discussed for the Room D samples. These variations are close to the 5 to 10% analytical variability proposed earlier in this memorandum. Overall, the concentrations in each borehole seem fairly constant across multiple samples; no trends are obvious from either Figure 8 or Figure 9.

No Evidence for Contamination of Salado Brine in Q-access Boreholes

The boreholes in the Q-access drift are located approximately 40 meters from the bottom of the Air Intake Shaft (AIS). Because brines from overlying formations collect in a sump at the bottom of the AIS, and because the sump has occasionally overflowed onto the floor of the excavations, there was concern that brines in Room Q and the Q-access drift could become contaminated with nonSalado brines. Indeed, this was part of the reason for the location of the Q-access boreholes.

The existing brine composition data provide no evidence that nonSalado brine has mixed with Salado brine, or that the brines collecting in the SSBIE boreholes have origins from other than the Salado Formation. Indeed, a comparison of the compositions of SSBIE samples in Figure 2 with those from brine weeps (Figure 2, Krumhansl et al., 1991) shows no significant differences. The brine weeps were located in drift walls one or several meters above the level at which the potential contamination mechanisms could be considered plausible. Thus, because the weep samples can be considered to represent uncontaminated Salado brines, and because the weep samples and the SSBIE samples have similar compositions, it appears that the SSBIE samples are also uncontaminated by brines from other formations.

Conclusions

The brines collected and analyzed as part of the Small Scale Brine Inflow Experiments do show compositional variation. However, much of the variation occurs in brines collected from the large (nominally 36" diameter) boreholes, and

appears to result from evaporation of water during the intervals between withdrawal of brine samples. This hypothesis, water evaporation during brine accumulation, accounts for the majority of compositional variation. Some small differences in element concentrations remain, and may be important if one is attempting to understand the origins of Salado brine. However, the SSBIE were originally intended to measure brine inflow rates; they were not intended to provide data for understanding brine origins or possible compositional variations. The study of brine origins and potential variations in brine compositions would be better conducted within a program specifically designed for those purposes.

The brine composition data examined in this memorandum appear to be an insufficient basis for drawing conclusions about transport in the Salado. Furthermore, these data do not suggest ways in which additional brine composition data may contribute to the development of inferences about brine transport in the Salado. Therefore, there do not appear to be any transport-related technical reasons for continuing to store and analyze brine samples from the SSBIE.

Acknowledgment

K.L. Robinson performed many of the PHRQPITZ simulations presented in this memorandum.

References

- Chem-Nuclear Geotech Analytical Laboratory. 1990. "Analytical Report." Grand Junction, Colorado. Chem-Nuclear Geotech Analytical Laboratory. (copy on file at Quality Assurance Records/Notebook System, Sandia National Laboratories, Carlsbad, New Mexico.)
- Chem-Nuclear Geotech Analytical Laboratory. 1991. "Analytical Report." Grand Junction, Colorado. Chem-Nuclear Geotech Analytical Laboratory. (copy on file at Quality Assurance Records/Notebook System, Sandia National Laboratories, Carlsbad, New Mexico.)
- Felmy, A.R., and J.H. Weare. 1986. "The Prediction of Borate Mineral Equilibria in Natural Waters: Application to Searles Lake, California." *Geochimica et Cosmochimica Acta* vol. 50: 2771-2783.
- Finley, S.J., D.J. Hanson, and R. Parsons. 1992. *Small-Scale Brine Inflow Experiments—Data Report Through 6/6/91*. SAND91-1956. Albuquerque, New Mexico: Sandia National Laboratories.

- Harvie, C.E., and J.H. Weare. 1980. "The Prediction of Mineral Solubilities in Natural Waters: The Na-K-Mg-Ca-Cl-SO₄-H₂O System from Zero to High Concentration at 25°C." *Geochimica et Cosmochimica Acta* vol. 44: 981-997.
- Harvie, C.E., N. Møller, and J.H. Weare. 1984. "The Prediction of Mineral Solubilities in Natural Waters: The Na-K-Mg-Ca-H-Cl-SO₄-OH-HCO₃-CO₃-CO₂-H₂O System to High Ionic Strength at 25°C." *Geochimica et Cosmochimica Acta* vol. 48: 723-751.
- Krumhansl, J.L., K.M Kimball, and C.L. Stein. 1991. *Intergranular Fluid Compositions from the Waste Isolation Pilot Plant (WIPP), Southeastern New Mexico*. SAND90-0584. Albuquerque, New Mexico: Sandia National Laboratories.
- McCaffrey, M.A., B. Lazar, and H.D. Holland. 1987. "The Evaporation Path of Seawater and the Coprecipitation of Br⁻ and K⁺ with Halite." *Journal of Sedimentary Petrology* vol. 57 #5: 928-937.
- Perry, R.H., and C.H. Chilton, editors. 1973. *Chemical Engineers Handbook*. Fifth Edition. New York: McGraw-Hill.
- Plummer, L.N., D.L. Parkhurst, G.W. Fleming, and S.A. Dunkel. 1988. *A Computer Program Incorporating Pitzer's Equations for Calculation of Geochemical Reactions in Brines*. Water-Resources Investigations Report 88-4153. Reston, Virginia: U.S. Geological Survey.
- Stein, C.L. 1985. *Mineralogy in the Waste Isolation Pilot Plant (WIPP) Facility Stratigraphic Horizon*. SAND85-0321. Albuquerque, New Mexico: Sandia National Laboratories.
- Stein, C.L., and J.L. Krumhansl. 1988. "A Model for the Evolution of Brines in Salt from the Lower Salado Formation, Southeastern New Mexico." *Geochimica et Cosmochimica Acta* vol. 52: 1037-1046.
- UNC Geotech Analytical Laboratory. 1990. "Analytical Report." Grand Junction, Colorado. UNC Geotech Analytical Laboratory. (copy on file at Quality Assurance Records/Notebook System, Sandia National Laboratories, Carlsbad, New Mexico.)

Copies to:

6100	R.W. Lynch	6300	D.E. Ellis
6115	P.B. Davies	6303	W.D. Weart
6115	M.D. Siegel	6305	S.A. Goldstein
6118	H.R. Westrich	6341	A.L. Stevens
6119	F. Gelbard	6342	D.R. Anderson
6119	C.F. Novak	6345	R.C. Lincoln
6119	H.W. Papenguth	6345	E.J. Nowak
6119	K.L. Robinson	6348	J.T. Holmes
6119	File	6348	L.H. Brush
6121	J.R. Tillerson	SWCF	RC/BC 1.1.4.2

Table 1. Analyzed concentrations of brine samples from the Small Scale Brine Inflow Experiments

Borehole	Nominal Diameter, inches	Collection Date	Analysis Report*	B, mM	Br, mM	Ca, mM	Cl, mM	K, mM	Mg, mM	Na, mM	SO ₄ , mM
DBT 10	4	16 Dec 87	UNC1	132	19.5	8.68	5571	394	1037	3509	192
DBT 10	4	15 Feb 90	UNC2	136	20.4	8.66	5571	409	1043	3226	197
DBT 10	4	20 Mar 90	UNC1	130	19.5	7.31	5543	407	1053	3326	190
DBT 10	4	21 Jun 90	UNC2	133	20.2	7.13	5557	402	1008	3278	192
DBT 11	4	11 May 88	UNC1	131	19.4	7.33	5614	399	1033	3530	192
DBT 11	4	20 Mar 90	UNC1	136	19.4	6.33	5571	399	1006	3430	190
DBT 11	4	21 Jun 90	UNC3	134	20.2	6.63	5529	422	1064	3307	190
DBT 12	4	18 Jan 90	UNC1	150	20.9	6.71	5543	412	1084	3189	200
DBT 12	4	20 Mar 90	UNC2	133	20.2	7.06	5571	391	1012	3298	191
DBT 12	4	21 Jun 90	UNC2	125	19.5	6.53	5557	380	1004	3389	187
DBT 13	4	21 Jun 90	UNC3	129	19.6	6.48	5529	399	1021	3313	186
DBT 14	4	28 Sep 88	UNC1	127	19.5	8.1	5557	395	1021	3396	188
DBT 14	4	17 May 89	UNC2	130	19.6	6.68	5557	376	992	3339	185
DBT 14	4	1 Nov 89	UNC2	131	20	6.53	5529	381	1008	3333	188
DBT 14	4	16 May 90	UNC2	129	20	6.63	5529	382	1002	3326	186
DBT 14	4	16 Aug 90	UNC3	130	20.1	6.53	5472	398	1025	3254	184
DBT 15	4	27 Jul 88	UNC1	139	20.5	8.03	5585	428	1097	3289	200
DBT 15	4	16 Aug 90	UNC3	139	20	6.43	5585	409	1029	3283	188
DBT 31	4	16 Mar 88	UNC1	153	22	8.08	5599	471	1163	3217	210
DBT 31	36	16 May 90	UNC2	241	38.2	2.52	5966	720	1994	1757	335
DBT 31	36	16 Aug 90	UNC3	215	31.8	3.74	5698	664	1621	2185	276
DBT 32	4	9 Mar 88	UNC2	138	20.2	9	5491	419	1056	3057	197
DBT 32	36	6 Apr 89	UNC1	188	26.8	6.16	5698	541	1533	2687	251
DBT 32	36	16 May 90	UNC2	171	26.5	5.21	5684	504	1374	2678	249
DBT 32	36	16 Aug 90	UNC3	167	25.4	5.09	5585	490	1288	2759	232
QPB 01	2	16 Aug 90	UNC3	138	18.1	7.53	5501	426	776	3463	160
QPB 01	2	20 Sep 90	UNC3	144	18.8	7.88	5614	448	817	3554	166
QPB 02	2	4 Oct 89	UNC2	139	18.5	7.93	5571	431	813	3596	166
QPB 02	2	13 Dec 89	UNC1	149	18.8	9.43	5529	453	866	3676	177
QPB 02	2	20 Jul 90	UNC3	144	18.8	7.83	5472	453	842	3493	165
QPB 02	2	16 Aug 90	UNC3	145	18.7	7.98	5444	458	819	3443	164
QPB 02	2	20 Sep 90	UNC3	144	18.6	10.17	5585	436	825	3637	166
QPB 03	2	16 Jan 90	UNC1	96	13.1	12.64	5487	312	611	4148	133
QPB 03	2	20 Jul 90	UNC3	140	18.6	7.78	5557	453	842	3633	169
QPB 03	2	16 Aug 90	UNC3	141	18.6	7.88	5416	460	809	3391	164
QPB 03	2	20 Sep 90	UNC3	146	18.6	7.68	5529	435	825	3493	165
QPB 04	2	27 Apr 90	UNC2	130	17.5	9.88	5501	399	767	3650	171
QPB 04	2	20 Jul 90	UNC3	143	18.6	7.58	5416	472	823	3435	165
QPB 04	2	16 Aug 90	UNC3	140	18.5	8.83	5501	451	821	3596	168
QPB 04	2	20 Sep 90	UNC3	144	18.6	11.17	5642	431	821	3639	169
QPB 05	2	27 Apr 90	UNC2	132	17.4	9.53	5529	409	784	3678	177
QPB 05	2	15 Jun 90	UNC2	137	18.2	8.03	5501	416	813	3537	164
QPB 05	2	20 Jul 90	UNC3	140	18.5	8.88	5585	451	821	3554	170
QPB 05	2	16 Aug 90	UNC3	146	18.8	7.83	5501	427	825	3430	165
QPB 05	2	20 Sep 90	UNC3	147	18.5	7.81	5360	460	823	3428	164
L4B01	4	21 Jun 89	UNC1	150	19.1	7.98	5529	464	912	3559	178
L4B01	4	14 Dec 89	UNC2	137	18.2	7.78	5543	428	829	3628	171
L4X01	36	13 Jul 89	UNC2	257	35.2	2.54	5853	674	1809	2015	361
L4X01	36	19 Jul 89	UNC1	242	32.7	2.99	5797	726	1831	2309	337
L4X01	36	15 Jun 90	UNC2	239	34.3	3.54	5825	716	1576	2304	291
L4X01	36	20 Jul 90	UNC3	201	29	5.19	5755	646	1265	2728	245

* UNC1: analysis date 20 Jun 90 (UNC Geotech Analytical Laboratory, 1990)
 UNC2: analysis date 21 Nov 90 (Chem-Nuclear Geotech Analytical Laboratory, 1990)
 UNC3: analysis date 29 Jan 91 (Chem-Nuclear Geotech Analytical Laboratory, 1991)

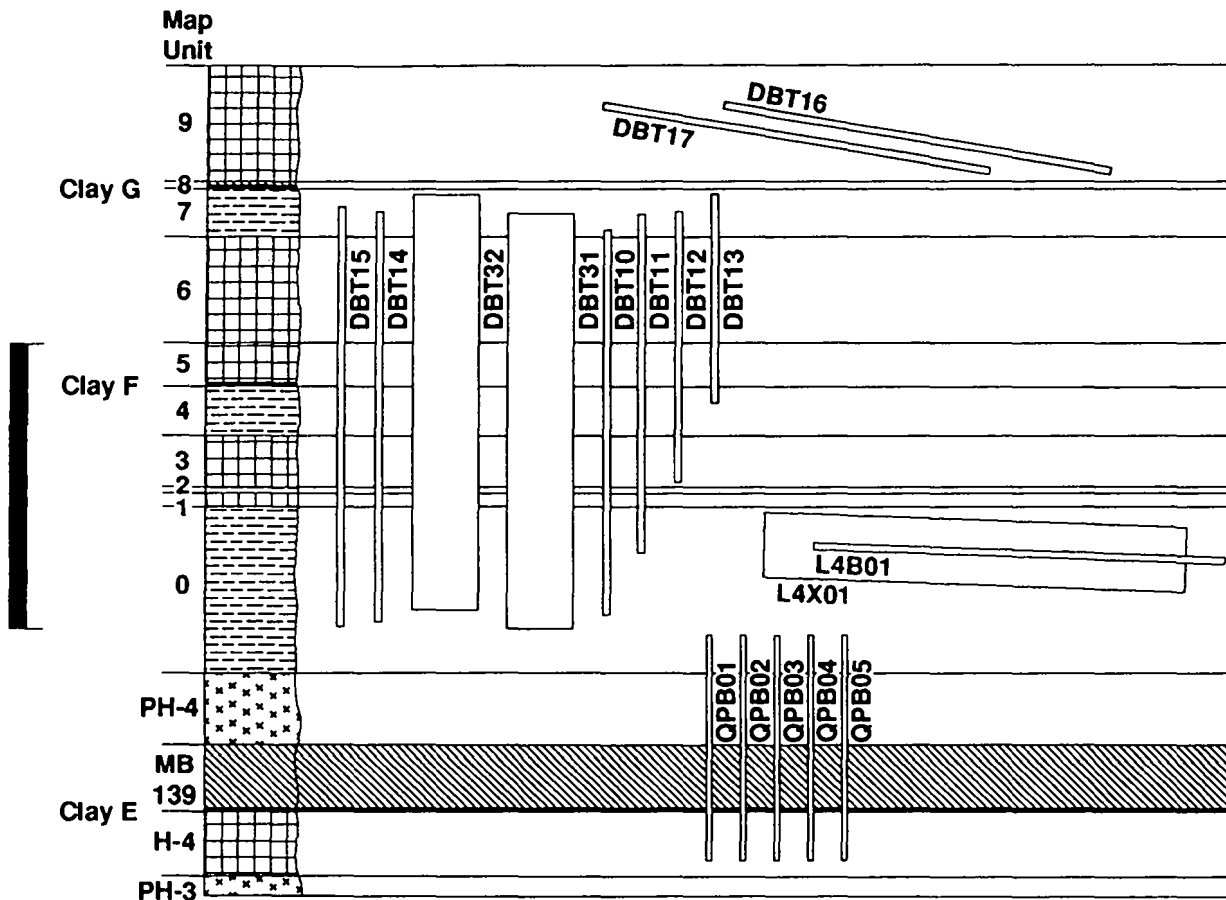
Table 2. Final borehole diameters and lengths, calculated void volumes within boreholes, and the required mass of water necessary to provide 75% relative humidity in the borehole (75% is approximately equilibrium with the initial brines).

Borehole	Diameter, cm	Length, cm	Volume, liters	g H ₂ O needed to saturate air to 75% relative humidity [§]
DBT10	10.2	530	43.3	0.82
DBT11	10.2	460	37.6	0.71
DBT12	10.2	370	30.2	0.57
DBT13	10.2	280	22.9	0.43
DBT14	10.2	560	45.8	0.86
DBT15	10.2	580	47.4	0.90
DBT31	91.4	560	3670	69.44
DBT32	91.4	570	3740	70.68
QPB01	5.1	300	6.13	0.12
QPB02	5.1	310	6.33	0.12
QPB03	5.1	310	6.33	0.12
QPB04	5.1	310	6.33	0.12
QPB05	5.1	310	6.33	0.12
L4B01	10.2	580	47.4	0.90
L4X01	91.4	570	3740	70.68







§ A value of 0.0189 grams H₂O per liter moist air (75% relative humidity) was estimated from the psychrometric chart on p. 20-6 of Perry and Chilton (1973).

Table 3. Calculation of the mass of H₂O required to saturate the air in the SSBIE boreholes to 75% relative humidity, and the ratio of this mass to the mass of water in the brine sample.

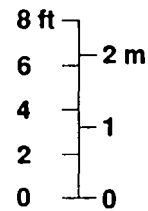
Borehole	Nominal Diameter, inches	Collection Date	g Brine in Sample	g H ₂ O needed to saturate air to 75% relative humidity	Ratio of g H ₂ O to reach 75% relative humidity to mass of water in brine sample
DBT 10	4	16 Dec 87	92	0.82	1.2%
DBT 10	4	15 Feb 90	194	0.82	0.6%
DBT 10	4	20 Mar 90	246	0.82	0.4%
DBT 10	4	21 Jun 90	871	0.82	0.1%
DBT 11	4	11 May 88	69	0.71	1.4%
DBT 11	4	20 Mar 90	294	0.71	0.3%
DBT 11	4	21 Jun 90	967	0.71	0.1%
DBT 12	4	18 Jan 90	173	0.57	0.4%
DBT 12	4	20 Mar 90	149	0.57	0.5%
DBT 12	4	21 Jun 90	510	0.57	0.1%
DBT 13	4	21 Jun 90	306	0.43	0.2%
DBT 14	4	28 Sep 88	78	0.86	1.5%
DBT 14	4	17 May 89	144	0.86	0.8%
DBT 14	4	1 Nov 89	200	0.86	0.6%
DBT 14	4	16 May 90	153	0.86	0.8%
DBT 14	4	16 Aug 90	514	0.86	0.2%
DBT 15	4	27 Jul 88	146	0.90	0.8%
DBT 15	4	16 Aug 90	120	0.90	1.0%
DBT 31	4	16 Mar 88	88	0.86	1.3%
DBT 31	36	16 May 90	430	69.44	21.5%
DBT 31	36	16 Aug 90	588	69.44	15.7%
DBT 32	4	9 Mar 88	79	0.87	1.5%
DBT 32	36	6 Apr 89	76	70.68	124.0%
DBT 32	36	16 May 90	520	70.68	18.1%
DBT 32	36	16 Aug 90	590	70.68	16.0%
QPB 01	2	16 Aug 90	147	0.12	0.1%
QPB 01	2	20 Sep 90	207	0.12	0.1%
QPB 02	2	4 Oct 89	191	0.12	0.1%
QPB 02	2	13 Dec 89	56	0.12	0.3%
QPB 02	2	20 Jul 90	2486	0.12	0.0%
QPB 02	2	16 Aug 90	2164	0.12	0.0%
QPB 02	2	20 Sep 90	66	0.12	0.2%
QPB 03	2	16 Jan 90	235	0.12	0.1%
QPB 03	2	20 Jul 90	445	0.12	0.0%
QPB 03	2	16 Aug 90	666	0.12	0.0%
QPB 03	2	20 Sep 90	1027	0.12	0.0%
QPB 04	2	27 Apr 90	55	0.12	0.3%
QPB 04	2	20 Jul 90	103	0.12	0.1%
QPB 04	2	16 Aug 90	80	0.12	0.2%
QPB 04	2	20 Sep 90	107	0.12	0.1%
QPB 05	2	27 Apr 90	74	0.12	0.2%
QPB 05	2	15 Jun 90	1214	0.12	0.0%
QPB 05	2	20 Jul 90	2117	0.12	0.0%
QPB 05	2	16 Aug 90	1713	0.12	0.0%
QPB 05	2	20 Sep 90	2316	0.12	0.0%
L4B01	4	21 Jun 89	30	0.90	4.0%
L4B01	4	14 Dec 89	74	0.90	1.6%
L4X01	36	13 Jul 89	115	70.68	81.9%
L4X01	36	19 Jul 89	108	70.68	87.3%
L4X01	36	15 Jun 90	98	70.68	90.2%
L4X01	36	20 Jul 90	84	70.68	102.2%



Legend

-  Halite
-  Anhydrite
-  Polyhalitic Halite
-  Argillaceous Halite
-  Clay Seam
-  Waste Facility Horizon

Vertical Scale
(No Horizontal Scale)



TRI-6344-553-0

Figure 1. A schematic representation of the small-scale brine inflow boreholes and the stratigraphic units tested in each borehole (p.3, Finley et al., 1992).

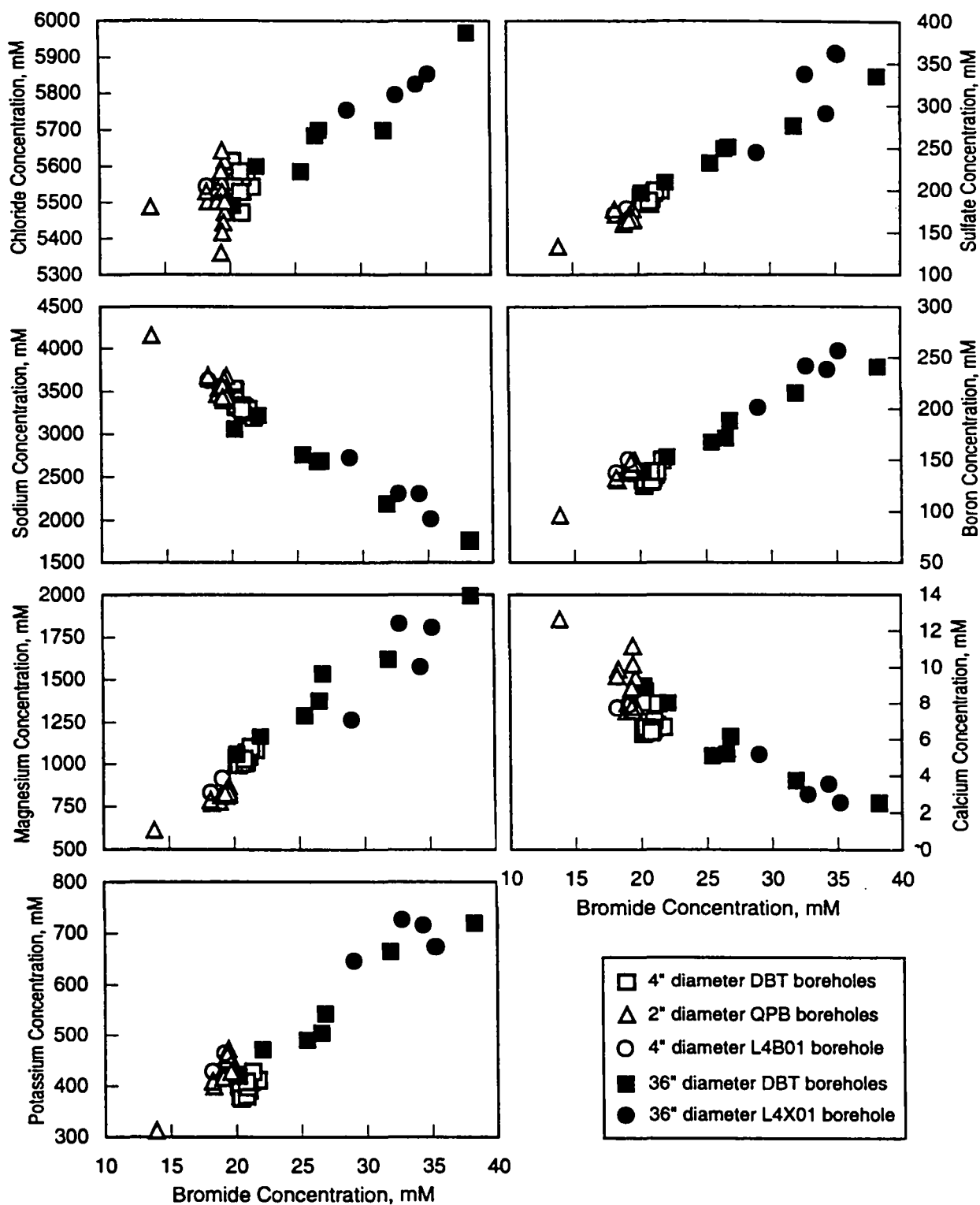


Figure 2. Analyzed concentrations from small (open symbols) and large (filled symbols) boreholes as a function of bromide concentration, which is assumed to be conservative.

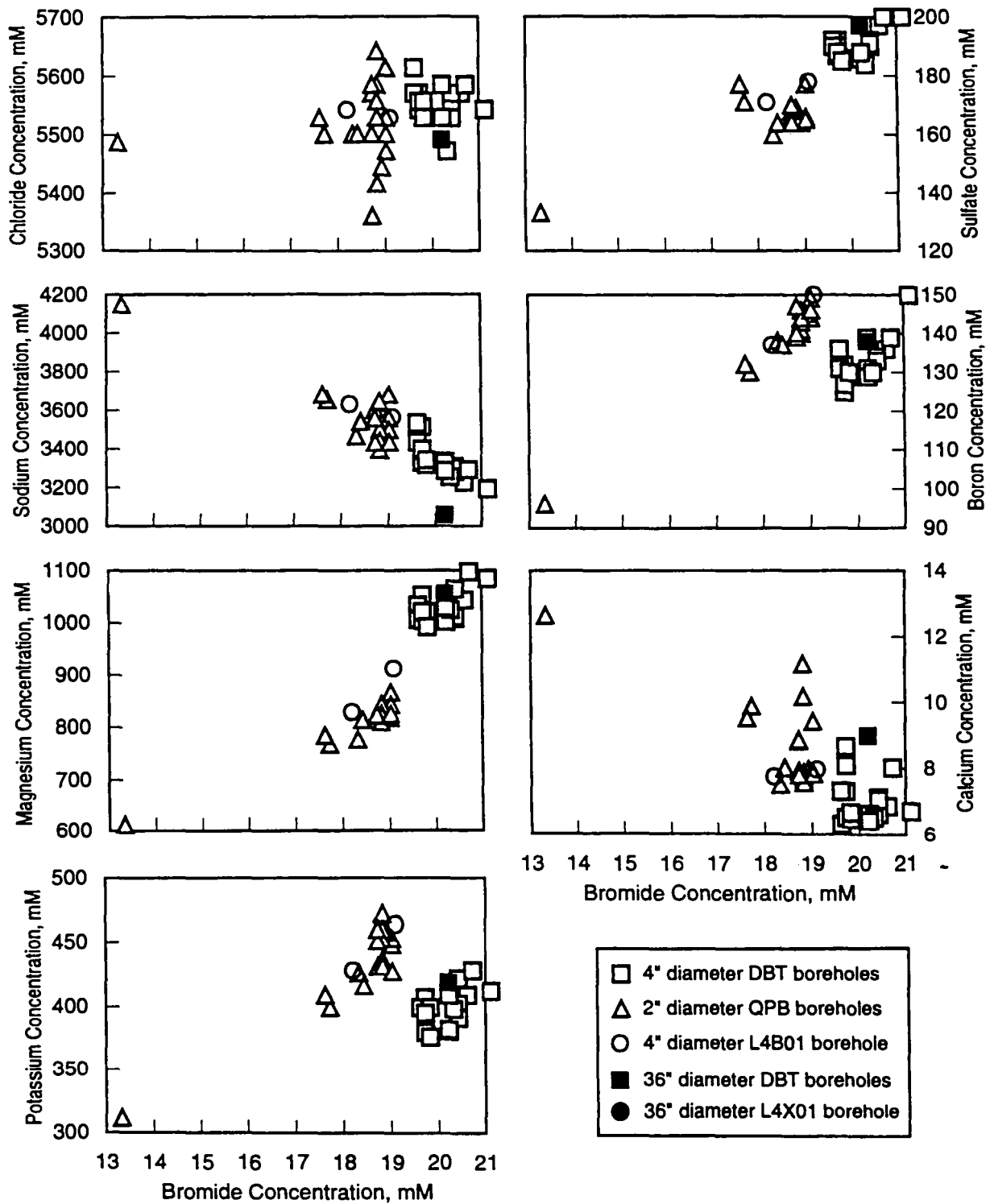


Figure 3. Expanded view of analyzed concentrations from small (open symbols) and large (filled symbols) boreholes as a function of bromide concentration, c.f., Figure 2, showing two apparent populations of brine compositions.

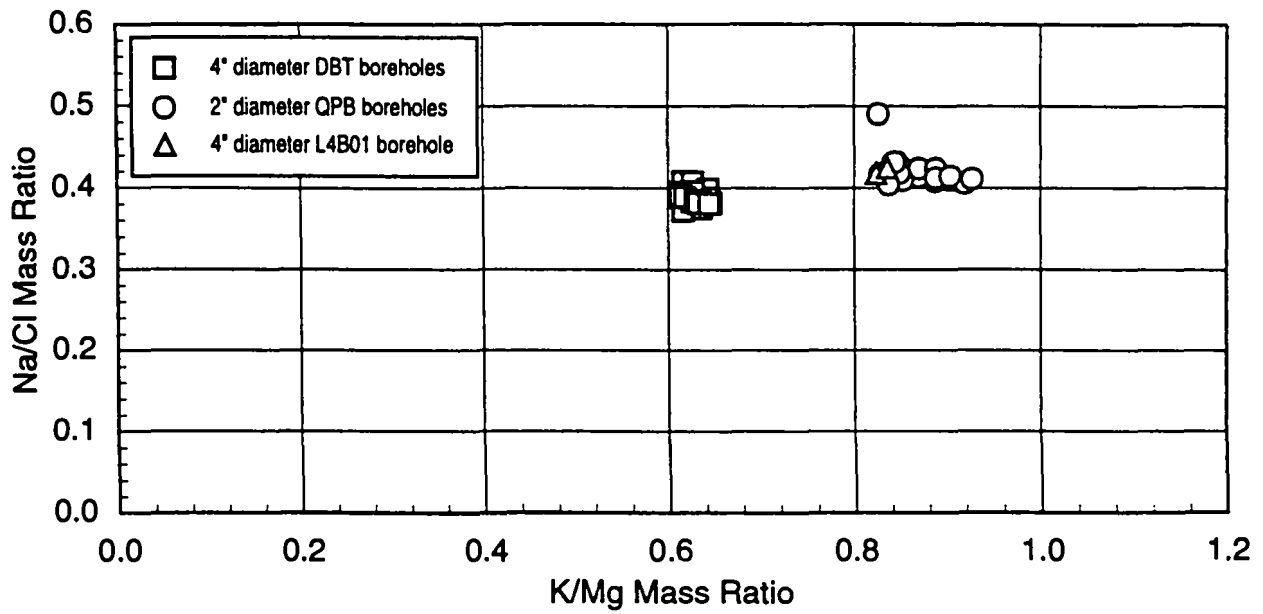


Figure 4. Plot of mass ratios of major solutes for the small diameter boreholes.

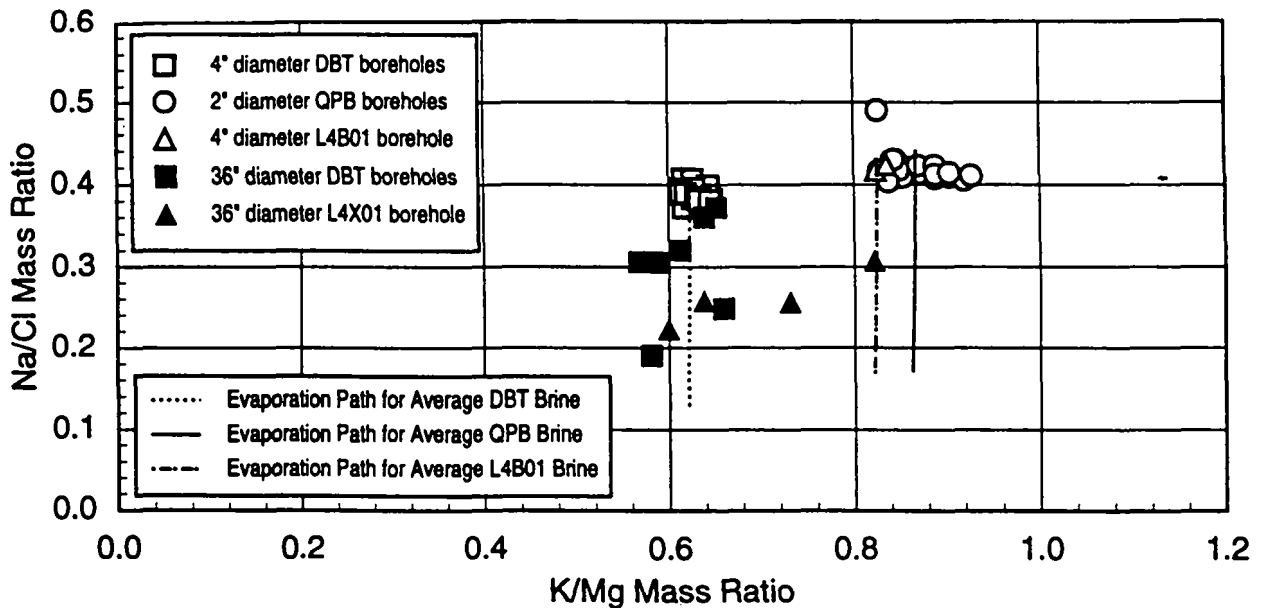


Figure 5. Plot of mass ratios of major solutes for small and large diameter boreholes, with calculated evaporation paths for average brines calculated from the small diameter borehole samples from Rooms D and L4, and the Q-access drift.

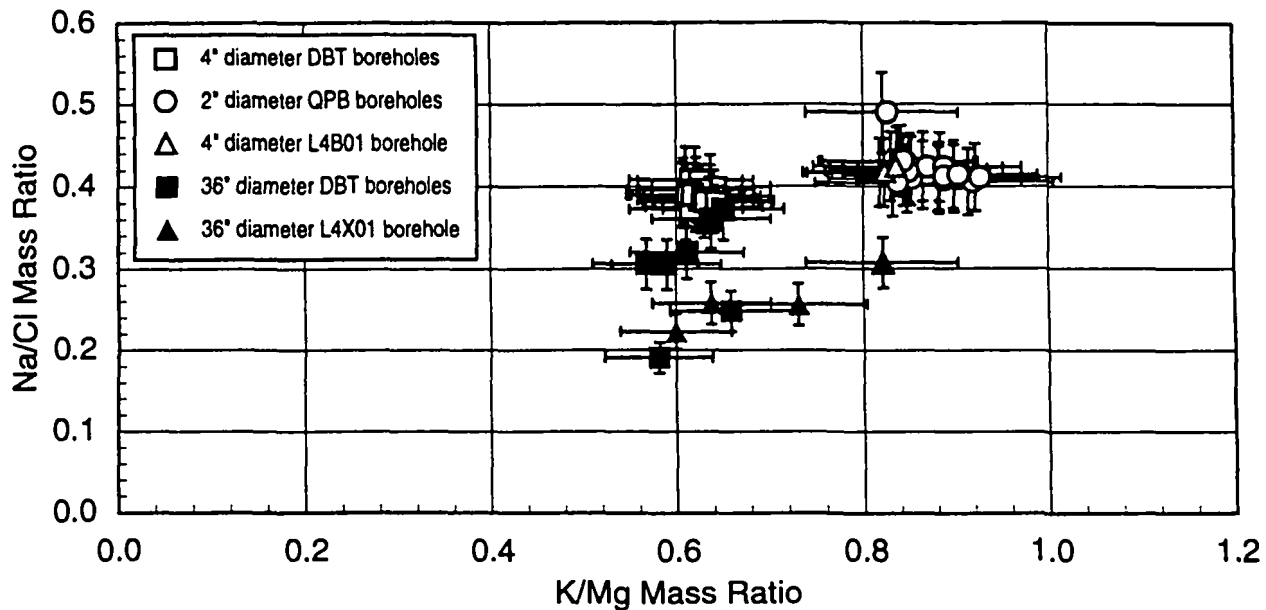


Figure 6. Plot of mass ratios of major solutes for both small and large diameter boreholes, showing the "error bars" that would result from a $\pm 5\%$ analytical accuracy in concentrations.

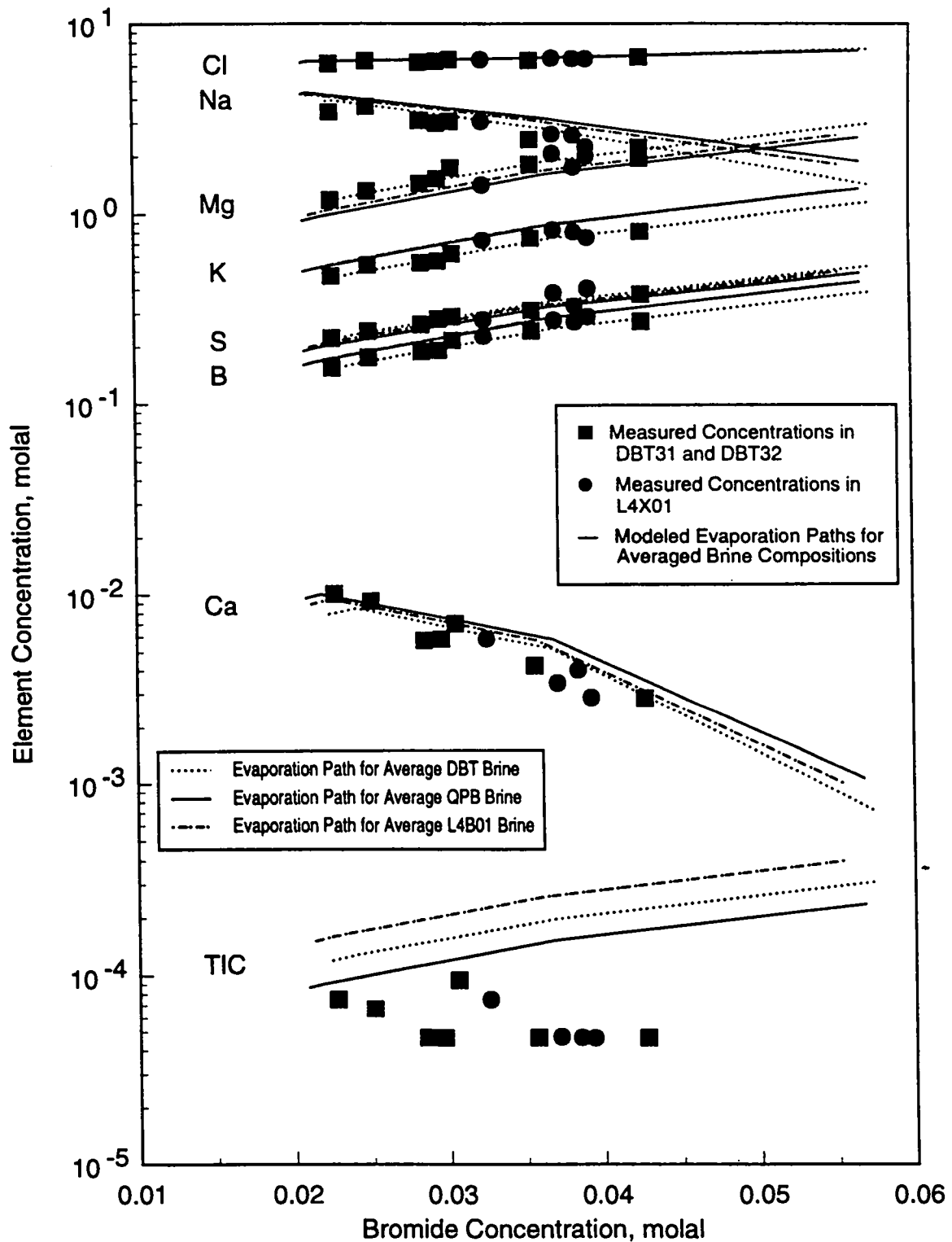


Figure 7. Comparison of modeled evaporation of average small borehole brines with concentration data from large boreholes.

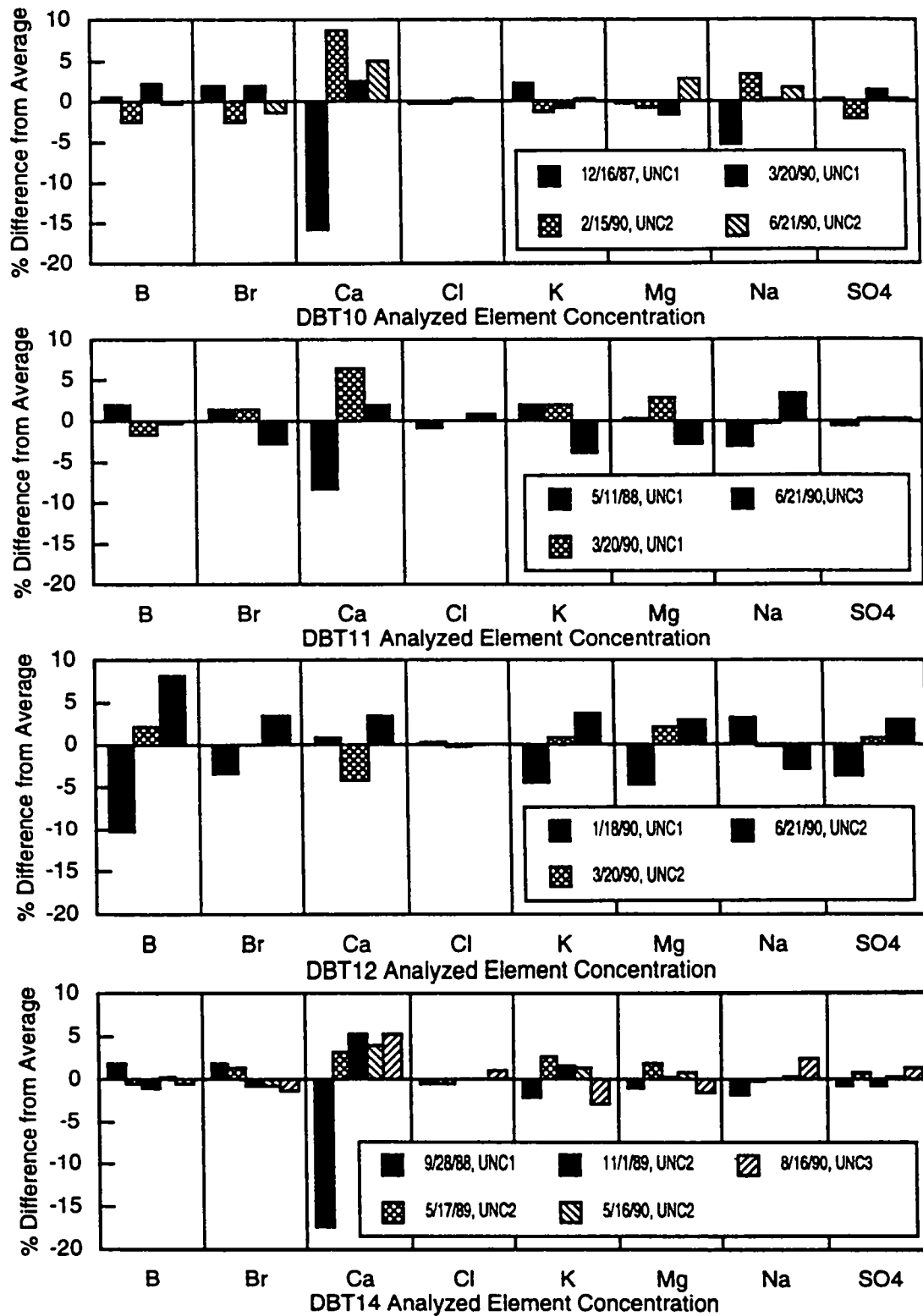


Figure 8. Percent difference in concentration of analyzed elements in DBT brines as a function of time.

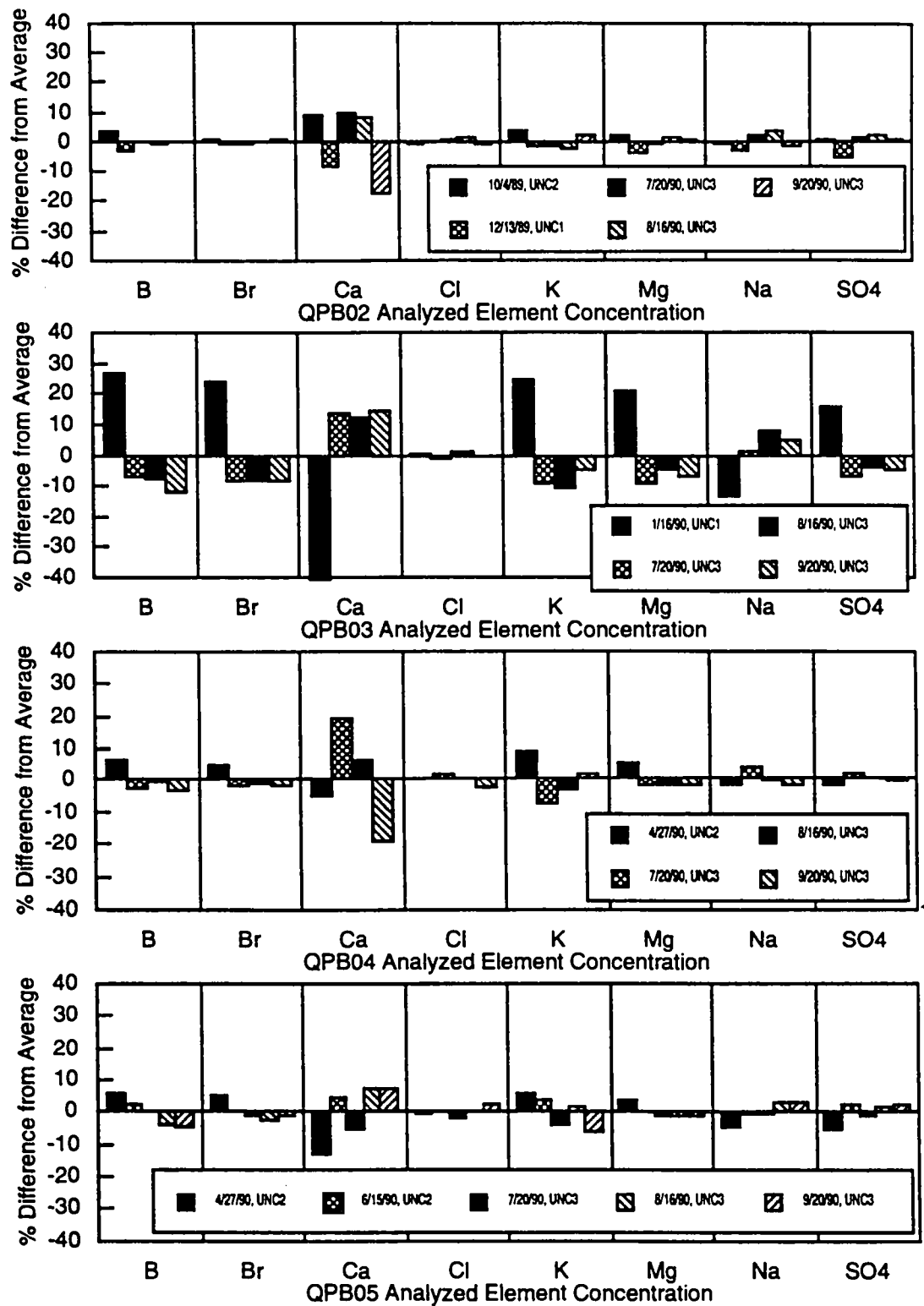
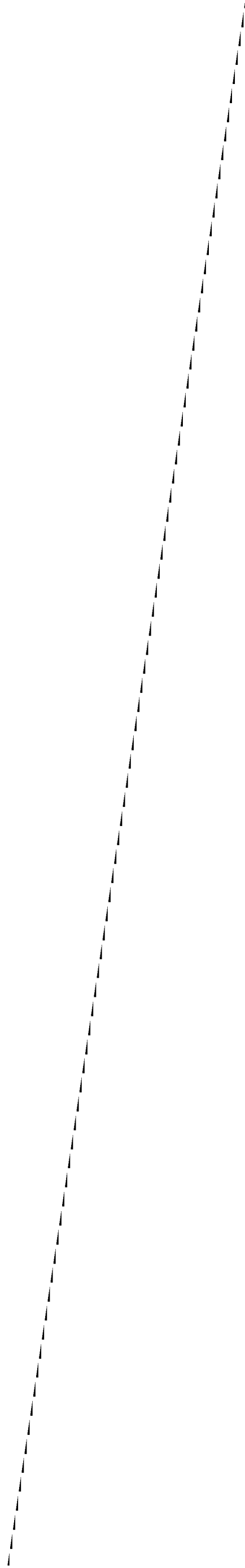


Figure 9. Percent difference in concentration of analyzed elements in QBP brines as a function of time.

D-42

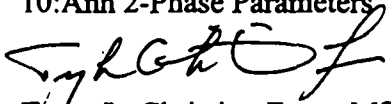


Appendix E.
PA Parameter Package: Salado Data/Parameters: Anhydrite Two-Phase Parameters.
Tracy Christian-Frear to SWCF-A, January 31, 1996.

The following information is provided as Appendix E of this document.

Sandia National Laboratories

Albuquerque, New Mexico 87185-1341

date: January 31, 1996
to: SWCF-A Records Center, SWCF-A:WBS 1.2.07.1:PDD:QA:SALADO:PKG
10:Anh 2-Phase Parameters

from: Tracy L. Christian-Frear, MS-1324 (6115)
subject: SALADO PARAMETER PRINCIPAL INVESTIGATOR
DOCUMENTATION PACKAGE FOR: ANHYDRITE TWO-PHASE
PARAMETERS

The attached record package contains the anhydrite two-phase values for the capillary and relative permeability models, the residual gas and brine saturation, the initial brine saturation, pore size distribution parameter and the threshold pressure.

The parameter information provided in this record package was collected by Principal Investigators for input to the WIPP Data Entry Form and for use by Performance Assessment personnel making parameter estimates. The record package was prepared in accordance with WIPP Quality Assurance Procedure (QAP) 17-1, Rev. 1, WIPP QA Records Source Requirements.

Please call me at 848-0704 if you have any questions.

RECORD PACKAGE:

**SALADO PARAMETER PRINCIPAL INVESTIGATOR
DOCUMENTATION PACKAGE FOR:**

ANHYDRITE TWO-PHASE PARAMETERS

Purpose: The parameter information in this package was collected by Principal Investigators for input to the WIPP Data Entry Form and for use by Performance Assessment personnel making parameter estimates.

Date of Record: January 31, 1996

Author/Organization: Tracy L. Christian-Frear
SNL Department 6115 (MS 1324)
(505) 848-0704

Recipient: SWCF-A Records Center

File Code: SWCF-A:WBS 1.2.07.1:PDD:QA:SALADO:PKG 10:Anh 2-Phase Parameters

RECORD PACKAGE:

SALADO PARAMETER PRINCIPAL INVESTIGATOR DOCUMENTATION PACKAGE FOR:

ANHYDRITE TWO-PHASE PARAMETERS

SWCF-A:WBS 1.2.07.1:PDD:QA:SALADO:PKG 10:Anh 2-Phase Parameters

Table of Contents

Record Number	Contents	Number of Pages
1	SALADO DATA/PARAMETERS : ANHYDRITE TWO-PHASE PARAMETERS (Date: December 22, 1996)	7
2	Attachment 1. Capillary Pressure Model Parameters Calc. Sheet	37
3	General Correspondence	0
4	Technical Review of Record Package	1
5	Roadmap to Supporting Documentation	0
6	Memo to PA Parameter Task Leader (attachment not included--same as record 1)	1

Total Number of Pages in Record Package

RECORD 1

SALADO DATA/PARAMETERS : ANHYDRITE TWO-PHASE PARAMETERS

Anhydrite Laboratory Data for two-phase parameters

I. Parameter No. (id):

CAP_MOD: 559, 579, 520
PC_MAX: 561, 582, 522
RELP_MOD: 575, 596, 536
SAT_IBRN: 576, 597, 537
SAT_RBRN: 577, 598, 538
SAT_RGAS: 578, 599, 539
PTHRESH: 573, 594, 534
PCT_A: IDPARAM Unknown at this time
PCT_EXP: IDPARAM Unknown at this time

II. Data/Parameter:

CAP_MOD: Capillary Pressure Model
PC_MAX: Maximum Capillary Pressure
PORE_DIS: Brooks-Corey Pore Distribution Parameter (lambda)
RELP_MOD: Relative Permeability Model
SAT_IBRN: Initial Brine Saturation
SAT_RBRN: Residual Brine Saturation
SAT_RGAS: Residual Gas Saturation
PTHRESH: Threshold Pressure
PCT_A: Threshold Pressure Linear Parameter
PCT_EXP: Threshold Pressure Exponential parameter

III. Parameter id (idpram):

CAP_MOD
PC_MAX
PORE_DIS
RELP_MOD
SAT_IBRN
SAT_RBRN
SAT_RGAS
PTHRESH
PCT_A
PCT_EXP

IV. Material:

Anhydrite

V. Material Id (idmtrl):

S_MB138, S_MB139, S_ANH_AB

VI. Units:

CAP_MOD: None
PC_MAX: Pa
PORE_DIS: None
REL_P_MOD: None
SAT_IBRN: None
SAT_RBRN: None
SAT_RGAS: None
PTHRESH: Pa
PCT_A: Pa/(m²PCT_EXP)
PCT_EXP: None

VII. Distribution Information:

The following are Model Parameters with recommendations:
CAP_MOD: Limit Capillary Pressure to PC_MAX
REL_P_MOD: 50% mixed B/C and 50% vG/P characteristic curves
PC_MAX: 1.0 E8 Pa
SAT_IBRN: 1.00

A. Category

PORE_DIS: Normal
SAT_RBRN: Normal
SAT_RGAS: Log Normal
PTHRESH: Normal
PCT_A: Constant
PCT_EXP: Constant

B. Mean

PORE_DIS: 0.6436
SAT_RBRN: 0.084
SAT_RGAS: 0.077
PTHRESH: 5.418 x 10⁵ Pa
PCT_A: 0.26 Pa/m^{-0.348*2}
PCT_EXP: -0.348

C. Median

PORE_DIS: 0.6536
SAT_RBRN: 0.071
SAT_RGAS: 0.055
PTHRESH: 4.958 x 10⁵ Pa
PCT_A: NA
PCT_EXP: NA

SALADO DATA/PARAMETERS : ANHYDRITE TWO-PHASE PARAMETERS

D. Std Deviation

PORE_DIS: 0.1189
SAT_RBRN: 0.055
SAT_RGAS: 0.070
PTHRESH: 1.875 x 10⁵ Pa
PCT_A: NA
PCT_EXP: NA

E. Maximum

PORE_DIS: 0.842
SAT_RBRN: 0.174
SAT_RGAS: 0.197
PTHRESH: 7.8 x 10⁵ Pa
PCT_A: NA
PCT_EXP: NA

F. Minimum

PORE_DIS: 0.491
SAT_RBRN: 0.008
SAT_RGAS: 0.014
PTHRESH: 3.29 x 10⁵ Pa
PCT_A: NA
PCT_EXP: NA

G. Number of data points

6

VIII. Data Collection and Interpretation Information:

A. Data Source Information:

1. Data Source:

WIPP Observational Data

2. Supporting Explanation/Justification for selection in #1 if other than WIPP
Observational Data:

NA

3. References for selection in #1 above if other than WIPP Observational Data:

NA

B. Data Collection (for WIPP Observational Data):

1. Data Collection and Test Method:

Unstressed capillary pressure tests were performed on 6 pairs of specimens. One specimen underwent centrifuge capillary pressure tests and the other specimen underwent mercury injection capillary pressure tests. Prior to the capillary pressure tests, the specimens underwent permeability and porosity testing. The specimens ranged in size from 12.05 to 12.65 cc's. The specimens were cut from whole core taken from 6 underground boreholes at the WIPP. Two of the cores were taken outside Room L3 and the other 4 from E140 Drift at the intersection of N1100 Drift.

2. Assumptions Made During Testing:

- 1) Cores were assumed to be 100% saturated at initiation of capillary pressure tests.**
- 2) Used 140° contact angle for correcting mercury-air data to brine-air repository conditions**
- 3) The data provided here was done using tests conducted at ambient conditions (no stress) and that this data is adequate to describe two-phase conditions at stress.**

3. Standard Error of Measurement of Tests Performed:

Errors are derived from formal propagation of random and systematic errors. Source of errors include pressure transducer accuracy, accuracy of injection rates (time and volume), caliper accuracy, uncertainty in fluid viscosity and uncertainty to the interpretive method. An approximate 10% error in capillary pressure measurements is assumed for these tests.

4. Form of Raw Data:

Pressures, time, lengths and volumes

5. References Related to Data Collection:

Contract numbers:

Rock Physics Assoc. (who contracted Core Labs) AF-3945

PI name(s):

Susan Howarth

Title of approved Test Plan under which data was collected:

Test Plan: Two-Phase Flow Laboratory Program for the Waste Isolation Pilot Plant

SALADO DATA/PARAMETERS : ANHYDRITE TWO-PHASE PARAMETERS

SAND report number:
SAND94-0472

Sandia WIPP Central Files (SWCF) file code for non-SAND references:
SWCF-A:1.1.4.1:HYD/TPF

SWCF code for data package(s):
SWCF-A:1.1.4.1:HYD/TPF

6. QA Status of Data:

a. Are all of the data qualified (Yes or No?)
If Yes, answer questions below to identify method of qualification.
If No, list those data which are not yet qualified.
Yes

b. Was data qualified by QAP 20-3 (Yes or No?)
If Yes for "a" above, give SWCF of qualified data package.
No

c. Was the data the subject of audit/surveillance by SNL or DOE?
(Yes or No; and SNL or DOE?)
If Yes for "c" above, give audit reference number.
Yes – Core Labs audit 94-04

d. Was the data collected under an SNL approved QA Program?
(Yes or No?) If Yes, give title and approval dates of the QA
Program(s)
Yes
***Test Procedures and Quality Assurance Plan: Porosity, Permeability, and
Capillary Pressure Measurements in Anhydrite Samples from the WIPP
Approved by Susan Pickering on 5/28/93***

C. Interpretation of Data:

1. Was the interpretation made by reference to previous work (Yes or No?)
If yes, give reference and answer #3 below.
**Yes. Air-mercury to air-brine raw data corrected at 140° contact
angle made by Joel Walls as outlined in SAND94-0472.**

2. Was the interpretation made by using newly performed calculations
(Yes or No?) If yes, answer questions 3-9 below.
Yes

3. Form of Interpreted Data: (Example: histogram, table of interpreted values)
Tables of data, Curve fits, Histograms, Probability graphs

4. Assumptions Made During Interpretation:
 - 1) **Cores were assumed to be 100% saturated at initiation of capillary pressure tests.**
 - 2) **Used 140° contact angle for correcting mercury-air data to brine-air repository conditions**
 - 3) **The data provided here was done using tests conducted at ambient conditions (no stress) and that this data is adequate to describe two-phase conditions at stress.**
 - 4) **The centrifuge data is inadequate to describe Pt and Slr, thus these test results are not used here to determine two-phase parameters.**
 - 5) **The threshold pressures reported in SAND94-0472 are actually entry pressures (first gas bubble in to a 100% liquid saturated rock). The threshold pressures derived by curve fits to the data (as presented here) are the threshold pressure at the critical (residual) gas saturation. These threshold pressures are consistent with the Brooks and Corey and the vanGenuchten/Parker definition of threshold pressure.**

5. Name of Code(s)/Software used to Interpret Data:
Microsoft Excel v. 4.0 and KaleidaGraph v. 3.0.3b2 on a Power Macintosh 8100 using system 7.5.

6. QA Status of Code(s) used to Interpret Data: For Sandia Codes:
 - a. Was the code qualified under QAP 19-1(Yes or No?) **NA**
 - b. QAP 9-1 (Yes or No?) **NA**

7. References Related to Data Interpretation:
 - Contract numbers:
Rock Physics Assoc. (who contracted Core Labs) AF-3945

 - SAND report number:
SAND94-0472

 - Sandia WIPP Central Files (SWCF) file code for non-SAND references:
SWCF-A:1.1.4.1;HYD/TPF

 - SWCF code for data package(s):
SWCF-A:1.1.4.1;HYD/TPF

SALADO DATA/PARAMETERS : ANHYDRITE TWO-PHASE PARAMETERS

8. For interpretations made by using newly performed calculations provide documentation that you followed the requirements of QAP 9-1 Appendix B.
NA

9. For routine calculations (not using code) did you follow requirements of QAP 9-5 (Yes or No?) **Yes**

IX Correlation with other Parameters (List only those not statistically independent of the parameter documented here):

**See Attachment 1:
 Sgr and Pt
 Pt and permeability**

X. Limitations or qualifications for usage of data by Performance Assessment (PA):
Data was only measured on specimens from MB139 taken from intact rock.

XI. Attachments:

Attachment 1. Capillary Pressure Model Parameters Calc. Sheet
Guidance documents are located in the following SWCF:
 SWCF-A: ^{WBS:} 1.2.07.1:PDD:QA:SALADO:CORR:Guidance Documents

TC 12/2/95

X11. Data

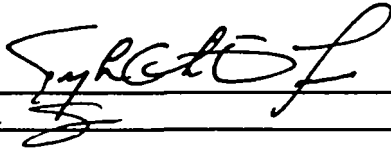
Sample	Pt (MPa)	Slr (%)	Sgr (%)	Lambda
5	0.54132	7.262	12.159	0.655
7	0.78	6.986	7.7729	0.66452
11	0.45026	17.401	1.3981	0.55775
13	0.75274	10.861	19.719	0.652
21	0.32914	0.77846	2.5201	0.49053
23	0.39724	6.8842	3.2177	0.84178
Statistics				
	Pt (MPa)	Slr (%)	Sgr (%)	Lambda
Minimum	0.329	0.778	1.398	0.491
Maximum	0.780	17.401	19.719	0.842
Sum	3.251	50.173	46.265	3.862
Points	6	6	6	6
Mean	0.5418	8.3621	7.7108	0.6436
Median	0.4958	7.1240	5.4953	0.6536
Std Deviation	0.1875	5.4908	7.0228	0.1189
Variance	0.0351	30.1492	49.3195	0.0141
Std Error	0.0765	2.2416	2.8670	0.0486
Skewness	0.4327	0.5632	1.1346	0.6365
Kurtosis	-1.8573	1.4753	0.5853	1.2579

12/96

RECORD 2

Attachment 1. Capillary Pressure Model Parameters Calc. Sheet

Calculation Tracy Christian-Frear



Date: 12/20/95

Checked By: Susan Howarth

Date: 12/21/95

Purpose:

To determine the two-phase capillary pressure characteristic curve that best fits the data, and the parameters for BRAGFLO calculations.

Specific Parameters are: Threshold pressure (Pt), residual brine and gas saturation (Sbr and Sgr),
and the pore size distribution parameter (lambda)

The following is a list of the paramters:

CAP_MOD
PC_MAX
PORE_DIS
RELP_MOD
SAT_IBRN
SAT_RBRN
SAT_RGAS
PCT_A
PCT_EXP**Calculation Description:**

Using the 140 degree contact angle corrected mercury injection core data found in SAND94-0472

determine the following by using the standard mixed B/C and vG/P formulas added to the general curve fit equations of KaledaGraph software (off the shelf software

- The two-phase characteristic curve (either Brooks/Corey (B/C) or vanGenuchten (vG/P)) that best fits the data;
- The Brooks and Corey (B/C) parameters of Pt, Sgr, Slr, and lambda that best fit the data.
(BRAGFLO generates vG/P parameters from the B/C parameters)
- Determine the initial brine saturation
- Determine the maximum capillary pressure, Pc.
- Based on the value of Pt determine PCT_A and PCT_EXP

I did not start with the values of Pt found in Table 12 of SAND94-0472 because the Pt values are actually entry pressure values (Pe at Saturation=0.999), not threshold pressure as used in the Brooks and Corey or vanGenuchten/Parker characteristic curves (Pt at liquid saturation =1-Sgr).

I did not start with the values of Slr found in Table 12 of SAND94-0472 because those values may be the result of equipment limitations.

Equations:

Mixed Brooks and Corey (Appendix E of SAND94-0472):

$$P_c = P_t / S_e^{1/\lambda} \quad \text{eqn 1}$$

$$S_e = (S - S_{lr}) / (1 - S_{lr} - S_{gr}) \quad \text{eqn 2}$$

vG/P:

$$P_c = 1/\alpha \left((S_e')^{(-1/m)} - 1 \right)^{1-m} \quad \text{eqn 3}$$

$$m = \lambda / (\lambda + 1) \quad \text{eqn 4}$$

$$S_e' = (S - S_{lr}) / (1 - S_{lr}) \quad \text{eqn 5}$$

$$\alpha = (1 / (P_t / 0.5^{1/\lambda})) \left((0.5^{(-1/m)} - 1) \right)^{1-m} \quad \text{eqn 6}$$

Threshold Pressure:

$$P_t = PCT_A * k^{PCT_EXP} \quad \text{eqn 7}$$

$$\text{if } PCT_EXP = 0, \text{ then } PCT_A = P_t$$

Capillary Pressure Model Params
Calculation Sheet

Variables:	Description	Determination	KaleidaGraph Curve fit variable
Pc	Capillary Pressure	data	
Pt	Threshold Pressure	data fit	m 1
S	Saturation of brine	data	
Slr	Residual liquid saturation	data fit	m 2
Sgr	Residual gas saturation	data fit	m 3
lambda	pore-size distribution param	data fit	m 4
m	vanGenuchten parameter 1	Fit and calculated from lambda	m 6
alpha	vanGenuchten parameter 2	calc and fit	m 5
Se and Se'	Effective Saturation	calculated	
k	Permeability	data	

Assumptions:

- 1) The centrifuge data is assumed to be inadequate to define the threshold pressure and other parameters because the initial speed was too high to determine Pt, and equipment limitations were such that Slr could not be adequately defined.
- 2) Cores were assumed to be 100% saturated with liquid at initiation of capillary pressure test.
- 3) 140 degree contact angle was best for correcting Mercury-air data to brine-air repository conditions
- 4) The data provided here was done using tests conducted at ambient conditions (no stress) and that this data is adequate to describe two-phase conditions at stress.
- 5) The threshold pressures reported in SAND94-0472 are actually entry pressures (first gas bubble in to a 100% liquid saturated rock). The threshold pressures derived by curve fits to the data (as presented here) are the threshold pressure at the critical (residual) gas saturation. These threshold pressures are consistent with the Brooks and Corey and the vanGenuchten/Parker definition of threshold pressure.

Process:

Verified that Kaliedagraph curve fits were working as required.

Curve fit steps:

1. Using KaliedaGraph general curve fit routine, define the vG/P equation for mixed relative permeability (eqn 3 except Se' is defined as in eqn 2) and solve for all 4 variables (Alpha, Slr, Sgr, m) based upon Pc vs Saturation data.
2. Check the curve fit R2 and chisq. R2 > 0.99 and chisq < 10. (Also see if the curve fit looks adequate)
 - If they are OK— goto 3
 - If they are not OK— Eliminate data points (usually choose data with less than 40% saturation and one low sat. point) and goto 1.
3. Check for values with an error less than 12%. Use that (those) values in subsequent curve fits until you get a Slr and Sgr that has less than 10% error.
4. Put the Slr and Sgr determined in the previous steps into the mixed B/C curve fit (eqn 1) and fit the data.
5. Obtain v: 3 variables (Pt, Slr, lambda). If neither is negative, find the variable that has the least error and fix that variable
6. Determine the vG/P parameter m from lambda (eqn 4), and alpha from Pt, lambda, m (eqn 6).
7. Using eqn 1 define Pc data that fit the parameters determined for B/C and add the data to the graph.
8. Using eqn 3 define Pc data that fit the parameters determined for vG/P and add the data to the graph.
9. Curve fit the B/C generated data to check the software.
10. Curve fit the vG/P generated data to check the software.
11. Equate PCT_A to the value determined for Pt, and equate PCT_EXP to 0 (see eqn 7).

Solution: The values found are provided in Table 1.
Each curve fit data and errors sheet are provided as indicated in Table 1.

No definitive data exists to recommend one set of characteristic curves over the other. However the data does show that either B/C or vG/P can be used to describe the data.

Figure 1 a, b, c, d, e, f show that there is possibly a relationship between Pt and Sgr (Fig. 1b)

Figure 2 shows box diagrams indicating that there are data that may be considered statistical outliers.

Figures 3, 4, 5 and 6 show the histograms and probability distribution for Pt, Slr, Sgr and lambda, respectively.

Figure 7 shows the curve for the mean values

Figures 8 though 13 are the curve fits for each specimen (including data)

Figure 14 shows the relationship between the Pt determined, the Davies equation and the entry pressures determined for the specimens.

Recommendations:

1. use 50% mixed B/C and 50% mixed vG/P characteristic curves (Pc and rel perm).
2. The mean value of Sgr is: Sgr=7.71%
3. The mean value of Pt is: Pt=0.54 MPa
4. The mean value of Slr is: Slr=8.36%
5. The mean value of lambda is: lambda= 0.644
6. The maximum Pc should be 100 Mpa (seems adequate to provide full data realization)
7. The initial brine saturation should be 100% (no evidence for anything else).
8. The Davies relationship ($Pt=0.26 \cdot k^{-0.348}$) appears to be adequate in relating threshold pressure to permeability for the anhydrites. PCT_A=.26 Pa: PCT_EXP=-.348

TABLE 1. Capillary Pressure Curve Fit Values

Sample	Pt (MPa)	Slr (%)	Sgr (%)	Lambda	m	Alpha (1/MPa)	Pc Max (MPa)	Figure	Perm (m2)
5	0.54132	7.262	11.042	0.655	0.3958	1.646	100	8	5.10E-19
7	0.78	6.986	7.7729	0.66452	0.3992	1.141	100	9	9.50E-19
11	0.45026	17.401	1.3981	0.55775	0.3580	2.010	100	10	1.80E-18
13	0.75274	10.861	19.719	0.652	0.3947	1.184	100	11	1.60E-18
21	0.32914	0.77846	2.5201	0.49053	0.3291	2.785	100	12	7.70E-19
23	0.39724	6.8842	3.2177	0.84178	0.4570	2.201	100	13	1.30E-18
Statistics	Pt (MPa)	Slr (%)	Sgr(%)	Lambda					
Minimum	0.329	0.778	1.398	0.491					
Maximum	0.780	17.401	19.719	0.842					
Sum	3.251	50.173	46.265	3.862					
Points	6	6	6	6					
Mean	0.5418	8.3621	7.7108	0.6436	0.391591	1.648	100		
Median	0.4958	7.1240	5.4953	0.6536					
Std Deviation	0.1875	5.4908	7.0228	0.1189					
Variance	0.0351	30.1492	49.3195	0.0141					
Std Error	0.0765	2.2416	2.8670	0.0486					
Skewness	0.4327	0.5632	1.1346	0.6365					
Kurtosis	-1.8573	1.4753	0.5853	1.2579					

Verification of Software as per QAP 9-1:

1. Software used:
MicroMicrosoft Excel v. 4.0 and KaleidaGraph v. 3.0.3b2 on a PowerMacintosh with system 7.5.
2. All software is considered "off the shelf" and thus can be verified in use.
3. Kaleidagraph was verified by computing the characteristic curve values and then applying the appropriate curve fit. The R2 value of the curve fit should equal 1. (shown on each graph)
4. Hand calculations of equations for Excell. An audit of the worksheet is provided from page 20 through 37 at the end of this calc sheet which includes a map, formulae, and contents.

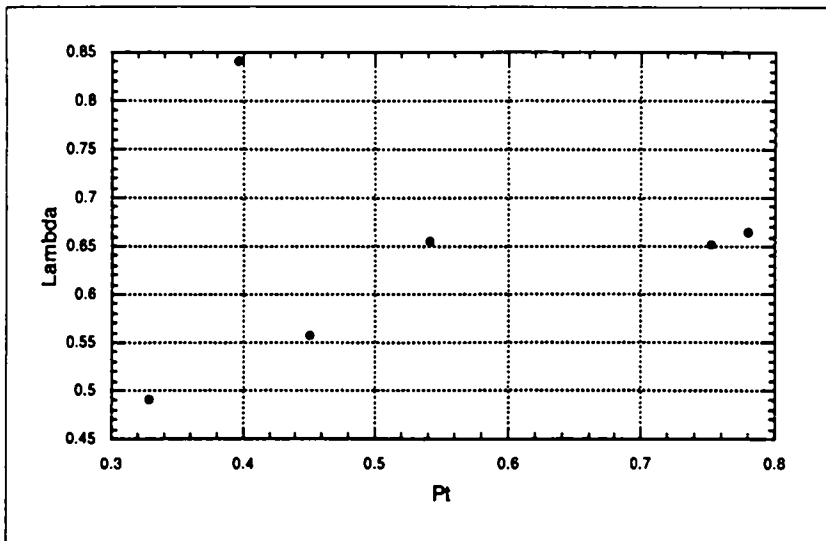


Figure 1a

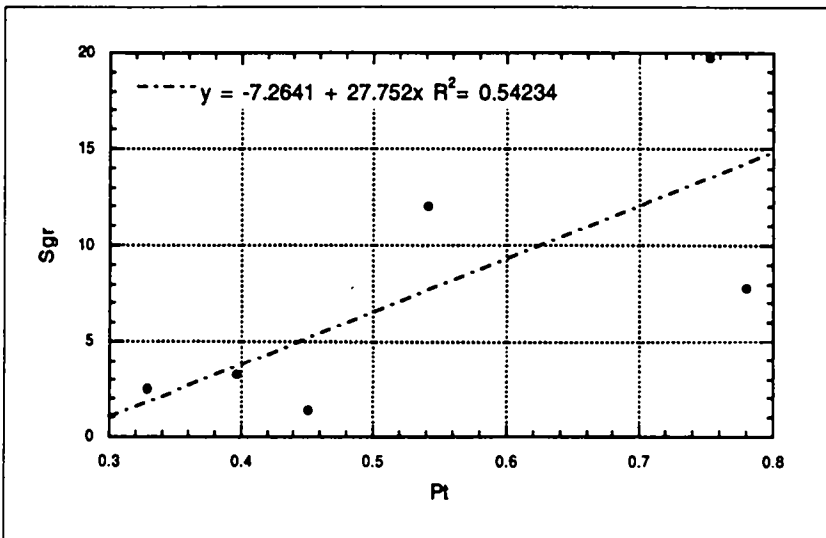


Figure 1b

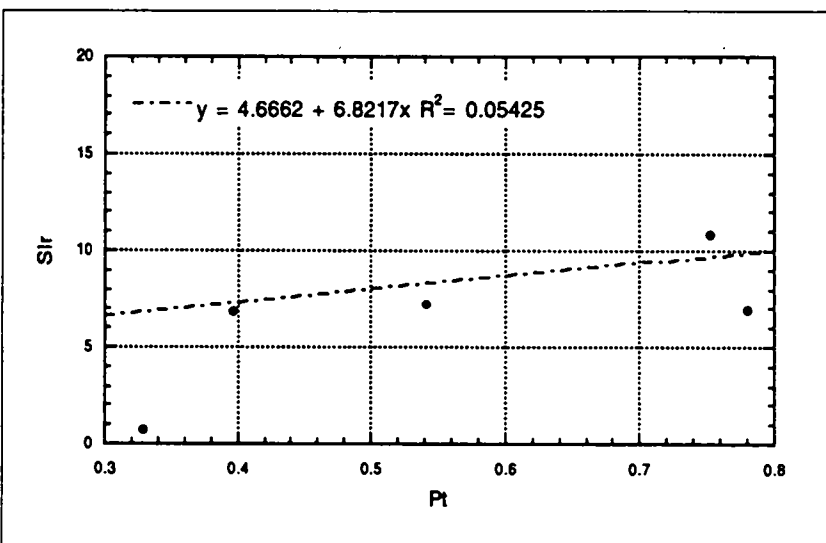


Figure 1c

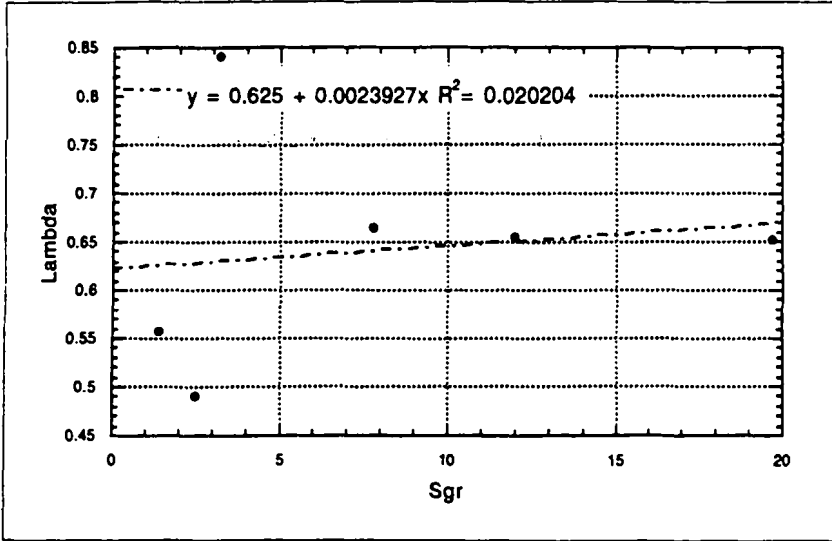


Figure 1d

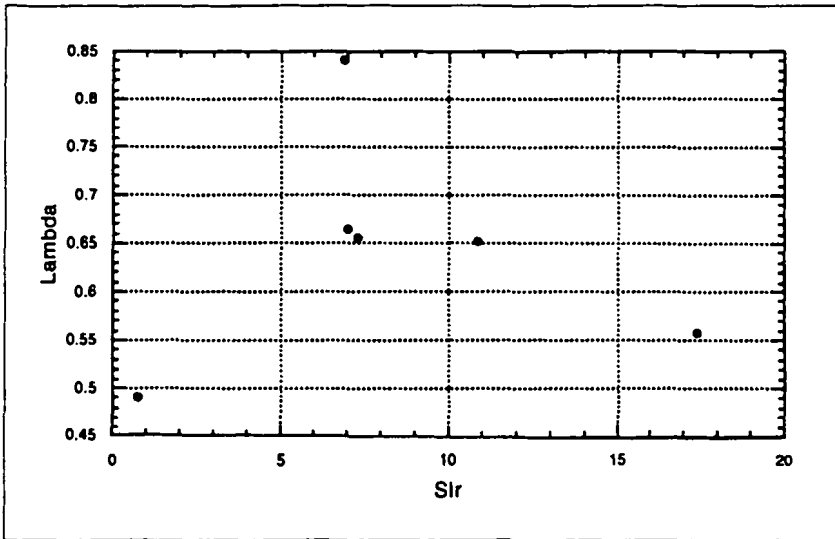


Figure 1e

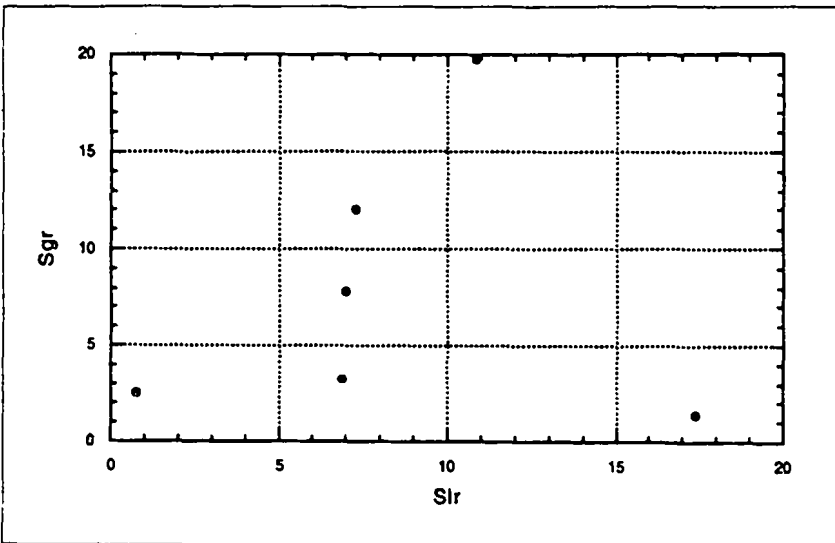


Figure 1f

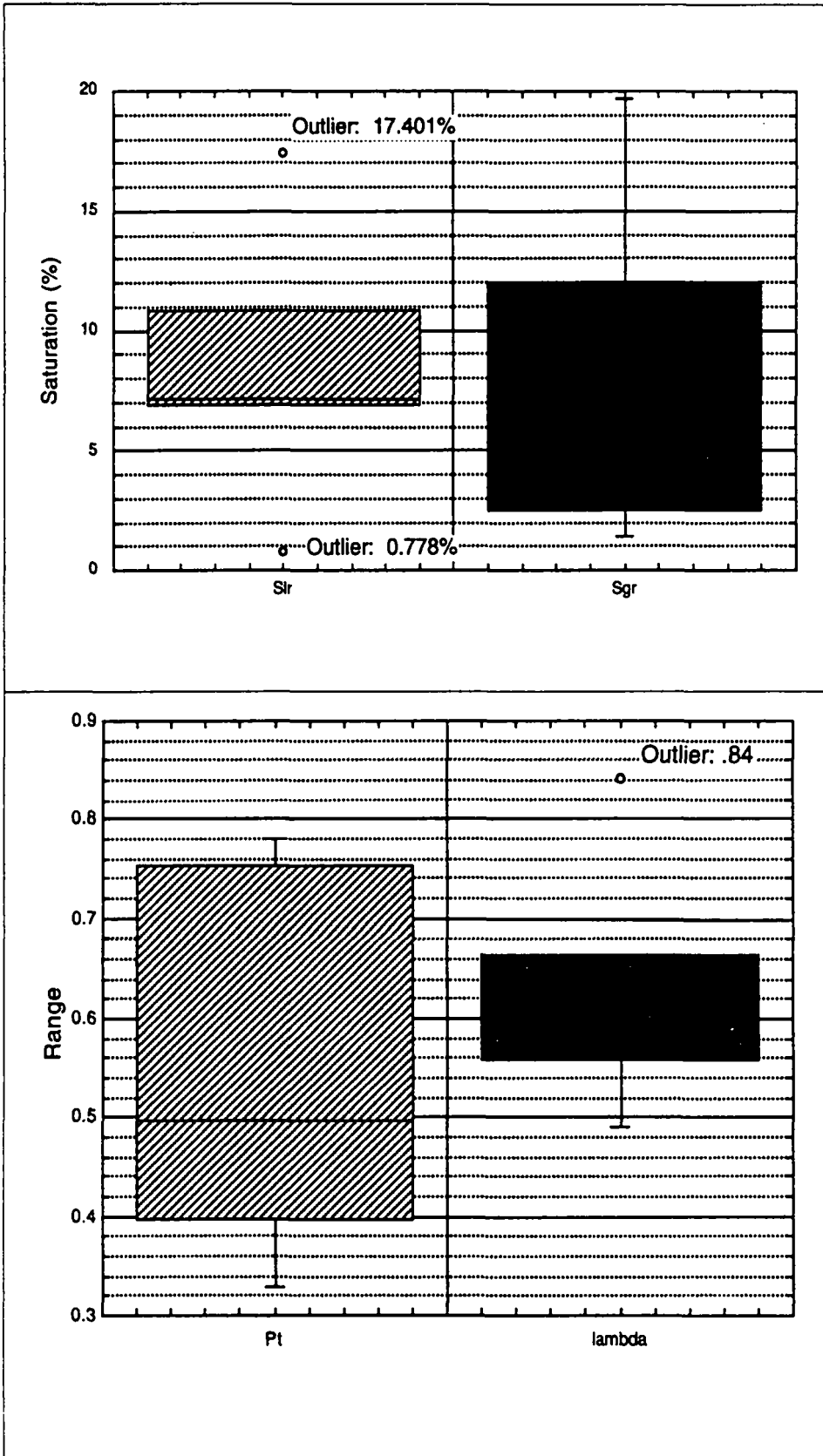


Figure 2. Box diagrams

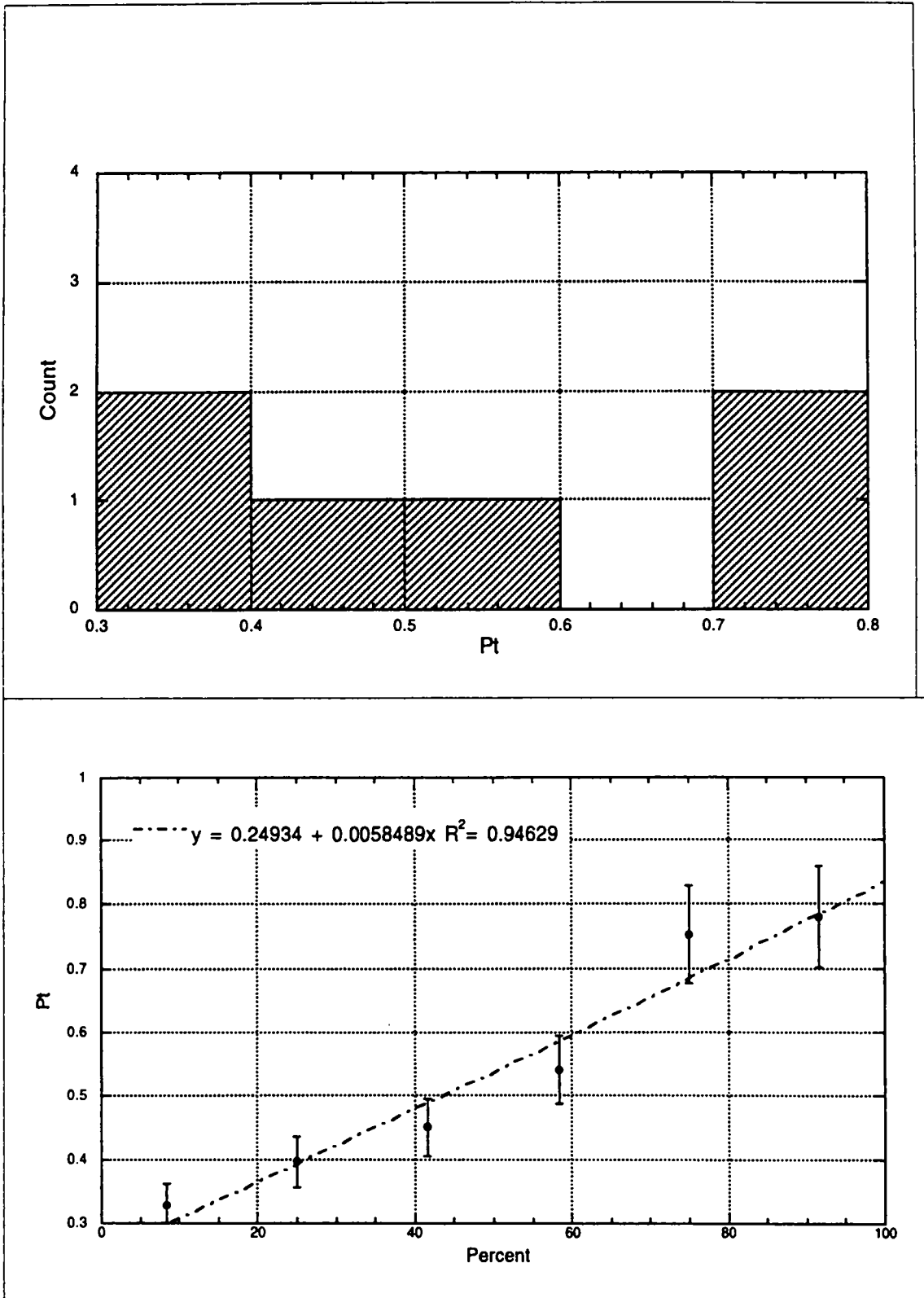


Figure 3. Pt histogram and probability graphs

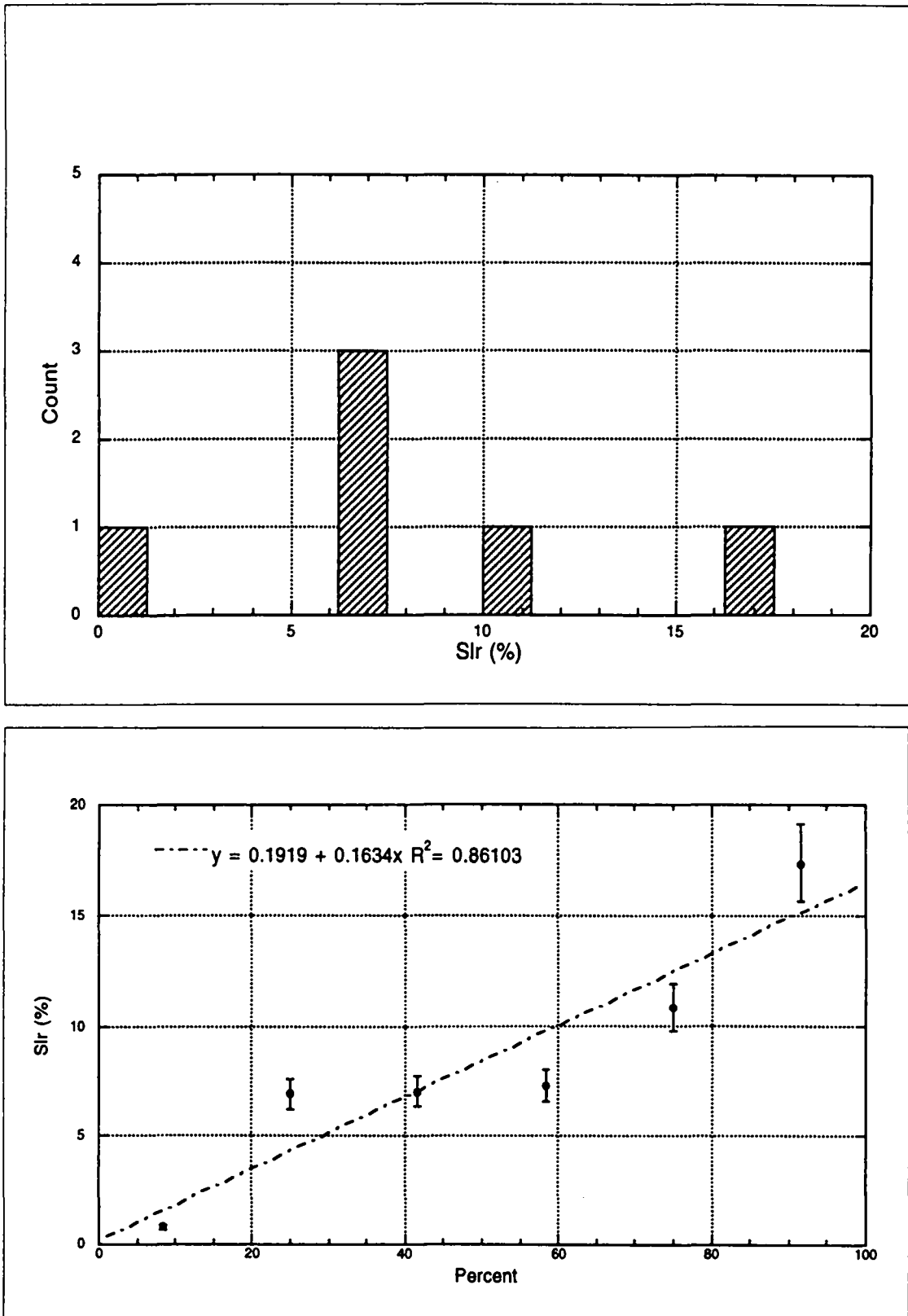


Figure 4. Slr histogram and probability graph

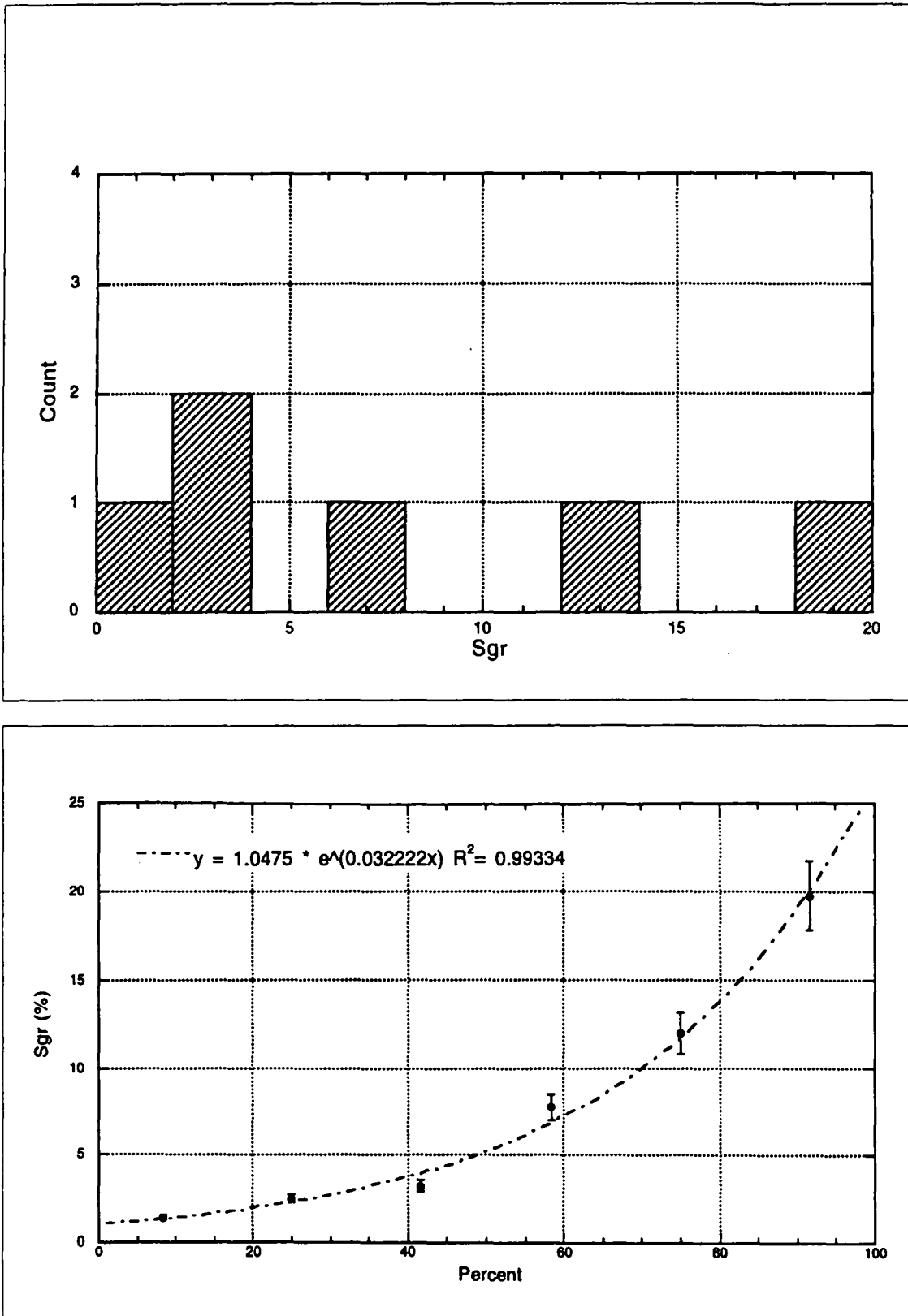


Figure 5. Sgr histogram and probability graphs

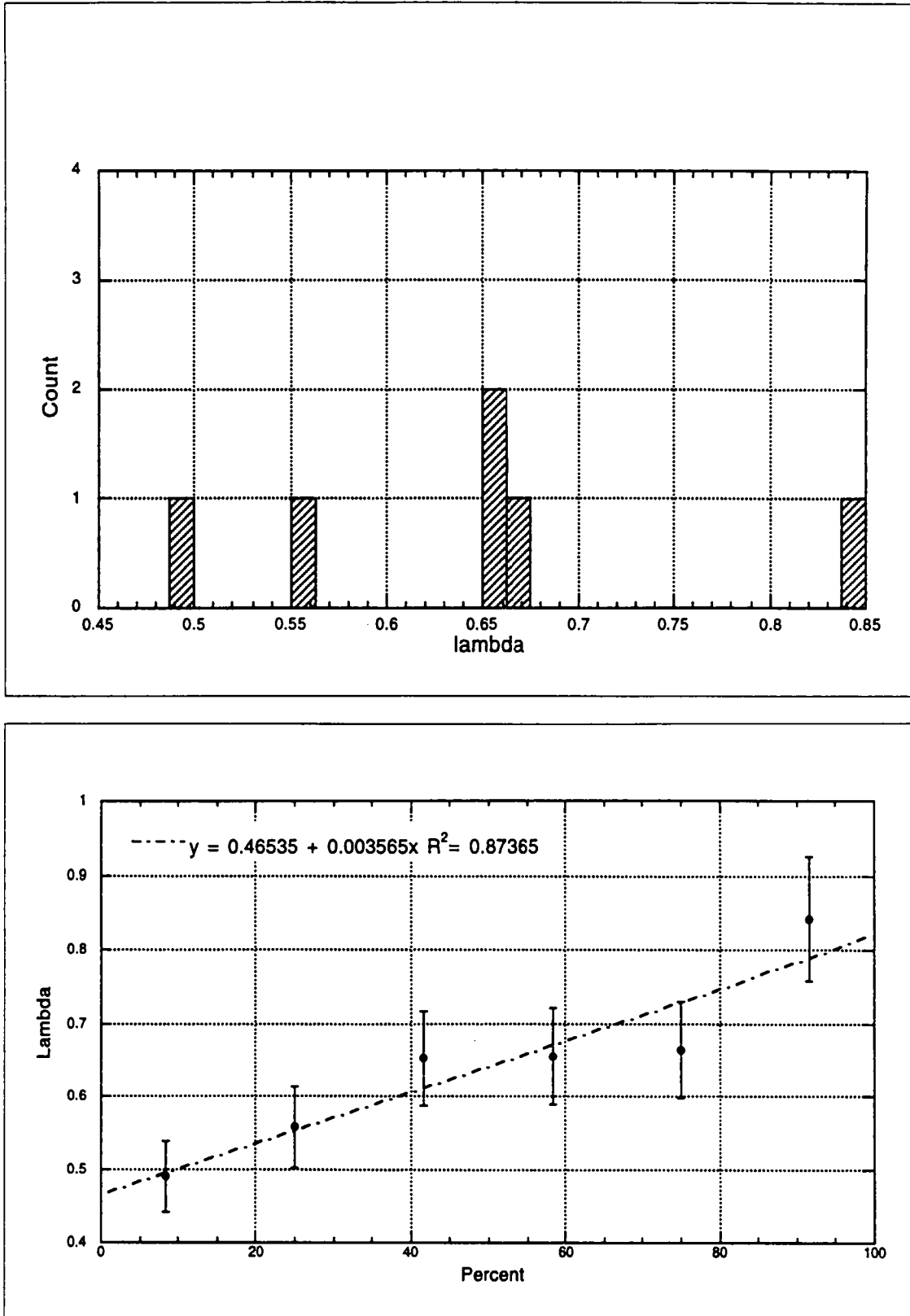


Figure 6. Lambda histogram and probability graphs

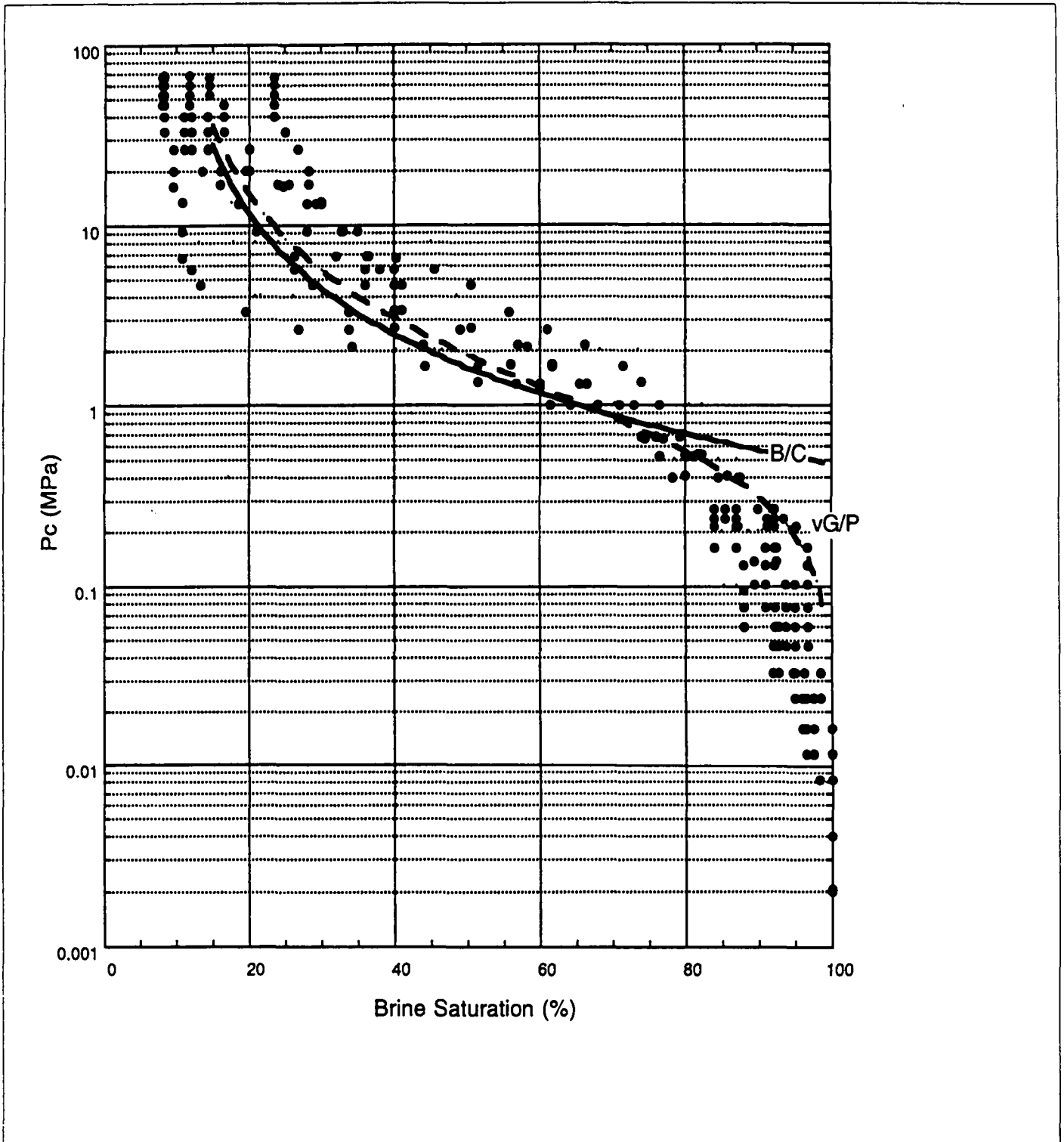
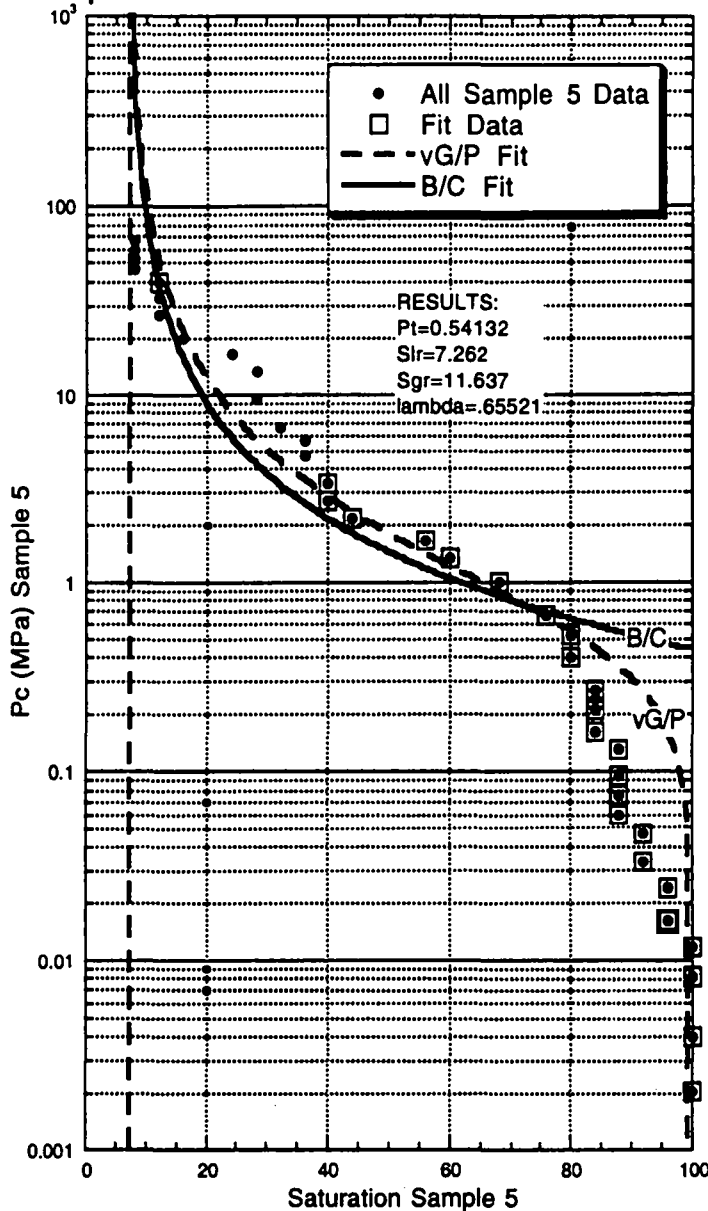


Figure 7. Mean values characteristic curves

Sample 5 Data 11:57:09 AM 12/14/95 vG/P



$$y = (1/m5)^{((((m0-m2)/(100-...))$$

	Value	Error
m2	7.262	1.2759
m3	11.637	0.65159
m5	1.0531	0.10894
m6	0.42977	0.027708
Chisq	0.41455	NA
R ²	0.99973	NA

$$y = (1/m5)^{((((m0-m2)/(100-...))$$

	Value	Error
m2	7.262	0.10451
m5	1.0531	0.028209
Chisq	0.41455	NA
R ²	0.99973	NA

B/C

$$y = m1/((m0-7.262)/(100-7.26...))$$

	Value	Error
m1	0.5413	0.06774
m4	0.65521	0.019205
Chisq	5.1848	NA
R ²	0.99657	NA

$$y = m1/((m0-7.262)/(100-7.26...))$$

	Value	Error
m1	0.54132	0.0061217
Chisq	5.1848	NA
R ²	0.99657	NA

vG/P: Validation of Software: m6 should =.3958

$$y = (1/1.646)^{((((m0-7.262)...))$$

	Value	Error
m6	0.3958	3.2804e-12
Chisq	8.4361e-13	NA
R ²	1	NA

B/C: Validation of Software: m4 should=.65521

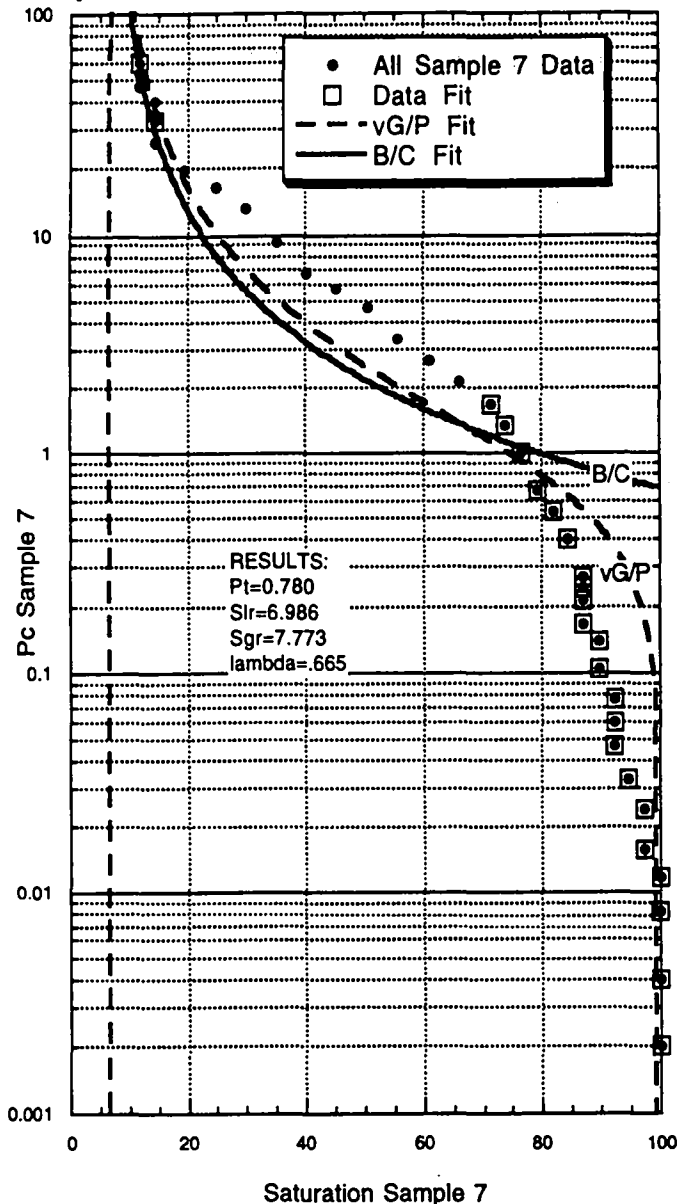
$$y = .54132/((m0-7.262)/(100-...))$$

	Value	Error
m4	0.65521	5.3358e-11
Chisq	1.6523e-11	NA
R ²	1	NA

General Curve Fit "vG/P 1"	$(1/m5)^{((((m0-m2)/(100-m2-m3))^{(1/m6)}-1)^{(1-m6))}$
General Curve Fit "vG/P 2"	$(1/m5)^{((((m0-m2)/(100-m2-11.637))^{(-1/1.42977)}-1)^{(1-1.42977))}$
General Curve Fit "vG/P 3"	$(1/1.646)^{((((m0-7.262)/(100-7.262))^{(-1/m6)}-1)^{(1-m6))}$
General Curve Fit "Brooks/Corey"	$m1/((m0-7.262)/(100-7.262-11.637))^{(1/m4)}$
General Curve Fit "B/C2"	$m1/((m0-7.262)/(100-7.262-11.637))^{(1/1.65521)}$
General Curve Fit "B/C3"	$.54132/((m0-7.262)/(100-7.262-11.637))^{(1/m4)}$

Figure 8. Sample 5 curve fits

Sample_7.data 12:34:43 PM 12/14/95 vG/P



$y = (1/m5)^{((((m0-m2)/(100-...))$

	Value	Error
m2	8.8747	1.0607
m3	23.094	3.6823
m5	0.21275	0.055392
m6	0.561	0.049125
Chisq	333.41	NA
R ²	0.9745	NA

$y = (1/m5)^{((((m0-m2)/(100-...))$

	Value	Error
m2	6.986	0.22449
m3	7.7729	0.23324
m5	0.80499	0.065639
m6	0.42739	0.0086918
Chisq	0.6288	NA
R ²	0.99985	NA

B/C

$y = m1/((m0-6.986)/(100-6.98...$

	Value	Error
m1	0.78033	0.10006
m4	0.66452	0.020229
Chisq	12.383	NA
R ²	0.99712	NA

$y = m1/((m0-6.986)/(100-6.98...$

	Value	Error
m1	0.78032	0.0083466
Chisq	12.383	NA
R ²	0.99712	NA

General Curve Fit "vG/P 1"
$(1/m5)^{((((m0-m2)/(100-m2-m3))^{(-1/m6)}-1)^{(1-m6))}$
General Curve Fit "vG/P 2"
$(1/1.141)^{((((m0-6.986)/(100-6.986))^{(-1/m6)}-1)^{(1-m6))}$
General Curve Fit "Brooks/Corey"
$m1/((m0-6.986)/(100-6.986-7.7729))^{(1/m4)}$
General Curve Fit "B/C2"
$m1/((m0-6.986)/(100-6.986-7.7729))^{(1/0.66452)}$
General Curve Fit "B/C3"
$.78032/((m0-6.986)/(100-6.986-7.7729))^{(1/m4)}$

vG/P: Validation of Software: m6 should =.3992

$y = (1/1.141)^{((((m0-6.986)...$

	Value	Error
m6	0.3992	1.3935e-10
Chisq	6.4558e-12	NA
R ²	1	NA

B/C: Validation of Software: m4 should=.66452

$y = .78032/((m0-6.986)/(100-...$

	Value	Error
m4	0.66452	2.3784e-10
Chisq	1.5711e-12	NA
R ²	1	NA

Figure 9. Sample 7 curve fits

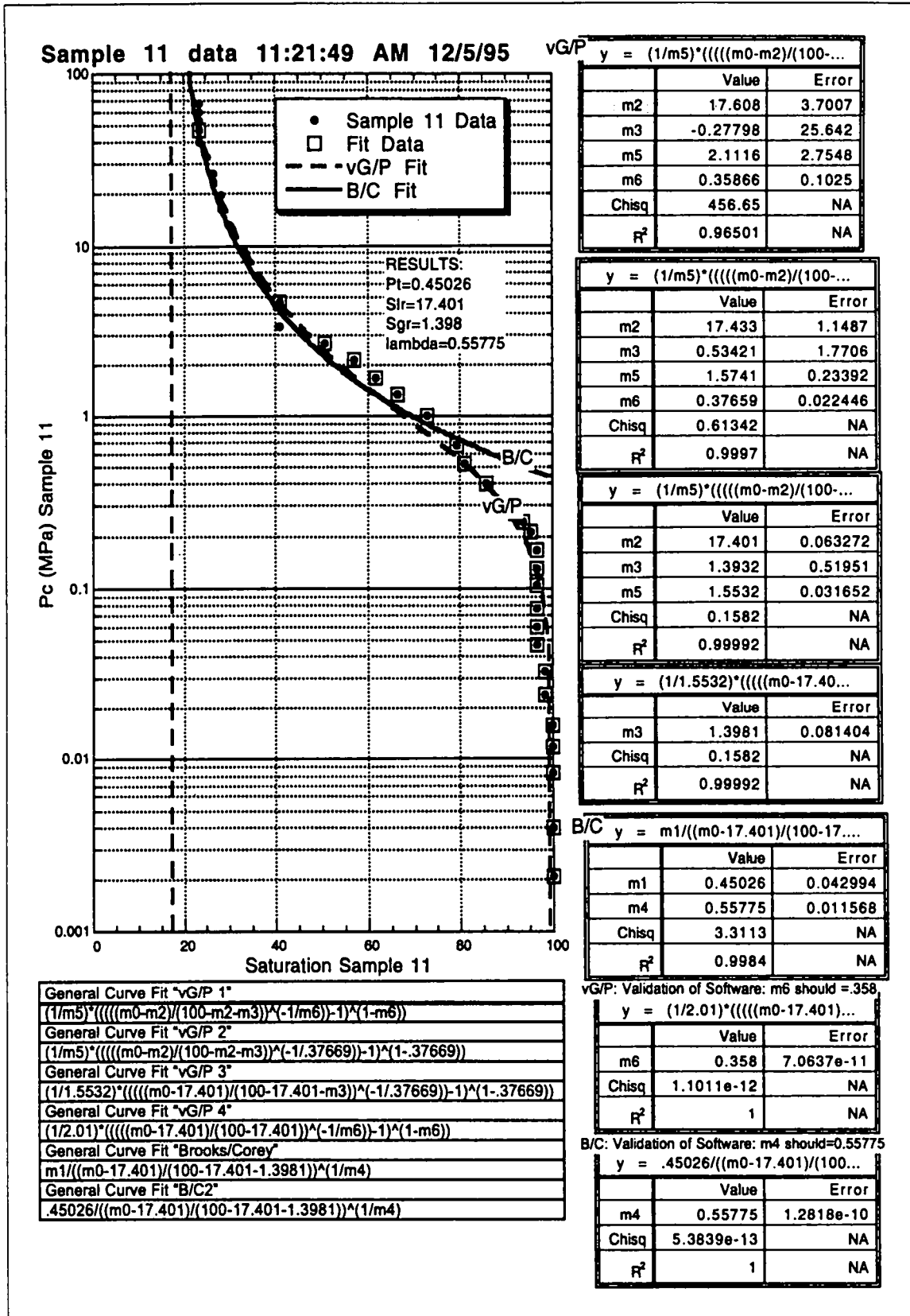
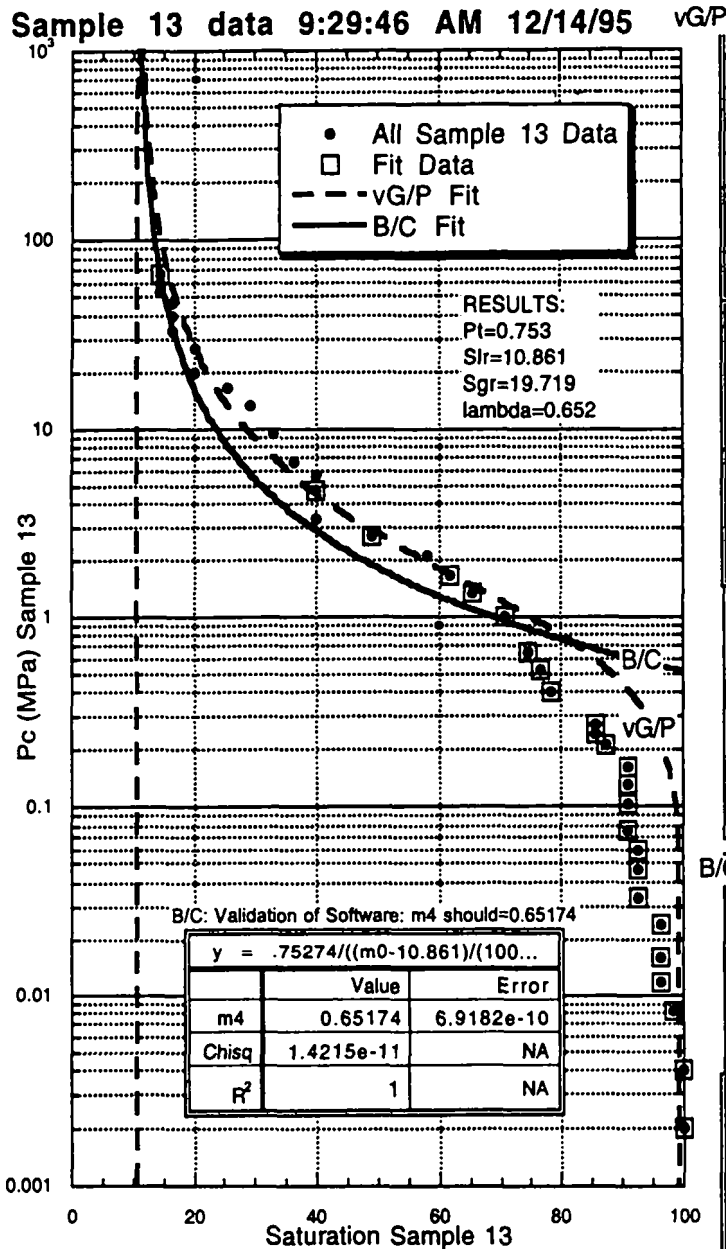


Figure 10. Sample 11 curve fits



$$y = (1/m5)^{((((m0-m2)/(100-...))^{1/m6}-1)^{1-m6})}$$

	Value	Error
m2	10.002	1.4335
m3	25.068	6.2913
m5	0.37471	0.1267
m6	0.45984	0.048036
Chisq	225.57	NA
R ²	0.98271	NA

$$y = (1/m5)^{((((m0-m2)/(100-...))^{1/m6}-1)^{1-m6})}$$

	Value	Error
m2	10.976	1.0028
m3	20.553	1.1045
m5	0.59574	0.062887
m6	0.44388	0.027805
Chisq	0.37516	NA
R ²	0.99991	NA

$$y = (1/m5)^{((((m0-m2)/(100-...))^{1/m6}-1)^{1-m6})}$$

	Value	Error
m2	10.861	0.079001
m3	19.719	0.94012
m5	0.61652	0.02239
Chisq	0.35013	NA
R ²	0.99992	NA

$$y = m1/((m0-10.861)/(100-10...))^{1/m4}$$

	Value	Error
m1	0.75275	0.10968
m4	0.65174	0.021272
Chisq	8.4475	NA
R ²	0.99799	NA

$$y = m1/((m0-10.861)/(100-10...))^{1/m4}$$

	Value	Error
m1	0.75274	0.0066906
Chisq	8.4475	NA
R ²	0.99799	NA

General Curve Fit "vG/P 1"	$(1/m5)^{((((m0-m2)/(100-m2-m3))^{1/m6}-1)^{1-m6})}$
General Curve Fit "vG/P 2"	$(1/m5)^{((((m0-m2)/(100-m2-m3))^{1/1.44021}-1)^{1-1.44021})}$
General Curve Fit "vG/P 3"	$(1/1.184)^{((((m0-10.861)/(100-10.861))^{1/m6}-1)^{1-m6})}$
General Curve Fit "Brooks/Corey"	$m1/((m0-10.861)/(100-10.861-19.719))^{1/m4}$
General Curve Fit "B/C2"	$m1/((m0-10.861)/(100-10.861-19.719))^{1/0.65174}$
General Curve Fit "B/C3"	$.75274/((m0-10.861)/(100-10.861-19.719))^{1/m4}$

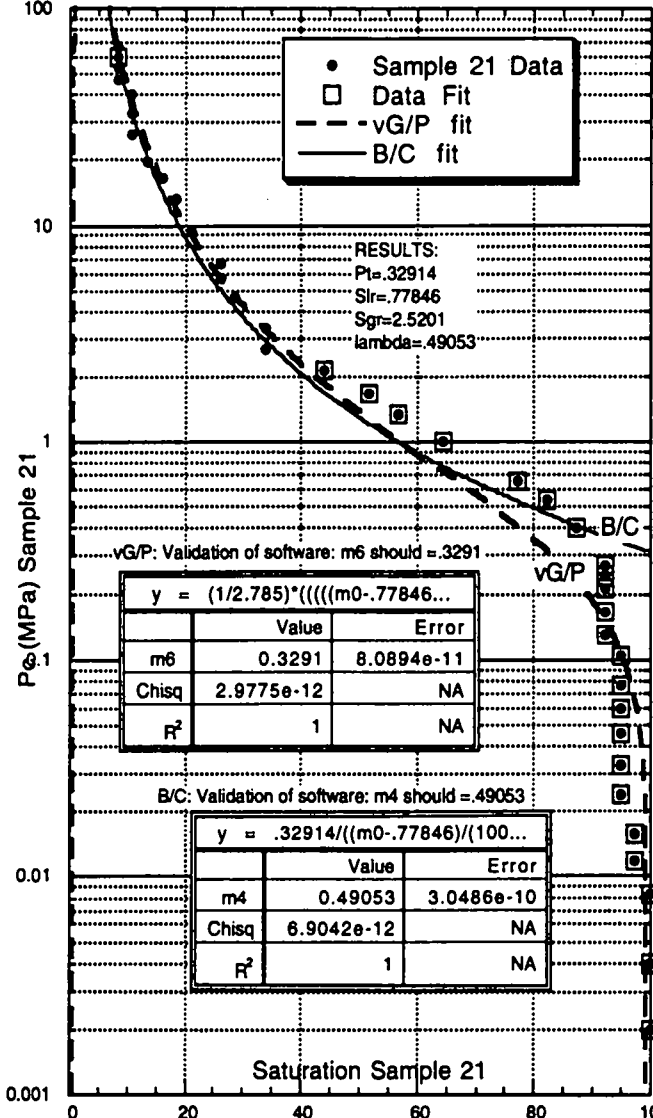
vG/P: Validation of Software: m6 should = .3946

$$y = (1/1.184)^{((((m0-10.861...))^{1/m6}-1)^{1-m6})}$$

	Value	Error
m6	0.3946	1.027e-10
Chisq	7.0805e-12	NA
R ²	1	NA

Figure 11. Sample 13 curve fits

Sample 21 Data 2:26:30 PM 12/5/95



$y = (1/m5)^{((((m0-m2)/(100-...))}$

	Value	Error
m2	0.55551	3.472
m3	2.4469	25.431
m5	1.9078	1.8813
m6	0.35058	0.073591
Chisq	321.57	NA
R ²	0.97535	NA

$y = (1/m5)^{((((m0-m2)/(100-...))}$

	Value	Error
m2	0.77834	1.5129
m3	2.5342	0.5038
m5	1.7947	0.16896
m6	0.35298	0.020812
Chisq	0.10557	NA
R ²	0.99997	NA

$y = (1/m5)^{((((m0-m2)/(100-...))}$

	Value	Error
m2	0.7785	0.10544
m3	2.5199	0.47547
m5	1.7966	0.048236
Chisq	0.104	NA
R ²	0.99997	NA

$y = (1/1.7966)^{((((m0-m2)/(...))}$

	Value	Error
m2	0.77846	0.034373
m3	2.52	0.40294
Chisq	0.104	NA
R ²	0.99997	NA

$y = (1/1.7966)^{((((m0-.7784...))}$

	Value	Error
m3	2.5201	0.058376
Chisq	0.104	NA
R ²	0.99997	NA

$y = (1/2.785)^{((((m0-.77846...))}$

	Value	Error
m6	0.3291	8.0894e-11
Chisq	2.9775e-12	NA
R ²	1	NA

$y = .32914/((m0-.77846)/(100-...))$

	Value	Error
m4	0.49053	3.0486e-10
Chisq	6.9042e-12	NA
R ²	1	NA

$y = m1/((m0-.77846)/(100-.77...))$

	Value	Error
m1	0.32913	0.038377
m4	0.49053	0.011018
Chisq	1.7003	NA
R ²	0.9995	NA

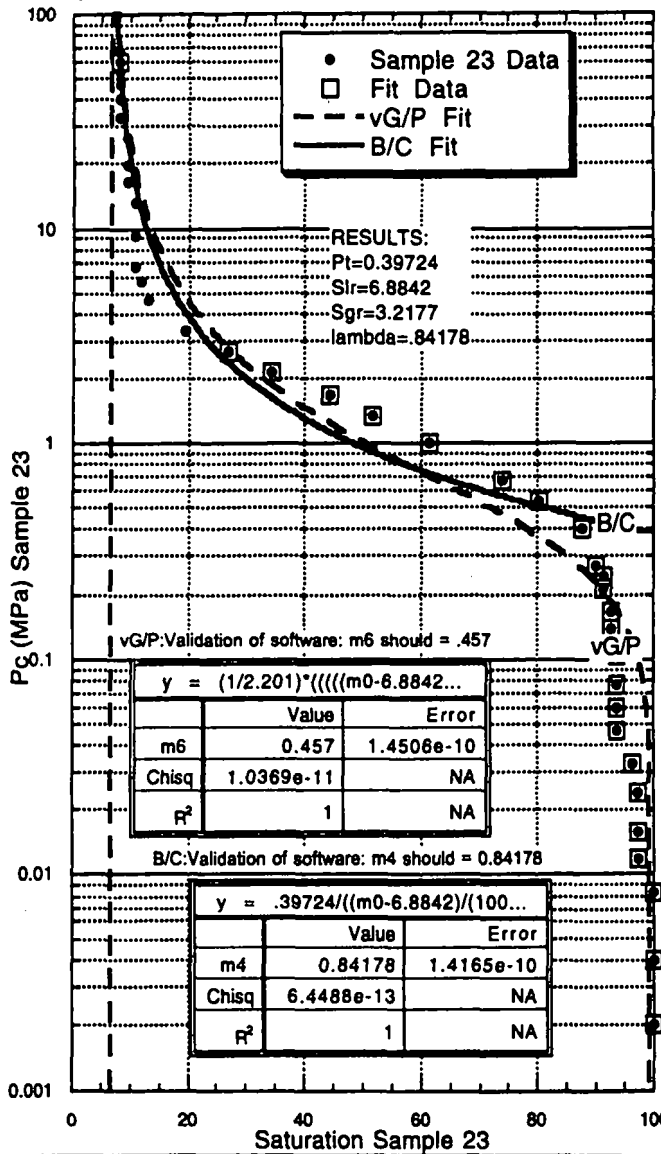
General Curve Fit "vG/P 1"	$(1/m5)^{((((m0-m2)/(100-m2-m3))^{1/m6}-1)^{1-m6})}$
General Curve Fit "vG/P 2"	$(1/m5)^{((((m0-m2)/(100-m2-m3))^{1/1.35298}-1)^{1-1.35298})}$
General Curve Fit "vG/P 3"	$(1/1.7966)^{((((m0-m2)/(100-m2-m3))^{1/1.35298}-1)^{1-1.35298})}$
General Curve Fit "vG/P 4"	$(1/1.7966)^{((((m0-.77846)/(100-.77846-m3))^{1/1.35298}-1)^{1-1.35298})}$
General Curve Fit "vG/P 5"	$(1/2.785)^{((((m0-.77846)/(100-.77846-0))^{1/m6}-1)^{1-m6})}$
General Curve Fit "Brooks/Corey"	$m1/((m0-.77846)/(100-.77846-2.5201))^{1/m4}$
General Curve Fit "B/C2"	$m1/((m0-.77846)/(100-.77846-2.5201))^{1/1.49053}$
General Curve Fit "B/C3"	$.32914/((m0-.77846)/(100-.77846-2.5201))^{1/m4}$

$y = m1/((m0-.77846)/(100-.77...))$

	Value	Error
m1	0.32914	0.0014887
Chisq	1.7003	NA
R ²	0.9995	NA

Figure 12. Sample 21 curve fits

Sample 23 data



vG/P $y = (1/m5)^{((((m0-m2)/(100-...))}$

	Value	Error
m2	6.4023	2.2757
m3	-67.739	10248
m5	56.143	6370.3
m6	0.36158	0.20869
Chisq	881.58	NA
R ²	0.93256	NA

$y = (1/m5)^{((((m0-m2)/(100-...))}$

	Value	Error
m2	6.8705	0.33304
m3	2.4815	0.26179
m5	1.7183	0.17424
m6	0.47663	0.01972
Chisq	0.36215	NA
R ²	0.99989	NA

$y = (1/m5)^{((((m0-m2)/(100-...))}$

	Value	Error
m2	6.8732	0.038617
m3	2.4813	0.25583
m5	1.7222	0.05475
Chisq	0.36206	NA
R ²	0.99989	NA

$y = (1/1.7222)^{((((m0-m2)/(...))}$

	Value	Error
m2	6.8842	0.016869
m3	3.2146	1.1258
Chisq	0.35812	NA
R ²	0.9999	NA

$y = (1/1.7222)^{((((m0-6.884...))}$

	Value	Error
m3	3.2177	0.16467
Chisq	0.35812	NA
R ²	0.9999	NA

B/C $y = m1/((m0-6.8842)/(100-6.8...))$

	Value	Error
m1	0.39723	0.044994
m4	0.84178	0.019069
Chisq	2.6033	NA
R ²	0.99924	NA

$y = m1/((m0-6.8842)/(100-6.8...))$

	Value	Error
m1	0.39724	0.0021747
Chisq	2.6033	NA
R ²	0.99924	NA

General Curve Fit "vG/P 1"	$(1/m5)^{((((m0-m2)/(100-m2-m3))^{(1-1/m6)}-1)^{(1-m6))}$
General Curve Fit "vG/P 2"	$(1/m5)^{((((m0-m2)/(100-m2-m3))^{(1-1/47663)}-1)^{(1-47663))}$
General Curve Fit "vG/P 3"	$(1/1.7222)^{((((m0-m2)/(100-m2-m3))^{(1-1/47663)}-1)^{(1-47663))}$
General Curve Fit "vG/P 4"	$(1/1.7222)^{((((m0-6.8842)/(100-6.8842-m3))^{(1-1/47663)}-1)^{(1-47663))}$
General Curve Fit "vG/P 5"	$(1/2.201)^{((((m0-6.8842)/(100-6.8842))^{(1-1/m6)}-1)^{(1-m6))}$
General Curve Fit "Brooks/Corey"	$m1/((m0-6.8842)/(100-6.8842-3.2177))^{(1/m4)}$
General Curve Fit "B/C2"	$m1/((m0-6.8842)/(100-6.8842-3.2177))^{(1/0.84178)}$
General Curve Fit "B/C3"	$.39724/((m0-6.8842)/(100-6.8842-3.2177))^{(1/m4)}$

Figure 13. Sample 23 curve fits

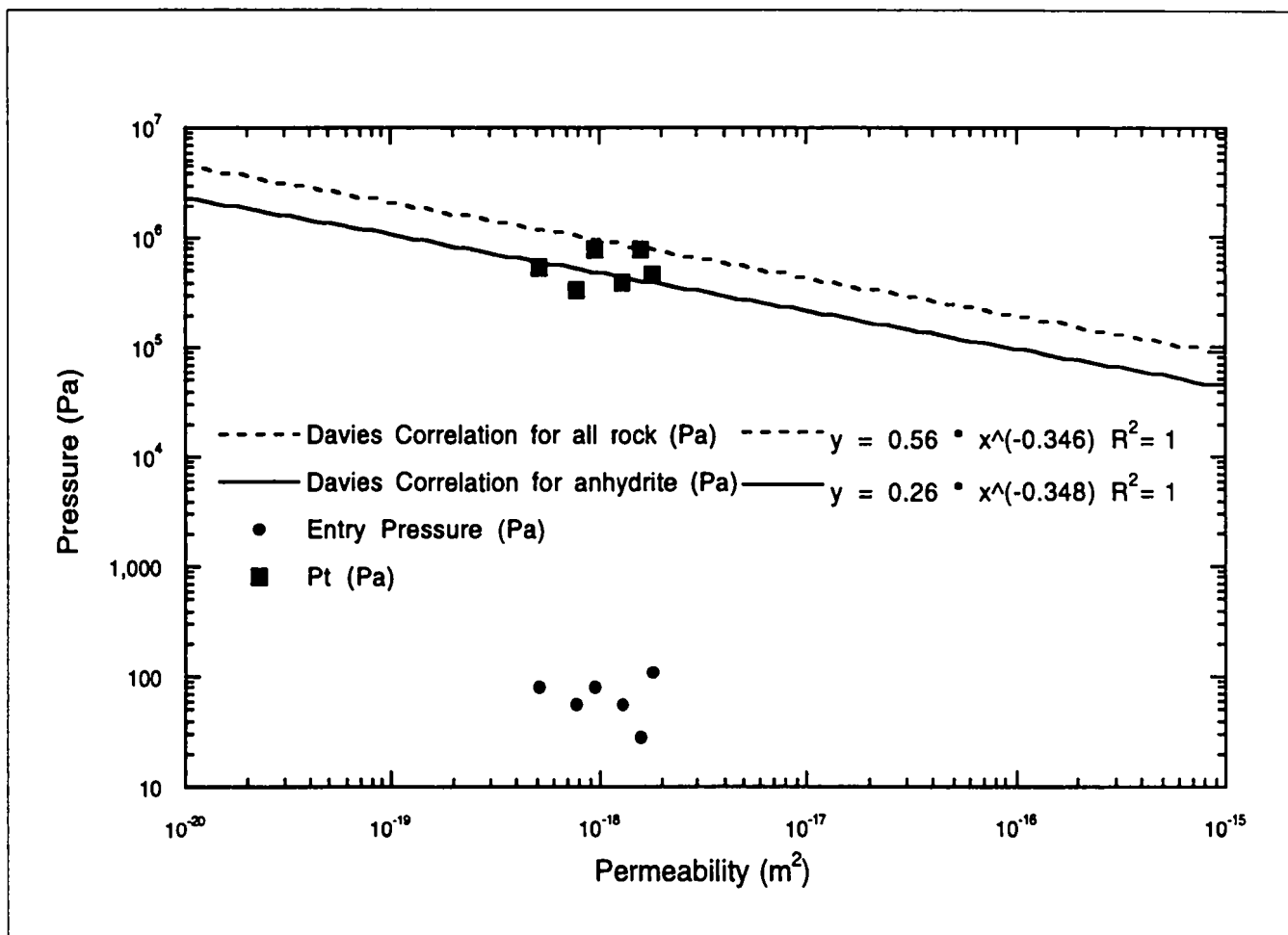


Figure 14. Permeability vs Threshold Pressure
Correlations found in SAND91-0893/3 page 2-13

Audit of Capillary Pressure Model Params

Worksheet Info		Map of Capillary Pressure Model Params											
			B	C	D	E	F	G	H	I	J	K	L
		1											
		2											
		3	T	T						T			
		4	T							T			
		5											
		6	T										
		7	T										
		8	T										
		9		T									
		10		T									
		11			T								
		12			T								
		13			T								
		14			T								
		15			T								
		16			T								
		17			T								
		18			T								
		19			T								
		20											
		21	T										
		22	T										
		23	T										
		24		T									
		25		T									
		26			T								
		27		T									
		28		T									
		29		T									
		30											
		31	T										
		32	T										
		33	T										
		34											
		35	T										
		36		T									
		37			T								T
		38			T								T
		39		T									
		40			T								T
		41			T								T
		42			T								T
		43			T								T
		44		T									
		45			T								T
		46			T								
		47											
		48											
		49	T		T			T		T			
		50		T	T			T					
		51		T	T			T			T		
		52		T	T			T					
		53		T	T			T			T		
		54		T	T			T			T		
		55		T	T			T			T		
		56		T	T			T			T		
		57		T	T			T			T		
		58		T	T			T			T		

LEGEND	
T	Text
F	Formula
9	Number
L	Logical
#	Error

Document Info

Name	Capillary Pressure Model Params
	No changes made since last save
Path	Dino:PA Parameters:2-Phase
Protection	None
Version	Microsoft Excel version 4.0
System	Macintosh 7.50

Worksheet Info

Active Area	830 rows by 11 columns
	9,130 cells
Blanks	8,812 (96.5%)
Constants	259 (2.8%)
Numbers	48 (0.5%)
Text	211 (2.3%)
Logicals	0 (0.0%)
Errors	0 (0.0%)
Formulas	59 (0.6%)
Names	30 total
	16 normal
	14 hidden
Objects	24

Audit of Capillary Pressure Model Params

Map of Capillary Pressure Model Params												
	B	C	D	E	F	G	H	I	J	K	L	
59		T	T			T						
60												
61	T											
62		T										
63		T										
64		T										
65		T										
66		T										
67		T										
68			T									
69		T										
70		T										
71		T										
72		T										
73												
74	T											
75		T										
76		T										
77		T										
78			T									
79			T									
80		T										
81			T									
82			T									
83			T									
84		T										
85			T									
86		T										
87		T	T									
88		T										
89		T										
90		T										
91		T										
92		T										
93		T										
94	T	T										
95		T										
96												
97		T										
98		T										
99		T										
100		T										
101		T										
102		T										
103		T										
104		T										
105			T									
106												
107	T											
108			T									
109			T									
110			T									
111			T									
112			T									
113			T									
114			T									
115			T									
116			T									

Audit of Capillary Pressure Model Params

Map of Capillary Pressure Model Params											
	B	C	D	E	F	G	H	I	J	K	L
117											
118		T									
119		T	T	T	T	T	T	T	T	T	T
120			T	T	T			T	T		T
121	T	9	9	9	9	9	F	F	9	9	9
122	T	9	9	9	9	9	F	F	9	9	9
123		9	9	9	9	9	F	F	9	9	9
124		9	9	9	9	9	F	F	9	9	9
125		9	9	9	9	9	F	F	9	9	9
126		9	9	9	9	9	F	F	9	9	9
127	T										
128	T		T	T	T	T					
129	T		F	F	F	F					
130	T		F	F	F	F					
131	T		F	F	F	F					
132	T		F	F	F	F					
133	T		F	F	F	F	F	F	F		
134	T		F	F	F	F					
135	T		F	F	F	F					
136	T		F	F	F	F					
137	T		F	F	F	F					
138	T		F	F	F	F					
139	T		F	F	F	F					
140											
141	T										
142		T									
143			T								
144											
145		T									
146		T									
147			T								
148		T									
149			T								
150											
151											
152											
153											
154											
155											
156											
157											
158											
159											
160											
161											
162											
163								T			
164											
165											
166											
167											
168											
169											
170											
171											
172											
173											
174											

Audit of Capillary Pressure Model Params

Map of Capillary Pressure Model Params												
	B	C	D	E	F	G	H	I	J	K	L	
175												
176												
177												
178								T				
179												
180												
181												
182												
183												
184												
185												
186												
187												
188												
189												
190												
191												
192												
193								T				
194												
195												
196												
197												
198												
199												
200												
201												
202												
203												
204												
205												
206												
207												
208								T				
209												
210												
211												
212												
213												
214												
215												
216												
217												
218												
219												
220												
221												
222												
223								T				
224												
225												
226												
227												
228												
229												
230												
231												
232												

Audit of Capillary Pressure Model Params

Map of Capillary Pressure Model Params												
	B	C	D	E	F	G	H	I	J	K	L	
233												
234												
235												
236												
237												
238								T				
239												
240												
241												
242												
243												
244												
245												
246												
247												
248												
249												
250												
251												
252												
253												
254												
255												
256												
257												
258												
259												
260												
261												
262												
263												
264												
265												
266												
267												
268												
269												
270												
271												
272												
273												
274												
275												
276												
277												
278												
279												
280												
281												
282												
283												
284												
285												
286												
287												
288												
289												
290												

Audit of Capillary Pressure Model Params

Map of Capillary Pressure Model Params												
	B	C	D	E	F	G	H	I	J	K	L	
291	T											
292												
293	T											
294												
295												
296												
297												
298												
299												
300												
301												
302												
303												
304												
305												
306												
307												
308												
309												
310												
311												
312												
313												
314												
315												
316												
317												
318												
319												
320												
321												
322												
323												
324												
325												
326												
327												
328												
329												
330												
331												
332												
333												
334												
335												
336												
337												
338	T											
339												
340												
341												
342												
343												
344												
345												
346												
347												
348												

Audit of Capillary Pressure Model Params

Map of Capillary Pressure Model Params												
	B	C	D	E	F	G	H	I	J	K	L	
349												
350												
351												
352												
353												
354												
355												
356												
357												
358												
359												
360												
361												
362												
363												
364												
365												
366												
367												
368												
369												
370												
371												
372												
373												
374												
375												
376												
377												
378												
379												
380												
381												
382												
383												
384	T											
385												
386												
387												
388												
389												
390												
391												
392												
393												
394												
395												
396												
397												
398												
399												
400												
401												
402												
403												
404												
405												
406												

Audit of Capillary Pressure Model Params

Map of Capillary Pressure Model Params												
	B	C	D	E	F	G	H	I	J	K	L	
407												
408												
409												
410												
411												
412												
413												
414												
415												
416												
417												
418												
419												
420												
421												
422												
423												
424												
425												
426												
427												
428												
429												
430	T											
431												
432												
433												
434												
435												
436												
437												
438												
439												
440												
441												
442												
443												
444												
445												
446												
447												
448												
449												
450												
451												
452												
453												
454												
455												
456												
457												
458												
459												
460												
461												
462												
463												
464												

Audit of Capillary Pressure Model Params

Map of Capillary Pressure Model Params

	B	C	D	E	F	G	H	I	J	K	L
465											
466											
467											
468											
469											
470											
471											
472											
473											
474											
475											
476	T										
477											
478											
479											
480											
481											
482											
483											
484											
485											
486											
487											
488											
489											
490											
491											
492											
493											
494											
495											
496											
497											
498											
499											
500											
501											
502											
503											
604											
505											
506											
607											
508											
509											
510											
511											
612											
513											
514											
515											
516											
517											
518											
519											
520											
521											
522											

Audit of Capillary Pressure Model Params

Map of Capillary Pressure Model Params												
	B	C	D	E	F	G	H	I	J	K	L	
523	T											
524												
525												
526												
527												
528												
529												
530												
531												
532												
533												
534												
535												
536												
537												
538												
539												
540												
541												
542												
543												
544												
545												
546												
547												
548												
549												
550												
551												
552												
553												
554												
555	T											
556												
557												
558												
559												
560												
561												
562												
563												
564												
565												
566												
567												
568												
569	T											
570												
571												
572												
573												
574												
575												
576												
577												
578												
579												
580												

Audit of Capillary Pressure Model Params

Map of Capillary Pressure Model Params

	B	C	D	E	F	G	H	I	J	K	L
581											
582											
583											
584											
585											
586											
587											
588											
589											
590											
591											
592											
593											
594											
595											
596											
597											
598											
599											
600											
601											
602											
603											
604											
605											
606											
607											
608											
609											
610											
611											
612											
613											
614											
615	T										
616											
617											
618											
619											
620											
621											
622											
623											
624											
625											
626											
627											
628											
629											
630											
631											
632											
633											
634											
635											
636											
637											
638											

Audit of Capillary Pressure Model Params

Map of Capillary Pressure Model Params												
	B	C	D	E	F	G	H	I	J	K	L	
639												
640												
641												
642												
643												
644												
645												
646												
647												
648												
649												
650												
651												
652												
653												
654												
655												
656												
657												
658												
659												
660												
661	T											
662												
663												
664												
665												
666												
667												
668												
669												
670												
671												
672												
673												
674												
675												
676												
677												
678												
679												
680												
681												
682												
683												
684												
685												
686												
687												
688												
689												
690												
691												
692												
693												
694												
695												
696												

Audit of Capillary Pressure Model Params

Map of Capillary Pressure Model Params												
	B	C	D	E	F	G	H	I	J	K	L	
697												
698												
699												
700												
701												
702												
703												
704												
705												
706												
707	T											
708												
709												
710												
711												
712												
713												
714												
715												
716												
717												
718												
719												
720												
721												
722												
723												
724												
725												
726												
727												
728												
729												
730												
731												
732												
733												
734												
735												
736												
737												
738												
739												
740												
741												
742												
743												
744												
745												
746												
747												
748												
749												
750												
751												
752												
753	T											
754												

Audit of Capillary Pressure Model Params

Map of Capillary Pressure Model Params												
	B	C	D	E	F	G	H	I	J	K	L	
755												
756												
757												
758												
759												
760												
761												
762												
763												
764												
765												
766												
767												
768												
769												
770												
771												
772												
773												
774												
775												
776												
777												
778												
779												
780												
781												
782												
783												
784												
785												
786												
787												
788												
789												
790												
791												
792												
793												
794												
795												
796												
797												
798												
799	T											
800												
801												
802												
803												
804												
805												
806												
807												
808												
809												
810												
811												
812												

Audit of Capillary Pressure Model Params

Map of Capillary Pressure Model Params												
	B	C	D	E	F	G	H	I	J	K	L	
813												
814												
815												
816												
817												
818												
819												
820												
821												
822												
823												
824												
825												
826												
827												
828												
829	T											
830	T											

E-49

	A	B	C	D	E	F	G	H	I	J	K
1											
2											
3	Calculation By:	Tracy Chris							Date:		
4	Checked By:								Date:		
5											
6	Purpose:										
7	To determine the two-ph										
8	Specific Parameters are										
9		and the po									
10		The followi									
11			CAP_MOD								
12			PC_MAX								
13			PORE_DIS								
14			REL_P_MOD								
15			SAT_IBRN								
16			SAT_RBRN								
17			SAT_RGAS								
18			PCT_A								
19			PCT_EXP								
20											
21	Calculation Descriptio										
22	Using the 140 degree C										
23	determine the following										
24		a) The two									
25		b) The Bro									
26			(BRAGFLO generate								
27		c) Determin									
28		d) Determin									
29		e) Based c									
30											
31	I did not start with the v										
32	not threshold pressure i										
33	I did not start with the v										
34											
35	Equations:										
36		Mixed Broc									
37			$P_c = P V S_e^{(1/\lambda)}$								eqn 1
38			$S_e = (S - S_{tr}) / (1 - S_{tr} - S_{gr})$								eqn 2
39		vG/P:									
40			$P_c = 1/\alpha ((S_e)^{-1} - 1)$								eqn 3
41			$m = \lambda / (\lambda + 1)$								eqn 4
42			$S_e = (S - S_{tr}) / (1 - S_{tr})$								eqn 5
43			$\alpha = 1 / (P V 0.5^{(1/\lambda)})$								eqn 6
44		Threshold									
45			$P_t = PCT_A^k * PCT_E$								eqn 7
46			if PCT_EXP=0, then								
47											
48											
49	Variables:		Description			Determination		KaleidaGraph Curve fit variable			
50		Pc	Capillary Pressure			data					
51		Pt	Threshold Pressure			data fit			m1		
52		S	Saturation of brine			data					
53		Sir	Residual liquid satur			data fit				m2	

	A	B	C	D	E	F	G	H	I	J	K
54		Sgr	Residual gas saturab			data fit			m3		
55		lambda	pore-size distribution			data fit			m4		
56		m	vanGenuchten param			Fit and calculated from k			m6		
57		alpha	vanGenuchten param			calc and fit			m5		
58		Se and Se	Effective Saturation			calculated					
59		k	Permeability			data					
60											
61	Assumptions:										
62		1) The cer									
63		because									
64		Sir couk									
65		2) Cores w									
66		3) 140 deg									
67		4) The dat									
68			and that this data is								
69		5) The thre									
70		liquid satur									
71		threshold p									
72		Brooks and									
73											
74	Process:										
75		Verified the									
76		Curve fit st									
77		1. Using K									
78			(eqn 3 except Se' is								
79			based upon Pc vs Sa								
80		2. Check t									
81			if they ar OK-- goto 3								
82			if they are not OK-- E								
83			and one low sat. poin								
84		3. Check									
85			until you get a Sir and								
86		4. Put the									
87		5. Obtain	3 variables (Pt, Sir, la								
88		6. Deferm									
89		7. Using e									
90		8. Using e									
91		9. Curve fit									
92		10. Curve f									
93		11. Equate									
94	Solution:	The values									
95		Each curve									
96											
97		No definitiv									
98		show that									
99		Figure 1 a,									
100		Figure 2 sh									
101		Figures 3,									
102		Figure 7 sh									
103		Figures 8 t									
104		Figure 14 d									
105			determined for the s								
106											

E-50

	A	B	C	D	E	F	G	H	I	J	K
107	Recommendations:										
108			1. use 50% mixed Bl								
109			2. The mean value of								
110			3. The mean value of								
111			4. The mean value of								
112			5. The mean value of								
113			6. The maximum Pc								
114			7. The initial brine sat								
115			8. The Davies ratio								
116			relating threshold pres								
117											
118		TABLE 1.									
119		Sample	Pt	S _{lr}	S _{gr}	Lambda	m	Alpha	Pc Max	Figure	Perm
120			(MPa)	(%)	(%)			(1/MPa)	(MPa)		(m2)
121	Mercury	5	0.54132	7.262	11.637	0.65521	=lambda/(1+lambda)	=1/(PV0.5*(1/lambda))*(((0.5*(1-m))-1)^(1-m))	100	8	5.1E-19
122	Injection	7	0.78	6.986	7.7729	0.66452	=lambda/(1+lambda)	=1/(PV0.5*(1/lambda))*(((0.5*(1-m))-1)^(1-m))	100	9	9.5E-19
123		11	0.45026	17.401	1.3981	0.55775	=lambda/(1+lambda)	=1/(PV0.5*(1/lambda))*(((0.5*(1-m))-1)^(1-m))	100	10	0.000000000000000018
124		13	0.75274	10.861	19.719	0.652	=lambda/(1+lambda)	=1/(PV0.5*(1/lambda))*(((0.5*(1-m))-1)^(1-m))	100	11	0.000000000000000016
125		21	0.32914	0.77846	2.5201	0.49053	=lambda/(1+lambda)	=1/(PV0.5*(1/lambda))*(((0.5*(1-m))-1)^(1-m))	100	12	7.7E-19
126		23	0.39724	6.8842	3.2177	0.84178	=lambda/(1+lambda)	=1/(PV0.5*(1/lambda))*(((0.5*(1-m))-1)^(1-m))	100	13	0.000000000000000013
127	Statistics										
128			Pt (MPa)	S _{lr} (%)	S _{gr} (%)	Lambda					
129	Minimum		=MIN(Pt)	=MIN(S _{lr})	=MIN(S _{gr})	=MIN(lambda)					
130	Maximum		=MAX(Pt)	=MAX(S _{lr})	=MAX(S _{gr})	=MAX(lambda)					
131	Sum		=SUM(Pt)	=SUM(S _{lr})	=SUM(S _{gr})	=SUM(lambda)					
132	Points		=COUNTA(Pt)	=COUNTA(S _{lr})	=COUNTA(S _{gr})	=COUNTA(lambda)					
133	Mean		=AVERAGE(Pt)	=AVERAGE(S _{lr})	=AVERAGE(S _{gr})	=AVERAGE(lambda)	=F133/(1+F133)	=1/(C133*0.5*(1/F133))*(((0.5*(1-G133))-1)^(1-G133))	=AVERAGE(I121:I126)		
134	Median		=MEDIAN(Pt)	=MEDIAN(S _{lr})	=MEDIAN(S _{gr})	=MEDIAN(lambda)					
135	Std Deviation		=STDEV(Pt)	=STDEV(S _{lr})	=STDEV(S _{gr})	=STDEV(lambda)					
136	Variance		=VAR(Pt)	=VAR(S _{lr})	=VAR(S _{gr})	=VAR(lambda)					
137	Std Error		=C135/(C132)^0.5	=D135/(D132)^0.5	=E135/(E132)^0.5	=F135/(F132)^0.5					
138	Skewness		=SKEW(Pt)	=SKEW(S _{lr})	=SKEW(S _{gr})	=SKEW(lambda)					
139	Kurtosis		=KURT(Pt)	=KURT(S _{lr})	=KURT(S _{gr})	=KURT(lambda)					
140											
141	Verification of Software										
142		1. Software									
143			Micro/Microsoft Excel								
144											
145		2. All software									
146		3. Kateda									
147			the appropriate curve								
148		4. Hand									
149			end of this calc sheet								
150											

E-51

RECORD 3

General Correspondence

RECORD 4

Technical Review of Record Package

January 31, 1996

Technical Review of Record Package

SALADO PARAMETER PRINCIPAL INVESTIGATOR DOCUMENTATION PACKAGE FOR: ANHYDRITE TWO-PHASE PARAMETERS

Technical Review Status:

Scientific Notebooks:

Not Applicable X ; Incomplete _____; Complete _____
(Give Date) (Give Date)

Interpretive Analyses:

Not Applicable ; Incomplete _____; Complete December 21, 1995
(Give Date) (Give Date)

Routine Calculations:

Capillary Pressure Model Parameters Calc. Sheet Incomplete _____; Complete December 21, 1995
(Give Date) (Give Date)

Qualification Status:

Data: Used WIPP Observational Data

Not Applicable _____; Incomplete 1/31/96 ; Complete _____
(Give Date) (Give Date)

NOTES:

Data must be technically reviewed and forwarded to SWCF (TLCF-1/31/96)

Codes

Microsoft Excell; Incomplete _____; Complete 12/21/95 (in use verification)
(Give Date) (Give Date)

KaleidaGraph; Incomplete _____; Complete 12/21/95 (in use verification)
(Give Date) (Give Date)

PARAMETER QUALIFIED: Incomplete: 1/31/96 ; Complete: _____
(Give Date) (Give Date)

RECORD 5

Roadmap to Supporting Documentation

January 31, 1996

RAODMAP FOR
SALADO PARAMETER PRINCIPAL INVESTIGATOR DOCUMENTATION PACKAGE FOR:
ANHYDRITE TWO-PHASE PARAMETERS

RECORD 6

Memo to PA Parameter Task Leader

Sandia National Laboratories

Albuquerque, New Mexico 87185-1341

date: January 31, 1996
to: PA Parameter Task Leader


from: Tracy L. Christian-Frear, MS-1324 (6115)

subject: SALADO PARAMETER PRINCIPAL INVESTIGATOR DOCUMENTATION
PACKAGE FOR: ANHYDRITE TWO-PHASE PARAMETERS

The attached record contains the anhydrite two-phase values for the capillary and relative permeability models, the residual gas and brine saturation, the initial brine saturation, pore size distribution parameter and the threshold pressure.

The title of the records package is: SALADO PARAMETER PRINCIPAL
INVESTIGATOR DOCUMENTATION PACKAGE FOR: ANHYDRITE TWO-
PHASE PARAMETERS

The SWCF is: SWCF-A:WBS 1.2.07.1:PDD:QA:SALADO:PKG 10:Anh 2-Phase
Parameters

The WPO is: 30643

The deficiencies in the parameter documentation are:
Data must be technically reviewed and forwarded to SWCF

Please call me at 848-0704 if you have any questions.

Attachment:

SALADO DATA/PARAMETERS : ANHYDRITE TWO-PHASE PARAMETERS

Appendix F.
Memorandum: S.W. Webb to P. Vaughn, August 29, 1995

The following information is provided as Appendix F of this document.

Appendix F

Memorandum: S.W. Webb to P. Vaughn, August 29, 1995.

Errata Sheet

The two citations in Appendix F:

Davies, SAND90-3246 on p. F-3 and

Davies (1991) on p. F-4

refer to the same report. A copy is on file in SWCF as WPO#26169.

Sandia National Laboratories

Albuquerque, New Mexico 87185

date: August 29, 1995

to: P. Vaughn, MS-1328 (6749)

from:  S.W. Webb, MS-1324 (6115)

subject: Mixed Brooks and Corey Two-Phase Characteristic Curves

The mixed Brooks and Corey two-phase characteristic curves have been used in SPM-2 calculations and will be recommended for future studies including the compliance application. The mixed Brooks and Corey model uses two definitions of the effective saturation to reflect the different saturation ranges for the relative permeabilities of the wetting and nonwetting phases. However, the approach used in SPM-2 was inconsistent with the definition of threshold pressure used in the Davies' correlation (Davies, SAND90-3246), partially due to the use of displacement pressure instead of threshold pressure in the original specification. The correct form of the mixed Brooks and Corey curves consistent with Davies' threshold pressure definition is summarized below.

In the mixed Brooks and Corey model, two separate effective saturations are used which are defined as

$$S_e = \frac{S - S_r}{1 - S_r} \quad (1)$$

$$S'_e = \frac{S - S_r}{S_c - S_r} \quad (2)$$

where

- S_e = effective saturation
- S = wetting phase saturation
- S_r = wetting phase residual saturation
- S_c = critical gas saturation = $1 - S_{r,nw}$
- $S_{r,nw}$ = nonwetting phase residual saturation.

S_e is the original Brooks and Corey definition while S'_e is a modified definition.

The capillary pressure relationship is

$$S_e' = \left(\frac{P_t}{P_c} \right)^\lambda \quad (3)$$

or

$$P_c = \frac{P_t}{S_e'^{1/\lambda}} \quad (4)$$

where P_t and P_c are the threshold pressure and the capillary pressure, respectively, and λ is the pore-size distribution parameter.

The wetting phase relative permeability expression is given by

$$k_{r,w} = S_e^{(2+3\lambda)/\lambda} \quad (5)$$

while the nonwetting phase relationship is

$$k_{r,nw} = (1 - S_e)^2 (1 - S_e^{(2+3\lambda)/\lambda}) \quad (6)$$

Therefore, consistent with Davies (1991), the threshold pressure is the capillary pressure when the saturation is equal to the critical gas saturation (S_c), or when S_e' equals 1.0.

If there are any questions, please contact me.

cc:

MS-1324 P.B. Davies (6115)
MS-1324 A.R. Lappin (6115)
MS-1324 T.L. Christian-Frear (6115)
MS-1328 D.R. Anderson (6749)
MS-1341 K.W. Larson (6747)

WIPP
UC721 - DISTRIBUTION LIST
SAND94-0472

Federal Agencies

US Department of Energy (4)
Office of Civilian Radioactive Waste Mgmt.
Attn: Deputy Director, RW-2
Acting Director, RW-10
Office of Human Resources & Admin.
Director, RW-30
Office of Program Mgmt. & Integ.
Director, RW-40
Office of Waste Accept., Stor., & Tran.
Forrestal Building
Washington, DC 20585

Attn: Project Director
Yucca Mountain Site Characterization Office
Director, RW-3
Office of Quality Assurance
P.O. Box 30307
Las Vegas, NV 89036-0307

US Department of Energy
Albuquerque Operations Office
Attn: National Atomic Museum Library
P.O. Box 5400
Albuquerque, NM 87185-5400

US Department of Energy
Research & Waste Management Division
Attn: Director
P.O. Box E
Oak Ridge, TN 37831

US Department of Energy (5)
Carlsbad Area Office
Attn: G. Dials
D. Galbraith
M. McFadden
R. Lark
J. A. Mewhinney
P.O. Box 3090
Carlsbad, NM 88221-3090

US Department of Energy
Office of Environmental Restoration and
Waste Management
Attn: M Frei, EM-30
Forrestal Building
Washington, DC 20585-0002

US Department of Energy (3)
Office of Environmental Restoration and
Waste Management
Attn: J. Juri, EM-34, Trevion II
Washington, DC 20585-0002

US Department of Energy
Office of Environmental Restoration and
Waste Management
Attn: S. Schneider, EM-342, Trevion II
Washington, DC 20585-0002

US Department of Energy (2)
Office of Environment, Safety & Health
Attn: C. Borgstrom, EH-25
R. Pelletier, EH-23 I
Washington, DC 20585

US Department of Energy (2)
Idaho Operations Office
Fuel Processing & Waste Mgmt. Division
785 DOE Place
Idaho Falls, ID 83402

US Environmental Protection Agency (2)
Radiation Protection Programs
Attn: M. Oge
ANR-460
Washington, DC 20460

Boards

Defense Nuclear Facilities Safety Board
Attn: D. Winters
625 Indiana Ave. NW, Suite 700
Washington, DC 20004

Nuclear Waste Technical Review Board (2)
Attn: Chairman
J. L. Cohon
1100 Wilson Blvd., Suite 910
Arlington, VA 22209-2297

State Agencies

Attorney General of New Mexico
P.O. Drawer 1508
Santa Fe, NM 87504-1508

Environmental Evaluation Group (3)
Attn: Library
7007 Wyoming NE
Suite F-2
Albuquerque, NM 87109

NM Environment Department (3)
Secretary of the Environment
Attn: Mark Weidler
1190 St. Francis Drive
Santa Fe, NM 87503-0968

NM Bureau of Mines & Mineral Resources
Socorro, NM 87801

Laboratories/Corporations

Battelle Pacific Northwest Laboratories
Battelle Blvd.
Richland, WA 99352

INTERA, Inc.
Attn: G. A. Freeze
1650 University Blvd. NE, Suite 300
Albuquerque, NM 87102

INTERA, Inc.
Attn: J. F. Pickens
6850 Austin Center Blvd., Suite 300
Austin, TX 78731

Los Alamos National Laboratory
Attn: B. Erdal, INC-12
P.O. Box 1663
Los Alamos, NM 87544

RE/SPEC, Inc.
Attn: A. Robb
4775 Indian School NE, Suite 300
Albuquerque, NM 87110-3927

RE/SPEC, Inc.
Attn: J. L. Ratigan
P. O. Box 725
Rapid City, SD 57709

Tech Reps, Inc. (3)
Attn: J. Chapman (1)
Loretta Robledo (2)
5000 Marble NE, Suite 222
Albuquerque, NM 87110

Westinghouse Electric Corporation (5)
Attn: Library
J. Epstein
J. Lee
B. A. Howard
R. Kehrman
P.O. Box 2078
Carlsbad, NM 88221

S. Cohen & Associates
Attn: Bill Thurber
1355 Beverly Road
McLean, VA 22101

Rock Physics Associates
Attn: J. Walls
4320 Steven Creek Blvd., Ste 282
San Jose, CA 95129

**National Academy of Sciences,
WIPP Panel**

Howard Adler
Oxyrase, Incorporated
7327 Oak Ridge Highway
Knoxville, TN 37931

Tom Kiess
Board of Radioactive Waste Management
GF456
2101 Constitution Ave.
Washington, DC 20418

Rodney C. Ewing
Department of Geology
University of New Mexico
Albuquerque, NM 87131

Charles Fairhurst
Department of Civil and Mineral Engineering
University of Minnesota
500 Pillsbury Dr. SE
Minneapolis, MN 55455-0220

B. John Garrick
PLG Incorporated
4590 MacArthur Blvd., Suite 400
Newport Beach, CA 92660-2027

Leonard F. Konikow
US Geological Survey
431 National Center
Reston, VA 22092

Carl A. Anderson, Director
Board of Radioactive Waste Management
National Research Council
HA 456
2101 Constitution Ave. NW
Washington, DC 20418

Christopher G. Whipple
ICF Kaiser Engineers
1800 Harrison St., 7th Floor
Oakland, CA 94612-3430

John O. Blomeke
720 Clubhouse Way
Knoxville, TN 37909

Sue B. Clark
University of Georgia
Savannah River Ecology Lab
P.O. Drawer E
Aiken, SC 29802

Konrad B. Krauskopf
Department of Geology
Stanford University
Stanford, CA 94305-2115

Della Roy
Pennsylvania State University
217 Materials Research Lab
Hastings Road
University Park, PA 16802

David A. Waite
CH₂ M Hill
P.O. Box 91500
Bellevue, WA 98009-2050

Thomas A. Zordon
Zordan Associates, Inc.
3807 Edinburg Drive
Murrysville, PA 15668

Universities

University of New Mexico
Geology Department
Attn: Library
141 Northrop Hall
Albuquerque, NM 87131

Libraries

Thomas Brannigan Library
Attn: D. Dresp
106 W. Hadley St.
Las Cruces, NM 88001

Government Publications Department
Zimmerman Library
University of New Mexico
Albuquerque, NM 87131

New Mexico Junior College
Pannell Library
Attn: R. Hill
Lovington Highway
Hobbs, NM 88240

New Mexico State Library
Attn: N. McCallan
325 Don Gaspar
Santa Fe, NM 87503

New Mexico Tech
Martin Speere Memorial Library
Campus Street
Socorro, NM 87810

WIPP Public Reading Room
Carlsbad Public Library
101 S. Halagueno St.
Carlsbad, NM 88220

Foreign Addresses

Atomic Energy of Canada, Ltd.
Whiteshell Laboratories
Attn: B. Goodwin
Pinawa, Manitoba, CANADA R0E 1L0

Francois Chenevier (2)
ANDRA
Route de Panorama Robert Schumann
B. P. 38
92266 Fontenay-aux-Roses, Cedex
FRANCE

Claude Sombret
 Centre d'Etudes Nucleaires de la Vallee Rhone
 CEN/VALRHO
 S.D.H.A. B.P. 171
 30205 Bagnols-Sur-Ceze
 FRANCE

Commissariat a L'Energie Atomique
 Attn: D. Alexandre
 Centre d'Etudes de Cadarache
 13108 Saint Paul Lez Durance Cedex
 FRANCE

Bundesanstalt fur Geowissenschaften und
 Rohstoffe
 Attn: M. Langer
 Postfach 510 153
 D-30631 Hannover
 GERMANY

Bundesministerium fur Forschung und
 Technologie
 Postfach 200 706
 5300 Bonn 2
 GERMANY

Institut fur Tieflagerung
 Attn: K. Kuhn
 Theodor-Heuss-Strasse 4
 D-3300 Braunschweig
 GERMANY

Gesellschaft fur Anlagen und Reaktorsicherheit
 (GRS)
 Attn: B. Baltes
 Schwertnergasse 1
 D-50667 Cologne
 GERMANY

Shingo Tashiro
 Japan Atomic Energy Research Institute
 Tokai-Mura, Ibaraki-Ken, 319-11
 JAPAN

Netherlands Energy Research Foundation ECN
 Attn: J. Prij
 3 Westerduinweg
 P.O. Box 1
 1755 ZG Petten
 THE NETHERLANDS

Svensk Karnbransleforsorjning AB
 Attn: F. Karlsson
 Project KBS (Karnbranslesakerhet)
 Box 5864
 S-102 48 Stockholm
 SWEDEN

Nationale Genossenschaft fur die Lagerung
 Radioaktiver Abfalle (2)
 Attn: S. Vomvoris
 P. Zuidema
 Hardstrasse 73
 CH-5430 Wettingen
 SWITZERLAND

AEA Technology
 Attn: J. H. Rees
 D5W/29 Culham Laboratory
 Abington, Oxfordshire OX14 3DB
 UNITED KINGDOM

AEA Technology
 Attn: W. R. Rodwell
 044/A31 Winfrith Technical Centre
 Dorchester, Dorset DT2 8DH
 UNITED KINGDOM

AEA Technology
 Attn: J. E. Tinson
 B4244 Harwell Laboratory
 Didcot, Oxfordshire OX11 0RA
 UNITED KINGDOM

Internal

<u>MS</u>	<u>Org.</u>	
1324	6115	P. B. Davies
1324	6115	T. L. Christian-Freear (5)
1324	6115	C. Boney
1324	6115	R. L. Beauheim
1324	6115	S. W. Webb
1320	6831	E. J. Nowak
1322	6121	J. R. Tillerson
1328	6849	D. R. Anderson
1328	6848	H. N. Jow
1335	6801	M. Chu
1335	6801	S. M. Howarth (15)
1341	6832	J. T. Holmes
1395	6800	L. Shephard
1395	6821	M. Marietta
0751	6117	L. S. Costin
0751	6117	N. S. Brodsky
0751	6117	J. T. Fredrich
0751	6117	D. J. Holcomb

0751	6117	D. H. Zeuch
0705	6116	D. J. Borns
1330	6811	K. Hart (2)
1330	4415	NWM Library (20)
9018	8940-2	Central Technical Files
0899	4414	Technical Library (5)
0619	12690	Review and Approval Desk (2), For DOE/OSTI